The Photolysis and Pyrolysis of Succinimide Vapor

by G. Choudhary,[1] A. M. Cameron,[2] and R. A. Back

Publication No. 10235 from the Division of Pure Chemistry, National Research Council of Canada, Ottawa, Canada
(Received March 18, 1968)

The photolysis of succinimide vapor at pressures of 5–20 torr and temperatures of 160–200° with light of wavelength of about 2300–2600 Å appears to proceed by four concurrent molecular processes: (1) $CH_2CH_2CONHCO + h\nu \rightarrow CO + HNCO + C_2H_4$ (~40%); (2) $CH_2CH_2CONHCO + h\nu \rightarrow CO_2 + HCN + C_2H_4$ (~40%); (3) $CH_2CH_2CONHCO + h\nu \rightarrow CO + H_2O + CH_2=CHCN$ (~10%); (4) $CH_2CH_2CONHCO + h\nu \rightarrow CO_2 + CH_3CH_2CN$ (~10%). It is suggested that these may occur through a common initial ring-opening step, followed by rearrangement and fragmentation. The pyrolysis of succinimide vapor followed first-order kinetics at temperatures of 425–500° and pressures of 100–300 torr, with Arrhenius parameters $E = 52$ kcal/mol and $A = 1.2 \times 10^{10}$ sec^{-1}. The products were similar to the photolysis, but with reactions 3 and 4 favored relative to 1 and 2. The photolysis and pyrolysis of N-methylsuccinimide appeared to proceed chiefly by the process analogous to reaction 1, yielding CO, C_2H_4, and CH_3NCO, with the analog of reaction 2 occurring to some extent. Reactions corresponding to 3 and 4 were not observed. Saturation vapor pressures of both compounds are reported. The absorption spectrum of succinimide vapor was measured at 2000–8000 Å and shows a maximum at ~2200 Å with a shoulder around 2450 Å.

Introduction

There has been considerable interest in recent years in the photolysis and the pyrolysis of simple ring compounds. Imides of dicarboxylic acids have apparently not been studied previously in this regard. Succinimide was of special interest as a possible source of NH radicals or of succinimidyl radicals. The present article describes a detailed study of the photolysis of succinimide vapor and a brief study of the pyrolysis. The photolysis and pyrolysis of N-methylsuccinimide were also investigated very briefly for comparison.

Experimental Section

The vapor was photolyzed in a cylindrical quartz cell, 5 cm in diameter and 10 cm long, mounted in a heated box which provided controlled temperatures up to 200°. Solid succinimide was kept in a storage tube within the heated box but was cooled to ~20°. Its temperature could be raised to provide succinimide vapor at any desired pressure, up to about 28 torr

(the vapor pressure at 200°). Tests showed that thermal decomposition of succinimide, either of the vapor up to 200° or of the solid or liquid during the vaporization procedure or of the solid stored for some weeks at 20°, was negligible.

The light source was a Hanovia S-500 medium-pressure mercury arc, unfiltered in most of the work. The absorption spectrum of the vapor was determined directly in the reaction vessel, using a McPherson 0.5-m grating monochromator equipped with a photomultiplier to measure the transmitted light.

The vapor pressure of succinimide was measured over a range of temperature using either a quartz spiral or, for more accurate data, a mercury manometer with both arms evacuated and sealed, having succinimide in

(1) National Research Council of Canada Postdoctorate Fellow, 1965–1967.

(2) National Research Council of Canada Summer Research Assistant, 1965.

a side tube attached to one arm, mounted in the heated box, and read with a cathetometer.

Succinimide was obtained from Eastman and was used in most experiments without further purification, other than prolonged pumping to remove water vapor and dissolved air. Succinimide recrystallized from ethanol or sublimed several times under vacuum showed behavior identical with that of the unpurified reagent.

The pyrolysis of succinimide vapor was done in small Pyrex tubes (2 cm in diameter and 12 cm long) sealed under vacuum and placed in a cylindrical furnace preheated to the desired temperature. Pressure in each tube was calculated from the known volume, temperature, and weight of succinimide. After pyrolysis, the tubes were attached by means of a break-seal to the vacuum line for analysis.

Photolysis and pyrolysis products were separated by means of suitable cold traps into three fractions. The first, volatile at −210°, was shown to be entirely CO. The second, volatile at −181°, was entirely C_2H_4. The third fraction, volatile at 25°, was a mixture of products which were analyzed further by gas chromatography and mass spectrometry and will be discussed later.

N-Methylsuccinimide was obtained from Frinton Laboratories and was studied by the same techniques employed with succinimide.

Results and Discussion

Vapor Pressure Data. Saturation vapor pressures of liquid succinimide and N-methylsuccinimide were found to be represented by the equations

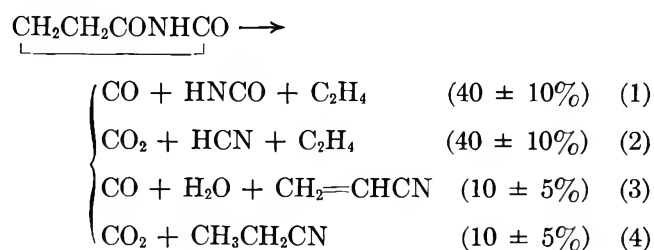$$\log p(\text{torr}) = 9.05 - (3530/T)$$

and

$$\log p(\text{torr}) = 5.05 - (1530/T)$$

for the temperature ranges 126–177° and 83–122°, respectively, from which may be derived molar heats of vaporization of about 4100 and 1800 cal. The higher heat of vaporization of succinimide, its lower volatility (10 torr at 166° *vs.* 10 torr at 105°), and its higher melting point (126 *vs.* 66°) all point to extensive hydrogen bonding of the imide hydrogen in liquid and solid succinimide, which is absent in the N-methyl derivative. There is no information about the extent of dimer formation in the vapor, but evidence from comparable systems suggests that it was probably of no consequence in the present experiments.

The Photolysis of Succinimide. Products. Products of the photolysis were CO, C_2H_4, HNCO, CO_2, HCN, C_2H_5CN, and C_2H_3CN, in approximately decreasing order of importance, together with trace amounts (≪1% of the total product) of n-C_4H_{10}, ethylene oxide, C_2H_5NCO, C_2H_6, C_2H_2, and butene. The products nonvolatile at −181° were analyzed by gas

chromatography, using for the most part dinonyl phthalate on firebrick and, on occasion, Porapak Q, dimethyl sulfolane, and silicone rubber columns. The identity of products was established by elution times and by direct analysis of the effluent gas with a mass spectrometer. The quantitative measurement of the nitrogenous products proved very difficult. HNCO and HCN were lost in an irregular fashion in the product traps by polymerization and perhaps by reaction with succinimide. They also disappeared in the inlet system and on the columns of the gas chromatograph. The nitriles were less troublesome, but in the product mixture there was some loss perhaps by copolymerization with HNCO. Probably the most accurate estimate of these products was obtained by admitting the sample directly to a mass spectrometer through a metal-free inlet system.

The relative product yields observed are approximately in accord with the occurrence of four concurrent processes

$$\overline{CH_2CH_2CONHCO} \longrightarrow$$

$$\begin{cases} CO + HNCO + C_2H_4 & (40 \pm 10\%) \quad (1) \\ CO_2 + HCN + C_2H_4 & (40 \pm 10\%) \quad (2) \\ CO + H_2O + CH_2{=}CHCN & (10 \pm 5\%) \quad (3) \\ CO_2 + CH_3CH_2CN & (10 \pm 5\%) \quad (4) \end{cases}$$

Wavelength of the Photolytic Light. The absorption spectrum of succinimide vapor, measured in the photolysis cell at a pressure of 9.8 torr at 190°, is shown in Figure 1. From this spectrum and that of the medium-pressure mercury arc, it is evident that a fairly broad range of wavelengths, from about 2000 to 2700 Å, was absorbed, with emission lines at 2652, 2571, 2537 (reversed), 2482, 2400, 2360, and 2300 Å being of major importance. This was confirmed by experiments with a Vycor filter (Corning 7910) which cuts off sharply at
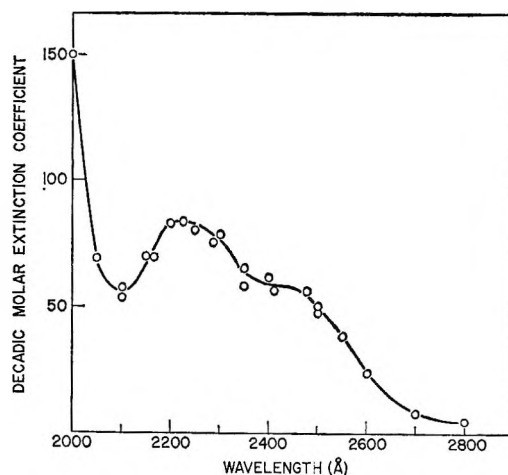

Figure 1. Absorption spectrum of succinimide vapor at 9.8 torr and 190°.

2200 Å, and had little effect upon the product yields, and with a Corex filter (Corning 9700) with a sharp cutoff at 2600 Å, which reduced yields to less than 5% of their original values. One experiment was performed with a mercury resonance lamp (2537 Å), which was

Reaction 1 then would occur by simple fragmentation into C_2H_4, HNCO, and CO. Reactions 2 and 4 could proceed through a splitting out of CO_2 followed by transfer of a hydrogen atom and decomposition, as shown below.
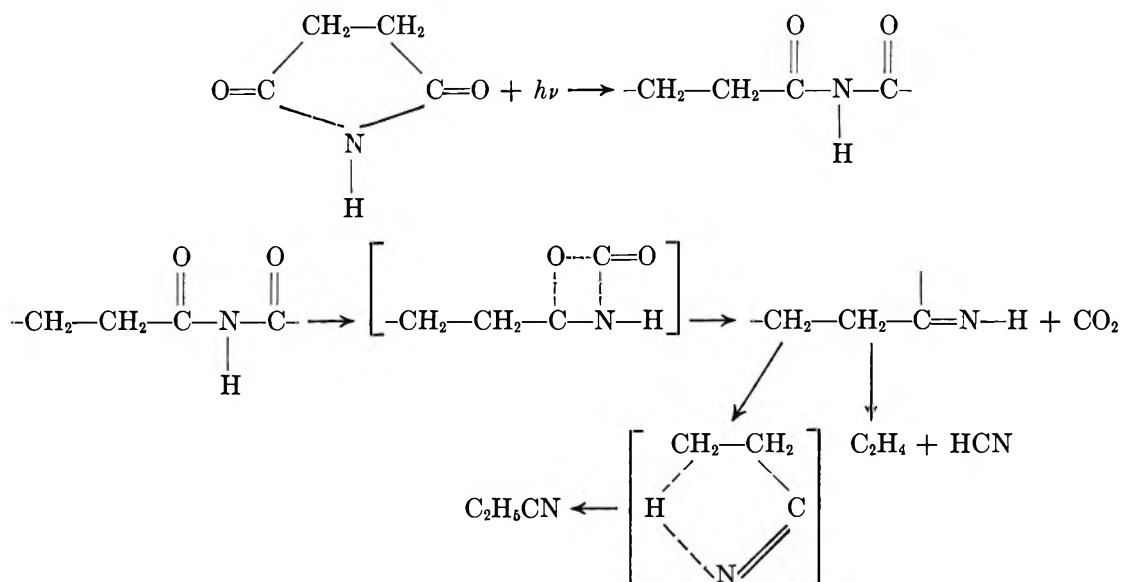
Reaction 3 could occur by successive loss of CO and H_2O
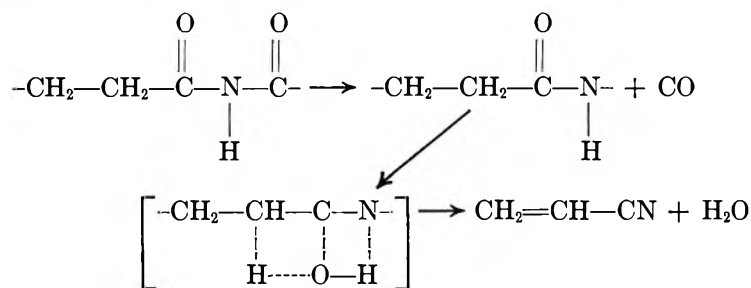
probably a mercury-sensitized decomposition rather than a direct photolysis.

Product ratios in all these experiments remained virtually unchanged within the uncertainties of the analysis. Thus the relative importance of reactions 1–4 appears largely unaffected by photon energy in this range.

The Mechanism of the Photolysis. Within the accuracy of the analysis, the ratios of the major products were observed to be independent of wavelength, pressure (5–20 torr), temperature (160–200°), conversion (3–20%), and light intensity (varied by a factor of 10) and were unaffected by the addition of propylene or ethylene.

These observations indicate that the photolysis was a unimolecular process rather than a free-radical one. The products observed strongly support this view, as it would be difficult to devise a free radical mechanism that would yield these products and no others. Reactions 1–4 can be reasonably rationalized in terms of a common initial ring-opening step.

The minor products, ethylene oxide and C_2H_5NCO, can also be accounted for by similar plausible processes.

The formation of *n*-butane and ethane as minor products suggests that hydrogen atoms were produced in the photolysis and added to ethylene (present as a product) to form ethyl radicals. This was confirmed by the production of propane and hexane instead of ethane and butane in the presence of 25 torr of propylene. The hydrogen atoms may have come from a primary process or possibly from secondary photolysis of HNCO. Their yield was less than 1% of the sum of reactions 1–4.

Formation of NH radicals was also apparently not important in the photolysis. Reactions of NH with ethylene should have yielded H_2 and CH_4, while other reactions might have been expected to produce at least some N_2; none of these products was observed.[3]

The Pyrolysis of Succinimide Vapor. The pyrolysis was studied from 425 to 500° at pressures from 100 to

(3) W. D. Woolley and R. A. Back, *Can. J. Chem.*, **46**, 295 (1965).

300 torr. The major products were the same as those of the photolysis, with an additional product, CH_3CN, appearing in amounts about 10% of the CO. There was relatively less ethylene produced than in the photolysis, suggesting that reactions 3 and 4 were favored relative to 1 and 2. This reduced fragmentation is understandable in view of the lower energy per molecule in the pyrolysis (~52 kcal/mol, see below) compared with 105–130 kcal/mol in the photolysis.

The decomposition rate, based on CO production, showed first-order kinetics independent of pressure and conversion up to at least 10%. First-order rate constants, each derived from a number of experiments at various pressures and times, are shown in Table I. From these data, Arrhenius parameters of $E = 52$ kcal/mol and $A = 1.2 \times 10^{10}$ sec^{-1} were obtained. While the sealed-tube technique is not conducive to precise kinetic measurements, the values of k in Table I are probably accurate to $\pm 10\%$.

Table I: First-Order Rate Constants for CO Production in the Pyrolysis of Succinimide

| Temp, °C	$k \times 10^7$
426	8.5
450	25
476	56
501	300

The similarity of the products of the pyrolysis to those of the photolysis suggests a similar mechanism. If the initial step is ring opening, as suggested, and if the activation energy of 52 kcal may be correlated with this process, it indicates considerable strain energy in the succinimide ring. Reaction 1, the main source of CO, could, on the other hand, be a more or less a concerted (rather than a stepwise) process, in which case no simple correlation with bond dissociation energy would be possible. The rather low A factor is probably compatible with either possibility, and no clear decision can be made from the present data.

The Photolysis and Pyrolysis of N-Methylsuccinimide. The photolysis was studied briefly at 120° and a pressure of about 11 torr. Carbon monoxide and ethylene were again major products, and, as with succinimide, quantitative analysis of the product fraction condensable at $-181°$ was difficult. A further complication

was the occurrence of extensive secondary photolysis and the polymerization of methyl isocyanate, a major product, which set in even at relatively low conversions. It is fairly clear, however, that the major process, probably accounting for 80 or 90% of the photolysis, is the reaction

$$\underline{CH_2CH_2CONCH_3CO} \longrightarrow$$

$$CO + CH_3NCO + C_2H_4 \quad (5)$$
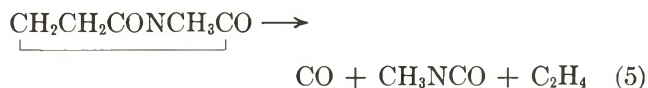
which corresponds to reaction 1 in the succinimide system. It is interesting to note that C_2H_5CN and C_2H_3CN, while detectable, were less than 1% of the CO, and their methyl-substituted analogs were not observed. This tends to support the imide-hydrogen transfer mechanism suggested for reactions 3 and 4, which would be blocked by methyl substitution. HCN was observed as a product, but it may well have come from secondary photolysis of CH_3NCO.[4] CH_3CN was a minor product, which suggests that the analog of reaction 2 may have occurred

$$\underline{CH_2CH_2CONCH_3CO} \longrightarrow C_2H_4 + CH_3CN + CO_2$$

$$(6)$$
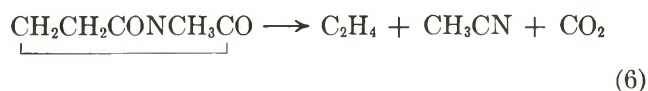
This would not require migration of a CH_3 group, as the reaction could proceed through formation of CH_3NC, followed by isomerization.

One other minor product was observed in both the photolysis and the pyrolysis. It was detected only when the fraction condensable at $-181°$ was admitted directly to the mass spectrometer through an all-glass inlet system; it did not emerge from any gas chromatography column and was lost by contact with metal surfaces. Reducing the electron-beam energy in the mass spectrometer showed clearly that the parent mass was 106, with prominent fragments at masses 91 and 77 appearing as the electron energy was increased. With this mass spectrum it cannot be a primary product, and it seems probable that it came from an addition reaction perhaps involving $N-CH_3$ formed by secondary photolysis of CH_3NCO. Its identity remains uncertain.

The pyrolysis was studied very briefly at 450° and a pressure of N-methylsuccinimide of about 460 torr. The products were the same as those of the photolysis, in roughly similar amounts, including the unidentified product of mass 106.

(4) R. A. Back and D. W. L. Griffiths, unpublished results.

Gravimetric Adsorption Studies of Thorium Oxide. III. Adsorption

of Water on Porous and Nonporous Samples[1,2]

by H. F. Holmes, E. L. Fuller, Jr., and C. H. Secoy

Reactor Chemistry Division, Oak Ridge National Laboratory, Oak Ridge, Tennessee 37830 (*Received July 7, 1967*)

The adsorption of water at 25.00° on two contrasting samples of thorium oxide has been investigated using a sensitive vacuum microbalance. Although the specific surface areas of the two samples were approximately equal (about 6 m²/g), their porosities were markedly different. Adsorption–desorption isotherms for water on one of the samples showed hysteresis due to capillary condensation in pores down to, and including, two molecular diameters in size. In contrast, no evidence of capillary condensation was found with the second sample. Outgassing studies on both samples showed that temperatures as high as 1000°, *in vacuo*, were required to dehydrate the surfaces completely. Both samples exhibited irreversible retention of water in amounts much greater than that required for complete hydroxylation of the bare surface. Application of the BET equation indicated that the amount of water required to form a physically adsorbed monolayer on top of the irreversibly adsorbed water was drastically different for the two samples. The results are interpreted in terms of hydration of the surface hydroxyl groups. Differences in the statistical monolayer capacities of the two samples are attributed to the spatial arrangement of the hydrating water molecules on the 100 and 111 crystal faces.

Introduction

Previous work[3] on the thorium oxide–water system demonstrated that the outgassed surface of thorium oxide could irreversibly adsorb water in quantities far in excess of that required to completely hydroxylate the bare surface. All of the previous calorimetric[4,5] and gravimetric[3] work has been performed with thorium oxide prepared by the thermal decomposition of thorium oxalate. Typically, this material consists of relatively large particles which are composed of much smaller crystallites.[6] This, of course, gives rise to a porous structure. The suggestion has been made[7] that our calorimetric work is needlessly complicated by this porous structure. Furthermore, it has been inferred[8] that the observed dependence of the heat of immersion on specific surface area[4] is merely a fictitious result caused by the microporous structure of oxalate-derived samples. It is the purpose of the present paper to explore some of the differences in the water adsorption characteristics of porous and nonporous thorium oxide powders.

Experimental Section

The gravimetric adsorption apparatus incorporating a sensitive vacuum microbalance has been described.[9] Water for the adsorption experiments was obtained by the thermal decomposition, *in vacuo*, of previously outgassed $BaCl_2 \cdot 2H_2O$. During the water adsorption measurements, the sample was maintained at 25.00° by means of a constant-temperature water bath controlled to ±0.001° (Hallikainen Instruments Thermotrol, Model 1053A). For outgassing studies the quartz sample tube was surrounded by a Marshall furnace

controlled to ±1° and capable of operating at temperatures up to, and including, 1000°.

Adsorbents. Sample C was a typical oxalate-derived thorium oxide which was prepared, in this case, by calcination at 1000°. The particle size, as determined by sedimentation analysis, was 2.7 μ while the crystallite size, as determined by X-ray line broadening, was only 680 Å.[10] The specific surface area of sample C, determined by nitrogen adsorption at −196° after outgassing the sample at 500°, was 5.50 m²/g.

Sample S was prepared[11] from an oxalate-derived oxide very similar to sample C. Briefly, this sample was prepared by digesting the starting material in hot nitric acid and then sizing the resulting product by centrifugation.[12] The X-ray crystallite size of sample

(1) Research sponsored by the U. S. Atomic Energy Commission under contract with the Union Carbide Corporation.

(2) Presented in part at the 153rd National Meeting of the American Chemical Society, Miami Beach, Fla., April 1967.

(3) E. L. Fuller, Jr., H. F. Holmes, and C. H. Secoy, *J. Phys. Chem.*, **70**, 1633 (1966).

(4) H. F. Holmes and C. H. Secoy, *ibid.*, **69**, 151 (1965).

(5) H. F. Holmes, E. L. Fuller, Jr., and C. H. Secoy, *ibid.*, **70**, 436 (1966).

(6) V. D. Allred, S. R. Buxton, and J. P. McBride, *ibid.*, **61**, 117 (1957).

(7) K. H. McCorkle, Ph.D. Thesis, University of Tennessee, 1966.

(8) J. A. G. Taylor and J. A. Hockey, *J. Phys. Chem.*, **70**, 2169 (1966).

(9) E. L. Fuller, Jr., H. F. Holmes, and C. H. Secoy, *Vacuum Microbalance Tech.*, **4**, 109 (1965).

(10) These data were obtained by the Analytical Chemistry Division of Oak Ridge National Laboratory.

(11) This sample was prepared and supplied through the courtesy of F. H. Sweeton of the Reactor Chemistry Division of Oak Ridge National Laboratory.

(12) F. H. Sweeton, Reactor Chemistry Division Annual Progress Report, ORNL-3127, Jan 31, 1961, p 71.

S was 880 Å.[10] After ougassing at 500°, sample S had a specific surface area of 5.96 m²/g, as determined by nitrogen adsorption at −196°.

Figures 1 and 2 are electron photomicrographs[13] of samples C and S, respectively. Figure 1 is typical of the structure of thorium oxide obtained by thermal decomposition of the oxalate.[14] In this case the dimensions of the large particle agree quite well with the sedimentation particle size of 2.7 μ. The porosity of sample C is evident from the structure observed in the center of the large particles. Apparently, the acid digestion process used to prepare sample S broke the large particles (similar to those in Figure 1) down into crystallites as the size of the individual particles shown in Figure 2 agrees quite favorably with the crystallite size of 880 Å. An interesting point is that electron diffraction patterns of relatively large single particles of thorium oxide obtained from a similar acid digestion process indicate that they are nearly perfect single crystals.[15]

Results

Two adsorption–desorption cycles for water on sample C at 25.00° are shown in Figure 3. It is very important to remember that the amount of adsorbed water for each isotherm is computed from the initial sample weight *in vacuo* at the beginning of that isotherm. Thus, on an absolute weight basis, isotherm II is above isotherm I. The results shown in Figure 3 are quite similar to those reported previously[3] for two other oxalate-derived materials of different specific surface area. Discontinuities in the isotherms are the result of overnight or weekend pauses in the experiment. Normally the data points were taken after a time lapse of 20 to 60 min after dosing. Considered by themselves, these discontinuities are indicative of a slow irreversible adsorption process.

Some data were taken with periods of time as long as 4 days between data points on both the adsorption and desorption branches. Except for minor differences in separation of the adsorption and desorption branches, the important characteristics of the isotherm were unchanged even with these long equilibration times. A further complicating factor was the slow pressure decrease with time on the adsorption branch and a corresponding slow pressure increase with time on the desorption branch. This phenomenon is due to adsorption–desorption on parts of the apparatus other than the sample. The phenomenon is an inherent property of the glass system since it also occurs in the absence of the Cahn RG Electrobalance. In the reported[3] reversible isotherm for the adsorption of water on thorium oxide we demonstrated that 6 months of repeated adsorption–desorption *cycles* were necessary to obtain this isotherm. Furthermore, this reversible isotherm was accurately reproducible even in the presence of the
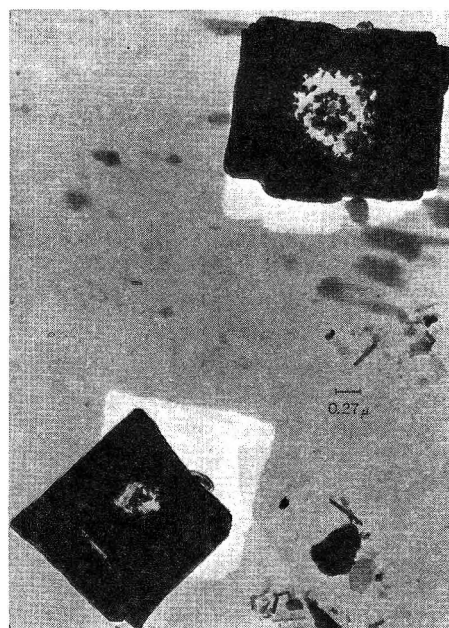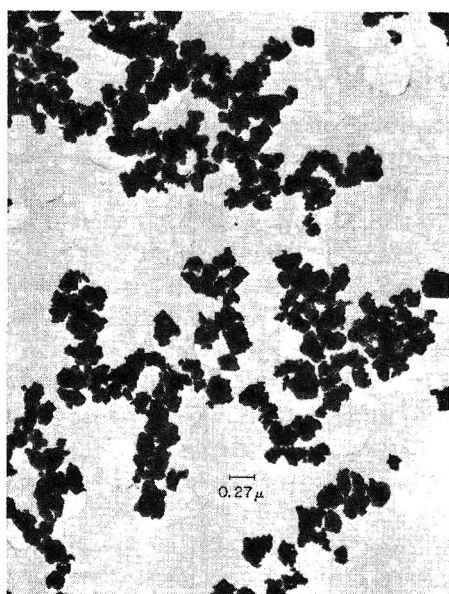

Figure 1. Electron photomicrograph of sample C.

Figure 2. Electron photomicrograph of sample S.

slow increases or decreases in the water vapor pressure in the system.

The importance of adsorption–desorption cycling was demonstrated by the following experiment. Sample S was outgassed for 24 hr at 25°. This resulted in a stable vacuum weight (at this point in the experimental sequence the sample contained about 460 μg/m² of irreversibly adsorbed water). The sample was then

(13) The electron microscopy was performed by T. E. Willmarth of the Analytical Chemistry Division of Oak Ridge National Laboratory.

(14) R. Beckett and M. E. Winfield, *Australian J. Sci. Res.*, **4A**, 644 (1951).

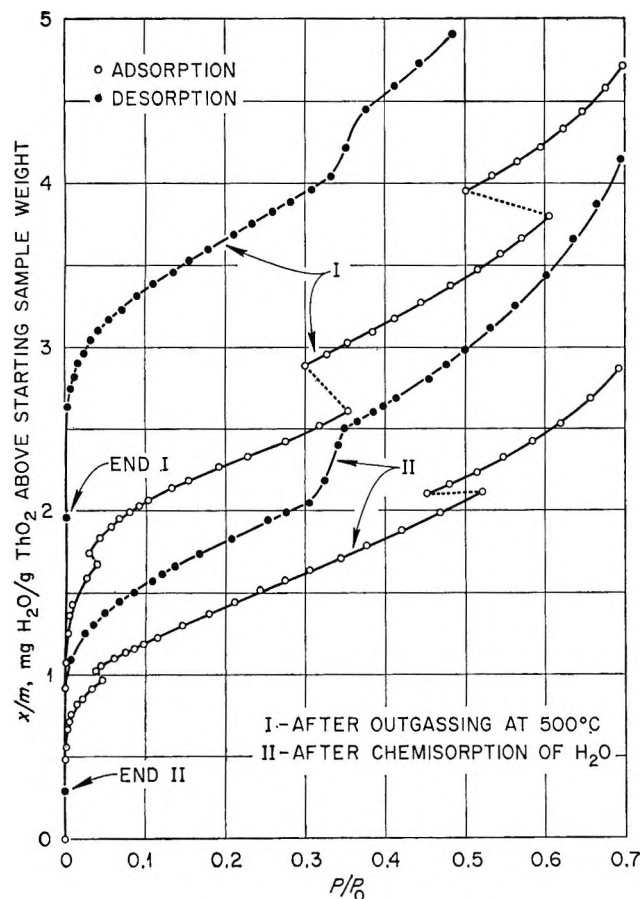(15) T. E. Willmarth, private communication.

Figure 3. Adsorption of H_2O on sample C at 25.00°.

exposed to a constant pressure (4.579 torr) of water vapor provided, and maintained, by a water reservoir surrounded by an ice bath. After an initial rapid weight gain which was complete in 20 min, the sample weight remained constant ($\pm$ 1 μg) for a period of 4 days. Water vapor pressure was then cycled four times by alternately immersing the water reservoir in a liquid nitrogen bath and then allowing it to warm to room temperature. The ice bath was then replaced around the water reservoir. Within 30 min the pressure and sample weight were constant. This sample weight was 16 μg *heavier* than the previous weight under 4.579 torr of water vapor. The sample weight remained constant for 3 days after which the pressure cycling process was repeated. This resulted in an additional 12-μg increase in the sample weight at a constant pressure of 4.579 torr. After an additional 3 days under 4.579 torr of water vapor, during which time the weight remained constant, the sample was outgassed for 24 hr. A stable vacuum weight was achieved which was 36 μg heavier than the original vacuum weight at the start of the experiment. The sample was maintained at 25.00° throughout the course of the experiment and the pressure was monitored to ascertain its constancy.

Desorption branches of both isotherms in Figure 3 have a well-defined classical capillary condensation

hysteresis loop closing at a relative pressure of about 0.35. This closure point corresponds to pores of about 10 Å radius as computed from the Kelvin equation. This pore size was also observed[3] in oxalate-derived thorium oxide which had been prepared by calcination at 650° but not in samples calcined at 1200°. It is somewhat surprising that these small pores are not removed by sintering until the calcining temperature is greater than 1000°. However, this does lend credit to our hypothesis[4] that the process responsible for the slow heat of immersion is the diffusive resistance to liquid water entering these small pores. For example, a slow heat of immersion was observed with all samples calcined at 1000° or less but not with samples which were calcined at temperatures in excess of 1000°.[4,5]

Obviously, the process responsible for the low-pressure hysteresis below 0.35 relative pressure is not complete after one adsorption–desorption cycle. Actually, isotherm II was the third consecutive isotherm at 25.00° without intervening outgassing at elevated temperatures. Actual amounts of water irreversibly retained by these samples will be discussed later.

Comparable adsorption–desorption cycles for sample S are depicted in Figure 4. Conspicuously absent in these two isotherms is the classical capillary condensation hysteresis loop which was observed with sample C. The isotherms for sample S gave no evidence for this type of pore system although there was some indication of interparticle condensation at very high relative pressures. Conversely, what is also obviously present is the same type of discontinuities and irreversible adsorption as was observed with sample C, although they are not as marked in the case of sample S. In reality, at any given relative pressure, sample S adsorbs substantially less water than sample C even though sample C has a smaller nitrogen surface area. Nevertheless, irreversible adsorption with sample S at low relative pressures persisted through at least five consecutive isotherms without intervening outgassing at elevated temperatures.

At this point, it is probably pertinent to give the experimental basis for referring to sample S as nonporous and to sample C as porous. The experimental nitrogen specific surface area for sample S (5.96 m²/g) agrees quite favorably with that computed from the X-ray crystallite size (6.8 m²/g), certainly to within the absolute uncertainty associated with the values. The nitrogen surface area for sample C (5.50 m²/g) differs substantially from that computed from the X-ray crystallite size (8.8 m²/g). Furthermore, the electron microscope particle size for sample S compares quite well with the X-ray crystallite size. Finally, sample C exhibits a well-defined capillary condensation hysteresis loop while none was ever observed for sample S.

BET plots of the adsorption data for both samples were quite linear over the usual relative pressure range (about 0.05 to 0.3). BET parameters obtained from
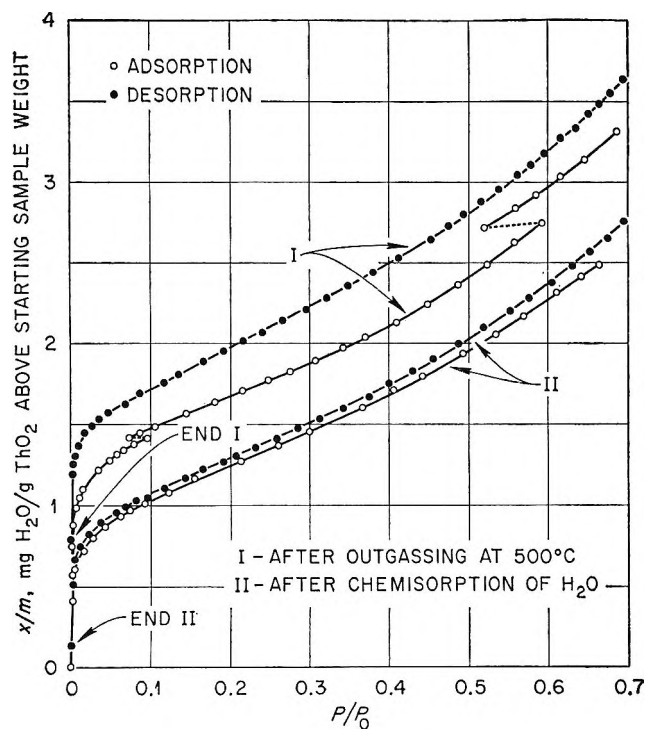
Figure 4. Adsorption of H_2O on sample S at 25.00°.

Table I: Summary of H_2O Adsorption on Samples C and S

Sample	$\Delta w,^a$ μg	$\Delta w/\sigma,^b$ $\mu g/m^2$	$\Sigma,^{c,e}$ m^2/g	$\Sigma/\Sigma_0{}^d$	BET C constant
C	466	170	6.66	1.21	360
C	1446	526	4.33	0.79	58
C	1548	563	4.13	0.75	107
S	166	139	4.79	0.80	620
S	218	183	4.50	0.76	175
S	351	295	3.67	0.62	95
S	379	318	3.27	0.55	94
S	380	319	3.78	0.63	208
S	439	369	2.67	0.45	40
S	497	418	2.44	0.41	46
S	512	430	3.10	0.52	67
S	545	458	2.25	0.38	39
S	606	509	2.94	0.49	96

^{a} Amount of water already irreversibly adsorbed on sample at the beginning of the experiment. Computed by using the vacuum weight at 1000° as zero. ^{b} Same as above but on a unit area basis by means of the nitrogen specific surface area after outgassing at 500°. ^{c} Computed on the basis of 10.6 $Å^2$ per adsorbed water molecule. ^{d} Reduced surface areas, i.e., the ratio of column 4 to the nitrogen specific surface area after outgassing at 500°. ^{e} Throughout this paper we have reported surface areas to three significant figures. This is not warranted on an absolute basis but is certainly valid for comparison on a relative basis.

the adsorption experiments are summarized in Table I. Admittedly, the data are perturbed by the underlying chemisorption. This is especially true for the data taken after outgassing at 500°. Data for subsequent isotherms probably give a rough estimate of the amount of water necessary to form a physically adsorbed monolayer as the underlying chemisorption is less rapid and less extensive in these cases. Ideally, in the BET range, one would like unperturbed data for true physical adsorption. On this basis one can make a strong argument for obtaining data in the BET range as rapidly as possible in order to minimize perturbations from the slow irreversible adsorption. Accordingly, in this study, data in the BET range were obtained in a period of 6 hr or less. Surface areas were computed by assuming that a physically adsorbed water molecule occupies 10.6 $Å^2$. This value, obtained from the density of liquid water,[16] is questionable in those cases where the possibility for site adsorption exists.

However, even with these limitations, it is surprising that the computed surface area for sample S, when outgassed at 500°, is only about 80% of the nitrogen area under the same outgassing conditions. For both samples it is difficult to explain the decrease in effective surface area after chemisorption of water without postulating that the chemisorbed water actually reduces the free surface area or that an adsorbed water molecule occupies an area other than 10.6 $Å^2$. This point will be discussed in more detail later. The decrease in adsorptive capacity after chemisorption of water is even more marked with sample S than with sample C.

Obviously, porosity alone cannot be responsible for the decrease in adsorptive capacity in the presence of chemisorbed water.

Discussion

Table I is a summary of our experiments with samples C and S. Vacuum weight at 1000° was chosen as zero since it was found necessary to outgas at this temperature in order to obtain a reasonably constant weight, independent of outgassing temperature. The 1000° vacuum weight was obtained at the conclusion of the experiments since samples C and S were originally prepared by calcination at 1000°. Nitrogen adsorption measurements showed that additional sintering did occur when the samples were heated to 1000° a second time. Exploratory experiments showed that after outgassing at 1000°, the samples showed the same slow irreversible adsorption and low-pressure hysteresis as was observed after outgassing at 500°. Furthermore, after these exploratory experiments it was found necessary to return to 1000° to remove the irreversibly adsorbed water. The highest outgassing temperature for an experiment given in Table I is 500°. At this temperature both samples contain approximately 100 $\mu g/m^2$ of chemisorbed water. When the sample temperature is lowered to conduct an adsorption experiment, additional water is chemisorbed even though the samples were continually pumped at 10^{-6} to 10^{-7}

(16) H. K. Livingston, J. Amer. Chem. Soc., 66, 569 (1944).

torr. This observation is identical with those reported previously.[3]

The persistence of hysteresis to very low vapor pressures is also associated with materials which have a laminar structure and swell on adsorption, e.g., clay minerals. However, even in these cases the hysteresis vanishes on evacuation; i.e., the vacuum weight is the same before and after the adsorption–desorption cycle. Obviously, this is not the case in the present system. Furthermore, the heat of immersion of clay-like materials as a function of adsorbed water has unique features which are associated with the swelling. Reported heat of immersion data for thorium oxide[5] do not show this feature. On the basis of the above discussion one must conclude that the hysteresis at low vapor pressures is not due to a variable pore geometry associated with a laminar structure.

A bare thorium oxide surface chemisorbs water by dissociative adsorption to form surface hydroxyl groups. The maximum quantity of water which thorium oxide can chemisorb in this manner is 221 μg/m^2 based on the 111 crystal face. The presence of any other face would tend to decrease this value. From Table I, we obviously have much more irreversibly adsorbed water than would be required for a simple rehydroxylation of the bare surface. Since this phenomenon occurs repeatedly with sample C, without intervening outgassing at elevated temperatures, and also occurs on the nonporous sample S, it cannot be ascribed to a simple irreversible retention of water in very small pores. We have previously described[3] this phenomenon as an associative adsorption to give the surface analog of a hydrated bulk hydroxide.

The existence of molecular water strongly associated with an oxide surface does not appear to be confined to the present system. A few examples will suffice to document this. Infrared studies have demonstrated the existence of molecular water on the surface of titanium dioxide after evacuation at 150°.[17] An outgassing temperature of 160° has been suggested[18] as "the best compromise between the maximum removal of the physically adsorbed water and the minimum loss of surface hydroxyl groups" in the case of silica. In the case of γ-alumina it is necessary to outgas at 400° in order to remove the adsorbed molecular water.[19] Data for one of the silica samples studied by Whalen[20] indicated that it had 2.2 "bound" water molecules per 100 Å^2 after outgassing at 110°. Studies[21] on the interaction of water with the surface of magnesium oxide have shown that the "primary physisorbed layer" of water can only be removed by evacuation at 200–250°. Water remaining on the surface of a silica–alumina catalyst after evacuation at 150° was termed "fixedly adsorbed" by Haldeman and Emmett.[22] Subsequent infrared studies by Basila[23] identified this "fixedly adsorbed" water as molecular water. Zettlemoyer and Chessick[24] have questioned

whether outgassing at 120–130° clearly separates physically adsorbed water from chemisorbed water.

A strongly associated surface layer of adsorbed molecular water has been demonstrated for many oxides. Furthermore, it has been shown that this water can only be removed by outgassing at elevated temperatures. Simple thermodynamics tells us that the equilibrium thermodynamic state of this water cannot be defined by an adsorption isotherm determined at 25°. This is because the true equilibrium pressure corresponding to this coverage cannot be attained at 25° by current techniques. The character of a 25° water adsorption isotherm on such an oxide (after outgassing at an elevated temperature) will depend in a marked manner on the kinetics of replacing this water from the vapor phase at 25°. If the kinetics are so slow that they are unobservable during the time span of the experiment, then the isotherm will appear to be truly reversible. On the other hand, if the kinetics are slow but observable, the isotherm will exhibit hysteresis over the entire range of pressures. An interesting case arises when the strongly associated molecular water is immediately and completely replaced from the vapor phase. In this case, the only observable hysteresis will be between the initial and final vacuum weights. As a matter of fact, the isotherm will be reversible in a strict thermodynamic sense except for the very important initial and final vacuum weights. Clearly, the thorium oxide–water system falls in the second category. This type of isotherm has also been observed[25] for water on Fe_2O_3, SnO_2, SiO_2, and TiO_2. In any event, none of the above isotherms, nor those shown in Figures 3 and 4, has a rigorous thermodynamic meaning. However, the isotherms are still valid for interpretive purposes provided that one is cognizant of the experimental conditions and does not attempt to extract thermodynamic data from the isotherms. The difficulties and inconsistencies resulting from the application of thermodynamics to such isotherms have been elegantly discussed by the late V. K. La Mer.[26]

The BET parameters listed in Table I form a con-

(17) D. J. C. Yates, J. Phys. Chem., 65, 746 (1961).

(18) R. L. Every, W. H. Wade, and N. Hackerman, ibid., 65, 26 (1961).

(19) J. B. Peri and R. B. Hannan, ibid., 64, 1526 (1960).

(20) J. W. Whalen, Advances in Chemistry Series, No. 33, American Chemical Society, Washington, D. C., 1961, p 281.

(21) P. J. Anderson, R. F. Horlock, and J. F. Oliver, Trans. Faraday Soc., 61, 2754 (1965).

(22) R. G. Haldeman and P. H. Emmett, J. Amer. Chem. Soc., 78, 2917 (1956).

(23) M. R. Basila, J. Phys. Chem., 66, 2223 (1962).

(24) A. C. Zettlemoyer and J. J. Chessick, Advances in Chemistry Series, No. 43, American Chemical Society, Washington, D. C., 1964, p 88.

(25) R. C. Asher, J. F. Goodman, and S. J. Gregg, Proc. Brit. Ceram. Soc., 5, 125 (1965).

(26) V. K. La Mer, J. Colloid Interface Sci., 23, 297 (1967).

sistent, if not very smooth, pattern. As expected, the large energy of adsorption on the outgassed surface is reflected in the relatively large BET C constant. However, in the case of the water-covered surface, the C value is surprisingly low for the adsorption of water on a "polar" surface. The physical significance of the computed surface areas is questionable in view of the uncertainty associated with the area occupied by an adsorbed water molecule. However, this does not alter the fact that the adsorptive capacity of both surfaces has been reduced by the presence of irreversibly adsorbed water. In the case of sample C this decrease could possibly be attributed to chemisorbed water blocking part of the pore volume. No such argument can be applied to the nonporous sample S where the decrease is even more marked than with sample C. The reduced surface area for sample S is similar to that observed for water on titanium dioxide which presumably was covered with chemisorbed water.[27] Even for the outgassed surface of sample S, the reduced surface area was only 0.8, which is somewhat surprising. The reduced surface area for the outgassed surface of sample C was larger than unity, which is what one would expect for data which include a substantial amount of chemisorbed water.

If one accepts the hypothesis that the process responsible for the irreversible adsorption of water in such large quantities is the formation of surface hydroxyl groups and the subsequent slow hydration of these on the basis of one water molecule per surface hydroxyl group, it is then possible to construct a tentative model. Since in the primary chemisorption process each water molecule forms two surface hydroxyl groups, the total quantity of water involved in this model is just the weight equivalent of the three chemisorbed monolayers referred to in the previous publication.[3] In addition to being consistent with the experimental results, the model will have to take into consideration the substrate lattice spacing and the hydrogen bonding characteristics of surface hydroxyls and water molecules. Since thorium oxide is a face-centered cubic crystal, we will assume, as has been done previously,[7] that the preferentially exposed face is either the 100 or the 111 face, or a combination of these.

Figure 5 is our proposed model for the completely hydrated 100 surface of thorium oxide. In an attempt at clarity, the size of the individual atoms has not been drawn to scale. However, the positions of the oxygen and thorium atoms, but not of the hydrogen atoms, have been drawn to scale. The surface hydroxyl groups occupy the same positions as oxygen ions in a normal 100 plane of the crystal. Hydrate water molecules lie in a plane above the surface hydroxyl groups. The prominent feature is the hydrogen bonding characteristics of this structure. Each surface hydroxyl group forms two hydrogen bonds with adjacent water molecules. Each hydrate water molecule
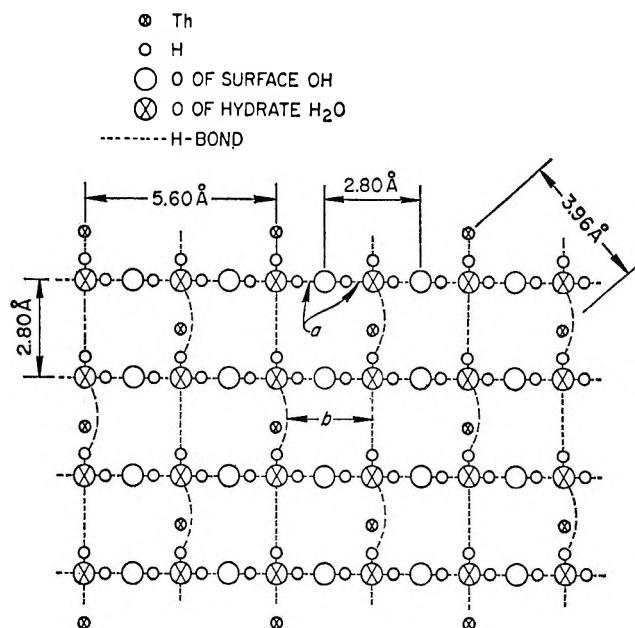

Figure 5. Model of hydrated 100 surface of ThO_2.

forms four hydrogen bonds, two with underlying surface hydroxyl groups and two with adjacent water molecules. There are two types of hydrogen bonds, differing in length and linearity. These are designated as a and b in Figure 5. For the sake of clarity, some of the b bonds are shown as curves. A salient feature of this model is that the hydrogen bonding capacity of the water molecule is completely satisfied. This means that no additional adsorption, either physical or associative, can occur by means of hydrogen bonding. The proposed model is similar to the explanation which has been made to account for the nonpolar character of nitrogen adsorption on ice.[28] In reality, on thorium oxide covered with a relatively large amount of irreversibly adsorbed water, nitrogen adsorbs with an abnormally low BET C constant.[29] Presumably, water adsorption on the fully hydrated 100 face would give a liquid-like layer with each water molecule occupying 10.6 $Å^2$.

Our proposed model for the fully hydrated 111 surface of thorium oxide is shown in Figure 6. In this case the thorium atoms are positioned at the corners of equilateral triangles which are 3.96 Å on a side. The surface hydroxyl groups are positioned over the centers of these triangles (same position as the oxide ions in the normal crystal structure). In the model each surface hydroxyl group again forms two hydrogen bonds with adjacent hydrate water molecules. However, each hydrate water molecule, located in a plane above the surface

(27) A. C. Zettlemoyer, R. D. Iyengar, and P. Scheidt, *J. Colloid Interface Sci.*, **22**, 172 (1966).

(28) A. W. Adamson and L. M. Dormat, *J. Amer. Chem. Soc.*, **88**, 2055 (1966).

(29) H. F. Holmes, E. L. Fuller, Jr., and C. H. Secoy, unpublished results.
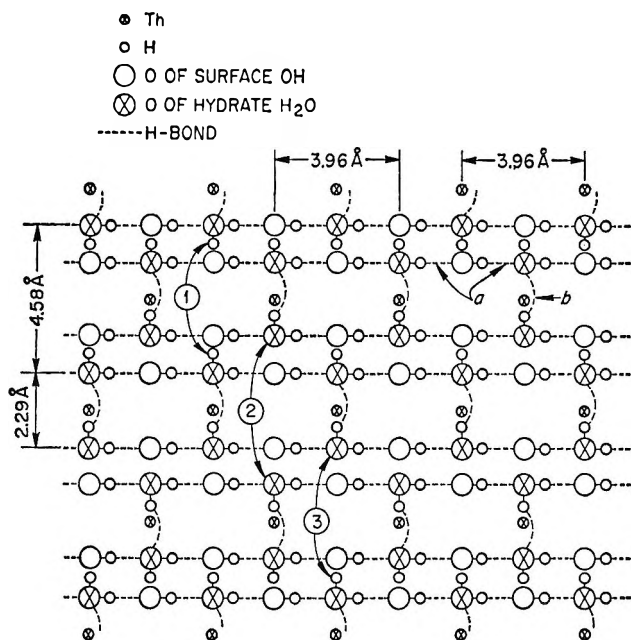
Figure 6. Model of hydrated 111 surface of ThO₂.

hydroxyls, can now form only three hydrogen bonds. Two of these are with underlying surface hydroxyl groups and one is with an adjacent water molecule. Again there are two types (*a* and *b*) of hydrogen bonds, differing in length and linearity.

Since each water molecule is capable of forming four hydrogen bonds, this arrangement leaves potential sites for further adsorption to occur by means of hydrogen bonding. Depending on the orientation of the hydrate water molecules at the opposite corners of a regular hexagon there are three types of such sites. These are designated as 1, 2, and 3 in Figure 6. Type 1 consists of two hydrogen atoms, type 2 of two pairs of nonbonding electrons, and type 3 of hydrogen atom and a pair of nonbonding electrons. The area of each of the regular hexagons is 13.6 $Å^2$. The prime restriction on the orientation of the hydrate water molecules is that any two rows joined by hydrogen bonds must be orientated in the same direction. Since this orientation should occur in a random manner, it is evident that there will be 25% type 1 sites, 25% type 2 sites, and 50% type 3 sites. Reversible adsorption on the hydrated 111 face will, in all probability, occur by hydrogen bonding. If all three types of sites are equally energetic, then an adsorbed water molecule will occupy an area of 13.6 $Å^2$ instead of the conventional 10.6 $Å^2$. However, if one considers hydrogen-bond formation as an electrostatic phenomenon involving polarization of the water molecule,[30] he is led to believe that a water molecule will preferentially interact with a type 3 site. This is what we will assume in the present model. Thus the reversible isotherm for water adsorption on the hydrated 111 surface should show a break (point "B") corresponding to a complete filling of all type 3 sites. Furthermore,

the effective area of an adsorbed water molecule in the first "monolayer" will be 27.2 $Å^2$. We further postulate that adsorption in the second and succeeding layers will be normal (10.6 $Å^2$/molecule). This assumption is prompted by the fact that the two isotherms in Figure 4 are parallel, indicating that multilayer adsorption is the same in both cases.

The proposed model is that the predominantly exposed crystal face is 100 in the case of sample C and predominantly 111 in the case of sample S. Agreement of the model with the experimental results is not perfect. For example, the reduced surface areas (Table I) for the water covered surface should be 1.00 for sample C and 0.39 in the case of sample S. However, a completely hydrated surface was never attained. In addition, one would hardly expect the crystal habit to be totally exclusive. In support of the model, electron diffraction studies[15] on relatively large single crystals of thorium oxide prepared in much the same manner as sample S indicated that about 80% of the exposed faces were the 111 plane with the remainder being the 100 plane. Unfortunately, the crystals of sample C and S are too small to permit such a study. The experimental adsorption data are certainly complicated by the very slow kinetics of irreversible bonding of water. An additional feature of the proposed model is that the rigid order imposed on the hydrate water molecules provides a ready explanation for the slow kinetics.

In construction of the present model, prime consideration was given to formation of the maximum number of hydrogen bonds. An additional restraint on the model is that the hydrogen bond distances and angles should be consistent with, but not necessarily equal to, those observed in other systems. Hydrogen bond *b* in Figure 5 is 2.80 Å in length. This is very consistent with the bond lengths quoted in Pimentel and McClellan[31] for hydroxides. However, this is a nonlinear bond, with the hydrogen being approximately 15° off a line connecting the oxygens for the least favorable orientation of the hydrate water molecules. Such deviations from linearity have been observed.[32] Obviously, the exact bond lengths and angles are not known, but the values quoted in this discussion are geometrically possible. The length of hydrogen bond *a* in Figure 5 will depend on the angle formed by the hydrate water molecule with the two underlying surface hydroxyl groups. If we arbitrarily set the length as 2.3 Å, then the angle is 75°. This assumes bond *a* is linear. Both of these values are just outside the lower limits quoted in Pimentel and McClellan.[31,33] Hydrogen bond *b* in Figure 6 is nonlinear with the

(30) C. A. Coulson in "Hydrogen Bonding," D. Hadzi, Ed., Pergamon Press, Ltd., London, 1959, p 339.

(31) G. C. Pimentel and A. L. McClellan, "The Hydrogen Bond," W. H. Freeman and Co., San Francisco, Calif., 1960, p 283.

(32) Reference 31, p 264.

(33) Reference 31, p 281.

deviation being approximately 15° for the least favorable orientation of the hydrate water molecules. At 2.29 Å this bond is 0.07 Å less than the shortest bond listed by Pimentel and McClellan.[31] The angle formed by the hydrate water molecule with the two underlying surface hydroxyl groups and the length of bond a (Figure 6) can have a wide range of acceptable values. For example, if the angle is 100°, then the bond length is 2.58 Å. Both of these values are roughly in the middle of the observed range.[31,33] It is our opinion that the deviations discussed above are not sufficiently large as to warrant rejection of the proposed model. It is hoped that current infrared investigations will provide additional information concerning the structure of the associatively adsorbed water on the surface of thorium oxide.

The Passivation of Mercury in Sulfide Ion Solutions

by R. D. Armstrong, D. F. Porter, and H. R. Thirsk

Department of Physical Chemistry, University of Newcastle upon Tyne, Newcastle upon Tyne, England

Accepted and Transmitted by The Faraday Society   *(July 14, 1967)*

The growth of thin anodic films of mercury sulfide on a mercury electrode in sulfide ion solutions and the effect of such films on the anodic dissolution of mercury have been studied using the potentiostatic method. In the initial stages of film growth, mercury sulfide (metacinnabarite) is deposited on the electrode in the form of two successive monomolecular layers, and the presence of each layer severely inhibits the rate at which mercury dissolves as the complex species $HgS_2{}^{2-}$. The current–potential relationship was found to exhibit discontinuities corresponding to the formation of each HgS monolayer and it is suggested that the passivation process at some solid metal electrodes may be of a similar nature.

Introduction

Previous articles have dealt with the anodic-dissolution reaction[1] and the specific anion adsorption[2] which occur at a mercury electrode polarized anodically in aqueous sulfide ion solutions. It was shown that the mercury dissolves as the complex ion $HgS_2{}^{2-}$ and that the sulfide ion is very strongly adsorbed at the electrode over a short potential range, causing the electrocapillary maximum to be found at relatively negative potentials.

The present work investigates the phenomena occuring at slightly more anodic potentials, where a solid-phase film is present on the electrode surface. Zhdanov and Kiselev[3] have examined this system using dilute $(10^{-3} M)$ solutions of sodium sulfide in 0.1 M KCl and have concluded that mercury sulfide is deposited in the form of successive monomolecular layers on the electrode surface, but these authors did not examine the kinetics of film growth nor did they positively identify the phase formed.

In an attempt to elucidate these factors, the film growth has been studied in a carbonate-buffered solution of sodium sulfide of pH 9.5. In this solution the dissolution reaction is considerably reduced,[2] facilitating the examination of the film growth alone. The effect of the film on the dissolution reaction in 1 M Na_2S solution was then examined.

Experimental Section

Kinetic and impedance measurements were made using the potentiostatic technique, details of which are given elsewhere.[1,4] Films of the anodic product were removed from a mercury-pool anode and were examined by electron diffraction and by electron microscopy[4] techniques. Potentials were measured with reference to an Hg–HgO electrode in 1 M NaOH solution *via* a liquid junction formed at a three-way tap.

The solutions used were 0.5 M Na_2S + 1 M $NaHCO_3$ ("buffered sulfide solution") and 1 M Na_2S, ("alkaline sulfide solution"), prepared in an atmosphere of purified nitrogen from Analar reagents and deoxygenated triply distilled water. Mercury was prepared by chemical cleaning followed by two successive distillations *in vacuo*.

The reversible potential of HgS in 0.5 M Na_2S + 1 M $NaHCO_3$ solution was found experimentally by setting

(1) R. D. Armstrong, D. F. Porter, and H. R. Thirsk, *J. Electroanal. Chem.*, **14**, 17 (1967).

(2) R. D. Armstrong, D. F. Porter, and H. R. Thirsk, *ibid.*, **16**, 219 (1968).

(3) S. I. Zhdanov and B. A. Kiselev, *Dokl. Akad. Nauk SSSR*, **155**, 651 (1964).

(4) M. Fleischmann and H. R. Thirsk, *Electrochim. Acta*, **9**, 757 (1964).

up Hg–HgS electrodes in this solution and by measuring their potentials with respect to Hg–HgO in 1 M NaOH solution *via* a liquid junction. These potentials were −0.692 V for the black form of HgS (metacinnabarite) and −0.698 V for the red HgS (cinnabar). In this work we shall designate the reversible potential of black HgS in this solution as E_r.

All measurements were made at room temperature, 24 ± 1°.

Results

Buffered Sulfide Solution. The formation of the solid film on the mercury electrode was observed potentiostatically by applying an anodic rectangular pulse of potential to the electrode, which was initially held at a potential 0.3 V negative to E_r. The resultant current–time transients for various pulse heights are shown in Figure 1.

The first feature attributable to the growth of a solid film was found on pulsing to a potential of $E_r + 6$ mV, where the current–time transient exhibited a "shoulder" (Figure 1A) which moved to progressively shorter times and higher current densities as the potential was increased (Figure 1B). The area under the shoulder was approximately constant and corresponded to a charge of 179 ± 16 μC cm⁻². On pulsing to potentials of $E_r = +23$ mV and above, a second feature appeared, taking the form of a peak in the current–time transient (Figure 1C, and D). The area under this peak was also approximately constant at 228 ± 23 μC cm⁻².

Reduction of the anodic phase was also observed, at the end of the formation period (~350 msec), by changing the potential stepwise to $E_r = -18$ mV. The resultant reduction transients are shown in Figures 1E, and F, and graphical integration yielded charges in agreement with those obtained from the formation transients for the same formation potentials.

Measurements of the impedance of the electrode were made in the buffered sulfide solution as a function of electrode potential, E (Figure 2). The admittance at potentials negative to that at which a film is formed is principally due to the adsorption of sulfide ions[2] and at low frequencies is purely capacitative. On increasing the electrode potential positive to this adsorption region, a discontinuous fall in the double-layer capacity, C_{dl}, from ~500 to ~35 μF cm⁻², was observed at a potential of $E_r = +6$ mV. A second discontinuity occurred at a potential of $E_r = +23$ mV, where the capacity fell to ~20 μF cm⁻². On subsequently decreasing the electrode potential, there was only one discontinuous capacity rise which occurred at $E = E_r$, and the capacity reverted to a high value ~500 μF cm⁻², corresponding to the specific anion adsorption.

The high capacities of the adsorption region were measured at 15 or 30 cps, low frequencies being necessary at high capacities to reduce the proportion of the measured impedance due to the solution resistance.[2]
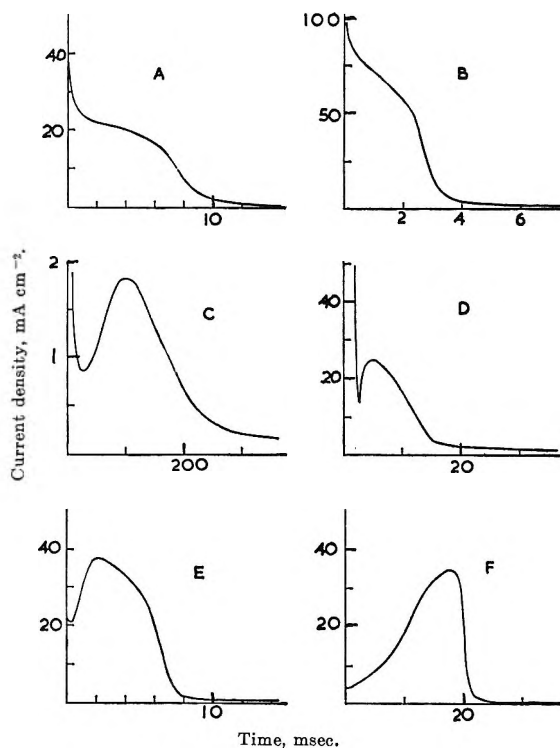

Figure 1. Current–time transients for the formation (A–D) and reduction (E and F) of HgS in 0.5 M Na₂S + 1 M NaHCO₃ solution, at overpotentials of (A) 6 mV, (B) 17 mV, (C) 23 mV, (D) 32 mV, (E) −18 mV, (F) − 18 mV. The reduction transients are for films formed for 350 msec at 12 mV (E) and 25 mV (F).

The impedance of the electrode at potentials positive to the adsorption region was measured at a higher frequency of 1 kcps, in order to reduce effects due to the dissolution reaction.[1] Though greatly reduced in this solution compared with the alkaline sulfide solution, the reaction is still sufficient to produce significant pseudo-capacities at low frequencies when the electrode double-layer capacity falls to values <50 μF cm⁻². The capacities shown in Figure 2 are considered to be, to a good approximation, the true thermodynamic double-layer capacities.

The buffered sulfide solution was used for the preparation of anodic films for examination by electron diffraction and electron microscopy techniques. Typical results are shown in Figure 3 for a film grown at $E_r = +50$ mV for a period of 1 min. Transmission electron diffraction at normal incidence to the film yielded a ring pattern (Figure 3A) from which the anodic phase was identified as the black cubic form of HgS, metacinnabarite (ASTM Card 6-0261). No evidence was found for the red hexagonal form, cinnabar. There were no missing rings, indicating that the deposit was probably randomly oriented. A pattern for a randomly oriented sample of black HgS is shown in Figure 3B as a comparison. The HgS was prepared by chemical precipitation and subsequent ultrasonic dispersion in 2-butanol.
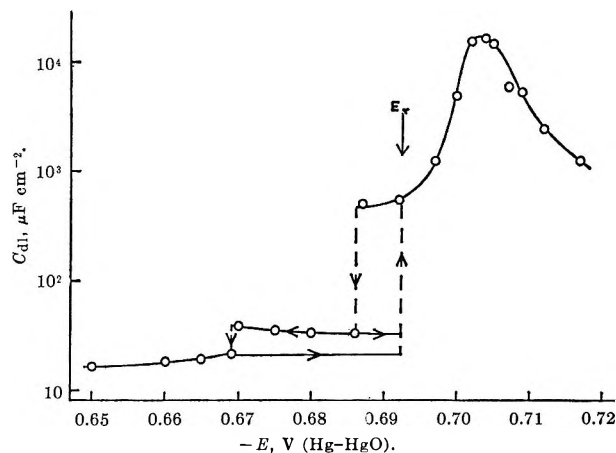
Figure 2. Potential dependence of the electrode double-layer capacity, C_{dl}, in 0.5 M Na$_2$S + 1 M NaHCO$_3$ solution, showing discontinuities attributable to the formation and reduction of HgS monolayers.
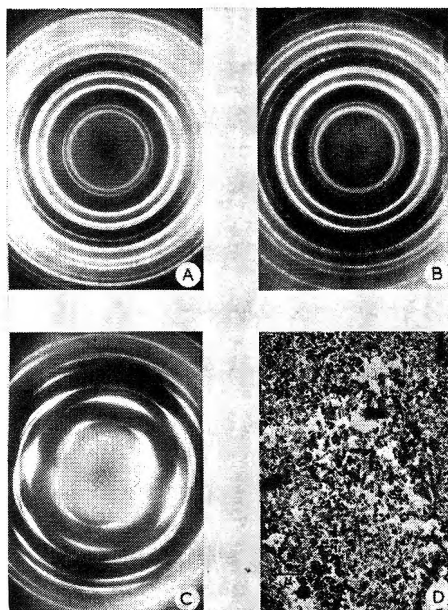

Figure 3. (A) Electron diffraction pattern at normal incidence for deposit formed at E_r + 50 mV for 1 min in 0.5 M Na$_2$S + 1 M NaHCO$_3$ solution; (B) pattern obtained from chemically prepared sample of black HgS; (C) deposit, same as in A, tilted at 45° to the electron beam, obtained for limited number of areas only; (D) electron micrograph of deposit formed the same as in A.

Figure 4. Current-time transients for the mercury electrode in 1 M Na$_2$S solution: (A) dissolution at -0.850 V; (B) effect of one HgS monolayer at -0.750 V; (C) the same as B at -0.740 V; (D) effect of two HgS monolayers at -0.740 V; (E) the same as D at -0.725 V; (F) test of the theoretical model applied to the case of E. Potentials on the Hg-HgO scale.

When the specimen was tilted, a limited number of small areas were found to give arced patterns (*e.g.*, Figure 3C), indicating some degree of orientation. These patterns were of the type which would be expected for 1 deg oriented material, but no consistent fiber axis could be found. However, the major part of the deposit gave no arcs, confirming that it was mainly of a random nature. No single-crystal spot patterns were obtained, indicating that the crystallite size of the deposit was considerably less than the diameter of the smallest beam aperture used, 2μ. This observation is
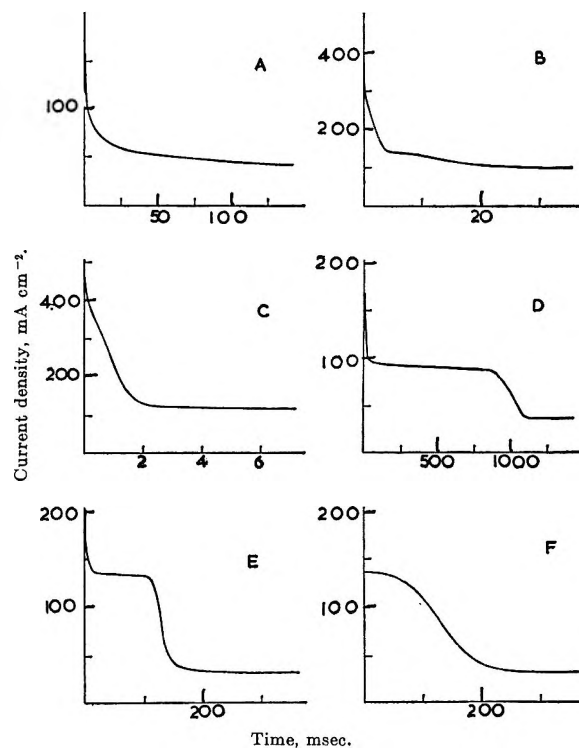
supported by an examination of the micrographs (*e.g.*, Figure 3D).

Alkaline Sulfide Solution. The potentiostatic behavior of the mercury electrode in the alkaline sulfide solution was examined in the same way as in the buffered sulfide solution. Figures 4A–E show typical current–time transients obtained in this system, and in all cases the dominating feature is the anodic-dissolution reaction.[1] At potentials negative to that at which a solid HgS film forms, the current due to this reaction decreased with time in the manner shown in Figure 4A. At $E \geq -0.75$ V (Hg–HgO), a "shoulder" was observed in the transient, after which the current decreased at a much lower rate and approximated to a steady-state dissolution current (Figure 4B and C). Values of this current were obtained at a series of potentials.

At $E = -0.74$ V (Hg–HgO), a second, well-defined shoulder was observed in the current at long times ($\sim$1 sec) and moved to shorter times as the potential was further increased (Figures 4D and E). The approximately constant current after this feature was also recorded as a function of potential.

The current densities are plotted against potential in Figure 5, together with values previously obtained at more negative potentials by the faradaic-impedance method.[1] The times at which the second shoulder
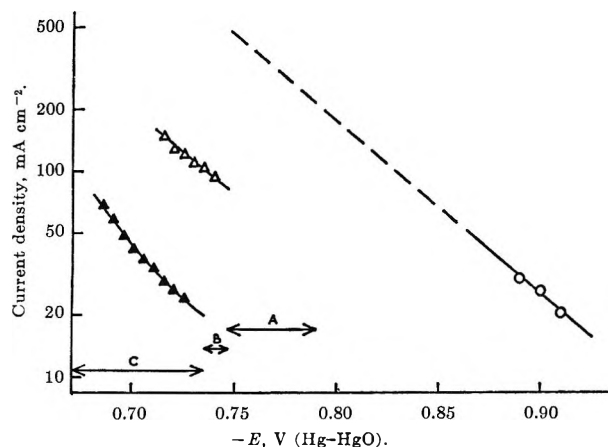
Figure 5. Potential dependence of dissolution current density in 1 M Na₂S solution: (A) region of strong adsorption of S²⁻ ion; (B) region of stability of first HgS monolayer only (on increasing potential anodically); (C) region of stability of first and second monolayers (increasing anodically); (B + C) the same as C (increasing cathodically); △, electrode covered with one HgS monolayer; ▲ two HgS monolayers; O, faradaic impedence measurements on film-free electrodes.
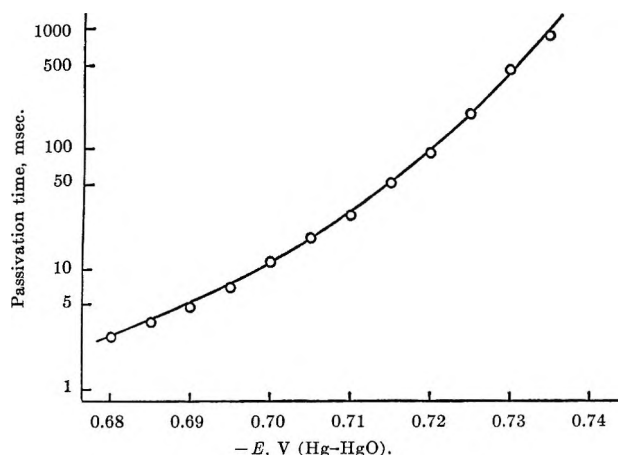

Figure 6. Potential dependence of time at which passivation due to the second HgS monolayer occurs in 1 M Na₂S solution.

occurred were also recorded as a function of potential and are shown in Figure 6. These passivation times could not be obtained for the first shoulder, since it was much less well defined.

Steady state impedance observations in the potential region of film formation were possible in this solution only in a qualitative form, owing to time-dependent effects introduced by reactant depletion at the electrode surface as a result of the very high rate of the dissolution reaction. The following features were observed.

(i) A discontinuous fall in the admittance on increasing the potential through $E = -0.747$ V (Hg–HgO). This discontinuity was very reversible, and the potential could be adjusted so that a 5-mV sinusoidal perturbation extended into both the regions prior to and after the discontinuity.

(ii) A second discontinuous fall in the admittance at $E = -0.735$ V (Hg–HgO). This change could be reversed only by reducing the potential to that of the first discontinuity, $E = -0.747$ V (Hg–HgO).

(iii) At low frequencies (<150 cps) in the potential region just prior to the first discontinuity (-0.79 to -0.75 V), the phase angle, θ, of the electrode impedance lay between -90 and $-180°$, whereas normally $0° > \theta > -90°$. This was considered most likely to be caused by a negative charge transfer slope resistance, which could have arisen if the adsorption of sulfide ions at the electrode inhibits the dissolution reaction. The effect is only observed at low frequencies, since the capacities in the adsorption region are very high[2] and the solution resistance makes a significant contribution to the impedance at all except the lowest frequencies.

The negative resistance effect of (iii) was confirmed by observing the current–time transients when the electrode potential was changed stepwise by ∼5 mV in the potential region of adsorption (-0.79 to -0.75 V), where a change in current of the opposite sign to the change in potential was observed. This procedure was facilitated by the use of the double-pulse technique.[5] An example is shown in Figure 7.

Discussion

Formation of the Solid Phase. The features observed in the buffered sulfide solution, both in the current–time transients and the impedance measurements, are consistent with the successive deposition of two monomolecular layers of a solid phase on the electrode, since they conform to the pattern of behavior observed in several other systems using liquid electrodes. These systems have been summarized elsewhere.[6]

The shape of the current–time transient for the first monolayer (Figures 1A and B) differs from that normally found in that no maximum is observed. This deviation from the theoretical transient shape for two-dimensional nucleation and growth[4] of a monolayer is probably attributable to the low concentration of sulfide ions present (1.5×10^{-5} M), which may give rise to a relaxation process in the film growth similar to that observed in the anion-adsorption process.[2]

The discontinuities in the capacity–potential relationship (Figure 2) provide further evidence for the formation of solid-phase monolayers on the electrode surface, and a clear distinction should be drawn here between the adsorbed layer of ions (disordered array) prior to the formation of the first monolayer and the solid-phase monolayer itself, which incorporates a lattice structure (ordered array). This distinction is not clear in parts of the work of Kiselev and Zhdanov,[3,7]

(5) R. D. Armstrong, M. Fleischmann, and H. R. Thirsk, *Trans. Faraday Soc.*, **61**, 2238 (1965).

(6) R. D. Armstrong and M. Fleischmann, *J. Polarog. Soc.*, **11**, 31 (1965).

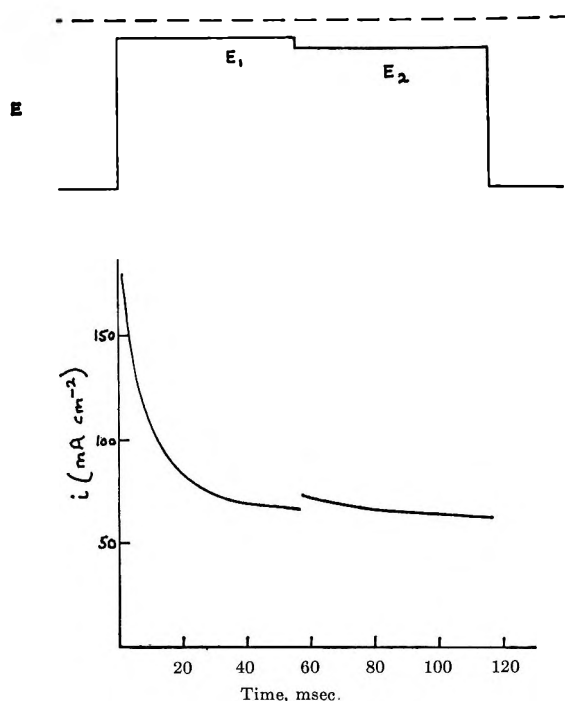(7) B. A. Kiselev and S. I. Zhdanov, *Elektrokhimiya*, **1**, 132 (1965).

Figure 7. Potential-time profile and the resultant
current-time transient in the region of strong adsorption of S^{2-}
ions for 1 M Na$_2$S solution: ---, reversible potential of
first HgS monolayer. Transient shown for $E_1 = -0.753$ V
and $E_2 = -0.758$ V (Hg–HgO).

who refer to both monomolecular layers of HgS and to
"adsorbed HgS."

The solid phase formed on the electrode surface was
identified as the black form of HgS, which has the face-
centered cubic structure. This structure is not of the
layer-lattice type, unlike many of the phases previously
investigated.[6] The question therefore arises as to
what structure a monomolecular layer of HgS may
assume. Clearly it must be a modification of the
bulk phase, since to obtain a monolayer in any plane of
the crystal lattice would require the breaking of pri-
mary bonds which would have to rearrange to a stable
configuration. An analogous situation may be found
in the surface structures of silicon and germanium
which have been examined by low-energy electron
diffraction techniques[8a,b] and have been shown to be
modifications of the bulk structure.

Evidence that the first and second monolayers are
probably not of the same structure is provided by the
following observations. (i) The second monolayer,
though formed separately, may be reduced only with
the first monolayer. This evidence, provided by both
the transient behavior (Figures 1E and F) and the
impedance observations (Figure 2), suggests a change
in structure of the film when the second monolayer is
deposited, insofar as the two layers become bonded
together. (ii) The charge required for the formation of
each monolayer is not the same, being less for the
first (179 ± 16 μC cm^{-2}) than the second (228 ± 23 μC

cm^{-2}). This suggests that the structure of the first
monolayer is less closely packed than that of the
second. These charges may be compared with that
calculated for a monolayer in the most closely packed
plane in the bulk phase, $i.e.$, a monolayer in the (111)
orientation, for which a value of 218 μC cm^{-2} is ob-
tained.

Passivation of the Electrode. The results obtained
using the alkaline sulfide solution indicate that mercury
sulfide is deposited on the electrode surface as two suc-
cessive monomolecular layers, in the same manner as has
been established for the buffered sulfide solution. The
effect of the growth of these monolayers on the rate of
anodic dissolution of the electrode must now be con-
sidered.

The current–time transients of Figure 4 show that
the growth of each monolayer on the electrode surface
results in a marked decrease in the dissolution current.
When the first monolayer is grown (Figures 4B and C),
the current becomes almost constant with time; $i.e.$,
the reaction is no longer to a large extent diffusion
controlled but is now controlled by the rate at which
mercury passes through the HgS layer. The effect of
the growth of the second monolayer is then observed as
a well-defined fall in the current (Figures 4D and E).
The current–potential relationship of Figure 5 shows
that each monolayer reduces the rate at which mercury
dissolves by a comparable factor of $\sim$5.

An attempt was made to interpret the current–time
transients for the effect of the growth of the second
monolayer (Figures 4D and E), for which the effects of
diffusion may be neglected. The current may then be
considered to be the sum of four components due to
(i) the formation of the second monolayer (i_1), (ii)
dissolution at the electrode surface covered with one
monolayer (i_2), (iii) dissolution at the electrode surface
covered with two monolayers (i_3), and (iv) dissolution at
the edges of growing centers (i_4).

These currents may be formulated on the basis of the
previously proposed model for the progressive nu-
cleation and growth of a two-dimensional mono-
molecular layer

$$i_1 = \frac{nF\pi Mk^2 Aht}{\rho} \exp\left(-\frac{\pi M^2 k^2 At^3}{3\rho^2}\right) \qquad (1)$$

where M is the molecular weight of the phase, ρ is its
density (in g cm^{-3}); h is the height (in cm); k is the
rate constant of crystal growth (in mol cm^{-2} sec^{-1});
and A is the rate constant of nucleation in nuclei
(in cm^2 sec^{-1})

$$i_2 = i_0' \exp\left(-\frac{\pi M^2 k^2 At^3}{3\rho^2}\right) \qquad (2)$$

(8) (a) J. J. Lander, $Surface$ $Sci.$, 1, 125 (1964); (b) R. Seiwatz,
$ibid.$, 2, 473 (1964).

where i_0' is the dissolution rate per square centimeter of electrode covered with one monolayer

$$i_3 = i_0'' \left[1 - \exp\left(-\frac{\pi M^2 k^2 A t^3}{3\rho^2} \right) \right] \quad (3)$$

where i_0'' is the dissolution rate per square centimeter of electrode covered with two monolayers

$$i_4 = i_p k^2 A t^2 \exp\left(-\frac{\pi M^2 k^2 A t^3}{3\rho^2} \right) \quad (4)$$

where i_p is a constant (with units of C cm⁴ mol⁻² nuclei⁻¹) relating to the catalytic activity per unit edge.

The partial currents represented by eq 1–4 are shown schematically in Figure 8 together with the form of the resultant total current of $i_2 + i_3$.

In order to test the experimentally obtained transients (Figures 4D and E), the currents i_2 and i_3 were assumed to be the dominant terms and i_1 and i_4 were neglected. The point of inflection in the resultant transient then coincides with the maxima in i_1 and i_4 which occur at a time

$$t_m = \left(\frac{2\rho^2}{\pi M^2 k^2 A} \right)^{1/3} = \beta^{1/3} \quad (5)$$

Combining eq 5 with 2 and 3

$$i_2 = i_0' \exp\left(-\frac{2}{3\beta} t^3 \right) \quad (6)$$

$$i_3 = i_0'' \left[1 - \exp\left(-\frac{2}{3\beta} t^3 \right) \right] \quad (7)$$

The sum of i_2 and i_3 was calculated using values of t_m and i_0''/i_0' estimated from the transient of Figure 4E, obtained at a potential of −0.725 V (Hg–HgO). The resultant current–time curve (Figure 4F) gives only approximate agreement with the experimental result; this may be due partly to the assumptions made above and partly to the distortion of the experimental transient arising from the high currents involved. Such currents become limited by resistance overpotential and also may lead to reactant depletion at the electrode surface, resulting in changes in the reversible potential of HgS on the electrode.

Relationship of the Present Work to the Mechanism of Passivation. The mechanism of the passivation of metals has been extensively discussed with particular reference to the behavior of iron.[9] It has been variously suggested that passivity is caused by (a) the adsorption of anions, (b) the formation of a two-dimensional film, (c) the formation of a three-dimensional film, and most recently[10] (d) the tranformation of a three-dimensional ionically conducting film to an electronically conducting film. In dealing with the transition metals, considerable complications arise because of the variable valency states which are found.
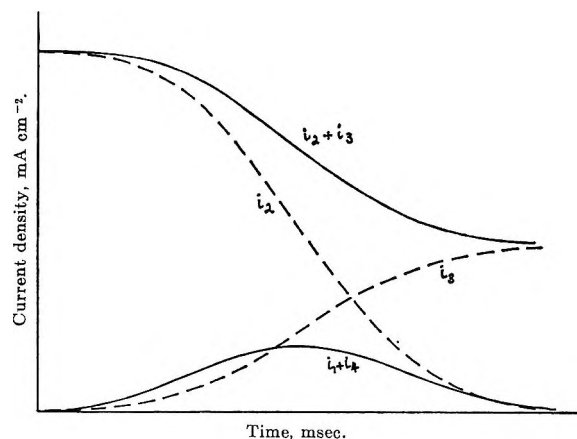

Figure 8. Schematic transients for component currents due to monolayer growth (i_1), and simultaneous anodic dissolution at the electrode covered with one monolayer (i_2) and two monolayers (i_3). i_4 represents the current due to dissolution at the edges of growing centers.

The present work has established that in the case of mercury in sulfide ion solution, there is only one solid anodic phase formed, and its growth on the electrode surface as a monomolecular two-dimensional film severely inhibits the dissolution reaction. The formation of a second monolayer further inhibits the reaction.

The most important aspect of the experimental results is the evidence that the current–potential curve is discontinuous (Figure 5). In most previous discussions of passivation, it has been assumed that the current–potential curve shows a region of "negative" Tafel slope, and theories have been proposed to account for this phenomenon (*e.g.*, Gilroy and Conway[11]). It seems likely that such regions which are associated with the formation of a solid phase arise either from the recording of nonsteady-state measurements or from a blurring of the individual discontinuities associated with relatively perfect crystal faces by the use of polycrystalline material. A schematic representation of the current–potential relationship for such a case is shown in Figure 9.

It has been shown in the present system that it is possible to distinguish between adsorbed sulfide ions and a two-dimensional film of HgS. Unfortunately, in the potential region in which strong adsorption of sulfide ions occurs in 1 M Na₂S solution, the dissolution current is too high to permit accurate measurements to be made. However, the observation of a negative charge-transfer resistance in this region indicates that a small region of negative Tafel slope may exist cathodic to the potential at which the first monolayer of HgS is formed.

(9) L. Young, "Anodic Oxide Films," Academic Press Inc., New York, N. Y., 1961, p 227.

(10) J. O'M. Bockris, A. K. N. Reddy, and B. Rao, *J. Electrochem. Soc.*, **113**, 1133 (1966).

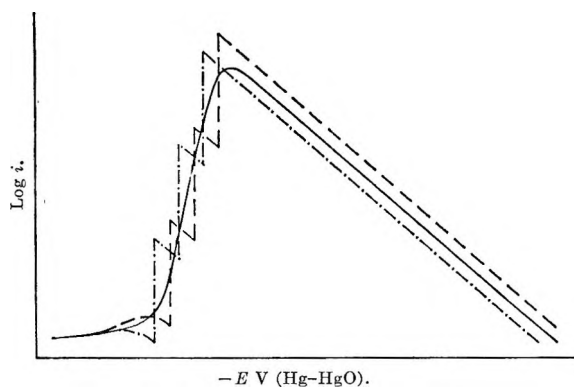(11) D. Gilroy and B. E. Conway, *J. Phys. Chem.*, **69**, 1259 (1965).

Figure 9. Schematic potential dependence of the dissolution current density in the passivation of a solid metal electrode: ----, face A; ----, face B; ———, polycrystalline.

In summary, the present measurements suggest that (a) the severe inhibition of the dissolution of a metal is associated in the first instance with the formation of a two-dimensional film on the electrode surface, and (b) the adsorption of anions does not cause a change in the dissolution rate of orders of magnitude, although it may have some effect.

Finally, it is of interest to consider the passivating effect of a solid anodic phase resulting from the electrostatic-potential drop in the phase. For any given thickness of film, the rate of dissolution of mercury at film–solution interface is equal to the rate at which mercury is transported through the film, when the steady state has been reached. Thus it may be seen that even if the "intrinsic" dissolution rate is the same at the HgS–solution interface as it is at the mercury–solution interface, the current is likely to be smaller, since there will now be an electrostatic-potential drop in the HgS. The possible situations are illustrated in Figure 10, where the potential–distance profile is shown for the case where the film has an electronic conductivity comparable with that of a metal (Figure 10b) and where the electronic conductivity is appreciably less (Figure 10C).

Thus if the dissolution rate in the absence of the film is

$$i_M = i_0 \exp\left[\frac{\alpha nF}{RT}(\phi_M - \phi_S)\right] \qquad (8)$$

in the presence of the film, it will be

$$i_F = i_0' \exp\left[\frac{\alpha nF}{RT}(\phi_F - \phi_S)\right] \qquad (9)$$

(See Figure 10).

We should only expect $i_M \approx i_F$ if the film were a good electronic conductor and $\bar{\mu}_e{}^M = \bar{\mu}_e{}^F$. In general, however, there will be an electrostatic-potential gradient in the film (Figure 10C) (there must be an
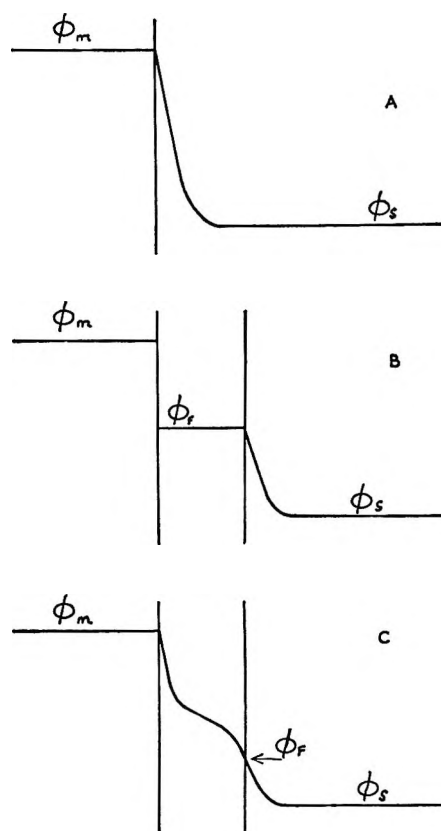

Figure 10. Electrostatic potential–distance profiles for the dissolution of a metal: (A) in the absence of a film; (B) in the presence of a film with good electronic conductivity and $\bar{\mu}_e{}^m = \bar{\mu}_e{}^f$; (C) in the presence of a film with poor electronic conductivity.

electrochemical-potential gradient for the metal ions across the film, in order to maintain a constant film thickness) causing $i_M > i_F$.

The view of Bockris, et al.,[10] that passivation is primarily concerned with the change of a three-dimensional film from an ionic conductor to an electronic conductor can only be true if either (a) i_0' for the ionically conducting film is considerably greater than i_0' for the electronically conducting film or (b) the ionically conducting film is discontinuous while the electronically conducting film is continuous. These points are not considered by Bockris, et al.

Neither of these differences in film behavior would be expected to be intimately connected with the conductivity of the films, and, moreover, adsorption measurements at visible frequencies cannot be used unambiguously to predict dc conductivities.

The Thermal Dissociation of Oxygen Difluoride. I.

Incident Shock Waves

by Jay A. Blauer and Wayne C. Solomon

Air Force Rocket Propulsion Laboratory, Edwards, California 93523 (*Received July 25, 1967*)

The thermal dissociation of OF_2 behind incident shock waves was investigated with an Ar diluent in the temperature range 860–1300°K. The course of the dissociation was followed by means of uv absorption spectroscopy utilizing a light beam centered at 220 mμ. The dissociation exhibits two phases: a slow initiation phase followed by an accelerating rate. Initial slope measurements gave a second-order rate constant of $k = 10^{14.2}e^{-31,500/RT}$ cm^3/mol sec. The results are interpreted as being indicative of a chain mechanism.

Introduction

The thermal dissociation of OF_2 has been the subject of at least two independent studies in the past.[1,2] The over-all second-order rate constant for the reaction

$$M + OF_2 \longrightarrow F + OF + M$$
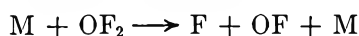
below its high pressure limit was given as

$$k = 10^{17.7}e^{-39,900/RT} \text{ cm}^3 \text{ mol}^{-1} \text{ sec}^{-1}$$

by Koblitz, *et al.*[1] Dauerman[2] also reports an activation energy of 40 kcal for the reaction.

Although both of the cited studies consider the reaction as a simple cleavage of an OF bond, there is much current speculation that the actual reaction proceeds by means of a chain mechanism.[3,4] Recently a thorough investigation of this reaction was undertaken at this laboratory in conjunction with studies of the OF_2–H_2 and OF_2–CH_4 systems. Sufficient data have now been collected to make a valid comparison with the previously published results. The investigation proceeded by two paths. The high-temperature (*ca.* 860–1300°K), high-pressure (*ca.* 10–20 atm) region was investigated behind incident shock waves. The low-temperature (*ca.* 500–650°K), low-pressure (*ca.* 0–10 atm) region was investigated by means of a static reactor coupled to a mass spectrometric sampling system.

Experimental Section

The shock tube, designed at Avco Corp., Wilmington, Mass., is of stainless steel and has an inside diameter of 3.75 cm. The downstream section has a length of 7.5 m and its entire inside surface is finished to a grade-8 smoothness. The driver, having an over-all length of 1.7 m, was separated from the downstream section by means of a scribed-steel or aluminum diaphragm. The downstream section was, in turn, separated from a 220-l. dump tank by means of a thin sheet of Mylar.

Shock detection was by means of moderate response (*ca.* 7 μsec) piezoelectric detectors[5] having a spatial

resolution of 2 mm and placed at intervals of 76.2 cm along the entire length of the downstream section. The detector outputs were displayed on a Tektronix Model 535 oscilloscope equipped with a raster sweep and a Radionics Model TWM crystal-driven timing generator. The observation port was equipped with sapphire windows held in compression by close-fitting brass collets. Window to shock tube sealing was effected with indium wire gaskets. The windows were polished to a tolerance of 1 wavelength of the Na D line.

The course of the dissociation was followed by means of a once-through, single-light-path, ultraviolet absorption spectrometer.[6]

The ultraviolet source was a Beckman deuterium arc lamp. Spectral isolation was by means of a Baird atomic interference filter centered at 2200 ± 250 Å. Detection was by means of a Type 1P28 photomultiplier tube. The instrument has a spatial resolution of 2 mm and an overrelaxation time of about 3 μsec.

Argon having a stated purity of 99.998% was purchased from Matheson and subjected to mass analysis, which confirmed high purity. Gaseous OF_2, purchased from Allied Chemical Corp., was filtered through a column of NaF pellets (previously purged of HF by maintaining above 350° for several hours) and condensed in a prepassivated Monel flask at 77°K. A vacuum was then applied to the material for at least 1 hr, after which a 0.9 fraction of the residue was slowly distilled into a second Monel flask held at 77°K. Mass analysis of the purified gas with argon as an internal

(1) W. Koblitz and H. J. Schumacher, *Z. Physik. Chem.* (Leipzig), **B25**, 283 (1934).

(2) L. Dauerman, G. Salser, and Y. A. Tajima, private communication.

(3) K. J. Laidler, "Chemical Kinetics," 2nd ed, McGraw-Hill Book Co., Inc., New York, N. Y., 1965, pp 170, 171.

(4) A. F. Trotman-Dickenson, "Gas Kinetics," Butterworth and Co. Ltd., London, 1955, p 80.

(5) Purchased from Kistler Instrument Corp., Model No. 601.

(6) Furnished by Rocketdyne, Canoga Park, Calif., under Contract No. AF 04(611)-5963.

standard indicated 0.7% O_2 and 1.8% N_2 as the only significant impurities.

Mixtures of OF_2 and Ar were prepared by pressure difference utilizing Bourdon gauges.[7] Prior to each test, the OF_2 content of the sample was determined by measurement of its optical density at 220 mμ with a Beckman DK-2 spectrophotometer. The results were closely approximated by Beer's law. No change in concentration was observed on standing, even for several days. All gaseous mixtures were used within 1 week of their preparation.

Data Analysis

A typical absorption trace is shown in Figure 1. These traces were extrapolated linearly to the shock front to obtain the optical densities under conditions of negligible dissociation, which conditions were described by the Rankine–Hugoniot relations. The concentration of OF_2 immediately behind the shock front was varied by a factor of 9 (see Table I). Beer's law describes these results closely, the temperature dependence of the extinction coefficient being illustrated in Figure 2. A small initial "blip" lasting for 30–50 μsec was observed for data taken below 900°K (see Figure 1). Its presence was ignored in the extrapolation.

Table I: Incident Shock Parameters and Initial Reaction Rates

Shot no.	OF_2, %	$10^4 (OF_2)_2$,[a] mol/cm³	P_2, atm	T_2, °K	$10^3 (Ar)$, mol/cm³
38	10.0	0.1804	12.5	856	0.1624
44	5.0	0.0898	14.8	1003	0.171
46	5.0	0.0890	14.8	1012	0.169
47	2.5	0.0434	14.8	1041	0.169
48	2.5	0.0457	19.0	1264	0.178
51	2.5	0.0408	12.1	905	0.159
55	7.5	0.1320	12.9	892	0.163
61	5.0	0.0830	11.8	863	0.158
68	5.0	0.0480	10.2	1290	0.091

[a] The subscript 2 refers to the initial state of the gas (after passage of the shock wave).

During the course of the dissociation, gaseous F_2 is formed. Since fluorine resulting from dissociation also absorbs radiation in the range considered, its presence must be accounted for. This was accomplished in two ways. Binary mixtures of F_2 and Ar were shocked to temperatures covering the entire range of interest. This procedure gave an extinction coefficient of 9370 ± 600 cm³/mol, which was found to be statistically independent of temperature. A second procedure involved use of the equilibrium conditions behind the shock wave. At all temperatures considered, OF_2 was completely dissociated.[8] As a consequence, the extinction coefficient for F_2 can be obtained from the equilibrium voltage of the oscillogram. This procedure gave a
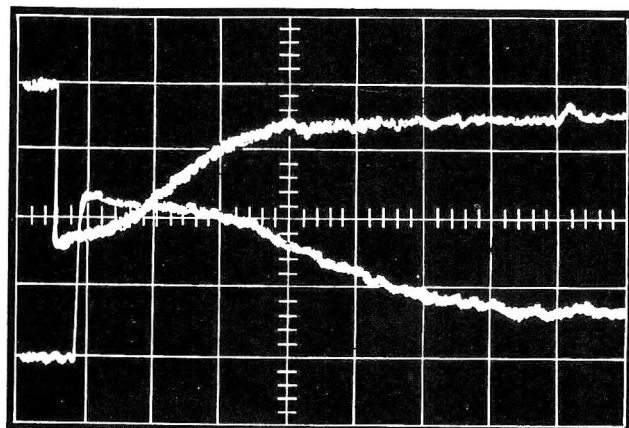

Figure 1. Absorption trace for shot no. 61: 5.0% F_2O, 0.1-V ordinate divisions, 100-μsec fast-sweep, 200-μsec slow-sweep abscissa divisions, 863°K, 11.8-atm incident shock pressure.
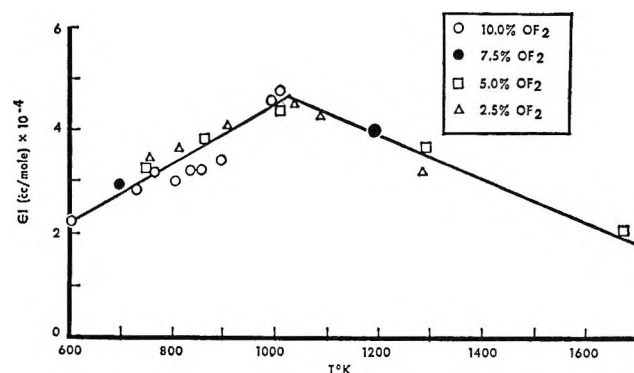
Figure 2. Temperature dependence of molar extinction coefficients for F_2O at 220 mμ.

value of 10,390 ± 750 cm³/mol for the extinction coefficient which was also independent of temperature. The slightly higher values in this instance can be ascribed to a slight absorption owing to O_2.

Other possible molecules which may absorb radiation in the spectral range of interest are O_2F_2, O_2F, and OF. The large first-order rate constant for the decomposition of O_2F_2[9]

$$k = 5.9 \times 10^{12} e^{-17,300/RT} \text{ sec}^{-1}$$

assures that its concentration will remain negligibly small. Arkell[10] has prepared OF in an Ar matrix at liquid He temperatures. When the system was allowed to warm above 40°K, the OF was found to disappear rapidly. These results, coupled with its exothermic reaction with OF_2 (ca. 12 kcal/mol), indi-

(7) Purchased from Heise Company, Newton, Conn.

(8) "JANAF Thermochemical Tables," Dow Chemical Co., Midland, Mich., 1967.

(9) H. J. Schumacher and F. Frisch, Z. Physik. Chem. (Leipzig), B24, 332 (1934).

(10) A. Arkell, R. R. Reinhard, and P. J. Larson, J. Amer. Chem. Soc., 87, 1016 (1965).

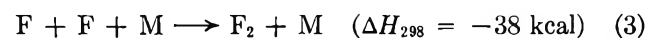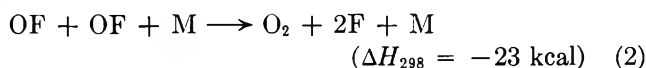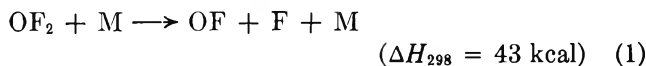cate that OF will exhibit a high degree of reactivity and will not be present in the reaction mixture to any appreciable extent. Pimentel[11] found similar results for O_2F. Accordingly, it would seem that only OF_2 and F_2 will be present in amounts large enough to absorb significant amounts of radiation from the source.

An adiabatic, nonequilibrium computer program[12] was used to obtain an analytical description of the initial portions of a series of reaction profiles by a procedure of numerical integration. The following reaction mechanism was assumed in these calculations

$$OF_2 + M \longrightarrow OF + F + M$$
$$(\Delta H_{298} = 43 \text{ kcal}) \quad (1)$$

$$OF + OF + M \longrightarrow O_2 + 2F + M$$
$$(\Delta H_{298} = -23 \text{ kcal}) \quad (2)$$

$$F + F + M \longrightarrow F_2 + M \quad (\Delta H_{298} = -38 \text{ kcal}) \quad (3)$$

Here 5.8 and 29.7 kcal are taken as the heats of formation of OF_2 and OF, respectively.[13] The value for k_3 was taken from the recent work reported by Diesen.[14] The analytical procedure used involved adjusting the activation parameters of steps 1 and 2 until the best description of the data over the entire range of experimental conditions was obtained.

Results and Discussion

The analytical description of the data which resulted from the computer analysis is illustrated in Figure 3. Here normalized optical density is plotted against laboratory time for nine separate reaction profiles. The experimental conditions for each test are listed in Table I.

The expression obtained for k_1 from this analysis, i.e.

$$k_1 = 10^{14.2}e^{-31,500/RT} \text{ cm}^3/\text{mol sec}$$

is in reasonable agreement with the recent results of Wagner,[15] i.e.

$$k_1 = 10^{15.1}e^{-34,200/RT} \text{ cm}^3/\text{mol sec}$$

However, they are in poor agreement with the very recent results of Dauerman,[16] who reports

$$k_1 = 10^{12.78}e^{-32,500/RT} \text{ cm}^3/\text{mol sec}$$

The results are even in fair agreement with the results of Schumacher[1] when one accounts for the differences in both the activation energy and the frequency factor. An actual comparison with the results of Schumacher would require a knowledge of the temperature dependence of the preexponential factor to allow a reasonable extrapolation over a temperature span of approximately 500°.

It has been suggested by a referee that the acceleration in reaction rate observed in oscillograms such as that shown in Figure 1 is due to heat released as fluorine atoms recombine. This point was checked with the
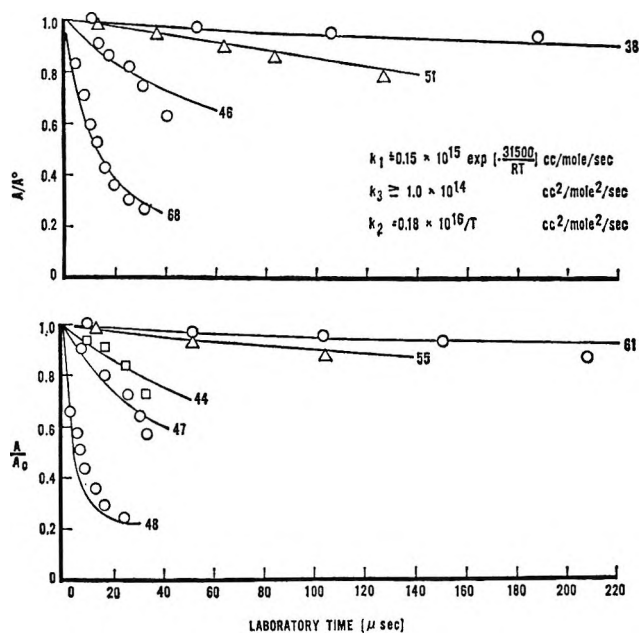

Figure 3. Adiabatic numerical integrations for the initial reaction rate. (The values of k_2 and k_3 should be interchanged; i.e., $k_2 \geq 1.0 \times 10^{14}$ and $k_3 = 0.18 \times 10^{16}/T$.)

computer program described above. It was found that no combination of steps 1–3 could give any apparent acceleration in reaction rate unless the activation energy to step 1 was in the region of 100 kcal/mol. As a consequence, it must be assumed that the reaction is autocatalytic, probably proceeding by means of a chain mechanism.

Although the other investigators cited above saw no direct evidence of a chain mechanism, it seems reasonable that at the high reagent concentrations used in this study, a reaction such as the following might begin to compete with step 1, i.e.

$$F + OF_2 \longrightarrow OF + F_2 \quad (\Delta H_{298} = 4 \text{ kcal}) \quad (4)$$
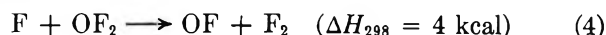
Steps 1–4 would then constitute a chain reaction with fluorine atoms as the chain carrier. Furthermore, at temperatures below the point of significant dissociation of F_2, the addition of molecular fluorine to the reaction mix should inhibit the reaction due to the reversible nature of step 4. This effect has actually been observed and is illustrated in Figure 4. Here the normalized optical density has been corrected for the presence of

(11) R. P. Spratley, J. J. Turner, and G. C. Pimentel, J. Chem. Phys., 44, 2063 (1966).

(12) Furnished by Dr. T. A. Jacobs of Aerospace Corp., El Segundo, Calif.

(13) R. King and G. Armstrong, National Bureau of Standards, private communication, 1967.

(14) R. W. Diesen, Fourth International Fluorine Symposium, Estes Park, Colo., 1967.

(15) H. Wagner, private communication, 1967.

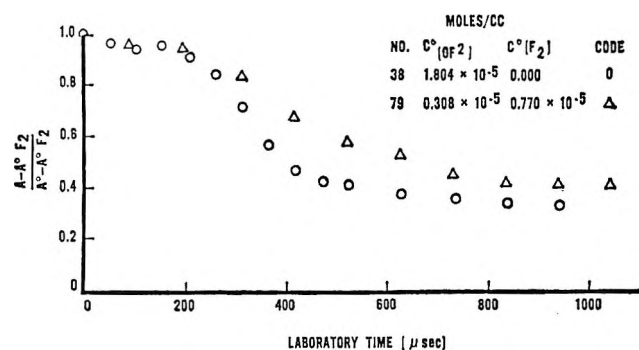(16) L. Dauerman, G. Salser, and Y. Tajima, J. Chem. Phys., 71, 3999 (1967).

Figure 4. Illustration of the effect of added fluorine upon the reaction profile at 855°K with an incident shock pressure of 12 atm.

Figure 5. Illustration of the effect of initial reactant concentration upon the reaction profile at $T = 900 \pm 5$°K for binary mixtures of argon and oxygen difluoride at an incident shock pressure of 12 ± 1 atm.

initial fluorine to allow a direct comparison of the two sets of data. At higher temperatures, this inhibition due to F_2 was found to decrease and finally vanish at temperatures above 1200°K.

Of course, it must be demonstrated that the effect illustrated in Figure 4 is not due simply to the concentration difference of the two tests cited. Accordingly, the normalized profiles for two separate tests conducted with mixes of very different concentration levels are compared in Figure 5. The results demonstrate that within the range of concentrations considered (ca. 0.4 $\times$ 10^{-5} to 0.2 $\times$ 10^{-4} mol/cm^3), the normalized reaction profiles are independent of the initial concentration of reactant.

Gatti, et al.,[17] have presented photochemical evidence that reaction 4 must have an activation energy in excess of 15 kcal/mol; however, these workers neglected any contribution from the reverse of reaction 4 in their analysis.

Conclusions

It presently appears that the dissociation of OF_2 occurs by means of a chain mechanism which becomes particularly important at high reagent concentrations (ca. >10^{-6} mol/cm^3). The chain termination probably occurs by recombination of F atoms and/or by interaction of OF radicals. It must be concluded that until the real nature of this decomposition has been demonstrated, no reliance should be placed upon the activation parameters derived for step 1.

(17) R. Gatti, E. Staricco, J. Sirce, and H. Schumacher, *Z. Physik. Chem.* (Leipzig), **35**, 343 (1962).

The Thermal Dissociation of Oxygen Difluoride. II. Static Reactor

by W. C. Solomon, J. A. Blauer, and F. C. Jaye

Air Force Rocket Propulsion Laboratory, Edwards, California 93523 (*Received July 25, 1967*)

The thermal decomposition of oxygen difluoride has been investigated in aluminum reactors at 563–634°K. The reaction has an induction period followed by an apparent first-order decay in the pressure region of 10–5500 mm. The observed first-order constant is $10^{9.0}e^{-30,100/RT}$ sec^{-1}. The data are discussed in terms of decomposition proceeding *via* a chain reaction.

Introduction

The preceding paper in this series dealt with the dissociation of OF_2 in argon at temperatures between 900 and 1400°K using the shock-tube technique.[1] Since these results were at some variance with earlier reports,[2,3] reexamination of this important reaction in the chemical reactor was also undertaken. The conclusions drawn from these two studies have bearing on more complex systems involving oxygen difluoride and fluorine. From the available information on oxygen difluoride decomposition, one would anticipate it to be at least as reactive as fluorine.[2] In contrast to the fluorine reactivity with reducing agents,[4,5] mixtures of oxygen difluoride with hydrogen or methane are stable even at elevated temperatures.[6] If the decomposition of OF_2 proceeds by simple dissociation, it could provide a better basis for understanding unimolecular decompositions. However, this study makes it seem that the thermal decomposition of OF_2 proceeds in a complex fashion.

Experimental Section

The OF_2 was purified by vacuum distillation at 77°K. The helium and argon purities were 99.99% and the fluorine purity was 98.5%. The nitrogen, which was the diluent in many experiments, was Matheson preparative grade. The oxygen used for these studies was aviators' breathing oxygen (99.5%).

The gases were handled and mixed using passivated stainless steel vacuum lines and Monel or stainless steel vessels. The corrosive gas systems were equipped with Hoke Y-440 valves and Autoclave 10V-4071 valves. After passivation with elemental fluorine, the systems were maintained at 10^{-3} to 10^{-6} mm when not in use. Pressure measurements for gas transfers were made with two calibrated Wallace and Tiernan FA-145 precision manometers. The manometers were constructed with Ni-Span C capsules having pressure ranges of 0–800 and 0–7600 mm, respectively.

The two reactor systems which were used here consisted of a 31-cm³ welded aluminum cylinder and a 70-cm³ aluminum sphere (1100-series aluminum). Swagelok fittings were welded to the opposite ends of

each of the reactors. At one end, a short piece of aluminum tubing which was connected to an adjustable leak (Granville-Phillips variable leak) furnished sample to a mass spectrometer. The opposite end of the vessel was connected to the gas-handling system by aluminum tubing through a Hoke Y-440 vacuum valve. The good mechanical behavior of the leak allowed study of the reaction over a pressure range of 10–6000 mm in the reactor. Although the above system was not line-of-sight, the reaction mixture was admitted directly into the analyzer section without the necessity of differential pumping. The pressure drop to 10^{-5} mm effectively inhibited further thermal reaction. Temperature control was maintained to ±0.25° by use of a full proportional temperature controller (F & M 240-M25). This unit sensed the air-bath oven temperature with a chromel–alumel thermocouple. Measurements with the same thermocouple in the circulating air stream and inside the reactor itself disclosed less than a 0.5° temperature variation. The oven was cylindrical, with three planar heater elements incorporating radiation shields between the heaters and the reactor. Circulation was by a Varian Model 18-001 fan and motor.

The aluminum reactor chamber was degreased with chloroform; then it was baked out under vacuum and was checked for leaks (2×10^{-7} mm with continuous pumping). The chamber was filled with fluorine to 350 mm and the temperature was gradually increased to 625°; this was followed by a similar treatment with 500 mm of undiluted oxygen difluoride. The progress of this passivation was monitored with the mass spectrometer. The oxygen balance indicated formation of aluminum fluoride by action of the fluorine, followed by partial reconversion to an oxide or oxyfluoride when OF_2 was introduced.

(1) Part I: J. A. Blauer and W. C. Solomon, *J. Phys. Chem.*, **72**, 2307 (1968).

(2) W. Koblitz and H. J. Schumacher, *Z. Physik. Chem.* (Leipzig), **25B**, 283 (1934).

(3) L. Dauerman, G. Salser, and Y. A. Tajima, *J. Phys. Chem.*, **71**, 3999 (1967).

(4) J. B. Levy and B. K. W. Copeland, *ibid.*, **67**, 2156 (1963).

(5) J. B. Levy and B. K. W. Copeland, *ibid.*, **69**, 408 (1965).

(6) W. C. Solomon and F. C. Jaye, unpublished results.

As already indicated, the time *vs.* concentration data were obtained by analysis of the gas mixtures with a CEC 130 mass spectrometer. The spectrometer introduction system was stainless steel and Monel. The instrument background never exceeded 1% when compared to the sample under measurement. The reaction gas entered the analyzer *via* continuous flow through the leak.[7] Argon was used as an internal standard in all mixtures and its pressure was normally maintained at 0.25 times the initial OF_2 pressure. The argon peak at m/e 40 could be compared to the peaks for OF_2 at 35 and 54, oxygen at 32, and fluorine at 38 in about 10 sec. The ratios of intensities (corrected for relative mass spectral sensitivities) provided the time *vs.* concentration data. This analysis also provided a complete and continuous material balance of all the stable species in the system. Rates measured in this manner agreed closely with those determined by subjecting the entire sample to analysis.

Results and Discussion

The stoichiometry of the decomposition is that which had been reported by Koblitz[2] for quartz vessels. The over-all reaction can be characterized by eq 1 and no deviations from this are detected in a

$$OF_2 \longrightarrow {}^1/_2O_2 + F_2 \qquad (1)$$
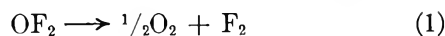
properly treated aluminum vessel (*vide supra*). The measured rates are taken from observations of the OF_2 peaks. Surface effects seem to be relatively unimportant, since no rate changes are noted on going from a cylindrical to a spherical reactor (a change in surface to volume ratio by a factor of 2).

The reaction exhibits some of the features of a true unimolecular decomposition. The kinetics for the most part are nicely described by first-order decay curves. For this reason, all of the data are reported in terms of apparent first-order rate constants. Table I gives these constants and the conditions under which they are obtained. The time *vs.* concentration curves for all of these measurements are quite smooth. Rate constants are taken from lines drawn visually through data points in plots of the logarithm of OF_2 pressure *vs.* time. Typical data from these experiments are plotted in Figure 1. After a short induction time, these logarithmic plots are seen to be linear for a period (at least 75% reaction) sufficient to establish an order very close to 1. The induction period as well as the first-order rate is found to be a function of temperature. The presence of this induction period, which has not been observed by the earlier workers,[2,3] is inconsistent with a mechanism involving a single elementary reaction. The time to first observation in the early work may have obscured the presence of the induction period. Moreover, it is also found that the rate constant increases with increasing pressure up to a value above 5500 mm (see Figure 2).[8] Therefore, all of the rate

Figure 1. Rate of decomposition of OF_2 as a function of temperature. All rate measurements were made in nitrog (680 mm) at a total system pressure of 800 mm.
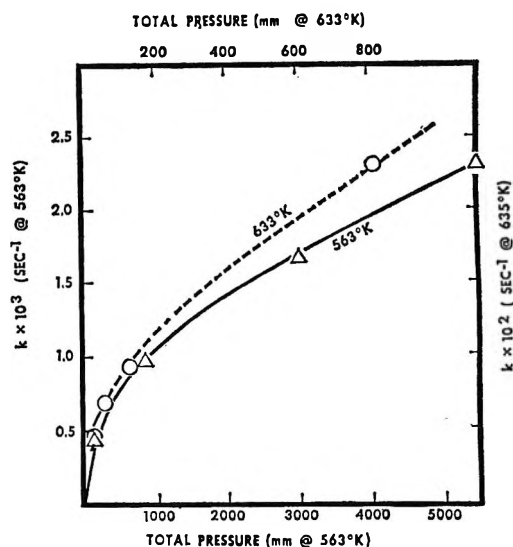
Figure 2. Pressure dependence of the rate constant at constant temperature. Nitrogen was the added diluent in all cases.

measurements in this study seem to have been made in a pressure-dependent region of at least one of the elementary steps. The observed changes in decomposition rates which are presented in the form of the pressure *vs.* rate constant curve (Figure 2) appear to be unrelated to the initial OF_2 concentration and seem to be the result of the regular alterations in total pressure. This conclusion is reinforced by the observation (*cf.* runs numbered 8, 9, 16–19, 28, and 33–35) that a change in the partial pressure of OF_2 on going from 600 to 1 mm at nearly *constant total pressure* has no no-

(7) Continuous time *vs.* concentration plots were observed as long as the pressure in the ion source of the mass spectrometer was constant. Measurements made when the pressure varied by more than one-half order of magnitude were discarded.

(8) The high-pressure experiments were limited to a maximum of 5500 mm by the design of the reaction chamber.

Table I: Reaction Parameters

Run	Total pressure, mm	Pressure of OF₂, mm	Pressure of Ar, mm	Diluent	Temp, °K	Apparent rate constant, sec⁻¹ × 10³
24B	10	9.0	1.0	OF_2	633	4.6
24A	50	45	5.0	OF_2	633	6.6
19	115	15	4	N_2	563	0.63
20	120	109	11	OF_2	563	0.53
21	120	109	11	OF_2	593	2.1
22	120	109	11	OF_2	611	4.2
23	120	109	11	OF_2	633	9.2
8	705	100	25	N_2	563	1.13[a]
9	705	100	25	N_2	563	1.07
17A	705	100	25	N_2	563	0.89
17B	705	100	25	N_2	563	0.89
18	705	100	25	N_2	563	0.92[a,b]
19	705	100	25	N_2	563	0.91[b]
33	695	10	5.0	N_2	563	0.77[c]
35	682	2.0	...	N_2	563	1.5[c]
34	681	1.0	...	N_2	563	1.1[c]
10	705	100	25	N_2	594	5.5
11	705	100	25	N_2	614	10.7
13A	705	100	25	N_2	634	18[b]
13B	705	100	25	N_2	634	23
31	760	100	10	N_2 (325)–F_2 (325)[d]	563	0.59
14	685	100	25	F_2	574	1.75
29	760	100	10	F_2	563	0.49
15	750	650	100	OF_2	574	2.75
16	750	650	100	OF_2	564	1.20
28	780	600	180	OF_2	563	0.89
6	725	100	25	He	563	0.90
7	725	100	25	Kr	563	0.62
8A	725	100	25	CF_4	563	1.05
4	775	100	25	O_2	563	1.20[c]
32	800	400	50	N_2	563	0.77
30	1670	100	10	F_2	563	0.58
26	3020	400	40	N_2	563	1.64
25A	5600	400	40	N_2	563	2.31
25B	5600	400	40	N_2	563	2.30

[a] Conducted in a 31-cm³ cylinder; all others carried out in a 70-cm³ sphere. [b] Determined by extracting about 20% of the total reaction mixture into a cold vacuum line followed by analysis of the mass spectrometer. [c] Because of the low partial pressures of OF₂ and Ar, the error of these measurements is considerably greater than the others in the report. They are estimated to be no better than ±25%, whereas the rest of the rate constants are considered to be reproducible to within ±10%. [d] Numbers in parentheses indicate a pressure of 325 mm.

ticeable effect on either the rate or the form of the kinetics.

An effort has been made to gain more insight into the reaction mechanism through examination of the effect of added gases. Most of the study has been done using nitrogen as an added inert. None of the added gases is found to change the observed kinetics, although large-scale decomposition of CF_4 is observed in the case where it is the added diluent. Moreover, one can see that the effects of gases on the reaction rate are generally quite small (Table II). One of the products (oxygen) has no noticeable effect and the other product (fluorine) acts moderately to retard the reaction. The effect of added fluorine seems to be one of inhibition, since the addition of 1560 mm of fluorine does not retard the rate more (within the

experimental error) than the addition of 325 mm of F_2. This observed inhibition contrasts with an acceleration found by the earlier workers.[2] Indeed, the high efficiency of helium in the decomposition is probably the only surprising observation. Truly unimolecular decompositions are reported[9] to be much more sensitive to added helium than is observed here; however, larger effects might be noted at lower pressures.

The Arrhenius parameters which are found here are important to subsequent analysis of the data. In the present work we have obtained the relationship seen in eq 2. The parameters reported here are least-

$$k = 10^{9.0 \pm 0.4} e^{-30,100 \pm 1000/RT} \text{ sec}^{-1} \qquad (2)$$

(9) K. J. Laidler, "Chemical Kinetics," 2nd ed, McGraw-Hill Book Co. Inc., New York, N. Y., 1965, p 171.

Table II: Effects of Added Gases

Added gas	k_x/k_{OF_2} (623°K)[a]	k_x/k_{OF_2} (800 mm and 563°K)[b]
OF_2	1.0	1.0
O_2	1.13	1.0
N_2	1.01	1.0
SiF_4	0.88	...
CF_4	...	0.80
He	0.40	0.75
F_2	1.13	0.64
Ar	0.82	...
Kr	...	0.52

[a] Taken from ref 2. [b] This work.

squares values for ten measurements taken at a pressure of 800 mm. The data from runs made at 120 mm are plotted in Figure 3, along with data at various pressures from references 1, 2, 3, and 10. Although there are not enough of the low-pressure data for a least-squares value, it is apparent that the activation energy at 120 mm is substantially the same as that measured at the higher pressure. This allows for comparison of activation energies with the shock measurements.[1] The activation energy of 31.5 kcal/mol which has been observed in the shock-tube study[1] is substantially that which is found here for the static reactor. The respective Arrhenius parameters, 1.5 × 10^{14} and 3.0 × 10^{14} cm/mol sec. are also comparable. The close relationship between these energetics would make it appear that the same chemical process is being measured. If either one or both of the reactions are complex, such similar results would not necessarily be expected. The shock-tube result[1] is merely for the initial portion of reaction, whereas the value reported here represents the apparent first-order reaction after an initial delay period. Figure 3 allows for comparison of our values with those of Koblitz and Schumacher,[2] Troe, Wagner, and Weden,[10] and Dauerman, Salser, and Tajima.[3] As has been pointed out,[1] the first two sets of results are in reasonable agreement with our findings, while the latter set (flow-reactor data) seems to be at appreciable variance. The large difference has been noted by Dauerman, but no explanation is evident. One would anticipate that the flow-reactor data (taken at higher temperatures) would be less subject to surface phenomena than either of the two static-reactor studies and thus should give closer agreement with shock-tube observations. Turning again to a comparison of the studies done in these laboratories, one thing stands out in both. The delay periods encountered here and the turnover observed in shock-tube experiments imply a mechanism more complex than simple bond rupture. Moreover, it is difficult to rationalize the inhibiting effects of added fluorine on the basis of a single elementary step such as

$$OF_2 + M \longrightarrow OF + F + M \qquad (3)$$

As pointed out in the previous study, we think that a reasonable estimate for the energy to break the first bond in OF_2 might be 43 kcal/mol (*vide infra*). The consequence of using 30 kcal/mol (our activation energy) has profound significance on the bond energy of the newly formed OF radical. This consideration leads to a bond dissociation energy of 62 kcal/mol for the OF radical. The aforementioned value is 13 kcal/mol higher than that which has been derived from infrared studies[11] or theoretical work.[12,13] A value of 62 kcal/mol seems even more unreasonable when compared to the value of 24 kcal/mol which was obtained from electron-impact studies.[14]

A recent independent observation made in these laboratories may also have bearing on possible reaction mechanisms. During the course of the rate measurements in the aluminum reaction chamber, two very small peaks at masses 70 and 51 were detected. These are most intense in the presence of excess fluorine. The peak at mass 70 has been made the subject of a high-resolution mass spectrometric study to determine its exact mass.[15] A peak at mass 69.986 ± 0.003 is observed
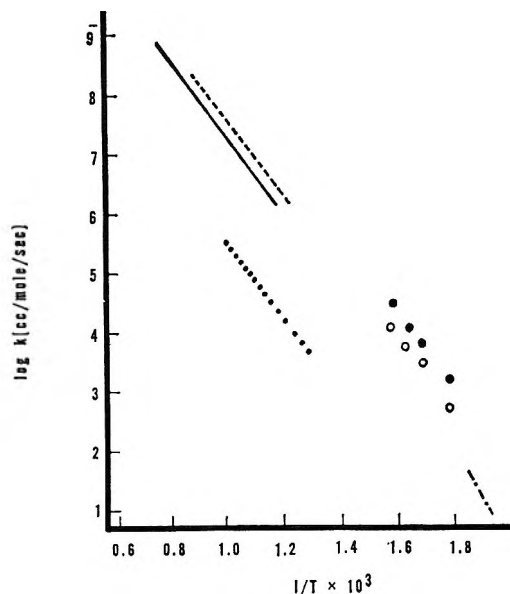
Figure 3. Temperature dependence of apparent second-order rate constants: − − − −, Wagner;[10] ———, Blauer;[1] ○, this work (P = 120 mm); ●, this work (P = 705 mm); − · — · —, Schumacher;[2] . . . . , Dauerman.[3]

(10) J. Troe, H. Gg. Wagner, and G. Weden, private communication, 1967.

(11) A. Arkell, R. R. Reinhard, and L. P. Larson, *J. Amer. Chem. Soc.*, **87**, 1016 (1965).

(12) G. Glockler, *J. Chem. Phys.*, **16**, 605 (1948).

(13) W. C. Price, T. R. Passmore, and D. M. Roessler, *Discussions Faraday Soc.*, **35**, 207 (1963).

(14) V. H. Diebler, R. M. Reese, and J. L. Franklin, *J. Chem. Phys.*, **27**, 1296 (1957).

and can reasonably be assigned to O_2F_2 (69.988). The temperature for these experiments is far above that normally encountered in the usual synthesis of dioxygen difluoride.[16] Therefore, its observation under these conditions implies that it may be one of the intermediate species[17] in a chain decomposition of OF_2. The decomposition of the O_2F radical resulting from O_2F_2 has been the subject of several researches[18,19] and may offer a key to the over-all reaction.

A number of steady-state solutions to free-radical systems involving OF_2, OF, F, and O_2F_2 have been considered. In testing these possibilities, we have assumed the thermochemistry indicated in ref 1. In most of the possibilities which have been considered, step 4 is assumed to be the chain-carrying mechanism.

$$F + OF_2 \rightleftarrows OF + F_2 \qquad (4)$$

We have used as boundary conditions the experimental observations that we are dealing with an M-dependent reaction which is approximately first order in OF_2. Several mechanistic schemes obtain to provide M-dependent solutions which are either first or $^4/_3$ 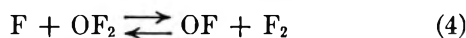order in OF_2. In some cases, estimates of activation energies for individual steps provide reasonable numbers for the activation energy. The observed delay periods can be accounted for simply as the time required for chain carrier to achieve a steady-state concentration. The problem with such an approach is that the pressure dependence is not accurately described, and the fluorine inhibition cannot be accounted for quantitatively. Further, with the available data it is difficult to distinguish between several of the more plausible steady-state approximations.

Conclusions

It has been pointed out by Dauerman[3] that if we equate the experimental activation energies with the energy required to dissociate the first bond, then OF should be considerably more stable than OF_2. In fact, this assumption requires that the second OF bond be about twice as strong as the first. Our analysis has assumed a more equal distribution of bond strengths.

There may be good reason to think that the second bond is actually weaker than the first. Dauerman[3] has cited some of these arguments. The electron-impact data would support this thought.[14] Referring to the model compound Cl_2O, however, one finds that the first ClO bond is considerably weaker than the second.[20,21] Moreover, the fact that four separate studies made over a broad range of concentrations and temperatures provide essentially the same activation energy and Arrhenius preexponential is startling. If one wishes to build a case for changing mechanisms, one might anticipate greater differences in these kinetic parameters than is found.

(15) High-resolution work was conducted using a line-of-sight reaction chamber coupled to a CEC-110 double-focusing mass spectrometer. Two small peaks were resolved at mass 70. The peak at mass 69.969 ± 0.003 is assigned to SF_2^+, from a major impurity (SF_6) in the fluorine used. The peak at 69.986 ± 0.003 is assigned to O_2F_2. A possible contribution from $F_3{}^{13}C^+$ to this assignment is negligible from consideration of the known ^{12}C:^{13}C isotope ratio and the observed low intensity of the $F_3C_{12}^+$ peak.

(16) A. D. Kirshenbaum, A. V. Grosse, and J. G. Aston, *J. Amer. Chem. Soc.*, 81, 1277 (1959).

(17) It has been suggested to us by Dr. Sydney Benson that the O_2F_2 observed here could as well be the result of recombination, concomitant with supersonic flow and expansion through the leak to the ion source of the spectrometer.

(18) R. D. Spratley, J. J. Turner, and G. C. Pimentel, *J. Chem. Phys.*, 44, 2063 (1966).

(19) P. H. Kassai and A. D. Kirshenbaum, *J. Amer. Chem. Soc.*, 87, 3069 (1965).

(20) G. Herzberg and D. A. Ramay, *Discussions Faraday Soc.*, 9, 80 (1950).

(21) W. H. Evans, T. R. Munson, and D. D. Wagman, *J. Res. Nat. Bur. Stand.*, 55A, 147 (1955).

Thermodynamics of Ternary Systems.   The Quasi-Chemical Approximation

by K. Hagemark[1]

North American Aviation Science Center, Thousand Oaks, California   91360   (*Received July 31, 1967*)

Based on the quasi-chemical approximation, values have been calculated for the partial excess free energies (activity coefficients) of one of the components comprising a ternary solution.   Only the nearest-neighbor interaction has been included.   Within the ternary concentration range, the problem could not be solved explicitly in terms of concentrations, and an iteration method had to be used.   However, an explicit expression has been derived for the partial excess free energy of a third component in dilute solution in a binary mixture. The results are in good agreement with the experimental data for Cd-Bi-Pb, Cd-Sn-Pb, and Al-Bi-Pb.

I. Introduction

Guggenheim[2a] has treated the problem of multicomponent systems by a quasi-chemical method.   His treatment was based on nearest-neighbor interactions. In general, the results for the free energy of mixing cannot be expressed explicitly in terms of the concentration and interaction parameters.   However, the problem can be solved in special cases.   In this article, a simple equation describing the behavior of the partial excess free energy (activity coefficient) of a third component in dilute solution in a binary mixture will be discussed. In addition, equations are given from which values for the partial excess free energy of one component will be calculated for compositions within the ternary system by numerical methods.

Recently, Lupis and Elliott[2b] have applied the quasi-chemical theory to obtain terms called first- and second-order free energy interaction coefficients from an analytical expansion of the excess free energy in terms of mole fractions of the solute components.   The solvent in their case was a single component containing a dilute solution of two or more solutes.

Results from the present treatment will be compared with experimental data for the systems Cd-Bi-Pb, Cd-Sn-Pb,[3] and Al-Bi-Pb.[4]

II. Theoretical Treatment

A ternary system consists of the components A, B, and C.   The partial molar free energy $\bar{G}_C$ (or chemical potential μ_C) of component C is defined by

$$\bar{G}_C = \mu_C = \left(\frac{\partial nG}{\partial n_C}\right)_{n_A, n_B, P, T} \tag{1}$$

where n is the total number of moles, G is the molar free energy, n_i the number of moles of species i, P is the total pressure, and T is the temperature.   The partial molar excess free energy of solution of component C will be defined by

$$\bar{G}^E_C = \bar{G}_C - G^\circ_C - RT \ln N_C \tag{2}$$

where G°_C is the free energy of one mole of pure C, N_C is the mole fraction of C given by

$$N_C = \frac{n_C}{n} \tag{3}$$

R is in cal deg^{-1} mol^{-1}, and T is in degrees Kelvin.

The quasi-chemical method has been explained in several textbooks, and in the present treatment, the notation of Hill[5] is used.

The partition function for the canonical ensemble of systems containing $\mathfrak{N}_A$, $\mathfrak{N}_B$, and $\mathfrak{N}_C$, the number of atoms of species A, B, and C, respectively, is

$$Q(\mathfrak{N}_i, T) = \Pi_i \, (q_i(T))^{\mathfrak{N}_i} \sum_{\mathfrak{N}_{ij}} g(\mathfrak{N}_i, \mathfrak{N}_{ij}) \exp\left(-\frac{E(\mathfrak{N}_{ij})}{kT}\right) \tag{4}$$

where $\mathfrak{N}_i$ is the number of atoms of species i, $\mathfrak{N}_{ij}$ is the number of nearest-neighbor pairs of i and j, $E(\mathfrak{N}_{ij})$ is the configurational energy, k is the Boltzmann constant, $g(\mathfrak{N}_i, \mathfrak{N}_{ij})$ is the number of ways $\mathfrak{N}_i$ atoms can be distributed on $\Sigma\mathfrak{N}_i$ sites forming $\mathfrak{N}_{ij}$ pairs, and $q_i(T)$ is the partition function of an isolated atom on a site.

By following the scheme utilized by Hill,[5] the function $g(\mathfrak{N}_i, \mathfrak{N}_{ij})$ can approximately be written

$$g(\mathfrak{N}_i, \mathfrak{N}_{ij}) = C(\mathfrak{N}_i) w(\mathfrak{N}_i, \mathfrak{N}_{ij}) \tag{5}$$

where

$$w(\mathfrak{N}_i, \mathfrak{N}_{ij}) = \frac{\left(\frac{z}{2}\Sigma\mathfrak{N}_i\right)!}{\Pi_i (\mathfrak{N}_{ii}!) \Pi_{i \neq j}\left[\left(\frac{1}{2}\mathfrak{N}_{ij}\right)!\right]^2} \tag{6}$$

which is the number of ways of distributing $\mathfrak{N}_{ij}$ pairs if they were independent of each other, z is the coordina-

(1) Address correspondence to the author at 3M Company, Central Research Laboratories, St. Paul, Minn. 55101.

(2) (a) E. A. Guggenheim, *Proc. Roy. Soc.*, A169, 134 (1938); (b) C. H. P. Lupis and J. F. Elliott, *Acta Met.*, **14**, 1019 (1966).

(3) J. F. Elliott and J. Chipman, *J. Amer. Chem. Soc.*, **73**, 2682 (1951).

(4) T. C. Wilder and J. F. Elliott, *J. Electrochem. Soc.*, **111**, 352 (1964).

(5) T. L. Hill, "An Introduction to Statistical Thermodynamics," Addison-Wesley, Reading, Mass., 1960, p 252.

tion number (the number of sites which are nearest neighbors to a given site).

$$C(\mathfrak{N}_i) = \left[\frac{\left(\sum_i \mathfrak{N}_i \right)!}{\prod_i \mathfrak{N}_i!} \right]^{1-z} \quad (7)$$

is a normalization factor taking into account the fact that $w(\mathfrak{N}_i, \mathfrak{N}_{ij})$ overcounts the number of configurations.

The configurational energy is expressed as

$$E(\mathfrak{N}_{ij}) = \sum_{i \geq j} \mathfrak{N}_{ij} \epsilon_{ij} \quad (8)$$

where ϵ_{ij} is the interaction parameter for the nearest-neighbor pairs of i and j.

The six unknown variables $\mathfrak{N}_{ij}$ are determined by three coupled linear equations

$$z\mathfrak{N}_A = 2\mathfrak{N}_{AA} + \mathfrak{N}_{AB} + \mathfrak{N}_{AC} \quad (9a)$$

$$z\mathfrak{N}_B = 2\mathfrak{N}_{BB} + \mathfrak{N}_{AB} + \mathfrak{N}_{BC} \quad (9b)$$

$$z\mathfrak{N}_C = 2\mathfrak{N}_{CC} + \mathfrak{N}_{AC} + \mathfrak{N}_{BC} \quad (9c)$$

and three coupled equations to the second degree (obtained by maximizing the partition function)

$$\frac{4\mathfrak{N}_{AA}\mathfrak{N}_{BB}}{\mathfrak{N}_{AB}^2} = e^{-\frac{\Delta\epsilon_{AB}}{kT}} \quad (10a)$$

$$\frac{4\mathfrak{N}_{AA}\mathfrak{N}_{CC}}{\mathfrak{N}_{AC}^2} = e^{-\frac{\Delta\epsilon_{AC}}{kT}} \quad (10b)$$

$$\frac{4\mathfrak{N}_{BB}\mathfrak{N}_{CC}}{\mathfrak{N}_{BC}^2} = e^{-\frac{\Delta\epsilon_{BC}}{kT}} \quad (10c)$$

where $\Delta\epsilon_{AB} = \epsilon_{AA} + \epsilon_{BB} - 2\epsilon_{AB}$, etc, and is positive when pairs of unlike atoms are preferred.

The free energy of the system is calculated from

$$G \approx A = -kT \ln Q \approx -kT \ln Q_{max} \quad (11)$$

where A is the Helmholtz free energy. Furthermore, the partial molar excess free energy of component C (excess chemical potential μ^E_C or $RT \ln\gamma_C$, where γ_C is the activity coefficient) is

$$\bar{G}^E_C = \mu^E_C = \frac{\partial A}{\partial n_C} - G^\circ_C - RT \ln N_C \quad (12)$$

$$\bar{G}^E_C = \mu^E_C = \frac{z}{2} RT \ln \frac{\alpha_{CC}}{N_C^2} \quad (12)$$

where

$$\alpha_{CC} = \frac{\mathfrak{N}_{CC}}{\frac{z}{2} \sum_i \mathfrak{N}_i} \quad (13)$$

$\mathfrak{N}_{CC}$ represents the number of nearest-neighbor pairs of component C. For random mixing ($\Delta\epsilon_{ij} = 0$), $\alpha_{CC} = N_C^2$ and $\mu^E_C = 0$. Thus μ^E_C being greater than or less

than zero is related to $\mathfrak{N}_{CC}$ being larger or smaller than the number of C–C nearest neighbor pairs obtained by random mixing of the components A, B, and C.

Similar expressions are derived for the partial molar excess free energy of the components A and B. Thus the molar excess free energy of solution can formally be written as

$$G^E = \Sigma N_i \bar{G}^E_i = \frac{z}{2} RT \sum_i N_i \ln \frac{\alpha_{ii}}{N_i^2} \quad (14)$$

The partial molar excess free energy of component C may also be written as

$$\bar{G}^E_C = \frac{z}{2} RT \ln \frac{1 - \dfrac{\alpha_{AC} + \alpha_{BC}}{N_C}}{N_C} \quad (15)$$

where α_{AC} is defined by

$$\alpha_{AC} = \frac{\mathfrak{N}_{AC}}{z \sum_i \mathfrak{N}_i} \quad (16)$$

and α_{BC} is similarly defined. The values for the α's are obtained by solving eq 9a–c and 10a–c. From combinations of these equations, using the definitions of the α's and mole fraction

$$N_i = \frac{\mathfrak{N}_i}{\sum_i \mathfrak{N}_i}$$

the following equations are obtained

$$\left(1 - e^{-\frac{\Delta\epsilon_{AC}}{kT}}\right)\alpha_{AC}^2 -$$
$$[(N_A + N_C) - \alpha_{BC} - \alpha_{AB}]\alpha_{AC} +$$
$$(N_A - \alpha_{AB})(N_C - \alpha_{BC}) = 0 \quad (17a)$$

$$\left(1 - e^{-\frac{\Delta\epsilon_{BC}}{kT}}\right)\alpha_{BC}^2 -$$
$$[(N_B + N_C) - \alpha_{AC} - \alpha_{AB}]\alpha_{BC} +$$
$$(N_B - \alpha_{AB})(N_C - \alpha_{AC}) = 0 \quad (17b)$$

$$\left(1 - e^{-\frac{\Delta\epsilon_{AB}}{kT}}\right)\alpha_{AB}^2 -$$
$$[(N_A + N_B) - \alpha_{AC} - \alpha_{BC}]\alpha_{AB} +$$
$$(N_A - \alpha_{AC})(N_B - \alpha_{BC}) = 0 \quad (17c)$$

In general the equations can only be solved by numerical methods.

Two cases will be discussed here: (a) $\bar{G}^E_C$ as a function of x ($x = N_B/(N_A + N_B)$) for the case in which $N_C = 0$ and (b) $\bar{G}^E_C$ as a function of N_C when $x = 0.5$. The first case, corresponding to a third component in dilute solution in a binary mixture, can be solved explicitly in terms of concentrations and interaction parameters.

$\bar{G}^E{}_C$ *in Dilute Solution in AB.* Instead of using the mole fractions N_A, N_B, and N_C (only two of them are independent), it will prove more convenient to represent $\bar{G}^E$ as function of the variables N_C and

$$x = \frac{N_B}{N_A + B_B} \qquad (18)$$

Notice that $x \to N_B$ for $N_C \to 0$. The mole fractions of A and B are given by

$$N_A = (1 - x)(1 - N_C) \qquad (19)$$

$$N_B = x(1 - N_C) \qquad (20)$$

An expression for $\bar{G}^E{}_C$ in the binary AB is obtained from eq 15 from the equation

$$\bar{G}^E{}_C(AB) = \frac{z}{2} RT \ln \left[\lim_{N_c \to 0} \left(\frac{1 - \dfrac{\alpha_{AC} + \alpha_{BC}}{N_C}}{N_C} \right) \right]$$
$$(x = \text{constant}) \qquad (21)$$

The derivation is given in Appendix A, which is exact except for the approximate nature of the quasi-chemical theory itself. The result is

$$\bar{G}^E{}_C(AB) = -zRT \ln$$

$$\left[\sqrt{1 - x - \alpha^\circ{}_{AB}} \, e^{\frac{\Delta \epsilon_{AC}}{2kT}} + \sqrt{x - \alpha^\circ{}_{AB}} \, e^{\frac{\Delta \epsilon_{BC}}{2kT}} \right] \qquad (22)$$

where

$$\alpha^\circ{}_{AB} = \frac{2x(1 - x)}{1 + \sqrt{1 - 4x(1 - x)\left(1 - e^{-\frac{\Delta \epsilon_{AB}}{kT}}\right)}} \qquad (23)$$

The expression for $\bar{G}^E{}_C(AB)$ can be written in a more convenient form (see Appendix B)

$$\bar{G}^E{}_C(AB) = (1 - x)\bar{G}^E{}_C(A) +$$
$$x\bar{G}^E{}_C(B) - G^E{}_{QC}(AB) + f(x) \qquad (24)$$

where $\bar{G}^E{}_C(A)$ and $\bar{G}^E{}_C(B)$ are the partial excess molar free energies of C in pure A and in pure B, respectively. $\bar{G}^E{}_{QC}(AB)$ is the excess molar free energy of the binary AB calculated from the quasi-chemical theory and is expressed in eq B8. The function $f(x)$ is given by

$$f(x) = -zRTx(1 - x) \times$$

$$\left[\frac{1}{1 - x} \ln \left(1 + (1 - x)(ye^\Delta - 1) \right) + \right.$$

$$\left. \frac{1}{x} \ln \left(1 + x \left(\frac{1}{y} e^{-\Delta} - 1 \right) \right) \right] \qquad (25)$$

where

$$y = \sqrt{\frac{1 - x - \alpha^\circ{}_{AB}}{x - \alpha^\circ{}_{AB}}} \, \frac{x}{1 - x} \qquad (26)$$

and

$$\Delta = \frac{\Delta \epsilon_{AC} - \Delta \epsilon_{BC}}{2kT} \qquad (27)$$

The expression for $\bar{G}^E{}_C(AB)$ given in eq 24 disagrees somewhat with an expression presented by Alcock and Richardson.[6] The disagreement is explained by the approximations introduced in their derivations. However, if $f(x)$ is negligible, the expression in eq 24 reduces to an approximate form

$$\bar{G}^E{}_C(AB) \approx (1 - x)\bar{G}^E{}_C(A) +$$
$$x\bar{G}^E{}_C(B) - G^E(AB) \qquad (28)$$

suggested by Alcock and Richardson.[7] $G^E(AB)$ is the actual measured excess free energy of the A–B binary system.

If, for example, the binary AB shows negative deviations from ideality, this approximate expression suggests that $\bar{G}^E{}_C(AB)$ as a function of x exhibits a positive deviation from linearity. The deviation, represented by the term $-G^E(AB)$, which is of the form $x(1 - x)b(x)$, is in this case characterized by the properties of the system A–B only. Any third component C should accordingly exhibit the same deviation from linearity of $\bar{G}^E{}_C(AB)$ as function of x. This, of course, seems unrealistic from a physical point of view. The behavior of $\bar{G}^E{}_C(AB)$ as function of x should also depend on the interactions between the components A and C and between B and C. In the present treatment, these interactions are taken into account by the last term $f(x)$. The nearest-neighbor interaction parameters $\Delta \epsilon_{AC}$, $\Delta \epsilon_{BC}$, and $\Delta \epsilon_{AB}$ are obtained by fitting the quasi-chemical expression to each of the binaries, AC, BC, and AB, respectively.

Before the results are compared with experimental data the function $f(x)$ given in eq 25 will be discussed briefly. The function $f(x)$ is dependent on the parameter Δ(defined by eq 27), which represents the difference between the interaction parameters for the binaries AC and BC. If these two systems exhibit identical deviations from ideality, then $\Delta = 0$ and $f(x)$ is symmetric about $x = 0.5$. Furthermore, the function $f(x)$ is always negative (or zero for random mixing) and becomes more negative (and asymmetric about $x = 0.5$) with increasing absolute values of Δ. Thus an increasing difference between the binary systems AC and BC results in a negative contribution to $\bar{G}^E{}_C(AB)$, *i.e.*, there is a decrease in the positive deviation from linearity (or an increase in negative deviation from linearity) calculated from the approximate expression given in eq 28.

III. Comparison with Experimental Values

The calculated values for $\bar{G}^E{}_C$ will be compared with experimental data for the systems Cd–Bi–Pb, Cd–Sn–

(6) C. B. Alcock and F. D. Richardson, *Acta Met.*, **8**, 882 (1960).

(7) C. B. Alcock and F. D. Richardson, *ibid.*, **6**, 385 (1958).

Pb[3] and Al–Bi–Pb,[4] with Cd (or Al) chosen as the C component and Pb as the B component. These systems are chosen not only because there are very few ternary systems that have been investigated systematically, but also because they are illustrative, since the binary Bi–Pb exhibits negative deviations from ideality whereas Sn–Pb shows positive deviations. Furthermore, the term Δ is larger in the system Al–Bi–Pb than in Cd–Bi–Pb.

The experimental values used in these calculations are given in Table I. Equations B6 and B7 determine

Table I: Experimental Values[3,4] and Corresponding Interaction Parameters

System AB	$G^E_{x=0.5}$(AB), cal	$\Delta\epsilon_{AB}/kT$
Bi–Pb (773°K)	−300	0.153
Bi–Pb (1173°K)	−300	0.102
Sn–Pb (773°K)	350	−0.187

Solvent i	$\bar{G}^E_C$(i), cal	$\Delta\epsilon_{C-i}/kT$
	C = Cd	
Bi (773°K)	0	0
Sn (773°K)	900	−0.117
Pb (773°K)	1880	−0.245
	C = Al	
Bi (1173°K)	4010	−0.344
Pb (1173°K)	7830	−0.672

the parameters $\Delta\epsilon_{AC}$ and $\Delta\epsilon_{BC}$. The parameter $\Delta\epsilon_{AB}$ is determined from the relation

$$G^E_{x=0.5} \text{ (AB)} = -\frac{z}{2} RT \ln\left[\frac{1}{2}\left(e^{\frac{\Delta\epsilon_{AB}}{2kT}} + 1\right)\right] \quad (29)$$

The value for z, the number of nearest-neighbor sites next to a particular site, is chosen equal to 10. This choice is only significant in computing the function $f(x)$ (eq 25).

In Figure 1, the calculated values (from eq 24) are compared with the experimental data for $\bar{G}^E_{Cd}$ in Bi–Pb and in Sn–Pb and for $\bar{G}^E_{Al}$ in Bi–Pb. In agreement with the experiments, $\bar{G}^E_C$ as a function of x shows positive (negative) deviation from linearity when $\bar{G}^E$(AB) is negative (positive). Note that $\bar{G}^E_{Al}$ shows less positive deviations from linearity than does $\bar{G}^E_{Bi}$ in the same binary solution Bi–Pb. This trend is correctly predicted by the quasi-chemical theory and is due to the term $f(x)$ (see eq 25). As pointed out, $f(x)$ becomes more negative with increasing values of 2Δ, the difference between the interaction parameters for the binaries AC and BC. The values for $f(x = 0.5)$ are −8, −30, and −80 cal for the systems Cd–Sn–Pb ($\Delta = 0.064$), Cd–Bi–Pb ($\Delta = 0.123$), and Al–Bi–Pb ($\Delta = 0.164$), respectively. The effect is even larger experimentally.
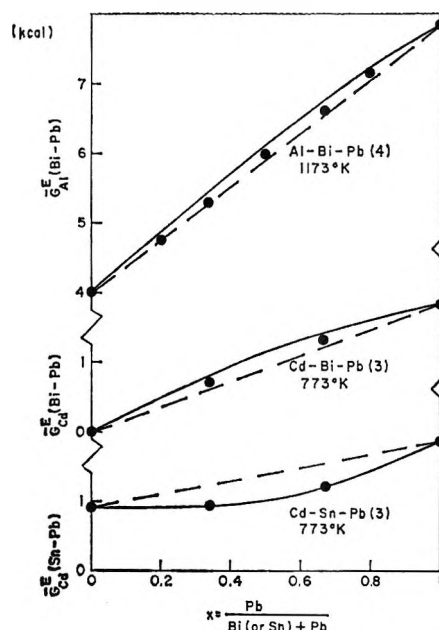

Figure 1. Calculated and experimental values[3,4] for the partial excess free energy of component C as a function of $x = N_B/(N_A + N_B)$ in dilute solution in the binary A–B (Cd in Bi–Pb or Sn–Pb and Al in Bi–Pb): ●, experimental; —, calculated.

$\bar{G}^E_C$ as a Function of N_C. $\bar{G}^E_C$ can be expressed as

$$\bar{G}^E_C = (1 - x)\bar{G}^E_C(AC) + x\bar{G}^E_C(BC) + \Delta\bar{G}^E_C \quad (30)$$

where $\bar{G}^E_C$(AC) ($=\bar{G}^E_C(x = 0, N_C)$) and $\bar{G}^E_C$(BC) ($=\bar{G}^E_C(x = 1, N_C)$) are the partial excess free energy of C in the binaries AC and BC, respectively. $\Delta\bar{G}^E_C$ represents the deviation from linearity of $\bar{G}^E_C$ as function of x at constant N_C. Based on a treatment by Darken,[8] it may be shown that

$$\int_0^1 \frac{\Delta\bar{G}^E_C}{(1 - N_C)^2} dN_C = -\bar{G}^E(AB)$$

$$(x = \text{constant}) \quad (31)$$

Thus the average value of $\Delta\bar{G}^E_C/(1 - N_C)^2$ at constant x is equal to $-G^E$(AB). This is a useful constraint that is discussed in more detail in another paper.[9]

From eq 30 using eq 15 obtained from the quasi-chemical approximation, the expression

$$\frac{\Delta\bar{G}^E_C}{(1 - N_C)^2} = \frac{\frac{z}{2} RT}{(1 - N_C)^2} \times$$

$$\left[\ln \frac{1 - \frac{\alpha_{AC} + \alpha_{BC}}{N_C}}{N_C} - (1 - x)\ln\frac{1 - \frac{\alpha^\circ_{AC}}{N_C}}{N_C} - x\ln\frac{1 - \frac{\alpha^\circ_{BC}}{N_C}}{N_C}\right] \quad (32)$$

(8) L. S. Darken, *J. Amer. Chem. Soc*, **72**, 2909 (1950).

(9) J. Guion, M. Blander, D. Hengstenberg, and K. Hagemark, *J. Phys. Chem.*, **72**, 2086 (1968).

is derived. The $\alpha°_{AC}$ and $\alpha°_{BC}$ are given by expressions obtained from the expression for $\alpha°_{AB}$, eq 23, by replacing x by N_C and $\Delta\epsilon_{AB}$ by $\Delta\epsilon_{AC}$ or $\Delta\epsilon_{BC}$. Values for α_{AC} and α_{BC} are solved on a computer using the Gauss–Seidel iteration method.[10] Initial guesses for α_{AC} and α_{BC} were made

$$\alpha^i{}_{AC} = N_A N_C$$

$$\alpha^i{}_{BC} = N_B N_C$$

corresponding to random mixing. Usually less than ten iterations were necessary in order to obtain the α's with five significant figures. Having solved for α_{AC} and α_{BC}, the values for $\Delta \bar{G}^E{}_C/(1 - N_C)^2$ are calculated from eq 32.

In Figure 2, calculated values for $\Delta \bar{G}^E/(1 - N_C)^2$, $x = 0.5$, are compared with experimental data for Cd–Bi–Pb and Cd–Sn–Pb.[3] The agreement is good, particularly for the latter system. Note that in both systems the average value of $\Delta \bar{G}^E{}_C/(1 - N_C)^2$ is equal to $-G^E(AB)$, 300 and -350 cal, respectively. The large immiscibility range in Al–Bi–Pb excludes a comparison. However, although it is not shown here, the quasi-chemical approximation predicts qualitatively the existence of immiscibility in this system.

IV. Conclusion

From the quasi-chemical theory, based on nearest-neighbor interactions, a simple expression has been derived for $\bar{G}^E{}_C(AB)$, the excess partial free energy of a third component, C, in dilute solution in a binary mixture, AB. The theory suggests that the deviation from linearity of $\bar{G}^E{}_C(AB)$ as a function of x (mole fraction of B in dilute solutions of C) is determined by two factors. 1. The pair interactions of A–B lead to a contribution equal in magnitude to $\bar{G}^E(AB)$, but with opposite sign. 2. The difference between the pair interaction of A–C and B–C results in a negative contribution to $\bar{G}^E{}_C(AB)$ and consequently leads to an increase in a negative deviation from linearity of
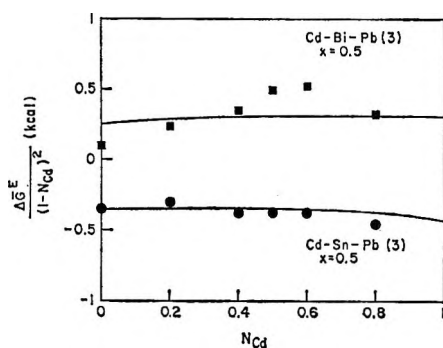

Figure 2. Calculated and experimental values[3] for $\Delta \bar{G}_C{}^E/(1 - N_C)^2$, defined by eq 32 in the text, as a function of N_C at constant $x = N_B/(N_A + N_B)$: ■, experimental (Cd–Bi–Pb); ●, experimental (Cd–Sn–Pb); —, calculated. The average value of $\Delta \bar{G}_C{}^E/(1 - N_C)^2$ has to be equal to $-G^E(AB) \cdot (G^E(Bi-Pb) = -300$ cal and $G^E(Sn-Pb) = 350$ cal).

$\bar{G}^E{}_C(AB)$ as a function of x (or a decrease in a positive contribution).

These features are demonstrated in the systems Cd–Sn–Pb, Cd–Bi–Pb,[3] and Al–Bi–Pb,[4] Cd or Al being the C component. By using a numerical method, values for $\bar{G}^E{}_C$ have also been calculated within the ternary system. In this case, no simple analytical expression is given.

In order to really test the significance of the present treatment, ternary systems exhibiting considerably larger deviations from ideality, for example molten salt systems, should be examined. Expressions derived here are also valid for ternary ionic salt systems with a common anion (or cation). The theory is then based on next nearest neighbor interactions between the cations (or the anions). This is explored in another article.[9]

A more general discussion of the limitations of the quasi-chemical approximation to mixtures is given by Oriani and Alcock[11] and by Darken.[12] It should, however, be added that the quasi-chemical approximation in its usual form assumes the atoms (or ions) to be distributed over the same kind of sites. Thus for example, it cannot be applied to mixtures of oxygen (or sulfur) and metals (mixtures of anions and cations) without considering at least two different kinds of sites.

Appendix A

Equations 17a and 17b can be expressed in the form

$$\left[1 - e^{-\frac{\Delta\epsilon_{AC}}{kT}}\right]\alpha_{AC}\frac{\alpha_{AC}}{N_C} -$$

$$[(1 - x)(1 - N_C) + N_C - \alpha_{BC} - \alpha_{AB}]\frac{\alpha_{AC}}{N_C} +$$

$$[(1 - x)(1 - N_C) - \alpha_{AB}]\left[1 - \frac{\alpha_{BC}}{N_C}\right] = 0 \quad (A1)$$

and

$$\left[1 - e^{-\frac{\Delta\epsilon_{BC}}{kT}}\right]\alpha_{BC}\frac{\alpha_{BC}}{N_C} -$$

$$[x(1 - N_C) + N_C - \alpha_{AC} - \alpha_{AB}]\frac{\alpha_{BC}}{N_C} +$$

$$[x(1 - N_C) - \alpha_{AB}]\left[1 - \frac{\alpha_{AC}}{N_C}\right] = 0 \quad (A2)$$

For $N_C \to 0$, $\alpha_{AC} = \alpha_{BC} = 0$ and eq A1 (or A2) yields

$$\left(\frac{\alpha_{AC}}{N_C}\right)_{N_C=0} + \left(\frac{\alpha_{BC}}{N_C}\right)_{N_C=0} = 1 \quad (A3)$$

(10) D. D. McCracken, "A Guide to FORTRAN IV Programming," John Wiley and Sons, Inc., New York, N. Y., 1965, p 74.

(11) R. A. Oriani and C. B. Alcock, *Trans. Met. Soc. AIME*, **224**, 1104 (1962).

(12) L. S. Darken, *ibid.*, **239**, 80, 90 (1967).

Thus

$$\lim_{N_C \to 0} \frac{1 - \dfrac{\alpha_{AC} + \alpha_{BC}}{N_C}}{N_C} = -\frac{\partial}{\partial N_C}\left(\frac{\alpha_{AC} + \alpha_{BC}}{N_C}\right)_{N_C=0}$$

$$(x = \text{constant}) \quad (A4)$$

From a partial derivative of eq A1 with respect to $\partial/\partial N_C$, taking the limit $N_C \to 0$ and making use of the relation

$$\lim_{N_C \to 0}\left(\frac{\alpha_{AC}}{N_C}\right) = \left(\frac{\partial \alpha_{AC}}{\partial N_C}\right)_{N_C=0}$$

one obtains

$$\frac{\partial}{\partial N_C}\left(\frac{\alpha_{AC} + \alpha_{BC}}{N_C}\right)_{N_C=0} =$$

$$-\frac{1}{1 - x - \alpha^\circ_{AB}}\left[\left(\frac{\alpha_{AC}}{N_C}\right)_{N_C=0}\right]^2 e^{-\frac{\Delta\epsilon_{AC}}{kT}} \quad (A5)$$

where α°_{AB} and α_{AB} in the binary AB. A similar expression is obtained from eq A2

$$\frac{\partial}{\partial N_C}\left(\frac{\alpha_{AC} + \alpha_{BC}}{N_C}\right)_{N_C=0} =$$

$$-\frac{1}{x - \alpha^\circ_{AB}}\left[\left(\frac{\alpha_{BC}}{N_C}\right)_{N_C=0}\right]^2 e^{-\frac{\Delta\epsilon_{BC}}{kT}} \quad (A6)$$

These two expressions have to be equal and thus

$$\frac{1}{1 - x - \alpha^\circ_{AB}}\left[\left(\frac{\alpha_{AC}}{N_C}\right)_{N_C=0}\right]^2 e^{-\frac{\Delta\epsilon_{AC}}{kT}} =$$

$$\frac{1}{x - \alpha^\circ_{AB}}\left[\left(\frac{\alpha_{BC}}{N_C}\right)_{N_C=0}\right]^2 e^{-\frac{\Delta\epsilon_{BC}}{kT}} \quad (A7)$$

From eq A3 and A7, one can solve for $(\alpha_{AC}/N_C)_{N_C=0}$

$$\left(\frac{\alpha_{AC}}{N_C}\right)_{N_C=0} =$$

$$\frac{\sqrt{1 - x - \alpha^\circ_{AB}}\, e^{\frac{\Delta\epsilon_{AC}}{2kT}}}{\sqrt{1 - x - \alpha^\circ_{AB}}\, e^{\frac{\Delta\epsilon_{AC}}{2kT}} + \sqrt{x - \alpha^\circ_{AB}}\, e^{\frac{\Delta\epsilon_{BC}}{2kT}}} \quad (A8)$$

The solution for $\{\partial/\partial N_C[(\alpha_{AC} + \alpha_{BC})/N_C]\}_{N_C=0}$ is then calculated from eq A5 (or A6) and the result for $\bar{G}^E_C(AB)$ is given in eq 22.

Appendix B

The expression for $\bar{G}^E_C(AB)$ in eq 22 can be rearranged by writing

$$\ln[R] = (1 - x)\ln[R] + x\ln[R] \quad (B1)$$

where

$$\ln[R] = \ln\left[\sqrt{1 - x - \alpha^\circ_{AB}}\, e^{\frac{\Delta\epsilon_{AC}}{2kT}} + \sqrt{x - \alpha^\circ_{AB}}\, e^{\frac{\Delta\epsilon_{BC}}{2kT}}\right] \quad (B2)$$

Equation B2 can be written as

$$\ln[R] = \ln e^{\frac{\Delta\epsilon_{AC}}{2kT}} + \ln\frac{\sqrt{1 - x - \alpha^\circ_{AB}}}{x} +$$

$$\ln\left(1 + x\left(\frac{1}{y}e^{-\Delta} - 1\right)\right) \quad (B3)$$

or as

$$\ln[R] = \ln e^{\frac{\Delta\epsilon_{BC}}{2kT}} + \ln\frac{\sqrt{x - \alpha^\circ_{AB}}}{x} +$$

$$\ln(1 - (1 - x)(ye^\Delta - 1)) \quad (B4)$$

where y and Δ are defined by eq 26 and 27, respectively. Introducing these two expressions for the first and second $\ln[R]$, respectively, on the right side in eq B1, one obtains

$$\bar{G}^E_C(AB) = -zRT(1 - x)\ln e^{\frac{\Delta\epsilon_{AC}}{2kT}} - zRTx\ln e^{\frac{\Delta\epsilon_{BC}}{2kT}} -$$

$$zRT\left[(1 - x)\ln\frac{\sqrt{1 - x - \alpha^\circ_{AB}}}{1 - x} +$$

$$x\ln\frac{\sqrt{x - \alpha^\circ_{AB}}}{x}\right] - zRTx(1 - x) \times$$

$$\left[\frac{1}{1 - x}\ln(1 + (1 - x)(ye^\Delta - 1)) +$$

$$\frac{1}{x}\ln\left(1 + x\left(\frac{1}{y}e^{-\Delta} - 1\right)\right)\right] \quad (B5)$$

The first three terms in the expression for $\bar{G}^E_C(AB)$ have a simple thermodynamic interpretation

$$\lim_{N_C \to 0} \bar{G}^E_C(AC) = \bar{G}^E_C(A) = -zRT\ln e^{\frac{\Delta\epsilon_{AC}}{2kT}} \quad (x = 0)$$

$$(B6)$$

and

$$\lim_{N_C \to 0} \bar{G}^E_C(BC) = \bar{G}^E_C(B) = -zRT\ln e^{\frac{\Delta\epsilon_{BC}}{2kT}} \quad (x = 1)$$

$$(B7)$$

The third term is the molar excess free energy of the binary solvent system A–B

$$G^E_{QC}(AB) = zRT \times$$

$$\left[(1 - x)\ln\frac{\sqrt{1 - x - \alpha^\circ_{AB}}}{1 - x} + x\ln\frac{\sqrt{x - \alpha^\circ_{AB}}}{x}\right]$$

$$(B8)$$

calculated from the quasi-chemical theory. From eq B5-B8, the expression

$$\bar{G}^E{}_{QC}(AB) = (1 - x)\bar{G}^E{}_C(A) +$$
$$x\bar{G}^E{}_C(B) - G^E{}_{QC}(AB) + f(x) \quad (B9)$$

is obtained, where $f(x)$ represents the last term in eq B5 and is discussed in more detail in the text.

Electrolytic Oxidation of 9,10-Diphenylanthracene and

Properties of Its Free Radical Cation and Anion

by R. E. Sioda[1]

Department of Chemistry, University of Kansas, Lawrence, Kansas 66044 *(Received August 4, 1967)*

The visible spectra of the free radical cation and anion of 9,10-diphenylanthracene (DPA) in acetonitrile solution were measured. The free radical cation (DPA$^+$) is stable (half-life $\sim$ 50 min) in the presence of air under anhydrous conditions. It reacts with water to form *trans*-9,10-dihydroxy-9,10-dihydro-9,10-diphenyl-anthracene: $2DPA^+ + 2H_2O \rightarrow 2H^+ + DPA + DPA(OH)_2$. The reaction is of the first order with respect to DPA$^+$ and water. The free radical cation undergoes electron transfer with iodide and bromide ions: $2DPA^+ + 2X^- \rightarrow 2DPA + X_2$. Reactions of DPA$^+$ with other reagents, such as methanol, phenol, Cl$^-$, CH$_3$COOK, KCNS, etc., were investigated spectrophotometrically. Chemiluminescence is produced in the reactions of DPA$^+$ with potassium acetate and sodium methoxide.

Introduction

Many data have been published on the electrolytic oxidation of aromatic compounds.[2-5] Aside from hypothetical assumptions, little was known about the initial oxidation mechanism. Lund assumed that two electrons are removed in the initial oxidation stage of aromatic hydrocarbons.[2b] Hoijtink, by analogy with chemical oxidations, postulated a one-electron electrolytic oxidation.[3] The latter prediction was confirmed experimentally in the case of certain compounds, such as *p*-phenylenediamine,[6,7] derivatives of phenothiazine,[8,9] 9,10-dimethylanthracene, and others.[10] The initial formation of a free radical cation was also postulated by Friend and Ohnesorge[11] for the process of the oxidation of anthracene in acetonitrile in the presence of ethanol.

Recently, Visco and Chandross,[12] and Peover and White[10b] described stepwise cyclic voltammetric oxidation of 9,10-diphenylanthracene (DPA). In acetonitrile, DPA undergoes two one-electron oxidations. The first one-electron process corresponds to the formation of a free radical cation, DPA $-$ e $\rightarrow$ DPA$^+$, and the second one corresponds to a free radical cation oxidation, DPA$^+$ $-$ e $\rightarrow$ DPA^{2+}. The free radical cation was stable for at least 10 sec.[12] The esr spectrum of the free radical cation was determined.[13,14]

The formation of the free radical cation of DPA was also found during electrolytic oxidation of DPA in nitrobenzene[15,16] and methylene chloride[17] solutions. Nitrobenzene proved to be a good solvent for con-

(1) Address correspondence to the author at Instytut Chemii Fizycznej PAN, Warszawa, ul. Kasprzaka 44, Poland.

(2) (a) M. J. Allen, "Organic Electrode Processes," Chapman and Hall Ltd., London, 1958; (b) H. Lund, *Acta Chem. Scand.*, 11, 1323 (1957).

(3) G. J. Hoijtink, *Rec. Trav. Chim.*, 77, 555 (1958).

(4) E. S. Pysch and N. C. Yang, *J. Amer. Chem. Soc.*, 85, 2124 (1963).

(5) S. Wawzonek, *Science*, 155, 39 (1967).

(6) M. T. Melchior and A. H. Maki, *J. Chem. Phys.*, 34, 471 (1961).

(7) L. H. Piette, P. Ludwig, and R. N. Adams, *Anal. Chem.*, 34, 916 (1962).

(8) J.-P. Billon, G. Cauguis, J. Combrisson, and A.-M. Li, *Bull. Soc. Chim. Fr.*, 2062 (1960).

(9) J.-P. Billon, G. Cauguis, and J. Combrisson, *J. Chim. Phys.*, 61, 374 (1964).

(10) (a) T. A. Gough and M. E. Peover, "Proceedings of the Third International Polarography Congress, Southampton, 1964," The Macmillan Co., Ltd., London, 1965, p 1017; (b) M. E. Peover and B. S. White, *J. Electroanal. Chem.*, 13, 93 (1967).

(11) K. E. Friend and W. E. Ohnesorge, *J. Org. Chem.*, 28, 2435 (1963).

(12) R. E. Visco and E. A. Chandross, *J. Amer. Chem. Soc.*, 86, 5350 (1964).

(13) L. O. Wheeler, K. S. V. Santhanam, and A. J. Bard, *J. Phys. Chem.*, 70, 404 (1966).

(14) R. E. Sioda and W. S. Koski, *J. Amer. Chem. Soc.*, 87, 5573 (1965).

ducting electrolytic oxidations. Several other aromatic hydrocarbons dissolved in this solvent were investigated to determine their ability to form free radical cations.[15,16] The free radical cations of aromatic hydrocarbons play decisive roles in the phenomenon of electroluminescence.[12,18,19]

The purpose of the present investigation is to determine the stability of the free radical cation of DPA in acetonitrile and to determine its reactivity toward different reagents.

Experimental Section

The preparations of solutions of the free radical ions of 9,10-diphenylanthracene and of its two-electron-oxidation product were carried out in a new electrolytic cell utilizing a flowing solution. The cell was described earlier.[20] The working electrode consisted of an 80-mesh platinum grid. The flow velocities ranged from 1 to 2 ml/min. A usual starting concentration of DPA was $1.3 \times 10^{-3}\ M$. The employed supporting electrolyte was $0.1\ M$ tetraethylammonium perchlorate (TEAP) in acetonitrile (ACN). The solutions were not deaerated prior to electrolysis, except in the case of production of the free radical anion of DPA, when dry nitrogen was bubbled through the solution. The experiments were carried out at room temperature (22°).

Cyclic voltammetric curves were recorded using the potentiostat and the triangular-wave generator described earlier.[21] A Beckman platinum button model (No. 39273) was used as the working electrode.

Optical spectra were recorded with a Cary Model 1115 spectrophotometer. The spectrum of the solution of DPA⁻ reactive toward oxygen was measured in a special optical cell. A usual optical quartz cell (1-cm² cross-sectional area) was covered with a Plexiglass lid sealed with wax. Three glass tubes were put through the lid to introduce the solution and to remove air by passing nitrogen through the solution. Small metal clips attached to Tygon tubes served to cut off the flow of nitrogen and of the solution. The cell was then disconnected from the supply of nitrogen and the solution and was put into the spectrophotometer.

The Reaction of DPA⁺ with Water. A $1.3 \times 10^{-3}\ M$ solution of DPA in a solution of $0.1\ N$ TEAP in acetonitrile was electrooxidized at the potentials of the limiting current of the first wave (~1.3 V *vs.* sce; see Figure 1D). The effluent from the cell was deep blue. About 50 ml of the effluent containing DPA⁺ was added to 1 ml of water. The DPA⁺ decomposed rapidly and the solution became colorless. The solvent was evaporated under vacuum and the TEAP in the residue was removed with water. The matter insoluble in water was dried in air. Its weight was about 80% of the content of DPA in the 50 ml of the solution before electrolysis. This substance was dissolved in 3 ml of benzene and was introduced into a
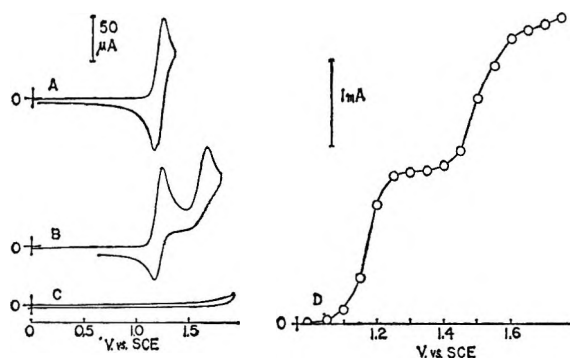

Figure 1. (A) Cyclic voltammetric curves of oxidation on a Beckman platinum electrode of $1.3 \times 10^{-3}\ M$ DPA in a supporting electrolyte of $0.1\ N$ TEAP in ACN; (B) cyclic voltammetric curves of oxidation on a Beckman platinum electrode of $1.3 \times 10^{-3}\ M$ DPA in a supporting electrode of $0.1\ N$ TEAP in ACN; (C) the curve for the supporting electrolyte (voltage scan rate = 10 V/min); (D) voltammetric curve of oxidation of $1.5\ 10^{-3}\ M$ DPA on the platinum-grid electrode in the flow apparatus (supporting electrolyte as above; flow velocity 0.0136 ml/sec).

neutral alumina (Voelm) chromatographic column. The DPA in the sample was easily removed from the column by benzene. Bright fluorescence in uv light served as a DPA indicator. The column was then eluted with methanol. Methanol was evaporated from the effluent and the yellowish residue was crystallized twice from toluene. White crystals and some oily residue were obtained. The melting point of the crystals was 263°. The melting point of *trans*-9,10-dihydro-9,10-diphenylanthracene (diol)
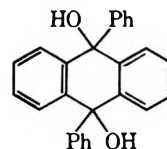
is 263°.[22] The results of the elemental analysis of the product, calculated for the diol, are given. *Anal.* Calcd for $C_{26}H_{20}O_2$: C, 85.7; H, 5.5. Found: C, 85.3; H, 5.9 ± 0.4.

The Reaction of DPA²⁺ with Water. A $1.3 \times 10^{-3}\ M$ solution of DPA in acetonitrile was oxidized at the potentials of the diffusion current of the second wave (~1.7 V *vs.* sce). According to the magnitude of the

(15) P. A. Malachesky, L. S. Marcoux, and R. N. Adams, *J. Phys. Chem.*, **70**, 2064 (1966).

(16) L. S. Marcoux, I. M. Fritsch, and R. N. Adams, *J. Amer. Chem. Soc.*, **89**, 5766 (1967).

(17) J. Phelps, K. S. V. Santhanam, and A. J. Bard, *ibid.*, **89**, 1752 (1967).

(18) D. M. Hercules, *Science*, **145**, 808 (1964).

(19) D. M. Hercules, R. C. Lansbury, and D. K. Roe, *J. Amer. Chem. Soc.*, **88**, 4578 (1966).

(20) R. E. Sioda, *Electrochem. Acta*, **13**, 375 (1968).

(21) J. R. Alden, J. Q. Chambers, and R. N. Adams, *J. Electroanal. Chem.*, **5**, 152 (1963).

(22) Ch. Pinazzi, *Ann. Chim.* (Paris), **7**, 397 (1962).
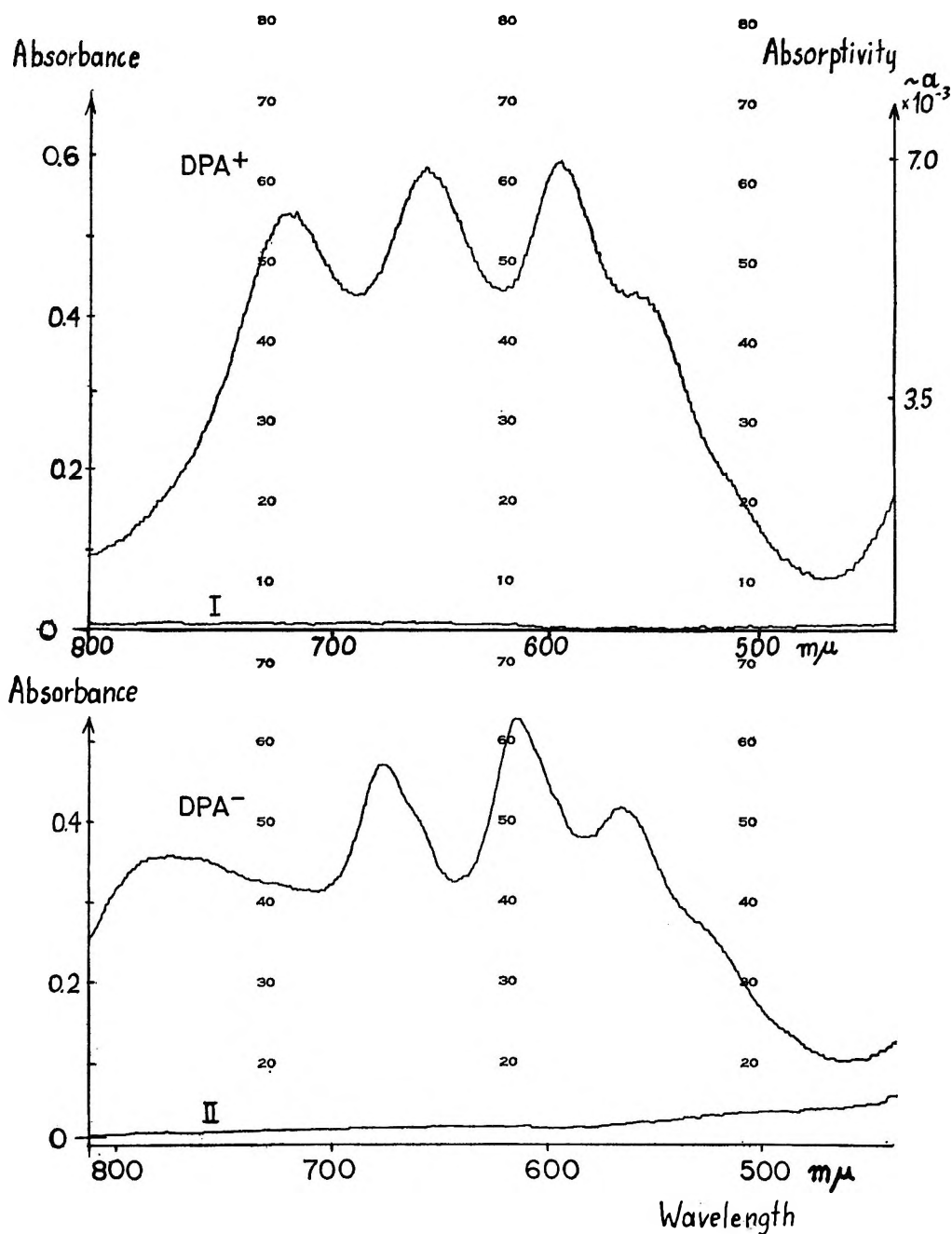
Figure 2. The visible spectra of the free radical ions of DPA in the basic solution in ACN. Curves I and II represent the spectra of the respective solutions after decomposition of the radical ions. Cell length =: 1 cm. The concentration of DPA$^+$ was determined from the passage of oxidation current.

electrolytic current, approximately 90% of the DPA in the starting solution underwent two-electron oxidation. About 50 ml of the solution after electrolysis was added to 1 ml of water. The solvent was evaporated under vacuum and the residue was fractionated in the manner described above. The isolated crystalline colorless product had a melting point of 261–263°. No melting point depression was obtained with the product from reaction of DPA$^+$ with water.

In another procedure the solution, after two-electron oxidation of DPA, was left to evaporate in contact with air. No water was added. The isolated product

had a melting point of 261–263° and was indistinguishable from the product of the first procedure.

Chemicals. The 9,10-diphenylanthracene was used as purchased from K & K Laboratories, Inc. Acetonitrile, a Matheson Coleman and Bell product, was distilled at normal pressure from P_2O_5. It contained less than 0.03% water. The tetraethylammonium perchlorate was purified by several crystallizations from water.[23]
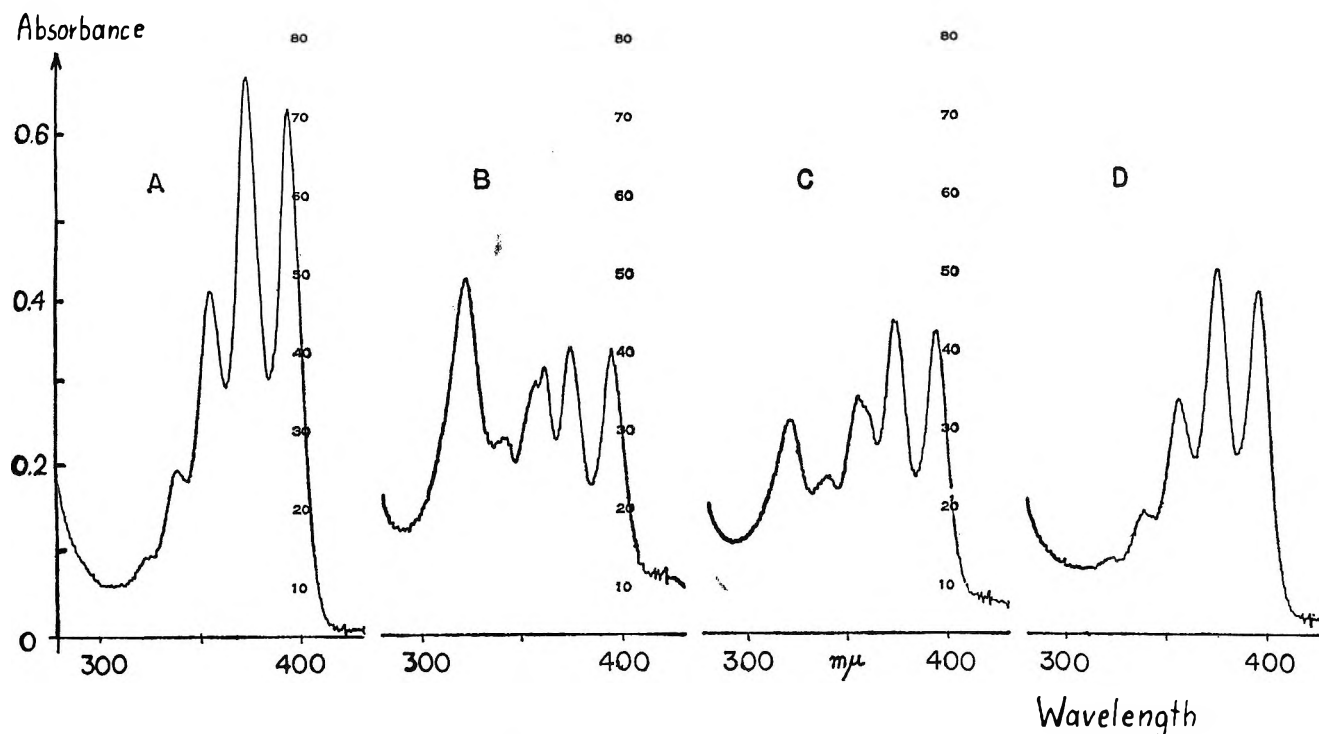
Figure 3. (A) The uv spectrum of starting solution of 1.3×10^{-3} M DPA, diluted 2.5 times with ACN, in the supporting electrolyte of 0.1 N TEAP in ACN; (B) spectrum of the starting solution diluted 2.5 times with ACN, shortly after being oxidized at the potentials of the first wave of DPA; the current passed was approximately 0.75 electron/molecule of DPA; visible new peaks of DPA[+] at 361 and 322 mμ; (C) spectrum of this solution after further decomposition of DPA[+] under influence of water; (D) spectrum of the solution after full decomposition of DPA[+] with water (the over-all loss of absorption of DPA in the process corresponds to one-half of the generated concentration of DPA[+]; the length of the cell = 0.1 cm).

Results

Voltammetric curves of oxidation of 9,10-diphenyl-anthracene in acetonitrile are presented in Figure 1. The oxidations were carried out in the cell with a flowing solution and on a platinum button in a stationary solution. The magnitudes of the limiting currents of the oxidation waves obtained in the cell with the moving solution depended upon the flow velocity according to the relation $I_1 \sim V^{0.97}$.[20]

The waves and peaks in Figure 1 correspond to one-electron oxidations. The first stage of oxidation at $E_{1/2} = 1.18$ V is reversible and leads to the formation of a stable free radical cation: DPA $-$ e $\rightarrow$ DPA[+]. The second oxidation stage at $E_{1/2} = 1.5$ V is irreversible.[10b,12-15] The probable initial oxidation product is the doubly charged cation: DPA[+] $-$ e $\rightarrow$ DPA[2+].[10b,12]

The visible spectrum of the solution of DPA[+] obtained by electrolysis at the potentials of the limiting current of the first oxidation wave is presented in Figure 2. The radical cation also shows absorption in the uv region, with peaks at 361 and 322 mμ (Figure 3 B and C). Under anhydrous conditions, in the presence of air the DPA[+] is quite stable in the acetonitrile solution (half-life $\sim$50 min). Its concentration immediately after electrolysis reaches about 85% of the initial concentration of DPA. This value was

calculated from the magnitude of the electrolytic current and was also determined chemically (the reaction of DPA[+] with I[-]).

When electrolysis is carried out at the potential of the limiting current of the second wave (1.7 V vs. sce), the electrolyzed solution is yellow-orange. Its absorption spectrum contains a peak at 440 mμ (Figure 4). The color disappears instantly after the addition of a small amount of water to the solution.

Figure 2 represents the visible spectrum of the blue solution of the free radical anion of DPA. The anion is formed during the one-electron reduction of DPA: DPA $+$ e $\rightarrow$ DPA[-], at a potential of $\sim$$-1.8$ V vs. sce.[12,24] The electrolysis was carried out in the cell with a flowing solution. The anion is stable for at least 5 min under anhydrous conditions and in the absence of air.

Spectrophotometry was employed in a study of the decomposition of DPA[+] in the presence of various reagents. The DPA shows an absorption band between 310 and 410 mμ (Figure 3A), characteristic for the anthracene nucleus.[25] Positions 9 and 10 in

(24) K. S. V. Santhanam and A. J. Bard, J. Amer. Chem. Soc., 87, 139 (1965); 88, 2669 (1966).

(25) H. H. Jaffé and M. Orchin, "Theory and Applications of UV Spectroscopy," John Wiley and Sons, Inc., New York, N. Y., 1962, pp 316-321.
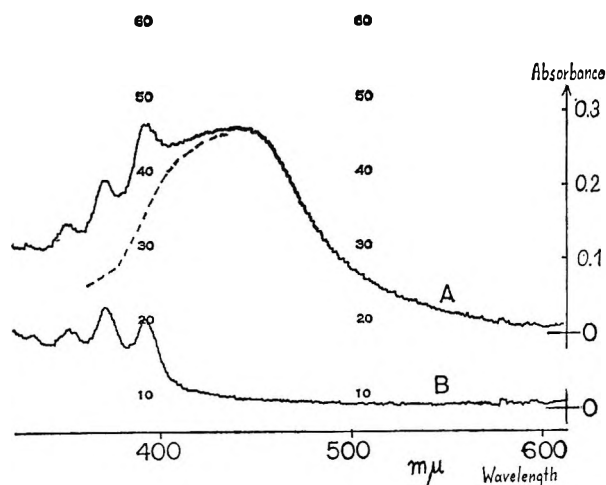
Figure 4. (A) The spectrum of the solution after oxidation of 1.3×10^{-3} M DPA at the potential of the limiting current of the second oxidation wave, $\sim$1.7 V vs. sce (charge consumed, approximately 1.8 electrons/molecule); (B) the same solution after adding water, 0.5% (the cell length = 0.1 cm).

DPA are the most reactive toward addition reactions.[26-28] The 9,10 addition causes a disappearance of the characteristic anthracene ring absorption band; this makes possible spectrophotometric determination of the addition process.

The reaction of DPA$^+$ with water was most thoroughly investigated. Figure 3 presents the uv spectra of a solution of DPA$^+$ in different stages of decomposition in the presence of water. The characteristic bands of the radical cation at 322 and 361 mμ disappear and in their place bands of DPA are restored. The amount of DPA restored is equal to one-half of the original concentration of generated DPA$^+$. The solution after completion of the decomposition reaction contains protons in an amount approximately equal to the quantity of generated DPA$^+$. The proton concentration was roughly obtained by pH determination of the solution, diluted four times with water, after the reaction. The most probable equation for the reaction is 2DPA$^+$ + 2 H$_2$O $\rightarrow$ DPA + DPA(OH)$_2$ + 2H$^+$. The attachment of OH groups takes place at the 9 and 10 positions, causing the disappearance of the characteristic uv band of DPA.

trans - 9,10 - Dihydroxy - 9,10 - dihydro - 9,10 - diphenylanthracene was isolated as a crystalline product of the reaction of DPA$^+$ with water (see the Experimental Section).

We investigated the kinetics of the reaction of DPA$^+$ with water. The decomposition of DPA$^+$ was followed spectrophotometrically at an arbitrary wavelength λ 625 mμ. The reaction was first order both in respect to DPA$^+$ and in respect to water (Figures 5 and 6). Figure 5 represents the semilogarithmic plot of the time change of the optical absorption of DPA$^+$ in a solution containing a 2.6 M concentration of water.

Figure 5. The semilogarithmic plot of decomposition vs. time of DPA$^+$ in the presence of a 2.6 M concentration of water. The vertical axis corresponds to decimal logarithm of optical absorption of DPA$^+$ at 625 mμ. Length of the cell = 1 cm.

Figure 6. Dependence of the pseudo-first-order kinetic rate constant (k_1) of the decomposition of DPA$^+$ on the molar concentration of water in the solution.

The plot is linear and is characteristic for a first-order process described by the equation $\log c/c_0 = -k_1 t$, where c and c_0 are the momentary and initial concentrations, k_1 is the kinetic constant, and t is the time. Figure 6 represents the dependence of the pseudo-first-order rate constant of the DPA$^+$ decomposition on the water concentration. Except for small water concentrations, the dependence is linear. The over-all kinetic equation of the reaction of DPA$^+$ with water is $v = -d[\text{DPA}^+]/dt = (0.083 [\text{H}_2\text{O}] - 0.056)[\text{DPA}^+]$.

Even when no water was added to a solution of DPA$^+$, a decomposition of the radical cation took place. The plot of the change of concentration of DPA$^+$ with time was first order. The half-life of the radical was about 50 min. One-half of the original concentration of DPA$^+$ was transformed into DPA. It is probable that the decomposition was caused by small (less than 0.03%) impurities of water in acetonitrile.

(26) Ch. K. Ingold and Ph. G. Marshall, J. Chem. Soc., 3080 (1926).
(27) Ch. Dufraisse and A. Etienne, Compt. Rend., 201, 280 (1935).
(28) A. L. J. Bechwith, R. O. C. Norman, and W. A. Waters, J. Chem. Soc., 171 (1958)

The reaction of DPA$^+$ with the iodide anion from potassium iodide can be used for analytic determination of the concentration of DPA$^+$ in solution. In this reaction iodine is liberated instantaneously according to the equation 2DPA$^+$ + 2I$^-$ → 2DPA + I$_2$. The iodine is titrated with water solution of sodium thiosulfate. The bromide ion reacts similarly: 2DPA$^+$ + 2Br$^-$ → 2DPA + Br$_2$. The chloride anion behaves in a different way. Most probably, addition of chloride takes place in the 9,10 positions of the DPA structure, according to the equation 2DPA$^+$ + 2Cl$^-$ → DPA + DPACl$_2$. A loss of the characteristic anthracene ring optical absorption of DPA was observed in the solution after the reaction. The loss corresponded to one-half of the concentration of DPA$^+$ before the reaction. The reactions of DPA$^+$ with both Br$^-$ and Cl$^-$ (from tetraethylammonium salts) were fast. No kinetic data can be given at the moment.

The reaction of H$_2$S, KCNS, and p-hydroquinone with DPA$^+$ was similar to that of the iodide anion with DPA$^+$. All characteristic anthracene ring absorptio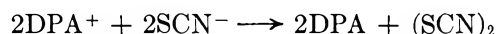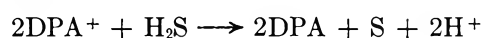n was restored after decomposition of DPA$^+$. The decomposition was fast. The probable reactions of the transformation of DPA$^+$ into DPA are

$$2DPA^+ + H_2S \longrightarrow 2DPA + S + 2H^+$$

$$2DPA^+ + 2SCN^- \longrightarrow 2DPA + (SCN)_2$$

and

$$DPA^+ + p\text{-HOC}_6H_4OH \longrightarrow$$
$$DPA + p\text{-HOC}_6H_4O \cdot + H^+$$
$$DPA^+ + p\text{-HOC}_6H_4O \cdot \longrightarrow$$
$$DPA + p\text{-OC}_6H_4O + H^+$$

In the reaction of DPA$^+$ with p-hydroquinone, the end product is probably quinone, and the transition product is the semiquinone radical.

Reactions of DPA$^+$ with several other reagents were carried out. DPA$^+$ in solution reacted readily with methanol, ethanol, cyclohexanol, phenol, ethylamine, t-butylamine, and n-butylamine, ammonia, potassium acetate, and dimethylformamide. Only one-half of the original concentration of DPA$^+$ restored the characteristic uv spectrum of DPA after the decomposition, as in the reaction with water.

Possibly diethers of 9,10-dihydroxy-9,10-dihydro-9,10-diphenylanthracene were the products of the reaction of DPA$^+$ with the alcohols and phenol: 2DPA$^+$ + 2ROH → DPA + DPA(OR)$_2$ + 2H$^+$. Such ethers were prepared by Pinazzi.[22] t-Butyl alcohol did not react with DPA$^+$. As reported by Pinazzi, no diether was formed from the reaction between 9,10-dihydro-9,10-dichloro-9,10-diphenylanthracene and t-butyl alcohol, contrary to the behavior of primary and secondary alcohols.[22]

In the case of the reaction of DPA$^+$ with potassium acetate, possibly 9,10-diacetoxy-9,10-dihydro-9,10-diphenylanthracene[22] is formed: 2DPA$^+$ + 2R$^-$ → DPA + DPAR$_2$.

The reaction course of DPA$^+$ with dimethylformamide, the amines, and ammonia is unclear. In the case of the last two reagents, it may be that a bond is formed between the nitrogen of the amine or ammonia group and the 9,10 positions of the DPA$^+$ with exclusion of a proton.

Sodium methoxide and a 10% solution of tetraethylammonium hydroxide in water reacted with DPA$^+$ readily. The last reaction was instantaneous. Sodium methoxide, which is negligibly soluble in acetonitrile, reacted somewhat slower and after mixing.

The solutions after the decomposition of DPA$^+$ were slightly yellow. Approximately 60% of the initial concentration of DPA$^+$ restored the characteristic uv absorption of DPA after decomposition. In the case of 10% tetraethylammonium hydroxide in water, the initial reaction of DPA$^+$ was caused primarily by hydroxide ions. The water content of the reagent was too small to cause the instantaneous decomposition of DPA$^+$.

Acids like sulfuric acid, 70% perchloric acid, acetic acid (added in a concentration of 0.5-1%), and benzoic acid did not influence appreciably the speed of the decomposition of DPA$^+$. About 50% of the initial concentration of DPA$^+$ restored the characteristic anthracene ring absorption after the decomposition, as in the case of decomposition under the influence of water. The solution after two-electron irreversible oxidation of DPA was yellow-orange. From the solution $trans$-9,10-dihydroxy-9,10-dihydro-9,10-diphenylanthracene was isolated (see the Experimental Section). The solution after oxidation diluted with water contained protons in an amount approximately equal to the quantity of electrons passed into the solution during the oxidation process. The most probable initial oxidation product is the dipositive cation, DPA^{2+}. It reacts with the trace amounts of water in the solution to produce the $trans$-9,10-diol: DPA^{2+} + 2H$_2$O → DPA(OH)$_2$ + 2H$^+$.

The chemiluminescent behavior of DPA$^+$ solutions with several reagents was briefly studied. A formation of white-blue light was observed on mixing DPA$^+$ solutions with acetonitrile solutions of ethylamine, n-butylamine, t-butylamine, tetraethylammonium hydroxide, dimethylformamide, potassium acetate, and sodium methoxide.

Discussion

Molecular orbital theory developed by Hückel and others offers a quantum-mechanical explanation for the formation of free radical ions of aromatic compounds.[29]

(29) A. Streitwieser, Jr., "Molecular Orbital Theory for Organic Chemists," John Wiley and Sons, Inc., New York, N. Y., 1961.

Free radical cations are formed by removing an electron from the highest π-bonding level. Free radical anions are formed by adding an electron to the lowest π-antibonding orbital. In the case of alternant hydrocarbons, the bonding and antibonding orbitals are symmetrical. Consequently, one can expect a similarity of optical absorption spectra of free radical anions and cations of an alternant hydrocarbon.[30,31]

These theoretical predictions were supported by measurements of spectra of hydrocarbon ions by Hoijtink and coworkers.[32,33] A close similarity between the absorption spectra of the anthracene anion and the cation was noted. Both ions show their main visible absorption around 700 mμ.[33] The anthracene cation has two strong uv bands of absorption at 310 and 355 mμ, similar to that of the two DPA$^+$ bands at 322 and 361 mμ.

DPA belongs to the group of even alternant hydrocarbons. Its near-uv absorption spectrum resembles closely that of anthracene. The phenyl substituents at positions 9 and 10 are twisted out of the plane of the anthracene ring by at least 57°, owing to a steric overlap of the phenyl o-hydrogen atoms with the nearest hydrogens of the anthracene ring.[34] The lack of planarity inhibits conjugation in the molecule, and the phenyl substituents cause only small bathochromic shifts of the anthracene bands. Analogous to anthracene, the absorption band of DPA at 260 mμ can be classified as a $^1B_b \leftarrow {}^1A$ transition, and the group of bands of DPA between 310 and 410 mμ corresponds to different vibrational levels of the $^1L_a \leftarrow {}^1A$ transition.[25]

The visible absorption spectrum of DPA$^+$ (Figure 2) corresponds most probably to the $\psi_2 \leftarrow \psi_1$ transition, where ψ_2 and ψ_1 are the two highest bonding levels (Figure 7). The band is subdivided into four peaks, which are separated by an average vibrational frequency of 1370 cm^{-1}, similar to that of the ^1L_a bands of DPA (1350 cm^{-1}) and of anthracene (1430 cm^{-1}).[25]

The visible absorption spectrum of DPA$^-$ (Figure 2) exhibits four peaks and exhibits an inflection at 530 mμ. The average separation is 1500 cm^{-1} and corresponds most probably to the vibrational frequency. The band represents the $\psi_{-2} \leftarrow \psi_{-1}$ transition, where ψ_{-2} and ψ_{-1} are the lowest antibonding molecular orbitals (Figure 7).

We calculated the molecular orbital energies of DPA$^+$ and DPA$^-$, repeating the results of Bard and coworkers.[13] These authors determined the angles between anthracene and phenyl rings in DPA$^+$ and DPA$^-$ employing the esr data and molecular orbital calculations. The following angles (θ) were determined: 68° for DPA$^-$ and 61° for DPA$^+$. The resonance integrals (β) of the bonds between the anthracene and the phenyl rings in the ions were

Figure 7. The calculated middle molecular orbitals of DPA$^+$ (A) and DPA$^-$ (B). The electronic transitions corresponding to the visible absorption bands of the radical ions are shown. Orbitals ψ_2 and ψ_{-2} are sixfold degenerate.

calculated from the relation $\beta = \beta_0 \cos \theta$, where β_0 is a resonance integral of the bonds in the rings.

The calculated energy difference between the two highest bonding orbitals of DPA$^+$, ψ_1 and ψ_2, is $0.616\beta_0$. The corresponding energy difference for DPA$^-$ is $0.605\beta_0$. The longest wavelength absorption band of DPA$^+$ is at 13,850 cm^{-1}, and that of DPA$^-$ is at 12,900 cm^{-1}. By comparing these two values with the above-calculated orbital-energy differences, one obtains $\beta_0 = 21,900 \pm 600$ cm^{-1}. β_0 values, ranging from 16,000 to 24,000 cm^{-1}, were obtained from different sources.[29]

DPA has a structure resembling the triarylmethyl radicals.[26] The 9 and 10 carbons of DPA correspond to the radical centers. These positions are most susceptible to addition reactions.[26-28] The 9 and 10 positions are also reactive in DPA$^+$. The density of the positive charge in DPA$^+$ is the highest at the 9 and 10 carbons, according to molecular orbital calculations. The net positive charge is 0.179. It is probable that nucleophilic reagents attack primarily the 9 and 10 carbons of DPA$^+$. This view is supported by the spectrophotometric data on reactions of DPA$^+$ with different reagents leading to the disappearance of the uv band of DPA.

The following mechanism can be proposed for these reactions

(30) M. J. Dewar and H. C. Lonquet-Higgins, Proc. Phys. Soc., A67, 795 (1954).

(31) A. D. McLachlan, Mol. Phys., 4, 49 (1961).

(32) G. J. Hoijtink and W. P. Weijland, Rec. Trav. Chim., 76, 836 (1957).

(33) W. I. Aalbersberg, G. J. Hoijtink, E. L. Mackor, and W. P. Weijland, J. Chem. Soc., 3049, 3055 (1959).

(34) R. N. Jones, J. Amer. Chem. Soc., 67, 2127 (1945).

$$DPA^+ + R^- \longrightarrow C_6H_4 \underset{Ph}{\overset{Ph \quad R}{\diamondsuit}} C_6H_4$$

I

or $DPA^+ + RH \rightarrow I + H^+$. The neutral radical I is oxidized immediately by DPA^+ to form a carbonium ion

$$I + DPA^+ \xrightarrow{fast} C_6H_4 \underset{Ph}{\overset{Ph \quad R}{\diamondsuit^+}} C_6H_4 + DPA$$

II

The carbonium ion, II, reacts with another molecule of reagent RH or R^- to form a 9,10-disubstituted 9,10-dihydro-9,10-diphenylanthracene $(DPAR_2)$

$$II + R^- \longrightarrow DPAR_2$$

or

$$II + RH \longrightarrow DPAR_2 + H^+$$

The above mechanism is supported by the kinetic data of the reaction of DPA^+ with water and by the isolation of the product. The reaction is first order in respect to DPA^+ and water. In agreement with the kinetic data, the rate-determining step of the reaction is propably an attack of the DPA^+ radical ion by a dipole of water

$$DPA^+ + H_2O \longrightarrow \left[C_6H_4 \underset{Ph}{\overset{Ph \quad O \cdots H}{\diamondsuit^+}} C_6H_4 \right] \longrightarrow$$

$$C_6H_4 \underset{Ph}{\overset{Ph \quad OH}{\diamondsuit}} C_6H_4 + H^+$$

The radical DPAOH· then reacts fast with DPA^+ and water to form the diol

$$DPAOH· \underset{-DPA}{\overset{+DPA^+}{\rightleftarrows}} C_6H_4 \underset{Ph}{\overset{Ph \quad OH}{\diamondsuit^+}} C_6H_4 \xrightarrow{H_2O} C_6H_4 \underset{HO \quad Ph}{\overset{Ph \quad OH}{\diamondsuit}} C_6H_4 + H^+$$

Some of the reagents $(I^-, Br^-, CNS^-, H_2S,$ and hydroquinone) do not form adducts with DPA^+ but are oxidized instead; e.g., $DPA^+ + 2I^- \rightarrow 2DPA + I_2$.

Sodium methoxide and tetraethylammonium hydroxide (10% solution in water) seem to exhibit both types of reactivity. Approximately 60% of the initial concentration of DPA^+ restores the spectrum of

DPA in the presence of these reagents. This may indicate that besides the 9,10 addition some amount of DPA^+ (about 10%) undergoes an electron-transfer reaction with a transient formation of hydroxyl and methoxyl radicals: $DPA^+ + R^- \rightarrow DPA + R·$.

The primary oxidation product of DPA at the second wave is the cation DPA^{2+}. This cation is unstable, as is apparent from the irreversibility of the second oxidation peak of DPA (Figure 1B). Most probably it reacts with the water present as an impurity in acetonitrile or with acetonitrile itself. trans-9,10-Di-hydroxy-9,10-dihydro-9,10-diphenylanthracene was isolated as a product of the two-electron oxidation process: $DPA^{2+} + H_2O \rightarrow DPA(OH)_2 + 2H^+$.

The solution immediately after the two-electron oxidation, is yellow-orange and exhibits a band of absorption at 440 mμ (Figure 4). The color disappears immediately after the addition of a small amount of water (0.2%). The location of the absorption band is similar to those of the diphenylmethyl cation (440 mμ)[35] and of the cation obtained by protonation of anthracene in the 9 position (425 mμ).[35]

It seems possible that the yellow-orange coloration of the solution after two-electron oxidation of DPA is caused by carbonium ions similar in structure to the anthracene protonated at position 9. A carbonium ion can be produced, for example, in the reaction of the initially formed DPA^{2+} with one molecule of water

$$DPA^{2+} + H_2O \longrightarrow C_6H_4 \underset{Ph}{\overset{Ph \quad OH}{\diamondsuit^+}} C_6H_4 + H^+$$

The phenyl substituents at positions 9 and 10 are out of the plane of the rest of the molecule and do not influence significantly the location of the absorption band of the carbonium ion.

Using the extinction coefficent of the protonated anthracene (32,000),[35] we calculated the possible concentration of the carbonium ions from the optical absorption of the solution after two-electron oxidation of DPA. The concentration was $\sim 8 \times 10^{-5}$ M, i.e., 7% of the full concentration of DPA oxidized by the two-electron process $(1.15 \times 10^{-3} M)$.

When water is added to the solution, the color disappears as the carbonium ion is transformed into the 9,10-diol: $DPAOH^+ + H_2O \rightarrow DPA(OH)_2 + H^+$.

Several papers have described the chemiluminescent reactions of radical ions of DPA and other hydrocarbons.[12,18,19,36-38] The emitted light had char-

(35) V. Gold and F. L. Tye, J. Chem. Soc., 2172 (1952).

(36) E. A. Chandross and F. I. Sonntag, J. Amer. Chem. Soc., 86, 3179 (1964).

(37) E. A. Chandross, J. W. Longworth, and R. E. Visco, ibid., 87, 3259 (1965).

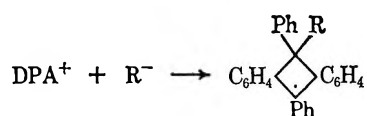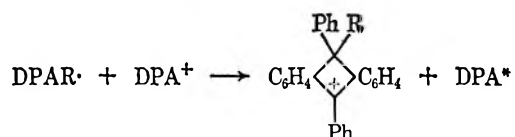(38) E. A. Chandross and F. I. Sonntag, ibid., 88, 1089 (1966).

acteristics similar to those of fluorescence of hydrocarbons.[12,18,19,28] The light is produced during the annihilation of positive and negative radical ions or during their reactions with different reagents. Hercules, et al.,[19] described chemiluminescence resulting from reactions of radical cations of rubrene, 9,10-diphenylanthracene, perylene, and 3,5,8,10-tetraphenylpyrene with amines, water, and dimethylformamide. The formation of excited states of hydrocarbons in these reactions was explained by an elaborate mechanism involving a production of neutral radicals by hydrogen abstraction from acetonitrile. Those radicals react with the hydrocarbon radical cations, leading to the formation of the excited states: $\cdot CH_2CN + R^+ \rightarrow R + CHCN^+$. It is possible that a similar mechanism is operative in the chemiluminescent reactions of DPA^+ with CH_3ONa and tetraethylammonium hydroxide. There is an indication that $OH\cdot$ and $CH_3O\cdot$ radicals are produced in these reactions and that they may abstract a hydrogen from the solvent or produce the hydrocarbon excited state in another way.

A possibility that other transient radicals participate in the formation of an excited state of the hydrocarbon should be taken into account. Radicals probably are formed as intermediates in the 9,10 addition reactions of DPA^+, e.g.

This radical may undergo a reaction with DPA^+, in which the excited state DPA^* is formed.

A somewhat similar mechanism was proposed for the chemiluminescent reactions of DPA^-.[38]

Radiolysis of Aqueous Chromium and Vanadium in Their +2 and +3 Oxidation States

by P. A. P. Lykourezos, A. Kanellopoulos, and D. Katakis

Nuclear Research Center "Democritos," Aghia Paraskevi, Attikis, Athens, Greece

In the radiolysis of aqueous Cr^{II}, the product Cr^{III} appears in the form of various complexes, depending on the oxidizing agent. In perchloric acid solutions, monomeric and dimeric Cr^{III} are the sole products, their yields increasing with increasing $HClO_4$ concentration. In H_2SO_4 the products are the Cr^{III} monomer and the sulfate complex. The chloro complex in the acid region studied is formed only if Cl^- is added to the initial Cr_{aq}^{2+} solution, the yield depending on the $(Cl^-):(Cr^{2+})$ ratio, the total $G(Cr^{III})$ remaining constant for a given $HClO_4$ concentration; all evidence points to the conclusion that this complex is formed only by paths catalyzed by chloride. The hydrolysis of the Cr^{III} dimer and the chloro complex is accelerated by radiation, but it does not compete with Cr^{2+} oxidation. In the radiolysis of V^{2+}, deaerated V^{3+}, and air-saturated V^{3+} solutions, the G values are 8.2, 0.9, and 15.5, respectively. The results with the $Cr^{II}-Cr^{III}$ system are discussed with a bias toward its characteristics that seem useful in studying unknown intermediates.

Introduction

In our attempt to find new systems which could give more information about the species formed in the radiolysis of aqueous solutions, we tried V^{II}, V^{III}, Cr^{II}, and Cr^{III}. These systems are expected to have many similarities with the corresponding iron pair, and indeed it turns out to be so. On the other hand, they also have some rather interesting differences which could be very useful. In particular, the $Cr^{II}-Cr^{III}$ system has the well-known property[1] that while Cr^{II} is

(1) See, for example, H. Taube, *Advan. Inorg. Chem. Radiochem.,* **1,** 1 (1959)

generally labile, Cr^{III} is substitution inert, and thus intermediates formed in the radiolysis are "trapped" in the form of readily detectable complexes without changing the physical environment, as in the case of freezing down the solutions. The Cr^{III} complexes give direct information about the composition of the activated complex and, therefore, the species from which they were formed. In the present work, we give a brief demonstration of the exploitation of this property in radiation chemistry. For methodological reasons, the demonstration is made with intermediates for which the formation and subsequent reactions are fairly well understood, but once the method has been tested and some of its details have been worked out, it can be applied to the much more interesting cases where the intermediates are unknown and must be identified, particularly those formed from more or less complex organic molecules.

Experimental Section

Dosimetry. The irradiations were done in Spectrosil cells with Co^{60} γ rays. The dose rate was determined with the Fricke dosimeter using $G(Fe^{3+}) = 15.5$ and ϵ_{305} 2174 at 24°.

Reagents and Solutions. The water was triply distilled. All reagents were of analytical grade and used without further purification.

The oxygen-sensitive chromous and vanadous solutions were prepared in an inert gas atomosphere or under vacuum. Air was also excluded in all subsequent manipulations of these solutions.

Chromous ion solutions were prepared by reduction of chromic ion with a zinc amalgam, by electrolytical methods, or by the dissolution of chromium metal of high purity in the appropriate acid.[2] In the reduction with zinc amalgam, the solutions were passed through sintered glass in order to filter out pieces of zinc. In the electrolysis, the cathode was a mercury pool and the anode was a platinum pool. The metal ion was in the cathode region, which was separated from the anode region by sintered glass. The current density during the electrolysis was 30–50 mA/cm². The method of preparation of Cr^{2+} does not have any effect on the results reported in this paper; the presence of zinc or mercury ions does not interfere.

Chromic perchlorate solutions were prepared from $K_2Cr_2O_7$ solutions of from CrO_3 suspensions in $HClO_4$ by reduction with H_2O_2 and destruction of the excess peroxide. Aqueous dimeric Cr^{III} was prepared by air oxidation of Cr_{aq}^{2+}.

Vanadous ion is formed by the electrolysis of a V_2O_5 suspension in the appropriate acid. The conditions of electrolysis were similar to those used for chromous ion. The storage of the V^{2+} solutions was made at low temperature to minimize the reaction with the acid.

V^{3+} was prepared by mixing equimolar amounts of

V^{2+} and VO^{2+}. The test for excess V^{2+} or VO^{2+} was made spectrophotometrically. VO^{2+} solutions were prepared by partial electrolytic reduction of V_2O_5.

Analytical Procedures. Chromous solutions were titrated with[3] Cu^{2+} or[4] Fe^{3+} using a Beckman expanded-scale pH meter. Alternatively, the chromous content was determined by oxidation with air and by spectrophotometric measurement of the chromic dimer formed, taking into account the small initial decrease in optical density illustrated in Figure 1. It is noted that after this initial period, the hydrolysis of the product of oxidation of Cr^{2+} by oxygen is extremely slow and in the time scale of Figure 1 is taken as constant. The correction is not affected by Cl^-.

The chromic yields were determined spectrophotometrically with Beckman DU and Cary 14 spectrophotometers at the peak, around 400 mμ. The extinction coefficients of the various chromic species at this wavelength region were obtained from the literature;[5,6] Cr^{2+} does not absorb in this region. The over-all yield was calculated using an average extinction coefficient of the various chromic species present, after chromatographic determination of their relative amounts. Alternatively, the analysis was made by titrating the remaining Cr^{2+} and by estimating the Cr^{III} formed by subtraction from the initial concentration of Cr^{2+}. The acid content was measured by titration with alkali using a pH meter.

The ion-exchange separation of the chromic species was done on DX50 purified as described in the literature.[7] In most of the samples, the original Cr^{2+} had been oxidized. The elution of the monomer, $Cr(H_2O)_6^{3+}$, was made with 1.5 M $HClO_4$, and the elution of the dimer was made with 0.2 M $La(ClO_4)_3$. Higher polymers were formed in negligible amounts, if at all. The chloro complex $(H_2O)_5CrCl^{2+}$ and the sulfato complex $(H_2O)_5CrOSO_3H^{2+}$ are eluted first with 0.4 M and 0.1 M $HClO_4$, respectively. The column was cooled with ice during the separation in order to minimize hydrolysis of the complexes. The eluted fractions were measured spectrophotometrically.

V^{3+} was measured spectrophotometrically at 400 mμ, where its extinction coefficient was taken as 8.1 and the extinction coefficient of V^{2+} was taken as 0.8. VO^{2+} was determined at 760 mμ using ϵ 17; the other vanadium species present do not absorb at this wavelength.

Results

Oxidation Yields of Cr^{2+}. In a solution containing 2×10^{-2} M Cr^{2+} and 0.145 M $HClO_4$, the G value of the

(2) J. M. Crabtree, *J. Chem. Soc.*, 46 (1946).

(3) J. J. Lingane and R. Pecsok, *Anal. Chem.*, 20, 425 (1949).

(4) J. J. Lingane, *ibid.*, 20, 797 (1949).

(5) J. A. Laswick and R. A. Plane, *J. Amer. Chem. Soc.*, 81, 3564 (1959).

(6) P. J. Elving and B. Zemel, *ibid.*, 79, 1281 (1957).

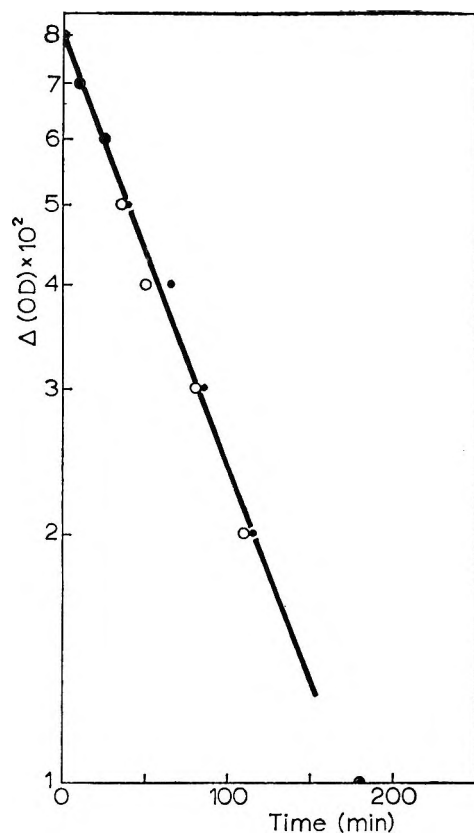(7) R. C. Thompson and G. Gordon, *Inorg. Chem.*, 5, 557 (1966).

Figure 1. Hydrolysis of the product of oxidation of Cr^{2+} by air at room temperature: ●, without 1.5 M Cl^-; ○, with 1.5 M Cl^-; initial Cr^{2-}, 33 mM; $HClO_4$, 0.5 M; $\Delta(OD) = (OD)_0 - (OD)_t$ at 415 mμ; 1-cm cell.

Table I: Effect of Chloride on the Yields of Cr^{III} Complexes

Concn of Cr^{II}, mM	Concn of $HClO_4$, M	Concn of NaCl, M	Monomer	Dimer	Chloro complex	Total G
43	0.64	...	9.3	0.55	...	9.85
33	0.55	0.049	7.8	0.35	1.55	9.7
44	0.56	0.405	6.6	...	2.8	9.4
55	0.96	...	10.35	0.65	...	11.0
40	0.96	0.054	10.1	0.5	0.6	11.2
55	1.9	...	12.5	1.4	...	13.9
42	1.9	0.254	9.1	0.6	4.2	13.9
29	1.9	2.18	5.1	0.7	8.6	14.4

chromic equivalents formed was found to be 8.3 ± 0.3. The irradiations were carried out with a dose rate of 3.1 × 10^{19} eV/l. min. The concentration $vs.$ dose curve was a straight line up to almost complete conversion. With 0.8 N H_2SO_4, instead of $HClO_4$, we obtained a G value of 8.4 ± 0.3.

Figure 2 gives the yields of dimer and total chromic species as a function of the $HClO_4$ concentration. The concentration $vs.$ dose curves were linear. The dose rate was ∼5 × $10^{2)}$ eV/l. min, corrected for the variation of electron density of the solutions. From 20 to 80 mM, no appreciable influence of the Cr^{2+} concentration on $G(Cr^{III})$ was observed. Decreasing the dose rate by a factor of ∼10 also had no effect. The chloro complex was not detected even at the highest perchloric acid concentrations used, namely 2.8 M. When chloride is added to the initial Cr^{2+} solution, considerable amounts of $(H_2O)_5CrCl^{2+}$ are formed on irradiation at a dose rate of ∼5 × 10^{20} eV/l. min. Figure 3 gives the percentage of the chloro complex over the total Cr^{III} equivalents as a function of the amount of the Cl^- added, at various $HClO_4$ concentrations. The chloro complex is formed at the expense of both the monomer and the dimer, as illustrated in Table I; the over-all yields do not seem to be affected.

After what appears to be complete oxidation of Cr^{II}

to Cr^{III}, the possibility of having small, steady-state amounts of Cr^{II} or Cr^{VI} still must be examined. All our attempts, however, to detect such concentrations failed; even when H_2-saturated instead of deaerated solutions are used, $G(Cr^{III})$ remains the same and steady-state Cr^{2+} is not found.

In the radiolysis of Cr^{2+} in 0.8 N H_2SO_4, the monomer and the sulfate complex are formed in approximately equal amounts.

Radiolysis of Cr^{III} Solutions. In order to interpret the results on the radiolysis of Cr_{aq}^{2+} some information must be obtained on the effect of γ rays on Cr^{III} solutions and on the thermal behavior of these solutions under the conditions of our experiments. Thus in a blank containing 50 mM Cr_{aq}^{3+}, 1 M $HClO_4$, and 2 M Cl^-, compared with the radiolysis experiments, no change in optical density was detected over a long period. Thermal formation of the dimer from $Cr(H_2O)_6^{3+}$ is unimportant, and hydrolysis of the dimer and chloro complex is also negligible under the conditions of our experiments.

Hydrogen-saturated, air-saturated, or deareated solutions of Cr_{aq}^{3+} (0.02 M Cr_{aq}^{3+} and 0.2 M $HClO_4$) are unaffected, even under irradiation: neither dimer nor Cr^{2+} is formed. In the presence of Cl^-, no chloro complex was found. These observations indicate that the respective complexes in the radiolysis of Cr_{aq}^{2+} are formed from the oxidation of Cr^{2+} rather than by a radiation-induced dimerization or by introduction of the anion into the Cr^{III} coordination sphere.

With the dimer and the chloro complex under irradiation, the situation is different. There is again no net oxidation–reduction change of Cr^{III}, but there is hydrolysis. In a solution containing a 3 mM dimer and 0.1 M $HClO_4$, the average $G(-dimer)$ for a dose of 3 × 10^{22} eV/l. was found to be ∼1.6. The initial $G(-dimer)$ is somewhat higher, decreasing with dose. The G of hydrolysis decreases when air, H_2O_2, or $Cr^3_{aq}^+$ is added.

Irradiation of an air-saturated 5 × 10^{-4} M $(H_2O)_5$-$CrCl^{2+}$–0.05 M $HClO_4$ solution containing Cl^- gave, for a dose of 10^{22} eV/l., an average $G(-chloro complex) = ∼2$.
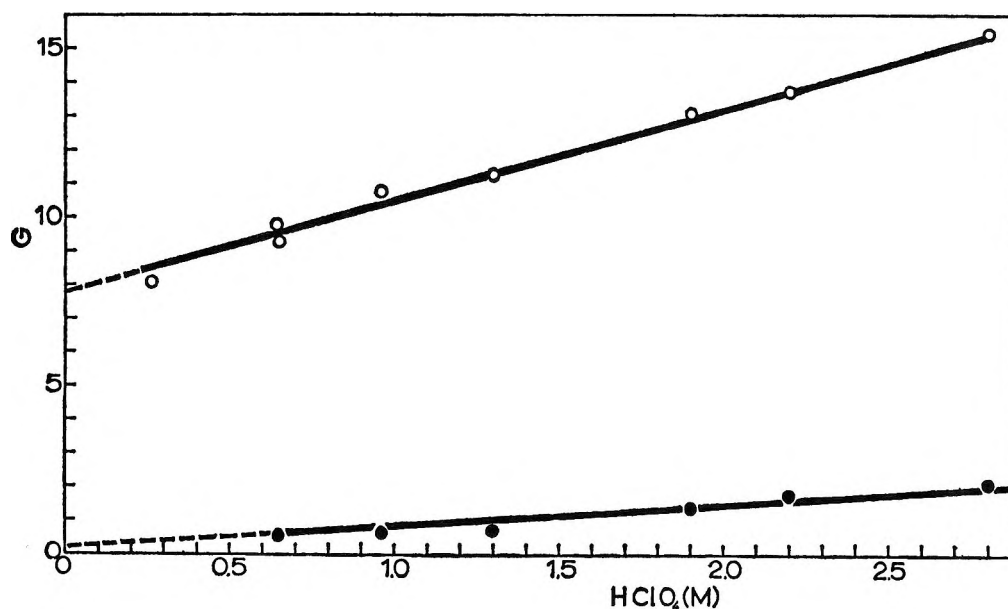
Figure 2. Total Cr^{III} (O) and dimeric Cr^{III} (●) formed in the radiolysis of Cr^{II} solutions as a function of the $HClO_4$ concentration.
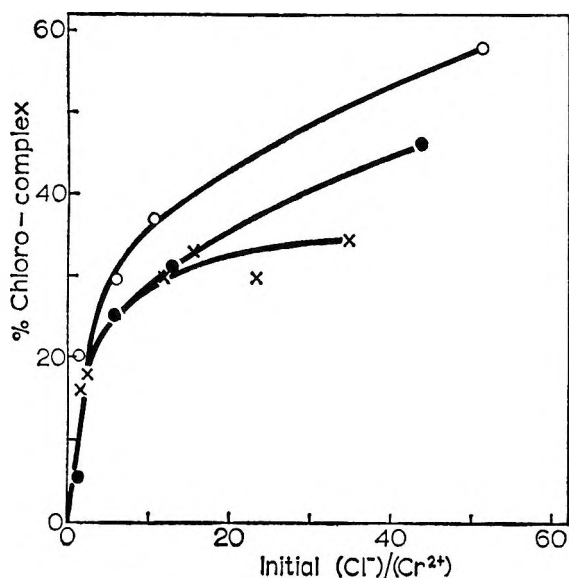

Figure 3. The percentage of the chloro complex over total Cr^{III} formed in the radiolysis of Cr^{II} solutions vs. the initial $(Cl^-):(Cr^{2+})$ ratio. Perchloric acid concentration: O, 1.9 M; ●, 0.96 M; ×, 0.5 M.

Since the radiation-induced hydrolysis of Cr^{III} complexes is possible, we must examine how important it is in the radiolysis of Cr^{2+} solutions. Such information is necessary in order to establish the correspondence between the measured complexes and the intermediates we want to study. We are interested not in the net amount of complex left but rather in the amount left plus that which was perhaps destroyed during the radiolysis. Fortunately in the case of the chloro complex and the dimer, hydrolysis does not seem to compete with the oxidation of Cr^{2+}. The evidence for the

previous statement includes the following. After the consumption of the Cr^{2+} there is no appreciable change in optical density on continuing irradiation both with and without Cl^-, presumably because of accumulation of products that suppress hydrolysis. The failure to detect steady-state Cr^{2+} also indicates that the Cr^{III} reactions cannot compete with the Cr^{2+} oxidation. Dimeric Cr^{III} present initially in concentrations up to ~50% of the Cr^{2+} concentration does not affect $G(Cr^{III})$. $G(Cr^{III})$ is also essentially unaffected by the initial Cr^{2+} concentration both in the presence and in the absence of Cl^-. Finally, it is noted that the optical density vs. dose curves do not seem to deviate from linearity up to very high conversion of Cr^{2+}, whereas hydrolysis would be expected to cause such deviation even though it does not involve net redox change.

Miscellaneous Observations. A number of relevant miscellaneous semiquantitative observations were also made to clarify certain aspects of the Cr^{II}–Cr^{III} system.

In the thermal oxidation of Cr^{2+} by ClO_3^- in $HClO_4$, if large excess of Cr^{2+} is used (which is closer to the conditions of radiolysis) no chloro complex is formed, in contrast to results obtained with small excess of Cr^{2+} or excess oxidizing agent.[8] The fraction of chromium III obtained in the form of dimer also seems to be smaller than that reported in the literature.[7]

In the oxidation of Cr^{2+} by air in 0.8 N H_2SO_4, we find that the formation of the dimer is suppressed. The products are the monomer and the sulfate complex. Oxidation of a Cr^{2+} solution containing 1.5 M NaCl gave no indication of interference by the chloride (Figure 1).

(8) M. Ardon and R. A. Plane, *J. Amer. Chem. Soc.*, **81**, 3197 (1959).

Radiolysis of V^{2+} *and* V^{3+} *Solutions.* Only deaerated V^{2+} solutions were irradiated, as V^{2+} is oxidized rapidly by air. The G value of formation of V^{3+} was found to be equal to 8.2 ± 0.3 and to be independent of the V^{2+} (10–46 mM) and perchloric acid concentration in the range 0.26–0.425 M. It was also found to be independent of the $V^{3+}:V^{2+}$ and of the $V^{3+}:H^{+}$ ratios, up to complete conversion. Change in the dose rate from 1.87 to 3.45×10^{19} eV/l. min had no measurable effect. Addition of 1 mM Cl^{-} or Br^{-} also had no effect.

In the radiolysis of deaerated solutions of V^{3+} in $HClO_4$, $G(VO^{2+})$ was found to be equal to 0.9 and to be independent of acid and dose rate. When air is present, we obtain $G(VO^{2+}) = 15.5 \pm 0.2$. The thermal oxidation of V^{3+} by air within the time period required for the performance of the radiolysis experiments is negligible.

Discussion

The interpretation of the vanadium data is straightforward. The $G(V^{3+})$ in the radiolysis of V^{2+} solutions is essentially equal to the G value of oxidation of ferrous ion in deaerated 0.8 N H_2SO_4. A similar mechanism should, therefore, be postulated, and thus neglecting the oxidation due to the ClO_4^{-} decomposition products, we have

$$G(V^{3+}) = G_H + G_{OH} + 2G_{H_2O_2} = 8.2 \pm 0.3$$

The hydrogen atoms react with V^{2+} rather than with V^{3+}, up to almost complete conversion. After the consumption of V^{2+}, the V^{3+} is oxidized further to VO^{2+}. Formation of complex ions with Cl^{-} or Br^{-} is not important. In deaerated V^{3+} solutions, VO^{2+} is formed from OH and H_2O_2 and is reduced by H either directly or through formation of V^{2+}, which is known[9] to react rapidly with VO^{2+} to give V^{3+}

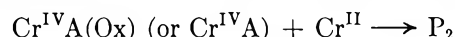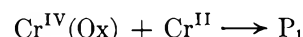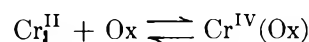$$G(VO^{2+}) = -G_H + G_{OH} + 2G_{H_2O_2} = 0.9 \pm 0.1$$

In aerated V^{3+} solutions, the reaction must be analogous with those in the Fricke dosimeter and, therefore

$$G_{air}(VO^{2+}) = 3G_H + G_{OH} + 2G_{H_2O_2} = 15.5$$

From the above equations, we obtain the values $G_H = 3.65$ and $G_{OH} + 2G_{H_2O_2} = 4.55$, in good agreement with literature[10] values.

The Cr^{II}–Cr^{III} system seems to be more interesting, as it reveals some characteristics that are not observable in a labile system. A simple explanation of the data reported in the Results contains the following general features. The dimeric Cr^{III} obtained at low $HClO_4$ concentrations originates in the oxidation of Cr^{2+} by H_2O_2. This oxidation is known[8] to give a mixture of monomeric and dimeric species. The small amount of dimeric Cr^{III} found under these conditions does not leave room for postulation of a source other than H_2O_2.

Thus the free radicals must give Cr_{aq}^{3+}, a conclusion which was, after all, not unexpected. At higher $HClO_4$ concentrations, new oxidizing agents come into the picture, originating in the so-called "direct" decomposition of ClO_4^{-} by radiation. Although some hydrogen–oxygen species may be included in these products, the major part are chlorine–oxygen compounds.[11] The increased monomer and dimer yields (Figure 2) may be attributed to these agents. In the presence of Cl^{-}, we also have formation of the chloro complex from an attack of Cr^{2+} by chlorine atoms formed in the reaction of $Cl^{-} + OH$. An estimate of the ratio of the rate constants of OH with Cl^{-} and Cr^{2+} at 0.5 M $HClO_4$, obtained from Figure 3, is $\sim 1:3$. At higher concentrations of $HClO_4$, additional chloro complex is formed by the oxidation of Cr^{2+} by the ClO_4^{-} decomposition products. In the last case it is interesting to note that there is a significant difference between the stoichiometry reported in the literature and that which we obtain here. Thus we obtain chloro complex only in the presence of Cl^{-}, whereas Ardon and Plane[8] and Thompson and Gordon[7] report high yields of this complex even without Cl^{-} added initially. This difference provides us with an important clue to understanding better both cases. This clue points to the conclusion that the chloro complex is formed only by Cl^{-} catalyzed paths. In the experiments reported in the literature, the chloro complex is formed even without addition of Cl^{-}, because there is enough of a supply of it in the reduction of the oxychlorine compounds. In our case, the amount of these compounds is insufficient for providing with the necessary Cl^{-}. Pursuing this line of reasoning, we propose the following general scheme which can account for at least a large part of the oxidation of Cr^{II} by two-electron oxidizing agents

$$Cr_l^{II} + Ox \rightleftharpoons Cr^{IV}(Ox)$$

$$Cr^{IV}(Ox) + Cr^{II} \longrightarrow P_1$$

$$Cr^{IV}(Ox) + A \longrightarrow Cr^{IV}A(Ox) \quad (or \ Cr^{IV}A)$$

$$Cr^{IV}A(Ox) \ (or \ Cr^{IV}A) + Cr^{II} \longrightarrow P_2$$

In this schematic representation, the products P_1 and P_2 may, in general, be different, and A is a complexing agent (*e.g.*, anion). The key to this scheme is the formation of Cr^{IV} stabilized by the reduced oxidizing agent that remains attached to it or by an added complexing agent; such intermediates can also be viewed as complexes of Cr^{III} with free radicals. Underlying is the idea that we may have a variety of Cr^{IV} species, depending upon the oxidizing agent, each one of them behaving differently toward various complexing agents, as seems to be the case with HSO_4^{-} and Cl^{-} in relation

(9) T. W. Newton and F. B. Baker, *J. Phys. Chem.*, **68**, 228 (1964).

(10) A. O. Allen, "The Radiation Chemistry of Water and Aqueous Solutions," D. Van Nostrand Co., Inc., New York, N. Y., 1961.

(11) D. Katakis and A. O. Allen, *J. Phys. Chem.*, **68**, 3107 (1964).

to their effect on the oxidation of Cr^{II} by H_2O_2 and air. Gaps in our knowledge of the exact distribution of the various oxidation states of chlorine in the radiolytic decomposition of ClO_4^- do not affect the general arguments given above, since what was said applies to all possible products of decomposition of ClO_4^-.

In concluding, instead of giving a summary of the findings reported in the paper, we give a more or less equivalent résumé of the procedure to be followed in the application of the Cr^{II}-Cr^{III} system for the study of unknown intermediates. The acid used is $HClO_4$ at low concentrations ($\sim$0.2 M should be all right). Higher concentrations of $HClO_4$, as well as other acids such as H_2SO_4, lead to formation of complex ions which may introduce unnecessary complications unless a competition study is desired. The complexes formed are separated and are identified; then their individual G values are determined at various initial conditions. Finally, we assess the importance of the thermal or radiation-induced hydrolysis and ligand reactions or the formation of the Cr^{III} complexes in order to establish their quantitative correspondence to the intermediates.

Analysis of Experimental Term Energies[1]

by Norman Padnos

Department of Chemistry, North Carolina College at Durham, Durham, North Carolina (*Received August 23, 1967*)

If the energy of a state be known for several isoelectronic monatomic species, the average potential energy of interaction of one electron, or of several electrons, with the nucleus and with the remaining electrons can be estimated. For one electron, these are, respectively: $E_n^1 = Z(dT/dZ)$ and $E_e^1 = 2T - E_n^1$. T is the energy of the state considered, taking as zero the energy of the species with the electron completely removed, and Z is the atomic number. The above expressions are derived using the Hellmann–Feynman theorem and the virial theorem and neglecting magnetic interactions (spin-orbit, etc.).

Introduction

A criterion which is commonly used in evaluating an approximate atomic wave function is agreement of the energy calculated from the wave function with the spectroscopically observed energy. The calculated energy can be analyzed into contributions from the kinetic energy, the electron–nucleus potential energy $E_n = \sum_i \langle Ze^2/r_i \rangle$, and the electron–electron potential energy $E_e = \sum \langle e^2/r_{ij} \rangle$. The virial theorem enables one to analyze the observed energy into contributions from kinetic energy and from potential energy. The present work develops and illustrates a method of analyzing the potential energy thus derived from observation into electron–nucleus and electron–electron contributions. Thus three energy quantities, kinetic energy, E_n, and E_e, derived from any approximate wave function can be compared to experimental data.

We start with the Hamiltonian

$$H = -\frac{\hbar^2}{2m} \sum_i \nabla_i^2 - \sum_i \frac{Ze^2}{r_i} + \sum_{j>i} \frac{e^2}{r_{ij}} \quad (I)$$

where the indices i and j refer to electrons. The Hellmann–Feynman theorem[2] states that

$$\frac{\partial E}{\partial Z} = \left\langle \frac{\partial H}{\partial Z} \right\rangle = \sum \left\langle \frac{-e^2}{r_i} \right\rangle$$

Thus, the nuclear contribution to the energy

$$E_n = \Sigma \langle -Ze^2/r_i \rangle = Z \frac{\partial E}{\partial Z} \quad (II)$$

This is the total energy of attraction of the nucleus for all the electrons in the atom if E represents the energy required to remove all the electrons. If only the term energy, T, be known, we still have $T = E - E_{ion}°$, and

$$Z \frac{\partial T}{\partial Z} = E_n - E_{n,ion}° \equiv E_n^1 \quad (III)$$

This is approximately $\langle Ze^2/r \rangle$ for the electron re-

(1) This work was supported in part by a Dupont Summer Grant for Teachers in Chemistry.

(2) (a) R. P. Feynman, *Phys. Rev.*, **56**, 340 (1939); (b) H. Hellmann, "Einführung in die Quantenchemie," Franz Deuticke, Leipzig, 1937.

Table I: Ne I Series

	$-T$, kK	$\sqrt{-T}$	$d\sqrt{-T}/dZ$[a]	$-E_n{}^1$, kK	$|E_n{}^1/E_e{}^1|$	$Z/(n-1)$	$\langle 1/r \rangle^{-1}$, Å	r_{ionic}
Ne I	173,932	417.05	211.69	1766	1.24	1.111	0.658	...
Na II	381,528	617.68	191.73	2604	1.41	1.222	0.490	0.97
Mg III	646,364	803.97	182.16	3515	1.58	1.333	0.396	0.66
Al IV	967,783	983.76	177.88	4550	1.74	1.444	0.332	0.51
Si V	1,345,100	1159.78						

[a] Estimated using a five-point Lagrange formula.[6]

moved to form the ion.[3] In this way, we can estimate, from the observed energy of a state in an isoelectronic series, the potential energy of an electron in the field of the nucleus.

The virial theorem[4] states that, for the Hamiltonian I, $V = 2E$, where V is the potential energy, and E is the total energy. Since the potential energy is the sum of the electron–nucleus and electron–electron contributions, we have for the latter

$$E_e{}^1 = E_e - E_e{}^\circ(\text{ion}) = 2T - Z(dT/dZ) \quad \text{(IV)}$$

Using the same sort of approximation as before, we can interpret this as the energy of interaction of the electron removed, with the other electrons.

In expressions III and IV, the derivative, dT/dZ, is not strictly measurable since we can only make measurements at integral values of Z. An estimate can be made, however, from a formula for term values such as[5]

$$(T/R)^{1/2} = (Z - \sigma)/n$$

or by numerical differentiation of a set of data.[6] Probably the best estimate can be obtained by a combination of these procedures, finding $\sqrt{T}$ and differentiating this more nearly linear function numerically. This is the procedure followed here.

Calculations

In order to illustrate the use of the formulas given and to see if they give reasonable results, we have estimated $E_n{}^1$, $E_e{}^1$, $|E_n{}^1/E_e{}^1|$, and a mean radius $\langle 1/r \rangle^{-1}$ for some species. We would expect that $|E_n{}^1/E_e{}^1|$ be of the order of the ratios of the atomic number to the number of electrons less one, $Z/(n - 1)$, e.g., for Li II $3/1 = 3.0$, for He I $2/1$, for Pd II $46/44 = 1.045$. $\langle 1/r \rangle^{-1}$ should be less than the radius of the species.

One-Electron Ions. This case is trivial, since $E_e = 0$, but serves as a check on the theory developed here. The observed energies are

$$T = Z^2R/n^2$$

The calculated E_n is

$$ZdT/dZ = Z(2ZR/n^2) = 2T$$

in accord with the virial theorem, and the calculated E_e is $2T - 2T = 0$, also the correct value.

Ions Isoelectronic with Ne I: the Ground States. The ground state of these ions is $2p^6({}^1S)$. They ionize to give $2p^5({}^2P)$. Table I gives the ionization energies[7a] and the square root of the ionization energy for the first five members of this series and calculated quantities for the first four members. The calculated radii are smaller than the (crystal) ionic radii and vary in the same sense from Na II to Al IV. The $|E_n{}^1/E_e{}^1|$ ratios are consistently larger than the charge ratios and vary in the same manner.

Pd II; the $4d^8({}^3F)$ 5s (^4F) State. The ionization energies from this state for Rh I, Pd II, and Ag III are[7c,8] -58.71, -129.53, and -215.01 kK. E_n is -3660 kK and E_e is 3410 kK. The ratio $|E_n{}^1/E_e{}^1|$ is 1.08, compared with $Z/(n - 1) = 1.045$.

He I and Li II: Ground State, $2s({}^3S)$, $4s({}^3S)$, $4d({}^3D)$ States. The ionization energies[7a] for He I, Li II, and

Table II: He I and Li II

State	$-T$, kK	$\sqrt{-T}$	$d\sqrt{-T}/dZ$	$|E_n{}^1/E_e{}^1|$	$Z/(n-1)$
He I 1s²	198.305	14.08	10.66	2.95	2.00
Li II 1s²	610.097	24.70	10.57	4.52	3.00
Be III 1s²	1241.2	35.23			
He I 2s	38.45	6.20	5.42	2.34	2.00
Li II 2s	134.03	11.58	5.33	3.62	3.00
Be III 2s	248.7	16.87			
He I 4s	8.013	2.831	2.655	2.14	2.00
Li II 4s	30.097	5.486	2.655	3.23	3.00
He I 4d	6.866	2.620	2.621	2.00	2.00
Li II 4d	27.467	5.241	2.621	3.00	3.00

(3) This approximation should be most accurate when the electron is in a highly excited state to begin with, as its removal in this case would not be expected to greatly change the other r_i's.

(4) H. Eyring, J. Walter, and G. E. Kimball, "Quantum Chemistry," John Wiley and Sons, Inc., New York, N. Y., 1944, pp 355–358; W. Kauzmann, "Quantum Chemistry," Academic Press, New York, N. Y., 1957, pp 229–233.

(5) H. E. White, "Introduction to Atomic Spectra," McGraw-Hill Book Co., Inc., New York, N. Y., 1934, Chapter 17.

(6) Z. Kopal, "Numerical Analysis," 2nd ed, John Wiley and Sons Inc., New York, N. Y., 1961, pp 87–92, 554–556.

(7) C. E. Moore, "Atomic Energy Levels," National Bureau of Standards Circular 467, U. S. Government Printing Office, Washington, D. C.: (a) Vol. I, 1949; (b) Vol. II, 1952; (c) Vol. III, 1958.

(8) The values given are averaged over the four possible J values for the quartet states.

Be III were used to evaluate the derivatives for the first two states, but data on He I and Li II only were used for the other states. Table II shows data and calculated quantities. From Table II, it is evident that, as the electron becomes more excited, the ratio, $|E_n{}^1/E_e{}^1|$ approaches $Z/(n-1)$.

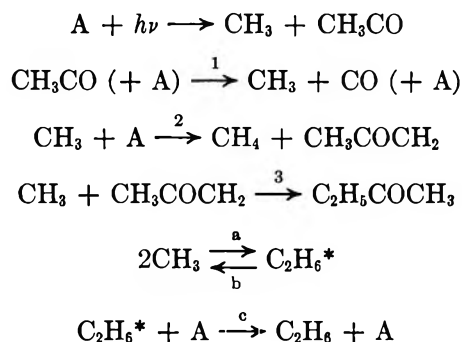# The Photochemistry of Gaseous Acetone

by Henry Shaw and Sidney Toby

School of Chemistry, Rutgers University, New Brunswick, New Jersey 08903   *(Received August 28, 1967)*
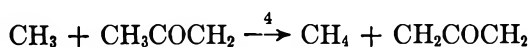
The photochemistry of acetone was reinvestigated in the temperature range 121–298° and the pressure range 0.1–220 torr. The quantum yield of carbon monoxide production was independent of pressure over the large pressure range studied. Data were obtained giving the variation of quantum yields of methane, ethane, methyl ethyl ketone, 2,5-hexanedione, and a number of minor products as a function of pressure and temperature, and a mechanism is proposed which accounts for the major products. The behavior of methane formation at low pressures suggests that intramolecular formation of methane is important under some conditions. The quantum yield for acetone disappearance was unity at low pressures but increased rapidly at pressures of acetone greater than 10 torr. After taking energy-transfer considerations into account, excellent agreement was obtained with published values of $k_2/k_a{}^{1/2}$ for the reactions $CH_3 + A \xrightarrow{2} CH_4 + CH_3COCH_2$ and $2CH_3 \xrightarrow{a} C_2H_6{}^*$. By correcting literature values of k_a, the high-pressure limit was found to be $k_{a\infty} = (2.0 \pm 0.15)10^9 T^{1/2}$ l. mol^{-1} sec^{-1}. This yields $k_2 = (3.3 \pm 1.5)10^8 \exp[(-9440 \pm 350)/RT]$ l. mol^{-1} sec^{-1}.

Introduction

The photolysis of gaseous acetone (A) has been extensively studied because it is one of the principle sources of quantitative data on the kinetics of methyl radical reactions. The mechanism was postulated by Dorfman and Noyes[1] and may be written

$$A + h\nu \longrightarrow CH_3 + CH_3CO$$

$$CH_3CO\ (+ A) \xrightarrow{1} CH_3 + CO\ (+ A)$$

$$CH_3 + A \xrightarrow{2} CH_4 + CH_3COCH_2$$

$$CH_3 + CH_3COCH_2 \xrightarrow{3} C_2H_5COCH_3$$

$$2CH_3 \underset{b}{\overset{a}{\rightleftarrows}} C_2H_6{}^*$$

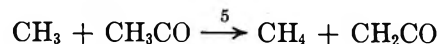$$C_2H_6{}^* + A \xrightarrow{c} C_2H_6 + A$$

Reactions a, b, and c were shown to be important at low pressures by Dodd and Steacie,[2] and the asterisk indicates vibrationally excited ethane. More recently, Darwent, Allard, Hartman, and Lange[3] determined that reaction 2 was not sufficient to account for all of the methane produced in the photolysis of acetone above 200°. They speculated on the additional abstraction reaction

$$CH_3 + CH_3COCH_2 \xrightarrow{4} CH_4 + CH_2COCH_2$$

but they did not obtain any direct evidence for this reaction.

Henderson and Steacie[4] also observed more methane than would be predicted from reaction 2 only. They attributed this methane to a reaction of methyl radicals with excited acetone. They presented strong evidence to show that the source of this additional methane was not due to methyl radicals abstracting from ethane. Ausloos and Steacie[5] clearly demonstrated that at 27° additional methane was produced from the reaction

$$CH_3 + CH_3CO \xrightarrow{5} CH_4 + CH_2CO$$

They observed ketene in their product gases and found a product dependency on the square root of the incident intensity. O'Neal and Benson[6] demonstrated that the acetyl radical is sufficiently long lived to react with hydrogen iodide at temperatures above 200°.

The photolysis of gaseous acetone at low pressures is

(1) L. M. Dorfman and W. A. Noyes, Jr., *J. Chem. Phys.*, **16**, 557 (1948).

(2) R. E. Dodd and E. W. R. Steacie, *Proc. Roy. Soc.* (London), **A223**, 283 (1954).

(3) B. deB. Darwent, M. J. Allard, M. F. Hartman, and L. J. Lange, *J. Phys. Chem.*, **64**, 1847 (1960).

(4) J. F. Henderson and E. W. R. Steacie, *Can. J. Chem.*, **38**, 2161 (1960).

(5) P. Ausloos and E. W. R. Steacie, *ibid.*, **33**, 47 (1955).

(6) E. O'Neal and S. W. Benson, *J. Chem. Phys.*, **36**, 2196 (1962).

Table I: Quantum Yields of Products at 121°[a]

$10^4[A]$, mol l.$^{-1}$	Photolysis time, sec × 10^{-3}	Φ_M	Φ_E	$10^2\Phi_{70}$	$10^2\Phi_{MEK}$	$10^2\Phi_{86}$	$10^3\Phi_{98}$	$10^4\Phi_{112}$	Φ_{114}	$10^9 R_{CO}$, mol/l. sec^{-1}	$^1/_2\Phi_M + \Phi_E^{1/2}$	$\Phi_E^{1/2} + \Phi_{114}^{1/2}$	$\Phi_E + ^1/_2\Phi_M + ^1/_2\Phi_{MEK}$
89.3	1.00	0.976	0.478							4.78	1.18		
74.6	1.10	0.887	0.525							4.70	1.16		
58.1	1.25	0.792	0.596							4.17	1.17		
42.5	1.50	0.687	0.658							3.54	1.15		
33.0	1.80	0.553	0.648							3.17	1.08		
24.6	2.20	0.526	0.749							2.48	1.12		
17.2	2.30	0.399	0.781							1.88	1.08		
7.97	2.50	0.301	0.890							0.916	1.09		
2.08	3.50	0.184	1.02							0.274	1.10		
1.14	5.00	0.147	1.07							0.146	1.10		
0.574	7.50	0.102	0.993	1.1	5.4	0.7	2	6	...	0.074	1.05	1.00	1.07
0.38	10.0	0.10	1.1	1.3	4.8	0.8	4	5	...	0.043	1.10	1.05	1.17
0.23	12.0	0.097	1.1	1.1	4.0	0.9	2	4	...	0.033	1.10	1.05	1.17
0.11	18.5	0.11	1.2	1.5	3.2	1.4	2	2	...	0.014	1.15	1.10	1.27
0.083	22.0	0.11	1.3	2.0	3.3	1.8	2	4	...	0.0094	1.20	1.14	1.37
0.040	25.0	0.17	1.3	4.2	3.0	4.6	7	8	...	0.0046	1.22	1.14	1.40

[a] Blanks indicate that no analysis was performed and dots indicate that no product was detected.

of interest as an energy-transfer system[2,7] and can be used to provide data to test unimolecular rate theory.[8] Since methane is an important product even at low pressures, it is necessary to evaluate quantitatively all sources of methane additional to step 2. It is then possible to correlate much previous work on the acetone photolysis and obtain more accurate Arrhenius parameters. For these rate data to be obtained on an absolute basis, the rate of dimerization of methyl radicals should be accurately known. By taking energy-transfer considerations into account, it has been possible to correlate much of the published work on this reaction.

Experimental Section

A conventional high-vacuum apparatus, with greaseless valves in the photolysis and product fractionation sections, was used. The cylindrical, quartz photolysis cell, volume 558 cm³, was thermostated in a modified convection oven within ±0.5° up to 300°.

The beam from an Osram HBO-75W high-pressure mercury arc, made parallel with a quartz lens, completely filled the photolysis cell. A mirror at the back of the cell increased light intensity and uniformity. The 3130-Å region was isolated with a solution filter,[9] and the potassium biphthalate solution was changed whenever the light output decreased by a few per cent.[10] Light intensity was varied with neutral density filters. In some experiments a less monochromatic but more intense beam was obtained using a Kimax plate with a Corning 7-54 filter. When corrected for intensity differences, both solution and glass filters gave the same results.

Spectroquality (Matheson Coleman and Bell) acetone was distilled from a Linde 5A[11] molecular sieve and then was distilled from bulb to bulb.

Products were fractionated at low temperature. Carbon monoxide, methane (M), and ethane (E) were analyzed gas chromatographically using a silica gel column at 25°. The less volatile products were analyzed using a mass spectrometer. Conversions were kept below 5%, except for the four lowest pressure runs at 298°.

Results

Results are summarized in Tables I–III. Products giving mass spectrometric parent peaks of 70, 86, 98, 112, and 114 were not unambiguously identified, but comparisons with API spectra indicated that the peaks were due to methyl vinyl ketone, biacetyl, mesityl oxide, 2,5-hexenedione, and 2,5-hexanedione, respectively. Analysis for the heavier products were not accurate, since these products were present as a very small fraction of the unreacted acetone.

A dark reaction was carried out for 15 hr at 298° with 200 torr of acetone. The rate was less than 0.01% of the corresponding photoreaction.

The quantum yield for carbon monoxide production, Φ_{CO}, was assumed unity at 216°.[12] Φ_{CO} at the other temperatures were determined using the Beer–Lambert law for slab geometry.[13] The absorption coefficients at

(7) G. B. Kistiakowsky and E. K. Roberts, *J. Chem. Phys.*, 21, 1637 (1953).

(8) H. Shaw, J. H. Menczel, and S. Toby, *J. Phys. Chem.*, 71, 4180 (1967).

(9) W. A. Noyes, Jr., and P. A. Leighton, "The Photochemistry of Gases," Reinhold Publishing Corp., New York, N. Y., 1941.

(10) M. Venogapalan, G. O. Pritchard, and G. H. Miller, *Nature*, 200, 563 (1963).

(11) K. S. Howard and F. P. Pike, *J. Phys. Chem.*, 63, 311 (1959).

(12) J. G. Calvert and J. N. Pitts, Jr., "Photochemistry," John Wiley and Sons, Inc., New York, N. Y., 1966.

(13) H. Shaw and S. Toby, *J. Chem. Educ.*, 43, 408 (1966).

Table II: Quantum Yields of Products at 216°ᵃ

$10^4[A]$, mol l.⁻¹	Photolysis time, sec × 10⁻³	Φ_M	$10^2\Phi_E$	$10^2\Phi_{70}$	Φ_{MEK}	$10^2\Phi_{86}$	$10^3\Phi_{98}$	$10^2\Phi_{112}$	Φ_{114}	$10^9 R_{CO}$, mol/l. sec⁻¹	$\frac{1}{2}\Phi_M + \Phi_E^{1/2}$	$\Phi_E^{1/2} + \Phi_{114}^{1/2}$	$\Phi_E + \frac{1}{2}\Phi_M + \frac{1}{2}\Phi_{MEK}$
72.3	1.25	1.74	4.29	...	0.64	...	...	180	0.82	6.36	1.08	1.12	1.23
60.8	1.50	1.67	4.63	...	0.53	...	...	73	0.73	6.09	1.04	1.06	1.14
40.2	2.50	1.56	7.04	...	0.53	...	...	41	0.41	5.15	1.04	0.90	1.11
30.3	2.60	1.53	9.30	...	0.47	...	...	110	(3.2)	4.20	1.07		1.09
20.4	2.80	1.40	12.1	...	0.51	...	...	20	0.73	3.29	1.05	1.20	1.07
12.4	1.10	1.30	15.1	...	0.68	...	...	79	Trace	2.00	1.04	0.39	1.14
7.53	6.00	1.20	16.2							0.838	1.00	0.40	
3.53	2.00	1.10	27.9	...	0.35	...	...	...	...	0.655	1.03	0.53	1.00
1.27	3.10	0.869	34.5	...	0.29	...	...	...	...	0.252	1.02	0.59	0.92
0.646	3.60	0.774	42.8	1.8	0.24	1.6	4	0.8	...	0.131	1.03	0.65	0.93
0.412	4.00	0.761	48.9	2.6	0.21	1.4	4	0.9	...	0.079	1.08	0.70	0.98
0.24	6.10	0.73	50	1.6	0.16	0.7	2	0.4	...	0.047	1.07	0.71	0.95
0.12	11.0	0.72	51	1.6	0.10	0.9	2	0.4	...	0.023	1.07	0.71	0.92
0.065	20.0	0.77	36	2.4	0.043	1.8	4	0.5	...	0.011	0.98	0.60	0.70
0.029	30.0	0.93	49	2.8	0.063	2.5	4	0.5	...	0.005	1.16	0.70	1.00

ᵃ Blanks indicate that no analysis was performed and dots indicate that no product was detected.
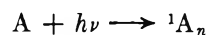
Table III: Quantum Yields of Products at 298°ᵃ

$10^4[A]$, mol l.⁻¹	Photolysis time, sec × 10⁻³	Φ_M	$10^2\Phi_E$	$10^2\Phi_{70}$	Φ_{MEK}	$10^2\Phi_{86}$	$10^3\Phi_{98}$	$10^2\Phi_{112}$	Φ_{114}	$10^9 R_{CO}$, mol/l. sec⁻¹	$\frac{1}{2}\Phi_M + \Phi_E^{1/2}$	$\Phi_E^{1/2} + \Phi_{114}^{1/2}$	$\Phi_E + \frac{1}{2}\Phi_M + \frac{1}{2}\Phi_{MEK}$
59.7	0.50	1.94	0.316	...	...	...	Trace	Trace	(...)	5.01	0.92		0.86
56.3	0.75	1.92	0.369							4.27	1.02		
51.6	1.60	1.95	0.501	...	0.21	...	...	63	0.6	6.10	1.04	0.84	1.08
42.3	1.20	1.90	0.501	...	...	...	Trace	Trace	(...)	4.20	1.02		0.95
36.9	2.30	1.88	0.651	...	0.21	...	...	31	1.0	5.26	1.02	1.08	1.05
29.4	1.50	1.83	0.416							2.36	0.97		
26.0	2.40	1.87	0.879	...	0.18	...	...	33	2.1	4.24	1.02	1.5	1.04
20.3	2.50	1.88	1.16	...	0.16	...	...	30	1.2	3.57	1.05	1.21	1.03
13.9	1.50	1.94	1.03							2.04	1.07		
11.9	3.33	1.76	1.80		0.25	...	...	15	1.3	2.41	1.01	1.27	1.01
8.77	4.00	1.73	1.35							1.41	0.98		
6.17	4.50	1.71	1.97	...	0.20	...	...	34	0.7	1.02	0.99	0.98	0.97
3.39	6.00	1.59	2.85	...	0.14	...	...	...	...	0.627	0.96	0.17	0.89
1.85	7.50	1.62	3.79	...	0.14	...	...	...	...	0.344	1.00	0.19	0.92
1.23	10.0	1.50	5.43	...	0.14	...	...	...	...	0.248	0.98	0.23	0.87
0.891	13.3	1.48	6.52	...	0.13	...	...	...	...	0.175	1.00	0.26	0.87
0.441	18.0	1.43	8.42	...	0.11	...	...	...	...	0.090	1.00	0.29	0.85
0.280	18.0	1.69	5.60	1.4	0.03	1.2	3	0.4	...	0.0215	1.08	0.24	0.92
0.24	13.0	1.4	12	1.4	0.11	0.6	1	0.2	...	0.054	1.05	0.35	0.87
0.19	14.0	1.4	12	1.3	0.08	0.6	1	0.2	...	0.043	1.05	0.35	0.86
0.093	66.0	1.1	5.8	1.0	0.015	0.8	1	0.2	....	0.012	0.79	0.24	0.61
0.076	61.0	1.4	5.7	1.4	0.014	1.1	4	0.2	....	0.0074	0.94	0.24	0.76
0.051	76.0	1.2	6.0	2.0	0.007	...	...	1.4	....	0.007	0.84	0.24	0.66
0.031	60.0	1.1	4.3	2.0	0.012	2.4	2	0.4	....	0.0033	0.76	0.21	0.59

ᵃ Blanks indicate that no analysis was performed and dots indicate that no product was detected.
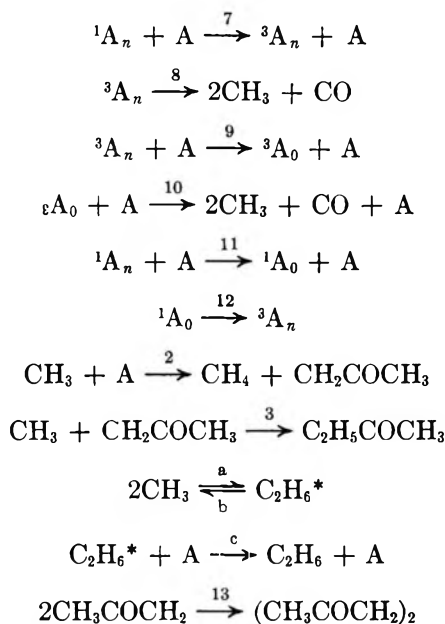
the temperatures of this study were determined from the data of Caldwell and Hoare.[14] Φ_{CO} was 0.86 at 121° and 1.0 at 298°. Plots were made for the rate of carbon monoxide production (R_{CO}), calculated from the Beer–Lambert law, as a function of acetone concentration. These plots gave excellent agreement with experimental values of R_{CO}, except that at the highest pressures of this study the experimental values of R_{CO} were consistently slightly lower than the calculated values.

A reaction mechanism which accounts for the major products is

$$A + h\nu \longrightarrow {}^1A_n$$

(14) J. Caldwell and D. E. Hoare, J. Amer. Chem. Soc., 84, 3987 (1962).

$$^1A_n + A \xrightarrow{7} {}^3A_n + A$$

$$^3A_n \xrightarrow{8} 2CH_3 + CO$$

$$^3A_n + A \xrightarrow{9} {}^3A_0 + A$$

$$\varepsilon A_0 + A \xrightarrow{10} 2CH_3 + CO + A$$

$$^1A_n + A \xrightarrow{11} {}^1A_0 + A$$

$$^1A_0 \xrightarrow{12} {}^3A_n$$

$$CH_3 + A \xrightarrow{2} CH_4 + CH_2COCH_3$$

$$CH_3 + CH_2COCH_3 \xrightarrow{3} C_2H_5COCH_3$$

$$2CH_3 \underset{b}{\overset{a}{\rightleftharpoons}} C_2H_6{}^*$$

$$C_2H_6{}^* + A \xrightarrow{c} C_2H_6 + A$$

$$2CH_3COCH_2 \xrightarrow{13} (CH_3COCH_2)_2$$

The superscripts refer to the lowest excited singlet and the triplet state; the subscripts refer to thermal (0) and higher-than-thermal (n) vibrational levels of the electronically excited states. Making the usual steady-state assumption for the transient species and assuming[15,16] that $k_3/k_a{}^{1/2}k_{13}{}^{1/2} = 2$, we have for the high-pressure region the following relationships for the major products

$$\Phi_E{}^{1/2} + \Phi_{114}{}^{1/2} = 1 \tag{1}$$

$$^1/_2\Phi_M + {}^1/_2\Phi_{MEK} + \Phi_E = 1 \tag{2}$$

$$^1/_2\Phi_M + \Phi_E{}^{1/2} = 1 \tag{3}$$

The experimental values for equations 1–3 are shown in Tables I–III. Good agreement in the high-pressure region is seen and the few scattered values are clearly due to our inaccurate analyses for Φ_{114}.

At constant incident intensity, as [A] increases most of the methyls disappear by reactions 2 and 3, whereas at low values of [A] reactions a–c become more important. The limiting low- and high-pressure quantum yields would then be given by

$$\Phi_M{}^0 = 0; \quad \Phi_E{}^0 = 1; \quad \Phi_{MEK}{}^0 = 0;$$

$$\Phi_{114}{}^0 = 0; \quad -\Phi_A{}^0 = 1 \tag{4}$$

$$\Phi_M{}^\infty + \Phi_{MEK}{}^\infty = 2; \quad \Phi_E{}^\infty = 0;$$

$$\Phi_{114}{}^\infty = 1; \quad -\Phi_A{}^\infty = 3 \tag{5}$$

The quantum yields of methane, ethane, methyl ethyl ketone formation and acetone disappearance are given in Figures 1–4 as a function of acetone concentration. The correlation between anticipated and actual values will be discussed shortly.

High-Pressure Rate Constants. The mechanism leads to the previously obtained[2,7] relation

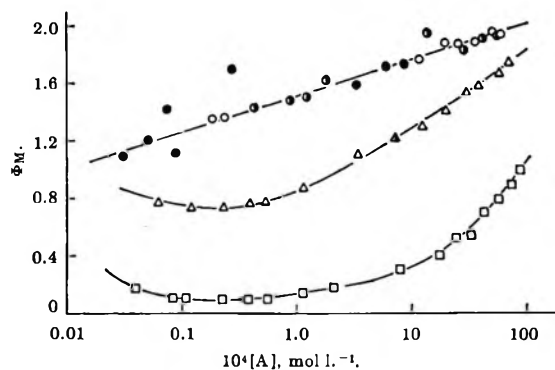$$\frac{R_M}{R_E{}^{1/2}[A]} = \frac{k_2}{k_a{}^{1/2}}\left(1 + \frac{k_b}{k_c[A]}\right)^{1/2} \tag{6}$$

Figure 1. Plot of the quantum yield of methane formation against the acetone concentration: $\square$, 121° ($I_0 = 1.75 \times 10^{-10}$ einstein cm^{-2} sec^{-1}); $\blacktriangle$, 216° ($I_0 = 1.35 \times 10^{-10}$ einstein cm^{-2} sec^{-1}); $\triangle$, 216° ($I_0 = 1.75 \times 10^{-10}$ einstein cm^{-2} sec^{-1}); $\bullet$, 298° ($I_0 = 0.66 \times 10^{-10}$ einstein cm^{-2} sec^{-1}); $\mathbb{O}$, 298° ($I_0 = 1.35 \times 10^{-10}$ einstein cm^{-2} sec^{-1}); $\bigcirc$, 298° ($I_0 = 1.75 \times 10^{-10}$ einstein cm^{-2} sec^{-1}).
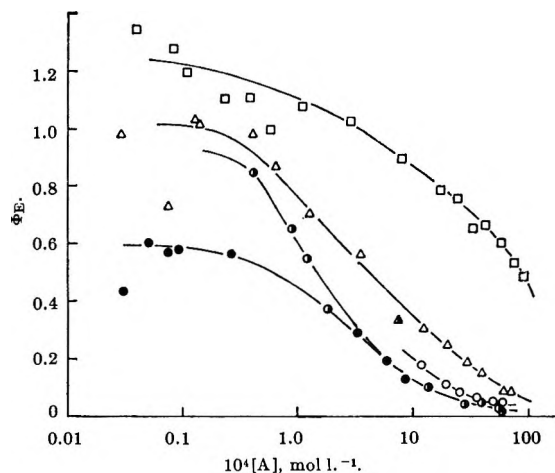

Figure 2. Plot of the quantum yield of ethane formation against acetone concentration: $2\Phi_E$, 216°; $10\Phi_E$, 298°. Symbols the same as in Figure 1.

A Lindemann–Hinshelwood plot of our data as well as that of various literature sources gave us the values of $k_2/k_a{}^{1/2}$ as [A] $\rightarrow \infty$. Figure 5 is the Arrhenius plot for a large body of data from different laboratories. It shows excellent agreement and yields for the high pressure limits

$$E_2 - {}^1/_2E_a = 9.44 \pm 0.35 \text{ kcal mol}^{-1}$$

$$\log (A_2/A_a{}^{1/2}) = 3.17 \pm 0.17$$

(units of A factors are l. mol^{-1} sec^{-1}; probable errors are given.)

The Methyl Combination Rate Constant. The absolute value of k_2 requires a knowledge of k_a. The latter constant has been measured by a large number of investigators under a variety of conditions, but there has

(15) R. K. Brinton, *J. Amer. Chem. Soc.*, **83**, 1541 (1961).

(16) J. A. Kerr and A. F. Trotman-Dickenson, *Progr. Reaction Kinetics*, **1**, 105 (1961).
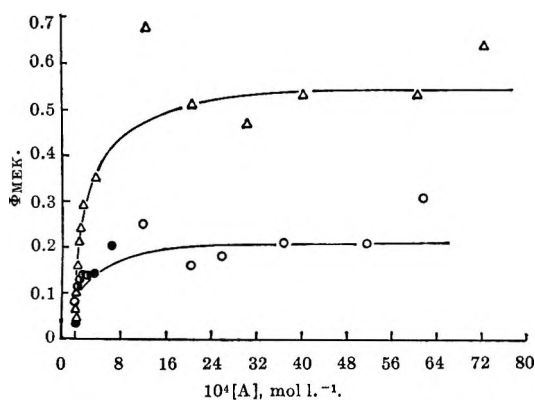
Figure 3. Plot of the quantum yield of methyl ethyl ketone formation against the acetone concentration. Symbols the same as in Figure 1.
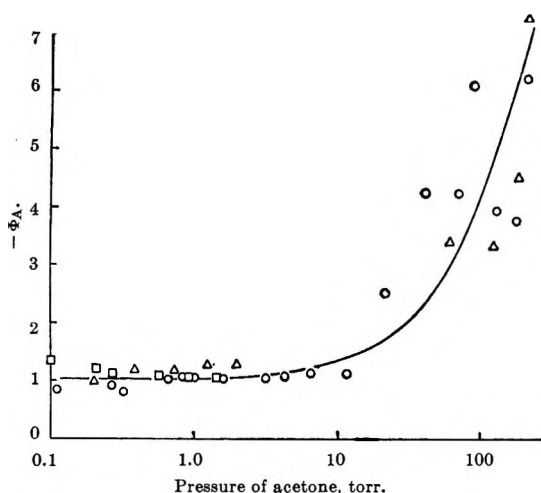

Figure 4. Plot of the quantum yield of acetone disappearance against the acetone pressure. Symbols the same as in Figure 1.

Figure 5. Arrhenius plot of $k_2/k_{a\infty}^{1/2}$: ●, A. F. Trotman-Dickenson and E. W. R. Steacie, *J. Chem. Phys.*, **18**, 1097 (1950); □, R. H. Linnell and W. A. Noyes, Jr., *J. Amer. Chem. Soc.*, **73**, 3986 (1951); ✕, Kistiakowsky and Roberts;[7] △, Darwent, *et al.*;[3] ▲, Brinton;[16] ○, this work.

Figure 6. Plot of the methyl dimerization rate constant against the temperature.

been no systematic attempt to correct all the data for energy-transfer effects. We have obtained the infinite-pressure value of k_a for all published data. The Lindemann mechanism is, of course, a poor approximation at lower pressures and our corrections were made using the data of Setser and Rabinovitch,[17] which were calculated from RRKM unimolecular rate theory. The values are given in Table IV and are plotted in Figure 6 as a function of temperature.

There is considerable scatter, but a better fit is obtained with a $T^{1/2}$ dependence.

Assuming no activation energy for the high-pressure rate constant the best value is

$$k_a = (2.0 \pm 0.15) \times 10^9 T^{1/2} \text{ l. mol}^{-1} \text{ sec}^{-1}$$

Hence

$$k_2 = (3.3 \pm 1.5) \times 10^8 e^{(-9440 \pm 350)/RT} \text{ l. mol}^{-1} \text{ sec}^{-1}$$

Discussion

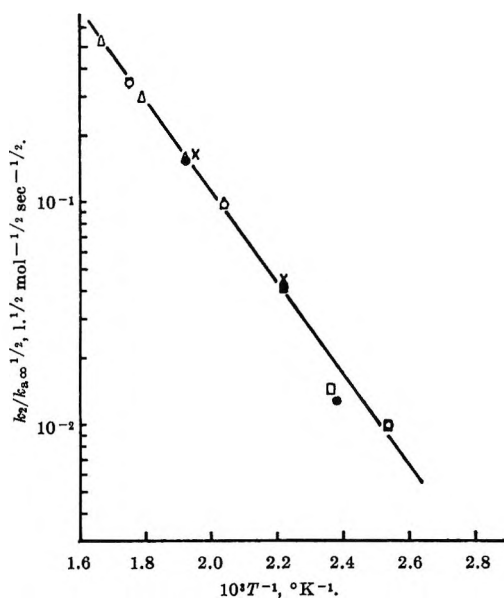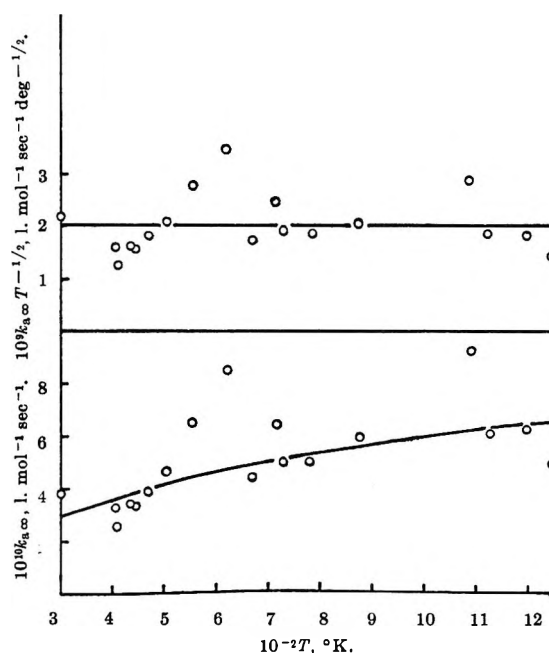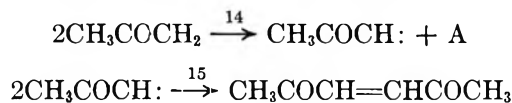*High-Pressure Mechanism.* The high-pressure quan-

tum yields predicted by eq 5 are well obeyed by our data. At higher pressures than used in this study $\Phi_M^\infty \to 2$. We have not shown a plot of Φ_{114}, since our values are rather scattered, but the trend in Tables I–III is clear. The quantum yield for acetone disappearance shown in Figure 4 is based on a carbon balance and, therefore, includes the yield of 2,5-hexene-

(17) D. W. Setser and B. S. Rabinovitch, *J. Chem. Phys.*, **40**, 2427 (1964).

dione. This product was not included in the mechanism because of a large uncertainty in its origin, and if it is omitted from the carbon balance, then $-\Phi_A$ at high pressures is closer to 3, the expected value. The liquid product of a dark reaction contained this unsaturated product. Majer and Simons[18] observed 2,5-hexenedione in the photolysis of halogenated ketones and assumed that it was produced by the reactions

$$2CH_3COCH_2 \xrightarrow{14} CH_3COCH: + A$$

$$2CH_3COCH: \xrightarrow{15} CH_3COCH{=}CHCOCH_3$$

Brinton[15] photolyzed acetone in the range 300–475° and found no 2,5-hexenedione. The other products found in this study were in general agreement with Brinton's findings, although it is clear that ethylene is only formed in appreciable amounts above 300°.[15,19]

Low-Pressure Mechanism. The low-pressure quantum yields predicted by eq 4 correlate well with the experimental results, with the exception of $\Phi_M{}^\circ$ which is nonzero and may be unity (Figure 1). In addition, $\Phi_E{}^\circ$ at 121° appears to be somewhat greater than unity, although, as seen in Figure 2, the points at pressures less than 0.3 torr are rather scattered.

The existence of an additional methane-forming step at low pressures is strongly suggested by a plot of $R_M/R_E{}^{1/2}$ against [A]. This is shown in Figure 7, where a positive intercept not predicted by eq 6 is found, in agreement with previous work.[3] We cannot reconcile previous suggestions[3–5] for the source of the extra methane with our data, and we postulate an additional primary step

$$^1A_n \xrightarrow{6} CH_4 + CH_2CO$$

Equation 6 then becomes

$$\frac{R_M}{R_E{}^{1/2}} = \frac{k_6 I_a}{(k_6 + k_7[A] + k_{11}[A])R_E{}^{1/2}} +$$

$$\frac{k_2[A]}{k_a{}^{1/2}}\left(1 + \frac{k_b}{k_c[A]}\right)^{1/2} \quad (7)$$

At *sufficiently low pressures*, we may write

$$R_E = \frac{k_a k_c[A][CH_3]^2}{k_b} = \frac{I_a(k_7 + k_{11})[A]}{k_6 + k_7[A] + k_{11}[A]}$$

where steps 2 and 3 can be neglected in the steady-state equation of methyl radicals. Substitution into eq 7 gives the intercept, λ, in Figure 7 as

$$\lambda = \frac{k_6 I_a{}^{1/2}}{[(k_6 + k_7[A] + k_{11}[A])(k_7 + k_{11})[A]]^{1/2}} \simeq$$

$$\left(\frac{k_6 I_0 \epsilon}{k_7 + k_{11}}\right)^{1/2}$$

which accounts for the finding of Darwent, *et al.*, that the intercept varies with the square root of the incident intensity.
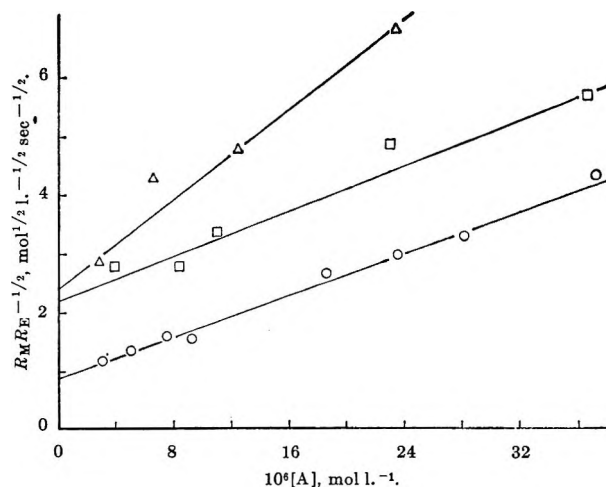
Figure 7. Plot of $R_M/R_E{}^{1/2}$ against the acetone concentration at low pressures. Symbols the same as in Figure 1. Ordinate is multiplied by 10^7, 10^6, and 10^6 at 121, 216, and 298°, respectively.
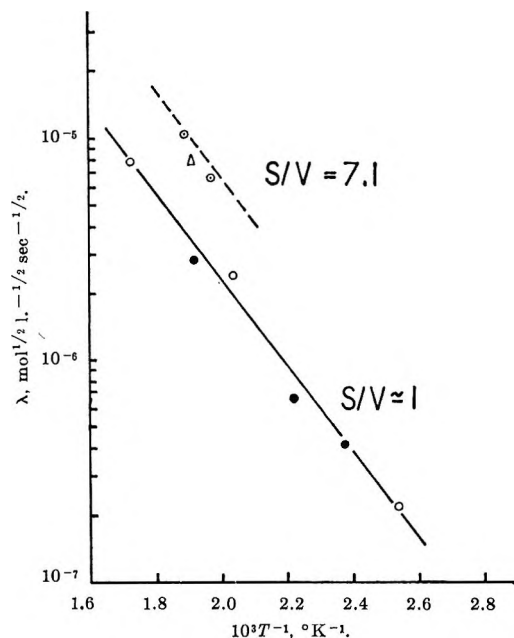

Figure 8. Arrhenius plot of λ (defined in text): ●, Dodd and Steacie[2] ($s/v = 1.1$ cm^{-1}); △, Dodd and Steacie[2] ($s/v = 7.1$ cm^{-1}); ⊘, Ausloos and Steacie[5] ($s/v = 7.1$ cm^{-1}); ○, this work ($s/v = 0.9$ cm^{-1}).

Figure 8 shows an Arrhenius plot for λ using data presented here and the data of Dodd and Steacie[2] and Ausloos and Steacie.[5] The slope corresponds to an activation energy of 9.4 kcal mol^{-1} and an apparent surface effect is seen. We believe this effect is spurious, since an Arrhenius plot of k_6 (assuming collision numbers for k_7 and k_{11}) shows considerable scatter but no surface effect, suggesting that packing the reaction vessel may have changed the effective incident intensity. Al-

(18) J. R. Majer and J. P. Simons, *Advan. Photochem.*, **2**, 137 (1964).
(19) L. Mandelcorn and E. W. R. Steacie, *Can. J. Chem.*, **32**, 331 (1954).

though the occurrence of heterogeneous effects affords a possible explanation for the intercepts in Figure 7, we believe an intramolecular process is more likely.

The fate of the ketene produced in reaction 6 is uncertain. We found traces of ketene in some of the mass spectrographic analyses, but this molecule is very reactive and may have been consumed in a CO-forming polymerization reaction.[20] The primary photochemical reactions proposed here are similar to those previously considered[21] with the addition of reaction 6, a molecular elimination reaction, important at low pressures.

The production of molecular entities in photochemical reactions has been observed in the photochemistry of acetaldehyde where methane is produced presumably from an excited singlet state.[12] Also, in the photoxidation of acetone, methane is produced in the presence of oxygen,[20,22] suggesting an intramolecular process.

Φ_{CO} was unity at the higher temperatures of this study; at 121° the quantum yield was 0.86 in agreement with Cundall and Davies[23a] and Pearson.[23b]

The Rate Constants. Step 6 is unimportant at high pressures and at the intensities employed in our work and has little effect on Figure 5. The third-body effect is, however, important in obtaining the high-pressure[24] value $k_2{}^2/k_{a\infty}$. It is important to note that the assumption that $E_a = 0$ is only valid at high pressures, for at low pressures E_a will have an apparently negative value.[25]

The high-pressure correction to convert k_a to $k_{a\infty}$ varied considerably, as shown in Table IV. The values of $k_{a\infty}/k_a$ ranged from near unity at low temperatures to more than 20 at the highest temperatures. In the case of the mass spectrometric determinations the helium carrier gas was assumed to be $^1/_{15}$th as efficient as acetone in stabilizing excited ethane.

The scatter of the data is too great to decide whether or not the simple collision theory $T^{1/2}$ dependence is a better fit than a Gorin model[26] which leads to a $T^{1/6}$ dependence.

It is interesting to note that using simple collision theory with a collision diameter $\sigma(CH_3) \simeq 3.8$ Å $= \sigma(CH_4)$,[27] assuming that σ is not a function of temperature[28] and that there is an electronic steric factor of 0.25, we obtain a value for the dimerization rate constant of $k_{a\infty}T^{-1/2} = 1.8 \times 10^9$. The value obtained in averaging all 18 determinations in Table IV is $k_{a\infty}T^{-1/2} = 2.0 \times 10^9$.

Table IV: Observed (k_a) and Corrected $(k_{a\infty})$ Rate Constants for Dimerization of Methyl Radicals

Foot-note	Temp, °K	$10^{10}k_a$, l. mol^{-1} sec^{-1}	$10^{10}k_{a\infty}$ l. mol^{-1} sec^{-1}
a	298	3.81	3.81
b	403	2.40	3.23
c	407	2.30	2.56
d	434	1.36	3.40
b	443	2.00	3.33
d	466	1.17	3.90
d	502	1.16	4.64
d	551	0.973	6.49
d	617	0.853	8.53
e	669	0.673	4.49
d	713	0.646	6.46
e	726	0.753	5.02
e	779	0.753	5.02
d	872	0.590	5.90
d	1087	0.462	9.24
e	1123	0.302	6.03
f	1198	0.311	6.23
f	1248	0.248	4.96

a F. Moseley and J. C. Robb, *Proc. Roy. Soc.*, **A243**, 130 (1957). *b* A. Shepp, *J. Chem. Phys.*, **24**, 939 (1956); G. B. Kistiakowsky and E. K. Roberts, *ibid.*, **21**, 1637 (1953); R. Gomer and G. B. Kistiakowsky, *ibid.*, **19**, 85 (1951). *c* R. E. March and J. C. Polanyi, *Proc. Roy. Soc.*, **A273**, 360 (1963). *d* K. U. Ingold, I. H. S. Henderson, and F. P. Lossing, *J. Chem. Phys.*, **21**, 2239 (1953); K. U. Ingold and F. P. Lossing, *ibid.*, **21**, 1135 (1953). *e* F. P. Lossing and A. W. Tickner, *ibid.*, **20**, 907 (1952). *f* F. P. Lossing, K. U. Ingold, and A. W. Tickner, *Discussions Faraday Soc.*, **14**, 34 (1953).

(20) D. E. Hoare and G. S. Pearson, *Advan. Photochem.*, **3**, 83 (1964).

(21) J. Heicklen, *J. Amer. Chem. Soc.*, **81**, 3863 (1959); J. Heicklen and W. A. Noyes, *ibid.*, **81**, 3858 (1959); R. E. Rebbert and P. Ausloos, *ibid.*, **86**, 4803 (1964); C. W. Larson and H. E. O'Neal, *J. Phys. Chem.*, **70**, 2475 (1966).

(22) D. E. Hoare and D. A. Whytock, *Can. J. Chem.*, **45**, 865 (1967); A. Cohen, *J. Chem. Phys.*, **47**, 3828 (1967).

(23) (a) R. B. Cundall and A. S. Davies, *Proc. Roy. Soc.*, **A290**, 563 (1966); (b) G. S. Pearson, *J. Phys. Chem.*, **67**, 1686 (1963).

(24) L. Endrenyi and D. J. LeRoy, *ibid.*, **71**, 1334 (1967), have recently measured and reviewed the Arrhenius parameters for reaction 2. We obtain excellent agreement with their values, which were obtained under conditions where energy-transfer effects are unimportant.

(25) F. W. Schneider and B. S. Rabinovitch, *J. Amer. Chem. Soc.*, **84**, 4215 (1962).

(26) E. Gorin, *Acta Physiocochim. URSS*, **6**, 691 (1938); H. S. Johnston and P. Goldfinger, *J. Chem. Phys.*, **37**, 700 (1962).

(27) J. O. Hirschfelder, C. F. Curtiss, and R. B. Bird, "Molecular Theory of Gases and Liquids," John Wiley and Sons, New York, N. Y., 1965.

(28) B. H. Mahan, *J. Chem. Phys.*, **32**, 362 (1960).

Analysis of Proton Magnetic Resonance Spectra of *trans*-2,5-Dimethylpiperazine

and Its Hydrochlorides.   Effect of Amine Substituents on

Chemical Shifts and Coupling Constants[1]

by J. L. Sudmeier

Contribution No. 2109, Department of Chemistry, University of California, Los Angeles, California   90024
(Received September 12, 1967)

Proton magnetic resonance spectra of *trans*-2,5-dimethylpiperazine, *trans*-2,5-dimethylpiperazine mono-hydrochloride, and *trans*-2,5-dimethylpiperazine dihydrochloride are recorded at 60 and 100 MHz in aqueous solution. All spectra are of the $ABCX_3$ type and are fully analyzed with the aid of computers. The axial and equatorial protons undergo nearly equal protonation shifts. Surprisingly, the vicinal-coupling constants exhibit positive shifts with increasing substituent electronegativity, and the geminal-coupling constants exhibit negative shifts. That is, the vicinal-coupling constant of the ring protons is larger for the hydrochlorides, contrary to the usual trend. The geminal-coupling constant of the methylene protons is smaller (more negative) for the hydrochlorides, suggesting that the β substituent effect is greater than the opposing α substituent effect in these compounds.

It is well known that protonation of a basic site in a molecule leads to downfield chemical shifts for neighboring –CH protons.[2] The magnitude of the protonation shift depends upon (1) the nature of the substituent, (2) the distance (number of bonds) from the substituent,[3] and (3) the spatial relationship (*e.g.*, dihedral angle) of the substituent and the particular –CH proton. The primary cause of protonation shifts is generally the increase in electronegativity of the protonated substituent, and this satisfactorily accounts for factors 1 and 2. Protonation shifts which depend upon the dihedral angle, however, are caused either by an angular dependence of the electron-withdrawing effect or by changes in the local anisotropic magnetic shielding resulting from protonation.

The compounds studied in the present paper, *trans*-2,5-dimethylpiperazine (P), *trans*-2,5-dimethylpiperazine monohydrochloride (HP$^+$), and *trans*-2,5-dimethylpiperazine dihydrochloride (H$_2$P^{2+}) exist almost exclusively (greater than 98%)[4] in the diequatorial conformation I. In P, the conformation of electron

I
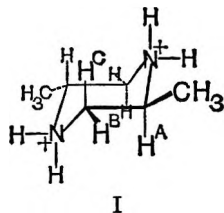
pairs is uncertain,[5] as will be discussed later.

A knowledge of protonation shifts is essential in studies of microscopic acid–base equilibria,[3,6] whose results depend heavily upon the assumed protonation-shift values.

Considerable interest has been shown in the effect of substitutents on coupling constants.[7] For a large number of compounds, the vicinal-coupling constants are inversely proportional to the sum of the substituent-atom electronegativities,[8] in agreement with the valence-bond theory of vicinal coupling.[9]

In studies of rotational isomerism of α-amino acids at various pH values, the effect of amine substituents on the coupling constants is of primary importance. Calculation of residence times depends upon assumed values of J_t and J_g, the *trans*- and *gauche*-vicinal-coupling constants. Pachler,[10] for example, showed

(1) This research was supported by National Institutes of Health Grant No. 1-R01-AM10889-01.

(2) E. Grunwald, A. Loewenstein, and S. Meiboom, *J. Chem. Phys.*, **27**, 630, 641 (1957).

(3) See, for example, J. L. Sudmeier and C. N. Reilley, *Anal. Chem.*, **36**, 1698 (1964).

(4) E. L. Eliel, N. L. Allinger, S. J. Angyal, and G. A. Morrison, "Conformational Analysis," Interscience Publishers, Inc., New York, N. Y., 1965.

(5) (a) M. Aroney and R. J. W. LeFevre, *J. Chem. Soc.*, 3002 (1958); N. L. Allinger and J. C. Tai, *J. Amer. Chem. Soc.*, **87**, 1227 (1965); N. L. Allinger, J. G. D. Carpenter, and F. M. Karkowski, *ibid.*, **87**, 1232 (1965); J. B. Lambert and R. G. Keske, *ibid.*, **88**, 620 (1966); E. L. Eliel and M. C. Knoeber, *ibid.*, **88**, 5347 (1966); (b) J. B. Lambert, R. G. Keske, R. E. Carhart, and A. P. Jovanovich, *ibid.*, **89**, 3761 (1967).

(6) See, for example, (a) A. Loewenstein and J. D. Roberts, *ibid.*, **82**, 2705 (1960); (b) D. E. Leyden and D. B. Walters, 152nd National Meeting of the American Chemical Society, New York, N. Y., Sept 1966.

(7) For a recent review, see A. A. Bothner-By, "Advances in Magnetic Resonance," Vol. I, J. S. Waugh, Ed., Academic Press Inc., New York, N. Y., 1965.

(8) R. J. Abraham and K. G. R. Pachler, *Mol. Phys.*, **7**, 165 (1964).

(9) M. Karplus, *J. Amer. Chem. Soc.*, **85**, 2870 (1963); H. S. Gutowsky, M. Karplus, and D. M. Grant, *J. Chem. Phys.*, **31**, 1278 (1959).

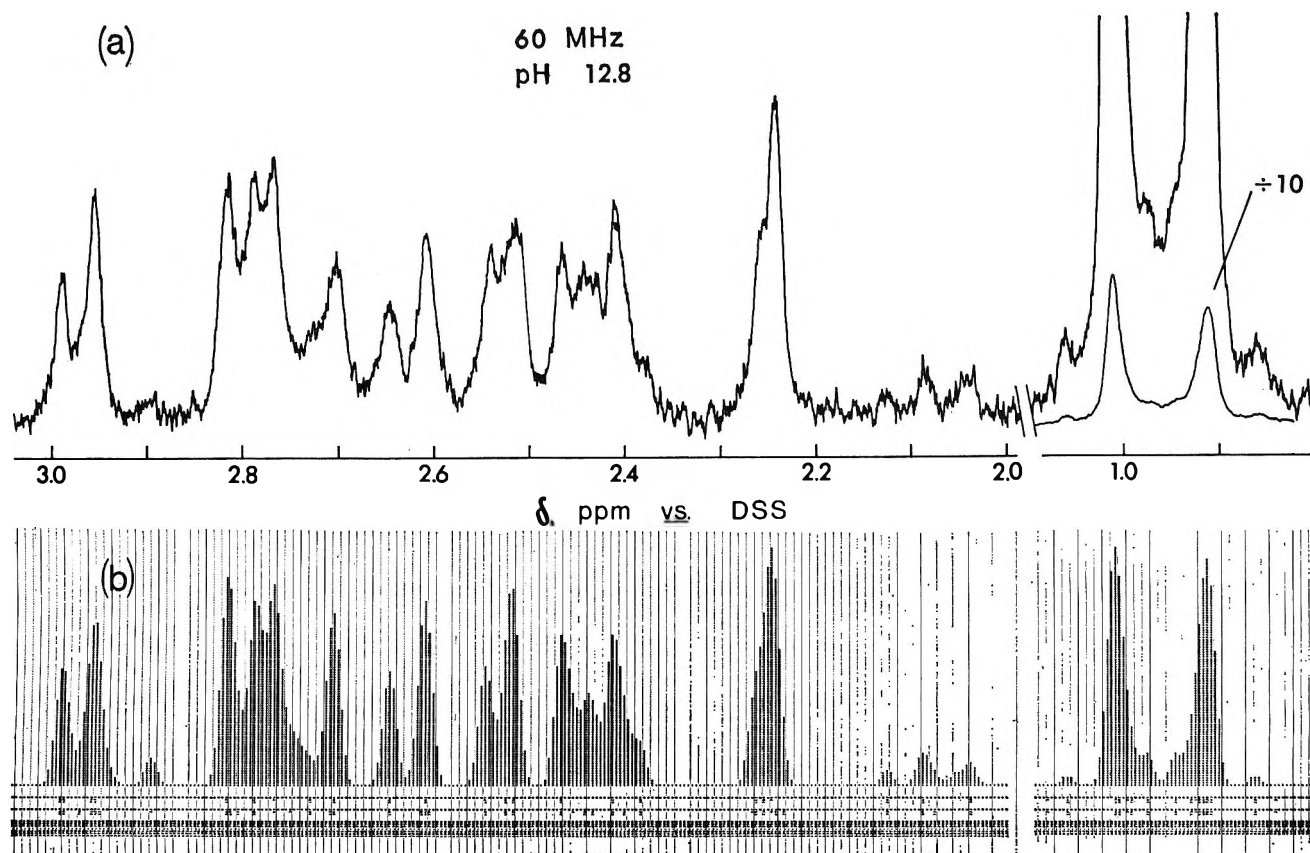(10) K. G. R. Pachler, *Spectrochim. Acta*, **20**, 581 (1964).

Figure 1. Nuclear magnetic resonance spectra of *trans*-2,5-dimethylpiperazine (P) at 60 MHz: (a) observed;   (b) calculated.

that J_t = 13.56 cps and J_g = 2.60 cps are justifiable values for amino acids in alkaline solution, and that residence times could be calculated on this basis. Knowledge of these coupling constants at lower pH values, however, is lacking. The compounds employed in the present study permit the observation of amine substituent effects in the absence of changes in rotamer population.

The molecular orbital treatment of Pople and Bothner-By[11] for geminal coupling predicts that the values of geminal-coupling constants, J_{gem}, should be directly proportional to the electronegativity of an α substituent.   For β substituents, a dependence on the dihedral angle is predicted, such that as the electronegativity of substituent X increases, J_{gem} becomes larger (more positive) in II, and smaller (more negative)

in III.   The positive shift for a given substituent in II, however, is approximately one-half as large as the negative shift in III, so that in rotationally averaged compounds the net effect is negative.

Protonation of a secondary amine group causes an appreciable increase[12] in electronegativity, which is easily achieved by decreasing the solution pH.

Experimental Section

trans-2,5-Dimethylpiperazine was obtained from Aldrich Chemical Co. and was recrystallized from benzene. A solution of approximately 0.4 M was prepared using deionized water. This solution was passed through a column of Bio-Rad Chelex 100 chelate resin to remove any paramagnetic metals, which could broaden the spectral lines. Potentiometric titration with 4 M HCl yielded values of pK_2 = 10.20 and pK_1 = 5.85. The pH values of solutions corresponding to P, HP$^+$, and H$_2$P^{2+} are 12.8, 7.7, and 1.3, respectively.

The spectra at 60 MHz were recorded using a Varian A-60 nmr spectrometer. All samples were run at probe temperature ($\sim$44°). A sweep width of 100 cps (1 cm = 2 cps) and a scan rate of 0.2 cps/sec were employed. A radiofrequency field strength of 0.02 mG gave optimal signal-to-noise without saturation. Chemical shifts were measured relative to internal t-butyl alcohol but reported relative to 2,2-dimethyl-2-silapentane 5-sulfonic acid, sodium salt (DSS), whose methyl resonance lies 1.233 ppm upfield of t-butyl alco-

(11) J. A. Pople and A. A. Bothner-By, *J. Chem. Phys.*, **42**, 1339 (1964).

(12) Values of 2.85 and 3.03, respectively, on the group-electronegativity scale of Cavanaugh and Dailey (J. R. Cavanaugh and B. P. Dailey, *ibid.*, **34**, 1099 (1961)) derived from data from aqueous solutions given in ref 3. Primary and tertiary amine substituents yield similar values: -NH₂, 2.86; -⁺NH₃, 3.01; -NR₂, 2.81; and -⁺NHR₂, 3.09.
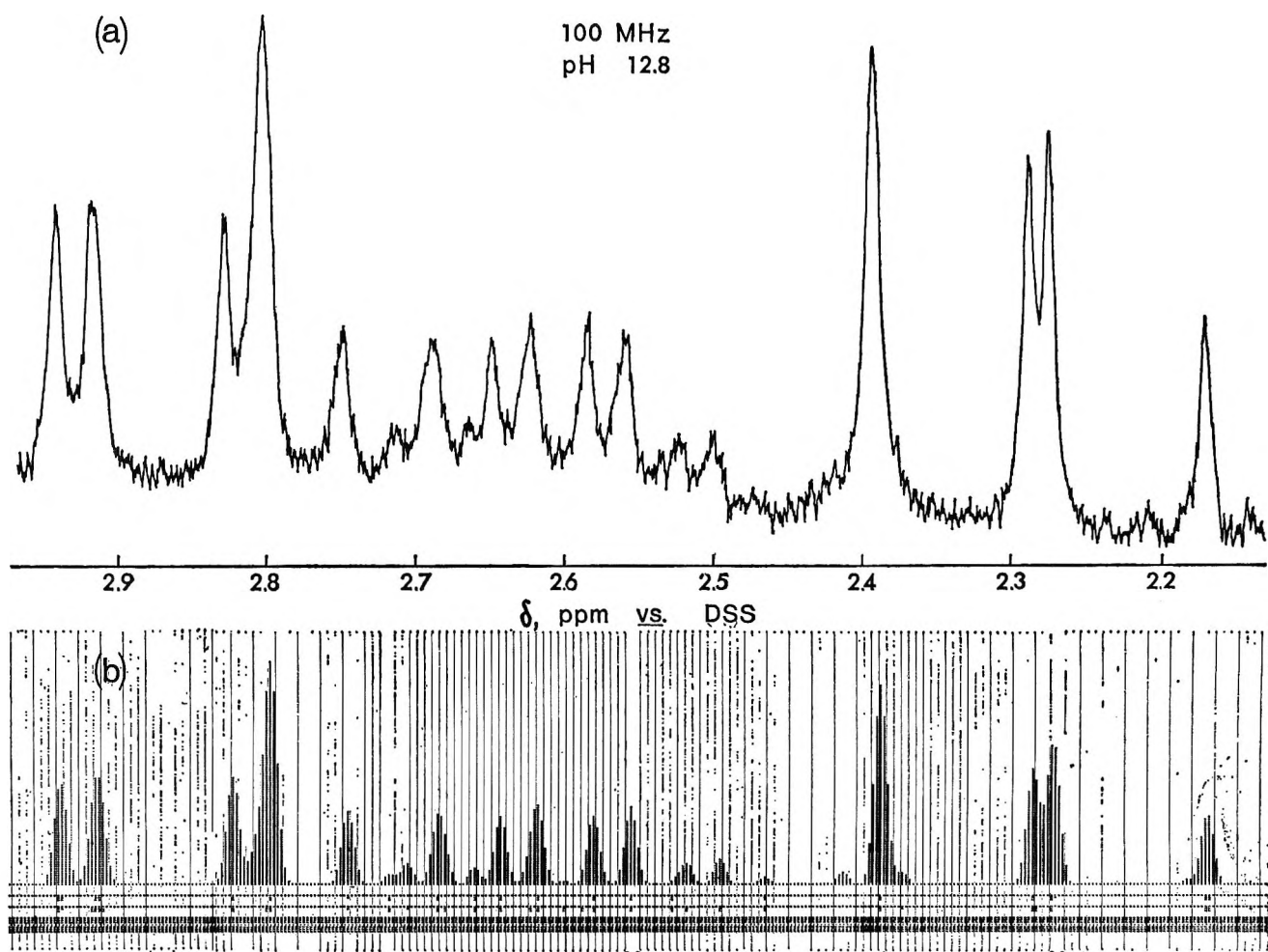
Figure 2.   Nuclear magnetic resonance spectra of *trans*-2,5-dimethylpiperazine (P) at 100 MHz: (a) observed;   (b) calculated.

hol. Sweepwidth linearity was checked after recording each spectrum, and any deviation from correct linearity (that producing the CHCl₃ proton resonance at 435.5 cps downfield of TMS (tetramethylsilane) on the 100-cps sweep width using offset) was corrected for. Spectral-line positions are estimated accurate to ±0.2 cps. Removal of dissolved oxygen produced negligible line sharpening and was omitted thereafter. The 100-MHz spectra were recorded on a Varian HA-100 nmr spectrometer, and linearities were checked by the usual audio side-band method. Computation of spectra was performed on the IBM 7094,[13] using LAOCOON II[14] with modifications by Maddox[15] (combining parts I and II) and by the present author (plot subroutine).

Results

P exists in greater than 98% abundance as the di-equatorial conformer shown in I for H₂P²⁺. This structure exhibits C_i symmetry, with pairs of equivalent methyl groups, methine protons, and two methylene protons related by reflection through the center of symmetry. Because of rapid exchange, the –NH proton resonance merges with that of water, and the

–NH and –CH protons are effectively decoupled[2] under the conditions reported herein.

The nmr spectrum of P at 60 MHz is shown in Figure 1a. ABCX₃ spectra for 1,2-disubstituted propaneg have been reported.[16] The high-field doublet, containins an area equal to that of the low-field portion, is readily assigned to the methyl protons in P, and the low-field portion is assigned to the methine and methylene protons labeled A, B, and C in I. The spectral lines in Figure 1a, like those in all remaining figures, are somewhat broad, probably due to quadrupole relaxation by N¹⁴ and/or to unresolved long-range coupling through the nitrogen atoms.

The ABC portion of the nmr spectrum of P at 100 MHz, shown in Figure 2a, is the easiest to interpret by inspection. The four-line pattern at high fields consists roughly of doublets of doublets with repeated

(13) We thank the UCLA Computing Facility for generously providing computer time and programming assistance.

(14) S. Castellano and A. A. Bothner-By, *J. Chem. Phys.*, **41**, 3863 (1964).

(15) M. Maddox, Ph.D. Thesis, University of California, Los Angeles, Calif., 1966.

(16) H. Finegold, *Proc. Chem. Soc.*, 213 (1962).

spacings of ~12 and ~10 cps. One of these values must arise from geminal coupling, and the other from *trans*-vicinal coupling. The only proton which could be so coupled is proton C in structure I. This assignment is further supported by the high-field chemical shift of this proton, characteristic of axial protons such as C. The proton-B resonance is also expected to consist of doublets of doublets, split by the geminal coupling constant of ~10 or ~12 cps (absolute value) and by a smaller *gauche*-vicinal-coupling constant. The four lines at lowest field strengths fit this description, exhibiting repeated spacings of ~12 and ~3 cps, and are thus assigned to proton B. Both proton B and C are four bonds removed from the methyl protons and are thus not expected to couple strongly with them. The proton-A resonance is expected to be split into quartets by the three vicinal methyl protons, with a coupling constant of ~6 cps, the separation of the methyl doublet peaks. In addition, the proton-A resonance should be split into doublets by proton C with the *trans*-vicinal-coupling constant, now known to be ~10 cps, and further split into doublets by proton B with the *gauche*-vicinal-coupling constant of ~3 cps, and is thus expected to be quite complex.

The first stage in the computation of spectral parameters with LAOCOON II is computation of a trial spectrum, using only part I (with plot output). The use of known spectral parameters from analogous compounds is invaluable in making the first approximations. For example, the signs of the geminal- and vicinal-coupling constants in similar compounds are opposite.[17] Although this condition was assumed for the initial computations, the excellent fit of spectra at both 60 and 100 MHz confirms the relative signs of the coupling constants.

The parameters were then refined by trial and error until 1:1 matching of computed and observed lines was possible. Typically, 110 calculated lines, many of which are triply degenerate, were matched out of the total of 972 calculated lines—the unmatched lines generally being very low in intensity. The second stage of the computation utilizes both parts I and II of LAOCOON II, in which the program optimizes all parameters so that a "best fit" of calculated and observed lines is obtained by least squares. Additional refinement at the second stage was generally needed, as unusually large deviations revealed the presence of improper assignments.

Table I gives the best parameters obtained for P, HP+, and H₂P²⁺. The average and root-mean-square errors in the fit of observed and calculated lines and the probable errors in the individual parameters were always less than and hence limited by the error (estimated ±0.2 cps) in determining the positions of these rather broad lines.

Initially, the unresolved long-range couplings due to J_{BX} and J_{CX} were set equal to zero. At a later stage,

Table I: Chemical Shifts and Coupling Constants of *trans*-2,5-Dimethylpiperazine and Its Hydrochlorides

	P (pH 12.8)	HP+ (pH 7.7)	H₂P²⁺ (pH 1.3)
δ_A (±0.003), ppm	2.644	3.103	3.693
δ_B (±0.003), ppm	2.859	3.248	3.728
δ_C (±0.003), ppm	2.293	2.700	3.239
δ_X (±0.003), ppm	0.960	1.180	1.422
J_{AB} (±0.2), cps	2.9	3.0	3.4
J_{AC} (±0.2), cps	10.8	11.5	12.2
J_{AX} (±0.2), cps	6.4	6.2	6.1
J_{BC} (±0.2), cps	−12.5	−13.5	−14.2
J_{BX} (±0.2), cps	−0.1	−0.1	−0.2
J_{CX} (±0.2), cps	−0.2	−0.3	−0.3

these restrictions were removed, and small negative values resulted.

Figures 1b and 2b show computed spectra of P at 60 and 100 MHz obtained from part I with the parameters given in Table I, with plot output, using an interval of 0.25 cps and a peak half-width of 1.00 cps. The methyl resonance in Figure 1b is arbitrarily reduced in scale relative to the remainder of the spectrum.

Figures 3a and 4a give the observed spectra of HP+ and H₂P²⁺ at 100 MHz. Similar procedures were employed in calculating the parameters shown in Table I. Figures 3b and 4b give the computed spectra of HP+ and H₂P²⁺ at 100 MHz, using parameters in Table I. The observed and calculated spectra of HP+ and H₂P²⁺ (not shown) also exhibit good agreement.

Discussion

Chemical Shifts. The protonation shifts occur in two unequal steps, with the change produced in going from P to HP+ being ~20% smaller than those produced in going from HP+ to H₂P²⁺. The magnitudes of these protonation shifts, in order of decreasing pH values, are: for proton A, 0.46 and 0.59 ppm; for proton B, 0.39 and 0.48; for proton C, 0.41 and 0.53; and for proton X, 0.22 and 0.24. Unsubstituted piperazine exhibits the same effect with corresponding values of 0.40 and 0.48 ppm,[3] the reason for which is unclear. The total protonation shift of A, 1.05 ppm, is larger than that of protons B or C, in agreement with the larger substituent effects often found for methine protons. The total protonation shifts of B and C, 0.87 and 0.94 ppm, are almost identical, indicating negligible dependence of the dihedral angle of the substituents.

The chemical-shift difference $\Delta\delta_{BC}$ is 0.57 ppm in P, 0.55 ppm in HP+, and 0.49 ppm in H₂P²⁺. According to Lambert, *et al.*,[5b] a difference in the chemical shifts of axial and equatorial protons, $\Delta\delta_{ae}$, of 0.40–0.50 ppm in piperidine derivatives indicates that the lone

(17) J. W. Emsley, J. Feeney, and L. H. Sutcliffe, "High Resolution Nuclear Magnetic Resonance Spectroscopy," Vol. 1, Pergamon Press Ltd., New York, N. Y., 1965, pp 172–174.
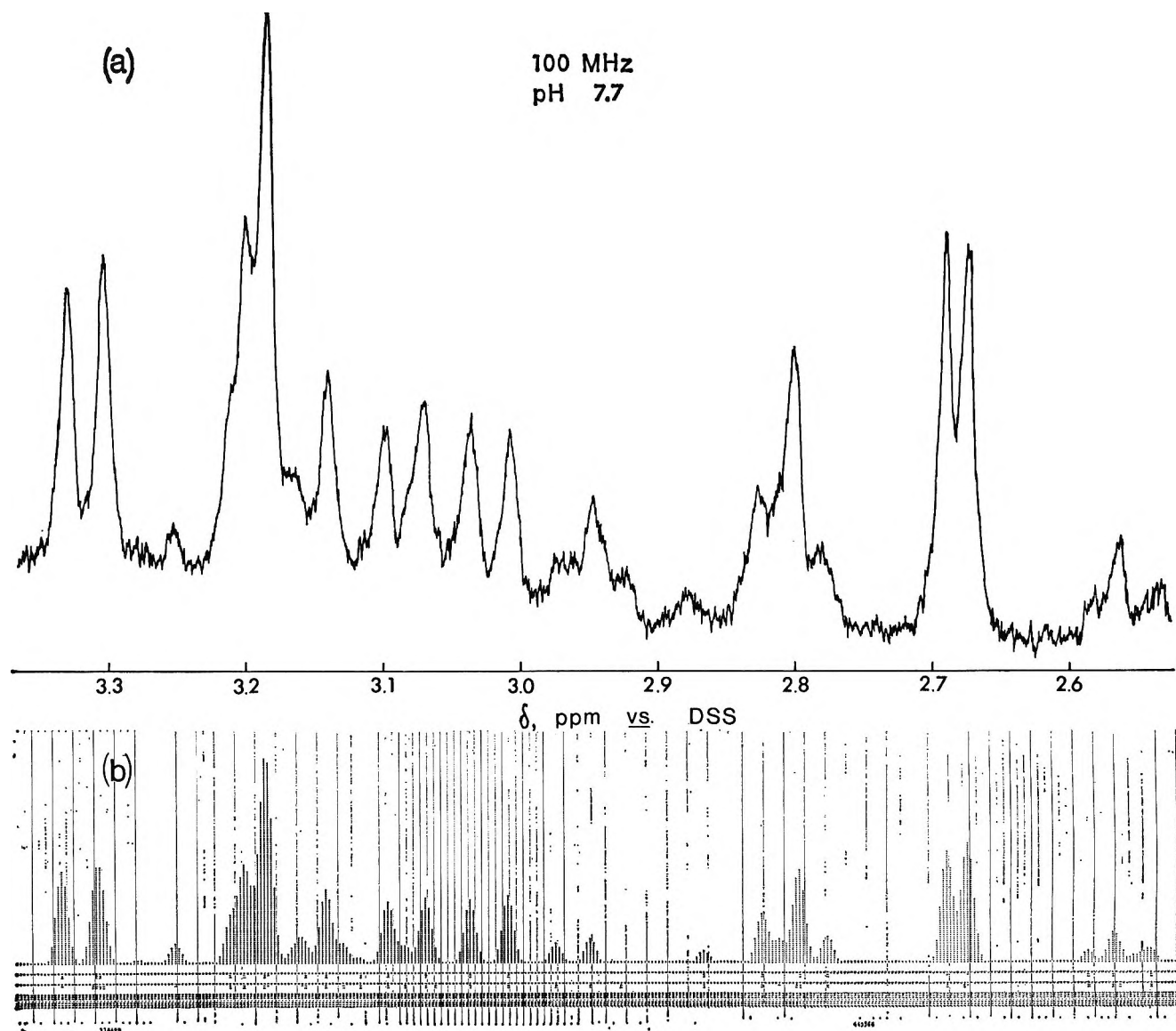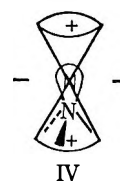
Figure 3. Nuclear magnetic resonance spectra of *trans*-2,5-dimethylpiperazine monohydrochloride (HP$^+$) at 100 MHz: (a) observed; (b) calculated.

pair is equatorial, and a difference of 0.80–0.94 ppm indicates that the lone pair is axial. However, the situation is more complex in piperazine derivatives, apparently because of deshielding of axial protons by axial lone pairs on the β nitrogen. This 1–3 deshielding interaction is deduced from the value of $\Delta\delta_{ae} = 0.63$ ppm for N,N'-dimethylpiperazine at low temperatures.[18] The lone pairs in this compound are predominantly axial, and the α substituent is expected to contribute as much as 0.94 to $\Delta\delta_{ae}$, the value found in N-methylpiperidine at low temperatures. The decrease of $\sim$0.3 ppm is attributed to the deshielding of axial protons by the axial β lone pairs. Because the shielding contributions of axial lone pairs on the α and β nitrogen atoms in piperazine derivatives are opposite, $\Delta\delta_{ae}$ tends to be independent of the lone-pair conformation. By analogy with recent findings

for piperidine,[4b] however, the lone pairs in P are probably largely equatorial.

The anisotropic shielding of nitrogen lone pairs discussed here can be represented by the model, IV, where the plus sign indicates increased magnetic shielding and the minus sign indicates deshielding.[19,19a]

IV

(18) R. K. Harris and R. A. Spragg, *Chem. Commun.*, 314 (1966).

(19) For a similar derivation of a carbonyl group shielding model, see G. J. Karabatsos, G. C. Sonnichsen, N. Hsi, and D. J. Fenoglio, *J. Amer. Chem. Soc.*, **89**, 5067 (1967).
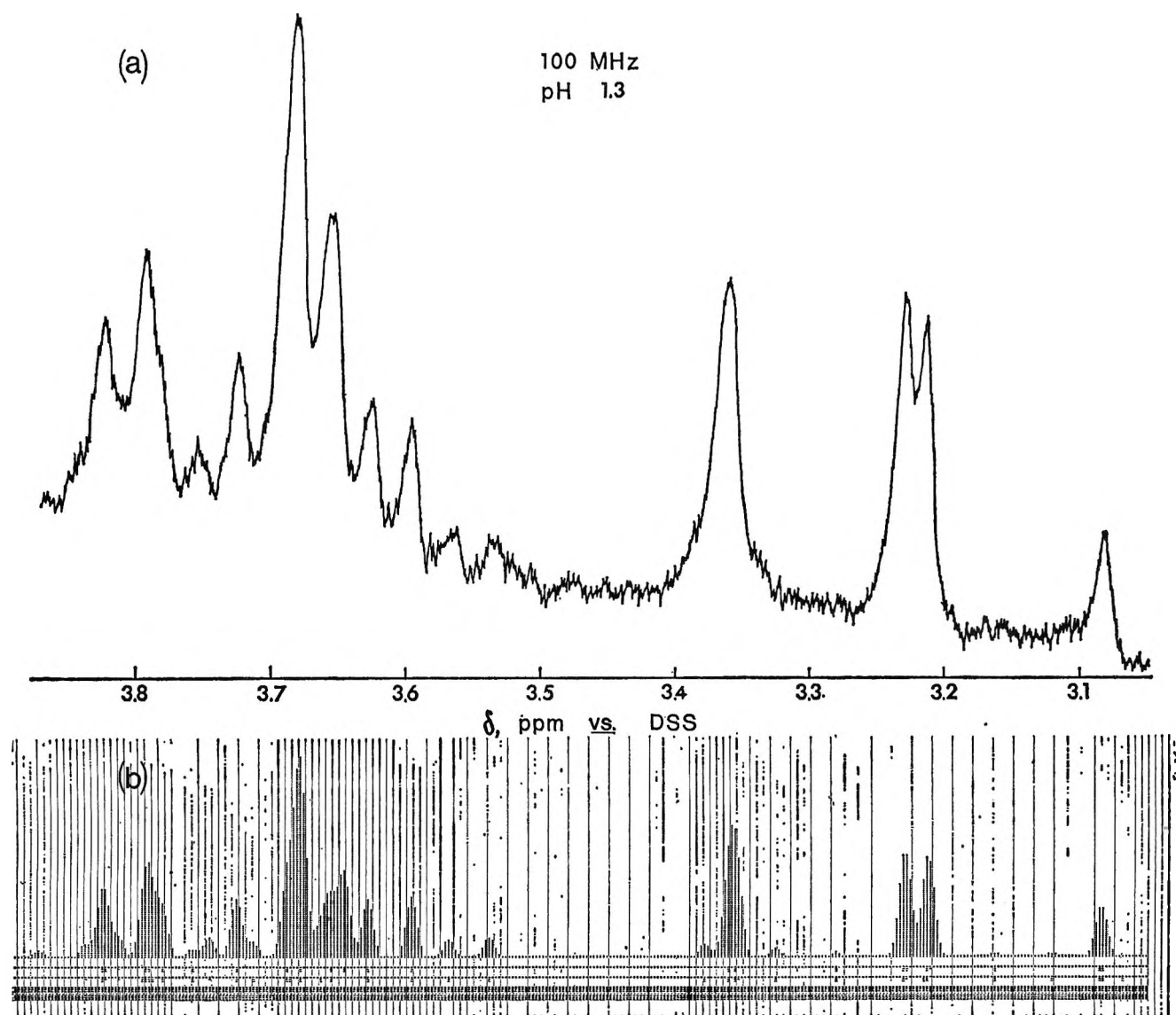
100 MHz
pH 1.3

(a)

(b)

δ, ppm vs. DSS

Figure 4. Nuclear magnetic resonance spectra of trans-2,5-dimethylpiperazine dihydrochloride (H_2P^{2+}) at 100 MHz: (a) observed; (b) calculated.

Vicinal-Coupling Constants. The vicinal-coupling constants J_{AB} and J_{AC} are almost certainly positive[7,17] and increase in going from P to H_2P^{2+}. This trend is contrary to that predicted by valence-bond theory,[9] which states that vicinal-coupling constants should be inversely proportional to the substituent electronegativities.

A possible explanation for this anomalous substituent effect may be found in ring deformations caused either by rehybridization of the nitrogen atoms with protonation or by electrostatic repulsion between the positive charges in H_2P^{2+}. The latter cause can apparently be ruled out, being inconsistent with the monotonic trend in coupling constants of the series P, HP⁺, and H_2P^{2+}.

Rehybridization of the nitrogen atoms with protonation places greater s character in the C–N bonds and tends to (1) increase the C–N–C bond angle,[20] (2) de-

crease the ring N–C–C bond angles, (3) slightly decrease the H–C–C bond angles (ring carbon atoms),[21] and (4) decrease ring H–C–C–H dihedral angles. Factor 3 argues in favor of the observed increase in the vicinal-coupling constants and factor 4 argues in favor of the increase in J_{AB} and against the increase in J_{AC}. Thus if factor 3 is predominant, it would account for the anomalous substituent effect.

Recent nmr studies,[20] however, indicate that the extent of nitrogen rehybridization is only a few per cent

(19a) NOTE ADDED IN PROOF. This model agrees with recent chemical shift data from aziridines: H. Saitô, K. Nukada, T. Kobayashi, and K. Morita, *J. Amer. Chem. Soc.*, 89, 6605 (1967).

(20) G. Binsch, J. B. Lambert, B. W. Roberts, and J. D. Roberts, *ibid.*, 86, 5564 (1964).

(21) Provided that the orthogonality rules are obeyed (*e.g.*, see K. Mislow, "Introduction to Stereochemistry," W. A. Benjamin, Inc., New York, N. Y., 1965, p 17), the H–C–C bond angle decreases ~0.5° per increase or decrease of ~9° in the N–C–C bond angles.

Table II: Spectral Parameters of Some α-Amino Acids

Compound	n	J_{BC}, cps	J_{AB}, cps	J_{AC}, cps	δ_A, ppm	δ_B, ppm	δ_C, ppm	Ref
Phenylalanine[a]	0	−13.45	5.34	7.75	3.47	3.00	2.27	f
Phenylalanine	1	−14.50	5.14	8.00	3.97	3.27	3.10	f
Phenylalanine	0	−13.7	5.5	7.8	0.000	−0.482	−0.686	g
Phenylalanine	2	−14.7	5.6	7.7	0.000	−1.014	−1.137	g
Cystine[b]	0	−13.7	4.8	7.7	0.000	−0.448	−0.662	g
Cystine	4	−15.4	4.2	8.2	0.000	−1.035	−1.175	g
Aspartic acid[c]	0	−15.4	3.8	9.9	3.56	2.63	2.28	h
Aspartic acid	0.5[d]	−17.0	3.5	8.3	3.78	2.73	2.53	h
Aspartic acid[b]	0	−15.5	4.1	9.7	0.000	−0.927	−1.252	g
Aspartic acid	3	. . .	5.4	5.4	0.000	−1.258	−1.258	g
Cysteine[e]	0	−12.8	3.3	9.5	−3.26	−3.55	−3.92	i
Cysteine	0.5	−13.2	3.6	8.7	−3.05	−3.52	−3.79	i
Cysteine	1.0	−13.9	3.9	8.2	−2.83	−3.49	−3.64	i
Cysteine	2.0	. . .	5.1	5.1	−2.53	−3.47	−3.47	i

[a] Chemical shifts converted to ppm vs. DSS by the present author (t-butyl alcohol set at 1.233 ppm vs. DSS). For all values above, δ increases with decreasing field strength. [b] Chemical shifts converted to ppm vs. δ_A by the present author. [c] All parameters obtained by first-order analysis and thus are approximate. Chemical shifts obtained by interpolation of graphical data and reported vs. DSS. [d] Value of n approximated by the present author, using graphical interpolation. [e] Chemical shifts (vs. external benzene) converted to ppm by the present author. Bulk-susceptibility corrections were not made. [f] J. R. Cavanaugh, J. Amer. Chem. Soc., **89**, 1558 (1967). [g] K. G. R. Pachler, Spectrochim. Acta., **19**, 2085 (1963). [h] F. Taddei and L. Pratt, J. Chem. Soc., 1553 (1964). [i] R. B. Martin and R. Mathur, J. Amer. Chem. Soc., **87**, 1065 (1965).

in s character between NH_3 and $NH_4{}^+$ ion. The same result for secondary amines is evidenced by the C–N–C bond angles from the following electron and X-ray diffraction data (dimethylamine (g), 111 $\pm$ 3°;[22] and piperidine hydrochloride (s), 112.3°) which lies well within the range of internal angles (109.8 to 113.4°) in this compound.[23]

Geminal-Coupling Constants. The geminal-coupling constants are almost certainly negative[7,17] and decrease from −12.5 to −13.5 to −14.2 cps in P, HP^+, and H_2P^{2+}. The methylene groups are each situated between two amine substituents, one directly attached (α) and one a carbon–carbon single bond removed (β). Because the theory of geminal coupling[11] states that α substituent effects are positive and β effects in this case are negative, our results tend to indicate that the β effect is greater than the α effect, as previously suggested for 1,2-disubstituted ethanes and propanes.[8]

Ring deformations due to nitrogen rehybridization with protonation tend to decrease the internal N–C–C angle and increase the geminal H–C–H angle. The resultant increase in s character of the C–H bonds tends to increase the value of J_{BC} rather than decrease its value as observed.

It is quite possible that the α substituent effect for amines is anomalous in the sense that back-donation of nonbonding electrons on nitrogen atoms may have a greater effect than the increased inductive effect of protonated nitrogen atoms. That is, withdrawal of σ

electrons from the symmetric bonding orbital as the nitrogen is protonated may be more than compensated by the loss of nonbonding electrons back-donated into the antisymmetric bonding orbital by the unprotonated nitrogen atom, with the result that nitrogen protonation could yield a negative α substituent effect. At present, there is no literature data on this point.

However, there is independent evidence (Table II) to support the contention that the β inductive effect alone is sufficient to account for a decrease in J_{BC} of the magnitude (1.7 cps) observed in going from P to H_2P^{2+}. Data for phenylalanine and cystine in Table II show that J_{BC} in these compounds undergo decreases of 1.0 and 1.7 cps, respectively, on protonation of the amine group. The labeling of protons A, B, and C is given in V, which is the most abundant rotamer in both alkaline and neutral solutions.

V
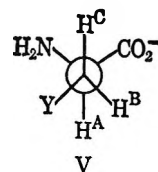
For some of the comparisons in Table II, the value of n, the number of equivalents of H^+ added to the fully unprotonated form of the compound, changes rather abruptly (e.g., from 0–4 in cystine), indicating pro-

(22) P. W. Allen and L. E. Sutton, Acta Crystallogr., **3**, 46 (1950).
(23) P. C. Rerat, ibid., **13**, 72 (1960).

tonation of carboxylate and other groups in addition to amine groups. Nearly all the observed change in J_{BC}, however, is caused by the amine protonation alone, shown, for example, in the data for phenylalanine. The absence of significant changes in rotamer populations, particularly in the case of phenylalanine, is shown by the constancy of the vicinal-coupling constants. (Note also the absence of positive changes in the amino acid vicinal-coupling constants with increased protonation, as were found in the present study.) When 1 equiv of H^+ is added to cysteine, a decrease of 1.1 cps in the geminal-coupling constant is observed. The first equivalent of H^+ added to cysteine protonates not only amino groups but also mercaptide groups with roughly equal distributions.[6b,24] Once again, the posi-

tive contribution of increasing the electronegativity of the α substituent ($-S^-$ to $-SH$) must be negligibly small compared to the positive contribution of increasing the electronegativity of the β substituent ($-NH_2$ to $-^+NH_3$). Some redistribution in rotamer populations may be indicated by the small changes in the vicinal-coupling constants in cysteine from $n = 0$ to $n = 1$, but rotamer V undoubtedly remains the predominant one.

(24) D. P. Wrathall, R. M. Izatt, and J. J. Christensen, *J. Amer. Chem. Soc.*, 86, 4780 (1964).

Solutions of N-Substituted Amino Acids. III. The Influence of Solvent on the Tautomeric Equilibrium

by David A. Horsma[1] and Charles P. Nash

Department of Chemistry, University of California, Davis, California 95616 *(Received September 15, 1967)*

Dielectric constant measurements have been made on solutions of N,N-di-*n*-butyl-β-aminopropionic acid in seven nonaqueous solvents. The results lead to dipole moments for the monomeric acid which vary from 6.3 D in benzene to 12 D in methanol. Intermediate values are interpreted on the basis of shifts in the equilibrium between the zwitterion and the classical tautomers of the amino acid. The equilibrium constants thus obtained are compared with the predictions of continuum electrostatic theory and the deviations are rationalized on the basis of specific solute–solvent interactions.

Introduction

It has been accepted for some 30 years that two tautomeric forms of an amino acid, neither of which carries a net charge, can exist in solution in equilibrium. In aqueous solutions of naturally occurring aliphatic amino acids, the dipolar ion (zwitterion) tautomer outnumbers the "chargeless" form by a factor of about 1 million. In alcohol–water mixtures, however, the ratio may be reduced to a few hundred.[2]

It is evident that a study of this simple tautomerization reaction in media having different macroscopic dielectric constants would be a worthwhile test of the extent to which essentially electrostatic processes contribute to the over-all free energy change for a model chemical reaction. Spectroscopic investigations by Barrow[3] and Cook[4] have shown, in a qualitative way, that N,N-dialkylated amino acids are soluble in a wide range of solvents and that the tautomeric equi-

librium can be made to shift within readily observable limits. It has also been shown that in nonpolar media, dimeric and higher aggregates, in which proton transfers also occur, form very readily.[4,5]

The present paper reports dielectric constant measurements on solutions of N,N-di-*n*-butyl-β-aminopropionic acid in seven solvents over concentration ranges in which unimolecular solute species dominate. The apparent dipole moments thus obtained are interpreted in terms of solvent effects on the tautomeric equilibrium.

(1) NDEA Predoctoral Fellow 1962–1965.

(2) J. T. Edsall and M. H. Blanchard, *J. Amer. Chem. Soc.*, 55, 2337 (1933).

(3) G. M. Barrow, *ibid.*, 80, 86 (1958).

(4) D. B. Cook, Ph.D. Thesis, University of California, Davis, Calif., 1965.

(5) C. P. Nash, E. L. Pye, and D. B. Cook, *J. Phys. Chem.*, 67, 1642 (1963).

Experimental Section

Solvents. The solvents employed were acetonitrile, benzene, chloroform, ethylene chloride, methylene chloride, methanol, and nitromethane. In each case commercial materials (Eastman White Label or Baker and Adamson reagent grade) were purified by accepted procedures, pains being taken to exclude moisture.[6] In each case the physical properties of the purified materials agreed with values cited in standard compendia to within ±0.0007 g/cm³ for the density and ±0.0004 for the refractive index.

Solute. N,N-Di-*n*-butyl-β-alanine (NDBBA) was prepared by adding 100 g of ethyl acrylate slowly to a cooled solution of di-*n*-butylamine (140 g) in absolute ethanol (180 ml). The reaction mixture was stored for 1 week in the dark, after which the ethyl ester of NDBBA was recovered by fractional distillation at reduced pressure. The ester was refluxed with distilled water for 48 hr, after which three-fourths of the solvent was stripped at reduced pressure. The concentrated mixture was shaken with diethyl ether to remove unhydrolyzed ester, the remaining solvent was stripped, and the crude solid acid was recrystallized repeatedly, first from ether and finally from cyclohexane. (*Anal.* Calcd for $C_{11}H_{23}O_2N$: C, 65.7; H, 11.5; N, 7.0. Found: C, 65.5; H, 11.3; N, 6.9).

Dielectric Constant Determinations. The dielectric constants of solutions of NDBBA in benzene were calculated from capacitances measured by the heterodyne beat method at 1 MHz using apparatus of conventional design[7] incorporating an oscilloscope as a zero-beat detector. A General Radio Type 722-D precision capacitor was used, hence the precision of the method is ±0.1%. The cell used was of the triple concentric cylinder type constructed of gold-plated brass with Teflon spacers. The cell was immersed in a grounded thermostat held at 30 ± 0.01°. The air capacitance of the cell, determined by using purified benzene, carbon tetrachloride, and cyclohexane as calibration liquids,[8] was 26.22 pF, while the stray and lead capacitance was 4.97 pF.

In the other solvents, traces of conductance forced the use of bridge methods. Impedances were measured with a General Radio Type 1606-A RF bridge fed by a General Radio Type 1330-A bridge oscillator operated between 0.5 and 30 MHz. The detector was a communications receiver with an oscilloscope as a null senser. Above 15 MHz the measured impedances were corrected for inductive effects. The over-all precision of the capacitance measurements we place at ±2%. Two different cells were used, each consisting of a pair of concentric cylinders of sand-blasted platinum enclosed in a glass vessel, which in turn was surrounded by a jacket through which water at 30 ± 0.2° was circulated. The air capacitances of the two cells were 3.82 and 13.7 pF, while the stray capacitances were 1.68 and 3.2 pF, respectively. Nitrobenzene and

ethylene chloride were purified and used as calibration liquids.[8]

Miscellaneous. Solutions for dielectric constant measurements were prepared by standard volumetric techniques and were used within a few hours. Densities were determined with a Christian Becker Model SG-1 specific gravity balance. Molecular weight measurements were made with a Mechrolab Model 301-A vapor-phase osmometer at 37° using biphenyl as a calibration standard. Infrared spectra were recorded by either a Perkin-Elmer 521 or a Beckman IR 12 spectrophotometer using calibrated sodium chloride cells. The sample temperature in the beam of these instruments was measured with a thermocouple to be ∼33°. The temperature of 30° at which the dielectric constant studies were made was selected as a compromise between solubility limitations of the solute and volatility problems with some of the solvents.

Results

For all the solvents except benzene, radiofrequency bridge measurements were required to obtain dielectric constants of NDBBA solutions. Measurements were made between 0.5 and 30 MHz for each solution. The results in chloroform are typical of those obtained throughout these investigations. In Figure 1 are shown apparent dielectric constants of several solutions as functions of frequency. The apparent dielectric constant is defined by the ratio of the capacitance of the cell full of solution to its air capacitance, each measured value having been corrected for the capacitance of the leads.

The pronounced curvatures displayed in Figure 1 are most readily attributed to electrode polarization effects. Semiempirical treatments of these effects[9,10] indicate that the true dielectric constant of a solution, ϵ_{12}, may be obtained as the ordinate intercept of a linear plot of the apparent dielectric constant against the reciprocal of the square of the frequency, as shown in Figure 2. The intercepts of the lines in Figure 2, determined by least-squares fits to the data points, are plotted against the molar concentrations of the several solutions in Figure 3. The slope of the line in Figure 3 is, by definition, the dielectric increment, δ, of NDBBA in chloroform.

In Table I are listed values of the dielectric increment of NDBBA in the six solvents studied by radiofrequency bridge methods, together with the probable errors

(6) Details may be found in D. A. Horsma, Ph.D. Thesis, University of California, Davis, Calif., 1966.

(7) J-Y. Chien, *J. Chem. Educ.*, **24**, 492 (1947).

(8) A. A. Maryott and E. R. Smith, "Table of Dielectric Constants of Pure Liquids," National Bureau of Standards Circular 514, U. S. Government Printing Office, Washington, D. C., 1951.

(9) J. F. Johnson and R. H. Cole, *J. Amer. Chem. Soc.*, **73**, 4536 (1951).

(10) H. P. Schwan in "Physical Techniques in Biological Research," Vol. 6, W. L. Nastick, Ed., Academic Press Inc., New York, N. Y., 1963, p 323.
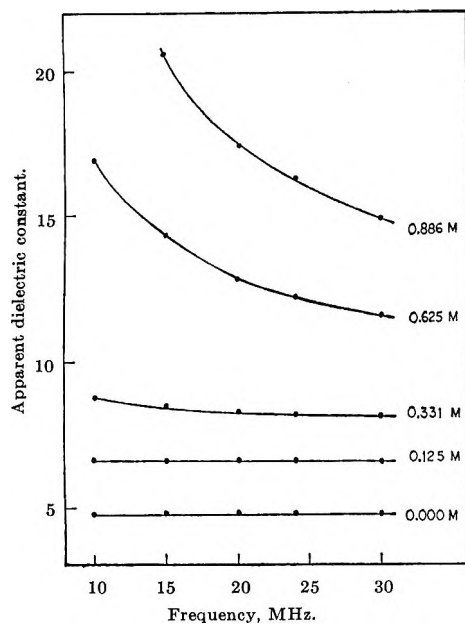
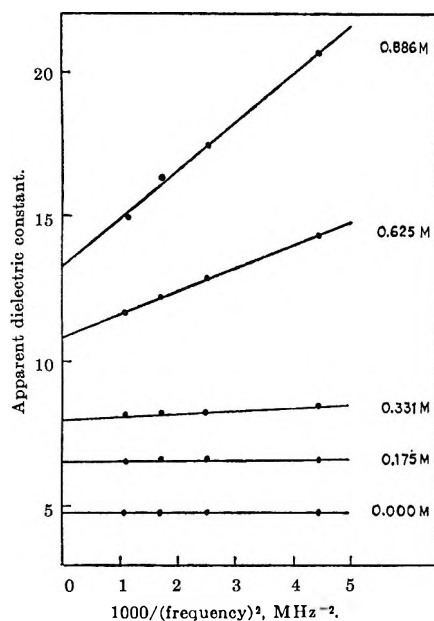Figure 1. Apparent dielectric constants of solutions of NDBBA in chloroform as functions of frequency.

Figure 2. Apparent dielectric constants of solutions of NDBBA in chloroform as functions of inverse-square frequency.

Table I: Dielectric Increments of NDBBA in Nonaqueous Solvents

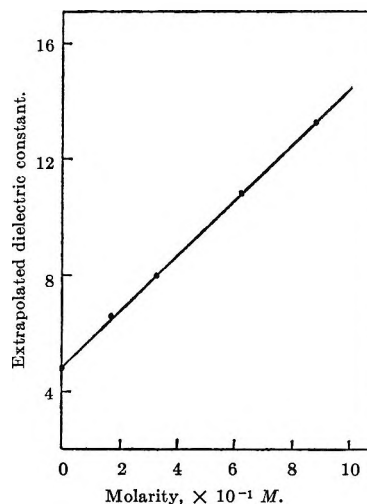| Solvent	δ, ./mol
Nitromethane	4.71 ± 0.16
Acetonitrile	5.10 ± 0.08
Ethylene chloride	8.32 ± 0.18
Methylene chloride	9.10 ± 0.13
Chloroform	9.38 ± 0.04
Methanol	20.8 ± 0.5

Figure 3. Concentration dependence of the extrapolated dielectric constants of solutions of NDBBA in chloroform.
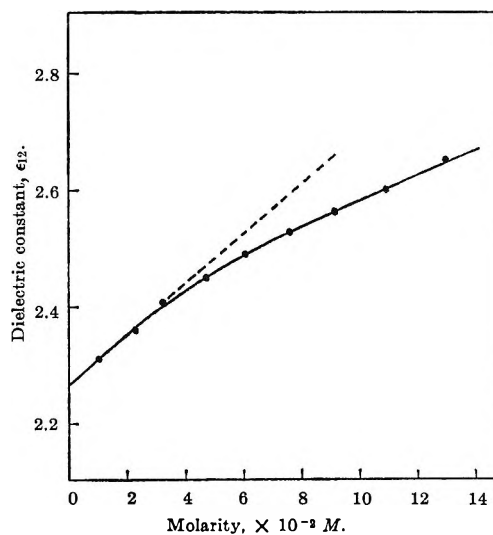

Figure 4. Dielectric constants of solutions of NDBBA in benzene at 1 MHz.

based on least-squares fits to the increment plots typified by Figure 3. The least-squares intercepts of the lines agreed in every case with the measured dielectric constant of the pure solvent to within the 2% accuracy that we ascribe to the method. Thus a two-parameter representation of the dielectric-increment values is entirely satisfactory.

The dielectric constants of solutions of NDBBA in benzene, determined by the heterodyne beat method, are shown in Figure 4. This plot, in contrast to Figure 3, shows a pronounced curvature over the concentration

range studied. The curvature is undoubtedly associated with the formation of dimeric and higher aggregates, since osmometric measurements show a continuous increase in the number-average molecular weight from the monomer value of 201 in 0.01 M

solution to 320 in 0.1 M solution. The present paper is confined to a discussion of monomeric systems, and hence only the zero-concentration limiting slope in Figure 4 is of interest. We find a value of δ in benzene of 4.27 l./mol. This value may be compared with the limiting value of 5.1 l./mol found by Edsall and Wyman[11] for the dielectric increment of N,N-dimethylanthranilic acid in benzene.

Discussion

We begin by developing the equations necessary to obtain the dipole moment of the amino acid molecule in the various solvents. We assume that the solutions may all be described by the Böttcher[12] modification of the Onsager[13] equation for a spherical dipolar molecule imbedded in a dielectric continuum.

The use of a spherical model requires some justification at the outset. Infrared spectra of solutions of NDBBA in all the solvents employed at concentrations in which the molecule is present only as the monomer show that the nondipolar ion tautomer exists in an intramolecularly hydrogen-bonded form. The ester of NDBBA has a prominent absorption band near 2810 cm^{-1} which is attributed to CH stretching vibrations perturbed by a free-electron pair on the nitrogen of a tertiary amine.[14] This band is not observed in solutions of the monomeric acid. Furthermore, we have recently concluded, on the basis of its ultraviolet spectrum, that the molecule N-ethyl-N-phenyl-β-aminopropionic acid (in which the basicity of the amine function is much lower than in NDBBA) exists as an intramolecularly hydrogen-bonded monomer in methylene chloride solution.[15] Examination of a molecular model of NDBBA in the intramolecularly H-bonded configuration shows that if the two butyl side chains are coiled, the molecule approximates a sphere. If they are fully extended, the molecule may be treated as a prolate spheroid of eccentricity ~2, in which the principal dipole is directed along a minor axis of the ellipsoid. Calculations based on the recent work of Weaver and Parry[12] show that dipole moments obtained from data on benzene solutions assuming spherical symmetry are 5% larger than those obtained for the alternative ellipsoidal configuration. In acetonitrile solution, our polar extreme, the discrepancy is at most 11%. By analogy with the properties of polymer solutions, however, it is unlikely that the hydrocarbon chains would be fully extended into a highly polar solvent. Moreover, thermal motions would probably also tend to make the cavity in which the molecule resides have roughly a spherical shape in all solvents. These considerations, together with the fact that the electrostatic interaction energy between a sphere bearing a dipole and a surrounding dielectric may be calculated for both real and point dipoles having arbitrary positions inside the sphere (vide infra), whereas much less general solutions are available for ellipsoidal geometry,

have led us to treat all our data within the framework of spherical symmetry.

Böttcher's equation for a mixture of components is

$$\frac{(\epsilon_{12} - 1)(2\epsilon_{12} + 1)}{12\pi\epsilon_{12}} =$$

$$\sum_i \frac{N_i}{1 - f_i\alpha_i}\left[\alpha_i + \frac{1}{3kT}\left(\frac{\mu_i^2}{1 - f_i\alpha_i}\right)\right] \quad (1)$$

where ϵ_{12} is the dielectric constant of the solution, N_i is the number density of molecules of species i, μ_i is their dipole moment, and kT has its usual significance. The factor α_i is approximated by

$$\alpha_i \cong 3R_i/4\pi\bar{N} \quad (2)$$

where R_i is the molar refraction of component i and $\bar{N}$ is Avogadro's number. The product $f_i\alpha_i$ is related to the refractive index of component i by

$$f_i\alpha_i = (2\epsilon_{12} - 2)(n_i^2 - 1)/(2\epsilon_{12} + 1)(n_i^2 + 2) \quad (3)$$

We now adopt the convention that $i = 1$ designates the solvent and $i = 2$ designates the solute, and

$$X_i \equiv [1/(1 - f_i\alpha_i)] \quad (4)$$

When eq 1 is differentiated with respect to the molar concentration, C, of solute and then the limit $C \to 0$ is taken, there results

$$\frac{2\epsilon_1^2 + 1}{12\pi\epsilon_1^2}\delta = N_1\alpha_1^2 X_1^2\left(\frac{\partial f_1}{\partial C}\right)_0 +$$

$$\alpha_1 X_1\left(\frac{\partial N_1}{\partial C}\right)_0 + \alpha_2 X_2\left(\frac{\partial N_2}{\partial C}\right)_0 +$$

$$\frac{\mu_2^2}{3kT}\left\{X_2^2\left(\frac{\partial N_2}{\partial C}\right)_0\right\} +$$

$$\frac{\mu_1^2}{3kT}\left\{2N_1\alpha_1 X_1^3\left(\frac{\partial f_1}{\partial C}\right)_0 + X_1^2\left(\frac{\partial N_1}{\partial C}\right)_0\right\} \quad (5)$$

The three derivatives on the right-hand side of eq 5 are found to be

$$\left(\frac{\partial f_1}{\partial C}\right)_0 = \frac{1}{\alpha_1}\left(\frac{n_1^2 - 1}{n_1^2 + 2}\right)\frac{6\delta}{(2\epsilon_1 + 1)^2} \quad (6)$$

$$\left(\frac{\partial N_1}{\partial C}\right)_0 = \frac{\bar{N}}{M_1}\left[\left(\frac{\partial d}{\partial C}\right)_0 - \frac{M_2}{1000}\right] \quad (7)$$

$$\left(\frac{\partial N_2}{\partial C}\right)_0 = 10^{-3}\bar{N} \quad (8)$$

(11) J. T. Edsall and J. Wyman, *J. Amer. Chem. Soc.*, **57**, 1964 (1935).

(12) C. J. F. Böttcher, "Theory of Electric Polarization," Elsevier Publishing Co., New York, N. Y., 1952. Subsequent developments have been summarized by J. R. Weaver and R. W. Parry, *Inorg. Chem.*, **5**, 703 (1966).

(13) L. Onsager, *J. Amer. Chem. Soc.*, **58**, 1486 (1936).

(14) K. Nakanishi, "Infrared Absorption Spectroscopy—Practical," Holden-Day, Inc., San Francisco, Calif., 1962, p 40.

(15) C. P. Nash, D. K. Fujita, and E. D. Retherford, *J. Phys. Chem.*, **71**, 3187 (1967).

where d is the density of the solution and M_i is the molecular weight of component i. Substitution of eq 2 and 6–8 into eq 5 and rearrangement yields the final equation

$$\frac{\bar{N}}{1000}\frac{(\mu_2 X_2)^2}{3kT} = \frac{2\epsilon_1^2 + 1}{12\pi\epsilon_1^2}\delta -$$
$$\frac{6\delta}{(2\epsilon_1 + 1)^2}\left(\frac{d_1}{M_1}\right)^2 X_1^2 R_1\left[\frac{2X_1\mu_1^2\bar{N}}{3kT} + \frac{3R_1}{4\pi}\right] -$$
$$\frac{X_1}{M_1}\left[\left(\frac{\partial d}{\partial C}\right)_0 - \frac{M_2}{1000}\right]\left[\frac{X_1\mu_1^2\bar{N}}{3kT} + \frac{3R_1}{4\pi}\right] - \frac{3R_2X_2}{4000\pi} \quad (9)$$

Equation 9 is equivalent to the expression derived by Scholte[16] to treat polar molecules in a nonpolar solvent if $\mu_1 = 0$ and our molar concentrations are converted to mole fractions.

If the solute may be obtained as a pure liquid, all the terms in eq 9 are, in principle, easily evaluated. In the present instance, however, the zero concentration limit of X_2 depends upon the dielectric constant of the solvent and the refractive index of a solute which is a solid. To estimate the n_2-dependent factor, we observe that density measurements in seven solvents give a molar volume for NDBBA of 215 ± 10 ml. This, together with the molar refraction of 55 ml, yields $(n_2^2 - 1)/(n_2^2 + 2) = 0.25$.

An additional problem attaches to the proper value to be used for μ_1, particularly in acetonitrile and nitromethane. In all the other solvents, the terms in μ_1 are sufficiently small that uncertainties attending the choice among gas-phase, pure-liquid, or solution values are negligible. For these systems we have used vapor-phase values from McClellan.[17] With acetonitrile and nitromethane, however, the third term on the right-hand side is an appreciable fraction of the total, and the influence of μ_1 on its value is by no means negligible. The most sensible choices are between the vapor-phase value and the effective moment calculated from the Onsager equation for the pure dipole liquid, as tabulated by Böttcher.[12]

In Table II are presented values of the dipole moment of NDBBA in seven solvents as calculated from eq 9. In each case, the first of the two entries for acetonitrile and nitromethane derives from the use of a vapor-phase solvent moment, and the second from the pure-liquid effective value. Table II also contains our measured values for the dielectric constants of the seven solvents at 30°.

For comparison, when the data in benzene are treated by Hedestrand's[18] method (with the assumption that the electronic polarization may be obtained by summing group refractions and that the atomic polarization is negligible), we find a dipole moment for the amino acid molecule of 6.0 D. Edsall and Wyman,[11] whose method of calculating μ from their δ value was unspecified, reported a dipole moment of 6.3 D for N,N-dimethylanthranilic acid in benzene.

Table II: Dipole Moments of NDBBA in Nonaqueous Solvents at 30°

Solvent	ϵ	μ, D
Benzene	2.26	6.3
Ethylene chloride	10.11	7.7
Methylene chloride	8.64	8.1
Chloroform	4.78	8.2
Nitromethane	36.7	8.5–8.8
Acetonitrile	36.2	9.5–9.0
Methanol	33.6	12.0

The dipole moments that we find for the extreme cases of benzene and methanol we assign to the nondipolar and dipolar ion tautomers, respectively, each tautomer being in a cyclic configuration. To justify the assignment of a 6-D moment to the nondipolar tautomer, we note first that the infrared spectrum of NDBBA in very dilute benzene solutions shows no evidence of a carboxylate species. In a recent study of equimolar mixtures of tertiary amines with carboxylic acids, Bauge and Smith[19] found moments for the assumed 1:1 complexes of about 4 D. Carbonyl bands were also present in the infrared spectra of their mixtures. Inspection of molecular models reveals that the moment of an intramolecularly H-bonded amino acid should be greater than that of the analogous bimolecular complex. In Figure 5 we show schematically the expected geometry of the skeletons of the two systems. In the intramolecular case, the C=O bond, whose moment is ~2.4 D,[20] has a large component along the direction of the N$^+$—O$^-$ axis, whereas in the bimolecular case these two dipoles are opposed.

The 12-D moment which we attribute to the dipolar ion tautomer is found in methanol solutions which fail to show a carbonyl absorption at any concentration. A moment of this magnitude is clearly within the 11–15-D range found by several investigators[21–23] for the ion pairs of tetraalkylammonium salts of picric and carboxylic acids in benzene.

Since the dipole moment of β-alanine in water solution is about 20 D,[24] there is little doubt that the dipolar ion of NDBBA in methanol remains in the cyclic configuration illustrated in Figure 5b. This conclusion is

(16) T. G. Scholte, *Rec. Trav. Chim. Pays-Bas*, **70**, 50 (1951).

(17) A. L. McClellan, "Tables of Experimental Dipole Moments," W. H. Freeman and Co., San Francisco, Calif., 1963.

(18) G. Hedestrand, *Z. Physik. Chem.*, **B2**, 428 (1929).

(19) K. Bauge and J. W. Smith, *J. Chem. Soc., A*, 616 (1966).

(20) C. P. Smyth, "Dielectric Behavior and Structure," McGraw-Hill Book Co., Inc., New York, N. Y., 1955, p 306.

(21) A. A. Maryott, *J. Res. Nat. Bur. Stand., A*, **41**, 1 (1948).

(22) M. Davies and G. Williams, *Trans. Faraday Soc.*, **56**, 1619 (1960).

(23) K. Bauge and J. W. Smith, *J. Chem. Soc.*, 4244 (1964).

(24) E. J. Cohn and J. T. Edsall, "Proteins, Amino Acids and Peptides," Reinhold Publishing Corp., New York, N. Y., 1943, Chapter 6.

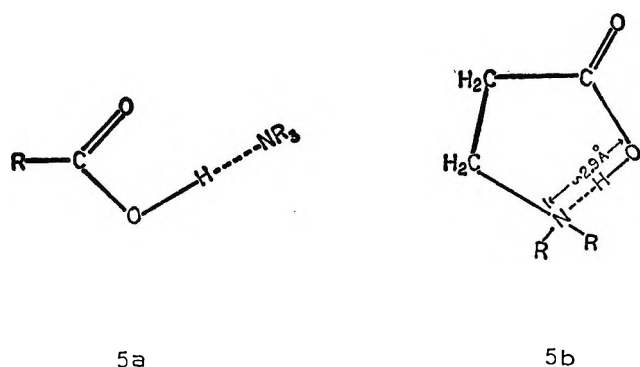5a   5b

Figure 5. Inter- and intramolecular hydrogen bonding of carboxylic acid and amine entities.

further supported by an estimate of the charge separation, r_c, in this form. The measured dipole moment of the zwitterion is the vector sum of er_c, the various group moments in the molecule, and an induced moment arising from the existence of the real charges. Davies and Williams[22] cite a moment for the R_3NH^+ function ~ 0.9 D with H positive. If the moment of the C∴O bond is taken to be the mean of C=O and C—O, we estimate a group moment for the CO_2^- function ~ 1.7 D directed along the bisector of the OCO angle, with C positive. Based on a planar skeleton with the configuration of Figure 5b, we then estimate the vector sum of er_c and the induced moment to be $\mu_{eff} \approx 11.3$ D. If a crude approximation is used, the effective dipole moment is related to the effective polarizability and the charge separation by

$$\mu_{eff} \approx er_c\left(1 - \frac{\alpha_{eff}}{r_c^3}\right) \approx 11.3 \text{ D} \qquad (10)$$

There is no way a priori to estimate α_{eff} other than to note that its upper bound is set by the optical polarizability of 22 $\mathring{A}^3$, deduced from the molar refraction of the molecule.

Suffice it to say that values of α_{eff} between 6 and 22 $\mathring{A}^3$ in eq 10 yield r_c values between 3.0 and 3.9 $\mathring{A}$. These distances, when scaled from the center of the nitrogen atom, intersect the bisector of the OCO angle at what seem to be reasonable places for the center of the negative charge density to reside.

Infrared spectra of solutions of NDBBA in the remaining solvents (except nitromethane, which is opaque) show carbonyl intensities which decrease as the measured dipole moment increases. We therefore conclude that the measured moment is a root-mean-square average from which we may deduce the equilibrium constant for the tautomeric equilibrium. That is, the factor $N_2\mu_2^2$ in eq 1 is more properly written

$$N_2\mu_2^2 = N_n\mu_n^2 + N_d\mu_d^2 \qquad (11)$$

where n connotes the nondipolar tautomer and d connotes the dipolar tautomer. Then from the moments 6.3 and 12.0 D for the tautomers, we evaluate

$K = N_d/N_n$, as shown in Table III. The entries for acetonitrile and nitromethane were calculated for the means of the values listed in Table II.

Table III: Tautomeric Equilibrium Constants

Solvent	K
Benzene	<0.05[a]
Ethylene chloride	0.23
Methylene chloride	0.33
Chloroform	0.36
Nitromethane	0.53
Acetonitrile	0.78
Methanol	>20[a]

[a] Based on estimated levels of detection of the infrared bands of the carbonyl and carboxylate functional groups.

It is instructive to compare the values in Table III with the predictions of electrostatic theory. Two equations have been derived to describe the free energy of transfer of a sphere of radius b containing a dipole of moment μ from the gas phase to a continuous medium of dielectric constant ϵ. Both these equations may be written in the form

$$\Delta G_t = \frac{1 - \epsilon}{2\epsilon + 1}\left(\frac{\mu^2}{b^3}\right)(1 + B) \qquad (12)$$

where B is a function of ϵ and of the position and orientation of the dipole within the sphere. This function vanishes if the dipole is centered. Böttcher's[12] equation describes an ideal point dipole at distance s from the center with moment directed along the radius through point s. Kirkwood's[25] equation admits real dipoles which may have any position and orientation within the sphere. We have compared the two models and have found that for radial dipoles they give substantially the same numerical B values when $s/b \leq 0.5$. When the dipole is symmetrically disposed perpendicular to a radius, B is smaller than in the parallel configuration. For example, when $s/b = 0.4$, $B_{||} = 0.9$ and $B_\perp = 0.6$, and when $s/b = 0.25$, $B_{||} = 0.28$ and $B_\perp = 0.20$.

An examination of the molecular model shows that the dipole in NDBBA is approximately in the perpendicular orientation; so we adopt this form of Kirkwood's[25] theory, which gives

$$B = \frac{9}{2}\left(\frac{s}{b}\right)^2\left(\frac{2\epsilon + 1}{3\epsilon + 2}\right) + \left[12 - \frac{3}{2}\left(\frac{R}{s}\right)^2 + \frac{1}{8}\left(\frac{R}{s}\right)^4\right]\left(\frac{s}{b}\right)^4\left(\frac{2\epsilon + 1}{4\epsilon + 3}\right) + \text{higher terms} \qquad (13)$$

where R is the charge separation.

If the equilibrium constant for the tautomerization

(25) J. G. Kirkwood, J. Chem. Phys., 2, 351 (1934).

reaction in the gas phase is K_g and in solution is K_s and if the only effect of the solvent is electrostatic, it follows from eq 12 that

$$\bar{N}k \ln \frac{K_s}{K_g} = \left(\frac{\epsilon - 1}{2\epsilon + 1}\right)(1 + B)\left(\frac{\mu_d^2 - \mu_n^2}{b^3 T}\right) =$$

$$\beta\left(\frac{\mu_d^2 - \mu_n^2}{b^3 T}\right) \quad (14)$$

while the equilibrium constants in two different solvents are related by

$$\bar{N}k \ln \frac{K_2}{K_1} = (\beta_2 - \beta_1)\left(\frac{\mu_d^2 - \mu_n^2}{b^3 T}\right) \quad (15)$$

If we choose b in the range 5.3–6.2 Å, s/b between zero and 0.4, and R as the apparent charge separation, i.e., 12 D/e, we find eq 15 gives an excellent fit to the equilibrium constants in ethylene chloride and nitromethane and predicts only 1% dipolar ion in benzene. A value for $s/b > 0.4$ is unreasonable, on the basis of the molecular model. From the apparent molar volume of NDBBA ∼215 ml, we find an apparent molecular radius $r \sim 4.5$ Å. The discrepancy between b and r is easily rationalized, since the dielectric continuum could scarcely be expected to begin nearer than the approach distance of the first shell of solvent molecules, some 2 Å.

Values of K together with the predictions of continuum theory are plotted in Figure 6. Clearly continuum theory provides a lower bound to the set of equilibrium constants for the proton-transfer reaction under study. Values of K in excess of the theoretical values may be explained on the basis of well-documented chemical evidence for the stabilization of the carboxylate anion function by certain classes of solvents.

In nonhydroxylic media, conductance maxima are observed near half-neutralization of acids by amines.[26–29] The addition of traces of methanol increases the conductance of acid–amine mixtures,[27] while a large amount of added H-bonding agent eliminates the conductance maximum.[29] These results all show that H-bonding agents, including excess acid itself, stabilize a carboxylate anion. Direct evidence for the stabilization of carboxylate by chloroform is given by Barrow and Yerger,[30] who found that 1:1 complexes of acetic acid and triethylamine gave only carbonyl absorption in carbon tetrachloride but only carboxylate absorption in chloroform. The 2:1 complexes showed carboxylate in both media. Again a hydrogen bond from either solvent or excess acid is found to promote proton transfer. In the present systems, methanol and chloroform are unquestionably hydrogen-bonding agents, and Klemperer, et al.,[31] give evidence for a weak interaction between methylene chloride and the carbonyl group of N-methylacetamide.

The efficiency of acetonitrile in assisting the proton-transfer reaction apparently has its origin in the
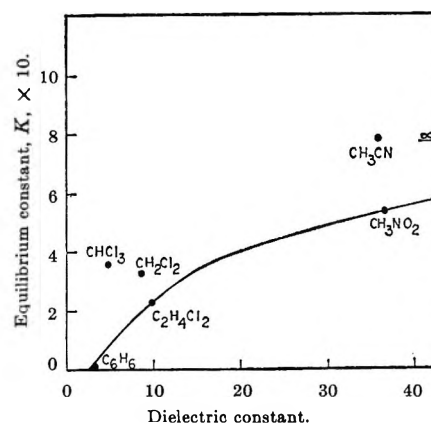

Figure 6. Tautomeric equilibrium constants as functions of solvent dielectric constants. The solid curve, which approaches the asymptotic limit designated by ∞, is derived from electrostatic theory.

existence of its compact dipole. Coplan and Fuoss[32] found that the single-ion conductance of anions is smaller in acetonitrile than in nitromethane, the effect decreasing with increasing ionic size. This behavior strongly suggests the formation of ion–dipole solvates. Keefer and Andrews[33] have found that chlorination reactions which require electrophilic solvation of the activated complex proceed at eight times the rate in acetonitrile as in nitromethane; and, further, that reactions requiring nuclophilic solvation showed the rate of reaction to be virtually the same in these two solvents. Some evidence exists that nitriles will interact specifically with the carbonyl group. Becker[34] found that acetonitrile causes nearly as large a shift in the n → π* transition of benzophenone as does chloroform. Spectra of benzonitrile–benzophenone mixtures showed an isosbestic point giving strong evidence for a specific interaction between the nitrile positive carbon and the carbonyl oxygen.

In summary, Figure 6 documents the relative importance of bulk electrostatic effects and specific solvent effects, of either the hydrogen-bonding or the ion–dipole type, in determining the position of a simple proton-transfer reaction. In the best hydrogen-bond-

(26) V. K. La Mer and H. C. Downes, J. Amer. Chem. Soc., 53, 888 (1931).

(27) A. A. Maryott, J. Res. Nat. Bur. Stand., A, 38, 527 (1947).

(28) P. J. R. Bryant and A. W. H. Wardrop, J. Chem. Soc., 895 (1957).

(29) I. M. Kolthoff and M. K. Chantooni, J. Amer. Chem. Soc., 85, 2195 (1963).

(30) G. M. Barrow and E. A. Yerger, ibid., 76, 5211 (1954).

(31) W. Klemperer, M. W. Cronyn, A. H. Maki, and G. C. Pimentel, ibid., 76, 5846 (1954).

(32) M. A. Coplan and R. M. Fuoss, J. Phys. Chem., 68, 1177 (1964).

(33) R. M. Keefer and L. J. Andrews, J. Amer. Chem. Soc., 84, 3635 (1962).

(34) R. S. Becker, J. Mol. Spectrosc., 3, 1 (1959).

ing medium, *i.e.*, methanol, electrostatic effects are completely insignificant.

Apparent and Partial Molal Volumes of Na-Kaolin

and NaCl in Kaolin Suspensions

by A. K. Helmy, F. F. Assaad, M. Naguib Hassan, and H. Sadek[1]

Faculty of Agriculture, Alexandria University, Egypt

Apparent and partial molal volumes of NaCl and Na-kaolin as a function of electrolyte and clay concentration were determined by density measurements. It was found that the apparent and partial molal volume of NaCl is greater in 5% Na-kaolin than in water. The apparent and partial molal volume of kaolin increases with particle concentration both in water and in 0.5 M NaCl and is larger in NaCl than in water. Satisfactory correspondence is found between calculated and experimental values for the departure of Na-kaolin in NaCl from ideal behavior.

Apparent and partial molal volumes of electrolytes vary with the ionic strength in a manner predictable by the Debye–Hückel theory.[2] The presence of other substances, such as kaolin particles, probably affects the above-mentioned volumes of electrolytes.

In this paper measurements on the apparent and partial molal volumes of NaCl and Na-kaolin as a function of electrolyte and clay concentration are reported.

Materials and Methods

The kaolin used is a product of Merck, Darmstadt, Germany. Fine particles having an effective diameter less than 2 μ were separated by sedimentation and decantation methods with the help of the Stokes formula. This fine material was found to have a cation-exchange capacity of 6.4 mequiv/100 g, as determined by the difference between total calcium and total chloride in a given amount of homoionic suspension. It had an *o*-phenanthroline specific surface area of 38 m²/g.[3] The particles were sodium saturated by repeated washings with 0.5 M NaCl until the concentrations of added and decanted solution became identical. It was washed with water until almost free of electrolyte, was dried on a water bath then in an oven at 40°, was ground in a porcelain mortar, and was kept in a well-stoppered bottle. A portion of this material (2.5 g) in 40 ml of water showed a NaCl concentration of 0.0005 M.

For the determination of density, use was made of a 50-ml pycnometer kept in an air thermostat adjusted to 30°. Four replications or measurements were always made near each given particle concentration. Usually the clay was added first and weighed, followed by the water or the electrolyte. The pycnometers were put for about 1 hr in an evacuated desiccator in order to exclude air bubbles then left overnight in the incubator before weighing again.

Results and Discussion

Apparent and partial molal volumes of Na-kaolin and NaCl at different concentrations of particles and NaCl are given in Tables I and II. The necessary calculations were done using the following relations[4]

For a single solute

$$\phi = (V - V_0)/n = \frac{1000/d - (1000 - g)/d_0}{g/M} \quad (1)$$

where ϕ is the apparent molal volume; V and V_0 are the volumes of the solution and the water, respectively; n is the number of moles; g is the weight of solute in 1000 g of solution having a molecular weight M; and

(1) Professor of Physical Chemistry, Faculty of Science, Alexandria University, Egypt.

(2) O. Redlich and D. M. Meyer, *Chem. Rev.*, **64**, 221 (1964).

(3) D. C. Lawrie, *Soil Sci.*, **92**, 188 (1961).

(4) D. A. MacInnes and M. O. Dayhoff, *J. Amer. Chem. Soc.*, **75**, 5219 (1953).

Table I: Partial and Apparent Molal Volume of NaCl (ml) in H_2O and in a 5% Na-Kaolinite Suspension

| Molality, m | | App mol vol in | | | | Partial mol vol in | |
| NaCl | Kaolin | Kaolin | | Water | | Kaolin | Water |
		Exptl	Calcd	Exptl	Calcd	Kaolin	Water
1.0	0.0952	20.4	20.1	18.7	18.6	22.7	19.9
0.8	0.0961	20.0	19.5	18.3	18.3	21.7	19.5
0.7	0.0960	19.1	19.3	18.3	18.1	21.2	19.4
0.6	0.0955	18.7	19.0	18.2	18.1	20.7	19.0
0.5	0.0955	18.3	18.7	18.0	17.7	20.2	18.9
0.4	0.0961	18.0	18.4	17.8	17.5	19.6	18.7
0.2	0.0965	17.8	17.7	17.4	17.1	18.5	18.0
0.1	0.0962	17.7	17.3	17.2	16.8	17.7	17.6

Table II: Partial and Apparent Molal Volume (ml) of Na-Kaolinite in Water and in 0.5 M NaCl

| Molality, m | | App mol vol in | | | | Partial mol vol in | |
| Kaolin | NaCl | NaCl | | Water | | NaCl | Water |
		Exptl	Calcd	Exptl	Calcd	NaCl	Water
0.0192	0.5	179.1	180.2	178.8	179.2	181.4	181.3
0.0379	0.5	182.3	182.1	181.5	181.6	187.0	187.0
0.0577	0.5	185.8	185.0	184.9	184.6	194.4	193.7
0.0763	0.5	188.3	188.2	187.0	187.6	201.8	200.4
0.0948	0.5	192.4	191.6	190.9	190.7	209.6	207.1

d or d_0 are the densities of the solution and of the water, respectively.

For one solute when two solutes are present

$$\phi_1 = (V - (n_0 \bar{V}^0 + n_2\phi_2))/n_1$$

$$= \left(\frac{1000}{d} - \frac{1000 - g_1 - g_2}{d_0} - \frac{g_2}{M_2}\phi_2\right)\frac{M_1}{g_1} \quad (2)$$

where g_1 and g_2 are the number of grams of the two solutes in 1000 g of solution; M_1 and M_2 are the corresponding molecular weights; n_0 is the number of moles of water; and $\bar{V}^0$ is the volume occupied by 1 mol of pure solvent. For calculating partial molal volumes, $\bar{V}$, the following relation was used

$$\bar{V} = \phi + m\frac{d\phi}{dm} \quad (3)$$

where ϕ is the apparent quantity and m is the molality.

Although eq 1 and 2 are usually used for dissolved materials, nothing precludes their use for colloidal materials. The molecular weight of kaolin was taken equal to 516.34, according to the ideal formula Si_4Al_4-$O_{10}(OH)_8$. This molecular weight and, subsequently, the apparent volumes are not sensitive to the small isomorphous substitution of Al for Si or the atomic weight of the saturating cation. This is because of the small cation-exchange capacity and the small difference between the atomic weights of Al and Si.

The apparent and partial molal volumes could be summarized in the following statistical relations which relate these quantities to their molalities and which were calculated from the experimental data using a least-square method. For NaCl in water

$$\phi(NaCl) = 16.542 + (1.693m^{1/2}) + (0.405m) \quad (4)$$

$$\bar{V}(NaCl) = 16.542 + (2.540m^{1/2}) + (0.810m) \quad (5)$$

For NaCl in a 5% kaolin suspension

$$\phi(NaCl) = 16.620 + (1.659m^{1/2}) + (1.786m) \quad (6)$$

$$\bar{V}(NaCl) = 16.620 + (2.489m^{1/2}) + (3.572m) \quad (7)$$

For Na-kaolin in water

$$\phi(Na\text{-}kaolin) =$$
$$179.317 - (32.214m^{1/2}) + (225.071m) \quad (8)$$

$$\bar{V}(Na\text{-}kaolin) =$$
$$179.317 - (48.321m^{1/2}) + (450.142m) \quad (9)$$

For Na-kaolin in 0.5 M NaCl

$$\phi(Na\text{-}kaolin) =$$
$$183.363 - (63.582m^{1/2}) + (293.308m) \quad (10)$$

$$\bar{V}(Na\text{-}kaolin) =$$
$$183.363 - (95.373m^{1/2}) + (586.616m) \quad (11)$$

The partial quantities are related to the apparent ones in the same way as an increment is related to the differential in calculus. The discussion will, therefore, be confined to the partial volumes.

Equations 4 and 5 are similar but not identical to those given by Klotz.[5] The difference is not large and we have been able to reproduce our results several times so that the data reported are self-consistent.

The data presented in Tables I and II indicate that

(5) I. M. Klotz, "Chemical Thermodynamics," Prentice-Hall, Inc., Englewood Cliffs, N. J., 1950, p 194.

the partial molal volumes increase with concentration. This behavior is attributed to the variation in the structure of water as a result of the presence of electric fields around charged particles. Raising the concentration of solute increases the interaction between electric fields and between electrostricted water molecules, with the result that the constrictive force per particle is diminished.

The presence of 5% kaolin particles causes a further increase in the partial molal volume of NaCl. This finding is important because free energy, ion-exchange constants, and other thermodynamic quantities require knowledge of the partial volumes of electrolyte in colloidal systems. This increase in $\bar{V}$ might even become more significant as the particle concentration increases, as is the case with thick suspensions or soils.

The partial molal volume of Na-kaolin increases with increase in particle concentration in the range 1–5%. The presence of 0.5 M NaCl causes further increase in the partial molal volume of the particles. In order to get an idea about the diminution of volume of solvent caused by the particles, use is made of the relation

$$V = U - \bar{V}^0$$

where U is the physical volume (194.8 ml/mol for kaolin of density 2.65 g/cm^3), and $\bar{V}^0$ is the partial molal volume at infinite dilution. The diminution in volume V is found equal to 13.5 ml/mol. This volume is of the same order of magnitude as that caused by monovalent ions.[6]

The departure of kaolin from ideal behavior with respect to volume V_e is equal to[7]

$$V_e = n_2(\phi - \phi^0) \tag{12}$$

where n_2 is the number of moles of kaolin; ϕ is the volume of kaolin in 0.5 M NaCl, and ϕ^0 is the apparent molecular volume of kaolin in 0.5 M NaCl at infinite dilution. V_e could be calculated from the standard double-layer theory as follows

$$V_e = \frac{dG}{dp} = \frac{dG}{d\Psi_0}\frac{d\Psi_0}{dp} \tag{13}$$

where G is the free energy of the double layer per mole and Ψ_0 is the surface potential.

For 1 mol of kaolin (516.34 g) in a (1:1) electrolyte, G is found equal to[8,9]

$$G = -\sqrt{\frac{8\epsilon R^3 T^3 C v^2}{\pi F^2}}\left(\cosh\frac{F\Psi_0}{2RT} - 1\right) \tag{14}$$

where ϵ is the dielectric constant of water; C is the concentration (mol/cm^3) of NaCl; v is a factor used to convert free energy per square centimeter to that per mole of kaolin and equals 1.96 × 10^8 cm^2/mol; the other symbols have their usual meanings.

$$\frac{dG}{d\Psi_0} = -\sqrt{\frac{2\epsilon RTCv^2}{\pi}}\left(\sinh\frac{F\Psi_0}{2RT}\right) \tag{15}$$

In eq 15 the assumption of constant ϵ cannot be very accurate for the high field near the charged surface, but the error is small for $\epsilon \gg 1$.[10] The equilibrium of the kaolin–electrolyte system requires that at every point the gradient of the hydrostatic pressure and the force on the space charge balance each other.[11] Therefore

$$d\rho + \rho d\Psi_0 = 0$$

$$\frac{d\Psi_0}{d\rho} = -1/\rho \tag{16}$$

where ρ is the charge density and, for a 1:1 electrolyte, is equal to

$$\rho = -2CF\sinh\frac{F\Psi_0}{RT} \tag{17}$$

Substitution of eq 17 into 16 and combination with eq 15 and rearrangement gives

$$V_e = -\sqrt{\frac{\epsilon RTv^2}{8\pi F^2 C}}\left(\cosh\frac{F\Psi_0}{2RT}\right)^{-1} \tag{18}$$

The surface potential Ψ_0 is calculated from the surface charge σ using the relation

$$\sigma = \sqrt{\frac{2\epsilon CRT}{\pi}}\left(\sinh\frac{F\Psi_0}{2RT}\right) \tag{19}$$

The calculated values of V_e are shown together with some experimental values in Table III. The calcu-

Table III: Calculated and Experimental Departure of Na-Kaolin in NaCl from Ideal Behavior

NaCl, M	Surface potential, mV	V_e, ml/mol Calcd	V_e, ml/mol Exptl
1	56	3.6	...
0.8	60	3.8	...
0.5	70.5	4.0	−4.3–8.2
0.1	108.5	4.4	−5.6–4.6[a]

[a] F. F. Assaad, unpublished data.

(6) S. W. Benson and C. S. Copeland, *J. Phys. Chem.*, **67**, 1194 (1963).

(7) R. S. Harned and B. B. Owen, "The Physical Chemistry of Electrolytic Solutions," Reinhold Publishing Corp., 1958, p 392.

(8) J. Th. G. Overbeek, "Colloid Science," H. R. Kruyt, Ed., Elsevier Publishing Co., Amsterdam, The Netherlands, 1952, p 141.

(9) A. K. Helmy, *Trans. Intern. Congr. Soil Sci.*, **3**, 271 (1964).

(10) G. N. Lewis and M. Randall, "Thermodynamics," 2nd ed, McGraw Hill Book Co., Inc., New York, N. Y., 1961, p 503.

(11) Reference 9, p 255.

lated values are of the right order of magnitude for small particle concentrations. The descrepancy between the experimental and calculated values is not considered serious because of the ideality of the double-layer model assumed, *viz.*, point charges, infinitely large flat plates, and uniform surface charge.

Transpiration Vapor Pressure Measurements for the Molten Salt

Systems PbCl$_2$ + CsCl and CdCl$_2$ + CsCl

by H. Bloom and J. W. Hastie

Chemistry Department, The University of Tasmania, Hobart, Australia (*Received October 16, 1967*)

A transpiration method has been used to obtain partial pressure data over a range of compositions for molten PbCl$_2$ + CsCl and CdCl$_2$ + CsCl mixtures. The data have been interpreted to indicate the formation of complex ions in the melts. Vapors in equilibrium with the molten PbCl$_2$ + CsCl mixtures contain the complex molecule CsPbCl$_3$ as well as CsCl and PbCl$_2$ while in the CdCl$_2$ + CsCl system there is the complex molecule CsCdCl$_3$ together, probably, with CsCd$_2$Cl$_5$, in equilibrium with the components.

Introduction

For all the PbCl$_2$ + ACl and CdCl$_2$ + ACl systems yet investigated,[1-6] (where A is Na, K, Rb, or Cs), none forms simple ionic mixtures in any phase, with the exception of solid mixtures of PbCl$_2$ + NaCl. Thermodynamic activities for the two components of each binary system, calculated from transpiration measurements, are not consistent with the Gibbs–Duhem relationship,[6] if the vapors are assumed to be the simple unassociated components. In these systems, the activities of ACl deviate in a positive sense from the Raoult and Henry laws, while large negative deviations are found for PbCl$_2$ or CdCl$_2$. Previous workers have attributed these to vapor association equilibria, *e.g.*, for the PbCl$_2$ + CsCl system

$$PbCl_2 + CsCl \longrightarrow CsPbCl_3 \qquad (1)$$
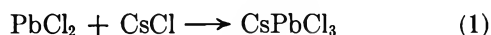
Hagemark, Hengstenberg, and Blander[7] have recently inferred, by measuring pressure–temperature relations, the presence of KPbCl$_3$ and RbPbCl$_3$ in the vapor systems KCl + PbCl$_2$ and RbCl + PbCl$_2$, respectively.

In a comprehensive study of a number of systems by mass spectrometry, Bloom and Hastie[8] have directly verified the existence of complex molecules over molten salt mixtures, including CsPbCl$_3$ in the CsCl + PbCl$_2$ system and CsCdCl$_3$ in the CsCl + CdCl$_2$ system.

Experimental Section

The transpiration apparatus and method which were used have been described by other investigators.[6,9] The carrier gas was purified argon and flow rates were

kept within ranges for which it had been verified that derived partial pressures of the components were independent of flow rate. For example, for the equimolar mixture PbCl$_2$ + CsCl at 700°, the various partial pressures were found to be independent of the rate of flow of argon over the range 0–60 ml/min.

Errors due to thermal diffusion (significant only at very low flow rates or at high pressures) were shown to be mostly absent under the selected conditions of measurement, but corrections where made where necessary by making duplicate runs at zero flow rate. Temperature was measured by 13% Rh–Pt—Pt thermocouples calibrated at the melting points of metals and sodium chloride.

Salts were of analytical reagent quality and, except for Cs, standard chemical methods of analysis were

(1) H. H. Landolt and R. Bornstein, "Zahlenwerte und Funktionen," Vol. II, Part 3, Springer-Verlag, Berlin, 1956.

(2) F. G. McCarty and O. J. Kleppa, *J. Phys. Chem.*, **68**, 3846 (1964).

(3) A. G. Bergman and Zh. V. Misler, *Russ. J. Inorg. Chem.*, **10**, 696 (1965).

(4) B. F. Markov, Iu. K. Delimarskii, and I. D. Panchenko, *Zh. Fiz. Khim.*, **28**, 1987 (1954).

(5) I. I. Il'yasov, A. G. Bergman, and N. I. Chaurskii, *Russ. J. Inorg. Chem.*, **10**, 679 (1965).

(6) J. L. Barton and H. Bloom, *Trans. Faraday Soc.*, **55**, 1792 (1959).

(7) K. Hagenmark, D. Hengstenberg, and M. Blander, *J. Phys. Chem.*, **71**, 1819 (1967).

(8) H. Bloom and J. W. Hastie, *Aust. J. Chem.*, **19**, 1003 (1966).

(9) C. Beusman, "Activities in the KCl-FeCl$_2$ and LiCl-FeCl$_2$ Systems," ORNL Report 2323, Oak Ridge, Tenn., 1957.

used. For Cs, which often had to be determined in small amounts, the γ-active ^{137}Cs isotope was used to label the CsCl and its concentration was determined by standard procedure using a Geiger liquid counter.

Results and Discussion

In this article, only the measurements at 650° will be discussed, as this was the only temperature at which all the salt-mixture compositions were investigated.

Isothermal (650°) Properties of the PbCl$_2$ + CsCl System. Values of apparent and corrected partial pressures obtained by transpiration (at mole fraction x) are listed in Table I.

Table I: Partial Pressures and Activities for the System PbCl$_2$ + CsCl at 650°

Composition (x_{PbCl_2}), mol fraction	Transpiration results P_{PbCl_2}(trans), mm	P_{CsCl}(trans), mm	Cor partial pressures (P_{PbCl_2}(true)), mm	True activities of PbCl$_2$ (a)
0.000	0	0.126	0	0
0.299	0.550	0.368	0.182	0.018
0.503	2.320	0.761	1.559	0.158
0.507	2.360	0.801	1.559	0.158
0.598	3.470	0.569	2.901	0.294
0.690	5.240	0.530	4.710	0.478
0.796	6.850	0.250	6.600	0.669
0.891	7.830	0.150	7.680	0.779
1.000	9.860	0	9.860	1.000

It will be noticed that the transpiration partial pressures of PbCl$_2$ deviate from the Raoult-law values in a negative sense, but those of CsCl are all much higher than the ideal values; *e.g.*, for the mixture 0.507 mol fraction of PbCl$_2$ + 0.493 mol fraction of CsCl, the apparent partial pressure of CsCl was found to be 0.801 mm by analysis of Cs instead of 0.0621 mm, which would be expected if the system were to behave as ideal mixtures of Cs$^+$, Cl$^-$, and Pb^{2+}, according to the model of molten salt mixtures devised by Temkin.[10]

It has been shown[6,11] that for each component of the binary molten salt system PbCl$_2$ + ACl, the activities, a (*i.e.*, P_i/P_i^0, where P_i is the partial pressure of component i, of the mixture, and P_i^0 is the total vapor pressure of the pure salt at the same temperature) are very much smaller over a considerable part of the composition range than the Temkin activities. The latter for an ideal binary mixture would be the same as the mole fraction. Thus the true partial pressures of CsCl over the liquid mixtures are actually very small over most of the composition range, in contrast to the transpiration values which are the combined pressures of CsCl and CsPbCl$_3$. This has been confirmed by the mass spectrometry results.[8]

Since

$$P_{CsPbCl_3} = P_{CsCl}(trans) - P_{CsCl}(true) \quad (2)$$

and

$$P_{CsCl}(trans) \gg P_{CsCl}(true) \quad (3)$$

the values of P_{CsCl}(trans) for the mixtures in Table I can be regarded as being the actual vapor pressures of CsPbCl$_3$ in the vapor. The true vapor pressures of PbCl$_2$ above the mixtures are thus given by

$$P_{PbCl_2}(true) = P_{PbCl_2}(trans) - P_{CsPbCl_3}$$

$$\quad (4)$$

$$P_{PbCl_2}(true) = P_{PbCl_2}(trans) - P_{CsCl}(trans)$$

These values of true partial pressures of PbCl$_2$ above the liquid mixtures are shown also in Table I, together with the activities of PbCl$_2$ calculated from corrected vapor pressures. Activity coefficients of PbCl$_2$ ($\gamma_{PbCl_2} = a_{PbCl_2}/x_{PbCl_2}$) are plotted as a function of melt composition in Figure 1. This figure illustrates the errors in activity coefficient which would be caused by neglecting compound formation in the vapor phase in these transpiration measurements.

For ideal mixing, *e.g.*, of AX with BX$_2$, the Temkin model would allow the calculation of activities of components of a binary molten salt system as follows

$$a_{AX} = N_{A^+} N_{X^-} \quad (5)$$

and

$$a_{BX_2} = N_{B^{2+}} N_{X^-}^2 \quad (6)$$

where the ionic fractions N_{A^+}, etc., are given in terms of mole fractions of ions by the equations

$$N_{A^+} = x_{A^+}/(x_{A^+} + x_{B^{2+}})$$

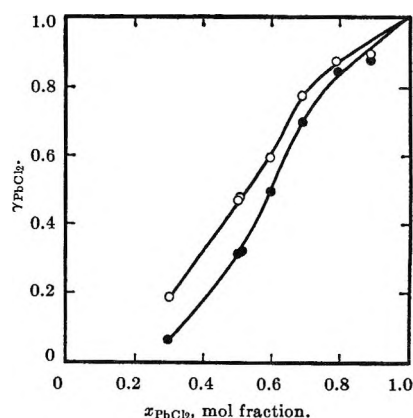etc. This simple behavior has been confirmed for several molten salt systems.[11]

Figure 1. Activity coefficients for PbCl$_2$ in the PbCl$_2$ + CsCl system at 650°: ○, uncorrected for compound formation in vapor; ●, corrected for compound formation in vapor.

(10) M. Temkin, *Acta Physicochim. URSS*, **20**, 411 (1945).

(11) H. Bloom, *Pure Appl. Chem.*, **7**, 389 (1963).

Bredig[12] has shown that for the systems $CdCl_2$ + KCl and $CdBr_2$ + KBr, the activities can be calculated using the Temkin model only if allowance is made for complex ions in the mixtures, e.g., $CdCl_4{}^{2-}$ in the chloride system. Perfect curve fitting could not, in any case, be achieved by Bredig without assuming equilibria between complexed and uncomplexed ions rather than reactions to completion.

In order to calculate activities and hence activity coefficients of CsCl and $PbCl_2$, we use Temkin equations, analogous to eq 5 and 6 putting the ionic fractions

$$N_{Cs^+} = x_{Cs^+}/(x_{Cs^+} + x_{Pb^{2+}})$$

and

$$N_{Cl^-} = x_{Cl^-}/(x_{PbCl_3^-} + x_{Cl^-})$$

If $PbCl_3{}^-$ is the only complex ion present in the system and if it mixes ideally with the ions from $PbCl_2$ and CsCl, the activity of $PbCl_2$ can be shown by the use of the Temkin equation to be given by

$$a_{PbCl_2} = \frac{kx_{PbCl_2} - 2 + 2[1 - kx_{PbCl_2}x_{CsCl}]^{1/2}}{kx_{PbCl_2}} \quad (7)$$

where the constant $k = 4K/(K + 1)$, and the equilibrium constant is given by

$$K = a_{CsPbCl_3}/a_{CsCl}a_{PbCl_2} \quad (8)$$

Through iteration it was found that a value of $K = 30$ fits the experimental activity and activity coefficient (Figure 1) curves within the estimated uncertainty of $\pm 4\%$ over the whole of the composition range. Similar calculations were made for other complex species, such as $PbCl_4{}^{2-}$ or $PbCl_6{}^{4-}$, but none of these agreed with the experimental curve. Hence it seems reasonable to postulate that $PbCl_3{}^-$ is the major species in the mixtures responsible for the nonideal behavior.

Additional information on complex-ion formation in this system can be drawn from a consideration of the partial molar excess entropies of $PbCl_2$ ($\bar{S}^E{}_{PbCl_2}$) in these mixtures. These values, obtained from a combination of McCarty and Kleppa's[2] partial molar excess enthalpy data with our partial molar excess free energy (from activity) data, are plotted in Figure 2.

As was found by Kleppa and McCarty[13] for the $MgCl_2$ + KCl system, the partial excess entropies of MCl_2 vary from positive to negative values, and this trend parallels that of the partial excess molar volumes. Formation of complex ions would be expected to lead to negative values of the partial molar excess entropies. This is reflected in a minimum in the integral entropy at the equimolar composition accompanying the formation of $PbCl_3{}^-$, owing to the high relative degree of local order at the equimolar composition.

The formation of $CsPbCl_3$ in the vapor state is most likely related to the ability of Pb^{2+} to form $PbCl_3{}^-$ in the liquid state. It is suggested that the vapor-phase
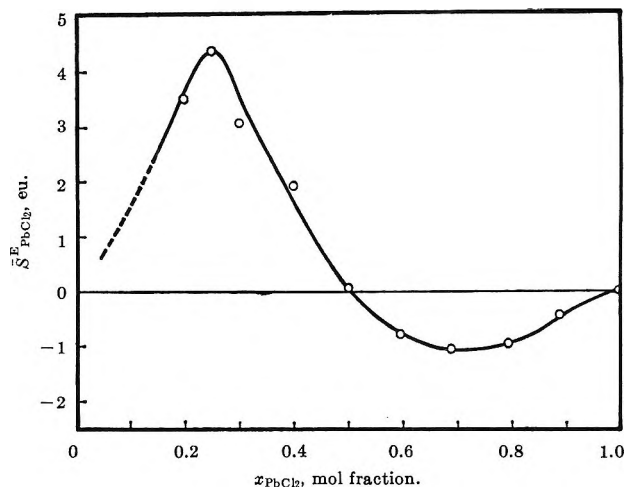

Figure 2. Partial molar excess entropies of $PbCl_2$ in the $PbCl_2$ + CsCl system at 650°.

$CsPbCl_3$ molecule is essentially $Cs^+PbCl_3{}^-$ and that the structure of $PbCl_3{}^-$ is similar in both the liquid and the vapor states. The structure of $PbCl_3{}^-$ in $PbCl_2$ + KCl melts has been found from Raman spectra to be pyramidal (point group C_{3v}).[14] We suggest a similar structure for the $CsPbCl_3$ molecule, Cs forming three Cs–Cl bridges to Pb.

The recent identification of the pyramidal $SnCl_3{}^-$ complex ion in $SnCl_2$ + KCl mixtures suggests that the formation of complex ions and possibly complex molecules (in the vapor state) could be general for all group IVa metal–halide systems.[15]

The $CdCl_2$ + CsCl System. In this system the partial pressures of $CdCl_2$ were found to be very much larger than those of the vapor compound $CsCdCl_3$, hence the transpiration vapor pressures of $CdCl_2$ are also the true vapor pressures. The carrier-gas flow rates used for this system were ca. 10 ml/min. The results for 650° together with the activities of $CdCl_2$ calculated using the vapor pressure of pure $CdCl_2$ at this temperature, measured by Bloom and Welch,[16] are shown in Table II.

For this system, the equilibrium constant for the formation of $CsCdCl_3$ ($a_{CdCl_3}/(a_{CdCl_2}a_{CsCl})$) required to give a good fit of the experimental activity coefficient curve at 650° was $K = 130$. The experimental and calculated results are shown in Figure 3, where the broken lines show deviations of the calculated values at the extremes of composition. The assumption that $CdCl_3{}^-$ is the only complex ion formed in this system is thus inadequate over parts of the composition range.

(12) M. A. Bredig, *J. Chem. Phys.*, **37**, 451 (1962).

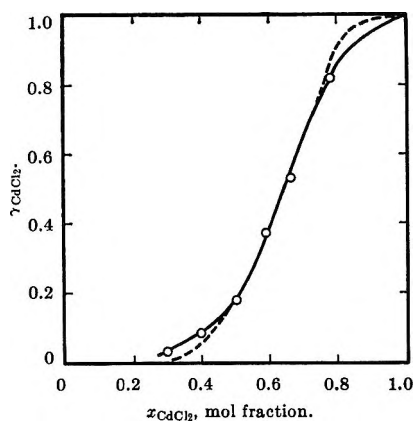(13) O. J. Kleppa and F. G. McCarty, *J. Phys. Chem.*, **70**, 1249 (1966).

(14) K. Balasubrahmanyam and L. Nanis, *J. Chem. Phys.*, **40**, 2657 (1964).

(15) J. H. R. Clarke and C. Solomons, Abstracts, 153rd National Meeting of the American Chemical Society, Miami Beach, Fla., April 1967.

(16) H. Bloom and B. J. Welch, *J. Phys. Chem.*, **62**, 1594 (1958).

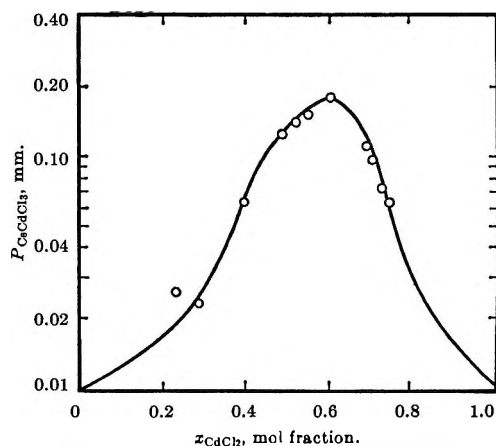**Table II:** Partial Pressures and Activities for
the System $CdCl_2$ + CsCl at 650°

Composition (x_{CdCl_2}), mol fraction	Transpiration vapor pressures P_{CdCl_2}(trans), mm	P_{CsCl}(trans), mm	Activities of CdCl$_2$ (a)
0.000	0	0.126	0.000
0.226	...	0.0455	...
0.279	0.0925	0.0354	0.009
0.388	...	0.067	...
0.398	0.355	...	0.033
0.489	...	0.123	...
0.500	0.96	...	0.090
0.512	...	0.138	...
0.540	...	0.154	...
0.562	...	0.169	...
0.591	2.38	...	0.222
0.610	...	0.180	...
0.662	3.80	...	0.354
0.690	...	0.109	...
0.705	...	0.094	...
0.725	...	0.071	...
0.738	...	0.066	...
0.770	...	0.022	...
0.780	6.87	...	0.640
1.000	10.72	0	1.000

Figure 4. Partial pressures of CsCdCl$_3$ in the CdCl$_2$ + CsCl
system at 650°, calculated from eq 9.

Figure 3. Activity coefficients for $CdCl_2$ in the $CdCl_2$ +
CsCl system at 650°.

A possible explanation of these deviations may be due to
other complex ions, e.g., $CdCl_4^{2-}$ and $CdCl_6^{4-}$, being
present also in these liquid mixtures.

Vapor Pressures of the Compounds at 650°. From
Table I the vapor pressures of $CsPbCl_3$, i.e., P_{CsCl}
(trans), at 650° are known as a function of composition.
The values are symmetrical about the equimolar compo-
sition. This is thermodynamically consistent with the
formation of $CsPbCl_3$ as the sole vapor-phase com-
pound in this system.

For the $CdCl_2$ + CsCl system, the vapor pressures of
$CsCdCl_3$ at various compositions can be calculated as
follows: P_{CdCl_2}(trans) is very much greater than
P_{CsCl}(trans) over most of the composition range (Table
II), hence the true values of P_{CdCl_2} can be regarded as
the same as the transpiration values. From the ac-

tivities of $CdCl_2$, true activities of CsCl are calculated
by graphical integration of the Gibbs–Duhem equation.
From these values for the mixtures and the partial
pressure of pure CsCl at the same temperature, the true
partial pressures of CsCl are calculated. The values of
P_{CsCdCl_3} can then be obtained from the equation

$$P_{CsCdCl_3} = P_{CsCl}(\text{trans}) - P_{CsCl}(\text{true}) \qquad (9)$$

These P_{CsCdCl_3} results at 650° are shown plotted
against molar composition in Figure 4. The curve is
not symmetrical about the equimolar composition,
hence there is at least one other vapor-phase compound
containing more than one molecule of $CdCl_2$ for each
molecule of CsCl. The formation of some dinuclear
compound $CsCd_2Cl_5$ at mole fractions of $CdCl_2$ greater
than 0.5 mol fraction could lead to the observed results.
It is estimated from Figure 4 that the partial pressure
of $CsCd_2Cl_5$ would reach a maximum of ca. 0.03 mm
at 0.66 mol fraction of $CdCl_2$. Unfortunately no mass
spectrometric evidence is available to prove the ex-
istence of the $CsCd_2Cl_5$ species. Previous mass spectro-
metric measurements[8] were made over the composi-
tion range 0.3 mol fraction < x_{CdCl_2} < 0.5 mol fraction,
in which the pressure of $CsCd_2Cl_5$ would be very small
and difficult to detect in mass spectrometric experi-
ments.

It is significant that the transpiration data[6,11] for the
$CdCl_2$ + NaCl system are exactly analogous to the
present data. In particular, the apparent P_{NaCl} vs.
x_{CdCl_2} curve shows similar dissymmetry about the
x_{CdCl_2} = 0.5 mol fraction composition, hence the vapors
above $CdCl_2$ + NaCl mixtures could also be considered
to contain the complex species $NaCd_2Cl_5$ as well as
$NaCdCl_3$.

The data of Schrier and Clark[17] for the $MgCl_2$ + KCl
system also indicate an unsymmetrical P_{KMgCl_3} vs.
x_{MgCl_2} curve, which may be regarded as the superposi-
tion of two curves: one due to $KMgCl_3$ and one due to
KMg_2Cl_5 in the vapor at compositions greater than

(17) E. E. Schrier and H. M. Clark, *J. Phys. Chem.*, **67**, 1259 (1963).

x_{MgCl_2} = 0.5 mol fraction. The maximum pressure of KMg_2Cl_5 would be about 3 mm, compared with a value of 21 mm for $KMgCl_3$.

The absence of corresponding species such as $CsPb_2Cl_5$ and KPb_2Cl_5 from both transpiration and mass spectrometric[8] evidence is possibly related to the inability of $PbCl_2$ to dimerize, in contrast to $MgCl_2$ and $CdCl_2$ (although only to a small extent in the latter case[17,18]).

(18) F. J. Keneshea and D. D. Cubiciotti, *J. Chem. Phys.*, **40**, 1778 (1964).

A Multilayer Model for the Surface Transport of Adsorbed Gases

by Weldon K. Bell and Lee F. Brown

Department of Chemical Engineering, University of Colorado, Boulder, Colorado 80302 (*Received October 20, 1967*)

A model for the multilayer flow of adsorbed gases is developed and its application to surface migration in microporous media is investigated. Transport within an individual layer is viewed as resulting from a two-dimensional spreading-pressure gradient, and momentum exchange between adjacent layers is represented by a simplified law. Equations for the concentration of each layer are developed within the framework of BET adsorption theory. Employing a circular-pore geometry, a two-parameter relation results which describes the adsorbed flux. The model is applied to published experimental data. The values obtained for the two parameters exhibited concentration dependence, temperature dependence, and relationship with each other in agreement with physical expectations. The quantitative values of the parameters are dependent upon the assumed number of adsorbed layers, however, and this represents a weakness of the model.

Introduction

Previous investigators of the surface transport of adsorbed gases have described it by a single-phase flow utilizing a spreading pressure or with models based on random molecular movement between adsorbed sites. These models do not consider the possible multilayer nature of adsorption nor do they allow for the dilute-liquid behavior of these adsorbed layers. This article presents a multilayer model for the flow of adsorbed gases and investigates its application to surface transport in microporous media.

For many years the transport of adsorbed gases has been generally accepted and has come to be known as "surface migration" or "surface diffusion." A recent review of the surface diffusion of adsorbed molecules is that by Dacey.[1] Hayward and Trapnell[2] provide a fairly complete discussion of the surface mobility of chemisorbed species.

In Dacey's review, four regions for surface flow in porous solids are considered. The first region occurs at very low pressures where surface coverages are very small. At somewhat higher surface concentrations, a region of less-than-monolayer coverage occurs. Multilayer coverage is significant in the third region, while capillary condensation exists in the fourth.

To explain the surface flow in these regions, several models have been proposed.[3-8] While none correlates the data in all regions, the models proposed by Smith and Metzner[6,7] and by Gilliland, *et al.*,[4,5] have had fair success. Smith and Metzner's equation for surface flow was derived from a basis of random molecular motion between adsorbed sites and fits data well at low coverage. Gilliland, *et al.*, proposed a single-phase flow resulting from a spreading pressure and obtained the best results at low- and intermediate-adsorbed concentrations. Both assumed only a single surface layer.

Since multilayer coverage begins to assume significant

(1) J. R. Dacey, *Ind. Eng. Chem.*, **57**, 27 (1965).

(2) D. O. Hayward and B. M. W. Trapnell, "Chemisorption," 2nd ed, Butterworths and Co. Ltd., Washington, D. C., 1964.

(3) S. Kruyer, *Koninkl. Ned. Akad. Wentenschap. Proc.*, **56B**, 274 (1952).

(4) J. S. Russell, Sc.D. Thesis, Massachusetts Institute of Technology, Cambridge, Mass., 1963.

(5) E. R. Gilliland, R. F. Baddour, and J. S. Russell, *A.I.Ch.E.* (*Amer. Inst. Chem. Eng.*) *J.*, 4 (1958).

(6) R. K. Smith, M.Ch.E. Thesis, University of Delaware, Newark, Del., 1963.

(7) R. K. Smith and A. B. Metzner, *J. Phys. Chem.*, **68**, 2741 (1964).

(8) J. A. Weaver and A. B. Metzner, *A.I.Ch.E.* (*Amer. Inst. Chem. Eng.*) *J.*, **12**, 655 (1966).

proportions at concentrations far below that corresponding to a BET monolayer, it was decided to study theoretically the possible behavior of surface flow in multimolecular layers.

Derivation of the Model

A. Basic Assumptions. This section presents a simplified model for the multilayer flow of adsorbed molecules utilizing a two-dimensional "spreading pressure" within the different layers. The model is based on the following assumptions.

(1) The net transport within an individual layer is caused by a gradient in the spreading pressure.

(2) The two-dimensional pressure in a layer is a function only of the concentration within that layer.

(3) The momentum possessed by a given layer is proportional to the product of the concentration and velocity of that layer. The momentum exchanged between two layers is proportional to the difference in the momenta of the two layers.

(4) The concentration within a layer is equal to that predicted by the BET adsorption theory.

(5) The two-dimensional pressure is characterized by a two-dimensional equation of state.

(6) The thickness of each adsorbed layer equals the diameter of the adsorbed molecule as calculated from the critical volume.

In order to determine the concentrations of each layer, the multilayer adsorption theory developed by Brunauer, Emmett, and Teller (BET)[9] is used. In the BET derivation s_i is defined as the area of surface which is covered by only i layers of molecules (*i.e.*, s_0 is the free area and s_1 is the area covered by *only* one layer but not the total area of the first layer). It is also shown that

$$\varepsilon_i = z s_{i-1} = z^{i-1} s_1 \qquad (1)$$

This relationship according to the BET theory holds for any number of layers.

B. Concentration within an Individual Layer. If the BET theory of multilayer adsorption is accepted, the concentration of any layer can be found as a function of the total adsorbed concentration and the relative pressure. The concentration within a layer, x_j, is proportional to the sum of the BET areas covered by j or more layers. Thus

$$x_j \propto s_j + \ldots + s_n = s_1(z^{j-1} + \ldots + z^{n-1}) \qquad (2)$$

The total adsorbed concentration, y, is then the sum of the individual-layer concentrations, so that in general

$$x_j = y\left(\frac{\sum_{i=j}^{n} z^{i-1}}{\sum_{i=1}^{n} i z^{i-1}}\right) \qquad (3)$$

C. Flux within Circular Pores. The adsorbed flow in an individual layer is proportional to the product of
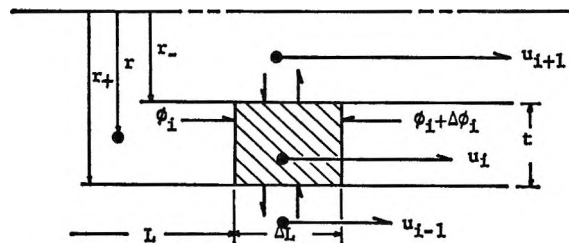

Figure 1. Momentum balance for the circular pore.

the concentration of that layer and its average net velocity. The total adsorbed flow is the sum of the flows in each layer.

It is possible to describe surface flow in a catalyst pellet by a circular-pore geometry. The momentum-balance diagram for multilayer flow in a circular pore is shown in Figure 1. Since the momentum exchange between two layers is assumed proportional to the difference in the momenta of the layers, a momentum balance on layer i yields the following rates of momentum exchange: at r_+

$$\text{in} \qquad +k_2 2\pi r_+ x_{i-1} u_{i-1} \Delta L$$

$$\text{out} \qquad -k_2 2\pi r_+ x_i u_i \Delta L$$

at r_-

$$\text{in} \qquad +k_2{}^* 2\pi r_- x_{i+1} u_{i+1} \Delta L$$

$$\text{out} \qquad -k_2{}^* 2\pi r_- x_i u_i \Delta L \qquad (4)$$

at L

$$\text{in} \qquad +k_3 2\pi r t x_i u_i$$

at $L + \Delta L$

$$\text{out} \qquad -k_3 2\pi r t (x_i u_i + \Delta x_i u_i)$$

The forces in the direction of flow are: at L, $2\pi r t \phi_i$; and at $L + \Delta L$, $2\pi r t (\phi_i + \Delta\phi_i)$. The term $\Delta x_i u_i$ in eq 4 is equal to zero because it is assumed that there is no net transfer of material from one layer to the next. Hence from continuity considerations $x_i u_i$ is constant. It is also assumed that the rate of momentum exchange between any two layers has the same proportionality constant, so that $k_2 = k_2{}^*$.

Summing the terms and taking the limit as ΔL approaches zero

$$\frac{d\phi_i}{dL} = k_2\left(\frac{r_+}{r} x_{i-1} u_{i-1} - \frac{r_+ + r_-}{r} x_i u_i + \frac{r_-}{r} x_{i+1} u_{i+1}\right) \qquad (5)$$

in which the ratios r_+/r and r_-/r are evaluated for each layer. If n layers are allowed to fill the catalyst pore, these ratios become

$$\left(\frac{r_+}{r}\right)_i = \frac{(n + 1 - i)}{(n - 1/2 - i)} \equiv c_i \qquad (6)$$

(9) S. Brunauer, P. H. Emmett, and E. Teller, *J. Amer. Chem. Soc.*, **60**, 309 (1938).

$$\left(\frac{r_-}{r}\right)_i = \frac{(n-i)}{(n-1/2-i)} \equiv e_i \qquad (7)$$

For the first layer, the momentum balance is

$$\frac{d\phi_1}{dL} = -(k_1 + k_2)c_1 x_1 u_1 + k_2 e_1 x_2 u_2 \qquad (8)$$

The constant describing momentum exchange between the first adsorbed layer and the solid (k_1) is assumed to be different from that between adjacent layers (k_2).

de Boer[10] shows the spreading pressure can be expressed in terms of concentration by the use of two-dimensional equations of state analogous to those for three-dimensional gases. An equation of state analogous to the Volmer equation was chosen for study. This enabled some compensation for nonidealty. The van der Waals equation of state was not used because of uncertainty in the attractive force constant under adsorbed conditions.

For the Volmer equation of state

$$\phi_i(A - \bar{n}_i b) = \bar{n}_i RT \qquad (9)$$

and, noting that $\bar{n}_i/A = x_i/S$

$$\frac{d\phi_i}{dL} = \frac{RT}{S} \frac{1}{\left(1 - \frac{b}{S}x_i\right)} \frac{dx_i}{dL} \equiv \frac{RT}{S}\left(g_i \frac{dx_i}{dL}\right) \qquad (10)$$

By using the set defined by eq 5 and 8, a system of n simultaneous equations determining the velocities of each of the n layers in terms of their concentrations and spreading-pressure gradients can be obtained. This set of equations in matrix form is

$$k_1 \underline{A}\,\underline{u} = \underline{\phi} \qquad (11)$$

in which

$$\underline{A} = \begin{bmatrix} -(c_1 + fe_1)x_1 & fe_1 x_2 & & \\ fc_2 x_1 & -f(e_2 + c_2)x_2 & fe_2 x_3 & \\ & & \cdots & \\ & & fc_n x_{n-1} & -fe_n x_n \end{bmatrix} \qquad (12)$$

and

$$\underline{\phi} = (RT/S)[g_i dx_i/dL] \qquad (13)$$

In the above, $f = k_2/k_1$.

The expression for the total adsorbed flux in terms of the concentrations and surface velocities of each layer is

$$N/A_{cs} = \rho \sum_{1}^{n} x_i \hat{u}_i \qquad (14)$$

Because the adsorbed molecules follow a tortuous path through the microporous plug, the surface velocity and distance along the surface can be related to their average components by the tortuosity factor. So $L = \tau L_p$ and $\hat{u}_i = (1/\tau)u_i$. Writing eq 14 in vector notation

$$N/A_{cs} = (\rho/\tau)\underline{x}\cdot\underline{u} \qquad (15)$$

Solving eq 11

$$\underline{u} = \left(\frac{1}{k_1}\right)\underline{A}^{-1}\underline{\phi} \qquad (16)$$

Combining eq 13, 15, and 16

$$\frac{N}{A_{cs}} = \left(\frac{\rho RT}{Sk_1\tau^2 L_p}\right)\underline{x}\underline{A}^{-1}\left[g_i \frac{dx_i}{dL_p}\right] \qquad (17)$$

Separating variables and integrating

$$\frac{N}{A_{cs}} = \frac{\rho RT}{Sk_1\tau^2 L_p}\int_{r_i}^{r_t}\underline{x}\underline{A}^{-1}[g_i dx_i] \qquad (18)$$

Equation 18, relating the catalyst properties, the momentum-transfer constants, pressure, pressure drop, and adsorbed concentration to the adsorbed flux, is the basic equation for the multilayer surface-transport theory proposed in this paper.

The two-dimensional constants for the Volmer equation of state can be evaluated from its three-dimensional counterpart as presented by de Boer[10]

$$b = \frac{3b_3}{4d} \qquad (19)$$

where $d = d(3b_3/2N_{av})^{1/3}$.

In order to obtain a measure of the thickness of an adsorbed layer, an effective diameter based on volumetric measurements is used. This relation, presented by Moore,[11] is

$$t = \sqrt[3]{\frac{0.74v_c}{\frac{\pi}{6}N_{av}}} \qquad (20)$$

For the circular-pore geometry, the maximum number of layers filling the pore is given by

$$n = D/2t \qquad (21)$$

Once n is determined, the matrix and vector elements of the integrand in eq 18 may be evaluated.

Investigation and Discussion of the Multilayer Model

In order to investigate the multilayer model and to compare it with previous models, data in the form of observed fluxes and the pressure drops at several mean adsorbed concentrations were required. The adsorbed-flow measurements selected, which were believed to be the most complete currently available, were those presented by Russell.[4] In addition to surface-flow measurements for ethylene, propylene, and isobutane on Vycor at three temperatures, the required adsorp-

(10) J. H. de Boer, "The Dynamical Character of Adsorption," Oxford University Press, London, 1953.

(11) W. J. Moore, "Physical Chemistry," Prentice-Hall Inc., Englewood Cliffs, N. J., 1962.
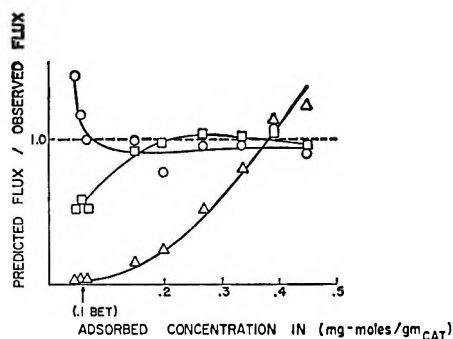
Figure 2. Flux ratios for propylene at 298°K.:   O, multilayer; □, Russell; △, Smith.

tion isotherms and the physical description of the adsorbent were included.

The parameters for all models were evaluated at the minimum of the sum of the squares of the differences between the predicted and observed values of the surface flux. For the models requiring a single parameter, a linear least-squares method was used. For the multilayer model a search technique was employed to find the values of k_1 and k_2 corresponding to the minimum of the sum of the error squared. No prior assumptions were made concerning the values of or relationships between k_1 and k_2. The technique is fully described by one of the authors.[12]

Comparison with Other Models. Typical results obtained for the multilayer model and the models of Smith[6] and Russell[4] are shown in Figure 2. If the entire concentration range is considered, Smith's model gave by far the poorest results. Because this model was derived for a unimolecular layer, it might be expected to correlate the data only at low coverage. At low adsorbed concentrations, the slope of the flux-ratio curve approached zero, indicating that Smith's model gave its best results in this range. Russell's model was found to fit the data most satisfactorily at the higher coverage ranges but showed negative deviations at low concentrations.

The multilayer model fits the data in the higher concentration regions as well as the prior models but at low surface coverages predicts fluxes considerably higher than those observed. The breakdown of the present multilayer surface-diffusion model within this range is not unreasonable. In this model, the momentum exchange between the first adsorbed layer and the surface is characterized by k_1. This parameter is probably related to the attraction of the adsorbed molecule to the surface. Young and Crowell[13] indicate that heats of adsorption, also related to the attraction of the adsorbed molecule to the surface, can vary considerably with coverage at low concentrations. While no precise correlation between the heat of adsorption and k_1 is suggested, it is probable that on the surface a distribution of the attraction between the surface and the adsorbed molecule exists; at low coverage the value

of k_1 would be concentration dependent. At lower concentrations the higher energy sites would be selectively filled, and k_1 would be expected to decrease with increasing coverage. Because k_1 was found by considering all the data from a given run, the value used to predict the fluxes at low concentrations would be smaller than it should have been, and fluxes that were too large resulted. At higher coverage the possible leveling of the distribution of the attracting sites would eliminate this effect.

Behavior of Parameters k_1 and k_2. Comparison of k_1 and k_2 for each data set in Table I indicates that k_2 is smaller in every case. This would be expected, since the molecules in the first layer would be attracted strongly to the solid surface and a momentum exchange with the solid more rapid than that between adjacent layers would result.

Table I: Momentum-Transfer Coefficients for the Multilayer-Model Volmer Equation of State

Temp, °K	$10^{-10}k_1$, sec^{-1}	$10^{-10}k_2$, sec^{-1}
	Ethylene	
273	5.818	0.1060
298	6.935	0.0469
313	5.940	0.0459
	Propylene	
273	3.783	0.2417
298	3.107	0.1740
313	3.749	0.0826
	Isobutane	
273	5.897	0.5390
298	1.879	0.4721
313	1.875	0.3016

The value of k_2 decreases steadily with temperature in all three of the cases studied. The momentum transfer between adsorbed layers is indicated to decrease with increasing temperature much as the momentum transfer within liquids decreases, as evidenced by the change of viscosity with temperature. (In gases, on the other hand, viscosity increases with temperature.) The liquidlike behavior between adjacent layers is not unreasonable. Within an adsorbed layer, molecules may be relatively far apart resulting in gas behavior. However, the distances between the centers of molecules in adjacent layers in the direction normal to the surface is of the order of the molecular diameter—the same separation as in liquids.

Inspection of the parameter k_1 indicates no apparent trend with temperature. It is believed that the opti-

(12) W. K. Bell, M.S. Thesis, University of Colorado, Boulder, Colo., 1967.
(13) D. M. Young and A. D. Crowell, "Physical Adsorption of Gases," Butterworths and Co. Ltd., London, 1962.

mization techniques used to find these parameters would disguise all but strong trends in the data, and thus a hidden temperature dependence for k_1 may exist.

Effect of the Number of Layers. Because fewer than the maximum number of adsorbed layers could exist during surface migration, a more satisfactory relation for the circular-pore model was considered possible if fewer than this number was assumed. To investigate the effect of the number of layers, two sets of data (isobutane at 40° and ethylene at 25°) were examined. The number of adsorbed layers was varied from one to the maximum in each case. The results are presented in Figure 3 and Table II.

Table II: Effect of the Number of Layers in Multilayer Model

	No. of layers				
	$10^7 E$				
	1	2	3	4	5
Ethylene 298°K	2.32	0.382	0.393	0.397	0.398
Isobutane 313°K	0.81	0.49	0.51	0.54	

When the effect of the number of layers from two to the maximum is considered, the differences in mean errors are small and the greatest deviations occur at the low-concentration range, where the model has been shown to err. Since optimum values of the momentum-exchange parameters were chosen, the effect of increasing the number of layers was just offset by increases in k_1 and k_2. Because the data are correlated with approximately the same accuracy for any number of adsorbed layers between 2 and 5, absolute values for k_1 and k_2 must be considered unreliable. This insensitivity to the number of layers must be regarded as a weakness of the model in its present form.

When a single adsorbed layer is considered, the multilayer model contains only one adjustable parameter. Although with one layer the present model is similar to Russell's single-phase model, this model differs from Russell's single-parameter model in two fundamental respects.

(1) The momentum transfer between the adsorbed gas and the solid for the Russell model is proportional to only the velocity of the phase, while in the present study it is proportional to the product of the concentration and the velocity.

(2) For the present model the gradient in spreading pressure is related to the gas pressure *via* the adsorption isotherm and a two-dimensional equation of state. In the Russell case, the Gibbs adsorption isotherm relates gas-phase pressure to spreading pressure.

For the isobutane the deviation of the single-layer

limit is smaller than for the Russell model, but the opposite is true for the ethylene data (see Table II). These comparisons show that if the present theory were limited to one layer, thus possessing the advantage of only one parameter, it is possible that this model would predict results as satisfactorily as those of Russell.

Extension to a Flat Plate. If the number of adsorbed layers is large, a flat-plate geometry may better describe the surface. Assuming a flat plate the area correction elements, c_i and e_i, of matrix $\underline{A}$ become unity. Also, if the number of adsorbed layers is allowed to become very large, the terms in eq 3 may be approximated by their infinite sums resulting in further simplification.

The flux on a flat surface resulting from migration in n adsorbed layers can now be considered. Because of the symmetry of $\underline{A}$, a general relation for the inverse can be found. The total adsorbed flux can then be obtained as a function of adsorbent properties, spreading-pressure gradients in each layer, momentum-exchange parameters, and the number of adsorbed layers by using eq 16. This procedure has been carried out by one of the authors.[12] The resulting flux relation is

$$N/A_{cs} = \frac{-f}{Kk_1}\left[n\dot{\phi}_1 + \{n + (n-1)K\}\dot{\phi}_2 + \right.$$
$$\left. \cdots + \left\{n + \sum_{j=1}^{n-1} jK\right\}\dot{\phi}_n \right] \quad (22)$$

where $K = 1/f$.

If the spreading-pressure gradient in the first layer is nonzero, the total flux increases without limit as n becomes large, if only the first term in the series is considered. Since all additional terms are positive, these remaining terms only aggravate the situation. Finite values of the flux are thus unattainable if k_1 is finite and n increases without limit. The flat-plate model using an infinite number of adsorbed layers, therefore, cannot be considered a reasonable approximation of an existing physical situation describing surface flow.

Comparison of Equations of State. In order to estimate the effects of the Volmer correction for nonideality, the results of using a two-dimensional ideal equation of state were compared with the results of using the Volmer equation. The results using a two-dimensional van der Waals equation of state were also obtained to estimate the value of further corrections for nonideality. A typical comparison of the predicted:observed flux ratio as a function of adsorbed concentration for the three equations of state is shown in Figure 4. All three equations present similar curves, although the Volmer equation does give somewhat better results than the other two. Poorest behavior is shown by the van der Waals equation, presumably caused by the difficulty of determining a realistic value for the two-dimensional attractive-force constant. The superiority of the
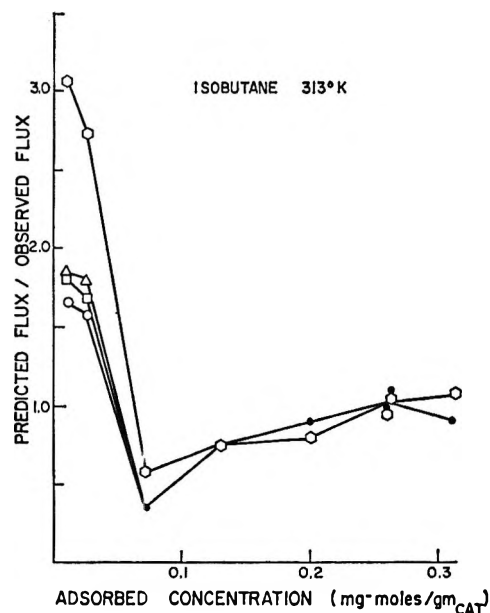
Figure 3. Effect of the number of layers on the multilayer model: ○, 1 layer; ⊙, 2 layers; □, 3 layers; △, 4 layers; ●, 2, 3, and 4 layers.

Volmer equation, though slight, existed in seven of the nine cases studied.

It should be pointed out that there are some internal inconsistencies in the model presented here. The BET adsorption theory assumes localized adsorption in all layers, yet this model assumes completely mobile molecules in the adsorbed layers, with concentrations derived from BET theory. A second inconsistency lies in the use of an equation of state to determine the spreading pressure. Once the concentration within a two-dimensional adsorbed phase is known, the spreading pressure in theory can be obtained from the Gibbs adsorption equation. When this is applied to the present system, the resulting equations are quite complicated, and the simpler picture was adopted to obtain a mathematically tractable system. It is still believed, in spite of these inconsistencies, that this model presents a useful approach to the problem of surface transport.

Conclusions

In the development of the multilayer model, transport within individual adsorbed layers is viewed as a result of a gradient in a two-dimensional spreading pressure. This spreading pressure is found through the use of simple two-dimensional equations of state. A simplified representation of momentum transfer between adjacent layers is devised, and equations are developed to describe the concentrations of the individual layers using the BET adsorption theory. Relations describing the adsorbed flux are then derived. Two geometries describing the adsorbent surface are considered—a flat plate and a circular pore.
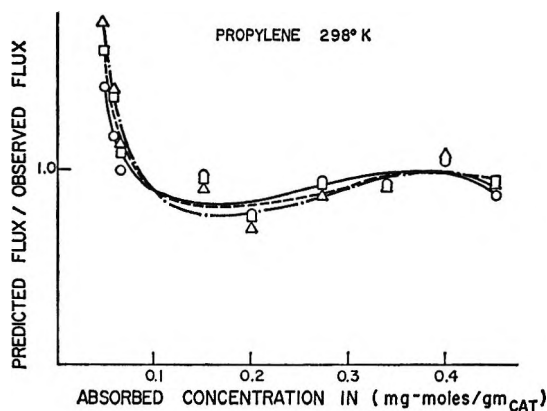

Figure 4. Comparison of equations of state for the multilayer model: − − −, ideal (□); ———, Volmer (○); —·—·, van der Waals (△).

Within a circular pore, the number of layers is limited, and the model predicts finite fluxes. The equations describing the flux are applied to data for surface flow. Comparison with previous models indicates that the multilayer model correlates the data as accurately as the best of the previous models in regions of intermediate and high surface coverage. At low adsorbed concentrations the multilayer model predicts fluxes higher than those observed. This deviation at low coverage is attributed to surface nonuniformity.

No prior assumptions are made regarding the quantitative values or properties of the coefficients describing momentum transfer. Values of these coefficients are obtained by comparing the theory with experimental data. Behavior of the two parameters with relation to each other and to surface coverage and temperature is in agreement with physical reality. The model's principal weakness is that the calculated values of the momentum-transfer parameters depend strongly upon the number of adsorbed layers.

Notations

A_{cs}	Cross-sectional area of the plug, cm²
a	Two-dimensional van der Waals repulsion term, ergs cm²/mol
a_3	Three-dimensional van der Waals repulsion term, ergs cm³/mol
b	Two-dimensional Volmer correction, cm²/mol
b_3	Three-dimensional Volmer correction, cm³/mol
C_R	Coefficient of resistance, g/sec cm²
c_i	Ratio of the outer radius to the mean radius in layer i
D	Diameter of the pore, cm
d	Molecular diameter, cm
E	Square root of the average error in the flux squared, mg-mol
e_i	Ratio of the inner radius to the mean radius in layer i
f	Momentum-exchange ratio, k_2/k_1
g_i	Nonideality spreading pressure gradient correction
K	$1/f$

$k_1, k_2,$ k_2^*, k_3	Momentum-exchange rate constants, sec^{-1} or $(g/g\text{-}mol)(g_{cat}/cm^2)\ sec^{-1}$	t	Thickness of adsorbed layer, cm
L	Length in the direction of flow *on* the surface, cm	u_1	Velocity of layer 1 on the surface, cm/sec
L_p	Length in the direction of flow through the plug, cm	u_i	Velocity of layer i in the direction of the plug axis, cm/sec
N	Molar flow rate, mg-mol/sec	v_c	Critical volume, cm^3
N_{av}	Avogadro's number of molecules, molecules/mol	x_i	Concentration of layer i, mg-mol/g_{cat}
n	Number of layers	y	Total adsorbed concentration, mg-mol/g_{cat}
$\bar{n}_i$	Number of moles, mol	z	Relative pressure, p/p_0
p	Gas-phase pressure, mm		
p_0	Vapor pressure, mm	*Greek Letters*	
R	gas constant, mg cm^2/sec^2 mg-mol deg	ρ	Apparent catalyst density, g_{cat}/cm^3
S	Specific surface area, cm^2/g_{cat}	τ	Tortuosity factor
s_i	BET areas, cm^2	ϕ_i	Spreading pressure in layer i, dyn/cm
T	Temperature, °K	$\dot{\phi}_i$	Spreading-pressure gradient in layer i, dyn/cm^2

Infrared Spectrum, Surface Reaction, and Polymerization of

Adsorbed Hydrogen Cyanide on Porous Glass

by M. J. D. Low, N. Ramasubramanian, P. Ramamurthy, and A. V. Deo

Department of Chemistry, New York University, New York, New York 10453 (*Received October 25, 1967*)

Infrared spectra of HCN sorbed on highly dehydroxylated porous glass as well as on pure and boria- and alumina-impregnated silica were recorded. Some HCN dissociates, boria on the porous glass acting as the adsorption and dissociation center, and new B–OH and Si–OH groups are formed. Physical adsorption of HCN occurs by hydrogen bonding to both types of surface OH groups and to oxygen atoms through the HCN hydrogen atom. HCN is also bound through the nitrogen atom to aluminum ions present as an impurity on the porous glass surface. Polymerization occurs, the aluminum acting as reaction center.

In their report of the study of the infrared spectrum and surface polymerization of HCN adsorbed on porous glass, Kozirovski and Folman[1] noted that the band due to surface OH groups may appear as a closely spaced doublet if the glass was degassed at 900°. The reason for the appearance of the doublet was not clear to them, but they suggested that one of the bands may have been due to OH groups attached to boron atoms present in small amounts in the glass (the other being due to surface silanols). Later work showed the validity of their suggestion. A sharp band at 3748 cm^{-1} due to free surface silanol groups and a second, sharp band at 3703 cm^{-1} due to surface B–OH groups were reported.[2,3] Kozirovski and Folman noted the adsorption of HCN occurring on two different sites at small surface coverage as well as the hydrogen bonding of adsorbed HCN to two types of OH groups at higher coverage, but they did not give any further consideration to surface B–OH groups. It has been found, however, that the presence of boron affects the silica skeleton of the glass. Surface boron acts as an ad-

sorption and reaction center in the hydration of porous glass,[4,5] and provides Lewis-acid-type sites for the adsorption and reaction[6] of NH_3. We have consequently studied the sorption of HCN.

The present work was carried out with highly degassed porous-glass specimens in order to be able to observe clearly the changes occurring in the B–OH band, whereas a part of Kozirovski and Folman's work was done with specimens degassed at 450°. The B–OH band is not developed[3] unless an appreciable amount of water is removed by degassing above 600°, but high-temperature treatments lead to a diffusion of

(1) Y. Kozirovski and M. Folman, *Trans. Faraday Soc.*, **60**, 1532 (1964).

(2) M. J. D. Low and N. Ramasubramanian, *Chem. Commun.*, 499 (1965).

(3) M. J. D. Low and N. Ramasubramanian, *J. Phys. Chem.*, **70**, 2740 (1966).

(4) M. J. D. Low and N. Ramasubramanian, *ibid.*, **71**, 730 (1967).

(5) M. J. D. Low and N. Ramasubramanian, *ibid.*, **71**, 3077 (1967).

(6) M. J. D. Low, N. Ramasubramanian, and V. V. S. Rao, *ibid.*, **71**, 1726 (1967).

boron to the surface.[3,4,7] Work on NH_3 sorption, however, shows that appreciable amounts of boron exist on glass surfaces degassed at relatively low temperatures.[6,8-10] Consequently, although the glass surfaces used in the present study would have been enriched because of the migration of boron, comparison can be made of the present spectra with previous ones.

Experimental Section

Most of the general procedures employed were described elsewhere.[3-6] Porous glass,[11] Corning Code 7930, was purchased from Corning Glass Co. in the form of 1 mm thick sheets. Specimens 1 × 2.5 cm were cut, were installed in the infrared cell,[3] were heated in oxygen (*ca.* 60 torr) at 700° for 3-4 hr in order to remove carbonaceous impurities, and were then degassed at 850° for 14-30 hr. Palladium-diffused D_2 was used to deuterate the surfaces, a specimen being exposed to D_2 at approximately 850° until more than 90% of the OH groups had been converted to OD groups. HCN was prepared and tested as described by Kozirovski and Folman.[1] Boria- and alumina-impregnated samples of Cab-O-Sil[12] were prepared by the well-known incipient-wetness method, using boric acid and an $Al(NO_3)_3$ solution of appropriate concentrations and volumes. Alumina-enriched porous glass was prepared in a similar fashion by soaking glass in $Al(NO_3)_3$ solution, wiping off excess liquid, and then drying and degassing the specimens *in vacuo*. Leached porous glass specimens were prepared following the method of Little, Klauser, and Amberg.[13]

Spectra were recorded with Perkin-Elmer Models 521 or 621 spectrophotometers. The ordinates of the various figures are arbitrary and are displaced in order to avoid the overlapping of spectra.

Results and Discussion

Various experiments were carried out with highly degassed, but otherwise untreated, porous glass, with deuterated glass surfaces as well as with a variety of other adsorbents, some of which had been deliberately contaminated. The spectra recorded indicated that adsorption, dissociation, and polymerization of HCN occurred in a complex, simultaneously occurring set of reactions. A detailed examination of the various effects is consequently necessary. For simplicity, some interactions are considered individually.

Generation of Surface Hydroxyls. The prominent features of the spectrum of a highly degassed porous glass are an intense band near 3748 cm^{-1} (hereafter called the Si-OH band), generally attributed to surface silanols, and a less intense but sharp band near 3703 cm^{-1} (hereafter called the B-OH band), attributed to the OH stretching of surface B-OH groups.[2,3] Spectrum A of Figure 1 is an example. When an exhaustively dehydrated specimen was exposed to HCN at room temperature, significant changes occurred in the
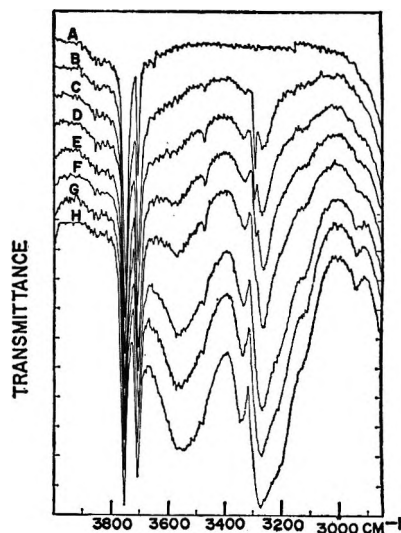

Figure 1. HCN sorption. After the background spectrum, A, of the clean glass had been obtained, spectra were recorded at the following pressures, in torr, in the presence of HCN at room temperature: B, 4; C, 8; D, 13; E, 20.5; F, 44; G, 58; H, 81.

OH region. With increasing HCN pressure there were minor changes in the Si-OH band, but the B-OH band broadened and increased in intensity (spectra B-J, Figures 1 and 2). Further increases occurred when the sorbed HCN was removed at low temperatures (spectra K-N, Figure 2). The B-OH band then decreased somewhat if the sample was degassed at progressively higher temperatures up to 600°. The B-OH band intensity after an adsorption-desorption cycle was greater than that preceding the cycle.

It is doubtful if any quantitative relation between the relative intensities of B-OH and other bands is valid for spectra recorded in the presence of gaseous or adsorbed HCN, because small but significant changes in the B-OH-band intensity occurred with time. For example, when a freshly degassed sample was exposed to HCN at room temperature and the spectra were recorded at various times up to 5 hr, the B-OH band increased in intensity and broadened slowly and progressively. Small changes in other bands are considered later. The changes occurring in the Si-OH band were smaller and less well defined than those found with the B-OH band. The Si-OH band broadened slightly and shifted to lower wave numbers

(7) T. H. Elmer, I. D. Chapman, and M. E. Nordberg, *J. Phys. Chem.*, **67**, 2219 (1963).

(8) N. W. Cant and L. H. Little, *Can. J. Ceram.*, **42**, 802 (1964).

(9) I. D. Chapman and M. L. Hair, *Trans. Faraday Soc.*, **61**, 1507 (1965).

(10) M. L. Hair and I. D. Chapman, *J. Amer. Ceram. Soc.*, **49**, 651 (1966).

(11) M. E. Nordberg, *ibid.*, **27**, 299 (1944).

(12) G. Cabot Co., Boston, Mass.

(13) L. H. Little, H. E. Klauser, and C. H. Amberg, *Can. J. Chem.*, **39**, 42 (1961).
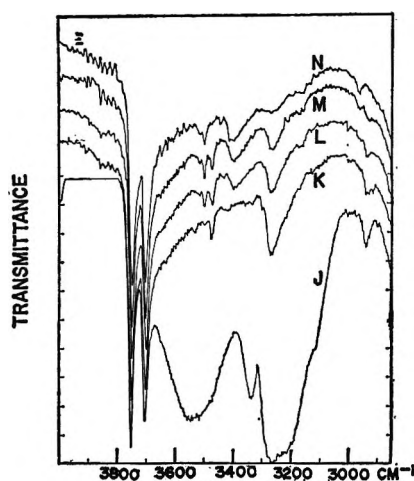
Figure 2. HCN desorption. Continuation of the sequence of Figure 1. After HCN sorption at 103 torr (spectrum J), degassing was as follows: K, 5 min at room temperature; L, 1 hr at room temperature; M, 2–5 hr at room temperature; N, 30 min each at 60, 120, and 200°.
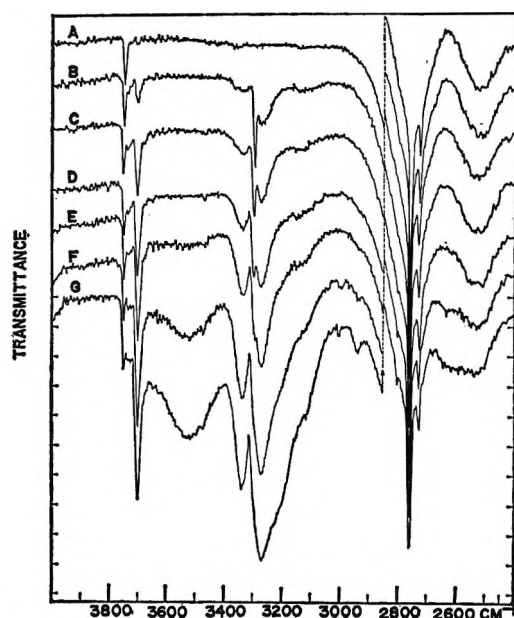

Figure 3. HCN sorption, deuterated glass. After the background spectrum, A, of the deuterated specimen had been recorded, spectra were recorded at room temperature in the presence of HCN at the following pressures, in torr: B, 2; C, 7.5; D, 14.5; E, 29.5; F, 61; G, 94.

by approximately 2 cm^{-1} with increasing HCN pressure. However, it is not possible to define precisely the changes in intensity of the Si-OH band, especially when appreciable amounts of HCN were sorbed, because HCN sorption caused a reversible increase in the sample transmittance, most evident in the 4000–3800-cm^{-1} region (spectra H and J, Figures 1 and 2). After a complete cycle of HCN sorption followed by degassing at high temperature, however, the original "background" was restored, the Si-OH band resuming its original location at 3748 cm^{-1} but with slight increases in intensity and half-width.

Analogous results were obtained with deuterated porous glass. Spectrum A of Figure 3 of a deuterated specimen shows the remnant of the previously prominent Si-OH band, indicating that the conversion of OH to OD groups was not far from completion. The Si-OD band at 2760 cm^{-1} and the B-OD band at 2728 cm^{-1} of spectrum A are superimposed on a broad band of the adsorbent.[3] The B-OH band appeared when the sample was exposed to HCN and grew in intensity with increasing HCN pressure (spectra A-G, Figure 3). The Si-OH band increased only slightly with increasing pressure, but there were no significant changes in the Si-OD and B-OD bands. Complex changes occurred in both the OH and OD regions when the adsorbent was degassed (Figure 4). The B-OD and Si-OD bands first increased slightly as physically adsorbed HCN was removed and then decreased on pumping at successively higher temperatures. Simultaneously, the B-OH band decreased and the Si-OH band increased continuously. There were no shifts in band positions larger than approximately 2 cm^{-1}.

Experiments using differential techniques with other deuterated samples which were exposed to HCN at
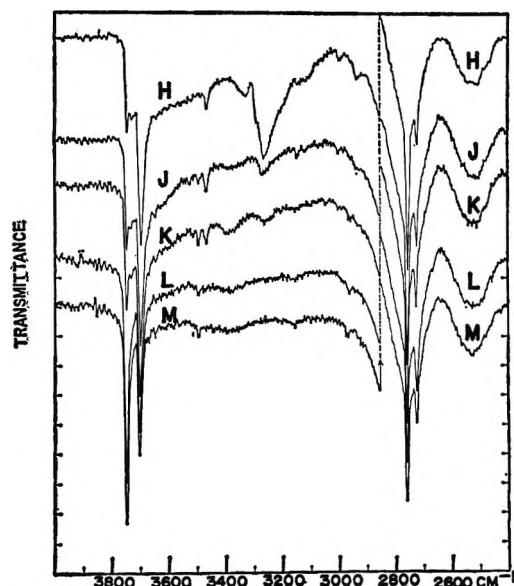

Figure 4. HCN desorption, deuterated glass. Continuation of the sequence of Figure 3. Spectrum H was recorded after the pressure had been reduced to 10 torr. The specimen was then degassed as follows: J, 4.5 hr at room temperature; K, 30 min at 65°; L, 30 min at 160°; M, 30 min at 250°.

room temperature for several hours confirmed that the changes in the OH region, particularly the growth of the B-OH band, occurred without significant changes in the Si-OD and B-OD bands. Similarly, large changes which would indicate an extensive conversion from OD to OH were not found even after long exposures to HCN. A deuterated specimen was exposed to HCN at

room temperature for 5 days and was then degassed; a large decrease of the OD bands occurred only when the temperature was raised appreciably above room temperature. Also, a distinct band near 2618 cm^{-1} owing to the ν_3 vibration of the DCN molecule[1] was not observed.

The various results show that the exchange reaction at room temperature between gaseous or adsorbed HCN and surface OD groups occurred very slowly, in distinct contrast to the results reported by Kozirovski and Folman.[1] They reported that, within a few minutes after exposure of a deuterated specimen to HCN, new bands appeared at 4545, 3745, 3571, and 2618 cm^{-1}, and they concluded that the exchange was quite fast. As their 3745-cm^{-1} OH band grew, the 2762-cm^{-1} OD band weakened. The 2618-cm^{-1} band had been ascribed to the ν_3 vibration of DCN formed by the exchange. However, they had deuterated their adsorbent by adsorbing D_2O vapor and by heating at 100° for 1 hr with subsequent desorption at 450°, repeating this treatment three or four times until practically all the OH groups were replaced by OD. In comparing their spectra of samples before and after deuteration, they reported that the band at 3745 cm^{-1} due to surface OH groups nearly disappeared, and in its place appeared a band of comparable intensity due to surface OD groups. However, it was shown[3-6] that degassing at 450° does not remove adsorbed H_2O or D_2O completely, and if the exchange reaction is carried out with D_2 (or with D_2O followed by adequate degassing), the OD bands are much smaller than the corresponding OH bands.[3-6] Such results indicate that the Kozirovski and Folman exchange experiments had been carried out with surfaces containing appreciable amounts of adsorbed D_2O. Hydrogen bonding of HCN to such D_2O as well as to OD groups would then bring about a band on the low-frequency side of the OD band, in direct analogy to a band near 3572 cm^{-1} ascribed[1] to hydrogen bonding of HCN to OH groups. Examples of such broad bands near 2600 cm^{-1} are shown in Figure 3. In view of such results, it seems unlikely that the 2618-cm^{-1} band was caused by the ν_3 vibration of DCN, except that Kozirovski and Folman observed effects similar to those described above involving the dissociation of HCN with the attendant formation of hydroxyl groups.

Further results which point to the importance of boron to the hydroxyl generation reaction came from experiments with adsorbents other than porous glass. Spectra obtained with highly degassed samples of the pure silica Cab-O-Sil[12] show that the prominent band at 3750 cm^{-1} due to isolated OH groups broadened slightly and shifted to approximately 3748 cm^{-1}, and a broad band formed near 3550 cm^{-1}, when HCN was adsorbed. The broad band disappeared and the silanol band was restored when the HCN was desorbed. In contrast, when HCN was adsorbed and then de-

sorbed on Cab-O-Sil impregnated with boria, the B–OH band at 3702 cm^{-1} grew in intensity, broadened, and shifted by approximately 5 cm^{-1}; also, the 3750-cm^{-1} silanol band increased slightly. The results are thus similar to those observed with porous glass. However, the results observed in the OH region when HCN was adsorbed on a Cab-O-Sil sample impregnated with 2% alumina were identical with those obtained with pure silica.

The various results described, particularly those with silicas, indicate the generation of surface hydroxyls to be due to an abstraction of hydrogen from the adsorbate rather than to the effects of traces of water contaminant. The relatively large increases found in the B–OH band of porous glass, as well as the results obtained with silicas, show that the dissociation reaction occurs predominantly with surface boron and is mainly independent of HCN adsorption and polymerization on other parts of the surface. This suggests that the principal reaction involves the breaking of B–O–B bridges. A similar reaction in which HCN reacts directly with siloxane bridges would be expected to occur to a much smaller extent, in view of the results found with pure silica. Also, the breaking of Si–O–B bridges, involving individual boron atoms linked to the silica structure, would make a minimal contribution to the over-all hydroxyl generation because such a reaction would require a larger buildup of Si–OH groups than the relatively small increase which was observed. These observations lend some support to the suggestion that small B_2O_3 aggregates or islands exist on the porous glass surface,[5] because the disruption of a B–O–B bridge would not lead to the formation of Si–OH groups. The fate of the CN fragments is uncertain.

A comparison of the results obtained with pure and with boron-containing silica indicates that the presence of boron increases the reactivity of the adsorbent to HCN, much as boron increases the reactivity of the otherwise inert silica to H_2O.[5] Also, the results with deuterated surfaces show that B–OH groups are formed to a larger extent during the initial reaction. When the temperature is raised, there seems to be a growth of Si–OH groups at the expense of B–OH groups. There is, also, a slow growth of the Si–OH band with respect to the B–OH band during long exposures to HCN. These effects suggest that boria islands act not only as adsorption and reaction sites but also as reservoirs from which the products of the reaction may migrate to the silica.

Bonding to Surface Hydroxyls. A broad absorption band appears in the 3600–3500-cm^{-1} region when HCN is taken up by the porous glass. Kozirovski and Folman mentioned a similar effect and, with a specimen degassed at 900°, noted that the band was composed of two overlapping bands at 3571 and 3484 cm^{-1}

which were ascribed to hydrogen bonding between the adsorbed HCN and two types of OH groups.

Two distinct bands were not observed in the present work. As shown in the sequence of spectra A–J of Figures 1 and 2, HCN sorption first caused a very broad absorption in the 3650–3500-cm^{-1} region and then a distinct, although broad, band near 3580 cm^{-1} (spectrum D). Contrary to prior observations, the absorption on the low wave number side of the band became relatively stronger with increasing pressure, as if a second, broad band were growing along with the first band; simultaneously, the center of the entire band moved to lower wave numbers near 3550 cm^{-1}. An analogous band was formed in the OD region near 2620 cm^{-1}, but the band was weaker and less well defined than the bands in the OH region. The broad band was near 3550 cm^{-1} if the Si–OH band was larger with respect to the B–OH band, $i.e.$, for surfaces containing a large proportion of Si–OH groups. With Cab-O-Sil, containing only Si–OH groups, the band was near 3560 cm^{-1}. Conversely, with surfaces containing a large number of B–OH groups with respect to the number of Si–OH groups, the band was near 3520 cm^{-1}, $e.g.$, spectra F and G, Figure 3. That the species producing the band were weakly held is shown by the ease with which the band could be diminished. Reductions in gas pressure reduced the band (spectra G and H, Figures 3 and 4), and short pumping at room temperature decreased the 3550-cm^{-1} absorption greatly with porous glass (spectra J and K, Figure 2) and also with Cab-O-Sil. Such behavior suggests that hydrogen bonding of HCN to Si–OH and to B–OH groups, respectively, contributed to the absorption at the high- and low-frequency portions of the broad 3550-cm^{-1} band.

$HCN\ Adsorption.$ Four bands due to adsorbed HCN molecules were reported.[1] A weak band at 4000 cm^{-1} was assigned to the $\nu_2 + \nu_3$ combination. This band was not observed during the present work, probably because of the increased transmission and background distortion in the 4000–3800-cm^{-1} region produced by relatively high HCN pressures (spectra H and J, Figures 1 and 2). A weak band at 2105 cm^{-1} observable at high coverage was assigned[2] to the ν_1 vibration, and a very weak band at 2137 cm^{-1} was assigned to $3\nu_2$. In the present work the small ν_1 and $3\nu_2$ bands were detected only at relatively high HCN pressures. The low intensities and consequent small utility of these bands focus attention on the more intense ν_3 vibration.

An absorption due to the ν_3 vibration (CH stretching mode) was previously reported[1] at 3268 cm^{-1} with porous glass degassed at 450°; with samples degassed at 900°, the ν_3 vibration appeared as a doublet with a spacing of 30 cm^{-1}. On further adsorption, only the lower frequency band continued to increase; in parallel, the broad bands due to hydrogen bonding increased. The doublet suggested HCN adsorption on
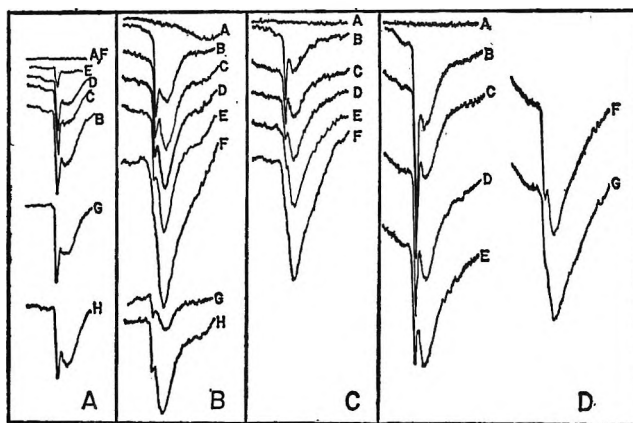

Figure 5. Spectra of the ν_3 region: (Part A) Degassed porous glass. After the background spectrum, A, was recorded, 3.5 torr of HCN was admitted, and after 2 min the pressure was reduced to below 1 torr (spectrum B). The specimen was then degassed, as follows: C, 2 min at room temperature; D, 15 min at room temperature; E, 30 min at 100°; F, 1 hr at 200°. The specimen was then exposed to 10 torr of HCN and the pressure was reduced to below 1 torr after 2 min (spectrum G). The specimen was then degassed for 1 hr at 200° and was exposed to HCN at 65 torr, and the pressure was reduced to below 1 torr after 2 min (spectrum H). The spectra were recorded at 1× ordinate expansion for part A but was recorded at 5× for other parts. (Part B) Degassed porous glass. After the background spectrum, A, had been recorded, the sample was exposed to HCN at room temperature for 5 min at the following pressures, in torr: B, 2; C, 5; D, 14; E, 24; F, 60. The sample was then degassed for 2 hr at room temperature (spectrum G) and, after additional degassing had removed residual bands, was reexposed to 14 torr of HCN for 5 min (spectrum H). (Part C) Leached porous glass. After the background spectrum, A, had been recorded, the sample was exposed to HCN at room temperature for 5 min at the following pressures, in torr: B, 2; C, 4; D, 14; E, 24; F, 64. (Part D) Al-impregnated porous glass. After the background spectrum, A, had been recorded, the sample was exposed to HCN at room temperature for 5 min at the following pressures, in torr: B, 2; C, 4; D, 14; E, 24; F, 44; G, 64.

two different sites. Frequency shifts and band shapes of the ν_3 absorption indicated that at high surface coverage, the hydrogen atom of the adsorbed HCN molecule was greatly affected and at least a fraction of the molecules was adsorbed via their hydrogen atoms. Kozirovski and Folman suggested for that case that the strong HCN dipole may be oriented with its positive end to the surface, with the hydrogen bound to surface oxygens; for low surface coverages, where the absorption band is much narrower, the molecules were adsorbed on OH groups via the nitrogen atom, leaving the hydrogen relatively little affected. The present results support the suggestion of dual adsorption modes. However, the behavior of the ν_3 doublet is complex and is partly obscured by changes of background, time, pressure, and polymerization effects, so that a variety of data must be considered.

The general behavior of the ν_3 absorption with increases in pressure is shown by Figures 1, 3, and 5.

When a fresh, highly degassed porous-glass specimen was exposed to HCN at low pressure, the ν_3 absorption consisted of a sharp band at 3294 cm^{-1} and a slightly asymmetric band centered at 3260 cm^{-1}. The latter increased in intensity, broadened, and apparently obscured the 3294-cm^{-1} band. The growth of the band in the 3700–3400-cm^{-1} region paralleled that of the 3260-cm^{-1} band (Figures 1 and 3). The spectra clearly showed that the positions of the band maxima did not change with increasing surface coverage, although the 3260-cm^{-1} band became more asymmetric with increasing pressure. Unfortunately, the unavoidable changes in adsorbent transmission with increased adsorption preclude a quantitative evaluation of the band intensities. The latter are also affected by time.

During the course of the work, several spectra were occasionally recorded at various times after a sample had been exposed to HCN at constant pressure. The time intervals varied from fractions of 1 hr to several hours or days. In general, the changes observed in HCN bands were small; e.g., several per cent transmittance at the highest pressures, most of the increase occurring during the first hour. The changes were slight at the lower pressures but were significant in that the intensity ratio of the doublet bands varied. For example, during the course of a 280-min exposure to HCN at 4 torr, the 3294-cm^{-1} band decreased while the 3260-cm^{-1} band increased slightly. At higher pressures the change with time of the intensity ratio was not clearly observable because the 3294-cm^{-1} band was obscured by the 3260-cm^{-1} band, but some effect of time and pressure could be deduced from desorption experiments.

A variety of experiments was carried out in which the sample was exposed to HCN for short times, and, to avoid time effects and changes of the surface due to polymerization, spectra were recorded only over a short interval. For Figure 5A, for example, after the background spectrum, A, of the degassed sample had been recorded, the sample was exposed to 5.5 torr of HCN for 2 min, the pressure was reduced to below 1 torr, and spectrum B was recorded. Spectra G and H were recorded after similar 2-min exposures to HCN at higher pressures. Spectra B, G, and H of Figure 5A, as well as other spectra, showed that the 3294-cm^{-1} band could be observed over the entire pressure range if the contact time was short. Both doublet bands were readily observable, and both bands declined continuously on degassing, subsequent to a short exposure to HCN at low pressure (spectra A–F, Figure 5A). Conversely, spectra recorded at various stages of degassing subsequent to exposure to HCN for many hours showed that the 3294-cm^{-1} band was diminished. If the pressure was reduced subsequent to an adsorption sequence, such as that of Figure 2 or 3, a weak 3294-cm^{-1} band could be detected, as in spectrum K of

Figure 2, but the small band was removed on further degassing. The sharp 3294-cm^{-1} band was not detected on degassing specimens which had been exposed to HCN for 5 days. For in-between cases, i.e., relatively short exposures at high pressures or long exposures at low pressure, the 3294 cm^{-1} band was small with respect to the 3260-cm^{-1} band; spectrum G of Figure 5B is an example.

In summary, the various data indicate that there was a change in the intensities of the two ν_3 bands. At constant pressure, the broad band grew slowly with the passage of time at the expense of the sharp band. Increasing the pressure increased the decline of the sharp band and increased the intensity of the broad band.

There was also a "poisoning" effect. All bands were removed and the transmittance was restored, except for changes in the OH region noted earlier, when an HCN-treated sample was degassed at high temperature. Degassing at 200° or below removed the ν_3 absorptions completely but did not precisely restore the sample transmittance in the 3500–3000-cm^{-1} range; depending upon the time of exposure, minor bands due to polymerized material remained. On exposing a sample to HCN, removing adsorbed HCN molecules by low-temperature degassing, and then reexposing the sample to HCN, the intensity ratio of the ν_3 bands was affected. Changes in background make it uncertain precisely as to what extent the 3260-cm^{-1} band was changed, but it is clear that the 3294-cm^{-1} band was diminished with respect to the 3260-cm^{-1} band. An example is shown in Figure 5B, spectra C and H. Such results indicate a decrease in the number of adsorption sites at which the species responsible for the 3294-cm^{-1} absorption could form. However, it seems unlikely that the site was a surface hydroxyl.

The relatively low adsorption of HCN on silica as well as on boron-impregnated silica and Kozirovski and Folman's observation that polymerization became more rapid with decreasing surface hydroxyl concentration suggested that some species other than surface boron, oxide, or hydroxyls may be involved. As porous glass contains some R_2O_3 impurities,[11] some spectra were recorded of HCN sorption on alumina-impregnated Cab-O-Sil and on alumina-enriched, as well as on leached, porous glass. A sharp band at 3294 cm^{-1} was formed when HCN was taken up by the alumina-impregnated Cab-O-Sil; this band was not found with pure or boria-impregnated Cab-O-Sil. With the treated porous glass, only the 3400–3100-cm^{-1} region was scanned after a sample was first exposed to HCN, in order to avoid time and polymerization effects. The pressure was then increased, the second short scan was begun, and so on, so that the sample was exposed to HCN for only 5 min at each pressure. Sequences of spectra recorded under comparable conditions with three samples are shown in parts B–D of

Figure 5. Observations of the OH region prior to HCN sorption showed the samples to be in comparable stages of dehydration. Comparison of the spectra shows that leaching, which reduces the R_2O_3 impurities,[13] diminished both ν_3 bands. Conversely, with the Al_2O_3-enriched sample, the sharp 3294-cm^{-1} band was markedly increased at the lower pressures. The broad 3260-cm^{-1} band was slightly enhanced, but changes in background at higher pressures again introduce some uncertainty. However, the intensity of the sharp band with respect to the broad band appeared to be increased over the entire pressure range. Such results suggest that the alumina impurity of porous glass, perhaps with some contribution from other R_2O_3 traces, was, to a significant extent, responsible for the formation of the HCN surface species causing the 3294-cm^{-1} absorption. The latter is sharp and is not subject to frequency shifts and is, consequently, assigned in great part to the little-perturbed ν_3 vibration of HCN bonded to surface aluminum ions *via* the nitrogen atom. The broader ν_3 band is attributed to hydrogen bonding of HCN through the hydrogen to surface oxygens and to hydroxyls.

Polymerization. Polymerization of HCN yields a black solid from which a crystalline compound can be recovered. The latter is a tetramer, was thought to be aminoiminosuccinonitrile (I),[14] but is now established to be diaminomaleonitrile (II).[15-19] The dimer iminoacetonitrile (III) was also suggested[20] for the crystals, but this structure was shown[19] to be based on an incorrect interpretation of X-ray diffraction data.

When HCN was polymerized on porous glass, the infrared bands detected led Kozirovski and Folman to suggest that both compounds II and III were formed but that compound I was absent.[1] HCN polymerization was also found in the present study which may be summarized as follows. (a) A small band at 3470 cm^{-1} was found even at low pressures, *e.g.*, spectrum A, Figure 1, and grew slightly with increasing pressure. Simultaneously, a broader band grew at 2940 cm^{-1}. (b) On pumping at room temperature, the 3470- and 2940-cm^{-1} bands decreased slightly, a broad band grew at 3400 cm^{-1}, and a relatively sharp band appeared at 3490 cm^{-1}. (c) When the temperature was raised above ambient, the 3470-cm^{-1} band decreased and vanished. The 2940-cm^{-1} band declined, but a band near 2960-cm^{-1} appeared. Both the 2940- and 2960-cm^{-1} bands declined with increasing temperature; the 2940-cm^{-1} band vanished before the 2960-cm^{-1} band. A small band was frequently, but not always, observed at 3510 cm^{-1}. Bands formed at 3490 cm^{-1} and near 2220 cm^{-1} in the CN region; occasionally a second CN band was found near 2250 cm^{-1}. The decline of the 2470- and 2940-cm^{-1} bands and growth of the other bands coincided with a change of the color of the adsorbent from yellowish to red-

brown. (d) The 3490-, 3470-, 3400-, and 2220-cm^{-1} bands at first became more prominent but then declined, and the color of the adsorbent deepened, with increasing severity of degassing. All bands were removed above 250°. (e) With adsorbents which had been exposed to HCN for 5 days, the absorption near 3500 cm^{-1} was more intense than with samples exposed for shorter times. The absorption appeared to be a composite one, the small but relatively sharp 3510- and 3490-cm^{-1} bands being superimposed on a broader band peaking near 3490 cm^{-1}.

Assignment of the various bands on the basis of group frequencies[21] is reasonable. The 2960- and 2940-cm^{-1} bands fall in the CH stretching region, and the 2220- and 2250-cm^{-1} bands fall in the C≡N region. The single 3470-cm^{-1} band, which is accompanied by the 2940-cm^{-1} band, falls in the range for secondary amines but is somewhat higher than the 3400–3300-cm^{-1} range mentioned for imines. A dimer such as compound III or an intermediate bearing secondary amine groups may thus exist. The other NH bands could be due to primary or secondary amines. The empirical relation of Bellamy and Williams[22] between the symmetric and asymmetric $-NH_2$ stretching frequencies fits reasonably well to the 3490- and 3400-cm^{-1} bands. These may thus indicate the presence of structures such as compound I and/or II, although differenecs in intensities and shapes of the bands make this assignment uncertain. However, it is interesting to note that two CH bands and two C≡N bands were detected. These, in conjunction with the apparent relation between the 3420-cm^{-1} NH band and the 2940-cm^{-1} CH band and also that between other NH bands and the 2960 cm^{-1} CH band, might suggest the existence of two different structures, such as compounds I and III, incorporating CH bands. The various results thus suggest that the surface polymer was a mixture of at least three materials and could be changed in composition by degassing.

Kozirovski and Folman found that the polymerization rate increased when the porous glass was dehy-

(14) L. E. Hinkel, G. O. Richards, and O. Thomas, *J. Chem. Soc.*, 1432 (1937); L. E. Hinkel and T. I. Watkins, *ibid.*, 2206 (1940).

(15) E. Gryszkiewicz-Trochimowski, *Roczniki Chem.*, **8**, 165 (1928).

(16) R. L. Webb, S. Frank, and W. C. Schneider, *J. Amer. Chem. Soc.*, **77**, 3491 (1955).

(17) M. P. Hartschorm and J. Vaughn, *Chem. Ind.* (London), 632 (1961).

(18) P. S. Robertson and J. Vaughn, *J. Amer. Chem. Soc.*, **80**, 2691 (1958).

(19) B. R. Penfold and W. N. Lipscomb, *Tetrahedron Lett.*, **6**, 17 (1960); *Acta Crystallogr.*, **14**, 589 (1961).

(20) T. Wadsten and S. Andersson, *Acta Chem. Scand.*, **13**, 1069 (1959).

(21) L. J. Bellamy, "The Infrared Spectra of Complex Molecules," 2nd ed, John Wiley and Sons, Inc., New York, N. Y., 1960, p 248 ff.

(22) L. J. Bellamy and R. L. Williams, *Spectrochim. Acta*, **9**, 341 (1957).

droxylated at increasingly higher temperatures, and they suggested that the polymerization was a base-catalyzed reaction with oxygen atoms acting most probably as adsorption sites, the HCN molecule being adsorbed through the hydrogen. The second HCN for dimerization would then come from the gas phase, adsorption of the second reacting HCN on OH groups being unlikely because the polymerization was enhanced by dehydroxylation.[1] However, the present results point to another mechanism. The bonding of HCN to aluminum ions and the poisoning effect described earlier suggest that aluminum ions acted not only as adsorption sites but also as centers for the polymerization. After HCN had adsorbed on an aluminum site, a second HCN could come from a neigh-

boring oxygen atom. The polymer thus formed could block the center and lead to the observed poisoning. The polymerization would be enhanced because increased dehydroxylation would lead to the formation of a greater number of oxygen atoms at which HCN could adsorb. Alternatively, or in addition to this, the progressive degassing may lead to the formation of additional centers through the migration of aluminum to the glass surface, in analogy to the enrichment of boron on the surface *via* migration from the bulk of the glass.[3,4,7]

Interactions of Propionic and Acetic Acids with Germania

by J. C. McManus and M. J. D. Low

Department of Chemistry, New York University, New York, New York 10453   (*Received February 16, 1968*)

Infrared spectra were recorded from 4000 to 1000 cm^{-1} of acetic and propionic acid sorbed on partially hydrated, dehydroxylated, and deuterated germania surfaces, and also after degassing at temperatures up to 600°. In general, the same results were obtained with both acids. Some HPr was physically adsorbed at high surface coverage, hydrogen bonded to surface Ge–OH groups, and could be desorbed at 100°. Dissociative chemisorption resulted in the formation of surface esters. At least some of the acids reacted with Ge–O–Ge bridges to yield the ester and Ge–OH structures, but the extent of a direct esterification reaction of acids with preexisting Ge–OH groups is uncertain. A small amount of Ge–H and propionate ion may be formed. The surface esters decomposed above 300°. Various data suggest that the surface ester decomposed to form surface carbonate and ketone within the pores of the gel. The ketone then formed a ketene, which became chemisorbed.

There have been several infrared studies on the interactions of carboxylic acids with oxide surfaces.[1] It was shown with formic acid adsorbed on NiO, ZnO, Al_2O_3, and MgO that ionic formate species were formed, but the results with SiO_2 were not so clear. Hirota, *et al.*,[2] claimed that formic acid was not dissociated and was present in monomeric form on SiO_2, while Eischens[3] suggested that carboxylic acids were sometimes dissociatively adsorbed on SiO_2 with the formation of a covalently bonded carboxylate radical. These interpretations were not unequivocal, because the opacity of the SiO_2 samples prevented examining the spectral region where C–O stretching and OH deformation would occur. Germania is, however, reasonably transmitting to 1000 cm^{-1}. We have consequently recorded infrared spectra over the 4000–1000 cm^{-1} region of the interactions of propionic and acetic acids with germania gel.

Experimental Section

Germania gel was prepared in a manner similar to that described by Laubengayer and Brandt,[4] except that double the amount of water recommended by them was used. The gel was air dried at 110° for 3 hr, was ground, and was compressed at approximately 25 tons/in.^{2} to form self-supporting disks. Sample disks (approximately 25 mg/cm^2) were degassed in a cell[5] by pumping for 12–14 hr, at temperatures from 450 to 600°, depending upon the degree of dehydroxylation

(1) L. H. Little, "Infrared Spectra of Adsorbed Species," Academic Press Inc., New York, N. Y., 1966.

(2) K. Hirota, K. Kuwata, T. Otaki, and S. Asai, *Proc. Intern. Congr. Catalysis, 2nd, Paris, 1960* 809 (1961).

(3) R. P. Eischens, *Science*, 146, 486 (1964).

(4) A. W. Laubengayer and P. L. Brandt, *J. Amer. Chem. Soc.*, 54, 549 (1932).

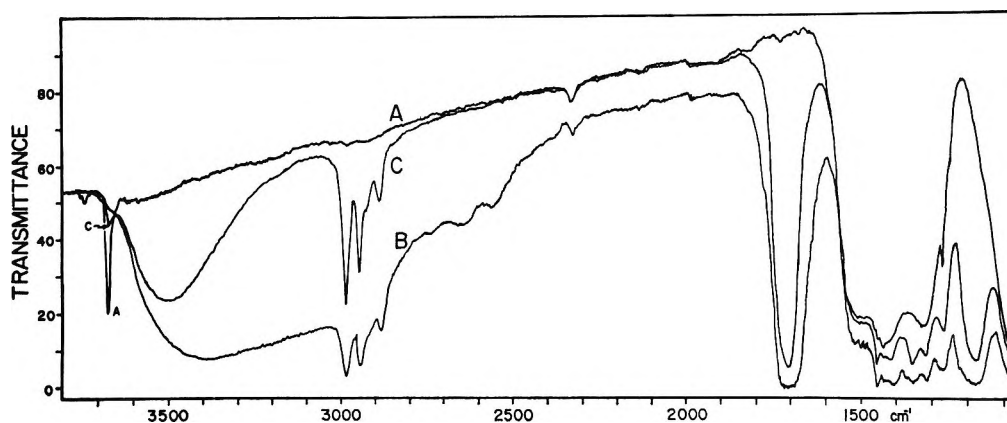(5) J. B. Peri and R. B. Hannan, *J. Phys. Chem.*, 64, 1521 (1960).

Figure 1. Propionic acid on hydroxylated germania: (A) background spectrum of gel after degassing; (B) after exposure to 10 torr of HPr for 2 min and degassing for 30 min at 25°; (C) after degassing for 30 min at 122° and 30 min at 153°.

required. To remove carbonaceous material, the samples were heated in 10 torr of oxygen for 2 hr, at the temperature used for degassing.

Propionic acid (HPr) was degassed by alternate freezing and thawing *in vacuo* until no pressure burst was detected by a Pirani gauge. Acetic acid (HAc) was dried by $CuSO_4$ and vacuum distillation and was degassed by means of freezing–thawing cycles. Each acid was always degassed before use.

Acids were sorbed at 25°. Spectra were recorded with the samples at room temperature using a Perkin-Elmer Model 621 spectrophotometer. A second cell was used in the reference beam of the instrument.

Results and Discussion

Various sorption experiments were made with HPr and HAc at pressures up to 10 torr on partially hydrated, dehydroxylated, and deuterated surfaces. Spectra were also recorded after various heat treatments up to 600° subsequent to adsorption. The results obtained with the two acids were similar, and several reactions were observed. However, the data clearly show that two temperature regions were involved, in that the nature of the surface species changed drastically above 300°. Consequently, each of the temperature regions is considered separately.

The Nature of the Adsorbed Layer (25–300°). Spectra of specimens which had been degassed and oxygen treated below 550° showed sharp bands at 3672 cm⁻¹ and a broad band near 3500 cm⁻¹, e.g., Figure 1, spectrum A. The sharp 3672-cm⁻¹ band, hereafter termed the Ge–OH band, is attributed to the O–H stretching fundamental of isolated Ge–OH surface structures,[6,7] while the broader absorption is ascribed to hydrogen-bonded hydroxyls.[7] The hydroxyls could be removed by outgassing at 600° (Figure 2, spectrum A) or could be converted to OD groups by exchange with D_2O (Figure 3, spectrum A). With some specimens a band was observed at 2330 cm⁻¹, which could not be removed by further degassing or oxygen treatment; it
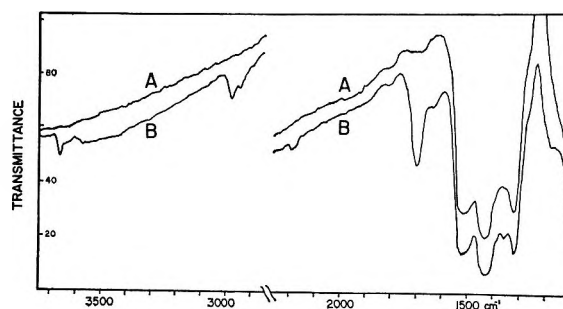

Figure 2. Propionic acid on dehydroxylated germania: (A) germania gel dehydroxylated at 620°; (B) after exposure to 0.6 torr of HPr for 20 min and degassing for 5 min at 25° (the trace is slightly displaced to avoid overlapping).

was probably caused by CO_2 trapped in closed pores.[7,8] Strong absorptions below 1550 cm⁻¹ were caused by the adsorbent.

Changes occurred over the entire spectral range when acids were sorbed. Some effects produced by HPr are shown in Figure 1, spectrum B. On exposing a partially hydroxylated surface to 10 torr of HPr, the Ge–OH band disappeared and the transmittance decreased from 3600 to 1800 cm⁻¹. The broad absorption peaked near 3400 cm⁻¹ and showed satellite bands in the 2800–2400-cm⁻¹ region. Bands formed at 2986, 2950, and 2890 cm⁻¹ in the C–H region. A pronounced, somewhat asymmetric, band formed near 1700 cm⁻¹ (approximately 1730–1696 cm⁻¹). Other bands occurred near 1462, 1420, 1380, 1360, 1320, 1276, 1230, and 1180 cm⁻¹. Degassing under relatively mild conditions substantially reduced some of the absorptions. As shown by the example (Figure 1, spectrum C), a short degassing removed most of the 3600–1800-cm⁻¹ absorption. A broad band remained near 3500 cm⁻¹ and the Ge–OH band reappeared. The

(6) M. J. D. Low and P. Ramamurthy, *Chem. Commun.*, 609 (1967).

(7) M. J. D. Low and P. Ramamurthy, to be submitted for publication.

(8) The air-dried gel contains some adsorbed ethanol which partly desorbs and decomposes on heating the solid.
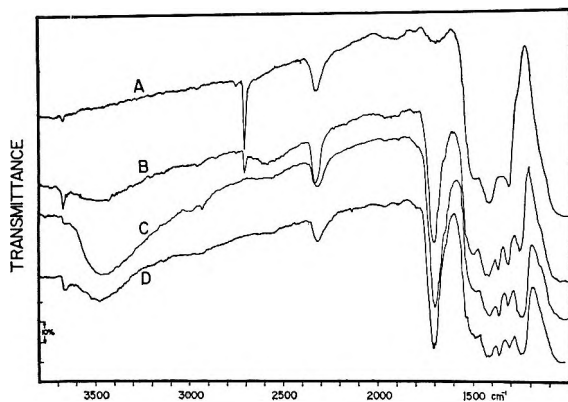
Figure 3. Acetic acid on deuterated germania: (A) gel subsequent to degassing at 500°, after deuteration and degassing at 420°, (B) after exposure to 5 torr of HAc for 21 min; (C) after exposure to 10 torr of HAc for 35 min and degassing for 1 hr at 25°; (D) after degassing for 30 min at 210°. (The ordinates are displaced to avoid overlapping of traces.)

bands in the C–H region became more distinct. The intense band near 1700 cm^{-1} lost some of its asymmetry on its low wave number side and appeared near 1720 cm^{-1}. Other bands occurred near 1462, 1360, 1273, and 1180 cm^{-1}. An additional weak band was found at 1080 cm^{-1} in some spectra. The various "residual" bands, i.e., those remaining after an initial degassing at 100–150°, decreased continuously and in concert on progressive degassing up to approximately 300°. Residual bands at the same positions and exhibiting the same behavior on degassing were observed on exposing the adsorbent to lower HPr pressures, e.g., Figure 2. The intense 3600–1800 cm^{-1} absorption and 1418-, 1380-, and 1230-cm^{-1} bands were not observed at low surface coverage. Also, on first exposing a fresh, hydroxylated specimen to HPr at low pressure, e.g., a fraction of 1 torr, the Ge–OH band increased slightly but then decreased with increasing HPr pressure and surface coverage.

Essentially the same behavior was observed when a hydroxylated sample was exposed to HAc and was then degassed, except that the broad absorption was not so extensive and the satellite bands were not found. Distinct bands indicating that physical adsorption had occurred were not observed. The bands subsequent to degassing at 100–150° were at 3028, 2940, 1715, 1370, and 1250 cm^{-1}. The spectrum of HAc adsorbed on a deuterated surface is shown in Figure 3. The band in the 2700–2400-cm^{-1} region is attributed to perturbed surface deuteroxyls (Figure 3, spectrum B).

With HPr sorption at 10 torr, the band positions observed were like those found with liquid HPr, with the exception of the 1360- and 1180-cm^{-1} bands. Liquid HPr also exhibits a broad absorption in the 3700–2000-cm^{-1} region. These absorptions could easily be decreased, and in the case of those at 1418, 1380, and 1230 cm^{-1}, can be removed entirely, by pumping at

relatively low temperature. Also, the apparently reversible behavior of the Ge–OH band was typical of that exhibited by surface hydroxyls in the presence of a weakly bound adsorbate. In view of such behavior, some of the effects observed at high surface coverage are ascribed to physically adsorbed HPr. The satellite bands in the 2800–2400-cm^{-1} region, found in the spectra of dimeric fatty acids,[9] indicate that at least a part of the physically adsorbed HPr was dimeric.

The bands produced by sorbing acid at low pressure, where no significant amounts of physically adsorbed material were detected, and the identical bands observed on degassing subsequent to exposure to acids at high pressure, indicate the existence of more tightly bound species. However, the possibility of HPr or HAc adsorption in undissociated, monomeric form must be considered, as Hirota, et al.,[2] have suggested this to be the case for formic acid adsorbed on SiO$_2$.

There has been some controversy about the assignments and positions of bands of monomeric fatty acids. Wilmshurst claimed that ν(C–O) occurred at 1279 cm^{-1} for HAc and at 1200 cm^{-1} for formic acid, while the corresponding bands for δ(OH) occurred at 1192 and 1105 cm^{-1}, respectively.[10] These assignments were criticized,[11,12] and now it appears that the situation is more complex. For example, it is thought[13] that the ν(C–O), δ(OH), and δ(CH$_3$) vibrations of HAc interact but that a band at 1182 cm^{-1} can be assigned primarily to ν(C–O), while another at 1264 cm^{-1} resulted mainly from δ(OH). Hadzi and Pintar[12] found two characteristic bands in the spectra of monomeric acids in the regions 1380–1280 cm^{-1} and 1190–1075 cm^{-1} and concluded that while there is much coupling, the first band is due mainly to δ(OH) and second band is due to ν(C–O).

For adsorbed HAc, the intense 1250-cm^{-1} band might be attributed to ν(C–O). That absorption occurs at 1190 cm^{-1} with the free monomer, but an upward shift would be expected if the monomer were held to the surface by hydrogen bonding. However, there was no band ascribable to δ(OH). The latter is of medium intensity under conditions of medium[9,13] hydrogen bonding and is absent[12] when hydrogen bonding is strong, and this might account for the absence of such a band. For adsorbed HAc, however, hydrogen bonding was weak, as evidenced by the relatively small perturbation of surface hydroxyls. Also, if the 1728-cm^{-1} band of adsorbed HAc is taken as ν(C=O), its shift from 1788 cm^{-1} for gaseous[12] HAc would be 2–3 times the shift usually found[14] for that band under conditions of weak hydrogen bonding.

The situation is more difficult for adsorbed HPr,

(9) D. Hadzi and N. Sheppard, Proc. Roy. Soc., A216, 247 (1953).
(10) J. K. Wilmshurst, J. Chem. Phys., 25, 478, 1171 (1956).
(11) R. C. Millikan and K. S. Pitzer, ibid., 27, 1305 (1957).
(12) D. Hadzi and M. Pintar, Spectrochim. Acta, 12, 162 (1958).
(13) M. Haurie and A. Novak, J. Chim. Phys., 62, 137 (1965).

because monomeric HPr does not appear to have been examined. However, from results for HAc and butyric acid,[13] ν(C–O) would be expected near 1190–1150 cm^{-1} and δ(OH) would be expected near 1380–1320 cm^{-1}. For adsorbed HPr it seems most likely that the 1180-cm^{-1} band is due to ν(C–O), because it is intense. However, for monomeric HPr held to the surface by hydrogen bonding, ν(C–O) would be expected at frequencies higher than the observed 1180 cm^{-1}. Also, δ(OH) would be shifted to higher wave numbers by hydrogen bonding; the observed 1280-cm^{-1} band is lower than would be expected.

The spectral evidence thus outlined does not favor the concept of HAc or HPr adsorption in undissociated, monomeric forms, and this is supported by chemical evidence. In view of the relatively small perturbation of surface hydroxyls, shown by the shift of only approximately 200 cm^{-1}, more extensive desorption would be expected if the adsorbed layer consisted of monomeric acid molecules. As the adsorbed layer was retained at 300°, more tightly bound species are indicated.

Comparison of what were earlier termed the residual bands with spectra of organic esters[15,16] and silyl esters[17] shows remarkably good agreement in band positions in the 1800–1000-cm^{-1} region. Also, the relative band intensities are of the same order of magnitude as those for organic esters.[16] Unfortunately, there appear to be no published spectra of germyl esters, but such compounds exist[18] and have similar properties to their silicon and carbon counterparts; also, germanium tetraacetate exists.[19] In the absence of preferable alternatives, the present results can be best explained in terms of analogous surface structures. The residual bands of the tightly bound species are consequently attributed to surface esters. The prominent bands at 1715 and 1720 cm^{-1} are attributed to ν(C=O) modes, and those at 1260 and 1180 cm^{-1} are attributed predominantly to ν(C–O) modes of acetate and propionate surface esters, respectively. Assignments for other bands follow those outlined by Katritzky, et al.,[16] who point out that there is a great deal of coupling. Thus the 1278-cm^{-1} band of propionate ester may have some contribution from the ν(C–O) mode.

Ester formation could occur in two ways
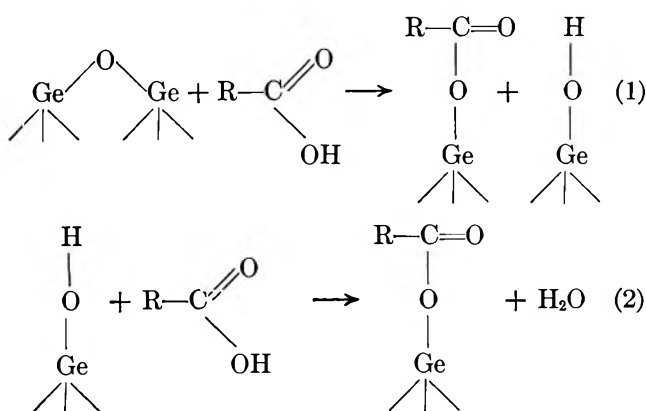
In an attempt to distinguish between these mechanisms, other sorption experiments were made. On addition of acid to deuterated surfaces (Figure 3), the Ge–OH band was observed along with bands of hydrogen-bonded OH groups, free Ge–OD groups at 2707 cm^{-1}, and hydrogen-bonded OD groups and those of the adsorbate. However, those results are not unequivocal, because exchange reactions[7] may have occurred. Conversely, acid addition to completely dehydroxylated germania (Figure 2) clearly showed that free Ge–OH groups and hydrogen-bonded ones were formed. Thus reaction 1 is definitely operative. The extent of the esterification reaction (eq 2) remains uncertain. Occasionally small bands at 2190 and 1633 cm^{-1} were observed when small quantities of HPr were added to either hydroxylated or dehydroxylated surfaces. The bands appeared together and declined and vanished on degassing at 200° and were removed by exposure to H_2O; they were not formed with HAc. The bands are shown in spectrum B of Figure 2, but these are more intense than those normally observed. Other work has shown that a band can form in the region 2170–2190 cm^{-1} when H_2, H_2O, or NH_3 are adsorbed on germania under certain conditions, and by comparison with the spectra of various germanes, the band was attributed to surface Ge–H species.[7,20] The 2190-cm^{-1} band of spectra of adsorbed HPr can be similarly assigned, but the cause of its comparison band is uncertain. Carboxylate species would give rise to bands near 1650–1550 cm^{-1} and 1440–1360 cm^{-1}, the latter being the less intense.[21] The present spectra showed no additional absorption near 1400 cm^{-1}, but the germania itself was highly absorbing in that region, so that detection of a weak band would be difficult. However, the general behavior of the 2190- and 1633-cm^{-1} bands leads to the speculation that propionate ions were responsible for the 1633-cm^{-1} band. A reaction of acid leading to carboxylate ions and Ge–H structures might occur at a nonstoichiometric portion of the germania surface. The ions may be precursors of the ester species. As the compound germanium tetraacetate exists, the formation of bulk esters must be considered. Taking the surface area[7] as 80 m^2/g, it can be deduced that the surface coverage by adsorbed species did not exceed one monolayer at acid pressures of 1 torr (the amount adsorbed could not be measured,

(14) S. Bratoz, D. Hadzi, and N. Sheppard, *Spectrochim. Acta*, **8**, 249 (1956).

(15) H. W. Thompson and P. Torkington, *J. Chem. Soc.*, 640 (1945).

(16) A. R. Katritzky, J. M. Lagowski, and J. A. T. Beard, *Spectrochim. Acta*, **16**, 964 (1960).

(17) A. G. E. Robiette and J. C. Thompson, *ibid.*, **21**, 2023 (1965).

(18) H. H. Anderson, *J. Amer. Chem. Soc.*, **72**, 2089 (1950).

(19) H. Schmidt, C. Blohm, and G. Jandes, *Angew. Chem.*, **A59**, 233 (1947).

(20) M. J. D. Low and K. Matsushita, to be submitted for publication.

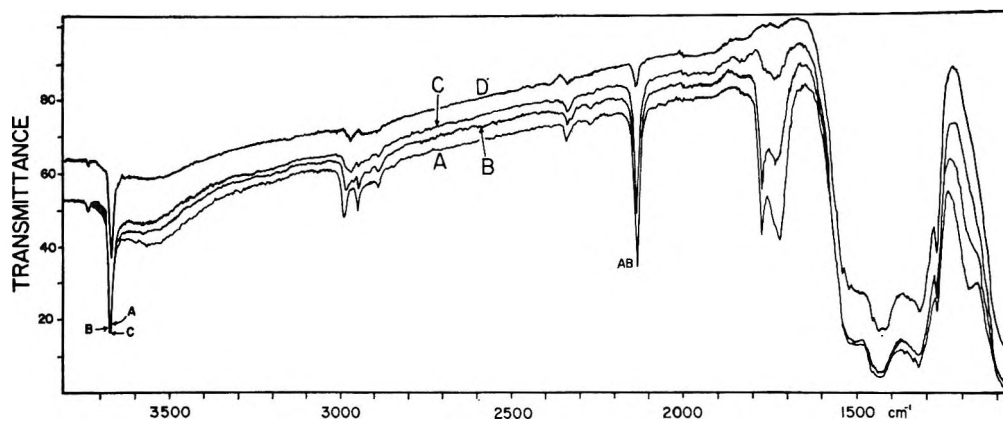(21) N. B. Colthup, *J. Opt. Soc. Amer.*, **40**, 397 (1950).

Figure 4. Propionic acid on hydroxylated surface. Continuation of the sequence of spectra of Figure 1. The spectra were recorded after degassing at the following temperatures and times (in min): (A) 398°, 30; (B) 433°, 30; (C) 490°, 45; (D) 527°, 105 plus 569°, 60. The D ordinate is displaced.

and the values of extinction coefficients for the surface species are unknown and must be estimated). However, the skeleton of the spectrum of bulk germania was retained when acids were added, and considerable amounts of unreacted acid remained on the surface after acid addition at high pressure. Thus if bulk ester is formed at these high pressures, it must be limited to only a few monolayers.

Behavior of the Adsorbed Layer above 300°. When hydroxylated samples were treated with acid and subsequently degassed, the bands ascribed to the surface ester decreased and new bands appeared. Bands formed at 2131 and 1767–1769 cm^{-1} at 300–320° with HPr-treated samples. The bands were not related, *e.g.*, the intensity of the 2131-cm^{-1} band reached a maximum on heating to 420°, while the other band had begun to decline. The 2131-cm^{-1} band could be detected after all ester bands and the second band had disappeared. Some spectra of a degassing sequence are shown in Figure 4. On degassing from 300 to 600°, the Ge–OH band at first increased but then decreased continuously with increasing temperature; the broad band due to hydrogen-bonded hydroxyls decreased continuously. The C–H bands also declined and, at the highest degassing temperature, changed slightly in position and relative intensities. HAc-treated hydroxylated samples exhibited very similar behavior, except that bands formed at 2150 cm^{-1} and at 1769–1776 cm^{-1}.

In general, the intensities of the new bands depended on the original outgassing temperature of the adsorbent and on the history of the sample. The bands were intense with a fresh sample outgassed at relatively low temperature but, as the sample was subjected to sorption–degassing cycles, became less prominent. Also, the relative intensities changed, the bands near 1770 cm^{-1} decreasing to a lesser extent than the other bands. The new bands were not observed at all with samples which had been completely dehydroxylated by degassing at high temperature. However, when a completely dehydroxylated sample was rehydroxylated by reaction

with H$_2$O, the new bands were also not observed. Such effects would indicate that it is the texture of the adsorbent rather than the concentration of surface hydroxyls which governs the concentration of decomposition products. Assignments for the two pairs of bands are made difficult by the lack of other bands. Some spectra tended to show quite weak absorptions near 1180 cm^{-1} for adsorbed HAc and near 1120 cm^{-1} for adsorbed HPr during the desorption process, but such results are of little value because the sloping background in that region obviates reliable measurements of very weak bands. However, the similarities of the two pairs of intense bands suggest that the products of the decomposition of each ester must have very similar structures; this assumption is implicit in the interpretation adopted.

The single, fairly intense band at 2150 or 2130 cm^{-1} caused by one of the products might be attributed to either the Ge–CO or Ge–H structures. The latter is rejected because the band position is a function of the nature of the acid and the band intensities and positions are much different from those observed for the Ge–H bands. It is also unlikely that the bands were caused by adsorbed CO. The observation of the bands both above and below the frequency of ν(C–O) for gaseous CO would indicate peculiar behavior of the C–O bond of a hypothetical Ge–CO structure. There are no published data for CO adsorption on germania, but Bennett and Tompkins[22] have shown that CO is weakly adsorbed on oxidized germanium. It is unlikely that CO would remain adsorbed on germania above 100°. In view of these objections, it seems that the 2150- and 2131-cm^{-1} bands are best interpreted in terms of ketenic structures.

It is suggested that the decomposition of the acetate and propionate esters produces adsorbed ketene and methyl ketene, respectively. Some indirect support

(22) M. J. Bennett and F. C. Tompkins, *Trans. Faraday Soc.*, **58**, 816 (1962).

for this suggestion comes from reports that methyl ketene is produced[23] by the pyrolysis of HPr, and that ketene is formed when HAc is passed[24] over $ZrO_2-Al_2O_3$. There is strong absorption in the ketene spectrum[25] near 2150 cm^{-1}, owing to $\nu(C{=}C{=}O)$; with methyl ketene,[23] $\nu(C{=}C{=}O)$ absorbs at 2150 cm^{-1}, although the data are meager. The $\nu(C{=}C{=}O)$ absorption of ketene is also approximately one order of magnitude more intense than other ketene absorptions,[25] and this can readily explain the absence of other bands in the present spectra. In view of the similarity of the band positions, the surface structures

$$
\begin{array}{cc}
H_3C \diagdown && H \diagdown \\
\quad C{=}C{=}O & \quad\quad C{=}C{=}O \\
| && | \\
Ge && Ge \\
\diagup | \diagdown && \diagup | \diagdown
\end{array}
$$

are suggested. The hydrogen abstracted on adsorption of ketenes would form surface hydroxyls.

Assignments of the bands near 1770 cm^{-1} are again made difficult because of the absence of other bands. However, the similarities of position and behavior of the bands derived from two different acids suggest that one surface structure is responsible for one 1770-cm^{-1} band. Organic carbonates absorb near that frequency,[26] and it is suggested that a surface carbonate

$$
\begin{array}{c}
O \\
\| \\
C \\
\diagup \quad \diagdown \\
O \quad\quad O \\
| \quad\quad | \\
Ge \quad Ge \\
\diagup|\diagdown \;\; \diagup|\diagdown
\end{array}
$$

is formed, giving rise to the 1770-cm^{-1} band. Indirect support for this suggestion comes from the observation that ketones formed[27] from fatty acids over germania at 360–450°. Detailed kinetic studies were not made, but mixed ketones occurred when acid mixtures were used, indicating a bimolecular process.[27] Ketones were not observed in the present study, but these would not be expected to bond strongly to the surface. A similar bimolecular process is suggested for the present thermal decompositions

$$
\begin{array}{ccccc}
R{-}C{=}O & R{-}C{=}O & O & & O \\
| & | & \| & & \| \\
O & + & O & \rightarrow & C & + O & C \\
| & | & \diagup \diagdown & & \diagup \diagdown \\
Ge & Ge & R \;\; R & & O \quad\quad O \\
\diagup|\diagdown & \diagup|\diagdown & & & | \quad\quad | \\
& & & & Ge \;\; Ge \\
& & & & \diagup|\diagdown \; \diagup|\diagdown
\end{array}
$$

$$(3)$$

resulting in the formation of ketone and the postulated

Figure 5. Propionic ester decomposition. After the gel had been degassed at 530° (spectrum A), it was exposed to 1 torr of HPr for 5 min and then degassed for 1.5 hr (spectrum B). The sample was then heated in the isolated cell for 30 min at the following temperatures: (C), 325°, 365°; (D) 410°, 480°. Spectra were recorded with the sample at 25°. The ordinates are displaced.

surface carbonate. The latter would decompose to Ge–O–Ge bridges and CO_2 at high temperatures.

The formation of ketenes, and the subsequently adsorbed ketenes, could occur through the decomposition of the surface ester, e.g.

$$
\begin{array}{ccc}
H_3C{-}C{=}O & & H \\
| & & | \\
O & \longrightarrow & O & + H_2C{=}C{=}O \\
| & & | \\
Ge & & Ge \\
\diagup|\diagdown & & \diagup|\diagdown
\end{array}
$$

$$(4)$$

or from a ketone, e.g.

$$
\begin{array}{c}
O \\
\| \\
C_2H_5{-}C{-}C_2H_5 \xrightarrow{GeO_2} H_2CHC{=}C{=}O + C_2H_6
\end{array}
$$

$$(5)$$

In view of the earlier generalizations relating the intensities of the 1770- and 2150–2130-cm^{-1} bands to the sample history and pretreatments, it is suggested that most of the ketenes were derived from ketones produced, held, and allowed to react within the pores of the gel. This would readily explain why ketenes were not observed with samples which had been subjected to very severe degassing and consequently were sintered. Some experiments were carried out in which an acid-treated sample was heated with the cell isolated from the pumping system. Spectra were recorded after the

(23) P. G. Blake and K. Hole, J. Phys. Chem., 70, 1464 (1966).

(24) V. I. Yakerson, L. I. Lafer, A. L. Klyachko-Gurvich, and A. M. Rubinshtein, Izv. Akad. Nauk SSSR, Ser. Khim., 1, 83 (1966).

(25) F. Halverson and V. A. Williams, J. Chem. Phys., 15, 552 (1947).

(26) B. M. Gatehouse, S. E. Livingstone, and R. S. Nyholm, J. Chem. Soc., 3137 (1958).

(27) P. Mastagli, P. Lambert, C. Hirigoyen, and J. Pourriere, Compt. Rend., 250, 1507 (1960).

sample had cooled. Some results are shown in Figure 5. On progressive heating, the following occurred. (a) The ester concentration decreased, but more slowly than when the cell was evacuated. This suggests that some ester decomposed by the reverse of reaction I; the ester would re-form when the adsorbent cooled. (b) Free and hydrogen-bonded hydroxyls increased and bands in the C–H region changed. The band at 2990 cm^{-1} shifted to 2976 cm^{-1}, while the relative intensity of the 2890-cm^{-1} band increased, indicating the formation of a new surface structure. It is known that acetone is decomposed to 2-methylpropene,

CO_2, and H_2O over the SiO_2–Al_2O_3 catalyst.[28] A similar reaction is suggested, ketone being formed from surface ester and decomposing to yield chemisorbed water and olefin. (c) The 2130-cm^{-1} band was very small and the 1770-cm^{-1} band was absent. The decrease in ketene bands could result from reaction of the ketene with a neighboring OH to form the surface ester or with the acid to yield the ketone and CO_2. The surface carbonate could be destroyed by reaction with the acid produced by the reversal of eq 1.

(28) M. Demorest, D. Mooberry, and J. D. Danforth, *Ind. Eng. Chem.*, **43**, 2569 (1951).

Lead Bromide Photochemistry: Reduction of Lead Ion and Oxidation of Leucocrystal Violet

by H. E. Spencer and Jennifer O. Darlak

Research Laboratories, Eastman Kodak Company, Rochester, New York 14650   (*Received October 25, 1967*)

Ultraviolet irradiation of microcrystals of lead bromide at 22° produces metallic lead and induces the oxidation of adsorbed leucocrystal violet to crystal violet. In terms of incident quanta, the sensitivity for production of either lead or crystal violet is higher at 313 and 335 mμ than at 254 or 366 mμ. The quantum yield for crystal violet production is 0.15 molecule/absorbed quantum at 254 mμ and 0.31 molecule/absorbed quantum at 313, 335, and 366 mμ. Adsorbed 3,3'-diethylthiacyanine ethyl sulfate and 3-carboxymethyl-5-(3-ethyl-2-benzothiazolinylidene)rhodanine spectrally sensitize crystal violet production, but not lead production, to about 500 mμ. The rates of production of lead and of crystal violet are proportional to the first power of the intensity of irradiation. Increasing the temperature to 100° appreciably changes the sensitivity for lead production only at the longer wavelengths at which absorption of radiation is increased. Possible mechanisms are discussed in terms of the band structure of $PbBr_2$.

Introduction

Among the recent papers dealing with the photodecomposition of inorganic solids are those concerned with lead halides, namely: PbF_2,[1] $PbCl_2$,[2-4] $PbBr_2$,[4] and PbI_2.[4,5] In this paper we shall discuss the photochemistry of lead bromide.

Wells[6] first observed that lead bromide blackens when exposed to sunlight. Norris[7] showed that lead was formed and that bromine was lost during irradiation. Sanyal and Dhar[8] also reported a loss of bromine. Using an optical method for measurement, Verwey[4a,d] calculated the quantum efficiency of lead production in irradiated single crystals. No measurements have been made of the quantum yield (Φ) for the production of bromine or for the production of either bromine or lead when microcrystals of lead bromide are used.

Because microcrystals have a large surface-to-volume ratio, they are particularly suited to the study of solid-state reactions which occur at surfaces. Micro-

crystalline lead bromide dispersions were, therefore, used in this work.

The electron–hole pair created in a solid by the absorption of radiation can react further; electrons can cause reduction, whereas holes can cause oxidation. We shall report here an electron reaction, the reduction of lead ion to lead, and a hole reaction, the oxidation of

(1) D. A. Jones, *Proc. Phys. Soc.*, **B68**, 165 (1955).

(2) W. C. Tennant, *J. Phys. Chem.*, **70**, 3523 (1966).

(3) A. Kaldor and G. A. Somorji, *ibid.*, **70**, 3538 (1966).

(4) (a) J. F. Verwey, *J. Phys. Chem. Solids*, **27**, 468 (1966); (b) J. F. Verwey and J. Schoonman, *Physica*, **35**, 386 (1967); (c) J. Arends and J. F. Verwey, *Phys. Status Solidi*, **23**, 137 (1967); (d) J. F. Verwey, Ph.D. Thesis, University of Utrecht, 1967.

(5) (a) R. I. Dawood and A. J. Forty, *Phil. Mag.*, **7**, 1633 (1962); (b) R. I. Dawood and A. J. Forty, *ibid.*, **8**, 1003 (1963); (c) M. R. Tubbs and A. J. Forty, *Brit. J. Appl. Phys.*, **15**, 1553 (1964).

(6) H. L. Wells, *Amer. J. Sci.*, **45**, 121 (1893).

(7) R. S. Norris, *Amer. Chem. J.*, **17**, 189 (1895).

(8) A. K. Sanyal and N. R. Dhar, *Z. Anorg. Allgem. Chem.*, **128**, 212 (1923).

leucocrystal violet (LCV) to crystal violet (CV). Preliminary experiments in our laboratory demonstrated that CV is produced by 366-mμ irradiation of a lead bromide dispersion to which LCV has been added. Oster and Yamamoto[9] recently utilized the oxidation of LCV to CV in studying the photochemistry of zinc oxide.

Experimental Section

Dispersions of lead bromide in polyvinyl alcohol–water solutions were prepared at room temperature by a double-jet scheme[10] in which 25 ml of a 3.0 M KBr solution and 25 ml of a 1.5 M Pb(NO$_3$)$_2$ solution were pipetted simultaneously into a well-stirred, 50-ml, 0.5 wt % polyvinyl alcohol–water solution. The two salt solutions were pipetted into two funnels connected to capillary tubing, the bore and length of which were adjusted so that the time of delivery was about 210 sec.[11]

Several different varieties of Du Pont Elvanol polyvinyl alcohol were found to give a dispersion which was stable for days; Du Pont Elvanol polyvinyl alcohol (PVA), 70–05, was used for all the quantitative investigations reported here. The PVA was purified by repeated soaking in ethanol and ethanol–water mixtures.[12] Some dispersions were prepared in the absence of PVA. These dispersions coagulated in a few minutes if the double-jet scheme was used, but a stable dispersion was obtained if the lead nitrate solution was poured quickly into the potassium bromide solution.

Reagent grade Baker and Adamson potassium bromide and lead nitrate were used without further purification.

Coatings of lead bromide were prepared by pouring a few milliliters of the dispersion onto glass plates. The dispersion was spread with a stirring rod and allowed to dry in room air.

The radiation from a PEK 200-W, high-pressure mercury lamp was passed through a Jarrel-Ash 0.25-m Ebert monochromator with 5-mm entrance and exit slits, and the output was focused by a quartz lens. A suitable Corning glass filter was always used to remove scattered light. The radiation intensity was calibrated with a ferrioxalate actinometer.[13] The ferrioxalate solution was placed in the same type of beaker used for the irradiation of the liquid dispersion.

These liquid dispersions were irradiated in a rotating 50-ml Pyrex glass or quartz beaker containing 25 ml of the dispersion which was stirred mechanically. For exposure of the coated films, the apparatus for rotating the 50-ml beakers was removed, and a coated glass plate inserted at about the same distance from the exit slit of the monochromator. Red or yellow safelights were used in all experiments.

A few milligrams of Eastman LCV was dissolved in 2 or 3 ml of acetone and was added, with stirring, to 25 ml of dispersion. Two slightly different methods

were used for the determination of CV. In the first method, ethanol (10 ml) was stirred into 25 ml of irradiated sample for a few minutes. The desorbed CV was separated from the microcrystals, or grains, by centrifugation, and its concentration in the supernatant liquid was determined spectrophotometrically. This method was used if spectrally sensitizing dyes were adsorbed to the grains. In the second method, the alcohol was added before, rather than after, irradiation.

The diffuse reflectivity of the liquid dispersion was measured relative to BaSO$_4$ in either a 1- or a 4.5-cm cell, and nearly identical results were obtained. No detectable radiation was transmitted through the 1-cm cell. The diffuse reflectivity of the coatings was measured in a similar manner; again, no transmitted radiation was detected.

To obtain the measurements of both reflectivity and lead production at 100°, the liquid dispersion was poured on a flattened side of a 50-ml beaker and dried. Boiling water in the beaker provided a constant-temperature bath for the 100° measurements.

A few milligrams of a sensitizing dye was dissolved in either a few milliliters of methanol or water containing 1 or 2 drops of pyridine. A few milliliters of solution was poured into 25 ml of PbBr$_2$ dispersion and stirred for several minutes.

Results

Dispersion. Electron micrographs of the microcrystals or grains of the PbBr$_2$ reveal needles several tens of microns long and <1 μ in each of the shorter dimensions. X-Ray analysis of dried coatings of the dispersion on glass plates, where the needles are constrained to lie parallel to the plane of the glass, showed that the long axis of the needles is parallel to the shortest unit-cell axis of the orthorhombic crystal structure. Presumably this needlelike structure accounts for the stability of the liquid dispersion: the needles form a kind of brush pile, which coagulates with difficulty.

We found no qualitative differences between results obtained with dispersions prepared either with or without PVA. For the dispersion without PVA, however, the results were less reproducible. Also the value of Φ for CV production was generally about half that found for the PVA dispersion. Since the value of Φ was independent of the PVA concentration between 0.5 and 2.5 wt %, it is presumed that the absence of PVA did not affect the value of Φ. In the absence of PVA, the grains are larger than the grains precipitated

(9) G. Oster and M. Yamamoto, *J. Phys. Chem.*, **70**, 3033 (1966).

(10) C. R. Berry and D. C. Skillman, *Photogr. Sci. Eng.*, **6**, 159 (1962).
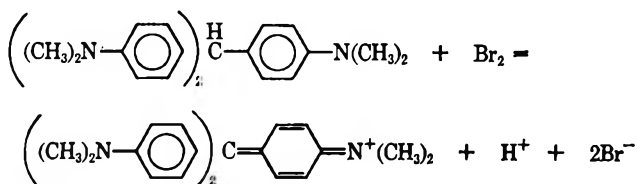
(11) The use of capillary tubing was suggested by R. W. Berriman of the Research Laboratories of Kodak Ltd., Harrow, England.

(12) A. V. Buettner, *J. Chem. Phys.*, **44**, 1398 (1967).

(13) C. G. Hatchard and C. A. Parker, *Proc. Roy. Soc.* **A235**, 518 (1958).

in the presence of PVA, and, although we have not actually measured the dependence of Φ on grain size, it is possible that the value of Φ decreases with decreasing surface-to-volume ratio of the grains.

Positive-Hole Detection. LCV can be oxidized to CV by bromine water, presumably according to the equation

$$\left((CH_3)_2N-\langle\bigcirc\rangle\right)_2 \overset{H}{\underset{}{C}}-\langle\bigcirc\rangle-N(CH_3)_2 + Br_2 =$$

$$\left((CH_3)_2N-\langle\bigcirc\rangle\right)_2 C=\langle\bigcirc\rangle=N^+(CH_3)_2 + H^+ + 2Br^-$$

This reaction can be followed spectrophotometrically, since LCV is colorless in aqueous solution and CV has an absorption maximum at 592 mμ (molar extinction coefficient 9×10^4 M^{-1} cm^{-1}). Instead of one bromine molecule, two bromine atoms or two positive holes can be used in balancing this equation. We do not know which of these three reactions occurs in our system. However, the reaction occurs principally during irradiation. Usually, the LCV was added before irradiation. When the LCV was added immediately after irradiation, only about one-tenth as much CV was produced.

When the LCV-containing PbBr$_2$ dispersion was centrifuged, more than half the LCV was found in the sediment, presumably adsorbed to the PbBr$_2$ grains. For all the wavelengths investigated, irradiation of a control mixture containing all components, but the PbBr$_2$ produced negligible amounts of CV. If PbBr$_2$ was present, the number of CV molecules was proportional to the number of incident quanta. The quantum yield for CV production was independent of several variables: LCV concentration between 10^{-4} and 10^{-3} M, intensity between 2.9×10^{14} and 1.2×10^{16} quanta/sec, and CV concentration up to at least 10^{-5} M. In a few experiments, nitrogen was bubbled through the dispersion; the amount of CV produced was unchanged by this treatment. Although this represents only a limited investigation of the effect of oxygen, there is no evidence that oxygen is important in this system, in contrast to the case of ZnO–LCV.[9]

We have not been able to produce CV by irradiation of a dried coating of LCV-containing PbBr$_2$ dispersion. This suggests that water plays some role in the oxidation of LCV to CV.

The second technique for desorbing the CV formed during irradiation, adding the alcohol before irradiation, yielded some 40% more CV than if the alcohol was added after irradiation, the first method of desorption. At least one reason for this increased yield is that all the CV is not desorbed by the first method. Visual inspection of the solid sediment after centrifugation revealed some characteristic blue color of CV. Hence the second method was used, except when sensitizing dyes
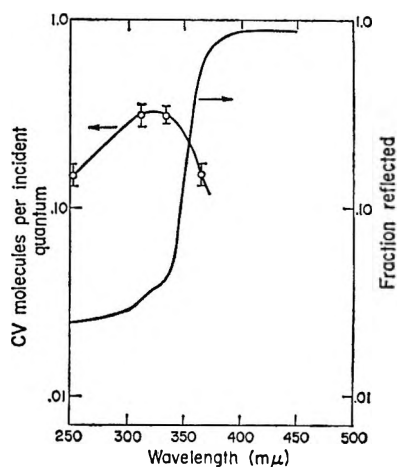
Figure 1. Spectral dependence of CV production and of reflection; diffuse reflection relative to BaSO$_4$: bars above and below experimental points indicate average deviation.

were present, because of the possibility of desorbing some of the sensitizing dyes by the alcohol. In the absence of sensitizing dyes, the shapes of the Φ–wavelength curves were the same for the first and second methods of CV desorption, and, presumably, this would be true if sensitizing dyes were present. For the present purposes, the absolute value of Φ in the spectrally sensitized region is unimportant: the emphasis here is placed on the relative CV yields in the shorter wavelength region and in the spectrally sensitized region.

Spectral Dependence of Reflection and CV Production. The spectral dependences of reflectivity and CV production are shown in Figure 1. The increasing reflection at long wavelengths represents decreasing absorption and is accompanied by a long-wavelength drop in number of CV molecules per incident quantum. From these data, the number of CV molecules per absorbed quantum, here called quantum yield, Φ, can be calculated. The values of Φ and their average deviations at 254, 313, 335, and 366 mμ are 0.15 ± 0.02, 0.31 ± 0.04, 0.31 ± 0.03, and 0.31 ± 0.04, respectively. Negligible amounts of CV were produced at 405 mμ, consistent with the negligible absorption at 405 mμ.

Identification of Lead. Sufficient exposure of the white, milky PbBr$_2$ dispersion, in either liquid state or dry form on a glass plate, produced a dark photoproduct. In the coated films, this photoproduct was bleached by ferric nitrate solution. Ferric ferricyanide solution also bleached the photoproduct and produced a blue material.[14] We conclude that the photoproduct is metallic lead.

Spectral Dependence of Reflection and Lead Production. In Figure 2 are shown the spectral dependence of reflectivity and that of lead production at 22 and 100° in

(14) F. Feigl, "Spot Tests in Inorganic Analysis," 5th ed, Elsevier Publishing Co., New York, N. Y., 1958, p 363.

coated films. Not shown are similarly shaped curves at 22° for a dried PVA-free coating of $PbBr_2$ on glass. The spectral reflectance of the coated films at 22° is similar to the reflectance curve for the liquid dispersion in Figure 1.

We used a semiquantitative method to determine the sensitivity for lead production. The minimum number of quanta necessary to produce visible lead in about a 4-cm^2 area was determined from a series of different times of exposure at each wavelength. Half of this minimum number of quanta produced no visible lead. The reciprocal of the number of quanta necessary to produce lead was utilized as a measure of sensitivity. The bars on the points in Figure 2 indicate the minimum and one-half the minimum number of quanta necessary to produce visible lead.

In Figure 2 it can be seen that increasing the temperature to 100° causes both increased absorption and increased sensitivity for lead production at wavelengths between 350 and about 400 mμ; the absorption and sensitivity increase in a parallel manner.

Intensity Dependence of Lead Production. Figure 3 shows the dependence on intensity at 366 mμ of the rate of lead production at room temperature. The reciprocal of the time necessary to produce just-visible lead is used as a measure of the rate of lead production. The slope of the line is 1; the rate is proportional to the first power of intensity. This same linear dependence was found for irradiation at the shorter wavelengths.

Dye Sensitization. The sensitivity of $PbBr_2$ for CV production, but not for lead production, was extended into the visible region by adsorbed dyes. Figures 4 and 5 show this spectral sensitization, respectively, for the two dyes 3,3'-diethylthiacyanine ethyl sulfate (I) and 3-carboxymethyl-5-(3-ethyl-2-benzothiazolinyl-idene)rhodanine (II)
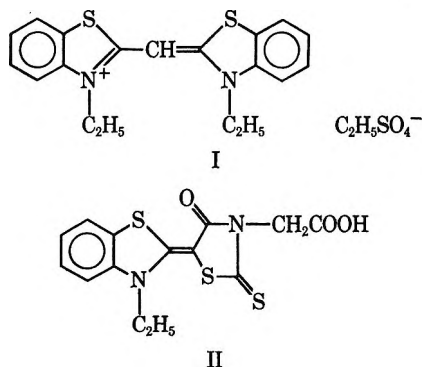
Both of these dyes exhibit absorption maxima at wavelengths shorter than 500 mμ. Qualitative observations of some other dyes, which also had maxima at wavelengths shorter than 500 mμ, indicated CV production when irradiated, whereas still other dyes, with absorption maxima beyond 500 mμ, were tried unsuccessfully as spectral sensitizers.

Control experiments showed that insignificant
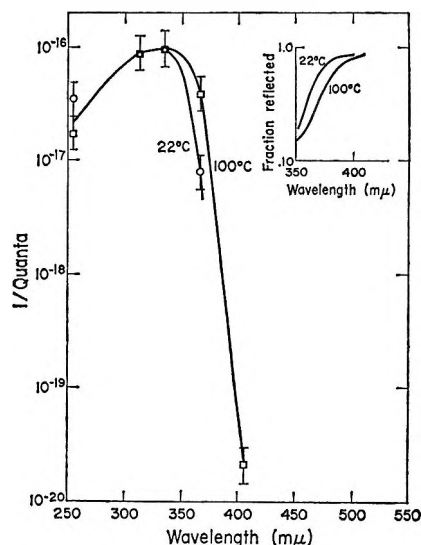
Figure 2. Spectral dependence of reflectivity and of lead production: see text.
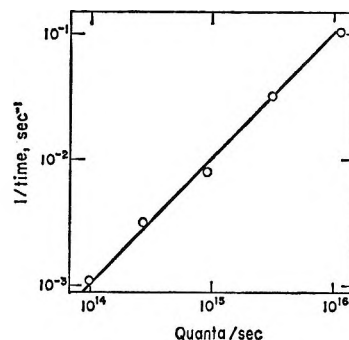
Figure 3. Intensity dependence of rate of lead production as measured by the reciprocal of the time necessary to produce visible lead (wavelength, 366 mμ).

amounts of CV are produced unless $PbBr_2$ is present. There is no appreciable dark reaction between the dyes and LCV. Provided some LCV and some dye are present, the value of Φ is independent of either LCV or dye concentration. However the value of Φ in the spectrally sensitized region is only 20–25% of the value in the 313–366-mμ region. For dye I, Φ is independent of the intensity of irradiation at least between 4×10^{15} and 1.3×10^{16} quanta/sec at 405 mμ.

Discussion

In Figure 1 the reflectance spectrum exhibits a shoulder at about 325 mμ. This shoulder arises because of a maximum in the absorption coefficient at about 335 mμ and a minimum at 320 mμ.[15] This long-wavelength band has been described as an exciton band by Illmas, *et al.*[16] They concluded that the band and a

(15) H. Fesefeldt, *Z. Phys.*, **64**, 741 (1930).

(16) E. Illmas, R. Kink, G. Lüdja, and A. Malysheva, *Tr. Inst. Fiz. i Astron., Akad. Nauk Est. SSR* **26**, 112 (1964); see also K. J. DeVries and J. H. Van Santen, *Physica*, **30**, 2051 (1964).
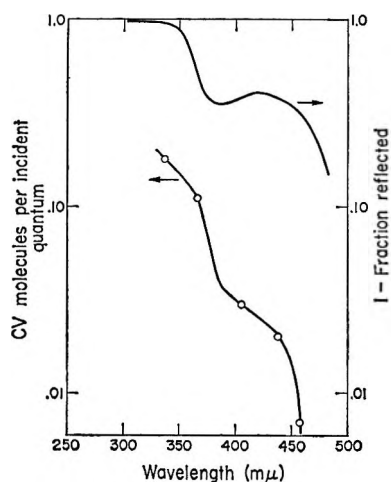
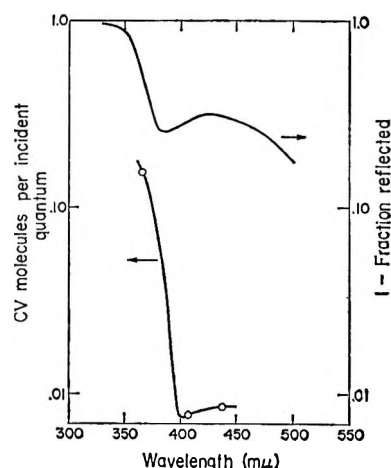Figure 4. Absorption and spectral sensitization (dye I, 10^{-4} M).

Figure 5. Absorption and spectral sensitization (dye II, 2×10^{-4} M).

similar one in $PbCl_2$ are due to a $6S^2 \rightarrow 6S6P$ electronic transition in the lead ion. In contrast, Best[17] explains the $PbCl_2$ band as an electronic transition from a Cl^- anion to a $PbCl^+$ cation. We agree with Illmas, *et al.*, not only because of their extensive study of the optical properties of the lead halides but also because we have detected similar bands in PbC_2O_4 (282 mμ) and $PbSO_4$ (291 mμ) and a shoulder in $PbCO_3$ (305 mμ).

Although there are some quantitative differences between the CV per incident quantum curve in Figure 1 and the lead-production curve at 22° in Figure 2, the two curves have the same shape qualitatively. Both drop at short and at long wavelengths, and on both the 313- and 335-mμ points are at almost equal values of the ordinate.

Radiation absorbed by the 335-mμ exciton band produces CV in the liquid dispersion and lead in the coated films. This suggests that the band structure of $PbBr_2$ is such that the exciton can dissociate into both an electron in the conduction band and a hole in the

valence band. Probably the bands are of such shapes that there exists a phonon-assisted, indirect transition at an energy equal to the exciton energy.

A possible interpretation of the lower yields of CV and lead at 254 mμ relative to the yields at longer wavelengths is that the absorption coefficient is higher and the radiation is absorbed in a smaller crystal thickness at 254 mμ than at longer wavelengths. Thus there is a higher probability of recombination at 254 mμ than at longer wavelengths.

The parallel manner in which the sensitivity for lead production and absorption increases between 22 and 100° is in contrast to similar measurements made on evaporated $PbCl_2$ films by Kaldor and Somorji.[3] They reported that the minimum energy required to induce the photoreaction at temperatures above 40° is always less than the energy at the absorption edge of $PbCl_2$. This is unusual and interesting behavior which, unfortunately, we do not find for our samples of $PbBr_2$.

Quantum yields of 0.15–0.31 CV molecule/quantum indicate that 0.30–0.62 hole/quantum is detected, since the oxidation of LCV to CV involves two electrons. Verwey calculated values of Φ for lead production in $PbCl_2$[4a,d] and in $PbBr_2$[4d] and found 0.1 and 0.25 lead atom/quantum, respectively. Thus in $PbBr_2$ lead production accounted for one-half of the electrons. We have not yet measured Φ for lead production. The fate of the undetected holes is not known, although recombination is a probable process and, undoubtedly, occurs to some extent.

The rate of production of both lead and CV depends upon the first power of the intensity of irradiation. This suggests that, independent of intensity, each electron has a certain probability of reducing lead ions and each hole has a certain probability of oxidizing LCV. Arends and Verwey[4c] found esr evidence for the formation of Pb^+ ions in the initial step of the photochemical decomposition of $PbBr_2$ at 80°K. They also state that at very short irradiation times the rate of photolysis is a linear function of the intensity of irradiation. If one-electron reduction, such as the reduction of Pb^{2+} to Pb^+, and one-electron oxidation were the rate-limiting steps, the intensity dependence should be linear, as we have found. In contrast, Kaldor and Somorji[3] reported a different relationship between the optical density of photoproduct and the intensity of irradiation. They found two regions: a low-intensity region in which the optical density was proportional to the 0.17 power of the intensity, and a high-intensity region in which the power was 3.2. Our intensities correspond to the low-intensity region of Kaldor and Somorji. The reasons for these differences in intensity dependence are not understood.

Lead bromide has long been considered as an inert substrate for dyes;[18] however, spectral sensitization is

(17) K. J. Best, *Z. Phys.*, **163**, 309 (1961).

reported in this paper for the first time. In Figure 4 it can be seen that the sensitivity for CV production is dropping abruptly at about 460 mμ, although the adsorbed dye is absorbing light at longer wavelengths. This fact and the previously mentioned qualitative observation that effective dyes have absorption maxima at wavelengths shorter than 500 mμ suggest some sort of limit of spectral sensitization.

One such limit is suggested by the Gibbs free energy of dissociation of $PbBr_2$. This value is 62.24 kcal/mol[19] or converted into equivalent wavelength is 459 mμ. It would be of significance to show that the limit of spectral sensitization is related to the free energy of dissociation into the elements, but whether or not such a fundamental upper wavelength limit does exist for this spectral sensitization cannot be decided from these limited results.

It appears that light absorbed by the adsorbed dyes, I and II, produces CV but not lead. It is possible, of course, that lead is present in some undetectable form. However, if lead is not formed but CV is, the results can be explained by the relative location of the energy levels.[20] Light absorbed by a dye molecule excites an electron from the ground state to an excited state. If the partially empty level from which the electron was excited lies below the top of the $PbBr_2$ valence band, an electron could be transferred from the valence band to the partially empty dye energy level. Thus a hole is injected into the $PbBr_2$ valence band; this hole could oxidize LCV. In this scheme, the energy level of the excited electron in the dye must lie below the bottom of the $PbBr_2$ conduction band, because the energy difference between ground and excited states in the dye is less than the energy separation between the valence and conduction bands of $PbBr_2$. Thus an excited electron in the dye would be unlikely to transfer to the $PbBr_2$ conduction band and would be unavailable for reduction of lead ion to lead.

Another possible mechanism for producing CV involves some form of resonant energy transfer between the excited dye molecules and $PbBr_2$ energy levels. The lack of lead production could be explained in this case by trapping of the electron in some localized energy level below the conduction band.

Whatever the exact mechanism, the lower Φ for CV production in the dye-sensitized region, relative to the Φ at shorter wavelengths, suggests that the energy of electron transfer is not fully efficient.

(18) See E. Clementi and M. Kasha, *J. Chem. Phys.*, **26**, 959 (1957); W. West in "Scientific Photography," H. Sauvenier, Ed., Pergamon Press Ltd., London, 1962, p 557; W. West and A. L. Geddes, *J. Phys. Chem.*, **68**, 837 (1964).

(19) "Selected Values of Chemical Thermodynamic Properties," National Bureau of Standards Circular 500, U. S. Government Printing Office, Washington, D. C., 1950.

(20) For similar consideration of energy levels in the spectral sensitization of solids, see, for example: R. W. Gurney and N. F. Mott, *Proc. Roy. Soc.*, **A164**, 151 (1938); R. C. Nelson, *J. Phys. Chem.*, **71**, 2517 (1967).

The Heat and Products of Detonation of Cyclotetramethylenetetranitramine,

2,4,6-Trinitrotoluene, Nitromethane, and Bis[2,2-dinitro-2-fluoroethyl]formal[1]

by Donald L. Ornellas

Lawrence Radiation Laboratory, University of California, Livermore, California 94550 *(Received October 26, 1967)*

Three pure CHNO explosives covering a wide range of oxygen balance and one fluorine-containing explosive were fired in a detonation calorimeter. Product compositions and heat releases were obtained that are representative of the isentropic expansion of the detonation products. Energies ranged from 1095 to 1480 cal/g. Products varied from those containing no solid carbon to those containing more than 50% of the total carbon as solid. Observed products were compared to those calculated with the best available thermodynamic–hydrodynamic computer codes.

Introduction

Calorimetric measurements combined with product analysis offer a precise method for obtaining fundamental information about the detonation process. This information can then be used to provide normalization and boundary conditions for thermodynamic–hydrodynamic codes that predict explosive performance.

Three pure CHNO explosives and one fluorine-containing explosive were investigated. This work is an extension of the work reported[2] for PETN. Jointly, these studies span the range of oxygen balance[3] in explosives that is of greatest interest.

Previous detonation calorimetric work with 2,4,6-trinitrotoluene (TNT)[4-7] and cyclotetramethylenetetranitramine (HMX)[8] is not amendable to theoretical interpretation because of the geometries used or the lack of reliable product information. No information concerning the experimental determination of the heat and products of detonation of nitromethane (NM) and bis[2,2-dinitro-2-fluoroethyl]formal (FEFO) has been found in the literature.

Experimental Section

Apparatus and Operation. The apparatus and its operation have been described;[2] however, some changes have been made.

The thermometric system is a quartz thermometer which has a sensitivity of $10^{-4°}$ for differential measurements, is easily calibrated, and has direct digital readout.

The heat equivalent of the standard instrument, taken as the average of six calibration runs, was $15,193 \pm 2$ cal/deg. All errors quoted are twice the estimated standard deviation of the mean.

Charges are now completely confined by a 1.27-cm thickness of gold. Formerly the ends of the confining cylinder were left open. Since the bottom of the interior of the bomb was most damaged by flying

fragments, it was protected by a stainless steel disk, 0.64 cm thick and 6.4 cm in diameter, which we replaced after each experiment.

In order to contain NM under vacuum conditions, we sealed the gold cylinder 1.27 cm from each end with a translucent film which is a laminate of 0.025-mm polyethylene and 0.013-mm Mylar. A vacuum-tight seal was obtained by compressing the film between appropriately machined gold surfaces. The weight of film averaged 0.017 g/experiment.

All charges were fired using the detonator previously described.[2] Because of differences in the initiation characteristics of the explosives studied, various sizes of boosters were required. Boosters were made of PETN having a density of 1.71 g/cm^3, and their weight was kept to a minimum. No booster was required for the TNT experiments, since initiation was effected by means of the detonator alone. HMX and FEFO required 0.3-g boosters and NM required a 0.75-g booster.

Explosive Materials. Military specification, grade II HMX was used. Analyses by thin layer chroma-

(1) Work performed under the auspices of the U. S. Atomic Energy Commission. Work presented in part at the Joint Symposium of the Divisions of Fuel and Physical Chemistry on Detonations and Reactions in Shock Waves, 154th National Meeting of the American Chemical Society, Chicago, Ill., Sept 1967.

(2) D. L. Ornellas, J. H. Carpenter, and S. R. Gunn, *Rev. Sci. Instrum.*, **37**, 907 (1966).

(3) If the generalized molecular formula of an explosive is $C_aH_bN_cO_dF_e$, then the oxygen balance to the carbon dioxide level is OB (%) = $d - 2a - 0.5(b - e)$/mol wt 1600. The oxygen balances of the explosives studied are thus -22% (HMX), -74% (TNT), -15% (NM), and -9% (FEFO).

(4) A. Y. Apin, N. F. Velina, and Y. A. Lebedev, *Zh. Prikl. Mekhan. i Tekhn. Fiz.*, **5**, 96 (1962).

(5) ARE Memo No. 1/51, U. K. Ministry of Supply, Armament Research Establishment, Fort Halstead, Kent, England, April 1951.

(6) R. Robertson and W. E. Garner, *Proc. Roy. Soc.*, **A103**, 539 (1923).

(7) ARDE Report (S)4/56, U. S. confidential and U. K. restricted, as quoted by D. Price, *Chem. Rev.*, **59**, 801 (1959).

(8) H. W. Sexton, private communication.

tography showed about 0.5% cyclotrimethylene-trinitramine (RDX) and less than 1% each of an incompletely characterized linear nitramine (compound C) and 1-N-acetal-3,5,7-trinitrocyclotetranitramine (SEX). The melting point was 278–282°. Charges were machined from billets which had been prepared with a special solvent-pressing technique.

Granular TNT, military specification, grade III, was used. Analysis by thin layer chromatography showed less than 2% impurities. These were identified as 2,4,5-trinitrotoluene, 2,4-dinitrotoluene, and trinitrobenzoic acid. Elemental analyses for carbon, hydrogen, and nitrogen were in agreement with theory for pure TNT within the limits of the analyses. The melting point was 82.0°. Charges were pressed in increments to a density at which TNT detonates reliably in small diameters.

Commercial grade NM was used. Chromatographic analysis showed a purity of 96.7%. The impurities were: nitroethane, 0.94%; 2-nitropropane, 2.5%; 1-nitropropane, 0.03%; and water, 0.1%. The empirical formula on which results are based was calculated from the above analyses and adjusted to 1.00 for carbon.

We deaerated NM to avoid the formation of an air bubble between the booster and liquid when the bomb was evacuated. A large air bubble is undesirable because it acts as an attenuator between the booster and the main charge. Deaeration was accomplished by subjecting frozen NM to vacuum, sealing the container, and then thawing the NM. This procedure was repeated several times.

FEFO was available only in research quantities. It is a liquid with a vapor pressure of about 40 μ at 90°. The sample was determined to be 97.4% pure by chromatographic analyses. The principle impurity is bis[2,2-dinitro-2-fluoroethyl]diformal and it contains 0.1% water as received.

Water was removed by vacuum distillation in order to avoid loss of FEFO from the confining cylinder when the calorimeter was evacuated. The empirical formula on which results are based was calculated from elemental analyses and was adjusted to 5.00 for carbon.

Product Determination. The vacuum system built to measure total volume and to permit sampling of gaseous detonation products has been described.[2] Only minor changes were required to permit quantitative determination of the new products.

Carbon dioxide (CO_2), carbon monoxide (CO), nitrogen (N_2), hydrogen (H_2), methane (CH_4), ethane (C_2H_6), and acetylene (C_2H_2) were determined quantitatively by mass spectrometry. The amounts of the minor products CH_4, C_2H_6, and C_2H_2 were sometimes checked by glpc. Water was determined gravimetrically. Ammonia was determined by wet analysis of the two H_2O traps, a third trap containing sulfuric acid, and the calorimeter bomb washings. Hydrogen cyanide, hydrofluoric acid (HF), and total fluoride were

determined by wet analyses of the water traps and the bomb washings. Solid carbon (C(s)) was determined by the difference.

About 65% of the total fluorine in FEFO was recovered as HF and about 23% was recovered as metal fluoride in solution. Because no other products containing fluorine could be detected, we concluded that all of the fluorine must appear as HF in the detonation products and that the fluorine which was not observed as HF reacted with the stainless steel bomb. The observed heat of detonation and products for FEFO were corrected for these reactions.

Results and Discussion

Products from Heavily Confined Charges. Studies[2,4,9] indicate that the products from heavily confined charges represent those found on the Chapman-Jouguet (CJ) isentrope at temperatures in the range 1500–1800°K. Table I lists these products and the heats of detonation for HMX, TNT, NM, and FEFO.

As one proceeds down the scale of oxygen balance, FEFO, HMX, and TNT, the proportion of carbon which appears as C(s) increases and which appears as CO_2 and CO decreases. Also, the proportion of

Table I: The Heat and Products of Detonation of Heavily Confined Charges of Explosives[a,b]

	HMX	TNT	NM[c]	FEFO[d]
		Density, g/cm³		
	1.89	1.53	1.13	1.60
		Charge weight, g		
	25	22	15	25
		ΔH,[e] cal/g		
	1479 ± 12	1093 ± 7	1227 ± 7	1279 ± 12
		Amt of product, mol/mol of explosive		
CO_2	1.92	1.25	0.261	3.16
CO	1.06	1.98	0.550	1.88
C(s)[f]	0.97	3.65	0.095	Not detected
N_2	3.68	1.32	0.394	1.99
H_2O	3.18	1.60	0.882	2.14
H_2	0.30	0.46	0.294	0.046
HF	0	0	0	1.87[g]
NH_3	0.395	0.162	0.118	0.023
CH_4	0.039	0.099	0.083	0.001
HCN	0.008	0.020	0.008	Not detected
C_2H_6	0.001	0.004	0.001	Not detected

[a] Cylindrical charges, 1.27 cm in diameter, completely confined in 1.27 cm of gold. [b] Corrected for PETN in the initiation system. [c] NM = $C_{1.00}H_{2.96}N_{0.96}O_{1.92}$ by analysis and was adjusted to 1.00 for C. Trace amounts of acetylene were observed. [d] FEFO = $C_{5.00}H_{5.74}N_{4.09}O_{10.06}F_{1.87}$ by analysis and was adjusted to 5.00 for C. Results are corrected for reaction of HF with stainless steel. Charge not confined on the ends. [e] H_2O(l), 298°K. [f] Determined by difference. [g] From total fluorine contained in FEFO.

(9) H. Jones and A. R. Miller, *Proc. Roy. Soc.* **A194**, 480 (1948).

Table II: Comparison of the Calculated CJ Isentrope Products with the Observed Products from Heavily Confined Charges of HMX

Products	Obsd (heavily confined)	Amt of product, mol/mol of HMX			
		Calcd			
		BKW CJ isentrope		LJD CJ isentrope	
		1520°K	1800°K	1490°K	1760°K
N_2	3.68	3.97	3.97	3.98	3.97
H_2O	3.18	3.11	3.67	2.90	3.06
CO_2	1.92	2.39	2.13	2.16	2.01
CO	1.06	0.10	0.071	0.77	0.93
C(s)	0.97	1.13	1.68	0.73	0.81
NH_3	0.395	0.076	0.073	0.047	0.063
H_2	0.30	0.005	0.001	0.36	0.34
CH_4	0.039	0.38	0.11	0.34	0.26
HCN	0.008	0	0	Not allowed	Not allowed
C_2H_6	0.001	Not allowed	Not allowed	Not allowed	Not allowed

Table III: Comparison of the Calculated CJ Isentrope Products with the Observed Products from Heavily Confined Charges of TNT

Products	Obsd (heavily confined)	Amt of product, mol/mol of TNT			
		Calcd			
		BKW CJ isentrope		LJD CJ isentrope	
		1505°K	1835°K	1500°K	1870°K
C(s)	3.65	3.57	4.50	3.52	3.80
CO	1.98	0.56	0.32	1.60	1.58
H_2O	1.60	1.06	1.87	1.33	1.64
N_2	1.32	1.49	1.48	1.50	1.50
CO_2	1.25	2.19	1.91	1.53	1.39
H_2	0.46	0.043	0.017	0.48	0.40
NH_3	0.162	0.026	0.047	Not allowed	Not allowed
CH_4	0.099	0.68	0.27	0.34	0.23
HCN	0.020	3.6×10^{-6}	1.3×10^{-6}	Not allowed	Not allowed
C_2H_6	0.004	Not allowed	Not allowed	Not allowed	Not allowed

Table IV: Comparison of the Calculated CJ Isentrope Products with the Observed Products from Heavily Confined Charges of NM

Products	Obsd (heavily confined)	Amt of product, mol/mol of NM			
		Calcd			
		BKW CJ isentrope		LJD CJ isentrope	
		1520°K	1835°K	1500°K	1800°K
H_2O	0.88	0.75	0.77	0.81	0.85
CO	0.55	0.18	0.21	0.43	0.48
N_2	0.39	0.47	0.47	0.5	0.5
H_2	0.29	0.049	0.027	0.32	0.29
CO_2	0.26	0.49	0.47	0.38	0.33
NH_3	0.12	0.017	0.027	Not allowed	Not allowed
C(s)	0.095	0	0	0	0
CH_4	0.083	0.33	0.32	0.19	0.18
HCN	0.008	0	0	Not allowed	Not allowed
C_2H_6	0.001	Not allowed	Not allowed	Not allowed	Not allowed

hydrogen appearing as H_2 increases. NM, a low-density explosive with a high hydrogen-to-carbon ratio, is the exception of these trends. It lies between FEFO and HMX in oxygen balance, yet proportionally more carbon appears as CO and less appears as CO_2 and C(s) and proportionally more hydrogen appears as H_2 than one might expect from the FEFO and HMX

results. In addition, greater amounts of CH_4 are present in the NM products than for any of the other explosives.

It is noteworthy that all of the fluorine in FEFO appears as HF. Carbon tetrafluoride or other compounds containing the C–F structure were not observed.

The products from heavily confined charges attain

equilibrium under nonideal gas conditions, since the pressure at 1500–1800°K is of the order of 5000–50,000 atm. In order to calculate the product composition along the CJ isentrope, one must, therefore, use complex thermodynamic–hydrodynamic calculations. Calculations were made by using the two best equations of state available, the Becker–Kistiakowsky–Wilson (BKW) equation[10] in the RUBY computer code[11] and the LJD equation.[12] The comparisons of observed products with calculated products for the four explosives studied (Tables II–V) are fair. Data of this type will be used to improve equations of state for detonation products.

Table V: Comparison of the Calculated CJ Isentrope Products with the Observed Products from Heavily Confined Charges of FEFO

| | Amt of product, mol/mol of FEFO | | |
| | Obsd (heavily confined) | Calcd (BKW CJ isentrope) | |
Products		1520°K	1820°K
CO_2	3.16	3.92	3.82
H_2O	2.14	1.38	1.57
N_2	1.99	2.04	2.03
CO	1.88	0.83	0.85
HF	1.87	1.87	1.85
H_2	0.046	0.045	0.025
NH_3	0.023	0.018	0.026
CH_4	0.001	0.24	0.16
CF_4	0	0	0.005
C(s)	0	0	0.17

The Effect of Heavy End Confinement. The ideal experiment to allow isentropic expansion of detonation products is an infinitely long, heavily confined, open-ended charge. For such a configuration, end effects would be negligible. However, charge length is limited by the calorimeter dimensions, and end effects are such that some of the detonation products that jet from the open ends of the confining cylinder are sufficiently shock heated on colliding with the calorimeter wall to cause reequilibration. Reequilibration of these products can be avoided by confining the ends of the charge. However, end confinement presents the undersirable possibility of causing a significant amount of the detonation products to be shocked to an isentrope above the CJ isentrope as a result of reflections generated by a head on detonation impinging against the gold end confinement.

We fired heavily confined TNT charges with and without end confinement to investigate the magnitude of this effect. Results are presented in Table VI. The experiments with end confinement show the following: (1) an increase in the heat of detonation and (2) an increase in the species representative of a lower temperature isentrope (C(s), H_2O, and CO_2) and a corresponding decrease in the species repre-

Table VI: The Effect of Variations in Confinement on the Heat and Products of Detonation of Heavily Confined Charges of TNT[a,b]

	Method of cylindrical confinement	
	Both ends confined[c]	Both ends open
	ΔH detonation,[d] cal/g	
	1093 ± 7	1032 ± 7
Products	Amt of product,[e] mol/mol of TNT	
C(s)[f]	3.65	3.28
CO	1.98	2.56
H_2O	1.60	1.40
N_2	1.32	1.34
CO_2	1.25	1.07
H_2	0.46	0.74

[a] TNT: density, 1.53 g/cm³; 1.27 cm in diameter; 22-g charges confined in 1.27 cm thick gold cylinders. [b] Corrected for 0.25 g of PETN in the initiation system. [c] End confinement was 1.27 cm thick gold. [d] $H_2O(l)$, 298°K. [e] Minor products, NH_3, CH_4, HCN, and C_2H_6, were omitted. [f] Determined by difference.

Table VII: Comparison of the Calculated Equilibrium Products at Constant Volume with the Observed Products from Unconfined Charges of HMX[a]

| | Amt of product, mol/mol of HMX | | |
| | Obsd (unconfined) | Calcd for ideal gas | |
Products		1500°K	1800°K
N_2	4.01	4.00	4.00
CO	2.65	2.36	2.52
H_2O	2.50	2.36	2.52
H_2	1.53	1.64	1.48
CO_2	1.44	1.65	1.49
HCN	0.0006	2×10^{-5}	2×10^{-5}
NH_3	Not detected	0.0006	0.0002
CH_4	Not detected	0.0004	0
C(s)	Not detected	0	0

[a] Charges (25 g) at a density of 1.89 g/cm³ and 2.45 cm in diameter.

sentative of a higher temperature isentrope (CO and H_2) when the two isentropes are compared at the same volume.

This evidence indicates that the undesirable effect of end confinement is very small and that products from charges with end confinement are more nearly representative of those along the CJ isentrope than products from charges without end confinement. For this reason we adapted heavy end confinement to our standard configuration. All explosives except FEFO were fired in this configuration. For explosives of high oxygen balance, such as PETN or FEFO,

(10) C. L. Mader, Report LA-2900, Los Alamos Scientific Laboratory, 1963.

(11) H. B. Levine and R. E. Sharples, Report UCRL-6185, Lawrence Radiation Laboratory, Livermore, Calif., 1962.

(12) W. Fickett, Report LA-2712, Los Alamos Scientific Laboratory, 1962.

there is no significant difference in results with and without end confinement.

Products from Unconfined Charges. It has been shown[2] that the temperature at which equilibrium becomes frozen can be found by comparing observed detonation products from unconfined charges with products calculated with ideal gas laws. Work with PETN and the calculations of Jones and Miller[9] indicated a freeze-out temperature of 1500–1800°K. Unconfined charges of HMX and TNT were fired and products were compared (Tables VII and VIII) to those calculated. The agreement is good, confirming the earlier work.

The TNT data indicate that C(s) equilibrates rapidly during the reshocking of products that occurs with unconfined charges. The value for C(s), frozen out in the initial isentropic expansion, is 3.65 mol/mol of TNT (from Table I). If it were not equilibrating, the amount found in the products from unconfined charges (1.01 mol/mol of TNT, Table VIII) should be at least as large as that found in the products from heavily confined charges.

Acknowledgments. The author wishes to thank Dr. John W. Kury for his assistance and guidance in

Table VIII: Comparison of the Calculated Equilibrium Products at Constant Volume with the Observed Products from Unconfined Charges of TNT[a]

	Obsd (unconfined)	Calcd for ideal gas	
Products		1500°K	1800°K
CO	5.89	5.97	6.00
H_2	2.31	2.10	2.36
N_2	1.36	1.49	1.47
C(s)	1.01	0.81	0.90
H_2O	0.17	0.007	0.003
CO_2	0.063	0.009	0.003
HCN	0.024	0.018	0.056
NH_3	0.022	0.0005	0.0003
CH_4	0.0092	0.192	0.053

[a] Charges (25 g) at a density of 1.53 g/cm³ and 1.27 and 2.54 cm in diameter.

Studies in the Aqueous Radiation Chemistry of Cysteine.   I.

Deaerated Acidic Solutions[1,2]

by Adnan Al-Thannon, Richard M. Peterson,[3] and Conrad N. Trumbore[4]

Department of Chemistry, University of Delaware, Newark, Delaware

Accepted and Transmitted by The Faraday Society   *(November 3, 1967)*

Results of studies on the cobalt-60 γ radiolysis of acidic cysteine (RSH) solutions, pH 1.0 and 0.5, are reported. Irradiation products which have been identified are H_2, H_2S, RSH, and H_2O_2 with radiation yields at $10^{-3} M$ cysteine of 3.2, 0.95, 3.0, and 0.68 molecules/100 eV absorbed.   Alanine was also observed qualitatively as a radiation product.   Yields for the disappearance of the thiol group were measured polarographically during the irradiation and $G(-RSH)$ was found to be 7.0 at $10^{-3} M$ cysteine.   A mechanism is postulated for strongly acid cysteine solutions on the basis of competition kinetics, material balances, and comparison with theoretical yields.   Analysis of results of competition studies provides evidence for a rate constant of approximately 3×10^{10} l. mol^{-1} sec^{-1} for the reaction of the hydrated electron with the protonated-amine form of cysteine.   Results of scavenger studies at concentrations higher than $10^{-2} M$ cysteine require that additional processes be postulated in order to account for high H_2S yields.

Introduction

In a previous article,[5] evidence for the rapid reaction of the hydrated electron and the hydroxyl radical with cysteine (RSH) in neutral solutions was presented. Armstrong and coworkers[6] have recently proposed a mechanism for the cobalt-60 γ radiolysis of 1 N perchloric acid solutions of cysteine. We have independently studied this system at higher pH and we provide evidence here on yields and competition studies which are in agreement with their yields and which support, quantitatively, certain steps in their proposed mechanism. In addition, studies are reported which provide evidence that at higher cysteine concentrations there is very efficient scavenging of the hydrated electron by cysteine in competition with the hydronium ion. A diffusion-limited rate constant for this scavenging by cysteine is in contrast with the earlier reported rate constant for the neutral species, thus demonstrating the enhancing effect of the nearly complete protonation of the amine group in strong acid. Solutions were studied at pH 1 and 0.5 in order to limit the number of cysteine species to essentially only the amine-protonated one with the structure $HSCH_2$-$CH(NH_3{}^+)COOH$.[7]   Air-free solutions were studied in order to prevent possible chain reactions.[8,9]

Experimental Section

All irradiations were carried out at 25° in a Gammacell 220 (Atomic Energy of Canada, Ltd.) cobalt-60 irradiation unit. Absorbed dose rates in solutions in this study were approximately 10^3 rads/min. All aqueous solutions were swept with Ar, labeled 99.995% pure, supplied by Linde Air Products Co. and were irradiated in preirradiated Pyrex vessels supplied with standard tapers so that solutions could be transferred

from the Ar bubbler in a manner similar to that described by Swinnerton and Cheek.[10]   Dose rates were obtained using ferrous sulfate solutions irradiated in the same vessels.   All water was triply distilled.   In all cases solutions were prepared immediately before use to minimize air oxidation of cysteine.   pH measurements were carried out with a Beckman expanded-scale pH meter and spectrophotometric measurements were made with a Zeiss PMQ II spectrophotometer.

Cysteine (RSH), cystine (RSSR), and alanine (RH) were of the highest purity available from Nutritional Biochemicals Co. and Calbiochemical Co. Only the free-base forms of the amino acids were used in this work. Perchloric acid was either Merck or Baker reagent grade and KNO_3 was Baker and Adamson reagent grade. p-Chloromercuribenzoic acid was from Aldrich Chemical Co.

The rate of disappearance of the cysteine thiol

(1) This research was supported by the U. S. Atomic Energy Commission and is AEC Document NYO-3383-9.

(2) Based in part upon the Ph.D. dissertations of A. Al-Thannon and R. M. Peterson, University of Delaware, Newark, Del., 1967 and 1968, respectively.

(3) Deceased July 17, 1967.

(4) To whom correspondence should be addressed.

(5) A. El Samahy, H. L. White, and C. N. Trumbore, *J. Amer. Chem. Soc.*, 86, 3177 (1964).

(6) V. G. Wilkening, M. Lal, M. Arends, and D. A. Armstrong, *Can. J. Chem.*, 45, 1209 (1967).

(7) J. T. Edsall and J. Wymann, "Biophysical Chemistry," Vol. I, Academic Press Inc., New York, N. Y., 1958; J. N. Butler, "Ionic Equilibrium," Addison-Wesley, Inc., Reading, Mass., 1964.

(8) A. J. Swallow, *J. Chem. Soc.*, 1334 (1952); J. E. Packer, *ibid.*, 2320 (1963).

(9) A. Al-Thannon, R. M. Peterson, and C. N. Trumbore, unpublished results.

(10) J. W. Swinnerton, V. J. Linnebom, and C. H. Cheek, *Radiat. Res.*, 19, 636 (1963).

group, as well as the rate of buildup of the radiolytic products, H_2S and RSSR, was followed polarographically using a Sargent Model XV recording polarograph. The polarographic cell employed a dropping-mercury electrode and a saturated calomel reference electrode. An agar plug, prepared according to Meites,[11] was used between the reference electrode and the salt bridge (KCl) which contacted cysteine solutions (thermostated to 25 ± 0.1°) through a porous glass frit. In all cases the supporting electrolyte was perchloric acid. Sulfuric acid was found to give poorer polarographic waves for cysteine and cystine.

The main technique for gathering polarographic data was that of direct polarography of solutions during irradiation. A special thermostated cell containing the solution to be irradiated and analyzed, the dropping-mercury electrode, the salt bridge, and the standard cell was designed to fit inside the Gammacell irradiation chamber. With this cell it was possible to monitor during the irradiation the changes in concentration of cysteine, H_2S, and cystine at 0.15, -0.15, and -0.56 V; all voltages refer to the saturated calomel electrode.

Solutions to be simultaneously irradiated and polarographed were first bubbled with Ar until all traces of polarographically detectable oxygen were removed. The solution was then polarographed at a given constant voltage while outside the irradiation zone to establish a horizontal "base line" for the desired compound. Polarography continued as the lead drawer containing the sample and the polarographic cell were lowered into the irradiated zone.

Polarographic calibration curves for cystine were found to be dependent upon the amount of cysteine present with the known amounts of cystine.

The half-wave potentials of RSH, RSSR, and H_2S are separated widely enough to monitor independently during the irradiation concentration changes of a single compound. However, since H_2S and RSH waves are both anodic-oxidation waves,[12] any decrease in RSH during radiolysis was in competition with an increase in H_2S concentration. Thus the H_2S buildup was monitored in a separate experiment when it was desired to obtain $G(-RSH)$ and appropriate corrections were made on cysteine polarographic data.

Independent measurements of the yield of destruction of cysteine were carried out using a modification of the technique described by Boyer[13] using measurements at pH 1 rather than with an acetate buffer. These experiments were not as reliable as polarographic methods but, within the larger experimental error, gave qualitatively the same results as the polarographic measurements.

Yields of cystine obtained from polarographic studies were not as precise as those available from directly following the optical density of the cystine at

248 nm, where there is negligible absorbance from the cysteine and irradiation products other than cystine.

In addition to polarographic determination of H_2S at lower cysteine concentrations, the yields of this irradiation product were determined colorimetrically based upon the formation of methylene blue from the careful oxidation of freshly prepared p-aminodimethylaniline in acidic solution.[14] Hydrogen peroxide yields were determined using titanous sulfate.[15] Hydrogen was analyzed gas chromatographically using a 13 X molecular-sieve column maintained at 0° and using Ar as the carrier gas. Samples were injected into the chromatograph according to the technique of Swinnerton, et al.,[10] except for the addition of a Drierite column to remove water from the stripped gases from the 3-ml irradiation sample and to allow continuous sweeping of the liquid with Ar.

Attempts were made to develop a thin-layer chromatographic procedure employing radioisotope tracers which would separate cysteine from its radiation products. Even using glove-bag procedures and plate predevelopment to exclude oxygen, there was still oxidation of the cysteine to cystine during the chromatographic development period causing tailing. However, cystine and alanine could be qualitatively determined using 1-butanol–acetic acid–water (3:1:1 v/v/v) on MN-Polygram (Brinkmann) Sil S-HR, 110-μ layer on a plastic backing.

In experiments with added p-nitrosodimethylaniline, separate experiments were performed to ensure that the radiolysis product H_2S did not react with p-nitrosodimethylaniline.

Results

The primary kinetic products of the γ radiolysis of air-free aqueous cysteine solutions found and measured in this study were H_2, H_2S, H_2O_2, and RSSR, and from chromatography, RH. In addition, yields for the disappearance of the cysteine thiol group, $G(-RSH)$, were measured polarographically. These yields are reported in Table I along with those from other workers for comparison. In all cases the yields reported from this work are based upon linear yield vs. dose plots or, in a very few cases, upon initial-slope data where noticeable curvature in these plots developed at low doses and low cysteine concentration.

The H_2 and H_2S yields are especially sensitive to RSH concentration at concentrations above 3×10^{-3} M RSH. Yields from other workers are in most cases

(11) L. Meites, "Polarographic Techniques," 2nd ed, John Wiley and Sons, Inc., New York, N. Y., 1965, p 63.

(12) I. M. Kolthoff and C. Barnum, J. Amer. Chem. Soc., 63, 520 (1941); N. Matsuura, K. Muroshima, and M. Takizawa, Jap. Analyst, 13, 324 (1964).

(13) P. D. Boyer, J. Amer. Chem. Soc., 76, 4331 (1954).

(14) M. S. Budd and H. A. Bewick, Anal. Chem., 24, 1536 (1952); L. Gustafsson, Talenta, 4, 227 (1960).

(15) A. C. Egerton, et al., Anal. Chim. Acta, 10, 422 (1954).

Table I: Radiolytic Product Yields[a] in Air-Free Aqueous Cysteine Solutions, pH 1 $(HClO_4)^b$

(RSH), M	$G(-RSH)^c$	$G(H_2)$	$G(H_2S)^d$	$G(RSSR)^e$	$G(H_2O_2)$	$G(RH)$
1×10^{-4}	5.4	3.05	0.8	2.9		
4×10^{-4}		3.12	0.9			
5×10^{-4}	6.8		0.95	3.0		
6×10^{-4}		3.15				
1×10^{-3}	7.0 ± 0.5	3.22 ± 0.1	0.95 ± 0.1	3.0 ± 0.3	0.68	
	(7.6 ± 0.3)	(3.1 ± 0.1)	(0.75 ± 0.05)	(3.1 ± 0.2)		(0.77 ± 0.05)
	$(6.7)^f$			2.8 ± 0.5^g		
2×10^{-3}	7.0		0.95			
2.5×10^{-3}				3.0		
4×10^{-3}		3.27	1.0			
5×10^{-3}			1.0			
1×10^{-2}		3.05	1.2	$3.8, 3.0^g$	0.68	
	(7.8 ± 0.3)	(3.35 ± 0.1)	(0.78 ± 0.05)	$(3.3, 4.2)$		(0.87 ± 0.05)
	$(7.0)^f$					
2×10^{-2}		2.75	1.5			
3.5×10^{-2}			1.8			
4×10^{-2}			2.0			
5×10^{-2}		2.40				
6×10^{-2}			2.4			
1×10^{-1}		1.82	3.3			
2×10^{-1}		1.70				
4×10^{-1}		1.40				

[a] All yields are calculated from initial slopes of dose *vs.* yield plots which were normally linear. [b] Values in parentheses are taken from ref 6 unless otherwise noted. [c] Obtained polarographically; averages of several points except at 10^{-3} M where the average of eight determinations is given. [d] Average values of polarographic and colorimetric determinations given between 10^{-4} and 10^{-3} M RSH. [e] Polarographic data. [f] Obtained from N. Matsuura and K. Muroshima, *Sci. Papers Coll. Gen. Educ., Univ. Tokyo*, **14**, 183 (1964); 0.8 N H_2SO_4. [g] Colorimetric data.

in agreement, within the combined experimental error, with those reported in the present work.

In Table II are presented data from a more limited study of the hydrogen yields in air-free perchloric acid (pH 0.5) solutions of cysteine at varying RSH concentrations. It may be noted that these yields are slightly higher than similar ones at pH 1 but that the same basic trend in RSH concentration dependence is followed.

Table II: Hydrogen Yields from Irradiated Air-Free Aqueous Cysteine Solutions at pH 0.5 $(HClO_4)$

Initial concn of RSH, M	$G(H_2)$
1.0×10^{-4}	3.10
5.0×10^{-4}	3.30
1.0×10^{-3}	3.40
5.0×10^{-3}	3.57
1.0×10^{-2}	3.40
5.0×10^{-2}	3.10
1.0×10^{-1}	2.60

In an experiment in which a 5×10^{-4} M RSH solution was made 5×10^{-5} M in *p*-nitrosodimethylaniline, the hydrogen yield was only slightly reduced from a normal yield of 3.1–3.0, whereas the hydrogen

sulfide yield dropped from a value of 0.95 to below the detectable limit of the analytical method employed. However, this sensitivity of $G(H_2S)$ to additives was not found when solutions which were 5×10^{-5} and 10^{-3} M in RSH, respectively, were each made 10^{-3} M in glycine. No change in $G(H_2S)$ from that obtained in the absence of glycine was observed.
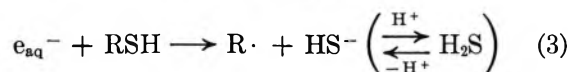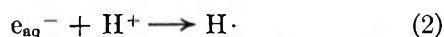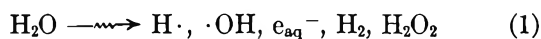
In the thin layer chromatographic experiments, alanine was identified through its R_f value. No other chromatographically detectable products were observed either through ninhydrin tests or through radioisotopic-labeling techniques.

Solutions of 10^{-5} M RSH and 10^{-2} M H_2O_2 showed no detectable reaction after standing for 3 hr, whether they were air saturated or Ar degassed.

Discussion

The yields of products found in our work and those of Armstrong and coworkers[6] agree, within the combined errors of the experimental measurements. A satisfactory sulfur and material balance between $G(-RSH)$ and the measured products is obtained and agrees well with the following mechanism, which is slightly different from those presented by earlier workers.[16]

(16) A. El Samahy, H. L. White, and C. N. Trumbore, *J. Amer. Chem. Soc.*, **86**, 3177 (1964); V. G. Wilkening, M. Lal, M. Arends, and D. A. Armstrong, *Can. J. Chem.*, **45**, 1209 (1967), and references therein.

$$H_2O \xrightarrow{} H\cdot, \cdot OH, e_{aq}^-, H_2, H_2O_2 \qquad (1)$$

$$e_{aq}^- + H^+ \longrightarrow H\cdot \qquad (2)$$

$$e_{aq}^- + RSH \longrightarrow R\cdot + HS^- \left(\overset{H^+}{\underset{-H^+}{\rightleftarrows}} H_2S \right) \qquad (3)$$

$$H\cdot + RSH \longrightarrow H_2 + RS\cdot \qquad (4)$$

$$H\cdot + RSH \longrightarrow R\cdot + H_2S \qquad (5)$$

$$R\cdot + RSH \longrightarrow RH + RS\cdot \qquad (6)$$

$$H\cdot + RSH \longrightarrow RH + HS\cdot \qquad (7)$$

$$HS\cdot + RSH \longrightarrow H_2S + RS\cdot \qquad (8)$$

$$\cdot OH + RSH \longrightarrow H_2O + RS\cdot \qquad (9)$$

$$RS\cdot + RS\cdot \longrightarrow RSSR \qquad (10)$$
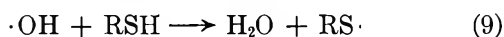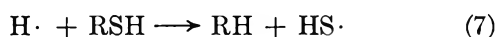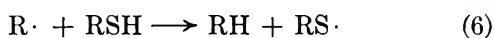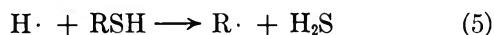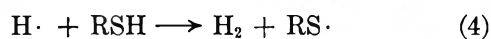
It will be noted that there are presented in this mechanism three different pathways for reaction of the hydrogen atom, $H\cdot$, with cysteine, RSH. Reaction 4 leads directly to the production of H_2. Both pathway a [reactions 5 and 6] and pathway b [reactions 7 and 8] lead to the same net over-all reaction products, namely, one molecule of H_2S and one molecule of RH. In this reaction mechanism the precursors to formation of H_2 and H_2S are both H atoms.

In the experiment with added *p*-nitrosodimethylaniline, known for its scavenging of OH radicals,[17] the H_2 and H_2S yields are affected in markedly different manners. If the *p*-nitrosodimethylaniline does not react with a precursor of the $H\cdot$ and yet cuts down the H_2S yield to very low values, it would tend to eliminate pathway a, since H_2S is formed directly in step 5. If pathway b is considered, the $HS\cdot$ intermediate could react with *p*-nitrosodimethylaniline completely to eliminate the H_2S yield and yet not affect the H_2 yield. If this is so, it may also be concluded that the reaction rate of the H atom with RSH is competitive with that for reaction with the *p*-nitrosodimethylaniline molecule, which could easily add the H atom to the aromatic ring.

From the above mechanism, the following sulfur balance may be derived: $G(-RSH) = 2G(RSSR) + G(H_2S)$. An over-all theoretical mass balance may also be derived: $G(-RSH) = G_{OH} + G_{e_{aq}^-} + G_H + G(H_2S)$. In addition $G(H_2S)$ must equal $G(RH)$. Within the limits of the combined experimental errors involved in Table I, the data presented are consistent with these relationships at RSH concentrations greater than 4×10^{-4} M, if commonly accepted values for acid solutions are taken for G_{OH} and $G_{e_{aq}^-}$.[18] It is, therefore, probable that all of the major primary radiolysis products in the γ radiolysis of acid solutions of cysteine have been accounted for.

Since the pK for the ionization of the carboxyl group of the cysteine equals 1.8,[7] it was necessary to maintain a pH of 1 or lower in order to have essentially only one form of the cysteine present to react with

radiolytic intermediates. Since abundant evidence has been presented that the hydrated electron reacts with the neutral (zwitterion) form of cysteine,[5,6,19] it was of interest to acquire evidence for the same reaction rate constant for the acid form present at pH 1 and below. The pulse-radiolysis method is presented with formidable problems in this region because of the very short lifetime of the hydrated electron in these strongly acid solutions. If the rate constant for reaction of RSH with e_{aq}^- is diffusion limited, there should be a competition for the hydrated electron represented by reactions 2 and 3, which should become important above 10^{-2} M RSH. Since the reaction product of eq 3 is the same as one of the products from the series of reactions arising from eq 2, a more complex relationship than simple competition was anticipated as reflected in eq 11, which is derived on the basis of reactions 2–4, 7, and 8

$$G(H_2) = G_H \left[\frac{1}{1 + \dfrac{k_7}{k_4}} \right] + $$
$$G_{e_{aq}^-} \left[\frac{1}{1 + \dfrac{k_3(RSH)}{k_2(H^+)}} \right] \left[\frac{1}{1 + \dfrac{k_7}{k_4}} \right] + 0.45 \qquad (11)$$

G_H represents the "residual" hydrogen atom yield, commonly reported to equal 0.6.[18] $G_{e_{aq}^-}$ may be taken equal to 3.3, which is higher than commonly reported for neutral solutions[18] but gives a value which is sufficiently high enough to give the experimental hydrogen yields at lower cysteine concentrations.

It is seen from Table I that the sum of $G(H_2)$ and $G(H_2S)$ is essentially a constant between 10^{-3} and 2×10^{-2} M RSH and is equal to 4.3 at pH 1. This is approximately equal to the sum of the reducing-radical yield (at higher solute concentration) for acid solutions plus the molecular hydrogen yield of 0.45.[18] If at relatively low RSH concentration, the predominant reaction of the hydrated electron is with the hydrogen ion to form the hydrogen atom as in eq 2, the ratio $G(H_2S)/[G(H_2)_{measd} - G(H_2)_{molecular}]$ should equal k_7/k_4, the ratio of rate constants for reactions 7 and 4, assuming pathway b is operative rather than pathway a.

If a value of 2.2×10^{10} l. mol^{-1} sec^{-1} is taken for k_2,[20] the only unknown quantity in eq 11 is the value of k_3, the electron-scavenging rate constant for the acid form of cysteine. Figure 1 shows the agreement

(17) I. Kraljić and C. N. Trumbore, *J. Amer. Chem. Soc.*, **87**, 2547 (1965).

(18) Proceedings of the Fifth International Conference on the Radiation Chemistry of Water, Notre Dame University, Notre Dame, Ind., Oct 1967, p 27.

(19) R. Braams, *Radiat. Res.*, **27**, 319 (1966).

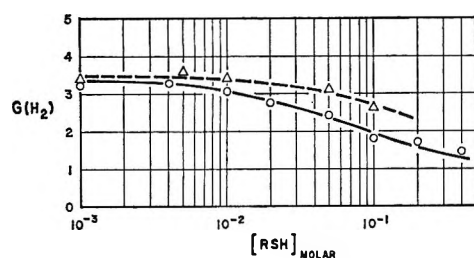(20) M. Anbar and P. Neta, *J. Appl. Radioact. Isotopes*, **16**, 227 (1965).

Figure 1. Comparison of experimental vs. theoretical (eq 11) radiolysis yields of hydrogen for acid solutions of cysteine as a function of cysteine concentration: O, pH 1 (experimental results); —, pH 1 (predicted $G(H_2)$, assuming $G_{e_{aq}^-} = 3.3$, $G_H = 0.6$, $k_7/k_4 = 0.33$, $k_3/k_2 = 1.36$, $G_{H_2} = 0.45$); △, pH 0.5 (experimental results); – – –, pH 0.5 (predicted $G(H_2)$, assuming same rate constants and yields as above, except that $G_{e_{aq}^-} = 3.4$).

Figure 2. Comparison of experimental $G(H_2S)$ yields at pH 1 from irradiated cysteine solutions with those predicted from the proposed mechanism and eq 11: O, experimental yields; – – –, predicted from eq 11 using the same yields and rate constant ratios as in Figure 1 (pH 1).

between the experimental and the calculated results based upon eq 11 when the value of k_3 is assumed to be 3×10^{10} l. mol^{-1} sec^{-1}. Only at higher RSH concentrations of 10^{-1} M RSH and above are there deviations which are slightly outside the limit of experimental error. In the same figure is shown the agreement between predicted and experimental values of $G(H_2)$ for the data in Table II at pH 0.5. In this calculation all values for yields and rate constants were the same as above, except that $G_{e_{aq}^-}$ was taken to be 3.4 in order to account for the higher yields of hydrogen at low (RSH). Again good agreement is found over the more limited region of RSH concentration covered.

It would, therefore, appear that, if the assumptions made are correct, the rate constant for the scavenging of the hydrated electron by the acid form is higher by about a factor of 4 than that for the zwitterion. The positive charge of the amino group may be responsible for this increased effectiveness of trapping the negatively charged entity.[21] However, it is interesting to note that the eventual product of this reaction is not ammonia, as is the case with amino acids which do not contain the –SH group,[22] but instead is H_2S. It would, therefore, appear that if the positive ion is neutralized at the amine site, the neutralization product must live long enough to allow delocalization of the electron in the molecule. It is also possible that the positive charge only serves to accelerate the reaction rate but that the attack of the electron is still directly on the sulfur orbitals.[23]

Again in contrast with the nonsulfhydryl-containing amines, there appears to be no *net* abstraction of the hydrogen attached to the amino carbon, although this may be the result of secondary reactions.

In the mechanism proposed above, the sum of $G(H_2S)$ and $G(H_2)$ should equal a constant, namely, about 4.3. Therefore, it should be possible to calculate very simply from the predicted values of $G(H_2)$ those anticipated for $G(H_2S)$ and to compare them with the experimental ones. Such a comparison is shown in Figure 2. It is
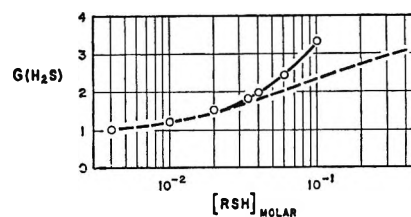
seen that there is an obvious deviation from predicted values above 2×10^{-2} M RSH and that the deviation becomes greater the greater the RSH concentration. In this concentration region a "scavenging of the spur" would be expected to play an increasingly important role, especially if the electron-scavenging rate constant is as high as 3×10^{10} l. mol^{-1} sec^{-1}. However, this would be internally inconsistent, since the hydrogen yields should be much lower than predicted in the same concentration region, and if anything they are slightly higher, as seen in Figure 1. At 10^{-1} M RSH the deviation from the expected $G(H_2S)$ yield is a relatively high value of about $G = 1$. It is entirely possible that a direct effect producing molecular hydrogen from RSH is becoming important, but the concentrations would appear to be rather low for such a phenomenon to occur except through a long-range energy-transfer mechanism. Another possibility is that the chain reaction producing H_2S observed in studies[9] of oxygen-containing cysteine solutions may be important even though the oxygen concentration is estimated to be less than 10^{-6} M. Unfortunately other H_2S analysis methods tried during this study were not found to be as reliable as that one used in the low-concentration range where initial yields are measured. Thus no analytical cross-checks were possible on the H_2S yields, but since blanks were used containing the same RSH concentrations, the only possible interference would come from irradiation products. It is, therefore, thought that the large excess hydrogen sulfide yields reported are valid.

Hydrogen peroxide yields found in this study are those normally anticipated for molecular H_2O_2 yields and again indicate the high efficiency of the cysteine in scavenging reactive intermediates.

(21) R. Braams, *Radiat. Res.*, **31**, 8 (1967).

(22) B. M. Weeks, S. A. Cole, and W. M. Garrison, *J. Phys. Chem.*, **69**, 4131 (1965).

(23) D. C. Wallace, J. E. Hesse, and F. K. Truby, *J. Chem. Phys.*, **42**, 3845 (1965).

the Government of Iraq held during the tenure of this research. The authors also wish to acknowledge helpful advice from and discussions with Drs. W. McCurdy, H. Bell, and I. Kraljić.

Conformational Properties of Optically Active Poly-α-olefins in Solution

by P. L. Luisi and P. Pino

Istituto di Chimica Organica Industriale dell'Università di Pisa,
Centro Nazionale di Chimica delle Macromolecole del C. N. R., Sezione IV, Italy

The molar ratio of monomeric units spiraled in the right-handed (ω_r) and left-handed (ω_s) screw sense has been related at each temperature to the molar rotatory power of isotactic poly((S)-4-methyl-1-hexene) in solution. The parameters ΔE and ΔU, in terms of which ω_r and ω_s are expressed by a statistical treatment previously reported, are hence evaluated by a best-fitting procedure. All the other conformational properties defined by ΔE and ΔU, such as the end-to-end distance, the number of inversions between the two screw senses, and the length of the regularly spiraled sequences in each screw sense, are calculated and compared with those of isotactic nonoptically active poly-α-olefins having an analogous structure.

Introduction

The molar rotatory power of optically active vinyl polymers in solution has been interpreted by assuming that the main chain of the macromolecule consists of alternated left-handed and right-handed sequences, one of the two screw senses, on the average, being prevalent, depending upon the absolute configuration of the asymmetric carbon atom of the side groups and its distance from the main chain.[1-3]

Birshtein and Luisi[4] and, independently, Corradini, Allegra, and Ganis[5] have expressed the conformational properties of these macromolecules in solution by a statistical treatment in which the conformation of the monomeric units and their mutual interactions are taken into account.

The statistics developed by Birshtein and Luisi is in terms of the two parameters

$$g = e^{-\Delta E/RT} \qquad p = e^{-\Delta U/RT} \qquad (1)$$

where

$$2\Delta E = E_{r,r} - E_{s,s}$$

$$2\Delta U = E_{r,s} + E_{s,r} - (E_{s,s} + E_{r,r}) \qquad (2)$$

where $E_{s,s}$ and $E_{r,r}$ are the free energies of a pair of monomeric units when included in a left-handed and a right-handed sequence, respectively; $E_{r,s}$ and $E_{s,r}$ are free energies of a pair of monomeric units of which the former is, respectively, right-handed and left-handed spiraled and the latter is, respectively, left-handed and right-handed spiraled.

Birshtein and Ptitsyn have given a rough estimation of ΔE on the basis on the relationship[6,7]

$$\Delta E = RT \ln (n_s/n_r) \qquad (3)$$

where n_s and n_r are the number of conformations allowed to the monomeric unit when included in a left-handed and in a right-handed sequence, respectively; the number of conformations can be determined on the basis of conformational analysis.[1]

As far as ΔU is concerned, a value ranging between 600 and 1500 cal/mol can be estimated for some nonoptically active poly-α-olefins on the basis of the data obtained[8] for the energy at the conformational reversals (inversions from one sense of spiralization to the other one).

In this paper, an independent evaluation of ΔE and ΔU is given, starting from the experimental molar rotatory power and its temperature coefficient and

(1) P. Pino, F. Ciardelli, G. P. Lorenzi, and G. Montagnoli, *Makromol. Chem.*, **61**, 207 (1963).

(2) P. Pino, *Advan. Polym. Soc.*, **4**, 393 (1965); P. Pino, P. Salvadori, E. Chiellini, and P. L. Luisi, *J. Pure Appl. Chem.*, in press.

(3) P. Pino and P. L. Luisi, *J. Chim. Phys.*, **65**, 130 (1968).

(4) T. M. Birshtein and P. L. Luisi, *Vysokomol. Soedin.*, **6**, 1238 (1964).

(5) G. Allegra, P. Corradini, and P. Ganis, *Makromol. Chem.*, **90**, 60 (1966).

(6) T. M. Birshtein and O. B. Ptitsyn, Conformations of Macromolecules," Interscience Publishers, New York, N. Y., 1966.

(7) Such a procedure, which assumes that all the allowed conformations have the same energy and neglects the higher energy ones, although sufficient to give the order of magnitude of ΔE, is not sufficient for an approach to the problem in more quantitative terms, particularly when use should be made of relationships involving the dependence of ΔE on temperature.

from the energy differences between the different conformations of bonds, known in low molecular weight compounds.

Relationship between Optical Activity and Conformation in Optically Active Isotactic Vinyl Polymers

The molar rotatory power, $[\phi]_D^T$, of the optically active, ideally isotactic vinyl polymer can be expressed by the equation[9]

$$[\phi]_D^T = M_s \omega_s + M_r \omega_r \tag{4}$$

where M_r and M_s are the molar rotations and ω_r and ω_s are the molar fractions of the monomeric units included in the right-handed and the left-handed spiraled sequences, respectively, at temperature T.[10]

M_r and M_s can be expressed by

$$M_s = \frac{\sum_i^i M_i e^{-\varepsilon_i/RT}}{\sum_i e^{-\varepsilon_i/RT}} \qquad M_r = \frac{\sum_j^j M_j e^{-\varepsilon_j/RT}}{\sum_j e^{-\varepsilon_j/RT}} \tag{5}$$

where i and j are the number of conformations allowed to the monomeric unit when it is included in a left-handed or right-handed spiraled sequence, respectively, and ε_i and ε_j are the energies and M_i and M_j are the molar rotatory powers of the ith and jth conformation, respectively.

The problem of determining ΔE and ΔU from the optical activity experimental data by using eq 4 and 5 can be solved only if the number of conformations of the monomeric unit and their relative energy can be evaluated. Until now, only in the case of low molecular weight paraffins could a reliable conformational analysis be performed. According to such an analysis, only staggered *trans* and *gauche* conformations of bonds are considered, and on the basis of simple rules, the conformations which are "allowed" and the ones which are "forbidden," because of high-energy interactions between nonbonded atoms, can be predicted.[11-14] Experimental and theoretical investigations indicate that the energy difference between a *trans* and a *gauche* conformation of bonds is about 600–800 cal/mol, and the energy difference between a full *trans* and a forbidden conformation is about 2700–3000 cal/mol for each high-energy interaction.[12-14]

Since these data can be reasonably extended to high molecular weight paraffins, optically active poly-α-olefins can be suitably investigated in these terms. Furthermore, we have to consider that in the case of poly-α-olefins, which can be dissolved and investigated in hydrocarbons, the influence on $[\phi]_D^T$ of the solvent–polymer interaction is considered to be fairly low.

For these reasons we started to investigate poly((S)-4-methyl-1-hexene), the most isotactic fraction of this polymer being highly soluble in hydrocarbons in a wide range of temperatures (Figure 1). Furthermore, per-
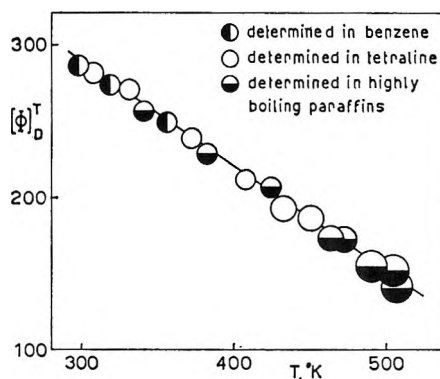
Figure 1. The molar rotatory power at different temperatures of highly isotactic poly((S)-4-methyl-1-hexene).

forming for such a polymer the conformational analysis previously mentioned, we conclude that only three conformations are allowed to the monomeric unit inserted in an isotactic sequence,[1] two (S_1 and S_2) when the sequence is left-handed spiraled and one (R_1) when the sequence is right-handed spiraled. These three conformations can be visualized in terms of internal-rotation angles, as indicated in Table I. In Table II the Newman projections of bonds are shown. We shall state that e' is the energy difference between S_1 (considered as the most stable conformation) and S_2 and that e is the energy difference between S_1 and R_1.

In Table I the conformations having one (S_3–S_5 and R_2–R_7) and two high-energy interactions (S_6–S_{13} and R_8–R_{14}) are reported for the monomeric unit included in an isotactic sequence left-handed and right-handed spiraled.

We have faced the problem of evaluating ΔE and ΔU of poly((S)-4-methyl-1-hexene) on the basis of the

(8) P. Debye and F. Bueche, *J. Chem. Phys.*, **19**, 589 (1951); W. R. Krigbaum and P. J. Flory, *J. Polym. Sci.*, **11**, 37 (1953); K. E. Fattakov, *Zh. Tekhn. Fiz.*, **24**, 1401 (1954); W. R. Krigbaum and D. Carpenter, *J. Phys. Chem.*, **59**, 1166 (1955); F. Danusso, G. Moraglio, and G. Gianotti, *Rend. Ist. Lombardo Sci. Lettere*, **A93**, 666 (1959); P. Corradini and G. Allegra, *Atti Accad. Nazl. Lincei, Rend., Classe Sci. Fis. Mat. Nat.*, **30**, 516 (1961); P. de Santis, E. Giglio, A. M. Liquori, and A. Ripamonti, *Nuovo Cimento*, **26**, 616 (1962); N. P. Borisova and T. M. Birshtein, *Vysokomol. Soedin.*, **6**, 1234 (1964).

(9) In the papers concerning the optical activity of synthetic polymers, $[\phi]_D^T$ is generally referred to one monomeric unit, as it is independent from molecular weight, provided that a polymerization degree higher than 20–30 is considered.[2]

(10) ω_r and ω_s are expressed in terms of ΔE and ΔU by the relationships[4,6] $\omega_r = (r - q)/2r$ and $\omega_s = (r + q)/2r = 1 - \omega_r$, where $r^2 = q^2 + p^2 g$ and $q = (1 - g)/2$.

(11) M. V. Volkenstein, "Configurational Statistics of Polymeric Chains," Interscience Publishers, New York, N. Y., 1963.

(12) N. L. Allinger and M. A. Miller, *J. Amer. Chem. Soc.*, **83**, 2145 (1961); M. Hanack, "Conformation Theory," Academic Press Inc., New York, N. Y., 1965; R. A. Scott and M. A. Sheraga, *Biopolymers*, **4**, 237 (1966); A. Abe, R. L. Jernigan, and P. J. Flory, *J. Amer. Chem. Soc.*, **88**, 631 (1966).
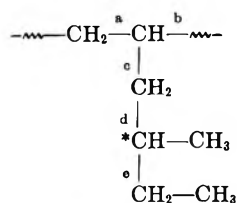
(13) J. H. Brewster, *ibid.*, **81**, 5475 (1959).

(14) K. S. Pitzer, *J. Chem. Phys.*, **8**, 711 (1940); K. Ito, *J. Amer. Chem. Soc.*, **75**, 2430 (1953); W. B. Person and C. G. Pimentel, *ibid.*, **75**, 532 (1953); S. Mizushima, "Structure of Molecules and Internal Rotation," Academic Press Inc., New York, N. Y., 1954; L. S. Bartell and D. A. Kohl, *J. Chem. Phys.*, **39**, 3097 (1963).

Table I:[a] Conformational Analysis of a Monomeric Unit of Poly((S)-4-methyl-1-hexene) Included in a Left-Handed and a Right-Handed Sequence

$$-\text{ww}-\overset{a}{CH}-\overset{b}{CH_2}-\text{ww}-$$
$$\overset{c}{|}$$
$$CH_2$$
$$\overset{d}{|}$$
$$*CH-CH_3$$
$$\overset{e}{|}\ \ ^f$$
$$CH_2-CH_3$$

Conformations	a	b	c	d	e	f	Relative energy	Molar rotation according to Brewster	Conformations	a	b	c	d	e	f	Relative energy	Molar rotation according to Brewster
S_1	T	G	T	G	T	G	0	300	R_1	G′	T	G′	T	G′	T	e	−300
S_2	T	G	T	G	T	T	e'	180	R_2	G′	T	G′	G	T	G	ε	60
S_3	T	G	T	G	T	G′	ε	240	R_3	G′	T	G′	G	T	T	ε	−60
S_4	T	G	T	G	G′	T	ε	60	R_4	G′	T	G′	T	T	G	ε	−60
S_5	T	G	T	T	G′	T	ε	−60	R_5	G′	T	G′	T	T	T	ε	−180
S_6	T	G	T	G′	T	G	2ε	240	R_6	G′	T	G′	T	G′	G′	ε	−180
S_7	T	G	T	G′	T	T	2ε	120	R_7	G′	T	G′	T	G′	G	ε	−240
S_8	T	G	T	G	G′	G′	2ε	120	R_8	G′	T	G′	G	T	G′	2ε	0
S_9	T	G	T	T	G′	G	2ε	0	R_9	G′	T	G′	T	T	G′	2ε	−120
S_{10}	T	G	T	T	G′	G′	2ε	60	R_{10}	G′	T	G′	G′	T	T	2ε	−120
S_{11}	T	G	T	G′	G′	T	2ε	0	R_{11}	G′	T	G′	G′	G	G	2ε	0
S_{12}	T	G	T	G	G	G′	2ε	120	R_{12}	G′	T	G′	G′	G′	T	2ε	−240
S_{13}	T	G	T	G	G	T	2ε	120	R_{13}	G′	T	G′	T	G	G	2ε	−120
									R_{14}	G′	T	G′	T	G	T	2ε	−240

[a] On the basis of the commonly accepted rules (P. Corradini, P. Ganis, and P. Oliviero, *Atti Accad. Nazl. Lincei, Rend. Class. Sci. Fis. Mat. Nat.*, **33**, 320 (1962)), the rotation angles of each C–C bond is evaluated according to the plane defined by the two previous C–C bonds, proceeding clockwise and assuming as the zero angle the complanar *cis* position: T = 180°, G = 60°, and G′ = −60°.

Table II: Newman Projections of a Monomeric Unit of Poly((S)-4-methyl-1-hexene) Included in the Main-Chain Sequences Left-Handed and Right-Handed Spiraled

$$-\text{ww}-\overset{a}{CH_2}-\overset{b}{CH}-\text{ww}-$$
$$\overset{c}{|}$$
$$CH_2$$
$$\overset{d}{|}$$
$$*CH-CH_3$$
$$\overset{e}{|}$$
$$CH_2-CH_3$$

energy interaction have all the same energy excess ε, and the conformations having two high-energy interactions have all the same energy excess 2ε; (c) e, e', ε, M_s, and M_r are independent of temperature in the range investigated (300–500°K, see Figure 1).[15]

On the basis of these assumptions, ΔE can be written in the form (see eq 2)

$$\Delta E = \frac{RT}{2}\ln$$
$$\frac{1 + 2e^{-e'/RT} + e^{-2e'/RT} + 12e^{-\varepsilon/RT} + 41e^{-2\varepsilon/RT}}{e^{-2\varepsilon/RT} + 12e^{-\varepsilon/RT} + 50e^{-2\varepsilon/RT}}$$

(6)

In fact, according to conformational analysis, a pair of monomeric units included in a left-handed-spiraled sequence may exist in 3 × 4 conformations having one high-energy interaction (excess energy ε) and in (3^2 + 4 × 8) conformations having two high-energy interactions (excess energy 2ε); similarly, it is easy to verify that in the right-handed screw sense, a pair of

following assumptions: (a) only the allowed conformations and the conformations with one and two high-energy interactions are taken into account; (b) relative to S_1, the conformations having one high-

(15) We can obtain an indication of the reasonability to consider M_r and M_s independent of temperature by studying the dependence of eq 5 on temperature on the basis of the Brewster[13] values for M_i and M_j (from Table I) and for a set of reliable values for e, e', and ε. In the range of e and e' from 0 to 500 cal/mol, and with ε ranging from 2000 to 3500 cal/mol, M_s and M_r change with respect to temperature, in the range 300–500°K, by far less than the experimental indetermination on $[\phi]_D^T$.

monomeric units may exist in 2×6 conformations having one high-energy interaction and in $(6^2 + 7 \times 2)$ conformations having two high-energy interactions (see Table I).

Similarly, ΔU can be written in the form

$$\Delta U = \frac{RT}{2} \ln$$

$$\frac{1 + 2e^{-e'/RT} + e^{-2e'/RT} + e^{-2e/RT} + \begin{array}{c} 24e^{-\varepsilon/RT} + 91e^{-2\varepsilon/RT} \end{array}}{14e^{-\varepsilon/RT} + 59e^{-2\varepsilon/RT}}$$

(7)

Concerning the denominator of eq 7, there are no allowed conformations for a pair of monomeric units involved in a conformational reversal. Furthermore, for each given sequence, the two kinds of inversion (left to right and right to left) do not have the same energy: the conformational reversal in one case can be realized in 4 ways with an excess of energy ε and in 32 ways with an excess of energy 2ε; in the other case, it can be realized 10 ways with an excess of energy ε and in 27 ways with an excess of energy 2ε.

We must remark that in eq 6 and 7 the terms with energy ε and 2ε cannot be neglected, because their cumulative statistical weight considerably affects the values of ΔE and ΔU and the temperature dependence of the conformational properties.

The problem of determining ΔE and ΔU on the basis of eq 4–7 has been solved with a computer, it being assumed that ε ranges between 2500 and 3000 cal/mol and that e' ranges between 0 and 300 cal/mol.[16,17]

For any values of ε and e' in these ranges, values for e, M_r, and M_s can be found such that the set of these parameters reproduces the experimental values of $[\phi]_D{}^T$ in the range experimentally investigated (Figure 1). In Figure 2, the relationship among the e, e', and ε values which gives the best fit with the experimental data in terms of eq 4 is shown.

It must be remarked that for $\varepsilon \leqslant 2000$ cal/mol or $\varepsilon \geqslant 4000$ cal/mol, no values of e and e' in the range from -800 to 800 cal/mol can be found in such a way that the experimental data of molar rotatory power in the whole range of temperature are reproduced by eq 4 within the limit of experimental errors (4–5% between 300 and 400°K, 7–8% above 400°K).

Results

On the basis of e, e', and ε values reported in Figure 2, eq 6 gives a range for ΔE between 300 and 500 cal/mol, and eq 7 gives a range for ΔU between 800 and 1100 cal/mol. A value for M_s between 320 and 340 and a value for M_r between -220 and -360 can be calculated from eq 4.

These results are quite reasonable; not only does the range obtained for e agree with our expectations, which suggest a value of the order of e', but also M_r
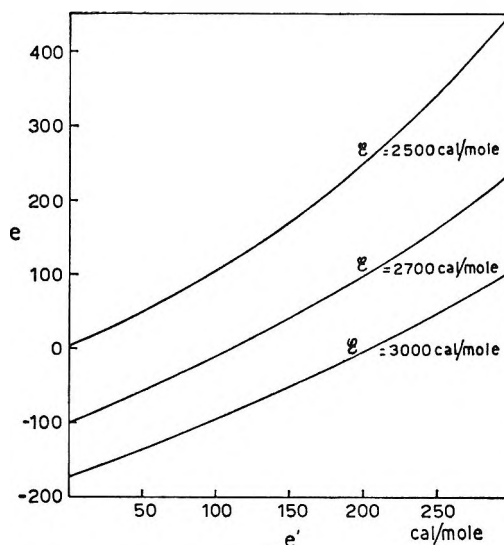

Figure 2. The relationship among e, e', and ε values which are best fitting, on the basis of eq 4, with experimental values of $[\phi]_D{}^T$ in the range 300–500°K.
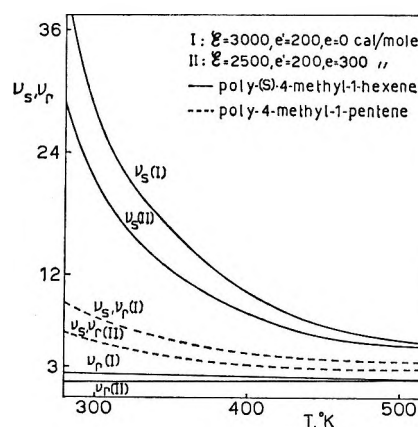

Figure 3. The temperature dependence of the average number of monomeric units included in the main-chain sections regularly spiraled in the left-handed (ν_s) and the right-handed (ν_r) screw sense.

and M_s are close to the values obtained on the basis of the Brewster semiempirical calculations[13] (see Table I). Furthermore, the value of ΔU is in the range of the values which have been determined for some isotactic nonoptically active poly-α-olefins.[6,8]

The dependences on temperature of the molar fraction of monomeric units spiraled in the left sense (ω_s) and the right sense (ω_r), respectively (Figure 5), of the average number of monomeric units included in the sequences spiraled in the left-handed (ν_s) and the right-

(16) This last assumption derives from the consideration that e', being an energy difference between two *gauche* conformations, must be a small fraction of 600–800 cal/mol, which is the value commonly indicated as the energy difference between a *trans* and a *gauche* conformation in the case of linear hydrocarbons.[14] Some data obtained from low molecular weight model compounds[17] confirm that the free-energy difference between S_1 and S_2 is fairly low.

(17) S. Pucci, P. L. Luisi, M. Aglietto, and P. Pino, *J. Amer. Chem. Soc.*, **89**, 2787 (1967).
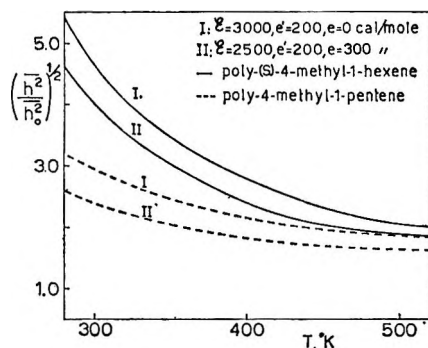
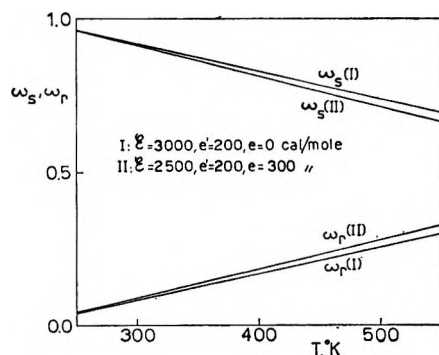Figure 4. The temperature dependence of the characteristic ratio $(\bar{h}^2/\bar{h}_0^2)^{1/2}$.

Figure 5. Temperature dependence of the molar fraction of monomeric units spiraled in the left-handed (ω_s) and the right-handed (ω_r) screw sense.

handed (ν_r) sense (Figure 3), and of the characteristic ratio $(\bar{h}^2/\bar{h}_0^2)^{1/2}$ (Figure 4) are reported for the two limit cases: $\mathcal{E} = 2500$ cal/mol, $e' = 200$ cal/mol, and $e = 300$ cal/mol; and $\mathcal{E} = 3000$ cal/mol, $e' = 200$ cal/mol, and $e = 0$.

Any other set of "solutions" in the range indicated in Figure 2 gives values for the conformational properties included between those reported in Figures 3-5.

From Figure 5 one can see that the macromolecules of poly((S)-4-methyl-1-hexene) are spiraled about 91-92% in the left-handed-screw sense at 300°K; at 400°K this is reduced to 81-83%.

One can also calculate that, for the range of e, e', and $\mathcal{E}$ previously indicated, the macromolecules of poly((S)-4-methyl-1-hexene) are, on the average, composed at 300°K of left-handed sequences of 22-28 monomeric units and alternated by right-handed sequences of about 2 or 3 monomeric units.[18] The dependence on the temperature is shown in Figure 3. It must be remarked that ν_s decreases considerably with temperature (at 400°K ν_s is reduced to 8-10 monomeric units) while ν_r remains practically constant. Consequently, by increasing the temperature we have in the macromolecules a considerable increase of the number of conformational reversals: at 300°K we can calculate about 7 or 8 conformational reversals for 100 monomeric units; at 500°K we can calculate 22-28.

For the same range of limit values of e, e', and $\mathcal{E}$, the characteristic ratio $(\bar{h}^2/\bar{h}_0^2)^{1/2}$ of poly((S)-4-methyl-1-hexene) is 4.1-4.8 at 300°K; this value decreases with the temperature, reaching 2.4-2.8 at 400°K (Figure 4).[19]

The meaning of these values of the conformational properties of poly((S)-4-methyl-1-hexene) appears more evident when they are compared with those of a nonoptically active polymer having an analogous structure, such as poly (4-methyl-1-pentene).[20,21] For such a polymer, the following expression for ΔU can be obtained

$$\Delta U = \frac{RT}{2} \ln \frac{2 + 12e^{-\mathcal{E}/RT} + 30e^{-2\mathcal{E}/RT}}{7e^{-\mathcal{E}/RT} + 28e^{-2\mathcal{E}/RT}} \qquad (8)$$

In fact, according to the same rules of conformational analysis, in a pair of monomeric units of poly(4-methyl-1-pentene) in an isotactic enchainment, a conformational reversal can be obtained in 7 ways with only one high-energy interaction and in 28 ways with two high-energy interactions. Furthermore, for each of the two main-chain screw senses, a pair of monomeric units in an isotactic enchainment may exist in one "allowed" conformation (zero energy), in 6 conformations having one high-energy interaction (energy excess $\mathcal{E}$), and in 15 conformations having two high-energy interactions (energy excess $2\mathcal{E}$).

Equation 8 gives, in the range of $\mathcal{E}$ from 2500 to 3000 cal/mol, $\Delta U = 900$-1100 cal/mol at 300°K and $\Delta U = 800$-1000 cal/mol at 400°K. The average dimensions[20,21] of the macromolecules of these polymers and their dependence on temperature are shown in Figures 3 and 4.

The characteristic ratio is 3.0-2.4 at 300°K and slightly decreases with temperature; the macromolecules consist at 300°K of alternate left-handed and right-handed sequences of 6-8 monomeric units, a value which slightly decreases by increasing the temperature.

Final Remarks

On the basis of the adopted procedure, in the case of poly(4-methyl-1-pentene), a value of $\bar{h}^2$ can be cal-

(18) The average length of regularly left-handed (ν_s) and right-handed sequences (ν_r) is expressed as[4,6] $\nu_s = [1 + (r - q)]/(r - q)$ and $\nu_r = [1 + (r - q)]/(r + q)$, where r and q are the parameters previously defined.[10]

(19) The end-to-end distance is expressed by the following equation for optically active vinyl polymers:[6] $\bar{h}^2 = (4/3)Nl^2[(q^2 + 2r^2) \times (1 - q)^2 + q^2r^2]/r(1 - q)(r^2 - q^2)$, where N is the number of C–C bonds, l is their length, and r and q are the parameters previously defined.[10] In ref 5 a less precise equation is given for $\bar{h}^2$.

(20) For isotactic nonoptically active vinyl polymers, the conformational properties are expressed in terms of p as[6,11,21] $\omega_s = \omega_r = (1 + p)/p$ and $\bar{h}^2 = (8/3)Nl^2(1/p)$, where $p = \exp(-\Delta U/RT)$ and N and l have the same meanings previously defined.

(21) T. M. Birshtein and O. B. Ptitsyn, Zh. Tekhn. Fiz., 29, 1048 (1959); T. M. Birshtein, Y. Y. Gotlib, and O. B. Ptitsyn, J. Polym. Sci., 52, 77 (1961); G. Allegra, P. Ganis, and P. Corradini, Makromol. Chem., 61, 225 (1963).

culated which is in the range of those obtained by different authors for some isotactic vinyl polymers.[22] This confirms the validity of the conformational analysis used in order to evaluate ΔU and indirectly supports the results obtained for poly((S)-4-methyl-1-hexene) in which the conformational equilibrium has been related to optical activity.

In this case, a remarkable prevalence of one of the two main-chain screw senses on the other one can be obtained as predicted qualitatively in previous papers[4-6] with a low ΔE value and a ΔU value of the order of that calculated for nonoptically active vinyl polymers. This causes the macromolecules of poly((S)-4-methyl-1-hexene) to consist of relatively long left-handed sequences alternated by very short right-handed ones and causes a remarkable enhancement of the end-to-end distance and its temperature coefficient with respect to the corresponding properties of nonoptically active polymers having similar structure.

Experimental work is now in progress in our institute in order to verify these predictions.

Experimental Section

Optical Activity Measurements. The sample of poly((S)-4-methyl-1-hexene) (diisopropyl ether soluble, diethyl ether insoluble fraction) has been obtained and characterized as already reported[1] ($[\phi]_D^{25}$ 288, mp 210–215°, and $[\eta]$ 3.18 dl./g at 120° in decalin).

For the determination of optical activity, the tubes, 1 or 2 dm long, provided with glass sleeves for the circulation of highly boiling hydrocarbons as thermostating fluid, were kept during the measurements in an air thermostat where the temperature could be kept constant within ±0.5° in the range 20–100° and within *ca.* ±1° above 100°.

The measurements have been performed in benzene between 20 and 60°, in tetralin between 20 and 140°, and in highly boiling paraffins between 20 and 220° (fraction A-33 of Shell commercial oil, purified by vacuum fractionation, bp above 280°, d^{20} 0.8865,

n^{25}D 1.4798, $\alpha_{l=1}^{20}$ 2.33, $\Delta\alpha_{l=1}\Delta T = -0.002$ between 20 and 200°). The correction due to the solvent refractive index has not been taken into account, as it is less than the experimental uncertainty (which is 4–5% in the range 300–400°K and 7–8% above 400°K, determined by the least-square-minimum method).

Computing Program

From eq 4 at two temperatures, T_1 and T_2, we can obtain

$$M_r = \frac{[\phi]_D^{T_2} r_2 (r_1 + q_1) - [\phi]_D^{T_1}(r_2 + q_2) r_1}{r_2 q_1 - r_1 q_2} \quad (9)$$

where $[\phi]_D^{T_1}$ and $[\phi]_D^{T_2}$ are the experimental values of molar rotation at T_1 and T_2, and r_1 and q_1 and r_2 and q_2 are the parameters previously defined[10] at T_1 and T_2, respectively.

For a given value of ε, for each pair of e and e' in the ranges −500 to 500 and 0 to 300 cal, respectively, the M_2 value on the basis of eq 9 and the corresponding M_s value on the basis of eq 4 at T_1 were calculated by a computer (IBM 7090 of the University of Pisa). For each set of e, e', M_r, and M_s values so obtained, the $[\phi]_D$ values for the whole range 300–500°K were calculated (eq 4) and were compared with the experimental ones, the best-fitting criterion being the standard deviation calculated by the least-square method at 300, 325, 350, 400, 450, and 475°K.

Another independent best-fitting criterion has been obtained when it is considered that the e and e' values, which solve our problem consistently with the initial hypothesis, should give the same value of M_r, according to eq 9, independently of the temperature pair T_1 and T_2 (M_r being independent of the temperature). This criterion has been found to be in good agreement with the first one.

(22) E. Kunst, *Rec. Trav. Chim. Pays-Bas*, **69**, 125 (1950); G. T. Fox, Jr., and P. J. Flory, *J. Amer. Chem. Soc.*, **73**, 1909 (1951); W. R. Krigbaum and P. J. Flory, *J. Polym. Sci.*, **11**, 37 (1953); C. C. Bawn and R. D. Patel, *Trans. Faraday Soc.*, **52**, 1669 (1956); G. Moraglio, *Polym. Lett.*, **2**, 1105 (1964).

# Kinetic Analysis of Thermogravimetric Data

by J. Zsako

Department of Chemistry, Babes-Bolyai University, Cluj, Rumania

Accepted and Transmitted by The Faraday Society (*February 1, 1968*)

The trial-and-error method of Doyle was modified. Instead of curve fitting, the calculation of standard deviation is suggested. The integrals of eq 11 are tabulated as a function of temperature and of activation energy. Testing of different kinetic equations and estimating of apparent activation energy, frequency factor, and activation entropy are discussed. The suggested method is compared with the methods given by Horowitz and Metzger and by Freeman and Carroll using experimental data obtained for two cobalt(III)–dimethylglyoxime complexes.

Theoretical Section

The thermal decomposition of solids is a very complex process even in the simple case expressed by the stoichiometric equation

$$A(s) = B(s) + C(g)$$
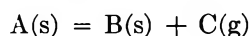
This process takes place in several stages, *e.g.*: the chemical act of breaking of bonds; destruction of the initial crystal lattice; formation of the crystal lattice of the solid product B, consisting of the formation of crystallization centers and the growth of these centers; adsorption–desorption of the gaseous product C; diffusion of C; heat transfer.

The rate of the thermal decomposition is determined by the rate of one or more of these stages. Sometimes the rate-determining stage at the beginning of the pyrolysis can lose its significance later and another stage can take its place. Thus pyrolysis rate depends not only upon the nature of the studied substance but also upon many other factors, such as particle size, weight of the sample, shape of the crucible, etc. When investigated under the conditions obtained in thermogravimetric analysis, the heating rate has a decisive part too.

Taking into account the complexity of the process, there is little chance to find a general equation able to describe the kinetics of all thermal decomposition reactions, especially in the case when kinetics varies during the process.

Many attempts have been made to obtain kinetic equations, mainly for cases where the process is governed by a unitary kinetic law. Using these equations, a considerable number of techniques for deriving kinetic data from thermogravimetric curves has been developed.[1]

The decomposition rate can be defined as $d\alpha/dt$, where α stands for the fraction of the initial compound reacted. In isothermal conditions, we can presume this reaction rate to depend only upon the fraction reacted

$$\frac{d\alpha}{dt} = kf(\alpha) \tag{1}$$

where $f(\alpha)$ is a certain function of α, and k can be considered to be a rate constant.

When pyrolysis takes place under the conditions of thermogravimetric analysis, k cannot remain constant and will depend upon temperature. The validity of the Arrhenius equation can be presumed for this dependence

$$k = Z \exp\left(-\frac{E_a}{RT}\right) \tag{2}$$

where Z is the frequency factor and E_a is the activation energy. Since thermogravimetric analysis is carried out with a constant heating rate, $q = dT/dt$, the substitution $dt = dT/q$ can be made, and from eq 1 and 2, the following differential equation is obtained

$$\frac{d\alpha}{f(\alpha)} = \frac{Z}{q} \exp\left(-\frac{E_a}{RT}\right) dT \tag{3}$$

The equation of thermogravimetric curves could be obtained by integration of eq 3, but here two main difficulties arise: the analytical form of function $f(\alpha)$ is generally unknown, and the right side of eq 3 cannot be integrated in finite form.

The analytical form of the function $f(\alpha)$ depends upon the mechanism of the thermal decomposition. Considerable efforts have been made to deduce this function using various models. One of the most general equations able to describe various solid-state reactions is

$$f(\alpha) = \alpha^a (1 - \alpha)^b \tag{4}$$

with a and b constants, called frequently homogeneity factors.

A large number of cases were discussed by different

(1) J. Sestak, *Silikaty*, **11**, 153 (1967).

authors on the basis of both theoretical and experimental investigations. The most simple forms of eq 4 are those with $a = 0$. In this case, eq 1 has the same form as the kinetic equation of a b-order homogeneous reaction, and, consequently, b can be considered an apparent reaction order

$$f(\alpha) = (1 - \alpha)^b \qquad \frac{d\alpha}{dt} = k(1 - \alpha)^b \qquad (5)$$

Equations of the same form as eq 5 are considered to be the most simple laws of the dissociation of solids.[2]

Equation 5 with $b = {}^2/_3$ was found theoretically for the first time by Roginsky and Schulz,[3] and later by many other authors, both theoretically and experimentally.[4-6] It is considered to be the fundamental law of topochemical reactions.[7]

Different authors have considered also the following b values: $0, {}^1/_3, {}^1/_2, 1,$ and $2.$[8]

For a group of reactions, kinetic equations with $b = 0$, i.e.

$$f(\alpha) = \alpha^a \qquad (6)$$

were found to be valid. The a values, proposed by different authors[8] are 1 and ${}^2/_3$.

An equation the same type as (4) with $a \neq 0$ and $b \neq 0$, namely

$$f(\alpha) = \alpha(1 - \alpha) \qquad (7)$$

was found for the first time by Lewis[9] and was obtained theoretically by Prout and Tompkins.[10] Equations of this type have been discussed also for the cases $a < 1$, $b = 1$; and $a = {}^2/_3, b = {}^2/_3$.[8]

Concerning the integration of the right side of eq 3, some authors have tried to approximate the exponential factor by integrable functions. Thus Horowitz and Metzger[11] have made an asymptotic expansion of $1/T$ at a conveniently chosen temperature, and neglecting all the terms, except the first two, they obtained an integrable form for eq 3.

Taking the logarithm of the function

$$g(\alpha) = \int_0^\infty \frac{d\alpha}{f(\alpha)} \qquad (8)$$

they have found this to vary linearly with temperature. From the slope of the corresponding straight line, the activation energy, E_a, can be computed. Since a thermal decomposition step takes place frequently over a temperature range of 60–80°, this asymptotic expansion is not quite justifiable. Our calculations showed indeed that log $g(\alpha)$ does not vary linearly over such a large temperature range. The slope of the theoretical curve log $g(\alpha)$ vs. T shows a variation of about 25–30%, which introduces a large error in the activation energy data.

Thus the accurate integration of eq 3 is absolutely necessary. Some attempts have been made in this

direction too. Introducing the notation $u = E_a/RT$, eq 3 can be written as

$$\frac{d\alpha}{f(\alpha)} = -\frac{ZE_a}{Rq} \frac{e^{-u}}{u^2} du \qquad (9)$$

Integration of this equation from the absolute-zero temperature up to the actual one of the sample leads to the equation

$$g(\alpha) = -\frac{ZE_a}{Rq} \int_\infty^x \frac{e^{-u}}{u^2} du \qquad (10)$$

where x means the value of u at the temperature of the sample. The values of the integral

$$p(x) = -\int_\infty^x \frac{e^{-u}}{u^2} du = \frac{e^{-x}}{x} - \int_x^\infty \frac{e^{-u}}{u} du \qquad (11)$$

have been calculated and tabulated by Doyle[12] for x values covering the range from 10 to 50. The equation of the thermogravimetric curves given by Doyle is

$$g(\alpha) = \frac{ZE_a}{Rq} p(x) \qquad (12)$$

The main difficulty in applying eq 12 consists in the dependence of $p(x)$ on both temperature and activation energy. Doyle has suggested a trial-and-error curve-fitting method for the determination of activation energy. He discussed reactions for which function $f(\alpha)$ was known, and thus $g(\alpha)$ values could be computed from thermogravimetric data. Under such conditions this author obtains the approximate value of E_a from the slope of the thermogram and calculates the theoretical curve by means of eq 12. By modifying the presumed E_a value, the agreement between the theoretical and the experimental curves can be imporved. The activation energy value which ensures the best consistency will be the required one.

Ozawa[13] has suggested a method based on the eq 12 for determining the activation energy. This author has shown that the activation energy can be graphically

(2) M. T. Trambouze and B. Imelik, *J. Chim. Phys.*, **57**, 656 (1960).

(3) S. Roginsky and E. Schulz, *Z. Phys. Chem.*, **A138**, 21 (1928).

(4) K. L. Mampel, *ibid.*, **A187**, 43, 235 (1940).

(5) P. W. M. Jacobs and F. C. Tompkins in "Chemistry of the Solid State," W. E. Garner, Ed., Butterworth and Co. Ltd., London, 1955, p 184.

(6) G. F. Hüttig, *Monatsh. Chem.*, **85**, 365 (1954).

(7) W. E. Garner, *Chem. Ind.* (London), 1010 (1951).

(8) E. A. Prodan and M. M. Pavlyuchenko in "Heterogeneous Chemical Reactions," M. M. Pavlyuchenko and E. A. Prodan, Ed., Nauka i tekhnika, Minsk, U.S.S.R., 1965, p 20.

(9) G. M. Lewis, *Z. Phys. Chem.*, **52**, 310 (1905).

(10) E. G. Prout and F. C. Tompkins, *Trans. Faraday Soc.*, **40**, 488 (1944).

(11) H. H. Horowitz and G. Metzger, *Anal. Chem.*, **35**, 1464 (1963).

(12) C. D. Doyle, *J. Appl. Polym. Sci.*, **15**, 285 (1961).

(13) T. Ozawa, *Bull. Chem. Soc. Jap.*, **38**, 1881 (1965).

Table I:　−Log p(x) Values Corresponding to Different Temperatures and Activation Energies

Temp. °C	10	12	14	16	18	20	22	24	26	28	30	32	34	36
100	8.175	9.498	10.798	12.083	13.348	14.610	15.862	17.108	18.349	19.584	20.811	22.038	23.262	24.784
100	8.002	9.294	10.559	11.812	13.052	14.283	15.505	16.716	17.926	19.132	20.333	21.530	22.719	23.910
112	7.833	9.099	10.338	11.561	12.770	13.999	15.163	16.347	17.527	18.701	19.871	21.043	22.206	23.366
130	7.678	8.908	10.121	11.318	12.503	13.672	14.838	15.996	17.149	18.294	19.438	20.579	21.716	22.845
140	7.523	8.731	9.917	11.090	12.243	13.391	14.530	15.658	16.785	17.908	19.023	20.136	21.248	22.351
150	7.383	8.565	9.725	10.865	11.997	13.118	14.232	15.341	16.440	17.536	18.628	19.716	20.802	21.885
160	7.241	8.402	9.537	10.659	11.765	12.860	13.952	15.033	16.112	17.182	18.252	19.315	20.376	21.434
170	7.110	8.244	9.357	10.458	11.542	12.615	13.681	14.740	15.792	16.845	17.890	18.930	19.947	21.002
180	6.984	8.096	9.186	10.261	11.328	12.380	13.423	14.461	15.491	16.518	17.545	18.564	19.579	20.592
190	6.862	7.953	9.025	10.078	11.118	12.153	13.175	14.190	15.204	16.209	17.214	18.211	19.205	20.200
200	6.744	7.818	8.864	9.900	10.923	11.935	12.940	13.934	14.926	15.913	16.896	17.876	18.848	19.821
210	6.632	7.683	8.717	9.730	10.731	11.727	12.709	13.691	14.661	15.626	16.592	17.550	18.504	19.461
220	6.524	7.558	8.569	9.566	10.549	11.523	12.493	13.451	14.405	15.353	16.296	17.237	18.179	19.100
230	6.417	7.438	8.432	9.411	10.377	11.333	12.281	13.222	14.158	15.089	16.015	16.938	17.862	18.779
240	...	7.317	8.294	9.259	10.208	11.147	12.077	13.001	13.919	14.838	15.746	16.652	17.555	18.454
250	...	7.206	8.165	9.113	10.044	10.965	11.883	12.789	13.695	14.591	15.487	16.375	17.260	18.147
260	...	7.095	8.042	8.972	9.885	10.794	11.693	12.587	13.475	14.358	15.232	16.107	16.979	17.848
270	...	6.989	7.918	8.834	9.735	10.631	11.513	12.388	13.264	14.130	14.991	15.853	16.707	17.559
280	...	6.887	7.803	8.702	9.590	10.468	11.337	12.200	13.057	13.910	14.754	15.603	16.444	17.283
290	...	6.790	7.688	8.574	9.450	10.314	11.166	12.016	12.860	13.700	14.535	15.362	16.190	17.017
300	...	6.693	7.583	8.452	9.313	10.160	11.004	11.841	12.667	13.494	14.316	15.130	15.945	16.758
310	...	6.601	7.473	8.333	9.181	10.015	10.846	11.670	12.483	13.297	14.106	14.907	15.709	16.504
320	...	6.509	7.372	8.220	9.055	9.875	10.693	11.504	12.304	13.104	13.901	14.693	15.478	16.264
330	...	6.422	7.271	8.106	8.928	9.740	10.544	11.342	12.134	12.921	13.705	14.484	15.255	16.028
340	...	...	7.175	7.997	8.810	9.609	10.401	11.185	11.963	12.742	13.512	14.279	15.042	15.802
350	...	...	7.085	7.893	8.692	9.483	10.261	11.037	11.803	12.568	13.325	14.083	14.833	15.584
360	...	...	6.996	7.793	8.579	9.357	10.126	10.889	11.646	12.398	13.147	13.891	14.633	15.371
370	...	...	6.908	7.693	8.471	9.235	9.996	10.746	11.494	12.233	12.973	13.705	14.437	15.163
380	...	...	6.821	7.598	8.363	9.118	9.866	10.661	11.347	12.077	12.803	13.527	14.246	14.963
390	...	...	6.739	7.503	8.259	9.006	9.745	10.477	11.199	11.921	12.639	13.353	14.064	14.768
400	...	...	6.657	7.413	8.160	8.893	9.624	10.348	11.061	11.774	12.479	13.184	13.882	14.582
410	...	...	6.581	7.327	8.061	8.790	9.508	10.218	10.927	11.627	12.323	13.020	13.709	14.395
420	...	...	6.504	7.241	7.968	8.682	9.395	10.097	10.793	11.485	12.171	12.860	13.541	14.218
430	...	...	6.427	7.155	7.873	8.584	9.284	9.977	10.664	11.347	12.025	12.705	13.376	14.046

obtained by following thermogravimetrically the decomposition at different heating rates.

In the present paper we have tried to simplify Doyle's trial-and-error method and to find new applications of eq 12 in the kinetic analysis of thermogravimetric curves. If the logarithm of eq 12 is found, the following expression is obtained

$$\log \frac{ZE_a}{Rq} = \log g(\alpha) - \log p(x) = B \qquad (13)$$

where B depends only upon the nature of the compound studied and upon the heating rate, but not upon the temperature. The value of $g(\alpha)$ for a given temperature can be calculated from the experimental data if $f(\alpha)$ is known. Similarly, $p(x)$ for the same temperature can be found if the activation energy is known. The constancy of the difference $\log g(\alpha) - \log p(x)$ enables us to suggest a quantitative method of testing the validity of different kinetic equations of the same type as eq 3 and of determining the apparent activation energy, consistent with a given function $f(\alpha)$.

This method consists of the following. By pre-

suming the validity of a function $f(\alpha)$ and using thermogravimetric data, $g(\alpha)$ values are calculated for different temperatures. By means of a trial-and-error method, the apparent activation energy can be estimated by finding the E_a value which ensures the maximum constancy of $B = \log g(\alpha) - \log p(x)$.

The agreement between experimental data and presumed E_a can be characterized quantitatively by the standard deviation of individual B_i values from their arithmetical mean $\bar{B}$. This will be defined as

$$\delta = \sqrt{\frac{(B_i - \bar{B})^2}{r}} \qquad (14)$$

where r is the number of experimental data used for the calculation of $\bar{B}$. The minimum of δ indicates the best E_a value. At the same time, this least value, δ_{min}, is a measure of the consistency of the decomposition process with the presumed function $f(\alpha)$. By presuming other kinetic equations and by calculating the corresponding δ_{min} values, the minimum of δ_{min} will indicate that function $f(\alpha)$, among the tested ones, which ensures the maximum consistency with ex-

E_a, kcal/mol														
38	40	42	44	46	48	50	52	54	56	58	60	62	64	66
25.702	26.919	28.129	29.342	30.552	31.761	32.968	34.175	35.375	36.579	37.782	38.984	40.184	41.382	42.581
25.097	26.284	27.464	28.646	29.826	31.004	32.164	33.353	34.528	35.701	36.869	38.040	39.211	40.380	41.548
24.524	25.679	26.834	27.986	29.135	30.283	31.430	32.574	33.724	34.867	36.008	37.150	38.290	39.429	40.568
23.978	25.107	26.235	27.356	28.480	29.602	30.722	31.837	32.954	34.073	35.183	36.298	37.413	38.524	39.635
23.457	24.560	25.661	26.757	27.855	28.951	30.041	31.124	32.226	33.313	34.403	35.491	36.579	37.663	38.747
22.963	24.041	25.115	26.190	27.257	28.327	29.396	30.462	31.528	32.592	33.657	34.719	35.781	36.841	37.904
22.487	23.543	24.592	25.643	26.690	27.738	28.780	29.822	30.865	31.904	32.945	33.983	35.023	36.057	37.094
22.038	23.067	24.095	25.120	26.145	27.161	28.192	29.211	30.229	31.246	32.267	33.282	34.296	35.309	36.322
21.602	22.610	23.620	24.624	25.625	26.627	27.627	28.626	29.625	30.619	31.613	32.606	33.599	34.592	35.583
21.189	22.174	23.162	24.145	25.129	26.109	27.086	28.066	29.041	30.014	30.991	31.962	32.941	33.907	34.877
20.793	21.761	22.723	23.688	24.651	25.612	26.573	27.527	28.484	29.440	30.395	31.345	32.298	33.250	34.201
20.410	21.361	22.306	23.249	24.194	25.134	26.073	27.014	27.950	28.888	29.822	30.753	31.689	32.619	33.552
20.044	20.975	21.902	22.827	23.751	24.678	25.598	26.519	27.437	28.354	29.270	30.189	31.103	32.015	32.927
19.693	20.606	21.516	22.424	23.330	24.235	25.138	26.041	26.942	27.846	28.744	29.642	30.538	31.434	32.328
19.556	20.250	21.143	22.034	22.922	23.815	24.701	25.585	26.469	27.351	28.237	29.117	29.996	30.875	31.753
19.026	19.907	20.784	21.661	22.533	23.407	24.276	25.143	26.013	26.879	27.747	28.610	29.476	30.337	31.199
18.715	19.579	20.437	21.298	22.156	23.013	23.869	24.723	25.571	26.424	27.275	28.125	28.973	29.819	30.665
18.413	19.260	20.104	20.952	21.793	22.632	23.475	24.312	25.147	25.986	26.820	27.657	28.489	29.320	30.151
18.128	18.953	19.784	20.615	21.443	22.270	23.095	23.919	24.741	25.562	26.383	27.203	28.022	28.794	29.656
17.839	18.655	19.474	20.291	21.107	21.916	22.728	23.538	24.348	25.152	25.959	26.766	27.572	28.374	29.177
17.564	18.371	19.178	19.976	20.779	21.580	22.374	23.172	23.964	24.759	25.553	26.343	27.135	27.926	28.714
17.302	18.096	18.885	19.675	20.465	21.248	22.034	22.814	23.597	24.380	25.156	25.936	26.717	27.492	28.268
17.048	17.825	18.605	19.383	20.159	20.929	21.702	22.474	23.244	24.009	24.777	25.544	26.307	27.073	27.837
16.799	17.568	18.334	19.100	19.862	20.624	21.384	22.143	22.900	23.652	24.407	25.161	25.914	26.668	27.419
16.564	17.320	18.073	18.825	19.575	20.323	21.075	21.820	22.564	23.307	24.050	24.795	25.535	26.275	27.014
16.329	17.076	17.821	18.559	19.301	20.035	20.774	21.507	22.242	22.972	23.706	24.434	25.165	25.894	26.623
16.107	16.841	17.573	18.303	19.031	19.757	20.483	21.207	21.929	22.651	23.371	24.090	24.809	25.525	26.243
15.890	16.615	17.334	18.055	18.770	19.488	20.200	20.915	21.625	22.338	23.045	23.756	24.461	25.269	25.875
15.677	16.393	17.104	17.812	18.517	19.223	19.926	20.629	21.330	22.034	22.732	23.430	24.126	24.823	25.518
15.473	16.176	16.878	17.578	18.271	18.967	19.661	20.355	21.047	21.734	22.424	23.115	23.801	24.487	25.172
15.274	15.968	16.656	17.348	18.037	18.720	19.416	20.085	20.770	21.448	22.131	22.805	23.484	24.160	24.836
15.084	15.765	16.449	17.127	17.803	18.481	19.155	19.825	20.501	21.170	21.838	22.510	23.176	23.842	24.511
14.893	15.570	16.241	16.910	17.578	18.247	18.912	19.575	20.237	20.897	21.561	22.220	22.877	23.534	24.196
14.712	15.376	16.038	16.702	17.362	18.018	18.674	19.328	19.980	20.638	21.289	21.938	22.587	23.235	23.882

perimental data. If the minimum value, δ_{min}, is small enough, we can assume the validity of a kinetic equation of the same type as eq 3, with the corresponding f(α) and the found E_a value as the apparent activation energy of the process.

The obtained $\bar{B}$ value can be used for the calculation of the apparent frequency factor Z, according to the equation

$$\log Z = \bar{B} + \log Rq - \log E_a \quad (15)$$

derived from eq 13. An apparent activation entropy can be calculated too, using the equation

$$S^{\ddagger} = 2.303 \log \frac{Zh}{kT} \quad (16)$$

From these calculations for T can be taken the temperature $T_{1/2}$, at which the weight loss is half of the total weight loss during the considered step.

Applying the above method, the first problem is to calculate g(α) from the experimental data, presuming different analytical forms for f(α). The simplest cases are equations of the same type as (5). An-

alytical forms of g(α) and of B for the case of validity of equations of this type, calculated by means of eq 8 and 13, respectively, are listed below for different b values in the equation f(α) = $(1 - \alpha)^b$

$$b = 0 \quad g_0(\alpha) = \alpha \quad B_0 = \log \alpha - \log p(x) \quad (17)$$

$$b = 1/3$$

$$g_{1/3}(\alpha) = 3/2 [1 - \sqrt[3]{(1 - \alpha)^2}] \quad B_{1/3} =$$
$$\log 3/2 + \log [1 - \sqrt[3]{(1 - \alpha)^2}] - \log p(x) \quad (18)$$

$$b = 1/2$$

$$g_{1/2}(\alpha) = 2[1 - \sqrt{1 - \alpha}] \quad B_{1/2} =$$
$$\log 2 + \log [1 - \sqrt{1 - \alpha}] - \log p(x) \quad (19)$$

$$b = 2/3$$

$$g_{2/3}(\alpha) = 3[1 - \sqrt[3]{1 - \alpha}] \quad B_{2/3} =$$
$$\log 3 + \log [1 - \sqrt[3]{1 - \alpha}] - \log p(x) \quad (20)$$

$b = 1$

$g_1(\alpha) = -\ln (1 - \alpha)$

$$B_1 = \log \left(\ln \frac{1}{1 - \alpha} \right) - \log p(x) \quad (21)$$

$b = 2$

$$g_2(\alpha) = \frac{\alpha}{1 - \alpha} \qquad B_2 = \log \frac{\alpha}{1 - \alpha} - \log p(x) \quad (22)$$

If the thermogravimetric step corresponds to a unitary process, the fraction of the initial compound reacted can be given as the ratio of the actual weight loss to the total weight loss during the considered step, i.e.

$$\alpha = \frac{W_0 - W}{W_0 - W_t} \quad (23)$$

where W, W_0, and W_t are the actual, initial, and final weights of the sample, respectively. Equation 23 enables us to calculate $g(\alpha)$ for different presumed kinetic equations.

To facilitate the obtaining of the activation energy, we have tabulated the integrals $p(x)$ for temperatures between 100 and 430° and for activation energies between 10 and 66 kcal/mol. The $-\log p(x)$ values, given in Table I, have been calculated by using Doyle's tabulated values and, in the case $x > 50$, by using the approximate formula

$$p(x) \approx e^{-x}\left(\frac{1}{x^2} - \frac{2}{x^3} \right) \quad (24)$$

For intermediate E_a values, the corresponding $-\log p(x)$ can be found by means of linear interpolation.

The suggested trial-and-error method consists in calculating B_i for different $f(\alpha)$ functions and different E_a values with the help of Table I and formulas 17–22 or by means of the corresponding $g(\alpha)$ function, obtained according to eq 8 from the presumed $f(\alpha)$, for all the temperatures at which the weight of the sample was measured. By means of eq 14, the standard deviation, δ, will be calculated, and the minimum of this will indicate the best $f(\alpha)$ and the corresponding E_a value.

The apparent frequency factor can be calculated by means of eq 15, and an apparent activation entropy can be also obtained by means of eq 16.

Applications

In our earlier papers[14-17] the kinetics of the thermal decomposition of complexes of the type $[Co(DH)_2Am_2]X$ have been studied: $(DH)_2$ is dimethylglyoxime or cyclohexanedione dioxime; Am is different aromatic amines; and X is Cl, Br, I, or NCS. The first step of the decomposition of the above complexes is the substitution of an amine molecule by the external-sphere anion, which leads to the volatilization of the aromatic

amine and to the formation of the nonvolatile nonelectrolyte $Co(DH)_2AmX$ as a quite stable intermediate product, accordingly to the equation

$$[Co(DH)_2Am_2]X = Co(DH)_2AmX + Am$$

The corresponding thermogravimetric steps were studied by means of the Horowitz and Metzger method.

We give now two examples for the application of the above-explained method, using experimental data published in our earlier paper.[15] The two complexes we take here are

$[Co(dimethylglyoxime)_2(p-ethylaniline)_2]NCS \quad (I)$

$[Co(dimethylglyoxime)_2(\gamma-picoline)_2]NCS \quad (II)$
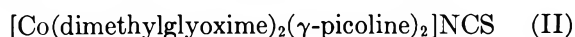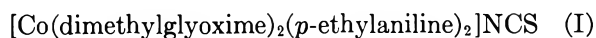
Using the Horowitz and Metzger method, we have found the following kinetic data for these compounds, where b is the apparent reaction order, corresponding to eq 5

$b = 2; \quad E_a = 42 \text{ kcal/mol}; \quad S^{\ddagger} = -22 \text{ eu} \quad (I)$

$b = 1; \quad E_a = 33 \text{ kcal/mol}; \quad S^{\ddagger} = +1 \text{ eu} \quad (II)$

For applying the above-suggested method, we have calculated $g_b(\alpha)$ for these compounds, presuming zero-, first-, and second-order reactions. The weight of the sample, W, at different temperatures and the corresponding $g_b(\alpha)$ values are given in Table II.

Table II: Sample Weight and Log $g(\alpha)$ Data for Compounds I and II at Different Temperatures

Compound	Temp, C	W, mg	Log α	Log [ln $1/(1 - \alpha)$]	Log $\alpha/(1 - \alpha)$
I[a]	160	99.3	-1.469	-1.464	-1.454
	170	97.9	-0.992	-0.969	-0.945
	180	95.9	-0.701	-0.654	-0.605
	190	92.4	-0.433	-0.337	-0.233
	200	87.9	-0.231	-0.053	0.153
	210	82.1	-0.061	0.308	0.821
	220	81.1	-0.037	0.395	1.046
II[b]	140	101.4	-1.948	-1.948	-1.945
	150	101.2	-1.648	-1.643	-1.648
	160	100.9	-1.406	-1.397	-1.388
	170	100.2	-1.104	-1.087	-1.069
	180	98.2	-0.719	-0.674	-0.627
	190	95.5	-0.465	-0.377	-0.283
	200	91.2	-0.233	-0.057	0.148
	210	86.0	-0.057	0.320	0.851
	220	84.3	-0.012	0.553	1.539

[a] $W_0 = 100.0$ mg; $W_t = 79.4$ mg. [b] $W_0 = 101.6$ mg; $W_t = 83.8$ mg.

(14) J. Zsakó, Cs. Várhelyi, and E. Kékedy, Studia Univ. Babes-Bolyai, Chem., 2, 7 (1965).

(15) J. Zsakó, Cs. Várhelyi, and E. Kékedy, Analele Univ. Bucuresti, Ser. Stiint. Nat., 14, No. 15 (1965).

(16) J. Zsakó, Cs. Várhelyi, and E. Kékedy, J. Inorg. Nucl. Chem., 28, 2637 (1966).

(17) J. Zsakó, Cs. Várhelyi, and E. Kékedy, Acta Chim. Acad. Sci. Hung., 51, 53 (1967).

In order to determine which of the three tested b values is the most consistent with experimental data, we had to calculate for different presumed E_a and those b values that we wanted to test. On the basis of eq 17, 21, and 22, and by means of tabulated $-\log p(x)$ values in Table I we have calculated B_0, B_1, and B_2 for all the temperatures. In each case the arithmetical mean of B was calculated and δ was obtained accordingly to eq 14.

In the case of complex I, we obtained the following intermediate results

E_a, kcal/ mol	δ	E_a, kcal/ mol	δ	E_a, kcal/ mol	δ
	$b = 0$		$b = 1$		$b = 2$
20	0.1149	26	0.0900	38	0.0917
22	0.1086	28	0.0714	40	0.0900
24	0.1192	30	0.0755	42	0.1044

These data are sufficient to see that standard deviations are less if we presume a first-order reaction. Thus we can consider that from the tested b values $b = 1$ is the best. Using interpolated $-\log p(x)$ values for the case $b = 1$, we have

	E_a, kcal/mol		
	28.8	28.9	29.0
δ	0.0694	0.0693	0.0698

i.e., δ has a minimum value for $E_a = 28.9$ kcal/mol. This corresponds to $\bar{B}_1 = 16.291$. By means of eq 15, we obtain $\log Z = 11.712$. Apparent activation entropy can be estimated using relation 16, and we obtain $S^{\ddagger} = -5.84$ eu. We can see that the considered method gives quite different results from that obtained by means of the Horowitz and Metzger method. Even the found reaction order is 1 and not 2.

In the case of complex II the minimum values of standard deviation are

	$b = 0$	$b = 1$	$b = 2$
δ_{min}	0.0767	0.0610	0.0743

i.e., this reaction seems to be of first order, too. The corresponding activation energy is $E_a = 28.3$ kcal/mol, the frequency factor $\log Z = 11.446$, and the activation entropy $S^{\ddagger} = -7.06$ eu. These values are also flatly different from those obtained by means of Horowitz and Metzger's method.

Apparent reaction order and activation energy have

been calculated also by means of the Freeman and Carroll method,[18] using the same experimental data. In Table III are compared the b and E_a values, obtained by means of the three methods.

Table III: Reaction Order b and Activation Energy E_a in the First Thermogravimetric Step of the Complexes I and II

Method	Complex I b	Complex I E_a, kcal/ mol	Complex II b	Complex II E_a, kcal/ mol
Modified Doyle	1	28.9	1	28.3
Freeman–Carroll	1.16	29.2	0.82	28.7
Horowitz–Metzger	2	42	1	33

We can see that the data given by the Freeman and Carroll method are in good agreement with those found by means of our method, but the Horowitz and Metzger method gives quite different results. The Freeman and Carroll method can be used successfully, though it is based on graphical determination of thermogravimetric-curve slopes. It gives nearly the same results as our more accurate method. We cannot say the same about the Horowitz and Metzger method, which is affected by considerable errors.

Conclusions

The suggested method, using the real values of the integral $p(x)$, is free from the errors introduced by the approximative Horowitz and Metzger formulas. Meanwhile, the statistical way of working up experimental data and the minimization of standard deviation ensures an accuracy in estimating apparent activation energy which is consistent with the presumed kinetic equation. This method is more expeditive than the initial Doyle method. Calculations can be carried out relatively simply using Table I and can be easily programmed for electronic computers.

Since the standard deviation, δ, is a quantitative measure of the consistency between experimental data and the presumed kinetic equation, the suggested method can be very useful in testing the validity of different kinetic equations and thus can be applied in the study of solid-state reaction mechanisms.

(18) E. S. Freeman and B. Carroll, *J. Phys. Chem.*, **62**, 394 (1958).

The Wettability of Gold[1]

by Robert A. Erb

Chemistry Department, The Franklin Institute Research Laboratories, Philadelphia, Pennsylvania 19103
(Received November 13, 1967)

Experiments were run to determine the inherent wettability of gold by water. Measurements in pure steam at 101° gave a contact angle on gold of about 65° after 23,648 hr of continuous condensation. Radiotracer studies with oleic acid added to the refluxing water showed 0.209 monolayer on filmwise copper and 0.013–0.015 monolayer on dropwise gold, indicating that the nonwetting behavior of gold is not caused by organic contamination. The average contact angle on freshly electropolished gold surfaces was found to be 62.6 ± 3.4°. Heating experiments in quartz apparatus showed three sources of erroneously low contact angles that could readily be present in this type of experiment: (1) inorganic contamination of the surface; (2) surface roughness; and (3) equilibrium not established with water vapor. Cumulative evidence indicates that the equilibrium contact angle of water on a clean, smooth gold surface is between 60 and 65°.

Introduction

In 1962 we undertook a program to develop permanent systems for producing dropwise condensation of steam on metal condenser surfaces.[2] This program has been aimed toward the goal of increasing the heat-transfer efficiency of distillation processes for desalination. Early in the study we were surprised to find that silver produced dropwise condensation of steam despite extensive measures taken toward maintaining the purity of the refluxing water and the cleanliness of the apparatus. This experience was contrary to the statement[3] that all pure liquids would spread spontaneously on high-energy surfaces, with the exception of certain organic liquids which were "autophobic" or hydrolyzed on contact with the solid surface. Nevertheless, because of the persistence of the results with silver, we predicted that gold also (from Cu–Ag–Au in the periodic table) would exhibit some hydrophobic behavior. Earlier experimental papers had reported both high (Plaksin and Bessonov,[4] 61–62°) and low (Bartell and Smith,[5] 7°) contact angles of water on gold. White[6] then produced new experimental evidence for a high contact angle of water on an oxide-free surface of gold and for a sharp contrast between results on gold and results on base metals. New concepts by Fowkes[7] have provided a theoretical basis for understanding the nonwetting behavior on gold by consideration of the dispersion-force nature of the interaction between water and the oxide-free metal surface. Our continuous-condensation experiments in pure steam confirmed that gold was nonwettable under these conditions.[8] In addition, other noble metals, such as palladium and rhodium, were also seen to produce dropwise condensation. This is in contrast to some 13 different base metals tested, all of which produced filmwise condensation. Table I lists the average advancing contact angles[9] measured on the same 99.9% gold sample after 3650 hr and after 23,648 hr under continuous-con-

densing conditions. The average angle varied less than 1° in more than 2 years.

In 1965, Bewig and Zisman[10] published experimental results in which there were consistent 0° contact angles of water on gold and platinum after heating treatments in high-purity atmospheres. They concluded that if a water drop does not spontaneously wet a "clean" metal surface, it is probably an indication of measurable contamination by a hydrophobic organic impurity.

The following three experimental sections describe some of our programs designed to help clarify the situation by giving additional information toward the following questions: (1) is the dropwise condensation on gold caused by preferential attachment of organic contamination (as compared with filmwise base metals); (2) what factors cause lowering of the contact angle on gold, particularly in the heating-type experiments; (3) what is the best value for the equilibrium contact angle of water on a clean, smooth gold surface?

(1) Paper presented at the Symposium on Wettability of Metal Surfaces, Division of Colloid and Surface Chemistry, 153rd National Meeting of the American Chemical Society, Miami Beach, Fla., April 1967.

(2) R. A. Erb and E. Thelen, *Ind. Eng. Chem.*, **57**, No. 10, 49 (1965).

(3) H. W. Fox, E. F. Hare, and W. F. Zisman, *J. Phys. Chem.*, **59**, 1097 (1955).

(4) I. N. Plaksin and S. V. Bessonov, *Dokl. Akad. Nauk SSSR*, **61**, 865 (1948).

(5) F. E. Bartell and J. T. Smith, *J. Phys. Chem.*, **57**, 165 (1953).

(6) M. L. White, *ibid.*, **68**, 3083 (1964).

(7) F. M. Fowkes, *ibid.*, **67**, 2583 (1963); *Ind. Eng. Chem.*, **56**, No. 12, 40 (1964).

(8) R. A. Erb, *J. Phys. Chem.*, **69**, 1306 (1965).

(9) The "advancing" and "receding" angles on the vertical surface in ref 8 are both advancing in the sense that the drops are always growing; they actually are "upper" and "lower" angles which are smaller and greater, respectively, than the equilibrium contact angle on a horizontal surface because of the gravitational distortion. An average of the "upper" and "lower" angles is used in Table I as the reported contact angle.

(10) K. W. Bewig and W. A. Zisman, *J. Phys. Chem.*, **69**, 4238 (1965).

Table I: Contact Angle of Water on 99.9% Gold under Continuous-Condensing Conditions (101°)

|	Time, 3650 hr (0.42 year)	Time, 23,648 hr (2.7 year)
Lower angle, deg	85 ± 3	77.6 ± 1.0
Upper angle, deg	46 ± 2	51.8 ± 1.9
Av advancing angle, deg	65.5	64.7

Figure 1. Radiotracer study of the pickup of oleic acid contamination by surfaces of gold and other materials under continuous condensing conditions: (left-hand side) surface coverage 10 days after adding 0.0311 mg of oleic acid to 6 l. of refluxing water, 101°; (right-hand side) surface coverage after two subsequent changes of water.

Experimental Program. I. Radiotracer Studies under Continuous Condensing Conditions

An experimental procedure was devised to resolve the question as to whether gold as a condensing surface in steam picks up and retains organic hydrophobic materials more readily than base metals (a possible explanation for its dropwise behavior). Oleic acid, a classical promoter of dropwise condensation, was chosen to be used in a radiotracer study. Oleic acid-1-^{14}C with a specific activity of 9.0 mCi/mmol (Tracerlab Inc.) was used in this study. A solventless 0.0331-mg (0.001 mCi) sample was introduced into 6 l. of pure water (redistilled from alkaline permanganate) refluxing in a closed system at 101°, giving a concentration of 0.005 mg/l. Previously, 16 flats, 2.5 × 7.5 cm, had been attached to a cooled core.

At a period of 30 min after the introduction of the tagged oleic acid, small samples of steam and water were taken from the apparatus and were found to be radioactive. After 10 days the radioactivity in the water was greatly diminished, indicating that adsorption of the oleic acid had taken place on walls and condensing surfaces. Measurements of the surface concentration of oleic acid were made on the samples in a cell with fixed geometry by means of a Geiger counter with the substrate types previously calibrated for backscatter. Fractional monolayer coverages were calculated by using a value of 40 Å^2/molecule for a close-packed monolayer, which corresponds to 2.5 × 10^{14} molecules/cm^2.

Figure 1 shows some of the experimental results. The surface concentration was 0.209 monolayer on a copper condensing surface (which showed the usual filmwise condensation) and only 0.015 and 0.013 monolayer on two gold surfaces (with the usual dropwise condensation). This is a strong indication that the nonwetting behavior of gold is not caused by organic contamination.

The highest surface coverage was noted on the sample which is a mixture of poly(tetrafluoroethylene) (TFE) and aluminum oxide (Tufram, General Magnaplate). However, the oleic acid is mostly removed from the surface of the TFE polymer after one change of water. The chromium is an example of a wettable system which shows low adsorption of the oleic acid. Titanium,
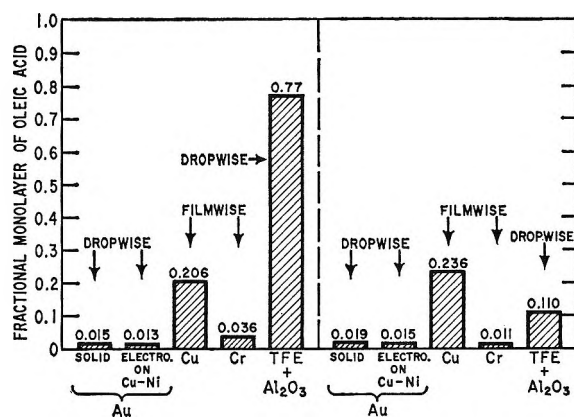
molybdenum, and type 316 stainless steel samples also showed wettable behavior and low adsorption. Palladium and rhodium, on the other hand, showed dropwise behavior and low adsorption, tending to confirm the conclusion that the nonwettability of noble metals under continuous-condensation conditions is not due to organic contamination.

Experimental Program II: Wettability of Electropolished Gold Surfaces

The basic problem in the measurement of the contact angle of water on gold is in the preparation of a smooth surface which is free from both hydrophobic organic contamination and from hydrophilic inorganic contamination. One way to accomplish this is by deep electropolishing, in which 50 μ or more of the surface is removed after the last mechanical polishing step. This technique was used by Trevoy and Johnson,[11] who obtained angles of 0–11° for water on aluminum, copper, nickel, zinc, and other metals.

We experimented with several types of electropolishing baths for gold and found that the most consistent results were obtained with the Meakin[12] solution, which is made of glacial acetic acid, hydrochloric acid, and water. This produces smooth, specularly bright surfaces, which are free of possible residues from phosphoric acid or potassium ferrocyanide such as are found in cyanide baths. We operated the electropolishing at room temperature at applied potentials of from about 20 to 23 V and at currents of 450–800 mA for the small cylindrical samples which are about 0.6–0.7 cm in diameter and 0.4–0.7 cm in height.

After electropolishing, the sample is rinsed in water, with the final rinse in water which has been redistilled by alkaline permanganate. The water is shaken off the

(11) D. J. Trevoy and H. Johnson, *J. Phys. Chem.*, **62**, 833 (1958).
(12) J. D. Meakin, *Rev. Sci. Instrum.*, **35**, 763 (1964).

sample and the contact angle of an applied sessile drop is measured rapidly, with a telemicroscope with a protractor eyepiece.

The following gold materials were studied: (1) 99.99% pure monocrystalline gold (Semi-Elements Inc.), (2) 99.999% pure monocrystalline gold (Materials Research Corp.); and (3) 99.9999% pure polycrystalline gold (Semi-Elements Inc.). The measured contact angle of water on gold (average for six samples, 21 drops) on surfaces freshly electropolished with removal of 50-μ surface layer, was 62.6 ± 3.4°. There did not appear to be any significant wettability differences between mono- and polycrystalline surfaces or among the three levels of purity. The only great deviations (lowered angles) from the 60–65° region were observed when the sample surface became discolored, hazy, or roughened from improper current density or from improper agitation during the electropolishing process.

Experimental Program III: Wettability Studies on Gold Heated in Pure Atmospheres

As noted above, our experiments under continuous-condensing conditions and with freshly electroplated surfaces support a contact angle of water on gold of about 60–65°. However, the experimental results of Bewig and Zisman,[10] with zero contact angles on gold samples heated to near the melting point in pure atmospheres, have raised many basic questions, not the least of which is, "Is the inherent equilibrium contact angle zero or isn't it?"

White and Drobek[13] have provided some insight into the divergence of results with their recent paper on the effect of residual abrasives on the wettability of polished gold surfaces. Residual aluminum oxide abrasives, shown to be present by electron diffraction, were seen to cause lowered contact angles. They measured angles of 62° on clean, vacuum-deposited gold with and without heating to 1000° in oxygen. (Even with residual oxides present, the reported values were not less than 34°.)

Two new apparatus were built for our study. Figure 2 shows a quartz apparatus for the induction heating of the gold sample in pure atmospheres and for the measuring of the contact angle without opening the system to the laboratory air. The second quartz apparatus, shown in Figure 3, uses a vertical tube furnace for heating the sample, which is then elevated to a cooler zone for measurement of contact angles. One function of the second apparatus was to determine whether any special surface phenomena were caused by *induction* heating *per se*. No differences were found between the two methods.

As steps to avoid organic contamination: (1) grease-free fittings were used throughout; (2) all inner surfaces of the apparatus were cleaned with sodium dichromate–sulfuric acid; and (3) all helium and hydrogen
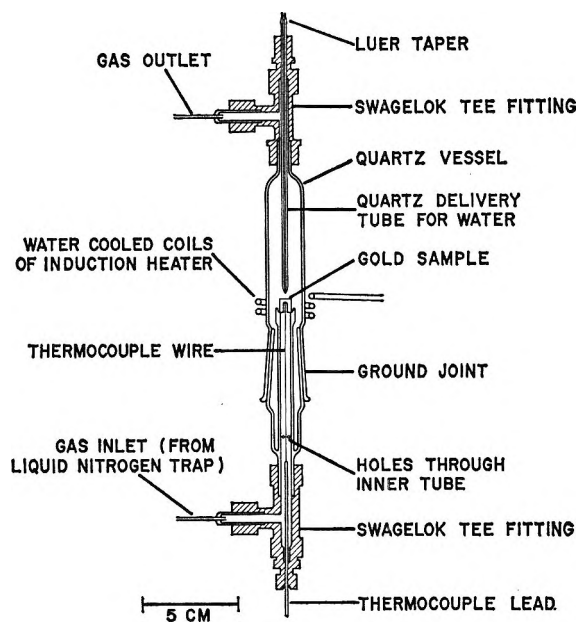
Figure 2. Quartz apparatus for the induction heating of gold specimens in pure atmospheres and for the measuring of wettability without subsequent openings.
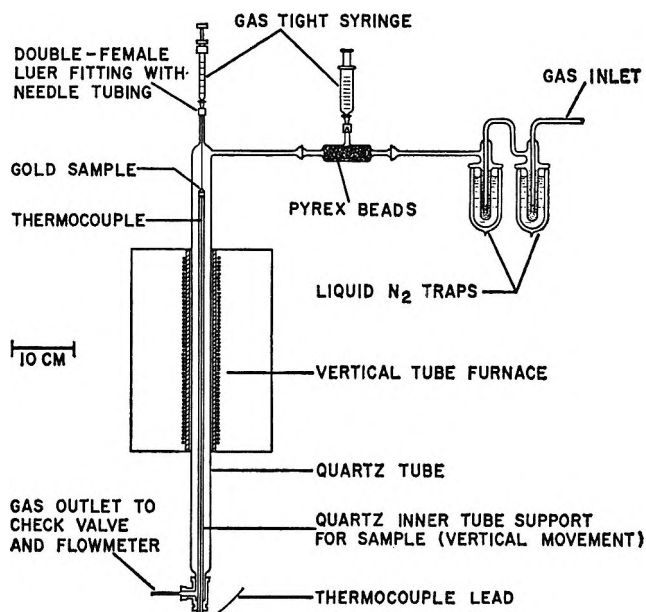
Figure 3. Quartz apparatus for heating gold sample in the tube furnace in a pure atmosphere, with subsequent movement of the sample to a cool zone for wettability measurement.

gas flows were passed through a double liquid nitrogen trap filled with glass beads. (Dry Ice–acetone was used with oxygen.) The contact angles were measured at room temperature in the gas stream flowing at about 100 cm³/min.

Table II gives some results on gold samples which had been prepared with a final step of deep electropolishing (greater than 50-μ removal) to avoid the

(13) M. L. White and J. Drobek, *J. Phys. Chem.*, **70**, 3432 (1966).

presence of abrasive residue on the surface. The samples were held at the indicated temperature for 3 min. A number of things can be noted in the table. First, no zero angles were obtained on any of these gold samples. However, the angles observed, mostly in the range from 6 to 21°, were consistently lower than these obtained in our other experiments, or those of White and Drobek.[13] Other things of note are: (1) there was a very irregular trend toward lower angles with high

Table II: Contact Angles after Heat Treatment[a]

Sample	Atmosphere	Temp, °C	Range angles, deg
1. 6-9's polyxn gold (sequence without repolishing)	Helium	500	14.7-19.3
	Helium	600	18.3
	Helium	700	7.1-16.3
	Helium	800	6.0-14.3
	Helium	900	15.1-30.5
	Helium	1000	5.0-19.7
	Oxygen	1000	12.5
	Oxygen with water in the base of the cell	500	30.6-37.7
2. 6-9's polyxn gold	Helium	1000	15.0-20.8
3. 5-9's monoxn gold (sequence)	Helium	400	25.0
		700	9.9-18.0
		950	13.6
4. 99.45% nickel, final diamond polish (sequence)	Oxygen	1000	0
	Helium	1000	0
	Hydrogen	1000	9.5-21.0

[a] Measured at room temperature in the dry gases given in the table; the gold was mechanically polished, followed by Meakin electropolish.

temperatures; (2) there were no great differences between monocrystalline and polycrystalline gold; (3) when a second drop was placed over a first drop, the contact angle of the second drop was always higher than that of the first drop; (4) the highest angle was for the one experiment in which water was kept in the base of the induction-heating cell during heating and angle measurement (these results in (3) and (4) pointed to the important effect of water vapor, which is discussed later); and (5) the nickel samples heated in oxygen and helium produced a zero contact angle, indicating freedom from organic contamination after heating and reduction; in hydrogen, nonzero angles were obtained, which might be attributed to the nonwettability of an oxide-free metal surface, as seen with gold.

Table III lists eight possible causes of reduced contact angle on gold surfaces. The first five are related to inorganic (hydrophilic) contamination of the surface. The effect of residues of abrasives has been covered well by White and Drobek.[13] This can be readily avoided by their methods or by deep electro-

polishing. Another, very serious, contamination possibility comes from concentration of oxide-forming bulk impurities at the surface when the sample is heated to near its melting point. Plumb and Thakkar[14] indicate that even at room temperature a gold sample containing only 0.01% copper will rapidly become coated with a layer of copper oxide. The diffusion coefficients increase greatly with increasing temperature, and it might be reasonable to expect that bulk impurities, even as low as 1 ppm, could lead to serious surface contamination of a thick gold sample when heated to just below the melting point (1063°). In the work of Bewig and Zisman,[10] where zero angles were obtained, the solid-gold samples were heated "white hot," which was described as a condition just at the edge of melting. In their work, finite contact angles were observed when the samples were heated to "dull red heat" (which is roughly from 605 to 850°). This difference might be explained in large part as due to surface contamination by bulk impurities.

Table III: Sources of Reduced Contact Angle

Experimental problem	Solution
I. Inorganic Contamination of Surface	
1. Residues of abrasives	Deep electropolishing (>50 μ)
2. Impurities from bulk moving to surface under elevated temperatures	Use high-purity gold (6-9's); avoid too high temperatures
3. Deposition of material from wall of vessel under high temperatures	Use quartz rather than borosilicate glass
4. Deposition of material from gas stream (fibrous glass or trap packing)	Avoid presence of finely divided material in gas stream
5. Nonvolatile residues from electropolishing baths (such as those containing phosphoric acid, ferrocyanide)	Use volatile electropolishing reagent (e.g., Meakin solution)
II. Surface Roughness	
1. Surface not smooth as prepared	Smoothing by polishing or otherwise
2. Surface roughening by thermal etching	Check surface by electron microscopy; avoid conditions of temperature and atmosphere which produce thermal etching
III. Equilibrium Not Established with Water Vapor	
1. Gold sample heated and then cooled and contact angle measured in gas stream free from water vapor (passed through liquid nitrogen trap); contact angle observed is not the equilibrium contact angle	Introduce saturating vessel in gas stream past the cold trap

(14) R. C. Plumb and N. Thakkar, *J. Phys. Chem.*, **69**, 439 (1965).
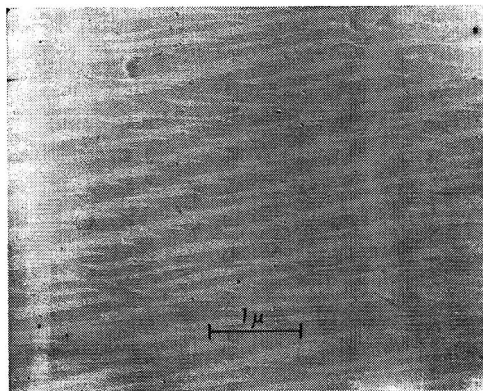
Figure 4. Electron micrograph of surface of previously electropolished 99.9999% gold specimen after heating for 3 min in oxygen at 1000°.

Contamination of the sample surface by deposition from borosilicate walls, by fibrous glass particles, and by electropolishing residues are also listed. We have observed particles of fibrous glass on one sample, with resulting lowered contact angles, and have replaced this packing with glass beads in the saturating vessel in Figure 3. We have also noticed adverse effects from nonvolatile residues from electropolishing in cyanide baths.

The second section in Table III lists sources of reduced contact angle from surface roughness. The roughness may be considered to be related to contact angle by Wenzel's law,[15] which states that the roughness $r = \cos \theta_{apparent}/\cos \theta_{true}$. We have observed a number of instances in which a detectable roughness was introduced in electropolished gold surfaces by heating in pure atmospheres (oxygen and helium). Figure 4 is an electron micrograph of the surface of one 99.9999% gold sample after heating to 1000° in oxygen for 3 min. The faceted surface structure indicates that thermal etching has taken place.

The third section in Table III lists one of the most serious sources of error leading to the reporting of abnormally low contact angles in the heating type of experiment. For an *equilibrium* contact angle to be measured, the measuring cell should be essentially saturated with water vapor. The heating experiments (ours included) in which liquid nitrogen traps are used have no water in the flowing atmosphere, and after the heating has driven all adsorbed water from the gold surface, there is no opportunity for the adsorbed water to be restored. When a drop is placed on the gold substrate in the flowing stream of dry helium, water only then becomes present in the system, although at a very low partial pressure in the flowing gas atmosphere; this presence of water is associated with a higher contact angle when a second drop is placed on the surface, as noted earlier. Table IV shows an example of what happens when water vapor is introduced directly into the gas stream after heating and cooling is complete.

In our various experiments, the contact angle upon addition of water vapor has increased by 20-40° over the angle measured upon cooling in the dry gas.

Table IV: Effect of Addition of Water Vapor to the Atmosphere for the Measurement of Contact Angle

Sample: Monocrystalline gold (5-9's), electropolished; heated in helium at 960°; cooled under dry helium
Contact angles under dry helium: 11.9-13.8°
Contact angle 15 min after water vapor added to helium stream: 53.2°

The basis for the apparently substantial effect of water vapor on the contact angle of water on a previously heated surface of gold is not clearly understood. However, it would be reasonable to expect a higher contact angle if the solid-to-gas interfacial tension of gold is lowered, as it would be by adsorption of water in the presence of a high partial pressure of water vapor. It is to be noted that a duplex layer of water on the gold is not present (which would lead to liquid water spreading over bulk water, with a resultant 0° contact angle).

These sources of lowered contact angle are cumulative and can indeed cause erroneous zero angles. To illustrate, we heated one 99.9999% gold sample, previously electropolished, just up to the melting point in helium such that the edges were seen to deform slightly before the temperature was reduced. Surface roughening could be seen under an optical microscope, and we would also suspect migration of base metals from the bulk to the surface. When the sample was cooled in flowing dry helium, a zero contact angle was observed. However, one of the contributing factors to the low angle was removed by adding water to the

Table V: Summary of Experimental Values Supporting the 60-65° Contact Angle on Clean, Smooth Gold

Investigators	Angle, deg	Experimental conditions
Plaksin and Bessenov (1948)	61	In oxygen
	61	In nitrogen
	62	In CO₂
Erb (1965)	65.5	Condensation, 3650 hr (101°)
White and Drobek (1966)	62	Vacuum deposited, with and without heating in O₂ at 1000°
	61	Diamond polished and heated in O₂ at 1000°
Erb (1967)	64.7	Condensation, 23,648 hr (101°)
	62.6	Electropolished (Meakin solution)

(15) R. N. Wenzel, *Ind. Eng. Chem.*, **28**, 988 (1936).

saturating vessel. The contact angle was measured after 30 min and was found to be no longer zero but 31.7°.

Conclusion

The experimental evidence discussed here helps to provide an explanation for low contact angles of water on gold which have previously been reported in the literature and supports a conclusion that water has a high equilibrium contact angle on a smooth, uncontaminated surface of gold. Table V is a compilation of results from several different investigators and experimental procedures. The best value for the equilibrium contact angle of water on gold at room temperature appears to be about 62°. A value of this magnitude is also in line with theoretical considerations of Fowkes[7] and Thelen[16] on the interfacial relationships with oxide-free metal surfaces.

(16) E. Thelen, *J. Phys. Chem.*, **71**, 1946 (1967).

Focused, Coherent Radiation (Laser)-Induced

Degradation of Aromatic Compounds

by Richard H. Wiley and P. Veeravagu

Department of Chemistry, Hunter College of the City University of New York, New York, New York 10022
(Received November 20, 1967)

The principal gaseous decomposition products formed from aromatic compounds in a focused laser beam experiment are methane and acetylene. Minor amounts of ethane, ethylene, propane, propene, allene, and a four-carbon acetylenic hydrocarbon are also formed. The ratio of methane to acetylene is very low (4:85) for polycyclic types (naphthalene, anthracene, phenanthrene, and biphenyl) and higher (40:10) for monocyclic (toluene, xylene, and mesitylene) types. This difference suggests a reactant-dependent decomposition mechanism. The possibility of a nonsource-dependent, energetic carbon plasma-type reaction is suggested by the formation of high yields of acetylene from dissimilar substances and the absence of marked differences for decompositions run in the presence of nitrogen, oxygen, or hydrogen.

The physical conditions existing at the focal point of a focused, coherent radiation (laser) beam have been the subject of some speculation.[1-5] In theory the beam can be focused to a 10^{-6} cm^2 area to provide, from normal (millisecond) burst, power densities of 10^{15} W/cm^2 and electromagnetic field (optical wavelengths) of 10^6 V/cm. The temperature rise associated with this phenomenon is difficult to estimate,[1,2] and "temperature" assignments of $10^9 °K$ are probably not meaningful. Electrical breakdown occurs[6,7] and the phenomenon presumably involves plasma formation.[3] Some experiments designed to evaluate the nature and magnitude of these effects have been reported. From a chemical point of view, the exposure of a material to such an intense power concentration should (and in fact does) result in extensive degradation.[8]

It is of some interest to determine, if possible, whether such focused-laser degradations show product patterns which correlate with extrapolated thermodynamic data or with data on reactions of fragments and atoms

(1) A. L. Shawlow, *Science*, **149**, 13 (1965).

(2) C. H. Townes, *Biophys. J.*, **2**, 325 (1962).

(3) J. Berkowitz and W. A. Chupka, *J. Chem. Phys.*, **40**, 2735 (1964); see also ref 4.

(4) M. W. Dowley, K. B. Eisenthal, and W. L. Peticolas, *Phys. Rev. Lett.*, **18**, 531 (1967). These authors describe conditions involving laser-produced dielectric breakdown in liquids. These data indicate, and the authors are indebted to a reviewer for pointing this out, degradation in solids *via* internal scattering and absorption of energy on the interfaces. It is difficult to see, however, how crystal structures can survive under these conditions so as to participate in controlling energy-transfer schemes.

(5) R. H. Wiley, *Ann. N. Y. Acad. Sci.*, **122**, 685 (1965).

(6) R. C. Rosen, M. K. Healy, and W. F. McNary, Jr., *Science*, **142**, 236 (1963).

(7) A. G. Meyerand, Jr., and A. F. Haught, *Phys. Rev. Lett.*, **11**, 401 (1963).

(8) R. H. Wiley, N. Dunski, and T. K. Venkatachalam, *J. Heterocyclic Chem.*, **3**, 117 (1966).

Table I: Relative Peak Areas of Gaseous Products[a]

	CH_4	C_2H_6	C_2H_4	C_2H_2	C_3H_8	C_3H_6	C_3H_4[b]	$C_4H_4,$ C_4H_2[c]
Benzene	56	1.5	21	16		T	T	
Under N	53	1.2	18	27				
Toluene	38	<1	10	51		T	T	
p-Xylene	42	<1	9	48		T	T	
Mesitylene	46	<1	13	40		T	T	
Biphenyl	7	T	6	84		T	T	3
Naphthalene	4	T	4	87		T	T	5
Under N	3		5	86				5
Anthracene	4	T	3	85		T	T	8
Under H	2		3	84		1		11
Under O	5		5	82				8
Phenanthrene	2	T	1	91		T	T	6
Benzoic acid	3	T	1	85		T	T	11
Benzil	15	1	19	65		T	T	
Anthraquinone	3	T	2	86		T	T	9
N,N-Dimethylaniline	77	5	12	2	2	1	T	
N,N-Diethylaniline	51	7	26	9	6	1	T[d]	
Methyl yellow	28	7	8	57	T	T	T	T
Methylene blue	44	3	8	43	T	T	T	2

[a] Values are the relative amounts of the gaseous components obtained by laser irradiation (intensity = 3.5 ± 0.5 J) of the listed compounds. The analysis of the gaseous mixtures was done by gas chromatography based on peak-area values determined as described in the Experimental Section. The exposures were made in air except as indicated: H, hydrogen; N, nitrogen; and O, oxygen. [b] Allene. [c] Vinylacetylene and diacetylene, respectively. [d] Also some unidentified C_4H_{10} fraction.

with excess kinetic energy. The data available on thermal degradation reactions[9,10] and the characteristic reactions of energetic atoms[11-14] are not, however, directly relatable to the focused-laser experiment. The extrapolations are excessive and the experimental conditions are different. For these reasons and because the focused-laser experiment itself is not as yet as well defined as might be desired, it is premature to try to establish correlations and mechanisms. It is presumably of some interest, however, to record the description of focused-laser experiments as a contribution to the development of further understanding of the conditions involved. It is to be noted that the focused-laser experiment[3-5,15,16] is thus to be distinguished from the photochemical laser experiment.[17,18] It is also to be recognized that absorption by the reacting species is involved in the focused-laser experiment, not in the usual photochemically energy-transfer sense but in partial interference in achieving maximum focusing intensity.

It is the purpose of this paper to describe a chemical experiment with focused, coherent (laser) radiation which presents evidence upon which some conclusions as to the characteristics of the phenomenon can be determined. For this purpose a 4-10-J ruby laser operating in the normal (burst) mode at 6943 Å was focused through a lens on a sample contained in a tube. The degradation under these conditions was extensive. Analyses of the gaseous products gave characteristic groups of compounds identified, and their relative amounts determined quantitatively, by gas chro-

matographic analysis. The compounds degraded, the products formed, and the quantitative data on the relative amounts of the products are listed in Table I.

The principal products formed in these degradations are methane and acetylene. Although these are products often observed in thermal degradations, presumably because of their thermodynamic stability at elevated temperatures, there are differences in the data for the two sets of conditions. Thus it has been noted that although acetylene is formed from benzene, it is not commonly observed in pyrolyses.[8] There are three categories of methane-acetylene formation patterns in our laser experiments. One group of com-

(9) G. M. Badger, *Progr. Phys. Org. Chem.*, **3**, 1 (1965).

(10) C. D. Hurd, A. R. Macon, J. I. Simon, and R. V. Levetan, *J. Amer. Chem. Soc.*, **84**, 4509 (1962).

(11) A. P. Wolf, *Advan. Phys. Org. Chem.*, **2**, 201 (1964); also P. B. Shevlen and A. P. Wolf, *J. Amer. Chem. Soc.*, **88**, 4735 (1966); H. J. Ache and A. P. Wolf, *ibid.*, **88**, 888 (1966).

(12) R. Wolfgang, *Ann. Rev. Phys. Chem.*, **16**, 15 (1965); *Progr. Reaction Kinetics*, **3**, 97 (1965); also R. Wolfgang, *et al.*, *J. Amer. Chem. Soc.*, **86**, 4741, 4747 (1964); **87**, 3008 (1965); **88**, 1064, 1065, 1610 (1966).

(13) R. R. Engel and P. S. Skell, *ibid.*, **87**, 4663 (1965).

(14) J. L. Sprung, S. Winstein, and W. F. Libby, *ibid.*, **87**, 1812 (1965).

(15) W. B. Tiffany, A. W. Moos, and A. L. Shawlow, *Science*, **157**, 40 (1967).

(16) R. M. Danziger, K. H. Bar-Eli, and K. Weiss, *J. Phys. Chem.*, **71**, 2633 (1967).

(17) W. A. Chupka and J. Berkowitz, unpublished data.

(18) R. Rocherolles, French Patent 1,370,722 (1964); *Chem. Abstr.*, **62**, 1148e (1965).

pounds forms considerably more acetylene than methane (biphenyl, naphthalene, anthracene, phenanthrene, benzoic acid, benzil, anthraquinone, and methyl yellow); a second group gives about equal amounts of methane and acetylene (toluene, p-xylene, mesitylene, and methylene); and the third group gives more methane than acetylene (benzene, N,N-dimethylaniline, and N,N-diethylaniline).

In addition to methane and acetylene, a few other compounds are regularly observed in our experiments. Ethylene is formed in relatively low amounts but more is formed in those samples giving the higher methane to acetylene ratios. An unsaturated four-carbon fraction is formed in significant amounts from those compounds giving low methane yields. A three-carbon fraction is formed in traces only, and former evidence[5] for its formation is attributable to the difference in experimental conditions (one, not many exposures; optical path; and different modes from Brewster angle vs. total internal reflecting ruby) and methods of analysis (different column which allows separations not made previously). Allene is formed in trace amounts in all experiments. The four-carbon fragment has been identified by mass spectroscopy as a mixture of vinylacetylene and diacetylene and is free of butadiene. Butadiene is reported[9] to be formed from many hydrocarbons on pyrolysis. Hydrogen and also carbon monoxide and nitrogen from some sources are also formed. There is a residue of carbon and, often, apparently unchanged starting material.

The products thus identified in the focused-laser experiment are, in general, those associated with thermal degradations and those to be predicted from thermodynamic data from studies in the usual high-temperature ranges. Such reactions should, however, follow customary fragmentation patterns via radical or ionic mechanisms characteristic of the structures being degraded.[9,10] Such structurally related fragmentation patterns are not consistently observed in the focused-laser degradations and some peculiarities are to be noted. Thus it is difficult to rationalize the distinct differences in methane:acetylene ratios obtained for the benzene–biphenyl pair and for the benzene–benzoic acid pair. Mechanistically one would perhaps predict the degradation of any of the aromatics to give acetylene predominantly, and it is mechanistically atypical to find methane as a significant product of nonmethylated structures such as benzene and benzil. The pattern resembles that of the previously noted[13] formation of toluene from benzene but seems to have gone further.

The alternatives to thermal degradations are those of energetic carbon and energetic hydrogen reactions within a plasma. The reactions characteristic of these systems are insertion and abstraction.[11,12] It is characteristic of these reactions also that acetylene is a principal product, and high yields of acetylene from dissimilar substances have been considered previously

as evidence of carbon insertion reactions. Methane is also formed under some conditions. It is further characteristic that these products are formed in the reactions which are not primarily substrate (reactant) dependent and that they show effects when moderated by the presence of inert[10,11] or reactive[12] gases. The energetic carbon inserts either a singlet (1D) state or triplet (3P) state to give intermediates which decompose to give allene (from the singlet) or acetylene (from the triplet) as the principal characteristic products.

Some features of these patterns are observed in the focused-laser experiments. The formation of relatively large amounts of acetylene from all compounds except the N,N-dimethyl and C-methyl types is noteworthy. The presence of methane in the amounts observed suggests the presence of enhanced amounts of a methine, methylene, or methyl radical, the significance of which has been discussed before,[11] or of especially enhanced abstraction processes leading to more highly hydrogenated products such as toluene[14] in a reaction characteristic of aromatic materials and less common in reactions of olefins. The absence of any marked difference in the kinds or amounts of products produced in presumably reactive (oxygen and hydrogen) gases or an inert gas (nitrogen) is consistent with a plasma-type reaction.

The conclusion thus derived from the present data is that there are observations best accounted for on the assumption that the reactions in focused-laser degradations are not simply those of a pyrolysis but are characteristic of the special conditions involved and are free of some of the problems, such as radiation damage,[11] encountered in other high-energy reactions.

Experimental Section

Materials Used for Irradiation. All compounds used were obtained from Eastman Organic Chemicals. The solids, biphenyl, naphthalene, anthracene, phenanthrene, anthraquinone, methyl yellow, benzil, and benzoic acid, were purified by recrystallization. The liquids, benzene, toluene, p-xylene, mesitylene, N,N-dimethylaniline, and N,N-diethylaniline, were freshly distilled before use. Methylene blue was purified by the procedure described by Bergman and O'Konski.[19]

Laser Irradiation of Samples. The laser used was a 6-in. ruby pumped with two xenon flash tubes in a double-elliptical cavity with water cooling (Lear Siegler Instruments Model No. LS-212). The housing for this instrument is so designed as to nearly completely exclude stray flash-lamp light reaching the target. The output was monitored twice daily, before and after a series of exposures, with a photodiode beam-splitting monitor (Lear Siegler, Energy Monitor, Model M1-2). The performance of the crystal was monitored monthly

(19) K. Bergman and C. T. O'Konski, *J. Phys. Chem.*, **67**, 2169 (1963).
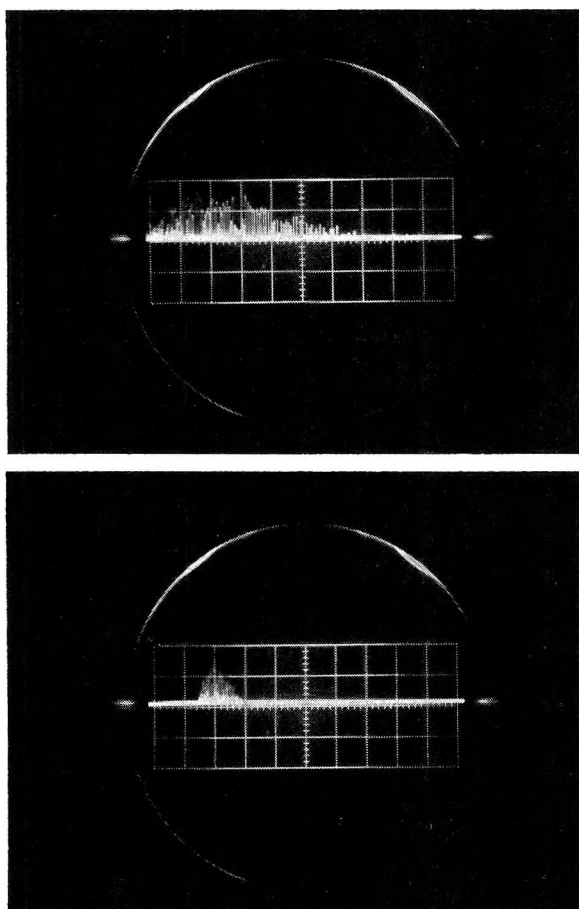
Figure 1. Laser operations. Oscilloscope trace at 9-J
(burst) output at 60.6 kW/V: top, 0.1 msec/cm;
bottom, 0.5 msec/cm.

by displaying and recording photographically its output
on a fast-rise oscilloscope (Tektronics Model 585A)
with a fast-rise, high-gain unit (Tektronics Model 86).
A typical response is shown in Figure 1. The mode
pattern was not determined and no filters were used to
remove harmonics. The laser beam was used at the
following two intensities: (a) 3.5 ± 0.5 J and (b)
10.0 ± 0.5 J. All the experiments summarized in
Table I were carried out with a beam of intensity
3.5 ± 0.5 J and in the normal (burst) mode. Results
from less complete experiments carried out with a
beam intensity of 10.0 ± 0.5 J and all of the compounds
(except benzil) in Table I were similar to those obtained
with a beam of intensity 3.5 ± 0.5 J. The same prod-
ucts were found in not significantly different relative
amounts and no other compounds were observed.
More extensive degradation, often fracturing the tube,
was observed with 10-J bursts. Each sample was
exposed to only one burst.

Pyrex capillary tubes, 8 cm long, 3 mm o.d., and
2 mm i.d., were used throughout this work. The tubes
were cleaned with chromic acid cleaning solution and
distilled water and were dried at 120°. Each tube
was sealed at one end. It was charged with 5–10 mg

of the sample and was stoppered with a serum-bottle
(needle-puncture) rubber stopper. A series of samples
of naphthalene and of benzene run under prepurified
(Matheson Co.) nitrogen and a series of anthracene
samples run under hydrogen and under oxygen showed
no marked difference in relative amounts of products
formed. The data are in Table I. The solid samples
were packed firmly into the bottom of the tube with a
metal rod. For the liquid samples, the stoppered tube
containing the sample was frozen in liquid nitrogen
imediately before irradiation. The laser radiation
usually had no effect on the unfrozen liquid samples.[4]
The laser beam was focused, with an 8.4 cm focal length
lens, on the sample. The lens and the sample holder
were mounted in an optical bench and the focal point
was located by observing the size of the hole burned in
a black-tape target. A minimum diameter of about
1 mm was burned at the apparent focal point. Hazards
in observational laser alignment and handling preclude
simple adaptations of optical procedures for this
measurement.

Gas Analysis. All gas chromatographic analysis in
this work was performed on a Perkin-Elmer Corp.
Model 154D vapor fractometer. The detector system
was either a flame-ionization unit or a thermistor ther-
mal-conductivity unit. Helium was used as the carrier
gas.

Most gas analyses were carried out with a 1-m silica
gel column (Perkin-Elmer J column). The detection and
estimation of gases were made at a column temperature
of 70° and with a helium flow rate of 70 ml/min. At
70° the retention times (alone or in mixtures) of
standard methane, ethane, ethylene, propane, acety-
lene, propene, and allene were 0.3, 1.4, 2.2, 4.7, 4.9, 12.6,
and 14.2 min, respectively. For the detection of
gaseous products of higher molecular weights, the silica
gel column was operated at 100° with a helium flow
rate of 70 ml/min. At 100° the retention times (alone
or in mixtures) of standard methane, ethane, ethyl-
ene, propane, acetylene, propene, allene, butane,
butene-1, methylacetylene, and butadiene were, re-
spectively, 0.2, 0.9, 1.5, 3.3, 3.3, 7.2, 8.5, 10.8, 29.2,
30.8, and 36.0 min.

A satisfactory separation of acetylene from propane
could not be obtained with the silica gel column. How-
ever, they were separated on a 1-m dimethylsulfolane
column (Perkin-Elmer I column). The I column was
not, however, useful for the resolution of other lower
gaseous components. The retention times (alone and
in mixtures) on this column for methane, ethane, ethyl-
ene, propane, propene, and acetylene at 30° and at a
helium flow rate of 5 ml/min were, respectively, 1.2,
1.4, 1.5, 1.8, 2.5, and 4.0 min.

Samples (2–5 µl) of the gaseous products formed on
laser irradiation were removed from the radiated
sample tube with a 10-µl Hamilton syringe (Model
N) and were injected into the gas chromatograph. The

areas of the peaks in the gas chromatograms were measured with a planimeter (Ott, Type 31). Duplicate area measurements gave values agreeing within ±1%. The relative amounts of the individual components were calculated from the ratio of the peak areas. For each of the compounds studied, the irradiation and subsequent gas chromatographic analysis were repeated five times to give the data recorded in Table I. Naphthalene was rerun ten times by this procedure and five times under nitrogen Benzene was run under nitrogen and under air. Anthracene was run under hydrogen, oxygen, and air. The deviation from the average in the relative amounts of the major component, acetylene, in the gas mixtures from the solid hydrocarbons and from anthraquinone, benzil, and benzoic acid, for five repetitive experiments was from 1 to 12% (average, 5%). The liquid hydrocarbons, methyl yellow, and methylene blue, yielded methane and acetylene as the two major components. In the five individual experiments with the liquid hydrocarbons, the deviation from the average in the yield of methane was from 13 to 68% (average, 38%) and the deviation for the yield of acetylene was from 10 to 40% (average, 23%). The deviation in the case of methyl yellow and methylene blue, for methane, was from 14 to 34% (average, 23%) and for acetylene was from 7 to 33% (average, 18%). Both N,N-dimethylaniline and N,N-diethylaniline gave methane as the major product and the deviation was from 1 to 20% (average, 12%). Much of this variation can probably be attributed to variations in the modal operation of the ruby crystal. If so, gas laser data should be less variable.

Hydrogen is also formed in these degradations as has been demonstrated by analysis of the gaseous products from naphthalene radiations. For this analysis, an activated-carbon column (Perkin-Elmer M column) was used at 44 cm³/min helium and at 30°; the hydrogen retention time was 1 min. Carbon monoxide (retention time = 6 min) was also demonstrated as a product from the anthraquinone and benzil radiation. These products, hydrogen and carbon monoxide, were not included in the survey experiments because they are not separated on the gas chromatographic column used for hydrocarbon product analysis.

As noted in Table I some of the compounds formed a product with a rentention time of 38.0 min on silica gel column at 100° and at a helium flow rate of 70 ml/min. This was not butadiene, the retention time of which was 36.0 min under the same conditions. Mass spectrographic analysis (Consolidated Electrodynamics Corp. residual-gas analyzer Model 21-614) of the gases obtained from irradiation of anthracene gave four peaks (in the four carbon range) of mass numbers 49, 50, 51, and 52, respectively. The m/e 50 peak was the largest of the four. Based on these data, it was concluded that the product with a rentention time of 38 min was a mixture of diacetylene (m/e 50) and monovinylacetylene (m/e 52). Standards of these for gas chromatographic analysis were not available. The results obtained in the experiments at 3.5–4.5 J are summarized in Table I.

To determine the amount of material reacted during a typical experiment, a sample of 9.3 mg of anthracene was exposed to a 4-J burst. The exposed tube and its contents were dissolved in absolute ethanol and made up to a standard volume (100 ml). The uv maximum of 2520 mμ was found to be 82.6% that of a solution of 9.3 mg of anthracene in 100 ml of absolute ethanol. The gas chromatographic analysis of the product gases, made before dissolution, was typical of other runs. On the basis of the amounts of gaseous products as sampled in other experiments, these data give a fair estimate (1–3 mg) of the amount of reactant decomposed in the experiments listed in Table I.

Prediction of Heats of Formation

by W. Schotte

*Engineering Technology Laboratory, E. I. du Pont de Nemours and Co., Inc.,
Wilmington, Delaware 19898* *(Received November 27, 1967)*

Semiempirical quantum-mechanical equations have been developed to calculate energies of different types of bonds. These equations have been used in Mulliken's method for the prediction of heats of formation and the energies required to dissociate molecules into gaseous atoms. The scheme has been applied to 24 binary compounds of C, H, Cl, and N. Heats of formation of some of these were used to establish parameters appearing in the theory. Good agreement has been obtained between predicted values and the known heats of formation of the other compounds.

I. Introduction

Heats of formation of many compounds, particularly unstable molecules and free radicals, are not known. Group-contribution methods are frequently helpful to predict heats of formation of many types of molecules, but they are usually not applicable for calculations involving free radicals. Mulliken[1] proposed a simplified quantum-mechanical procedure to predict the energy of atomization, *i.e.*, the energy required to dissociate the molecule into gaseous atoms. Mulliken's method has many good features and explains qualitatively the various bond energies and repulsions which contribute to the energy of atomization. Pedley[2,3] modified Mulliken's method somewhat to simplify the calculations and to obtain satisfactory agreement between predicted and known energies of atomization. Pedley used the following equation for simple hydrocarbons

$$\Delta H_a = \sum X_H + \sum X_C - \sum H_1 H_1 - \sum H_1 H_2 - \sum C_1 H_2 - \sum C_1 C_3 - \sum Y - V \quad (1)$$

X_H and X_C are, respectively, the energies of carbon–hydrogen and carbon–carbon bonds; $\sum H_1 H_1$ is the sum of repulsions between hydrogen atoms on the same carbon atom; $\sum H_1 H_2$ is the sum of repulsions between hydrogen atoms on adjacent carbon atoms; $\sum C_1 H_2$ is the sum of repulsions between carbon atoms and nonbonded hydrogen atoms; $\sum C_1 C_3$ is the sum of repulsions between nonbonded carbon atoms; and Y is the repulsion between a free electron of an atom and an electron of an adjacent atom. Finally, the total energy, ΔH_a, is corrected by the sum of the valence-stage energies of the atoms, V.

Pedley adopted Mulliken's equations for the bond energy

$$X_{ij} = \frac{A I_{ij} S_{ij}}{1 + S_{ij}} \quad (2)$$

and made a small change in the empirical constant in Mulliken's equation for the repulsion between two electrons in orbitals i and j

$$Y_{ij} = 0.25 A I_{ij} S_{ij}{}^2 \quad (3)$$

where A is an empirical constant, I_{ij} is the average ionization potential, and S_{ij} is the overlap integral. To simplify calculations, Pedley used an empirical equation to estimate repulsions between atoms. For H atoms

$$H_1 H_1 = \frac{B}{r_{HH}{}^4} \quad (4)$$

where B is an empirical constant and r_{HH} is the distance between H atoms. Equation 1 gives good results for alkanes and their radicals, such as CH_4, CH_3, CH_2, CH, C_2H_6, C_2H_5, C_3H_8, C_3H_7, etc. However, one runs into difficulties when the method is applied to alkenes, alkynes, aromatics, and nonhydrocarbons, which may also have double bonds, triple bonds, three-electron bonds, coordinate bonds, and resonance.

II. Bond Energies for Different Types of Bonds

1. Covalent, Two-Electron Bond. This is the usual type of bond in simple organic molecules. The equation developed by Mulliken[1] and also used by Pedley[2,3] is quite satisfactory

$$X_{12} = \frac{A I_{12} S_{12}}{1 + S_{12}} \quad (5)$$

2. One-Electron Bond. Mulliken[1] proposed that a one-electron bond has one-half of the bond energy of a two-electron bond

$$X_{12} = (^1/_2) \frac{A I_{12} S_{12}}{1 + S_{12}} \quad (6)$$

This has also given satisfactory results.

3. Coordinate Bond. A coordinate bond is formed when both bonding electrons come from one atom. For example, there may be a coordinate bond between a lone pair of electrons in an orbital of chlorine and a

(1) R. S. Mulliken, *J. Phys. Chem.*, **56**, 295 (1952).
(2) J. B. Pedley, *Trans. Faraday Soc.*, **57**, 1492 (1961).
(3) J. B. Pedley, *ibid.*, **58**, 23 (1962).

vacant orbital of carbon. A simplified derivation of the bond-energy equation can be made by considering a C atom, a Cl^{2+} ion, and two electrons. The wave function for an electron will be approximated as a linear combination of Slater atomic orbitals

$$\Psi = C_1\Psi_1 + C_2\Psi_2$$

The electron energy can then be obtained by solving the secular determinant

$$\begin{vmatrix} H_{11} - E & H_{12} - ES_{12} \\ H_{12} - ES_{12} & H_{22} - E \end{vmatrix} = 0 \quad (7)$$

It is helpful to define the following symbols

$$\bar{E} = {}^1\!/_2(H_{11} + H_{22}) \quad (8)$$

$$\delta = {}^1\!/_2(H_{22} - H_{11}) \quad (9)$$

$$\beta = H_{12} - S_{12}\bar{E} \quad (10)$$

which can be used to modify the determinant to

$$\begin{vmatrix} \bar{E} - E - \delta & \beta + S_{12}(\bar{E} - E) \\ \beta + S_{12}(\bar{E} - E) & \bar{E} - E + \delta \end{vmatrix} = 0$$

This can be solved for the electron energy

$$E = \bar{E} + \frac{-\beta S_{12} \pm \beta\sqrt{1 + (1 - S_{12}{}^2)\delta^2/\beta^2}}{1 - S_{12}{}^2} \quad (11)$$

The Hamiltonian for electron 1 can be written as

$$H = h_1 + u_2 + u_{12}$$

where h_1 is the Hamiltonian with respect to the C atom, u_2 is the potential energy with respect to Cl^{2+}, and u_{12} is the potential energy with respect to electron 2. Then

$$H_{11} = \int\Psi_1 h_1\Psi_1 \, d\tau + \int\Psi_1 u_2\Psi_1 \, d\tau + \int\Psi_1 u_{12}\Psi_1 \, d\tau \quad (12)$$

where

$$u_{12} = \int\Psi\frac{e^2}{r_{12}}\Psi \, d\tau$$

Mulliken[4] has approximated $\Psi\Psi$ by the expression

$$\Psi\Psi = {}^1\!/_2(1 - Q)\Psi_1\Psi_1 + {}^1\!/_2(1 + Q)\Psi_2\Psi_2$$

where $Q = C_2{}^2 - C_1{}^2$, which is an indication of the polarity of the bond. Defining also the symbols

$$P_{11} = \int\Psi_1\Psi_1\frac{e^2}{r_{12}}\Psi_1\Psi_1 \, d\tau$$

and

$$P_{12} = \int\Psi_1\Psi_2\frac{e^2}{r_{12}}\Psi_1\Psi_2 \, d\tau$$

one obtains

$$\int\Psi_1 u_{12}\Psi_1 \, d\tau = {}^1\!/_2(1 - Q)P_{11} + {}^1\!/_2(1 + Q)P_{12}$$

which can be substituted into eq 12 to give

$$H_{11} = E_1 + \int\Psi_1 u_2\Psi_1 \, d\tau + \\ {}^1\!/_2(1 - Q)P_{11} + {}^1\!/_2(1 + Q)P_{12} \quad (13)$$

where $E_1 = \int\Psi_1 h_1\Psi_1 \, d\tau$ is the kinetic plus the potential energy of electron 1 with respect to the C atom. Similarly

$$H_{22} = E_2 + \int\Psi_2 u_1\Psi_2 \, d\tau + \\ {}^1\!/_2(1 - Q)P_{12} + {}^1\!/_2(1 + Q)P_{22} \quad (14)$$

Here, u_1 is the potential of electron 2 in the field of a neutral C atom. This is nearly zero: $u_1 \approx 0$. One can write

$$\int\Psi_1 u_2\Psi_1 \, d\tau = \int\Psi_1 v_2\Psi_1 \, d\tau - \int\Psi_1\Psi_2\frac{e^2}{r_{12}}\Psi_1\Psi_2 \, d\tau$$

where v_2 is the potential energy of electron 2 with respect to a Cl^+ ion. As a rough approximation

$$\int\Psi_1 v_2\Psi_1 \, d\tau = -\int\Psi_1\frac{e^2}{r}\Psi_1 \, d\tau = -\frac{e^2}{r}$$

where r is the distance between C and Cl^{2+}. In that case

$$\int\Psi_1 u_2\Psi_1 \, d\tau = -\frac{e^2}{r} - P_{12}$$

Equations 13 and 14 become

$$H_{11} = E_1 - \frac{e^2}{r} - P_{12} + \\ {}^1\!/_2(1 - Q)P_{11} + {}^1\!/_2(1 + Q)P_{12}$$

$$H_{22} = E_2 + {}^1\!/_2(1 - Q)P_{12} + {}^1\!/_2(1 + Q)P_{22}$$

The coordinate bond is frequently weak. Both electrons will be largely a part of the Cl atom and $Q \approx 1$. Then

$$H_{11} = E_1 - \frac{e^2}{r}$$

$$H_{22} = E_2 + P_{22}$$

where E_2 is the kinetic plus the potential energy of electron 2 with respect to Cl^{2+}. P_{22} is the potential energy of electron 2 with respect to electron 1. The sum of these is just the opposite of the ionization potential of Cl

$$E_2 + P_{22} = -I_{Cl}$$

E_1 is the kinetic plus the potential energy of electron 1 with respect to C. This is the electron affinity of C

$$E_1 = A_e$$

Then

$$H_{11} = A_e - \frac{e^2}{r} \qquad H_{22} = -I_{Cl}$$

(4) R. S. Mulliken, *J. Chim. Phys.*, **46**, 497 (1949).

and

$$2\delta = -I_{Cl} - A_e + \frac{e^2}{r}$$

$$2\bar{E} = -I_{Cl} + A_e - \frac{e^2}{r}$$

The ionization potential is the ground-state ionization potential, I_{Cl}^0, corrected for the difference in valence-state energies between Cl^+ and Cl

$$I_{Cl} = I_{Cl}^0 + V(Cl^+) - V(Cl)$$

Similarly

$$A_e = A_e^0 + V(C^-) - V(C)$$

The final expressions for δ and $\bar{E}$ are then

$$2\delta = -I_{Cl}^0 - A_e^0 + \frac{e^2}{r} -$$
$$V(Cl^+) + V(Cl) - V(C^-) + V(C) \quad (15)$$

$$2\bar{E} = -I_{Cl}^0 + A_e^0 - \frac{e^2}{r} -$$
$$V(Cl^+) + V(Cl) + V(C^-) - V(C) \quad (16)$$

Mulliken[1] found for the covalent bond that β could be approximated by

$$\beta = -\tfrac{1}{2}AIS \quad (17)$$

The same relationship will be assumed for the co-ordinate bond. In that case, eq 11 for the lower-energy state becomes

$$E = \bar{E} + \frac{AI_{Cl}S_{12}^2 - \sqrt{A^2 I_{Cl}^2 S_{12}^2 + (1 - S_{12}^2)(2\delta)^2}}{2(1 - S_{12}^2)}$$

The bond energy is

$$X_2 = E_1^0 + E_2^0 - 2E$$

where E_1^0 ($=E_2^0$) is the energy of electron when it is not bonded, *i.e.*, the energy of the electron as part of Cl^+

$$E_1^0 = E_2^0 = -I_{Cl}^0 - V(Cl^+) + V(Cl)$$

The equation for the bond energy becomes finally

$$X_2 = 2\delta +$$
$$\frac{-AI_{Cl}S_{12}^2 + \sqrt{A^2 I_{Cl}^2 S_{12}^2 + (1 - S_{12}^2)(2\delta)^2}}{1 - S_{12}^2} \quad (18)$$

where 2δ can be calculated from eq 15.

4. Three-Electron Bond. Three-electron bonds are usually weak. They may involve two electrons from a lone-pair electron orbital of one atom and a single electron from an orbital of a second atom. The Hamiltonian for electron 1 is

$$H = h_1 + u_2 + 2u_{12}$$

and

$$H_{11} = E_1 + \int\Psi_1 u_2\Psi_1 \, d\tau + 2\int\Psi_1 u_{12}\Psi_1 \, d\tau$$

Similarly

$$H_{22} = E_2 + \int\Psi_2 u_1\Psi_2 \, d\tau + 2\int\Psi_2 u_{12}\Psi_2 \, d\tau$$

As an example, the system consisting of C^+, Cl^{2+}, and three electrons will be considered. The potential energy of electron 1 in the field of a neutral Cl atom is

$$v_2 = u_2 + 2\int\Psi_2\frac{e^2}{r_{12}}\Psi_2 \, d\tau$$

This is small and will be neglected: $v_2 \approx 0$. Then

$$\int\Psi_1 u_2\Psi_1 \, d\tau = -2P_{12}$$

The potential energy of electron 2 in the field of a neutral C atom is

$$v_1 = u_1 + \int\Psi_1\frac{e^2}{r_{12}}\Psi_1 \, d\tau \approx 0$$

or

$$\int\Psi_2 u_1\Psi_2 \, d\tau = -P_{12}$$

As before

$$\int\Psi_1 u_{12}\Psi_1 \, d\tau = \tfrac{1}{2}(1 - Q)P_{11} + \tfrac{1}{2}(1 + Q)P_{12}$$
$$\int\Psi_2 u_{12}\Psi_2 \, d\tau = \tfrac{1}{2}(1 - Q)P_{12} + \tfrac{1}{2}(1 + Q)P_{22}$$

Then

$$H_{11} = E_1 - 2P_{12} + (1 - Q)P_{11} + (1 + Q)P_{12}$$
$$H_{22} = E_2 - P_{12} + (1 - Q)P_{12} + (1 + Q)P_{22}$$

This gives

$$2\delta = E_2 - E_1 + (1 - 2Q)P_{12} +$$
$$(1 + Q)P_{22} - (1 - Q)P_{11}$$

Let

$$\eta = \tfrac{1}{2}(P_{11} + P_{22}) - P_{12}$$

Then

$$2\delta = E_2 - E_1 - (1 - 2Q)\eta - \tfrac{1}{2}P_{11} + \tfrac{3}{2}P_{22}$$

Usually η will be small. $Q = 0$ for a covalent bond involving one electron from each atom, while $Q = 1$ when there is no bond. In the present case, Q will probably be close to 0.5. Therefore, $(1 - 2Q)\eta$ will be close to zero and

$$2\delta = E_2 - E_1 - \tfrac{1}{2}P_{11} + \tfrac{3}{2}P_{22}$$

The various terms on the right-hand side of the equation can be written in terms of ionization potentials and electron affinities: $E_2 = -I_{Cl^+}$, the second ionization potential of Cl; $E_2 + P_{22} = -I_{Cl}$; $E_1 = -I_C$; and $E_1 + P_{11} = A_e$. Using ground-state values

$$2\delta = \tfrac{1}{2}[I_{Cl^+}^0 - 3I_{Cl}^0 +$$
$$I_C^0 - A_e^0 + V(Cl^{2+}) - 4V(Cl^+) +$$
$$3V(Cl) + V(C^+) - V(C^-)] \quad (19)$$

Equation 11 for the electron energy still holds. This gives for the total energy of the three electrons

$$E_t = 3\bar{E} + \frac{-3\beta S_{12} + \beta\sqrt{1 + (1 - S_{12}{}^2)\delta^2/\beta^2}}{1 - S_{12}{}^2} \quad (20)$$

where $\beta = -\frac{1}{2}AI_{12}S_{12}$. In the derivation of the equation for the coordinate bond, $\bar{E}$ was determined. However, a simplification will be used with eq 20. There is no bond when $S_{12} = 0$

$$E_1{}^0 + E_2{}^0 + E_3{}^0 = 3\bar{E} - \delta$$

The bond energy is

$$X_3 = E_1{}^0 + E_2{}^0 + E_3{}^0 - E_t$$

Therefore

$$X_3 = -\delta +$$
$$\frac{-3AI_{12}S_{12}{}^2 + \sqrt{A^2I_{12}{}^2S_{12}{}^2 + (1 - S_{12}{}^2)(2\delta)^2}}{2(1 - S_{12}{}^2)} \quad (21)$$

The absolute value of δ, calculated from eq 19, should be used.

5. Resonance. Resonance occurs when there are different molecular structures which have nearly the same energy. An example is CCl_3 where the three-electron bond between C and Cl may be considered to resonate between the three Cl atoms. Only the three-electron bonds will be considered here. Each Cl atom contributes two electrons and the C atom contributes one electron. There are seven electrons distributed over four orbitals. Each orbital can be represented by an approximate wave function

$$\Psi = C_1\Psi_1 + C_2\Psi_2 + C_3\Psi_3 + C_4\Psi_4$$

where Ψ_1, Ψ_2, Ψ_3, and Ψ_4 are wave functions for the atomic orbitals.

The secular determinant becomes, after appropriate simplifications

$$\begin{vmatrix} \bar{E} - \delta - E & \beta + S_{12}(\bar{E} - E) \\ \beta + S_{12}(\bar{E} - E) & \bar{E} + \delta - E \\ \beta + S_{12}(\bar{E} - E) & 0 \\ \beta + S_{12}(\bar{E} - E) & 0 \end{vmatrix}$$

$$\begin{vmatrix} \beta + S_{12}(\bar{E} - E) & \beta + S_{12}(\bar{E} - E) \\ 0 & 0 \\ \bar{E} + \delta - E & 0 \\ 0 & \bar{E} + \delta - E \end{vmatrix} = 0$$

which can be worked out to give

$$(\bar{E} - \delta - E)(\bar{E} + \delta - E)^3 -$$
$$3(\bar{E} + \delta - E)^2[\beta + S_{12}(\bar{E} - E)]^2 = 0$$

This equation has four solutions corresponding to the energies of the four orbitals. Two of these are the same

$$E = \bar{E} + \delta \quad (22)$$

and the other two give after substitution of the expression for β

$$E = \bar{E} +$$
$$\frac{3AI_{12}S_{12}{}^2 \pm \sqrt{3A^2I_{12}{}^2S_{12}{}^2 + (1 - 3S_{12}{}^2)(2\delta)^2}}{2(1 - 3S_{12}{}^2)} \quad (23)$$

There are seven electrons. Six of these can go in the three lower energy orbitals and one is left for the highest energy orbital. The total energy is, therefore

$$E_t = 7\bar{E} + 4\delta +$$
$$\frac{9AI_{12}S_{12}{}^2 - \sqrt{3A^2I_{12}{}^2S_{12}{}^2 + (1 - 3S_{12}{}^2)(2\delta)^2}}{2(1 - 3S_{12}{}^2)}$$

There are no three-electron bonds if $S_{12} = 0$. Therefore

$$E^0 = 7\bar{E} + 3\delta$$

The bond energy is then

$$X_{R3} = E^0 - E_t$$

or

$$X_{R3} = -\delta +$$
$$\frac{-9AI_{12}S_{12}{}^2 + \sqrt{3A^2I_{12}{}^2S_{12}{}^2 + (1 - 3S_{12}{}^2)(2\delta)^2}}{2(1 - 3S_{12}{}^2)} \quad (24)$$

where δ is the absolute value of the result from eq 19. Comparison of eq 21 and 24 shows that the three-electron bond energy with resonance, X_{R3}, is similar to the three-electron bond energy without resonance, X_3, except that $S_{12}{}^2$ is replaced by $3S_{12}{}^2$.

Another case of interest is that where resonance occurs between two structures, such as in the CCl_2 triplet. In a similar fashion, as shown above, one can derive

$$X_{R3} = -\delta +$$
$$\frac{-6AI_{12}S_{12}{}^2 + \sqrt{2A^2I_{12}{}^2S_{12}{}^2 + (1 - 2S_{12}{}^2)(2\delta)^2}}{2(1 - 2S_{12}{}^2)} \quad (25)$$

Resonance can also occur with coordinate bonds, such as in the CCl_2 singlet. In that case

$$X_{R2} = 2\delta +$$
$$\frac{-2AI_{Cl}S_{12}{}^2 + \sqrt{2A^2I_{Cl}{}^2S_{12}{}^2 + (1 - 2S_{12}{}^2)(2\delta)^2}}{1 - 2S_{12}{}^2} \quad (26)$$

where δ is given by eq 15.

6. Double and Triple Bonds. The presence of a π bond in addition to a σ bond, such as in a double bond, or two π bonds in addition to a σ bond, such as in a triple bond, leads to a complication. Mulliken[1] calculated separate bond energies for the σ bond and the π bond from eq 5 and added these to obtain the total bond energy. However, he found it necessary to use an empirical constant, A_π, for the π bond different from

A_σ for the σ bond to get meaningful results. This is not satisfactory.

The double bond between atom A, having orbitals 1 and 2, and atom B, having orbitals 3 and 4, will be considered. There is a σ bond, owing to overlap of orbitals 1 and 3, and a π bond, owing to the overlap of orbitals 2 and 4. An approximate wave function for the system of four orbitals and four electrons will be

$$\Psi = C_1\Psi_1 + C_2\Psi_2 + C_3\Psi_3 + C_4\Psi_4$$

The total energy of the σ and π bonds can be derived in the usual manner, giving

$$X_{\sigma\pi} = \frac{AI_{13}S_{13}}{1 + S_{13}} + \frac{AI_{24}S_{24}}{1 + S_{24}}$$

This would make it appear that it is possible to calculate separate σ- and π-bond energies from Mulliken's equation (eq 5) and to add these numerically. It should be noted, however, that the bond energies are considered relative to the energies of the atoms in their valence states. Therefore, the valence-state energies of the atoms are substracted in eq 1. The valence-state energy includes interactions between the electrons which belong to a particular atom. However, the interaction, H_{12}, between the electrons in orbitals 1 and 2 of atom A has been included in the derivation of the equation for the bond energy. The same holds for the interaction, H_{34}, of the electrons in orbitals 3 and 4 of atom B. These interactions should not be included again in the valence-state energies of atoms A and B. However, it is more convenient to use conventional valence-state energies and to apply the correction to the bond-energy equation. The interactions are exchange integrals, $^1/_2K_{ij}$. Applying the exchange-integral corrections

$$X_{\sigma\pi} = X_\sigma + X_\pi - \frac{1}{2}K_{12} - \frac{1}{2}K_{34} \qquad (27)$$

where

$$X_\sigma = \frac{AI_{13}S_{13}}{1 + S_{13}}$$

and

$$X_\pi = \frac{AI_{24}S_{24}}{1 + S_{24}}$$

For a triple bond, a similar equation is obtained

$$X_{\sigma\pi} = X_\sigma + 2X_\pi - \frac{1}{2}(K_{12} +$$
$$K_{13} + K_{23} + K_{45} + K_{46} + K_{56}) \qquad (28)$$

where atom A has bonding electrons in orbitals 1–3 and atom B has bonding electrons in orbitals 4–6.

III. Calculation of Energies of Atomization

The general expression for the energy of atomization of binary compounds can be written by expanding eq 1 to include the different types of bonds which have been

discussed earlier. Although the following equation is written for a compound of the type C_2Cl_n, the same type of expression can be used for other compounds as well

$$\Delta H_a = \sum X_{Cl} + X_C + \sum X_2 + \sum X_3 - \sum Cl_1Cl_1 -$$
$$\sum Cl_1Cl_2 - \sum C_1Cl_2 - \sum Y - V \qquad (29)$$

where X_{Cl} is a covalent carbon–chlorine bond which can be calculated from eq 5. The carbon–carbon bond, X_C, may include both σ and π bonds

$$X_C = X_\sigma + \sum X_\pi - \frac{1}{2}\sum K \qquad (30)$$

The coordinate bond is represented by X_2, which, if present, can be calculated from eq 18. However, X_{R2}, as calculated from eq 26, should be used if resonance can occur. X_3 represents possible three-electron bonding. This is calculated from eq 21. Resonance can be included by using X_{R3} from eq 24 or 25 in place of X_3. Cl_1Cl_1 represents a repulsion between Cl atoms on the same C atom. Cl_1Cl_2 is a repulsion between Cl atoms on adjacent C atoms, and C_1Cl_2 is a repulsion between a C atom and a Cl atom on the adjacent C atom. These repulsions can be calculated from expressions of the type of eq 4. Y can be calculated with eq 3. Strictly speaking, $\sum Y$ should include all electron interactions which have not been accounted for in the bonds or in the valence-state energy. However, it is simpler to include only the electron repulsions which cannot be conveniently accounted for otherwise. For example, chlorine–chlorine repulsions have already been accounted for in the Cl_1Cl_1 and Cl_1Cl_2 terms. Some of the carbon–chlorine interactions can be included in the empirical bond-energy constant, A. However, Y should include repulsions between free C electrons and electrons of the Cl atoms which are bonded to the C atom. Again, C–Cl interactions for nonbonded atoms can be accounted for in the C_1Cl_2 terms. Finally, Y should also include electron repulsions of adjacent C atoms.

The valence-state energy, V, for C_2Cl_n is

$$V = 2V(C) + nV(Cl) \qquad (31)$$

where the valence-state energies of the atoms, $V(C)$ and $V(Cl)$, can be calculated by the method of Van Vleck.[5] Many of the atomic constants, needed for the calculation of V, have been listed by Pilcher and Skinner[6] or Hinze and Jaffe.[7] The constants used in this study were calculated directly from atomic energy levels tabulated by Moore[8] using the procedure given by Slater.[9] Exchange integrals, K, are used both in the

(5) J. H. Van Vleck, *J. Chem. Phys.*, **2**, 20 (1934).

(6) G. Pilcher and H. A. Skinner, *J. Inorg. Nucl. Chem.*, **24**, 937 (1962).

(7) J. Hinze and H. H. Jaffe, *J. Chem. Phys.*, **38**, 1834 (1963).

(8) C. E. Moore, "Atomic Energy Levels," National Bureau of Standards Circular 467, U. S. Government Printing Office, Washington, D. C., 1949.

(9) J. C. Slater, "Quantum Theory of Atomic Structure," Vol. 1, McGraw-Hill Book Co., Inc., New York, N. Y., 1960.

valence-state energy calculations and in some of carbon–carbon bond calculations (see eq 30). For electrons in orbitals i and j

$$K_{ij} = \alpha_i^2 \alpha_j^2 (F_0^{ss} + F_0^{pp} -$$
$$2F_0^{sp} + 4F_2^{pp} - 4G_1^{sp}) +$$
$$(\alpha_i^2 + \alpha_j^2)(G_1^{sp} - 3F_2^{pp}) + 3F_2^{pp} \quad (32)$$

where F_0^{ss}, F_0^{sp}, F_0^{pp}, F_2^{pp}, and G_1^{sp} are the coulomb and exchange integrals for electrons in pure s and p orbitals. The degree of hybridization, α_i^2, is that from the wave function for the hybridized orbital i

$$\Psi_i = \alpha_i \Psi(s) + \sqrt{(1 - \alpha_i^2)} \Psi(p) \quad (33)$$

Another convenient method of expressing eq 33 is

$$\Psi_i = \frac{\Psi(s) + \lambda_i \Psi(p)}{\sqrt{1 + \lambda_i^2}} \quad (34)$$

Therefore

$$\alpha_i^2 = \frac{1}{1 + \lambda_i^2}$$

The detailed calculations of the bond energies, X, and repulsion energies, Y, require a knowledge of overlap integrals, S_{12}, and ionization potentials, I_{12}. A general expression for the overlap integral is

$$S_{12} = \{ S(2s, 3s) + \lambda_1 S(2p\sigma, 3s) \cos \gamma_1 +$$
$$\lambda_2 S(2s, 3p\sigma) \cos \gamma_2 +$$
$$\lambda_1 \lambda_2 [S(2p\sigma, 3p\sigma) \cos \gamma_1 \cos \gamma_2 +$$
$$S(2p\pi, 3p\pi) \sin \gamma_1 \sin \gamma_2] \} /$$
$$\sqrt{(1 + \lambda_1^2)(1 + \lambda_2^2)} \quad (35)$$

where γ is the angle which a p orbital makes with respect to the bond axis. Equation 35 is expressed in terms of overlap integrals between pure s and pure p orbitals, such as $S(2s, 3s)$. Approximate Slater orbitals have been used in this study. Mulliken[10] has tabulated equations and numerical data for the appropriate integrals which are needed. As proposed by Mulliken[1] and Pedley,[2] the ionization potential is the mean value for the two electrons in each of their atomic orbitals

$$I_{12} = \frac{1}{2}(I_1 + I_2) \quad (36)$$

The determination of the bond-energy constants, A, and the repulsion constants, B remains. They should be calculated from the known energies of atomization (or heats of formation) of some of the compounds. For compounds of the type C_2Cl_n, a bond-energy constant A_C for C–C bonds, A_{Cl} for C–Cl bonds, a repulsion constant B_C for C–Cl repulsions, and B_{Cl} for Cl–Cl repulsions need to be estimated. This will be explained in more detail below. An approximate estimate of the bond lengths is necessary to calculate the overlap integrals and the repulsions between atoms. Bond lengths

are usually fairly well known or can easily be estimated. A small error can be made without significant effect on the prediction of the energy of atomization.

IV. Results

1. System: CH_4–CH_3–CH_2–CH. Calculations for methane and its radicals were made by Pedley[3] but were repeated in this study to obtain a consistent set of constants, A_H and B_H, for further calculations. Heats of formation listed in the JANAF Tables[11] were used to obtain energies of atomization and bond distances for CH_4, $\Delta H_a(298°K) = 17.223$ eV/g-mol and $r_{C–H} = 1.094$ Å, and for CH_3, $\Delta H_a = 12.803$ eV and $r_{C–H} = 1.079$ Å. These energies of atomization could be used to calculate $A_H = 1.131$ and $B_H = 2.833$. Calculations were then made to predict energies of atomization as a function of the hybridization coefficient, λ, for the CH_2 singlet, the CH_2 triplet, and CH. Pedley's finding that the CH_2 triplet is the stable state was confirmed and ΔH_a was calculated to have a maximum of 7.862 eV for $\lambda = 1$ (bond angle of 180°) at a given bond distance of 1.03 Å.[12] Calculations for CH gave $\Delta H_a = 3.510$ eV for $\lambda = 1.84$ at a bond distance of 1.113 Å.[13]

2. System: C_2H_6–C_2H_5–C_2H_4–C_2H_3–C_2H_2–C_2H–C_2. This is a more complex system which gave Mulliken[1] some difficulties and which was not completely covered by Pedley[2,3] because of the π-bond energy. There is a second carbon atom and four empirical constants are needed. The value of $A_H = 1.131$ can be used from the previous calculations. It is not wise to use the previously determined value of B_H, since the H–H repulsions will be affected by the electrons of the added C atom. For example, the C electrons may cause some shielding which would reduce B_H. A new value of B_H should be determined. In addition, a bond-energy constant, A_C, for the C–C bond and a repulsion constant, B_C, for the repulsions between nonbonded C and H atoms are needed. Values of A_C, B_H, and B_C can be calculated from the known energies of atomization of C_2H_6, C_2H_4, and C_2H_2.

The following bond distances were used in the calculations: C_2H_6: C–C, 1.54 Å; C–H, 1.100Å;[14] C_2H_5: C–C, 1.54 Å; C_1–H_1, 1.100 Å; C_2–H_2, 1.095 Å (estimated); C_2H_4: C–C, 1.336 Å; C–H, 1.085 Å;[14] C_2H_3: C–C, 1.322 Å; C_1–H_1, 1.085 Å; C_2–H_2, 1.08 Å (estimated); C_2H_2: C–C, 1.205 Å; C–H, 1.059 Å;[14] C_2H: C–C, 1.220 Å; C–H, 1.062 Å;[15] C_2: C–C, 1.242 Å.[16]

(10) R. S. Mulliken, *et al.*, *J. Chem. Phys.*, **17**, 1248 (1949).

(11) "JANAF Thermochemical Tables," The Thermal Research Laboratory, Dow Chemical Co., Midland, Mich., 1960–1966.

(12) G. Herzberg, *Proc. Roy. Soc.*, A262, 291 (1961).

(13) G. Herzberg, "Molecular Spectra and Molecular Structure. I. Spectra of Diatomic Molecules," 2nd ed, D. Van Nostrand Co., Inc., New York, N. Y., 1950.

(14) L. E. Sutton, "Tables of Interatomic Distances and Configuration in Molecules and Ions," The Chemical Society, London, 1958. Also, Supplement 1956–1959, publ. 1965.

Table I: Terms for the Energy of Atomization (298°K) of Hydrocarbons

	λ_1	λ_2	X_{H_1}	X_{H_2}	X_σ	ΣX_π	$\frac{1}{2}\Sigma K$	ΣHH	ΣCH	ΣY	V	ΔH_a
C_2H_6	1.94	1.94	6.228	6.228	9.838	...	...	1.779	1.938	0.505	13.738	29.249
C_2H_5	1.94	1.57	6.228	6.610	10.070	...	...	1.107	1.503	0.460	13.894	25.011
C_2H_4	1.62	1.62	6.582	6.582	11.416	3.584	1.310	0.573	1.491	0.552	14.083	23.320
C_2H_3	1.62	1.06	6.582	7.328	11.823	3.666	1.378	0.256	0.999	0.475	14.388	18.486
C_2H_2	1.07	1.07	7.376	7.376	12.625	8.497	3.462	0.018	0.594	0.115	14.695	16.989
C_2H	1.23	1.06	7.382	...	12.492	6.334	2.336	...	0.288	0.527	11.395	11.661
C_2	1.27	1.27	...	...	12.191	4.156	1.199	...	...	0.985	7.808	6.354

The heat of formation of C_2H_6 was obtained from API Research Project 44[17] and was converted to ΔH_a(298°K) = 29.252 eV. Heats of formation of C_2H_4 and C_2H_2 were obtained from the JANAF Tables[11] and were converted to values of H_a = 23.315 eV and ΔH_a = 16.988 eV, respectively. Trial values of A_C, B_C, and B_H were tried to maximize ΔH_a as a function of the hybridization coefficients of the C orbitals until calculated and actual ΔH_a values finally matched. This gave A_C = 1.535, B_H = 2.222, and B_C = 7.809. Predicted energies of atomization were then obtained for C_2H_5, C_2H_3, C_2H, and C_2. The energy terms which appear in eq 29 for ΔH_a, using H in place of Cl, are shown in Table I for the optimum values of the hybridization coefficients, λ_1 and λ_2, for the two C atoms.

3. System: CCl_4–CCl_3–CCl_2–CCl. This is a more complex system which has not been covered in the literature, since the Cl atom has 17 electrons, while H has only 1. However, only the 7 electrons in the 3s and 3p orbitals of the valence shell are of interest here. Some hybridization of the bonding p electron and the lone-pair s electrons should be considered, since this may lead to stronger bonding. Again, the bond-energy constant, A_{Cl}, and the repulsion constant, B_{Cl}, have to be determined from the known energies of atomization of CCl_4 and CCl_3. Values of ΔH_a = 13.57 eV and r_{C-Cl} = 1.760 Å were obtained for CCl_4 from the JANAF Tables.[11] Results of Farmer,[18] Reed,[19] Goldfinger,[20] Fox,[21] and Benson[22] were averaged to obtain the heat of formation of 18 kcal/g-mol (ΔH_a = 10.41 eV) for CCl_3. A bond distance of 1.74 Å was estimated. Values of A_{Cl} = 1.237 and B_{Cl} = 34.43 were calculated from the energy equations for CCl_4 and CCl_3. Predictions of ΔH_a were then made for the CCl_2 triplet, the CCl_2 singlet, and CCl. Estimated bond distances of 1.71 Å for the CCl_2 triplet and 1.67 Å for the CCl_2 singlet were used. Verma and Mulliken[23] have determined a bond distance of 1.645 Å for CCl. Values of the energy terms which make up ΔH_a are shown in Table II for the optimum values of the hybridization coefficient, λ, of the C atom and the degree of hybridization, α^2, of the Cl atoms. For weak hybridization of Cl, it is more convenient to use α^2 because λ goes to infinity when there is no hybridization of the 3p orbital of Cl.

It is of interest to note in Table II that the three-electron bond in CCl_3 gives negative energy which indicates that there is a slight repulsion. This is not surprising, since three-electron bonds form only when the energy difference, δ, between the electrons is small. The three-electron bond is either weak or gives a repulsion when the energy difference is appreciable. Table II shows also that the CCl_2 singlet is more stable than the CCl_2 triplet and is, therefore, the ground state. This differs from CH_2 where the triplet is the ground state. The difference is largely due to the fact that that a coordinate bond can be formed in CCl_2 but not in CH_2.

4. System: C_2Cl_6–C_2Cl_5–C_2Cl_4–C_2Cl_3–C_2Cl_2–C_2Cl. The calculations for this system include again a second carbon atom and require four empirical constants. The bond-energy constant for the C–Cl bonds, A_{Cl} = 1.237, and for the C–C bond, A_C = 1.535, have already been determined in the calculations for the CCl_4 system and the C_2H_6 system. The repulsion constants for Cl–Cl repulsions, B_{Cl}, and for C–Cl repulsions, B_C, remain to be estimated by substituting known energies of atomization into the equations for C_2Cl_6 and C_2Cl_5.

The following bond distances have been used in the calculations: C_2Cl_6: C–C, 1.56 Å; C–Cl, 1.77 Å;[24] C_2Cl_5: C–C, 1.56 Å; C_1–Cl_1, 1.77 Å; C_2–Cl_2, 1.75 Å (estimated); C_2Cl_4: C–C, 1.33 Å; C–Cl, 1.72 Å;[14] C_2Cl_3: C–C, 1.33 Å; C_1–Cl_1, 1.71 Å; C_2–Cl_2, 1.69 Å (estimated); C_2Cl_2: C–C, 1.195 Å; C–Cl, 1.64 Å;[25] C_2Cl: C–C, 1.22 Å; C–Cl, 1.64 Å (estimated). Puyo[26]

(15) M. N. Plooster and T. B. Reed, *J. Chem. Phys.*, **31**, 66 (1959).

(16) E. A. Ballik and D. A. Ramsay, *Astrophys. J.*, **137**, 84 (1963).

(17) "Selected Values of Properties of Hydrocarbons and Related Compounds," American Petroleum Institute Research Project 44, Thermodynamics Research Center, Texas A & M University, College Station, Texas, 1952.

(18) J. B. Farmer, *et al.*, *J. Chem. Phys.*, **24**, 348 (1956).

(19) R. I. Reed and W. Snedden, *Trans. Faraday Soc.*, **54**, 301 (1958).

(20) P. Goldfinger and G. Martens, *ibid.*, **57**, 2220 (1961).

(21) R. E. Fox and R. K. Curran, *J. Chem. Phys.*, **34**, 1595 (1961).

(22) S. W. Benson, *ibid.*, **43**, 2044 (1965).

(23) R. D. Verma and R. S. Mulliken, *J. Mol. Spectrosc.*, **6**, 419 (1961).

(24) A. Almenningen, *et al.*, *Acta Chem. Scand.*, **18**, 603 (1964).

(25) O. Hassel and H. Viervoll, *ibid.*, **1**, 149 (1947).

(26) J. Puyo, *et al.*, *Compt. Rend.*, **256**, 3471 (1963).

Table II: Terms for the Energy of Atomization (298°K) of Chlorocarbons

	$\lambda_1(C)$	$\lambda_3(C)$	$\alpha^3(Cl)$	$\alpha_2^2(Cl)$	X_{Cl}	X_{Cl_2}	X_C	ΣX_2	ΣX_3	$\Sigma ClCl$	ΣCCl	ΣY	V	ΔH_a
CCl₄	1.732	…	0.032	…	6.201	…	…	…	…	3.028	…	…	8.203	13.573
CCl₃	1.414	…	0.034	…	6.596	…	…	…	-0.029	1.252	…	…	8.095	10.410
CCl₂ (triplet)	1.000	…	0.037	…	7.192	…	…	…	0.234	0.252	…	…	7.860	6.505
CCl₂ (singlet)	1.860	…	0.042	…	6.744	…	…	1.233	…	0.666	…	0.816	5.223	8.017
CCl	1.800	…	0.042	…	6.922	…	…	0.749	0.139	…	…	0.409	2.963	4.439
C₂Cl₆	2.08	2.08	0.030	0.030	5.901	5.901	10.284	…	…	1.854	3.816	0.386	15.782	23.852
C₂Cl₅	2.08	1.66	0.030	0.030	5.901	6.291	10.406	…	0.132	1.149	2.988	0.367	15.591	20.729
C₂Cl₄	1.71	1.71	0.034	0.034	6.401	6.401	14.029	…	…	0.666	2.940	0.487	15.613	19.927
C₂Cl₃	1.70	1.10	0.035	0.035	6.455	7.160	14.222	…	0.194	0.274	1.972	0.418	15.552	16.270
C₂Cl₂	1.10	1.10	0.041	0.041	7.417	7.417	17.851	…	…	0.031	1.230	0.102	15.585	15.737
C₂Cl	1.23	1.10	0.040	…	7.406	…	16.531	…	…	…	0.594	0.513	11.830	11.001

and Goldfinger[20] have given heats of formation of C_2Cl_6 for which $\Delta H_a = 23.849$ eV. The heat of formation of C_2Cl_5 was obtained from Goldfinger and Martens'[20] data and was converted to $\Delta H_a = 20.726$ eV. Using these values, trial-and-error calculations were made to maximize ΔH_a with respect to hybridization of C and Cl orbitals for assumed values of B_{Cl} and B_C until agreement was reached. The results were $B_{Cl} = 12.295$ and $B_C = 39.742$. Energies of atomization were then predicted for C_2Cl_4, C_2Cl_3, C_2Cl_2, and C_2Cl. The energy terms of eq 29 are listed for optimum values of $\lambda(C)$ and $\alpha^2(Cl)$ in Table II.

5. System: NH_3–NH_2–NH. The nitrogen atom has five electrons in the valence shell. Hybridization can take place between the two electrons of the 2s orbital and the three electrons of the 2p orbitals. NH_3 will have some hybridization of all three 2p orbitals with the 2s orbital. However, NH_2 will show hybridization of only two of the 2p orbitals with the 2s orbital, since this requires less valence-state energy than for NH_3. For the same reason, NH will have hybridization between one 2p orbital and the 2s orbital.

The JANAF Tables[11] were used to obtain $\Delta H_a = 12.002$ eV for NH_3 at 0°K and a bond distance of 1.012 Å. Kerr and coworkers[27] have determined the heat of formation of NH_2 at 0°K for which $\Delta H_a = 7.653$ eV. The bond distance of 1.025 Å was taken from the JANAF Tables. Using this information, the following bond-energy and repulsion constants were determined: $A = 1.335$ and $B = 6.576$. The energy of atomization of NH was then predicted for a bond distance of 1.038 Å listed in the JANAF Tables. The energy terms are tabulated in Table III for the optimum values of λ.

Table III: Terms for the Energy of Atomization (0°K) of NH₃, NH₂, and NH

	λ	X_N	ΣHH	ΣY	V	ΔH_a
NH₃	1.546	8.630	2.336	0.245	11.307	12.002
NH₂	1.604	8.610	0.773	0.721	8.073	7.653
NH	1.883	8.176	…	0.918	3.664	3.593

V. Discussion

The utility of these simplified quantum-mechanical calculations can best be determined by comparing the predicted results with measured values or with other predictions reported in the literature. It is easier to compare heats of formation, since these are usually reported. Table IV shows the predicted heats of formation, corresponding to the energies of atomization, and the actual values.

The heat of formation of CH_2 seems uncertain. Some reviewers, such as Kerr,[28] give a value of about 90

(27) J. A. Kerr, *et al.*, *J. Chem. Soc.*, 3584 (1964).

Table IV: Heats of Formation (kcal/g-mol)

Compd	Temp. °K	Calcd	Actual
CH$_4$	298	...	−17.9
CH$_3$	298	...	31.9
CH$_2$	298	93.8	95
CH	298	142.0	142
CCl$_4$	298	...	−26
CCl$_3$	298	...	18
CCl$_2$	298	43.8	43
CCl	298	97.4	96
C$_2$H$_6$	298	...	−20.2
C$_2$H$_5$	298	25.5	25.7
C$_2$H$_4$	298	...	12.5
C$_2$H$_3$	298	71.8	72
C$_2$H$_2$	298	...	54.2
C$_2$H	298	124.9	123
C$_2$	298	195.2	197
C$_2$Cl$_6$	298	...	−34.7
C$_2$Cl$_5$	298	...	8.4
C$_2$Cl$_4$	298	−2.1	−3.5
C$_2$Cl$_3$	298	53.3	...
C$_2$Cl$_2$	298	36.7	...
C$_2$Cl	298	117.0	...
NH$_3$	0	...	−9.4
NH$_2$	0	...	39.3
NH	0	81.3	80

kcal/g-mol. However, a detailed review has been reported in the JANAF Tables[11] where it was concluded that it should be 95 kcal/g-mol. This value seems better substantiated. The heat of formation of CH is quite well established[6,28] at about 142 kcal/g-mol.

Blanchard and Le Goff[29] determined bond energies from which a heat of formation of 46 kcal/g-mol can be calculated for CCl$_2$. Reed and Snedden[19] made similar measurements, which result in a heat of formation of 42 kcal/g-mol. Shilov and Sabirova[30] measured an activation energy of 47 kcal for the dissociation of CHCl$_3$ to CCl$_2$ and HCl. This indicates that the heat of reaction will be about 44 kcal which gives ΔH_f(CCl$_2$) = 42 kcal/g-mol. An average of the three above values has been selected: ΔH_f(CCl$_2$) = 43 kcal/g-mol. Kuzyakov and Tetevskii[31] have determined a dissociation energy of 104 kcal for CCl, which gives a heat of formation of 96 kcal/g-mol. Ovcharenko[32] found from the CCl spectrum a dissociation energy of either 76 or 101 kcal. The value of 101 kcal appears to be the better one. This gives ΔH_f = 99 kcal/g-mol. Reed and Snedden's bond dissociation energy measurements[19] can be used to calculate a value of 93 kcal/g-mol. An average of the three results gives ΔH_f(CCl) = 96 kcal/g-mol.

Kerr's[28] review shows that the heat of formation of C$_2$H$_5$ is about 25.7 kcal/g-mol. He selected a heat of formation of 64 kcal/g-mol for C$_2$H$_3$, but his review is incomplete. Studies of mercury-photo-

sensitized reactions of ethylene, carried out by LeRoy and Steacie[33] and by Kebarle[34] indicate that the C$_2$H$_3$–H bond-dissociation energy should be about 112 kcal, giving ΔH_f(C$_2$H$_3$) = 72 kcal/g-mol. Steacie[35] has reviewed the reaction of H with C$_2$H$_4$ to give C$_2$H$_3$ and H. He has concluded that there is an activation energy of 10 kcal. This indicates that the heat of reaction will be about 8 kcal, giving ΔH_f(C$_2$H$_3$) = 73 kcal/g-mol. Lampe and Field[36,37] have made a number of electron-impact measurements which have led to heats of formation of 70, 82, and 86 kcal/g-mol. Harrison and Lossing's[38] electron-impact results give ΔH_f = 65 kcal/g-mol and Stevenson's[39] electron-impact measurements give 57 kcal/g-mol. The average heat of formation from the electron-impact studies is 72 kcal/g-mol. This compares well with the values of 72 and 73 kcal/g-mol estimated from the kinetic studies and appears to be a better value than that listed by Kerr. A similar uncertainty exists for C$_2$H. Kerr does not list a value, but Knox and Palmer[40] have made a review. They concluded that ΔH_f = 116 kcal/g-mol, but this was based on an unpublished prediction and not on experimental facts. Dibeler[41] has made electron-impact measurements which give ΔH_f = 122. Coats and Anderson[42] made electron-impact measurements on a variety of compounds which give heats of formation of 152, 153, 137, and 110 kcal/g-mol and an average of 138 kcal/g-mol. Cherton[43] concluded from photochemical studies that the bond-dissociation energy of C$_2$H–H is 121 kcal, which gives ΔH_f = 123 kcal/g-mol. The above results suggest that the heat of formation of C$_2$H is probably closer to 123 kcal/g-mol than to Knox and Palmer's value of 116 kcal/g-mol. Fortunately, the heat of formation of C$_2$ is better known. Brewer[44] has calculated a value of 195 kcal/g-mol at 0°K using

(28) J. A. Kerr, *Chem. Rev.*, **66**, 465 (1966).

(29) L. P. Blanchard and P. Le Goff, *Can. J. Chem.*, **35**, 89 (1957).

(30) A. E. Shilov and R. D. Sabirova, *Russ. J. Phys. Chem.*, **34**, 408 (1960).

(31) Y. Y. Kuzyakov and V. M. Tetevskii, *Izv. Vyssh. Ucheb. Zaved., Khim. Khim. Tekhnol.*, **3**, 293 (1960).

(32) I. E. Ovcharenko, *et al.*, *Opt. Spektrosk.*, **19**, 294 (1965).

(33) D. J. LeRoy and E. W. R. Steacie, *J. Chem. Phys.*, **10**, 676 (1942).

(34) P. Kebarle, *J. Phys. Chem.*, **67**, 716 (1963).

(35) E. W. R. Steacie, "Atomic and Free Radical Reactions," Vol. 1, Reinhold Publishing Corp., New York, N. Y., 1954, pp 439, 440.

(36) F. W. Lampe and F. H. Field, *J. Amer. Chem. Soc.*, **81**, 3238 (1959).

(37) F. H. Field, *J. Chem. Phys.*, **21**, 1506 (1953).

(38) A. G. Harrison and F. P. Lossing, *J. Amer. Chem. Soc.*, **82**, 519 (1960).

(39) D. P. Stevenson, *ibid.*, **65**, 209 (1943).

(40) B. E. Knox and H. B. Palmer, *Chem. Rev.*, **61**, 247 (1961).

(41) V. H. Dibeler, *et al.*, *J. Amer. Chem. Soc.*, **83**, 1813 (1961).

(42) F. H. Coats and R. C. Anderson, *ibid.*, **79**, 1340 (1957).

(43) R. Cherton, *Bull. Soc. Chim. Belges*, **52**, 26 (1943).

(44) L. Brewer, *et al.*, *J. Chem. Phys.*, **36**, 182 (1962).

the most recent spectral data. This gives a heat of formation of 197 kcal/g-mol at 298°K.

Puyo[26] has determined a value of -3.5 kcal/g-mol for C_2Cl_4. Unfortunately, there are no known values of the heats of formation of C_2Cl_3, C_2Cl_2, and C_2Cl.

The heat of formation of NH is somewhat uncertain. The JANAF Tables[11] list a predicted value of 79.2 kcal/g-mol. Franklin[45] found $\Delta H_f = 81$ kcal/g-mol from appearance-potential measurements. Seal and Gaydon[46] determined a value of 90.1 kcal/g-mol from spectroscopic measurements of NH in a shock tube. However, their results conflict with those of a similar study carried out by Harrington.[47] Calculations based on Harrington's data show rather good agreement with the thermodynamic properties listed in the

JANAF Tables. The best estimate at present is a value of about 80 kcal/g-mol.

There is good agreement between the predicted and actual heats of formation listed in Table IV. Actually, the differences appear to be smaller than the uncertainties in the measured data ranging from 2 to 5 kcal/g-mol. It is believed that the present method can give accurate results for a wide variety of molecules and free radicals. In some cases, however, it may be necessary to derive additional bond-energy equations, since not all possible types have been developed here.

(45) J. L. Franklin, *et al.*, *J. Amer. Chem. Soc.*, **80**, 298 (1958).
(46) K. E. Seal and A. G. Gaydon, *Proc. Phys. Soc.*, **89**, 459 (1966).
(47) J. A. Harrington, *et al.*, *J. Quant. Spectrosc. Radiat. Transfer.*, **6**, 799 (1966).

Kinetic Isotope Effects in the Hydrogen Electrode Reaction

by J. D. E. McIntyre

Bell Telephone Laboratories, Inc., Murray Hill, New Jersey

and M. Salomon

School of Chemistry, Rutgers University, New Brunswick, New Jersey   (Received December 26, 1967)

Partition function ratios for hydrogen and deuterium gases and the lyonium species $L_2O(l)$, L_3O^+, and OL^- (where L = H or D) have been reevaluated from recent spectroscopic and thermodynamic measurements. These values may be employed in predicting deuterium isotope effects in electrochemical reactions, in estimating the energies of transfer of anions between protium and deuterium oxide solutions, and in establishing an electrode-potential scale for heavy-water electrolytes. The results of measurements of the rate of hydrogen evolution on mercury electrodes in electrolytes of pure and mixed isotopic (H–D) composition are compared and are shown to be in accord with a mechanism involving a rate-determining proton-discharge step.

The effects of H–D isotopic substitution on the kinetics of the electrochemical evolution of hydrogen from aqueous electrolytes have recently been reexamined from a theoretical viewpoint.[1-9] It was shown that by properly accounting for zero-point energies in the activated complex, the low value of the separation factor, S_D, observed experimentally with mercury electrodes[10] was consistent with that predicted theoretically for a rate-determining proton-discharge step and not with the slow discharge of the molecule ion, H_2^+, as previously proposed.[11-13] The long-standing disagreement between the results of electrochemical kinetic studies and kinetic isotope effect investigations was thereby resolved.

The isotopic exchange reaction
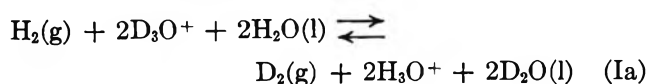
$$H_2(g) + 2D_3O^+ + 2H_2O(l) \rightleftharpoons$$
$$D_2(g) + 2H_3O^+ + 2D_2O(l) \quad (Ia)$$

may be represented as a hypothetical electrochemical cell *without* transference

$$(M)H_2|H_3O^+(H_2O)||D_3O^+(D_2O)|D_2(M) \quad (Ib)$$
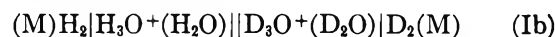
(1) B. E. Conway, *Proc. Roy. Soc.*, **A247**, 400 (1959).
(2) B. E. Conway, "Transactions of the Symposium on Electrode Processes," John Wiley and Sons, New York, N. Y., 1961, Chapter 15.
(3) J. O. M. Bockris and S. Srinivasan, *J. Electrochem. Soc.*, **111**, 844 (1964).
(4) J. O. M. Bockris and S. Srinivasan, *ibid.*, **111**, 853 (1964).
(5) J. O. M. Bockris and S. Srinivasan, *ibid.*, **111**, 858 (1964).
(6) B. E. Conway and M. Salomon, *Ber. Bunsenges. Phys. Chem.*, **68**, 331 (1964).
(7) M. Salomon and B. E. Conway, *ibid.*, **69**, 669 (1965).
(8) B. E. Conway and M. Salomon, *J. Chem. Phys.*, **41**, 3169 (1964).
(9) M. Salomon and B. E. Conway, *Discussions Faraday Soc.*, **39**, 223 (1965).
(10) M. Rome and C. F. Hiskey, *J. Amer. Chem. Soc.*, **76**, 5207 (1954).

may be represented as a hypothetical electrochemical cell *without* transference consisting of reversible hydrogen and deuterium electrodes. Knowledge of the emf of this cell is a prerequisite for investigations of electrochemical reaction mechanisms employing isotopic-substitution methods[14] and for estimating free energies of transfer of ions between light- and heavy-water electrolytes.[15] Since anion transfer energies are not accurately known, the emf of this cell must be evaluated by an indirect, statistical thermodynamic method. A reexamination of the recent calculations by Salomon and Conway[6-9] of S_D and the exchange current density ratio, R, for the hydrogen-evolution reaction (h.e.r.) has revealed errors in the values which they employed for the partition function ratio, q_{D_2}/q_{H_2}, and the emf of cell I.

In the present article, we have recalculated the partition function (pf) ratios for hydrogen and deuterium gases and those for the lyonium species $L_2O(l)$, L_3O^+, and OL^- (where L = H or D) and have obtained a corrected value for the emf of cell I. These calculations lead to closer agreement between the experimental values of S_D and R and those predicted theoretically, and they tend to substantiate the more recent conclusions[1-9] concerning the mechanism of the h.e.r.

Evaluation of Partition Function Ratios

The pf ratios for the lyonium species in aqueous solutions may be calculated from spectroscopic data, provided that the correct form of the liquid-state pf is known. This is generally not the case, however, particularly for hydrogen-bonded liquids. A somewhat more satisfactory procedure is to calculate an empirical pf ratio from thermodynamic measurements on isotopic-exchange reactions. The resulting pf ratios are then strictly valid only for ideal solutions. Since the activity coefficients of salts in nonideal light- and heavy-water electrolyte solutions are similar,[16] however, the effects of ion–solvent interactions on the partition functions of the isotopic lyonium species should be cancelled to a good approximation, in taking their ratio.

For H_2 and D_2 gases, the ratio of the reduced partition functions (exclusive of nuclear spin weights) for an equilibrium mixture can be evaluated conveniently from tabulated values[17] of the thermodynamic function, $-(G° - E_0°)/RT$, and the spectroscopic data of Herzberg.[18] The pf ratio $q_{D_2O(l)}/q_{H_2O(l)}$ can then be determined as a function of temperature from thermodynamic data[19] for the reaction

$$D_2(g) + H_2O(l) \rightleftarrows H_2(g) + D_2O(l) \quad (II)$$
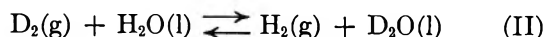
heat capacity data for H_2O[20] and D_2O,[21] and values of the function $-(H° - E_0°)/RT$ for $H_2(g)$ and $D_2(g)$.[17] For reaction II, the standard free energy and enthalpy

changes (expressed in units of calories) are given by the relations

$$\Delta G°_{II} = -2407.46 + 3.96623T -$$
$$(3.20533 \times 10^{-3})T^2 \quad (1a)$$

$$\Delta H°_{II} = 2407.46 + (3.20533 \times 10^{-3})T^2 \quad (1b)$$

The ratio $q_{D_3O^+}/q_{H_3O^+}$ may be obtained from the values of the equilibrium constant, L, of the exchange reaction

$$2D_3O^+ + 3H_2O(l) \rightleftarrows 2H_3O^+ + 3D_2O(l) \quad (III)$$
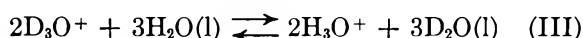
From mass spectrometric experiments, Heinzinger and Weston[22] determined a value of 8.9 for L at 13.5° but did not measure its temperature dependence. The temperature coefficient of L may be estimated from recent emf measurements[16] on the cell

$$(M)H_2|HCl(H_2O)|AgCl;Ag-Ag;$$
$$AgCl|DCl(D_2O)|D_2(M) \quad (IVa)$$
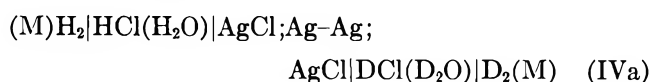
and the thermodynamic data for the reaction II. For cell IVa, the net reaction is

$$H_2(g) + 2D_3O^+ + 2H_2O(l) + 2Cl^-(D_2O) \rightleftarrows$$
$$D_2(g) + 2H_3O^+ + 2D_2O(l) + 2Cl^-(H_2O) \quad (IVb)$$
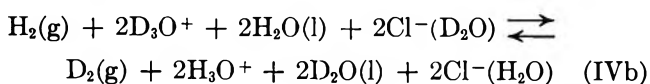
The standard free energy and enthalpy changes for reaction IV (expressed on the *mole fraction* scale in units of calories) are[16]

$$\Delta G°_{IV} = -1704.78 + 11.7447T -$$
$$(2.24618 \times 10^{-2})T^2 \quad (2a)$$

$$\Delta H°_{IV} = -1704.78 + (2.24618 \times 10^{-2})T^2 \quad (2b)$$

Hence at 13.5°, the free-energy change for the transfer process

(11) J. Horiuti, G. Okamoto, and K. Hirota, *Sci. Pap. Inst. Phys. Chem. Res.* (Tokyo), **29**, 233 (1936).

(12) J. Horiuti, T. Keii, and K. Hirota, *J. Res. Inst. Catalysis, Hokkaido Univ.*, **2**, 1 (1951).

(13) T. Keii and T. Kodera, *ibid.*, **5**, 105 (1957).

(14) J. D. E. McIntyre and M. Salomon, paper presented at the Symposium on Electrochemical Processes, 153rd National Meeting of the American Chemical Society, Miami Beach, Florida, April 1967, Abstract No. I73.

(15) J. D. E. McIntyre and M. Salomon, to be submitted for publication.

(16) R. Gary, R. G. Bates, and R. A. Robinson, *J. Phys. Chem.*, **68**, 1186 (1964).

(17) "Ideal Gas Thermodynamic Functions and Isotope Exchange Functions for the Diatomic Hydrides, Deuterides, and Tritides," National Bureau of Standards Monograph 20, U. S. Government Printing Office, Washington, D. C., 1961.

(18) G. Herzberg, "Molecular Spectra and Molecular Structure. I. Spectra of Diatomic Molecules," 2nd ed, D. Van Nostrand Co., Inc., New York, N. Y., 1950.

(19) F. D. Rossini, J. W. Knowlton, and H. L. Johnston, *J. Res. Nat. Bur. Stand.*, **24**, 369 (1940).

(20) N. S. Osborne, H. F. Stimson, and D. C. Ginnings, *ibid.*, **23**, 238 (1939).

(21) A. Eucken and M. Eigen, *Z. Elektrochem.*, **55**, 343 (1951).

(22) K. Heinzinger and R. E. Weston, Jr., *J. Phys. Chem.*, **68**, 745 (1964).

$$Cl^-(D_2O) \rightleftarrows Cl^-(H_2O) \qquad (V)$$
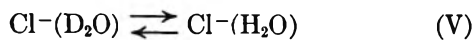
is $\Delta G^\circ_V(13.5^\circ) = -242.8$ cal mol^{-1}. The enthalpy of Cl$^-$ ion transfer is not yet known; it may be estimated[23,24] to be ca. -400 ± 200 cal mol^{-1}. Although the resulting uncertainty of ΔH°_{III} is ca. $\pm 40\%$, values of ΔG°_{III} can be computed with reasonable accuracy ($\pm 2\%$) at temperatures close to 13.5°. With $\Delta H^\circ_V = -400$ cal mol^{-1}, we have

$$\Delta G^\circ_{III} = -3312.24 + 14.6142T -$$
$$(2.56671 \times 10^{-2})T^2 \qquad (3a)$$

$$\Delta H^\circ_{III} = -3312.24 + (2.56671 \times 10^{-2})T^2 \qquad (3b)$$

At 25°, the corresponding value for L_N is 8.06. This value is slightly lower than that calculated by Heinzinger and Weston,[22] since we have employed a larger value of ΔH°_{III} and have taken its temperature variation into account.

In order to evaluate the pf ratio $q_{D_3O^+}/q_{H_3O^+}$, it is necessary to convert values of ΔG°_{III} and L_N from a mole fraction to a *molarity* scale. Thus

$$L_c = \left(\frac{d^\circ_{H_2O}}{d^\circ_{D_2O}}\right)^2 \left(\frac{W_{D_2O}}{W_{H_2O}}\right)^2 L_N \qquad (4)$$

where $d^\circ_{H_2O}$, $d^\circ_{D_2O}$, W_{H_2O}, and W_{D_2O} represent the densities[25] and molecular weights of the light- and heavy-water solvents. Finally, the ratio, q_{OD^-}/q_{OH^-}, can be evaluated from thermodynamic data[26] for the ionization of light and heavy water.

The corrected values of the partition function ratios (with zero-point energy terms *included*) are listed in Table I for four selected temperatures,[27] together with values of L_c. The values at 50 and 75° should be regarded as approximate only, owing to the extrapolations involved. It may be noted, in particular, that the values of the ratio q_{D_2}/q_{H_2} differ significantly from those employed by Salomon and Conway;[6-9] their values involve a computational error. Values of the ratio q_{OD^-}/q_{OH^-} given in Table I also differ considerably from those previously employed.[6-9,28] The former value of 21.15 for q_{OD^-}/q_{OH^-} at 25° was based on a value[29] for the ionization constant of D$_2$O which is now thought to be too large.[26] The pf ratios for the lyonium species, L$_2$O and L$_3$O$^+$, calculated[30] on the basis of the model assumed by Swain and Bader for aqueous solutions[23] and spectroscopically observed vibrational and librational frequencies are slightly higher than the empirical pf ratios listed in Table I.

Standard Cell Emf's

For cell I, the standard emf (on the *molarity* scale) expressed in terms of partition functions is

$$\varphi^\circ_{D_2/D^+} - \varphi^\circ_{H_2/H^+} =$$
$$\frac{RT}{F} \ln\left[\left(\frac{q_{D_3O}}{q_{H_3O}}\right)\left(\frac{q_{D_2}}{q_{H_2}}\right)^{1/2} \bigg/ \left(\frac{q_{D_3O}}{q_{H_3O}}\right)\right] \qquad (5)$$

Table I: Partition Function Ratios

Temp, °C	$q_{D_2(g)}/$ $q_{H_2(g)}$	$q_{D_2O(l)}/$ $q_{H_2O(l)}$	$q_{D_3O^+}/$ $q_{H_3O^+}$	$q_{OD^-}/$ q_{OH^-}	L_c
0	143.193	2550.9	41,035	18.55	9.858
25	109.048	1394.2	18,267	14.39	8.122
50	86.662	842.58	9,075	11.55	7.263
75	71.187	550.46	4,910	9.61	6.920

Similarly, for standard alkaline electrolytes, the corresponding emf is

$$\varphi^\circ_{D_2,OD^-} - \varphi^\circ_{H_2,OH^-} =$$
$$\frac{RT}{F} \ln\left[\left(\frac{q_{OD^-}}{q_{OH^-}}\right)\left(\frac{q_{D_2}}{q_{H_2}}\right)^{1/2} \bigg/ \left(\frac{q_{D_2O}}{q_{H_2O}}\right)\right] \qquad (6)$$

In Table II, values of these emf's are given as a function of temperature. Knowing these values, we may proceed to establish a scale of standard-electrode potentials in deuterium oxide electrolyte solutions which is referred to the standard hydrogen electrode potential in protium oxide solutions.[31] It is interesting to note that while the emf of the standard acid cell I decreases with increasing temperature, that of the standard alkaline cell remains virtually constant.

Table II: Standard Cell Emf's

Temp, °C	$\varphi^\circ_{D_2/D^+} - \varphi^\circ_{H_2/H^+}$, mV	$\varphi^\circ_{D_2,OD^-} - \varphi^\circ_{H_2,OH^-}$, mV
0	-6.964	-57.47
25	-5.828	-57.83
50	-4.061	-57.34
75	-1.666	-57.47

Deuterium Separation Factor

Using the revised value for the difference in standard potentials of the reversible hydrogen and deuterium electrodes, we now compare the results of measurements of the rate of hydrogen evolution on mercury electrodes in electrolytes of pure and mixed isotopic (H–D) composition.

For a rate-determining proton-discharge step, the

(23) C. G. Swain and R. F. W. Bader, *Tetrahedron*, **10**, 182 (1960).

(24) P. Salomaa and V. Aalto, *Acta Chem. Scand.*, **20**, 2035 (1966).

(25) T. L. Chang and L. H. Tung, *Chinese J. Phys.*, **7**, 230 (1949).

(26) A. K. Covington, R. A. Robinson, and R. G. Bates, *J. Phys. Chem.*, **70**, 3820 (1966).

(27) The melting point of D$_2$O is 3.81°.

(28) M. Salomon, *J. Electrochem. Soc.*, **114**, 922 (1967).

(29) W. F. K. Wynne-Jones, *Trans. Faraday Soc.*, **32**, 1397 (1936).

(30) C. G. Swain, R. F. W. Bader, and E. R. Thornton, *Tetrahedron*, **10**, 200 (1960).

(31) J. D. E. McIntyre and M. Salomon, to be submitted for publication.

ratio of rate constants at constant electrode potential is given by[6-9,32]

$$\left(\frac{k_\mathrm{H}}{k_\mathrm{D}}\right)_\varphi = R_\eta \exp\left(-\frac{\beta\Delta\varphi^\circ F}{RT}\right) \quad (7)$$

where $\Delta\varphi^\circ = \varphi^\circ{}_\mathrm{D} - \varphi^\circ{}_\mathrm{H}$; R_η is the current ratio, $i_{\mathrm{H}_2}/i_{\mathrm{D}_2}$, at a given (constant) overpotential, η; and β is the cathodic transfer coefficient. The ratio $(k_\mathrm{H}/k_\mathrm{D})_\varphi$ is obtained from the measured value of R_η and the value of $\Delta\varphi^\circ$ determined above. At 25°, the value of R_η measured by Post and Hiskey[33] at an overpotential of 1.00 V is 2.48; the corresponding value of $(k_\mathrm{H}/k_\mathrm{D})_\varphi$ is then 2.77.

Assuming the rule of the geometric mean to be applicable, a value of $(k_\mathrm{H}/k_\mathrm{D})_\varphi$ can also be evaluated from the relation for the deuterium separation factor

$$S_\mathrm{D} = \left(\frac{k_\mathrm{H}}{k_\mathrm{D}}\right)_\varphi \left(\frac{N_\mathrm{H}}{N_\mathrm{D}}\right)_\mathrm{s} \left(\frac{3C_{\mathrm{H}_3\mathrm{O}^+} + 2C_{\mathrm{H}_2\mathrm{DO}^+} + C_{\mathrm{HD}_2\mathrm{O}^+}}{3C_{\mathrm{D}_3\mathrm{O}^+} + 2C_{\mathrm{HD}_2\mathrm{O}^+} + C_{\mathrm{H}_2\mathrm{DO}^+}}\right) \quad (8)$$

where $(N_\mathrm{H}/N_\mathrm{D})_\mathrm{s}$ is the atomic ratio of H and D in the bulk solution and the C_j terms represent the concentrations of the lyonium species. From the value of S_D equal to 3.75 measured by Rome and Hiskey[10] at 25°, we obtain a value for $(k_\mathrm{H}/k_\mathrm{D})_\varphi$ of 2.71.

The above comparison is based on the results of independent experimental measurements and involves no assumptions concerning the specific form of the activated complex. The close agreement tends to confirm a path for the h.e.r. proceeding via a rate-determining proton-discharge step on mercury electrodes.

(32) J. D. E. McIntyre and M. Salomon, to be submitted for publication.

(33) B. Post and C. F. Hiskey, *J. Amer. Chem. Soc.*, **73**, 161 (1951)

Vapor Pressure and Heats of Sublimation of Calcium Nitride[1]

by Roy C. Blair and Zuhair A. Munir

Department of Materials Science, San Jose State College, San Jose, California 95114 (Received December 1, 1967)

The sublimation pressure of calcium nitride was measured by the torsion–effusion and torsion–Langmuir methods. The vapor pressure, as measured by the torsion–effusion method in the temperature range 994–1190°K, is given by $\log P = -(1.127)10^4/T + 6.009$, where P is the pressure in atmospheres and T is the Kelvin temperature. Based on the reaction $\mathrm{Ca_3N_2(s)} = 3\mathrm{Ca(g)} + \mathrm{N_2(g)}$, second-law and third-law heats of sublimations at 298°K were found to be 217.3 ± 10.9 and 227.9 kcal/mol, respectively. Torsion–Langmuir measurements in the temperature range 1152–1479°K gave the following expression for the free-surface vapor pressure of calcium nitride: $\log P_\mathrm{L} = -(1.108)10^4/T + 3.528$, where P is the pressure in atmospheres and T is the absolute temperature.

Introduction

The sublimation of calcium nitride was first investigated by Kraus and Hurd[2] by means of a static vapor pressure method. In interpreting their results they had assumed an equilibrium between solid calcium, gaseous nitrogen, and solid calcium nitride. However, observing that metallic calcium was distilling on the cooler regions of their apparatus, these investigators expressed doubt in the validity of their assumption and hence the significance of their results. Since no free surface sublimation studies or recent determinations of the equilibrium vapor pressure of calcium nitride have been made, and in view of the results of recent free surface sublimation studies on other metallic nitrides,[3-6] information regarding the stability of calcium nitride would be of considerable interest.

Experimental Section

The torsion method for the determination of vapor pressures has been discussed in a number of publications,[3,7,8] and the apparatus used in this investigation has been described in detail in a recent paper.[9]

(1) From the thesis submitted by R. C. Blair in partial fulfillment of the requirements for the degree of Master of Science in Materials Science, San Jose State College, San Jose, Calif.

(2) C. A. Kraus and C. B. Hurd, *J. Amer. Chem. Soc.*, **45**, 2559 (1923).

(3) Z. A. Munir and A. W. Searcy, *J. Chem. Phys.*, **42**, 4223 (1965).

(4) B. A. Blank, Ph.D. Thesis, University of California at Berkeley, Berkeley, Calif., UCRL-16018, April 1965.

(5) C. L. Hoenig and A. W. Searcy, *J. Amer. Chem. Soc.*, **50**, 460 (1967).

(6) R. C. Schoonmaker, A. R. Venkitaraman, and P. K. Lee, *J. Phys. Chem.*, **71**, 2676 (1967).

(7) Z. A. Munir and A. W. Searcy, *J. Electrochem. Soc.*, **111**, 1170 (1964).

Cylindrical torsion–effusion cells were made using National Carbon ZT101 Grade graphite and Type 316 stainless steel. The graphite cells were made with tight friction-fitted lids. Previous experimentation has proved the absence of leakage around lids of identical cells.[9] Thin-walled stainless steel cells, made with the same design, had lids which were permanently closed by welding. These cells were loaded by funneling powder samples through the orifices.

Torsion–Langmuir cells consisted of graphite blocks, each with two sample wells located eccentrically on two opposite sides. Geometric descriptions of these cells have been given elsewhere.[9]

The calcium nitride which was purchased in lamp form from Alfa Inorganics was analyzed by X-ray diffraction. The resulting Debye–Scherrer pattern showed calcium nitride lines only. The congruency of sublimation of this compound was established by X-ray analysis of samples heated *in vacuo* at temperatures and heating periods corresponding to about 20–30% weight loss from each sample. In every attempt the resulting pattern indicated the existence of Ca_3N_2 only. Since this nitride is hygroscopic, all preparation steps were carried out under an argon atmosphere in a vacuum drybox. To obtain wafers of calcium nitride for the Langmuir studies, screened powder was compressed under a pressure of approximately 180,000 psi at room temperature under an inert atmosphere.

As a check on the reliability of the measurements made with this apparatus, the vapor pressures of zinc and tin were redetermined in the range from 10^{-6} to 10^{-3} atm using techniques identical with those described above. Third-law heat of sublimation of zinc at 298°K was calculated from the results of 33 vapor pressure determinations obtained with three cells having orifice areas differing by a factor of 6. The calculated value was 31.6 ± 0.2 kcal/mol, which is in reasonable agreement with that of 31.2 kcal/mol as reported by Hultgren, *et al.*[10] Vapor pressure values (28) of tin, obtained from measurements using three cells with orifice areas differing by a factor of 4, gave a third-law value of $\Delta H°_{298}$ of 72.4 ± 0.1 kcal/mol, which agrees very favorably with 72.2 kcal/mol listed in ref 10.

Results

A. Torsion–Effusion Studies. Figure 1 shows the results of more than 60 torsion–effusion vapor pressure determinations which were made in the temperature range 994–1383°K using graphite and stainless steel cells having six orifice sizes. Since the validity of such results depends on the applicability of molecular-flow equations,[11–13] ratios of the mean free path to the orifice diameter, λ/d, were calculated using the hard-sphere approximation and the molecular diameter of nitrogen.[14] These calculations showed a systematic deviation of the vapor pressure results as the ratio
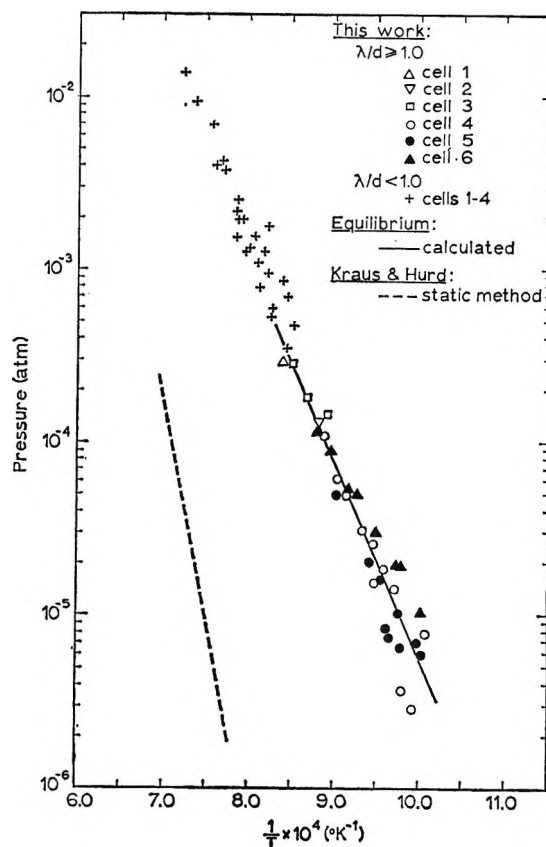
Figure 1. Vapor pressure of calcium nitride, torsion–effusion method.

λ/d fell significantly below 1. Thus only those vapor pressure values for which $\lambda/d \geq 1.0$ were included in the calculations of the least-square fit and consequently all the thermodynamic functions.

Based on the following sublimation

$$Ca_3N_2(s) = 3Ca(g) + N_2(g) \qquad (1)$$
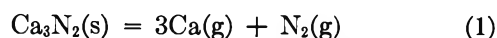
a least-square fit of the results for which $\lambda/d \geq 1.0$ gave the following expression for the equilibrium constant, K_{eq}, between 994 and 1190°K

$$\log K_{eq} = -(4.508)10^4/T + 23.059 \qquad (2)$$

The heat of sublimation of calcium nitride was calculated by the second-law and third-law methods. The second-law heat at 298°K, $\Delta H°_{298}$, was found to be 217.3 ± 10.9 kcal/mol. Third-law heat values were

(8) A. N. Nesmeyanov, "Vapor Pressure of the Chemical Elements," Elsevier Publishing Co., New York, N. Y., 1963.

(9) W. T. Lee and Z. A. Munir, *J. Electrochem. Soc.*, **114**, 1236 (1967).

(10) R. Hultgren, R. L. Orr, P. D. Anderson, and K. K. Kelley, "Selected Values of Thermodynamic Properties of Metals and Alloys," John Wiley and Sons, Inc., New York, N. Y., 1963.

(11) H. W. Liepmann, *J. Fluid Mech.*, **10**, 65 (1961).

(12) A. W. Searcy and D. A. Schulz, *J. Chem. Phys.*, **38**, 772 (1963).

(13) K. D. Carlson, P. W. Gilles, and R. J. Thorn, *ibid.*, **38**, 2064 (1963).

(14) S. Dushman, "Scientific Foundations of Vacuum Technique," John Wiley and Sons, Inc., New York, N. Y., 1962.

Table I: Third-Law Heats of Sublimation of Calcium Nitride—Torsion-Effusion Data

Temp, °K	P, atm	λ/d	ΔH°_{298}, kcal/mol	Temp, °K	P, atm	λ/d	ΔH°_{298}, kcal/mol
A. Cell 1				**D. Cell 4**			
1190	2.90×10^{-4}	2.01	225.9	994	8.07×10^{-6}	169	225.2
1226	1.28×10^{-3}	0.47	216.6[a]	1008	2.94×10^{-6}	46	236.1
1248	1.35×10^{-3}	0.45	218.9[a]	1021	3.75×10^{-6}	36	236.6
1269	1.99×10^{-3}	0.31	218.5[a]	1031	1.45×10^{-5}	9.6	227.3
1275	2.19×10^{-3}	0.27	217.3[a]	1044	1.86×10^{-5}	7.5	227.6
1308	3.87×10^{-3}	0.17	215.3[a]	1055	1.59×10^{-5}	9.1	230.8
1314	4.12×10^{-3}	0.16	214.8[a]	1059	2.66×10^{-5}	5.3	227.1
1358	9.40×10^{-3}	0.07	211.3[a]	1073	3.11×10^{-5}	4.8	228.1
1383	1.41×10^{-2}	0.05	209.4[a]	1092	5.07×10^{-5}	2.9	227.0
B. Cell 2				1107	6.38×10^{-5}	2.3	227.5
1135	1.36×10^{-4}	2.09	225.0	1129	1.12×10^{-4}	1.3	225.9
1174	4.92×10^{-4}	0.68	218.8[a]	1153	1.76×10^{-4}	0.85	225.2[a]
1183	6.97×10^{-4}	0.48	216.6[a]	1167	2.31×10^{-4}	0.69	224.9[a]
1192	8.57×10^{-4}	0.40	215.9[a]	1213	5.42×10^{-4}	0.30	223.2[a]
1208	6.11×10^{-4}	0.45	212.5[a]	**E. Cell 5**			
1216	9.53×10^{-4}	0.42	218.1[a]	1001	6.01×10^{-6}	21.1	230.1
1218	1.18×10^{-3}	0.38	216.4[a]	1004	7.12×10^{-6}	17.5	228.3
1235	1.11×10^{-3}	0.33	219.2[a]	1023	6.65×10^{-6}	19.1	232.3
1241	1.57×10^{-3}	0.31	216.5[a]	1027	1.03×10^{-5}	12.6	229.5
1253	1.31×10^{-3}	0.27	219.7[a]	1037	7.43×10^{-6}	17.5	233.9
1264	2.00×10^{-3}	0.18	216.9[a]	1042	8.49×10^{-6}	15.6	233.8
1272	2.55×10^{-3}	0.14	215.3[a]	1084	1.65×10^{-5}	8.1	229.3
1298	3.74×10^{-3}	0.01	214.5[a]	1063	2.05×10^{-5}	6.5	230.0
1305	4.31×10^{-3}	0.01	213.9[a]	1108	5.15×10^{-5}	2.7	229.5
1327	6.94×10^{-3}	0.005	211.4[a]	**F. Cell 6**			
C. Cell 3				999	1.05×10^{-5}	12.0	224.3
1121	1.42×10^{-4}	1.95	222.5	1023	1.96×10^{-5}	6.0	223.5
1153	1.81×10^{-4}	1.57	225.1	1029	2.01×10^{-5}	6.0	224.3
1176	2.90×10^{-4}	1.0	224.0	1055	3.21×10^{-5}	3.8	225.0
1186	3.58×10^{-4}	0.85	223.4[a]	1079	5.11×10^{-5}	2.5	224.9
1230	7.93×10^{-4}	0.38	221.6[a]	1090	5.53×10^{-5}	2.3	226.1
1274	1.56×10^{-3}	0.20	220.6[a]	1118	9.04×10^{-5}	1.4	226.1
				1138	1.17×10^{-4}	1.2	226.9

[a] Data for which λ/d < 1.0 were not included in the calculation of ΔH°_{298} average.

calculated using tabulated free-energy functions for Ca(g) and N_2(g),[10,15] and calculated free-energy functions for Ca_3N_2(s) using specific heat data.[16] These values which are shown in Table I gave an average ΔH°_{298} of 227.9 kcal/mol. Second-law calculations of the entropy of sublimation at 298°K, ΔS°_{298}, gave a value of 121.1 ± 4.5 eu.

B. Torsion-Langmuir Studies. The results of free-surface vapor pressure determinations in the temperature range 1152–1479°K are plotted in Figure 2 as log P_L vs. $1/T$. Based on eq 1, a least-square fit of these data gave the following expression for the apparent equilibrium constant

$$\log K^* = -(4.432)10^4/T + 13.135 \qquad (3)$$

From this equation the second-law heat of sublimation under free surface conditions was calculated to be $\Delta H^{\circ}_{298}* = 219.4 \pm 12.0$ kcal/mol. Third-law calculations of this heat are shown in Table II, from which

an average value at 298°K, ΔH_{298}°, was found to be 275.4 kcal/mol of calcium nitride. The second-law free surface sublimation entropy at 298°K was found to be 80.3 ± 4.1 eu.

The sublimation coefficient, α, calculated by combining the torsion–Langmuir with the torsion–effusion data, was found to vary from 5.12×10^{-3} at 1000°K to 4.79×10^{-3} at 1200°K.

Discussion

The availability of graphite cells as well as the suggested use of graphite as a crucible material for melting calcium[17,18] led to the initial use of these cells for the

(15) "JANAF Thermochemical Data," Dow Chemical Co., Midland, Mich., 1963.

(16) K. K. Kelley, U. S. Bureau of Mines Bulletin 476, U. S. Government Printing Office, Washington, D. C. 1949.

(17) M. F. Culpin, *Proc. Phys. Soc.*, **B70**, 1079 (1957).

(18) J. Bockris, J. L. White, and J. D. Mackenzie, "Physicochemical Measurements at High Temperatures," Butterworth and Co. Ltd., London, 1959, p 337.
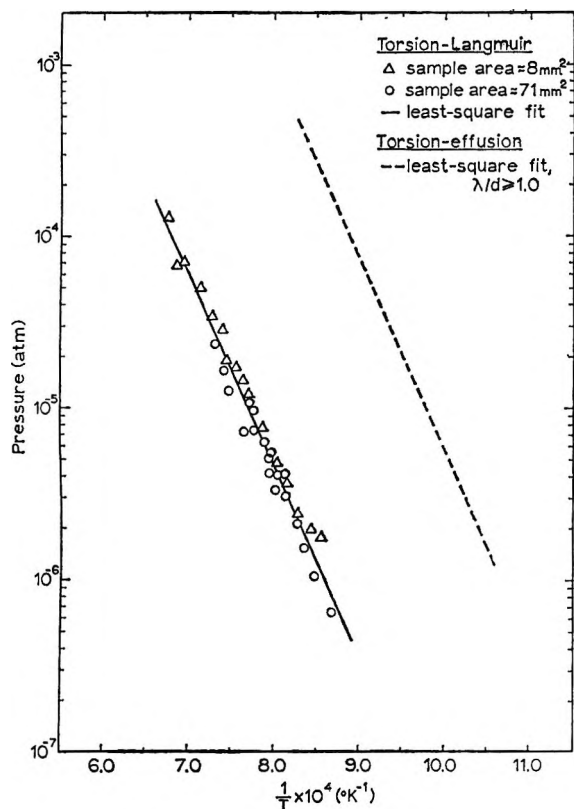
Figure 2. Vapor pressure of calcium nitride, torsion–Langmuir method.

Table II: Third-Law Heats of Sublimation of Calcium Nitride(s)—Torsion–Langmuir Data

Temp, °K	P, atm	$\Delta H°_{298}$*, kcal/ mol	Temp, °K	P, atm	$\Delta H°_{298}$*, kcal/ mol
A. Sample Diameter, 3.175 mm					
1168	1.77×10^{-6}	270.2	1324	1.72×10^{-5}	273.9
1186	1.97×10^{-6}	272.4	1344	1.90×10^{-5}	276.6
1208	2.43×10^{-6}	274.3	1353	2.88×10^{-5}	273.1
1229	3.64×10^{-6}	274.2	1373	3.44×10^{-5}	274.0
1246	4.82×10^{-6}	274.4	1404	5.00×10^{-5}	274.4
1271	7.70×10^{-6}	273.9	1442	7.08×10^{-5}	275.7
1298	1.20×10^{-5}	273.7	1458	6.80×10^{-5}	278.5
1310	1.44×10^{-5}	273.9	1479	1.28×10^{-4}	273.8
B. Sample Diameter, 9.525 mm					
1152	6.50×10^{-7}	276.4	1259	4.16×10^{-6}	278.1
1180	1.05×10^{-6}	277.4	1260	5.06×10^{-6}	276.3
1196	1.52×10^{-6}	276.6	1269	6.34×10^{-6}	275.5
1208	2.16×10^{-6}	275.6	1288	7.49×10^{-6}	277.0
1232	3.08×10^{-6}	276.4	1289	9.60×10^{-6}	274.6
1234	4.21×10^{-6}	273.6	1298	1.08×10^{-5}	274.8
1244	4.11×10^{-6}	275.6	1308	7.21×10^{-6}	280.7
1248	3.34×10^{-6}	278.3	1339	1.25×10^{-5}	279.9
1253	4.80×10^{-6}	275.6	1349	1.65×10^{-5}	278.5
1258	5.45×10^{-6}	275.2	1370	2.37×10^{-5}	277.7

torsion–effusion experiments. A closer examination of Figure 1 shows that the vapor pressure measured with both graphite and Type 316 stainless steel cells are randomly distributed about the least-square fit. When third-law calculations were made for the 19 points obtained with the graphite cells, a value of $\Delta H_{298}°$ of 227.8 kcal/mol resulted. This compares with $\Delta H_{298}°$ of 227.9 kcal/mol calculated from 14 vapor pressure values obtained with stainless steel cells. Since it is highly improbable that reactions would reduce the activity of calcium in graphite and in steel by the same amounts, the excellent agreement between the third-law heats supports the belief that the pressures characteristic of congruent calcium nitride sublimation have been measured.

The existence of equilibrium pressures inside the torsion cell was tested by varying the orifice size. If nonequilibrium conditions exist for a certain orifice size, then the use of a smaller orifice will lead to high pressure. The results from six orifice areas, differing by a factor of 16, showed no systematic dependence of the vapor pressure on the effusion area.

Total pressures of calcium nitride were calculated for reaction 1 from existing thermodynamic data.[10,14,19]

These results, shown in Figure 1, are in excellent agreement with those obtained in this investigation.

The second-law heat of free-surface sublimation, $\Delta H°_{298}$* of 219.4 kcal/mol is appreciably lower than the third-law value, 275.4 kcal/mol. However, the second-law heat of free-surface sublimation is not significantly different from that obtained by the torsion-effusion method, 217.3 kcal/mol. From these comparisons, therefore, it can be concluded that the existence of an activation barrier of about 48 kcal/mol is due almost entirely to entropy effects.

A possible source of error in free surface sublimation studies is the presence of cracks and fissures in the surfaces of sample wafers. Examination of samples used in this work under $150\times$ magnification revealed the absence of such surface defects both in the as-pressed and the heated wafers. However, since these dense wafers were not pore-free (i.e., single crystals), reported values for the apparent free-surface pressures, sublimation coefficients, and sublimation entropy must be regarded only as upper limits.

(19) K. K. Kelley, U. S. Bureau of Mines Bulletin 407, 1937.

The Reaction Products of γ-Picoline and Iodine

by I. Haque and J. L. Wood

Imperial College of Science and Technology, Imperial Institute Road, London, England

Accepted and Transmitted by The Faraday Society *(June 21, 1967)*

Solutions of iodine in γ-picoline contain the (γ-PicI-γ-Pic)$^+$ ion. In the presence of free γ-picoline this reacts to give solid Ia established by infrared and nmr spectra. Further reaction produces solid Ib and also solid Ic. The protons eliminated in these reactions are incorporated in the (γ-PicH-γ-Pic)$^+$ ion.

Introduction

Two distinct solid compounds can be isolated from solutions of iodine in γ-picoline.[1] The first, which is rapidly formed on mixing, is soluble in γ-picoline and other organic solvents but is insoluble in water. Both crystal-structure studies[2] and the infrared spectrum show this to be the charge-transfer complex γ-PicI$_2$. The second compound is formed more slowly and eventually precipitates from the γ-picoline solution. It is insoluble in many organic solvents but is soluble in water. This compound (compound I of Glusker and Miller) was shown by these authors to contain no I–I distance shorter than 3.0 Å, and the authors suggested structure A. Hassel, *et al.*,[2] however, proposed that B was more probable, by analogy with the corresponding pyridine salt.
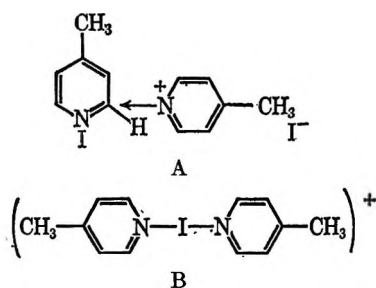
We have recently determined the infrared and Raman spectra of various iododi-γ-picolinium salts.[3] Comparison with the infrared spectrum of the water-soluble compound shows decisively that Hassel's conjecture is untenable. (See Figure 1.)

We have, therefore, sought to determine the structure of this product and the nature of the process by which compound I is formed, largely using spectroscopic means. The situation turns out to be appreciably more complicated than initially envisaged—nevertheless, many features have been elucidated.

The Reaction Process

If equimolar proportions of γ-picoline and iodine are mixed in an inert solvent, *e.g.*, *n*-hexane or benzene, the molecular charge-transfer complex γ-picoline–I$_2$ is formed, the equilibrium strongly favoring the complex.[4]

At room temperature these solutions show no spectroscopic changes, either in daylight or the dark, at least over a period of ≈12 hr, provided no excess γ-picoline is present. The presence of excess, and consequently free, I$_2$ also does not lead to reaction in inert solvents. In polar solvents and also in CS$_2$ to a lesser extent, partial ionization takes place[5]

$$2\gamma\text{-PicI}_2 \rightleftharpoons (\gamma\text{-Pic}_2\text{I})^+ + \text{I}_3^- \qquad (1)$$
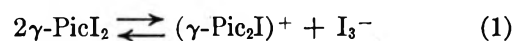
the cation being the iododi-γ-picolinium ion. When I$_2$ is added to excess γ-picoline in an inert solvent, or when γ-picoline is itself the solvent—in both cases necessarily implying the possibility of ionization, spectroscopic changes are immediately apparent, culminating in the precipitation of the water-soluble solid. Owing to the opacity of the solution, it is not possible to fix a time at which precipitation commences, but it is apparent within 30 min.

The spectroscopic changes are most clearly shown in the 500–700-cm^{-1} region, which in the freshly made up solution contains only bands at 515 cm^{-1} (ν_{6a}[6] of free γ-picoline), 536 cm^{-1}, the corresponding band of γ-PicI$_2$, and 546 cm^{-1}, that of (γ-Pic$_2$I)$^+$. The changes in this frequency range are shown in Figure 2 and display the rise in a strong band at ∼605 cm^{-1}, one of the most characteristic features of the spectrum of the product. The band at 546 cm^{-1} due to (γ-Pic$_2$I)$^+$ rapidly disappears and eventually the band at 515 cm^{-1} also decreases in intensity, a consequence of the utilization of γ-picoline in forming the product. The retention of the 535-cm^{-1} band arising from the γ-picoline–I$_2$ complex is apparently irreconcilable with the disappearance of γ-Pic$_2$I$^+$, since the equilibrium is found to be rapidly

$$2\gamma\text{-PicI}_2 \rightleftharpoons (\gamma\text{-Pic}_2\text{I})^+ + \text{I}_3^-$$
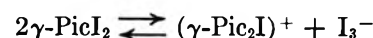
(1) D. L. Glusker and A. Miller, *J. Chem. Phys.*, **26**, 331 (1957).

(2) O. Hassel, C. Romming, and T. Tufte, *Acta Chem. Scand.*, **15**, 967 (1961).

(3) I. Haque and J. L. Wood, unpublished data.

(4) R. F. Lake and H. W. Thompson, *Proc. Roy. Soc.* (London), **297A**, 440 (1967).

(5) I. Haque and J. L. Wood, *Spectrochim. Acta*, **23A**, 2523 (1967).

(6) J. H. S. Green, *et al., ibid.*, **19**, 549 (1963).
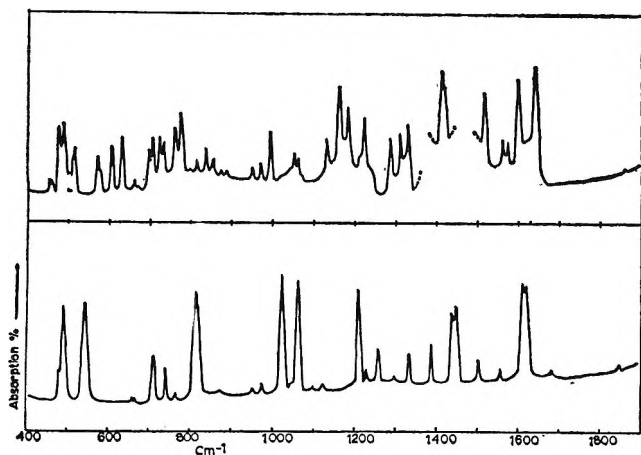
Figure 1. Upper: infrared spectrum of reaction product of I_2 with γ-picoline, washed with ethanol to remove excess γ-picoline but not otherwise treated (Nujol mull). Lower: composite infrared spectrum of $(\gamma Pic_2I)^+$ ion, from data using the BF_4^- and PF_6^- salts (Nujol and HCBD mulls).
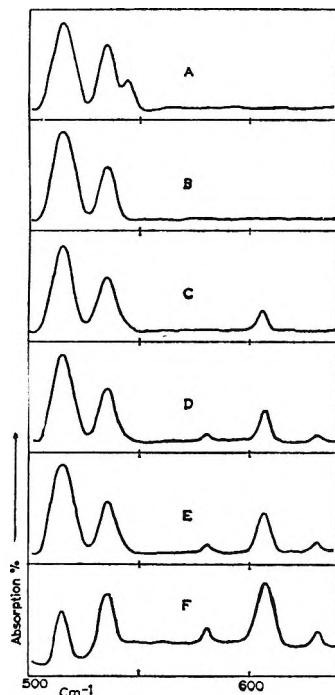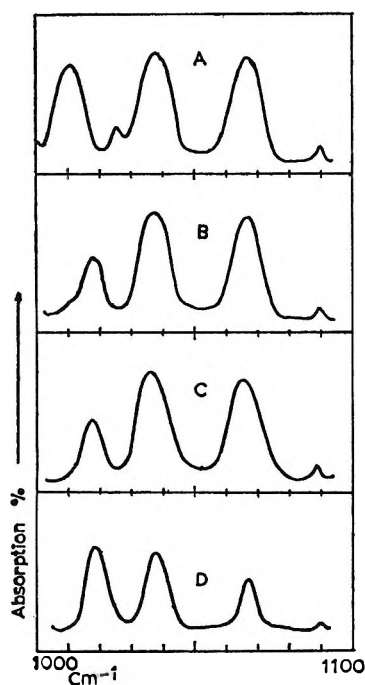

Figure 2. Scans of the 500–650-cm^{-1} range of a nearly saturated solution of I_2 in γ-picoline at successive periods after preparation: A, 5 min; B, 25 min; C, 40 min; D, 65 min; E, 2 hr; F, 24 hr after mixing. The cell containing the solution remained in the beam for the first five scans. The final scan refers to a sample kept throughout in a closed flask until examined.

set up, i.e., within the time that the first observations can be made, so that the concentrations of γ-PicI$_2$ and γ-Pic$_2$I$^+$ should keep proportionate. The difficulty is resolved by examination of the spectral range around 1000 cm^{-1}. The charge-transfer complex γ-PicI$_2$ has a single sharp band at 1011 cm^{-1} in γ-picoline solution (this is ν_1[6] of the complex). The corresponding band of

$(\gamma-Pic_2I)^+$ is at 1025 cm^{-1}. As reaction proceeds, both the 1011- and 1025-cm^{-1} bands disappear and are replaced by a sharp band of the product at 1018 cm^{-1} (Figure 3). This shows that as reaction proceeds, the 535-cm^{-1} band is no longer due to γ-PicI$_2$ and therefore arises from a product. Further, it is apparent that the bands at 1011 and 1025 cm^{-1} disappear and the band at 1018 cm^{-1} appears before the appearance of the 605-cm^{-1} band. It will be seen later that the bands at 605 and 1018 cm^{-1} arise from different products. The 1018 cm^{-1} band is still present in old solutions which also show the 605-cm^{-1} band, and is consequently not due to a forerunner of the 605-cm^{-1} product. The changes of the spectrum in other frequency ranges are generally complex, but it is significant that in the low-frequency range the strong band initially present at 137 cm^{-1}, due to the I$_3^-$ ion,[5] the band at ~162 cm^{-1} which comprises both the I–I stretching of the un-ionized complex (162 cm^{-1}), and the antisymmetric (N–I–N) stretching of $(\gamma-PicI_2)^+$ (168 cm^{-1}) disappear, and the lower frequency range (100–300 cm^{-1}) becomes devoid of all bands except a weak band at ~210 cm^{-1}. The rate of reaction, as shown by the intensity of the 606-cm^{-1} band, is the same in the dark and in daylight. These observations do not permit us to distinguish whether it is the ion $(\gamma-Pic_2I)^+$ or the complex γ-PicI$_2$ which reacts with γ-picoline. It is easy to demonstrate that at least the $(\gamma-Pic_2I)^+$ cation reacts with γ-picoline to give a product containing the bands at 535, 606, and 1018 cm^{-1} (Figure 4). The characteristic $(\gamma-Pic_2I)^+$ bands at 545 and 168 cm^{-1} (not shown) rapidly disappear. The accompanying anion (BF$_4^-$ or PF$_6^-$) remains unchanged. The reaction of $(\gamma Pic_2I)^+$ salts with γ-picoline can also be demonstrated in CH$_2$Cl$_2$ solution, forming the same product. Examination of the electronic spectrum shows that no free I$_2$ is formed. Further, the $(\gamma Pic_2I)^+$ cation (in the form of the fluoroborate salt) is stable in a polar solvent (nitrobenzene) for at least 24 hr, and there is also no reaction when free I$_2$ is added to $(\gamma Pic_2I^+ BF_4^-)$ in CH$_2$Cl$_2$, for at least 6 hr. The fact that $(\gamma-Pic_2I)^+$ reacts with γ-picoline does not exclude the possibility that in solutions γ-PicI$_2$ also reacts directly with γ-picoline. As it is not possible to have γ-PicI$_2$ alone present in γ-picoline solutions, since equilibrium[4] always provides $(\gamma-Pic_2I)^+$, a detailed kinetic investigation is required to decide whether γ-PicI$_2$ is also reacting directly with γ-picoline. We shall adopt, simply to economize on hypotheses, that the reaction is due to the $(\gamma-Pic_2I)^+$ ion.

$$(\gamma-Pic_2I)^+ + \gamma-Pic \longrightarrow products \qquad (2)$$
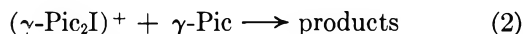
Although for simplicity we have referred so far to "the product," this turns out to comprise several chemical species, and the proportions can vary with the reaction conditions.

The observation that the I$_3^-$ counterion disappears in the original process could be easily accounted for, using

Figure 3. Scans of the 1000–1050-cm^{-1} range of a nearly saturated solution of I_2 in γ-picoline at successive periods after preparation: A, 5 min; B, 15 min; C, 2 hr; D, 24 hr. The cell containing the sample remained in the beam throughout.
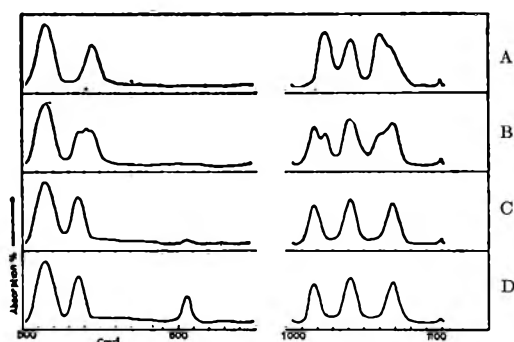
Figure 4. The reaction of $(\gamma$-Pic$_2$I$)^+$ with γ-picoline: A, 5 min; B, 20 min; C, 40 min; D, 3 hr. Both the BF$_4^-$ and PF$_6^-$ salts were examined. Anion bands are omitted.

equilibria which are known to occur in γ-picoline solution.

$$I_3^- + \gamma\text{-Pic} \rightleftarrows \gamma\text{-PicI}_2 + I^-$$

$$2\gamma\text{-PicI}_2 \rightleftarrows (\gamma\text{-Pic}_2\text{I})^+ + I_3^- \tag{3}$$

$$(\gamma\text{-Pic}_2\text{I})^+ + \gamma\text{-Pic} \longrightarrow \text{products}$$
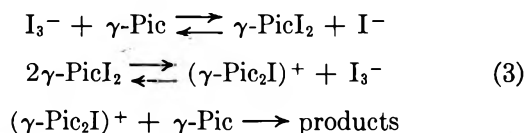
This possibility can be tested directly by dissolving (NAlk$_4$)$^+$, I$_3^-$ in γ-picoline. After 1 day the characteristic product bands at 535 and 1018 cm^{-1} are clearly present (Figure 5), while the 137-cm^{-1} band disappears. Neither the 1011-cm^{-1} γ-PicI$_2$ nor the 1025-cm^{-1} $(\gamma$-Pic$_2$I$)^+$ bands can be picked up in rapid scans of this frequency range (Figure 5), but the speed with which

these bands disappear from γ-picoline $+ I_2$ solutions (Figure 3) shows that their absence is not inconsistent with the reaction scheme 3.

The reaction of I_3^- with γ-picoline suggests that IBr$_2^-$ should also react to give the same product, since the corresponding equilibria (eq 4) would produce the

$$\text{IBr}_2^- + \gamma\text{-Pic} \rightleftarrows \gamma\text{-PicIBr} + \text{Br}^-$$

$$2\gamma\text{-PicIBr} \rightleftarrows (\gamma\text{-Pic}_2\text{I})^+ + \text{IBr}_2^- \tag{4}$$
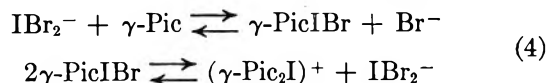
$(\gamma$-Pic$_2$I$)^+$. This expectation is borne out, as the spectrum of a solution (NAlk$_4$)$^+$, IBr$_2^-$ in γ-picoline after 1 day (Figure 6) shows. The IBr$_2^-$ band at 174 cm^{-1} (not shown) correspondingly disappears. In this case scans of the 1000-cm^{-1} region of freshly prepared solutions show evidence of the transient presence of γ-PicIBr, which has a sharp band at 1019 cm^{-1}.[5] This band rapidly decreases at first (Figure 6), the weaker permanent residuum being ascribed to 1018 cm^{-1} of the product.

We have also examined the reaction of γ-PicICl with γ-picoline. Since $(\gamma$-Pic$_2$I$)^+$ is formed in this solvent[5] the same product can be expected. Figure 7

$$2\gamma\text{-PicICl} \rightleftarrows (\gamma\text{-Pic}_2\text{I})^+ + \text{ICl}_2^-$$
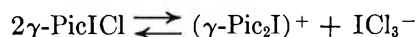
shows that both γ-PicICl and $(\gamma$-Pic$_2$I$)^+$ disappear from a solution in γ-picoline, as evidenced by the disappearance of the 545-cm^{-1} band (the frequency corresponding to ν_{6a} is almost the same in the two compounds, a reflection of the similarity of the electron transfer from the γ-picoline ring). The characteristic product band at 606 cm^{-1} arises but is now accompanied by other bands at 570 and 630 cm^{-1}, indicating the production of further species.

Taken together, these observations show that $(\gamma$-Pic$_2$I$)^+$ reacts with γ-picoline to form a product or products which are comprised in "compound I." The possibility of other reactions, e.g., directly between γ-PicI$_2$ or γ-PicICl and γ-picoline, cannot be excluded.

The Nature of the Reaction Product

The only previous examination of the reaction product is by Glusker and Miller,[1] and we quote their description: "A saturated solution of resublimed iodine in pure γ-picoline was prepared under anhydrous conditions. It set to a solid mass after approximately 2 hr. The mixture was partially soluble in ethyl alcohol. The insoluble residue (I) which proved to be water soluble, and insoluble in the common organic solvents, was washed with ether and recrystallized from water–alcohol mixtures as a light brown microcrystalline solid. Its melting point is 223–224° with decomposition, and its density is approximately 1.9 g/cm^3. Chemical analysis and the equivalent weight determined from the freezing point depression of water solutions were consistent with an ionic formula $C_{12}H_{14}N_2I^+, I^-$. A precipitate of silver iodide is formed immediately upon the addition of acidified silver nitrate solution to an aqueous solution of I."
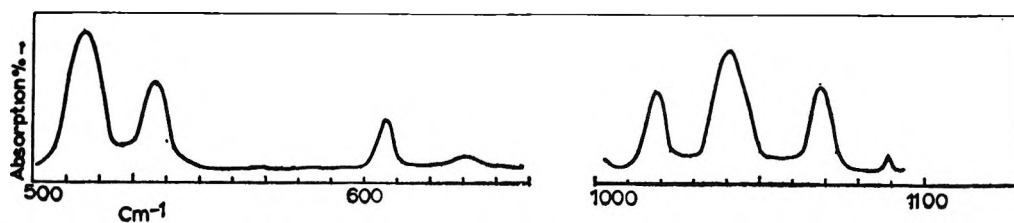
Figure 5. NBu₄⁺, I₃⁻ in γ-picoline after 1 day *in vitro*.
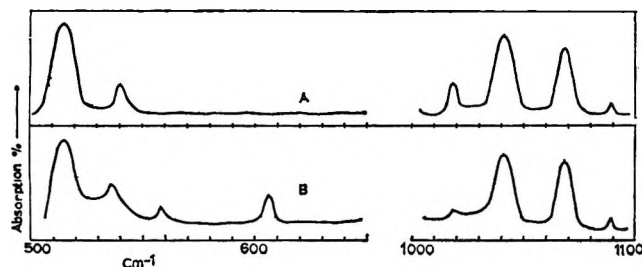
Figure 6. NMe₄⁺, IBr₂⁻ in γ-picoline: A, 5 min (note the bands at 540 and 1019 cm⁻¹, characteristic of γ-PicIBr); B, after one day *in vitro*. Note the bands of the reaction product at 536, 606, and 1018 cm⁻¹. The band at 558 cm⁻¹ has not been accounted for.
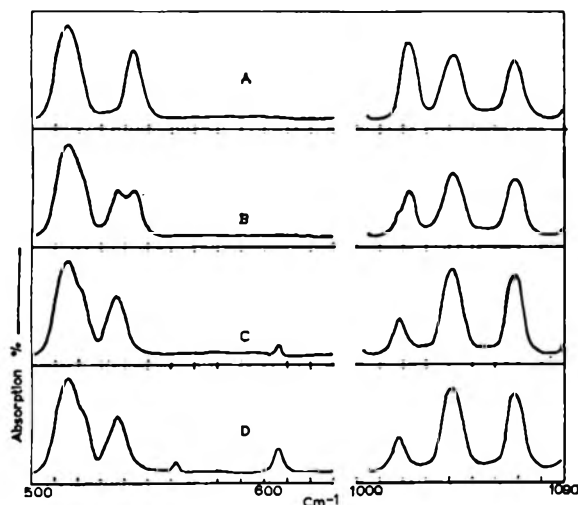
Figure 7. γ-PicICl in γ-picoline: A, 5 min; B, 25 min; C, 45 min; D, 2 hr. The bands at 545 (γ-Pic₂I⁺ and γ-PicICl) 1022 (γ-PicICl), and 1025 cm⁻¹ (γ-Pic₂I)⁺ disappear and product bands at 536, 570, 608, and 1018 cm⁻¹ arise.

Figure 8. Product Ia, as in C but after metathesis of anion with NO₃⁻ (* indicates NO₃⁻ bands); B, product Ia obtained by reaction of (γ-Pic₂I)⁺, PF₆⁻ with γ-picoline (* indicates PF₆⁻ bands); C, product Ia obtained by reaction of I₂ with γ-picoline.

Extraction of our I₂–γ-picoline reaction product with ethanol gave a solution from which addition of ether precipitated a cream-colored solid (Ia), mp 175° and very soluble in water, which gives an analysis (Table I) corresponding more nearly to 2γ-Pic:I, in contrast to Glusker and Miller's result. The infrared spectrum of this substance, shown in Figure 8, contains the characteristic 606-cm⁻¹ band but not bands near 535 or 570–580 cm⁻¹. The product of the reaction of (γ-Pic₂I)⁺ PF₆⁻ with γ-picoline, when worked up in the same way, gives an identical infrared spectrum (Figure 8), if allowance is made for the presence of (PF₆)⁻

bands. Both observations suggest that compound Ia is the salt (2γ-Pic),⁺ X⁻. The analysis of the product from the second reaction bears this out (Table I), showing that PF₆⁻ has partially replaced I⁻. This hypothesis was supported by dissolving the Ia iodide in water and adding aqueous AgNO₃ solution, which gave

Table I: Analyses[a]

	C	H	I	N	(PF₆)⁻
Ia from γ-Pic + I₂	45.7	4.43	42.8	8.15	
C₁₂H₁₃N₂I requires	46.1	4.16	40.7	8.97	
Ia from (γ-Pic₂I)⁺, PF₆⁻ + γ-Pic	43.6	4.76	32.0	8.15	11.6
Empirical formula	12	15.8	0.84	1.93	0.26
Ib	38.5	3.53	46.9	7.38	
C₁₈H₁₉N₃I₂ requires	40.67	3.57	47.8	7.9	
Ic	37.79	3.26	47.6	7.52	
C₂₄H₂₅N₄I₃ requires	38.4	3.30	50.8	7.46	

[a] Given in per cent.
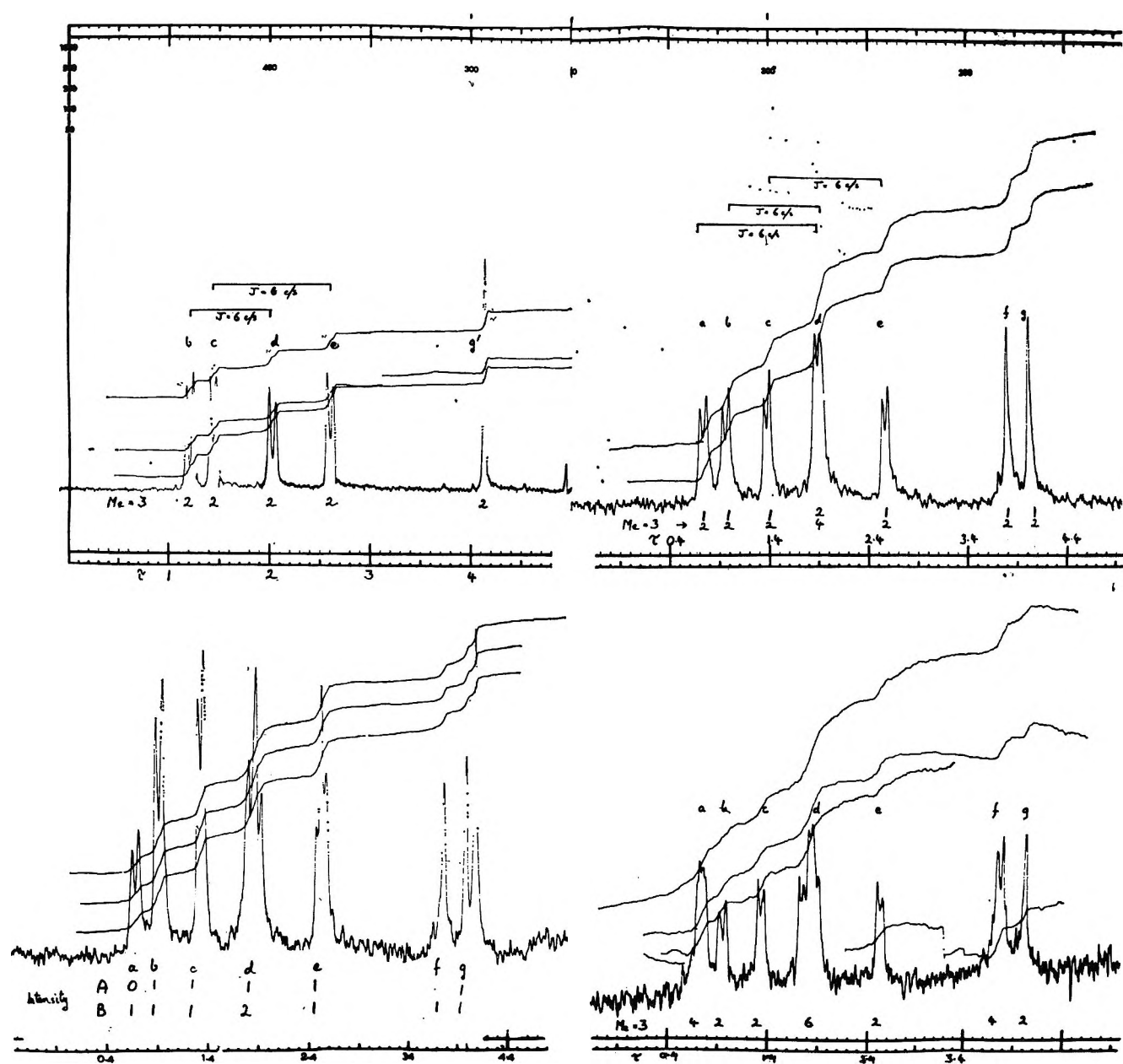
Figure 9. Top left, nmr spectrum of Ia (intensities relative to Me equal to 3 protons indicated); top right, nmr spectrum of Ib; bottom left, nmr spectrum of a mixture of Ia and Ib; bottom right, nmr spectrum of Ic.

an immediate of AgI. On extraction, a noncrystalline residue was obtained, which contained no iodine. The presence of nitrate bands is clearly shown in the infrared spectrum. The remaining bands, although bearing a general similarity to those of solid Ia, show shifts of up to 10 cm^{-1}. We take this to indicate that the Ia infrared spectrum does not depend on the presence of iodine, and that the nitrate salt is rather unstable, as indicated by its slow brownish discoloration.

To determine the nature of the cation more precisely, the nmr spectrum of the Ia iodide was examined (Figure 9). Decoupling experiments show the doublets d and b were coupled, likewise the doublets e and c, each individual doublet representing two protons, relative to

Me equal to 3 protons. This indicates the structure Ia as shown, the d–b pair of doublets being assigned to the

$$CH_3 \overset{d\ b}{\underset{}{\text{—}}} \overset{+}{N} \overset{g'}{\underset{}{\text{—}}} CH_2 \overset{e\ c}{\underset{}{\text{—}}} N \quad I^-$$

Ia
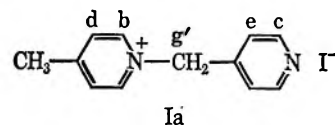
ring bearing the formal charge. The structure is consistent with the analytical results. The absence of an $^+$NH stretching vibration in the infrared and the overall cation:anion ratio shows the cation is the free base and bears only a single unit charge. Although we have not attempted a complete vibrational assignment of the infrared spectrum (see Table II), comparison with

closely related compounds[5-7] shows that it is consistent with structure Ia; in particular the 605-cm^{-1} band is identified as a CH$_2$ deformation mode. The mass spectrum (see Table III) generally supports the structure shown, the peaks assigned to CH$_2$-4-C$_5$H$_4$N at m/e 92 and CH$_3$-4-C$_5$H$_4$N at m/e 93 being particularly prominent. The peaks at m/e 184 and 185 suggest the presence of CH$_2$-4-C$_5$H$_4$NCH$_2$-4-C$_5$H$_4$N and CH$_3$-4-C$_5$H$_4$NCH$_2$-4-C$_5$H$_4$N. In view of the pronounced thermal instability of Ia (see the following section), the agreement with the proposed structure appears reasonable.

In earlier work on the product, we followed Glusker and Miller's procedure and recrystallized from ethanol-water mixtures. The light brown product (mp 218°, decomposition) gave an infrared spectrum having strong, sharp bands at $\sim$580 and $\sim$606 cm^{-1}. The variation in the relative intensities of these two bands indicated that a mixture was present. Repeated recrystallization to constant infrared spectrum gave a product Ib containing sharp bands at 580 and 608 cm^{-1} of nearly equal intensity (Figure 10). Despite the close coincidence of many bands in the spectrum with bands of Ia, there are many distinct lines in the Ia infrared spectrum that have no counterparts in Ib (see Table II) and *vice versa*. Consequently, if Ia and Ib are single species (which we believe because of the constancy of their infrared and nmr spectra), they must be distinct.

The nmr spectrum of Ib is shown in Figure 9. The lines b, c, d, e, and g found in Ia are still present, with the same intensity relative to Me, the same coupling, and almost the same positions. There are, in addition, a further pair of two-proton doublets a–d and a two-proton resonance at f. As with the infrared spectra, one is concerned whether or not the sample could be a mixture of Ia and a 6-proton species X giving the new lines. In samples recrystallized to a constant infrared spectrum, the intensity ratio of the common and new lines would represent equimolar proportions of Ia and X—this is unlikely to arise fortuitously in a mixture. Decisive proof that Ib is not a mixture of Ia and X is provided by the nmr of a nearly equimolar mixture of Ia and Ib (Figure 9). If Ib already contained Ia, line g would be simply enhanced. In fact, two lines are seen; hence Ib contains no Ia and is a distinct species. The nmr spectrum is readily assigned to the structure Ib shown.

Ib
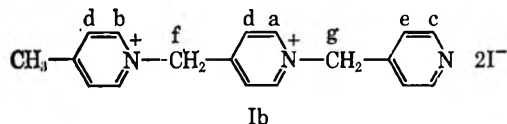
Structures involving substitution in the rings would involve a single-proton resonance, which is not observed. Further, the spectrum of Ib indicates that still only a single methyl group is present, so that an alternative such as (CH$_3$-4-C$_5$H$_4$NCH$_2$-4-C$_5$H$_4$N-I-NC$_5$H$_4$-4-CH$_3$)$^{2+}$ can be eliminated. If structure Ib is adopted,

Table II: Infrared Spectra of Solids Ia, Ib, and Ic as the Iodides

Solid Ia	Solid Ib	Solid Ic
1639 s	1631 s	1633 s
1600 sh	1598 ms	1597 m
1592 ms	...	...
1562 w	1560 m	1561 m
1513 ms	...	1513 m
...	1504 ms	1504 ms
1428 s	...	...
1416 ms	1413 s	1415 ms
1333 w		
1307 m	1295 s	1295 w
1239 w		
1231 w	1233 w	1233 sh
1224 w	1224 m	1222 w
1207 m	1205 w	1207 m
		1190 w
1172 s	...	...
...	1162 ms	1165 ms
...	1148 ms	1156 ms
1131 w	1131 w	
		1095 sh
1070 w	1073 w	1071 w
1044 w	1048 w	1050 w
...	1031 w	1034 w
1015 sh	...	...
...	1000 m	...
...	...	996 w
993 m	...	991 w
...	...	961 (broad) m
947 w	947 sh	
...	...	884 ms
869 vw		
858 sh		
847 w		
...	838 ms	838 w
...	826 s	824 ms
816 s	816 sh	814 sh
799 ms	...	...
...	...	773 m
758 s	765 s	759 s
...	735 ms	...
724 m	721 ms	724 s
...	711 ms	...
704 m	704 sh	705 m
666 w	668 w	666 w
663 w	662 w	
605 s	608 s	608 s
...	582 s	
...	...	577 s
...	521 ms	
...	...	514 ms
509 ms	500 sh	...
490 s	487 ms	489 s
454 m	455 m	
...	417 m	

the similarities in the nmr spectrum to that of Ia are readily explicable, as are also the positions and coupling of the new lines. The composition Ib is also supported

(7) E. Spinner, *J. Chem. Soc.*, 3860 (1963).

Table III: Mass Spectra[a]

Mass ratio, m/e	Solid Ia (as iodide) rel abun-dance	Solid Ib (as iodide) rel abun-dance	Tentative assignment
38	6.0	7.5	
39	22.5	33.0	
40	8.6	12.5	
41	3.6	7.0	
50	5.0	6.0	Py ring fragments[b]
51	9.0	11.0	
52	5.8	7.0	
53	5.4	6.9	
54	7.1	8.1	
62	3.0	2.8	
63	8.3	6.3	
64	5.6	10.0	
65	30.8	26.5	γ-Picoline ring fragments
66	30.0	34.0	
67	6.6	7.0	
78	4.8	6.1	C_5H_4N
91	1.9	2.1	$CH\text{-}4\text{-}C_5H_4N$
92	84	55.0	$CH_2\text{-}4\text{-}C_5H_4N$
93	100	100	γ-Picoline
94	6.6	10.0	Isotope
127	10.9	35	I
128	15.5	60	HI
157	nil	2.8	64 + 93 or 65 + 92 fragment
182	1.3	0.5	
184	3.7	0.7	$CH_2\text{-}4\text{-}C_5H_4NCH_2\text{-}4\text{-}C_5H_4N$
185	1.8	...	$CH_3\text{-}4\text{-}C_5H_4NCH_2\text{-}4\text{-}C_5H_4N$
219	15.3	6.5	$CH_2\text{-}4\text{-}C_5H_4N\text{-}I$
220	1.0	0.4	Isotope
254	8.2	47.0	I_2
275	1.0	...	

[a] Peaks with relative abundance less than 1% in both solids are omitted. [b] J. E. Collin and R. Cahay, *Bull. Acad. Roy. Belg.*, **52**, 606 (1966).

by the analysis (Table I). Further, the similarities in the infrared spectra of Ia and Ib are now simply explained. The band at 608 cm⁻¹ (the slight change in frequency is apparent on detailed examination) can be assigned to the end CH₂ group, while 580 cm⁻¹, of almost equal intensity, can be ascribed to the new CH₂ group. The 580-cm⁻¹ line is often much weaker than the line near 605 cm⁻¹ in the infrared spectra of the initial reaction products, and it appears that Ib has largely been produced as a result of the heating involved in the recrystallization. The mass spectrum (see Table III) resembles that of Ia and, while supporting the close relationship of Ia and Ib, appears to be indecisive in confirming the detailed proposal for Ib. The larger proportion of iodine in this compound is apparent.

In some earlier samples we noticed that the band near 580 cm⁻¹ was more intense than at ∼606 cm⁻¹. This could not result from a mixture of Ia and Ib. Recrystal-
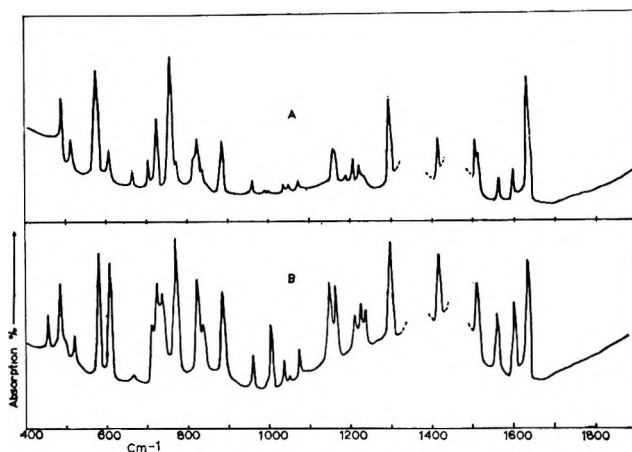
Figure 10. A, Infrared spectrum of Ic (mull); B, Infrared spectrum of Ib (mull). Mull bands omitted.

lization from methanol also resulted in a solid Ic (mp 227°, decomposes) with the 580-cm⁻¹ band stronger than the 605 cm⁻¹ in the infrared spectrum, shown in Figure 10. The nmr spectrum is shown in Figure 9. It corresponds closely to that of Ib, with the addition of a yet further pair of two-proton doublets at the a–d position, and also a further two-proton resonance at f′. Assignment to the "tetramer" structure Ic is suggested

Ic
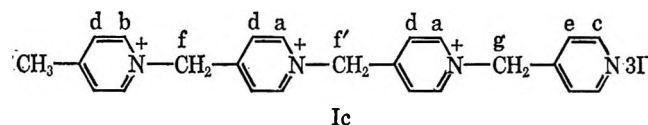
by comparison with Ib. The absence of further lines at g, together with the nearly integral intensity ratios shows Ic does not contain Ib or Ia. The elemental analysis (Table I), however, is not very satisfactory and indicates that Ic has not been cleanly isolated. The frequency and relative intensity of the CH₂ modes in the infrared spectrum further support this structure; there are now two chain CH₂ groups, contributing to the 580 cm⁻¹ band, for one end CH₂ group.

The proposed structures for Ia, Ib, and Ic also explain the surprising absence of any marked absorption bands in the low-frequency range; the sole weak band at 210 cm⁻¹ is due to the end Me group.[5]

It is notable that more prolonged refluxing was entailed in the recrystallization from methanol, further supporting the view that polymerization proceeds in the recrystallization process.

As the chain length of the polycation increases, the empirical formula approaches $(C_6H_7NI)_n$, if the counterion is entirely iodide. This is the composition observed by Glusker and Miller, suggesting that the substance isolated by them was the polymer. The cryoscopic depression observed by these authors also agrees with this interpretation, as do the remainder of their observations (see quotation). In the species we have examined, the presence of the Me group and

the general features of the nmr spectra show there is no appreciable ring closure to give polymers such as shown.
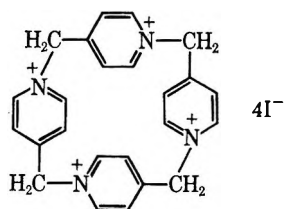
This, however, cannot be excluded as the substance reported by Glusker and Miller.

Finally, we return to the nature of the reaction product which gives rise to the bands at 536 and 1018 cm^{-1}, present in aged solutions of I_2 in γ-picoline (product II). These bands are absent in solids Ia, Ib, and Ic, and presumably have been eliminated in the washing involved in working-up these solids. Direct spectroscopic examination of a CH_2Cl_2 wash of the reaction product confirms the presence of both the 536- and 1018-cm^{-1} bands. Owing to the presence in the solution spectrum of bands due to unreacted γ-picoline and some dissolved solid Ia, only a few further characteristic bands of product II can be identified. These are at 478 cm^{-1} and a broad band centered about 2720 cm^{-1}, with a smaller shoulder near 3376 cm^{-1}. These bands strongly suggest that II is an H-bonded γ-picoline species. We have, therefore, examined the infrared spectrum of γ-picoline hydrogen iodide dissolved in an equimolar mixture of CH_2Cl_2 and γ-picoline. The frequency, intensity, and contours of all four identifiable bands of compound II are reproduced, showing this to be a solution of γ-PicHI and accounting for the proton eliminated in the reaction.

$$(\gamma\text{-Pic}_2I)^+ \longrightarrow (Ia)^+ + I^- + H^+$$
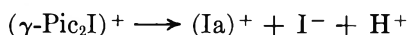
Comparison of the spectra with those of pyridinium salts in solutions containing pyridine[8] indicates that the H-bonded species II is (γ-PicH-γ-Pic)$^+$, I$^-$ rather than (γ-PicH)$^+$, I$^-$.

Conclusion

No attempt has been made to formulate a detailed course or to quantitatively examine the kinetics of the reactions. The absence of a direct reaction between I_2 (in excess) and γ-picoline, the absence of reaction in nonpolarizing solvents, and the lack of any notable distinction between the rates in daylight and the dark suggest that a heterolytic rather than a homolytic process is involved. Electron transfer from the γ-picoline ring increases in the series (γPic$_2$I)$^+$ > γPicI$_2$ > γ-picoline,[3,5] and the following reaction scheme involving the removal of a proton from the (γPic$_2$I)$^+$ ion by the free γ-picoline base present may be tentatively proposed.[9]
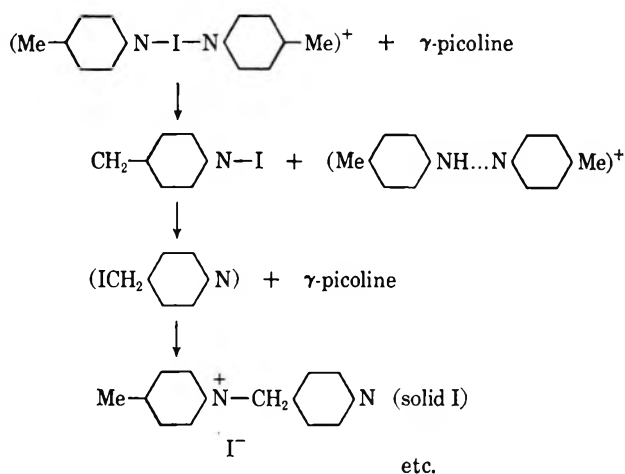
Establishment of the detailed mechanism of the reaction process requires extensive investigation beyond the objectives of the present examination, which has been to explain the main temporal changes in the spectra of solutions of iodine in γ-picoline and the nature of the products formed.

Experimental Section

Materials. BDP γ-picoline was first dried over sodium sulfate (anhydrous) and then over barium oxide, and then was fractionated. The purity of γ-picoline thus obtained and examined by vpc, was found to be 99%. AR Iodine was used without further purifications.

Reaction. A saturated solution of iodine in γ-picoline was prepared and kept for 24 hr, when it had become a solid mass. This was washed several times with ethanol and finally with sodium-dried ether, and dried. Column chromatography of this solid showed the presence of three components.

Product Isolation. Solid Ia. A saturated solution of iodine in γ-picoline was kept for about 3 hr. Two volumes of ethanol were added, the solid remaining was removed by filtration, and again was washed with ethanol. On adding ether to the combined filtrates, a precipitate was obtained, separated, washed, dried, and recrystallized from ethanol. The solid was then dissolved in hot ethanol and was cooled in an ice–salt freezing mixture; the light microcrystalline substance obtained was separated by filtration. To the *filtrate*, dried ether was added until precipitation was complete. This ppt was washed with sodium-dried ether and dried *in vacuo* (mp 175°).

Solid Ib. A saturated solution of iodine in γ-picoline was prepared and kept for 24 hr, becoming a solid mass. This was ground, was washed with alcohol several times, finally was washed with dried ether, and was dried. It was then dissolved in a mixture of water and alcohol (1:100), was boiled for 1 min, and then was filtered.

(8) T. R. Singh and J. L. Wood, unpublished data.

(9) J. H. Ridd, private communication.

The filtrate was cooled in Dry Ice for 2 hr—a microcrystalline light-brown solid was precipitated, filtered, washed, dried, and again crystallized (mp 218°, decomposition).

Solid Ic. A saturated solution of iodine in γ-picoline was kept for about 6 hr. The solid thus obtained was filtered, was washed several times with ethanol and then ether. The dried substance was mixed with Analar methanol and boiled for 1 min., when most of the solid dissolved. The filtrate was then cooled in solid carbondioxide for 2 hr. The resulting precipitate was filtered, was washed with ethanol then ether, and was dried with dry nitrogen. It was again recrystallized from methanol, was washed, and was dried (mp 227°, decomposition).

Infrared Spectroscopy. Above 400 cm^{-1} infrared spectra were recorded using a Grubb–Parsons Spectromaster; below 400 cm^{-1} a vacuum grating spectrometer constructed in the department was used. In general KBr windows were used in the high-frequency region and polythene in the lower range. No differences were found between the spectra of samples kept in the cell and samples stored in flasks. Kinetic runs (Figure 2) showed similar development using KBr, AgCl, or polythene windows.

Mass Spectroscopy. Mass spectra were obtained with an AEI MS-9 spectrometer with direct insertion, at T = 200°, p = 5 × 10^{-7} torr; electron impact source, 75 eV and 18 μA. The main peaks above m/e 37 are tabulated in Table III.

Nmr Spectroscopy. Most of the mmr Spectra were recorded using a Varian HA100 nmr spectrometer. Solutions in both dimethyl sulfoxide (dimethyl sulfoxide used as lock signal) and in D$_2$O (tetramethylsilane used as external lock signal) were examined.

The n-Donor Complex Formation and Polymorphic Transformation

of Zinc Phthalocyanine in Organic Suspension Media

by Takashi Kobayashi, Natsu Uyeda, and Eiji Suito

Institute for Chemical Research, Kyoto University, Uji, Kyoto-Fu, Japan   (*Received December 11, 1967*)

The polymorphic transformation process of zinc phthalocyanine dispersed in various organic suspension media was studied by X-ray diffraction, differential thermal analysis, and infrared absorption spectroscopy. Strong n-donor solvents, such as heterocyclic and normal amines, dioxane, and dimethyl sulfoxide, were found to form stoichiometric molecular compounds with zinc phthalocyanine in the solid phase. The compositions were determined by weight-loss measurements and from the thermal behavior of the addition compounds as observed by DTA analysis and X-ray diffraction. The decomposition temperature ranged from 70 to 240°, above which the crystallites were converted into the β form. Solvents other than n donors caused the α form to undergo an ordinary transformation into the β form. The process was found to be consecutive and two different new polymorphs (χ and θ) appeared as the intermediate phases, depending upon whether the suspension media consisted of electron donors or electron acceptors. The infrared absorption spectra assigned to the fundamental bands of the adduct molecules showed large shifts toward higher frequencies, which suggested that the coordination in the complexes could be interpreted in terms of a charge-transfer mechanism.

Many phthalocyanine compounds show a conspicuous polymorphic behavior. For example, a serious difficulty in the production of stable coloring materials in the pigment industry results from the dimorphic transformation of α-copper phthalocyanine to the β form and the consequent spontaneous crystal growth in vehicle solvents. A stepwise mechanism of the transformation in various organic suspension media has been observed[1] by X-ray diffraction and by electron microscopy.

When the experiment was extended to similar systems with zinc phthalocyanine, preliminary electron

(1) E. Suito and N. Uyeda, *Kolloid. Zh.*, **193**, 97 (1963).

microscopic examination showed that, unlike ordinary solvents which usually caused the dimorphic α–β transformation, as in the case of copper phthalocyanine, pyridine produced unusual crystallites which greatly differed in crystal habit and structure from the ordinary slender crystallites of the β form. Differential thermal analysis and infrared spectroscopy indicate that this final product was apparently an additional compound with the pyridine molecules included in it. As is well known, pyridine can be a strong electron donor, particularly when it forms a charge-transfer complex with a suitable acceptor such as iodine. Not only pyridine but many other heterocyclic and normal amines are often referred to as being strong n donors, in the sense that their characteristic electron-donating properties are considered to be due to their nonbonding electron pairs whose orbitals are ready to overlap with those of the electron acceptors. Several investigators[2] have reported that some metal derivatives of phthalocyanine form addition complexes, especially with some n-donor molecules. As for zinc phthalocyanine, spectroscopic evidence of solvation was presented by Whalley[3] for the pyridinium salt formed in a pyridine solution. On the other hand, zinc phthalocyanine is known to play the part of the electron donor for strong acceptors, such as 2,4,6-trinitrotoluene, sym-trinitrobenzene, and 2,4,7-trinitro-9-fluorenone, as shown by McCartin[4] in a spectroscopic investigation of the donor–acceptor equilibria in solution.

This behavior of phthalocyanine compounds suggested that the donor–acceptor interaction between the solvent and zinc phthalocyanine dispersed in it would have a certain influence on the dimorphic transformation and also that a suitable choice of solvent would lead to the formation of stable crystallites of other addition compounds.

Also, phthalocyanine compounds are of great interest because of their charge-transporting properties and their possible use as organic semiconductors. To date, most studies have been concerned with the unsolvated species. Formation of stable complexes of solvents and metal phthalocyanine derivatives could be used to vary the electric properties of the organic solid.

With these points in mind, the polymorphic transformation of zinc phthalocyanine in the presence of various organic dispersion media is investigated. Of particular interest is the behavior of some oxy compounds and various amines as n donors in the formation of stable crystalline complexes.

Experimental Section

A. Preparation of the Samples. The zinc phthalocyanine was synthesized by heating a stoichiometric mixture, composed of pure zinc and phthalonitrile purified by sublimation under reduced pressure, at 270–350° for about 5 hr and with constant stirring. The crude zinc phthalocyanine was purified by first

washing for 24 hr with pure acetone in a Soxhlet extractor and then by repeated sublimation in a silica tube, 3-cm i.d., with a nitrogen atmosphere flowing at 50 cm³/min. The resulting needlelike crystals were converted into a finely divided powder by the acid-paste method, which is widely used for obtaining coloring materials. It was pointed out by Robertson[5] in his investigation of metal-free, Be, Mn, Fe, Co, Ni, and Cu phthalocyanines that many phthalocyanines which assume a needlelike crystal habit when prepared by sublimation under reduced pressure have a conspicuous isomorphism. In this study, X-ray diffractometry suggests that the zinc derivative is also isomorphic. The needlelike crystals obtained in the present study are identified as the β form. The crystallographic modification of the zinc phthalocyanine powder prepared by the acid-paste method was shown by X-ray diffraction to assume the α form, which has been revealed[6] to be another isomorphic form for metal-free, Cu, Fe, Co, Ni, and Pt phthalocyanines.

The organic suspension media used in the present work are listed below, where the two groups are separated according to whether the resulting powder was the β form or some other form: group A: benzene, toluene, and xylene; ethyl alcohol, ethyl ether, and acetone; carbon tetrachloride and carbon disulfide; nitromethane, nitrobenzene, and thiophene; N-methylaniline and N,N-dimethylaniline; group B: pyridine, α-picoline, γ-picoline, piperidines, pyrazine, aqueous solutions of methylamine, dimethylamine, trimethylamine, and n-hexylamine; 1,4-dioxane and dimethyl sulfoxide (DMSO).

About 1 g of zinc phthalocyanine powder was dispersed in 10 ml of each solvent of the two groups and was left in stoppered glass tubes at 50° for 48 hr. The precipitated powder was separated from the individual media by filtration and was dried at 50–70° under reduced pressure. With pyrazine, which melts at 53°, the suspension was kept at 60° and the precipitate was separated while hot. The residual medium was evaporated at 80° in air.

B. Analysis Procedure. The crystal forms of the dried precipitates were identified from the X-ray-diffraction patterns taken with Ni-filtered Cu Kα radiation. The scanning speed was 2°/min and the time constant was set at 2.5 sec for automatic recording of the intensities of reflected X-rays. The diffraction patterns were also recorded with the powder separated from the dispersion medium at regular intervals of time

(2) F. H. Moser and A. L. Thomas, "Phthalocyanine Compounds," ACS Monograph 157, Reinhold Publishing Corp., New York, N. Y., 1963.

(3) M. Whalley, *J. Chem. Soc.*, 866 (1961).

(4) P. J. McCartin, *J. Amer. Chem. Soc.*, 85, 2021 (1963).

(5) J. M. Robertson, "Organic Crystals and Molecules," Cornell University Press, Ithaca, N. Y., 1953.

(6) M. Ashida, N. Uyeda, and E. Suito, *Bull. Chem. Soc. Jap.*, 39, 2616 (1966).

Table I: The X-Ray Diffraction Data for Zinc Phthalocyanine Complexes Formed in Various n-Donor Suspension Media

ZnPc (α form)		ZnPc (β form)		Pyridine (αPc-py)		Pyridine (βPc-py)		α-Picoline	
d, Å	I/I_0	d, Å	I/I_0	d, Å	I/I_0	d, Å	I/I_0	d, Å	I/I_0
12.99	vs	12.56	vs	12.99	vw	14.36	vs	13.18	s
12.30	s	9.50	vs	12.03	w	12.44	vw	10.63	s
10.10	w	8.34	m	10.33	s	11.55	s	9.10	m
9.54	m	7.03	m	8.99	w	9.50	m	7.25	m
8.90	w	6.37	w	8.35	m	8.38	vw	6.88	s
5.70	m	5.81	w	7.02	s	8.30	vw	6.68	w
5.51	m	4.86	m	5.90	vw	7.75	vw	5.92	s
4.28	w	4.74	m	5.71	s	6.75	vw	5.71	vw
3.46	s	4.53	w	5.48	m	5.73	w	5.53	m
3.42	s	4.40	w	5.15	m	5.63	vw	5.09	s
3.40	s	4.21	m	4.96	vw	5.42	s	4.97	m
3.23	m	4.10	w	4.79	w	5.27	w	4.86	m
2.92	m	4.00	w	4.64	w	4.99	vw	4.78	m
		3.88	m	4.33	w	4.79	w	4.67	w
		3.76	s	4.21	w	4.65	s	4.55	w
		3.39	s	4.14	m	4.13	w	4.36	m
		3.15	m	3.88	w	4.08	w	4.23	m
		3.02	w	3.78	m	3.98	m	4.17	w
		2.93	s	3.64	s	3.78	s	3.90	m
		2.84	w	3.52	m	3.60	vw	3.67	m
		2.77	w	3.41	vs	3.46	s	3.56	w
		2.69	w	3.32	m	3.25	vw	3.45	m
				3.24	m	3.19	m	3.38	vs
				3.08	m	3.10	w	3.25	m
				2.94	w	2.94	w	3.07	w

γ-Picoline		Pyrazine		Piperidine		Methylamine		Dimethylamine	
d, Å	I/I_0	d, Å	I/I_0	d, Å	I/I_0	d, Å	I/I_0	d, Å	I/I_0
11.94	s	16.98	vw	12.14	s	11.94	vs	11.78	s
11.04	s	13.70	vw	8.50	w	9.25	m	9.40	w
10.52	s	12.62	vs	7.75	vs	8.11	vs	8.18	vs
8.66	s	11.78	m	7.08	m	7.86	s	8.04	m
8.18	w	9.93	vs	6.13	m	7.25	vw	7.28	vw
7.52	vw	9.70	s	5.47	w	6.48	w	6.55	vw
6.25	vw	9.02	w	4.99	s	6.00	s	6.06	m
6.06	vw	8.58	m	4.79	m	5.68	w	5.71	w
5.62	s	8.33	m	4.62	w	5.03	m	5.06	m
5.29	vw	8.11	m	4.33	vs	4.86	s	4.90	s
5.14	s	7.28	s	4.19	s	4.50	m	4.57	m
4.74	s	6.91	m	4.08	m	4.41	m	4.44	m
4.62	vw	6.65	w	3.87	m	4.30	s	4.36	s
4.28	w	6.39	vw	3.78	w	4.00	s	4.07	m
4.16	m	5.94	w	3.54	w	3.97	m	3.97	m
4.07	m	5.75	m	3.39	w	3.63	m	3.88	w
3.94	s	5.60	s	3.22	vw	3.57	s	3.66	w
3.75	vw	5.32	m	3.16	vw	3.45	w	3.61	m
3.61	w	5.14	s	2.89	w	3.33	s	3.36	s
3.50	w	4.95	m	2.85	m	3.24	m	3.22	m
3.38	vs	4.87	s	2.70	w	3.17	m	3.05	vs
3.25	m	4.67	w	2.58	w	3.01	s	2.94	w
3.13	m	4.57	m	2.45	vw	2.87	w	2.87	w
3.03	w	4.49	m	2.37	vw	2.84	w	2.83	w
2.99	w	4.33	vw	2.35	vw	2.50	w		

Trimethylamine		n-Hexylamine		n-Hexylamine (140°)		DMSO		1,4-Dioxane	
d, Å	I/I₀	d, Å	I/I₀	d, Å	I/I₀	d, Å	I/I₀	d, Å	I/I₀
13.18	w	12.27	vs	17.66	vw	14.72	w	13.38	vs
11.40	vs	11.93	s	16.35	vw	13.09	w	12.62	w
10.00	m	9.78	w	12.80	w	10.27	m	9.60	w
8.34	s	8.75	m	12.40	w	9.71	s	9.11	m
8.08	s	8.22	w	11.55	s	8.93	m	7.25	vw
6.60	w	7.59	vw	11.18	m	8.79	s	6.28	w
6.02	w	7.08	vw	10.91	m	8.22	m	5.82	m
5.53	w	6.19	w	10.39	m	7.56	w	5.68	w
5.26	m	6.01	w	10.10	vs	7.37	m	5.30	w
4.96	s	5.71	vw	9.30	vw	7.07	w	5.21	vw
4.48	vs	5.58	vw	8.54	s	6.91	s	5.09	w
3.95	w	5.50	vw	7.78	w	6.27	w	4.88	vw
3.59	m	5.29	m	7.25	vw	6.21	w	4.77	w
3.31	vs	4.95	w	6.57	vw	6.04	w	4.57	m
3.27	s	4.71	m	6.37	w	5.86	w	4.39	w
3.20	m	4.53	m	6.32	m	5.80	w	4.21	w
3.04	m	4.46	w	5.98	vw	5.37	m	3.79	m
2.88	w	4.38	w	5.86	m	5.03	s	3.74	m
2.63	w	4.19	w	5.73	vw	4.88	m	3.49	w
		4.02	s	5.57	s	4.60	m	3.40	w
		3.86	vs	5.43	vw	4.39	m	3.18	m
		3.81	m	5.12	m	4.31	w	3.16	w
		3.74	w	4.92	w	4.16	m		
		3.62	w	4.79	m				
		3.53	w	4.53	w				

during the intermediate stages of reaction in the suspension.

When the resulting powder showed a new diffraction pattern which was distinctly different from either the α or β polymorph, differential thermal analysis using a conventional apparatus was applied to it to determine the behavior of the crystalline powder upon being heated. In these cases, a specimen of about 200 mg of each powder was heated to about 300° at a rate of 10°/min. A Pt—Pt–10% Rh thermocouple was used to detect the temperature difference between the sample and the α-alumina powder reference. Since one to three endothermic peaks appeared in most of the dta curves, weight loss due to the heat treatment was examined for all these specimens, in order to determine the formation of addition compounds. The crystallographic change caused by the heat treatment was detected by a second X-ray diffraction measurement of the specimens which were taken from the furnace right after the dta scanning produced a peak. Some specimens which gave rise to complicated thermal behaviors showing more than one dta peak were examined with a conventional high-temperature X-ray diffractometer in order to examine the crystal phase at elevated temperatures. The temperature of the furnace was controlled, with an accuracy of ±0.5°.

The infrared absorption spectra of the specimens were recorded with a Perkin-Elmer Model 521 grating spectrometer. The accuracy in frequencies was ±0.5

cm^{-1}, as calibrated with polystyrene film. The samples were prepared in Nujol with powder specimens of group B which had been dried under vacuum in order to eliminate the solvent molecules adsorbed on the surface of the crystallites.

Insomuch as it appeared that the solvents in group A simply changed the α form into the β form, whereas those in group B formed different crystal phases, the effect of group A was examined by redispersing the powder of the new crystal phases, for instance in acetone and ethyl ether.

Results and Discussion

A. X-Ray Diffraction. The X-ray powder diffraction patterns obtained from group A were identical with one another and suggested that the resulting powders had been all converted into the same β form. For example, the diffraction patterns of the specimens obtained in acetone and xylene are displayed in Figure 1 together with that of the original α form for comparison. Thus the phenomenon that took place in the solvent of group A was simply the α–β transformation, as in the case of the copper phthalocyanine. No addition compounds were formed with the solvated molecules.

The situation appeared to be much more complicated for the specimens produced in the solvents of group B. Several representative diffraction patterns are reproduced in Figure 2. The interplanar spacings of all the specimens are listed in Table I. The diffraction
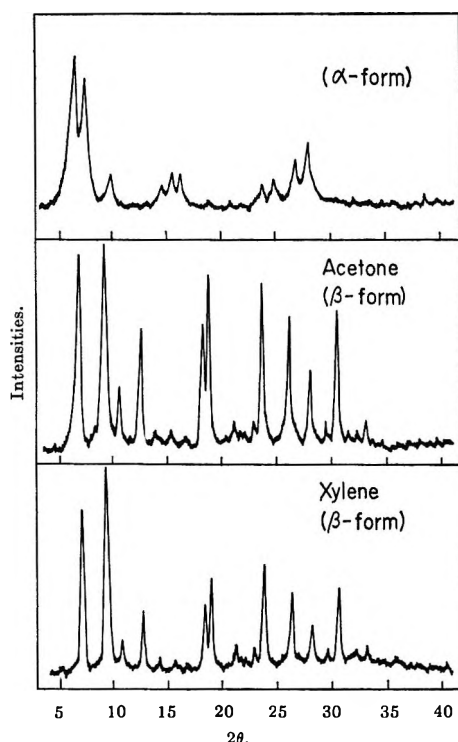
Figure 1. X-Ray powder diffraction patterns of the α and the β forms of zinc phthalocyanine.

data greatly differ not only from those of the α and β forms but also from one another, apparently indicating the formation of new phases which are closely associated with the difference in the treating solvent.

When β-zinc phthalocyanine powder prepared by pulverization of the needlelike crystals was used (instead of the α form) as the starting material, the same phase as that produced from the α form was brought about in every solvent of group B, with pyridine as an exception. The transition process from the β form was stepwise in pyridine, which produced at first another isolable phase, βPc–py, as shown by the diffraction data in Table I. A further treatment in pyridine finally gave rise to one identical with that from the α form, αPc–py.

Note that the characteristic feature of these diffraction patterns was that a great number of reflections were observed with the individual specimens. As there was a possibility that this effect might be due to the formation of a mixture of different crystal forms, electron microscopy was applied in order to examine the aspect of the individual crystallites. The results of the morphological observation and coordinated selected-area electron diffraction suggested that each specimen was uniform; the details will not be presented here. In some cases, particularly for n-hexylamine and DMSO, small microscopic single crystals were obtained, definitely triclinic in appearance. This suggested that the crystal symmetry was markedly lower than that of the β form. As the β form is known to be monoclinic,
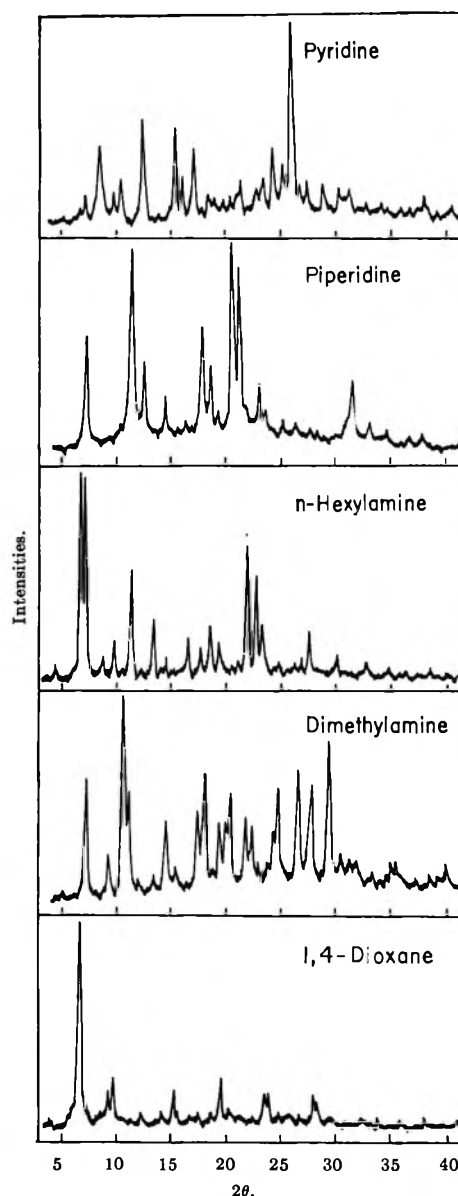
Figure 2. X-Ray powder diffraction patterns of zinc phthalocyanine complexes obtained in various n-donor suspension media.

$P2_1/c$, as pointed out by Robertson,[5] these new phases may be attributed either to the triclinic or to the monoclinic system with fewer symmetry elements. It is interesting to note that, among many different crystals of the new phases, the diffraction data of specimens obtained in methylamine and dimethylamine suggest a possible isomorphism and suggest that, in general, the interplanar spacings are slightly expanded for the specimen prepared in dimethylamine, which has a larger molecular size than methylamine.

B. The Differential Thermal Analysis of Solvated Complex Crystals. The differential thermal curves are reproduced in Figure 3, where the endothermic reactions are shown as downward deflections. With the specimens of group B, the dta curves generally showed at
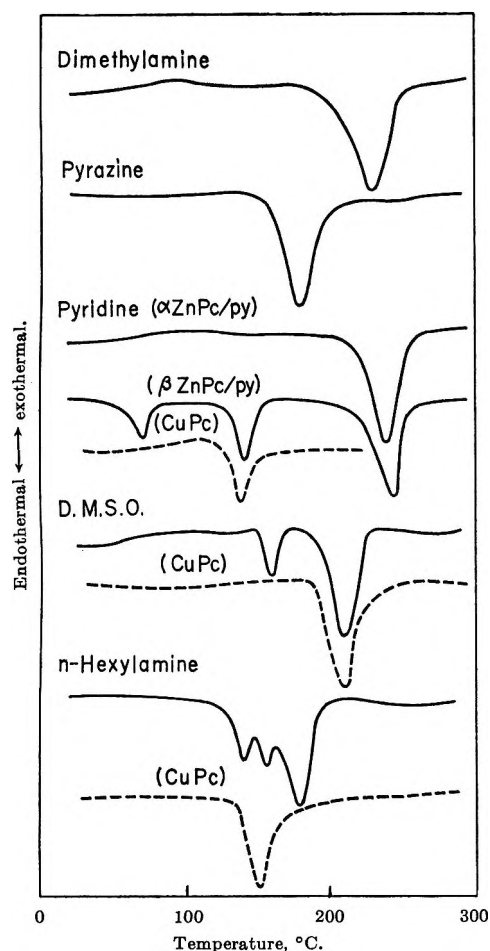
Figure 3. Differential thermal curves of zinc phthalocyanine complexes obtained in various n-donor suspension media. Rate of temperature elevation 10°/min.

Table II: Thermal Behavior and Composition of the Zinc Phthalocyanine Complexes Formed in Various n-Donor Solvents

Solvent component	Bp (solvent), °C	Temp (dec), °C	—Wt loss, %— Obsd	Calcd	Compn (ZnPc: solv)
Pyridine (αPc–py)	115	240	12.9	12.1	1:1
Pyridine (βPc–py)	115	70	10.2[a]	10.8[a]	1:2
		240	20.5	21.5	
α-Picoline	129	210	14.0	14.0	1:1
γ-Picoline	143	220	19.5	19.4	2:3
Piperidine	106	240	22.8	23.9	1:2
Pyrazine	116	180	16.5	17.2	2:3
Methylamine	−6.5	210	7.1	7.5	2:3
Dimethylamine	7.5	230	11.3	10.5	2:3
Trimethylamine	3.5	210	9.3	9.3	1:1
n-Hexylamine	130	140	b	b	b
		180	22.5	20.8	2:3
Dimethyl sulfoxide	189	160	16.3	16.8	2:3
1,4-Dioxane	101	110	7.1	7.1	2:1

[a] One molecule is released at 70°. [b] The intermediate product was not isolated.

least one distinct endothermic deflection peak and in a few cases two or three peaks were observed, all ranging between 70 and 240°, as listed in Table II. Since these changes were found to be thermally irreversible, X-ray diffraction was applied to the specimens which had been heated beyond the end point of an endothermic reaction in order to identify the new crystal form. The results indicated that all specimens with a single dta peak were converted into the β modification, independent of the initial treatment. This also occurred with other samples where more than one differential thermal peak appeared if the specimen was heated beyond the highest temperature peak. The specimen prepared in DMSO exhibited two peaks, at 160 and 210°. In this case, the crystal was already converted into the β form after the lowest temperature peak and the second peak was not associated with any additional change in crystal modification. As for βPc–py, which was the intermediate product prepared from the β form in pyridine, three peaks were observed, at 70, 140, and 240°, as shown in Figure 3. The crystal form of the powder which was heated at temperatures between the lowest and highest temperature peaks was shown to be the

same as that produced from the α form, αPc–py, regardless of the existence of the middle peak, as revealed by the X-ray diffractometry applied to the specimens after they were cooled to room temperature. Thus it may be reasonable to suggest that the shape and the position of the third peak is similar to the single peak of the αPc–py. A similar thermal behavior was found with the specimen obtained in n-hexylamine. The small middle peak had nothing to do with any phase transition. The crystal structures at both sides of the peak were identical but differed from either that of the initial crystal or that of the final β form. The middle peaks as well as the highest temperature peak for DMSO were considered to be associated with some property of the powder other than a crystallographic-phase change, as will be discussed in detail later.

When a known amount of each powder of group B was heated beyond the endothermic peak to the β form, the product showed a definite weight loss. The per cent weight losses are listed in Table II. Since the final products were all the pure β form of zinc phthalocyanine, the weight loss can be attributed to the release of some solvated molecules as deduced from the endothermic behavior of the specimen. Insomuch as no components other than the solvents themselves were involved in the system, it is obvious that the lost molecules were those of the solvents, and, in other words, the new crystal phases were all solvated complexes. With this assumption, the compositions were estimated as shown in Table II. The calculated per cent weight losses based on these molecular compositions are also presented for comparison. The compositions of these complexes were stoichiometric within the limits of experimental error. As for the pyridine complex,

βPc–py was found to have two solvated molecules. However, another stoichiometric addition compound with one solvated pyridine molecule was formed beyond the lowest temperature peak. A similar result was also obtained with the n-hexylamine complex, from which a certain number of molecules were reduced at the intermediate phase of the thermal treatment.

It is worth noting that the peak temperature of the dta curve is generally much higher than the boiling point of the adduct solvent. Thus the adduct molecules would be instantly discharged into the air whenever decomposition took place. However, for DMSO, n-hexylamine, and pyridine, the lowest peak position is lower than the boiling point or very close to it. In such cases, the released molecules would partly stay adsorbed on the surface of the produced crystallites. In order to demonstrate the behavior of the adsorbed molecules, copper phthalocyanine powder of the β form was kept slightly wet with these solvents and was examined by dta scanning. The curves which are reproduced with broken lines in Figure 3 clearly showed a single endothermic peak at 210° for DMSO, 150° for n-hexylamine, and 140° for pyridine, all slightly higher than the normal boiling points of the pure liquid solvents. The dta curves of the desorption of solvent molecules could well explain the appearance of the middle peaks at 155° for n-hexylamine and at 145° for pyridine, as well as the higher temperature peak at 210° for DMSO, all of which were not directly related to any subsidiary crystal change.

High-temperature X-ray diffractometry was applied in order to confirm the thermal behavior of the specimens in comparison with that revealed by differential thermal analysis. X-Ray diffraction was run at several constant temperatures, which were taken in ascending order. The results were generally consistent with those obtained by ordinary X-ray powder diffraction, although a few exceptions were found to occur and must be discussed in detail. When βPc–py powder was heated beyond the temperature of the lowest dta peak at 70°, the crystals were found to be the α form, instead of αPc–py as suggested by dta and ordinary diffraction. Upon further heating of the specimen stage, the crystals were transformed into the β form at about 150°, which was shown to be the monotropic, thermal-transition temperature of pure zinc phthalocyanine. A similar phenomenon also took place with the specimen prepared in 1,4-dioxane. The specimen heated beyond the temperature ascribed to the single dta peak was the α form, which was in turn converted into the β form above 150°. These results suggest that if the peak temperature of the dta curve was lower than the α–β transformation temperature, the crystal phase just over the peak temperature became the α form and was subsequently subject to the ordinary thermal α–β transition.

The discrepancy in thermal behavior with regard to

βPc–py may be due to the difference in the experimental circumstances. In the case of high-temperature X-ray diffractometry, the surface of the specimen prepared in the form of a thin disk was open to the air within a rather large vessel placed on the goniometer. Pyridine molecules were thus completely removed, leaving the α-form powder on the stage. On the other hand, in the dta studies the specimen was placed in a closed system and an equilibrium must have been attained between the powder and the vapor of released pyridine to form another crystal phase, αPc–py, without reaching complete decomposition.

In summary, the usual methods of preparation of the α-metal phthalocyanine have been either by the acid-paste method or by vacuum deposition onto a cool substrate. These studies of the decomposition behav-
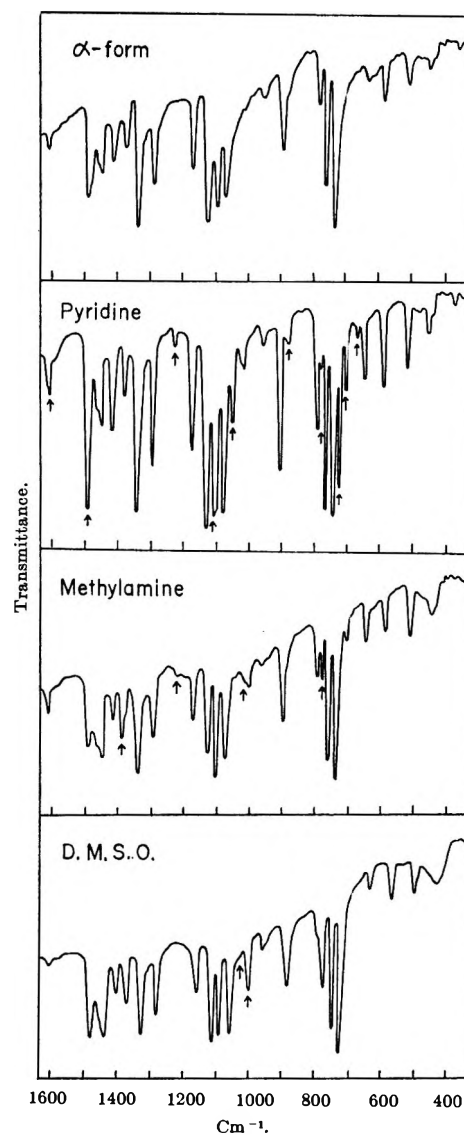
Figure 4. Infrared absorption spectra of zinc phthalocyanine complexes obtained in various n-donor suspension media. Arrows indicate the fundamental absorption bands of the adduct molecules.

Table III: Infrared Absorption Bands of Pyridine and γ-Picoline Involved in Zinc Phthalocyanine Complexes

| Frequency, cm⁻¹ | | | Assign- | Frequency, cm⁻¹ | | | Assign- |
ZnPc–py	Pyridine	Δf	ment[a]	ZnPc–γpic	γpic	Δf	ment[b]
675	650	25	4	539	515	24	6a
771	770	11	11	743	728	15	4
760	747	13	10b	810	800	10	12 + 10b
1008	991	17	1	1019	997	22	1
1035	1030	5	12	1118	1089	29	18b
1092	1067	25	18a	1230	1224	6	9a
1216	1217	−1	9a	1365	1364	1	14
1355	1350	5	6a + 10b	1618	1608	10	8a
1442	1436	6	19a				
1590	1578	13	8a				

[a] N. S. Gill, R. H. Nuttall, D. E. Scaife, and D. W. A. Sharp, *J. Inorg. Nucl. Chem.*, 18, 79 (1961). [b] M. Goodgame and P. J. Hayward, *J. Chem. Soc.*, A, 632 (1966).

ior of the complexes with dioxane and pyridine yield a new method of preparation of the α-zinc phthalocyanine powder from its β form.

C. *Infrared Spectroscopy.* In order to provide further evidence about the identity of the adduct molecules in individual complexes, the infrared absorption spectra of the specimens of group B were recorded. Some representative spectra are reproduced in Figure 4, where distinct absorption maxima of the solvent molecules are marked with arrows. The remaining absorption bands can mostly be assigned to zinc phthalocyanine, although the difference in crystal configuration caused slight shifts of the maxima as well as an intensity change of the absorption, as discussed by Ebert and Gottlieb.[7] In Figure 4, only the spectra of the α form are reproduced for the pure zinc phthalocyanine species. The positions of the observed absorption bands of pyridine and γ-picoline solvated in the respective complexes are listed in Table III. When compared with corresponding bands of pure pyridine and γ-picoline, most of the peak positions were shifted by 10–30 cm⁻¹ toward higher frequencies, as shown in Table III, where the data for pure species were based on those recently reported by Gill, Nuttall, Scaife, and Sharp[8] for pyridine and by Goodgame and Hayward[9] for γ-picoline. A close examination of the present data shows that apparently in both cases the larger shifts are mostly assigned to CH-bending vibrations of aromatic rings such as 10b, 11, 18a, and 18b.[8,9] The macromolecular ring of phthalocyanine with its more complicated absorptions masks many of those for the adduct molecules. However, similar shifts toward higher frequencies were observed with most of the adduct molecules such as α-picoline, piperidine, several aliphatic amines, and DMSO.

D. *Intermediate Stage of the α–β Transformation.* As stated in the previous sections, zinc phthalocyanine powder of the α form treated in the solvents of group A underwent a crystal transformation to the same β form in the final state. However, various crystal forms other

than the ordinary α and β forms were found to appear in the intermediate stage of a total transformation, as shown by X-ray diffractometry applied at definite intervals of time to the specimens treated in several suspension media of group A. For example, some X-ray diffraction patterns are reproduced in Figure 5, where the reflections due to the new phases are distinguished with arrows from the predominant β-form peaks. These new phases always appeared in a state of mixture with the α or β form, indicating the consecutive behavior of the transformation. A comparative examination of these diffraction patterns of the intermediate admixture revealed that they should be classified into three subgroups. The first subgroup contained the intermediate forms produced in methyl alcohol, acetone, ethyl ether, and carbon disulfide, all of which gave rise to an identical set of interplanar spacings for the crystallites of the intermediate form. The second contained those which appeared in nitromethane, nitrobenzene, carbon tetrachloride, and thiophene, which gave rise to another common crystal form.

Since these two new phases are common to the individual classes regardless of the type of solvent, it is reasonable to assume that the intermediate products are not the solvated complexes but are two modifications other than the α and β forms. Although these new phases have not been isolated, they may be tentatively named the χ and θ forms of zinc phthalocyanine for the first and the second subgroups. Infrared spectroscopy, as well as weight-loss measurements, indicated that no solvent molecules were in the specimens of these new phases.

A similar stepwise change has been observed for copper phthalocyanine[1] dispersed in various organic

(7) A. A. Ebert, Jr., and H. B. Gottlieb, *J. Amer. Chem. Soc.*, 74, 2806 (1952).

(8) N. S. Gill, R. H. Nuttall, D. E. Scaife, and D. W. A. Sharp, *J. Inorg. Nucl. Chem.*, 18, 79 (1961).

(9) M. Goodgame and P. J. Hayward, *J. Chem. Soc.*, A, 632 (1966).
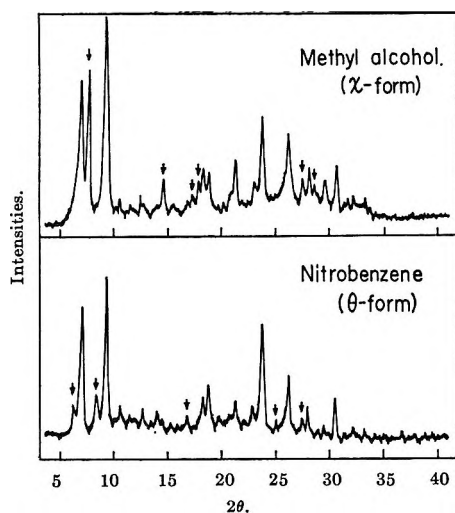
Figure 5. X-Ray diffraction patterns indicating two different new phases (arrows), χ and θ of zinc phthalocyanine mixed with the β form.

suspension media and for copper oxinate[10] dispersed in water. The intermediate product of the copper phthalocyanine system was identified to have the same α form as the reagent and this indicated that α-copper phthalocyanine simply underwent a preliminary crystal growth before the transformation into the β form. However, for copper oxinate, the intermediate form was observed to have a crystal form different from the α and β forms, although the composition of the crystal as copper oxinate dihydrate remained unchanged throughout the transformation.

On the other hand, when the solvents of the third group, N-methylaniline and N,N-dimethylaniline, were used as the dispersion media, the intermediate products gave different X-ray diffraction patterns which were neither identical with each other nor with those obtained from the other systems. These findings suggest the possible formation of new metastable intermediate addition compounds during the transformation process.

E. General Survey of the Transformation Process. It has been pointed out above that the transformation of zinc phthalocyanine occurs by various processes, depending upon the specificity of the suspension media. It may be worthwhile to classify the solvents used in the present work into appropriate groups, as listed in Table IV, according to the products and the behavior of zinc phthalocyanine in them. Generally speaking, the possibility of forming stable solvated crystallites with a definite composition has a close correlation to the fact that the adduct molecules are strong n donors, all having nonbonding electron pairs. As shown in section C, the large shifts of the fundamental absorption bands in the infrared spectra exhibit a general trend for most adduct molecules and indicate the possibility of a charge-transfer mechanism of complex formation. These shifts, most conspicuous for CH-

bending vibrations and aromatic ring deformations, show a trend simliar to those usually observed[11] for donor–acceptor complexes including oxygen- or nitrogen-containing n donors, although Friedlich and Person[12] note that one may not expect the shifts to be too large in such complexes. Zinc phthalocyanine is known to behave as an electron donor in solutions of 2,4,6-trinitrotoluene, sym-trinitrobenzene, and 2,4,7-trinitro-9-fluorenone, all of which are electron acceptors.[4] However, it must be playing the part of an electron acceptor with the ordinary electron donors used in the present work. Since metastable complexes have not been detected with other electron donors in subgroup A-1, such as benzene, toluene, and xylene, the concentrated electron clouds such as those of nonbonding lone pairs are likely to be necessary for the formation of stable complexes under the present experimental conditions.

Although detailed configurations of these complexes are still unknown, the solvated molecules are probably linked to the central metal ion by the use of the nonbonding electron pairs. Such a configuration has been proposed by Elvidge and Lever[13] from their spectroscopic studies of chromium and manganese phthalocyanines in pyridine solutions. A similar molecular pattern was also proposed by Assour[14] in his esr study of cobalt phthalocyanine in pyridine and many other heterocyclic amines. Although these examples were mostly investigated in solutions, it is plausible that similar coordination formulas may be assumed in the crystalline states. An X-ray crystallographic investigation recently reported by Vogt, Zalkin, and Templeton[15] clearly revealed the configuration of the pyridine complex of manganese phthalocyanine, where pyridine and oxygen are perpendicularly conjugated to the central Mn ion, as suggested by Elvidge and Lever[16] on the basis of infrared absorption spectra. In this study also, the infrared absorption data gave indirect evidence for such a configuration, since the general trend and degree of the blue shift in the absorption bands were quite similar to those reported by Gill, et al.,[8] and Goodgame, et al.,[9] in their studies of coordination complexes of metal halides with pyridine and γ-picoline.

Also it may well be that the orbital hybridization which defines the bonding of both molecules differs

(10) E. Suito, M. Arakawa, and T. Kobayashi, Kolloid. Zh., 212, 155 (1966); 213, 135 (1966).

(11) (a) D. L. Glusker, H. W. Thomson, and R. S. Mulliken, J. Chem. Phys., 21, 1407 (1953); (b) D. L. Glusker and H. W. Thomson, J. Chem. Soc., 471 (1955); (c) R. D. Kross, V. A. Fassel, and M. Margoshes, J. Amer. Chem. Soc., 78, 1332 (1956); (d) R. D. Kross and V. A. Fassel, ibid., 79, 38 (1957); (e) R. A. Zingaro and W. E. Tolberg, ibid., 81, 1353 (1959); (f) E. E. Ferguson and I. Y. Chang, J. Chem. Phys., 34, 628 (1961).

(12) H. B. Friedlich and W. B. Person, ibid., 44, 2161 (1966).

(13) J. A. Elvidge and A. B. P. Lever, J. Chem. Soc., 1257 (1961).

(14) J. M. Assour, J. Amer. Chem. Soc., 87, 4701 (1965).

(15) L. H. Vogt, Jr., A. Zalkin, and D. H. Templeton, Science, 151, 569 (1966).

(16) J. A. Elvidge and A. P. Lever, Proc. Chem. Soc., 195 (1959).

Table IV: Classification of Suspension Media and Their Effects in the Transformation and Complex Formation of Zinc Phthalocyanine

Class	Suspension media	Effect	Media type
A-1	Benzene, toluene, and xylene	The α form is directly transformed into the β form	π donors
A-2	Methyl alcohol, acetone, ethyl ether, and carbon disulfide	The α form is transformed into the β form, with consecutive formation of a metastable χ form at the intermediate stage of the total process	Weak n donors
A-3	Nitromethane, nitrobenzene, carbon tetrachloride, and thiophene	The α form is transformed into the β form, with consecutive formation of a metastable θ form at the intermediate stage of the total process	Acceptors
A-4	N-Methylaniline and N,N-dimethylaniline	The α form is transformed into the β form, with consecutive formation of an unstable solvated complex with the solvent	Strong n donors with steric hindrance
B	Pyridine, α-picoline, γ-picoline, piperidine, pyrazine, methylamine, dimethylamine, trimethylamine, n-hexylamine, dimethyl sulfoxide, and 1,4-dioxane	The α and β forms both give a solvated complex of stoichiometric composition with the respective solvent molecule	Strong n donors

according to the species of the central metal ion of the phthalocyanine derivatives, even when the molecular patterns of the complex are similar to one another. For instance, Assour[14] stated that the seventh 3d electron of Co^{2+} was spin unpaired in the $d_{3z^2-r^2}$ orbital which was coupled with the sp^2 orbital of the nitrogen atom of the solvated heterocyclic amines. As for zinc phthalocyanine, the 3d orbitals of the metal ion are wholly filled with ten electrons and the ion is forced by the rigid phthalocyanine macrocyclic ring to fit into the sp^2d orbital of the square-planar configuration, against its tendency to assume a more preferable sp^3 orbital of tetrahedral configuration. In such a case, the coordination of the solvated molecules will call for a hybridization of orbitals which is different from those of the phthalocyanine derivatives of other transition metals. In fact, preliminary investigations of the cobalt and iron phthalocyanines show that the crystal structures of the adduct complexes were different in most cases from the respective complexes with zinc derivatives.

As for methylaniline and dimethylaniline, they form only the intermediate complexes which finally disappear as the transformation proceeds, although they also have nonbonding electron pairs. The instability of these adduct compounds may be due to steric hindrance from the methyl group. A similar example for the methylated imidazole complexes of iron phthalocyanine was reported by Lagenbeck, Schubert, and Giesenmann.[17] However, steric hindrance seemed effective only during the formation of the stable solid and may be referred to as a packing hindrance in the crystal lattice, since the deeply colored greenish-blue appearance of the supernatant solvent suggested that
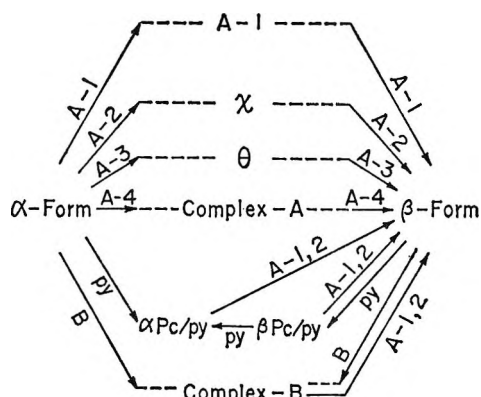
Figure 6. The diagram for total transformation processes of zinc phthalocyanine in various suspension media.

the molecules in solution remained solvated even after the α–β transformation was completed.

As already suggested, the appearance of nonsolvated intermediate phases in the solvents of subgroups A-2 and A-3 is similar to copper oxinate sediments[10] in a water suspension, where the metastable γ form in the course of the α–β transformation is produced. In the present case, however, it must be emphasized that different phases, χ and θ, appear, depending upon whether the solvent is a weak electron donor or an electron acceptor. Although zinc phthalocyanine is barely soluble in most of the solvents listed in Table IV, even the slightest solubility is an essential prerequisite for the occurrence of the transformation. Zinc phtha-

(17) W. Lagenbeck, H. Schubert, and H. Giesemann, Ann., 585, 68 (1954).

locyanine, when dissolved in these solvents, will form a loose complex with the solvent molecule. Such an interaction in solution would have a certain influence on the π-charge distribution of the zinc phthalocyanine in somewhat different ways, according to whether the solvated molecules act as donors or acceptors. Thus these molecules of zinc phthalocyanine which are influenced in different ways by the solvent would be expected to form nuclei of new phases that have molecular arrangements differing from those for the α or β form. The process in which the final β form is produced has not been fully determined at present and more elaborate application of X-ray diffractometry as well as electron microscopy may be necessary in order to approach a better understanding.

The total relationship of the transformation, solvation, and desolvation is schematically illustrated in Figure 6. It has been found that when the n-donor complexes are dispersed in a large quantity of ether or acetone, the precipitates are converted into the β form, in which the adduct molecules are released. Since the β form thus obtained is always ready to form solvated complexes with any solvent of group B, the repetitions of such alternative treatments with pure solvents will render a simpler and more reliable method than the vacuum evaporation or the acid-paste method for the purification of zinc phthalocyanine powder.

Infrared Evidence for FHF⁻ in Annealed LiF–HX Films[1]

by R. L. Redington and T. E. Redington

Department of Chemistry, Utah State University, Logan, Utah   84321, and Department of Chemistry, Texas Technological College, Lubbock, Texas   79409   (Received December 15, 1967)

Infrared spectra indicate that bifluoride ion is formed upon annealing vapor deposited LiF–HX solids. Approximately equimolar amounts of LiF vapor and HCl, DCl, HBr, DBr, or HI were simultaneously condensed onto a CsI window at about 77°K. Bifluoride ion absorptions appear in the spectra of the annealed samples; however, it is concluded that the solids are not well crystallized under the conditions of these experiments.

Introduction

Infrared spectra of FHF⁻ ion isolated as an impurity in several alkali halide lattices have been reported,[2] as well as spectra of crystalline $NaHF_2$[3] and KHF_2.[4,5] However, other bihalide ions have been prepared only in the presence of a large cation, such as tetraalkylammonium ion or Cs⁺ ion[6-12]. As described below, FHF⁻ appears to form upon annealing films formed by depositing LiF and HX from the vapor onto a cold surface. Preferential stability of FHF⁻ over XHX⁻ (X⁻ implies Cl⁻, Br⁻, or I⁻) in these solids is indicated and the influence of several new environments on the FHF⁻ spectra are observed.

Nibler and Pimentel[12] recently described a variation of this technique and demonstrate the power of direct formation of the bihalide ion species and low-temperature spectral studies. They propose a reassignment of the bending fundamental vibration frequency for ClHCl⁻, ClHBr⁻, and ClHI⁻, along with the statement that ClHCl⁻ probably does not possess a center of symmetry in their samples.

In view of the recent literature,[6-11,13] these ideas add considerably to the interest in studying these systems.

Experimental Procedure

The sample films were prepared by the simultaneous

(1) (a) This research was supported in part by the U. S. Army Research Office, Durham, N. C. (b) Direct correspondence to author at: Department of Chemistry, Texas Technological College, Lubbock, Texas   79409.

(2) J. A. A. Ketelaar, C. Haas, and J. vander Elsken, *J. Chem. Phys.*, 24, 624 (1956).

(3) A. Azman and A. Ocvirk, *Spectrochim. Acta*, A23, 1597 (1967).

(4) G. L. Coté and H. W. Thompson, *Proc. Roy. Soc.*, A210, 206 (1951).

(5) J. A. A. Ketelaar and W. Vedder, *J. Chem. Phys.*, 19, 654 (1949).

(6) T. C. Waddington, *J. Chem. Soc.*, 1708 (1958).

(7) J. A. Salthouse and T. C. Waddington, *ibid.*, 4664 (1964).

(8) J. A. Salthouse and T. C. Waddington, *ibid.*, 28 (1966).

(9) J. C. Evans and G. Y-S. Lo, *J. Phys. Chem.*, 70, 11 (1966).

(10) J. C. Evans and G. Y-S. Lo, *ibid.*, 70, 20 (1966).

(11) J. C. Evans and G. Y-S. Lo, *ibid.*, 70, 543 (1966).

(12) J. W. Nibler and G. C. Pimentel, *J. Chem. Phys.*, 47, 710 (1967).

(13) S. S. Chang and E. F. Westrum, *ibid.*, 36, 2571 (1962).

condensation of approximately equal amounts of gaseous LiF and HX onto a CsI crystal cooled to 77°K. A high vacuum was maintained at all times by continuous pumping. Spectra were recorded for various samples at temperatures ranging from extremes of 50°K to about 260°K. The spectra are completely different from those obtained by Nibler and Pimentel[12] on films initially made by depositing small amounts of HCl directly onto CsI or CsCl (e.g., at 183°K under 400 mm of gaseous HCl).

The HX and DX samples were deposited by standard methods from a glass vacuum system (with oil manometer) through a Teflon needle valve at a typical rate of 0.1 mmol/hr. The cryostat pressure was always about 5×10^{-5} mm during the deposition. The vacuum line was flushed with the sample gas before the experiments were run and was wrapped with aluminum foil for the HI preparations and experiments. The DBr and HI were prepared by allowing water, P_2O_5, and NaBr or KI to react. The DCl was prepared by allowing D_2O to react with CCl_3COCl, and HCl and HBr were obtained from the Matheson Co. All of the compounds were dried by trap-to-trap distillation at the lowest practical temperatures. The LiF effused from a 0.030-in. diameter hole in the end of a cylindrical iron furnace heated to about 880°. The furnace, held in position 3 in. from the deposition window by a tantalum cylinder, was 1 in. in diameter with 0.125 in. thick walls. Two radiation shields protected the cold deposition surface. Heating was provided by 15 coils (tantalum, B&S 24) which surrounded the furnace support cylinder. Chromel-p-alumel thermocouples were welded to the rear wall of the furnace and showed a temperature gradient of less than 10° between the furnace edge and its center at 880°. The LiF effusion rate was estimated by weighing the sample produced in extended calibration runs.

The sample temperatures during annealing were determined by a copper-constantan thermocouple imbedded in the CsI window. Spectra were recorded with a Beckman IR-12 spectrophotometer.

Spectral Observations and Discussion

Spectra of a freshly deposited, partially annealed, and fully annealed sample of LiF condensed with HCl are shown in Figure 1. Spectra of annealed samples of LiF condensed with HCl, DCl, HBr, DBr, and HI are shown in Figure 2. The spectra are discussed together in view of the similarities easily discerned in the figures.

Annealing induces similar spectral changes in all of the freshly deposited samples, finally leading to a pattern which merely loses intensity on continued treatment. The strong band at approximately 400 cm⁻¹ is most likely a lattice mode largely independent of the presence of hydrogen. The lattice vibration of normal LiF comes at 307 cm⁻¹. The remaining intense peaks closely resemble published spectra of bihalide ions in general appearance and frequency maxi—maincluding
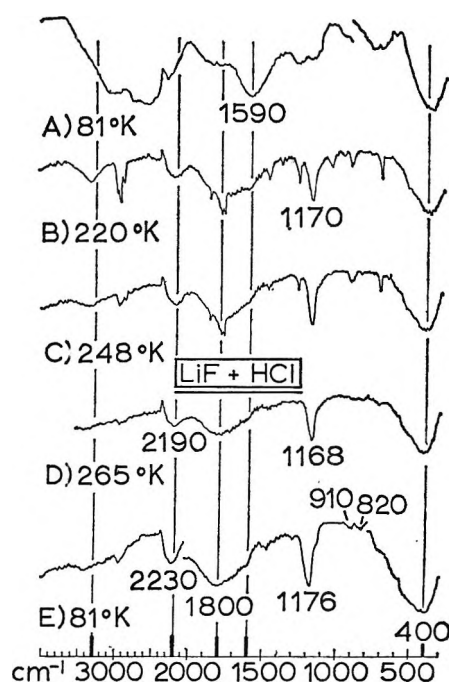
Figure 1. Spectra of[7] LiF-HCl solid film deposited from the vapor onto a CsI window: (A) spectrum of the freshly deposited sample, reference time 0.0 hr; (B) spectrum of the partially annealed sample, time 8.0 hr; (C) time 10.5 hr; (D) immediately after recooling the sample with liquid nitrogen, time 11 hr. The pressure in the system rose to approximately 10^{-4} mm for a short time as gas was pumped off around 200°K. It reached 10^{-4} mm again near 260°K but dropped on recooling to 81°K. The sharp bands evident in B are caused by trace moisture impurity and are particularly prominent in LiF-HCl spectra. Approximately 0.19 mmol of HCl was deposited in 100 min.

the deuterated samples. It is apparent that they are due to one or more of the ions: FHF⁻, FHX⁻, and XHX⁻. In addition to spectroscopic arguments given below, the known stability of FHF⁻ (37 kcal/mol,[14] compared to approximately one-third of this value for the other bihalides[15]) favors their assignment in the annealed solid as arising from FHF⁻ alone.

The Lattice Vibration. No sharp bands develop from the 400-cm⁻¹ absorption; any HD isotope effects are questionable, and this band is the only one to remain intense after overnight warmup of the sample to room temperature under continuous pumping. The band intensity appears greater at low temperatures than at high. The absorption maximum increases slightly in frequency on passing through the series LiF-HCl, -HBr, and -HI and does not appear intensely in samples with a deficiency of LiF. It is evidently due to a lattice vibration which remains essentially unchanged in the LiF-LiX residue which is present after warmup of the sample.

(14) S. A. Harrell and D. H. McDaniel, *J. Amer. Chem. Soc.*, **86**, 4497 (1964).

(15) D. H. McDaniel and R. E. Valley, *Inorg. Chem.*, **2**, 996 (1963).
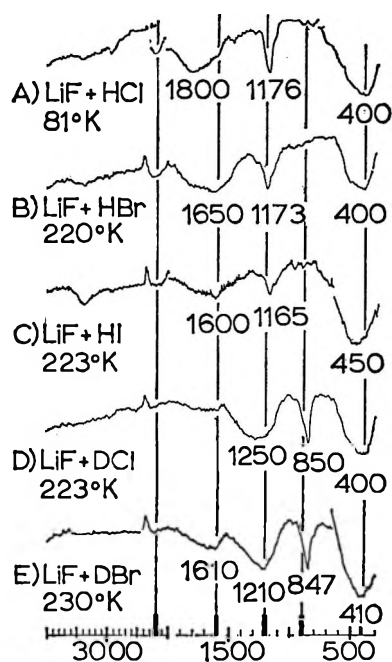
Figure 2. Spectra of annealed LiF–HX samples: (A) LiF–HCl (sample in Figure 1); (B) LiF–HBr, time 2.3 hr after stop of deposition; (C) LiF–HI, time 29 hr (this sample was warmed to 210°K for 5.0 hr, recooled with liquid nitrogen, held overnight, and warmed to 180°K for 28 hr; the pressure rose to 10^{-4} mm at $\sim$235°K and the sample started to deteriorate; recooling intensified the 450-cm^{-1} absorption); (D) LiF–DCl, time 2.0 hr after start of warmup; (E) LiF–DBr, time 2.0 hr (the sample was warmed to 270°K for 3.5 hr and was recooled to 82°K; the spectra resembled E except the bands weakened at the higher temperature; on recooling, the 400-cm^{-1} band regained intensity). Deposition amounts and rates were near those given in the caption to Figure 1.

Berthold[16] made infrared and X-ray studies of LiF and LiF + 20% KF deposited from the vapor at 20°K. In analogy to his results, the broadness and location of the 400-cm^{-1} absorption suggests an amorphous solid incorporating both LiF and HX. The broadness of the absorptions due primarily to hydrogen vibration suggests a great deal of disorder in the freshly deposited samples. In addition, the band widths in the annealed solids remain a few per cent wider than those of crystalline KHF$_2$,[4] and the high overtone and combination bands found there are not seen in any of the LiF–HX examples.

The frequency maximum of the 400-cm^{-1} band may vary somewhat in the initially deposited samples but always takes its characteristic value soon after annealing begins. This, in addition to the buildup of bihalide ion peaks, indicates at least a partial ordering rearrangement in the solid. However, diffraction studies of these solids must be done in order to convincingly establish the extent of detailed order which exists among the lithium, halide, and bihalide ions in these solids under various conditions.

The Journal of Physical Chemistry

The Bihalide Ion Vibrations. The data presented in Figures 1 and 2 can be compared with pertinent published infrared spectra.[3–5,7,8,10,11] It is found that FHX$^-$ ions are probably present in the initially deposited samples but that they quickly vanish on warming the solids. Broad bands occur near the known values[11] for FHX$^-$ ions in the H stretching and the 700-cm^{-1} regions.

The lack of clear bands in the 600-cm^{-1} region offers strong evidence against the occurrence of XHX$^-$ ions in the annealed samples, although a small absorption occurs in some partially annealed samples which might be due to ClHCl$^-$. Weak, sharp bands near 600 cm^{-1} are reported in the spectra[9,10,12] of ClHCl$^-$, BrHBr$^-$, ClHBr$^-$, and ClHI$^-$. Only two frequency values are reported for the other heavy anions, and, unfortunately, no details of the spectra are given.[6–8,14,15]

The absorption near 1175 cm^{-1}, reminiscent of the KHF$_2$ ν_2 (bending) vibration, sharpens and reaches a maximum intensity as the temperature is gradually raised and then decreases to vanish completely on warmup to room temperature. The frequency and intensity are mildly temperature dependent, as shown for the LiF–HCl sample in Figure 1. There is less of an effect with LiF–HBr, where spectra taken at 173°K are nearly superimposable on spectra taken at 77°K.

An absorption is apparent in the spectra near 1280 cm^{-1}. It usually vanishes completely at temperatures of 200°K or higher (with pumping) and does not reappear on recooling the sample to 77°K.

The absorption in the 1600-cm^{-1} region (bihalide ion ν_3 stretching vibration) broadens with annealing and the maximum shifts to higher frequencies. As expected, there appear to be more than one band present, but the absorption does not sharpen into several peaks upon cooling the annealed samples to 77°K. Significant sharpening of several bands was observed by Nibler and Pimentel[12] on cooling their samples to 20°K. Their observations, with sample molecules most likely located on the crystal surface, differ markedly from the results of Ferriso and Hornig[17] on systems more similar to the LiF–HX solids. These authors studied vapor-deposited HX–H$_2$O films and found no appreciable sharpening of the broad bands on cooling to 8°K.

The two strong bands at approximately 1175 and 1600 cm^{-1} in the LiF–HX solids could be assigned to XHX$^-$ ions. However, the relative intensity of the bands remains at a value observed for FHF$^-$ in several different environments.[2–5] It seems unlikely that the relative intensities and frequencies of ClHCl$^-$, BrHBr$^-$, and IHI$^-$ should be nearly identical in these solids. The relative intensity of the corresponding bands in ClHCl$^-$ and ClHBr$^-$ spectra is very sensitive to the environment.[9,10] The low-frequency band (attrib-

(16) G. Berthold, *Z. Phys.*, 185, 400 (1965).

(17) C. C. Ferriso and D. Hornig, *J. Chem. Phys.*, 23, 1464 (1955).

Table I: Spectra of FHF⁻ (FDF⁻) in Several Environments (cm⁻¹)

Sample	ν_2	ν_3	$\nu_3 + \nu_1$	$\nu_3 + \nu_1$
Annealed LiF–HCl[a]	1170 (850)	1800[e] (1250)	f	2190 (1600)
Annealed LiF–HBr	1173 (847)	1650 (1210)	f	2200 (1610)
Annealed LiF–HI	1163	1600	f	...
Crystalline NaHF₂[b]	1200 (860)	1550 (1140)	1880 (1560)	2110 (1720)
Crystalline KHF₂[c]	1223 (888)	1450 (1015)	1830	2055
NaBr matrix[d]	1247	1599		
KCl matrix[d]	1257	1570		
KBr matrix[d]	1258	1527		
KI matrix[d]	1239	1477		

[a] This work. [b] A. Azman and A. Ocvirk, *Spectrochim. Acta*, **A23**, 1597 (1967). [c] KHF₂ (G. L. Coté and H. W. Thompson, *Proc. Roy. Soc.*, **A210**, 206 (1955)); KDF₂ (L. H. Jones and R. A. Penneman, *J. Chem. Phys.*, **22**, 781 (1954)). [d] J. A. A. Kelelaar, C. Haas, and J. vander Elsken, *ibid.*, **24**, 624 (1956). [e] The value of 1700 cm⁻¹ seems more realistic; see text. [f] ν_3 and $\nu_2 + \nu_1$ are broad and overlap in these samples.

uted[12] to $2\nu_2$) was found to be much less intense than the high-frequency band by Nibler and Pimentel for ClHCl⁻, ClHBr⁻ (or possibly BrHBr⁻?[12]), and ClHI⁻.

The bihalide ion spectra in the various LiF–HX solids are similar but differ sufficiently to favor the presence of a single phase, rather than a mixture of, say, pure LiHF₂ and LiX crystals. This agrees with the previous discussion of the 400-cm⁻¹ lattice vibration.

The data for annealed samples are collected in Table I, along with the frequencies of FHF⁻ in the other available environments. The value of 1800 cm⁻¹ for ν_3 of FHF⁻ in the LiF–HCl solid seems rather high, considering the isotope effects, the $\nu_1 + \nu_3$ value, and the ν_3 values in the other solids. While a value of 1700 cm⁻¹ seems more realistic, the behavior shown in Figure 1 is reproduced in other charts too. The maximum frequency of the band in question increased dramatically and irreversibly as the temperature was raised.

There are trends in the spectral data presented in Table I which help to establish the presence of FHF⁻ in the annealed LiF–HX solids and which can provide tests for future frequency-shift calculations. Ignoring the different solid-state structures, the sets of ν_2 and ν_3 FHF⁻ vibration frequencies all fall in order on comparing the solid environments: (a) KCl, KBr, KI with LiF–HCl, LiF–HBr, LiF–HI; (b) KBr, NaBr, and LiF–HBr; (c) KHF₂, NaHF₂, and LiF–HCl (the smallest halide). The annealed LiF–HX solids should be basically Li₂(FHF)X. Although limited in number by the data, these comparisons indicate that ν_2 and ν_3 both increase as the atomic number of X⁻ increases, while ν_2 increases and ν_3 decreases as the atomic number of M⁺ increases. The ν_3 vibration is more sensitive to environment than ν_2.

Ketelaar, *et al.*, found that NaHF₂ would not form mixed crystals with KI and that KHF₂ and NH₄HF₂ did so with difficulty. It was difficult to obtain FHF⁻ ion spectra in the LiF–HI solids, and the FHF⁻ disappeared at much lower temperatures than in the corresponding HCl and HBr solids. In addition, the ν_2

frequency was shifted to lower values in the LiF–HI solid than in the others, analogous to the behavior in alkali halide lattices.

The intense hydrogen stretching band of H₃O⁺ near 3350 cm⁻¹ appeared during the annealing of all insufficiently dried samples. The LiF–HX films are especially sensitive to H₂O impurity, yielding a rich spectrum of sharp lines—some of which are seen rather weakly in Figure 1 in the partially annealed spectra. Also, as seen there, the initially small 3350-cm⁻¹ absorption was eliminated during the annealing process and did not reappear on recooling the sample with liquid nitrogen.

There is little evidence for H₂F₃⁻ species in the spectra. Bands occur in well-prepared samples near 820 and 910, 900 and 970, and 900 and 960 cm⁻¹ for annealed LiF–HCl, –HBr, and –HI solids, respectively. They do not correspond to known impurity bands and, owing to the large frequency shift required, may be unfavorably compared with bands at 1015 and 1105 cm⁻¹ tentatively assigned to H₂F₃⁻ in aqueous solution by Jones and Penneman.[18] Azman, *et al.*,[19] reported absorptions at 1020, 1050, and 1082 cm⁻¹ and at 1020, 1050, and 1150 cm⁻¹ for crystalline KH₂F₃, depending upon the sample preparation.

Conclusions

Evidence is presented that FHF⁻ ions are formed in annealed films of LiF–HCl, LiF–HBr, and LiF–HI. Samples deposited at about 77°K appear to be amorphous, with spectral evidence for the presence of (highly perturbed) FHX⁻. Annealing leads to clear FHF⁻ spectra; however, the bands are broad and the high-frequency overtone and combination bands were not observed with the sample thicknesses used. The spectra indicate that while considerable atomic rear-

(18) L. H. Jones and R. A. Penneman, *J. Chem Phys.*, **22**, 781 (1954).
(19) A. Azman, A. Ocvirk, D. Hadzi, P. A. Giguere, and M. Schneider, *Can. J. Chem.*, **45**, 1347 (1967).

rangement must occur in the solid during the course of an experiment, it never seems to attain a highly crystalline state under the given treatment.

It was observed that the lattice vibration of the LiF–HX solids occurs at considerably higher frequencies than for pure LiF. Pronounced environmental shifts of the FHF$^-$ vibration frequencies were observed, especially for ν_3.

There was no significant evidence in the spectra for the presence of XHX$^-$ (of course, assuming the primary band assignments to FHF$^-$ are correct), and, consequently, no statements concerning the linearity of those ions can be made. There is no evidence to suggest nonlinearity of FHF$^-$ in the given systems. (The integrity of the FHF$^-$ species in simple solids is indicated by the virtually identical F–F bond distance of 2.26 or 2.27 Å in LiHF$_2$,[20] NaHF$_2$,[21] KHF$_2$,[22] and NH$_4$-

HF$_2$[23]). There is no reliable spectral evidence for the presence of higher bifluoride ions, although bands occur which could possibly be assigned to these species.

The presence of moisture results in a large number of sharp absorption lines. While it is hoped that other bihalide ions may be formed in analogous solid mixtures, the present experience suggests that the solids may be amorphous and that the absorption bands may be too broad to yield accurate frequency values.

(20) L. K. Frevel and H. W. Rinn, *Acta Crystallogr.*, **15**, 286 (1962)

(21) B. L. McGaw and J. A. Ibers, *J. Chem. Phys.*, **39**, 2677 (1963).

(22) J. A. Ibers, *ibid.*, **40**, 402 (1964); S. W. Peterson and H. A. Levy, *ibid.*, **20**, 704 (1951).

(23) T. R. R. McDonald, *Acta Crystallogr.*, **13**, 113 (1960).

Electron Spin Resonance Study of Hydroperoxide on Zinc Oxide

by M. Codell, H. Gisser, J. Weisberg,

Pitman-Dunn Research Laboratories, Frankford Arsenal, Philadelphia, Pennsylvania

and R. D. Iyengar

Center for Surface and Coatings Research, Lehigh University, Bethlehem, Pennsylvania   (Received December 18, 1967)

The esr signal observed on zinc oxide (g 1.961) following oxygen treatment at 500° decreases in intensity on exposing the degassed sample to *t*-butyl hydroperoxide (TBHP) vapors. However, with samples vacuum outgassed at 500°, the adsorption of TBHP leads to the formation of two signals (g 1.965 and 1.961) in place of the original signal. No spectra of free radicals resulting from decomposition of TBHP have been observed. When vacuum-outgassed ZnO is treated with oxygen at 700 torr, reoutgassed at 25°, and left under vacuum for more than 24 hr, two signals are again observed which correspond to the two signals observed earlier on the TBHP treatment. The formation of the two signals and the variation in their intensities have been discussed in terms of oxygen ion vacancies and interstitial Zn$^+$ ions.

Introduction

Hydroperoxide association with the catalysis of oxidation of organic lubricants has long been known, and while the oxidation of these lubricants has been studied extensively, details of the mechanism of hydroperoxide participation are still not clear. Since metal surfaces exposed to lubricants are oxide coated, it was considered desirable to explore the interaction of hydroperoxides with metal oxides. Since the surface chemistry of zinc oxide has been extensively investigated,[1] zinc oxide was considered an appropriate experimental component.

Of the various techniques utilized in attempts to elucidate the nature of the surface species and defects on solids, the application of electron spin resonance has

been of considerable interest recently since it permits an analysis of different forms of chemisorbed paramagnetic species.

The esr spectrum of ZnO (vacuum outgassed as well as oxygen treated) has been studied by numerous investigators,[2–8] and signals corresponding to g values of

(1) For a summary of earlier work see: S. R. Morrison, *Advan. Catal.*, **7**, 213 (1955); G. Heiland, E. Mollwo, and F. Stöckman, *Solid State Phys.*, **8**, 191 (1959).

(2) J. H. Lunsford and J. P. Jayne, *J. Chem. Phys.*, **44**, 1487 (1966).

(3) Y. Fujita and J. Turkevich, *Discussions Faraday Soc.*, **41**, 407 (1966).

(4) K. M. Sancier, *J. Catal.*, **5**, 314 (1966).

(5) M. Sedaka and T. Kwan, *Bull. Chem. Soc. Jap.*, **38**, 1414 (1965).

(6) P. H. Kasai, *Phys. Rev.*, **130**, 989 (1963).

(7) R. J. Kokes, *J. Phys. Chem.*, **66**, 99 (1962).

1.96, 2.003, 2.008, 2.01, 2.04, and 2.049 have been reported. The triplet with g values 2.003, 2.008, and 2.049 has been attributed to an O_2^- species.[2,3] However, according to Sancier,[4] adsorbed O_2^- does not give any observable resonance, and the signal at 2.01 should be assigned to an O^- species. Kwan[5] attributes the signal at 2.003 to O^- ions which transform to O^{2-} ions above 370°. In support of this view, it has been observed[9] that the isobar for oxygen on ZnO reveals two peaks, corresponding to 170 and 370°.

The signal which appears in the vicinity of g 1.96 has been variously assigned to Zn^+ ions[3] possibly in shallow donor bands,[8] to oxygen vacancies,[6] and to conduction electrons.[7] Though the early work on ZnO[6-10] has revealed a complexity in the signal appearing at g 1.96, the emphasis in subsequent investigations has been clearly on adsorbed oxygen. In the present study the adsorption of t-butyl hydroperoxide was found to affect primarily the signal at g 1.96 and to modify it. This modification not only establishes clearly the complexity of the signal but also renders further investigations on zinc oxide possible. An attempt, therefore, has been made to elucidate the nature of the interaction between the hydroperoxide and zinc oxide by the observed effects of adsorption on the various resonance signals initially present on differently pretreated samples.

Experimental Section

Materials. Two zinc oxide samples, both prepared by the vapor-phase oxidation of zinc and furnished by the New Jersey Zinc Co. (Palmerton, Pa.), were used in this work. The first sample, designated Kadox-15, had a surface area of approximately 10 m^2/g. The second sample, designated SP 500, was of exceptionally high purity and had a surface area of $\sim$5 m^2/g. The chloride content of this sample as analyzed by the turbidimetric method was less than 1 ppm. Most of our experiments were done with SP 500. Essentially similar results were obtained in our studies with Kadox-15.

t-Butyl hydroperoxide, TBHP (Lucidol Division, Wallace and Tiernan Inc., Buffalo, N. Y.), was distilled at 18 mm and the fraction boiling between 36 and 37.5° was collected. The material was degassed by multiple freeze and thaw cycles prior to adsorption.

Apparatus. The vacuum treatment of ZnO and subsequent adsorption of oxygen and *t*-butyl hydroperoxide were carried out in a gas-handling apparatus attached to a mercury-diffusion pump backed by a mechanical pump (Welch Scientific Co.) and an ion gauge. A vacuum of 10^{-6} torr could be attained in this system. During outgassing, the ZnO samples were protected from mercury vapors by the use of a liquid-nitrogen trap.

The sample tubes were made of annealed Pyrex glass, 4-mm i.d., and were attached to the system through a vacuum stopcock and a detachable joint. Thus suc-

cessive treatments could be carried out on a single sample. Apiezon-N grease was used to lubricate all stopcocks and joints. Approximately 25 mg of the sample was taken in the tube for each experiment.

An esr spectrometer (Varian Model V-4500) with a TE-104 mode dual cavity at a frequency of approximately 9.3 kMcps was employed. The magnetic field was controlled by a Fieldial regulator V-FR-2100. 1,1-Diphenylpicrylhydrazyl (DPPH) was used as a standard for g measurements. All measurements were made at liquid-nitrogen temperature.

Procedure. Pretreated zinc oxide samples were exposed for 5 min to *t*-butyl hydroperoxide maintained at 25° (the vapor pressure of TBHP at 25° is 11 mm); the sample was then removed and the esr spectrum was recorded with and without subsequent degassing. Essentially the same spectrum was obtained. Extending the exposure time up to 30 min produced no changes in the spectrum.

Results

Oxygen-Treated Samples. Heating zinc oxide in oxygen at 1 atm for 2 hr at different temperatures in the range 100–500° does not completely eliminate the signal at g $\sim$1.96 (Figure 1a). The intensity of these signals increases somewhat on outgassing at room temperature for 30 min (Figure 1b). Oxygen treatment is also observed to produce a signal at g 2.012. The addition of TBHP to the sample at room temperature causes a decrease in the intensity of the signal at g $\sim$1.96; however, the peak to peak width of the signal remains constant (Figure 1c).
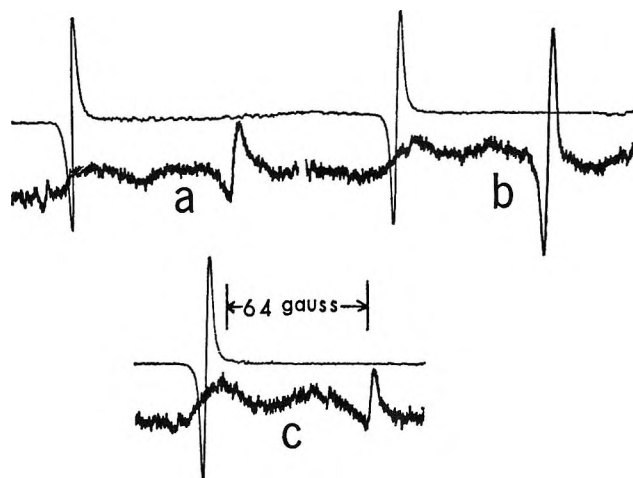
Figure 1. Esr (x-band) spectra of zinc oxide: (a) heated in oxygen for 2 hr at 500°; (b) outgassed at room temperature for 30 min; (c) exposed to *t*-butyl hydroperoxide (TBHP). DPPH (upper spectra) is used as a standard for the g value. The field increases from left to right.

(8) K. A. Muller and J. Schneider, *Phys. Lett.*, **4**, 2288 (1963).

(9) T. Kwan, personal communication.

(10) J. Schneider and A. Rauber, *Z. Naturforsch.*, **A16**, 712 (1961).
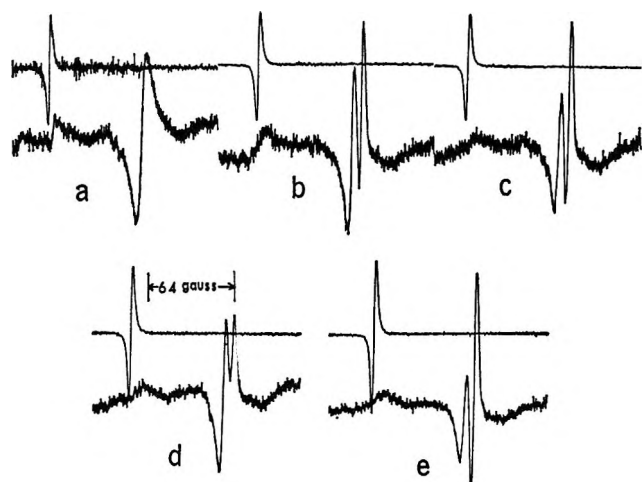
Figure 2. Esr spectra of ZnO: (a) outgassed at 500°; (b) TBHP added; (c) outgassed at 25° for 30 min; (d) Oxygen added (700 torr); (e) reoutgassed at 25° for 30 min. All spectra were recorded at the same signal level.

Figure 3. Esr spectra of zinc oxide outgassed for 2 hr at (a) 375°, (b) 400°, (c) 450°, (d) 525°, and (a', b', c', and d') after the addition of TBHP.

Figure 4. Esr spectra of zinc oxide vacuum outgassed for 2 hr at 500°: (a) 100 mm of oxygen added and reoutgassed 10 min at 25°; (b) after standing for 24 hr following treatment a; (c) after standing for 70 hr following treatment a.

Vacuum-Outgassed Samples. On subjecting zinc oxide to vacuum treatment at 500° for 2 hr, a broad signal (7.6 G) is observed at $g \sim 1.96$ (Figure 2a). On adding TBHP, the sample surprisingly showed the presence of two signals at g values of 1.965 and 1.961, respectively (Figure 2b). A series of experiments with zinc oxide outgassed at different temperatures in the range 100–525° revealed that the formation of two signals at $g \sim 1.96$ is observed only with samples outgassed at temperatures above 350°. The combined width of the two signals, however, appeared to be identical with the width of the signal prior to the addition of TBHP. The variation of the intensity ratio of the two signals (g 1.965 and 1.961) on subsequent oxygen treatment (Figure 2d) and vacuum treatment (Figure 2e) showed that the two signals were independent of each other and could not result from a single species.

The esr spectra (signal at $g \sim 1.96$) of zinc oxide, outgassed at 375, 400, 450, and 525°, and changes in the spectra as a result of TBHP adsorption are shown in Figure 3. Apparently the intensity of the signal shows a decrease at higher outgassing temperatures. The spectrum of the sample outgassed at 525° in addition indicates the presence of two signals at $g \sim 1.96$. A decrease in the intensity of the signal at $g \sim 1.96$ owing to the added TBHP is obvious for samples outgassed below 475° but is not so apparent at the higher temperatures, 500 and 525° (Figures 2 and 3). However, in all cases following TBHP adsorption, two signals are clearly observable.

Zinc oxide vacuum outgassed for 2 hr at 500° and subsequently treated with oxygen at room temperature and reoutgassed shows the typical spectrum of O_2^- (Figure 4a). (This spectrum is not observed on samples heated in oxygen at 500°.) The signal at $g \sim 1.96$ shows a decrease in intensity following the addition of oxygen, and two signals are not observed immediately.
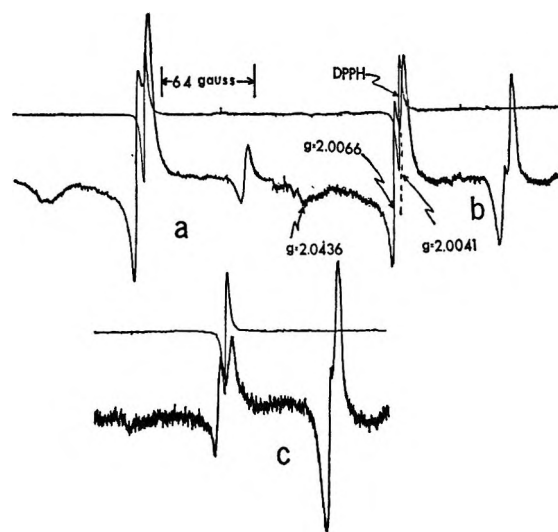
However on standing for 24 hr at room temperature, the sample shows the presence of two signals at $g \sim 1.96$. After 70 hr, the intensity of these signals increased with a simultaneous decrease in the signal for O_2^-. It appears that O_2^- is undergoing a surface transformation to a different species.

Samples which showed the presence of two signals at $g \sim 1.96$ as a result of treatment with TBHP or oxygen exhibited a restoration of the broad signal at $g \sim 1.96$ on being reoutgassed at 500° for 2 hr.

The Combined Effect of Oxygen and Hydrocarbons. While the addition of oxygen at 25° to zinc oxide vacuum outgassed at 500° does not immediately reveal the presence of two signals at $g \sim 1.96$, the presence of hydrocarbons in addition to oxygen leads to the immediate formation of two signals. In fact, it is not possible to differentiate between the spectra at $g \sim 1.96$ of samples treated with hydrocarbon + oxygen mixtures from those treated with TBHP. The results were

Table I: g Values and Signal Widths of Zinc Oxide Subjected to Various Treatments

Treatment	g values			Peak to peak widths		
	g	Std dev	No. of samples	Width, G	Std dev	No. of samples
Outgassed 2 hr at 500°	1.9657	0.0007	16	7.6	1.2	11
Outgassed 2 hr at 500°; O₂ added;	1.9660	0.0005	6	5.9	0.9	6
reoutgassed at 25°	1.9620	0.0007	6	3.0	0.5	6
Outgassed 2 hr at 500°; exposed to	1.9651	0.0009	16	4.4	1.0	15
TBHP vapors	1.9609	0.0007	16	3.0	0.6	16
Outgassed 2 hr at 500°; exposed to	1.9654	0.0007	16	4.6	0.9	12
TBHP vapors; outgassed 0.5 hr	1.9614	0.0007	16	3.4	1.3	13
at room temperature						
Outgassed 2 hr at 500°; exposed to	1.9655	0.0005	14	5.3	1.0	13
TBHP vapors; outgassed 0.5 hr	1.9617	0.0007	16	3.1	0.6	15
at room temperature; O₂ admitted						
Heated 2 hr in O₂ at 500°	1.9630	0.0005	3	6.1	0.4	3
Heated 2 hr in O₂ at 500°; exposed to TBHP vapors	1.9606	0.0006	5	3.2	0.8	4
Heated 2 hr in O₂ at 500°; outgassed at room temperature	1.9607	0.0006	12	3.7	0.8	12

Figure 5. Esr spectrum of zinc oxide outgassed at 500° and treated with methane containing 2% oxygen.

essentially the same for C_1 to C_4 hydrocarbons. Figure 5 shows the spectrum of zinc oxide treated with methane containing 2% oxygen.

Discussion

Schneider and Raüber[10] in their early experiments on vacuum-outgassed zinc oxide have reported a variation not only in the g values but also in the width of the principal signal. The observed g values varied from 1.956 to 1.962 and the peak to peak width of the signal ranged from 4.6 to 10.5 G at 300°K and from 2.7 to 6.1 G at 77°K. The g values reported in Table I show fluctuations of a similar magnitude to those of Schneider and Raüber in the range 1.961–1.966. The signal widths in the present investigation ranged from 3 G, for samples vacuum outgassed at 500° and exposed to TBHP vapors, to 7.6 G, for samples vacuum outgassed at 500° for 2 hr. These variations in signal width are also similar to those reported by Schneider and Raüber.

Kasai[6] has attributed the scattering of g values at $g \sim 1.96$ to the existence of two types of defects:

oxygen ion vacancies and halogen ions in substitutional positions (donors). The signal which he attributes to chloride ions in substitutional positions saturates at a power level of 16 mW. In the present investigation, no saturation was observed for either of the signals at $g \sim 1.96$ in the range 2.2–22 mW. It seems, therefore, that none of these signals can be due to chloride ions in substitutional positions, and the fluctuations observed in the present study do not result from halogen contamination.

A comparison of the two signals at $g \sim 1.96$ on vacuum-outgassed samples treated with oxygen (and reoutgassed at room temperature) with those obtained with the TBHP treatment shows that the g values compare within the limits of experimental error (Table I). The absence of any signal, with or without hyperfine structure, close to $g \sim 2$ on samples exposed to TBHP vapors indicates that no free radicals are formed from TBHP or any of its decomposition products. These observations suggest that the signals produced by the addition of TBHP arise from the interaction of either oxygen (O₂) or oxygen ions derived from TBHP.

Previous investigators have attributed the signal at $g \sim 1.96$ to ionic vacancies or interstitial Zn^+ ions. According to Thomas[11] most of the interstitial zinc in zinc oxide should be removed by oxygen treatment of the sample at 500° for a few minutes. Our observations that heating the sample in oxygen for 2 hr at 500° does not remove the signal at $g \sim 1.96$ clearly shows the presence of a defect other than Zn^+. The experiments of Kasai[6] suggest that the signal which survives the oxygen treatment can be attributed to electrons in oxygen vacancies. It appears that TBHP interacts

(11) D. G. Thomas, *J. Phys. Chem. Solids*, **3**, 229 (1957).

with the oxygen vacancies to restore stoichiometry as in

$$(CH_3)_3COOH \longrightarrow (CH_3)_3O \cdot + O^- + H^+ \quad (1)$$

$$O^- + e^- \text{ (oxygen vacancy)} \longrightarrow O^{2-} \quad (2)$$
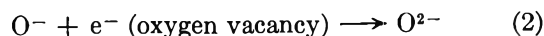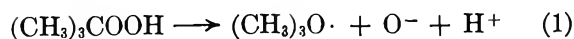
The H^+ ions can interact with lattice oxygen as in

$$O^{2-} + H^+ \longrightarrow OH^- \quad (3)$$

The formation of O^- at the surface, for example, resulting from the TBHP decomposition illustrated above, would explain the observed decrease in the intensity of the signals in samples heated in oxygen in the range 100–500°. The portion of the signal remaining after the addition of TBHP (g 1.961) to the sample heated in oxygen probably arises from anion vacancies in the bulk not readily accessible to the O^-.

A straightforward explanation of the other signal at g 1.965 is more difficult. It is possible that this signal is caused by zinc ions in interstitial positions. The absence of a hyperfine structure would then be due to the loosely bound electron in Zn^+.[10]

An explanation can now be offered for the formation of two signals at g ~1.965 and 1.961 either by oxygen treatment followed by outgassing or by TBHP treatment. The samples used were prepared at approximately 1000° by the oxidation of zinc vapors and contain anionic vacancies which are not removed by the oxygen treatment at temperatures below 900°[6] except at the surface. Vacuum outgassing at temperatures above 350° can be expected to produce additional anionic vacancies and interstitial zinc, the majority of which are at the surface. Adsorption of TBHP to the vacuum-outgassed sample leads to removal of Zn^+ as in

$$Zn^+ + O^- \text{ (from TBHP)} \longrightarrow Zn^{2+} + O^{2-}$$

This reaction leads to a decrease in the signal at g 1.965 and takes place in preference to the competing reaction

$$O^- + e^- \longrightarrow O^{2-}$$
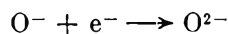
which leads to a decrease in the signal at g 1.961. Thus the decrease at g 1.965 is larger than the decrease at g 1.961 and the change in the relative intensity of the two signals leads to their resolution, making observation of the two signals possible.

Further, according to the above, a decrease in the intensity of the signal at g ~1.96 would normally be expected on the adsorption of TBHP. However, this is not obvious for samples outgassed at or above 500°, as seen in Figure 3. The reason for this behavior appears to be as follows: outgassing at higher temperatures produces a larger concentration of defects and the signal observed at g ~1.96 shows a decrease in amplitude and is comparatively broad because of the ensuing dipolar interactions. This can be seen in Figure 3b–d as the outgassing temperature of the sample is increased from 400 to 525°. If the subsequent interaction with TBHP reduces the concentration of the paramagnetic species just enough to eliminate the dipolar interactions, the increase observed in the intensity of the resolved signals can be explained.

The formation of two signals at g 1.96 on vacuum-outgassed samples subsequently exposed to oxygen (700 torr) and outgassed at room temperature is not immediate but occurs after a period of time. Simultaneously with the observation of two signals at g ~1.96, a decrease in the intensity of the O_2^- signal (g ~2) is also observed. It appears here that the O_2^- ions are desorbed as oxygen molecules leaving behind electrons. Thus

$$O_2^- \text{ (adsorbed)} \longrightarrow O_2 + e^- \text{ (to the surface)}$$
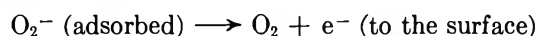
The electrons are localized at either the anionic vacancies or the Zn^{2+} ions, thereby contributing to an increase in the amplitude of the signals at g 1.961 and 1.965, respectively, as shown in Figure 4. The resulting increase in the concentration of Zn^- and oxygen ion vacancies accompanied by some broadening of the signals appears to be responsible for the poor resolution observed.

Zinc oxide vacuum outgassed and treated with a hydrocarbon containing oxygen (total pressure 700 torr) not only produced immediately the two signals corresponding to treatment with TBHP but also led to the formation of an O_2^- species. Hence it appears that both an O^- and an O_2^- species are formed. A possible mechanism involves the formation of a hydroperoxide through the activation of the hydrocarbon by an active site on zinc oxide. A mechanism for the formation of hydroperoxide from hydrocarbons has been suggested and discussed by Ingold.[12]

(12) K. U. Ingold, *Chem. Rev.*, **61**, 563 (1961).

Hydration of N-Methylacetamide in Carbon Tetrachloride

by R. D. Grigsby,

Research and Development Department, Continental Oil Company, Ponca City, Oklahoma

S. D. Christian, and H. E. Affsprung[1]

Department of Chemistry, The University of Oklahoma, Norman, Oklahoma (*Received December 18, 1967*)

The problem of investigating the hydration of functional groups common to proteins has been approached by studying the equilibrium between N-methylacetamide (NMA) and water in carbon tetrachloride solution. Hydration data were obtained by two independent methods: in one, the concentration of water in solution was measured as a function of NMA concentration at constant water activity; in the other, the concentration of NMA was held constant and the concentration of water was measured at increasing water activity. The relationship between NMA concentration, total water concentration, and water monomer concentration in solution was found to be the same as the Langmuir adsorption isotherm. The use of the Langmuir equation to explain the data is consistent with the assumption that NMA self-associates to form chains in dilute solution, with each chain containing multiple sites for the attachment of water molecules.

Introduction

The significance of hydrogen bonding in protein structure has been well established in recent years, although the role played by water is at present only partially understood.[2-4] Information has been obtained by studying proteins in their natural or partially denatured state[5] and by other methods; however, the large number and heterogeneity of possible hydration sites makes the interpretation of results difficult. For this reason, a number of investigators have attempted to study the hydrogen bonding and hydration of smaller, less complicated molecules which are chemically related to proteins. N-Methylacetamide has been the object of much investigation because it is the smallest molecule containing a single peptide group.[3,6-12] In the work to be described here, the hydration of NMA was investigated in CCl₄ solution to avoid the inherent difficulties encountered in studying hydration reactions in aqueous media. To our knowledge the hydration of NMA in nonpolar solvents has not been studied before, although the hydration of N,N-dimethylacetamide has been reported recently.[4,13] In addition, the hydration of 2-pyrrolidone and N-methyl-2-pyrrolidone has been investigated.[13,14]

Experimental Section

Materials. N-Methylacetamide (purchased from K & K Laboratories, Jamaica, N. Y.) was purified by vacuum distillation and fractional crystallization. The final product had a melting point of 30.5°. A Kjeldahl analysis showed a purity of 99%. The purified NMA was stored at 30.4° in a flask equipped with a P₂O₅ drying tube. Before use, any liquid phase present was withdrawn and was discarded.

Fisher Certified reagent carbon tetrachloride was purified by refluxing with mercury followed by distillation through a 30-plate Oldershaw column. The boiling point of the collected fraction was 77° corrected to 1 atm. Before the solvent was used, it was extracted with water to remove residual, water-soluble impurities.

Apparatus. The hydration of NMA in CCl₄ was studied by two independent methods, which gave nearly equivalent results. In the first, solutions of the amide in CCl₄ were suspended over constant-humidity solutions (dilute H₂SO₄) in closed containers thermostated at 25 ± 0.1°. After equilibrium was attained, samples of the NMA–CCl₄ solutions were withdrawn and were analyzed for total water content. A detailed description of the equilibrators and the technique has been given earlier.[15] The concentration of water in the samples was determined with a coulometric water

(1) Deceased August 5, 1967.

(2) C. Tanford, "Physical Chemistry of Macromolecules," John Wiley and Sons, Inc., New York, N. Y., 1961, p 130.

(3) I. M. Klotz and J. S. Franzen, *J. Amer. Chem. Soc.*, **84**, 3461 (1962).

(4) F. Takahashi and N. C. Li, *ibid.*, **88**, 1117 (1966).

(5) H. A. Scheraga in "Polyamino Acids, Polypeptides, and Proteins," M. A. Stahmann, Ed., The University of Wisconsin Press, Madison, Wis., 1962, p 241.

(6) S. Mizushima, T. Simanouti, S. Nagakura, K. Kuratani, M. Tsuboi, H. Baba, and O. Fujioka, *J. Amer. Chem. Soc.*, **72**, 3490 (1950).

(7) M. Davies and D. K. Thomas, *J. Phys. Chem.*, **60**, 767 (1956).

(8) L. A. LaPlanche, H. B. Thompson, and M. T. Rogers, *ibid*, **69**, 1482 (1965).

(9) F. Takahashi and N. C. Li, *ibid.*, **68**, 2136 (1964).

(10) F. Takahashi and N. C. Li, *ibid.*, **68**, 2140 (1964).

(11) F. Takahashi and N. C. Li, *ibid.*, **69**, 1622 (1965).

(12) F. Takahashi and N. C. Li, *ibid.*, **69**, 2950 (1965).

(13) D. D. Mueller, Ph.D. Dissertation, The University of Oklahoma, Norman, Okla., 1966.

(14) J. D. Worley, Ph.D. Dissertation, The University of Oklahoma, Norman, Okla., 1964.

(15) S. D. Christian, H. E. Affsprung, J. R. Johnson, and J. D. Worley, *J. Chem. Educ.*, **40**, 419 (1963).

analyzer similar to that described by Meyer and Boyd.[16] Hydration data were obtained for NMA solutions in CCl_4 ranging in concentration up to 0.0538 M and at water activities of 0.31, 0.47, 0.56, and 0.69.

The second method used to obtain hydration data involved the measurement of the total pressure of $NMA-H_2O-CCl_4$ solutions thermostated at 25 ± 0.1°. Water was added in milligram quantities to the initially dry $NMA-CCl_4$ solutions, whereupon the total pressure was measured at equilibrium. The apparatus and technique have been described elsewhere.[17] The concentration of NMA ranged up to 0.0612 M and the highest water activity studied was ~0 6.

Results

Figure 1 shows the data obtained from the constant-humidity equilibrators. The total water concentration, $[H_2O]_t$, of the $NMA-CCl_4$ solutions is plotted against the total amide concentration, $[NMA]_t$, at constant water activity. Because of phase separation, the data taken at a water activity of 0.69 could not be obtained much past an NMA concentration of 0.02 M.

In the analysis of the data it was assumed that the water monomer concentration is directly proportional to the water activity[18,19]

$$[H_2O]_m = 0.0098P/P^0 \ M \quad (25.0°)$$

The Henry's-law constant (0.0098 M) was determined from the slope of a plot (not shown) of water concentration vs. water activity for CCl_4 solutions containing no NMA.

The data taken from the total-pressure apparatus are shown in Figure 2. Total water concentration is plotted vs. water activity at constant NMA concentration. The vertical dotted lines represent water activities at which phase separations occur for the given concentrations. The lower line in the graph gives the concentration of water in solutions containing no NMA. From these data the Henry's-law constant was determined to be 0.0087 M; consequently, the water monomer concentration for this technique is given by

$$[H_2O]_m = 0.0087P/P^0 \ M \quad (25.0°)$$

The constant obtained here is about 11% lower than the value obtained from the equilibrator data. However, the smaller figure is believed to be more accurate and agrees with the value (0.0087 M) obtained by Johnson, et al.,[19] and by Clifford.[20]

Discussion

In the analysis of the data it is necessary to take into account the self-association of N-methylacetamide. Several independent studies have been conducted,[3,7,8,21] and it has been shown that the amide self-associates to form linear chains containing any number of monomeric units, depending on the total concentration of amide in solution. This process can be depicted as

$$A + A \underset{\longleftarrow}{\overset{\longrightarrow}{\rule{0pt}{0pt}}} A_2 \quad (K_2)$$

$$A_2 + A \underset{\longleftarrow}{\overset{\longrightarrow}{\rule{0pt}{0pt}}} A_3 \quad (K_n)$$

$$\vdots$$

$$A_{n-1} + A \underset{\longleftarrow}{\overset{\longrightarrow}{\rule{0pt}{0pt}}} A_n \quad (K_n)$$
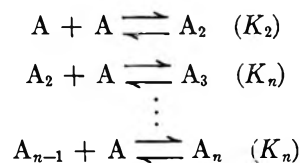
where only two constants, K_2 and K_n, are required to express the various equilibria.
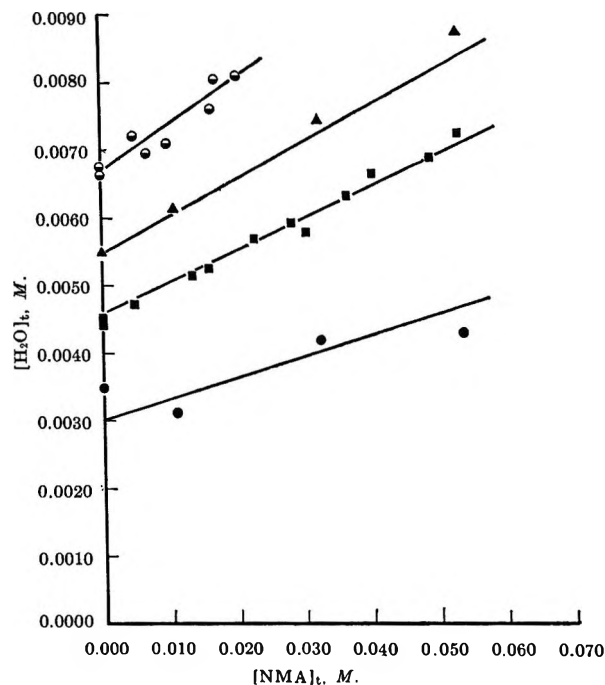
Figure 1. Total water concentration vs. total NMA concentration at constant water activity, P/P^0 (25 ± 0.1°): ●, 0.31; ■, 0.47; ▲, 0.56; ◒ 0.69. Lines are calculated with $K_{11} = 10.7$ l./mol and $B = 0.0098$ M.

Because of chain formation, it is reasonable to assume that each chain contains multiple sites of the attachment of water molecules. Based on this assumption, an equation was derived to explain the relationship between total amide concentration, total water concentration, and water monomer concentration in solution. The resulting equation was found to be a form of the Langmuir adsorption isotherm. Although the derivation of the Langmuir equation is readily available in a number of textbooks,[22,23] the steps leading

(16) A. S. Meyer and C. M. Boyd, *Anal. Chem.*, **31**, 215 (1959).

(17) A. A. Taha, R. D. Grigsby, J. R. Johnson, S. D. Christian, and H. E. Affsprung, *J. Chem. Educ.*, **43**, 432 (1966).

(18) J. R. Johnson, S. D. Christian, and H. E. Affsprung, *J. Chem. Soc.*, 1 (1965).

(19) J. R. Johnson, S. D. Christian, and H. E. Affsprung, *ibid.*, **77** (1966).

(20) C. W. Clifford, *Ind. Eng. Chem.*, **13**, 631 (1921).

(21) R. D. Grigsby, Ph.D. Dissertation, The University of Oklahoma, Norman, Okla., 1966.

(22) T. L. Hill, "An Introduction to Statistical Thermodynamics," Addison-Wesley, Inc., Reading, Mass., 1960, p 128.

(23) B. Jirgensons and M. E. Straumanis, "A Short Textbook of Colloid Chemistry," John Wiley and Sons, Inc., New York, N. Y., 1954, p 75.
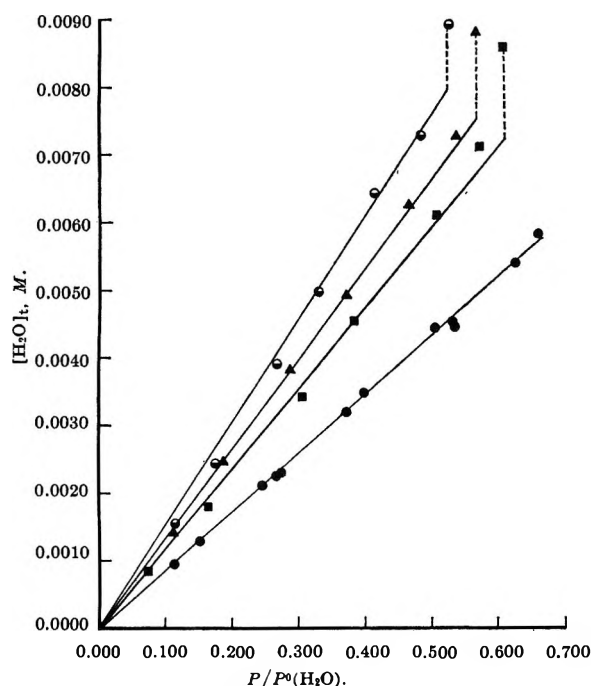
Figure 2. Total water concentration *vs.* water activity at constant NMA concentration, M (25 ± 0.1°); ●, 0.0000; ■, 0.0311; ▲, 0.0442; ⊖, 0.0612. Lines are calculated with $K_{11} = 12.8$ l./mol and $B = 0.0087$ M.

to the present form will be outlined below because the application of the equation to dilute-solution chemistry is somewhat removed from the usual gas–solid interaction studies.

If it is assumed that each chain contains n independent hydration sites, each of which can attach no more than one water molecule, then it can be shown that the equilibrium constant for the reaction

$$C\text{-}X_nW_{\nu-1} + W \rightleftharpoons C\text{-}X_nW_\nu$$

is given by

$$K_{n\nu} = \frac{n - \nu + 1}{\nu}K_{11} \tag{1}$$

where $C\text{-}X_n$ is a chain containing n hydration sites of type X and W is a molecule of water. The symbol $K_{n\nu}$ is thus the equilibrium constant for the reaction of one water with a chain having $\nu - 1$ attached water molecules. K_{11} is the equilibrium constant for the reaction of one water with a chain having only one possible hydration site. The number of attached water molecules in the product of the reaction cannot be greater than the number of possible hydration sites; *i.e.*, ν cannot be greater than n.

By using eq 1, an equation for the concentration of the species $C\text{-}X_nW_\nu$ can be derived in terms of the water monomer concentration and the concentration of $C\text{-}X_n$. The result is

$$[C\text{-}X_nW_\nu] = \frac{n!}{\nu!(n - \nu)!}(K_{11}[W])^\nu[C\text{-}X_n] \tag{2}$$

On the assumption that each monomeric unit, A, contains only one hydration site, the species $C\text{-}X_nW_\nu$ becomes A_nW_ν and eq 2 can be written

$$[A_nW_\nu] = \frac{n!}{\nu!(n - \nu)!}(K_{11}[W])^\nu[A_n] \tag{3}$$

The possibility of having more than one hydration site per monomer will be discussed later.

Using eq 3, an equation for the total concentration of water in solution can be derived. In terms of the water monomer concentration and all possible hydrated species present (assuming one hydration site per monomer), the total water concentration can be expressed as

$$[W]_t = [W] + [AW] + [A_2W] + [A_3W] + \ldots +$$
$$2[A_2W_2] + 2[A_3W_2] + 2[A_4W_2] + \ldots +$$
$$3[A_3W_3] + 3[A_4W_3] + 3[A_5W_3] + \ldots + \ldots$$

Similarly, the total amide concentration is

$$[A]_t = [A] + 2[A_2] + 3[A_3] + \ldots +$$
$$[AW] + 2[A_2W] + 3[A_3W] + \ldots +$$
$$2[A_2W_2] + 3[A_3W_2] + 4[A_4W_2] + \ldots + \ldots$$

By replacing the concentrations $[A_nW_\nu]$ with the right-hand expression in eq 3, the two series can be combined to give the final equation

$$[W]_t = [W] + \frac{K_{11}[W]}{1 + K_{11}[W]}[A]_t \tag{4}$$

which is a form of the Langmuir adsorption isotherm. Note that the self-association constants for the amide were not required in the derivation.[24]

Although eq 4 was derived on the assumption that each monomeric unit of the chain contains only one hydration site, the same result, except with the second term multiplied by 2, will be obtained if it is assumed that each monomer has two sites for hydration. Thus it becomes evident that it is not possible to determine the number of sites per monomer by simply fitting eq 4 to the experimental data.

It is interesting to note that eq 4 is also obtained if it is assumed that all of the amide is in the monomer form and that each monomer can attach one water. In fact it might be argued that at the concentrations considered

(24) An alternate derivation of eq 4 is simpler to follow and may shed light on the conclusion that values of the self-association constants of the amide are not required in the analysis of hydration data. It has been assumed that each amide molecule contributes exactly one hydration site (equivalent to and independent of all the other sites) regardless of the size of the polymeric unit in which it is found. Therefore, the number of sites is directly proportional to $[A]_t$, the total or formal amide concentration. The equilibrium constant for hydration of the sites may be written $K_{11} = [S\text{-}W]/\{[S][W]\}$, where $[S\text{-}W]$ is the concentration of hydrated sites and $[S]$ is the concentration of unhydrated sites. Of the total number of sites, a fraction $[S\text{-}W]/([S\text{-}W] + [S]) = K_{11}[W]/(1 + K_{11}[W])$ will be hydrated. The total concentration of bound water is thus equal to $K_{11}[W][A]_t/\{1 + K_{11}[W]\}$, which is a Langmuir-type relation involving the activity or monomer concentration of water. Since the concentration of bound water is equal to $[W]_t - [W]$, the expression leads directly to eq 4.

here, the amide exists almost entirely in the monomer state. We have, however, obtained data in our laboratory[21] to indicate that NMA is highly associated in dilute CCl_4 solutions. At 20° by a vapor pressure lowering technique, we have found $K_2 = 9.0 \pm 2.8$ l./mol and $K_n = 61.6 \pm 5.7$ l./mol. In addition, appreciable association was noted at 60 and 75° from data obtained by a liquid–vapor equilibrium technique (see Table I). The value of K_2 at 20° is in fair agreement with that of Klotz and Franzen (4.7 and 5.8 l./mol) obtained at 25°.[3] No value was given for K_n. Other values of K_2 and K_n obtained for various solvents by different investigators are summarized in Table I.

Table I: Self-Association of N-Methylacetamide in Various Solvents

Solution	Temp, °C	K_2, l./mol	K_n, l./mol	Ref
CCl_4	20	9.0 ± 2.8	61.6 ± 5.7	20
	25	4.7, 5.8	...	2
	60	2.7 ± 0.7	14.3 ± 1.5	20
	75	1.5 ± 0.4	13.8 ± 1.1	20
Benzene	25	6.7 ± 0.3^a	14.3 ± 0.2^a	6
	35	5.5 ± 0.2^a	11.5 ± 0.2^a	6
	49	4.2 ± 0.2^a	8.9 ± 0.2^a	6
$CDCl_3$	Room	1.25^a	1.35^a	7
Dioxane	25	0.52, 0.58	...	2
Water	25	0.005	...	2

^{a} Values were converted from mole fraction units.

Equation 4 can be tested directly with the data from the constant-humidity equilibrators, as shown in Figure 1. Using a least-squares computer program,[25] the best value of K_{11} was determined to be 10.7 ± 0.5 l./mol. The water monomer concentrations required in the calculations were obtained with a Henry's-law constant of 0.0098 M, as explained above.

After putting the equation into the form

$$[W]_t = \left(1 + \frac{K_{11}[A]_t}{1 + K_{11}[W]}\right)[W]$$

it can be tested with the data from the total-pressure apparatus (Figure 2). The least-squares value of K_{11} was found to be 12.8 ± 0.3 l./mol. A value of 0.0087 M for the Henry's law constant was used to obtain the water monomer concentrations (see Results).

The values of K_{11} (10.7 ± 0.5 vs. 12.8 ± 0.3 l./mol) obtained by the two independent methods are in reasonably good agreement. It might be supposed that part of the difference could be attributed to the difference in the Henry's law constants (0.0098 vs. 0.0087 M). However, an error analysis shows that this difference has little effect on the value of K_{11} if it can be assumed that the water concentrations from the two methods differ by a constant factor at all activities. Thus the difference in K_{11} must be attributed to unknown systematic errors.

Because the self-association constants for NMA do not appear in eq 4, it seems that the equation should apply to hydrated polymers in which the monomers are linked together by covalent instead of by hydrogen bonds. Thus it would be interesting to test the theory with data obtained for the hydration of small polyamides. If these molecules were found to hydrate in the same manner as N-methylacetamide, then with data from solutions of increasing dielectric constant it might be possible to formulate a model for hydrated proteins in aqueous media.

(25) S. D. Christian, *J. Chem. Educ.*, **42**, 604 (1965).

Concentration Dependence of the Nuclear Magnetic Resonance Spectral

Properties of Some N,N-Dimethylamides and -thioamides[1]

by Robert C. Neuman, Jr., William Snider, and Violet Jonas

Department of Chemistry, University of California, Riverside, California 92502 (*Received December 18, 1967*)

The effect of concentration on the nmr spectral properties of the amides N,N-dimethylacetamide (DMA) and N,N-dimethylformamide (DMF) and the thioamides N,N-dimethylthioacetamide (DMTA) and N,N-dimethylthioformamide (DMTF) in carbon tetrachloride have been studied and the results have been analyzed using a self-association equilibrium model. Evidence for hydrogen-bonding interactions involving the formyl protons of DMF and DMTF is presented.

Introduction

In the planar ground-state configuration of N,N-dimethylamides (I, X = O), N,N-dimethylthioamides (I, X = S), and related systems, the two NCH₃ groups

I
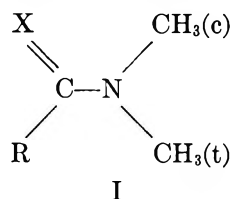
are in nonequivalent magnetic environments. Since the energy barriers to rotation about the central CN bond are relatively high owing to electron delocalization, two discrete NCH₃ resonances are often observed in nmr spectra of these compounds.[1b,2] When the group R contains protons α to the C=X carbon, spin–spin coupling with NCH₃(c) and NCH₃(t) has been frequently observed, and it seems that $J_{R,NCH_3(c)} > J_{R,NCH_3(t)}$.[1b,3,4] This unequal coupling acts as a label for the proton resonances corresponding to NCH₃(c) and NCH₃(t), and, in general, it has been found that the proton resonance for NCH₃(c) is at higher field than that for NCH₃(t).[1b,3-6] This can be seen in Figure 1 for N,N-dimethylacetamide (DMA), N,N-dimethylformamide (DMF), and N,N-dimethylthioformamide (DMTF). However, the relative shieldings of the NCH₃ protons in N,N-dimethylthioacetamide (DMTA) (Figure 1) appear to be reversed.[4,6] In addition, similar inversions have been observed for amides with more highly branched alkyl groups attached to nitrogen.[7]

It is well recognized that the nonexchanging chemical shift $\delta\nu(NCH_3)$ between the two NCH₃ groups of N,N-dimethylamides is significantly temperature, solvent, and concentration dependent, and this has been rationalized by proposing self-association of amides in solution.[1b,2-4,7,8] Possible supporting evidence includes cryoscopic molecular weight studies of DMA in benzene[9] and a large concentration dependence of the

activity of DMA in carbon tetrachloride.[10] That the relative shieldings of the two NCH₃ groups in such a compound might be different in the same solvent depending on whether the compound was a monomer or self-association dimer, however, has only recently been proposed.[2] This suggested that the apparent anomalous behavior of DMTA compared to the other compounds shown in Figure 1 might be a direct result of the extent of self-association in each system.[11]

In an attempt to answer this question, we have studied the effect of concentration on the chemical shifts of the various proton-resonance signals for DMA, DMF, DMTF, and DMTA in carbon tetrachloride. Although a previous extensive study of DMF in several solvents has been reported,[8] we felt obliged to repeat the experiments in carbon tetrachloride in order to verify our own observations and to extend the concentration range.[12]

An unavoidable aspect of studies of self-association

(1) (a) Part IV: Studies of Chemical Exchange by Nuclear Magnetic Resonance; (b) part III: R. C. Neuman, Jr., and V. Jonas, *J. Amer. Chem. Soc.*, **90**, 1970 (1968).

(2) R. C. Neuman, Jr., D. N. Roark, and V. Jonas, *ibid.*, **89**, 3412 (1967), and references therein.

(3) J. V. Hatton and R. E. Richards, *Mol. Phys.*, **3**, 253 (1960).

(4) R. C. Neuman, Jr., and L. B. Young, *J. Phys. Chem.*, **69**, 1777 (1965).

(5) F. A. L. Anet and A. J. R. Bourn, *J. Amer. Chem. Soc.*, **87**, 5250 (1965).

(6) B. B. Wayland, R. S. Drago, and H. F. Henneike, *ibid.*, **88**, 2455 (1966).

(7) A. G. Whittaker, D. W. Moore, and S. Siegel, *J. Phys. Chem.*, **68**, 3431 (1964).

(8) A. G. Whittaker and S. Siegel, *J. Chem. Phys.*, **42**, 3320 (1965).

(9) H. O. Chaplin and L. Hunter, *J. Chem. Soc.*, 1114 (1937).

(10) R. S. Drago, R. L. Carlson, N. J. Rose, and D. A. Wenz, *J. Amer. Chem. Soc.*, **83**, 3572 (1961).

(11) This possibility was also recognized independently by R. S. Drago and H. F. Henneike, private communication.

(12) The data previously reported[8] were given in terms of mole fraction of DMF in carbon tetrachloride. Although this precludes an exact comparison with our results, approximate conversion of mole fraction to molarity shows that our data are essentially identical. It should be noted that the previous study[8] was performed at 56.4 Mcps.

Table I: Chemical Shifts for the Proton Resonances of DMF, DMA, DMTF, and DMTA in Carbon Tetrachloride[a]

Cmpd	Concn[b]	CCH₃	CH	NCH₃(c)	NCH₃(t)	δν(NCH₃)[c]	NCH₃ doublet center
DMF (36 ± 1°)[d]	12.0		481.6	167.1	176.8	9.72 ± 0.10	172.0
	5.99		475.7	166.8	176.4	9.92 ± 0.10	171.6
	2.99		474.8	167.3	176.6	9.48 ± 0.11	172.0
	1.50		473.7	168.0	176.5	8.95 ± 0.10	172.3
	0.707		473.2	168.2	176.2	8.00 ± 0.10	172.2
	0.354		472.8	168.7	176.2	7.62 ± 0.20	172.5
	0.177		473.2	167.9	175.6	7.00 ± 0.10	171.8
	0.088		473.4	169.0	175.8	6.78 ± 0.10	172.4
DMA (36.5 ± 0.5°)	9.44	118.4		170.0	180.3	10.4₅	175.2
	8.66	118.1		169.8	180.3	10.5₅	175.1
	6.99	117.5		169.5	180.2	10.7₉	174.9
	5.91	117.4		169.2	179.8	10.9₁	174.5
	4.72	117.4		169.6	180.5	10.8₅	175.1
	3.49	117.2		169.6	180.2	10.7₁	174.9
	2.36	117.1		170.1	180.5	10.4₆	175.3
	1.75	117.1		170.1	180.2	10.1₉	175.1
	1.18	117.4		170.7	180.2	9.6₄	175.5
	0.590	117.9		171.7	180.4	8.7₉	176.1
	0.295	117.7		171.7	179.6	8.2₈	175.5
	0.148	117.5		171.4	179.3	7.8₄	175.4
	0.074	117.4		171.5	179.4	7.7₄	175.5
DMTF (34.5 ± 0.5°)	10.19		552.3	192.5	200.5	8.03 ± 0.10	196.5
	5.09		548.3	193.0	200.7	7.72 ± 0.10	196.9
	2.55		547.3	193.5	201.0	7.53 ± 0.13	197.3
	1.27		547.2	193.6	200.5	6.87 ± 0.10	197.1
	0.637		546.9	193.7	200.2	6.45 ± 0.10	197.0
	0.318		547.1	193.8	199.6	5.82 ± 0.10	196.7
	0.159		547.6	193.7	198.9	5.24 ± 0.10	196.3
	0.080		547.5	193.8	198.0	4.98 ± 0.10	195.9
DMTA (36.5 ± 0.5°)[e]	4.89	152.9		203.9	200.1	−3.70 ± 0.20	202.0
	2.44	153.7		204.3	200.1	−4.07 ± 0.10	202.2
	1.22	153.7		204.4	199.5	−4.67 ± 0.10	202.0
	0.611	154.0		204.6	199.2	−5.27 ± 0.12	201.9
	0.305	153.8		204.8	198.5	−5.83 ± 0.10	201.7
	0.153	154.0		204.6	198.1	−6.41 ± 0.10	201.4
	0.076	153.9		204.7	197.9	−6.59 ± 0.10	201.2

[a] Chemical shifts, in cps, at 60 Mcps; calibrated by the audio-side-band method. [b] Molar concentration assuming no aggregation. [c] Values of δν(NCH₃) are not the differences of the preceding two columns; see the text. See text for discussion of error limits. [d] Measured temperature range for the series of spectral measurements; see the text. [e] Significance of negative values discussed in the text.

is that the concentration of solute must be continuously increased in order to observe potential shifts in the equilibrium distribution of monomer and self-association aggregates. This leads to changes in the macroscopic properties of the system, such as viscosity, dielectric constant, etc., and such changes could well cause changes in δν(NCH₃) independent of the existence of any true self-association equilibrium that might exist. However, independent of the quantitative significance of the association equilibrium constants which we have derived, the effect of concentration on δν(NCH₃) is important, since studies of the magnetic anisotropy of the carbonyl and thiocarbonyl groups have been based on these relative chemical shifts[6,13−15] and little attention has been paid to the question of whether

or not they reflect the values for the unassociated monomer.

Results

Nmr Spectral Data. The data are tabulated in Table I. All of the chemical shifts were calibrated by superposition of the low-field audio side band of an internal tetramethylsilane sample, except for those listed as δν(NCH₃). These latter values were obtained from 50-cps sweep width traces and were calibrated using

(13) P. T. Narasimhan and M. T. Rogers, *J. Phys. Chem.*, **63**, 1388 (1959).

(14) D. L. Hooper and R. Kaiser, *Can. J. Chem.*, **43**, 2363 (1965).

(15) H. Paulsen and K. Todt, *Angew. Chem. Int. Ed. Engl.*, **5**, 899 (1966).
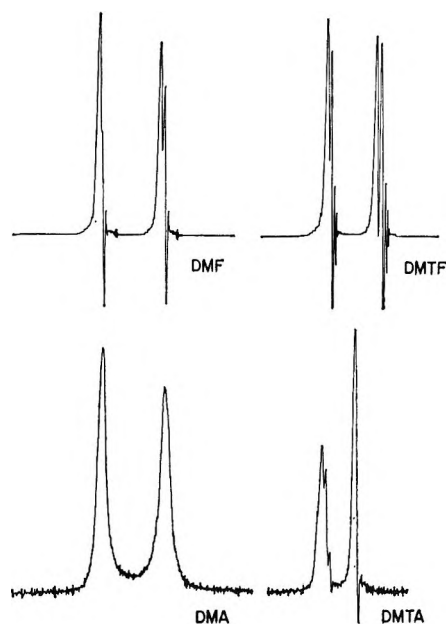
Figure 1. Typical nmr spectra of the NCH_3 resonance signals for carbon tetrachloride solutions of DMA, DMF, DMTF, and DMTA at ambient probe temperature. The magnetic field increases from left to right.

Figure 2. Experimental (points) and calculated (lines) dependence of $\delta\nu(NCH_3)$ on concentration in carbon tetrachloride solutions of DMTA; see text.

Figure 3. Experimental (points) and calculated (lines) dependence of $\delta\nu(NCH_3)$ on concentration in carbon tetrachloride solutions of DMTF; see text.

their own audio side bands. Although these values should be identical with the differences between the corresponding values of $\nu(NCH_3)_t$ and $\nu(NCH_3)_c$ (Table I), they are not, and this reflects the lower experimental accuracy associated with these latter two quantities determined from 250-cps sweep width spectra.

The values for $\delta\nu(NCH_3)$ represent the average of several determinations. Although the range of values observed in any given experiment was found to be less than 0.2 cps in many cases, we have assigned minimum error limits of ± 0.1 cps in these cases because smaller values seem to be unjustifiable. Larger error limits associated with the remaining values reflect the actual spread of the experimental data.

The data for all concentrations of a given compound were not determined on a single day. The temperature range reported thus reflects inaccuracies in measuring temperatures using the Varian-supplied standards and the temperature variation in the spectrometer between the various days in which the data were accumulated. Although the effect of temperature on $\delta\nu(NCH_3)$ for these compounds in carbon tetrachloride was not determined, available temperature-variation data for DMF in trichlorofluoromethane[8] indicate that variations in $\delta\nu(NCH_3)$ over the temperature range for DMF in our studies are well within the error limits quoted in Table I.

Values of $\delta\nu(NCH_3)$ have been arbitrarily assigned as negative numbers when the spectra showed the apparent NCH_3 shielding inversion as seen for DMTA (Figure 1). The values of $\delta\nu(NCH_3)$ for each compound have been plotted vs. log C in Figures 2-5. The

curves shown are calculated and will be discussed below.

Molecular Weight Determinations. Attempts to determine the apparent molecular weights of DMF and DMA in the solvent carbon tetrachloride by vapor pressure osmometry were not successful (see the Experimental Section). The nature of the results indicated that the vapor pressures of the solutes were too high, resulting in mass transfer of solute vapor into the initially pure reference solvent. This would lead to spuriously high molecular weights. The analogous
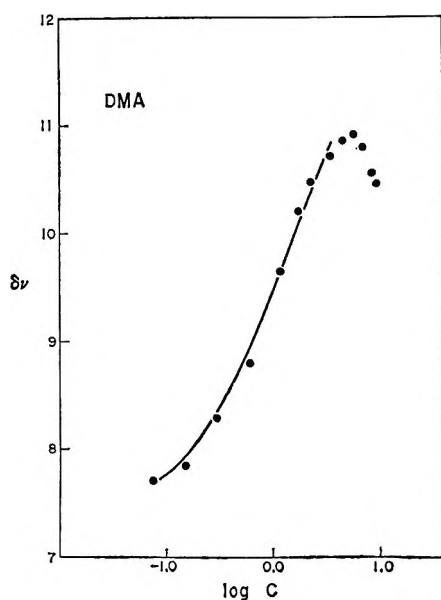
Figure 4. Experimental (points) and calculated (lines) dependence of $\delta\nu(NCH_3)$ on concentration in carbon tetrachloride solutions of DMA; see text.
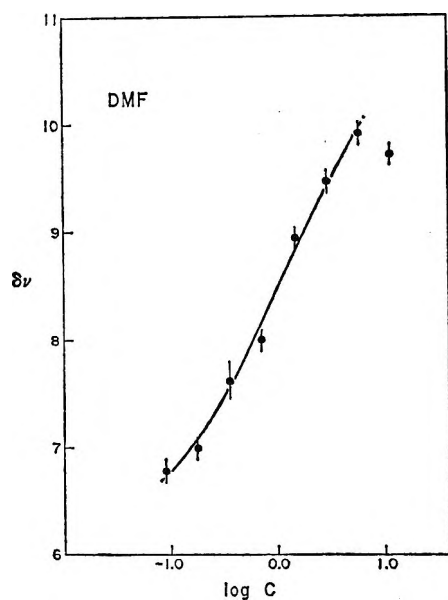
Figure 5. Experimental (points) and calculated (lines) dependence of $\delta\nu(NCH_3)$ on concentration in carbon tetrachloride solutions of DMF; see text.

thioamides DMTF and DMTA should have significantly lower vapor pressures, and molecular weight data obtained by Henneike by vapor pressure osmometry on carbon tetrachloride solutions of DMTF and DMTA indicate average molecular aggregates of 1.7 and 1.1 molecules/unit at formal concentrations of 0.03 and 0.05 M, respectively.[16] Additionally, we have previously determined the apparent molecular weight of the thioamide N,N-dimethylthiocarbamoyl chloride, $ClCSN(CH_3)_2$, in carbon tetrachloride by the same technique with no obvious experimental problems and

we have found the average molecular aggregate to be about 1.4 molecules at formal concentrations in the region of 0.05 M.[2]

Discussion

The general trends in $\delta\nu(NCH_3)$ for all four compounds as a function of concentration are quite similar (Figures 2-5). In each case the $NCH_3(c)$ resonance signals moved downfield as concentration was increased, and those for $NCH_3(t)$ moved upfield, Table I. Since the signal positions for DMTA are inverted compared with those of the other compounds, the net result is that the absolute value $\delta\nu(NCH_3)$ for DMTA decreased while those for DMTF, DMA, and DMF increased with increasing concentration. The relative shifts of NCH_3-(c) and $NCH_3(t)$ were such as to make the position of the doublet center reasonably independent of concentration (see the last column in Table I).

Although conclusive supporting evidence is not available, the trends observed for $\delta\nu(NCH_3)$ as a function of concentration could be associated with a self-association equilibrium between amide or thioamide molecules in solution. The self-association dimer could be held together by dipolar interactions. If such a monomer-dimer equilibrium existed, the values of $\delta\nu(NCH_3)$ would be described by eq 1, in which $\delta\nu_M$ and $\delta\nu_D$ are the nonexchanging chemical shifts between

$$\delta\nu(NCH_3) = (M\delta\nu_M + 2D\delta\nu_D)/(M + 2D) \quad (1)$$

the NCH_3 groups in pure monomer and dimer, respectively, and M and D are the respective molar concentrations. Since the association equilibrium constant K is equal to D/M^2 and the formal concentration, C, of solute in carbon tetrachloride is equal to $M + 2D$, eq 1 may be rearranged to give eq 2, which is useful for the computer analysis of the nmr data (Table I).[17]

$$[(8KC + 1)^{1/2} + 1]\delta\nu(NCH_3) =$$
$$2\delta\nu_M + [(8KC + 1)^{1/2} - 1]\delta\nu_D \quad (2)$$

The solid lines in Figures 2-5 represent the best-fit theoretical curves to the experimental data based on a monomer-dimer equilibrium model and the resulting parameters K, $\delta\nu_M$, and $\delta\nu_D$ are given (the numbers not in parentheses) in Table II. The signs of $\delta\nu_M$ and $\delta\nu_D$ are both negative for DMTA, while they are positive for the other compounds, and this implies that the extent of aggregation of the amide or thioamide systems is not responsible for the shielding inversion observed for DMTA (Figure 1). The value of $\delta\nu_D$ for DMTA is,

(16) H. F. Henneike, private communication.

(17) For a given value of K, a series of simultaneous equations can be generated by substitution of each C studied and the corresponding observed value $\delta\nu(NCH_3)$ (Table I). These equations may then be solved to obtain the best values of $\delta\nu_M$ and $\delta\nu_D$ corresponding to the value K. In addition the standard deviations of these best values $\delta\nu_M$ and $\delta\nu_D$ can be calculated, as well as an over-all standard deviation for the fit. Repetition of this procedure for a series of values K then allows a choice of the K giving values of $\delta\nu_M$ and $\delta\nu_D$ which show the smallest standard deviations.

Table II: Calculated Nonexchanging Chemical Shifts for the NCH_3 Proton Resonances in Monomer and Dimer and the Association Equilibrium Constants

Compd	K, l. m^{-1}	$\delta\nu_M$, cps	$\delta\nu_D$, cps
DMTA	0.64	−7.1	−1.8
	(0.24)	(−6.7)	(0.0)
DMTF	1.22	+4.3	+8.9
	(13.0)	(−0.3)	(+8.5)
DMA	0.37	+7.3	+13.8
DMF	0.60	+6.3	+11.6

however, very close to zero. In order to see if the experimental data might also reasonably fit a theoretical curve which led to inversion of shielding in going from monomer to dimer, best-fit curves just barely leading to such an inversion for DMTA and DMTF were calculated and are represented by the dashed lines in Figures 2 and 3. For DMTA, the dashed curve represents the results for $\delta\nu_D = 0.0$ ($\delta\nu_M = -6.7$), and for DMTF, the dashed curve was obtained with $\delta\nu_M = -0.3$ ($\delta\nu_D = 8.5$) (numbers in parentheses, Table II). In both cases, these dashed lines are not as good fits of the data as the solid curves not leading to inversion; however, the differences involved are quite small, especially for DMTA. The strongest supporting evidence for suggesting that inversion does not occur is the rather marked deviation from the dashed line of the highest concentration point for DMTA and the lowest concentration point for DMTF.

Although these analyses lead to numbers which accommodate the majority of the data reasonably well, it may be that this correspondence is fortuitous. Clearly, our simple model will not fit the high-concentration data for DMA and DMF (Figures 4 and 5). The behavior in these regions may be due to major deviations from ideality or could reflect the onset of additional association equilibrium processes. Additionally, the trends at lower concentrations might also be due to factors other than those considered here.

The available molecular weight data for DMTF and DMTA give values of K for DMTF and DMTA in carbon tetrachloride of 440 and 2.7 M^{-1}, respectively, compared with the values of 1.22 and 0.64 M^{-1} obtained from the nmr data. The greater disparity for the K's of DMTF, however, compared with those for DMTA suggests that the major discrepancy may reside in the molecular weight data rather than in the nmr results. While DMTA is a white, almost odorless, crystalline solid, DMTF is a liquid with a noticeable odor. Since solutes with finite vapor pressures will give rise to abnormally high molecular weights, the large K (440 M^{-1}) for DMTF may be due to such a problem. Additionally, this latter value of K is based on the apparent molecular weight at only one concentration.

Independent of the validity of the equilibrium anal-

ysis, it is important to note (see Figures 2–5) that the values of $\delta\nu(NCH_3)$ for all of these compounds at the lowest measured concentrations (0.07–0.08 M) do not yet represent the limiting chemical shifts for infinite dilution. This fact must be borne in mind when such data are used for magnetic anisotropy studies.

While no significant trends are apparent in the C–CH$_3$ resonance signals for DMA and DMTA as a function of concentration, there is a sudden relatively large downfield shift in the formyl proton resonance signal for both DMF and DMTF above concentrations of 5–6 M. We suggest that this is evidence for the participation of the formyl proton in hydrogen bonding

$$
\begin{array}{c}
X \\
\nearrow\!\!\!\!/ \\
B\text{--}H\text{---}C \\
\searrow \\
N(CH_3)_2 \\
II
\end{array}
$$
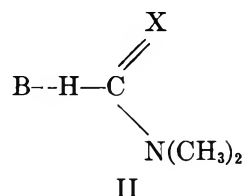
with some base represented by B.[18] In these systems, B must be another DMF or DMTF molecule and the basic site most certainly is the oxygen or sulfur atom, respectively.[19] A previous study of DMF over a more limited concentration range led to the conclusion that such an interaction was not important for DMF.[8]

Experimental Section

Materials. The amides DMF and DMA were commercial samples which had been purified and dried over molecular sieves. The syntheses of the thioamides DMTF and DMTA have been previously described.[4] An initial high-concentration sample of amide or thioamide in carbon tetrachloride was prepared and the lower concentration samples were prepared by volumetric dilution.

Nmr Spectral Data. The nmr spectra were determined at ambient probe temperature using a Varian A-60 nmr spectrometer. All resonance lines were calibrated by the audio-side-band method. Tetramethylsilane was used as an internal standard. Temperatures were determined using the Varian chemical thermometers.

Apparent Molecular Weight Studies. Attempts were made to determine the apparent molecular weights of DMA and DMF in carbon tetrachloride solution using a Mechrolab vapor pressure osmometer. Although no difficulty was encountered in calibration of the instrument with carbon tetrachloride solutions of benzil, the ΔT readings for samples of DMA or DMF in carbon

(18) Protons engaged in hydrogen bonding generally become deshielded relative to the nonhydrogen-bonded state: J. W. Emsley, J. Feeney, and L. H. Sutcliffe, "High Resolution Nuclear Magnetic Resonance Spectroscopy," Vol. I, Pergamon Press Ltd., London, 1965, pp 534–549.

(19) See, for example, D. P. Eyman and R. S. Drago, *J. Amer. Chem. Soc.*, **88**, 1617 (1966).

tetrachloride did not remain constant after initial calibration but decreased rapidly toward zero. For example using a 0.1 M sample of DMF in carbon tetrachloride, the ΔT reading 2 min after the sample drop was placed on the thermistor was 5.20, 1 min later it was 3.20, and after 15 min ΔT was 0.03. The rate of ΔT decrease for DMA solutions was slightly lower. This behavior would be expected with solutes whose vapor pressures were too high for study by this method and would lead to spuriously high molecular weights.

The Mean Activity Coefficient of Sodium Sulfate in Aqueous

Sodium Sulfate–Sodium Chloride Electrolytes

by John C. Synnott and James N. Butler

Tyco Laboratories, Inc., Waltham, Massachusetts 02154   (Received December 18, 1967)

The activity coefficient of Na_2SO_4 in aqueous Na_2SO_4–NaCl electrolytes at 25° and total ionic strength 1.0 has been measured using the cell

$$Pb(Hg)\,|\,PbSO_4(s)\,|\,Na^+,\ SO_4{}^{2-},\ Cl^-,\ H_2O\,|\,glass\ electrode$$
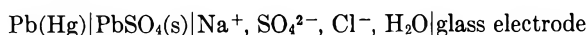
where the glass electrode is reversible to Na^+. If care is taken to exclude oxygen from the cell during preparation and measurements, reproducibility of the order of ±0.05 mV is obtained. Harned's rule was found to be obeyed within experimental error for Na_2SO_4 (component 2) in these mixtures, and the coefficient α_{21} at $I = 1$ was calculated by a least-squares method to be -0.035 ± 0.005. This agrees with the value of α_{21} calculated from published osmotic coefficients and activity coefficients of NaCl (component 1) in the corresponding mixtures.

Introduction

We have published[1] measurements of the activity coefficients of NaCl in NaCl (component 1)–Na_2SO_4 (component 2) electrolytes and have compared these with the measurements made using cation-sensitive glass electrodes.[2] From these measurements and from the known osmotic coefficients of the pure aqueous solutions of the pure components, we calculated the Harned rule coefficient for Na_2SO_4 in these mixtures (α_{21}). Since there was some discrepancy between the α_{12} values of various workers at ionic strength 1, it is of interest to measure α_{21} by an independent method.

We have made some measurements using a sulfate-reversible cell

$$Pb(Hg)\,|\,PbSO_4(s)\,|\,Na^+,\ SO_4{}^{2-},\ Cl^-,\ H_2O\,|$$

sodium ion-sensitive glass electrode
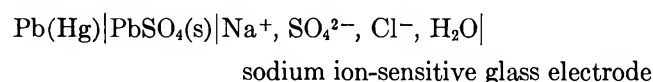
whose potential is given by

$$E = E° + \frac{RT}{2F} \ln\left(m_{Na}{}^2 m_{SO_4} \gamma_{21}{}^3\right) \qquad (1)$$

where γ_{21} is the mean activity coefficient of Na_2SO_4 in the mixed electrolytes, and the other symbols have their usual meanings.[1] The lead amalgam–lead sulfate electrode should not respond to chloride ion since the solubility of $PbCl_2$ is much larger than that of $PbSO_4$. The standard potential $E°$ includes the asymmetry potential of the glass electrode, and is expected to vary slowly with time. Therefore, the measurements were made by transferring the same glass electrode between two cells, one of which contained a reference solution of Na_2SO_4 without any added chloride.[3] This measurement is, in principle, the same as one using two sodium amalgam electrode cells, but is easier to apply because of the simplicity of working with the glass electrode. According to the work of Lanier,[2a] results of comparable precision should be obtained.

(1) J. N. Butler, P. T. Hsu, and J. C. Synnott, *J. Phys. Chem.*, **72**, 910 (1967).

(2) (a) R. D. Lanier, *ibid.*, **69**, 3992 (1965); (b) J. M. Gieskes, *Z. Physik. Chem.* (Frankfurt), **50**, 78 (1966).

(3) A. J. Zielen, *J. Phys. Chem.*, **67**, 1474 (1963).

Experimental Section

The glass electrode used was a Corning sodium ion electrode, Type NAS 11-18. It was connected to an Instrumentation Laboratories Model 135-A electrometer, which operated a Sargent Model SR recorder. Calibration was made with bias boxes differing in potential by a few millivolts. These were connected in place of the cell, and the change in deflection of the recorder was noted. The true potential difference was read from the bias boxes to ±0.005 mV on a Leeds and Northrup Model K-3 potentiometer. Another bias box was introduced in the recorder circuit so that the recorder zero could be offset by potentials large compared to its span. A switch allowed rapid comparison of the two sulfate-reversible electrodes incorporated in each cell.

All compounds used were reagent grade (Fisher Scientific) and were employed without further purification, since the manufacturer's analysis indicated no impurities expected to interfere with the measurements. Triply distilled water was used in preparation of solutions. Stock solutions of NaCl and Na₂SO₄ were prepared by weight and were analyzed for chloride by potentiometric titration with AgNO₃ and for sulfate by gravimetric analysis as BaSO₄.

The lead amalgam–lead sulfate electrodes were prepared as follows. Approximately 1% (by weight) of lead metal (Mallinkrodt Analytical Reagent) was dissolved in mercury (Doe and Ingalls, triple distilled) at 100°, with stirring, under an argon atmosphere in a glove box. The (saturated) amalgam was cooled to room temperature in a sealed flask with a stopcock and long tube for filling the cells. The long tube was filled with argon and sealed during transfer from the drybox to the cell.

The amalgam flask was removed from the drybox and the amalgam was introduced through the filling tube into each of the pool reservoirs of the two cells (which had been previously filled with argon). To avoid systematic differences in amalgam composition, first one reservoir in one cell, then one reservoir in the other cell, was filled, and the process was repeated. Dry lead sulfate was sprinkled over the top of the amalgam pools. The cells were then filled with solution, from which oxygen had been removed by bubbling prepurified argon gas (<1 ppm oxygen) through in a separate reservoir. The whole system was allowed to equilibrate under argon until the bias potential between the two pools was less than 0.05 mV. The glass electrode was then introduced through the top of the cell and its potential was measured as a function of time. A steady value was usually reached within 1 or 2 min. The glass electrode was then transferred to the other cell and the potential was read again. The potential of the glass electrode is extremely reproducible, and the precision of ΔE is better than ±0.05 mV. However, only by careful deoxygenation of the solutions, and by preventing any access of oxygen to the PbSO₄ electrode, could results of this precision be obtained.

The pH of the solutions was between 4 and 6. All measurements were made at 25.00 ± 0.05°.

Results and Discussion

The results obtained by this method for ΔE (the potential of the glass electrode in the cell containing only Na₂SO₄, less the potential of the same electrode in the cell containing the mixed electrolyte) and the activity coefficients calculated from these values (using eq 1) are given in Table I. γ_{21} is the activity coefficient for sodium sulfate in mixed electrolytes and is expected to be related to γ_{20} (activity coefficient for sodium sulfate in pure sodium sulfate solutions) by Harned's rule

$$\log \gamma_{21} = \log \gamma_{20} - \alpha_{21} X_1 I \qquad (2)$$

where $X_1 = 1 - X_2$ is the ionic strength fraction of NaCl in the mixed electrolyte and I is the total ionic

Table I: Mean Activity Coefficient of Na₂SO₄ in NaCl-Na₂SO₄ Electrolytes at 25°

Total ionic strength	Ionic strength % Na₂SO₄	ΔE, mV	$-\text{Log}\ \gamma_{21}$	$-\text{Log}\ \gamma_{21}$ (cor)
1.033	100.00	0	0.5079	0.5021
1.030	90.03	0.033	0.5028	0.4986
1.030	90.03	0.034	0.5028	0.4986
1.031	74.84	−0.125	0.4975	0.4928
1.031	74.84	0.174	0.5009	0.4062
1.029	50.18	1.774	0.4899	0.4852
1.029	50.18	1.771	0.4899	0.4852
1.028	26.23	6.649	0.4769	0.4722
1.027	9.58	18.31	0.4772	0.4727
1.027	9.58	18.19	0.4759	0.4713

strength. The activity coefficient values were corrected to ionic strength 1.000 using eq 2 and the known values of γ_{20} as a function of ionic strength[4] assuming $\alpha_{21} = -0.035$ as a provisional value[1] for the correction. The correction is not sensitive to the assumed value of α_{21} and a second iteration was not necessary, since the assumed value was verified by present experiments.

As the result of comments by a reviewer of this paper, we discovered that a misleading statement about the composition of the reference solution was made in the other papers of this series.[1,5] We said, "In all cases the reference solution was the first entry (100% ionic strength) in the table." This is only approximately correct, since several batches of reference solution were prepared, and these differed slightly in concentration. The first entry is a *representative* ionic strength value.

(4) R. A. Robinson and R. H. Stokes, "Electrolyte Solutions," Butterworth and Co., Ltd., London, 1959, Appendix 8.10.

(5) (a) J. N. Butler, R. Huston, and P. T. Hsu, *J. Phys. Chem.*, **71**, 3294 (1967); (b) J. N. Butler and R. Huston, *ibid.*, **71**, 4479 (1967).
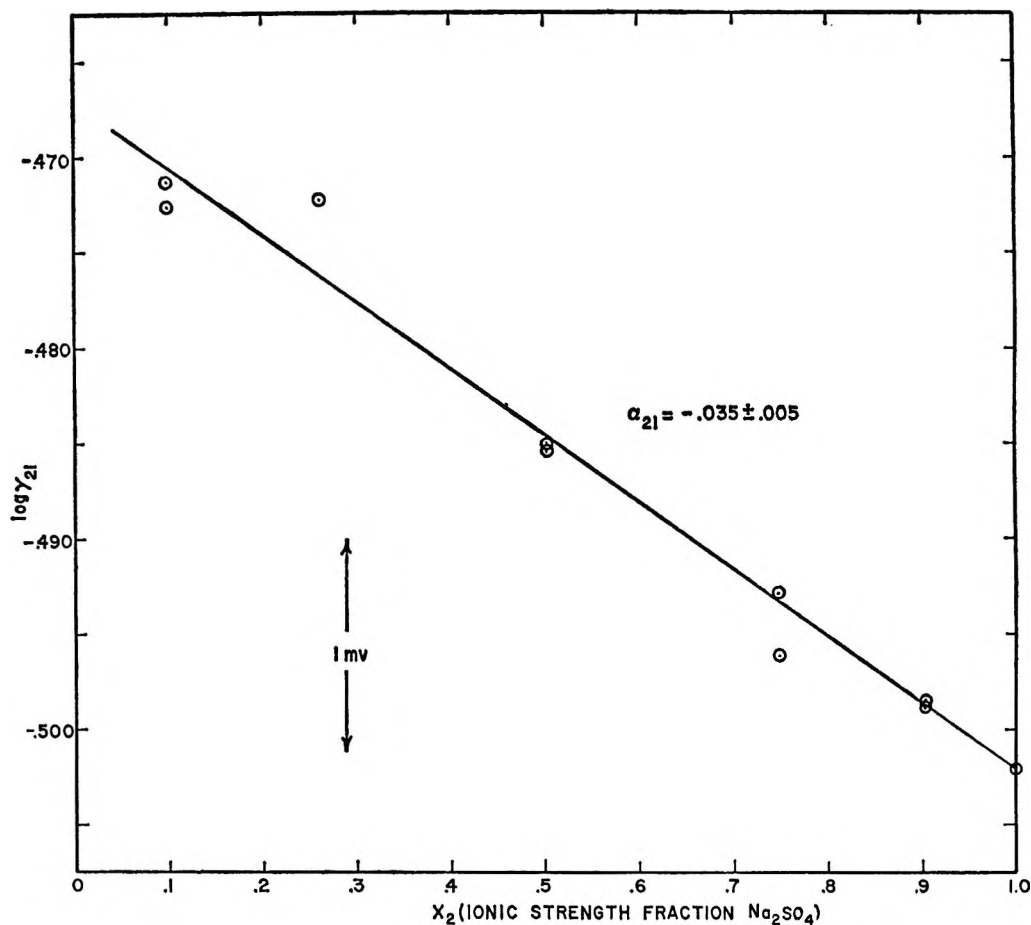
Figure 1. Activity coefficient of Na_2SO_4 in Na_2SO_4–NaCl electrolytes at $I = 1.000$ m. The straight line represents Harned's rule and was fitted by the method of least squares, allowing the intercept to vary.

When we did the calculations, we took account of these small variations in reference solution concentration, so that the tabulated values of activity coefficient are correct. It should be made clear that exact values of activity coefficients *cannot* be obtained from the tables of ΔE and solution composition, because the slight differences in reference solution composition were not given. The composition data in the tables thus may be considered as parameters on which the experimental values of activity coefficient may depend, but the activity coefficient values themselves must be considered the "raw data" of these papers.

Figure 1 shows the fit of the experimental activity coefficients (corrected to $I = 1.000$) to Harned's rule (eq 2). The straight line is the best fit by the method of least squares, in which the intercept is allowed to vary as one of the parameters. The best values obtained in this way were

$$\alpha_{21} = -0.035 \pm 0.005$$

$$\log \gamma_{20} = -0.502 \pm 0.003$$

where the errors are 95% confidence limits. The least-squares value for the intercept agrees with the literature value[4] ($\log \gamma_{20} = -0.5021$) to better than 99%

confidence. An alternative method of calculating the Harned rule coefficient is to fix γ_{20} at the literature value. Then each experimental point gives a value of α_{21} by means of eq 2. This method gives unequal weight to the points and is more subject to systematic errors in the measurement of solutions with X_2 close to unity. By this method, we obtained $\alpha_{21} = -0.034 \pm 0.004$, which agrees with the value obtained by the first method to well within the confidence limits.

Finally, we may compare these values of α_{21} with those calculated previously from measurements of α_{12} and the osmotic coefficients. From his glass electrode–silver chloride cell measurements, Lanier[2] calculated $\alpha_{21} = -0.0141$ at $I = 1$, and from our sodium amalgam–silver chloride cell measurements,[1] we calculated $\alpha_{21} = -0.0431$. On the assumption that the quantity

$$S' = 6\alpha_{12} + 3\alpha_{21} = 0.190$$

is independent of ionic strength, we calculated from osmotic coefficients[4] the value $\alpha_{21} = -0.035$ at $I = 1$. This agrees with the results obtained from the experiments reported in this paper, and confirms several statements made in our previous paper.[1] (a) Harned's rule is obeyed for both components of NaCl–Na_2SO_4 electrolyte mixtures. (b) The published value of os-

motic coefficients[4] can be used to predict the variation of α_{12} and α_{21} with ionic strength if $S' = 0.190$ (obtained at $I \geq 3$) is assumed to be independent of ionic strength. (c) The best values of the Harned rule coefficients in the ionic strength range from 1 to 6 are $\alpha_{12} = 0.048 \pm 0.003$ and $\alpha_{21} = -0.035 \pm 0.005$, essentially independent of ionic strength. There is no clear reason for the discrepancy between our measurements and those of Lanier, but we believe our values of Harned rule coefficients are more likely to be correct, since they have been obtained by two independent experiments using both chloride-reversible and sulfate-reversible electrodes, and are also consistent with a thermodynamically based extrap-

olation from higher ionic strengths, where our results are in agreement with those of Lanier.

The behavior of the Harned rule coefficients for this system at ionic strengths below 0.5 is not yet established. This is of theoretical rather than practical interest, since in this range even large deviations from the above values will not introduce appreciable error in calculated activity coefficients.

Evidence for Trimerization in Aqueous Solutions of Methylene Blue[1]

by Emory Braswell

Contribution No. 160 of the Institute of Cellular Biology, Biochemistry and Biophysics Section, University of Connecticut, Storrs, Connecticut 06268 (Received December 19, 1967)

The absorption spectra of aqueous solutions of methylene blue over the concentration range from 6×10^{-7} to 6×10^{-2} M can be described by assuming a simple reaction, *i.e.*, $3D^+ \underset{}{\overset{K_D}{\rightleftharpoons}} D_2^{2+} + D^+ \overset{K_T}{\rightleftharpoons} D_3^{3+}$, where the equilibrium constants are approximately the same. Vapor pressure osmometry measurements have confirmed that the degree of aggregation asymptotically approaches 3 as the dye concentration increases.

The behavior of the absorption spectra of certain basic dyes upon increasing the concentration of an aqueous solution of the dye is well known and usually evinces itself as a blue shift of the major absorption band. These deviations from the Beer–Bourget absorption law have been ascribed to the aggregation of the dye molecule (see, for example, ref 1–8), which presumably is brought about by dispersion forces arising from the delocalized π electrons.[1-3] The role of water in the formation of these aggregates, either as a dielectric sandwiching between the dye molecules[5,6] or as a former of hydrogen bonds[9,10] has been found to be of great importance. Most attempts to study this aggregation quantitatively have been limited to considering only dimerization,[2,4,6,10] even though many authors note that higher aggregates probably also form.[2,4,6,8,10]

In a series of articles, Hillson and McKay,[11,12] McKay and Hillson,[13,14] and McKay[15,16] presented evidence to back their belief that the metachromasia of dyes observed in solvents of low dielectric strength was due to strong interactions between dye ions and counterions to produce an undissociated dye in which the ions are

in intimate contact and are not separated by solvent molecules.[13] In one article they suggest that aggregation probably does not occur at all in solvents of very low dielectric strength,[14] even though metachromasia is

(1) G. Scheibe, *Angew. Chem.*, **50**, 212 (1937).

(2) G. Scheibe, *Kolloid Z.*, **82**, 1 (1938).

(3) G. Scheibe, *Angew. Chem.*, **52**, 631 (1939).

(4) E. Rabinowitch and L. F. Epstein, *J. Amer. Chem. Soc.*, **63**, 69 (1941).

(5) S. E. Sheppard and A. L. Geddes, *ibid.*, **66**, 1995 (1944).

(6) S. E. Sheppard and A. L. Geddes, *ibid.*, **66**, 2003 (1944).

(7) L. Michaelis and S. Granick, *ibid.*, **67**, 1212 (1945).

(8) T. Vickerstaff and D. R. Lemin, *Nature*, **157**, 373 (1946).

(9) G. R. Haugen and E. R. Hardwick, *J. Phys. Chem.*, **67**, 725 (1963).

(10) M. E. Lamm and D. M. Neville, Jr., *ibid.*, **69**, 3872 (1965).

(11) P. J. Hillson and R. B. McKay, *Trans. Faraday Soc.*, **61**, 374 (1965).

(12) P. J. Hillson and R. B. McKay, *Nature*, **210**, 297 (1966).

(13) R. B. McKay and P. J. Hillson, *Trans. Faraday Soc.*, **61**, 1800 (1965).

(14) R. B. McKay and P. J. Hillson, *ibid.*, **62**, 1439 (1966).

(15) R. B. McKay, *ibid.*, **61**, 1787 (1965).

(16) R. B. McKay, *Nature*, **210**, 296 (1966).

evident. In a later article, they imply that even when the dye is in the presence of a chromotrope in water that metachromasia occurs largely as a result of the interaction of the dye cation with the polyanion, resulting in a perturbation of the charge distribution of the dye cation.[12] In a recent paper, however, they concede that dimerization of the dye is an important cause of metachromasia in water and that this is due to the tendency of water molecules to self-associate, giving rise to strong hydrophobic bonding between dye molecules.[17]

Many studies have been limited to the consideration of dimer formation, because over the easily measured absorption range (corresponding to concentrations of from ca. 10^{-5} to ca. $10^{-3} M$), the long-wavelength absorption peak (α peak) decreases and the intermediate wavelength absorption peak (β peak) increases in such a manner as to form an isosbestic point, indicating that primarily there are present only two absorbing species. A second reason for considering only dimer formation has undoubtedly been the formidable calculations made necessary by higher aggregate models.

Examination of the experimental data for methylene blue (measured over a concentration range of from 6×10^{-7} to $6 \times 10^{-2} M$) clearly indicates the presence of at least three absorbing species (see lines in Figure 1). This study undertakes to test two models, each involving the presence of three absorbing species. The first model assumes that dye monomers, dye-aggregate end molecules, and dye-aggregate interior molecules each have their own characteristic absorption spectrum which obeys the Beer-Bourget absorption law. Therefore, the optical density of such a solution can be represented by

$$OD^\lambda = E_1^\lambda C_1 + E_2^\lambda C_2 + E_3^\lambda C_3 \qquad (1)$$

at any wavelength. In this equation E_1^λ and E_3^λ are the molar extinction coefficients per mole of dye monomer which can be obtained by extrapolating the observed extinction (OD/C_T, where OD is the observed optical density and C_T is the total molar concentration of dye in terms of monomer units) to zero and infinite concentrations, respectively. By realizing that each dye molecule has two reactive sites and by assuming the equilibrium
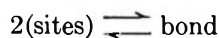
$$2(\text{sites}) \rightleftharpoons \text{bond}$$

$$K = \frac{[\text{bonds}]}{[\text{sites}]^2}$$

and

$$P = \frac{\text{reacted sites}}{\text{total sites}} = \frac{\text{bonds}}{C_T}$$

it follows that

$$K = \frac{P}{4C_T(1 - P)^2} \qquad (2)$$
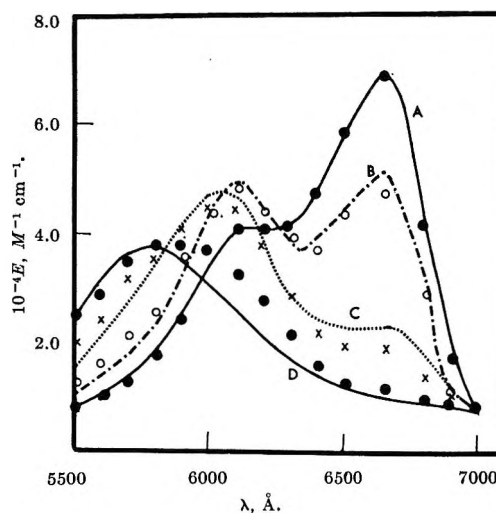
Figure 1. Absorption spectra of aqueous solutions of methylene blue at various dye concentrations. In each case the points represent the values calculated from the trimerization model and the lines represent the measured values: curve A, $3.45 \times 10^{-5} M$ (agreement was perfect at all concentrations below this, down to $6 \times 10^{-7} M$); curve B, $2.09 \times 10^{-4} M$; curve C, $3.02 \times 10^{-3} M$; curve D, $6.43 \times 10^{-2} M$.

To arrive at expressions for C_1, C_2, and C_3, one must evaluate the probability of the formation of each of these species. The expressions are

$$C_1 = C_T(1 - P)^2 \qquad (3)$$

$$C_2 = 2C_T P(1 - P) \qquad (4)$$

and

$$C_3 = C_T P^2 \qquad (5)$$

The problem then resolves itself into one of the solving five equations containing six unknowns (C_1, C_2, C_3, E_2^λ, P, and K) simultaneously. One cannot invoke a sixth relation using the conservation of mass principle; i.e., $C_T = C_1 + C_2 + C_3$, and this is already implicit in relations 3–5. Therefore, one must take the results of experiments at two concentrations to get enough equations to obtain solutions for all the unknown terms. This then reduces the problem to the simultaneous solution of two rather complicated quadratic equations.

The second model considered in this study is one involving the trimerization of the dye, wherein

$$2D^+ \rightleftharpoons D_2^{2+} \qquad D_2^{2+} + D^+ \rightleftharpoons D_3^{3+}$$

with the applicable equilibrium constants defined in the usual way, e.g.

$$K_2 = \frac{[C_2]}{[C_1]^2} \qquad (6)$$

and eq 7.

(17) R. B. McKay and P. J. Hillson, *Trans. Faraday Soc.*, **63**, 777 (1967).

$$K_3 = \frac{[C_3]}{[C_1]^3} \qquad (7)$$

The observed optical density is the sum of the contributions of each species and is

$$OD^\lambda = E_1^\lambda C_1 + 2E_2^\lambda C_2 + 3E_3^\lambda C_3 \qquad (8)$$

where E_1^λ, E_2^λ, and E_3^λ are defined as before, e.g., in terms of monomer units. Finally, one has the conservation of mass relation

$$C_T = C_1 + 2C_2 + 3C_3 \qquad (9)$$

This model, therefore, yields four equations and six unknowns (C_1, C_2, C_3, E_2^λ, K_2, and K_3), which could be reduced to one cubic equation with three unknowns. It is then possible, in principle at least, to make measurements at three different concentrations and to solve the three cubic equations simultaneously. In practice, however, this is hardly feasible and the techniques actually used will be described in a following section.

Consideration of activity coefficients leads to the conclusion that they can be ignored. They would normally be introduced, for example, into eq 6 in the following way

$$K_2 = \frac{\gamma_2[C_2]}{\gamma_1^2[C_1]^2} \qquad (10)$$

γ_3 would be introduced into eq 7 in a similar manner. If one assumes that the Debye–Hückel limiting law is valid, it can be shown that

$$\gamma_2 = \gamma_1^2 \qquad \gamma_3 = \gamma_1^3 \qquad (11)$$

Therefore, the ratios of activity coefficients that appear in the equilibrium equations are always equal to unity.

Experimental Methods and Results

I. Dye Purification. Attempts to prepare gram quantities of pure methylene blue by means of either silica gel or filter paper fiber column chromatography turned out to be impractical, although small quantities of relatively pure material could be so obtained. Instead, use was made of the familiar Hinsberg method (see, for example, ref 18) for separating primary, secondary, and tertiary amines. Therefore, the following procedure was used.

Methylene blue (6.7 g) was dissolved in 200 ml of warm water; to this was added 50 ml of benzene sulfonyl chloride, and the mixture was cooled. Then 200 ml of an aqeuous solution containing 50 g of KOH was added slowly while the mixture was cooled in running tap water. This mixture was then placed in the cold

room and was stored for several hours. This solution was filtered and the precipitate was washed with ether in order to remove the amides formed from the secondary amines. The precipitate was redissolved in water and the entire process was repeated. Finally, the precipitate was dissolved in water and was filtered; the pH was adjusted to 1.0 using HCl, and the solution was allowed to stand in the cold room for 3 hr. Filtration yielded 2.6 g of a semicrystalline black material which had a golden sheen.

Chromatographic analysis of the purified dye using Eastman thin-layer silica gel Chromagram sheets and methanol–acetic acid (9:1) as the developing solvent yielded a slowly moving intense blue spot which had an R_f value similar to that of the slowest spot found using commercial methylene blue. In addition a fainter, somewhat faster, incompletely resolved blue spot was also visible. Further cycles of purification did not perceptibly improve the purity of the dye. These results contrast with those obtained from samples of commercial dye which had been recrystallized from alcohol or water, for which as many as four spots were found. Elemental analysis (C, Cl, N, and S) of the purified dye yielded results that were low and were from 82 to 85% of theoretical, whereas the atom ratios were in good agreement with theory. Before purification, however, the N/C ratio was somewhat high, indicating the presence of compounds with lower degrees of methylation. Therefore, it was decided to use this partially purified material, but analysis for nitrogen was used to determine dye concentration in all solutions. The justification for using such samples is based on the thin layer chromatography results and the fact that the maximum absorption spectra of very dilute solutions was at 665 mμ, which is the longest so far observed (see Table I).

Table I: Comparative Results Obtained for Some Spectral Properties of Methylene Blue

Ref	Temp, °C	λ_{max}, mμ	$10^{-4}E_{max}$
Sheppard and Geddes[6]	30	. . .	7.2
Vickerstaff and Lemin[8]	. . .	656	6.1
Rabinowitch and Epstein[4]	27	656	4.0
Lewis, et al.[a]	30	660	8.5
Bergmann and O'Konski[b]	25	664	8.5, 9.5[c]
This study	30	665	7.8

[a] G. N. Lewis, O. Goldschmid, T. G. Magel, and J. Bigeleisen, *J. Amer. Chem. Soc.*, **65**, 1150 (1943). [b] K. Bergmann and C. T. O'Konski, *J. Phys. Chem.*, **67**, 2169 (1963). [c] The latter figure was obtained by correcting for dye absorption to the walls of the glass vessels and cells. None of the other results were corrected in this manner.

(18) R. L. Schriner and R. C. Fuson, "The Systematic Identification of Organic Compounds," John Wiley and Sons, Inc., New York, N. Y., 1948, p 91.

Since the azures and thionine have absorption maxima at successively shorter wavelengths, it would seem reasonable to assume that our sample is relatively free of these components. Another indication of purity is that the maximum molar extinction coefficient of these solutions was one of the higher ones observed (see Table I).

While this work was still in its final stages, Bonneau, Faure, and Joussot-Dubien[19] reported an elegant and efficient method for separating the various thiazine dyes by means of the differences in pK. A small amount of methylene blue purified in this manner showed almost identical properties to that prepared by our procedure. Because of its ease, however, future investigation will be done by this latter method.

II. Spectrophotometric Measurements. A. Measurement Technique. The absorption measurements were made by means of a Cary 14 spectrophotometer over a wavelength range of from 5500 to 7000 Å. The cells were thermostated at 30 ± 1°, and the cell size was chosen so that optical density measurements below 0.15 or above 1.5 were never made. This sometimes necessitated running two spectra on the same solution in cells of different sizes. The cells used had optical path lengths of from *ca.* 10 cm to *ca.* 0.005 cm. The exact relative size was determined by calibration at 373 mμ with alkaline K_2CrO_4 solution in relation to a 1-cm cell whose optical path length was assumed to be 1.000 cm. The size range of the cells made possible the use of dye solutions with concentrations of from *ca.* 6 × 10^{-7} to *ca.* 6 × 10^{-2} M. A total of 23 dye solutions was used to cover this concentration range. Tests to determine the time needed to reach equilibrium and the reversibility of the reaction were made. For the former, rapid dilution of a concentrated dye solution was made, followed by the measurement of the absorption as a function of time at a wavelength close to the expected absorption maximum for the diluted solution. If care was taken to keep the temperature constant, there was no observable change in the absorption with time, indicating that the reaction had apparently reached equilibrium in less than 1 min. The test for reversibility involved the measurement of the absorption spectrum of a dye solution first at 30°, then at 45°, and finally at 20°. The time for the solution to reach each temperature was about 15 min. This cycle was repeated several times and all the absorption spectra determined at any given temperature were identical.

B. Calculation Technique. The values of the observed molar extinction coefficients at 15 wavelengths of from 5500 to 7000 Å were independent of concentration at low dye concentrations and provided the value of E_1^λ. The extinctions at these wavelengths measured on dye solutions of high concentration were found to approach a limiting value asymptotically. Therefore the extinctions were plotted as E^λ vs. $1/CT$ and were extrapolated linearly by the computer to infinite concentration to provide the value of E_3^λ. Some repre-
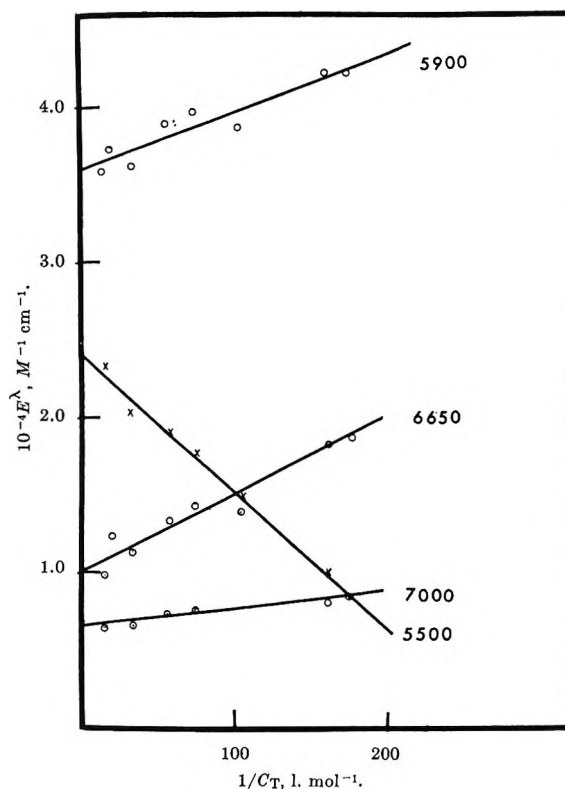
Figure 2. Extrapolation of absorption data at high methylene blue concentrations.

sentative extrapolations are shown in Figure 2, and the results of all of the extrapolations can be seen in Figure 3, curve C.

The polymerization model was tested first. Using eq 3–5 to eliminate C_1, C_2, and C_3, one can rewrite eq 1 in terms of C_T and P. Then by assuming a value for K, P is calculated using eq 2. This is then substituted into the rewritten quadratic eq 1 and this is solved for E_2. Eventually a value of K should be found which produces a value of E_2 which does not vary with concentration. If this value of K is constant with wavelength, the model successfully predicts the observed results. The reason this method was chosen rather than that of taking pairs of data for which an equation is written for each and is solved simultaneously is that in the latter case many of the pairs of data would fail to give solutions because of the sensitivity of the equations to small experimental errors. It was found impossible, however, to obtain a constant K, so the model was completely unacceptable.

One can make a great simplification in the trimerization model by first assuming that at low concentrations only the dimerization reaction need be considered. This is reasonable because, as stated previously, at low concentrations the α peak decreases while the β peak increases in such a manner that an isosbestic point is

(19) R. Bonneau, J. Faure, and J. Joussot-Dubien, *Talanta*, **14**, 121 (1967).
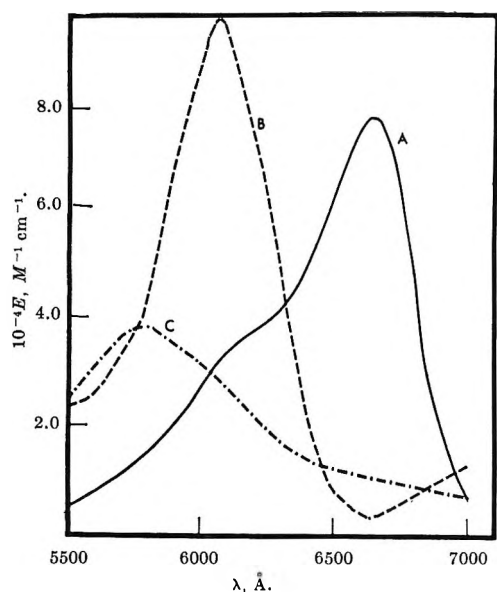
Figure 3. Absorption spectra of the three species present in aqueous solutions of methylene blue: curve A, monomer; curve B, dimer; curve C, trimer.

obvious. Using the iterative procedure described by de Maine and Seawright[20] which involves assuming a value for K_2, one then calculates a new value of K_2 which is reused, until successive calculated values of K_2 are insignificantly different. This procedure makes it easy to see if one has used data at too high dye concentration. One of the steps in this process involves fitting a straight line to a function of the data. If one first considers all the data, the high-concentration data deviate strongly from the straight line, indicating formation of higher species than dimers. By gradually removing the high concentration data, the fit gets better until the final value of K_2 and E_2 no longer change significantly as high concentration data are removed. In general, the values of K_2 obtained in the wavelength region of from 6400 to 7000 Å were highly constant, whereas those obtained in the region of from 5500 to 5800 Å were fair, and those from 5900 to 6300 Å were poor. The reason can be seen in Figure 3. This first wavelength region is one in which the monomer to dimer transition is accompanied by large absorption differences, followed by much smaller ones for the dimer to trimer transition. The region from 5500 to 5800 Å changes moderately on the formation of dimer but much less on the formation of trimer. The region from 5900 to 6200 Å involves a large increase of absorption on dimer formation and a large decrease on trimer formation. Therefore, the trimer reaction will appear significant at a fairly low dye concentration and the above mentioned simplification will not be valid over as large a concentration range as might be expected. It was not possible to obtain meaningful results at 6300 Å because this wavelength is near the isosbestic point for the monomer–dimer equilibrium. Therefore, for the

wavelength region 5900–6300 Å, a somewhat different procedure was used. The average value of K_2 determined in the range of 6400–7000 Å was assumed correct and from this the values of E_2^λ in the other regions were calculated.

The second step involves the calculation of K_3. Upon rewriting eq 8 and 9 using eq 6 and 7, one gets

$$OD^\lambda = E_1^\lambda C_1 + 2E_2^\lambda K_2 C_1^2 + 3E_3^\lambda K_3 C_1^3 \quad (12)$$

and

$$C_T = C_1 + 2K_2 C_1^2 + 3K_3 C_1^3 \quad (13)$$

which can be solved simultaneously, eliminating K_3, to yield a quadratic in C_1. Therefore, by using the data OD and C_T and the previously determined constants E_1^λ, E_2^λ and K_2, one can determine C_1. Substituting this back into eq 12, one can now solve for K_3. This was done by plotting a function of the data which yields a straight line, the slope of which is the value of K_3 at each wavelength. The values of K_3 were quite constant in the wavelength region of from 5900 to 6300 Å because of the relative importance of the dimer–trimer equilibrium, whereas they were rather poorly constant at other wavelengths. Therefore, the average value of K_3 obtained in this range was assumed correct. Finally, in order to test the model more thoroughly, the value of C_1 for each concentration was calculated from the cubic equation (eq 12). Then, using eq 12, the OD was calculated at each wavelength. The comparison of theory with experiment at a few representative concentrations is shown in Figure 1 and is a good indication of the ability of this model to describe the phenomena.

III. Vapor Pressure Osmometer Studies. At the time when it was evident that the polymerization model had failed, it was thought that a direct measurement of the molecular weight of the aggregates might suggest the proper model to be tested. Vapor pressure osmometry seemed suitable for these studies, and so the measurements were made with a Mechrolab Model 301A instrument using an aqueous probe at 30°. It was calibrated by using NaCl solutions of known concentration and osmotic coefficient. Four dye concentrations were studied over the range of from 0.017 to 0.055 M.

If one assumes that only the cation aggregates and that the Debye–Hückel limiting law applies, one can write the expression for the activity coefficient as

$$\ln \gamma_\pm = -0.52D\sqrt{1/2 C_T(D + 1)} \quad (14)$$

where D is the number average degree of polymerization of the dye cation. Of course it is assumed that the dye anion and the dye monomer cation are univalent, whereas the charge on the polymer cation is equal to D.

(20) P. A. D. de Maine and R. D. Seawright, "Digital Computer Programs for Physical Chemistry," Vol. I, The Macmillan Co., New York, N. Y., 1962, Chapter IV.

Using the relation between osmotic coefficient and activity coefficient,[21] one can write

$$\varphi - 1 = {}^{1}/{}_{3} \ln \gamma_{\pm} \qquad (15)$$

which can be rewritten using eq 14 as

$$\varphi = 1 - 0.3945D\sqrt{{}^{1}/{}_{2}C_{\mathrm{T}}(D + 1)} \qquad (16)$$

The resistance read from the osmometer is related to the molality of the polymerized dye cation by means of a calibration constant K, as is shown in the equation

$$R = Knm\varphi \qquad (17)$$

where m is the total molality of the variously polymerized dye molecules and n is the average apparent number of charged particles into which the polymerized molecule ionically dissociates (i.e., a dimer would yield three particles; a trimer would yield four; etc.). This can be rewritten as

$$R = K(D + 1)(C_{\mathrm{T}}/D)\varphi \qquad (18)$$

Rearranging eq 18, we get

$$\frac{R}{KC_{\mathrm{T}}} = \frac{D + 1}{D}\varphi \qquad (19)$$

The left side of eq 19 is what is measured. Therefore, substituting this into eq 16 gives us

$$\frac{R}{KC_{\mathrm{T}}} = (1 - 0.3945D\sqrt{{}^{1}/{}_{2}C_{\mathrm{T}}(D + 1)}) \frac{(D + 1)}{D}$$
$$(20)$$

To solve this, one merely varies D until eq 20 becomes an identity. The resulting final value of D is then the number-average degree of polymerization of the cation. A graph of D vs. C_{T} shows D rising rapidly and then leveling off asymptotically at high C_{T} near a value of 3 for D. A plot of the reciprocals $(1/D$ vs. $1/C_{\mathrm{T}})$ which linearize such a plot, gives the value of the asymptote more accurately, and the value of D is found to be 2.9 (see Figure 4). This indicates that the limiting form of aggregation is a trimer and is in good agreement with the conclusions arrived at from the spectral studies.

The only assumptions made here are that there is complete dissociation of the dye salt (regardless of degree of polymerization) and that the Debye–Hückel limiting law applies. These two assumptions must hold only over the concentration range studied to make this approach valid. The Debye–Hückel limiting law assumes that the ions are point charges with spherical symmetry. Since this conjugated molecule has its charge distributed over a considerable portion of the molecule and in view of the rather high concentrations studied (0.017–0.055 M), the validity of the assumptions made might be questionable.

Discussion

The results found here agree with those of Hillson and McKay,[11] who found by using polarographic methods
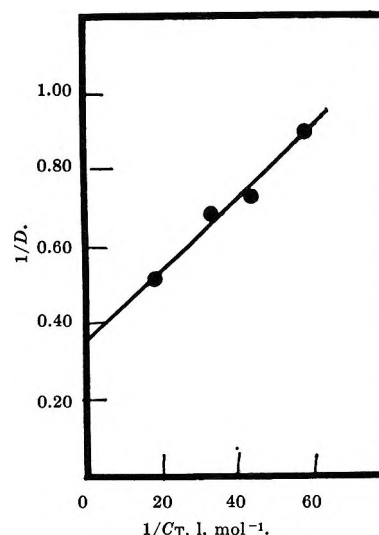
Figure 4. Vapor pressure osmometry study of concentrated solutions of methylene blue.

that the degree of aggregation of methylene blue at high concentrations was about 3.

The value which we observed for the equilibrium constant for the dimerization step, i.e., 2000 l. mol^{-1} at 30°, compares with those obtained by Rabinowitch and Epstein[4] and Bergmann and O'Konski,[22] 3600 l. mol^{-1} at 27° and 5900 l. mol^{-1} at 25°, respectively. The equilibrium constant for trimerization was found to have a value of about 6×10^{6} l.^{2} mol^{-2}. This means that it is at least as easy to add an additional dye monomer molecule to the dimer as it is to form the dimer. It may be that this simple trimerization model is incomplete, in that the presence of the anion in the equilibrium may be necessary. Haugen and Hardwick[9] have suggested that the dye dimerization may take place in the following manner

$$2D^{+} + A^{-} \xrightleftharpoons{\quad} D_{2}A^{+}$$
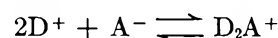
Lamm and Neville,[10] however, have found that it is impossible to distinguish by spectral means between this model and the simple dimerization model for acridine orange. The model involving anions in both the dimerization and trimerization step should and will be tested in the future by means of vapor pressure osmometry and spectrophotometry. However, if the simple trimerization model is correct, with the K for each stage being approximately equal, one might be able to detect still higher aggregates by studying aqueous solutions of methylene blue at lower temperatures, since studies at much higher dye concentrations than 0.06 M are limited by the solubility of the dye.

Acknowledgments. The dye purification and spectrophotometric measurements were performed by Mr.

(21) S. Glasstone, "Thermodynamics for Chemists," D. Van Nostrand Co., Inc., New York, N. Y., 1947, p 417.

(22) K. Bergmann and C. T. O'Konski, *J. Phys. Chem.*, **67**, 2169 (1963).

The Oxidation of Sodium, Potassium, and Cesium in Flames

by R. Carabetta

Space Sciences Laboratory, General Electric Company, Philadelphia, Pennsylvania 19101

and W. E. Kaskan[1]

Chemistry Department, State University of New York at Binghamton, Binghamton, New York 13901
(Received December 26, 1967)

The rates of oxidation of Na, K, and Cs have been measured in lean H_2–O_2–N_2 flames in the pressure and temperature ranges 100–1520 torr and 1420–1600°K. In all experiments, the reactions proceed *via* the mechanism alkali metal + O_2 + M $\xrightarrow{k_2}$ alkali superoxide + M. The rate constants, k_2, have been measured; average values are 0.82×10^{-33}, 1.02×10^{-33}, and 2.1×10^{-33} cm^6 particle^2 sec^{-1} for sodium, potassium, and cesium, respectively.

I. Introduction

The bulk of existing information on the behavior of alkali metals in fuel-rich flames is derived primarily from studies in which the metals were introduced into rich H_2–O_2–N_2 flames burned at atmospheric pressure.[2-6] On the basis of this work, it appears that the metals are involved in fast, equilibrated reactions of the type

$$A + H_2O \rightleftharpoons AOH + H \qquad (1)$$
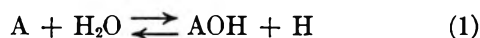
where A is an alkali metal.

In fuel-lean H_2–O_2–N_2 flames, however, the situation seems to be somewhat different. Kaskan's study[7] of Na and K in such flames indicates that the balanced reaction 1 does not apply but rather that the reaction of alkali metal with flame gases involves the formation of an alkali metal oxide. The conclusions drawn in this work were that the oxide is possibly AO, but most probably AO_2, which was formed *via* the forward reaction in the process

$$A + O_2 + M \underset{k_{-1}}{\overset{k_1}{\rightleftharpoons}} AO_2 + M \qquad (2)$$
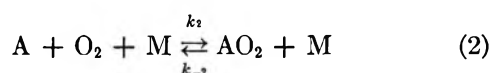
All of the work in ref 7 was performed at a single pressure (1 atm) so that the termolecular nature of eq 2 could not be proven but was assumed. McEwan and Phillips[8] have also reported that the kinetics for the re-action of both sodium and potassium are explicable in terms of process 2. The rate constants for the formation of the superoxides, k_2, were in good agreement, both for Na and K, with those reported by Kaskan.[7] In addition, they also reported measurements of the equilibrium constants for eq 2, when A is Na, at a number of temperatures, and from these measurements, they deduced the bond-dissociation energy, $D^0_{Na-O_2}$ (65 ± 3 kcal mol^{-1}).

Because the work on process 2 was carried out at atmospheric pressure, essentially at a constant (M), it was felt that the mechanism represented could be put on firmer ground if the termolecularity of the forward reaction could be demonstrated. In the present study,

(1) Consultant to the General Electric Space Sciences Laboratory, General Electric Co., Philadelphia, Pa. 19101.

(2) C. G. James and T. M. Sugden, *Nature*, **171**, 428 (1953).

(3) C. G. James and T. M. Sugden, *Proc. Roy. Soc.*, **A227**, 312 (1955).

(4) E. M. Bulewicz, C. G. James, and T. M. Sugden, *ibid.*, **A235**, 896 (1956).

(5) D. E. Jensen and P. J. Padley, *Trans. Faraday Soc.*, **62**, 2132 (1966).

(6) D. E. Jensen and P. J. Padley, *ibid.*, **62**, 2140 (1966).

(7) W. E. Kaskan, Tenth Symposium (International) on Combustion, Cambridge, England, The Combustion Institute, Pittsburgh, Pa., 1965, p 41.

(8) M. J. McEwan and L. E. Phillips, *Trans. Faraday Soc.*, **62**, 1717 (1966).

the rates of reaction of sodium, potassium, and cesium have been measured in a number of lean H_2-O_2-N_2 flames burned at pressures of from 100 to 1520 torr. It has been found that the reaction rate of the metal is first order in (A), in (O_2), and also in (M) and that the reaction rate constants, k_2, for both Na and K, are in good agreement with those reported in the two previous studies. In addition, k_2, for Cs, has been determined.

II. Experimental Section

The variable-pressure burner system is illustrated schematically in Figure 1. The burner was a water-cooled porous-metal type consisting of an inner circular part, 7.5 cm in diameter, surrounded by an annular part about 2.5 cm wide, each having a separate gas-inlet system. The burner, the characteristics of which have been described elsewhere,[9] was designed to provide a one-dimensional flow of unburned gas which would, in turn, provide a flat flame of diameter equal to that of the burner. The outer burner was used to support a shield flame, identical with that supported by the inner burner, but without alkali metal seeding. Metal was added to the inner flame by passing part of the gas stream to the inner burner through an atomizer bottle containing a solution of alkali metal salt, usually the chloride. Larger particles from the atomizer were separated from the smaller in a separate settling flask placed in the line between the atomizer and the burner. A wire-mesh screen placed above the burner head served to stabilize the column of hot flame gases so that after exiting from the reaction zone they would continue to flow perpendicular to the burner surface. With this arrangement, the vertical axis is also a time axis. The burner head was mounted on a pipe 5 cm in diameter which entered the lower portion of the chamber through an O-ring seal and both pipe and burner could be moved (in the vertical direction) with respect to the fixed axis of the optical system by means of a micrometer mechanism. Pressure inside the chamber was regulated by simultaneously admitting nitrogen into the system through a number of bleed valves and by adjusting a large gate valve leading to a vacuum pump. The gas flows to the burners were metered with calibrated critical flow orifices.

Figure 1 also shows a schematic of the optical system. Light from the source S was passed over the burner, parallel to its surface, *via* the mirror M1 and was refocused on the monochromator slit with the mirror M2. A tungsten strip filament lamp (filament dimensions 1 × 13 mm) served as a background source for alkali metal resonance–line absorption measurements. To measure OH concentrations and for OH rotational temperature determinations, the tungsten source was replaced by a water-discharge lamp.[10] For a typical flame, the spatial resolution in the vertical direction afforded by this arrangement of optics was about 1 mm.
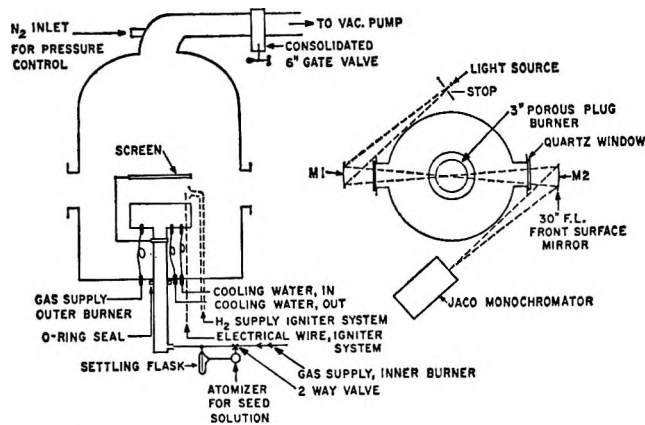
Figure 1. Schematic of burner and optical system.

Temperature profiles in the flames were measured with a silica-coated 0.0025-cm diameter Pt—Pt-10% Rh thermocouple and were corrected for radiation losses.[8] Occasionally, the thermocouple measurements were supplemented by measurement of ground-state OH rotational temperature. Agreement to within 50°K was always obtained.

Determination of the alkali metal atom concentrations in the flame gases from resonance–light-absorption measurements required the use of a set of calibration curves, one for each metal. Fuel-rich H_2-O_2-N_2 flames having equivalence ratios of 1.3 were chosen as calibration flames. In these flames, the alkali metal concentration did not change perceptibly with distance from the burner surface. Furthermore, based on the data for hydroxide formation provided by the work of Jensen and Padley,[5] the fraction (AOH)/(A) for Cs (the most favored of the three hydroxides) at the points of measurement in each of the calibration flames was computed to be less than could be measured with our apparatus, *i.e.*, less than 0.02. Calibrations were carried out in a plane in each flame at which the temperature was 1500°K; for all measurements, the tungsten background source was operated at a temperature of about 2500°K so that no emission correction for flame background was required.

The following procedure was used to establish the calibration curves. A concentrated solution containing equimolar quantities of NaCl, KCl, and CsCl was made up and diluted so as to produce a number of solutions, each less concentrated than the next by a factor of 2. Each of these solutions was used, in turn, to seed the calibration flame, and for each, the absorbance $(I_0 - I)/I_0$ was measured, where I_0 is the intensity of the background lamp and I is the intensity of the light transmitted through the gas at the wavelength of peak absorption. This was done for both the D_1

(9) W. E. Kaskan, Sixth Symposium (International) on Combustion, Yale University, Williams and Wilkins Co., Baltimore, Md., 1953, p 68.

(10) W. E. Kaskan, *Combust. Flame*, 2, 229 (1958).

and D_2 lines of Na and K and the D_2 line of Cs. The D_1 line for Cs could not, however, be conveniently measured because it lies just to the red side of the long wavelength cutoff of the monochromator. The absolute sodium atom concentration produced by each solution in each flame was deduced from the Van der Held curve of growth,[11] the a parameters suggested by the work of Sobolev, et al.,[12] the known f number of this line,[13] and the experimentally measured area under the absorption line. From this a calibration curve [log (absorbance) vs. log (concentration)] for sodium was established for the series of mixtures. Since the conditions of our experiments were such that at the planes of measurement equal quantities of the three metals were expected to be present, calibration curves based on the absorbance of the D_2 lines of Cs and K were obtained by plotting the measured absorbance of each against the absolute sodium concentration appropriate to the equimolar solution employed. Using this procedure, three smooth curves, one for each metal, were obtained at each pressure. Two checks were then carried out. First the absorbances of the Na D_1 and K D_1 lines for each solution were plotted at half the concentration appropriate to the corresponding D_2 lines (this, of course, was not done for Cs); for each metal, these points fell on the smooth curve defined by the absorbance measurements on the D_2 line, as would be expected. The second check made use of the fact that the absorption in the optically thin regime[13]

$$\frac{I}{L} \int \frac{I_0 - I}{I_0} d\nu = \frac{\pi e^2 N f}{mc^2} \tag{3}$$

where L is the path length and N is the number density of the absorbing species (m, c, e, and f have their usual meanings). Since the left-hand side of eq 3 can be experimentally measured for the three species, it is possible to solve for N. Using the smallest measurable values of absorbance for each species and eq 3, it was found that the absolute concentrations of the three metals were equal—as would be expected if virtually all of the alkali metal were converted to free metal in the calibration flame.

To measure the oxidation rates of the alkali metals, a solution containing equimolar quantities of the metals was used to introduce the alkalies into a number of H_2–O_2–N_2 flames having different equivalence ratios. Flames were burned at 5 pressures: 150, 250, 380, 760, and 1520 torr. In each experiment, the temperature profile through the flame was recorded, as was the alkali metal concentration profile. In seeding flames, solutions producing initial concentrations of ca. 10^{10} to 10^{11} alkali atoms/cm³ in the flame gases were used; thus the measurements of alkali metal profiles almost always involved the use of the nearly linear (and more sensitive) portions of the calibration curves.
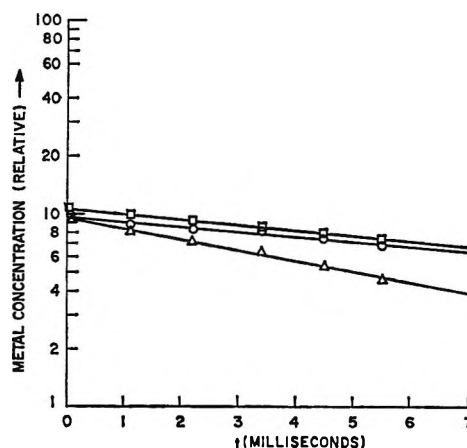
Figure 2. First-order reaction of Na, K, and Cs in flame 4: O, Na; □, K; △, Cs.
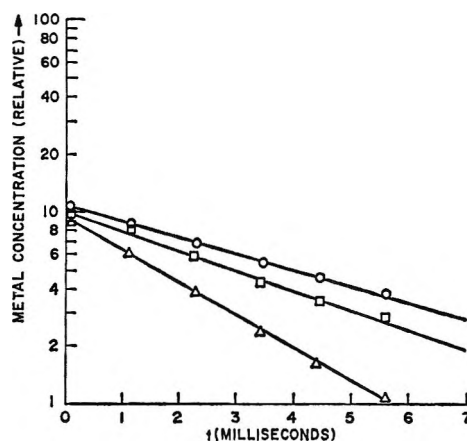
Figure 3. First-order reaction of Na, K, and Cs in flame 5: O, Na; □, K; △, Cs.

III. Results and Discussion

The flames employed to study the oxidation are listed in Table I. The gas compositions shown are nominal in that they were simply computed from the flame stoichiometry, assuming all H_2 was burned to H_2O. In each experiment, the kinetic measurements were limited to the burned-gas region, downstream of the reaction zone, where the temperature changes little with distance. In Table I the temperature shown (T) designates the average temperature in this region; similarly, $\bar{V}$ corresponds to the mean hot gas velocity in this region.

Some general statements can be made about the observations. In all cases, alkali atom concentrations are at a maximum in or near the reaction zone. In rich flames these concentrations remain constant downstream of the reaction zone, but in lean flames they

(11) E. F. M. Van der Held, Z. Phys., **70**, 508 (1931).

(12) N. N. Sobolev, E. M. Mezhericher, and G. M. Rodin, Zh. Eksperim. Teor. Fiz., **21**, 350 (1951).

(13) A. C. G. Mitchell and W. Zemansky, "Resonance Radiation and Excited Atoms," Cambridge University Press, London, 1961, Chapter 3.

Table I

Flame no.	ϕ^a	P, torr	$\bar{T}$, °K	$\bar{v}$, cm/sec	$10^{-17}(O_2)$, cm⁻¹	$10^{-17}(M)$, cm⁻¹	$10^{-17}(H_2O)$, cm⁻¹	$-d[\ln (A)]/dt$, sec⁻¹			$10^{11}k_2$, cm⁶ mol⁻² sec⁻¹			$10^{11}k_2'$, cm⁶ mol⁻² sec⁻¹		
								Na	K	Cs	Na	K	Cs	Na	K	Cs
1	0.38	100	1430	199	0.945	6.65	1.20	44.0	44.4	104	0.70	0.71	1.7	0.75	0.72	1.7
2	0.38	150	1450	202	1.41	10.0	1.64	121	141	280	0.86	1.0	2.0	0.88	1.0	2.1
3	0.38	250	1440	200	2.37	16.8	3.01	320	360	800	0.80	0.9	2.0	0.84	0.94	2.2
4	0.60	150	1565	190	0.817	9.25	2.65	61.8	56.6	136	0.82	0.75	1.8	0.84	0.76	1.8
5	0.60	250	1600	186	1.34	15.1	4.00	164	233	412	0.81	1.1	2.0	0.84	1.1	2.1
6	0.76	150	1540	134	0.404	9.40	2.60	b	b	44.7	b	b	1.2	b	b	1.4
7	0.76	250	1475	92.5	0.718	16.3	4.50	70.0	97.2	195	0.60	0.83	1.7	0.63	0.87	1.8
8	0.76	380	1420	58.6	1.14	25.8	7.10	195	230	435	0.66	0.78	1.5	0.86	0.96	1.9
9	0.76	380	1600	132	1.01	23.0	6.35	170	230	500	0.73	0.99	2.2	0.76	1.0	2.4
10	0.90	760	1575	126	0.77	48.2	13.6	290	528	850	0.78	1.4	2.3	0.81	1.5	2.7
11	0.95	760	1575	125	0.37	48.2	13.8	153	246	450	0.86	1.4	2.5	0.89	1.4	2.6
12	0.95	1520	1570	75.0	0.28	93.0	24.1	220	260	528	0.84	1.0	2.0	0.89	1.0	2.1

^{a} ϕ = equivalence ratio = (fuel/oxidant)(actual):(fuel/oxidant)(stoichiometric). ^{b} Slope was too small to permit accurate measurements.

decay downstream. At each pressure, these decays were found to be first order in the concentrations alkali, O_2, and M, and were found to be independent of the nature of the salt used (nitrates gave the same results as chlorides).

Some typical data are shown in Figures 2 and 3. Since the decay was found to be first order with respect to the metal, the metal concentrations shown are given in arbitrary units in order to facilitate the presentation of the data. In each of these plots, the first measurement (corresponding to that at $t = 0$) was made just downstream of the reaction zone where the temperature is within about 25°K of its peak value.

Assuming that the decay of alkali metals proceeds *via* the forward process 2, then

$$\frac{-d(A)}{dt} = k_2(A)(O_2)(M) \tag{4}$$

For constant (M) and (O_2)

$$\frac{-d[\ln (A)]}{dt} = k_2(O_2)(M) \tag{5}$$

The measured values for $-d[\ln (A)]/dt$ are contained in columns 9–11 in Table I. Columns 12–14 of this table contain the deduced values for k_2 as obtained from eq 5, uncorrected for the effects of diffusion.

Since the reaction rate is first order with respect to the metal, the following modified form of the diffusion equation was applied to our data[14]

$$D\frac{d^2(A)}{dX} - \bar{V}\frac{d(A)}{dX} - k_2'(A)(O_2)(M) = 0 \tag{6}$$

where D is the diffusion coefficient of A, X is the distance in the direction of gas flow in the flame, and k_2' is the true diffusion corrected third-order rate constant for the forward reaction in process 2. Integration of eq 6 for the boundary conditions, (A) = 0 at $X = \infty$ and (A) = $(A)_0$ at $X = X_0 = 0$ yields

$$k_2' = k_2\left(\frac{-D\, d\ln (A)}{\bar{V}^2\, dt} + 1\right) \tag{7}$$

Values for k' are given in the last three columns of Table I.

In applying the diffusion correction (eq 7) to our results, binary diffusion coefficients for the diffusion of the metal into N_2 were computed using the simple kinetic-theory approach[15] (D_{Na-N_2} (STP) = 0.191 cm² sec⁻¹, D_{K-N_2} (STP) = 0.134 cm² sec⁻¹, D_{Cs-N_2} (STP) = 0.098 cm² sec⁻¹). As a check, k_2 was measured for each of the metals in a number of flames differing primarily in $\bar{V}$. Flames 8 and 9 in Table I are two such flames. The fact that the k_2 values for the three metals, respectively, are comparable for both flames

(14) R. Friedman and J. Cyphers, *J. Chem. Phys.*, **23**, 1875 (1955).
(15) W. Jost, "Diffusion in Solids, Liquids and Gases," Academic Press Inc., New York, N. Y., 1952, Chapter X.

indicates that diffusion effects are relatively unimportant over the range of conditions in our experiments. This result is consistent with what would be predicted using the computed D values. The flames chosen in this study were in fact designed so as to minimize diffusion effects by experimentally minimizing the first term in the brackets of the right-hand side of eq 7.

The k_2' values for Na and for K listed in Table I are in excellent agreement with those reported by Kaskan[7] and are about a factor of 2 less than those reported by McEwan and Phillips.[8] In this work the reproducibility of a rate constant from a given experiment was about 10%. The experimental scatter in the results shown in Table I may well reflect differences in third-body efficiencies (see below).

The dependence of the rate of the forward reaction in process 2 on a third body is shown in Figure 4. The fact that the data fall on a fairly good straight line having a slope of 1 shows that the reaction is first order in (M).

In fuel-rich H_2-O_2-N_2 flames, the behavior of alkali metals has been interpreted in terms of process 1, involving alkali hydroxides. Kaskan has pointed out[7] that since eq 1 is postulated to be equilibrated,[4-6] then

$$\frac{(A)}{(AOH)} = \frac{(H)}{K_1(H_2O)} \tag{8}$$

where K_1 is the equilibrium constant for eq 1. Thus since the species H_2, OH, O, O_2, and H have been shown to be involved in fast equilibrated reactions[4,16] viz.

$$H_2 + OH \rightleftharpoons H_2O + H \tag{9}$$

$$H + O_2 \rightleftharpoons OH + O \tag{10}$$

$$O + H_2 \rightleftharpoons OH + H \tag{11}$$
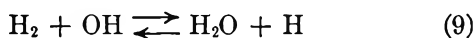
then

$$(H) = \frac{K_9}{K_{10}K_{11}} \frac{(OH)^3}{(H_2O)(O_2)} \tag{12}$$

so that

$$\frac{(A)}{(AOH)} = \frac{K_9}{K_1K_{10}K_{11}} \frac{(OH)^3}{(H_2O)^2(O_2)} \tag{13}$$

In Kaskan's work, it was possible to check relation 13, since both (OH) and the ratio (A)/(AOH) could be determined experimentally in those planes in the flame where the temperature and, therefore, the equilibrium constants in eq 13 changed but very slightly. The result was that (A)/(AOH) for Na and for K varied more nearly as the second power of (OH) than as the third power predicted by eq 13. It was pointed out[7] that this result is formally explicable in terms of the process

$$A + OH \rightleftharpoons AO + H \tag{14}$$
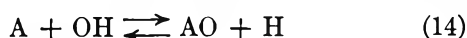
and as such, this possibility, rather than AO_2 formation, could not be ruled out.
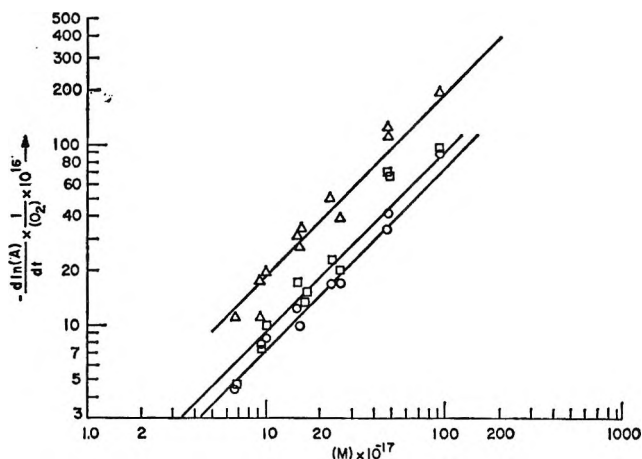
Figure 4. The pressure dependence of the reaction rate of A on (M): O, Na; □, K; △, Cs.

In the work carried out by Kaskan, there was no large variation in (H_2O). If the fair correlation of (A)/(AOH) with (OH)^2 were fortuitous, this might more clearly be shown from measurements in CO-O_2-N_2 flames containing a little added H_2, since in such flames (H_2O) is very much smaller than in H_2-O_2-N_2 flames. Such experiments were carried out and the data were treated in the following manner. Using the procedure previously described,[7] the quantities (OH) and (A)/(AOH) were first measured, as a check, in some atmospheric pressure H_2-O_2-N_2 flames. In computing (OH), the more recently reported value[17] for the oscillator strength was used; the line strengths used are those given by Dieke and Crosswhite[18] as corrected by Learner.[19] The concentration of AOH at a given location in the flame was deduced by difference from measurements of (A) and (A)$_0$. The quantity (A)$_0$ was deduced from measurements in similar rich flames having the same alkali salt delivery rate but in which no metal oxide or hydroxide was formed. For flames 10 and 11 in Table I, the results were found to be in agreement with Kaskan's, in that (A)/(AOH) seemed to correlate with (OH)$^{1.8-2.0}$ for both sodium and potassium.

In Figure 5 are shown the results obtained in an atmospheric pressure flame of unburned composition: H_2:CO:O_2:N_2 = 0.033:0.160:0.161:0.645; $\bar{T}$ = 1665°K. Clearly, in these flames, (A)/(AOH) does not correlate with any power of (OH). On this basis, it would seem reasonable to conclude that the observed correlation of this ratio with (OH)^2 in H_2-O_2-N_2 flames is fortuitous and that the equilibrated reaction 1 is not operative. The data from this flame were also

(16) W. E. Kaskan, Combust. Flame, 3, 49 (1959).

(17) R. G. Bennett and F. W. Dalby, J. Chem. Phys., 40, 1414 (1964).

(18) G. Dieke and H. M. Crosswhite, J. Quant. Spectrosc. Radiat. Transfer., 2, 97 (1962).

(19) R. C. M. Learner, Proc. Roy. Soc., A269, 311 (1962).
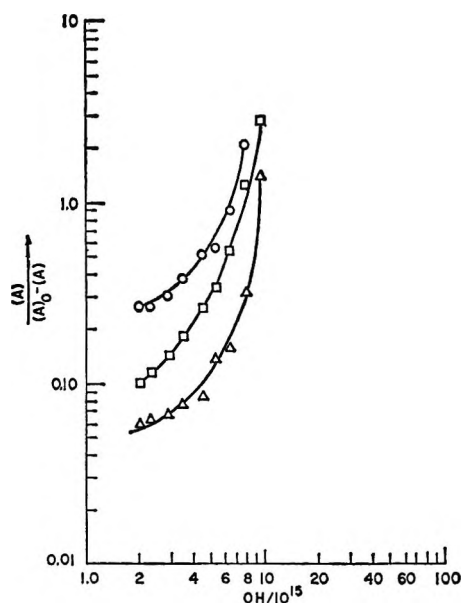
Figure 5. Correlation of $(A)/[(A)_0 - (A)]$ vs. (OH) in $H_2-CO-O_2-N_2$ flame: O, Na; □, K; Δ, Cs.

interpreted in terms of the superoxide formation; the third-order rate constants obtained for the three metals were a factor of 2 lower than the average for each listed in Table I. Although the difference could easily be explained in terms of the differences in efficiencies of H_2O and CO_2 as third bodies, this question was not pursued further (previous work[7] has indeed shown H_2O to be more effective than N_2 for the forward reaction 2).

The data from all of our experiments indicate that the mechanism responsible for the decay of alkali metals in lean flames is reaction 2 operating in the forward direction. It is interesting to note that in the atmospheric flame work reported by McEwan and Phillips[8] and Kaskan,[7] it was found that the compound-forming reaction did not go to completion; instead, following the initial first-order decay of (A), there was an apparent fall-off of the rate with time. In the work in ref 8, the fall-off is attributed to the reverse reaction in process 2, which makes its effect felt as the superoxide concentration increases. In the present work, the fall-off of the over-all oxidation rate was also observed in flames burned at pressures greater than 360 torr but not in the lower pressure flames. This result is consistent with the idea (but by no means a positive indication) that the reverse reaction is a function of (M). In our experiments, the O_2 concentration was adjusted in such a manner that the forward rate of reaction 2, $k_2(O_2)(M)(A)$, did not change much with pressure; thus a reverse reaction having a rate proportional to (M) × (concentration of final oxidation products) would be expected to become less favored relative to the forward reaction as the pressure and, therefore, (M) is reduced.

It is difficult to believe that MO_2 is the final species

produced. Indeed, if one assumes that the dissociation energy of NaO_2 is that reported by McEwan and Phillips,[8] then (based on JANAF data) the following exothermic and, therefore, conceivably, fast reactions could proceed

$$NaO_2 + O \longrightarrow NaO + O_2 \qquad (15)$$

$$NaO_2 + OH \longrightarrow NaOH + O_2 \qquad (16)$$

$$NaO_2 + H \longrightarrow NaOH + O \qquad (17)$$
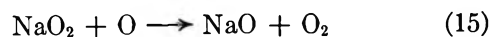
At equilibrium, in the highest temperature flame used by McEwan and Phillips to measure D_{Na-O_2} (T, 2030°K; unburnt gas composition, $H_2:O_2:N_2 = 1.5:1:1.3$; pressure, 1 atm) the concentrations of O, OH, and H are, respectively, 8.85×10^{14}, 1.12×10^{16}, and 1.58×10^{14} particles/cm³. Since the dissociation reaction requires a 65 kcal/mol activation energy, then at equilibrium in the flame in question, the concentration of H, O, and OH are certainly high enough so that if reactions 15–17 are operative, the final products would probably be NaO and/or NaOH rather than NaO_2. In an effort to help clarify this issue, some ancillary experiments involving the use of a mass spectrometer were carried out.

Available thermodynamic data[20] suggest that of the three superoxides, NaO_2 KO_2, and CsO_2, the last is the most stable (we note here that the heats of formation of these species are available only for the solid state and that their heats of sublimation are not known). Since the flame results show that CsO_2 is the most readily formed of the three in the gas phase, it seemed worthwhile to attempt to detect the presence of this species in the gas phase directly. To this end, crystalline cesium superoxide was placed into a platinum-lined Knudsen cell which would be heated by radiation and electron bombardment from a tungsten filament. The cell was also provided with an inlet system so that a pressure of about 1 torr of O_2 could be maintained over the superoxide. The temperature of the cell and its contents was measured with a thermocouple. After heating the cell, the gaseous products were allowed to effuse from the cell into the ion source of a time-of-flight mass spectrometer (Bendix Model 12).

In these experiments the cell was heated at temperatures of from 600 to 1300°K in approximately 100° steps. In each experiment, the electron-beam energy was varied from 0 to 70 eV. The cesium species, Cs^+, Cs_2^+, Cs_2O^+, and $Cs_2O_2^+$ were observed. However, CsO_2^+ could not be identified even at low energies where fragmentation is minimal.

On the basis of the foregoing, it would seem that although the forward reaction 2 is the rate-determining step in the oxidation of alkali metal atoms in lean flames, the superoxides may not be the final product.

(20) J. M. Mellor, Supplement to "Comprehensive Treatise on Inorganic and Theoretical Chemistry," Vol. II, Suppl III, Part II, John Wiley and Sons, Inc., New York, N. Y., 1961.

Finally, it must be stated that the results of these experiments are not in disagreement with the work in ref 2-6 in which process 1 has been postulated as operative. In the present study, the work was not only carried out in lean rather than rich flames but was carried out also at lower temperatures. In fact, the existence of a process such as eq 1 is demanded even in lean flames by the fact that the reverse of this reaction is most probably the type reaction responsible for the reduction of alkali metal compounds to free alkali atoms in the reaction zone. Thus although the reaction of alkali metals at relatively high O_2 concentrations and low temperatures has been shown to take place *via* AO_2 as a kinetically important intermediate, it is quite possible that an increase in temperature and/or a decrease in (O_2) (as with HO_2 in hydrocarbon oxidation) leads to conditions where process 1 is dominant. Based on the data of McEwan and Phillips,[8] it would appear that in a lean flame the change in kinetics would occur only at temperatures in excess of about 2000°K.

IV. Conclusions

The rates of reaction of sodium, potassium, and ce-

sium in lean H_2-O_2-N_2 flames, burned at pressures of from 100 to 1520 torr, scale with pressure in a manner such that the rate-determining step is shown to be

$$A + O_2 + M \longrightarrow AO_2 + M$$
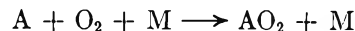
The rate constants computed for the reaction on this basis, for sodium and for potassium, are in excellent agreement with those measured at atmospheric pressure by Kaskan[7] and McEwan and Phillips.[8] It is questioned, however, whether the species AO_2 is the final product of the reaction.

Application of the WKB Method to the Dynamics of Anharmonic Oscillators[1]

by Robert Dubrow, Douglas Hatzenbuhler, William Marx, Eva Zahorian, and David J. Wilson

Department of Chemistry, University of Rochester, Rochester, New York 14627 (*Received December 26, 1967*)

The dynamical behavior of the Morse oscillator and the Fues oscillator is investigated by the WKB method. The results are compared with those obtained by using the exact-energy eigenfunctions (Morse oscillator) and with those obtained by using the linear-variation method with harmonic-oscillator basis functions (Fues oscillator). The WKB method yields results superior to those of the linear-variation method with harmonic-oscillator basis functions, and the results are in excellent agreement with those obtained using the exact-energy eigenfunctions as the basis set.

Introduction

The quantum dynamics of several anharmonic oscillators have been explored in earlier papers in this series.[2-6] The work of both Endres and Smyser indicated that the linear-variation method with harmonic-oscillator basis functions is not well adapted to dealing with wave packets having high vibrational energies. Neither the energies nor the approximate wave functions obtained by this method are of adequate accuracy to provide good results unless a very large number of functions are used. The form of the envelope to plots of $\langle r(t) \rangle$ vs. t (r is the coordinate of the oscillator) de-

pends upon the second differences of the energies. It is therefore necessary to have energies of quite high accuracy in order to obtain envelopes of even modest accuracy. The matrix elements of the coordinate and

(1) This work was supported by the National Science Foundation.
(2) E. Alterman, C. Tahk, and D. J. Wilson, *J. Chem. Phys.*, **44**, 451 (1966). See this paper for earlier references.
(3) R. Baetzold, C. Tahk, and D. J. Wilson, *ibid.*, **45**, 4209 (1966).
(4) P. F. Endres and D. J. Wilson, *ibid.*, **46**, 425 (1967).
(5) W. Smyser, Doctoral Dissertation, University of Rochester, Rochester, N. Y., 1967.
(6) P. F. Endres, *J. Chem. Phys.*, **47**, 798 (1967).

Table I: Exact and WKB Energies for Various One-Dimensional Oscillators

Potential	WKB energy	Exact energy
$2D\left[\dfrac{-r_e}{r} + \dfrac{r_e^2}{2r^2}\right]$	$\dfrac{-AD}{(n + 1/2 + \sqrt{A})^2}$ [a]	$\dfrac{-AD}{(n + 1/2 + \sqrt{A} + 1/4)^2}$ [a]
$D\{1 - \exp[-\beta(r - r_e)]\}^2$	$\beta h\sqrt{\dfrac{2D}{\mu}}(n + 1/2) - \dfrac{\beta^2\hbar^2}{2\mu}(n + 1/2)^2$	Same as WKB energy
$\left.\begin{array}{l}\infty, r < 0 \\ 0, 0 < r < a \\ \infty, r > a\end{array}\right\}$	$\dfrac{n^2\hbar^2}{8\mu a^2}$	Same as WKB energy
$1/2K(r - r_e)^2$	$(n + 1/2)\hbar\sqrt{\dfrac{K}{\mu}}$	Same as WKB energy
$\left.\begin{array}{l}\infty, r < 0 \\ ar, r > 0\end{array}\right\}$	$\left[\dfrac{3a(n + 3/4)h}{2^{5/2} \times \mu^{1/2}}\right]^{2/3}$	$\left[\dfrac{(a^2\hbar^2)}{6\mu}\right]^{1/3}\dfrac{3}{2^{2/3}}S_h^{2/3}$ [b]
$-V_0/\cosh^2(x/a)$	$-B[1/2\sqrt{A + 1} - (n + 1/2)]^2$ [c]	$-B[1/2\sqrt{A} - (n + 1/2)]^2$ [c]
$V_0\left(\dfrac{a}{r} - \dfrac{r}{a}\right)^2$	$B(n + 1/2)^d]$	$B[(n + 1/2) + 1/4(\sqrt{A + 1} - A)]^d$
$V_0\cot^2\dfrac{\pi x}{a}$	$B[(n + 1/2)^2 + 2(n + 1/2)\sqrt{A} + A] - V_0^e$	$B[(n + 1/2)^2 + 2(n + 1/2)\sqrt{A + 1} + A] - V_0^e$

[a] $A = 2D\mu r_e^2/\hbar^2$.   [b] S_n is tabulated by Watson[10] and is the nth root of $J_{1/3}(2u^{3/2}/3^{1/2}) + J_{1/3}(2u^{3/2}/3^{1/2})$.   [c] $A = 8\mu V_0 a^2/\hbar^2$; $B = \hbar^2/2\mu a^2$.   [d] $A = 8\mu V_0 a^2/\hbar^2$; $B = (2\hbar/a)(2V_0/\mu)^{1/2}$.   [e] $A = 2\mu V_0 a^2/\pi^2\hbar^2$; $B = \pi^2\hbar^2/2\mu a^2$.

the expansion coefficients of the initial wave packet are not subject to a variational principle (as are the energies); hence these matrix elements may introduce significant errors in $\langle r(t)\rangle$ even when the energies are calculated rather accurately by the linear-variation method.

The WKB method[7,8] yields extremely good values for the energy levels of a variety of anharmonic oscillators. We compared the exact and the WKB energies for the harmonic oscillator and for seven anharmonic oscillators; we use well depth, range, and mass parameters appropriate for hydrogen. (Most of these formulas may be found in the problem book by Gol'-dman and his collaborators.[9]) See Table I.[10] The agreement is extremely good in all cases and, as one would expect, improves at higher energies, in contrast to the linear-variation method. These results prompted us to investigate the use of WKB eigenfunctions for calculating the matrix elements and expansion coefficients needed to investigate the dynamical behavior of $\langle r(t)\rangle$.

The Fues potential (see the first expression in column 1 of Table I) yields a coulombic force at large distances and hence is useful for molecules which dissociate into ions. The Fues oscillator can be solved quantum mechanically,[11] and the exact and WKB energies are in excellent agreement for parameters chosen to simulate real molecules. The Fues potential is a slowly increasing potential for large r; hence the Fues potential provides one with a rather severe test for the linear-variation method with harmonic-oscillator basis functions.

We expanded the Fues potential in positive powers of $x = r - r_e$, yielding

$$V = D\left[\sum_{n=2}^{\infty}(-1)^n(n - 1)(x/r_e)^n\right] \quad (1)$$

The matrix elements of the Hamiltonian in the harmonic-oscillator basis set (for $V_{HO} = D x^2 r_e^2$) are

$$H_{nm} = \delta_{nm}(n + 1/2)h\nu_{HO} + \sum_{p=3} b_p \dfrac{x_{nm}^p}{r_e^p} \quad (2)$$

where $b_p = (-1^p(p - 1)D$ and $\nu_{HO} = (2D/\mu r_e^2)^{1/2}/2\pi$.

We note that some convergence questions arise if one extends the summations in eq 1 and 2 to infinity, owing to the singularity in V at $x = -r_e$; we evade this issue by redefining V as a truncated series similar to that in eq 1 and we choose our termination such that the final results are insensitive to the number of terms retained. This restricts us to wave packets, the amplitudes of which are negligible for $|x| \geq r_e$ and precludes the study of wave packets of really high energy (*i.e.*, $\langle E\rangle > 0.25D$), as will become apparent.

The initial wave packets were chosen to be gaussian minimum wave packets centered at various values, r_0,

(7) L. I. Schiff, "Quantum Mechanics," McGraw-Hill Book Co., Inc., New York, N. Y., 1955.

(8) L. D. Landau and E. M. Lifshitz, "Quantum Mechanics," Addison-Wesley Publishing Co., Reading, Mass., 1958.

(9) I. I. Gol'dman, V. D. Krivchenkov, V. I. Kogan, and V. M. Galitzkii, "Problems in Quantum Mechanics," Academic Press Inc., New York, N. Y., 1960.

(10) G. N. Watson, "Theory of Bessel Functions," Cambridge University Press, London, 1922.

(11) E. Fues, *Ann. Phys.*, **80**, 367 (1926).
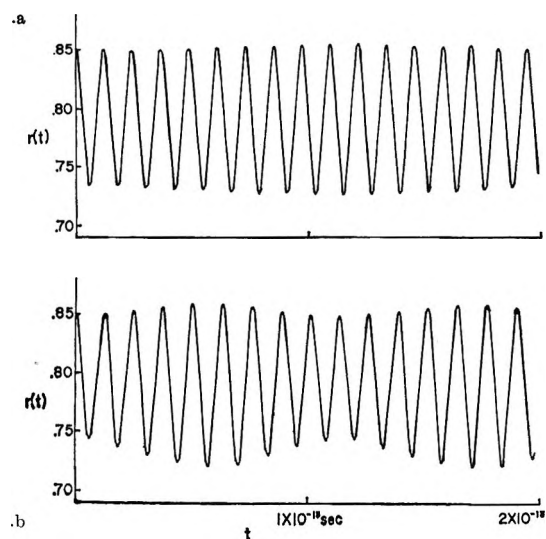
Figure 1. Expectation value of the coordinate as a function of time: (a) results obtained by the linear-variation method; (b) results obtained by the WKB method with the same parameters. Data given for the Fues oscillator: $r_e = 0.74$ Å; r_0 (the center of the initial wave packet) $= 0.85$ Å; $D = 0.7120 \times 10^{-11}$ erg/molecule; $\mu = 0.83 \times 10^{-24}$ g; the width parameter in the initial wave packet $= 0.1507$ Å; $\langle E \rangle_{initial} = -0.6781 \times 10^{-11}$ erg/molecule; $\langle E \rangle_{HO} = -0.6778 \times 10^{-11}$ erg/molecule; $\langle E \rangle_{WKB} = -0.6782 \times 10^{-11}$ erg/molecule; $N_{HO}^2 = 1.0000$; $N_{WKB}^2 = 0.9998$.

Figure 2. Expectation value of the coordinate as a function of time: (a) results obtained by the linear-variation method; (b) results obtained by the WKB method with the same parameters. Data given for the Fues oscillator: $r_e = 0.74$ Å; $r_0 = 0.95$ Å; $D = 0.7120 \times 10^{-11}$ erg/molecule; $\mu = 0.83 \times 10^{-24}$ g; the width parameter in the initial wave packet $= 0.1507$ Å; $\langle E \rangle_{initial} = -0.6595 \times 10^{-11}$ erg/molecule; $\langle E \rangle_{HO} = -0.6571 \times 10^{-11}$ erg/molecule; $\langle E \rangle_{WKB} = -0.6600 \times 10^{-11}$ erg/molecule; $N_{HO}^2 = 1.0000$; $N_{WKB}^2 = 0.9999$.

of the coordinate. The expansion coefficients for such wave packets in terms of the basis set used are well known.[12] The matrix of the Hamiltonian was diagonalized by the Jacobi method; the matrix of the coordinate was transformed into the new basis set of the approximate energy eigenfunctions; and the expansion coefficients of the initial wave packet were transformed into this new basis set. Then the expectation value of the coordinate as a function of time was calculated. The procedure used for these operations was essentially the same as that described in part A of ref 4.

The calculations outlined above were carried out on the IBM 7074 computer of the University of Rochester; this facility was also used to do the other computations described later in this paper. The results of some representative runs are given in Figures 1a–3a. In all the computations presented, the parameters D, μ, and r_e (and β for the Morse oscillator) were chosen to simulate H_2.

The dynamical behavior of the Fues oscillator was then investigated by the WKB method. The WKB energies were calculated by means of the appropriate formula in Table I, and the corresponding WKB wave functions were computed by use of the connection formulas[13] in the vicinities of the classical turning points and by means of numerical integration of Schiff's formula 28.19.[14] (Unsatisfactory results were obtained by terminating the wave functions in the classically allowed region and by neglecting the connection formulas.) Each wave function in the regions of the

turning points was then rescaled to make it continuous at the junctures of the regions of the turning points with the region including the bulk of the classically allowed values of the coordinate. The precise locations of the junctures did not significantly affect the results, provided that the junctures were sufficiently removed from the singularities at the classical turning points.

The resulting wave functions were then normalized. It was found that the functions were not quite orthogonal, so the Graham–Schmidt orthogonalization process[15] was used to force orthogonality and, thereby, to facilitate computation of the expansion coefficients of the initial wave packets. The functions were orthogonalized in order of increasing energy; ψ_n is orthogonalized with respect to $\psi_0, \psi_1, \ldots \psi_{n-1}$. Some of the resulting functions are plotted in Figure 4. The wave functions showed the appropriate number of nodes in

(12) See ref 7, p 67.

(13) See ref 7, p 188.

(14) See ref 7, p 191.

(15) R. Courant and D. Hilbert, "Methods of Mathematical Physics," Vol. I, Interscience Publishers, Inc., New York, N. Y., 1953, p 50.
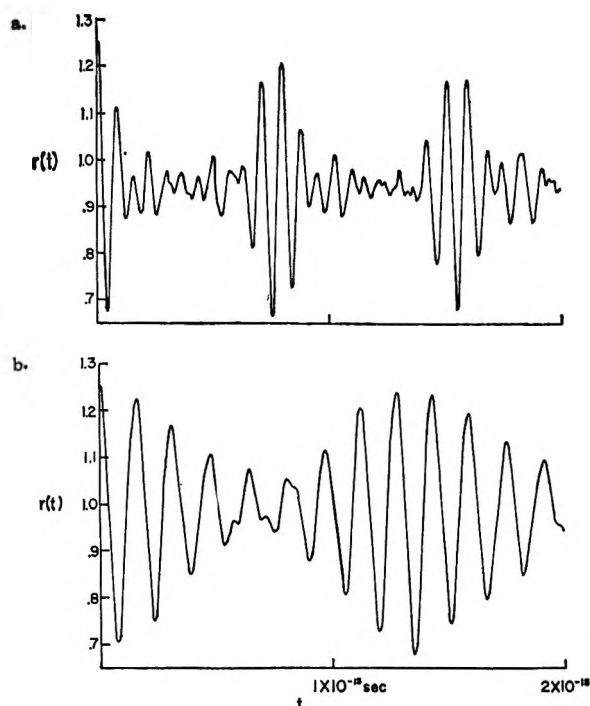
Figure 3. Expectation value of the coordinate as a function of time: (a) results obtained by the linear-variation method; (b) results obtained by the WKB method with the same parameters. Data given for the Fues oscillator: $r_e = 0.74$ Å; $r_0 = 1.25$ Å; $D = 0.7120 \times 10^{-11}$ erg/molecule; $\mu = 0.83 \times 10^{-24}$ g; the width parameter in the initial wave packet = 0.1507 Å; $\langle E \rangle_{initial} = -0.5793 \times 10^{-11}$ erg/molecule; $\langle E \rangle_{HO} = -0.2767 \times 10^{-11}$ erg/molecule; $\langle E \rangle_{WKB} = -0.5786 \times 10^{-11}$ erg/molecule; $N_{HO}^2 = 0.9991$; $N^2_{WKB} = 0.9999$.

all cases, and their graphs did not appear significantly different from plots of the functions before orthogonalization. All integrations were done numerically with the use of the simple trapezoidal rule; for the runs presented here, it was found that the results did not vary significantly with the spacing of the points when 200 or more points were used.

Initial gaussian minimum wave packets (as mentioned above) were employed in all runs; expansion coefficients were then calculated by numerical integration. The accuracy of the expansion is indicated by the closeness of the sum of the squares of the coefficients to unity; this sum is given for each of the runs plotted and was generally of the order of 0.9999.

Another test of the adequacy of the approximations used is the agreement obtained between $\langle r(0) \rangle$ and r^0, the location of the maximum of the initial gaussian wave packet. This agreement was to substantially better than 1% in all cases studied, both WKB and linear variation.

It should be noted that neither good normalization nor accurate agreement of $\langle r(0) \rangle$ and r_0 provides a very sensitive test of the validity of the computations; it was, therefore, felt advisable to calculate $\langle E \rangle$, the expectation value of the total energy, by means of the two formulas

$$\langle E \rangle = \int \psi^*(r, 0) H \psi(r, 0) \, dr \qquad (3)$$

and

$$\langle E \rangle = \sum_{n=0}^{\infty} c_n^* c_n E_n \qquad (4)$$

$\langle E \rangle$ calculated by eq 3 is denoted as $\langle E \rangle_{initial}$. It was found that disagreement between the results of eq 3 and those of eq 4 occurred for the linear-variation method with harmonic-oscillator basis functions even when normalization and agreement between $\langle r(0) \rangle$ and r_0 were quite good. The results of eq 3 and those of eq 4 were in good agreement for all computations carried out by the WKB method. The discrepancies
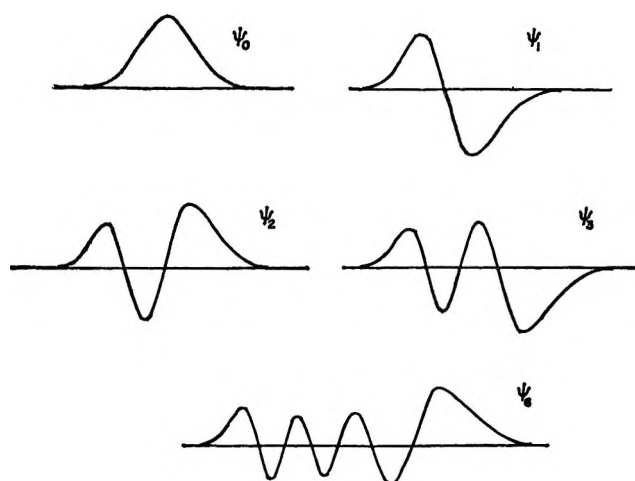
Figure 4. Plots of some WKB wave functions for the Fues oscillator: $r_e = 0.74$ Å; $D = 0.7120 \times 10^{-11}$ erg/molecule; $\mu = 0.83 \times 10^{-24}$ g.

observed with the linear-variation method are due to poor values of the energy levels, which in turn are due to (1) basis functions ill adapted to the Fues potential and (2) divergence of the series expansion used for the Fues potential in evaluating the matrix elements of the Hamiltonian. The exact, WKB, and linear-variation energies are given in Table II and constitute an impressive caveat against blind use of the linear-variation method. The failure of the linear-variation method to produce good values of the higher energies is not significantly improved by increasing either the number of basis functions or the number of terms retained in the power-series expansion of $V(r)$, although the lower energies are improved.

Plots of $\langle r(t) \rangle$ vs. t were calculated with the WKB method by computing the matrix elements of r in the basis of the WKB wave functions and then using

$$\langle r(t) \rangle = \sum_n \sum_m c_n^* c_m r_{nm} \exp \left[\frac{i(E_m = E_n)t}{\hbar} \right] \qquad (5)$$

where the c's are the expansion coefficients of the initial wave packet and the E's are the WKB energies. Re-

Table II: Energy Levels of the Fues Oscillator[a]

Energy (WKB), $\times 10^{-11}$ erg	Energy (exact), $\times 10^{-11}$ erg	Energy (linear variation), $\times 10^{-11}$ erg
−0.683328	−0.683389	−0.683071
−0.631091	−0.631109	−0.630510
−0.584579	−0.584600	−0.580883
−0.543026	−0.543053	−0.526483
−0.505751	−0.505790	−0.462627
−0.472186	−0.472223	−0.308343
−0.441855	−0.441900	−0.389505
−0.414355	−0.414403	−0.219938
−0.389345	−0.389394	−0.123958
−0.366533	−0.366583	−0.018130

[a] $\mu = 0.83 \times 10^{-24}$ g; $r_e = 0.74$ Å; $D = 0.712 \times 10^{-11}$ erg.

sults are shown in Figures 1b–3b, which differ from the results plotted in Figures 1a–3a only in that the WKB method was used rather than the linear-variation method.

The initial wave packet relevent to Figure 1 is of quite low energy, and we find that the two methods give essentially the same frequency of oscillation of $\langle r(t) \rangle$. However, even for this most favorable case, the frequencies of oscillation of the envelopes of the two plots are quite different, owing to the magnification of small differences in the energy levels yielded by the two methods when one calculates the second differences of the energies which determine the behavior of the envelopes.

Figures 2 and 3 compare runs made with initial wave packets with progressively increasing $\langle E \rangle$. In Figure 3 the frequencies of oscillation of $\langle r(t) \rangle$ are quite different and the envelopes of the curves bear no resemblance. The value of $\langle E \rangle$ calculated by the linear-variation method is grossly in error, while that obtained by the WKB method is in good agreement with the energy calculated by eq 3. The failure of the linear-variation method on this run is due to the failure of the series expansion for $V(r)$ to converge for sufficiently large r.

The Morse Oscillator

The Morse potential (see the second expression in column 1 of Table I) is a convenient and reasonably accurate approximation to a variety of bond-stretching potentials. We previously studied the dynamics of Morse oscillators by means of expansion in terms of the exact Morse eigenfunctions and by means of the linear-variation method with a harmonic-oscillator basis.[4] Expansion in terms of Morse eigenfunctions and the exact energies gives excellent results, provided that the initial wave packet can be adequately approximated by the bound-state eigenfunctions. The linear-variation method also gives good results, but only for wave

packets having $\langle E \rangle \leq 3\hbar\omega$, where ω is the angular frequency of the corresponding harmonic oscillator.

The availability of results for the Morse oscillator obtained by two independent methods (yielding good agreement) suggested that we test the WKB method by applying it to the same system. The WKB method gives the exact energies of the Morse oscillator, so the frequency of oscillation of $\langle r(t) \rangle$ and the frequency of oscillation of the envelope are of necessity correct. This test, therefore, checks the ability of the WKB wave functions to approximate the true values of the matrix elements and the expansion coefficients of the initial wave packet. Exact and WKB expansion coefficients for two runs are compared in Table III; these

Table III: Exact and WKB Expansion Coefficients of Initial Wave Packets

n	Expansion coef ($r_0 = 1.25$ Å), Exact	WKB	Expansion coef ($r_0 = 0.85$ Å), Exact	WKB
0	0.0579	0.0594	0.9051	0.8989
1	0.1848	0.1849	0.3984	0.4233
2	0.3800	0.3773	0.1480	0.1107
3	0.5573	0.5556	−0.0142	−0.0007
4	0.5803	0.5821	−0.0026	−0.0041
5	0.3929	0.3945	−0.0041	−0.0007
6	0.1222	0.1257	0.0049	0.0046
7	−0.0294	−0.0247	−0.0039	−0.0045
8	−0.0216	−0.0164	0.0022	0.0021
9	0.0106	0.0123	−0.0024	−0.0002
E	0.2974[a]	0.2972[a]	0.0585[a]	0.0585[a]

[a] E = value $\times 10^{-11}$ erg.

runs are plotted in Figures 5 and 6, one being of low energy ($r_0 = 0.85$ Å) and the other of high energy ($r_0 = 1.25$ Å). The agreement between corresponding expansion coefficients calculated by the two methods is rather good, and the agreement between the values of $\langle E \rangle$ is excellent. It is of particular interest to note that the WKB approximation appears to be at least as adequate at high energies as it is at lower energies, which is what one would expect; this conclusion was borne out by other runs not presented here.

The results of three representative runs (with parameters simulating H_2 and with the usual initial gaussian minimum wave packet) are shown in Figures 5–7. The figures labeled a pertain to the WKB method; those labeled b pertain to the expansion in exact energy eigenfunctions. In all three cases the plots are very similar, even down to rather small details. We note one discrepancy; the minimum values of $\langle r(t) \rangle$ for the WKB plots in Figures 5a and 7a are approximately 0.01 Å less than the corresponding minima for the exact eigenfunction plots in Figures 5b and 7b. This is due to the fact that the value of the magnitude of the slope at the left classical turning point is both rather small and rapidly increasing with decreasing r. This
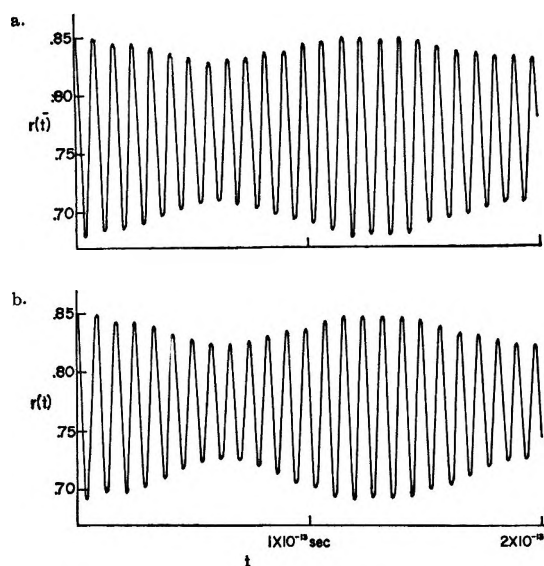
Figures 5. Expectation value of the coordinate as a function of time: (a) results obtained by the WKB method; (b) results obtained by expansion in terms of the exact Morse eigenfunctions (ME). β (the range parameter in the Morse potential) $= 0.1963 \times 10^9$ cm^{-1}; $r_e = 0.74$ Å; $r_0 = 0.85$ Å; $D = 0.7120 \times 10^{-11}$ erg/molecule; $\mu = 0.83 \times 10^{-24}$ g; the width parameter in the initial wave packet $= 0.1507$ Å; $\langle E \rangle_{initial} = 0.0585 \times 10^{-11}$ erg/molecule; $\langle E \rangle_{WKB} = 0.0586 \times 10^{-11}$ erg/molecule; $\langle E \rangle_{ME} = 0.0585 \times 10^{-11}$ erg/molecule; $N_{WKB}^2 = 0.9995$; N_{ME}^2 0.9999.

means that our use of the WKB connection formulas for calculating the first few wave functions in the left classically forbidden region must yield wave functions whose amplitudes are too large in this region of small r. The magnitude of the error greatly decreases as we consider wave functions of progressively higher energy, since the magnitude of the slope at the left side of the well becomes very large and the penetration of both exact and approximate wave functions into the classically forbidden region becomes less and less. This explains the fact that the discrepancy between the two methods at small $\langle r(t) \rangle$ is greatly reduced for the runs plotted in Figure 6. As is evident from Table III, the

Table IV: Morse Oscillator Energies

Energy (exact and WKB), $\times 10^{-11}$ erg	Energy (integration) $\times 10^{-11}$ erg	Energy (diagonalization) $\times 10^{-11}$ erg
0.0422	0.0547	0.0539
0.1228	0.1251	0.1247
0.1982	0.1993	0.1994
0.2685	0.2692	0.2693
0.3335	0.3346	0.3346
0.3955	0.3945	0.3946
0.4482	0.4498	0.4499
0.4978	0.5000	0.5003
0.5423	0.5460	0.5462
0.5816	0.5818	0.5820
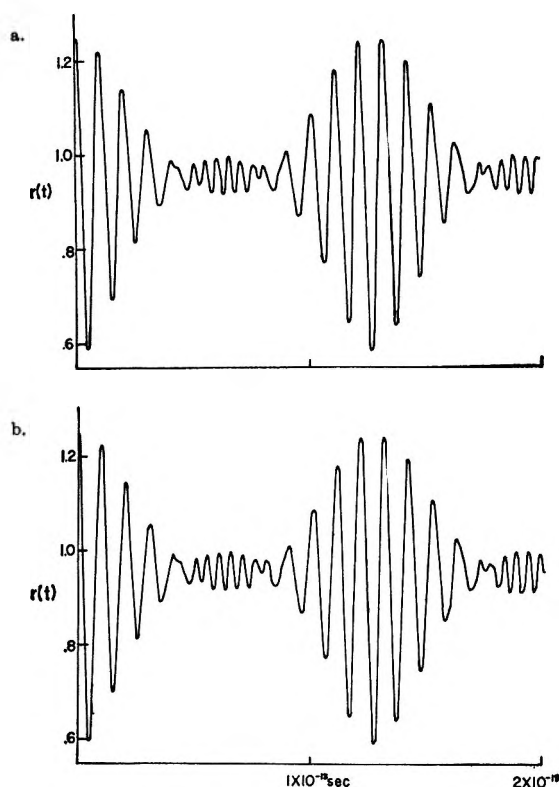
Figures 6. Expectation value of the coordinate as a function of time: (a) results obtained by the WKB method; (b) results obtained by the expansion in terms of the exact Morse eigenfunctions (ME). $r_e = 0.74$ Å; $r_0 = 1.25$ Å; $D = 0.7120 \times 10^{-11}$ erg/molecule; $\mu = 0.83 \times 10^{-24}$ g; the width parameter in the initial wave packet $= 0.1507$ Å; $\langle E \rangle_{initial} = 0.2968 \times 10^{-11}$ erg/molecule; $\langle E \rangle_{WKB} = 0.2972 \times 10^{-11}$ erg/molecule; $\langle E \rangle_{ME} = 0.2974 \times 10^{-11}$ erg/molecule; $N_{WKB}^2 = 1.0000$; $N_{ME}^2 = 0.9999$.

contributions of the first few eigenfunctions are quite small, so that this inaccuracy of the first couple of WKB wave functions introduces an error in $\langle r(t) \rangle$ smaller than was seen in Figures 5 and 7.

The accuracy of the WKB energies does not, unfortunately, imply similar accuracy of the WKB wave functions. We therefore tested the Morse WKB orthogonalized wave functions by using them as basis functions for calculating the matrix of the Hamiltonian. The diagonal matrix elements should be approximately equal to the Morse energy levels, and the off-diagonal elements should be approximately zero. The diagonal elements are given in Table IV in the middle column; the off-diagonal elements ranged from 0.01 to 0.79 $\times$ 10^{-13} erg. We then diagonalized the matrix of the Hamiltonian by means of an orthogonal transformation; this did not make any great changes in the energies, and the wave functions were not significantly changed. The energies resulting from this operation are listed in Table IV in the last column.

The energies calculated from the WKB wave functions are in rather good agreement with the exact ener-

Figures 7. Expectation value of the coordinate as a function of time: (a) results obtained by the WKB method; (b) results obtained by expansion in terms of the exact Morse eigenfunctions (ME). $r_e = 0.74$ Å; $r_0 = 0.95$ Å; $D = 0.7120 \times 10^{-11}$ erg/molecule; $\mu = 0.83 \times 10^{-24}$ g; the width parameter in the initial wave packet $= 0.1507$ Å; $\langle E \rangle_{\text{initial}} = 0.1037 \times 10^{-11}$ erg/molecule; $\langle E \rangle_{\text{WKB}} = 0.1030 \times 10^{-11}$ erg/molecule; $\langle E \rangle_{\text{ME}} = 0.1037 \times 10^{-11}$ erg/molecule; $N_{\text{WKB}}^2 = 0.9997$; $N_{\text{ME}}^2 = 0.9999$.

gies, except for the ground state. Here, of course, is where one would expect a semiclassical approximation to be in greatest difficulty. (FORTRAN decks of the computer programs used in this investigation are available from D. J. W. on request.)

Conclusions

The application of the linear-variation method with a harmonic-oscillator basis set to the Fues oscillator is fraught with some hazard, owing to the limited radius of convergence of the power-series expansion of the potential about the equilibrium internuclear distance. The situation may possibly be improved somewhat by use of the technique of Harris, Engerholm, and Gwinn;[16] we are currently looking into this. On the other hand, the application of the WKB method to the Fues oscillator may be expected to yield quite good results for all initial wave packets which can be adequately approximated by the bound state energy eigenfunctions of the oscillator. This permits one to investigate initial wave packets of far greater energy than is possible using the linear-variation method we employed.

The WKB method and the method of expansion in terms of exact-energy eigenfunctions yield extremely similar results for wave packets of both high and low energy, even for H_2, which is the most unfavorable case (the molecule for which the semiclassical approximation should be least adequate). For results of highest accuracy from the WKB method, it is necessary to take some care in calculating the wave functions in the classically forbidden region; for states of low energy, simply using the connection formulas throughout the classically forbidden region introduces small errors.

We note that the accuracy with which the WKB method approximates the energy levels of eight different oscillators, even at high energies, makes it an excellent approximation method for studying the quantum dynamics of anharmonic oscillators. We hope to use this method in developing a computationally tractable quantum theory of unimolecular reactions and a theory of inelastic collisions of molecules at rather high energies.

(16) D. Harris, G. Engerholm, and W. Gwinn, *J. Chem. Phys.*, **43**, 1515 (1965).

Divalent Transition Metal Complexes of Hydrolyzed

Ethylene–Maleic Anhydride Copolymer[1a]

by Betty J. Felber, Ernest M. Hodnett, and Neil Purdie[1b]

Chemistry Department, Oklahoma State University, Stillwater, Oklahoma 74074   (*Received December 26, 1967*)

In the alternating 1:1 copolymer of ethylene and maleic acid with molecular weight of 20,000–30,000, the two carboxyl groups have very different pk values; both are larger than those of succinic acid. Formation constants have been measured potentiometrically for the complexes between this copolymer and manganese(II), cobalt(II), nickel(II), copper(II), zinc(II), and cadmium(II) ions. The interionic attraction theory of electrolytes was useful in treatment of the data. The values are much larger than those previously reported for analogous systems in media of high ionic strength, where complexation occurs with the cation of the added electrolyte. A comparison is made with the corresponding metal–monosuccinate complexes; the differences in stabilities are discussed in terms of the enthalpy and entropy of complex formation.

Introduction

The binding of counterions to polymeric ions has been well established. The mechanism for binding may be[2] (1) electrostatic in character and therefore dependent upon the charge of the counterion or (2) site binding and therefore dependent upon complex formation. This distinction is analogous to the one made between ion pairs and complexes for metals with monomeric ligands. Results from kinetic studies of complex formation by relaxation techniques[3] suggest that ion pairs and complexes exist in equilibrium with each other and with the free aquated ions. Consequently, both mechanisms may operate, to a greater or lesser extent, depending upon the structure of the polymer. For example, alkali metal ions are poor participants in ion association unless the ligand is highly charged. The high degree of association in sodium polyacrylate is perhaps principally electrostatic in origin and the predominant interaction is ion pair formation in which the solvation spheres of the interacting ions remain intact. Preferential site binding can be expected to be really important when the same effect manifests itself at least to some degree in the low molecular weight or monomeric units of the polymer. Coulombic forces bring the metal ions into the sphere of influence of the polymer, as in ion pair formation, but the liberation of coordinated solvent molecules causes the equilibrium to lie predominantly in favor of a contact ion pair or metal chelate at the active site. As an illustration, hydrolyzed substituted ethylene–maleic anhydride copolymers[4] would be considered to form complexes by the site-binding mechanism, since the monomer succinic acid[5] forms stable complexes.

Previous reported studies of ion binding are restricted to the interactions of alkaline earth ions, especially copper(II) with polyacrylic acid[6] and analogs, with substituted ethylene–maleic anhydride copolymers and

with amino acids and proteins.[7] Most of the data available are for media of high ionic strength.

Any quantitative study of ion binding between metal ion and polymer is complicated by several properties of the polymer. Polyelectrolytes ionize considerably less than their monomeric counterparts. The actual degree of ionization depends upon concentration, the precise degree of neutralization (which may involve a configuration transition),[8] the molecular weight, and the ionic strength of the environment. If the analytical method is potentiometry, as in the present case, an additional complication may arise from competitive ion binding by the cation of the base used in titration.

It was our belief that the magnitude of the reported stability constants[4] (in the order of 100) seemed inconsistent with the extreme preference a polyelectrolyte or an ion-exchange resin might have for a divalent ion over a univalent ion. Moreover, we wanted to test the degree of applicability of the interionic-attraction theory of electrolytes to polyelectrolytes. It is relevant, for example, that the theory has been applied with some success to ion binding with micelles in aqueous solution.[9] Our preference was for a model syn-

(1) (a) Presented at the 154th Meeting of the American Chemical Society, Chicago, Ill., Sept 1967; (b) to whom communications should be directed.

(2) F. T. Wall, *J. Phys. Chem.*, **61**, 1344 (1957).

(3) M. Eigen and K. Tamm, *Z. Elektrochem.*, **66**, 93, 107 (1962).

(4) H. Morawetz, A. M. Kotliar, and H. Mark, *J. Phys. Chem.*, **58**, 619 (1954).

(5) A. McAuley, G. H. Nancollas, and K. Torrance, *Inorg. Chem.*, **6**, 136 (1967).

(6) M. Mandel and J. C. Leyte, *J. Polym. Sci.*, **A2**, 2883, 3771 (1964).

(7) H. Morawetz, "High Polymers," Vol. 21, Interscience Publishers, New York, N. Y., 1965, p 369 ff.

(8) M. Mandel, J. C. Leyte, and M. G. Stadhouder, *J. Phys. Chem.*, **71**, 603 (1967).

(9) C. W. Davies, "Ion Association," Butterworth and Co. Ltd., London, 1962, p 122.

thetic polymer in which site binding would be predominant. Our choice was hydrolyzed ethylene–maleic anhydride copolymer (HEMA), for which structural complications resulting from hydrophobic-bonding interactions are absent. Since competitive ion binding with the cation of the supporting electrolyte would interfere with the analysis of high ionic strength data, we have attempted to obtain thermodynamic stability constants by making activity corrections rather than by using the procedure of extrapolation to zero ionic strength.

Experimental Section

Grade A glassware and analytical reagents were used whenever possible. Metal perchlorates were obtained from G. Frederick Smith Chemical Co., and stock solutions were standardized by titration of the acid obtained after cation exchange with standard tetramethylammonium hydroxide. The copolymer, as the anhydride, was supplied by Monsanto Chemical Co. Hydrolysis to the acid was easily achieved by heating at 70–80° for a period of 2 hr. Polymer solutions were stored in Pyrex containers at 5°. The solutions were standardized potentiometrically. Emf measurements were made at 25 ± 0.05° with a cell of the type

Ag|AgCl, 0.2 M HCl|glass

Ag|AgCl, 0.2 M HCl|glass

soln | satd KCl calomel electrode
under |
study | satd KCl calomel electrode
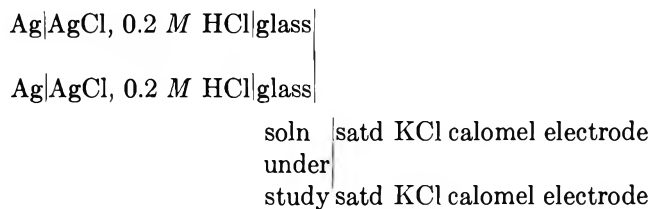
using a Beckman Research pH meter Model 1019. This arrangement allowed four emf measurements to be made at each point in the titration. The electrode systems were calibrated with standard Beckman buffer solutions of pH 4.01 and 9.18, respectively. Emf measurements were made in a nitrogen atmosphere.

Results and Discussion

Acid Dissociation Constants. The copolymer used has a molecular weight of 20,000–30,000. Its characterization has been outlined in Technical Bulletin I-261 of the Monsanto Chemical Co. From kinetic and infrared studies,[10] it has been shown to be an alternating 1:1 copolymer with no homopolymerized impurities, and the degree of sequence addition, when it occurs, is very small. Titration data show two distinct ionizable groups and essentially two molar equivalents of base consumption for each repeating unit of the polymer. It has been inferred that one carboxylic acid group from each adjacent pair is preferentially dissociated, leading to the first inflection in the titration curve. At neutralization the electrical charge density might be considered to be uniformly distributed throughout the molecule. From a comparison of the typical titration curves of the acid against
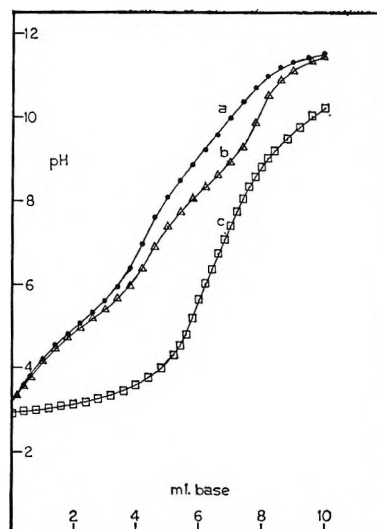
Figure 1. HEMA neutralization curves: (a) with quaternary ammonium hydroxide; (b) with potassium hydroxide; (c) with quaternary ammonium hydroxide and [HEMA]/[Cu(II)] = 2.

potassium hydroxide and tetramethylammonium hydroxide, the absence of a large inflection at the second equivalence point when the latter base is used as titrant might indicate that potassium is bound to the polymer in some way, Figure 1. This is not uncommon for univalent ions with carboxylic acid groups. Lithium and sodium ions are known to complex with acetic acid[11] when they are present in relatively high concentrations. In polyacrylic acid, low concentrations of lithium, sodium, and potassium ions have been observed to depress the pH titration curve compared to that of the symmetrical quaternary ammonium ions. This has been attributed to cation–polyion interactions rather than to specific salt effects.[12]

HEMA is a substituted polymeric succinic acid, but, unlike succinic acid, the buffer regions are quite distinct. The data were treated as the dissociation of two separate monobasic acids; the Katchalsky[13] form of the empirical Henderson equation corrected for activity coefficients was used

$$pH = pk_1 + n \log [\alpha/(1 - \alpha)] - 0.509I^{1/2} \quad (1)$$

for the first dissociation and

$$pH = pk_2 + n \log [\alpha/(1 - \alpha)] - 1.527I^{1/2} \quad (2)$$

for the second dissociation step. Here α is the degree of ionization. Plots of pH against log $[\alpha/(1 - \alpha)]$ for both buffer regions are linear with slopes $n = 1.5$ and $n = 2.2$, respectively. For substituted ethylene–

(10) S. Machi, T. Sakai, M. Gotoda, and T. Kagiya, *J. Polym. Sci.*, A4, 821 (1966).

(11) H. S. Harned and B. B. Owen, "Physical Chemistry of Electrolytic Solutions," Reinhold Publishing Corp., New York, N. Y., 1943, p 316.

(12) H. P. Gregor and M. Frederick, *J. Polym. Sci.*, 23, 451 (1957).

(13) A. Katchalsky and P. Spitnik, *ibid.*, 2, 432 (1947).
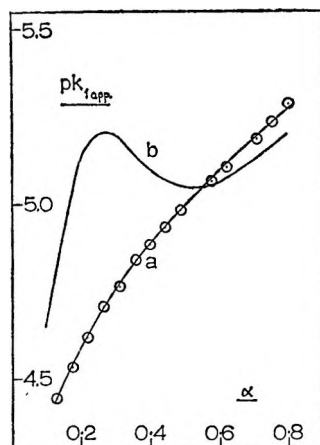
Figure 2. The dependence of the first dissociation constant on the degree of ionization for (a) HEMA and (b) the alternating 1:1 copolymer of hydrolyzed n-butyl vinyl ether and maleic anhydride: P. Dubin and U. P. Strauss, *J. Phys. Chem.*, **71**, 2757 (1967).

Table I

Vol of base, ml	1st ionization, %	$pk_{1,app}$[a]	Vol of base, ml	2nd ionization, %	$pk_{2,app}$[b]
1.80	42.5	4.847	5.80	36.8	9.119
2.00	47.2	4.913	6.00	41.6	9.234
2.20	52.0	4.971	6.20	46.3	9.318
2.40	56.7	4.998	6.40	51.0	9.415
2.60	61.4	5.044	6.60	55.7	9.515

[a] Mean $pk_{1,app}$ = 4.956; mean pk_1 = 4.965. [b] Mean $pk_{2,app}$ = 9.320; mean pk_2 = 9.602.

maleic anhydride copolymers, as a rule n is approximately 1 for the widely spaced first carboxyl groups and is greater than 2 for the ionization of the second carboxyl groups.[14]

The pk values from eq 1 and 2 relate to the ionization constants at the midpoints of the respective buffer regions. The manner in which the dissociation constant, pk_1, apparently varies with α is illustrated in Figure 2a, where $\alpha = 1$ corresponds to the half-neutralization point. The apparent dissociation constant, $pk_{1,app}$, is related to pH by the equation

$$pH = pk_{1,app} + \log[\alpha/(1 - \alpha)] - 0.509I^{1/2} \quad (3)$$

The smooth curve is an indication that the elongation of the polyion on neutralization is not complicated by an additional configuration transition; consequently the treatment of the data is simplified. For comparison, curve b is included. This curve is typical of the dependence of $pk_{1,app}$ on α when a compact coil to random coil transition is induced by ionization.[15] The curves are for analogous copolymers differing only in the side-chain substituents and should coincide at values of α greater than 0.7. They do not because activity coefficient corrections have been made only for HEMA. The apparent dissociation constants and the pk values are given in Table I.

The carboxylic oxygen atoms are more basic in HEMA than in succinic acid, owing in part to the inductive effect of the ethylene moiety of the polymer. No information is available in the literature for the dissociation of 2,3-dimethylsuccinic acid, which is structurally more comparable to the polymer. However in the series of dicarboxylic acids, $(CH_2)_x(COOH)_2$, the basicity is observed to increase with increasing x.[16] For the second dissociation in particular, the large difference in basicity also reflects the increased difficulty in removing a proton from the highly charged polyion.

Metal Complexes. The counterions studied were the divalent ions of the transition metals manganese, cobalt, nickel, copper, zinc, and cadmium. In Figure 1, a typical potentiometric curve is shown with the copper(II) ion present.

By analogy with the divalent transition metal succinates[5] at similar analytical concentrations of reagents, one might anticipate the two complex species MHA+ and MA to exist in solution for at least some of the metal ions

$$M^{2+} + HA^- = MHA^+ \qquad M^{2+} + A^{2-} = MA$$
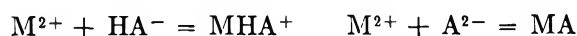
HA$^-$ and A^{2-} correspond to monomeric residues at different stages of ionization. However, analysis of the emf data from experiments in which the ratio of the analytical concentrations of metal and polymer were approximately 2:1, 1:1, and 1:2, which indicated that the system could be satisfactorily interpreted in all cases by the consideration of only one complex

$$M^{2+} + A^{2-} = MA \quad (4)$$

for which the thermodynamic stability constant expression is

$$K_{MA} = [MA]/[M^{2+}][A^{2-}] \times 1/f_2^2 \quad (5)$$

and f_2 is the mean activity coefficient of the divalent ions.

The concentration of ionic species may be calculated from equations for total metal ion concentration

$$m = [M^{2+}] + [MA] \quad (6)$$

for total polymer concentration in terms of moles of monomer

$$a = [H_2A] + [HA^-] + [A^{2-}] + [MA] \quad (7)$$

for electroneutrality

$$b + [H^+] + 2[M^{2+}] = [HA^-] + 2[A^{2-}] + 2m \quad (8)$$

(14) J. D. Ferry, D. C. Udy, F. C. Wu, G. F. Heeder, and D. B. Fordyce, *J. Colloid Sci.*, **6**, 429 (1951).

(15) P. Dubin and U. P. Strauss, *J. Phys. Chem.*, **71**, 2757 (1967).

(16) A. E. Martell and L. G. Sillen, "Stability Constants," Special Publication No. 17, The Chemical Society, London, 1964.

where b is the concentration of tetramethylammonium hydroxide, and for the thermodynamic dissociation constants for the ligand

$$k_1^0 = [H^+][HA^-](f_1^2/[H_2A]) \quad (9)$$

$$k_2^0 = [H^+][A^{2-}](f_2/[HA]) \quad (10)$$

The required stability constant is given by eq 5 and the ionic strength is given by

$$I = b + h + 3[M^{2+}] + [A^{2-}] \quad (11)$$

Activity coefficients were calculated using the Davies[9] equation

$$-\log f_i = 0.509z_i^2[I^{1/2}/(1 + Ba)I^{1/2} - CI] \quad (12)$$

where $Ba = 1$ and $C = 0.3$.

Because the acid dissociation constants are known to be concentration dependent,[2] the initial analytical concentration of polymer was kept constant in all titrations with metal ion present. At higher concentrations of A^{2-}, as would be obtained in the second buffer region, higher complexation is possible

$$MA + A^{2-} = MA_2^{2-}$$
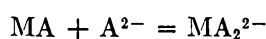
Analysis of the data was not always possible because of precipitation especially when the metal ion was in excess. The results of this calculation are not yet conclusive and are not reported.

It has been proposed[7] that the concept of ionic strength has meaning in polymer solutions only if the product $e\psi_{el}$ in the extended Henderson–Hasselbalch equation is less than kT.

$$pH = pk^0 + \log[\alpha/(1 - \alpha)] + 0.434e\psi_{el}/kT \quad (13)$$

In the present case the maximum value of $e\psi_{el}$ calculated from the last point used in the first buffer region is $0.7kT$. We therefore have some confidence in applying the interionic-attraction theory, and it is encouraging that even in its present form, without elaborating on the solution model, constant values for stabilities of metal complexes can be approached. Furthermore, when no activity corrections are made, the "stabilities" calculated are not by any means constant. It should be possible to vary the model by examining the dependence of K_{MA} on changing the parameters Ba and C in the Davies equation,[9] but this has not been attempted in the light of the more serious approximations made—for example, the use of the macroscopic dielectric constant for water in the vicinity of the polymer.

Equations 9 and 10 are really only applicable when the dibasic acid is monomeric and when k_1^0 and k_2^0 are true thermodynamic constants. Dissociation constants k_1 and k_2 derived from eq 1 and 2 were used to calculate K_{MA}, but this presumes that their dependence on α is determined by only a change in ionic strength, which is not the case. A considerable improvement was

Table II: Measurements at $I \to 0$

10^3a, M	10^3m, M	$10^{-4}K_{MA}$	Mean $10^{-4}K_{MA}$
Manganese–HEMA			
9.364	5.277	6.45	
9.364	5.277	6.46	
8.860	9.988	6.63	
8.860	9.988	6.10	6.41 ± 0.2
Cobalt–HEMA			
9.382	4.782	4.19	
9.382	4.782	4.28	
9.364	4.782	4.54	
8.880	9.052	4.21	
8.880	9.052	4.15	
8.262	9.052	4.73	
8.287	14.08	3.98	
8.287	14.08	3.81	
8.272	14.08	4.69	4.29 ± 0.3
Nickel–HEMA			
9.382	4.973	3.38	
9.382	4.973	3.65	
9.361	4.973	3.45	
9.361	4.973	3.71	
8.880	9.412	4.08	
8.880	9.412	4.07	
8.860	9.412	3.77	
8.860	9.412	3.63	
8.287	14.64	4.02	
8.287	14.64	3.86	3.76 ± 0.2
Copper–HEMA			
9.382	4.975	422	
9.382	4.975	432	
9.364	4.975	499	
9.364	4.975	476	
8.880	9.417	453	
8.880	9.417	486	
8.860	9.417	391	
8.860	9.417	377	
8.287	14.65	486	
8.287	14.65	475	
8.269	14.65	399	
8.269	14.65	372	
8.272	14.65	512	445 ± 42
Zinc–HEMA			
9.361	5.024	5.23	
9.361	5.024	5.33	
8.860	9.056	5.07	
8.860	9.056	5.08	
8.860	9.056	5.07	
8.269	14.80	4.67	
8.269	14.80	4.24	
8.269	14.80	5.07	4.97 ± 0.3
Cadmium–HEMA			
9.361	4.966	19.4	
9.361	4.966	19.8	
9.364	4.966	20.5	
8.860	9.396	22.4	
8.860	9.396	22.5	
8.862	9.396	23.0	
8.269	14.71	ppt.	21.3 ± 1.4

obtained if instead $k_{1,app}$ from eq 3 was used. In this way a correction was made for the dependence of the first dissociation constant on α in the complex-formation reaction. This was done by selecting data points from the first buffer region when metal was present to correspond with the points used in determining the apparent dissociation constant. A similar correction could not be made for k_2 in this part of the titration curve, and the average $k_{2,app}$ value was used. This probably contributes to the relatively large error in K_{MA} compared to the very precise succinate data of Nancollas, et al.[5]

Stability constants are given in Table II. Compared to the corresponding divalent metal monosuccinates, the stabilities of the mono-HEMA complexes are greater by at least six orders of magnitude. With the exception of manganese and cobalt the association constants for all the dicarboxylate complexes follow the Irving–Williams order of stability.[17] This result is consistent with the metal monosuccinate data. Copper–mono-HEMA as expected is again considerably more stable than the others, which is attributed to the contribution to the crystal field-stabilization energy from tetragonal distortion of the octahedral symmetry as a result of the Jahn–Teller effect.

The increase in stability in going to HEMA complexes is in part a result of the increased basicity of the coordinating oxygen atoms. This is directly related to the heat of formation of the complexes and indirectly, through ΔG, to the entropy of formation. It is difficult to predict what effect an increase in basicity will have upon the heat term. For example, the metal–dicarboxylate complexes are formed with an unfavorable positive enthalpy.[18] The complexes are therefore stabilized by a relatively large positive entropy, reflecting the liberation of coordinated water molecules from the interacting ions. As the basicity increases in going from oxalate to succinate, the enthalpy becomes progressively more positive. If this trend were to continue to HEMA, the entropy contribution would be considerable. On the other hand for the corresponding metal–glycinate complexes, where the nitrogen atom

has a basicity almost equal to the second oxygen in HEMA, the enthalpy is negative[18] and reinforces a smaller entropy term to produce much more stable complexes. It becomes necessary, therefore, to consider both possibilities. Compare as an example copper–succinate ($K_{MA} = 1.82 \times 10^3$) and copper–HEMA ($K_{MA} = 4.45 \times 10^{10}$). The literature values for the formation of copper–succinate are $\Delta H = 4.56$ kcal mol^{-1} and $\Delta S = 30.1$ eu at 25°. A similar ΔH for copper–HEMA would mean an entropy contribution of 64 eu/monomer. If, however, it is assumed that the entropy is unchanged (the chelate effect is small for a seven-membered ring), the calculated ΔH for copper–HEMA is -5.5 kcal mol^{-1}. The real situation is perhaps intermediate between these two extremes. Some credence to this conclusion is vindicated by the observed heat of formation of CuPAA,[19] $\Delta H = 1.6$ kcal mol^{-1}. A change in enthalpy would not explain exclusively the increase in stability over the succinates, and it is better to think of it in terms of an additional favorable entropy factor. This might indicate an additional configuration transition in going from an ordered hydrogen-bonded ligand species to a complex.

As expected, the stability constants are indeed much larger than any others previously reported for analogous systems. This is in part due to the difference in ionic strength, but perhaps more so to the fact that previously competitive ion binding by the added salt has been ignored.

(17) H. Irving and R. J. P. Williams, *J. Chem. Soc.*, 3192 (1953).
(18) G. H. Nancollas, "Interactions in Electrolyte Solutions," Elsevier Publishing Co., New York, N. Y., 1966, p 185.
(19) E. M. Loebl, L. M. Luttinger, and H. P. Gregor, *J. Phys. Chem.*, 59, 559 (1955).

Nuclear Quadrupole Resonance of Nitrogen-14 in Some Pyridine Derivatives

by Ryuichi Ikeda, Shinzaburo Onda, Daiyu Nakamura, and Masaji Kubo

Department of Chemistry, Nagoya University, Chikusa, Nagoya, Japan   *(Received January 2, 1968)*

The pure quadrupole resonance frequencies of ^{14}N in chloro-, cyano-, amino-, and methylpyridines and in aniline were determined at liquid nitrogen temperature. From the observed ν^I and ν^{II} frequencies, the quadrupole coupling constant and the asymmetry parameter were evaluated and assigned to ring nitrogen and nitrogen in substituents. The σ- and π-bond ionicities of ring N–C bonds were evaluated and were discussed in relation to the data of molecular orbital calculations.

Introduction

The electronic structure of heterocyclic compounds is complicated by the role of heteroatoms, as contrasted with the case of homocyclic compounds. In view of the ever increasing importance of nitrogen heterocycles, a number of experimental studies have been made on the electronic state of these compounds in the field of electronic absorption spectra, dipole moments, electron spin resonance, etc. The results have been used to check the adequacy of various parameters to be used in molecular orbital calculations.

^{14}N having a nuclear spin equal to unity is amenable to nuclear quadrupole resonance studies and permits the experimental determination of both the quadrupole coupling constant and the asymmetry parameter. Accordingly, from the observed data, one can obtain valuable information about the electronic states of various nitrogen-containing compounds of chemical interest. In fact, since Guibé[1] and others[2,3] succeeded for the first time in observing ^{14}N nuclear quadrupole resonance, a number of articles[4-6] have been published on the nuclear quadrupole resonance of aromatic nitrogen heterocycles. One of the characteristic features of ^{14}N quadrupole resonance data is that the asymmetry parameter is very high, as in pyridine (39%),[1] pyrazine (54%),[5] and *sym*-triazine (44%).[5] However, cyanuric chloride shows a small asymmetry parameter (1.7%).[3] This suggests the possibility of investigating the effect of substituents on ring nitrogen by nuclear quadrupole resonance. Since the quadrupole coupling constant and the asymmetry parameter can be correlated with the ionicity of N–C bonds regarding both σ- and π-bond character, one can evaluate the electronic population of σ and π electrons about a nitrogen nucleus and compare the results with those of molecular orbital calculations. The present investigation has been undertaken in order to elucidate the electronic state about nitrogen atoms in pyridine and its derivatives from the pure quadrupole resonance spectroscopy of ^{14}N.

Experimental Section

Apparatus. A modified Pound–Watkins-type spectrometer, already described,[7] was used for the observation of ^{14}N quadrupole resonance signals. Frequency modulation was employed for the determination of resonance frequencies, while Zeeman modulation was used for the assignment of observed lines to ν^I and ν^{II}. Field modulation was performed at a strength of about 100 G or less.

Materials. All the materials used were procured from commercial sources and were purified by distillation or recrystallization from organic solvents. Since 2- and 3-chloropyridines, 2- and 3-methylpyridines, and aniline are liquids at room temperature, they were frozen slowly in glass tubes and cooled with liquid nitrogen. 2-, 3-, and 4-aminopyridines, 2-, 3-, and 4-cyanopyridines, and 2,6-dichloropyridine, which are solids at room temperature, were melted in sample tubes to increase the filling factor and were allowed to solidify by gradual cooling.

2-Aminopyridine was dissolved in an approximately equal weight of heavy water and then water was allowed to evaporate in a vacuum desiccator. This process was repeated several times until the extent of deuteration was estimated to amount to about 90% of hydrogen in amino groups.

Results

Since ^{14}N has a nuclear spin equal to unity, one can usually observe two resonance frequencies, ν^I and ν^{II}, when the asymmetry parameter η is finite.

$$\nu^I = \frac{1}{4}eQq(3 + \eta)$$

$$\nu^{II} = \frac{1}{4}eQq(3 - \eta)$$

(1) L. Guibé, *Compt. Rend.*, **250**, 3014 (1960).

(2) H. Negita and P. J. Bray, *J. Chem. Phys.*, **33**, 1876 (1960).

(3) S. Kojima and M. Minematsu, *J. Phys. Soc. Jap.*, **15**, 355 (1960).

(4) L. Guibé, *Ann. Phys.* (Paris), **7**, 177 (1962).

(5) L. Guibé and E. A. C. Lucken, *Mol. Phys.*, **10**, 273 (1966).

(6) E. Schempp and P. J. Bray, *J. Chem. Phys.*, **46**, 1186 (1967).

(7) R. Ikeda, D. Nakamura, and M. Kubo, *J. Phys. Chem.*, **70**, 3626 (1966).

Here eQq denotes the quadrupole coupling constant in frequency units. Table I shows the resonance frequencies observed at liquid nitrogen temperature. Figure 1 shows the spectra of 2,6-dichloropyridine as an example. The absorption derivative curves taken by frequency modulation are not quite symmetric, owing to the saturation effect, the negative peak being stronger than the positive peak when scanning is made with increasing frequency. One can obtain more symmetric derivative curves by decreasing the power level of radiofrequency oscillation and/or increasing the sweep rate. For the accurate determination of resonance frequencies, it is desirable to employ the frequency modulation in the absence of saturation. In absorption curves recorded by Zeeman modulation, ν_I has a negative wing on the high-frequency side, while ν^{II} is accompanied by a negative wing on the low-frequency side.[8] Thus resonance lines can be assigned to ν^I and ν^{II} with the aid of line shapes. In general, ν^I was found to be stronger than ν^{II} in Zeeman modulation.[9] This rule does not necessarily hold when powder crystals are oriented in space.

Figure 1. Nuclear quadrupole resonance spectra of 2,6-dichloropyridine recorded by frequency modulation (top) and Zeeman modulation (bottom).

Table I: Quadrupole Resonance Frequencies, ν^I and ν^{II}, of ^{14}N in Some Pyridine Derivatives and Aniline at Liquid Nitrogen Temperature

Compound	ν^I, kcps	ν^{II}, kcps
2-Chloropyridine	3626.7 ± 0.1	3050.7 ± 0.1
3-Chloropyridine	3891.3 ± 0.1	3062.8 ± 0.1
2,6-Dichloropyridine	3304.8 ± 0.1	3079.1 ± 0.1
2-Cyanopyridine	3947.6 ± 0.1	3129.8 ± 0.1
	3039.8 ± 0.1	2898.4 ± 0.1
	3039.6 ± 0.2^a	2897.8 ± 0.2^c
3-Cyanopyridine	3899.7 ± 0.1	3050.2 ± 0.1
	3010.8 ± 0.1	2816.8 ± 0.1
4-Cyanopyridine	4099.4 ± 0.1	3057.6 ± 0.1
	2935.2 ± 0.1	2907.1 ± 0.1
	2935.3 ± 0.2^a	2907.3 ± 0.2^a
2-Aminopyridine	2841.8 ± 0.1	2776.1 ± 0.1
	2842^b	2776^b
	2970.3 ± 0.1	2355.2 ± 0.1
3-Aminopyridine	3810.4 ± 0.1	2934.4 ± 0.1
	3138.2 ± 0.1	2426.9 ± 0.3
4-Aminopyridine	2967.9 ± 0.1	2291.7 ± 0.1
	2915.5 ± 0.1	2755.5 ± 0.1
Aniline	3243.2 ± 0.2 ⎱	⎰ 2720.7 ± 0.2
	3183.7 ± 0.2 ⎰	⎱ 2649.8 ± 0.2
2-Methylpyridine	3712.6 ± 0.1	2975.0 ± 0.1
3-Methylpyridine	3920.5 ± 0.1	3009.9 ± 0.1

^{a} Reference 2. ^{b} Reference 4.

All chloro- and methylpyridines studied show a pair of resonance lines attributable to ν^I and ν^{II}. On the other hand, both cyano and amino derivatives of pyridine show two pairs of ν^I and ν^{II} lines. These facts indicate that the number of chemically nonequivalent nitrogen atoms in a molecule is equal to that of nonequivalent atomic sites of nitrogen in crystals at liquid nitrogen temperature. However, aniline shows two pairs of ν^I and ν^{II}, in spite of the presence of a single nitrogen atom in a molecule. This indicates that there are two crystallographically nonequivalent aniline molecules in crystals. Unfortunately, no crystallographic data are available for any of these compounds.

Previously, only one pair of lines has been detected for 2-cyano, 4-cyano, and 2-amino derivatives of pyridine.[2,4] Our results are in good agreement with these.

From observed frequencies, ν^I and ν^{II}, quadrupole coupling constants and asymmetry parameters were evaluated, as shown in Table II. For the chloro, cyano, and methyl derivatives of pyridine, they could be calculated in a straightforward manner. For the amino derivatives and aniline, however, an ambiguity remains as to whether ν^I of higher frequency should be combined with ν^{II} of higher frequency or whether the alternative correspondence should be made. The choice can be settled as follows. In the case of 2-aminopyridine, ν^I at 2970.3 kcps and ν^{II} at 2355.2 kcps were observable only under a high field strength of Zeeman modulation. The signals were sharp and were

(8) P. A. Casabella and P. J. Bray, *J. Chem. Phys.*, **28**, 1182 (1958); **29**, 1105 (1958).

(9) H. Negita, *ibid.*, **44**, 1734 (1966).

Table II: Quadrupole Coupling Constants, eQq, and Asymmetry Parameters, η, of ^{14}N in Some Pyridine Derivatives and Related Compounds at Liquid Nitrogen Temperature

Compound	eQq, kcps	η, %
2-Chloropyridine	4451.4 ± 0.2	25.87 ± 0.02
3-Chloropyridine	4636.1 ± 0.2	35.74 ± 0.02
2,6-Dichloropyridine	4255.9 ± 0.2	10.61 ± 0.02
2-Cyanopyridine	4718.2 ± 0.2	34.66 ± 0.02 (ring)
	3958.8 ± 0.2	7.14 ± 0.02 (cyano)
3-Cyanopyridine	4633.3 ± 0.2	36.67 ± 0.02 (ring)
	3885.0 ± 0.2	9.99 ± 0.02 (cyano)
4-Cyanopyridine	4771.3 ± 0.2	43.67 ± 0.02 (ring)
	3894.9 ± 0.2	1.44 ± 0.02 (cyano)
Cyanobenzene[a]	3885.4 ± 0.3	10.73 ± 0.02
2-Aminopyridine	3745.3 ± 0.2	3.51 ± 0.02 (ring)
	3550.3 ± 0.2	34.65 ± 0.02 (amino)
3-Aminopyridine	4496.5 ± 0.2	38.96 ± 0.02 (ring)
	3710.0 ± 0.3	38.35 ± 0.03 (amino)
4-Aminopyridine	3780.7 ± 0.2	8.46 ± 0.02 (ring)
	3506.4 ± 0.2	38.57 ± 0.02 (amino)
Aniline	3932	26.9 (av)
2-Methylpyridine	4458.4 ± 0.2	33.09 ± 0.02
3-Methylpyridine	4620.3 ± 0.2	39.42 ± 0.02
4-Methylpyridine[b]	4414.0	34.2
Pyridine[b]	4600	39 (av)

[a] Reference 2. [b] Reference 1.

Figure 2. Nuclear quadrupole resonance spectra of ring nitrogens in 2-aminopyridine (top) and 2-cyanopyridine (bottom) recorded by Zeeman modulation with modulation fields of 60 and 100 G, respectively. When the asymmetry parameter is small, negative wings are broad as in the spectrum of the former compound. Sharp negative wings observed for the latter compound are indicative of a large asymmetry parameter.

accompanied by a sharp negative wing, indicative of a large asymmetry parameter.[9] On the other hand, ν^I at 2841.8 kcps and ν^{II} at 2776.1 kcps could be observed even when the modulation field was weak. The accompanying negative wings were broad, suggesting that these lines correspond to each other to yield a small asymmetry parameter (Figure 2). In the case of 3-aminopyridine, ν^I lines at 3810.4 and 3138.2 kcps and a ν^{II} line at 2934.3 kcps were not detectable unless the Zeeman-modulation field was increased. Negative wings were sharp, indicating a fairly large asymmetry parameter. The line at 2426.9 kcps could not be observed by Zeeman modulation, although it could be located by frequency modulation. If ν^I of lower frequency is combined with ν^{II} of higher frequency, the resulting asymmetry parameter is small and contradicts the aforementioned line shapes recorded by Zeeman modulation. Therefore, ν^I of higher frequency must be combined with ν^{II} of higher frequency, as shown in Table I. In the case of 4-aminopyridine, ν^I at 2967.9 kcps and ν^{II} at 2291.7 kcps were not detected unless the Zeeman-modulation field was strong. They showed a sharp negative wing. On the other hand, ν^I at 2915.5 kcps and ν^{II} at 2755.5 kcps could be observed even under a weak modulation field and showed a broad negative wing. Accordingly, the correspondence between ν^I and ν^{II} is obvious. The same method is not applicable to aniline, because two ν^I lines as well as two ν^{II} lines are close to each other. Therefore,

the averages were taken for the calculation of the quadrupole coupling constant and the asymmetry parameter, errors being about 1.1% for eQq and 12% for η.

The two quadrupole coupling constants and the corresponding asymmetry parameters observed for cyanopyridines arise from ring nitrogen and nitrogen in cyano groups. By taking into account the data of pyridine[1] and cyanobenzene,[2] the higher values of eQq and η are attributed to ring nitrogen atoms, while the lower ones are assigned to nitrogen atoms in cyano groups.

Two sets of the quadrupole coupling constant and the asymmetry parameter observed for each of aminopyridine isomers surely correspond to the existence of two kinds of nitrogen atoms in a molecule. However, the assignment of the two sets to two different nitrogen atoms is not easy, because the observed resonance lines deviate from those of pyridine and aniline to a considerable extent, owing to a strong electronic interaction between the amino nitrogen and the ring nitrogen. Therefore, we have studied N-deuterated 2-aminopyridine in an attempt to obtain some clue to the solution of this problem. At liquid

nitrogen temperature, three weak lines were observed at 2992.5, 2843.2, and 2841.0 kcps within an accuracy of ±0.5 kcps. The last line was the weakest among the three lines and appeared as a shoulder on the second line. The lowest frequency agrees excellently with ν^{I} (2841.8 kcps) of the undeuterated compound within experimental errors, indicating the partial deuteration of amino groups. The highest frequency is about 22 kcps higher than one of the ν^{I} lines of normal compound at 2970.3 kcps, while the second frequency is very close to the other ν^{I} line (2841.8 kcps) of the undeuterated compound. It is expected that the resonance lines of deuterated amino groups shift to some extent, owing to the secondary hydrogen isotope effect,[10-12] whereas those of ring nitrogen atoms are affected to a lesser extent. Accordingly, the line of the highest frequency is attributed to nitrogen atoms in amino groups and the second line is presumed to be due to ring nitrogen atoms. Although ν^{I} lines could be observed, ν^{II} lines were undetectable, owing to their low intensity. Since 4-aminopyridine is analogous to 2-aminopyridine in many respects as a π-electron system, assignment can be made for the former compound on the basis of results for the latter by taking into account the relative magnitude of quadrupole coupling constants and especially asymmetry parameters. The two sets of eQq and η of 3-aminopyridine are close to each other; therefore, it is very difficult to make a conclusive assignment. However, since the eQq values of aniline and aliphatic amines are about 3.9 and 4.0 Mcps,[4,13] respectively, while that of pyridine is about 4.6 Mcps, it seems to be reasonable to assign $eQq = 3.710$ Mcps to amino nitrogen and $eQq = 4.497$ Mcps to ring nitrogen.

Discussion

In order to discuss the electronic structure of a nitrogen atom in a pyridine ring, let a coordinate system be taken with its origin at the nitrogen nucleus, the z axis being chosen along the negative direction of the bisector of $\angle CNC$ equal to 2θ. Let the x and y axes be perpendicular and parallel to the ring plane, respectively. As calculated by Guibé and Lucken,[5] the hybridized valency orbitals and the lone-pair orbital of nitrogen are given by

$$\psi_{\sigma 1} = \left(\frac{1 - \cot^2 \theta}{2}\right)^{1/2} \phi_s - \left(\frac{1}{2}\right)^{1/2}(\cot \theta)\phi_{pz} + \left(\frac{1}{2}\right)^{1/2}\phi_{py}$$

$$\psi_{\sigma 2} = \left(\frac{1 - \cot^2 \theta}{2}\right)^{1/2} \phi_s - \left(\frac{1}{2}\right)^{1/2}(\cot \theta)\phi_{pz} - \left(\frac{1}{2}\right)^{1/2}\phi_{py}$$

$$\psi_{1p} = (\cot \theta)\phi_s + (1 - \cot^2 \theta)^{1/2}\phi_{pz}$$

$$\psi_{\pi} = \phi_{pz}$$

Let the number of electrons occupying the two σ-bond orbitals and the π-bond orbital be denoted by $1 + i_{\sigma'}$, $1 + i_{\sigma''}$, and $1 + i_{\pi}$, respectively. The ionic character of the nitrogen atom is $i = i_{\sigma'} + i_{\sigma''} + i_{\pi}$. The lone-pair orbital is simply assumed to accommodate two electrons.[14] Then the occupation numbers, N_x, N_y, and N_z of the p_x, p_y, and p_z orbitals are given by

$$N_x = 1 + i_{\pi}$$

$$N_y = 1 + \frac{1}{2}(i_{\sigma'} + i_{\sigma''}) = 1 + i_{\sigma}$$

$$N_z = 2(1 - \cot^2 \theta) + (1 + i_{\sigma})\cot^2 \theta$$

Since the field gradient at the nitrogen nucleus originates mostly from electrons in these orbitals, let contributions from other electrons and nuclei be disregarded.[15,16] This approximation immediately leads to the coincidence of the principal axes of the field-gradient tensor with the geometric coordinate axes and the identity of q_{zz} with the principal value q of the field-gradient tensor having the largest absolute value. Accordingly, one has

$$|eQq_{zz}| = \left(N_z - \frac{N_x + N_y}{2}\right)\frac{|eQq_p|}{1 + i\epsilon} =$$
$$\left[1 - \cot^2 \theta + (\cot^2 \theta)i_{\sigma} - \frac{1}{2}(i_{\sigma} + i_{\pi})\right]\frac{|eQq_p|}{1 + i\epsilon}$$

$$\eta|eQq_{zz}| = \left[\left(N_x - \frac{N_y + N_z}{2}\right) - \left(N_y - \frac{N_x + N_z}{2}\right)\right]\frac{|eQq_p|}{1 + i\epsilon} = \frac{3}{2}|i_{\sigma} - i_{\pi}|\frac{|eQq_p|}{1 + i\epsilon}$$

Here, q_p is the field gradient at a nitrogen nucleus formed by the charge distribution of a single 2p electron in a neutral nitrogen atom along the symmetry axis. The denominator for $|eQq_p|$ takes into account a decrease in the electrostatic interaction between a valency p electron and the nucleus due to the expansion of the charge cloud in a negatively charged nitrogen, the screening constant ϵ being estimated by Townes and Schawlow at 0.3.[17] The valency angle $\angle CNC$ of nitrogen in a pyridine molecule has been determined as $2\theta = 116° 15'$ from microwave rotational spectra.[18]

(10) P. Love, *J. Chem. Phys.*, **39**, 3044 (1963).

(11) S. S. Lehrer and C. T. O'Konski, *ibid.*, **43**, 1941 (1965).

(12) R. H. Widman, *ibid.*, **43**, 2922 (1965).

(13) Y. Abe, *J. Phys. Soc. Jap.*, **18**, 1804 (1963).

(14) R. Hoffmann, *J. Chem. Phys.*, **40**, 2745 (1964).

(15) C. H. Townes and B. P. Dailey, *ibid.*, **17**, 782 (1949).

(16) T. P. Das and E. L. Hahn, "Solid State Physics," Suppl. 1, Academic Press Inc., New York, N. Y., 1958, p 119.

(17) C. H. Townes and A. L. Schawlow, "Microwave Spectroscopy," McGraw-Hill Book Co., Inc., New York, N. Y., 1955, p 225.

(18) B. Bak, L. Hansen-Nygaard, and J. Rastrup-Andersen, *J. Mol. Spectrosc.*, **2**, 361 (1958).

It is assumed that this value is unaltered in pyridine derivatives even in the solid state. The value of $|eQq_p|$ has been estimated at about 12 Mcps in our previous paper.[6,7,19] With these values, the bond ionicities, i_σ and i_π, can be calculated from the observed quadrupole coupling constants and the corresponding asymmetry parameters for two possible cases of $i_\sigma > i_\pi$ and $i_\sigma < i_\pi$. Table III shows the results obtained for the former choice as well as the alternative assumption. The latter is unreasonable in many respects. For instance, i_σ increases in the order of pyridine, 3-chloropyrindine, 2-chloropyridine, and 2,6-dichloro-pyridine, whereas the reverse order is expected because substituted chlorine atoms attract electrons from a pyridine ring through σ bonds. Therefore, one can rule out the second choice in agreement with the result of microwave measurement on pyridine[20] and with an anticipation presented by Guibé and Lucken[5,21] for nitrogen heterocycles. We have calculated i_π by the Pariser–Parr–Pople molecular orbital method also. Although the agreement is not excellent, relative magnitudes are quite satisfactory, in view of the different methods employed and the various assumptions made in the calculations. This and subsequent molecular orbital calculations have been performed by use of a Hitac 5020 computer. The following exchange-integral parameters have been used: $\beta_{C-C} = -2.39$ eV (ring), $\beta_{C-N} = -2.58$ eV (ring), $\beta_{C\equiv N} = -3.50$ eV, $\beta_{C-C} = -2.14$ eV (ring CN), and $\beta_{C-N} = -3.00$ eV (ring NH_2).

Table III: Calculated Values of i_σ and i_π

Pyridine derivatives	$i_\sigma > i_\pi$ ($|q_{yy}| > |q_{zz}|$) i_σ	i_π	i_π, (MO)	$i_\sigma < i_\pi$ ($|q_{yy}| < |q_{zz}|$) i_σ	i_π
Pyridine	0.320	0.195	0.176	0.164	0.282
2-Chloro-	0.308	0.227		0.206	0.283
3-Chloro-	0.310	0.195		0.167	0.275
2,6-Dichloro-	0.298	0.266		0.257	0.288
2-Cyano-	0.299	0.187	0.165	0.159	0.266
3-Cyano-	0.312	0.194	0.170	0.165	0.277
4-Cyano-	0.314	0.170	0.163	0.160	0.281
2-Amino-	0.343	0.334	0.257	0.331	0.340
3-Amino-	0.330	0.207	0.145	0.176	0.292
4-Amino-	0.348	0.325	0.221	0.317	0.340
2-Methyl-	0.322	0.219		0.192	0.288
3-Methyl-	0.319	0.193		0.161	0.281
4-Methyl-	0.329	0.223		0.195	0.296

Data shown in Table III indicate that the donation of π electrons from various substituents to ring nitrogen decreases in the order $NH_2 > Cl > CH_3 \sim H > CN$, whereas that of σ electrons decreases in the order $NH_2 > CH_3 \sim H > Cl \sim CN$.

It is interesting to note that i_π of 3-substituted pyridines is almost identical with that of pyridine, whereas those of 2- and 4-substituted pyridines are

quite different from that of pyridine. The same conclusion has been reached by Lucken[22] for some methylpyridines. Thus the π-electron distribution about ring nitrogen is practically unaffected by substitution at position 3, regardless of the kind of substituents. In fact, the observed pure quadrupole resonance frequency of ^{35}Cl in 3-chloropyridine is higher than those in 2- and 4-chloro derivatives,[23] indicating that the C–Cl π-bond character is the smallest for 3-chloropyridine.[24]

The data of cyano groups in cyanopyridines lead to the same conclusion. As in a previous article,[7] let the orbitals of nitrogen in a cyano group involved in bonding be expressed by

$$\psi_\sigma = (1 - s)^{1/2}\phi_{pz} + s^{1/2}\phi_s$$

$$\psi_{1p} = (1 - s)^{1/2}\phi_s - s^{1/2}\phi_{pz}$$

$$\psi_{\pi x} = \phi_{px}$$

$$\psi_{\pi y} = \phi_{py}$$

The sp-hybridized σ-bond orbital, ψ_σ, accommodates $1 + i_\sigma$ electrons, while the lone-pair orbital, ψ_{1p}, is fully occupied by a pair of electrons. The extent of s character has been estimated to be 0.2–0.3,[7] because Scherr[25] obtained $s = 26.1\%$ for a nitrogen molecule in his molecular orbital calculations. The average value, 25%, was taken. The π-bond orbitals, $\psi_{\pi x}$ and $\psi_{\pi y}$ having their axes perpendicular and parallel to the plane of the pyridine ring, respectively, are populated with $1 + i_{\pi x}$ and $1 + i_{\pi y}$ electrons, respectively. Calculations along the same line as for the foregoing ones yield

$$|eQq_{zz}| = \left[s + i_\sigma - si_\sigma - \frac{1}{2}(i_{\pi x} + i_{\pi y})\right]\frac{|eQq_p|}{1 + i\epsilon}$$

$$\eta|eQq_{zz}| = \frac{3}{2}(i_{\pi x} - i_{\pi y})\frac{|eQq_p|}{1 + i\epsilon}$$

Since there are three unknowns, i_σ, $i_{\pi x}$, and $i_{\pi y}$, whereas only two observables, eQq_{zz} and η, are available, let it be assumed that $i_{\pi y}$ is equal to 10% by taking into account the electronegativity difference vs. ionic-character curve of Townes and Dailey.[26] The calculated values of $i_{\pi x}$ are shown in Table IV, along with those from molecular orbital calculations. Again,

(19) L. Guibé and E. A. C. Lucken, *Compt. Rend.*, **263**, 815 (1966).

(20) G. Sørensen, *J. Mol. Spectrosc.*, **22**, 325 (1967).

(21) E. A. C. Lucken, *Trans. Faraday Soc.*, **57**, 729 (1961).

(22) E. A. C. Lucken, "Nuclear Quadrupole Resonance Spectroscopy," International Summer School on Theoretical Chemistry, Frascati, Italy, Oct 1967.

(23) P. J. Bray, S. Moskowitz, H. O. Hooper, R. G. Barnes, and S. L. Segel, *J. Chem. Phys.*, **28**, 99 (1958); M. J. S. Dewar and E. A. C. Lucken, *J. Chem. Soc.*, 2653 (1958).

(24) M. J. S. Dewar and E. A. C. Lucken, Special Publication No. 12, The Chemical Society, London, 1958, p 223.

(25) C. W. Scherr, *J. Chem. Phys.*, **23**, 569 (1955).

(26) B. P. Dailey and C. H. Townes, *ibid.*, **23**, 118 (1955).

$i_{\pi z}$ of the cyano nitrogen in 3-cyanopyridine is close to that of cyanobenzene, indicating the absence of the effect of the ring nitrogen as contrasted with the case of 2- and 4-cyanopyridines. It should be mentioned that this conclusion is unaltered by the choice of $i_{\pi y}$ in the vicinity of 10%.

Table IV: π Ionicity of CN Bonds

Compound	$i_{\pi z}$	$i_{\pi z}$ (MO)
2-Cyanopyridine	0.119	0.142
3-Cyanopyridine	0.126	0.150
4-Cyanopyridine	0.103	0.142
Cyanobenzene	0.127	0.149

The σ ionicity i_σ depends not so much on the kind and the position of substituents as i_π does. However, there is an unmistakable trend that it increases in the order of 2-, 3-, and 4-cyanopyridines and 2,6-, 2-, and 3-chloropyridines, as expected from the inductive effect of σ-electron-withdrawing substituents.

Hoffmann[27] has used an extended Hückel method of molecular orbital calculation to evaluate the electron population in the σ and π orbitals of pyridine and methylpryidines. The results are compared in Table V with $i = 2i_\sigma + i_\pi$ of the present investigation. Although the calculated values are greater than the observed values by about 10%, qualitative agreement is excellent.

Table V: Total Ionic Character i of a Nitrogen Atom in a Pyridine Ring

Compound	i	i (Hoffmann)
Pyridine	0.835	0.915
2-Methylpyridine	0.863	0.957
3-Methylpyridine	0.831	0.912
4-Methylpyridine	0.881	0.947

(27) R. Hoffmann, *J. Chem. Phys.*, **39**, 1397 (1963); **40**, 2480 (1964)

Comparison of Electrical Transport Properties of Anionic

Polyelectrolytes and Polysoaps[1]

by Raphael Varoqui[2] and Ulrich P. Strauss[3]

School of Chemistry, Rutgers, The State University of New Jersey, New Brunswick, New Jersey 08903
(Received January 2, 1968)

Two polysoap and three polyelectrolyte samples, prepared by the hydrolysis of copolymers of maleic anhydride with decyl vinyl ether and methyl vinyl ether, respectively, were compared by electrical transport studies at 0°. Conductometric titrations in aqueous saltless solutions gave the following results: (1) the equivalent conductance was smaller for the polysoap than for the polyelectrolyte samples and (2) while the equivalent conductance was independent of the degree of polymerization for the polyelectrolytes, it decreased with increasing degree of polymerization for the polysoaps. In 0.2 N LiBr solution, the polysoap conductance was again smaller than that of the polyelectrolytes. On the other hand, the electrophoretic mobility was identical for polysoaps and polyelectrolytes at each given LiBr concentration of the aqueous solvent medium and decreased as the LiBr normality increased from 0.04 to 0.8. The same invariance of the electrophoretic mobility to large changes in macroion configuration had previously been observed for cationic polyelectrolytes and polysoaps and thus appears to be a general phenomenon.

In a previous study[4] it was observed that the electrophoretic mobility of polyelectrolytes and polysoaps, derived from poly(4-vinylpyridine) by quaternization with alkyl bromides, was controlled only by the nature and the concentration of the simple electrolyte in the aqueous solvent medium. Specifically, the mobility was independent of the compactness of the polymer chain; *i.e.*, in any given electrolyte solution, polyelectrolytes and polysoaps whose intrinsic viscosities differed by more than an order of magnitude did not differ in their electrophoretic mobilities. These findings suggested similar experiments with other polyelectrolyte–polysoap systems in order to explore the generality of the observed phenomenon. The copolymers of vinyl alkyl ethers and maleic anhydride appeared especially promising for this purpose. The hydrolyzed polyacids act as typical polyelectrolytes when the alkyl group of the vinyl ether is short[5,6] and as typical polysoaps when the alkyl group is long.[7] Furthermore, the polyacids are alternating 1–1 copolymers. Thus their structure is known, and the backbones to which the fixed electrolyte groups are attached have the required identity for polyelectrolyte and polysoap.

Since very little is known concerning electrical transport properties of polysoaps, it was decided to supplement the electrophoresis with exploratory electrical-conductance studies. Hydrolyzed copolymers of maleic anhydride with vinyl methyl ether and with vinyl decyl ether were used as our polyelectrolyte and polysoap, respectively.

Experimental Section

Materials. Three 1–1 copolymers of vinyl methyl ether and maleic anhydride (VME–MA, our samples

G119, G139, and G169) were obtained from General Aniline and Film Corp. Each of the three compounds was purified several times by precipitation from dilute dimethylformamide solution into an excess of ethyl ether at room temperature. The products were dried *in vacuo*, first at room temperature, then at 100° for 24 hr, and were finally stored in a dry atmosphere. The absence of residual monomer and other low molecular weight material was verified by dialysis of small samples in an aqueous environment using Visking cellophane membranes. According to the supplier, the ranges of specific viscosities of 1% solutions in 2-butanone at 25° were 0.1–0.5, 1.0–1.4, and 2.6–3.5 for the low (G119), medium (G139), and high (G169) molecular weight samples, respectively. Since for our purposes we only needed to know that the molecular weights differed fairly widely, no attempt to measure the molecular weights of these samples was made.

One of the copolymers of vinyl decyl ether and maleic anhydride (VDE–MA, our sample S616) was prepared by refluxing in benzene under nitrogen an equimolar 7.5% mixture of the monomers with 0.1% azobisisobutyronitrile. After 4 hr of refluxing, the reaction

(1) The support of this research by a grant from S. C. Johnson and Son, Inc., is gratefully acknowledged. This paper was presented at the 154th National Meeting of the American Chemical Society, Chicago, Ill., Sept 1967.

(2) S. C. Johnson Postdoctoral Fellow, 1966.

(3) To whom inquiries concerning this paper should be directed.

(4) U. P. Strauss, N. L. Gershfeld, and H. Spiera, *J. Amer. Chem. Soc.*, **76**, 5909 (1954).

(5) J. D. Ferry, D. C. Udy, F. C. Wu, G. E. Heckler, and D. B. Fordyce, *J. Colloid Sci.*, **6**, 429 (1951).

(6) P. Dubin and U. P. Strauss, *J. Phys. Chem.*, **71**, 2757 (1967).

(7) K. Ito, H. Ono, and Y. Yamashita, *J. Colloid Sci.*, **19**, 28 (1964).

mixture was poured into five volumes of petroleum ether (bp 40–60°); the precipitated copolymer was dissolved in a minimum amount of tetrahydrofuran and was reprecipitated into pentane. After several reprecipitations, the product was dried *in vacuo* using the same procedure as for the VME–MA copolymers.

A higher molecular weight VDE–MA copolymer (our sample S703) was prepared by refluxing an equimolar 20% mixture of the monomers in benzene with 0.05% azobisisobutyronitrile at 63° for 5 hr. By a method similar to that used for the VME–MA copolymers, it was verified that copolymers S616 and S703 contained no remaining low molecular weight substances.

The weight-average degrees of polymerization, P_w, of VDE–MA copolymers S616 and S703 were determined from their intrinsic viscosity values in tetrahydrofuran at 30° by using the relation of Ito, *et al.*[7,8] These values were as follows: for VDE–MA S616, $[\eta] = 0.493$ dl/g and $P_w = 340$; for VDE–MA S703, $[\eta] = 3.30$ dl/g and $P_w = 9200$.

The VME–MA copolymers were hydrolyzed by heating their aqueous solutions at 80° for 2 hr followed by tumbling at room temperature for 24 hr. The dissolution of the VDE–MA copolymers in water, which proceeded with difficulty at room temperature, was accelerated by heating for 12 hr at 80°. Even then, clear fluid solutions were obtained only for sample S616, while sample S703 formed jellies at its low natural pH and could be brought to complete solution only by raising the pH above 7.

The intrinsic viscosity values of the hydrolyzed copolymers in 0.2 N LiBr, brought to pH 7.5 with LiOH, were 1.38 dl/g for VME–MA G119 and 0.042 and 0.20 dl/g for VDE–MA copolymers S616 and S703, respectively. The small intrinsic viscosities of the latter two compounds are typical of polysoaps in aqueous solutions and indicate that the macromolecules reach high degrees of compactness by intramolecular micellization.[9,10] In contrast, the much higher intrinsic viscosity of the vinyl methyl ether copolymer G119 is typical of ordinary polyelectrolytes.

Methods of Measurements. Electrical conductances were determined at 0° with a Shedlovsky-type bridge.[11,12] Resistance values were measured at 4 kcps with an accuracy of about 0.01%. Polarization errors were found to be negligible. All solutions were prepared with conductivity water obtained by passing distilled water through a mixed-bed ion-exchange resin. The specific conductivity of the water was 0.6 × 10⁻⁶ mho/cm.

Electrophoretic mobilities were determined at 0° in a Perkin-Elmer Model 38 Tiselius apparatus by the method previously described.[4] Cell currents ranged from 7 to 20 mA from the most dilute (0.04 N) to the most concentrated (0.8 N) LiBr solution. Average values of the mobilities of the ascending and descending
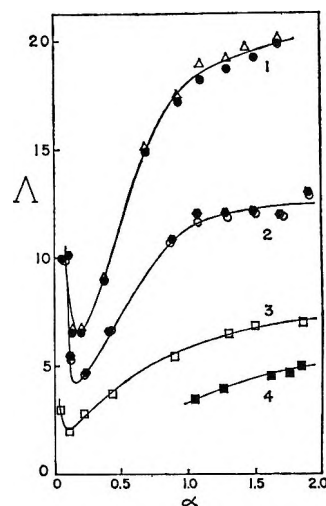
Figure 1. Equivalent conductance in the absence of a simple electrolyte: curve 1, VME–MA neutralized with KOH; ●, G119; △, G139; curve 2, VME–MA neutralized with LiOH; ○, G119; ●, G139; curve 3, VDE–MA neutralized with LiOH; □, S616; curve 4, VDE–MA neutralized with LiOH; ■, S703.

boundaries are used. Generally, the ascending boundary moved 5% faster than the descending boundary; however, in the 0.04 N LiBr solutions, the differences in the velocities of the two boundaries were of the order of 10%.

Results and Discussion

Conductometric Titration in Absence of Simple Electrolyte. The effect of added base on the conductivity of aqueous salt-free 0.02 N polyacid solutions is shown in Figure 1. The abscissa represents the degree of neutralization, α, defined by the equation

$$\alpha = [(MOH) + (H^+) - (OH^-)]/C_p \qquad (1)$$

where (MOH), (H⁺), and (OH⁻) are the concentrations of added base, hydrogen ion, and hydroxide ion, respectively, expressed in equivalents per liter, and C_p is the concentration of the polyacid expressed in monomoles per liter. (One monomole contains one maleic acid and one alkyl vinyl ether residue.) The hydrogen and hydroxyl ion concentration terms, which make significant contributions only at low and high pH, were calculated from the pH, the assumption being made that the activity coefficients were unity. With this definition $\alpha = 2$ at complete neutralization of the dibasic acid units. The ordinate represents the equivalent conductance, Λ, defined by the relation

(8) We have neglected a possible small error resulting from the fact that this relation was established for copolymers of maleic anhydride and vinyl dodecyl ether (instead of vinyl decyl ether).

(9) U. P. Strauss and E. G. Jackson, *J. Polym. Sci.*, **6**, 649 (1951).

(10) U. P. Strauss, N. L. Gershfeld, and E. H. Crook, *J. Phys. Chem.*, **60**, 577 (1956).

(11) T. Shedlovsky, *J. Amer. Chem. Soc.*, **52**, 1793 (1930).

(12) D. Edelson and R. M. Fuoss, *J. Chem. Educ.*, **27**, 610 (1950).

$$\Lambda = 1000\kappa_{sp}/2C_p \tag{2}$$

where κ_{sp} is the specific conductance due to the poly-electrolyte, *i.e.*, the difference between the specific conductance values of the solution and of the solvent. The data obtained by neutralizing the VME–MA copolymers G119 and G139 with KOH are given by curve 1; those obtained by neutralizing the same samples with LiOH are given by curve 2. The curves resemble those obtained with other weakly acidic polyelectrolytes, such as poly(acrylic acid) and poly-(methacrylic acid),[13,14] and their prominent features, such as the minimum at low α and the plateau at high α, have been discussed previously.[13,14] The observed independence of chain length is also characteristic of polyelectrolytes.[13,15]

Relevant molecular parameters derived from these conductance data are given in Table I. In the absence

Table I: Conductometric Titration Results in the Absence of Simple Salt

α	$i(G139)^a$	$10^4 u_p(G139)^a$, cm^2 V^{-1} sec^{-1}	$\Lambda(S616)/\Lambda(G139)$	$\Lambda(S703)/\Lambda(G139)$
0.2	0.086^b	2.3^b	0.553	...
0.4	0.14	2.5	0.570	...
0.6	0.19	2.5	0.543	...
0.8	0.24	2.5	0.515	...
1.0	0.30	2.1	0.520	...
1.2	0.34	1.7	0.525	0.319
1.4	0.36	1.4	0.550	0.348
1.6	0.37	1.4	0.565	0.372
1.8	0.40	1.2	0.575	0.400

^{a} Calculated by means of eq 3 and 4 (see text). ^{b} See ref 18.

of a rigorous theory, we have followed the usual procedure of considering part of the counterions bound to and traveling with the macroion and the remainder of the counterions completely free, *i.e.*

$$\Lambda = i(\mathfrak{F}u_p + \lambda_M) \tag{3}$$

where i is the fraction of ionized carboxylate groups, $\mathfrak{F}$ is the faraday, u_p is the mobility of the polyion, and λ_M is the equivalent conductance of the counterion. In addition we have used the relation

$$i = \frac{\Lambda_{KP} - \Lambda_{LiP}}{\lambda_K - \lambda_{Li}} \tag{4}$$

where Λ_{KP} and Λ_{LiP} refer to the equivalent conductances of the VME–MA polyacids partially neutralized with KOH and LiOH, respectively, to the same value of α. Relation 4 has been derived from eq 3 with the assumption that in the absence of simple electrolyte i and u_p are independent of the alkali metal ion and depend only upon α and C_p, an assumption which is supported by the findings that such a behavior is

indeed followed by poly(acrylic acid) and poly(methacrylic acid).[16] For λ_K and λ_{Li} we used the values at infinite dilution, 40.7 and 19.4, respectively.[17,18] The parameters i and u_p for VME–MA polyacid G139, which are given in the second and third columns of Table I as functions of α follow the same trends as observed for other polyacids.[14,19] The polymer charge fraction, i, increases rapidly at first and then more slowly, as with increasing neutralization an increasing number of counterions is attracted to the macroion. The decrease in the mobility, u_p, with increasing charge has been attributed to an increase in the friction coefficient caused by an extension of the molecular dimensions.[14,16] However, an increase in binding of alkali metal ions may also bring about this result.

Turning our attention now to the polysoaps, the effect on Λ of neutralizing the VDE–MA copolymers S616 and S703 with LiOH is shown by curves 3 and 4, respectively, of Figure 1. The behavior differs from that of the VME–MA polyelectrolytes in two aspects. First, the equivalent conductance of the polysoaps is smaller than that of the polyelectrolytes; second, whereas for typical polyelectrolytes the conductance is independent of chain length, for the polysoaps there appears to be an inverse dependence between the equivalent conductance and the degree of polymerization. The ratios of the equivalent conductance values of the polysoaps S616 and S703 to that of polyelectrolyte G139 are given in columns 4 and 5 of Table I. We note that these ratios show only small variations with changing α. We note further that since the friction coefficients must be smaller for the compact polysoap molecules than for the extended polyelectrolytes, the lower conductance of the polysoaps indicates a higher effective degree of counterion association. We shall discuss these effects further below.

Conductance and Electrophoresis in the Presence of Simple Electrolyte. The equivalent conductance of polyelectrolytes G119, G139, and G169 and polysoap S616 in 0.2 N LiBr solution is given as a function of the polymer concentration in Figure 2. Most of the

(13) W. Kern, *Z. Physik. Chem.* (Leipzig), **A181**, 249 (1938).

(14) J. R. Huizenga, P. F. Grieger, and F. T. Wall, *J. Amer. Chem. Soc.*, **72**, 2636 (1950).

(15) U. Schindewolf, *Z. Physik. Chem.* (Frankfurt), **1**, 134 (1954).

(16) H. Eisenberg, *J. Polym. Sci.*, **30**, 47 (1958).

(17) R. A. Robinson and R. H. Stokes, "Electrolyte Solutions," Academic Press Inc., New York, N. Y., 1955, p 454.

(18) At low pH the hydrogen ion makes a significant contribution to the equivalent conductance, and eq 3 must be modified to $\Lambda = i(\mathfrak{F}u_p + \lambda_M) + i_H(\lambda_H - \lambda_M)$, where $i_H = (H^+)/2C_p$ represents the contribution of the hydrogen ion to i. The left-hand side of eq 4 becomes $i - i_H$ under these circumstances. The magnitude of this contribution can be seen from the fact that without the modification the calculated values of i and u_p at $\alpha = 0.2$ would be 0.080 and 4.2, instead of the correct values given in Table I. The effect of the modification is very slight at $\alpha = 0.4$ and is completely negligible at higher values of α.

(19) F. T. Wall and R. H. Doremus, *J. Amer. Chem. Soc.*, **76**, 1557 (1964).
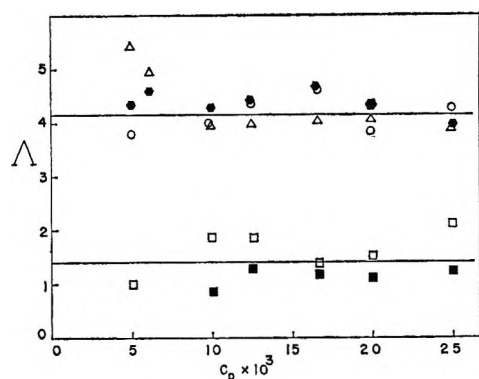
Figure 2. Equivalent conductance in 0.2 N LiBr at pH 7.0: O, VME-MA G119; ●, VME-MA G139; △, VME-MA G169; □ ■, VDE-MA S616 (two independent dilution runs).

Figure 3. Electrophoretic mobility as a function of LiBr concentration, m, at pH 8.8 (unless otherwise indicated): O, VME-MA G119; ●, VME-MA G139; □, VDE-MA S616; △, VDE-MA S703; ◑, VDE-MA S703 at pH 7.0.

results were obtained at pH 7.0 where α in this solvent is 1.5 for the polyelectrolyte and 1.2 for the polysoap. However, changes in pH up to 9 had no significant effect on Λ. For both the polyelectrolyte and the polysoap, the equivalent conductance shows no trend with varying polymer concentration, similar to previous findings with polyphosphates.[20] Neither is the influence of molecular weight noticeable for the three polyelectrolytes; however, as was the case in the absence of salt, Λ is significantly smaller for the polysoap than for the polyelectrolytes. (Unfortunately, the supply of polysoap S703 was not sufficient to permit the completion of these measurements and thus the effect of molecular weight on polysoap conductance in 0.2 N LiBr could not be determined.)

The results of the electrophoretic mobility determinations for polyelectrolytes G119 and G139 and for polysoaps S616 and S703 are presented in Figure 3 where the mobility u_p is given as a function of the LiBr concentration. Normally, the data were obtained with $C_p = 0.01$ and at pH 8.8. However, the effect of varying these parameters was also investigated. It is seen that in each given environment the electrophoretic mobility is identical for the extended polyelectrolyte and the compact polysoap molecules. The mobility is also independent of the concentration and the molecular weight of the polyelectrolytes and polysoaps and of the pH over the measured range from pH 7 to 8.8. (Some of the data were omitted from Figure 3 in order to avoid clutter.) In this range the mobility appears to be controlled only by the lithium bromide concentration. Thus we observe here the same type of behavior as has previously been found for the cationic polyelectrolytes and polysoaps derived from poly(4-vinylpyridine).[4]

The invariance of the electrophoretic mobility with macroion configuration thus appears to be a general phenomenon. Apparently, if a contraction of the molecular dimensions causes a decrease in the friction coefficient, such a decrease is compensated by a de-

crease in the effective electrical charge. It has been shown theoretically that the electrophoretic mobility for microscopic particles depends upon the charge density of their surface and on their ionic atmosphere. The theoretical results are usually represented by an equation of the type
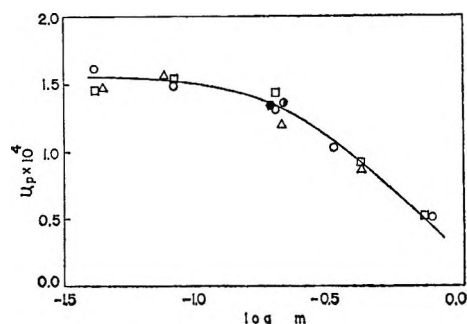
$$u = \frac{\epsilon \zeta}{C \eta} \qquad (5)$$

where ϵ and η are the dielectric constant and viscosity of the medium, respectively; C is a parameter ranging from 4π to 6π; and ζ, "zeta potential," is the potential at the surface of shear between the particle and medium.[21-23] It is well-known that, if microscopic particles of various sizes and shapes are coated with a protein, they assume the electrophoretic mobility of the protein.[24,25]

These considerations suggest that the compact polysoap molecules may be viewed as impermeable particles whose electrolytic behavior is determined by their surface. This surface contains the same hydrophilic groups as the chemically related polyelectrolyte; i.e., the polysoap molecules behave as if they were electroneutral particles covered with polyelectrolyte. This hypothesis would account for the fact that the polysoap and the polyelectrolyte have the same mobility and that the polysoap mobility is independent of molecular weight. The observation that the polysoap conductance is smaller than that of the polyelectrolyte would be attributable to the fact that the ionic groups which are buried in the micellar interior would not contribute to the conductance while the ionic groups in the surface contribute the same amount as if they were part of the polyelectrolyte.

(20) U. P. Strauss and S. Bluestone, *J. Amer. Chem. Soc.*, **81**, 5292 (1959).

(21) M. Smoluchowski, *Krak. Anz.*, 182 (1903).

(22) D. C. Henry, *Proc. Roy. Soc.*, **A133**, 106 (1931).

(23) F. Booth, *J. Colloid Sci.*, **6**, 549 (1951).

(24) H. A. Abramson, *J. Phys. Chem.*, **35**, 299 (1931).

(25) M. Mooney, *ibid.*, **35**, 331 (1931).

Table II: Molecular Dimensions and Surface Areas of Polysoap Molecules

Sample	DP	$[\eta]$, dl g^{-1}	ν	J	$\overset{\circ}{a}$	$\overset{\circ}{b}$	$10^{-2}S$, Å^2	S/DP, Å^2	$(S/DP)_{S616}/$ $(S/DP)_{S703}$
			Case 1: $v_{sp} = 1.00$ cm^3 g^{-1}						
S616	340	0.042	4.2	3.53	80.0	22.7	18.5	54.5	1.99
S703	9200	0.20	20	12.94	572	44.3	251	27.3	
			Case 2: $v_{sp} = 1.68$ cm^3 g^{-1}						
S616	340	0.042	2.5	1.00	41.3	41.3	21.4	63.0	1.84
S703	9200	0.20	11.9	8.87	533	60.0	317	34.4	

Thus the equivalent conductance ratios of polysoap to polyelectrolyte in Table I may be interpreted as the fraction of ionic groups in the surface of the polysoap molecules. Finally, the difference in equivalent conductance found for polysoaps S616 and S703 may then be due to a difference in exposed surface areas. To test this hypothesis, let us estimate the ratio of these surface areas from the available viscosity data.

The intrinsic viscosity may be related to the molecular dimensions by the Simha equation[26]

$$[\eta] = 0.01\nu v_{sp} \qquad (6)$$

where v_{sp} is the effective specific volume and ν is a shape factor, which for spheres equals 2.5 and which for prolate and oblate ellipsoids has been tabluated[27] as a function of the axial ratio J. It is clear that ν and v_{sp} cannot be uniquely obtained from eq 6. However, if we assume that the molecules of the two polysoaps are prolate ellipsoids with a common value of v_{sp} chosen arbitrarily, but realistically, to account for possible extents of solvent swelling, we find that the desired ratio of specific surface areas is affected only little by the choice of v_{sp}. As examples, the results of the calculations for two values of v_{sp} are given in Table II. Case 1 represents $v_{sp} = 1$ while case 2 represents $v_{sp} = 1.68$, the highest possible value consistent with

$\nu \geq 2.5$. While the values of the major and minor semiaxes, $\overset{\circ}{a}$ and $\overset{\circ}{b}$ (expressed in angstrom units), respectively, are seen to be quite sensitive to the chosen value of v_{sp}, the surface area, S, of the polysoap molecules is much less sensitive, and the figures in the last column which give the ratio of the specific molecular surface areas of both polysoap samples lie within 8% of one another. These figures represent the predicted value of the equivalent conductance ratio, $\Lambda(S616)/\Lambda(S703)$. The experimental value of this ratio obtained from the data in Figure 1 is 1.6 in the appropriate range of α ($\alpha \sim 1.4$).[28] The rather good agreement lends support to our hypothesis concerning the electrolytic behavior of polysoaps.

(26) R. Simha, *J. Phys. Chem.*, **44**, 25 (1940).

(27) J. W. Mehl, J. L. Oncley, and R. Simha, *Science*, **92**, 132 (1940).

(28) It should be noted that the molecular dimensions were obtained in 0.2 *N* LiBr, while the conductances were measured in the absence of simple electrolyte. Our procedure thus involves the not unreasonable assumption that the specific surface ratio of the two polysoap samples is insensitive to changes in the salt concentration of the solvent.

Solute–Solvent Interactions in Aqueous Media

by O. D. Bonner

Department of Chemistry, University of South Carolina, Columbia, South Carolina 29208   (*Received January 3, 1968*)

Spectroscopic measurements of the solvation of alkali halide salts in aqueous solutions are correlated with the colligative properties of these solutions as represented by their activity coefficients Evidence for ion pairing in some salts is based upon the concentration dependence of the absorption at 958 mμ. The spectra of the aromatic sulfonates and certain nonelectrolytes indicate that these solutes exert a "structure-breaking" effect upon the solvent. Solutions of all of the nonelectrolytes in this category are found to exhibit positive deviations from Raoult's law, in contrast to solvated solutes, such as dextrose, which have activity coefficients greater than unity. The small activity coefficients of the aromatic sulfonates also correlate with the spectral findings.

Preliminary studies of water and aqueous solutions in this laboratory,[1] in which the near-infrared absorbance of solutions is compared with that of pure water at the same temperature by a differential method, have yielded quantitative data on the solvation of both electrolytes and nonelectrolytes. The "solvation numbers" of the alkali metal chlorides were found to be unusual, in that the observed order of LiCl > CsCl > KCl > NaCl does not correspond with the lyotropic series of activity coefficients or cation-exchange equilibria. It is significant to note that for proton magnetic resonance measurements,[2,3] in which the magnitude of the effect of the ions on the water protons should be directly related to the chemical shift, the results are in complete qualitative agreement with those obtained from spectral measurements. As an explanation of the above unexpected findings, it was postulated that "hydration numbers" calculated from the colligative properties of the solution include both ion–solvent and ion–ion interactions, while those measured spectroscopically represent only the former. This article presents further experimental evidence to support this postulate.

Experimental Section

All spectra were recorded using a Cary Model 14M spectrophotometer. The differential technique which was used has been described previously.[1] All electrolytes except the sulfonates were reagent grade and were used without purification. The sulfonates were prepared and purified by methods which have been described in a previous publication.[4] Propylene carbonate and ethylene carbonate were triply distilled at reduced pressure, while dimethylurea was twice recrystallized from benzene.

Discussion

It has long been recognized that the structural properties of the solvent will need to be taken into account if the ultimate goal of electrolyte theory is reached. The "plausibility in the idea that water-structure influences play a part" in determining the activity co-

efficient–concentration curves of aqueous solutions of the alkali halides was discussed by Frank.[5] He pointed out, however, that many structural interpretations are available to explain each phenomenon and that more work needs to be done to clarify the picture. In the discussion of solutions, the solute–solvent interactions may be grouped together as "solvation" and the ion–ion interactions may be classified as "ion pairing." In an estimation of the relative importance of these two types of interaction in aqueous solutions of simple electrolytes, one must take into account several peculiarities in the order of activity coefficients of the alkali metal halides, nitrates, and sulfonates (Table I). The sequence for salts of any anion is Li$^+$ > Na$^+$ > K$^+$ > Rb$^+$ > Cs$^+$. If tetraalkylammoniums alts are included, the R$_4$N$^+$ ion follows Cs$^+$, as would be expected. If one notes a particular cation, however, it is observed that for the activity coefficients of lithium salts I$^-$ > Br$^-$ > Cl$^-$ > NO$_3^-$ > RSO$_3^-$ > OH$^-$. The sequence for the halide salts of Rb$^+$, Cs$^+$, and R$_4$N$^+$ is, on the other hand, the reverse of that of the lithium salts.

Results

Types of Solvation. The activity coefficient data are consistent with the solvation data[1] if the latter are interpreted in terms of the two types of solvation which have been postulated and the effect that this would be expected to have upon ion pairing. First consideration may be given to the halides of the two extreme alkali metal cations Li$^+$ and Cs$^+$. The smaller lithium ion should polarize the water molecules strongly and should orient them so that the oxygen end of the dipole is nearest the ion. The cesium ion, on the other hand,

(1) O. D. Bonner and G. B. Woolsey, *J. Phys. Chem.*, **72**, 899 (1968).

(2) J. C. Hindman, *J. Chem. Phys.*, **36**, 1000 (1962).

(3) M. S. Bergqvist and E. Forslind, *Acta Chem. Scand.*, **16**, 2069 (1962).

(4) O. D. Bonner and O. C. Rogers, *J. Phys. Chem.*, **64**, 1409 (1960).

(5) H. S. Frank, *Z. Phys. Chem.* (Leipzig), **228**, 364 (1965).

Table I: Activity Coefficients of Aqueous Solutions at 0.5 m Concentrations[a]

	OH	F	Cl	Br	I	NO₃	Tol[b]	Mes[c]
Li	0.583		0.739	0.753	0.824	0.726	0.659	0.632
Na	0.688	0.632	0.681	0.697	0.723	0.617	0.627	0.598
K	0.712	0.670	0.649	0.657	0.676	0.545	0.605	
Rb			0.634	0.632	0.629	0.534		
Cs	0.752		0.606	0.603	0.599	0.528		
Me₄N			0.597	0.558				
Et₄N			0.600	0.505	0.406			

[a] Data are from: R. A. Robinson and R. H. Stokes, "Electrolyte Solutions," Academic Press Inc., New York, N. Y., 1959; O. D. Bonner and O. C. Rogers, *J. Phys. Chem.*, **64**, 1499 (1960); S. Lindenbaum and G. E. Boyd, *ibid.*, **68**, 911 (1964).   [b] Toluenesulfonate.   [c] Mesitylenesulfonate.

because of its more shielded nuclear charge, is not so effective in polarizing the solvent but appears to enhance the structure of water around it in the manner of the tetraalkylammonium ion or the inert gases. The anions should not be nearly so effective as the lithium ion in orienting the water dipole, but the fluoride and hydroxide ions should be the most effective. One might expect that ion pairing would be almost nonexistent for the lithium salts, except perhaps for the cooperative type shown in Figure 1 which involves a solvent molecule. This model is consistent with the large activity coefficients of the lithium salts and with their order. Cesium salts should be much more susceptible to ion pairing, since the cation is not protected by a sheath of polarized solvent molecules. The chloride ion, because of its greater solvation, is more effective than bromide or iodide ion in resisting ion pairing, and the order of activity coefficients for the cesium salts results. The other alkali halides which are listed show behavior intermediates between lithium chloride and cesium iodide.

The hydration numbers which were reported in the first article[1] were those obtained by extrapolation of the data to infinitely dilute solutions. It was subsequently realized that, if the above postulated type of ion pairing occurred, it should be capable of experimental verification. The absorption at 958 mμ, which is used as a measure of the solvation of the solute, should change less rapidly with increased concentration of LiCl solutions, since the concentration of "free water" is decreasing and the lithium ion solvation in concentrated solutions is consequently decreased. Concentrated solutions of cesium salts should, however, exhibit increased solvation, since the water structure is enhanced around an increasing number of ion pairs which are larger than the individual ions. This behavior is verified in Figure 2, where a plot is given of I/C as a function of the concentration. Dextrose is included as an example of a highly solvated nonelectrolyte for which ion pairing is not possible. The slopes of the molal absorbance curves are found to have opposite arithmetic signs for the two different types of solvation.
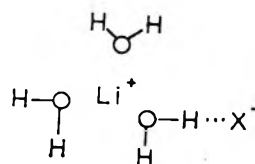
Figure 1.   A solvated ion-pair "model."
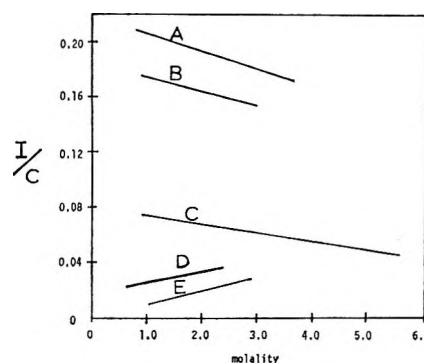
Figure 2.   Molal absorbance of solutions at 958 mμ: (A) LaCl₃, (B) dextrose, (C) LiCl, (D) CsI, (E) KNO₃.

It may also be noted that the two types of solvation postulated above offer a reasonable explanation of the behavior of the alkali halides at elevated temperatures.[6] Osmotic coefficients of LiCl are lower at 121° than at 25° because of a decrease in solvation (water polarization). The coefficients of CsCl increase with temperature since ion pairing, which is enhanced by the water structure at the lower temperature, decreases.

Structure-Breaking Solutes.   "Positive solvation," as evidenced by a decrease in the fraction of monomeric water in dilute solutions, was found for all of the salts except KNO₃ in the initial report. One other class of compounds for which activity coefficient data have been previously reported[4] appeared to be a good candidate for further investigation. Activity coefficients of the aromatic sulfonates are in the usual sequence, *i.e.*, $Li^+ > Na^+ > K^+$, etc., and those of the p-toluenesul-

(6) B. A. Soldano and C. S. Patterson, *J. Chem. Soc.*, 937 (1962).

fonates are of the same order of magnitude as the nitrates. With progressive substitution of the aromatic ring by methyl groups, the activity coefficients become quite small. This would indicate a type of "negative solvation" if one believes that the solvation of KNO_3 is nearly zero. This phenomenon was first observed by Sugden[7] from experiments in which acetic acid was distributed between salt solutions and amyl alcohol. The explanation which was proposed was a postulated depolymerizing effect on the water structure. This phenomenon is again capable of experimental verification. Pure water at 25° has been found to have an absorption maximum at 977 $m\mu$. Elevation of the temperature causes a shift of the maximum toward shorter wavelengths and it asymptotically approaches 958 $m\mu$, the characteristic band for liquid monomeric water. Solutions of salts which polarize the water molecule or solutes which cause an increase in the hydrogen bonding in water by enhancement of the structure cause a shift toward the limiting value of 986 $m\mu$. The data presented in Table II reveal that the band

Table II: Absorbance Maxima of Water and Certain Saturated Aqueous Solutions

Solution	Position of the $2\nu_1 + \nu_3$ band, $m\mu$
Magnesium chloride	986
Water	977
Sodium mesitylenesulfonate	974
Propylene carbonate	973

shift for aromatic sulfonates is in the direction *opposite* to that of the alkali metal halides. A more striking contrast of the behavior of the aromatic sulfonates and the alkali halides is shown in Figure 3. Solutions of sodium mesitylenesulfonate and potassium chloride are compared with water at 25° in the double-beam instrument with water in the reference beam. The water vs. aromatic sulfonate has a broad maximum at 990 $m\mu$, indicating that the pure water is hydrogen bonded to a greater extent than the water in the solution. The hump at about 960 $m\mu$ is due to the solvation of the sodium ion, with this band atop the shoulder of the broad band of hydrogen-bonded water. The water vs. KCl spectrum, on the other hand, has only the expected sharp peak at 958 $m\mu$. The spectroscopic evidence thus indicates that the lower activity coefficients of the aromatic sulfonates are related to their "structure-breaking" effect on the solvent and are not primarily due to ion pairing. While it is not possible to propose a definite "model" for this solute–solvent interaction, one may note that the sulfonate group is conjugated with the aromatic ring and that this permits the unit negative charge to be spread over a large area. The

Figure 3. Relative absorbance of solutions: (A) propylene carbonate, (B) sodium mesitylenesulfonate, (C) potassium chloride.

positive end of the water dipoles may be attracted sufficiently to "depolymerize" the water without substantial polarization of the molecules. The charge distribution on the large aromatic anions is quite different from that of the tetraalkylammonium cations which enhance the water structure in that the unit positive charge resides on the nitrogen atom of the R_4N^+ ion.

Nonelectrolytes. Solvation numbers of certain nonelectrolytes were also reported in the previous article. Sucrose and dextrose were found to be highly solvated and it was noted that their solutions exhibit negative deviations from Raoult's law. An equation relating the solvation of these solutes and their osmotic coefficients has been proposed by Stokes and Robinson.[8] No explanation other than "association" has been given, however, for nonelectrolytes, such as *sym*-dimethylurea,[9] in which the aqueous solutions exhibit positive deviations from Raoult's law.

It may be noted in Figure 3 that a nonelectrolyte, propylene carbonate, has a depolymerizing effect on the water structure. The spectra for solutions of ethylene carbonate and *sym*-dimethylurea are also quite similar and are, therefore, not included. It would be anticipated that osmotic and activity coefficients of aqueous solutions of ethylene carbonate would be substantially below unity, and preliminary results substantiate this expectation. Spectroscopic evidence of structure breaking by nonelectrolytes seems, in all cases, to be supported by colligative property measurements which indicate a positive deviation of the solutions from Raoult's law.

(7) J. N. Sugden, *J. Chem. Soc.*, 174 (1926).

(8) R. H. Stokes and R. A. Robinson, *J. Phys. Chem.*, **70**, 2126 (1966).

(9) O. D. Bonner and W. H. Breazeale, *J. Chem. Eng. Data*, **10**, 325 (1965).

Conclusions

Spectroscopic evidence presented above indicates two types of positive solvation by electrolytes.

(1) Small or highly charged ions, such as lithium and fluoride, are very effective in orienting the water molecules in their vicinity and tend to ion pair only with other ions having a high charge density.

(2) Larger ions, such as cesium and tetraalkylammonium, tend to enhance the water structure around them; i.e., the water is hydrogen bonded to a greater extent. These ions tend to form ion pairs, especially with other large ions having a lower charge density.

A type of negative solvation is exhibited by aromatic sulfonate anions which may be associated with a structure-breaking effect on the solvent. Nonelectrolytes are found to be both positively and negatively solvated, and, in all observed instances, the spectroscopic solvation evidence may be directly correlated with the direction of the deviation of their aqueous solutions from Raoult's law.

Nuclear Magnetic Resonance Study of Proton Exchange Involving

Methyl-Substituted Pyridinium Salts in Methanol

by Michael Cocivera

Bell Telephone Laboratories, Inc., Murray Hill, New Jersey 07974   (Received January 5, 1968)

The nuclear magnetic resonance line-broadening technique has been used to study proton-exchange reactions involving methyl-substituted pyridinium salts and methanol. For a reversible acid-dissociation reaction, $BH^+ + MeOH \underset{k_{-a}}{\overset{k_a}{\rightleftharpoons}} B + MeOH_2^+$, changing the position of the methyl group from the *para* position to the *ortho* position does not alter the value of either k_a or k_{-a}. In addition, the value of k_{-a} does not depend upon the degree of methyl substitution, and this value is comparable to the value expected for diffusion-controlled reactions. The reaction $BH^+ + MeOH + B \overset{k_2}{\rightarrow} B + MeOH + BH^+$ was found to involve only one methanol molecule. For the monomethyl compounds, the value of k_2 does not depend upon the position of the methyl group. For the dimethyl compounds, the value of k_2 depends upon the position of the methyl groups and indicates that the rate for this reaction is retarded when both methyl groups are *ortho* to the nitrogen of the pyridine ring.

Introduction

Nuclear magnetic resonance studies of proton exchange involving substituted ammonium salts and such solvents as water and methanol have revealed considerable information concerning the mechanisms by which the exchange can occur.[1] However, little information has been obtained concerning steric hindrance in these reactions. The only available evidence that steric effects can be significant in these reactions comes from a study of proton exchange involving triethylammonium ion in water.[2] In that study, Ralph and Grunwald concluded that the ethyl groups were sterically hindering one of the exchange reactions.

In the present article, the results of a study of the exchange involving methyl-substituted pyridinium salts in methanol are presented. The salts which were studied were the hydrochlorides of 2-picoline (I), 4-picoline (II), 2,4-lutidine (III), and 2,6-lutidine (IV).
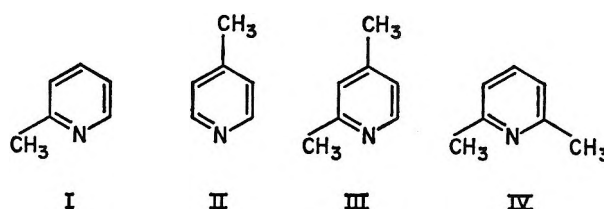
These salts were chosen because of the possibility that the methyl group could sterically hinder one or more of the exchange reactions when it is *ortho* to the nitrogen of the pyridine ring. The advantage of using these salts is that the pK_A of the salt does not change significantly when the methyl group is moved from the *ortho* to the *para* position on the pyridine ring. Consequently, the interpretation of the results is not

(1) For a brief review, see E. Grunwald and M. Cocivera, *Discussions Faraday Soc.*, **39**, 105 (1965).

(2) E. K. Ralph, III, and E. Grunwald, *J. Amer. Chem. Soc.*, **89**, 2963 (1967).

complicated by changes in acidity or basicity of the compounds when the methyl is moved from the *ortho* to the *para* position.

For each of the salts, the rates of the reactions given by eq 1–4 were measured. In these equations, B signifies the amine (I–IV).

$$MeOH + MeOH_2^+ \xrightarrow{k_+} MeOH_2^+ + MeOH \quad (1)$$

$$MeO^- + MeOH \xrightarrow{k_-} MeOH + MeO^- \quad (2)$$

$$BH^+ + MeOH \underset{k_{-a}}{\overset{k_a}{\rightleftarrows}} B + MeOH_2^+ \quad (3)$$

$$BH^+ + O\!-\!H + B \xrightarrow{k_2} B + H\!-\!O + BH^+ \quad (4)$$
$$\qquad\quad\; |\qquad\qquad\qquad\qquad\quad |$$
$$\qquad\;\; Me\qquad\qquad\qquad\qquad\; Me$$
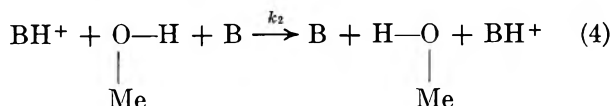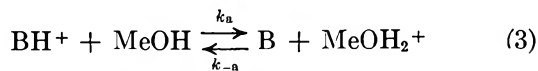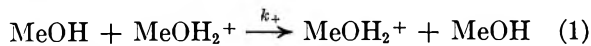
The values of k_+ and k_-, the rate constants for reactions 1 and 2, are known from previous studies.[3] Consequently, the pK_A of each pyridinium salt could be obtained from measurements of the rates of these reactions. The pK_A for each salt in methanol is nearly the same as the value in water. Comparison of the pK_A values, determined in the present study, with other methods is possible only for 4-picoline whose pK_A in methanol was determined to be 6.090 by the differential potentiometric method.[4] The value obtained in the present study is 6.05.

The *ortho* substitution of the methyl group was found to have little effect on k_a. The value of k_a for 2-picoline is almost the same as the value for 4-picoline. Similarly, there is no appreciable difference between the value for 2,6-lutidine and that for 2,4-lutidine. In addition, the position of the methyl group has little effect on k_{-a}. In fact, k_{-a} is essentially the same for all of the salts and is of the order of magnitude that one would expect for a diffusion-controlled reaction.

For the reaction given by eq 4, the position of the methyl group has an effect on the rate. The value of k_2 for 2,4-lutidine is more than three times the value for 2,6-lutidine. Since 2-picoline and 4-picoline have almost the same value for k_2, one methyl group in the *ortho* position apparently is not sufficient to retard the rate.

Experimental Section

Reagents and Solutions. The methyl-substituted pyridines were obtained from Aldrich Chemical Co. 2,6-Lutidine was purified according to the method of Brown.[5] The other amines were purified by distillation, and the boiling points agreed well with values reported in the literature. The nmr spectrum of each compound is as expected on the basis of its structure.

The hydrochloride of each amine was prepared by passing anhydrous HCl into a methanol solution containing the amine. After removing the methanol, each salt was recrystallized twice from either isopropyl alcohol or *n*-butyl alcohol. Each salt was analyzed

quantitatively for the chloride ion by using the Volhard method and for the methyl-substituted pyridinium ion by potentiometric titration. The equivalent weights determined by these analyses were in good agreement with the theoretical values.

Methanol was obtained from J. T. Baker Chemical Co. It was purified as described previously.[3] The solutions were prepared and analyzed by standard quantitative techniques.

Nmr Measurements. From slow-passage spectra, the chemical shifts were determined at five temperatures, −75, −50, −25, −15, and 0.8°, in the following manner. Using methanol solutions containing approximately 1 M salt and 2 M HCl, the chemical shift between the NH proton of the salt and the CH_3 protons of the methanol was determined. The chemical shift of the OH proton of methanol relative to the CH_3 protons was determined using acidified solutions containing tetramethylammonium chloride at concentrations which were to be used for the pyridinium salts in the kinetic studies. Assuming that the NH–CH_3 chemical shift is independent of the salt and HCl concentration, the NH–OH chemical shift is taken as the difference between the NH–CH_3 and the OH–CH_3 chemical shifts. The value of the NH–OH chemical shift above 0.8° was obtained by extrapolation. At 25.1° for 2-picolinium, 4-picolinium, 2,4-lutidinium, and 2,6-lutidinium ions, this chemical shift is 625, 632, 621, and 628 Hz, respectively, at 60 MHz. The NH-proton resonance occurs at a lower field relative to the OH.

The value of the transverse relaxation time, T_2, was obtained either by line-width measurements of resonance lines in slow-passage spectra or by means of a modified Carr–Purcell spin–echo scheme.[6–8] The longitudinal relaxation time was measured using the null method.[6]

Results

By means of nmr spectroscopy, exchange between the NH proton of the pyridinium salts and the OH proton of methanol was studied. The lifetime, τ, for proton exchange involving the OH proton of methanol was obtained from the determination of the quantity $(1/T_2) - (1/T_2^0)$, for either the OH- or the CH_3-proton resonance of methanol. T_2^0 is the transverse relaxation time in the absence of exchange and T_2 is the transverse relaxation time of the exchange-broadened line. A detailed description of the manner in which τ can be obtained from the line shape of OH- and CH_3-proton

(3) E. Grunwald, C. Jumper, and S. Meiboom, *J. Amer. Chem. Soc.*, **84**, 4664 (1962).

(4) C. Ritchie and P. Heffley, *ibid.*, **87**, 5402 (1965).

(5) H. Brown, S. Johnson, and H. Podall, *ibid.*, **76**, 5556 (1954).

(6) H. Carr and E. Purcell, *Phys. Rev.*, **94**, 630 (1954).

(7) S. Meiboom and D. Gill, *Rev. Sci. Instrum.*, **29**, 688 (1958).

(8) S. Alexander, *ibid.*, **32**, 1066 (1961).

resonance has been given elsewhere[3,9,10] and will not be repeated here. The slow-passage CH$_3$-proton resonance was analyzed in the manner discussed in ref 3. The T_2 of CH$_3$ determined by spin–echo was analyzed in the manner described in ref 10, with the exception that the relation $T_2^0 = T_1$ was not used (T_1 is the longitudinal relaxation time). This relationship was not used because, for both the OH- and CH$_3$-proton magnetic moments, the longitudinal relaxation rate depends upon the rate of OH-proton exchange.[11] Instead, the T_2 of the CH$_3$ of acidified methanol was used as T_2^0 since the CH$_3$ is not exchange broadened under these conditions. Measurements of the T_2 of the CH$_3$ of acidified methanol containing various amounts of tetramethylammonium chloride indicate that the concentration effect on T_2^0 is small and can be neglected over the range of concentrations used in the kinetic studies.

For the OH-proton resonance, the equation[9] describing the line broadening in a system involving exchange between a dominant line and a weak one was employed because the OH-proton resonance was always much larger than the NH-proton resonance; i.e., the NH-proton fraction, P_{NH}, was always less than 10^{-2} (P_{NH} is defined as $[NH]/([NH] + [OH])$, where the brackets signify molar concentrations). The analysis of the broadening of the dominant OH-proton resonance paralleled the analysis described in ref 10 and 12.

Measurements of the CH$_3$-proton resonance were made using buffered methanol solutions. Nine buffer ratios, $[BH^+]/[B]$, ranging from 8.36×10^{-3} to 1.982 were used in the study of 2,6-lutidine. For 2,4-lutidine, 2-picoline, and 4-picoline, two were used. For all of the salts the concentration, $[BH^+]$, was varied from 10^{-4} to 2×10^{-3} M. Both 2,6- and 2,4-lutidine were studied at -24.5, $+0.8$, and $+25.1°$. 2- and 4-picoline were studied only at $25.1°$.

Under these conditions, the NH–OH proton exchange was found to follow the rate law[10,12-15] given by

$$R = k_+[MeOH_2^+] + k_-[MeO^-] + nk_2[BH^+][B] \quad (5)$$

The brackets signify molar concentrations. For each buffer ratio, a plot of R vs. $[BH^+][B]$ was made. In each case the plot proved to be linear, and the least-squares intercept, R_{int}, was assumed to be equal to the quantity $k_+[MeOH_2^+] + k_-[MeO^-]$. By substitution, this expression is put in the form given by

$$R_{int} = k_+K_A \frac{[BH^+]}{[B]} + k_- \frac{K_{auto}[B]}{K_A[BH^+]} \quad (6)$$

In this equation

$$K_A = [B][MeOH_2^+]/[BH^+]$$

and

$$K_{auto} = [MeOH_2^+][MeO^-]$$

Since the values of k_+[3] and k_-[3,16] and K_{auto}[17] are known at 25.0 and $-0.7°$, the value of K_A could be calculated at 25.1 and 0.8° using eq 6 and the values of the intercept, R_{int}, obtained from the least-squares fit.[18] For each salt, the value of K_A at 25.1° along with $\Delta H°$ for each of the lutidinium salts is listed in Table I. For comparison, the value of K_A for 4-picoline obtained by the differential potentiometric method[4] is also listed. As can be seen agreement between the two methods is quite good.

The slope of the plot of R vs. $[BH^+][B]$ obtained by least squares was assumed to be equal to nk_2, where n is the number of solvent molecules involved in the reaction.[14,15] The quantity nk_2 is obtained from these measurements because the multiplet of the CH$_3$- or OH-proton resonance makes it possible to distinguish between methanol molecules. Consequently, the lifetime for the OH-proton exchange measured from the line shape of the CH$_3$- or OH-proton resonance is affected by exchange between methanol molecules. In the present case, n was found to be nearly equal to 1 for 2,6-lutidine and is assumed to be the same for the other compounds. The manner in which this value was determined is discussed in the following paragraph.

Measurements of the T_2 of the OH-proton resonance were made using buffered solutions of methanol for only one compound, 2,6-lutidine. The buffer ratio, 49.34, was chosen to make $k_+[MeOH_2^+]/[MeOH]$ large compared to the indirect spin–spin coupling constant between the OH and the CH$_3$ protons. Consequently, the OH multiplet is collapsed to a single line, which cannot be broadened by exchange between methanol molecules. Thus under these conditions, the NH–OH exchange involves one weak line (the NH) and one strong line (the OH), and one can use the equation[9] describing the line broadening in a system involving exchange between a dominant line and a weak one. Furthermore, under these conditions, only the reaction given by eq 4 is important since eq 1 and 2 cannot affect the line shape and eq 3 is slow compared to eq 4. In addition, because the OH multiplet is completely col-

(9) S. Meiboom, J. Chem. Phys., 34, 375 (1961).

(10) M. Cocivera, E. Grunwald, and C. Jumper, J. Phys. Chem., 68, 3234 (1964).

(11) M. Cocivera, J. Chem. Phys., 47, 1112 (1967).

(12) M. Cocivera, J. Amer. Chem. Soc., 88, 672 (1966).

(13) The kinetic analysis follows closely the analysis given in a number of other papers,[11,12,14,15] and details will not be discussed here.

(14) E. Grunwald, C. Jumper, and S. Meiboom, J. Amer. Chem. Soc., 85, 522 (1963).

(15) Z. Luz and S. Meiboom, J. Chem. Phys., 39, 366 (1963).

(16) E. Grunwald, J. Phys. Chem., 71, 1846 (1967).

(17) J. Koskikallio, Suomen Kemistilehti, B30, 111, 157 (1957).

(18) In this fit, activity coefficients were not included in the term containing k_- in eq 6 (as was done by Grunwald[11]), since they introduce a correction which is negligible in the present case. This correction is negligible because low concentrations were used and, more important, the contribution to R made by $k_-[MeO^-]$ is small compared to other two terms in eq 5.

Table I: Kinetic Parameters for Methyl-Substituted Pyridinium Salts in Methanol at 25.1°

	Compound			
	2-PiHCl[a]	4-PiHCl[b]	2,4-LuHCl[c]	2,6-LuHCl[d]
$10^7 K_A^0$, M	7.61	8.91 8.13[e]	1.36 ± 0.1	1.53 ± 0.2
$10^{-3} k_a^0$, sec^{-1}	9.08	10.6	1.32	1.15
$10^{-10} k_{-a}^0$, M^{-1} sec^{-1}	1.2	1.2	0.97	0.75
$-b_{BHCl}$, M^{-1}	0.86[f]	0.96	0.95	0.92
$10^{-7} n k_2$, M^{-1} sec^{-1}	28.9 ± 2.7	34.4 ± 1.2	29.7 ± 3.5	8.74 ± 0.90
$10^{-7} k_2$, M^{-1} sec^{-1}	...	...	...	9.26
$E_a(k_a^0)$,[g] kcal mol^{-1}	9.2	9.7	9.5	9.5
$E_a(k_2)$,[h] kcal mol^{-1}	...	...	4.9	4.2
$\Delta H°(K_A^0)$,[i] kcal mol^{-1}	...	...	5.6	6.1
$E_a(k_{-a}^0)$,[i] kcal mol^{-1}	...	...	3.9	3.4

[a] 2-Picolinium chloride. [b] 4-Picolinium chloride. [c] 2,4-Lutidinium chloride. [d] 2,6-Lutidinium chloride. [e] Reference 4. [f] The value of b_{HCl} (at 25.1°) is -0.76. [g] Calculated using values of k_a^0 at 0.8, 25.1, and 39.8°. [h] Calculated using values of k_2 at -23.3, 0.8, and 25.1°. [i] Calculated using values at 0.8 and 25.1°.

lapsed, the methanol molecules cannot be distinguished, and the lifetime, which is measured, is for exchange involving the NH and OH of only one methanol molecule.[14,15] As a result, $R/[BH^+][B]$ was found to be constant and was assumed to be equal to k_2. The value of k_2 obtained in this manner for 2,6-lutidine is given in Table I. In addition, values of $n k_2$ at 25.1° obtained from the CH$_3$-proton resonance are listed in this table for each salt. From this table, it is clear that the ratio $n k_2 / k_2$ is very nearly 1 for 2,6-lutidine. Since the other compounds are similar, the ratio probably is close to 1 for each of them also.

The OH-proton resonance also was studied using methanol solutions containing BH$^+$Cl$^-$ and HCl. Under these conditions the OH multiplet is collapsed to a single line. The concentration of BH$^+$ was kept low so that the dominant line equation was applicable. Because of the excess HCl, the concentration of B is very low and the acid-dissociation step of reaction 3 is the main contribution to the exchange rate. The maximum contribution made by reaction 4 under these conditions was 38%, and usually it was much less than that.

The rate constant for the acid-dissociation step of reaction 3 was found to be slightly dependent upon the concentration of salt at 39.8, 25.1, and 0.8°. Values of k_a at various salt concentrations for 2,4- and 2,6-lutidine are listed in Table II. This concentration dependence cannot be accounted for by assuming the formation of the ion pair BH$^+$Cl$^-$ which does not react as rapidly as the dissociated ion BH$^+$. First, if ion pairs were to occur and the dissociation constant were small, $R/[BH^+]^{1/2}$ would be constant. This ratio is not constant for any of the salts. Second, if the dissociation constant were not small, a plot of k_a vs. [BH$^+$] would be asymptotic at low concentrations and would have a negative curvature. In each case, the plots are not asymptotic at low concentration, and the curvature is positive.

Consequently, this concentration dependence was considered to be a "salt effect," and the data in Table II as well as the data for 2- and 4-picoline were fit to the equation.[19]

$$\log k_a = \log k_a^0 + b_{BHCl}[BHCl] \qquad (7)$$

The values of b_{BHCl} and k_a^0 at 25.1° are listed in Table I for each salt. Also given in Table I is the value of E_a, the activation energy, calculated using values of k_a^0 determined at 39.8, 25.1, and 0.8°. In addition, using the data given in Table II, the concentration effect of HCl on the k_a for 2-picoline was calculated using eq 7. The value -0.76 M^{-1} calculated for the b_{HCl} of this compound is very close to the values of b_{BHCl} for the salts.

Finally, the value of k_{-a}^0 is calculated as k_a^0/K_A and is listed in Table I for each salt. As can be seen, the

Table II: Values of k_a in Methanol at 25.1° as a Function of Salt and HCl Concentration

Salt	[BH$^+$], M	[HCl], M	$10^{-3} k_a$, sec^{-1}
2,4-LuHCl	0.1319	0.02510	0.990
	0.06595	0.02510	1.09
	0.03298	0.02510	1.23
	0.01649	0.02510	1.39
2,6-LuHCl	0.09916	0.01480	0.930
	0.04958	0.01480	0.995
	0.02479	0.01480	1.04
	0.01240	0.01480	1.12
	0.00620	0.01480	1.13
2-PiHCl	0.03112	0.2081	6.29
	0.03112	0.1040	7.49
	0.03112	0.0520	8.21
	0.03112	0.0260	8.16

(19) E. Grunwald, J. Phys. Chem., 67, 2211 (1963).

value of k_{-a} is large and is nearly the same for all of the compounds.

Discussion

For a study of steric effects on proton exchange, methyl-substituted pyridines are advantageous because a change in the position of the methyl group from *ortho* to *para* to the nitrogen does not change the acid dissociation constant K_A significantly. This lack of dependence can be seen in Table I; 2-picoline (*o*-methyl) has essentially the same K_A as 4-picoline (*p*-methyl), and the K_A for 2,6-lutidine (two *o*-methyl groups) is very close to the value for 2,4-lutidine (one *o*- and one *p*-methyl group). Thus in comparing 2-picoline with 4-picoline and 2,6-lutidine with 2,4-lutidine, differences in acidity and basicity as measured by K_A are negligible.

As can be seen in Table I, the position of the methyl group has an effect only on the value of k_2, the rate constant for reaction 4. The value of k_2 for 2,6-lutidine is about one-third the value for 2,4-lutidine. On the other hand, 2-picoline and 4-picoline have about the same value for k_2. Obviously, two methyl groups *ortho* to the nitrogen can retard the rate of reaction 4, and one *o*-methyl group is not sufficient. Whether this retarding effect is a steric effect cannot be decided on the basis of the present data. A reduction in the rate due to steric hindrance should be reflected in the activation energy. However, a factor of 3 in the rate constant corresponds to less than 0.6 kcal in the activation energy. This difference is comparable to the experimental error for $E_a(k_2)$.

Indirect evidence concerning the nature of the retarding effect can be obtained by considering the possible transition state for this reaction. As indicated by the data presented earlier, this reaction is termolecular, *i.e.*, involves BH^+, B, and one solvent molecule in the transition state. Most likely, in this transition state, the nonbonded p electrons of the oxygen of the methanol molecule are involved, and the oxygen is probably pyramidal as shown in Figure 1. The positive charge is probably spread over the three sites involved
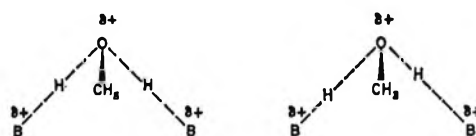
Figure 1. Possible transition states for reaction 4. B signifies the amine. The dashed lines indicate partial bonds.

in the reaction. Since the present data are consistent with a symmetrical (Figure 1a) and an unsymmetrical (Figure 1b) transition state, both possibilities are illustrated. For these transition states, models indicate that the two methyl groups of 2,6-lutidine can cause steric hindrance. Furthermore, the hindrance appears to be due mainly to the interaction of the methyl groups on one pyridine ring with the other pyridine ring and its methyl groups. The methyl group of the methanol molecule seems to be able to fit in with little difficulty. This conclusion is supported by the results obtained from a study of water solutions, which is presented in the following article.[20]

The values of $k_a{}^0$ are consistent with this conclusion. The value for 2,6-lutidine is almost the same as the value for 2,4-lutidine, indicating that any steric hindrance due to interaction between the methanol molecule and the two *o*-methyl groups of the 2,6-lutidinium ion is negligible in reaction 3.

The values of $k_{-a}{}^0$ given in Table I are of the same order of magnitude as values expected for diffusion-controlled reactions.[10,16] For comparison, the values of $k_{-a}{}^0$ for *p*-toluidine[10] and trimethylamine[16] are 1.04 $\times$ 10^{10} and 0.6 $\times$ 10^{10} M^{-1} sec^{-1}, respectively. The fact that $k_{-a}{}^0$ is essentially the same for all of these compounds is also consistent with a diffusion-controlled reaction. On the other hand, the activation energies for $k_{-a}{}^0$ listed in Table I are larger than might be expected for a diffusion-controlled reaction. Activation energies for viscous flow and for self-diffusion of methanol are about 2 kcal.[16]

(20) M. Cocivera, *J. Phys. Chem.*, **72**, 2520 (1968).

Nuclear Magnetic Resonance Study of Proton Exchange Involving

Methyl-Substituted Pyridinium Salts in Water

by Michael Cocivera

Bell Telephone Laboratories, Inc., Murray Hill, New Jersey 07974 (*Received January 5, 1968*)

The nuclear magnetic resonance line-broadening technique has been used to study proton-exchange reactions involving methyl-substituted pyridinium salts and solvent water. The results are compared with those obtained when methanol is the solvent. As in the case of methanol, only the reaction $BH^+ + H_2O + B \xrightarrow{k_2} B + H_2O + BH^+$ is found to depend upon the position of the methyl groups. The value of k_2 for each compound indicates that the rate is retarded when B has two methyl groups *ortho* to the nitrogen of the pyridine ring. Furthermore, the reduction in rate in water is almost the same as the reduction in methanol, indicating that the retarding effect of the methyl group of methanol is minor in this reaction. For the reaction $BH^+ + H_2O \underset{k_{-a}}{\overset{k_a}{\rightleftarrows}} B + H_3O^+$ neither k_a nor k_{-a} depends upon the position of the methyl groups. However, k_a depends upon the degree of methyl substitution, whereas k_{-a} does not. Also, the value of k_{-a} is of the order of magnitude expected for diffusion-controlled reactions. In contrast with methanol, the value of k_a in water is found to depend strongly upon the concentration of HCl. This dependence is consistent with a mechanism proposed by Grunwald, who found a similar effect for trimethylammonium ion in water.

Introduction

In the previous article,[1] the proton-exchange reactions given by eq 1-4 were studied for methyl-substituted pyridinium salts in methanol using the nmr line-broadening technique. In these equations, R

$$ROH + ROH_2^+ \xrightarrow{k_+} ROH_2^+ + ROH \quad (1)$$

$$RO^- + ROH \xrightarrow{k_-} ROH + RO^- \quad (2)$$

$$BH^+ + ROH \underset{k_{-a}}{\overset{k_a}{\rightleftarrows}} B + ROH_2^+ \quad (3)$$

$$BH^+ + \underset{R}{O-H} + B \xrightarrow{k_2} B + \underset{R}{H-O} + BH^+ \quad (4)$$
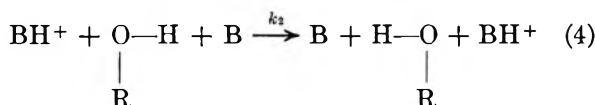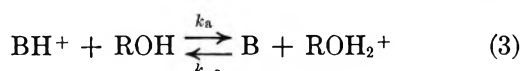
signifies the CH_3 group and B signifies the amines, 2-picoline, 4-picoline, 2,4-lutidine, and 2,6-lutidine. The structures of these amines are given in the previous article.[1] It was found that one methyl group *ortho* to the nitrogen of the pyridine ring had no retarding effect on reactions 3 and 4, whereas two *o*-methyl groups retarded reaction 4 but not reaction 3.

Since reaction 4 involves one methanol molecule,[1] steric hindrance owing to the methyl group of this molecule might be partially responsible for the observed retarding effect. Information concerning the importance of the retarding influence of this methyl group can be obtained by studying reaction 4 in water, since the methyl group is replaced by a hydrogen atom in this solvent. Thus if steric hindrance due to the methyl group of methanol is important in reaction 4, the relative rates for this reaction in water will differ from those observed in methanol. For this reason, a

study of reaction 4 in water was undertaken. To compare the effects of the two solvents, the other reactions were studied, also. The results of this study are presented in this article.

In this study, reaction 3 was found to depend upon the concentration of HCl. This effect was observed earlier by Grunwald[2] for proton exchange involving trimethylammonium ion and water, and the mechanism which he proposed was found to fit the data for the pyridinium salts

$$BH^+ \cdot \cdot OH_2 + H_2O \underset{k_{-a}}{\overset{k_a}{\rightleftarrows}} B \cdot \cdot HOH + H_3O^+$$

$$B \cdot \cdot HOH + H_2O \xrightarrow{k_H} B \cdot \cdot H_2O + HOH \quad (5)$$
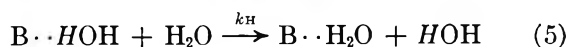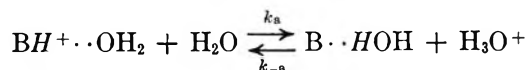
The first step of this mechanism is the reversible acid dissociation of BH^+. In this step, the proton of BH^+ jumps to a water molecule but remains attached to B through a hydrogen bond. The proton exchange occurs when the hydrogen bond is broken and is replaced by a hydrogen bond to a different proton (the second step of this mechanism).

In methanol,[1] the retarding effect of HCl appears to be a "salt effect," and the mechanism given by eq 5 could not be detected, indicating that k_H for the methyl-substituted pyridines is larger in methanol than in water. In other words, the lifetime for the hydrogen bond between the methyl-substituted pyridine and solvent is longer in water than in methanol. Also, the value of k_H is the same for both the mono- and dimethylpyridines, whereas K_A, the equilibrium constant

(1) M. Cocivera, *J. Phys. Chem.*, **72**, 2515 (1968).

(2) E. Grunwald, *ibid.*, **67**, 2211 (1963).

for the acid dissociation given by eq 3, decreases by a factor slightly over 5 when the number of methyls on the ring increases from 1 to 2. Thus the differences in basicity, as indicated by the differences in K_A, are not reflected in the relative lifetimes for the hydrogen bond between the methyl-substituted pyridines and water.

As in the case of methanol, only the reaction given by eq 4 is retarded when two methyl groups are *ortho* to the nitrogen of the pyridine ring. For k_2, the ratio 2,4-lutidine: 2,6-lutidine is about 3:1. The fact that this ratio is also about 3:1 when methanol is the solvent[1] indicates that the retarding effect of the methyl group of methanol is small in reaction 4.

Experimental Section

Reagents and Solutions. The methyl-substituted pyridines were prepared and were purified as described in the previous article.[1] Water was distilled twice in an all-glass apparatus. Water enriched in [17]O was obtained from Yeda.[3] Solutions were prepared and were analyzed by standard quantitative techniques.

Nmr Measurements. Measurement of the value of the transverse relaxation time, T_2, and the longitudinal relaxation time, T_1, were performed as described in the previous article.[1] For each salt, the chemical shift of the NH-proton resonance relative to the OH proton of water was obtained at 0.8 and 25.1° in the following manner. From a slow-passage spectrum of a water solution containing 12 M HCl, 1 M pyridinium salt, and 0.1 M tetramethylammonium chloride, the chemical shift of the NH proton relative to the CH₃-proton resonance of the tetramethylammonium ion was obtained. The chemical shift of the OH relative to the CH₃ of the tetramethylammonium ion was obtained from the slow-passage spectrum of a water solution containing 0.1 M tetramethylammonium ion. Assuming that the NH–CH₃ chemical shift is independent of the concentration of the salt and HCl, the NH–OH chemical shift is taken as the difference between the NH–CH₃ and the OH–CH₃ chemical shifts. At 25.1°, the values of this chemical shift for 2-picoline, 4-picoline, 2,4-lutidine, and 2,6-lutidine are 562, 549, 561, and 559 Hz, respectively, at 60 MHz. The NH-proton resonance occurs at lower field relative to the OH-proton resonance.

Results

As in the case of methanol,[1] exchange between the NH proton of the pyridinium salts and the OH proton of water was studied by means of nmr spectroscopy. Two nmr systems were studied. For each system, the analysis of the broadening was made using the equation derived by Meiboom[4] to describe the broadening due to exchange between a dominant line and a number of weak lines. In one system, the OH-proton resonance of water is the dominant line and the weak line is the

NH-proton resonance of the pyridinium salt. In the other system, the concentration of the pyridinium salt is very low and [17]O-enriched water is used. The exchange in this system involves a dominant [16]OH-proton line and six weak [17]OH-proton lines, since [17]O has a spin of ⁵/₂. The pyridinium salt catalyzes the exchange between [16]OH and [17]OH. A number of studies using [17]O-enriched water have been reported by Luz and Meiboom.[5] The broadening in these systems is described by[4]

$$\Delta = \frac{1}{T_2} - \frac{1}{T_2^0} = \tau \sum_{i \neq 1}^{n} \frac{p_i \delta_i^2}{1 + \tau^2 \delta_i^2} \qquad (6)$$

In this equation, T_2 is the transverse relaxation time of the exchange-broadened dominant line, T_2^0 is the transverse relaxation time of the dominant line in the absence of exchange, τ is the average lifetime between proton exchanges, δ_i is the chemical shift (in rad/sec) between the ith line and the dominant line, and p_i is the fraction of the protons in the ith environment and

$$\sum_{i=1}^{n} p_i = 1$$

The reaction given by eq 3 was studied using the system consisting of the dominant OH- and the weak NH-proton lines. The T_2 measurements were made using aqueous solutions containing the pyridinium salt and HCl. Because of the presence of HCl, the reaction given by eq 1 is very fast, so that the broadening due to proton exchange between H₂[16]O and the small amount of H₂[17]O occurring in unenriched water is negligible. In addition, because the HCl makes the concentration of the base B very small, the reaction given by eq 4 does not make an appreciable contribution to the line broadening. Thus only the rate of the acid dissociation reaction given in eq 3 is measured under these conditions. That is, R, the rate for proton exchange, is equal to $k_a[BH^+]$. (The brackets signify concentration.)

In contrast to methanol, the rate constant k_a for this reaction in water is not dependent upon the concentration of the salt. In Table I, the value of k_a at various salt concentrations is listed for 2,4- and 2,6-lutidinium chloride at 25.1 and 49.4°. As can be seen from the data in this table, k_a does not depend upon the concentration of salt. On the other hand, the value of k_a depends upon the concentration of HCl. This dependence can be seen in Table II, in which k_a at various concentrations of HCl is listed for each of the salts at 25.1°. As the HCl concentration is increased, k_a decreases monotonically.

(3) Yeda Research and Development Co., The Weizman Institute of Science, Rehovot, Israel.

(4) S. Meiboom, *J. Chem. Phys.*, **34**, 375 (1961).

(5) (a) Z. Luz and S. Meiboom, *ibid.*, **39**, 366 (1963); (b) Z. Luz and S. Meiboom, *J. Amer. Chem. Soc.*, **85**, 3923 (1963); (c) Z. Luz and S. Meiboom, *ibid.*, **86**, 4764 (1964); (d) Z. Luz and S. Meiboom, *ibid.*, **86**, 4766 (1964).

Table I: Values of k_a in Water at Various Concentrations of Salt

[2,6-LuHCl],[a] M	$10^{-3}k_a$, sec^{-1}	[2,4-LuHCl],[b] M	$10^{-3}k_a$, sec^{-1}
	25.1°		
0.3922	3.31	0.4169	4.67
0.1961	3.47	0.2084	4.33
0.09805	3.46	0.1042	4.05
0.04903	3.49	0.05210	5.11
0.02450	3.51	0.02610	5.13
	49.4°		
0.3888	15.6	0.4133	17.4
0.1944	15.0	0.2066	17.7
0.09722	14.8	0.1033	17.0
0.04861	14.3	0.05165	17.0
0.02430	15.4	0.02588	17.9

[a] 2,6-Lutidinium chloride; all solutions contained 0.02178 M HCl. [b] 2,4-Lutidinium chloride; all solutions contained 0.02178 M HCl.

Table II: Values of k_a in Water at 25.1° for Various HCl Concentrations

[HCl], M	2-PiHCl[a]	4-PiHCl[b]	2,4-LuHCl[c]	2,6-LuHCl[d]
		$10^{-2}k_a$, sec^{-1}		
2.310	35.3	34.5	6.67	6.18
1.155	95.0	109	21.9	15.2
0.5775	143	178	...	...
0.2888	179	223	...	...
0.1444	203	252	...	...
0.07220	219	280	42.1	33.2
0.03610	260	279	45.2	34.1

[a] 0.3030 M 2-picolinium chloride. [b] 0.2540 M 4-picolinium chloride. [c] 0.2968 M 2,4-lutidinium chloride. [d] 0.2970 M 2,6-lutidinium chloride.

Grunwald[2] has found a similar dependence on the HCl concentration for the k_a of trimethylammonium ion in water. He also found that k_a decreases slightly as the concentration of trimethylammonium chloride increases. This "salt effect" was fit to eq 7. He assumed that HCl also has a "salt effect" on k_a and that b_{HCl} for HCl is equal to b_{BHCl} for trimethylammonium chloride. After correcting for the HCl "salt effect," he found that k_a still is a function of the HCl concentration. He found that the mechanism given by eq 5 fits the data adequately. According to this mechanism, the dependence of k_a on the HCl concentration is given

$$k_a = k_a{}^0(1 + k_{-a}{}^0[\text{HCl}]/k_H)^{-1} \qquad (8)$$

The data given in Table II have been analyzed using this equation. In the treatment of these data, no correction was made for an HCl salt effect, since the

$$\log k_a = \log k_a{}^0 + b_{BHCl}[\text{BHCl}] \qquad (7)$$

data given in Table I indicate that k_a for the methyl-substituted pyridinium salts is not dependent on salt concentration up to a concentration of 0.4 M. A correction was made for the increase in viscosity of the solution caused by the HCl at each concentration. Data at 30° for the relative viscosity as a function of HCl concentration were obtained from Grunwald.[6] The viscosity of 2.31 M HCl is only 13% larger than the viscosity of pure water. Using eq 8 and the data in Tables I and II, $k_a{}^0$ and $k_{-a}{}^0/k_H$ were calculated for each salt. Since K_A, the acid-dissociation equilibrium constant, could be determined and since it is equal to $k_a{}^0/k_{-a}{}^0$, the values of $k_{-a}{}^0$ and k_H could be obtained for each pyridinium salt. The value at 25.1° for each of these rate constants and the value of K_A, which was determined in the manner described in the next paragraph, are listed in Table III. Activation energies are also listed in this table. For 2- and 4-picoline, $E_a(k_a{}^0)$ was calculated by least squares using values of k_a at four temperatures, 10.4, 25.1, 34.9, and 49.4°. Values of $k_a{}^0$ at 24.1, 34.9, 49.4, and 63.9° were used to calculate $E_a(k_a{}^0)$ for 2,4- and 2,6-lutidine. The values of $\Delta H°(K_A)$ and $E_a(k_{-a})$ for 2,4- and 2,6-lutidine were calculated using values of K_A and, consequently, $k_{-a}{}^0$ at 25.1 and 49.4°.

For 2,4- and 2,6-lutidine, the value of K_A was determined by measuring the rates of the reactions given by eq 1 and 2 in [17]O-enriched water which was buffered by the lutidine and its conjugate acid. Under these conditions, the reaction given by eq 3 is negligible, and R, the rate of proton exchange, is given by

$$R = k_+[\text{H}_3\text{O}^+] + k_-[\text{OH}^-] + nk_2[\text{BH}^+][\text{B}] \qquad (9)$$

In this equation, the brackets signify molar concentrations and n is the number of solvent molecules involved in reaction 4. As in the case of analysis of the CH$_3$-proton resonance of methanol,[1] the factor n occurs in eq 9 because the electron-coupled [17]OH spin–spin interaction makes it possible to distinguish between water molecules. The quantities k_+,[7] k_-,[7] and K_{auto}[8] are known, and the analysis used to determine K_A and nk_2 is identical with that employed in the methanol study.[1] For 2,4- and 2,6-lutidine, K_A and nk_2 at 25.1° are listed in Table III. The values of $\Delta H°(K_A)$ and $E_a(nk_2)$ listed in this table were calculated using values of K_A and nk_2 determined at 25.1 and 49.4°. For comparison, the values of K_A determined by other workers are listed also.[9-11] The values of K_A and nk_2

(6) E. Grunwald, Brandeis University, personal communication.

(7) Z. Luz and S. Meiboom, J. Amer. Chem. Soc., 86, 4768 (1964).

(8) H. Harned and R. Robinson, Trans. Faraday Soc., 36, 977 (1940).

(9) R. Andon, J. Cox, and E. Herington, ibid., 50, 923 (1954).

(10) H. Brown and X. Mihm, J. Amer. Chem. Soc., 77, 1723 (1955).

(11) H. Brown, D. McDaniel, and O. Hafliger in "Determination of Organic Structures by Physical Methods," E. A. Braude and F. C. Nachod, Ed., Academic Press Inc., New York, N. Y., 1955.

Table III: Kinetic Parameters for the Methyl-Substituted Pyridinium Salts in Water at 25.1°

	Compound			
	2-PiHCl	4-PiHCl	2,4-LuHCl	2,6-LuHCl
$10^7 K_A$, M	11.0[a]	10.5[a]	1.73	1.84
			2.29[a]	1.91[a]
			1.62[c]	1.78[b]
$10^{-3}k_a^0$, sec^{-1}	26.0	27.9	4.81	3.45
$10^{-10}k_{-a}^0$, M^{-1} sec^{-1}	2.36	2.66	2.78	1.88
$10^{-10}k_H$, sec^{-1}	1.4 ± 0.3	2.1 ± 0.9	1.7 ± 0.7	1.4 ± 0.4
$10^{-7}nk_2$, M^{-1} sec^{-1}	...	...	15.0	6.01
$E_a(k_a^0)$, kcal/mol	9.1[d]	8.1[d]	11.0[e]	11.4[e]
$E_a(nk_2)$,[f] kcal/mol	...	...	3.1	2.2
$\Delta H°(K_A)$,[f] kcal/mol	...	...	8.7	9.1
$E_a(k_{-a}^0)$,[f] kcal/mol	...	...	1.7	2.4

[a] R. Andon, J. Cox, and E. Herington, *Trans. Faraday Soc.*, **50**, 923 (1954). [b] H. Brown and X. Mihm, *J. Amer. Chem. Soc.*, **77**, 1723 (1955). [c] H. Brown, D. McDaniel, and O. Haflinger in "Determination of Organic Structures by Physical Means," E. A. Braude and F. C. Nachod, Ed., Academic Press Inc., New York, N. Y., 1955. [d] Calculated using values of k_a^0 at 10.4, 25.1, 34.9, and 49.4°. [e] Calculated using values of k_a^0 at 25.1, 34.9, 49.4, and 63.9°. [f] Calculated using values at 25.1 and 49.4°.

were not determined for the picolines, and as indicated, the K_A values listed in the table were obtained by other workers.[9]

Discussion

From Table III, it is clear that the position of the methyl group does not affect the value of K_A appreciably. The value of K_A for 2-picoline is essentially the same as the value for 4-picoline, and the value for 2,4-lutidine is almost identical with the value for 2,6-lutidine. On the other hand, for the lutidines, the value of nk_2 depends on the position of the methyl groups. The value of nk_2 for 2,6-lutidine is $1/2.5$ the value of 2,4-lutidine. Since these compounds have the same K_A, the difference in the rate of reaction 4 cannot be due to differences in the acidity or basicity of the reactants.

Whether this reduction in rate for 2,6-lutidine is due to steric hindrance caused by the two *o*-methyl groups cannot be decided on the basis of the present data. A reduction in rate due to steric hindrance should be reflected in the activation energies. However, a factor of 2.5 corresponds to a difference of less than 0.5 kcal in the activation energy, and this difference is comparable to the experimental error. Consequently, comparison of activation energies gives no conclusive information concerning the nature of the retarding effect. As mentioned in the previous article,[1] space-filling models indicate that the methyl groups could cause steric hindrance in a transition state such as the one illustrated in Figure 1. However, this information can only be regarded as very weak support for a steric hindrance model.

In methanol,[1] the value of k_2 for 2,6-lutidine is $1/3.3$ the value for 2,4-lutidine. The fact that the ratio in water in nearly the same as the ratio in methanol indicates that steric hindrance caused by the methyl group of methanol is minor for reaction 4.

Since the ratio $k_2(2,4\text{-Lu}):k_2(2,6\text{-Lu})$ is essentially

a   b
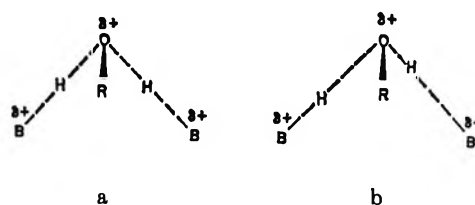
Figure 1. Possible transition states for reaction 4. B signifies the amine and R signifies either H or CH_3. The dashed lines indicate partial bonds.

the same in water and methanol, one can expect that the relative rates for 2- and 4-picoline will not change appreciably when the solvent is changed from methanol to water. For this reason, reaction 4 was not studied in water for the picolines. In methanol,[1] 2- and 4-picoline have essentially the same rate constant for this reaction, indicating that one methyl group *ortho* to the nitrogen is not sufficient to retard it. Thus, for the methyl-substituted pyridinium salts, two methyl groups *ortho* to the nitrogen of the ring are necessary to inhibit reaction 4, and the retarding effect of the methyl group of methanol is minor.

The values of k_a^0 listed in Table III indicate that the position of the methyl group(s) has little effect on the rate for the acid-dissociation reaction given in eq 3. The value for 2-picoline is almost the same as the value for 4-picoline. Likewise, there is no appreciable difference between the values for the lutidines. In comparing the picolinium salts with the lutidinium salts, the difference in rate parallels the difference in the K_A values, indicating that the difference in rate for this reaction is due mainly to the difference in the acidity of the salts.

For comparison, the values of k_a^0 in water and methanol at 25.1° are listed in Table IV. As can be seen, changing the solvent from water to methanol reduces the value of k_a^0 for all of the salts. The

present data give no information concerning the cause of this reduction. However, the results for reaction 4 indicate that the reduction probably is not due to steric hindrance caused by the methyl group of methanol. As shown earlier, the ratio $k_2(2,4\text{-Lu}):k_2(2,6\text{-Lu})$ is nearly the same in water and methanol, indicating that the retarding effect of the methyl group of methanol is minor in this reaction. Thus because steric hindrance by the methyl group is small for reaction 4, it probably is small for reaction 3.

Table IV: Values of $k_a{}^0$ aud $k_{-a}{}^0$ at 25.1° in Water and Methanol

Compd	$10^{-3}k_a{}^0$, sec^{-1}		$10^{-10}k_{-a}{}^0$, M^{-1} sec^{-1}	
	H$_2$O	MeOH[a]	H$_2$O	MeOH[a]
2-PiHCl	26.0	9.08	2.36	1.19
4-PiHCl	27.9	10.6	2.66	1.19
2,4-LuHCl	4.81	1.32	2.78	0.97
2,6-LuHCl	3.45	1.15	1.88	0.75
(Me)$_3$NHCl[b]	0.0047	0.0007	3.0	0.6

[a] Reference 1. [b] Trimethylammonium chloride.[12]

The values of $k_{-a}{}^0$ listed in Table IV are of order of magnitude expected for diffusion-controlled reactions.[12] For 2,4- and 2,6-lutidine, $E_a(k_{-a}{}^0)$ is 1.7 and 2.4 kcal/mol, respectively, in water, and in methanol it is 3.9 and 3.4 kcal/mol, respectively. These values were calculated using values of $k_{-a}{}^0$ determined at 25.1 and 49.4° in water and 0.8 and 25.1° in methanol. Activation energies for viscous flow and for self-diffusion of methanol are about 2 kcal.[12]

The values of k_H at 25.1° are listed in Table III for each salt. As indicated by the mean deviations listed in this table, all of these values are within experimental error of each other. According to the mechanism given by eq 5, k_H is the rate constant for breaking the hydrogen bond between the nitrogen of the amine and the proton bonded to the oxygen of the water molecule. On the basis of the K_A values given in Table III, the picolines are less basic than the lutidines. Thus the fact that k_H for the picolines is about the same as the k_H for the lutidines indicates that the rate for breaking the hydrogen bond is not determined solely by the basicity of the amine.

In a study of a series of alkyl-substituted amines in water, Grunwald and Ralph[13] also found that the relative k_H values did not correspond to the relative basicities of the amines. They suggested that the relative values of k_H might possibly depend mainly on the London dispersion interaction between the substituted amine and the solvent; i.e., as the dispersion interaction increases, k_H decreases. Since the dispersion interaction is expected to be nearly the same for all of the methyl-substituted pyridines, the lack of dependence of

k_H on the basicity is consistent with this suggestion. However, the k_H values are not in complete accord with this suggestion. Comparison of the values of k_H for these compounds with those of other amines suggests that the values for the methyl-substituted pyridines are larger than would be expected if the London dispersion interaction were mainly responsible for the relative k_H values. For example, for trimethylamine and triethylamine, the dispersion interaction is expected to be smaller than the interaction for the methyl-substituted pyridines. Consequently, k_H for the alkyl amines should be larger than the values for the pyridines. The k_H values for trimethylamine (10^{10})[13] and triethylamine (3.8×10^9)[13] are not consistent with this conclusion. Thus the results for the methyl-substituted pyridines indicate that neither the basicity of the amine nor the London dispersion interaction is the sole cause for the relative k_H values.

Most likely, both effects are important. While the dispersion effect is expected to be larger for the pyridines, the alkylamines are more basic (K_A for the pyridines is more than 10^3 larger than K_A for the alkylamines[13]). Thus the increased basicity of the alkylamines may compensate for their smaller dispersion interaction compared to the pyridines, to give the relative k_H values which are observed.

In the methanol study,[1] no evidence was obtained for the occurrence of reaction 5. Although the value of k_a decreases slightly as the concentration of HCl is increased, a comparable effect is observed when the concentration of the pyridinium salt is increased. In both cases, the concentration dependence was fit to eq 7. For all of the pyridinium salts, the value of b_{BHCl} is around -0.90. For 2-picolinium chloride, the value of b_{HCl} is -0.76. Thus, in methanol, the dependence of k_a on the concentration of HCl appears to be a salt effect.

The large concentrations of HCl used in water could not be used in methanol because of reaction of HCl with methanol. As a result, the maximum concentration of HCl was only 0.2 M in the methanol study. However, the data in Table II indicate that a decrease in addition to the decrease due to the salt effect should be observed at this concentration of HCl if the value of k_H in methanol were about the same as the value in water. The absence of this additional decrease in k_a indicates that the value of k_H in methanol is probably larger than the value in water.

In order to describe the transition states for the proton-exchange reactions in water, it is necessary to know the number of water molecules involved. For reaction 4, the experimental method used in the methanol study[1] could not be used because of experimental

(12) E. Grunwald, J. Phys. Chem., **71**, 1846 (1967).

(13) E. Grunwald and E. Ralph, III, J. Amer. Chem. Soc., **89**, 4405 (1967).

difficulties.[14] However, it seems likely that only one water molecule is involved in this reaction. This conclusion is based on the fact that when reaction 4 involves trimethylamine and its conjugate acid, only one solvent molecule is involved when the solvent is either water[5a] or methanol.[12] In view of this evidence, it seems reasonable to assume that one water molecule is involved for the methyl-substituted pyridines, since in methanol it was found[1] that one methanol molecule is involved for these compounds. Thus the transition state for this reaction is probably similar to the one suggested in the methanol article.[1] In the transition state, the nonbonded p electrons of the oxygen of the water are probably involved and the oxygen is probably pyramidal as shown in Figure 1. Whether this transition state is symmetric (a) or unsymmetric (b) cannot

be decided on the basis of the present information. As a result, both possibilities are illustrated in this figure.

The number of solvent molecules involved in the acid dissociation step given in eq 5 is not known. However, the fact that reaction 5 occurs indicates that at least two water molecules must be involved. Thus the transition state for the acid dissociation step may be identical with the one shown in Figure 1, with the exception that one B molecule is replaced by a water molecule which may or may not be hydrogen-bonded to other water molecules.

(14) The experiment which would indicate the number of solvent molecules involved in this reaction requires that $[BH^+]/[B] \geq 100$. Because the methyl-substituted pyridines are not sufficiently strong bases, it was not possible to determine accurately by potentiometric titration the value of [B] in solutions containing this buffer ratio.

Standard Partial Molal Heat Capacities of Sodium Tetraphenylboron

in Aqueous Solution from 0 to 90°.   Effect of Water

Structure and Hydrophobic Hydration

by S. Subramanian and J. C. Ahluwalia[1]

Department of Chemistry, Indian Institute of Technology, Kanpur, India   *(Received January 9, 1968)*

The standard partial molal heat capacities of sodium tetraphenylboron in aqueous solution from 0 to 90° have been determined by measuring the integral heats of solution as a function of temperature over the range 5–85°. ΔC_p^0 and $\bar{C}_{p2}^0$ values at all temperatures studied are positive and larger than those reported for any other solute. The plots of ΔC_p^0 and $\bar{C}_{p2}^0$ against temperature show two discontinuities which correspond to a minimum around 50° ($\Delta C_p^0 = 154$ cal deg^{-1} mol^{-1}) and a maximum around 70° ($\Delta C_p^0 = 245$ cal deg^{-1} mol^{-1}). The minimum is explained in terms of "hydrophobic interactions" and the maximum is presumed to be due to a reduction in the structure-making capacity of the solute above 70°. No quantitative interpretation for the discontinuities is available at present. This is the first instance that such pronounced discontinuities are observed in the temperature dependence of partial molal heat capacities of solutes (containing a large amphiphilic ion) in aqueous solution. This work suggests the need of more experimental data on the temperature dependence of thermodynamic properties of aqueous solutions of nonpolar solutes or solutes containing nonpolar groups in order to have a better understanding of the structure of aqueous solutions.

Introduction

The structural aspects of ion–solvent interactions in aqueous solutions have been discussed in great detail by Frank and Wen.[2] Relatively small and multivalent ions have a net structure-making effect, while most anions and large monovalent cations have a net structure-breaking effect on the water structure. That normal 1:1 electrolytes cause the disruption of water structure has been confirmed by various experimental

means.[2] Such electrolytes increase the viscosity of water and give rise to negative partial molal heat capacities in aqueous solutions.[2] As the temperature is increased, the net structure-breaking influence of such electrolytes decreases, thereby causing a diminishing of the viscosity enhancement[3] and the negative

(1) To whom all correspondence should be addressed.

(2) H. S. Frank and W. Y. Wen, *Discussions Faraday Soc.*, **24**, 133 (1957).

partial molal heat capacities. However, nonpolar solutes or solutes containing nonpolar groups in aqueous solutions display a behavior unlike those of normal electrolyte solutions. For example, the aqueous solutions of tetraalkylammonium halides have been found to give positive viscosity B coefficients[4] which are highly dependent on temperature, large apparent molal heat capacities,[2] peculiar activity coefficients,[5] anomalous concentration dependence of the partial molal volumes,[6] and characteristic mobilities for the ions.[7] These observations are in conformity with the view that nonpolar solutes and ions with large nonpolar groups promote the water structure by increasing its "ice-likeness" through the formation of Frank–Evans "icebergs."[8] It would be interesting to compare the structure-making capacity of sodium tetraphenylboron in aqueous solution with that of tetraalkylammonium halides. The former has a large nonpolar aromatic substituent in the symmetrical anion, while in the latter the substituents in the symmetrical cation are large nonpolar aliphatic hydrocarbon residues. This comparison would at once indicate the similarity and also variance, if any, in the two classes of compounds.

The partial molal heat capacities of solutes in aqueous solutions is a convenient property for studying the influence of the solutes on the structure of water. Since very little precise data are available on the temperature dependence of properties in aqueous solutions, the present work was undertaken to obtain accurate partial molal heat capacities of aqueous solutions of $NaBPh_4$ as a function of temperature over a large range of temperature. The results obtained from such an investigation are expected to be of great help toward a better understanding of the structure of aqueous solutions.

An easy and accurate method of determining the partial molal heat capacities of electrolytes at infinite dilution is the "integral-heat method"[9] which has specific and distinct advantages over the specific heat method, since in the latter the reliability of extrapolation from concentrated solutions to infinite dilution is subject to question. The integral-heat method involves measurements of the heat of solution at several temperatures. The heat involved in the dissolution of a solute in water is expressed as

$$\Delta H_s = n_1 \bar{H}_1 + n_2 \bar{H}_2 + n_1 \bar{H}_1^0 - n_2 H_2 \quad (1)$$

where $\bar{H}_1$ and $\bar{H}_2$ are the partial molal heat contents of water and the solute, respectively, $\bar{H}_1^0$ is the heat content of pure water, H_2 is the heat content of pure solute, and n_1 and n_2 represent the number of moles of water and solute, respectively. At infinite dilution

$$\Delta H_s^0 = n_2 \bar{H}_2^0 - n_2 H_2 \quad (2)$$

Over sufficiently small temperature intervals, the temperature coefficient of the above expression is

$$\left(\frac{d\Delta H_s^0}{dT}\right)_p = \Delta C_p^0 = n_2 \bar{C}_{p_2}^0 - n_2 C_{p_2} \quad (3)$$

where ΔC_p^0 is the change in the heat capacity for the dissolution, C_{p_2} is the heat capacity of the pure solute, and $\bar{C}_{p_2}^0$ is the partial molal heat capacity of the solute in solution at infinite dilution. So an accurate determination of ΔH_s^0 at various temperatures leads to values of partial molal heat capacities as a function of temperature.

Experimental Section

Apparatus. The submarine calorimeter used in this study was essentially similar to that used by Cobble, et al.[9,10] A 550-ml glass dewar-type flask was fitted to a standard 71/60 taper joint and an evacuated stopper. The stopper contained four 10-mm exit tubes extending to a height of 5 cm above the top of the stopper. One of the tubes was fused to a standard joint to which a precision-bore tubing was attached to house the stirrer shaft. The other three tubes were meant for introducing a heater, a thermistor, and an ordinary Pyrex tubing closed at one end to which the sample bulbs were attached. The stirrer was driven by an ac–dc motor at ~500 rpm. The sample bulbs could be broken by moving the tube vertically downward and by hitting the bulbs against the anvil at the bottom of the calorimeter. The calorimeter was immersed in a thermostat whose temperature was kept constant to $\pm 0.002°$ at lower temperatures and to $\pm 0.005°$ at higher temperatures using a Sargent Thermonitor. Extra heaters were used when working at higher temperatures.

The heating element was made by winding 2 ft of no. 36 manganin wire noninductively around 4-mm Pyrex tubing which was painted with Araldite and which was baked for several hours at 60°. Copper leads (no. 18) were used to carry the current. The potential leads for measuring the potential across the heater were attached to the midportion of the current-carrying leads. The lead wires of the precision thermistor (Yellow Springs Instruments, Yellow Springs, Ohio) were soldered to copper leads, which in turn were soldered to a two-core shielded cable connected to an amphenol in order to be fed into the Wheatstone-bridge circuit.

The Wheatstone bridge was constructed from precision decade resistors (Electro Scientific Industries, Portland, Ore.) and precision resistors. Three legs of

(3) M. Kaminsky, *Discussions Faraday Soc.*, **24**, 171 (1957).

(4) R. L. Kay, T. Vituccio, C. Zawoyski, and D. F. Evans, *J. Phys. Chem.*, **70**, 2336 (1966).

(5) S. Lindenbaum and G. E. Boyd, *ibid.*, **68**, 911 (1964).

(6) W. Y. Wen and S. Saito, *ibid.*, **68**, 2639 (1964).

(7) R. L. Ray and D. F. Evans, *ibid.*, **70**, 2325 (1966).

(8) H. S. Frank and M. W. Evans, *J. Chem. Phys.*, **13**, 507 (1945).

(9) C. M. Criss and J. W. Cobble, *J. Amer. Chem. Soc.*, **83**, 3223 (1961).

(10) J. C. Ahluwalia and J. W. Cobble, *ibid.*, **86**, 5377 (1964).

the Wheatstone bridge consisted of the thermistor (3 kilohms for low temperatures and 10 kilohms for higher temperatures), and the 1.2-kilohm dekastat (in 0.1-ohm steps) in series with a fixed 49.9-kilohm resistor. The fourth leg consisted of a 12-kilohm dekastat in (1-ohm steps). The 12-kilohm dekastat was used to match the thermistor at all temperatures for a rough balance, and finer manipulations were always done with the 1.2-kilohm dekastat. A mercury activator (1.35 V) was connected between the thermistor–dekastat junction and its opposite 49.9-kilohm resistor. The remaining junction points were connected to a Leeds and Northrup amplifier. The amplifier, in turn, drove a Sargent Model TR 0–2.5-mV recorder.

The power source for the manganin-wire calibration heater was a Sargent coulometric current source Model W with a built-in electronic timer which can be read with an accuracy of 0.02 sec. The current passed through the calibration heater was measured by measuring the voltage across a 10-ohm standard resistor (NBS Certified) using a precision K-3 potentiometer (Leeds and Northrup). The temperature sensitivity that could be detected over the whole range was $\sim 2 \times 10^{-6}°$.

Materials. All water used in the measurements was conductivity water obtained by passing distilled water through a Barnsted mixed-bed ion-exchange-resin column. Sodium tetraphenylboron was purchased from Fisher Scientific Co. (assay, 99.7%) and was purified by the method of Skinner and Fuoss.[11]

Procedure. The operating procedure was similar to that used previously.[9,10] Thin-walled sample bulbs having a diameter of 8 mm made from 6-mm Pyrex tubing were cleaned, dried, weighed, and filled with pure dry sodium tetraphenylboron and were weighed again. The bulbs with the sample were dried and were sealed with a very thin flame at the neck. Sample sizes ranged from 150 to 750 mg, resulting in calorimetric solutions of 10^{-3} to 5×10^{-3} m. The exact temperature of the water in the calorimeter at each operating temperature (at midpoints of the runs) was measured with the help of platinum resistance thermometer and a Mueller bridge. The runs were started when a linear time–temperature drift curve with a small slope was observed. Two electrical calibrations were made for each run, one before breaking the sample bulb and another after. A "best" straight line was drawn for each of the time–temperature curves and was extrapolated to the time at which either the sample bulb was broken or the calibration made. Several measurements of the heat of bulb breaking showed that the heat was negligible. The resistance of the calibration heater was measured at every temperature by measuring the voltage across a 10-ohm standard resistor connected in parallel to the calibration heater. The calorimeter was calibrated by measuring heats of solution of KCl. The values obtained were in good agreement (within 0.2%) with those reported by Gunn.[12]
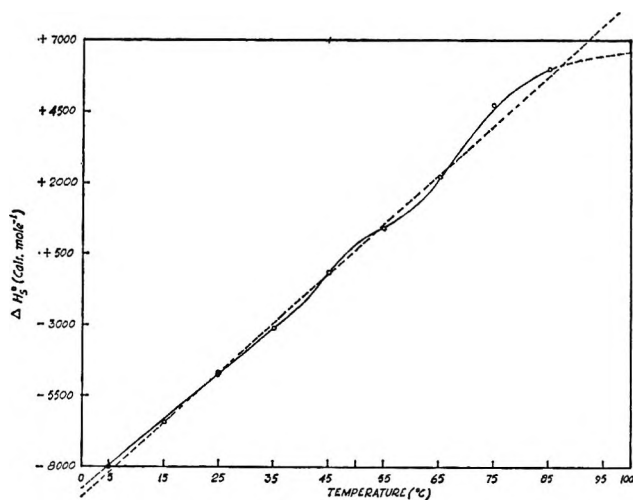
Figure 1. Heat of solution of NaBPh₄ at different temperatures.

Calculations and Results

The heats of solution at infinite dilution were obtained by extrapolating the plot of heat of solution as a function of molality at each temperature. The integral heats of solution, ΔH_s, at different molalities as well as the integral heats of solution at infinite dilution, ΔH_s^0, for NaBPh₄ at the various temperatures studied are listed in Table I. The standard deviations of ΔH_s values are also indicated in Table I. ΔH_s^0 values as a function of temperature over the range 5–85° are plotted in Figure 1. The dotted straight line in Figure 1 indicates the otherwise anticipated linear situation. The ΔC_p^0 values were calculated from ΔH_s^0 values at two adjacent temperatures; the temperature intervals were chosen such that there was no significant difference between $d\Delta H_s^0/dT$ and $\Delta(\Delta H_s^0)/\Delta T$. The ΔC_p^0 values were taken to represent the mean of the two adjacent temperatures.

The heat capacity of solid sodium tetraphenylboron, C_{p_2}, at each temperature was estimated by extrapolating linearly the values reported[13] for KBPh₄ up to 300°K and by making suitable correction for the difference between the K and Na salts. The extrapolation was justified on two grounds. The variation of C_{p_2} with temperature for the K salt was linear from 200 to 300°K. Also the differential thermal analysis on NaPBh₄ showed that there seems to be no break in the C_{p_2} vs. temperature curve for NaBPh₄ from room temperature up to more than 200°. The C_{p_2} values of NaBPh₄ at different temperatures were obtained from those of KBPh₄ by assuming that the difference would be constant between the two salts at all temperatures and further that the difference would be the same in

(11) J. F. Skinner and R. M. Fuoss, *J. Phys. Chem.*, **68**, 1882 (1964).

(12) S. R. Gunn, *ibid.*, **69**, 2902 (1965).

(13) T. Davies and L. A. Staveley, *Trans. Faraday Soc.*, **53**, 19 (1957).

Table I: Heats of Solution of NaBPh₄ in Water from 5 to 85°

Concn, $m \times 10^3$	$-\Delta H_s$, cal mol⁻¹	Concn, $m \times 10^3$	$-\Delta H_s$, cal mol⁻¹
Temp, 5.04°		**Temp, 15.10°**	
0.897	7992	0.8072	6289 ± 11
1.215	8033 ± 5[a]	0.8851	6325 ± 11
1.473	8023 ± 5	0.9854	6310 ± 11
1.614	7968 ± 5	1.1860	6308
1.760	7978 ± 5	2.1370	6306
1.850	8031 ± 13	2.4400	6247 ± 12
2.090	8005 ± 13	2.6190	6223 ± 12
2.546	7998	3.1031	6197 ± 31
$\Delta H_s{}^0 = -8000 \pm 16$ cal mol⁻¹		3.1870	6135 ± 31
		$\Delta H_s{}^0 = -6380 \pm 15$ cal mol⁻¹	
Temp, 25.12°		**Temp, 34.91°**	
1.490	4786	1.148	3091
1.615	4744 ± 13	1.370	3060 ± 21
1.650	4717 ± 13	1.378	3103 ± 21
1.964	4744 ± 14	1.533	3041 ± 24
2.059	4758 ± 14	1.793	3089 ± 24
2.064	4712 ± 14	1.975	3016 ± 1
2.252	4693 ± 11	1.975	3014 ± 1
2.360	4676 ± 11	2.058	3073
2.463	4715 ± 11	2.465	3061
2.580	4675 ± 10	2.808	3009
2.586	4696 ± 10	3.234	3002
2.676	4720	4.021	3007
2.980	4683	$\Delta H_s{}^0 = -3110 \pm 20$ cal mol⁻¹	
$\Delta H_s{}^0 = -4805 \pm 15$ cal mol⁻¹			
Temp, 44.73°		**Temp, 55.01°**	
1.736	1122 ± 2	2.104	−399 ± 7
1.927	1119 ± 2	2.250	−412 ± 7
2.442	1097 ± 3	2.752	−419 ± 7
2.533	1103 ± 3	3.184	−405 ± 7
2.802	1103 ± 12	3.400	−414 ± 2
2.902	1127 ± 12	3.408	−418 ± 2
3.023	1123 ± 8	3.641	−417
3.150	1108 ± 8	4.293	−411
3.366	1076	$\Delta H_s{}^0 = 410 \pm 4$ cal mol⁻¹	
3.694	1075		
$\Delta H_s{}^0 = -1150 \pm 8$ cal mol⁻¹			
Temp, 64.92°		**Temp, 75.17°**	
1.165	−2198	1.021	−4620 ± 15
1.522	−2077 ± 24	1.230	−4650 ± 15
1.764	−2130 ± 24	1.471	−4660 ± 4
2.008	−2150 ± 24	1.713	−4667 ± 4
2.410	−2052	2.210	−4652
2.883	−2116 ± 30	2.743	−4598 ± 6
2.984	−2056 ± 30	3.046	−4610 ± 6
3.139	−2003 ± 20	3.395	−4661
3.485	−2041 ± 20	$\Delta H_s{}^0 = 4670 \pm 17$ cal mol⁻¹	
$\Delta H_s{}^0 = -2235 \pm 30$ cal mol⁻¹			
Temp, 84.71°			
1.150	−5920 ± 10		
1.425	−5900 ± 10		
1.750	−5840 ± 35		
2.050	−5910 ± 35		
2.925	−5870		
3.550	−5880		
$\Delta H_s{}^0 = 5950 \pm 14$ cal mol⁻¹			

[a] Standard deviation of individual measurements from the average value of determinations at a close range of molalities.
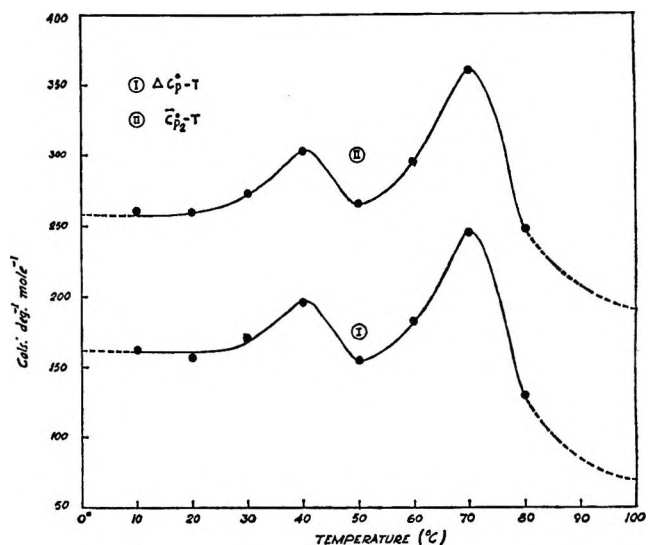
Figure 2. Standard partial molal heat capacities of NaBPh₄ in aqueous solutions at different temperatures.

various complex salts of Na and K. The estimated C_{p_2} values of NaBPh₄ are subject to correction whenever actual determinations are made. However, we believe that the uncertainty in the estimated value is probably not more than 2 cal deg⁻¹ mol⁻¹ and would not, in any significant manner, affect the trend of our results and the discussion in view of the large value observed for $\Delta C_p{}^0$. The partial molal heat capacities at infinite dilution, $\bar{C}_{p_2}{}^0$, were obtained by adding C_{p_2} and $\Delta C_p{}^0$ values. Table II gives the values of $\Delta C_p{}^0$, C_{p_2}, and $\bar{C}_{p_2}{}^0$ at various temperatures from 0 to 90°. The values at 0 and 90° are extrapolated ones. $\Delta C_p{}^0$ and $\bar{C}_{p_2}{}^0$ are plotted as functions of temperature from 0 to 90° in Figure 2. The accuracy of $\Delta C_p{}^0$ and $\bar{C}_{p_2}{}^0$ is better than ±3 cal deg⁻¹ mol⁻¹ at all temperatures except at 70°, where the uncertainty is ±4.5 cal deg⁻¹ mol⁻¹. The estimated uncertainties in the heat capacity values follow from those in the $\Delta H_s{}^0$ values indicated in Table I. Smoothed-out values of standard partial molal heat capacities of NaPBh₄ in aqueous solution from 0 to 90° are given in Table III.

Table II: Heat Capacity Data for Crystalline and Aqueous NaBPh₄[a]

Temp, °C	$\Delta C_p{}^0$	C_{p_2}	$\bar{C}_{p_2}{}^0$
0.0	162.0[b]	94.6	256.6[b]
10.1	162.0 ± 3.1	97.6	259.6 ± 3.1
20.1	157.5 ± 3.0	100.8	258.3 ± 3.0
30.0	169.5 ± 3.5	104.1	275.6 ± 3.5
39.8	196.0 ± 2.8	107.4	303.4 ± 2.8
49.9	156.0 ± 1.2	109.7	265.7 ± 1.2
60.0	182.5 ± 3.4	113.7	296.2 ± 3.4
70.0	244.0 ± 4.7	117.3	361.3 ± 4.7
90.0	85.0[b]	124.0	209.0[b]

[a] Units in cal deg⁻¹ mol⁻¹. [b] Extrapolated values.

Temp, °C	ΔC_p^{0b}	$\bar{C}_{p2}^{0b}$
0	162[c]	257[c]
10	160	257
20	160	260
30	168	272
40	196	303
50	154	264
60	182	295
70	245	360
80	130	248
90	85[c]	209[c]

[a] Units in cal deg^{-1} mol^{-1}. [b] The estimated error in ΔC_p^0 and $\bar{C}_{p2}^0$ values is less than ± 3 cal deg^{-1} mol^{-1} at all temperatures except 90°, where the uncertainty could be three times as large. [c] Extrapolated values.

Discussion

Figure 1 shows the variation of ΔH_s^0 of NaPBh$_4$ with temperature. The value of ΔH_s^0 at 25° is -4805 ± 15 cal mol^{-1}, which agrees perfectly well with that obtained by Wu and Friedman[14] and fairly closely with that of Arnett and McKelvey.[15] It may be seen from Figure 1 that ΔH_s^0 becomes more and more endothermic with increasing temperature. The increase in endothermicity is quite significant for ΔH_s^0 increases as much as by about 14 kcal on going from 5 to 85°, the values being -8000 cal at 5° and $+5950$ cal at 85°. The variation of ΔH_s^0 with temperature is linear only up to 50°. These results find some similarity in the temperature dependence of heats of solution of benzene in water as determined from solubility studies.[16] The ΔH_s^0 value of benzene in the aqueous medium increases linearly with temperature from a small exothermic value at subroom temperatures to $+2$ kcal mol^{-1} around 60°. The recent experimental data on the heats of solution of alkylhexoxyethylene glycol monoethers[17] at 25 and 40° show that the heats of solution and ΔC_p^0 become more positive with increase in temperature and also with increasing carbon chain length.

To explain the increase in endothermicity of heat of solution of NaBPh$_4$ with temperature as observed in the present investigation, we shall center all our discussions on the "flickering-cluster" model[2] for water structure to which a statistical treatment has been afforded by Némethy and Scheraga.[18] According to the flickering-cluster model, we have "icelike" (hydrogen-bonded) and "free" (unbonded) water molecules, the icelike patches enclosing within themselves void spaces. There is considerable support for the Frank–Evans hypothesis[8] that nonpolar solutes promote water structure through the formation of icebergs in aqueous solutions.[2] Like benzene and alkyl chain compounds, the

tetraphenylboride ion, being significantly nonpolar, seeks the icelike regions in water, gets enclosed in *partial* cages,[19] and interacts with the surrounding water molecules in such a way as to shift the equilibrium toward more icelikeness or more structuredness. That the nonpolar solute gets enclosed in cavities is known from the fact that the partial molal volumes of hydrocarbons are much less in water than in nonpolar solvents.[20] Now the enforcement of water structure by the formation of more hydrogen bonds should make the enthalpy of introduction of the solute in water negative. In addition there is a positive enthalpy contribution for the dissolution process arising from the formation of a tensile cavity around the nonpolar solute. The relative magnitudes of the two effects decide the sign and magnitude of ΔH_s^0 at any temperature. At low temperatures, since more structure will be present in water, there will also be more solvent cavities, which indicates that the enthalpy of solution will be predominantly controlled by structure promotion, whereas at higher temperatures, as the solvent structure is being broken down, the solvent cavitation energy takes precedence over the structure-making enthalpy making ΔH_s^0 more positive. Around 50° ΔH_s^0 is zero, implying a balance of positive and negative-enthalpy contributions. At still higher temperatures, solvent cavitation energy exceeds the negative-enthalpy term and hence ΔH_s^0 continues to be increasingly endothermic.

ΔC_p^0 *and* $\bar{C}_{p2}^0$ *vs. Temperature Curve.* The temperature dependence of ΔC_p^0 and $\bar{C}_{p2}^0$ of NaBPh$_4$ in aqueous solution over the temperature range 0–90° is shown in Figure 2. One finds large positive values of ΔC_p^0 and $\bar{C}_{p2}^0$ at all temperatures. ΔC_p^0 as well as $\bar{C}_{p2}^0$ increases with temperature, exhibiting a minimum around 50° and a maximum around 70°. $\bar{C}_{p2}^0$ values of various common electrolytes in aqueous solutions reported in the literature[2,9,10,21,22] all have negative values. These electrolytes have all been classed as structure breakers, leaving the solution less structured than water.[2]

The large positive values of ΔC_p^0 and $\bar{C}_{p2}^0$ of NaBPh$_4$

(14) Y. C. Wu and H. L. Friedman, *J. Phys. Chem.*, **70**, 501 (1966).

(15) E. M. Arnett and D. R. McKelvey, *J. Amer. Chem. Soc.*, **88**, 5031 (1966).

(16) R. L. Bohon and W. F. Claussen, *ibid.*, **73**, 1571 (1951).

(17) J. M. Corkill, J. F. Goodman, S. P. Harrold, and J. R. Tate, *Trans. Faraday Soc.*, **63**, 773 (1967).

(18) G. Némethy and H. A. Scheraga, *J. Chem. Phys.*, **36**, 3382 (1962).

(19) G. Némethy and H. A. Scheraga, *ibid.*, **36**, 3401 (1962).

(20) W. L. Masterton, *ibid.*, **22**, 1830 (1954).

(21) Thermal Properties of Aqueous Uni-univalent Electrolytes, National Bureau of Standards Annual Report NS RDS-NBS-2, U. S. Government Printing Office, Washington, D. C., 1965.

(22) (a) J. C. Ahluwalia and J. W. Cobble, *J. Amer. Chem. Soc.*, **86**, 5381 (1964); (b) R. E. Mitchell and J. W. Cobble, *ibid.*, **86**, 5401 (1964); (c) E. C. Jekel, C. M. Criss, and J. W. Cobble, *ibid.*, **86**, 5404 (1964).

in aqueous solution are in conformity with the earlier observation that nonpolar solutes or solutes with nonpolar groups like tetrabutylammonium bromide are structure makers and hence give rise to positive ΔC_p^0 values. It is interesting to compare the ΔC_p values of NaBPh$_4$ and n-Bu$_4$NBr in aqueous solution. ΔC_p^0 of NaBPh$_4$ at 25° is 164 $\pm$ 3 cal mol^{-1} deg^{-1}, while that reported[2] for n-Bu$_4$NBr is 120–150 cal deg^{-1} mol^{-1} at the same temperature. On the basis of the larger size of n-Bu$_4$N$^+$ (r = 4.94 Å)[23] as compared to that of BPh$_4^-$ (r = 4.2 Å)[24] and the fact that the nonpolar part in n-Bu$_4$N$^+$ is aliphatic while in BPh$_4^-$ it is aromatic, one would expect larger ΔC_p values for the n-Bu$_4$N$^+$ ion, but actually n-Bu$_4$NBr has a less positive ΔC_p than NaBPh$_4$. This could be because of the Br$^-$ ion which, being a structure breaker, might have reduced the effect due to the structure-making capacity of R$_4$N$^+$, while in NaBPh$_4$, Na$^+$ ion may enhance the structure-making capacity of BPh$_4^-$. It is also possible that the sign of the large ion and the aromatic substituent may have some influence.

The temperature dependence of ΔC_p^0 and $\bar{C}_{p_2}^0$ (Figure 2) of NaBPh$_4$ in aqueous solution is quite puzzling. ΔC_p^0 values continue to increase in the temperature range 0–40°, the increase being negligible from 0 to 20°, while from 20 to 40° it is as much as 38 cal deg^{-1} mol^{-1}. After 40° ΔC_p^0 and hence $\bar{C}_{p_2}^0$ begin to drop, giving rise to a minimum at about 50° followed by further increase resulting in a maximum at 70°. Above 70° the values drop again. The ΔC_p^0 values corresponding to the minimum and maximum are 155 and 245 cal deg^{-1} mol^{-1}, respectively.

The increase in ΔC_p^0 and $\bar{C}_{p_2}^0$ from 0 to 40° is in accord with the view[2] that more and more water structure promoted by the nonpolar solute is broken down with increasing temperature, thereby causing more heat to be absorbed, which enhances the heat capacity. A similar temperature behavior of ΔC_p^0 over the temperature range of 25–55° has been observed for potassium octanoate.[25]

As for the temperature dependence of ΔC_p^0 and $\bar{C}_{p_2}^0$ of the compound above 40° we have little doubt about the occurrence of the minimum and the maximum, because the uncertainty in the ΔC_p^0 values ($\pm$3 cal deg^{-1} mol^{-1}) is too small compared with the large drop (40 cal deg^{-1} mol^{-1}) in ΔC_p^0 from 40 to 50° and the large rise (88 cal deg^{-1} mol^{-1}) from 50 to 70°. Also it is very unlikely that any uncertainty in the estimated value of C_{p_2} obtained by extrapolation of known values between 200 and 300°K would rule out such pronounced discontinuities in the $\bar{C}_{p_2}^0$–T curve. Any discontinuity in the C_{p_2}–T curve is also ruled out from differential thermal analysis results.

The minimum around 50° suggests a drastic reduction in the structure around this temperature. Although there are feeble evidences for discontinuities[26] in the properties of water as a function of temperature,

the drop in ΔC_p is too much to be supported by the thermal anomalies. Formation of ion pairs is also ruled out from the conductometric and spectroscopic studies[27] of aqueous solutions of NaBPh$_4$. The possibility of water-structure-enforced ion pairing[28] causing any change does not arise, since the Na$^+$ ion is too small to cause a huge disturbance to water structure. Although precise data on the temperature dependence of partial molal heat capacities in the higher temperature range are available for a few aqueous electrolyte solutions,[9,10,22] we are not aware of any such data existing for aqueous solutions of electrolytes which contain nonpolar groups in the ions. We propose the following tentative qualitative explanation for the unusual behavior witnessed in the temperature range 40–70°.

There is ample evidence in the literature for the incidence of "hydrophobic interactions" and their consequential effects on the conformations of macromolecules. Advances in theoretical and experimental studies of hydrophobic interactions have been recently reviewed.[29] Hydrophobic interactions describe the tendency of nonpolar groups to associate in aqueous solution, thereby reducing the extent of contact with neighboring water molecules. Hydrophobic bonding is frequently invoked in the interpretation of various anomalies in protein structure and reactivity. The positive free energies of transfer of amino acid side chains from H$_2$O to D$_2$O indicates more extensive hydrophobic bonding in D$_2$O than in H$_2$O which is appropriate since D$_2$O is known to be a more structured solvent than water.[30] Similarly the transfer of hydrocarbons and tetraalkylammonium iodides from water to aqueous urea is accompanied by a negative free energy change, while ΔH^0 and ΔS^0 are positive, indicative of disruption of hydrophobic bonding by urea which means an increased solubility of hydrocarbons[31] and tetraalkylammonium iodides.[32]

If these examples are considered, it seems very likely that in order to reduce the interaction with water, the tetraphenylboride ions might associate, giving rise to hydrophobic interaction which would help minimize the solute–water contact to a considerable extent. The

(23) R. A. Robinson and R. H. Stokes, "Electrolyte Solutions," Butterworth and Co. Ltd., London, 1959, p 125.

(24) E. Grunwald, G. Baughman, and G. Kohnstam, *J. Amer. Chem. Soc.*, 82, 5801 (1960).

(25) P. White and G. C. Benson, *J. Phys. Chem.*, 64, 599 (1960).

(26) W. Drost-Hansen, presented at the First International Symposium on Water Desalination, Washington, D. C., Oct 1965.

(27) (a) A. K. Covington and M. J. Tait, *Electrochim. Acta*, 12, 113 (1967); (b) A. K. Covington and M. J. Tait, *ibid.*, 12, 123 (1967).

(28) R. M. Diamond, *J. Phys. Chem.*, 67, 2513 (1963).

(29) G. Némethy, *Angew. Chem. Int. Ed. Engl.*, 6, 195 (1967).

(30) G. C. Kresheck, H. Schneider, and H. A. Scheraga, *J. Phys. Chem.*, 69, 3132 (1965).

(31) D. B. Wetlaufer, S. K. Malik, L. Stoller, and R. L. Coffin, *J. Amer. Chem. Soc.*, 86, 508 (1964).

(32) F. Franks and D. L. Clarke, *J. Phys. Chem.*, 71, 1155 (1967).

enthalpy of hydrophobic interaction is slightly positive[33] at room temperature for amino acids involving aromatic and aliphatic side chains. It has been described in great detail[33] that although hydrophobic interaction is significantly maximal at low temperatures in view of the maximal structure of water, the endothermicity of hydrophobic bonding itself, $\Delta H_{H\phi}^0$, would make the interactions *stronger* with an increase of temperature. Calculations[33] show that for the interaction of a pair of phenylalanine side chains, which resemble the substituent in BPh_4^- ion, the hydrophobic interaction gains *maximal strength* around 42°. Since hydrophobic interaction is accompanied by a decrease in the heat capacity,[33,34] the temperature of maximum hydrophobic interactions would correspond to a maximum decrease in the ΔC_p value. For the tetraphenylboride ion, the temperature of maximum hydrophobic interactions might be anywhere between 45 and 55°, in which case the minimum in the $\Delta C_p^0 - T$ curve around 50° would be explained.

The foregoing evidence suggests convincingly, but not conclusively, the existence of hydrophobic interactions in $NaBPh_4$ aqueous solutions. With increase of temperature, ΔC_p increases owing to the thermal melting of icebergs but at the same time there is a concomitant decrease because of the increased strength of hydrophobic interactions. At temperatures below 40°, the temperature effect might be the predominating effect, giving rise to a positive slope to the curve. At $T > 40°$, hydrophobic interactions might supercede and submerge the temperature effect, thereby causing a net decrease in ΔC_p. This decrease is maximum around 50°, where the hydrophobic interactions are strongest. Above 50° while the temperature effect in increasing ΔC_p continues, the hydrophobic interactions might have withered away, either because of the changes setting in the molecular conformation of the tetraphenylboride

ion or because of natural attenuation, resulting from the lack of entropy-favored driving force, causing ΔC_p to rise once again till it reaches a maximum value at 70°. The decrease in ΔC_p above 70° may be due to the decrease in the structure-making ability of the solute at the highest temperatures where the solvent structure is nearing total collapse. It might be that this factor is responsible for the maxima observed in the $\bar{C}_{p_2}^0$ values for various electrolytes[9,10-24] in the region 50-70°. The $\bar{C}_{p_2}^0$ values of $NaBPh_4$ follow the same trend of ΔC_p^0 with regard to the temperature variation, although the temperature coefficient of C_{p_2} of solid $NaBPh_4$ is positive in the temperature range covered. The temperature coefficient is small enough (0.3 cal deg^{-1} mol^{-1}) to get submerged in the large changes in ΔC_p^0.

The opposing forces of temperature effect and hydrophobic interactions in determining the $\Delta C_p^0 - T$ curve finds a parallelism in the factors determining the thermal stability of proteins.[35]

The interplay of hydrophobic interaction in the aqueous solutions of solutes containing nonpolar groups in determining the temperature dependence of the partial molal heat capacity of the solute is a plausible interpretation of the results obtained in this investigation but is by no means a certainty. We believe much more work needs to be done with solutes of the type of $NaBPh_4$ on the temperature dependence of thermodynamic properties of aqueous solutions before anything could be said conclusively about the factors contributing to the structural changes in aqueous solutions with the change in temperature. We are presently continuing to investigate the same solute in aqueous solution by other studies which are in progress.

(33) G. Némethy and H. A. Scheraga, *J. Phys. Chem.*, **66**, 1773 (1962).

(34) G. C. Kresheck and L. Benjamin, *ibid.*, **68**, 2476 (1964).

(35) H. A. Scheraga, G. Némethy, and I. Z. Steinberg, *J. Biol. Chem.*, **237**, 2506 (1962).

Diffusion of Aromatic and Cycloparaffin Hydrocarbons

in Water from 2 to 60°

by L. Bonoli and P. A. Witherspoon

Department of Civil Engineering, University of California, Berkeley, California   (*Received January 15, 1968*)

Diffusion coefficients for benzene, toluene, ethylbenzene, cyclopentane, methylcyclopentane, and cyclohexane in water were measured starting with essentially saturated solutions at temperatures ranging from 2 to 60° using the capillary-cell method. Measurements with benzene at different initial concentrations show little effect of concentration. For a 40-fold decrease in concentration, the decrease in the diffusion coefficients of benzene averages about 10%. The diffusion coefficients of all six hydrocarbons can be correlated over the entire temperature range using the Wilke–Chang formula. Activation energies were found to be the same for all hydrocarbons, *viz.*, 4600 cal/mol.

Introduction

A project has been under way for some time in this laboratory to study the general problem of diffusion through water of the hydrocarbons found in petroleum. The first investigations were concerned with light paraffin hydrocarbons;[1-3] this work reports results on benzene, toluene, ethylbenzene, cyclopentane, methylcyclopentane, and cyclohexane.

In general, not many data on the diffusion of hydrocarbons in water have been published by others. Soviet workers[4] have reported results credited to Antonov for the diffusion of methane, ethane, propane, and *n*-hexane in water. Gubbins, *et al.*,[5] have reported data for methane as well as the effects of electrolytes on the diffusion of methane in water. With regard to other hydrocarbons, diffusion data have been reported only for acetylene in water,[6] propylene in water,[7] and ethylene, propylene, and butylene in water.[8] An extensive investigation on the solubility of hydrocarbons in water has been reported by McAuliffe.[9]

Experimental Section

The capillary-cell method of measuring diffusion coefficients perfected by Wang[10] has been modified for this work; the details have previously been reported.[2]

The aqueous solutions of liquid hydrocarbons[11] investigated in this study required a different method of preparation than that previously used with gases.[2,3] Since liquid hydrocarbons may form dispersions rather than true solutions in water, care had to be taken to avoid oversaturated solutions. The solubility data reported by McAuliffe[9] for various hydrocarbons in water at 25° were used. The amount of a specific hydrocarbon that could be dissolved in 250 cc of pure water at 25° was weighed and mixed with this volume in a 250-cc bottle. By minimizing the vapor space above the liquid, only slight amounts of hydrocarbons

could vaporize out of solution, thus leaving a slightly undersaturated solution. After mixing by magnetic stirrer, the solutions were allowed to equilibrate in a water bath at the same temperature as that of the diffusion measurements.

Since the increase in solubility for the aromatic hydrocarbons is only 5–10% over the range of 5–40°,[12,13] we used approximately the same initial concentrations at all temperatures. No data on the change in solubility with temperature are available for cycloparaffins, and since our objective was the measurement of diffusion coefficients, we did not attempt to determine the effect of temperature on solubility. We noted indirectly, however, during the course of this work, that the changes in the solubility of the cycloparaffins were about the same as those of the aromatics. Consequently, the same procedure was used for all hydrocarbons, and any concentrations cited below are only approximate.

(1) D. N. Saraf, P. A. Witherspoon, and L. H. Cohen, *Science*, **142**, 955 (1963).

(2) P. A. Witherspoon and D. N. Saraf, *J. Phys. Chem.*, **69**, 3752 (1965).

(3) J. J. Sahores and P. A. Witherspoon, paper presented at the Third International Meeting on Organic Geochemistry, London, Sept 1966, in press.

(4) A. A. Kartsev, *et al.*, "Geochemical Prospecting for Petroleum," University of California Press, Berkeley, Calif., 1959, p 69.

(5) K. E. Gubbins, *et al.*, *A.I.Ch.E. J.*, **12**, 548 (1966).

(6) G. Tammann and V. Z. Jensen, *Z. Anorg. Allgem. Chem.*, **179**, 125 (1929).

(7) J. E. Vivian and C. J. King, *A.I.Ch.E. J.*, **10**, 220 (1964).

(8) A. A. Unver and D. M. Himmelbau, *J. Chem. Eng. Data*, **9**, 428 (1964).

(9) C. McAuliffe, *J. Phys. Chem.*, **70**, 1267 (1966).

(10) J. H. Wang, *J. Amer. Chem. Soc.*, **73**, 510 (1951).

(11) All hydrocarbons used were pure grade, 99% pure or better, and were obtained from Phillips Petroleum Co., Bartlesville, Okla.

(12) R. L. Bohon and W. F. Claussen, *J. Amer. Chem. Soc.*, **73**, 1571 (1951).

(13) D. S. Arnold, C. A. Plank, E. E. Erickson, and F. P. Pike, *Ind. Eng. Chem., Chem. Eng. Data Ser.*, **3**, 253 (1958).

Table I: Results of Diffusion Measurements[a]

Hydrocarbon	2°	10°	20°	40°	60°
Benzene	0.58 ± 0.02	0.75 ± 0.02	1.02 ± 0.03	1.60 ± 0.05	2.55 ± 0.05
Toluene	0.45 ± 0.02	0.62 ± 0.02	0.85 ± 0.03	1.34 ± 0.05	2.15 ± 0.06
Ethylbenzene	0.44 ± 0.04	0.61 ± 0.05	0.81 ± 0.03	1.30 ± 0.05	1.95 ± 0.05
Cyclopentane	0.56 ± 0.02	0.64 ± 0.03	0.93 ± 0.02	1.41 ± 0.09	2.18 ± 0.07
Methylcyclopentane	0.48 ± 0.08	0.59 ± 0.06	0.85 ± 0.10	1.32 ± 0.12	1.92 ± 0.15
Cyclohexane	0.46 ± 0.04	0.57 ± 0.04	0.84 ± 0.05	1.31 ± 0.07	1.93 ± 0.12

[a] Diffusion coefficient, $D \times 10^5$ cm²/sec.

Table II: Results of Diffusion Measurements with Benzene at Different Initial Concentrations

—2°—		—10°—		—20°—		—40°—		—60°—	
Concn[a]	D[b]	Concn	D	Concn	D	Concn	D	Concn	D
1700	0.58 ± 0.02	1700	0.75 ± 0.02	1700	1.02 ± 0.03	1700	1.60 ± 0.05	1700	2.55 ± 0.05
210	0.56 ± 0.03	60	0.68 ± 0.04	40	0.82 ± 0.04	50	1.52 ± 0.05	45	2.39 ± 0.04
40	0.43 ± 0.02								

[a] Concentrations in ppm, approximate values. [b] $D \times 10^5$ cm²/sec.

During the course of this work, it was also necessary to have one solution with a constant concentration of hydrocarbons for reference purposes. This permitted us to determine if leakage of hydrocarbons was occurring from test solutions over prolonged periods and also provided a means of checking the reproducibility of the method of analysis. For this purpose, an ethane–water solution held at a constant temperature (22°) proved satisfactory.[3]

Since benzene has the highest solubility in water of any of the hydrocarbons studied, 1780 ppm at 25°,[9] it was possible to investigate the effects of concentration on diffusion. For this purpose, solutions with initial concentrations ranging from about 40 ppm to about 1700 ppm were prepared for investigation.

The results of diffusion measurements for essentially saturated solutions of all hydrocarbons are summarized in Table I. The results of diffusion with benzene at different initial concentrations are summarized in Table II, where the concentrations reported for the more dilute solutions were determined by measuring their relative concentrations with reference to the essentially saturated solutions (1700 ppm). The data represent averages of 10–15 repetitive runs, except for ethylbenzene at 60° where 27 runs were made. The precision shown is the standard deviation of the arithmetic mean.

Discussion

The results of Table II indicate that there is little effect of concentration on the diffusion of benzene in water. For a 30–40-fold decrease in concentration, the decrease in the diffusion coefficients averages about 10%, whereas the uncertainty in our results is about 3%.

These results suggest that over the range of concentrations studied, the benzene molecules move through water more or less independently of each other. This is not unexpected because at its maximum solubility, one molecule of benzene is surrounded by more than 2000 molecules of water. The same conclusion can be drawn from the results of Table I. Methylcyclopentane, for example, has the lowest solubility of the hydrocarbons studied, 42.6 ppm at 25°,[9] yet the diffusion coefficients for this hydrocarbon are only 20% lower than those of benzene. These lower results for methylcyclopentane may be explained by its larger molecular size and are not an effect of concentration. Hildebrand and coworkers[14-16] have supported the concept that movement by diffusion is a "random-walk" process, and later[17,18] have proposed that such a process should be controlled mainly by molecular cross section. Witherspoon and Saraf[2] have found the same results in studying the diffusion of light paraffin hydrocarbons.

Various attempts have been made to develop empirical equations that would enable one to predict diffusion coefficients.[19-21] Wilke and Chang[21] have pro-

(14) H. Watts, B. J. Alder, and J. H. Hildebrand, *J. Chem. Phys.*, **23**, 659 (1955).

(15) E. W. Haycock, B. J. Alder, and J. H. Hildebrand, *ibid.*, **21**, 1601 (1953).

(16) J. H. Hildebrand and R. L. Scott, "Regular Solutions," Prentice-Hall, Inc., New York, N. Y., 1962.

(17) M. Ross and J. H. Hildebrand, *J. Chem. Phys.*, **40**, 2397 (1964).

(18) K. Nokanishi, E. M. Voigt, and J. H. Hildebrand, *ibid.*, **42**, 1860 (1965).

(19) D. E. Othmer and M. S. Thakar, *Ind. Eng. Chem.*, **45**, 589 (1953).

(20) E. G. Scheibel, *ibid.*, **46**, 2007 (1954).

(21) C. R. Wilke and P. Chang, *A.I.Ch.E. J.*, **1**, 264 (1955).
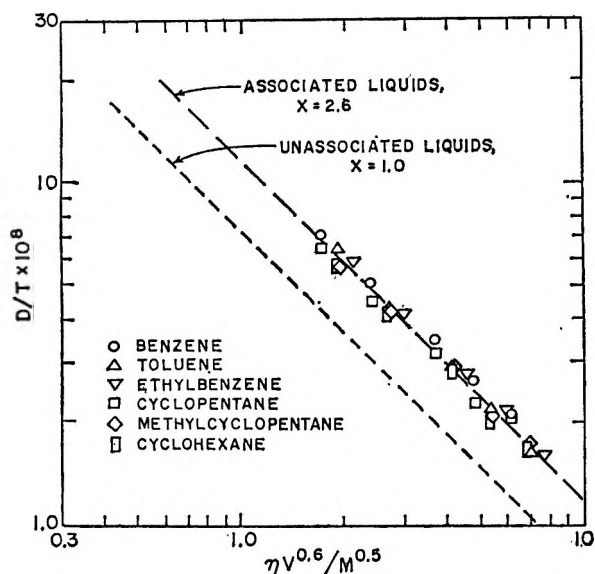
Figure 1. Correlation of diffusion coefficients in water.

posed the following equation for diffusion in either associated or unassociated liquids

$$D = 7.4 \times 10^{-8} \frac{(xM)^{0.5}T}{\eta V^{0.6}}$$

where x is the association parameter equal to 2.6 for water and 1.0 for unassociated liquids, M is the molecular weight of the solvent, T is the absolute temperature, η is the viscosity of the solvent at temperature T, and V is the liquid molal volume of the solute at its normal boiling point.

To examine the applicability of this equation to our results, we plotted D/T vs. $\eta V^{0.6}/M^{0.5}$ as shown in Figure 1. It will be noted that the data show a slight scatter about the correlation line for associated liquids when water is the solvent. However, the differences are within the limits of experimental error, and it would appear that the Wilke–Chang equation should provide a reliable means of predicting diffusion coefficients for aromatic and cycloparaffin hydrocarbons in water.

To obtain energies of activation for diffusion, an Arrhenius plot of the data of Table I was made as
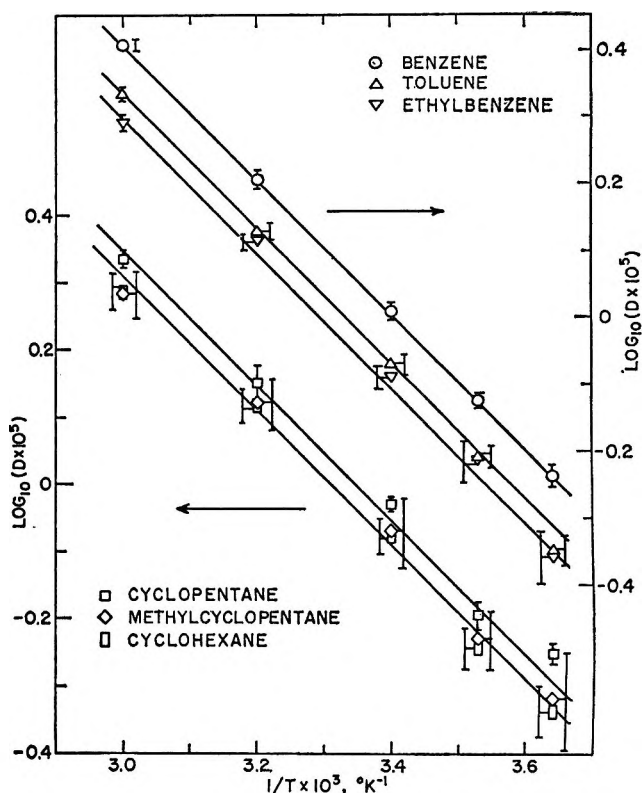
Figure 2. Arrhenius plot of D vs. $1/T$.

shown in Figure 2. It will be noted that within the limits of our experimental error, the data for any given hydrocarbon all fall on a straight line, at least between 10 and 60°. It is also important to note that the lines shown on Figure 2 are all parallel, which means that the activation energies are the same for each hydrocarbon, viz., 4600 cal/mol. Other workers[2,17] in studying the diffusion of several compounds in a single solvent have also obtained only one value for activation energy.

It appears in Figure 2 that below 10°, activation energies may be increasing. In studying the self-diffusion of water, Wang[10] has also reached the same conclusion. Between 5 and 50°, he obtained 4580 cal/mol, whereas at 0° he obtained 6400 cal/mol.

Investigation of Liquid Palladium–Tin Alloys

by J. R. Guadagno and M. J. Pool

Department of Metallurgy, University of Denver, Denver, Colorado (*Received January 15, 1968*)

The value of the heat of solution of palladium in liquid tin has been measured as a function of temperature and concentration in the dilute solution range and between 700 and 800°K. The partial heat of solution has been compared to the heats of formation of solid PdSn, $PdSn_2$, and $PdSn_4$. The similarity between the heat of solution and the heats of formation indicates that similar bonding may exist in all cases, and that each palladium atom in the liquid, like those in each of the compounds, is probably surrounded by four permanent tin neighbors. Density measurements of a 4% Pd liquid alloy show that a tetrahedral $PdSn_4$ molecule would have a Pd–Sn distance very close to that found in the intermetallic compounds.

Introduction

In liquid binary alloys a highly exothermic heat of solution of one element in the other appears to be a reasonable indication of a possible molecular structure.[1] While investigating the thermodynamic properties of solid silver–palladium alloys by means of liquid tin solution calorimetry in 1959, Chan[2] measured a value for the heat of solution of solid palladium in liquid tin of −26,400 cal/mol of Pd at 700°K. Later measurements at 775°K yielded a figure of −25,240 cal/mol.[3] This places the palladium–tin system along those which show strongest evidence of possible molecular structure.

The present work covers a more thorough investigation of the thermodynamic properties of this system. Heats of solution were measured at temperatures from 700 to 800°K and at concentrations from pure tin up to that of the liquidus. In addition, heats of formation of various solid intermetallic Pd–Sn compounds were measured, and the density of liquid tin and a 4% palladium alloy were determined.

Solution Colorimetry

The heat of solution of palladium in liquid tin was measured by using a liquid tin solution calorimeter, which has been described elsewhere.[4] Samples of high-purity (99.999%) palladium were cooled to 273°K and then dropped, *in vacuo*, into a bath of liquid tin (99.98% pure) maintained at the desired temperature. Dissolution of the palladium in the tin caused a positive temperature perturbation in the bath; after the reaction was completed, the temperature of the bath again returned to that of the surrounding heat sink, following a logarithmic decay curve. From such a curve, it is possible to calculate the heat evolved during the reaction,[5] provided both the rate at which the heat is transferred from the bath to the heat sink and the energy equivalent of the bath are known. The heat transfer rate can be determined from the curve itself (The rate used in the calculations is the average rate for all the runs in a series. It has been found that this procedure consistently produces less scatter than

using the heat transfer rates for the individual runs. It appears that the error involved in measuring the heat transfer rate for an individual run is greater than the difference in the actual rate between runs; it is therefore felt that the use of average rates leads to a truer measurement of the actual heat evolved.), while the energy equivalent can be determined by adding a sample whose heat content is known. In this case, pure (99.999%) tin was used as a calibration sample, the heat content being taken from Hultgren, Orr, Anderson, and Kelley.[6] Inert samples of tungsten were also used as a check when the bath contained an appreciable concentration of palladium. It was found, however, that the heat effect of the tin samples did not vary with composition, even though baths containing up to 10% palladium were used.

In each of the first six series of runs, the bath was maintained at a constant temperature, the temperatures chosen for the various series being 700, 725, 750, 762, 773, and 800°K. Repeated drops were made until, in most cases, the composition approached the liquidus. Before the liquidus could be reached, however, the reaction rate became too slow for accurate calculation of the heat effect.

In the last two series, runs were made while the temperature of the calorimeter was slowly increasing, in order to attempt to detect any dependence on temperature which might occur. Such a procedure is made

(1) J. R. Guadagno, Ph.D. Thesis, University of Denver, June 1967.

(2) J. P. Chan, P. D. Anderson, R. L. Orr, and R. Hultgren, 4th Technical Report, Task Order Contract No. 15, Minerals Research Laboratory, University of California, Berkeley, Calif., 1959.

(3) J. R. Guadagno, R. L. Orr, and R. Hultgren, 13th Technical Report, Task Order Contract No. 15, Minerals Research Laboratory, University of California, Berkeley, Calif., 1961.

(4) R. F. Peluso and M. J. Pool, "Heats of Solution of Praseodymium, Neodymium, and Samarium in Liquid Tin at 750°K," Proceedings of the 4th Rare Earth Research Conference, Phoenix, Ariz., 1964, p 269.

(5) R. L. Orr, A. Goldberg, and R. Hultgren, *Rev. Sci. Instr.*, 28, 767 (1967).

(6) R. Hultgren, R. L. Orr, P. D. Anderson, and K. K. Kelley, "Selected Values of Thermodynamic Properties of Metals and Alloys," John Wiley and Sons, Inc., New York, N. Y., 1963.

possible by the fact that the heat of solution of palladium in tin is invariant with concentration of palladium at all temperatures; thus any recorded change in heat effect must be due to the temperature change alone. When this procedure is followed, however, calculation of results is complicated by the fact that both heat transfer rate and energy equivalent vary considerably with temperature. These factors, coupled with uncertainty in measurement of the bath temperature, tend to make the results of these latter series less reliable.

The results of each series of additions are listed in Table I and refer to the reaction $Pd_{(s, T)} \rightarrow Pd_{(l, T, x_{Sn} = 1)}$. The data are shown graphically in Figure 1. Each point shown with limits is the average of several runs, and the limits indicate the probable error; points without limits represent only one to three runs each. The horizontal lines show the results of the variable temperature series.

Figure 1. Heat of solution of palladium in liquid tin.

Table I: Heat of Solution of Palladium in Liquid Tin

Temp, °K	No. of runs	$\overline{\Delta H}_{Pd}$, cal/g-atom	Ref
700	12	$-26,040 \pm 200$	...
725	14	$-26,020 \pm 260$	...
750	7	$-26,350 \pm 110$	...
763	13	$-25,870 \pm 130$	...
773	16	$-25,230 \pm 80$	...
797	3	$-25,050$	...
638–768	22	$-26,550$	...
727–791	14	$-27,060$	...
700	...	$-26,400$	2
775	...	$-25,240$	3

The magnitude of the heat of solution indicates strongly that the palladium forms permanent bonds with some of the tin atoms, probably according to the reaction

$$Pd_{(s,T)} + xSn_{(l,T)} \longrightarrow PdSn_{x(sol'n,T)}$$
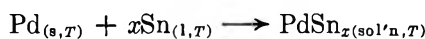
The lack of any variation in the partial molar heat of solution of palladium with solute concentration indicates that the same reaction takes place over the entire composition range covered. Thus, the $PdSn_x$ molecules already in solution have no apparent effect on the nature of the reaction of additional Pd atoms with the remaining tin matrix; the only observable effect of composition is a gradual decrease in the rate of reaction as both the number and mobility of the available unbound tin atoms decreases with increasing concentration of $PdSn_x$. The invariance of the heat effect of tin with composition also indicates strongly that the Pd–Sn bonds are permanent and that the tin added undergoes only a simple melting process.

If the palladium concentration in any of the experimental runs had exceeded that in $PdSn_x$, an abrupt change in the value of the heat of solution would surely
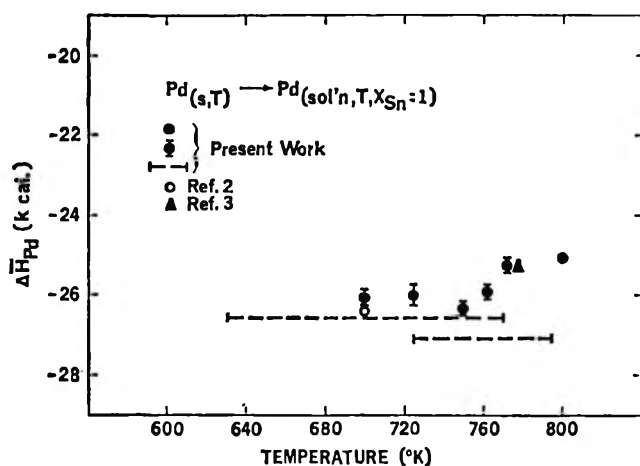
have been noted, since a different type of reaction must take place beyond this point. Thus the constancy of the measured data also shows that the value of x in $PdSn_x$ is less than the minimum ratio of Sn to Pd atoms reached in any of the experiments.

A different, and rather puzzling, result of the experimental data is the change in the value of the particular heat of solution between 750 and 773°K. This effect is also reflected in the independent work done earlier, although it was attributed at that time to differences in calorimetric technique. This change, however, did not show up in either of the two variable-temperature series of runs. In addition, heating and cooling curves for a liquid 4% palladium alloy failed to show a discontinuity at or near this temperature. Since the constant temperature data are considered more reliable, it is probable that some kind of structural change does take place, but it cannot be stated at this time whether the change is actually a second-order phase transformation or merely a weakening of the bond due to increasing temperature.

In order to investigate the possibility of a similarity between the structure of a postulated molecular species in the liquid phase and that of solid intermetallic compounds in the same system, the heats of formation of three of these compounds ($PdSn$, $PdSn_2$, and $PdSn_4$) were determined, also by means of liquid tin solution calorimetry, according to the relationships

$$Pd_{(s,273)} + XSn_{(l,T)} \longrightarrow PdSn_{x(sol'n,T)} \qquad \Delta H_1$$

$$Sn_{(s,273)} \longrightarrow Sn_{(l,T)} \qquad \Delta H_2$$

$$PdSn_{y(s,273)} + (x - y)Sn_{(l,T)} \longrightarrow PdSn_{x(sol'n,T)} \qquad \Delta H_3$$

$$Pd_{(s,273)} + ySn_{(s,273)} \longrightarrow PdSn_{y(s,273)} \qquad \Delta H_f$$
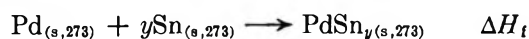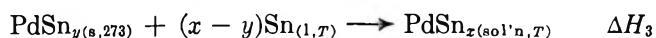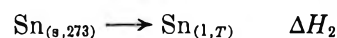
$$\Delta H_f = \Delta H_1 + y\Delta H_2 - \Delta H_3$$

where y represents the number of tin atoms per palladium atom in any of the intermetallic compounds. ΔH_1 and ΔH_3 can be measured experimentally, while ΔH_2 is taken from published data.[6] Five or six drops

Table II: Heats of Formation of Palladium–Tin Compounds at 273°K

Com-pound	ΔH_f, cal/g-atom	ΔH_f, cal/mol of Pd
PdSn	$-14,420 \pm 80$	$-28,840 \pm 160$
PdSn$_2$	$-10,450 \pm 60$	$-31,350 \pm 180$
PdSn$_4$	$-6,770 \pm 80$	$-33,850 \pm 400$

Figure 2. Density apparatus.

were made for each of the three compounds, and the results are listed in Table II.

The heats of formation of the three compounds, when calculated on a basis of 1 mol of palladium, are roughly equal and are just a few kilocalories more exothermic than the heat of solution of palladium in liquid tin, which can be taken as equal to the heat of formation of the molecular species formed in solution. This in itself is an indication that there may be a structural relation between the liquid and crystalline compounds.

A study of the structures of these three intermetallic compounds[7-9] shows that, in every case, each palladium atom has four tin atoms for its nearest neighbors. If we conclude from the similarity in heats of formation that the bonding in these three compounds is similar to that in the liquid alloys, then the molecular species existing in the liquid would most probably be PdSn$_4$. From the magnitude of the heat of solution of palladium in tin, it is obvious that the Pd–Sn bonds formed in the liquid are very strong in comparison with the Pd–Pd and Sn–Sn bonds which must be broken in the process. Since the heats of formation of the intermetallic compounds are 12–30% more exothermic than that found in the liquid, the above conclusion requires that the intermetallics, as well, have strong Pd–Sn and weak Sn–Sn and Pd–Pd bonds.

Table III shows the closest approach of like and unlike atoms in each of the three intermetallic compounds, as well as in the pure metals. (The derived metallic Pd–Sn distance is merely the sum of the atomic radii of the two metallic elements.) It can readily be seen that the Pd–Sn distance in each of the intermetallics is

considerably shorter than that derived from the pure crystalline structures, while the Pd–Pd and Sn–Sn distances are both longer than that found in the elements, indicating that the Pd–Sn bonds are, indeed, much stronger than the like-atom bonds in all of the compounds.

The manner in which the heat of formation varies from one intermetallic compound to another is also consistent with this supposition. As the tin content increases, the number of tin–tin bonds also increases (Pd–Pd distances are so great, except in PdSn, that the effect of Pd–Pd bonding can be neglected). Thus the bonding of each Pd atom with its four tin neighbors constitutes a decreasing (though still dominant) fraction of the total heat of formation of the compound.

Density Measurements

While the Pd–Sn distances in liquid alloys cannot be determined accurately without the use of diffraction studies, a rough idea of this distance can be derived from liquid alloy density measurements. A density apparatus (Figure 2) was constructed which employs a calibrated capillary. A 1-mm i.d. Vycor tube was formed into a coil, with both ends connected to straight sections leading to enlarged chambers, also of Vycor. The volume of the coiled section was determined by using a weighed amount of mercury, and the volumes of the linear sections were similarly calibrated as a function of length. In order to measure the volume of a metallic sample, the entire coiled capillary was inserted into the constant-temperature zone of a horizontal tube furnace, and the sample was melted in the upper chamber by an auxiliary heater and then pushed under argon gas pressure into the coil. The end points of the continuous liquid column were measured optically, using a telescope and prism arrangement; the volume occupied by the molten sample could then be determined to a high degree of accuracy. The liquid metal was then pushed out into a glass vial, cooled, and weighed.

The density of pure tin was measured as a function

Table III: Interatomic Distance in Palladium–Tin Compounds

Material	Pd–Pd, Å	Sn–Sn, Å	Pd–Sn, Å
Sn(c)	...	3.02	...
Pd(c)	2.74	...	...
Mechanical mixture	2.74	3.02	2.88
Sn(l)	...	3.26	...
PdSn	3.01, 3.18	3.17	2.68, 2.79
PdSn$_2$	4.59	3.11	2.43
PdSn$_4$	6.38	3.19	2.77
Model	...	...	2.70

(7) K. Schubert and H. Pfisterer, *Z. Metallk.*, **41**, 433 (1950).

(8) E. Hellner, *Z. Krist.*, **107**, 99 (1956).

(9) K. Schubert and U. Rösler, *Z. Metallk.*, **41**, 298 (1950).

of temperature over the range 623–793°K. From the experimental results, the following equation has been derived

$$\rho_{Sn} = 7.819 - 2.104(10^{-3})T + 9.6(10^{-7})T^2$$

The density of a liquid alloy containing 4% palladium was also determined as 6.965 g/cm³ at 785°K. The density of pure tin at this temperature is 6.759 g/cm³, and the density of a mechanical mixture containing 4% palladium, calculated from accepted atomic diameters,[10] would be 6.804 g/cm³. Thus the increase in density due to adding 4% palladium to liquid tin is more than four times what would be expected from a mechanical mixture of the two elements. This again confirms the existence of strong bonding between the palladium and tin atoms in the liquid.

From the experimental density data, it has been possible to calculate the palladium–tin interatomic distance, using a model based on the following assumptions. (a) The molecular species formed is $PdSn_4$. (b) The molecules are tetrahedral, with four tins surrounding a central palladium atom. This is the simplest form for a molecule of such composition. (c) The molecules are spherical.

This model yields a Pd–Sn distance of 2.70 Å, which is in close agreement with the values for the intermetallic compounds. This value is also listed in Table III.

Summary

The lack of direct methods of determining the structure of liquid palladium–tin alloys makes it necessary to postulate a structure, derive various properties from this model, and compare the derived properties with those measured experimentally. In order for the model to be considered valid, complete agreement must exist between derived and measured properties in all cases. At the present stage of development, neither theoretical nor experimental data are available in sufficient quantity and with sufficient precision to permit complete quantitative comparison. Therefore, the conclusions presented here must be considered tentative, subject to proof by further investigation.

From the evidence available, it appears that tin-rich liquid palladium–tin alloys, at temperatures between 600 and 800°K and at compositions ranging from pure tin up to the liquidus, consist of molecules composed of both palladium and tin atoms, these molecules being in equilibrium solution in a matrix of pure tin. While the exact composition of the molecules has not been conclusively determined, it is most probable that they fit the formula $PdSn_4$.

(10) C. S. Barrett and T. B. Massalski, "Structure of Metals," 3rd ed, McGraw-Hill Book Co., Inc., New York, N. Y., 1966, p 628.

Arrhenius Parameters for the Reactions of Atomic Nitrogen with Some Olefins and Acetylenes

by John T. Herron and Robert E. Huie

National Bureau of Standards, Washington, D. C. 20234 (*Received January 15, 1968*)

The rates of reaction of atomic nitrogen, produced in a flow system by means of a microwave discharge, with a series of olefins and acetylenes have been measured from 320 to 550°K. Preexponential factors and activation energies have been derived. In addition, upper limits are given for the rates of reaction of atomic nitrogen with several miscellaneous organic compounds.

Introduction

An earlier article from this laboratory reported rate constants at 340°K for the reactions of atomic nitrogen with a series of olefins.[1] These measurements have now been repeated over the temperature interval 320–550°K and have been extended to include data on a series of acetylenes and some miscellaneous compounds.

(1) J. T. Herron, *J. Phys. Chem.*, **70**, 2803 (1966).

Experimental Section

The experimental approach, which was to couple a discharge-flow system to a mass spectrometer to permit the direct measurement of the partial pressures of reactants and products, has been described in detail elsewhere.[1,2]

In the present work the reactor was a 20 mm i.d. Pyrex tube which could be heated to 550°K. The total pressure was about 2.5 torr. Reaction time, which could be adjusted by changing the distance between the reactant inlet and the sampling orifice of the mass spectrometer, was normally about 0.02 sec.

As noted previously,[1] secondary reactions, particularly of atomic hydrogen, necessitate working at very low reactant flows where the degree of conversion is small (e.g., 2–10%). At higher flows, reaction products cause additional reaction, leading to an apparent increase in rate constant. We have in all cases varied the initial partial pressures of the reactants over about a threefold range to be sure that our data were not complicated by secondary reactions. Under these conditions atomic nitrogen is in great excess, and the rate of the reaction is given by

$$k = \ln (R_0/R)/\int_0^t (N)\, dt \qquad (1)$$

where R_0 and R are the partial pressures of the reactants at times zero and t, respectively, and (N) is the atomic nitrogen concentration. Under our experimental conditions, loss of atomic nitrogen due to reaction or homogeneous recombination is negligible, the only significant loss mechanism being recombination on the walls of the reactor.

The atomic nitrogen partial pressure along the reaction tube was measured by titration with nitric oxide,[3] which also served to put the directly measured nitrogen atom partial pressure on an absolute basis.

The observed rate of decay of atomic nitrogen was sufficiently small so that the quantity $\int_0^t (N)\, dt$ in eq 1 could be repaced by $(N)_{av}t$, where $(N)_{av}$ is the average nitrogen atom concentration.[4] The latter typically corresponded to a partial pressure of about 0.005 torr.

When the reactor was operated at high temperatures, considerable outgassing occurred in the ion-source region of the mass spectrometer. This was reflected in a very great increase in background signal, which was particularly serious at masses less than 45.

In the case of ethylene and propene, this problem was avoided by using trideuterioethylene and hexadeuteriopropene, the parent ions of which are free from background interference. The measured rates will, therefore, reflect any kinetic isotope effects, although no effect was observed in a previous comparison of the propene and hexadeuteriopropene rate constants at 340°K.[1]

At least ten rate measurements were made for each compound studied. Assuming that the Arrhenius equation $k = A \exp(-E/RT)$ was applicable to these data, the parameters A and E, as given in Table I, were evaluated from a plot of $\log k$ vs. $1/T$. Computed uncertainties are standard deviations based on a least-squares treatment of the data. A plot of the deviations of the points from the computed line showed a random distribution, with no evidence of curvature.

Table I: Arrhenius Parameters for the Reactions of Atomic Nitrogen with Some Olefins and Acetylenes[a]

Reactant	Log A, cm³ mol⁻¹ sec⁻¹	E, cal mol⁻¹
	Olefins	
Ethylene, C_2HD_3	10.425 ± 0.208	760 ± 380
Ethylene[b]	10.204	700
Ethylene[c]	11.394	1900
Isobutene	10.893 ± 0.154	550 ± 270
Propene, C_3D_6	10.948 ± 0.145	1020 ± 270
Propene[b]	11.176	1650
2-Methyl-2-butene	10.966 ± 0.140	860 ± 250
1-Butene	11.190 ± 0.129	1310 ± 230
2,3-Dimethyl-2-butene	11.226 ± 0.099	1370 ± 170
cis-2-Butene	11.369 ± 0.082	1980 ± 150
trans-2-Butene	11.525 ± 0.071	2100 ± 125
	Acetylenes	
Acetylene[d]	$\cdots$	$\cdots$
Propyne	10.839 ± 0.153	1480 ± 280
2-Butyne	11.265 ± 0.133	1840 ± 250
1-Pentyne	11.468 ± 0.163	2080 ± 300
3-Hexyne	11.526 ± 0.122	2190 ± 220
1-Butyne	11.539 ± 0.114	2240 ± 210
1-Hexyne	11.664 ± 0.130	2450 ± 240

[a] This work, except as noted. [b] G. Paraskevopoulos and C. A. Winkler, J. Phys. Chem., **71**, 947 (1967). [c] L. I. Avramenko and V. M. Krasnen'kov, Izv. Akad. Nauk SSSR, Ser. Khim., 600 (1964). A and E were recomputed from the original date. [d] From 330 to 550°K, $k \leq 2 \times 10^9$ cm³ mol⁻¹ sec⁻¹. L. I. Avramenko and V. M. Krasnen'kov, Izv. Akad. Nauk SSSR, Ser. Khim., 822 (1964), give $k = (5.4 \times 10^8)T^{1/2} \exp[(-2300 \pm 299)/RT]$ cm³ mol⁻¹ sec⁻¹. At 550°K this leads to a rate constant approximately equal to our limiting value.

Results and Discussion

Arrhenius parameters for the reactions of atomic nitrogen with olefins and acetylenes are summarized in Table I. Our results are in good agreement with those of Paraskevopoulos and Winkler[5] for ethylene and

(2) F. S. Klein and J. T. Herron, J. Chem. Phys., **41**, 1285 (1964).

(3) G. B. Kistiakowsky and G. G. Volpi, ibid., **28**, 665 (1958).

(4) Assuming a first-order decay of atomic nitrogen, we calculate a recombination coefficient $\gamma = 2 \times 10^{-4}$ at 320 and 550°K. This value agrees quite well with γ(quartz) $= 5.5 \times 10^{-4}$ at 300°K reported by K. M. Evenson and D. S. Burch, J. Chem. Phys., **45**, 2450 (1966).

(5) G. Paraskevopoulos and C. A. Winkler, J. Phys. Chem., **71**, 947 (1967).

propene but differ from those of Avramenko and Kras-nen'kov[6] for the ethylene reaction. However, as can be seen from the table, our data for ethylene are of poor precision and it is difficult to compare them with the results of other workers, particularly in those cases where no indication of precision is given.

In the experiments of Paraskevopoulos and Winkler, the reaction was stopped at various times by means of a movable catalytic probe, and the rate constant was calculated from the over-all stoichiometry on the assumption that the hydrogen cyanide produced in the reaction was proportional to the atomic nitrogen consumed. Although the reaction is almost certainly so complex that the latter assumption is not strictly valid,[7] it does not appear to introduce any gross errors into the rate measurements.

Avramenko and Krasnen'kov base their rate measurements on the variation of product yield with reactant flow using a reactor having the walls coated with TiO_2. The assumptions required to derive rate data from this type of experiment are so open to question that it is difficult to have much confidence in their results.

The reactions of atomic nitrogen (^4S) with olefins and acetylenes to yield products in their ground electronic states are spin forbidden, and therefore the low A factors for these reactions are not unexpected.[8] Examination of the data of Table I does not reveal any obvious correlation between Arrhenius parameters and molecular structure. The only regularity in the data is the approximately linear dependence of the activation energy E on the preexponential factor A, which is the basis for ordering the data of Table I.

In addition to acetylene, we have found no measurable degree of reaction for CH_4, CH_3F, CH_3Cl, C_2HCl_3, $trans$-2-C_4F_8, and C_6H_6 (benzene). For these reactants, we estimate that at $500°K$, $k \leq 4 \times 10^9$ cm^3 mol^{-1} sec^{-1}. Although C_2H_3Cl and C_2H_3Br appeared to react at a rate comparable to that of ethylene, we have not studied these reactions in any detail.

The low degree of reactivity of atomic nitrogen suggests that these reactions could be initiated by highly reactive species, such as $N(^2S)$, $N_2(^3\Sigma_u^+)$, H, or O, produced in extremely minute quantities in the electrical discharge. However, evidence to support such a position has not been forthcoming. We have argued previously against atomic hydrogen or oxygen being

the initiating species,[1] and Starr and Shaw[9] have summarized the arguments against metastable nitrogen species originating in the discharge itself.[10] However, Campbell and Thrush[11] have now shown that $N_2(^3\Sigma_u^+)$ produced by the recombination of nitrogen atoms reacts with CO_2, NH_3, and N_2O. Furthermore, they have shown that the rate of reaction is directly proportional to the total pressure and to the square of the nitrogen atom partial pressure. We have attempted to observe similar rate dependencies in our work, with the results being shown in Table II. We find the rate constant to be essentially independent of initial atom concentration, time, or total pressure. If $N_2(^3\Sigma_u^+)$ were the initiating species, then we should expect that our observed rate constant would be directly proportional to $(N)P_{total}$, which clearly is not the case.

Table II: Rate Constant for the Reaction of Atomic Nitrogen with $trans$-2-Butene as a Function of Initial Atomic Nitrogen Partial Pressure, Total Pressure, and Reaction Time

T, °K	10^3t, sec	P_{total}, torr	10^3P_N, torr	Relative $P_N P_{total}$	$10^{-10}k$, cm^3 mol^{-1} sec^{-1}
319	16.7	1.77	3.57	1.0	1.19
319	24.7	2.62	5.68	2.4	1.35
337	22.8	2.90	5.51	2.5	1.55
319	38.0	4.03	5.15	3.3	1.36
337	22.8	2.90	7.43	3.4	1.42
364	16.0	4.17	11.3	7.5	1.31

Furthermore, we may note that if atomic hydrogen or oxygen were the initiating species, they would probably just as readily react with C_2H_2, C_2HCl_3, and $trans$-2-C_4F_8 as with any other unsaturated compound. Their lack of reactivity supports the conclusion that the reaction is not initiated by atomic hydrogen or oxygen.

(6) L. I. Avramenko and V. M. Krasnen'kov, *Izv. Akad. Nauk SSSR, Ser. Khim.*, 600 (1964).

(7) J. T. Herron, *J. Phys. Chem.*, **69**, 2736 (1965).

(8) H. G. V. Evans and C. A. Winkler, *Can. J. Chem.*, **34**, 1217 (1956).

(9) W. L. Starr and T. M. Shaw, *J. Chem. Phys.*, **44**, 4181 (1966).

(10) The arguments with respect to atomic hydrogen or oxygen apply only to the olefin reactions, inasmuch as they were partly based on a knowledge of the corresponding atomic hydrogen and oxygen rate constants. The equivalent data are not available for the acetylene reactions.

(11) I. M. Campbell and B. A. Thrush, *Chem. Commun.*, 932 (1967).

Study on the Kinetics of Fast Electrode Processes with

Pulse Technique and Electron Spin Resonance Methods

by Ryo Hirasawa, Takashi Mukaibo,

Department of Industrial Chemistry, the University of Tokyo, Bunkyo, Tokyo, Japan

Hideo Hasegawa, Noboru Odan, and Tetsuo Maruyama

Japan Electron Optics Laboratory, Akishima, Japan   (Received January 16, 1968)

Experiments have been carried out demonstrating a technique by which it is possible to observe, with esr methods, in a direct fashion the complete curve of the fast formation and the decay (in milliseconds) of radicals produced by pulse electrolysis. A loss of the signal-to-noise ratio for a rapid esr observation is compensated for by means of average accumulation with a spectrum computer. Some organic compounds such as dibutyl phthalate, anthracene, nitrobenzene, stilbene, diphenylacetylene, and tetraphenylethylene were treated with this method in acetonitrile solution with tetra-n-propylammonium perchlorate or bromide as the supporting electrolyte. There are three types of reactions in which the rate-determining step is in one of the following three consecutive processes: (i) in the electron transfer between the electrode and a depolarizer; (ii) in the desorption from the electrode; and (iii) following the reaction in the solution. The technique is useful not only in the investigation of kinetics and mechanisms of electrode processes but also for the study of the reactivity of paramagnetic species produced by the electrolysis.

Introduction

Techniques to determine the complete curve of the fast formation and the decay of radicals produced by pulse radiolysis[1] or the pulsed electron beam[2] were reported. A computer of average transients (C.A.T.)[1] or a "boxcar" integrator[2] in conjunction with an esr spectrometer for the enhancement of the signal-to-noise ratio of the curve was used. This paper is concerned with a technique for the study of the kinetics and mechanisms of short-lived paramagnetic intermediates (the lifetimes of which are longer than a few milliseconds) produced by *pulse electrolysis*. This technique is the combination of the recording of the esr signal intensity *vs.* time (*S–t* curve) at a fixed magnetic field and the use of a spectrum computer in treating the recordings of esr and the improvement of the signal-to-noise ratio. The pulse electrolysis technique, using a constant-current pulse, provided a powerful tool for the formation of organic intermediates[3] and was used in the measurement of the electric potential–time curve (*E–t* curve) for the study of mechanism of the electrode processes, the same as the galvanostatic-transient method.[4]

Some organic compounds such as dibutyl phthalate, nitrobenzene, anthracene, stilbene, diphenylacetylene, and tetraphenylethylene were treated with this method. It was possible to clarify the mechanism of the electrochemical formation of radicals generated from these substances and also to investigate the kinetics of decay behaviors of these radicals. The mechanisms, in all cases studied, are classified into three types according to the difference in the rate-determining step in the formation process of radicals.

Experimental Section

Equipment and Procedure. The block diagram of this method is given in Figure 1. Paramagnetic species are generated by the constant-current pulse electrolysis in an electrolytic cell placed directly into a microwave resonance cavity, so that it is possible to observe fast electrode processes involving adsorption and desorption on the electrode surface. The solution is pumped out through the electrolytic cell by a stroke pump or is circulated if the circulation of the solution does not affect any results. The electrode surface is renewed by the flow of the solution before the next pulse is charged. However, it was confirmed that the relation of the esr signal intensity to time was not influenced by the flow of solution during a certain time, which was determined by the flow rate of the solution. Only during the time, *e.g.*, 580 msec at 20 cm/sec, was it possible to observe a significant relation between the concentration of the paramagnetic substance and the time. The *S–t* curve was observed at a magnetic field fixed to the maximum or minimum intensity of a first-derivative signal under overmodulation. Because of the small amount of electricity in one shot pulse and the weak esr signal intensity of the rapid observation, which requires a spectrometer of short response time,

(1) L. H. Piette, presented at the Sixth International Symposium on Free Radicals, Cambridge, England, July 1963.

(2) R. W. Fessenden, *J. Phys. Chem.*, **68**, 1508 (1964).

(3) M. Fleischmann, I. N. Petrov, and W. F. K. Wynne-Jones, Proceedings of the First Australian Conference on Electrochemistry, Sydney, Australia, Feb 1963.

(4) P. Delahay, "New Instrumental Methods in Electrochemistry," Interscience Publishers, Inc., New York, N. Y., 1954, pp 179–216.
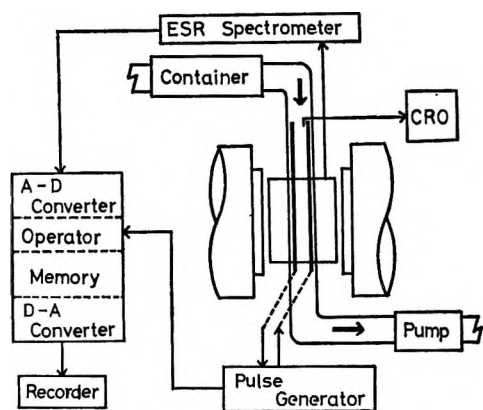
Figure 1. Schematic block diagram for the study of fast electrode processes.

Figure 2.　Esr signal intensity vs. time curves of the dibutyl phthalate anion radical, which was generated by the electrochemical reduction of 1.0×10^{-2} mol/l. of the parent molecule in acetonitrile with 0.1 mol/l. of tetra-n-propylammonium perchlorate: upper trace, one traverse; middle and lower trace, the results of the accumulation of 256 and 4096 traverses, respectively. The pulse width was 4 msec.

a spectrum computer is employed for the enhancement of the signal-to-noise ratio as an average-response computer.[5] The output from the esr spectrometer is transformed into digital numbers and is stored in a memory core of the spectrum computer triggered with a pulse generator. The summation of many transits is recorded, and the accumulated data are displayed on a recorder after the transformation from digital to analog. The signal-to-noise ratio is proportional to the square root of the response time and the square root of the number of the repetition of the experiments.[5] The effect of the accumulation is shown in Figure 2, which was obtained from the electrolytic pulse reduction of dibutyl phthalate in acetonitrile. A usual esr spectrum is composed by plotting S–t curves obtained at each point of different magnetic fields. Furthermore, for obtaining an esr spectrum, the rapid scanning of the magnetic field was combined with the technique described above successfully.[6] The relation of electric potential near the working electrode to time is observed with a cathode-ray oscilloscope and is recorded by a camera. Varying the pulse width and the current density, one may select any electrochemical condition corresponding to a potential plateau in the E–t curve.

The Pulse Generator. The pulse generator consists of two circuits of a monostable oscillator similar to a usual pulse generator[7] and supplies a rectangular constant-current pulse of 500 mA at the maximum. The pulse width and the pulse interval vary from 1 msec to 16 sec, independently.

The Electrolytic Cell. The electrolytic cell and its position in the microwave cavity are given in Figure 3. Both wire electrodes, platinum anode and silver cathode, are located in a quartz tube of which the inner and the outer diameter are 1.7 and 5 mm, respectively, and are kept strictly parallel with polyethylene resin, even outside of the resonance cavity with the same configuration as inside.[8] The working electrode, 0.5 mm in diameter and 8 cm in length, of which the lower 4.5 cm is placed in the resonance cavity, has an area of *ca.*

1.2 cm². The counter electrode has a radius of 0.3 mm. An aqueous saturated calomel electrode makes an electrolytic contact with the working electrode through a sintered-glass disk and a Luggin capillary. The resistance of the cell circuit was 12–15 ohms in the case of the solutions studied. The stroke-pump employed covers the flow-rate range from 1 to 250 cm/sec at the cell.

The Electron Spin Resonance Spectrometer. The esr spectrometer used in this study is partly different from the Japan Electron Optics Model 3BS-X, which has a Hall element to control the magnetic field and a vernier scale to set it. The output of the spectrometer is directly introduced from the end of the phase-sensitive detection unit, in which the capacitance is exchanged, so that the response time of the spectrometer becomes, theoretically, 0.5 msec.

The Spectrum Computer. The spectrum computer, Japan Electron Optics Model JRA-5, was used which has 4096 memories for the operation program and the

(5) M. P. Klein and G. W. Barton, Jr., *Rev. Sci. Instrum.*, **34**, 754 (1963).

(6) R. Hirasawa, T. Mukaibo, H. Hasegawa, Y. Kanda, and T. Maruyama, *ibid.*, in press.

(7) W. Jaenicke and H. Hoffman, *Ber. Bunsenges. Phys. Chem.*, **66**, 803 (1962).

(8) If the species generated at the counter electrode is observed with esr spectroscopy together with these at the working electrode, the counterion of the supporting electrolyte which is more depolarizable than the sample is required.
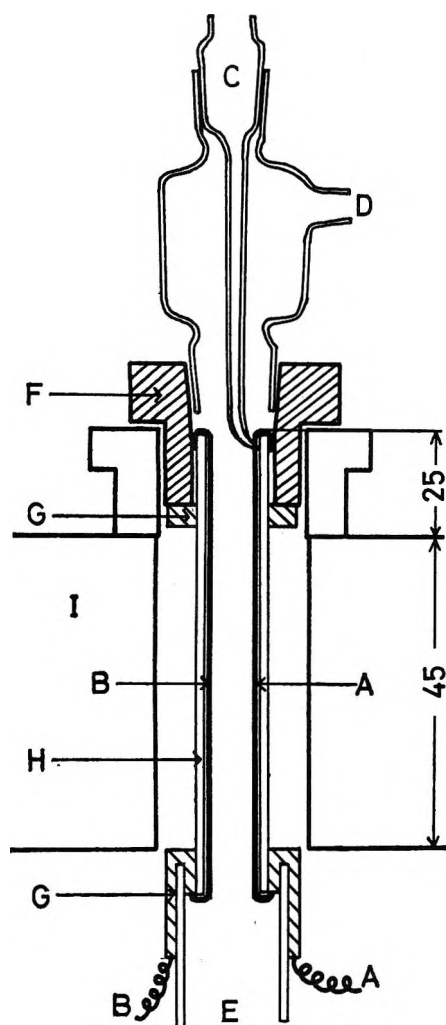
Figure 3. Electrolytic cell and its placement in the microwave resonance cavity: A, working electrode; B, counter electrode; C, Luggin capillary; D, inlet of solution; E, outlet; F, Teflon holder; G, polyethylene; H, quartz tube; I, resonance cavity.

data. The computer has a high speed A–D converter of successive comparison system and a D–A converter. The operating conditions are given in Table I.

The solution consists of a 1–10-mmol/l. depolarizer and a 0.1-mol/l. supporting electrolyte, both dissolved in acetonitrile. Reagent grade acetonitrile was puri-

Table I: The Operating Conditions of the Spectrum Computer

Program	Sampling period, μsec/point	Maximum number[a] of sampling points	Maximum number of accumulation times
A	20	2500	1,024
B	100	760	66,000
C	$360n^{b}$	3100	1,024

[a] The measuring time and the minimum experimental period are equal to the product of the sampling period and the number of sampling points employed. [b] $n = 1, 2, \ldots, 256$.

fied by the method of Coetzee, et al.[9] After distillation with phosphorus pentoxide, the solvent had a boiling point of 81.5° at 760 mm.

Tetra-n-propylammonium perchlorate, tetramethylammonium perchlorate, and tetra-n-butylammonium bromide, for use as supporting electrolytes, were prepared by neutralizing an aqueous solution of tetraalkylammonium hydroxide, obtained as a 10% aqueous solution from Tokyo Kasei Kogyo. These salts were purified by the method of Geske and Maki.[10] Dibutyl phthalate, nitrobenzene, anthracene, stilbene, diphenylacetylene, and tetraphenylethylene (all reagent grade) were used without further purification.

Discussion of the Experimental Method. The electrode process under study is expressed as

$$O + ne \xrightarrow{i} R \xrightarrow{k} P \tag{1}$$
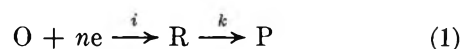
where O is the oxidant, R is the reductant, and P is the product. The flow of the solution is laminar in the method described above and is parallel to the electrodes, and the measuring time is so short as to allow one to suppose that the wire electrode employed is plane.[11] Thus the phenomenological equation involving diffusion, flow, and chemical reaction is

$$\frac{\partial C_R}{\partial t} = D_R \frac{\partial^2 C_R}{\partial r^2} - u \frac{\partial C_R}{\partial y} - kC_R \tag{2}$$

where C_R is the concentration of the reductant R, u is the flow rate of the solution parallel to the electrode, r is the perpendicular distance from the axis of the wire electrode (the y axis), D_R is the diffusion coefficient of the reductant, k is the rate constant of the first-order (or pseudo-first-order) reaction, and t is the time since the initiation of the pulse electrolysis. Since both wire electrodes are held parallel and only these lower parts are observed, one may assume that

$$\frac{\partial C_R}{\partial y} = 0 \tag{3}$$

during the time before no edge effect appears at the part of the electrode within the resonance cavity. Thus

$$\frac{\partial C_R}{\partial t} = D_R \frac{\partial^2 C_R}{\partial r^2} - kC_R \tag{4}$$

The initial and boundary conditions are: $C_R(r, 0) = 0$; $C_R(\infty, t) = 0$; and $-D_R C_R(r_0, t)/r = i/nF$, where r_0 is the radius of the electrode and i is current density. The esr signal intensity is given by solving eq 4

(9) J. F. Coetzee, G. P. Cunningham, D. K. McGuire, and G. R. Padmanabhan, *Anal. Chem.*, **34**, 1139 (1962).

(10) D. H. Geske and A. H. Maki, *J. Amer. Chem. Soc.*, **82**, 2671 (1960).

(11) P. Delahay, "New Instrumental Methods in Electrochemistry," Interscience Publishers, Inc., New York, N. Y., 1954, pp 68–70.

$$S \propto \int_{\tau_0}^{\infty} C_R \, dr = \frac{i}{nFk}(1 - e^{-kt}) \quad (t \le \tau) \quad (5a)$$

$$S \propto \int_{\tau_0}^{\infty} C_R \, dr = \frac{i}{nFk}(e^{k\tau} - 1)e^{-kt} \quad (t > \tau) \quad (5b)$$

where τ is the pulse width. For

$$kt \ll 1 \tag{6}$$

one obtains eq 7 from eq 5.

$$S \propto it/nF \quad (t \le \tau) \tag{7a}$$

$$S \propto i\tau/nF \quad (t > \tau) \tag{7b}$$

Relation 7 is also derived directly, under the condition that the current pulse is short compared with the flow of solution through the cell.

Nitrobenzene in acetonitrile solution undergoes an initial one-electron reduction near the half-wave potential of the first wave in the polarogram, as shown in reaction 1.[10] Since nitrobenzene anion radical is very stable in acetonitrile, relation 6 will be satisfied. Figure 4 is representative of the S-t curve of the nitrobenzene anion radical produced by the pulse electrolysis of nitrobenzene in a potential range corresponding to the first plateau in the galvanostatic transient. The signal intensity of the radical increases proportionally to the time elapsed since the beginning of the pulse electrolysis during the charging at a constant current and remains constant after the current is cut off. These behaviors agree with eq 7. However, this agreement is affected 580 msec after beginning to charge the pulse at the flow rate of 20 cm/sec. This suggests that the concentration profile along the y axis in the resonance cavity begins to change and eq 3 is not correct after this time.

It may be noted that if the additional magnetic field generated by the current through electrodes is large in comparison with the sharpness of the signal shape, the S-t curve is not available for kinetic studies so long as the pulse current is charged. For instance, the influence appeared in a measurement on the dibutyl phthalate anion radical overmodulated at 15 G in the case of the pulse current more than 350 mA.
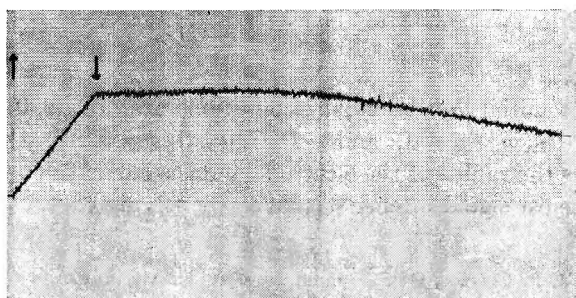
Figure 4. Formation curve (esr signal intensity $vs.$ time) of the nitrobenzene anion radical which was generated in the potential range of -0.5 to -0.6 V $vs.$ sce (the first plateau in the E-t curve). The pulse width was 150 msec.
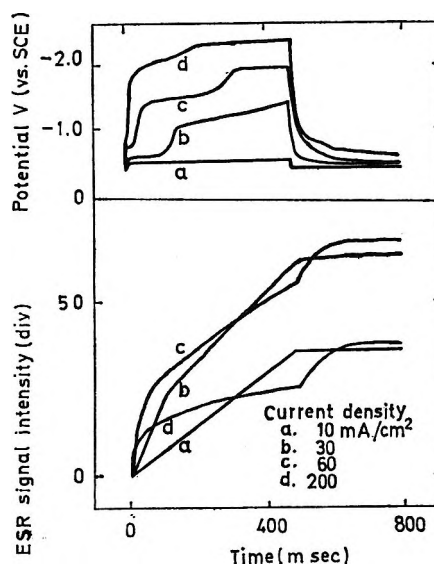
Figure 5. E-t and S-t curves in the pulse electrolysis of 1.6×10^{-2} mol/l. of nitrobenzene in acetonitrile with 0.1 mol/l. of tetra-n-propylammonium perchlorate at various current densities. The pulse width was 500 msec.

Results and Discussion

Typical S-t and E-t curves for the reduction of organic compounds are given in Figures 5 and 6 at several current densities and in Figure 7 for different pulse widths. The galvanostatic transient gives rise to several distinct plateaus in the E-t curves for various current densities and pulse widths. The behavior of the S-t curves corresponds to the difference of the plateaus.

As shown in Figure 5, for the reduction of nitrobenzene when the electric potential is on the first lowest plateau, the signal intensity of this radical increases linearly with time at several current densities, while in the second-plateau range, the velocity of the increase of the signal intensity becomes smaller than in the first, and if the potential is raised to the third stage, it discontinuously increases immediately after the current is cut off.[12] Similarly for anthracene, in the first plateau the signal intensity of the anthracene anion radical increases linearly with time, but in the second it decreases (Figure 6). In Figure 7, the S-t curves and the E-t curves for tetraphenylethylene are shown at various pulse widths. The signal intensity in the third plateau increases continuously even after the current is cut off. Similar observations were made for the reduction of dibutyl phthalate, stilbene, and diphenylacetylene.

(12) In the electrochemical reduction of nitrobenzene with tetra-n-butylammonium bromide, the same results as with tetra-n-propylammonium perchlorate were obtained. Even if the electrochemical reaction is made with a high current density and long pulse width, an esr signal was not observed for the reaction of tetra-n-butylammonium bromide only, while radicals were generated from perchlorate anion on an anode, as shown in Figure 10. Then we find that the supporting electrolyte does not affect the esr signal intensity under the condition employed for the reduction of nitrobenzene.
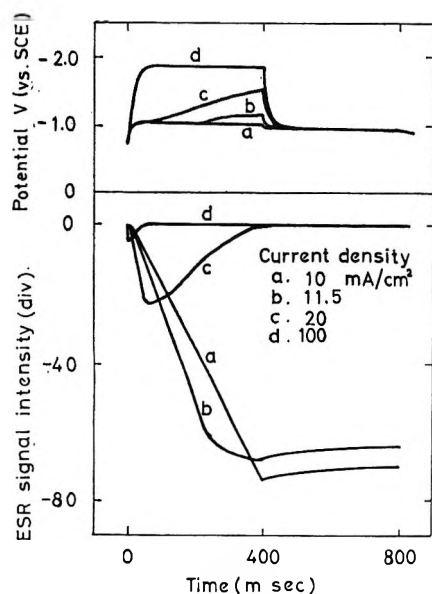
Figure 6. $E-t$ and $S-t$ curves in the pulse electrolysis of 1.0×10^{-2} mol/l. of anthracene in the same solution as nitrobenzene. The magnetic field was fixed at the field of minimum esr intensity of a first-derivative signal of the anion overmodulated at 5 G. The pulse width was 400 msec.
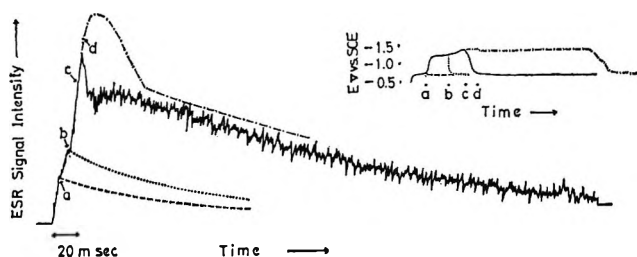
Figure 7. $E-t$ and $S-t$ curves in the pulse electrolysis of 6.0 $\times 10^{-2}$ mol/l. of tetraphenylethylene in the same solution as nitrobenzene for various pulse widths, indicated by a, b, c, and d. The current density was 10 mA/cm².

Figure 8. Three types of the esr signal intensity–time relation.
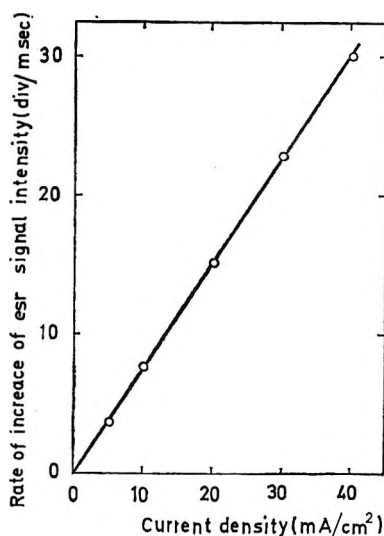
Figure 9. Rate of formation of the nitrobenzene anion radical *vs.* current density in the first-potential plateau.

A. *Formation Process of Radicals.* The formation processes of radicals observed by esr on each plateau of electric potentials are classified into three types, as shown in Figure 8, and are discussed below.

(*i*) *Direct Radical Formation Mechanism on the Electrode.* The first type of $S-t$ curve is shown in Figure 8a. The esr signal intensity increases in proportion to the time elapsed after beginning to charge the pulse current. The rate of increase of the esr signal intensity is proportional to the current density for the electrolysis, as shown in Figure 9, which was obtained in the electrochemical reduction of nitrobenzene at the first plateau of $E-t$ curve. On the basis of the eq 7, this result indicates that the rate of formation of radicals is controlled with the current density. Similar observations were made for the reduction of anthracene, dibutyl phthalate, stilbene, diphenylacetylene, and tetraphenylethylene on each potential plateau, as summarized in Table II.

(*ii*) *Desorption Mechanism from the Electrode.* In the second type, the signal intensity begins to increase immediately after the current is cut off, and then the depolarization on the electrode decreases, as shown in Figure 8b. The amount of radicals generated in this type is related to the depolarization potential. The reduction of nitrobenzene and also tetraphenylethylene at the third and the fourth plateau, respectively, belongs to this type. More typically, the oxidation of perchlorate anion demonstrates a similar behavior, as given in Figure 10. Both the amount of increase in the esr signal intensity of this radical,[13] ΔS, and the

(13) The esr spectrum of this radical agrees with that assigned to the perchlorate radical generated electrochemically in acetonitrile by Maki and Geske (A. H. Maki and D. H. Geske, *J. Chem. Phys.*, **30**, 1356 (1959)). The lifetime of this radical is about 10 sec in acetonitrile. Its hyperfine splitting of 17 G is small, in comparison with 50 and 72 G which were obtained from perchlorate radicals trapped in magnetically distinct sites in an irradiated crystal of KClO₄ (J. R. Morton, *J. Chem. Phys.*, **45**, 1800 (1966)), but is similar to the hyperfine splitting of ClO₂ radical in several solvents such as H₂O, H₂SO₄, and CCl₄, although the ClO₂ radical is stable in these solvents (N. Vanderkool, Jr., and T. R. Poole, *Inorg. Chem.*, **5**, 1351 (1966)).
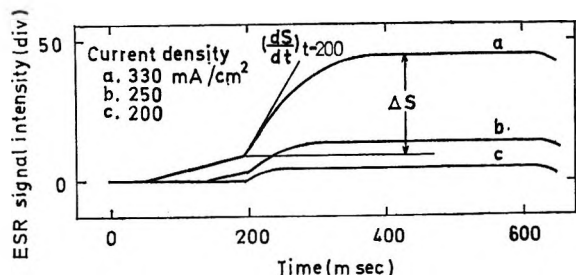
Figure 10. $E-t$ curves in the pulse electrolysis of 0.1 mol/l. of tetra-n-propylammonium perchlorate in acetonitrile at various current densities.

Figure 11. ΔS and $(dS/dt)_{t=200msec}$ vs. the amount of electricity for the oxidation of perchlorate anion.

Figure 12. Rapid-scan spectra observed in the first plateau (a) and in the third plateau (b).

velocity of increase immediately after the current is cut off, $(dS/dt)_{t=\tau}$, are proportional to the amount of the electricity for the oxidation at the first plateau in the potential range of 1.0–1.1 V vs. sce (Figure 11). Assuming that the amount of the electricity supplied on the anode surface is proportional to the amount of adsorption, these behaviors are explained kinetically when the desorption from the electrode is the rate determining factor.

(iii) *Following Reaction Mechanism in Solution.* The third type is shown in Figure 8c. As the signal intensity increases continuously even after the current is cut off, the rate-determining step is considered not to be directly related to the electron transfer. However, the maximum value of the $S-t$ curve increases with amount of electricity for the electrolysis in the potential plateau related to this type. For example, tetraphenylethylene reacts at the electrode in the first plateau with the electron-transfer mechanism in the third plateau, which is in a more negative potential range than the first one. At the potential on the third plateau and at a current density of 10 mA/cm², it is found that the concentration of radicals increases at two different rates even after the current is cut off, as given in Figure 7. At the higher current density or longer pulse width, it becomes impossible to distinguish these two processes in the $S-t$ curve. However, it was observed by means of the rapid scanning of the magnetic field during the electrolysis where the potential is on the third plateau that two radicals are detected almost overlapping each other in the esr spectrum, observed under the condition of the exchange broadening. On the other hand, in the first plateau, a kind of radical is produced, of which the spectrum coincides with that of a kind of radicals in the third plateau in respect to the peak-to-peak value of 6.2 G, as shown in Figure 12. On the basis of the foregoing evidence, it is appropriate to assume that these two radicals are produced by means of the chemical reaction between the reduction products, e.g., the tetraphenylethylene dianion, generated electrochemically in the third plateau, and the surrounding molecules. This assumption is consistent with the experimental results of the large-scale electrochemical reduction of tetraphenylethylene (5.0 g) to
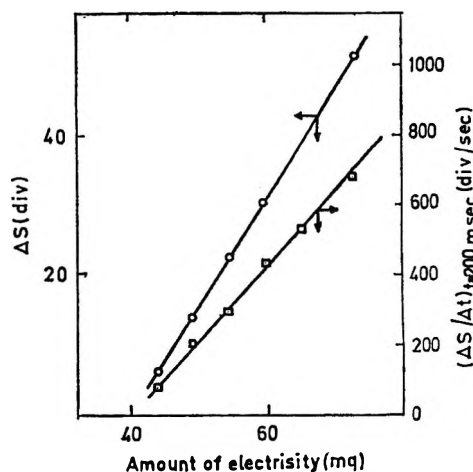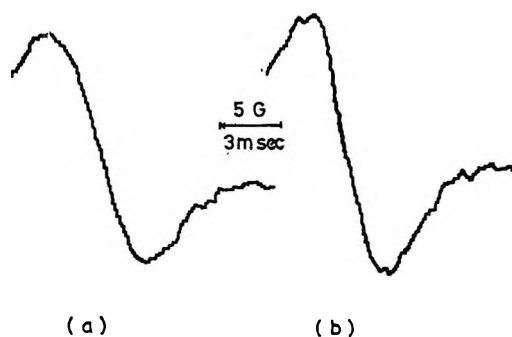
1,1,2,2-tetraphenylethane (2.4 g) and diphenylmethane (2.0 g) in acetonitrile with tetra-n-butylammonium iodide as the supporting electrolyte.[14] Thus in this third type of $S-t$ curve, the rate-determining step for the formation of radicals is regarded as a chemical reaction following the electron transfer and/or a charge transfer between reduced products and the surrounding molecules in the solution. All results of the pulse electrolysis for the compounds studied are summarized in Table II.

B. *Decay Process of Radicals.* In the case where the chemical reaction following the electron transfer is a first-order (or pseudo-first-order) reaction, the rate constant of the reaction for the radical produced in the direct radical formation mechanism is calculated from eq 5b.

For the dibutyl phthalate anion radical produced by the electrochemical reduction in acetonitrile, it was found from the decay behavior of the $S-t$ curve that the logarithm of the signal intensity is proportional to the time elapsed since the current is cut off. Because the reduction product is dihydrodibutyl phthalate, it seems

(14) S. Wawzonek, E. W. Blaha, R. Berkey, and M. E. Runner, *J. Electrochem. Soc.*, **102**, 235 (1955)

Table II: Results of Pulse Electrolysis[a]

Compound	Potential plateau	$E_{T/4}$[b] (V vs. sce)	Mechanism for formation of radicals	Half-life of radicals, msec
Nitrobenzene	1st	−0.6	c	i
	2nd	−1.4	f	i
	3rd	−2.0	d	i
Anthracene	1st	−1.0	c	i
	2nd	−1.6	g	
Dibutyl-phthalate	1st	−0.5	h	
	2nd	−1.2	c	27
Stilbene	1st	−1.0	h	
	2nd	−1.4	h	
	3rd	−1.7	c	120
	4th	−2.0	g	
Diphenyl-acetylene	1st	−0.9	h	
	2nd	−1.1	h	
	3rd	−1.7	c	i
	4th	−2.0	g	
Tetraphenyl-ethylene	1st	−0.7	c	180
	2nd	−1.2	f	180
	3rd	−1.4	e	∼180
			e	∼10
	4th	−1.7	d	

[a] All experiments performed at 22°. [b] Reference 4. [c] Direct radical formation. [d] Desorption. [e] Following chemical reaction. [f] The current efficiency for the formation of radicals is smaller than in the first potential plateau. [g] Anion radicals produced in the more positive potential plateau disappear in this plateau. [h] Independent of radicals. [i] The half-life of the radical is too long to be measured.

that the radical disappears according to a pseudo-first-order reaction between the solvent and the anion radical. The rate constant is 25.5 sec⁻¹. Similarly, the rate constant found for the pseudo-first-order
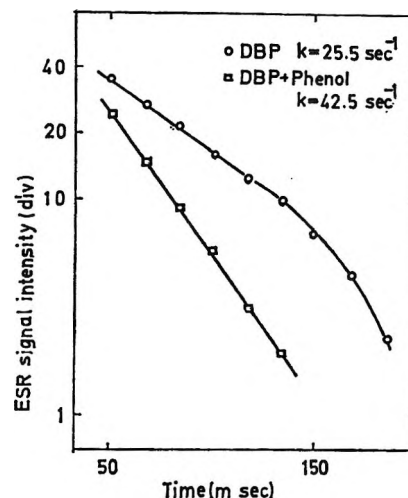
Figure 13. Rate of the decay process of the dibutyl phthalate anion radical in acetonitrile. The concentration of dibutyl phthalate and phenol was 2.0×10^{-3} and 0.1 mol/l., respectively.

disappearance of dibutyl phthalate anion radical in acetonitrile with phenol is 42.5 sec⁻¹ (Figure 13).

On the other hand, if the chemical reaction following the electron transfer is second order for radicals, we cannot investigate the kinetics of disappearance of these species in a direct fashion as described above. The conclusion is rather tentative regarding the "chemistry" as it is in most cases discussed in this article.

New Forms of McKay–Perring Equations

by Chai-fu Pan

Department of Chemistry, Alabama State College, Montgomery, Alabama   36101   (*Received January 17, 1968*)

Some new forms of McKay–Perring equations may be derived from McKay–Perring equations, equations of Randall and White, and Robinson and Sinclair. The derived equations can be applied to calculate the mean activity coefficients of electrolytes of the same charge type in mixed solutions if sufficient information about the osmotic coefficients of the mixture is available. This can be obtained from isopiestic vapor pressure measurements. At fixed total molality, the osmotic coefficients of the mixture may be expressed as a polynomial function of the stoichiometric molality fraction of an electrolyte, from which the integral parts in the derived equations can easily be evaluated. Alternate forms of these equations can also be used to obtain the relative activity coefficients if osmotic data for solutions in dilute region are not available.

Introduction

McKay[1] first pointed out that activities of nonvolatile solutes in a mixed solution can be determined from measurements of vapor pressure alone. In ternary aqueous systems, the activities of the three components are connected by the cross-differentiation equation. From a series of transformations and the application of the Gibbs–Duhem equation to the reference electrolyte, McKay and Perring[2] were able to derive equations which are suitable for integration to evaluate the mean activity coefficients of the component solutes by the isopiestic method. These equations are valid when isopiestic measurements are made on a number of mixtures in which electrolytes B and C are present in different concentration fractions but at constant water activity.

Robinson[3–6] has given numerical illustrations of the McKay–Perring equations. However, he limited himself to the case for which the reference electrolyte is solute B or C, a component in the test mixture. Electrolyte B or C should not be chosen as the reference if its thermodynamic properties (*e.g.*, osmotic or activity coefficients) are not available. Bonner and Holland[7] have given equations in a more general form, independent of the kind of electrolyte used as a reference. Nevertheless, following the original derivation of McKay and Perring,[2] they retain the function *m*, which is any linear combination of the molalities of electrolytes B and C in their equations. This makes the integral parts of their equations somewhat more complicated in numerical calculations.

New forms of McKay–Perring equations can be derived from McKay–Perring equations, equations of Randall and White, and Robinson and Sinclair. The derived equations may be applied to evaluate activity coefficients of electrolytes of the same charge type in mixed solutions if sufficient information about the osmotic coefficients of the mixture is available.

Derivation of Relations

For single electrolyte solutions, the mean activity coefficient of the solute, γ, is related to the practical osmotic coefficient of the solution, ϕ, by the Randall and White equation[8]

$$\ln \gamma = (\phi - 1) + \int_{m=0}^{m} (\phi - 1)\, \mathrm{d} \ln m \qquad (1)$$

where m is the molality of the solution. By applying the Gibbs–Duhem equation to a pair of isopiestic solutions, Robinson and Sinclair[9] were able to derive an equation to compute the mean activity coefficient of an electrolyte at any concentration providing the mean activity coefficient of the reference electrolyte is known. The Robinson and Sinclair equation is

$$\ln \gamma = \ln \gamma_R + \ln R + \int_{m_R=0}^{m_R} (R - 1)\, \mathrm{d} \ln (\gamma_R m_R) \qquad (2)$$

where R is the isopiestic ratio, γ is the mean activity coefficient of the test electrolyte at molality m, γ_R is the mean activity coefficient of the reference electrolyte at molality m_R, and m_R and m are the equilibrium molalities of the reference electrolyte and test electrolyte, respectively.

The McKay–Perring equations may be written in a more convenient form[5,7]

(1) H. A. C. McKay, *Nature*, **169**, 464 (1952).

(2) H. A. C. McKay and J. K. Perring, *Trans. Faraday Soc.*, **49**, 163 (1953).

(3) R. A. Robinson, *Trans. Faraday Soc.*, **49**, 1411 (1953).

(4) R. A. Robinson, *J. Phys. Chem.*, **65**, 662 (1961).

(5) R. A. Robinson and V. E. Bower, *J. Res. Nat. Bur. Stand.*, **69A**, 19 (1965).

(6) R. A. Robinson and V. E. Bower, *ibid.*, **69A**, 439 (1965).

(7) O. D. Bonner and V. F. Holland, *J. Amer. Chem. Soc.*, **77**, 5828 (1955).

(8) M. Randall and A. M. White, *ibid.*, **48**, 2514 (1926).

(9) R. A. Robinson and D. A. Sinclair, *ibid.*, **56**, 1830 (1934).

$$\ln \gamma_B = \ln \gamma_R + \ln R +$$
$$\int_0^{mR\phi R}\left[-\frac{y_C}{m_R}\left(\frac{\partial R}{\partial y_C}\right)_{a_w} + \frac{R-1}{m_R}\right]d\,(m_R\phi_R)$$

$$(3)$$

$$\ln \gamma_C = \ln \gamma_R + \ln R +$$
$$\int_0^{mR\phi R}\left[-\frac{y_B}{m_R}\left(\frac{\partial R}{\partial y_B}\right)_{a_w} + \frac{R-1}{m_R}\right]d\,(m_R\phi_R)$$

$$(3)$$

where γ_R is the mean activity coefficient of the reference electrolyte at molality m_R which is isopiestic with the mixture containing electrolytes B and C; the molalities of electrolytes B and C in the mixture are m_B and m_C, respectively; ϕ_R is the osmotic coefficient of the reference electrolyte at molality m_R; R is the isopiestic ratio, which is defined as

$$R = \frac{\nu_R m_R}{\nu_B m_B + \nu_C m_C} \qquad (4)$$

ν_i is the number of ions per "molecule" of electrolyte i; y_B and y_C are the stoichiometric ionic fraction of electrolytes B and C in the mixed solution respectively; i.e.

$$y_B = \frac{\nu_B m_B}{\nu_B m_B + \nu_C m_C} \qquad (5)$$

$$y_C = \frac{\nu_C m_C}{\nu_B m_B + \nu_C m_C}$$

By comparison of eq 2 with eq 3, it is easy to see that the contribution to $\ln \gamma_B$ and $\ln \gamma_C$, due to the presence of another solute, is given by the corresponding first term in the bracket in eq 3 over the interval of integration; i.e.

$$\int_0^{mR\phi R}\left[-\frac{y_C}{m_R}\left(\frac{\partial R}{\partial y_C}\right)_{a_w}\right]d\,(m_R\phi_R)$$

and

$$(6)$$

$$\int_0^{mR\phi R}\left[-\frac{y_B}{m_R}\left(\frac{\partial R}{\partial y_B}\right)_{a_w}\right]d\,(m_R\phi_R)$$

For simplicity, we limit ourselves to the case where B, C, and the reference electrolyte are all of the 1:1 charge type. That is $\nu_B = \nu_C = \nu_R = 2$; then $y_B = m_B/m$, $y_C = m_C/m$, and $R = m_R/m$, where $m = m_B + m_C$. At constant y_B, the terms in (6) can then be written as

$$y_C \int_0^{mR\phi R} \frac{1}{m_R}\left(\frac{\partial R}{\partial y_B}\right)_{a_w} d\,(m_R\phi_R)$$

and

$$(7)$$

$$-y_B \int_0^{mR\phi R} \frac{1}{m_R}\left(\frac{\partial R}{\partial y_B}\right)_{a_w} d\,(m_R\phi_R)$$

Recall the relationship for the isopiestic solutions in question

$$m\phi = m_R\phi_R$$

Thus

$$\left(\frac{\partial R}{\partial y_B}\right)_{a_w} = -\frac{m_R}{m^2}\left(\frac{\partial m}{\partial y_B}\right)_{a_w} = -\frac{m_R}{m^2}\left(\frac{\partial m}{\partial y_B}\right)_{m_R\phi_R} \qquad (8)$$

and

$$\left(\frac{\partial \phi}{\partial y_B}\right)_m = \frac{1}{m}\left[\frac{\partial(m_R\phi_R)}{\partial y_B}\right]_m \qquad (9)$$

From eq 8 and 9 and with the relationship

$$\left[\frac{\partial m}{\partial y_B}\right]_{m_R\phi_R}\left[\frac{\partial y_B}{\partial(m_R\phi_R)}\right]_m\left[\frac{\partial(m_R\phi_R)}{\partial m}\right]_{y_B} = -1 \qquad (10)$$

we obtain

$$\frac{1}{m_R}\left(\frac{\partial R}{\partial y_B}\right)_{a_w} d\,(m_R\phi_R) = \left(\frac{\partial \phi}{\partial y_B}\right)_m d \ln m \qquad (11)$$

at constant y_B. Thus, expression 7 becomes

$$y_C \int_{m=0}^m \left(\frac{\partial \phi}{\partial y_B}\right)_m d \ln m$$

and

$$(12)$$

$$-y_B \int_{m=0}^m \left(\frac{\partial \phi}{\partial y_B}\right)_m d \ln m$$

By placing a contribution term due to the presence of a "foreign" salt in the Robinson and Sinclair equation, the McKay–Perring equation can be formulated. The contribution terms have been transformed to be "harmonic" to the terms in the Randall and White equation. By adding the corresponding terms of expression 6 to the right-hand side of the Robinson and Sinclair equation, and expressing the left-hand side $\ln \gamma$ as $\ln \gamma_B$ or $\ln \gamma_C$, we obtain the McKay–Perring equation. Similarly, by adding the corresponding terms of expression 12 (equivalent to the terms in expression 6) to the right-hand side of the Randall and White equation (equivalent to the Robinson and Sinclair equation), and expressing the left-hand side $\ln \gamma$ as $\ln \gamma_B$ or $\ln \gamma_C$, new forms of McKay–Perring equations are obtained

$$\ln \gamma_B = (\phi - 1) + \int_{m=0}^m (\phi - 1) d \ln m +$$
$$y_C \int_{m=0}^m \left(\frac{\partial \phi}{\partial y_B}\right)_m d \ln m$$

$$(13)$$

$$\ln \gamma_C = (\phi - 1) + \int_{m=0}^m (\phi - 1) d \ln m -$$
$$y_B \int_{m=0}^m \left(\frac{\partial \phi}{\partial y_B}\right)_m d \ln m$$

From eq 13 it is easy to show that for two-salt solutions, eq 1 becomes

$$y_B \ln \gamma_B + y_C \ln \gamma_C =$$

$$(\phi - 1) + \int_{m=0}^{m} (\phi - 1) \, d \ln m \quad (14)$$

We also obtain a simple relationship between γ_B and γ_C

$$\ln \frac{\gamma_B}{\gamma_C} = \int_{m=0}^{m} \left(\frac{\partial \phi}{\partial y_B}\right)_m d \ln m \quad (15)$$

The integrations in eq 13 are performed at fixed values of y_B; the integrals may be evaluated by graphical methods. Equation 13 can be applied to single electrolytes as well as to mixtures containing electrolytes B and C of the 1:1 charge type. Following the above derivation, one can show that eq 13 is also valid for mixtures of B and C of the same charge type. The reference salt may be the same or different. As $y_B \rightarrow 0$ or $y_B \rightarrow 1$, eq 13 can be used to evaluate the limiting value of γ for a solute in a mixture of total molality m.

Discussion

Since the isopiestic method is not applicable in concentrations less than 0.1 m, extrapolations at lower concentrations yield crude estimates of the required area. Due to the difficulty of extrapolating, alternate forms of eq 13 may be used to evaluate the relative values of the mean activity coefficient of the solutes, i.e.

$$\ln \frac{\gamma_B}{\gamma_B'} = (\phi - \phi') + \int_{m=m'}^{m} (\phi - 1) \, d \ln m +$$
$$y_C \int_{m=m'}^{m} \left(\frac{\partial \phi}{\partial y_B}\right)_m d \ln m$$
$$(16)$$

$$\ln \frac{\gamma_C}{\gamma_C'} = (\phi - \phi') + \int_{m=m'}^{m} (\phi - 1) \, d \ln m -$$
$$y_B \int_{m=m'}^{m} \left(\frac{\partial \phi}{\partial y_B}\right)_m d \ln m$$

where γ_B' and γ_C' are activity coefficients of electrolytes B and C in the mixture at total molality m', respectively, and ϕ' is the osmotic coefficient of the mixture at total molality m', all at the same value of y_B as in the solution of molality m.

One advantage of the derived equations over McKay-Perring equations lies in the fact that theoretical guides for extrapolation to infinite dilution are more readily expressible in terms of ϕ than in terms of R.

The osmotic coefficient of the mixed solution at constant total molality may be expressed as a polynomial function of y_B.[10-12] The polynomial functions at different fixed values of m can be obtained by the interpolation of isopiestic data. If Harned's rule[11] holds for both electrolytes B and C, the osmotic coefficient of the mixture is a quadratic function of y_B. If a higher order β term is necessary to be added to mod-

ify Harned's rule, the osmotic coefficient in the mixture is then a cubic function of y_B. The osmotic coefficient in aqueous mixtures of NaOH–NaCl[13] and NaCl–KCl[4] should thus be expressed as cubic functions of y_B. Still higher terms are required to show the deviations from Harned's rule when larger chemical interaction is encountered.

For dilute 1:1 electrolyte solutions, the mean activity coefficient of the solute may be expressed by a modified Debye–Hückel law of the form

$$\ln \gamma = -\frac{2.3 A m^{1/2}}{1 + B \dot{a} m^{1/2}} + Cm + Dm^2 + \ldots \quad (17)$$

where $A, B, C, D, \ldots$ are constants for a given system at constant temperature; $\dot{a}$ is an average ion-size parameter assumed to be constant for a given solution. The constants A and B here are slightly different from the values tabulated by Robinson and Stokes[14] at different temperatures by a factor $d^{1/2}$; d is the density of solvent.[15] Constants $C, D, \ldots$ may be determined experimentally. The osmotic coefficient of the solution can then be derived by the relation[16]

$$\phi = 1 + \frac{1}{m} \int_{m=0}^{m} m \, d \ln \gamma \quad (18)$$

For very dilute solutions, ϕ may be expressed as a function of m in the form

$$\phi = 1 + K_1 m^{1/2} + K_2 m + K_3 m^{3/2} + \ldots \quad (19)$$

where K_i's are constants.

Equation 19 suggests that for very dilute 1:1–1:1 mixtures, ϕ retains the same form. However, the constants $K_2, K_3, \ldots$ are now functions of y_B; $(1 + K_1 m^{1/2})$ are Debye–Hückel limiting law terms, they should be independent of composition. Hence, at a fixed value of y_B, the function $(\partial \phi / \partial y_B)_m$ may be expressed as a polynomial in powers of $m^{1/2}$, but starting from a linear term in m; in the limit of very low concentration, the derivative is a linear function of m.

Scatchard's equation[17,18] for ϕ in 1:1–1:1 mixtures can be written as

$$\phi = y_B \phi_B^0 + y_C \phi_C^0 + \frac{1}{2} y_B y_C \beta_0 \quad (20)$$

(10) B. B. Owen and T. F. Cooke, Jr., *J. Amer. Chem. Soc.*, **59**, 2273 (1937).

(11) H. S. Harned and B. B. Owen, "The Physical Chemistry of Electrolytic Solutions," 3rd ed, Reinhold Publishing Corp., New York, N. Y., 1958, Chapter 14.

(12) G. N. Lewis and M. Randall (revised by K. S. Pitzer and L. Brewer) "Thermodynamics," 2nd ed, McGraw-Hill Book Co. Inc., New York, N. Y., 1961, pp 570, 571.

(13) H. S. Harned and M. A. Cook, *J. Amer. Chem. Soc.*, **59**, 1890 (1937).

(14) R. A. Robinson and R. H. Stokes, "Electrolyte Solutions," 2nd ed, Butterworth and Co. Ltd., London, 1959, p 468.

(15) Reference 12, p 338.

(16) Reference 14, p 34.

(17) G. Scatchard, *J. Amer. Chem. Soc.*, **83**, 2636 (1961).

(18) R. M. Rush and R. A. Robinson, *J. Tenn. Acad. Sci.*, in press.

where superscript 0 refers to a solution of a single salt at molality m; β_0 is a function of m but not of y_B, so that

$$\left(\frac{\partial \phi}{\partial y_B}\right)_m = \phi_B{}^0 - \phi_C{}^0 + \frac{1}{2}(y_C - y_B)\beta_0 \quad (21)$$

Thus from eq 13

$$\ln \gamma_B = y_B \phi_B{}^0 + y_C \phi_C{}^0 -$$
$$1 + \int_{m=0}^{m} (y_B \phi_B{}^0 + y_C \phi_C{}^0 - 1) \, d \ln m +$$
$$y_C \int_{m=0}^{m} (\phi_B{}^0 - \phi_C{}^0) \, d \ln m + \frac{1}{2} y_B y_C \beta_0 +$$
$$\frac{1}{2} \int_{m=0}^{m} y_B y_C \beta_0 \, d \ln m +$$
$$\frac{1}{2} y_C \int_{m=0}^{m} (y_C - y_B)\beta_0 \, d \ln m \quad (22)$$

At constant y_B, eq 22 can be simplified, *i.e.*

$$\ln \gamma_B = y_B \phi_B{}^0 + y_C \phi_C{}^0 -$$
$$1 + \int_{m=0}^{m} (\phi_B{}^0 - 1) \, d \ln m +$$
$$\frac{1}{2} y_B y_C \beta_0 + \frac{1}{2} y_C{}^2 \int_{m=0}^{m} \beta_0 \, d \ln m \quad (23)$$

but

$$\ln \gamma_B{}^0 = (\phi_B{}^0 - 1) + \int_{m=0}^{m} (\phi_B{}^0 - 1) \, d \ln m \quad (24)$$

Thus

$$2 \ln \frac{\gamma_B}{\gamma_B{}^0} = 2(\phi_C{}^0 - \phi_B{}^0) y_C + y_C \beta_0 +$$
$$y_C{}^2 \int_{m=0}^{m} \beta_0 \, d \ln m - y^2 \beta_0 \quad (25)$$

Scatchard has also defined a function B_0 such that

$$\beta_0 = \frac{dB_0}{d \ln m} \quad (26)$$

Hence

$$2 \ln \frac{\gamma_B}{\gamma_B{}^0} = 2(\phi_C{}^0 - \phi_B{}^0) y_C +$$
$$y_C \beta_0 + y_C{}^2 (B_0 - \beta_0) \quad (27)$$

This is Scatchard's equation for $\ln \gamma_B$, assuming that there is no term in $y_B y_C (y_B - y_C)$ in ϕ. Rush and Robinson[18] used Scatchard's equation to treat the Na-Cl–KCl–H$_2$O system. They evaluated functions of γ_B and γ_C which are consistent with the above derivations using the new forms of McKay–Perring equations.

Nuclear Magnetic Resonance Spectra of Mono- and Disubstituted

Benzenes Containing OH, SH, NH$_2$, and COOH

by H. B. Evans, Jr., A. R. Tarpley,[1] and J. H. Goldstein

Department of Chemistry, Emory University, Atlanta, Georgia 30322   *(Received January 18, 1968)*

Nmr spectra have been analyzed for four monosubstituted benzenes (OH, SH, NH$_2$, and COOH) and 13 disubstituted derivatives containing the same substituents. Substituent effects on the coupling parameters have been determined for all positions and have been found to be additive in the disubstituted compounds, the average deviation from additivity being 0.085 Hz for 62 couplings. A reasonably satisfactory additivity relation also holds for most of the chemical shifts. The effect of substituents on the coupling parameters, including previously obtained data, has been shown to correlate quite well with substituent (group) electronegativities. The results were also found to be useful in nmr spectral assignments and analysis for aromatic compounds.

Introduction

Considerable interest has been directed toward obtaining and interpreting the nmr parameters of the monosubstituted benzenes following the early work of Corio and Dailey.[2] Because of difficulties inherent in the analysis of the spectral patterns of these systems, simplification by selective deuteration has been resorted to by some investigators.[3-5] More recently, improvements in spectrometer performance and the availability of high-speed, iterative computer programs for nmr spectral analysis have greatly facilitated the study of these spectra.[5-11] One point of widespread interest has been the question of additivity of substituent effects on the chemical shifts in polysubstituted benzenes.[10-17] Recently, the existence of additivity relations for the proton–proton coupling parameters in various halogen substituted benzenes has also been established.[10,17,18] This latter development has stemmed, in large part, from a series of precise analyses of the monohalobenzene spectra and of the [13]CH satellite spectrum of benzene itself.[8,17,19] In this article we describe the results of nmr spectral analyses for phenol, benzoic acid, aniline, benzenethiol, and for 13 disubstituted benzenes derived from these compounds, all carried out under uniform experimental conditions. Precise and complete analyses for these compounds either have not been previously reported or the studies were performed under varying experimental conditions.[7,11,20-24] The results of this work indicate that additivity relations hold for both the chemical shifts and the couplings in the compounds studied.

Finally, we have established simple correlations between substituent electronegativity and the proton–proton coupling parameters in the corresponding monosubstituted benzenes, utilizing the new results described below, as well as previous data obtained here under quite similar conditions. These results extend con-

siderably the correlations of this type that have been previously observed.[8,11,17-20,23,24]

Experimental Section

All compounds used in this study were the commercially available materials and required no further purifi-

(1) NDEA Fellow, 1967–1968.

(2) P. L. Corio and B. P. Dailey, *J. Amer. Chem. Soc.*, **78**, 3043 (1956).

(3) H. Spiesecke and W. G. Schneider, *J. Chem. Phys.*, **35**, 731 (1961).

(4) J. L. Garnett, L. J. Henderson, W. A. Sollich, and G. V. D. Tiers, *Tetrahedron Lett.*, 516 (1961).

(5) R. E. Mayo and J. H. Goldstein, *Mol. Phys.*, **10**, 301 (1965).

(6) S. Castellano and J. Lorenc, *J. Phys. Chem.*, **69**, 3552 (1965).

(7) J. C. Schug and J. C. Deck, *J. Chem. Phys.*, **37**, 2618 (1962).

(8) J. M. Read, Jr., and J. H. Goldstein, *J. Mol. Spectrosc.*, **23**, 179 (1967).

(9) J. E. Loemker, J. M. Read, Jr., and J. H. Goldstein, *Mol. Phys.*, **13**, 433 (1967).

(10) R. W. Crecely, J. M. Read, Jr., R. S. Butler, and J. H. Goldstein, submitted for publication.

(11) J. M. Read, Jr., Ph.D. Dissertation, Emory University, Atlanta, Ga., 1967.

(12) J. S. Martin and B. P. Dailey, *J. Chem. Phys.*, **39**, 1722 (1963).

(13) P. Diehl, *Helv. Chim. Acta*, **44**, 829 (1961).

(14) J. B. Leane and R. E. Richards, *Trans. Faraday Soc.*, **55**, 707 (1959).

(15) W. B. Smith and G. M. Cole, *J. Phys. Chem.*, **69**, 4413 (1965).

(16) W. B. Smith and J. L. Roark, *J. Amer. Chem. Soc.*, **89**, 5018 (1967).

(17) J. E. Loemker, J. M. Read, Jr., and J. H. Goldstein, *J. Phys. Chem.*, **72**, 991 (1968).

(18) B. Dischler, *Z. Naturforsch.*, **20**, 888 (1965).

(19) J. M. Read, Jr., R. E. Mayo, and J. H. Goldstein, *J. Mol. Spectrosc.*, **22**, 419 (1967).

(20) R. R. Fraser, *Can. J. Chem.*, **44**, 2737 (1966).

(21) M. Ohnishi and Y. Kawazae, *Chem. Pharm. Bull.* (Tokyo), **12**, 938 (1964).

(22) I. Yamaguchi and N. Hayakawa, *Bull. Chem. Soc. Jap.*, **33**, 1128 (1960).

(23) P. F. Cox, *J. Amer. Chem. Soc.*, **85**, 380 (1963).

(24) S. Castellano and C. Sun, *ibid.*, **88**, 4741 (1966)

cation, as indicated by their nmr spectra, except for m-hydroxyphenol and m-aminobenzoic acid, which were recrystallized. A preliminary investigation of the physical properties of these compounds indicated that methanol would be a uniformly suitable solvent for the series. Therefore, the samples were prepared as approximately 5 mol % solutions in methanol and were degassed with a stream of nitrogen. All spectra were recorded on a Varian A-60-A nmr spectrometer. Calibrations were performed by the usual side-band technique using an audio oscillator constantly monitored by a frequency counter. The reported line frequencies are averages of at least three forward and three reverse traces and the mean deviation for a typical resonance line is approximately 0.05 Hz. The chemical shifts are referenced to external water in order to avoid possible errors arising from interactions of the internal reference with the solvent.

The chemical shifts were corrected for bulk susceptibilities which were determined according to the empirical method of Frei and Bernstein.[25] A calibration curve was constructed using five compounds, and a least-squares treatment of these data indicated that the bulk-susceptibility corrections were reliable to within about 0.50 Hz. It should be noted that the errors associated with the bulk-susceptibility corrections do not affect the coupling values.

Analysis and Calculations

All the spectra were analyzed using an iterative computer program patterned after the LAOCOON-II program of Bothner-By and Castellano.[26] Trial parameters for the monosubstituted benzenes were adopted from previous approximate analyses, where available, or from analyses of structurally similar compounds.[7,11,21] In the disubstituted compounds, trial chemical shifts were calculated assuming additivity of substituent effects in the corresponding monosubstituted benzenes. A similar procedure was used to calculate the coupling parameters. As is customary for benzene derivatives,[27,28] all the couplings were assumed to be positive. It is not possible in the AB_2C cases (symmetrical meta-disubstituted benzenes) to obtain the coupling between the two magnetically equivalent B protons. In addition, in AA′BB′ cases (symmetrical ortho or unsymmetrical para compounds) the analyses do not distinguish between $\nu_{A'}$ and $\nu_{B'}$ or between $J_{AA'}$ and $J_{BB'}$. In these cases the assignment followed that choice which best agreed with the additivity prediction. For example, two observed meta couplings in p-aminobenzoic acid are 2.14 and 2.42 Hz. The two corresponding additivity values are 2.15 and 2.40 Hz for the meta couplings adjacent to the carboxylic and amino groups, respectively. Consequently, the observed value of 2.14 Hz was associated with J_m adjacent to the carboxylic group.

The quality of the spectral fitting is indicated by the low root-mean-square deviations obtained, on the average ∼0.03 Hz between calculated and observed frequencies. Visual comparisons of observed spectra with theoretical Lorentz-shape patterns indicated that the computed intensities were satisfactory in each case. In general the largest uncertainties in the coupling values occurred for those cases involving chemically equivalent protons. This was most evident in the analysis of the collapsed benzenethiol spectrum.

Results

Table I lists the parameter values obtained in this study for benzoic acid, phenol, aniline, and benzenethiol. For subsequent use in correlations, the table also contains coupling values previously obtained under quite similar conditions in this laboratory for benzene and the halobenzenes, together with the electronegativities (E_X) for all substituents considered. The compounds are listed in order of increasing E_X. For convenience in discussing substituent effects, the shift values have been converted to an internal benzene reference $(-150.21$ Hz from external water). The substituent contributions shown in Table II are simply the appropriate parameter value minus the corresponding value in benzene. Tables III and IV give the parameters (shifts and couplings) obtained for 13 disubstituted benzenes together with the corresponding calculated values, in parentheses, based on the data of Table II and the assumption of additivity.

Discussion

Additivity of substituent effects on couplings was first noted by Dischler for the special case of J_m in para-disubstituted benzenes[18] and has recently been extended to a wider variety of disubstituted benzenes.[10,11,17] The present study provides data for four new substituents, OH, COOH, NH_2, and SH, and for 13 disubstituted benzenes containing these groups.

The results in Table IV indicate that the couplings follow the additivity relation quite satisfactorily. For the 62 couplings listed, the average deviation from additivity is 0.085 Hz and the largest deviation is 0.40 Hz. The largest deviations are observed in ortho-disubstituted structures. For example, with OH and COOH ortho to each other, the ortho couplings deviate by 0.1–0.3 Hz from additivity. In the corresponding meta compound, on the other hand, the largest deviation is 0.13 Hz for J_{56} and the average deviation is only 0.05 Hz.

For the chemical shifts, additivity of the substituent effects also turned out to be more satisfactory than had been anticipated from previous reports.[10–12,15–17] The

(25) K. Frei and H. J. Bernstein, J. Chem. Phys., 37, 1891 (1962).
(26) S. Castellano and A. A. Bothner-By, ibid., 41, 3863 (1964).
(27) R. W. Fessenden and J. S. Waugh, ibid., 31, 966 (1959).
(28) C. N. Banwell, Mol. Phys., 4, 265 (1961).

Table I: Chemical Shifts, Coupling Constants, and Group or Atom Electronegativity of the Monosubstituted Benzenes

	Chemical shifts[a]			Proton–proton coupling constants[a]						
Compd	ν_2	ν_3	ν_4	J_{23}	J_{24}	J_{25}	J_{26}	J_{34}	J_{35}	E_X[e]
Benzene[b]				7.54	1.37	0.69	1.37	7.54	1.37	2.07
Benzenethiol	−198.29	−144.19	−139.03	7.87	1.19	0.55	2.12	7.49	1.51	2.45
Benzoic acid	−195.34	−158.76	−165.48	7.84	1.30	0.64	1.84	7.50	1.35	2.54
Iodobenzene[c]				7.93	1.12	0.47	1.88	7.50	1.74	2.60
Bromobenzene[c]				8.07	1.10	0.46	2.08	7.49	1.73	2.94
Aniline	−117.96	−140.87	−116.69	8.06	1.07	0.51	2.42	7.35	1.68	2.99
Chlorobenzene[c]				8.15	1.14	0.50	2.24	7.57	1.71	3.19
Phenol	−121.59	−142.93	−121.59	8.20	1.08	0.46	2.64	7.39	1.77	3.51
Fluorobenzene[d]				8.40	1.10	0.42	2.65	7.45	1.74	3.93

[a] All values are in hertz; chemical shifts relative to external water. [b] Reference 18. [c] Reference 7. [d] Reference 8. [e] The E_X of the substituents are those reported by Dailey and Shoolery (B. P. Dailey and J. N. Shoolery, *J. Amer. Chem. Soc.*, **77**, 3977 (1955)) except for –H and –I, which were taken from Huggins (M. L. Huggins, *J. Amer. Chem. Soc.*, **75**, 4123 (1953)).

Table II: Substituent Contributions to Chemical Shifts and Proton–Proton Coupling Constants

	Substituent parameters[a]								
	Chemical shift			Proton–proton couplings					
Compd	S_o	S_m	S_p	S_{23}	S_{24}	S_{25}	S_{26}	S_{34}	S_{35}
Benzoic acid	−45.13	−8.55	−15.27	0.30	−0.07	−0.05	0.47	−0.04	−0.02
Phenol	28.62	7.28	28.62	0.66	−0.29	−0.23	1.27	−0.15	0.40
Aniline	32.25	9.34	33.52	0.52	−0.30	−0.18	1.05	−0.19	0.31
Benzenethiol	1.92	6.02	11.18	0.34	−0.18	−0.14	0.75	−0.05	0.14

[a] All values are in hertz.

Table III: Chemical Shifts for Disubstituted Benzenes

Substituent (position)[b]	Chemical shift[a]				
	ν_2	ν_3	ν_4	ν_5	ν_6
$CO_2H(1)$, $OH(2)$		22.10 (20.07)	−8.67 (−7.99)	25.39 (20.07)	−34.26 (−37.85)
$CO_2H(1)$, $OH(3)$	−16.51 (−16.51)		−13.86 (−16.51)	1.37 (−1.27)	15.83 (13.55)
$CO_2H(1)$, $OH(4)$	−36.69 (−37.85)	27.19 (20.07)		27.19 (20.07)	−36.69 (−37.85)
$CO_2H(1)$, $NH_2(2)$		30.97 (23.70)	1.71 (−5.93)	39.83 (24.97)	−34.70 (−35.79)
$CO_2H(1)$, $NH_2(3)$	−7.17 (−12.88)		20.94 (16.98)	5.83 (0.79)	−5.30 (−11.61)
$CO_2H(1)$, $NH_2(4)$	−30.90 (−35.79)	37.29 (23.70)		37.29 (23.70)	−30.90 (−35.79)
$OH(1)$, $NH_2(3)$	62.00 (60.87)		64.15 (60.87)	20.96 (16.62)	61.66 (62.14)
$OH(1)$, $OH(2)$		28.81 (35.90)	35.68 (35.90)	35.68 (35.90)	28.81 (35.90)
$OH(1)$, $OH(3)$	57.66 (57.24)		57.54 (57.24)	17.65 (14.56)	57.54 (57.24)
$NH_2(1)$, $NH_2(2)$		33.57 (41.59)	38.26 (42.86)	38.26 (42.86)	33.57 (41.59)
$NH_2(1)$, $NH_2(3)$	67.82 (64.50)		67.98 (65.77)	24.28 (18.68)	67.98 (65.77)
$CO_2H(1)$, $CO_2H(2)$		−26.27 (−53.68)	−16.25 (−23.82)	−16.25 (−23.82)	−26.97 (−53.68)
$CO_2H(1)$, $SH(2)$		−7.19 (−6.63)	−3.73 (−9.25)	5.72 (2.63)	−46.53 (−39.11)

[a] All values in hertz; chemical shifts relative to internal benzene. [b] According to convention of the "Handbook of Chemistry and Physics," C. D. Hodgman, Ed., The Chemical Rubber Co., Cleveland, Ohio, 1967.

large deviations from additivity in *ortho*-disubstituted compounds (up to 30 Hz for ν_o[12]) were not observed here, with but a single exception. The average deviation from additivity is ∼5 Hz for the 40 values listed in Table III, and in only three cases did the difference exceed 9 Hz. The most notable departures occur, not surprisingly, in the case of phthalic acid, ∼27 and ∼7.5 Hz. The other two large discrepancies were found in 2- and 4-aminobenzoic acid (∼15 Hz). It is tempting to think that in the series studied here the departures from additivity for the couplings might be related to the obvious hydrogen-bonding possibilities in these compounds. However, the corresponding chemical shifts do not regularly exhibit analogous deviations. Whatever may be the origin of the relatively small number of exceptions, on the whole the

Table IV: Proton–Proton Couplings for Disubstituted Benzenes

Substituent (position)	J_{23}	J_{24}	J_{25}	J_{26}	J_{34}	J_{35}	J_{36}	J_{45}	J_{46}	J_{56}
CO$_2$H(1), OH(2)	...	...	...	...	8.38 (8.16)	1.14 (1.06)	0.46 (0.41)	7.24 (7.35)	1.77 (1.70)	7.96 (7.69)
CO$_2$H(1), OH(3)	...	2.60 (2.57)	0.35 (0.41)	1.60 (1.55)	...	...	...	8.18 (8.16)	0.99 (1.01)	7.82 (7.69)
CO$_2$H(1), OH(4)	8.55 (8.50)	...	0.36 (0.41)	2.33 (2.24)	...	...	...	...	...	8.55 (8.50)
CO$_2$H(1), NH$_2$(2)	...	...	...	...	8.33 (8.02)	1.16 (1.05)	0.47 (0.46)	7.09 (7.31)	1.67 (1.61)	8.05 (7.65)
CO$_2$H(1), NH$_2$(3)	...	2.42 (2.35)	0.44 (0.46)	1.63 (1.54)	...	...	...	8.02 (8.02)	1.04 (1.00)	7.67 (7.65)
CO$_2$H(1), NH$_2$(4)	8.52 (8.36)	...	0.38 (0.46)	2.14 (2.15)	...	2.42 (2.40)	0.38 (0.46)	...	...	8.52 (8.36)
OH(1), NH$_2$(3)	...	2.16 (2.13)	0.39 (0.28)	2.34 (2.34)	...	...	...	7.93 (7.91)	0.90 (0.78)	8.04 (8.01)
OH(1), OH(2)	...	...	...	...	7.92 (8.05)	1.56 (1.48)	0.23 (0.23)	7.48 (7.24)	1.56 (1.48)	7.92 (8.05)
OH(1), OH(3)	...	2.33 (2.35)	0.31 (0.23)	2.33 (2.35)	...	...	...	8.07 (8.05)	...	8.07 (8.05)
NH$_2$(1), NH$_2$(2)	...	...	...	...	7.79 (7.87)	1.45 (1.38)	0.34 (0.33)	7.37 (7.16)	1.45 (1.38)	7.79 (7.87)
NH$_2$(1), NH$_2$(3)	...	2.14 (2.12)	0.39 (0.33)	2.14 (2.12)	...	...	...	7.88 (7.87)	...	7.88 (7.87)
CO$_2$H(1), CO$_2$H(2)	...	...	...	...	7.78 (7.80)	1.28 (1.28)	0.52 (0.59)	7.51 (7.46)	1.28 (1.28)	7.78 (7.80)
CO$_2$H(1), SH(2)	...	...	...	...	8.02 (7.84)	1.19 (1.17)	0.43 (0.50)	7.33 (7.45)	1.61 (1.43)	7.95 (7.79)

assumption of additivity turned out to be sufficiently valid to provide valuable assistance in the initial spectral assignments.

Water was selected as the external reference because it provided good signals in the coaxial cells used. The well-known sensitivity of the water shift to variations in temperature constitutes a potential source of uncertainty, although an examination of the calibrated data does not suggest this as serious in the present instance. There is, in addition, the possibility that the shifts might be affected by the hydrogen-bonding solvent methanol. For these reasons, the results obtained here for the chemical shifts should be viewed as more or less tentative. In any case, the principal interest in this study is the behavior of the coupling parameters, which are not affected by the reference under the conditions employed and are not expected to be appreciably sensitive to the medium.

Previous empirical efforts to interpret substituent effects on H–H couplings on aromatic systems have, as a rule, involved correlations with substituent electronegativity, E_X. Cox has reported a linear relation between J_{HH} and the sum of E_X in a series of disubstituted compounds.[23] Castellano and Sun observed a definite trend of coupling values with E_X (Pauling) in a study of 35 monosubstituted benzenes.[24] J_{23} and J_{26} were found to increase and J_{24} and J_{25} were found to decrease with E_X, and it was suggested that the inductive effect of the substituent was the principal factor involved. Fraser, on the other hand, from a consideration of J_o values in a series of monosubstituted derivatives, concluded that π contributions to J were at least as important as the inductive effect.[20] Read found that J_{23} and J_{26} in the halobenzenes increase with E_X but not linearly.[11] Recently it has been reported that in a series of halosubstituted fluorobenzenes the *ortho* H–F couplings vary linearly with E_X, the sign of the slope depending upon the position of the substituent.[9]

Utilizing the coupling data obtained for the four monosubstituted benzenes reported here, together with the other couplings previously determined in this laboratory, we have obtained the correlations shown in
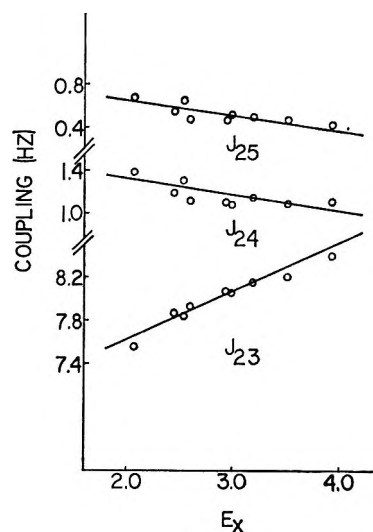
Figure 1. Plot of proton–proton couplings in monosubstituted benzenes vs. the electronegativity of the substituent.
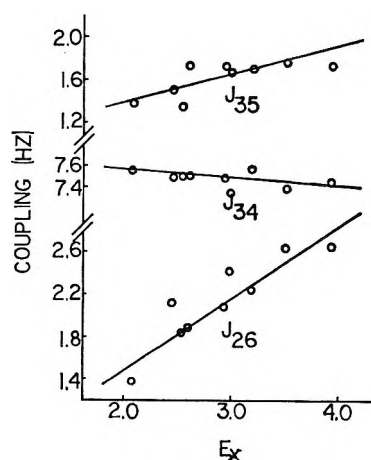
Figure 2. Plot of proton–proton couplings in monosubstituted benzenes vs. the electronegativity of the substituent.

Figures 1 and 2 as plots of J vs. E_X. These plots differ from those reported elsewhere, in that they include all the H–H couplings and employ group electronegativity values for the complex substituents. In all cases the

correlation appears to be monotonic and has been assumed to be linear. For some of the couplings (J_{24}, J_{25}, and J_{34}) the slopes are possibly in some doubt, but it can at least be inferred that the substituent effect here is quite small. The plots for J_{26}, J_{34}, and J_{35} exhibit somewhat more scatter than do the others. In the case of J_{26} (a *meta* coupling involving protons adjacent to the substituent) the points for SH, OH, and NH$_2$ all lie about 0.2 Hz above the correlation line. Whether this indicates an additional real effect is not clear.

Two aspects of the plots in Figures 1 and 2 appear to deserve comment. First, not surprisingly, the substituent effect is greater for coupled protons nearer the substituent, other factors being similar. This is evident, for example, by comparing the behavior of J_{23} and J_{26} with that of J_{34}. Second, positive slopes (J increasing with E_X) are noted where the lines linking the coupled protons are either parallel or perpendicular to the C–X bond; in all other orientations

the slope is either negative or nearly zero. This feature obviously suggests the possibility of an angle-dependent effect or interaction influencing the couplings, but whether it is real and significant is a question that will require further study.

These substituent effects on J values in aromatic systems are small ($\sim$1 Hz or less) and are correspondingly difficult to determine and investigate. Nevertheless, by extending these observations to more structures, such trends as are noted achieve increased significance on at least a statistical basis. Thus far it appears that inductive influences are significant, and perhaps dominant; additivity of the effects is reasonably well established; and the results can be quite useful in the preliminary analysis and assignments of aromatic nmr spectra.

Thermodynamic Properties of Gases in Propellants. III. Equilibria in

N$_2$H$_4$–1,1-N$_2$H$_2$(CH$_3$)$_2$ and He (or N$_2$)–N$_2$H$_4$–1,1-N$_2$H$_2$(CH$_3$)$_2$ Systems

by E. T. Chang and N. A. Gokcen

Chemical Thermodynamics Section, Aerospace Corporation, El Segundo, California   90045   (*Received January 19, 1968*)

Gas- and liquid-phase equilibria in N$_2$H$_4$, 1,1-N$_2$H$_2$(CH$_3$)$_2$, their mixtures, and the solubilities of He(g) and N$_2$(g) in the liquid mixtures have been measured. Excess volume of mixing of the mixtures has been determined as a function of composition. $\Delta G°$, $\Delta H°$, and $\Delta S°$ of vaporization have been obtained for the pure liquids. The measurements of vapor pressure and of liquid and gas compositions for the binary liquids have yielded the excess molar thermodynamic properties. An equation of the form $\Delta H = x_1 x_2 (a + bx_1 + cx_1^2)$ for the molar heat of solution in terms of the mole fractions, x_1, has been shown to be very convenient and useful and accounts for deviations from regularity. In the dilute regions, this equation assumes the "regular" form $\Delta H \cong ax_1 x_2$. The solubilities of He(g) and N$_2$(g) in the liquid mixtures were measured at various temperatures and pressures. It was found that the ternary "regular behavior" is obeyed for the dissolved gases and that the atmospheric solubility K (in mole fraction) follows the linear relationship log $K = e + fx_1$ in a wide terminal composition range. $\Delta G°$, $\Delta H°$, and $\Delta S°$ of solution have been computed for He and N$_2$ and have been closely estimated for Ar. The values of all the useful thermodynamic properties have been tabulated at convenient compositions of the liquid phase. Deviations from ideality have been briefly discussed from a molecular point of view.

Introduction

Mixtures of hydrazine, N$_2$H$_4$, and unsymmetrical dimethylhydrazine (UDMH), 1,1-N$_2$H$_2$(CH$_3$)$_2$, are frequently used as propellants, since the blending process is capable of retaining some of the desirable properties of the pure components and creating new attractive properties. A thermodynamic investigation of this system was carried out independently by the authors[1]

and by Pannetier and Mignotte[2] about the same period of time. The authors, however, observed difficulties which have been overlooked by other investigators,[2,3] *i.e.*, the observed vapor pressure of these compounds

(1) E. T. Chang and N. A. Gokcen, Report No. ATN-64(9228)-2, Aerospace Corp., El Segundo, Calif., 1964.

(2) G. Pannetier and P. Mignotte, *Bull. Soc. Chim. Fr.*, 982, 985 (1961); 2141 (1962); 694, 690, 701 (1963).

and their mixtures varied with time because of a slow decomposition, irrespective of the history of purification and the subsequent handling, contact with Teflon or small amounts of stopcock greases, and exposure to light. The rate of decomposition seemed to increase with temperature, but because of the increase in the vapor pressure with temperature, the fractional error due to decomposition appeared to be about the same for a given liquid composition. It was therefore necessary to pursue the earlier investigation[1] further in order to obtain closer results to the true equilibrium values for the gas–liquid binary-phase relationships.

Practical problems in pressurizing, storing, and pumping liquid propellants necessitate accurate data on the solubilities of gases in these liquid mixtures. Parts I and II of this series of investigations[4,5] dealt with the solubilities of gases in liquid N_2O_4, N_2H_4, $N_2H_3CH_3$, 1,1-, and 1,2-$N_2H_2(CH_3)_2$. The foregoing investigations were therefore extended to include the solubilities of He(g) and N_2(g) in the mixtures of N_2H_4 and 1,1-$N_2H_2(CH_3)_2$ at various pressures and temperatures. Very closely estimated data for Ar(g) in the mixtures were also obtained.

Reliable data[3,6] on the solubilities of gases in the liquid mixtures of N_2H_4–UDMH do not exist, except rough values for He and Ar at 0.50 wt fraction of hydrazine quoted by Liberto.[3] The data on the densities of the mixtures and on the total vapor pressure at various temperatures were also inadequate for the desired accuracy in the measurements of solubilities. It was therefore necessary to obtain such data concurrently with the measurements of solubilities.

Experimental Section

The apparatus and the procedure for solubility measurements were described in part I. Briefly, the apparatus consisted of three accurately calibrated volumes for the measurements of admitted gases, a calibrated container for the liquid which was vigorously stirred with a glass-enclosed magnet bar, and a mercury manometer for measuring the pressure with a microslide cathetometer. The volume occupied by the propellant was determined from the weight and the density determined by a method described elsewhere in detail.[7] The densities $\rho(i)$ are expressed in grams per milliliter as functions of temperature, t, in °C, as

$$\rho(x_2 = 0.7952) = 0.83450 - 0.001006t \quad (1)$$

$$\rho(x_2 = 0.6047) = 0.86286 - 0.000977t \quad (2)$$

$$\rho(x_2 = 0.3089) = 0.92569 - 0.000901t \quad (3)$$

$$\rho(x_2 = 0.1647) = 0.96589 - 0.000907t \quad (4)$$

In these equations x_2 is the mole fraction of UDMH. The corresponding equations for pure hydrazine and pure UDMH are given in part II. The gas and the liquid of known composition were brought to equilibrium at a selected constant temperature. The amount

of dissolved gas was found by subtracting the amount of remaining gas over the liquid from that of the admitted gas. The procedure was checked by measuring the solubility of nitrogen in water, and the resulting data agreed within 2% of published data. The change in the vapor pressure of the mixtures with time necessitated monitoring the pressure for 2 hr, after which further changes in pressure were found to be small. The vapor pressure during the solubility measurement was then obtained by extrapolating a plot of pressure vs. time. This procedure introduces an unavoidable error of about 0.2 mm in the vapor pressure and causes a negligibly small error in the solubility measurements.

The apparatus for solubility measurements was also suitable for the measurements of equilibrium pressure. However, a separate apparatus, completely immersed in a thermostat, was designed for the static measurements of the equilibrium pressure over each liquid mixture. This apparatus was equipped with a mercury manometer and Teflon stopcocks, which were later changed to all-glass stopcocks sparingly greased with various kinds of grease. A glass-coated magnet bar was used for gently stirring the liquid for quick equilibration. The mercury in the manometer was protected in some of the runs by admitting a small amount of nitrogen between the mercury and a stopcock before making a contact between the vapor and the nitrogen by opening the stopcock. The presence or the absence of nitrogen over the mercury showed no detectable effect on the observed pressure; hence the use of nitrogen was abandoned. The liquid of the desired composition was obtained by distilling the purified components of desired quantities directly into the apparatus. After the measurements of vapor pressure over a particular liquid, the vacuum was broken by admitting argon, and a sample of liquid was taken with a syringe and quickly placed in a Bausch and Lomb precision refractometer thermostated at 25°. The readings of the refractometer were calibrated with a sodium bulb by using separately prepared liquid mixtures of accurately known compositions. The index of refraction was plotted vs. composition on a very large chart for convenience in determining the composition. This plot may be represented accurately by

index of refraction = 1.4683 −

$$0.09806x_2 + 0.04685x_2{}^2 - 0.01199x_2{}^3 \quad (5)$$

(3) R. R. Liberto, "Titan II Storable Propellant Handbook," Report No. 8111-933003, Bell Aerosystems Co., Buffalo, N. Y., Air Force Flight Test Center, Edwards Air Force Base, Calif., 1961.

(4) E. T. Chang and N. A. Gokcen, J. Phys. Chem., 70, 2394 (1966).

(5) E. T. Chang, N. A. Gokcen, and T. M. Poston, ibid., 72, 638 (1968).

(6) "Pressurization System Design Guide," Vol. IIB, Aerojet-General Corp., Azusa, Calif., 1965; see also "Liquid Propellant Manual," CPIA (Confidential), Johns Hopkins University, Silver Spring, Md.

(7) A. I. Kemppinen and N. A. Gokcen, J. Phys. Chem., 60, 126 (1956).

where x_2 is the mole fraction of UDMH. Equation 5 also agrees very closely with similar data by Pannetier and Mignotte.[2]

The composition of gas in equilibrium with a liquid was obtained by using an apparatus in which Ar was used as a carrier gas bubbled at about 30 ml/min through a large amount of liquid mixture. The gas mixture was then passed through a U tube immersed in liquid nitrogen. The composition of gas phase was then determined by using a small portion of the completely melted condensate in the refractometer. Doubling the rate of flow of argon had no effect on the gas composition.

Results

N_2H_4. The vapor pressure of pure N_2H_4 was measured from 2.9 to 51.5° at suitable intervals of temperature. A total of 11 measurements after repeated evacuation and pressure readings were plotted as [ln P $- (\Delta C_p/R)$ ln T] vs. $1/T$ and were fitted to a straight line.

The integration of the Clausius–Clapeyron equation with $\Delta H_v°_T = B + T\Delta C_p$ yields the term $-(\Delta C_p/R)$ ln T and justifies the linearity of such a plot. In these expressions, $\Delta C_p = 11.0$ cal/mol is from the calorimetric measurements of Scott, et al.,[8] R is the gas constant, T is in °K and Δ refers to the difference corresponding to the vaporization process, i.e., gas minus liquid. The term B is simply an integration constant from $d(\Delta H) = \Delta C_p dT$. The resulting equation, based on the data fitted to the foregoing linear plot, yields

$$\Delta G° = -RT \ln P_{atm}(N_2H_4) =$$
$$13{,}837 + 25.328T \log T - 101.226T \quad (6)$$
$$\Delta H° = 13{,}837 - 11.0T \quad (7)$$

We obtain, for the vaporization, $\Delta H°_{298.15} = 10{,}557$ cal/mol and $\Delta S°_{298.15} = 27.55$ cal/deg mol from these equations as compared with 10,700 cal/mol and 28.00 cal/deg mol for $\Delta H°$ and $\Delta S°$, respectively, by Scott, et al., and $\Delta S°_{298.15} = 27.44$ cal/deg mol from spectroscopic methods. The agreement is excellent with Scott, et al., fairly good with Hieber and Woerner,[9] and fair with Pannetier and Mignotte.[2]

$1,1\text{-}N_2H_2(CH_3)_2$. The measurements of vapor pressure of UDMH were very difficult because of the fact that after successive evacuations of the space over the pure liquid, the pressure increased and finally reached a value that did not change by more than ±0.5 mm in 1 hr. When the same liquid was retained for 2 hr, the vapor pressure continued to increase slowly and in order to obtain the previous value of the vapor pressure during the first 0.5 hr, it was necessary to evacuate the space over the liquid several times. It appeared that a slow dissociation generates gases and increases the observed pressure over UDMH at a considerably larger degree than over hydrazine. Various pre-

cautions and methods of handling the liquid, the use of Teflon or greased stopcocks, protection from light, and even using a second similar apparatus with minor modifications, appeared to have no effect on this behavior. The set of data selected to be the best values, from −25 to 35° and consisting of 11 measurements, were used to obtain the following equations for UDMH

$$\Delta G° = -RT \ln P_{atm}(\text{UDMH}) =$$
$$12{,}973 + 39.604T \log T - 138.539T \quad (8)$$
$$\Delta H° = 12{,}973 - 17.2T \quad (9)$$

The value of ΔC_p used in these equations was estimated from the known values of ΔC_p for N_2H_4 and methylhydrazine from Aston, et al.[10] From eq 8 and 9, we obtain $\Delta H°_{298.15} = 7845$ cal/mol and $\Delta S°_{298.15} = 23.34$ cal/deg mol. Calorimetric values of Aston, et al.,[10] are $\Delta H°_{298.15} = 8366$ cal/mol and $\Delta S°_{298.15} = 24.96$ cal/deg mol, which are in poor agreement with the authors' values. The values of vapor pressure in this investigation agree better with the extrapolated values of Pannetier and Mignotte than those of Aston, et al.[10] All three measurements are identical at 51° and the authors' values are higher below 51° and lower above this temperature. In the range of −25–60°, maximum deviation of P in eq 8 from Pannetier and Mignotte is about 6%. We recommend the use of eq 8 up to the boiling point of UDMH, since beyond that temperature the disagreement among all three measurements becomes large.

N_2H_4–$N_2H_2(CH_3)_2$ System. The excess molar volumes of mixing of hydrazine and UDMH were computed from eq 1 to 4 and from the densities of pure components. The results are presented in Figure 1 and are compared with those of Pannetier and Mignotte. The difference between the two sets of data is largely due to the differences in the molar volumes of the pure components. The composition corresponding to $x_2 = 0.36$, which has equal weights of the components, is the densest mixture having the most practical uses in chemical propulsion.

The vapor pressure of the mixtures at selected compositions and temperatures was measured and the results are presented in Figure 2. The pressures for the pure components are from eq 6 and 8. The curves passing through the experimental points in Figure 2 are called the "bubble points." The dotted lines are the dew points and they are obtained from the measurements of liquid and gas compositions presented in Figure 3. Each pair of solid and dotted lines in Figure 2 represents the constant-temperature phase diagram. The results are compared with those of Pannetier and

(8) D. W. Scott, G. D. Oliver, M. E. Gross, W. N. Hubbard, and H. M. Huffman, J. Amer. Chem. Soc., 71, 2293 (1949).

(9) W. Hieber and A. Woerner, Z. Elektrochem., 40, 252 (1934).

(10) J. G. Aston, H. L. Fink, G. J. Janz, and K. E. Russel, J. Amer. Chem. Soc., 73, 1939 (1951).
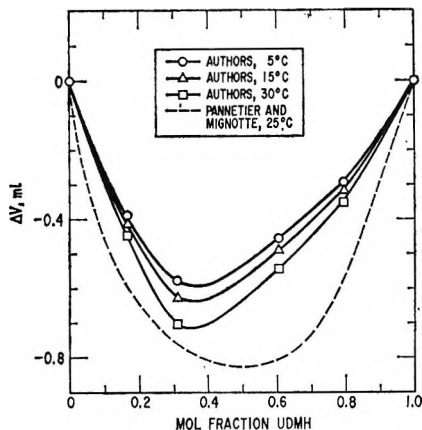
Figure 1. Excess volume of mixing, ΔV, in N_2H_4-1,1-$N_2H_2(CH_3)_2$ system. Abscissa is the mole fraction of 1,1-$N_2H_2(CH_3)_2$.
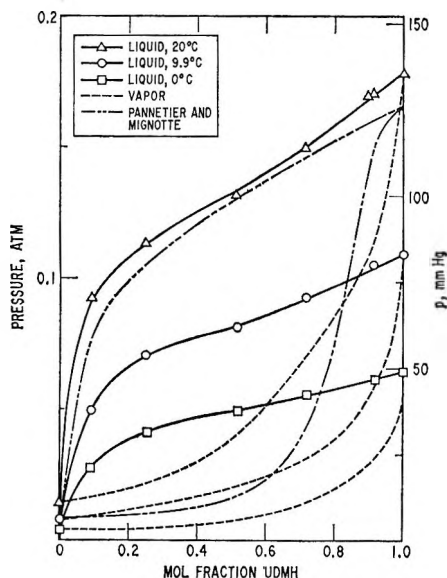
Figure 2. Vapor–liquid equilibria in N_2H_4-1,1-$N_2H_2(CH_3)_2$ system: solid lines total pressure *vs.* liquid composition (called "bubble points"); dotted lines, obtained from Figure 3 (called "dew points").

Figure 3. Liquid–gas composition relationships in N_2H_4-1,1-$N_2H_2(CH_3)_2$ systems.

Mignotte and it is seen that the agreement is good for the bubble points but only fair for the dew points. A similar set of curves in a handbook by Liberto[3] at 22.2° disagrees with Figure 2.

The selected thermodynamic properties of the liquid binary system have been obtained and the results are listed in Table I. The procedure in calculating these results is as follows. At the selected liquid compositions in the first column, *i.e.*, at the mol fractions, x_2, of UDMH, the mol fractions of UDMH in the gas, x_2', were obtained from a large plot of Figure 3 and are listed in the second column. The values of total pressure from Figure 2 were plotted for each composition as log P *vs.* $1/T$, and the best line passing through three points was used to obtain P in the third column at 0 and 20° directly from the linear plot.

Each pair of P for a given composition may be used to interpolate and extrapolate P with a good deal of accuracy in the range of -10–$40°$ by using log $P = (A/T) + B$, where the constants A and B are obtained by using the listed values of P at two temperatures. The constants A and B are assumed to be independent of temperature and pressure but dependent upon composition. The accuracy of the values obtained by such equations decreases outside the recommended temperature range. The values of activity a_i for each component may be computed by using $x_i'P/P_i^*$, where P_i^* is the pressure of the pure component.

The value of the activity coefficient γ_i may then be obtained from a_i/x_i. Extrapolation of γ_i from $x_i = 0.1$ to 0 can be accomplished by using log $\gamma_i = \alpha_i(1 - x_i)^2$, where the constant α_i is obtained by substituting the values of x_i and γ_i at $x_i = 0.1$, since it is well known that all dilute nonelectrolytic solutions obey this equation based on the regular solution theory. The foregoing procedure is accurate for UDMH because the vapor phase is predominantly rich in this component, but it is inaccurate for hydrazine; hence an alternative procedure was used to obtain the activity of hydrazine. For this purpose, the values of the activity coefficient γ_2 of UDMH were first calculated from a_2 and then the Gibbs–Duhem relation, x_1 d log $\gamma_1 + x_2$ d log $\gamma_2 = 0$, was integrated to obtain γ_1 for hydrazine. This procedure required a plot of $x_2/x_1 = 0$–9, bearing in mind that log $\gamma_1 = 0$ at $x_2 = 0$. The value of log γ_1 at $x_2 = 1$ or $x_2/x_1 = \infty$ was obtained by using log $\gamma_1 = \alpha_1 x_2^2$, where α_1 was obtained by using γ_1 at $x_2/x_1 = 9$. The excess partial molar excess Gibbs energy, $\bar{G}_i^{ex}$, was then obtained from $\bar{G}_i^{ex} = RT \ln \gamma_i$. The calorimetric data of Pannetier and Mignotte on the molar heat of mixing, ΔH, was fitted to

$$\Delta H = (308 + 0.72T)x_1x_2 + 470x_1^2x_2 - 310x_1^3x_2 \quad (10)$$

where $0.72T$, the temperature coefficient of heat of mixing, is based on a limited number of measurements at 25 and 50°, the bulk of measurements having been

Table I: Thermodynamic Properties of N_2H_4-$N_2H_2(CH_3)_2$[a]

x_2	x_2'	P, mm	$\bar{G}_1^{ex}$	$\bar{H}_1^{ex}$	$-\bar{S}_1^{ex}$	$\bar{G}_2^{ex}$	$\bar{H}_2^{ex}$	$-\bar{S}_2^{ex}$	ΔG^{ex}	ΔH	$-\Delta S^{ex}$
0.0	0.000	2.80	0	0	0	927	665	0.96	0	0	0
0.1	0.888	22.0	10	6	0.02	751	555	0.72	84	61	0.08
0.2	0.948	29.5	42	27	0.06	568	440	0.47	148	109	0.14
0.3	0.976	33.0	90	64	0.10	425	329	0.35	190	143	0.17
0.4	0.991	35.3	149	118	0.11	315	229	0.32	216	162	0.19
0.5	0.997	37.1	224	186	0.14	224	146	0.29	224	166	0.21
0.6	0.998	39.3	307	264	0.16	156	82	0.27	216	154	0.23
0.7	0.999	41.7	402	345	0.21	104	38	0.24	194	130	0.23
0.8	1.000	43.9	530	420	0.40	62	12	0.18	156	94	0.23
0.9	1.000	46.4	722	478	0.89	29	2	0.10	98	49	0.18
1.0	1.000	49.0	891	505	1.41	0	0	0	0	0	0
0.0	0.000	10.7	0	0	0	1051	683	1.26	0	0	0
0.1	0.836	70.1	12	6	0.02	851	570	0.96	96	63	0.11
0.2	0.900	82.5	59	27	0.11	586	452	0.46	164	112	0.18
0.3	0.922	89.9	115	65	0.17	413	338	0.26	205	147	0.20
0.4	0.941	95.5	179	120	0.20	294	268	0.20	225	166	0.20
0.5	0.950	99.9	260	190	0.24	194	150	0.15	227	170	0.19
0.6	0.960	106.0	340	270	0.24	129	85	0.15	213	159	0.19
0.7	0.970	112.7	429	353	0.26	81	39	0.14	185	134	0.18
0.8	0.978	120.4	529	431	0.33	48	13	0.12	144	97	0.16
0.9	0.989	128.2	677	492	0.63	22	2	0.07	88	51	0.12
1.0	1.000	135.9	836	523	1.07	0	0	0	0	0	0

[a] The first 11 rows are for 0° and the remaining rows are for 20°. ΔH is the same as ΔH^{ex} since in $\Delta H^{ex} = \Delta H - \Delta H$(ideal), the term ΔH(ideal) is zero. Note that ΔG^{ex} and $\bar{G}_i^{ex}$ and ΔH and $\bar{H}_i^{ex}$ are in cal/mol, and ΔS^{ex} and $\bar{S}_i^{ex}$ are in cal/deg mol.

carried out at 35°. Equation 10 is of the form $\Delta H = x_1x_2(a + bx_1 + cx_1^2)$, where the terms with b and c may be considered as perturbation terms, accounting for the deviation from regularity expressed by $\Delta H = ax_1x_2$. The data are represented well by eq 10 and it is seen that in the terminal regions $x_1 < 0.2$ and $x_1 > 0.8$, $\Delta H = ax_1x_2$ is very closely obeyed. Actually in the region of $x_1 = 0.1$-0.9, eq 10 is represented better than 15% in ΔH by $\Delta H = 685X_1X_2$, but the data appear to be considerably more accurate to justify a three-term equation. An interesting property of eq 10 is that the partial molar excess heats of solution, $\bar{H}_i^{ex}$, assume the convenient forms

$$\bar{H}_1^{ex} = (318 + 0.72T)x_2^2 - 920x_2^3 - 930x_2^4 \quad (11)$$

$$\bar{H}_2^{ex} = (-162 + 0.72T)x_1^2 + 1560x_1^3 - 930x_1^4 \quad (12)$$

The values of molar and partial molar quantities from eq 10–12 are also listed in Table I. The property $\bar{S}_i^{ex}$ was obtained from $\bar{G}_i^{ex} = \bar{H}_i^{ex} - T\bar{S}_i^{ex}$, and ΔG^{ex}, as well as ΔS^{ex}, from $\Delta G^{ex} = x_1\bar{G}_1^{ex} + x_2\bar{G}_2^{ex}$ and $\Delta S^{ex} = x_1\bar{S}_1^{ex} + x_2\bar{S}_2^{ex}$. Table I therefore summarizes all the useful thermodynamic properties of the binary liquid system hydrazine–UDMH.

The activities in this system at 20° are represented in Figure 4. It is seen that there is a fairly strong positive deviation from Raoult's law. The activities and the activity coefficients computed by the authors from the solid–liquid phase diagram[3] agree very well with this investigation and provide an independent check on
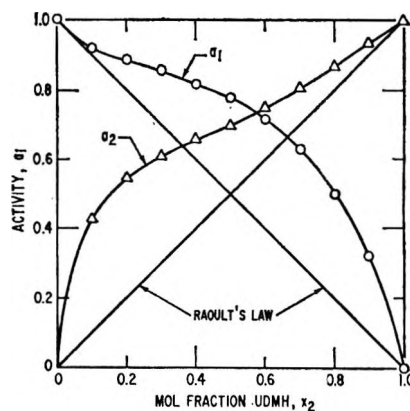
Figure 4. Activities in N_2H_4-1,1-$N_2H_2(CH_3)_2$ system.

the present results. Large positive deviations in Figure 4 are also consistent with the experimental fact that this system forms a eutectic diagram in the solid–liquid equilibrium regions at constant pressure, with no mutual solid solubility of one component in the other.

(He, N_2, and Ar)-N_2H_4-$N_2H_2(CH_3)_2$ Systems. The solubilities of gaseous He and N_2 in liquid mixtures of hydrazine and UDMH have been obtained at various pressures from 0.5 to 2.5 atm and at 0, 15, and 30°. The solubility process is simply

$$gas \rightleftharpoons \text{dissolved gas} \quad (K = x/P) \quad (13)$$
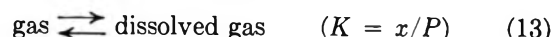
where K is the equilibrium constant; x is the mol fraction of dissolved gas, and P is the partial pressure
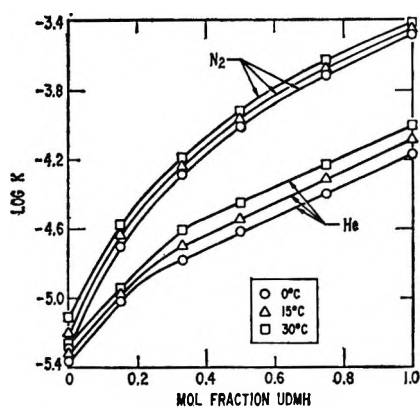
Figure 5. Solubilities of He(g) and N_2(g) in mixtures of N_2H_4-1,1-$N_2H_2(CH_3)_2$. $K = x/P$, where x and P are the mole fraction and the partial pressure of He or N_2 respectively.

Table II: $\Delta H°$ and $\Delta S°$ of Solution of He and N_2 in Liquid N_2H_4-UDMH Mixtures[a]

Mol fraction of UDMH	Helium		Nitrogen		Argon (estimated)	
	$\Delta H°$	$-\Delta S°$	$\Delta H°$	$-\Delta S°$	$\Delta H°$	$-\Delta S°$
0.0	1260	19.94	2360	15.60	2040[b]	15.61[b]
0.1	1230	19.02	1830	15.59	1490	15.6
0.2	1310	17.80	1450	15.60	1080	15.6
0.3	1900	15.03	1200	15.46	810	15.5
0.4	2150	13.71	1150	14.82	730	15.1
0.5	2210	13.09	1140	14.18	700	14.5
0.6	2220	12.63	1100	13.72	640	14.1
0.7	2200	12.29	1050	13.38	560	13.9
0.8	2170	11.99	980	13.16	470	13.8
0.9	2140	11.67	900	13.03	360	13.7
1.0	2110	11.36	800	13.00	240[b]	13.67[b]

[a] $\Delta G° = -RT \ln K = \Delta H° - T\Delta S°$ for the process of solution. See eq 13. [b] Experimental values; all other values for Ar are estimated.

of dissolved gas over the liquid. K also represents the atmospheric solubility of the gas. The average values of K at each composition and temperature are plotted as log K vs. the mol fraction, x_2, of UDMH in Figure 5. At each selected composition log K from a large plot of Figure 5 was read and plotted vs. $1/T$, and the best line passing through such points was represented by log $K = -(\Delta H°/4.5756T) + (\Delta S°/4.5756)$, yielding the values of $\Delta H°$ and $\Delta S°$ listed in Table II. The standard Gibbs energy of solution for each composition is then $\Delta G° = \Delta H° - T\Delta S°$. For argon, $\Delta H°$ and $\Delta S°$ were estimated very closely by plotting these quantities for nitrogen against the mol fraction of UDMH and the same quantities for argon in pure hydrazine and pure UDMH.[5] The intermediate values were then obtained by the compositional averaging of the known differences for the pure components.[6] This method is equivalent to drawing a curve similar to that for N_2 and satisfying the known terminal values for Ar. This procedure makes only small corrections on $\Delta H°$ and $\Delta S°$ for N_2 to obtain the corresponding values for Ar.

The regular solution theory[11,12] for a ternary system requires that the molar entalpy of the solution, H_{123}, must be related to the mole fractions, x_t, by $H_{123} = x_1^2 e_{11} + x_2^2 e_{22} + 2x_1 x_2 e_{12} + 2x_1 x_3 e_{13} + 2x_2 x_3 e_{23}$, where $e_{ij} = (ZN_0 E_{ij})/2$, where Z is the coordination number; N_0 is Avogadro's number, and E_{ij} is the bond energy. The molar heat of mixing is simply $H_{123} - x_1 e_{11} - x_2 e_{22} - x_3 e_{33}$. Let x_3 be the mole fraction of dissolved gas and remember that x_3 is very much smaller than x_1 and x_2; hence, $x_3 \rightarrow 0$. The partial molar heat of solution of component 3 in a mixture of 1 and 2, $\Delta \bar{H}_{3,12}$, is given by

$$\Delta \bar{H}_{3,12} = x_1 \Delta \bar{H}_{3,1} + x_2 \Delta \bar{H}_{3,2} - \Delta H_{12} \quad (14)$$

where $\Delta \bar{H}_{3,i}$ is the partial molar heat of solution of 3 in pure i. The quantity ΔH_{12} is the molar heat of solution of the binary liquid system 1 and 2. Sub-

stitution of $-RT \ln x_{3,1} = \Delta G°_{3,1} \approx \Delta \bar{H}_{3,1}$ and similar expressions for $x_{3,2}$ and $x_{3,12}$ into eq 14 gives

$$\log x_{3,12} = x_1 \log x_{3,1} +$$
$$x_2 \log x_{3,2} + \Delta H_{12}/(4.5756T) \quad (15)$$

where $x_{3,i}$ is the mol fraction of 3 in pure i, and $x_{3,12}$ is that in a mixture [13] of 1 and 2. Equation 15 is moderately successful in obtaining the solubility of a gas in a binary system from the solubilities in the pure liquid components and from the known values of ΔH_{12}. For example, log $x_{3,12}$ for He, N_2, and Ar is -4.632, -4.251 and 3.979, respectively, at $x_1 = x_2 = 0.50$ and 0° in hydrazine–UDMH system, whereas the actual values are -4.627, -4.016 and -3.729, respectively. The agreement is good for He but only fair for N_2 and Ar.

Figure 5 shows that the solubilities of He and N_2 follow a linear behavior on the N_2H_4-rich and on the UDMH-rich compositions, where ΔH_{12} becomes negligible so that eq 15 assumes the simple form

$$\log K = e + fx_2 \quad (16)$$

where e and f are independent of composition but vary with temperature. It is seen in Figure 5 that eq 16 is obeyed for nitrogen in limited terminal composition ranges of the liquid, but for helium in fairly large terminal composition ranges of the liquid. The values of e and f for each gas at each temperature are different for each terminal composition range, whereas eq 15 requires that e and f be the same for both terminal composition ranges.

(11) E. A. Guggenheim, "Mixtures," Oxford University Press, London, 1952.

(12) J. H. Hildebrand, "Solubility of Nonelectrolytics," Reinhold Publishing Corp., New York, N. Y., 1950; see also "Regular Solutions," Prentice-Hall, Inc., Englewood Cliffs, N. J., 1962.

(13) C. Wagner, Z. Phys. Chem., 132, 273 (1928); this paper gives a derivation of eq 15 for $\Delta H_{ij} = 0$.

A more successful scheme than the regular solution theory was found to be the use of Lennard-Jones potential outlined in a previous paper.[5] For this purpose it was necessary to make two more assumptions for the liquid mixtures. (a) The melting point of the mixture was assumed to be the compositional average of the melting points of the pure components in order that a reduced melting point can be obtained for the mixture in spite of the fact that a two-component liquid may have a melting range rather than a melting point. This assumption might appear to be questionable, but the use of either liquidus temperature or the average of liquidus and solidus temperatures does not affect the results greatly. (b) The hard core or the impenetrable spherical volume of the liquid was assumed to be the compositional average volume of the component molecules from which the impenetrable distance was computed. With only these new assumptions and following our previous procedure,[5] it was possible to calculate log K as a function of composition from a separate linear plot of log K vs. r^{-12}, where r is the distance between the solute molecule and the impenetrable sphere of solvent molecules. The calculations give the values of log K, or $\Delta G°$, at various compositions within a remarkably close range of about 2%. However, it is not our intention to claim that this procedure is applicable to solutions exhibiting unusual patterns in ΔG^{ex} and ΔH^{ex} of solution in the binary liquid systems. There is no molecular theory of solutions[11,12,14] capable of accounting for thermodynamic properties of all solutions at present. The success of our procedure is perhaps largely due to nearly regular behavior of N_2H_4–UDMH system. From a purely calculational point of view, it may be desirable to use the general form[15] of eq 16 with additional terms $gx_2^2 + hx_2^3 + \ldots$, particularly if the experimental data are limited.

(14) J. S. Rowlinson, "Liquid and Liquid Mixtures," Butterworth and Co., Ltd., London, 1959.
(15) For a similar equation see N. A. Gokcen, *Rev. Met.*, **57**, 261 (1960).

Electron Spin Resonance of α-Chromia–Alumina Solid Solutions

by Charles J. Carman and William J. Kroenke

The B. F. Goodrich Company, Research Center, Brecksville, Ohio 44141   (*Received January 22, 1968*)

Electron spin resonance (esr) was used to characterize the electronic environment of Cr^{3+} ions in a series of polycrystalline α-chromia–alumina solid solutions. The solid solutions were formed at 1350° and contained from 0.082 to 14.70 wt % Cr_2O_3. Esr resonances corresponding to electronically isolated Cr^{3+} ions, Cr^{3+} ions which are electronically coupled *via* weak exchange interactions, and Cr^{3+} ions which are electronically coupled *via* strong exchange interactions were found. Isolated Cr^{3+} ions predominate at low Cr_2O_3 concentration. The relative concentration of isolated to coupled Cr^{3+} ions decreases with increasing Cr_2O_3 concentration in a regular manner until all of the Cr^{3+} ions are strongly coupled. An explanation is proposed for the two resonances from coupled Cr^{3+} ions which occur at intermediate Cr_2O_3 concentrations. The results are compared to the esr studies of supported chromia–alumina catalysts which are reported in the literature.

Introduction

Many investigators have reported electron spin resonance (esr) studies of chromia–alumina systems. Their results have been summarized by Poole and MacIver in a recent review of the physical-chemical properties of chromia–alumina catalysts.[1a] Most of the esr studies have been made on catalysts consisting of mixtures of chromium oxides and γ-alumina,[1b] or on single crystals of ruby, dilute solid solutions of chromia in α-alumina, but no one had reported a detailed investigation of the esr of polycrystalline α-chromia–alumina solid solutions at low to moderate chromia concentrations.

O'Reilly and MacIver studied the esr at 77°K of impregnated chromia–alumina catalysts.[2] They studied both reduced and oxidized catalysts and reported three different "phases" of chromium ions: (1) δ phase,

(1) (a) C. P. Poole, Jr., and D. S. MacIver, *Advan. Catalysis*, **17**, 223 (1967). (b) These mixtures will be designated as either impregnated or coprecipitated chromia–alumina.
(2) D. E. O'Reilly and D. S. MacIver, *J. Phys. Chem.*, **66**, 279 (1962).

isolated Cr^{3+} ions; (2) β phase, clusters of electronically coupled Cr^{3+} ions; and (3) γ phase, Cr^{5+} ions.

Poole, Kehl, and MacIver report esr measurements of coprecipitated chromia–alumina catalysts.[3] They found the same three chromium ion phases reported by O'Reilly and MacIver, with one exception. At high chromia concentrations, ≥ 9.2 mol % chromia, they observed two β-phase resonances, β_W and β_N, associated with electronically coupled Cr^{3+} ions.

An esr spectrum of polycrystalline ruby ($\sim 1\%$ Cr_2O_3) was presented by O'Reilly and MacIver.[1a] Poole, Kehl, and MacIver observed the ruby spectrum in 0.87 and 1.80 mol % α-Cr_2O_3–Al_2O_3 solid solutions made at 1400°.[2] They also obtained the esr of α solid solutions containing 5.3, 9.2, and 19.6 mol % Cr_2O_3. These spectra were characterized by a major resonance which was assigned to β_N phase Cr^{3+} ions.

In this paper we report the results of a study of the esr of polycrystalline α-Cr_2O_3–Al_2O_3 solid solutions. The α-solid solutions, which were formed at 1350°, contained from 0.1 to 15% chromia. We observed a resonance attributed to isolated Cr^{3+} ions and two resonances resulting from electronically coupled Cr^{3+} ions. A qualitative explanation is presented to explain our results.

Experimental Part

Two methods of preparing the α-Cr_2O_3–Al_2O_3 solid solutions were used. One method consisted of impregnating Alcoa C-31 coarse hydrated alumina with reagent grade $Cr(NO_3)_3 \cdot 9H_2O$ dissolved in absolute ethanol. The resultant slurries were stirred continuously and heated to dryness over a steam bath. The dry, free-flowing impregnated aluminas were calcined in air for 16 hr at 660°. The resultant mixtures of chromium oxides and γ-alumina were passed through an 80 mesh screen, and they were fired in air for 16 hr at 1350° in platinum–10% rhodium crucibles.

The other preparative method was based on coprecipitating chromium–aluminum oxide gels. The hydrated gels were formed by rapidly injecting an aqueous stream of reagent grade chromium and aluminum nitrates into a vigorously agitated ammoniacal solution. They were recovered on a Büchner funnel and thoroughly washed with distilled water. After collapsing the gels by dehydrating them over a steam bath, they were fired in air for 8 hr at 1350° in platinum–10% rhodium crucibles.

X-Ray diffraction analysis of all of the samples fired at 1350° revealed that they were homogeneous solid solutions with the α-alumina, corundum, structure. No superlattice lines were observed, and although a quantitative evaluation was not made, the lattice parameters of the α-solid solutions appeared to increase regularly as the chromia content increased. X-Ray fluorescence spectrometry was used to determine the actual chromia concentrations to ± 10 ppm.

The esr spectra were obtained with a Varian E-3 esr spectrometer operating at 9.52 Gcps and 100 kcps modulation. The solid solutions were contained in 4-mm o.d. quartz tubes. Although all of the solid solutions were analyzed at room temperature, the temperature dependence of selected solid solutions was determined between 77 and 553°K.

The esr data discussed in this paper were obtained from the solid solutions prepared by the impregnation technique. Identical spectra were obtained from the solid solutions prepared using the sol–gel method. The particle sizes of the solid solutions used for esr analysis were between 53 and 63 μ.

Results

The esr spectra of 15 α-Cr_2O_3–Al_2O_3 solid solutions containing from 0.082 to 14.70% Cr_2O_3 were obtained at room temperature. The chemical composition and esr data of these solid solutions are summarized in Tables I and II.

Table I: Electronic Phases of α-Cr_2O_3–Al_2O_3 Solid Solutions Prepared at 1350°

Wt % Cr_2O_3	Mole % Cr_2O_3	Cr^{3+} ion phases	$\delta/\delta + \beta_N$[a]
0.082	0.055	Ruby	1.000
0.47	0.32	Ruby	1.000
0.94	0.63	Ruby; very weak β	...
1.48	1.00	Ruby; β_I; β_N	...
2.71	1.83	δ; β_I; β_N	0.827
3.79	2.58	δ; β_I; β_N	0.671
4.78	3.26	δ; β_I; β_N	0.499
5.80	3.97	δ; β_I; β_N	0.401
6.81	4.67	δ; β_N	0.275
7.73	5.32	δ; β_N	0.234
8.42	5.81	δ; β_N	0.197
9.75	6.76	δ; β_N	0.143
11.71	8.17	Very weak δ; β_N	0.101
14.70	10.36	No δ; β_N	0.000

[a] Relative ratio of isolated to coupled Cr^{3+} ions as defined in the text.

The solid solutions containing less than 1% Cr_2O_3 exhibited the characteristic esr spectrum of powdered ruby. It results from electronically isolated Cr^{3+} ions (δ phase).

Around 1.5% Cr_2O_3 two new resonances appear at $g = 1.99 \pm 0.01$. We attribute both of these resonances to Cr^{3+} ions electronically coupled with other Cr^{3+} ions. They apparently are related to the β phase resonances reported by other investigators.[1–4] The two β phase resonances, which we designated β_I and

(3) C. P. Poole, Jr., W. L. Kehl, and D. S. MacIver, Jr., *J. Catalysis,* 1, 407 (1962).

(4) C. P. Poole, Jr., and J. F. Itzel, Jr., *J. Chem. Phys.,* 41, 87 (1964).

Table II: Esr Parameters of α-Cr_2O_3-Al_2O_3 Solid Solutions

| Wt % Cr_2O_3 | δ phase $(\nu/H)_{max}$,[a] Gcps/G | β phase | |
		g	ΔH,[b] G
0.082	4.95×10^{-3}	. . .	. . .
0.47	4.98×10^{-3}	. . .	. . .
0.94	4.98×10^{-3}	. . .	. . .
1.48	4.95×10^{-3}	. . .	. . .
2.71	4.98×10^{-3}	1.987	498[c]
3.79	5.05×10^{-3}	1.979	476[c]
4.78	4.91×10^{-3}	1.977	500
5.80	5.05×10^{-3}	2.002	525
6.81	4.97×10^{-3}	1.992	525
7.73	5.06×10^{-3}	2.004	543
8.42	5.09×10^{-3}	2.004	533
9.75	4.78×10^{-3}	1.990	525
11.71	4.91×10^{-3}	1.999	500
14.70	. . .	1.999	438
	Av 4.97 ± 0.08 $\times 10^{-3}$	Av $1.993 \pm$ 0.01	

[a] Ratio of frequency to field of δ phase resonance maximum. [b] Separation between maximum and minimum of first derivative of absorption curve. [c] Cannot be accurately measured.

β_N are shown in Figure 1. We investigated the esr of solid solutions exhibiting both β_I and β_N resonances between 77 and 300°K. The observed temperature dependence indicates that the isolated Cr^{3+} ions and the Cr^{3+} ions responsible for both β phase resonances are paramagnetic. We suggest that the broad β_I resonance results from Cr^{3+} ions intermediate to isolated Cr^{3+} ions and Cr^{3+} ions which are strongly coupled electronically (β_N phase). It is interesting to note that the β_I resonance was found only in the solid solutions containing between 2 and 6% Cr_2O_3. The significance of the two β phase resonances and their origin is discussed in detail in the Discussion section.

As the Cr_2O_3 content increases, the β_N phase resonance increases in intensity. At approximately 4% Cr_2O_3 the resonances of the coupled and isolated Cr^{3+} ions appear to be equal. As the Cr_2O_3 content continues to increase, the number of coupled Cr^{3+} ions increases while the resonance from the isolated Cr^{3+} ions broadens and decreases in intensity. Finally, at 15 wt % Cr_2O_3, we were unable to detect any isolated Cr^{3+} ions. This can be seen in Figures 1 and 2.

Figure 3 is a plot showing the change in relative concentration of isolated Cr^{3+} ions (δ phase) to coupled Cr^{3+} ions (β_N phase) as a function of total Cr_2O_3 concentration. This ratio of the concentrations of the two types of Cr^{3+} ions was obtained by measuring the height from the base line to the maximum of the first derivative of the absorption for both the isolated Cr^{3+} resonance and the coupled Cr^{3+} resonance. The ratio is empirical. It does not provide an absolute measure of the number of spins contributing to the isolated Cr^{3+} resonance.
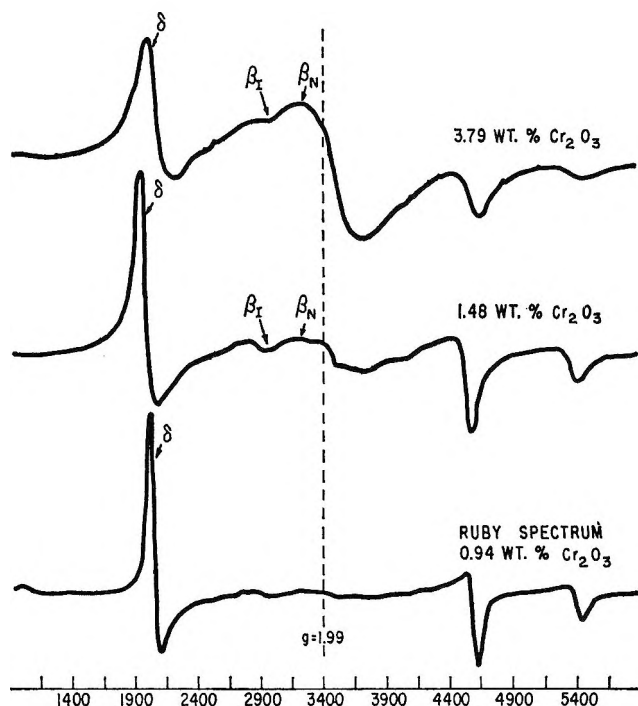
Figure 1. Appearance of coupled Cr^{3+} ions (β phase) with increasing Cr_2O_3 concentration in α-Cr_2O_3-Al_2O_3 solid solutions.
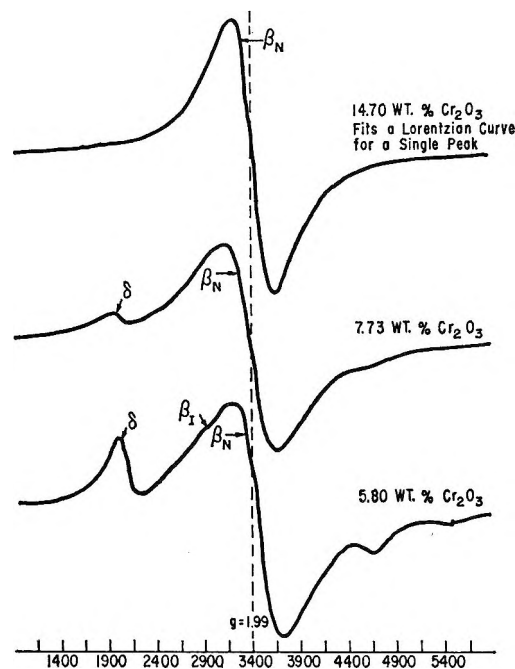
Figure 2. Disappearance of isolated Cr^{3+} ions (β phase) with increasing Cr_2O_3 concentration in α-Cr_2O_3-Al_2O_3 solid solutions.

The plot in Figure 3 indicates that the relative concentration ratio of the two Cr^{3+} phases varies in a smooth, nonlinear manner. An accurate measure of this ratio cannot be made below 2% Cr_2O_3 because of the low concentration of coupled Cr^{3+} ions. Similarly, the point at 11.71% Cr_2O_3 was subject to error because of the inaccuracy involved in measuring such a low con-
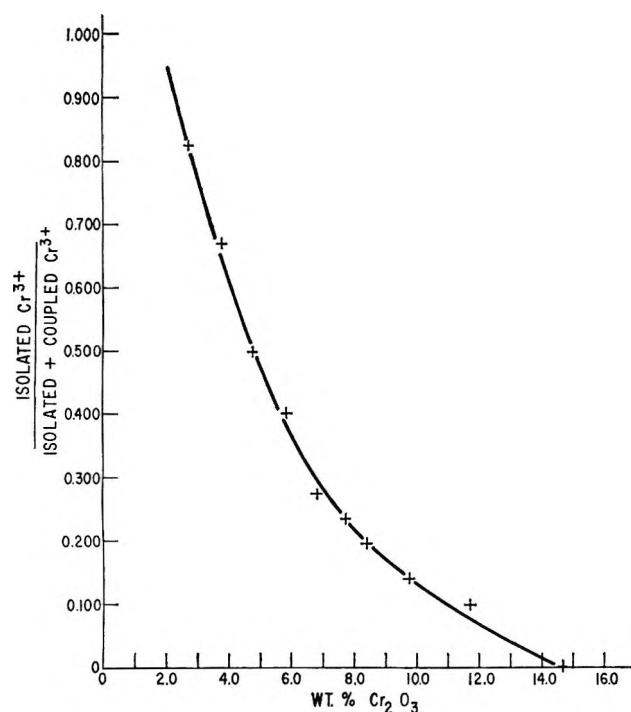
Figure 3. Variation in relative ratio of isolated to coupled Cr^{3+} ions as a function of composition.

centration of isolated Cr^{3+} ions. Besides its obvious analytical significance, this plot graphically shows the dependence of the two major Cr^{3+} ion phases on the total Cr$_2$O$_3$ concentration.

The esr data in Table II reveal that the peak to peak, full line width of the β_N phase resonance essentially remains constant between 2.5 and 15% Cr$_2$O$_3$. This result is in contrast to the variation in line width with increasing chromia content that has been reported previously for α-Cr$_2$O$_3$–Al$_2$O$_3$ solid solutions.[2,3] However, the other investigators have had to make a very large extrapolation since they only had two data points below 20 mole % Cr$_2$O$_3$. Thus, we think that the constancy of the line width of the β_N phase resonance which we established for eight different concentrations between 2.5 and 12% Cr$_2$O$_3$ is correct, and the slight decrease in line width of the 14.70% sample may be an indication of line narrowing with increasing Cr$_2$O$_3$ concentration. Additional data between 15 and 20% Cr$_2$O$_3$ would be required to establish if we are observing line narrowing in the 14.70% sample.

Discussion

The esr data in Table II show that the maximum of the derivative curve of the isolated Cr^{3+} ions (δ phase) major resonance is independent of Cr$_2$O$_3$ concentration. This means that in α-Cr$_2$O$_3$–Al$_2$O$_3$ solid solutions the origin of the δ phase is unchanged and its identifying peaks correspond to the major resonances in powdered ruby. The well-resolved symmetrical δ phase resonances in α-Cr$_2$O$_3$–Al$_2$O$_3$ solid solutions contrast with the

very broad δ phase resonance reported for impregnated and coprecipitated chromia–alumina catalysts.[2,3]

In the α-solid solutions the isolated Cr^{3+} ions are subjected to a strong axial crystal field in a highly ordered lattice. Consequently, in the dilute solid solutions the δ phase resonances are narrow, symmetrical, and well defined. In contrast, the δ phase resonance in impregnated and coprecipitated chromia–alumina catalysts is very broad. This is attributed to the imperfectly crystalline nature of the γ-alumina host lattice.[1a] γ-Al$_2$O$_3$ solid solutions may not be necessary to produce the broad δ-phase resonance since a δ-phase resonance was found in some catalysts which did not contain a detectable γ-Al$_2$O$_3$ solid solution phase.[1a] Cr^{3+} ions isolated on the surface also might produce a broad δ phase resonance since they would not be subjected to a regular crystalline field. In fact, it has been suggested that the isolated Cr^{3+} ions can exist either on the surface or in the bulk of the catalyst.[1a] Isolated Cr^{3+} ions in an amorphous matrix also could produce a broad δ phase resonance because of the absence of long-range order. For example, isolated Cr^{3+} ions in an amorphous phosphate glass matrix gave a broad δ phase resonance, even though they were subjected to a relatively strong axial field,[5] and indeed, the chromia–alumina catalysts are highly amorphous.[3]

We have observed two β-phase resonances (β_I and β_N) which we attribute to electronically coupled Cr^{3+} ions. We suggest that β_I results from Cr^{3+} ions which are close enough to couple electronically but far enough apart to experience only a weak exchange interaction. On the other hand, we suggest that β_N is a result of strong exchange interaction resulting from Cr^{3+}–Cr^{3+} ion pairs. Our interpretation of the origin of the β_I and β_N resonances is consistent with the results of esr measurements made on ruby single crystals.

Statz, et al., verified that the strongest electronic interaction in ruby single crystals is between Cr^{3+} ion pairs occupying adjacent lattice sites along the c axis.[6,7] Furthermore, they identified esr lines resulting from Cr^{3+} ion pairs. These would be centered at 3400 G at x-band frequencies. This result strengthens our assignment of the β_N phase resonance which is centered about 3420 G.

Statz, et al., also concluded that isotropic exchange interaction in Cr^{3+} ion pairs in α-Al$_2$O$_3$ can be present out to the eleventh neighbor shell with a magnitude of about 0.5 cm^{-1}.[7] For the third, fifth, and sixth neighbor shells the exchange interaction is of the order of 1 cm^{-1}. A sphere of radius 5.73 Å encompassing the 11 neighbor shells will contain about 42 cation sites.[7]

(5) R. J. Landry, J. T. Fournier, and C. G. Young, J. Chem. Phys., 46, 1285 (1967).

(6) H. Statz, L. Rimai, M. J. Weber, and G. A. DeMars, J. Appl. Phys., 32, 218S (1961).

(7) L. Rimai, H. Statz, M. J. Weber, G. A. DeMars, and G. F. Koster, Phys. Rev. Letters, 4, 125 (1960).

The significance of this hypothetical sphere is that if it contained two or more Cr^{3+} ions not forming nearest-neighbor ion pairs they still would be electronically coupled by exchange interactions. We suggest the more distant Cr^{3+} ions are weakly coupled by such electronic exchange interactions and result in the β_I phase resonance. In addition, in the cluster of ESR lines resulting from Cr^{3+} ion pairs the lines corresponding to the more distant neighbors are on the low-field side of the cluster.[7] β_I also appears on the low-field side of the β_N resonance and this is further evidence in support of our interpretation.

We used the equations given by Poole and Itzel[4] to calculate a 9 to 1 ratio of unpaired to nearest-neighbor paired Cr^{3+} ions for the 15% Cr_2O_3 solid solution which showed only a single symmetrical β_N resonance. Thus, in a statistical sense, the large increases in intensity we observed in the β_N resonance of α-solid solutions at higher Cr_2O_3 concentrations cannot be entirely accounted for in terms of simple nearest-neighbor ion pair formation. This is exactly what is expected based on the esr studies of ruby single crystals which showed that isotropic exchange interaction in Cr^{3+} ion pairs can be present out to the eleventh neighbor shell.[7] In other words, Cr^{3+} ion pairs other than nearest neighbors can contribute to the β_N resonance.

A narrow β phase resonance (also designated β_N) was found in coprecipitated chromia–alumina catalysts.[3] This antiferromagnetic β_N resonance was attributed to the presence of clumps or small crystallites of α-Cr_2O_3.[4]

The β_N phase resonance we observe in α-Cr_2O_3–Al_2O_3 solid solutions corresponds in g value, line shape, and line width to the β_N phase observed in coprecipitated chromia–alumina catalysts. However, there is one difference. We have found that the β_N phase resonance in α-Cr_2O_3–Al_2O_3 is paramagnetic up to about 10 mole % Cr_2O_3. This is in agreement with the report that the Neel points for a 9.2 and 19.6 mole % Cr_2O_3 solid solutions were too poorly defined to be measured.[4]

Another point to be considered is whether the β_I phase resonance we have found in α-Cr_2O_3–Al_2O_3 solid solutions is related to the β_W phase resonance reported in coprecipitated supported catalysts.[3,4] It was reported that the β_W resonance was paramagnetic and suggested that it might be associated with Cr^{3+} ions in solid solutions.[4] Our identification of the paramagnetic β_I resonance in α-Cr_2O_3–Al_2O_3 solid solutions strength-

ens this suggestion, especially since β_I and β_W have very similar g values and line widths. However, it was reported that the β_W resonance was independent of total Cr_2O_3 concentration,[3] and we have shown that β_I is concentration dependent, apparently existing only between about 1.5 and 6.0% Cr_2O_3. This suggests that if solid solutions of Cr_2O_3 and α-Al_2O_3 are responsible for the β_W resonance found in the coprecipitated catalysts, they probably will contain about 1.5 to 6% Cr_2O_3. Since β_W is apparently independent of concentration, perhaps the solubility limit of Cr_2O_3 in γ-Al_2O_3, under the conditions of forming the coprecipitated catalysts, is within this range. Because of the poorly crystallized nature of the γ-Al_2O_3 in coprecipitated chromia-alumina catalysts, it would be difficult to detect the formation of dilute solid solutions.

Conclusions

Three electronically different types of Cr^{3+} ions exist at low chromia concentrations in polycrystalline α-Cr_2O_3–Al_2O_3 solid solutions. These are isolated Cr^{3+} ions, Cr^{3+} coupled by weak electronic exchange interactions, and Cr^{3+} ions coupled by strong electronic exchange interactions. The relative ratio of isolated to coupled Cr^{3+} ions varies in a regular fashion.

We suggest a simple physical picture to explain the esr of polycrystalline α-Cr_2O_3–Al_2O_3 solid solutions. At low Cr_2O_3 concentrations (<1%) isolated Cr^{3+} ions in a strong axial field predominate. As the Cr_2O_3 concentration is increased, some of the Cr^{3+} ions locate close enough to other Cr^{3+} ions to couple by means of electronic exchange interaction. This results in the formation of two esr resonances, β_I and β_N. The β_I resonance is attributed to Cr^{3+} ions located within 11 neighbors of each other but far enough apart to experience only weak electronic exchange interactions. The β_N resonance results from first neighbor Cr^{3+} ion pairs and other Cr^{3+} ions located close enough to each other to experience strong electronic exchange interactions. As more Cr^{3+} ions are placed in the lattice, the number of strongly coupled Cr^{3+} ions increases and the resonance attributed to isolated Cr^{3+} ions and Cr^{3+} ions experiencing weak electronic exchange interactions decreases in intensity. Finally, around 15% Cr_2O_3 only a symmetrical resonance from the strongly coupled Cr^{3+} ions remains.

Quantum Deviations from the Principle of Corresponding States

by R. M. Gibbons

Air Products and Chemicals, Inc., Allentown, Pennsylvania 18105   (*Received January 22, 1968*)

An extension to the principle of corresponding states in terms of reduction by molecular constants is suggested which permits the calculation of consistent thermodynamic properties for simple molecules where quantum effects are important in the gas phase. The method correlates differences among the reduced properties of Ar, Ne, and ^{4}He with the reduced de Broglie wavelength. The thermodynamic properties of Ne, nH$_2$, and ^{3}He are calculated from empirical equations for Ar, Ne, and ^{4}He. The agreement with experimental data is good for the prediction of the properties of Ne and nH$_2$ but is less good for the properties of ^{3}He. The method fails for the liquid and critical regions of the phase diagram.

Introduction

The properties of light molecules deviate considerably from the classical principle of corresponding states at low temperatures and high densities. de Boer, *et al.*,[1] first suggested that these deviations were due to quantum effects and could be correlated with the reduced de Broglie wavelength; using this approach they were successful in the prediction of the critical properties and vapor pressure properties of ^{3}He. A similar approach has been used recently by Rodgers and Brickwedde[2] to predict the vapor pressure of tritium. Attention has also been given to the influence of quantum effects on phase equilibria[3] and critical-point behavior.[4] It is proposed here to examine the importance of quantum effects in the gas phase at higher temperatures than have been considered hitherto, with particular attention to the prediction of the PVT surface of ^{3}He.

The formulation of the law of corresponding states by de Boer, *et al.*,[1] in terms of reduction of properties by molecular units, derived from the collision diameter σ and the intermolecular potential constant ϵ, is the most suitable for examining the influence of quantum effects. de Boer showed if molecules had the same form of pairwise additive intermolecular potential, that in the reduced equation of state the reduced pressure was a function of the reduced temperature, volume, and de Broglie wavelength, $h/\sqrt{m\sigma^2\epsilon}$. The dependence on Λ^*, the reduced de Broglie wavelength, was not given explicitly and the effect of different statistics was ignored. In fact, de Boer, *et al.*, obtained the dependence property on Λ^* graphically, and similar methods were also used by Rodgers and Brickwedde.[2] For example, to obtain the vapor pressure curve of ^{3}He, de Boer, *et al.*,[1] plotted P^* *vs.* Λ^* at constant T^* for Ar, Ne, H$_2$, and ^{4}He; V^* was not held constant. The formulation used here is slightly different in that T^* and V^* are held constant in determining the dependence of P^* on Λ^* and the dependence on Λ^* is represented analytically instead of graphically. The method by which this was done is outlined in the following section.

The Dependence of P^* on Λ^*. The parameters used

to obtain the reduced properties are all listed in Table I. The two basic parameters for each substance σ and ϵ were obtained from second virial coefficient data[5] assuming a Lennard-Jones potential. The three reduction parameters ϵ/σ^3, $N\sigma^3$, and ϵ/k are not mutually independent, and the reduced PVT surface for a given molecule does not appear to be particularly sensitive to the choice of ϵ and σ, so the errors associated with using inexact constants should not be great.

To obtain the dependence of P^* on Λ^*, plots of P^* *vs.* f(Λ^*) at several T^* and V^* values were made to find a form so that P^* varies linearly with f(Λ^*). The plot of P^* *vs.* Λ^{*2} in Figure 1 shows P^* to vary linearly with Λ^{*2}, so that approximately the equation

$$P^* = \mathrm{f_c}(V^*, T^*) + \Lambda^{*2}\mathrm{f_2}(\Lambda^*, T^*) \qquad (1)$$

represents the dependence of P^* on Λ^* for fixed T^* and V^*. $\mathrm{f_c}(V^*, T^*)$ is a universal classical function and the term $\Lambda^{*2}\mathrm{f_2}(V^*, T^*)$ represents the total quantum effects. Rigorously, quantum effects can be represented by a series expansion $\Sigma\Lambda^{*n}\mathrm{f_n}(V^*, T^*)$ wherever such series converge; here this series is approximated by $\Lambda^{*2}\mathrm{f_2}(V^*, T^*)$. To obtain $\mathrm{f_c}$ and $\mathrm{f_2}$ at a given T^* and V^*, the actual pressures of Ar or Ne and ^{4}He are substituted into eq 1, which can than be solved for $\mathrm{f_c}$ and $\mathrm{f_2}$. It is possible that the differences in reduced pressures are due to other effects, such as nonadditivity of the intermolecular interactions or errors in the pressures of Ar and ^{4}He; for convenience, any differences in reduced pressures will be referred to as quantum effects, though it must be borne in mind that other causes can contribute too. Naturally, when quantum effects become

(1) J. D. de Boer, *Physica*, **14**, 138 (1948); J. D. de Boer and R. J. Lunbeck, *ibid.*, **14**, 510, 520 (1948).

(2) J. D. Rodgers and F. G. Brickwedde, *J. Chem. Phys.*, **42**, 2822 (1965).

(3) R. H. Sherman and L. Hammel, *Phys. Rev. Lett.*, **15**, 9 (1965).

(4) M. E. Fisher, *ibid.*, **16**, 11 (1966).

(5) J. O. Hirschfelder, C. F. Curtiss, and R. B. Bird, "Molecular Theory of Gases and Liquids," John Wiley and Sons, Inc., New York, N. Y., 1964, pp 1110, 1212.
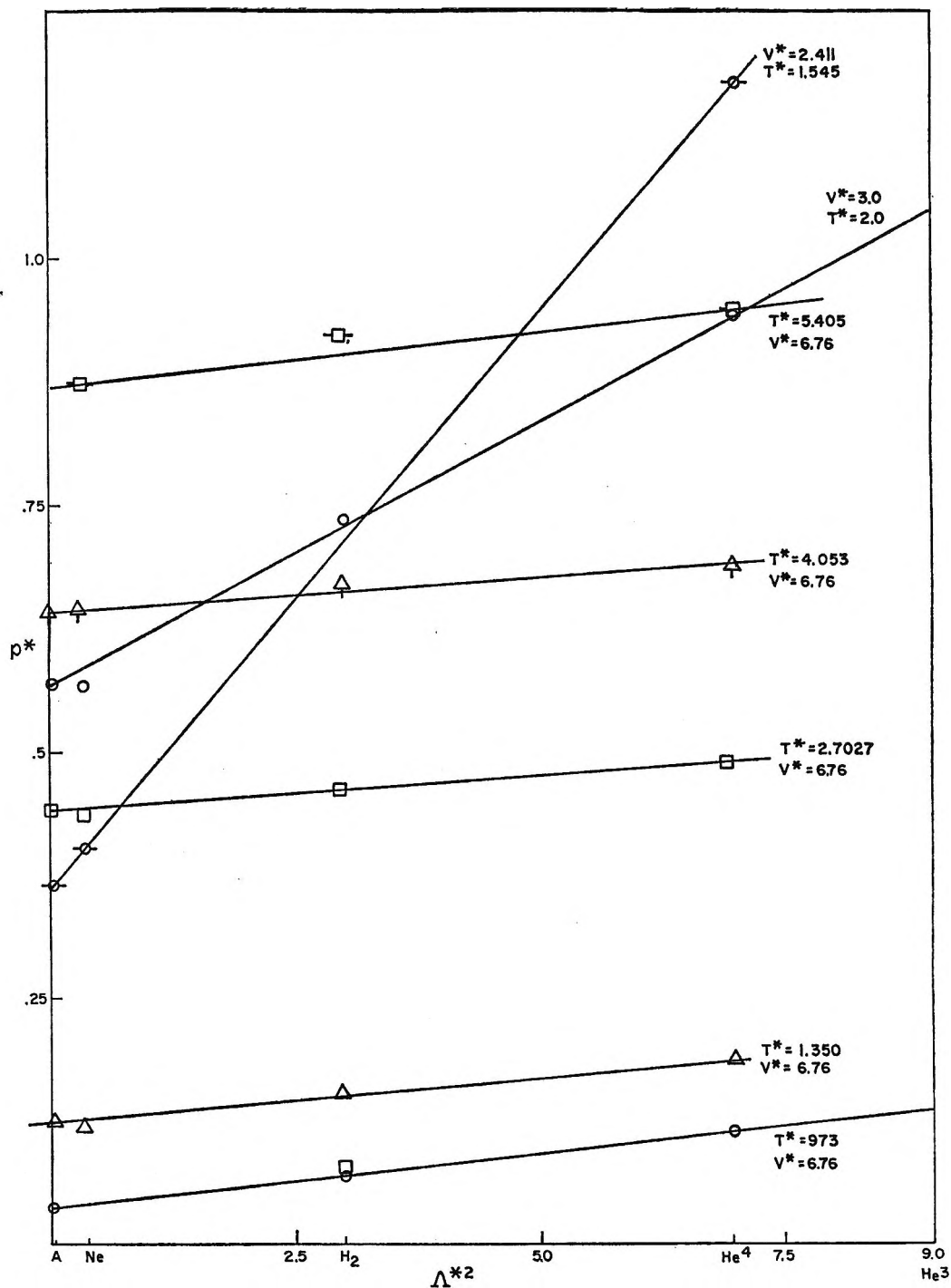
Figure 1.   Reduced pressure vs. reduced de Broglie wavelength at fixed reduced temperature and pressure.

gross, this simple representation will no longer be adequate to describe the dependence of P^* on Λ^* but the method should be of much greater accuracy than the classical form of the law of corresponding states by itself.   The enthalpy and entropy can be derived from the equation of state by standard thermodynamic arguments.[6]   This implies the same dependence on Λ^{*2} for H and S as has been shown by the pressure.

It remains then to generate consistent PVT, SVT, and HVT surfaces of the substances used to determine

f_c and f_2.   In this way, a consistent set of values for the thermodynamic properties can be obtained for other similar substances.   The modified Strobridge equations for ^{4}He,[7] Ar,[8] and Ne[9] are suitable.   These equations

(6) J. G. Hust and A. L. Gosman, Advan. Cryog. Eng., 9, 227 (1964).

(7) D. B. Mann, National Bureau of Standards Technical Note 154, U. S. Government Printing Office, Washington, D. C., 1962.

(8) A. L. Gosman, J. G. Hust, and R. D. McCarty, National Bureau of Standards Report 8293, U. S. Government Printing Office, Washington, D. C., 1964.
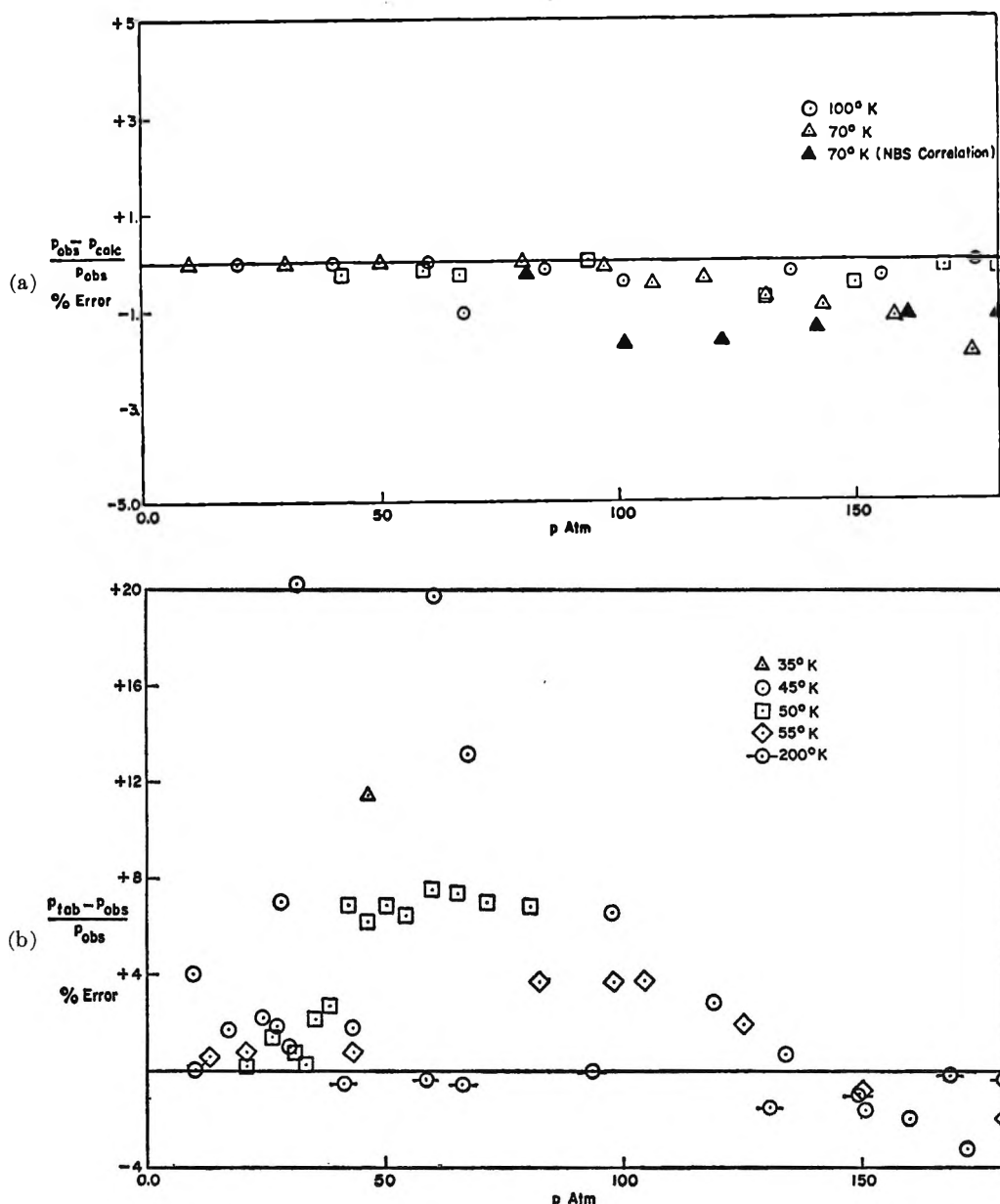
Figure 2. (a) The percentage error in the computed pressure vs. the experimental pressure at 70 and 100°; (b) the difference between the computed pressure and the pressure obtained from the McCarty–Stewart equation at 200, 55, 50, and 45°K.

Table I: Values of Molecular and Reference-State Constants

a. Molecular Constants

	ϵ/k, °K	σ, Å	ϵ/σ^3, atm	$N\sigma^3$, cc/mol	Λ^{*2}
Ar	119.8	3.405	413.54	23.778	0.034969
Ne	35.6	2.749	233.40	12.5127	0.349281
^{4}He	10.22	2.556	83.3795	10.05796	6.9696
^{3}He	10.22	2.556	83.3795	10.05796	9.025
H_2	37.0	15.11961	200.807	15.1196	2.9929

b. Reference-State Constants

	T_0, °K	S_0, J/g mol deg	H_0, J/g mol
Ar	87.28	129.826	9530.76
Ne	27.09	68.6195	1863.85
^{4}He	4.2144	37.0714	146.3425
H_2	20.39	80.1069	1486.50
^{3}He	3.1905	34.0131	66.3771

have restricted ranges but are suitable in most cases. The Ar equation has the smallest temperature range being limited to $T^* < 2.5$, but both the Ne and ^{4}He equations have ranges extending to $T^* > 9.0$. All these equations are inaccurate in the critical region. The equations for Ar[7] and ^{4}He[8] have been used in conjunction with eq 1 and the reduction parameters of Table I to calculate thermodynamically consistent properties of Ne and H_2. Similarly, calculations using the equations for Ne[9] and ^{4}He[8] have been made to obtain thermodynamically consistent properties for ^{3}He. These calculations will now be discussed.

(9) R. D. McCarty and R. B. Stewart, "Advances in Thermophysical Properties at Extreme Temperature and Pressure," American Society of Mechanical Engineers, McGraw-Hill Book Co., Inc., New York, N. Y., 1965, p 84.

The Properties of Neon. There is only a very limited amount of *PVT* data available for Ne with which comparisons can be made. The data of Michels, *et al.,*[10] at room temperature and above are the main source, together with the recent data of Sonntag and Sullivan[11] in the region 70–120°K. In addition, there is the equation of McCarty and Stewart,[9] which is more comprehensive but is not based upon experimental data at temperatures below 55°K, since none were available when the correlation was developed. Neon is normally thought of as a gas which obeys the classical version of corresponding states closely. However, Figure 1 shows that for $V^* = 2.411$ and $T^* = 1.545$, quantum effects can be as large as 10%. At low densities the influence of quantum behavior rapidly becomes very small especially at high temperatures.

Figure 2a shows an error plot for the values of P predicted by our correlation compared with the experimental results of Sonntag, *et al.,*[11] at 70 and 100°K. The average error in the predicted values of our correlation was <0.5%, with a maximum of 1.95%. Also shown in Figure 2a are comparisons of the values predicted by the McCarty–Stewart equation[9] at 70°K, which is more than ~1.2% too low at pressures >100 atm. Figure 2b shows plots of differences between the values predicted by the McCarty–Stewart equation and the present correlation. At 200°K the average difference is <0.3%, but for the three isotherms at 45, 50, and 55° there is an average difference of 5.9%. The largest errors in each isotherm always occur in the region near the critical point where the pressure changes very slowly with volume. The points in this region for each of the isotherms show errors of up to 25%; the isotherm at 45°K being less than 1°K from the critical temperature has the largest error. If this isotherm is excluded, the average difference between the McCarty–Stewart equation and the present correlation for the 100 points examined is 1.6%.

In examining the McCarty–Stewart equation at 70°K, it was found that this equation predicts lower reduced pressure than the argon equation[8] at the same reduced temperature and volume. Since quantum effects appear always to produce reduced pressures larger than the classical values, the McCarty–Stewart equation would seem to be too low by ~0.5% at 70°K. At 50°K, however, the McCarty–Stewart equation predicts reduced pressures greater than the corresponding reduced pressures for argon, as is normally expected. Figure 3 compares the predictions of the present correlation and classical corresponding states using the table of Pitzer and Brewer[12] with the McCarty–Stewart equation at 50 and 70°K. The McCarty–Stewart equation predicts values that lie between the classical values and those from the present correlation. The Pitzer correlation uses the critical properties as reduction parameters which leads to slightly different reduced forms than are obtained using molecular parame-
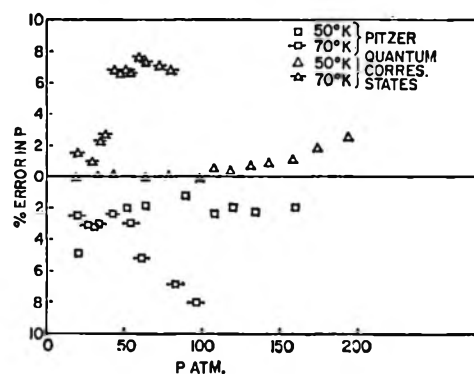
Figure 3. Comparison of the McCarty–Stewart equation with the present correlation and predictions from the classical version of corresponding states at 70 and 50°K.
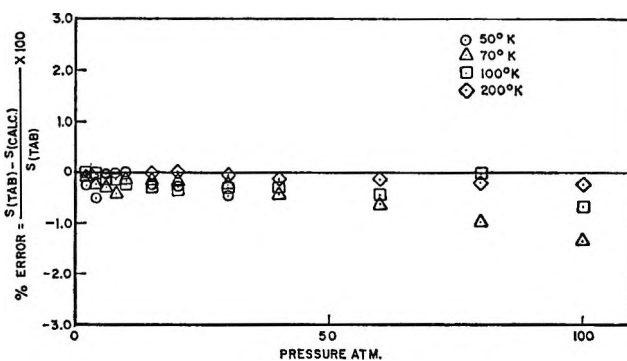
Figure 4. Comparison of the enthalpy from the present correlation with enthalpies from the McCarty–Stewart equation for neon.

ters. The present correlation has an average error of 4.4% at 50°K, while the Pitzer correlation is an average 4.4% too low. It is not possible to decide which is correct, but the present approach does suggest a way of checking the consistency of correlations with the principle of corresponding states.

Via standard thermodynamic arguments, as outlined by Hust and Gosman,[6] the same empirical equations can be used to obtain the entropy and enthalpy for Ar and [4]He. Proceeding in the same way as previously, the entropy and enthalpy of neon were obtained at 50, 70, 100, and 200°K and compared with the values of entropy and enthalpy generated from the McCarty–Stewart equation. Figure 4 shows the difference between the entropies of neon calculated by the present method and by the McCarty–Stewart equation. The agreement is better than 1% at 200, 100, and 70°K, but at 50°K, though there is agreement up to 30 atm, above this there are differences of up to 4%. Similar differences of up to 6% at 50°K can be observed for the

(10) A. Michels, T. Wassenaar, and P. Lourverse, *Physica*, **26**, 539 (1960).

(11) R. E. Sonntag and J. A. Sullivan, *Advan. Cryog. Eng.*, **12** (1966).

(12) K. S. Pitzer and L. Brewer, "Thermodynamics," McGraw-Hill Book Co., Inc., New York, N. Y., 1961, p 613.
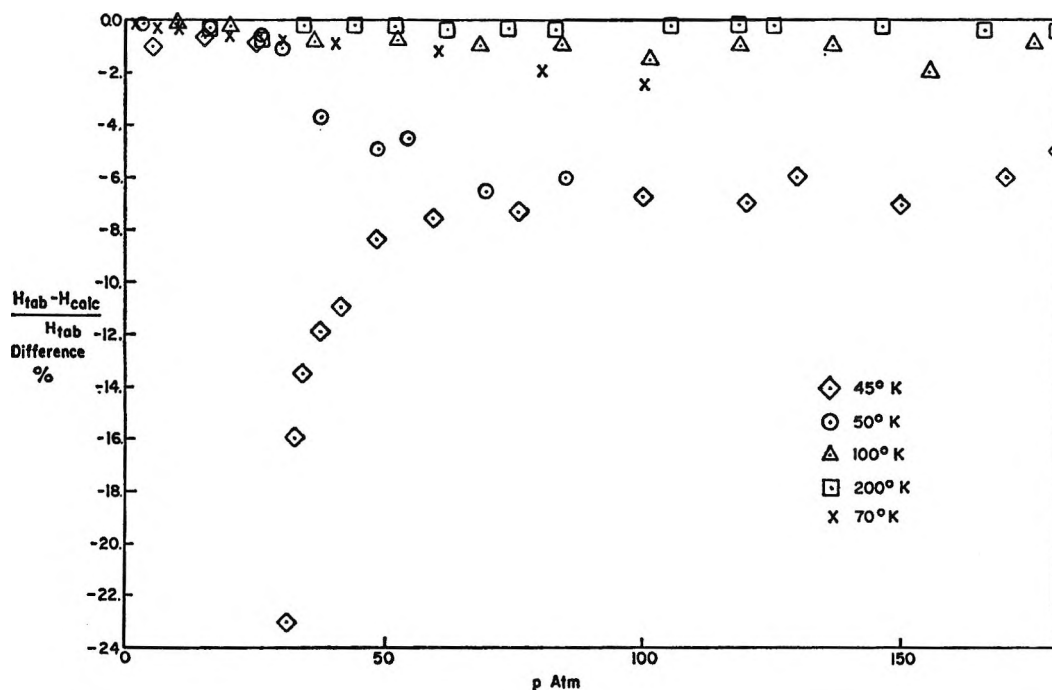
Figure 5. Comparison of the entropy from the present correlation with entropies from the McCarty–Stewart equation for neon.
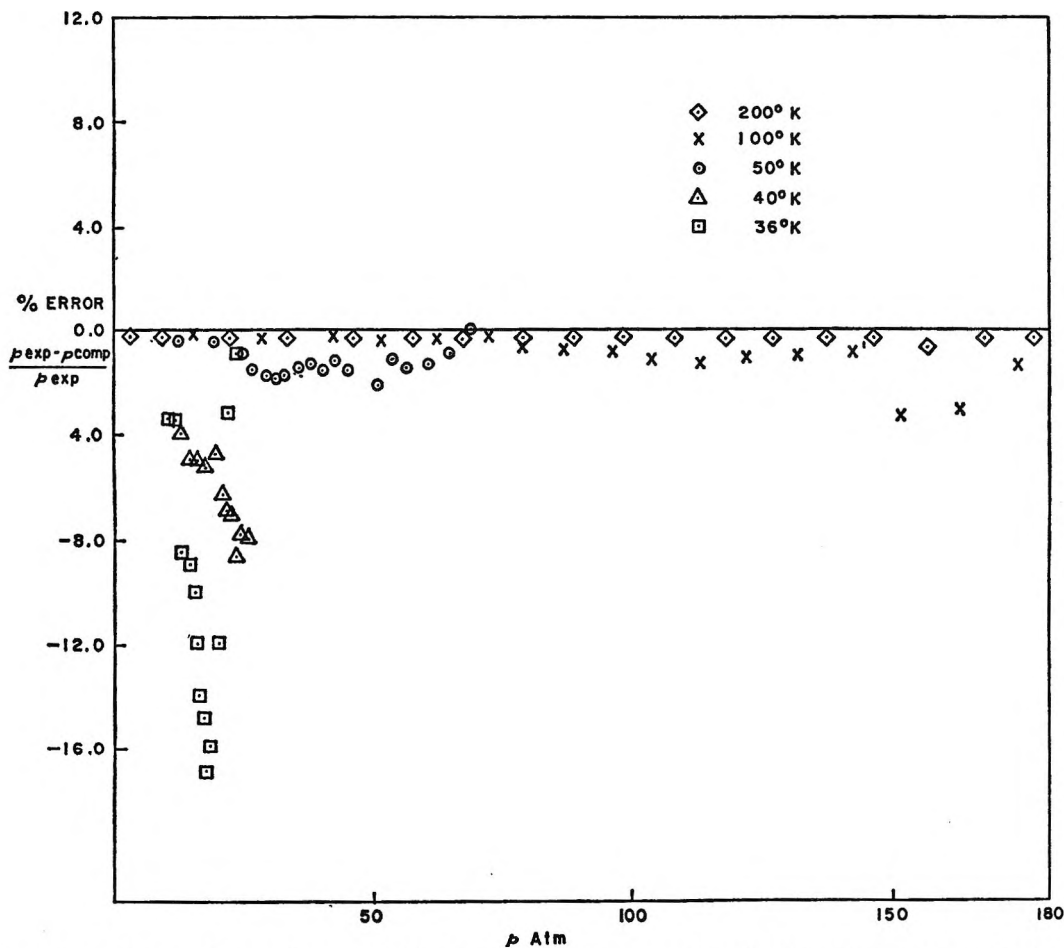
Figure 6. Comparison of the experimental pressure of hydrogen with the pressures predicted by the present correlation.

enthalpy of neon which is shown in Figure 5. The discrepancies at 50°K in the values of S and H between the two correlations merely reflect the differences in the values of the pressure and temperature derivatives of the pressure in the two correlations.

In conclusion, except perhaps for the critical region,
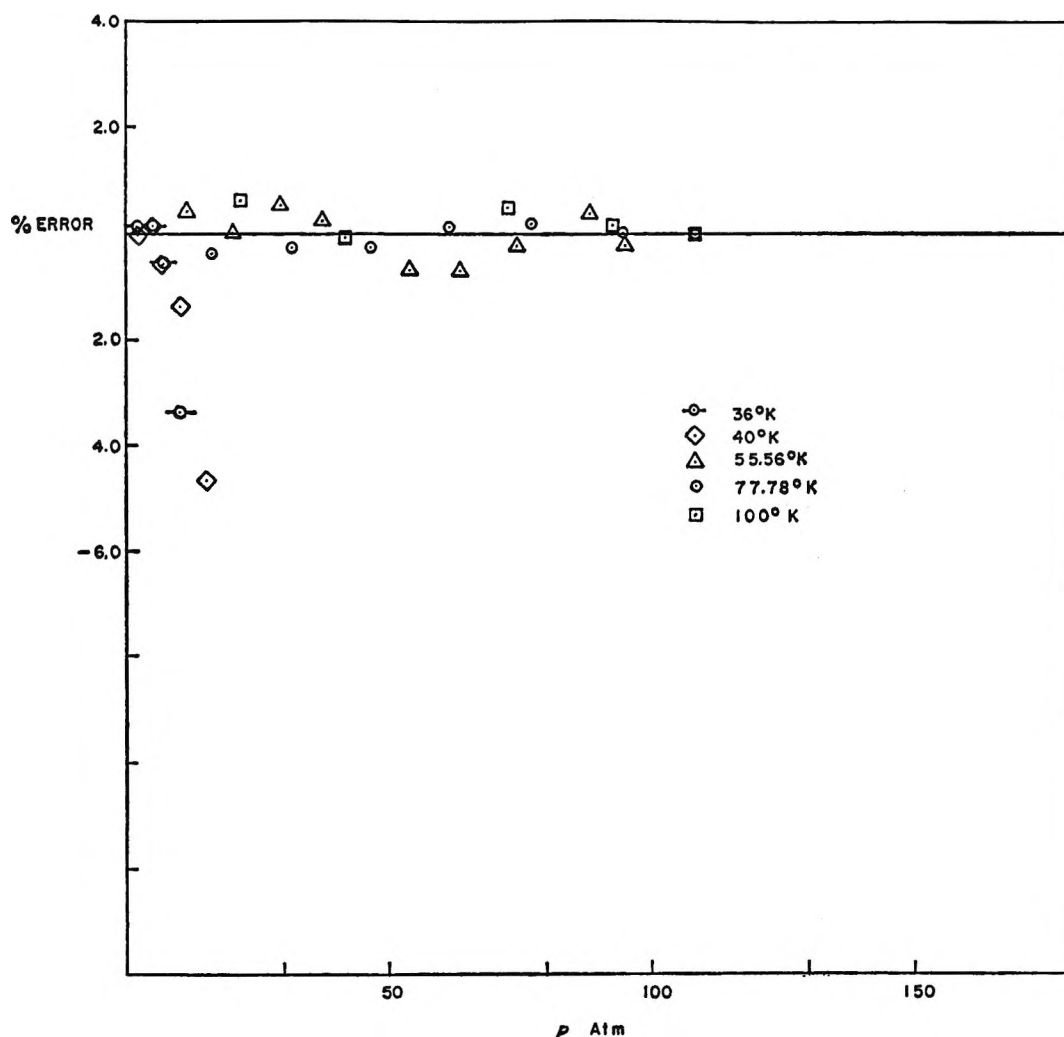
Figure 7. Comparison of the experimental enthalpy of hydrogen with the enthalpies predicted by the present correlation.

the present correlation can be used to obtain pressure data for Ne accurate to <1% and entropy and enthalpy data accurate to about 1% also. Because of the absence of data, neon is not suitable for testing the present correlation near the critical region. However, there are data available for low-temperature H_2 which can be used to test this approach in the critical region and this is discussed in the following section.

The Properties of Hydrogen. Hydrogen is the lightest of all molecules and it is well known that it shows considerable deviations from the classical law of corresponding states. The extensive tabulations of Wooley, Scott, and Brickwedde[13] cover the entire range from 10 to 600°K and pressures of up to 500 atm. However, there are difficulties in applying corresponding states to hydrogen. First, hydrogen is not monoatomic and the Lennard-Jones potential does not describe the molecular interactions as well as for the inert gases. There are also the difficulties associated with the ortho:para ratio being a function of temperature and the possible changes in the force constants resulting. As noted before, the effect of statistics is ignored in the formula-

tion of corresponding states. The predictions below apply then only to normal hydrogen and no account is taken of changes in the ortho:para ratio.

The differences between the values of the pressure produced by the present correlation and the experimental tabulations of Wooley, *et al.*,[13] are shown in Figure 6. The high-temperature isotherms at 100 and 200°K show excellent agreement, but, as with neon, the region near the critical is not reproduced well by this correlation. The errors for the 36°K isotherm has a maximum error of 16% at 15.5 atm, but this is close to the critical point where large changes in the pressure occur for small changes in volume. Over-all, for the 150 random points computed and compared with the experimental data, the agreement was good to 3%. If the isotherm at 35°K is excluded, the average deviation is 1%, which compared well with the recent correlation of Prausnitz, *et al.*[14]

(13) F. Wooley, R. B. Scott, and F. G. Brickwedde, *J. Res. Nat. Bur. Stand.*, **41**, 379 (1948).

(14) J. M. Prausnitz, R. D. Gunn, and P. L. Chueh, *A.I.Ch.E. J.*, **12**, 937 (1966).
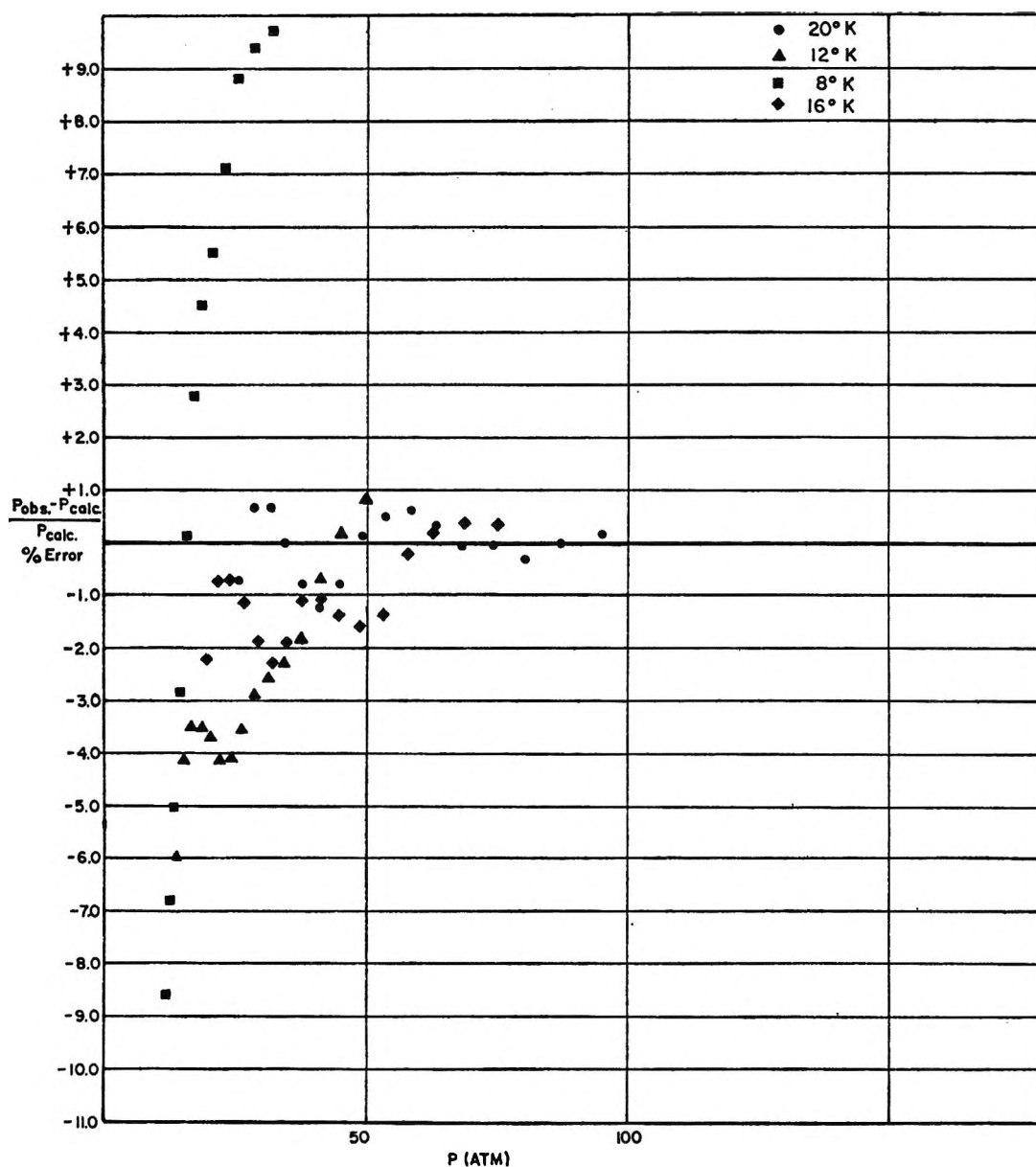
Figure 8. Comparison of the experimental pressures for ³He with the pressures predicted by the present correlation.

Figure 7 shows the comparison of the enthalpy predicted by the present correlation with the data of Wooley, et al.[13] The agreement is seen to be good for the high-temperature isotherms at 55.56, 77.78, and 100°K, but again there is poor agreement near the critical region for the isotherms at 36 and 40°K. The average difference between the 100 computed points and the experimental data was 0.4%, with a maximum error ~5.0%.

The Properties of ³He. The only gaseous data with which comparisons can be made are the recent data obtained at Air Products and Chemicals, Inc., under contract to the USAF[15] for the *PVT* properties of ³He. Figure 8 shows a comparison of the predicted values with the experimental values using Ne and ⁴He equations as the basis functions. The isotherms from 12 to 20°K show agreement with an average error of 1.5% and a

maximum error of 5.0% over the pressure range covered. Below 10°K, however, the disagreement becomes increasingly serious, culminating in the inversion of the 6°K isotherm with respect to the 8°K isotherm. The correlation fails completely therefore at the lowest temperatures. This is not too surprising, as ³He has the largest quantum effects of all the molecules and furthermore obeys statistics different from those for ⁴He and Ar. This simple approach is therefore not applicable to ³He at temperatures below ~12°K.

However, Figure 8 does show that at temperatures above 12°K the correlation is in very good agreement with the experimental data between 12 and 20°K. It is, therefore, reasonable to expect that at temperatures

(15) R. M. Gibbons and D. I. Nathan, "Thermodynamic Properties of He³," USAF Contract No. AF 33(615)-2870, Materials Research Laboratory, Wright-Patterson Air Force Base, Ohio, 1967.
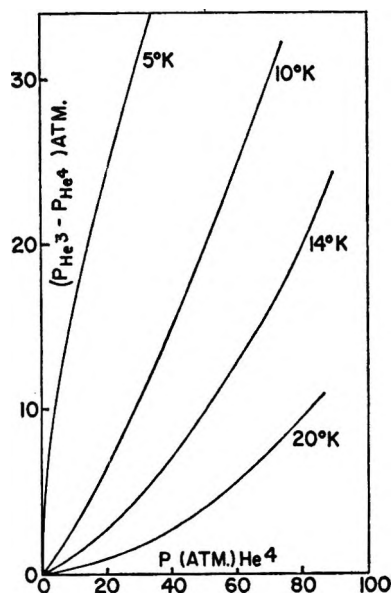
Figure 9. The difference in the pressures of ^{3}He and ^{4}He vs. the pressure of ^{4}He at 5, 10, 14, and 20°K.

Figure 10. Comparison of calculated and experimental enthalpies of ^{3}He.

above 20°K the correlation will predict values of the PVT surface accurate to ~1.0%, as the same approach gives excellent agreement at high temperatures for neon and hydrogen. Since quantum effects become important at high densities, it is instructive to plot the difference between the experimental pressures of ^{3}He and ^{4}He as a function of density at several temperatures, which is shown in Figure 9. It is seen that this difference increases with increasing density at all given temperatures and decreases to zero at low density as expected. The upper limit of 100°K is imposed upon the present correlation, as this is the highest reduced temperature at which the neon equation is applicable. By using experimental data rather than a correlated equation, one can, of course, continue this analysis to higher temperatures, until such a temperature that both ^{3}He and ^{4}He behave classically. At that temperature, the molar properties of the two molecules become identical.

Figures 10 and 11 show comparisons of the calculated and experimental enthalpies and entropies for ^{3}He. The values are not accurate enough to warrant showing in terms of plots of percentage error and are shown as direct comparisons. It can be seen that the enthalpy differs by up to ~5 J/g from the experimental enthalpy in Figure 10. The difference between the calculated and experimental entropies in Figure 11 is ~0.4 J/g deg. The absolute accuracy, therefore, is ~5% above 16°K. As with the predictions for Ne and H_2, better agreement should be obtained at higher temperatures.

Discussion

The present approach is of general utility in dealing with the quantum deviations from the law of corresponding states in the gas phase. It fails in the critical
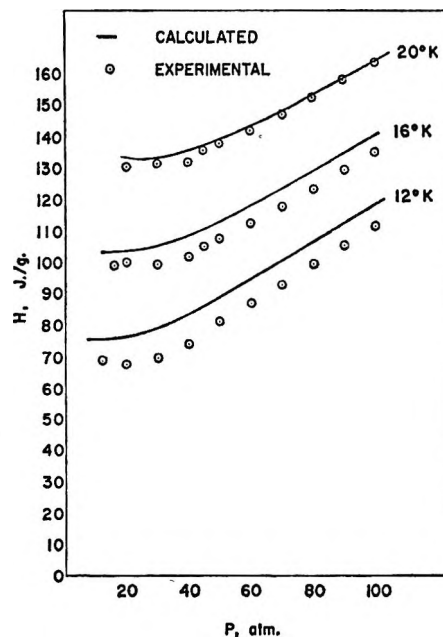
region for several reasons. In the first place, the dependence on Λ^* of P^* is represented too simply, but this could be corrected, assuming that the expansion in Λ^* converges in this region, by using a more complex form to represent this dependence. Also at the higher densities near the critical point, moderate values of the pressure of neon correspond to very large pressures of ^{4}He which lie beyond the range of the equation of Mann,[7] and uncertain errors can arise from this. The biggest difficulty, however, is that the liquid domes in the PVT plots for Ar, Ne, and ^{4}He do not occupy the same values of the reduced temperature and volume for all substances. As a result the pressure obtained for values of T and V lying within the dome, which is without physical meaning, may be used in the calculation of a pressure. Because of this difficulty, the present is only applicable in the gas phase or wherever all the pressures used have a physical meaning.

A further assumption implicit in this approach is that the Lennard-Jones potential describes adequately the interaction between molecules. This is not true and can give rise to uncertain errors at high densities where multibody interactions are important.

Conclusion

A general method of treating the quantum deviations from the law of corresponding states of light molecules has been presented and has been shown to be applicable to the gaseous region but is less successful in dealing with the liquid region. The dependence of a property on Λ^* is suggested as a useful test of the consistency of correlated data when experimental data are not available. The main result, however, is that this approach can be utilized to predict reliably the properties of gaseous
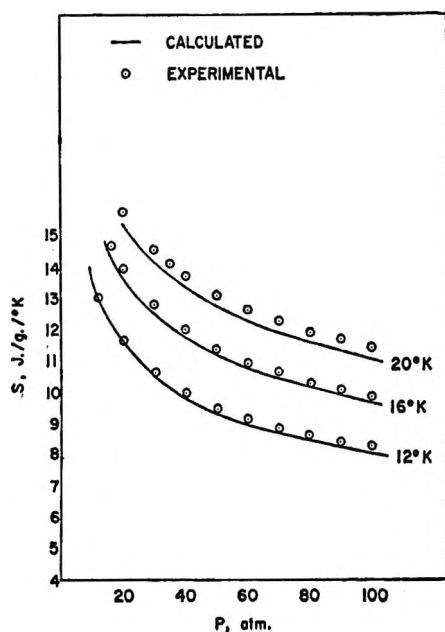
Figure 11. Comparison of calculated and experimental entropies of ^{3}He.

^{3}He in the region 20–100°K at pressures up to 100 atm. This general method will be used to generate data for ^{3}He in the region up to 100°K, which in combination with the experimental results in the lower temperature region will permit the correlation of the properties of ^{3}He from 1 to 100°K.

The present approach does suggest a way of improving the agreement between experimental data and the predictions of the law of corresponding states for any group of molecules which form a family. Using the data from two substances and a reduced plot in terms of molecular parameters, the dependence of the reduced properties on a parameter natural to the family can be determined. For example, for hydrocarbons the chain length might be used as an additional parameter,[16] or for polar molecules the reduced dipole or quadrupole moments could be used. The biggest difficulty in this sort of treatment would be in obtaining a three-constant intermolecular potential function which adequately described the interaction.

Another use of the quantum version of corresponding states is to extend the range for which data can be accurately predicted for a substance. For example, using the equations for neon and ^{4}He as a basis, the present correlation is able to predict consistent properties of argon to 1080°K at pressures of up to ~400 atm. This can be a useful supplement to experimental data.

Notations

h	Planck's constant
σ	Collision diameter
Λ^*	$h/\sqrt{m\sigma^2\epsilon}$, the reduced de Broglie wavelength
P^*	$p\sigma^3/\epsilon$, the reduced pressure
V^*	$V/N\sigma^3$, the reduced volume
T^*	kT/ϵ, the reduced temperature
S	Entropy
H	Enthalpy
T_0, S_0, and H_0	Reference-state constants

(16) E. A. Guggenheim and C. J. Wormald, *J. Chem. Phys.*, **42**, 3775 (1965).

Simultaneous Electrochemical and Internal-Reflection

Spectrometric Measurements Using Gold-Film Electrodes

by Arnold Prostak,[1a] Harry B. Mark, Jr.,[1b]

Department of Chemistry, The University of Michigan, Ann Arbor, Michigan 48104

and Wilford N. Hansen

Science Center, Aerospace and Systems Group, North American Rockwell Corporation, Thousand Oaks, California 91360
(Received January 22, 1968)

A vacuum-evaporated, uniform, transparent, commercially available thin-film gold electrode is described which permits transmission-like internal-reflection spectra to be obtained during an electrochemical reaction. Optical spectra of eosin Y and tris(4,7-dimethyl-1,10-phenanthroline)iron(II) sulfate are shown and the results are given of measurements made during potentiometric, potential-step, cyclic-voltammetry, and chrono-potentiometric experiments. The results are, with two exceptions, quantitatively understood.

Several authors have described the use of electrically conductive and optically transparent materials which can be used simultaneously as an electrode in an electrochemical cell and as an internal-reflection element to obtain spectra of absorbing–species that are close to or at the surface of the electrode.[2-6] Glass coated with the semiconductor tin oxide is the only electrode so far reported that has yielded spectra that can be quantitatively explained. However, because the thickness of the tin oxide film is comparable to the radiation wavelength, interference or optical-resonance effects cause very severe distortion of the spectra as compared with either transmission or conventional internal-reflection spectroscopy.[2,5] Indeed, as yet, no transmission-like internal-reflection spectrum made with the use of tin oxide coated glass has been reported. In addition, the electrochemical properties of tin oxide seem to be erratic.[2,4] Germanium electrodes are too chemically active to be generally useful and the reported non-uniform platinum-film electrodes give surprising but, as yet, unexplained results.

This paper describes the use, as a transparent electrode, of a thin (*ca.* 5 nm) uniform gold film deposited on glass. The advantages of gold are that it is already well known as an electrode[7] and its favorable optical and electrical constants[8,9] permit the use of a film sufficiently thin so that there are no optical-resonance effects from the film. Spectra and quantitative experimental data are given which illustrate some of the results which can be obtained with these gold films.

Experimental Section

Deposition of Gold Films. If pure gold is vacuum evaporated onto clean glass in an attempt to obtain a gold film thinner than about 20 nm, the result is a very high resistance deposit which has a bluish color in transmitted light. This is because such small amounts of

gold per unit area deposit as discontinuous "islands" rather than as a continuous film.[10,11] However, it has been reported that if a film of any one of several oxides, such as Bi_2O_3, is first deposited on the glass by reactive sputtering or a vacuum evaporation, then a continuous gold film of thickness 6 nm or less can be deposited on the undercoat by vacuum evaporation or sputtering.[12-16] Thin gold films with a PbO or a Bi_2O_3 undercoat were successfully prepared by following the vacuum-evaporation procedure of Ennos,[15] although occasionally the Bi_2O_3 decomposed during the evaporation giving a dark

(1) (a) National Science Foundation Graduate Fellow. (b) This research was supported in part by a grant from the National Science Foundation, NSF GP-4620.

(2) W. N. Hansen, T. Kuwana, and R. A. Osteryoung, *Anal. Chem.*, **38**, 1810 (1966).

(3) H. B. Mark, Jr., and B. S. Pons, *ibid.*, **38**, 119 (1966).

(4) B. S. Pons, J. S. Mattson, L. O. Winstrom, and H. B. Mark, Jr., *ibid.*, **39**, 685 (1967).

(5) V. S. Srinivasan and T. Kuwana, *J. Phys. Chem.*, **72**, 1144 (1968).

(6) N. J. Harrick, "Internal Reflection Spectroscopy," Interscience Publishers, New York, N. Y., 1967.

(7) (a) F. Baumann and I. Shain, *Anal. Chem.*, **29**, 303 (1957); (b) H. Khalifa and A. M. Daess, *Z. Anal. Chem.*, **159**, 272 (1958).

(8) G. Hass and L. Hadley in "American Institute of Physics Handbook," D. E. Gray, Ed., 2nd ed, McGraw-Hill Book Co., Inc., New York, N. Y., 1967, pp 6–112.

(9) J. Bardeen in "Handbook of Physics," E. U. Condon and H. Odishaw, Ed., McGraw-Hill Book Co., Inc., New York, N. Y., 1958, p 4–74.

(10) R. S. Sennett and G. D. Scott, *J. Opt. Soc. Amer.*, **40**, 203 (1950).

(11) O. S. Heavens, "Optical Properties of Thin Solid Films," Dover Publications, New York, N. Y., 1965, p 186.

(12) E. J. Gillham, J. S. Preston, and B. E. Williams, *Phil. Mag.*, **46**, 1051 (1955).

(13) L. Holland and G. Siddall, *Vacuum*, **3**, 375 (1953).

(14) L. Holland and G. Siddall, *Brit. J. Appl. Phys.*, **9**, 359 (1958).

(15) A. E. Ennos, *ibid.*, **8**, 113 (1957).

(16) W. H. Colbert, A. R. Weinrich, and W. L. Morgan, U. S. Patent 2,628,927 (1953).

rather than a colorless oxide film. These films had good optical properties and a resistance of about 35 ohms/square, as measured with a four-point probe.[17,18]

Two vendors were found who commercially supply substrates coated with thin gold films.[19,20] Sheet glass coated with Type 81-E coating with no overcoat on the conductive coating was procured from Liberty Mirror[19] (LM) by special order. The composition of the coating is considered proprietary by the vendor, but it appears to be essentially a gold film with no indication of a bismuth oxide undercoat. The undercoat might be a very thin film of a partially oxidized metal. Colorimetric analysis using o-toluidine reagent[21] of the gold content of one sample of this film gave a mass per unit area of gold equivalent to a 5-nm thickness of gold. The resistance of the gold film that was used was 24 ohms/square and the transmittance at normal incidence of the gold-coated glass was 76% at the 550-nm wavelength. The glass was 2.36 mm thick and its index of refraction, n_D, was 1.519. When this material was heated to 300° for about 15 min, its resistance decreased 24% and its transmittance increased by a few per cent, but this improved "annealed" material was not used in the experiments reported here. Sheet-glass substrate was specified because it was felt that the fire-polished surface of the sheet glass would have a smaller height gradient than plate glass.[22]

Gold films were also made by spin coating Hanovia Liquid Bright Gold No. 6854[23] on glass, followed by heating. The resulting film is essentially gold with small amounts of other metallic oxides to improve bonding to the substrate and had a resistance of about 5 ohms/square. In an unsuccessful attempt to make a thinner film, 1 part of Liquid Bright Gold was diluted with 0.4 part of xylene before spin coating. The resulting film had an extremely high electrical resistance.

Electrochemical Cells. The multiple-reflection cell used was similar to the one described by Hansen, et al.,[2,24] except that two gold-wire auxilliary (or counter-) electrodes connected in parallel were used. Each auxiliary electrode was in a separate compartment connected to the main cell compartment by a fine-porosity fritted glass disk. The reference electrode was also in a separate compartment connected to the main cell compartment with a similar fritted disk. Electrical contact to the gold film was made with conducting silver paint that was painted only on the bottom and side edges of the gold film. The silver paint did not contact the electrolysis solution. Four reflections at the solution side were used. The single-reflection variable-angle cell used was similar to the multiple-reflection cell, except that it had a smaller gold-electrode area and used the variable-angle optical scheme previously described by Hansen.[25] For some preliminary experiments, the electrolyte was deaerated by bubbling nitrogen through it, and the sample compartment in the spectrometer was also purged with nitrogen. However, the purge did not seem to make any difference in these experiments, and it was discontinued for the experiments reported here. (Caution must be employed in deciding not to deaerate, as many experiments will be air sensitive.)

Spectrometer and Recorder. A Cary Model 14R recording spectrophotometer with a high-intensity tungsten-iodine lamp was used and was modified to reduce beam divergence in the sample area by the installation of an additional pair of slits.[26] An expanded-scale slide-wire was used when desirable. A transmitting ten-turn potentiometer was geared to the slide-wire drive gear to provide a signal for an external recorder. A Hewlett-Packard Model 2FA two-pen recorder (x, y, and y' axes) simultaneously recorded electrochemical and optical data on the same chart.

Electrochemical Instrumentation. A Jaissle potentiostat was used for all experiments. When a potential step was employed, a Rubicon portable potentiometer provided the external step input to the potentiostat. For cyclic voltammetry studies, a Hewlett-Packard Model 202A low-frequency function generator provided a triangular wave for the external input to the potentiostat. Chronopotentiometric measurements were made using the galvanostatic operating mode of the Jaissle instrument. A Philbrick Researches Model P75 operational amplifier was used as a voltage follower to measure the potential between the reference and the indicator electrodes and the reference electrode was a Beckman fiber-junction calomel reference electrode (sce) from a Model G pH meter.

Chemicals. All solutions were made with triple-distilled water. Sodium sulfate solution, 0.1 M, was prepared from reagent grade crystalline sodium sulfate and the pH was adjusted to 5 by the addition of sulfuric acid.

Tris(4,7-dimethyl-1,10-phenanthroline)iron(II) sulfate (4,7-dimethyl ferroin, DM ferroin) was prepared from 4,7-dimethyl-1,10-phenanthroline obtained from the G. Frederick Smith Chemical Co. and reagent grade ferrous sulfate.[27,28] The solution was made 0.1 M in

(17) L. B. Valdes, *Proc. I.R.E.*, **42**, 420 (1954).

(18) F. M. Smits, *Bell System Tech. J.*, **37**, 711 (1958).

(19) Liberty Mirror Division, Libbey-Owens-Ford Glass Co., Brackenridge, Pa. 15014.

(20) The Sierracin Corp., Sylmar, Calif. 91342.

(21) E. Sandell, "Colorimetric Determination of Traces of Metals," Interscience Publishers, New York, N. Y., 1959, p 506.

(22) L. Holland, "The Properties of Glass Surfaces," John Wiley and Sons, Inc., New York, N. Y., 1964, Chapter 1.

(23) Hanovia Liquid Gold Division, Engelhard Industries, Inc., East Newark, N. J.

(24) W. N. Hansen and J. A. Horton, *Anal. Chem.*, **36**, 783 (1964).

(25) W. N. Hansen, *ibid.*, **37**, 1142 (1965).

(26) J. A. Horton and W. N. Hansen, *ibid.*, **39**, 1097 (1967).

(27) G. F. Smith and F. Richter, "Phenanthroline and Substituted Phenanthroline Indicators," The G. Frederick Smith Chemical Co., Columbus, Ohio, 1944, p 23.

Na_2SO_4 and then was adjusted to a pH of 5 by the addition of sulfuric acid.

The eosin Y solution used had an approximate concentration of 100 g/l.

Results and Discussion

Stability of Gold Film. Gold films with an undercoat of Bi_2O_3 made by the Ennos procedure[15] were not affected by immersion in 0.1 *N* NaOH, were destroyed by 0.1 *M* HCl, and after several hours of immersion were very slightly affected by 0.01 *M* HCl. Similar films with a PbO undercoat seemed to be less resistant to acid.

The Liberty Mirror gold film was removed by 24 hr of immersion in 0.1 *M* HCl, but 0.01 *M* HCl had no effect. These films were not affected by 16 hr of immersion in acetonitrile or dimethylformamide. After several days of immersion in aqueous solution, the films sometimes deteriorated at the air–liquid interface, even though the body of the film was unaffected. (This did not affect the electrical or optical behavior, inasmuch as the interface was kept above the optical path.) It was noted that after about 1 week of use during which time the films were stable, some of the LM films would slowly become thinner if kept at 0.95 V in DM ferroin solution.

The films prepared from Liquid Bright Gold seemed to be exceptionally resistant to chemical and mechanical attack but, as will be seen, were optically unsatisfactory.

Spectra. Figure 1 shows internal-reflection spectra (in terms of reflection absorbance, *i.e.*, -log (reflectance)) of a fairly concentrated eosin Y solution, which is known not to adsorb on glass. An angle of 72° was used because it is sufficiently far from the critical angle so that "distortion" is minimized and transmission-like spectra are obtained. The absorbance of the dye solution is taken as the additional absorbance when dye solution is in the cell compared to the absorbance under the same conditions but when distilled water is in the same cell. The absorbance of the gold film is the additional absorbance when the film is on the glass and water is in the cell compared to the absorbance under the same conditions but using the same glass without the gold film.

It will be noted that with no gold film on the glass the absorbance is greater with parallel than with perpendicular polarization. This effect is well known,[6] but, in the case of parallel polarization, the addition of the gold film further increases the absorbance per reflection while with perpendicular polarized light the opposite is true. This somewhat surprising effect is, however, in accordance with the calculated absorbance, as shown in Table I. These calculations were made with a high-speed digital computer and Hansen's equations for the reflectance from a stratified three-layer (glass–gold–solution) system.[29] With these equations, the optical

constants of each layer, and the thickness of the middle layer, one can calculate the reflectance and transmittance of the system as functions of the angle of incidence and plane of polarization of the incident radiation.

Table I: Comparison of Calculated and Experimental Absorbance

	Calcd[a]		Exptl	
	$A_{\parallel}$	$A\perp$	$A_{\parallel}$	$A\perp$
Gold film	0.101	0.130	0.22	0.27
Eosin Y on glass	0.31	0.26	0.33	0.28
Eosin Y on gold film	0.50	0.111	0.60	0.13
A_{gold}/A_{glass}, eosin Y	1.6	0.43	1.8	0.46

[a] Calculated for 72° angle of incidence, 5 nm thick gold film, and optical constants for the 520-nm wavelength; glass: $n = 1.52$ and $k = 0$ (the complex refractive index $n = n + ik$); gold: $n = 0.7$ and $k = 2.24$; eosin Y solution: $n = 1.368$ and $k = 0.0569$; water: $n = 1.335$ and $k = 0$. Optical constants of eosin Y solution from ref 25 after correcting ordinates of Figure 6 of ref 25 by dividing by 2.

Figure 2 shows a single-reflection spectrum of a concentrated solution of eosin B[24] using a gold film on glass prepared by spin coating Liquid Bright Gold. This film is substantially thicker than the vacuum-evaporated gold films. Note that for this thicker film the absorbance of the dye using parallel polarization is negative compared with the absorbance obtained with water in the cell, and the dye spectrum apparently is a function both of the absorption coefficient and the index
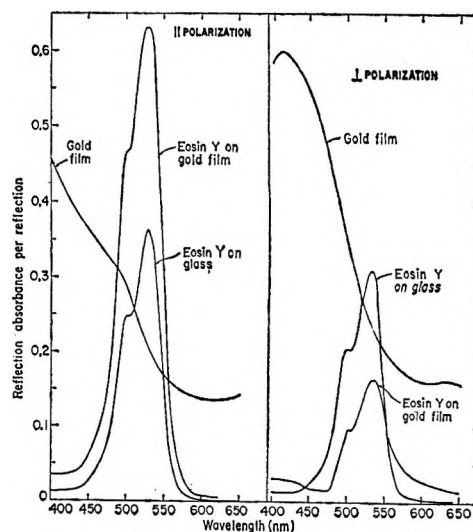
Figure 1. Internal-reflection spectra given as the reflection absorbance, *i.e.*, −log (reflectance): 100 g/l. of eosin Y, LM gold film, 72°, four reflections.

(28) W. W. Brandt and G. F. Smith, *Anal. Chem.*, **21**, 1313 (1949).
(29) W. N. Hansen, *J. Opt. Soc. Amer.*, **38**, 380 (1968).
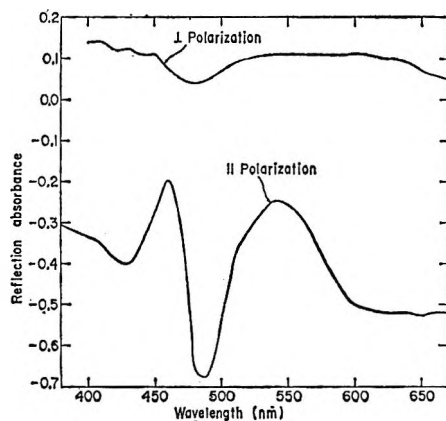
Figure 2. Internal-reflection spectra of a concentrated solution of eosin B using a relatively thick gold film prepared from Liquid Bright Gold: 72°, one reflection.

of refraction of the dye solution. Calculations using Hansen's equations[29] also show that for parallel polarization and gold-film thickness in the range from 10 to 90 nm, the absorbance decreases as the index of refraction of the solution increases. In part, the physical explanation of the negative absorbance is that the presence of the dye solution (with its higher index of refraction than water) against the gold decreases the radiant power absorbed in the gold film and this effect more than compensates for the radiation absorbed in the dye solution. In a very thin gold film, the radiant power absorbed in the gold film is sufficiently small so that small changes in this gold-film absorption due to changes in the index of refraction of the solution have relatively little effect. These considerations show that it is necessary to use gold films thinner than about 10 nm in order to get transmission-like spectra.

Figure 3 shows transmission and internal-reflection spectra of a 0.0125 M solution of 4,7-dimethyl ferroin with 0.1 M Na_2SO_4 as the supporting electrolyte and the pH adjusted to 5. At a potential of 0.379 V, the DM ferroin is in its fully reduced (colored) form, while at 0.94 V (which is not corrected for iR potential drop in the gold film) it should be in its oxidized (relatively colorless) form (dimethyl ferroin). Note that the internal-reflection spectrum on the LM gold film has essentially the same shape as the transmission spectrum. It would be impossible to see this reduction in absorbance in a conventional transmission measurement because the thin, relatively colorless oxidized layer is backed by the very highly absorbing solution. There is also a residual absorbance at the shorter wavelengths which may be due to adsorption. From the measured transmission absorption coefficient maximum at the 512-nm wavelength, we calculate that our DM ferroin solution ϵ is 13,700 l./mol cm, which agrees well with the reported value of ϵ 14,000 l./mol cm.[28] Table II compares the measured internal-reflection absorbances at 512 nm with calculated values. As the
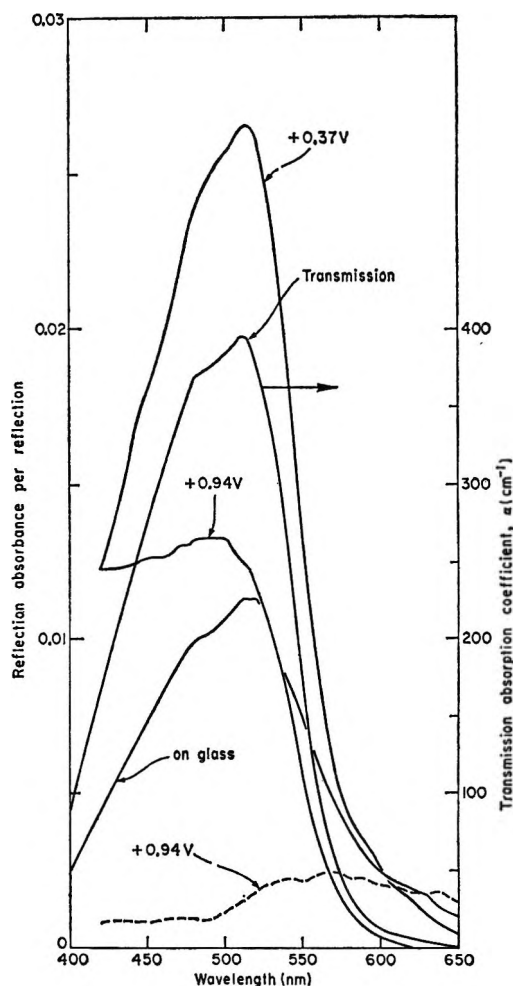
Figure 3. Spectra of 12.5 mM 4,7-DM ferroin solution and supporting electrolyte (0.1 M Na_2SO_4): ———, DM ferroin; – – –, Na_2SO_4 only (for internal-reflection spectra). LM gold film, parallel polarization, 72°, four reflections (for transmission spectrum), cell thickness 55 μm.

Table II: Comparison of Calculated and Experimental Absorbance for DM Ferroin Solution

	Calcd[a] $A_{||}$	Exptl $A_{||}$
On glass	0.0083	0.0112
On gold film	0.013	0.0265
A_{gold}/A_{glass}, DM ferroin	1.5	2.4

[a] Calculated for 72° angle of incidence, 5 nm thick gold film, and optical constants for the 512-nm wavelength; glass: $n = 1.52$ and $k = 0$ (the complex refractive index $n = n + ik$); gold: $n = 0.8$ and $k = 2.0$; DM ferroin solution: $n = 1.346$ and $k = 0.00160$; Na_2SO_4 solution: $n = 1.346$ and $k = 0$.

measured absorbances were higher than the calculated values, this suggests that DM ferroin adsorbs on glass and yet more strongly on gold.

In Figure 3 one can see a change in reflectance with potential (the dashed curve is the absorbance at 0.94 V relative to 0.34 V) when only colorless supporting
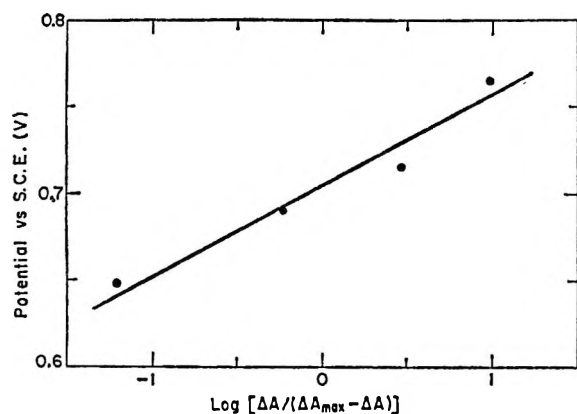
Figure 4. Graph of Nernst equation: 12.5 mM DM ferroin solution, LM gold film, 13.3-cm^2 area, 512-nm wavelength, parallel polarization, 72°, four reflections.

Figure 5. Potential step from 0.37 to 0.94 V and back to 0.37 V: 12.5 mM DM ferroin solution, LM gold film, 13.3-cm^2 area, 512-nm wavelength, parallel polarization, 72°, four reflections.

electrolyte is present, although the change here is small and is almost within the noise level. This effect will be discussed further below.

Potentiometry. The potential of the LM gold film in DM ferroin solution was maintained at each of several values and the current and the absorbance at the 512-nm wavelength were measured at each potential. The measured potential was corrected for iR drop in the film. The film and uncompensated electrolyte resistance was found to be about 10 ohms and was measured by applying a 5-mA current step to the cell and noting the magnitude of the potential rise. It can be shown by applying the Nernst equation that

$$E = E_0' + (2.3RT/nF) \log [\Delta A/(\Delta A_{max} - \Delta A)]$$

where ΔA is the change in absorbance obtained when stepping from less than 0.5 V to the potential E, and ΔA_{max} is the change in absorbance when the potential is stepped from 0.5 to 0.94 V (surface concentration of reduced DM ferroin is essentially zero at 0.94 V). A plot of E vs. the logarithmic term is shown in Figure 4. The slope of the least-squares-fitted straight line should be $2.3RT/nF$, which for the one-electron oxidation expected for DM ferroin[30] is 0.059 V. The experimentally determined slope is 0.052 V. The experimental formal potential of this couple given by this plot is 0.70 V with respect to an sce, which compares favorably with the recently reported potential of 0.695 V vs. the SCE for DM ferroin in an aqueous 0.1 M lithium perchlorate solution.[31]

Potential Step. Figure 5 shows the result of a potential-step experiment (anodic current is positive). As with tin oxide coated glass, the absorbance does not increase as rapidly as might be expected.[2] From the data in this figure, the equation describing the current density as a function of time, from $t = 1$ sec to $t = 20$ sec, is $i/A = 0.977$ mA cm^{-2} sec$^{1/2}$ $t^{-1/2}$, with a standard deviation of the data points from this straight line of 0.003 mA/cm^2. The slope of this straight line,
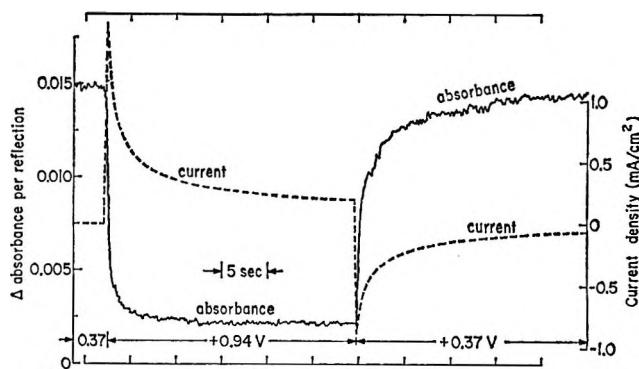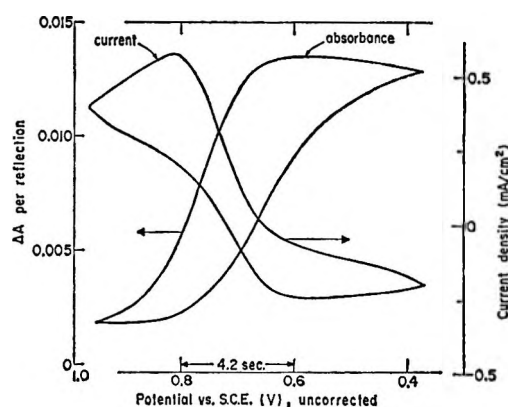
Figure 6. Cyclic voltammetry: 12.5 mM DM ferroin solution, LM gold film, 13.3-cm^2 area, 512-nm wavelength, parallel polarization, 72°, four reflections, 48 mV/sec.

0.977 mA cm^{-2} sec$^{1/2}$, is equal to $nFCD_{red}^{1/2}/\pi^{1/2}$ (see ref 2), from which we calculate $D_{red}^{1/2} = 1.43 \times 10^{-3}$ cm/sec$^{1/2}$.

Cyclic Voltammetry. Figure 6 shows the result of cyclic voltammetry. The potential axis is uncorrected for the effect of iR drop ($R \approx 10$ ohms) in the gold film. Because of this iR drop, the true potential sweep was not linear with time, the potentials shown are in varying error (proportional to the current) up to 75 mV, and the potential of the electrode is somewhat nonuniform and, therefore, not uniquely defined. However, as can be seen from the quantitatively satisfactory potentiometry and chronopotentiometry results, this nonuniformity of potential does not appear to have greatly affected the optical results.

Chronopotentiometry. The data shown in Figure 7 were obtained by optically monitoring the surface concentration of DM ferroin at 512 nm. The equations of the straight lines should be given by[32]

(30) Reference 27, p 30.
(31) F. Farha, Jr., and R. T. Iwamoto, *Anal. Chem.*, **38**, 143 (1966).
(32) P. Delahay, "New Instrumental Methods in Electrochemistry," Interscience Publishers, New York, N. Y., 1954, p 180.

$$\Delta A = \frac{\Delta A_{max} 2i}{CnFAD_{red}^{1/2}\pi^{1/2}} t^{1/2}$$

where ΔA_{max} is the ΔA at the transition time and $D_{red}^{1/2}$ was calculated from data obtained during a potential step. The slope of the line for $i = 5$ mA should be

$$\frac{(0.0138)(2)(5 \times 10^{-3}) \sec^{-1/2}}{(12.5 \times 10^{-6})(1)(9.65 \times 10^{4})(13.3)(1.43 \times 10^{-3})(1.77)} = 3.39 \times 10^{-3} \sec^{-1/2}$$

while similarly the slope of the line for $i = 7.5$ mA should be $5.08 \times 10^{-3} \sec^{-1/2}$. The experimentally determined slopes are 3.49×10^{-3} and 5.27×10^{-3} $\sec^{-1/2}$, respectively.

Transparent Solution. As is well known, one must use highly absorbing solutions in internal-reflection spectroscopy because of the small penetration depth of the radiation into the solution and the consequent small "effective thickness."[2,6] Therefore, it was surprising that colorless 0.1 M sodium sulfate solution gave a reflectance change as the potential of the gold electrode changed. This effect has also been seen with other transparent supporting electrolyte solutions. Figure 8 shows the results of cyclic voltammetry at 0.04-cps sweep rate with a simultaneous single-reflection measurement.

Figure 9 shows the absorbance change for one reflection during cyclic voltammetry from 0.34 to 0.94 V as a function of the angle of incidence and the plane of polarization. This potential range is approximately the same as was used with DM ferroin (it is inadvisable to go much above 0.94 V because of oxidation of the gold[33]). For perpendicular polarization just beyond

Figure 8. Cyclic voltammetry: 0.1 M Na$_2$SO$_4$, LM gold film, 5.8-cm^2 area, 480-nm wavelength, perpendicular polarization, 62°, one reflection, 48 mV/sec.
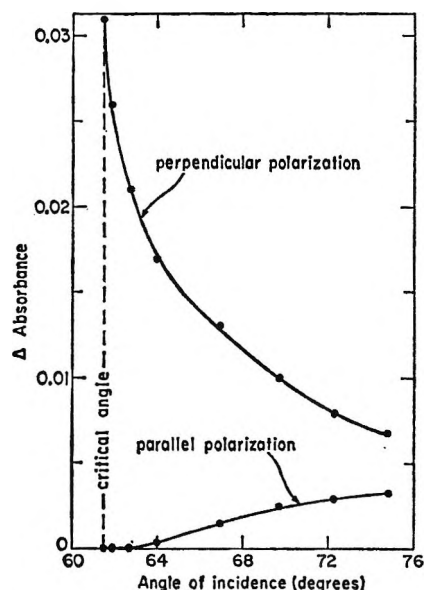
Figure 9. Peak-to-peak reflection absorbance change with angle during cyclic voltammetry: 0.1 M Na$_2$SO$_4$, LM gold film, 480-nm wavelength, one reflection, 0.04-cps triangular wave from 0.34 to 0.94 V, 48 mV/sec.

the critical angle, the absorbance change is quite large and could be further increased by increasing the potential sweep range. This effect is being investigated in several ways, but, as yet, no satisfactory explanation has been found. However, this effect is quite small (see Figure 2) for parallel polarization at 72° angle of incidence, which were the usual conditions for making measurements on absorbing aqueous solutions. Thus no corrections, or at most, only small corrections, are necessary for studies of this type.

Conclusions

In summary, thin-film gold electrodes are quite promising for optical observation of the electrode-electrolyte interfacial region and have important ad-

Figure 7. Chronopotentiometry: 12.5 mM DM ferroin solution, LM gold film, 13.3-cm^2 area, 512-nm wavelength, parallel polarization, 72°, four reflections.

(33) W. E. Reid and J. Kruger, *Nature*, **203**, 402 (1964).

vantages over previously reported materials for this purpose. These advantages include the suitability of gold as an electrode material, and, because of the absence of optical interference bands, recognizable transmission-like spectra can be obtained. These experimentally obtained spectra are consistent with spectra calculated from the applicable optical constants.

The Photoperoxidation of Unsaturated Organic Molecules. I. Relaxation

and Oxygen-Quenching Parameters of the Sensitizer Singlet State

by B. Stevens[1] and B. E. Algar

Department of Chemistry, Sheffield University, England   (*Received January 22, 1968*)

Fluorescence quantum yields, γ_F, lifetimes, τ_F, and oxygen-quenching rate constants, k_Q, are reported for a series of eight aromatic hydrocarbons in benzene at $25 \pm 2°$. The independence of k_Q on oxygen concentration is accepted as a criterion of stationary concentration gradients of the diffusing species over the period of observation, and the viscosity dependence of k_Q, reported previously (Ware), and the variation of k_Q with fluorescent solute in the same solvent are interpreted in terms of a nondiffusion-limited quenching process.

Introduction

The photosensitized addition of molecular oxygen to an unsaturated organic molecule in solution requires primary excitation of the lowest electronically excited singlet state of the sensitizer which is subject to radiative and nonradiative relaxation to the ground state with rate constants k_F and k_{IC}, intersystem crossing to the triplet state, k_{ISC}, and quenching by oxygen with bimolecular rate constant k_Q. These rate constants, which appear in photostationary expressions for the over-all quantum yield of photoperoxidation, are related to the experimentally accessible fluorescence quantum yield γ_F, the radiative relaxation constant $\tau_F{}^{-1}$, and the Stern–Volmer quenching constant K_Q of the sensitizer by the expressions

$$\gamma_F = k_F/(k_F + k_{IC} + k_{ISC}) \qquad (1)$$

$$\tau_F = 1/(k_F + k_{IC} + k_{ISC}) \qquad (2)$$

$$F_0/F = 1 + K_Q[Q] = 1 + k_Q\tau_F[Q] \qquad (3)$$

where F_0 and F denote relative fluorescence intensities in the absence and presence of dissolved oxygen at concentration [Q].

Rate constants k_Q measured for bimolecular quenching in solution have been interpreted in terms of a diffusional process at different levels of approximation. The development of the diffusional model based on con-

centration gradients[2] requires that the initial rapid quenching of those fluorescent molecules adjacent to a quenching site in a random solute distribution at $t = 0$ is characterized by a frequency kc_j and reduces the fluor concentration at this site from the average bulk concentration c_0 to c_ρ such that the reduced quenching frequency kc_ρ is equal to the molecular flux $\Phi(t)$ to the quenching site under the influence of the resulting concentration gradient. The solution of Fick's second diffusion law subject to the boundary conditions

$$c(r, 0) = c_0$$

$$c(\infty, t) = c_0$$

$$c(\rho, t) = c_\rho$$

where r denotes the distance from the quenching site and ρ is a quenching encounter diameter, yields an expression for c_ρ which is substituted in the flux equation

$$\Phi(t) = kc_\rho = k_Q(t)c_0$$

to obtain the following expression for a time-dependent

(1) Correspondence should be addressed to Professor Brian Stevens, Department of Chemistry, University of South Florida, Tampa, Fla. 33620.

(2) *Cf.* R. M. Noyes, *Progr. Reaction Kinetics*, 1, 129 (1961).

rate constant $k_Q(t)$ measured in terms of the bulk fluor concentration c_0

$$k_Q(t) = \frac{4\pi\rho DkN'}{k + 4\pi\rho D} \times$$

$$\left\{1 + \frac{k}{4\pi\rho D} \exp(x^2)\ \mathrm{erfc}(x)\right\}\ M^{-1}\ \sec^{-1} \quad (4)$$

where ρ is the sum of the fluor and the quencher encounter radii r_F and r_Q, D, the sum of the appropriate diffusion coefficients D_F and D_Q, characterizes the diffusional approach of fluor to a stationary quenching site, N' is the number of molecules per millimole, $x = [1 + (k/4\pi\rho D)]\sqrt{Dt}/\rho$, and $\exp(x^2)\ \mathrm{erfc}(x) = (1/x\sqrt{\pi})\cdot(1 - (1/2x^2) + (3/4x^4) - \ldots)$. The time t of measurement of $k_Q(t)$ is invariably of the order of $\tau_F > 5 \times 10^{-9}$ sec, which defines the rate of competing unimolecular relaxation; together with typical values of $D \sim 5 \times 10^{-5}\ cm^2\ sec^{-1}$ for the more fluid solvents this establishes the inequality

$$\sqrt{D\tau_F} \gtrsim 5 \times 10^{-7} > \rho \sim 5 \times 10^{-8}\ cm \quad (5)$$

and insofar as

$$k > 4\pi\rho D \quad (6)$$

higher terms in the expansion of $\exp(x^2)\ \mathrm{erfc}(x)$ may be neglected in the reduction of eq 4 to

$$k_Q(t) = \frac{4\pi\rho DkN'}{k + 4\pi\rho D} \times$$

$$\left\{1 + \frac{\rho k}{(k + 4\pi\rho D)\sqrt{\pi Dt}}\right\}\ M^{-1}\ \sec^{-1} \quad (7)$$

The time-dependent term in eq 7 is significant over the interval required to establish a stationary concentration gradient of the diffusing species, during which the fluorescence decay is nonexponential according to

$$F(t) = F(0)\exp(-(t/\tau_F) - tk_Q(t)[Q]) \quad (8)$$

and the Stern–Volmer quenching constant exhibits a dependence on quencher concentration [Q] expressed as[3a]

$$K_Q = [(F_0/F) - 1]/[Q] =$$

$$[k_Q\tau_F + (W/[Q])](1 - W)^{-1} \quad (9)$$

where $W = w\pi^{1/2}\exp(w^2)\ \mathrm{erfc}(w)$, $w = \{k_Q[Q]\rho k/(k + 4\pi\rho D)\}\{\tau_F/(1 + k_Q\tau_F[Q])\pi D\}^{1/2}$, and $k_Q = k_Q(t \to \infty) = 4\pi\rho DN'k/(k + 4\pi\rho D)$. Ware and coworkers[3a,b] have used eq 8 and 9 to describe the quenching of anthracene by carbon tetrabromide[4] and of perylene by N,N-dimethylaniline in solvents of low dielectric constant.

Further reductions of eq 7 are based on the following assumptions.

(a) The stationary concentration gradient is rapidly established compared with the time of measurement, i.e.

$$\rho \ll (\pi D\tau_F)^{1/2} \quad (10)$$

This condition removes the time dependence of k_Q, which is expressed by

$$k_Q = 4\pi\rho DkN'/(k + 4\pi\rho D)\ M^{-1}\ \sec^{-1} \quad (11)$$

The exponential fluorescence decay is restored and the quenching constant becomes independent of quencher concentration.

(b) The rate of quenching during an encounter vastly exceeds the encounter rate, i.e.

$$k \gg 4\pi\rho D \quad (12)$$

which leads to the time-dependent and time-independent expressions

$$k_Q(t) = 4\pi\rho DN'[1 + (\rho/\sqrt{\pi D\tau_F})] \quad (13a)$$

$$k_Q = 4\pi\rho DN' \quad (13b)$$

(c) The diffusion coefficient D_i of species i is given by the Stokes–Einstein equation

$$D_i = \frac{kT}{6\pi\eta\sigma_i}\left[\frac{1 + (3\eta/\beta\sigma_i)}{1 + (2\eta/\beta\sigma_i)}\right] \quad (14)$$

which is valid for diffusing spheres of radius σ_i and the coefficient of sliding friction β in a continuous medium of low or moderate viscosity η.[5] If the radii σ_F and σ_Q are approximately equal and identical with the encounter radii r_F and r_Q, eq 8b reduces to the limiting forms

$$k_Q(\eta \gg \beta\sigma) = 8RT/2000\eta \quad (15a)$$

$$k_Q(\eta \ll \beta\sigma) = 8RT/3000\eta \quad (15b)$$

for a diffusion-controlled process with and without "slipping," respectively.

Rate constants computed from eq 15 are in good agreement with those observed for singlet–singlet energy transfer from aromatic hydrocarbon donors to a biacetyl acceptor[6-8] and for triplet–triplet transfer between aromatic molecules with large energy separation of donor and acceptor triplet states.[9-11] In both types of system the low acceptor transition moment limits the long-range resonance transfer,[12] and the diffusion-limited rate constant is given by eq 15a.

(3) (a) W. R. Ware and J. S. Novros, J. Phys. Chem., 70, 3246 (1966); (b) W. R. Ware and H. P. Richter, 153rd National Meeting of the American Chemical Society, Miami Beach, Fla., April 1967.

(4) E. J. Bowen and W. S. Metcalf, Proc. Roy. Soc., A206, 437 (1951).

(5) Cf. A. D. Osborne and G. Porter, ibid., A284, 9 (1965).

(6) J. T. Dubois and B. Stevens, "Luminescence of Organic and Inorganic Materials," Kallmann and Spruch, Ed., John Wiley and Sons, Inc., New York, N. Y., p 115.

(7) J. T. Dubois and M. Cox, J. Chem. Phys., 38, 2536 (1963).

(8) J. T. Dubois and R. L. Van Hamert, ibid., 40, 923 (1964).

(9) G. Porter and F. Wilkinson, Proc. Roy. Soc., A264, 1 (1961).

(10) B. Stevens and M. S. Walker, Proc. Chem. Soc., 26 (1964).

(11) K. Sandros, Acta Chem. Scand., 18, 2355 (1964).

(12) Th. Forster, Ann. Physik, 2, 55 (1948); Discussions Faraday Soc., 27, 7 (1959).
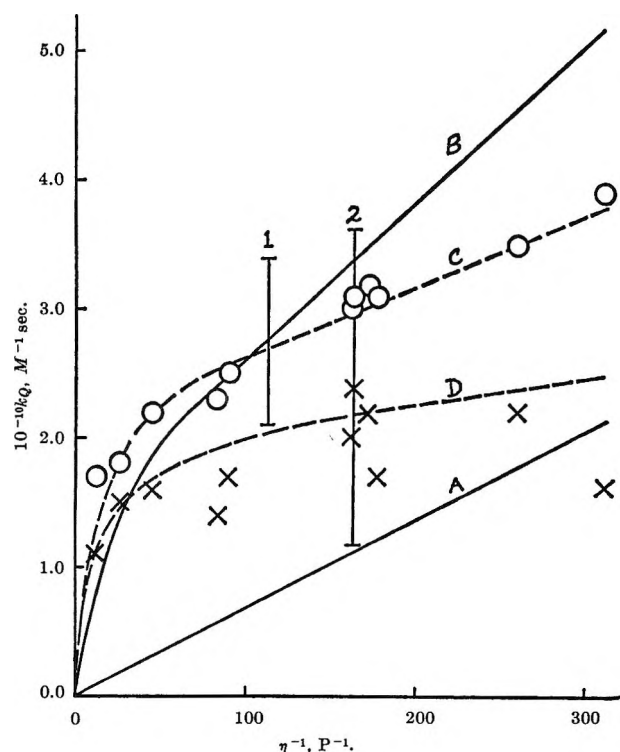
Figure 1. Summary of oxygen-quenching data: O, experimental points[14] for anthracene; X, experimental points[14] for 9,10-dichloroanthracene; curves A and B, drawn in accordance with reduced expressions 15b and 13b (with ρ = 6 Å and reported values for D); curves C and D, drawn from eq 11 (with ρ = 11 Å and vaues of k quoted in text) for anthracene and 9,10-dichloroanthracene, respectively. Vertical lines cover the range of k_Q values measured by Berlman[16] for cyclohexane solutions (1) and data reported in Table I for solutions in benzene (2).

On the other hand, the oxygen quenching of excited singlet states is characterized by rate constants which exceed[13] those computed from eq 15b by a viscosity-dependent factor of from ~2 to ~4,[14,15] as shown in Figure 1. Ware has shown[14] that the Stokes–Einstein eq 14 seriously underestimates the diffusion coefficient of the much smaller O_2 molecule and that the use of eq 13a and b with directly measured diffusion coefficients and realistic encounter radii leads to improved agreement with experimental data obtained for certain aromatic hydrocarbons in solvents of varying viscosity. As shown in Figure 1, eq 13a and b are less satisfactory at lower viscosities and, in the case of 9,10-dichloroanthracene, fail to account quantitatively for the quenching constants observed over most of the viscosity range examined.

Insofar as D_F and r_F are mutually compensating solute parameters, the ratio of fluorescence intensities, F_0/F, measured at a constant oxygen concentration for different solutes in the same solvent should be a linear function of solute lifetime, r_F (eq 3). This is confirmed by the extensive data reported by Berlman,[16] although the variation in k_Q computed from these (cf. Figure 1)

exceeds that attributable to variations in the diffusion coefficient D_F of the solute (see the Discussion below).

It is concluded that the dependence of oxygen-quenching constants on both solvent viscosity and unspecified solute parameters can be measured directly with greater reliability than that afforded by the approximate eq 13 and 15. The partial failure of eq 15 may result from the invalidity of condition 12 for those fluorescent molecules which are not immediately quenched on encountering a quenching site or from a time dependence of k_Q, which should be manifest experimentally as either a nonexponential fluorescence decay in the presence of oxygen or an oxygen concentration dependence of the measured Stern–Volmer constant. An examination of the latter alternative requires that decay curves be recorded directly by the pulsed-flash technique and that oxygen-quenching data be measured at more than one concentration of dissolved oxygen. These measurements, together with those of the fluorescence parameters γ_F and r_F, are reported and discussed below for a series of aromatic hydrocarbons used in the photoperoxidation studies.[17]

Experimental Section

Materials. Rubrene and 9,10-dimethylanthracene, from L. Light and Co., and naphthacene, donated by Dr. E. J. Bowen, were fractionally sublimed in a current of dry nitrogen as described by Melhuish;[18] 9,10-diphenylanthracene, L. Light and Co., was twice recrystallized from BDH spectroscopic grade ethanol; perylene, L. Light and Co., and anthanthrene, donated by Dr. E. Clar, were chromatographed on activated
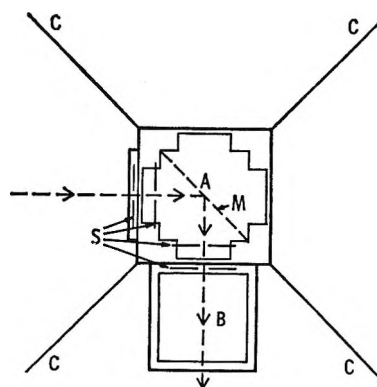
Figure 2. Plan of the modified cell compartment of the Aminco-Keirs spectrophotofluorimeter: A and B, alternative cell positions; M, plane mirror; S, slits; C, light baffles.

(13) E. J. Bowen, *Trans. Faraday Soc.*, **50**, 97 (1954).

(14) W. R. Ware, *J. Phys. Chem.*, **66**, 455 (1962).

(15) B. Stevens and J. T. Dubois, *Trans. Faraday Soc.*, **59**, 2813 (1963).

(16) I. B. Berlman, "Handbook of Fluorescence Spectra of Aromatic Molecules," Academic Press Inc., New York, N. Y., 1965.

(17) B. Stevens and B. E. Algar, to be submitted for publication.

(18) W. H. Melhuish, *Nature*, **183**, 1933 (1959).

Table I: Fluorescence and Oxygen-Quenching Data for Aromatic Hydrocarbons in Benzene at $25 \pm 2°$

	Concn, M	γ_F	τ_F, nsec	K_{O_2}, M^{-1}	$10^{-10}k_{O_2}$ $(=k_Q)$, M^{-1} sec^{-1}	$10^{-10}k$, M^{-1} sec^{-1}
9,10-Dimethylanthracene	1×10^{-5}	0.90 ± 0.04	13.9 ± 0.5 $(11)^a$	440 ± 20	3.15 ± 0.20	6.0
9,10-Diphenylanthracene	2×10^{-5}	0.91 ± 0.05 $(0.84)^b$	6.8 ± 0.4 $(8.2,^c$ $7.3^d)$	250 ± 15 $(210)^b$	3.62 ± 0.25 $(2.8)^c$	8.0
9,10-Dimethyl-1,2-benzanthracene	2×10^{-5}	0.36 ± 0.03	24.4 ± 1.0 $(26.5)^e$	670 ± 40	2.76 ± 0.16	4.7
Naphthacene	2×10^{-5}	0.19 ± 0.02 $(0.21)^f$	5.2 ± 0.2 $(5.5)^g$	120 ± 15 $(159)^h$	2.38 ± 0.18	3.8
Rubrene	1.5×10^{-5}	0.98 ± 0.02 $(1)^h$	16.4 ± 0.4 $(16.4,^i$ $15.4^j)$	194 ± 10 $(308)^h$	1.18 ± 0.08	1.5
Perylene	8×10^{-6}	0.89 ± 0.05 $(0.89)^b$	5.6 ± 0.4 $(4.9,^d$ $5.2^c)$	150 ± 10 $(210,^b$ $176^k)$	2.71 ± 0.30 $(3.2)^c$	4.6
Anthanthrene	5×10^{-6}	0.73 ± 0.05	3.8 ± 0.6	135 ± 10	3.55 ± 0.60	7.9
Decacyclene	1×10^{-5}	0.30 ± 0.04	31.9 ± 1.5	540 ± 25	1.69 ± 0.10	2.3

[a] A. S. Cherkasov, V. A. Molchanov, T. M. Vember, and K. G. Voldaikina, *Soviet Phys. Dokl.,* **1,** 427 (1956). [b] Melhuish.[19] [c] Ware.[14] [d] J. B. Birks and D. J. Dyson, *Proc. Roy. Soc.,* **A275,** 135 (1963). [e] J. B. Birks, D. J. Dyson, and T. A. King, *ibid.,* **A277,** 270 (1964). [f] I. B. Berlman.[16] [g] D. J. Dyson, Ph.D. Thesis, Manchester, 1963. [h] E. J. Bowen and A. H. Williams, *Trans. Faraday Soc.,* **35,** 765 (1939). [i] L. Brewer, C. G. James, R. G. Brewer, F. E. Stafford, R. A. Berg, and G. M. Rosenblatt, *Rev. Sci. Instrum.,* **33,** 450 (1962). [j] W. R. Ware, *J. Amer. Chem. Soc.,* **83,** 4374 (1961). [k] Bowen.[13]

alumina in the dark using a benzene–ligroin eluent. Hopkins and Williams benzene (Analar grade) was used as solvent for all measurements, and nitrogen and oxygen were supplied by the British Oxygen Co.

Fluorescence Quantum Yields. Fluorescence quantum yields of the compounds examined at the stated concentrations (Table I) were measured relative to that of a standard solution (quinine bisulfate in 0.1 M sulfuric acid) of the same optical density; the procedure adopted is described with reference to Figure 2 which illustrates the cell compartment of the Aminco-Keirs spectrophotofluorimeter modified to accommodate a nonfluorescent $1 \times 1 \times 5$ cm quartz cell in either of the positions A or B. Cells of the sample solution and of quinine bisulfate were placed in turn in the holder B with a precision-ground plane mirror in cell holder A as shown, and the transmission of the excitation beam by each solution was recorded as a function of emission monochromator wavelength setting; the optical densities of sample and standard solutions were equalized in the region of 0.3 by changes in excitation frequency and solute concentration, both solutions were diluted by a factor of 20, and the fluorescence signal from each solution in turn was recorded without change in excitation wavelength with the cell in position A. The fluorescence recordings were corrected for the wavelength sensitivity of the emission monochromator-detector assembly, integrated planimetrically, and compensated for oxygen quenching of the air-saturated sample solution and for the difference in refractive index of both solvents, to obtain the fluorescence

quantum yield of the sample solution relative to that of 0.546 reported for the quinine bisulfate standard.[19]

Fluorescence Decay Constants. Fluorescence decay constants τ_F^{-1} were computed from decay curves traced on an X–Y recorder (Advance Model HR-95) coupled to the pulse-sampling oscilloscope (Hewlett-Packard Model 185B) of a pulsed-flash fluorimeter similar to that described previously.[20] The source, an electric discharge in air at atmospheric pressure between tungsten-ball and platinum-whisker electrodes, was operated at a frequency of 1500 cps; this generates radiation pulses of 5-nsec half-intensity width and 2-nsec decay time originating from the $N_2(C^3\pi_u \rightarrow B^3\pi_g)$ fluorescence at 300–420 mμ. Complimentary filters were used to isolate the solute fluorescence intercepted by the detector at an angle of 90° to the excitation pulse.

Oxygen-Quenching Constants. Oxygen-quenching constants are estimated from fluorescence recordings for sample solutions equilibrated with N_2–O_2 gas mixtures of different composition at atmospheric pressure; these gases were fed separately through flowmeters, calibrated in the range 4–50 cm³ min^{-1}, into a mixing chamber and solvent presaturator with blow off to regulate the total gas flow, and introduced into the solution by a capillary tube through the stopcock of an 0.8 cm in diameter, cylindrical Pyrex cell; after a flow period of 1 hr the capillary was withdrawn and the stopcock was closed

(19) W. H. Melhuish, *J. Phys. Chem.,* **65,** 229 (1961).

(20) R. Bennett, *Rev. Sci. Instrum.,* **31,** 1275 (1960).
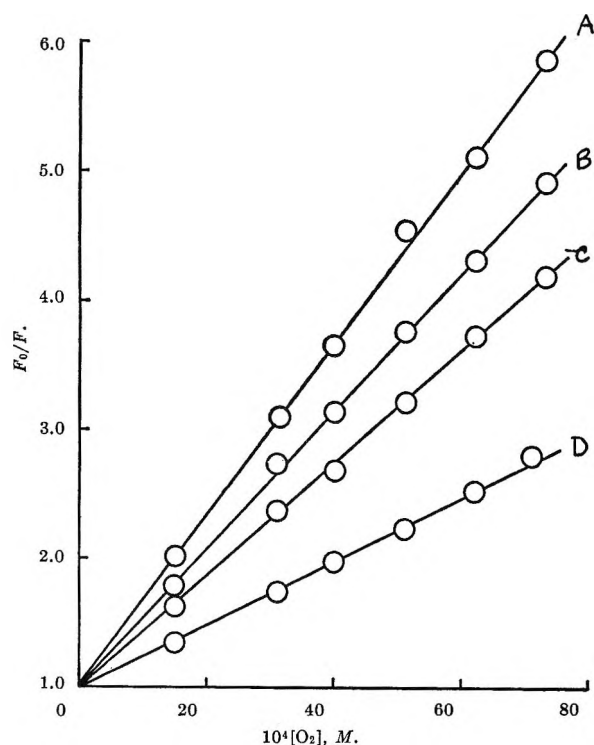
Figure 3. Plot of experimental oxygen-quenching data (eq 3) for the following in benzene at 25 ± 2°: A, 9,10-dimethyl-1,2-benzanthracene; B, decacylene; C, 9,10-dimethylanthracene; D, 9,10-diphenylanthracene.
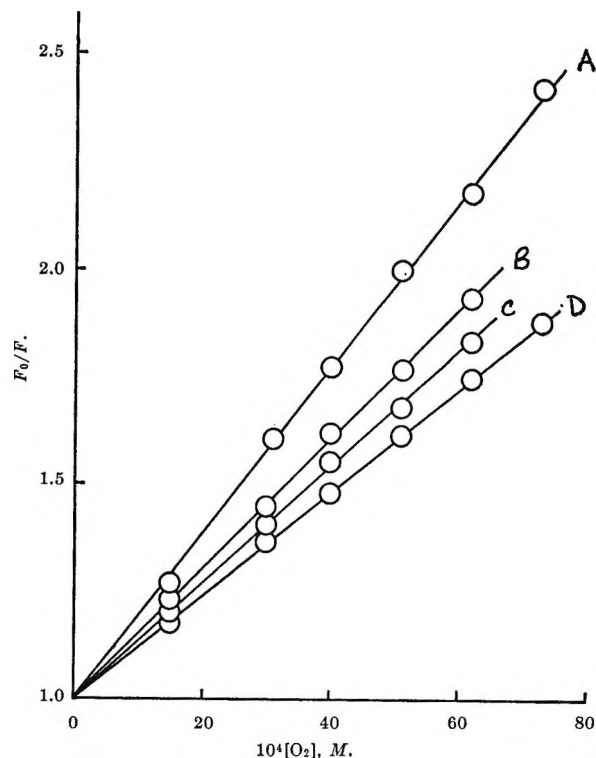
Figure 4. Plot of experimental oxygen-quenching data (eq 3) for the following in benzene at 25 ± 2°: A, rubrene; B, perylene; C, anthanthrene; D, naphthacene.

to seal the cell prior to its insertion in a machined cell holder in the spectrophotofluorimeter cell compartment. A series of preliminary measurements confirmed that the fluorescence intensity assumed a constant value well within the flow period used and varied by less than 2% with the position of the cell in the cell holder.

Concentrations of dissolved oxygen in the benzene solutions were estimated from the relative flow-rates of oxygen and nitrogen in the gas stream and from the oxygen solubilities reported for this solvent.[21]

Results

The oxygen-quenching data are plotted in accordance with the Stern–Volmer equation (eq 3) in Figure 3; quenching and rate constants K_Q and k_Q are listed in Table I together with values obtained for the fluorescence quantum yields, γ_F, and lifetimes, τ_F, of the eight compounds studied. All data refer to solutions of the same low concentrations in benzene at 25 ± 2°.

Fluorescence decay curves recorded for nitrogen- and oxygen-saturated solutions proved to be exponential to within 2% over a period of at least 3 half-lives, although at short time intervals after the flash, where time-dependent effects should be most pronounced in the presence of dissolved oxygen, the fluorescence decay profile is distorted by the time dependence of the excitation pulse. This distortion is responsible for an increase in the percentage limits of error in τ_F below 5 nsec.

Discussion

The threefold variation in experimental values of k_Q, listed in Table I, for different fluorescent solutes in the same solvent further illustrates the inadequacy of eq 15 when applied to the oxygen-quenching process (cf. Figure 1). Equations 13a and b accommodate variations in k_Q with the diffusion coefficient, the lifetime, and the encounter radius of the solute, and the maximum values measured for k_Q are consistent with those computed from eq 13b with measured values[5,14] of $D_F = 2.2 \times 10^{-5}$ cm² sec⁻¹ (for anthracene) and $D_Q = 5.7 \times 10^{-5}$ cm² sec⁻¹ and an encounter diameter of 6 Å. However, insofar as the diffusion coefficient of molecular oxygen exceeds that of the aromatic hydrocarbon by a factor of 2.6 in this solvent, the maximum reduction in k_Q due to a reduction in solute diffusion coefficient ($D_F \rightarrow 0$) is less than 30%, and the transient term $1 + (\rho/\sqrt{\pi D \tau_F})$ does not exceed 1.1 for the values of ρ and D quoted and the shortest lifetime measured ($\tau_F = 3.8$ nsec for anthanthrene). Moreover the lack of correlation between k_Q and the solute size or the lifetime (Table I) confirms the relative unimportance of these parameters in accounting for differences in measured rate constants, k_Q, for the various solutes.

In reverting to lower approximations of eq 7 the assumptions 10 and 12 must be examined. Although

(21) P. Schläpfer, T. Audykowski, and A. Bukowieki, Schweiz. Arch. Angew. Wiss. Tech., 15, 299 (1949).

the possibility of a nonexponential contribution to the fluorescence decay curves obtained in the presence of dissolved oxygen is not eliminated at short postflash intervals, the linearity of the Stern–Volmer plots up to the highest concentrations of oxygen used (Figures 3 and 4) confirms the validity of condition 10 over this concentration range which corresponds to a reduction in τ_F to ~3 nsec in most cases. It is concluded that a stationary concentration gradient is established within this time interval in this solvent and that the solute dependence of k_Q must be sought in terms of eq 11 for a nondiffusion-limited process.

A plot of previously published data[14] according to eq 11 in its reciprocal form

$$1/k_Q = (1/k) + (1/4\pi D\rho) \quad (11)$$

confirms the linear variation of $1/k_Q$ with D^{-1} and provides the approximate values

$$k \sim 6 \times 10^{10}\ M^{-1}\ \text{sec}^{-1} \quad \text{(anthracene)}$$

$$k \sim 3 \times 10^{10}\ M^{-1}\ \text{sec}^{-1} \quad \text{(9,10-dichloroanthracene)}$$

$$k \sim 5 \times 10^{10}\ M^{-1}\ \text{sec}^{-1} \quad \text{(9,10-diphenylanthracene)}$$

$$k \sim 7 \times 10^{10}\ M^{-1}\ \text{sec}^{-1} \quad \text{(perylene)}$$

with $\rho \approx 11$ Å in each case. The broken curves drawn in Figure 1 for anthracene and 9,10-dichloroanthracene according to eq 11 with values of k and ρ cited closely reproduce the observed trend in k_Q over the whole viscosity range, while the k value for anthracene is of the same magnitude as k_Q ($= 1.75 \times 10^{11}\ M^{-1}\ \text{sec}^{-1}$) measured[22] for the same system in the gas phase at 300°. It is further noted that with $k \sim 4\pi\rho D$ the condition

$$[1 + (k/4\pi\rho D)]\sqrt{Dt}/\rho \gg 1$$

necessary for the reduction of eq 4 to 7 remains valid when condition 10 is established from linear Stern–Volmer behavior.

The interpretation of the viscosity dependence of k_Q in terms of eq 11 affords a ready explanation of the variation in k_Q with fluorescent solute in the same solvent. Table I lists the values of k, computed from k_2 using eq 11 with an encounter diameter of 11 Å, which, insofar as oxygen quenching of the sensitizer S does not

lead to electronic excitation of the oxygen molecule,[23] describes the rate of collision-induced intersystem crossing represented by

$$^1S^* + {}^3O_2 \longrightarrow {}^3S^* + {}^3O_2 \quad (16)$$
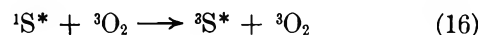
The absence of any direct correlation between k and the unimolecular intersystem crossing constant k_{ISC} given by

$$(k_{ISC})_{k_{IC}=0} = (1 - \gamma_F)/\tau_F$$

may reflect the sensitivity of the collision-induced process to the position of the charge-transfer state $^3CT(S^+O_2^-)$ relative to those of the initial $^3\Gamma(^1S^*,\ O_2,\ ^3\Sigma\mu^-)$ and final $^3\Gamma(^3S_n^*,\ O_2,\ ^3\Sigma\mu^-)$ states of the sensitizer-oxygen complex,[24] which must await identification of higher triplet states $^3S_n^*$ of the sensitizer.

The encounter diameter of 11 Å, which is necessary to account quantitatively for the viscosity dependence of k_Q in terms of eq 11, exceeds the expectation value for an aromatic hydrocarbon and oxygen in solution. In view of the nature of the quenching process 16, it may be argued that no oxygen concentration gradient is established, that the use of the combined coefficient to describe the diffusion of a fluorescent molecule to a stationary quenching site is of questionable validity, and that the migration of quenching sites through the solvent is better described by the theory of random flights.[1]

(22) W. R. Ware and P. T. Cunningham, *J. Chem. Phys.*, **43**, 3826 (1965).

(23) B. Stevens and B. E. Algar, *Chem. Phys. Lett.*, **1**, 58, 219 (1967).

(24) H. Tsubomura and R. S. Mulliken, *J. Amer. Chem. Soc.*, **82**, 5966 (1960).

Potassium Chloride Conductance in Aqueous Solution of a

Structure-Forming Nonionic Solute, Hexamethylenetetramine[1]

by G. Barone, V. Crescenzi, and V. Vitagliano

Laboratorio di Chimica Fisica, Istituto Chimico, Università di Napoli, Naples, Italy   (*Received January 23, 1968*)

Conductance data of KCl in aqueous solutions of hexamethylenetetramine and data on the "structural temperature" of hexamethylenetetramine aqueous solutions, evaluated by a spectroscopic technique, are reported. It is proposed that the observed reduction of the KCl limiting equivalent conductivity in the hexamine solutions be accounted for in terms both of a different structure of the water in these solutions with respect to pure water and of an obstruction effect of the hexamine molecules.

In previous papers from this laboratory, it was shown that equilibrium and transport properties of hexamethylenetetramine (HMT) aqueous solutions may be explained in terms of marked solute–solvent interaction.[2-4] As a result of these studies, it was concluded that HMT is a distinct structure-forming solute in water. Furthermore, it was thought worthwhile to investigate how the limiting equivalent conductivity of a simple electrolyte is altered in HMT solutions with respect to the limiting equivalent conductance in pure water. Such a study might, in fact, be of interest in connection with studies on the mechanism whereby nonpolar solutes which are heavily solvated and which also markedly increase the viscosity of water (such as HMT) modify ionic motion.

Studies of electrolytic conductance in aqueous solutions of a number of nonionic compounds have shown that limiting equivalent conductivities, Λ_0, of common electrolytes are higher than predictable from the macroscopic viscosity of the solutions.[5] An approach in which the ions are considered as electrical carriers of negligible dimensions moving through a medium containing obstructions—the nonelectrolyte molecules (depicted as insulating spheres)—leads conversely to estimated values which are too high, as compared to experimental data.[6] Comparison of HCl conductance data in aqueous sucrose solutions at 25° with those in water for different temperatures also suggested that correlation of conductance data in terms of a "structural temperature" of water would not be feasible.[7]

Our data on the limiting equivalent conductivity of KCl in HMT aqueous solutions reveal a pattern similar to that found with other nonelectrolyte solutions, in the sense that neither of the above-mentioned approaches appears to correlate satisfactorily with the observed reduction of KCl conductance. It is suggested, however, that in the case of HMT solutions, the reductions in the KCl limiting conductivity may be related to the structural temperature of the solutions, as evaluated by the spectroscopic procedure of Worley

and Klotz,[8] once the obstruction effect of the hexamine molecules is also taken into account.

Experimental Section

Hexamethylenetetramine, a Merck product, was recrystallized from ethanol and vacuum dried. KCl was a C. Erba (Milan, Italy) reagent grade product. D_2O was a Fluka (Buchs, Switzerland) product, 99.7% D_2O. HMT solutions were always prepared immediately before use in order to minimize hydrolysis of the hexamine. The conductance of HMT solutions was close to that of the redistilled water used to prepare them. It was found, however, that if cells with platinized electrodes were employed, the conductance of the HMT solutions slowly increased with time. This effect was not observed with cells having bright platinum electrodes, which, therefore, had to be employed in all measurements with KCl. For these measurements, a concentrated KCl aqueous solution (0.5 N) was added in small amounts, with a microsyringe, directly into the conductance cell containing *ca.* 60 ml of HMT solution. Resistance readings were taken after each KCl addition, after thorough mixing of the solution and temperature equilibration. Dilution of the HMT solutions with increasing KCl concentration (from about 5×10^{-4} to 10^{-2} equiv/l.) was neglected.

(1) This research has been carried out with the financial support of the Italian Consiglio Nazionale delle Ricerche (Contract No. 115.1385.0495).

(2) V. Crescenzi, F. Quadrifoglio, and V. Vitagliano, *J. Phys. Chem.*, **71**, 2313 (1967).

(3) L. Costantino, V. Crescenzi, and V. Vitagliano, *ibid.*, **72**, 149 (1968).

(4) V. Crescenzi, F. Quadrifoglio, and V. Vitagliano, *Ric. Sci.*, **37**, 529 (1967).

(5) R. H. Stokes and R. Mills, "Viscosity of Electrolytes and Related Substances," Pergamon Press Ltd., Oxford, 1965.

(6) B. J. Steel, S. M. Stokes, and R. H. Stokes, *J. Phys. Chem.*, **62**, 1514 (1958).

(7) R. A. Robinson and R. H. Stokes, "Electrolyte Solutions," Butterworth and Co. Ltd., London, 1959, p 307.

(8) J. D. Worley and I. M. Klotz, *J. Chem. Phys.*, **45**, 2868 (1966).

Table I: Experimental Values of KCl Equivalent Conductivity in Aqueous Hexamethylenetetramine Solutions ($t = 24.93°$)[a]

Molarity of HMT, M							
0.5		1.0		1.5		2.0	
$10^2\sqrt{c}$	Λ	$10^2\sqrt{c}$	Λ	$10^2\sqrt{c}$	Λ	$10^2\sqrt{c}$	Λ
4.401	127.12	1.847	107.38	1.776	88.08	3.781	68.81
5.822	125.81	2.768	106.39	2.812	87.11	3.941	69.02
7.154	124.58	3.327	106.05	3.443	86.97	5.270	68.85
7.916	123.86	4.018	105.39	3.972	86.78	5.276	68.32
8.602	123.16	4.696	104.90	4.439	86.36	5.848	68.65
9.397	122.70	5.347	104.65	4.857	86.35	6.433	68.02
		6.234	104.55	5.314	86.16		
		7.434	104.01	5.870	85.83		
		8.551	102.74				
		9.462	102.29				
		10.31	101.95				
		11.49	101.36				
Λ^{0b}	131.08 ± 0.079		108.05 ± 0.24		88.77 ± 0.13		70.01 ± 0.22

[a] Corrected for the conductivity of the solvent. [b] Λ^0 is the limiting equivalent conductivity obtained by least squares from the experimental Λ values. The Λ^0 has been divided by 1.022 to obtain the Λ^0_{HMT} given in Table III.

Conductances were measured at two temperatures (24.93 and 33.46°) with a Leeds and Northrup Jones bridge using two Leeds and Northrup cells with constants 10 and 1 cm^{-1}. All runs were taken in a Townson and Mercer thermostatic bath ($\pm 0.01°$).

The limiting equivalent conductivity of KCl in aqueous solution was measured using both black platinum electrodes and bright platinum electrodes. The $\Lambda^0_{H_2O}$ measured with black platinum electrodes was in agreement with the literature data within 2 ppt (see ref 7, Appendices 6.1 and 6.2, pp 463–465). The data obtained with bright platinum electrodes were

$$\Lambda^0_{br\ Pt} = 1.022\Lambda^0_{H_2O} \quad (24.93°)$$

$$\Lambda^0_{br\ Pt} = 1.007\Lambda^0_{H_2O} \quad (33.46°)$$

where $\Lambda^0_{H_2O}$ is the literature value.

The KCl limiting conductivity values in HMT–water mixtures have been obtained by a least-squares extrapolation of experimental data (corrected for the conductivity of the solvent, plotted as a function of $\sqrt{c}$. (See Table I and II.) The limiting conductivities have been divided by the correction factor 1.022 at 24.93° and 1.007 at 33.46°; the corrected data are given in Table III.

Near-infrared spectra of 5% H_2O in D_2O against pure D_2O have been taken as a function of temperature, by using the technique of Worley and Klotz.[8] For the measurements with HMT, the same amounts of HMT were put in the dilute H_2O solution and in the D_2O reference solution, and the spectra were recorded from 1350 to 1700 mμ. A Beckman DK-2 spectrophotometer, equipped with a circulating-water thermostat, was used. Structural temperatures of water in the presence of HMT were evaluated according to Worley and Klotz, who proposed that equal structural temperatures for different solutions correspond to equal

Table II: Experimental Values of KCl Equivalent Conductivity in Aqueous Hexamethylenetetramine Solutions ($t = 33.46°$)[a]

Molarity of HMT, M			
0.5		1.0	
$10^2\sqrt{c}$	Λ	$10^2\sqrt{c}$	Λ
2.326	150.96	1.833	128.35
2.978	150.34	2.902	127.33
3.021	150.26	3.670	126.50
3.712	149.93	4.494	125.99
3.707	149.78	5.475	125.46
4.205	149.38	6.040	124.99
4.351	149.08	6.654	124.44
4.641	148.93		
4.908	148.73		
5.464	147.97		
5.676	147.76		
6.002	147.43		
6.688	147.15		
Λ^{0b}	153.16 ± 0.12		129.59 ± 0.13

[a] Corrected for the conductivity of the solvent. [b] The Λ^0 values have been divided by 1.007 to obtain the Λ^0_{HMT} given in Table III.

values of the ratio of the optical density of HDO solutions at 1556 mμ to that at 1416 mμ.

Results and Discussion

Application of Worley and Klotz's[8] analysis to our near-infrared data for HMT aqueous solutions leads to the water structural-temperature values which are reported in Figure 1 as a function of HMT concentration. These data strongly suggest that HMT acts as a structure-maker solute in water, in agreement with earlier indications. Our conductivity data also indicate that the limiting equivalent conductance of KCl in HMT, Λ^0_{HMT}, is markedly reduced with respect to

Table III

	Molarity of HMT, M					
	0.5		1.0		1.5	2.0
	Molality of HMT, m					
	0.53		1.13		1.80	2.57
	Temp, °C					
	24.93	33.46	24.93	33.46	24.93	24.93
$\Lambda^0_{HMT}{}^a$	128.3	152.1	105.7	128.7	86.9	68.5
$R_{KCl}{}^b$	0.857	0.866	0.706	0.733	0.594	0.457
$\eta_0/\eta_{HMT}{}^c$	0.819	0.823	0.658	0.667	0.517	0.397
$t^{*,d,g}$ °C	17.5	25.7	9.3	17.7	2.9	~-5.3
$(\Lambda^0_{H_2O})_0{}^e$	132.9	157.6	114.2	139.1	101.2	83.1
$t,^f$ °C	19.2	27.6	12.4	21.3	7.6	0.6
$t_{ir},^{g,h}$ °C	19.4	27.4	13.5	20.6	7.1	0.1

[a] Limiting equivalent conductance of KCl in HMT aqueous solutions. [b] Limiting equivalent conductivity ratio: $R_{KCl} = \Lambda^0_{HMT}/\Lambda^0_{H_2O}$. [c] Relative fluidity of HMT aqueous solutions, taken from ref 2 and 3. [d] Temperature of water for which $(\Lambda^0_{H_2O})_t{}^* = \Lambda^0_{HMT}$. (See text.) [e] Values derived from eq 2, with a molar volume of 130 cm^3/mol for HMT. [f] Temperature of water at which $\Lambda^0_{H_2O} = (\Lambda^0_{H_2O})_0$ for KCl (eq 2, see text). [g] The values of t^* and t were calculated from eq i and ii in the text. [h] Structural temperature of HMT aqueous solutions (see Figure 1) obtained from spectroscopic data.
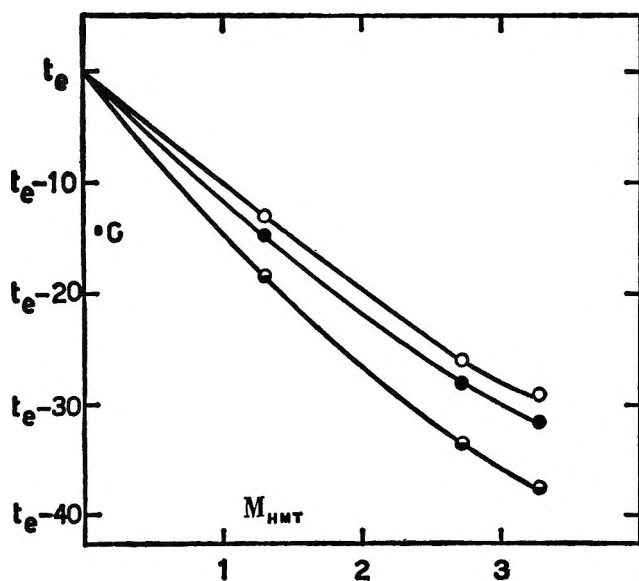
Figure 1. Structural temperature of HMT aqueous solutions, as measured from near-ir spectra[8] as a function of the HMT molality: O, $t_e = 25°$; ●, $t_e = 33.46°$; ◐, $t_e = 50°$.

that in pure water, $\Lambda^0_{H_2O}$ (see Table III). However the value of the ratio $R_{KCl} = \Lambda^0_{HMT}/\Lambda^0_{H_2O}$ is in all cases higher than the relative fluidity of the solutions. In our opinion a possible explanation of these data may be advanced as follows. Since HMT increases the degree of local order in water, ions will move in HMT aqueous solutions at a temperature t in a medium having a structure corresponding to that of pure water at a lower temperature t^*. The value of t^* should thus correspond to the structural temperature of HMT aqueous solutions. If this assumption were taken literally and if no other complicating effects were present, the temperature t^* would be that for which

$$(\Lambda^0_{H_2O})_t{}^* = (\Lambda^0_{HMT})_t \quad (1)$$

(or $R_{KCl} = 1$). From the known dependence of $\Lambda^0_{H_2O}$ for KCl on temperature, values of t^* were derived for each HMT concentration considered. [Limiting equivalent conductivity of KCl aqueous solutions and related temperatures (taken from ref 7, Appendix 6.2, p 454) have been fitted by a least-squares method to give the equations (i) $\Lambda^0_{H_2O} = 81.66 + 2.480t + 0.01087t^2 - (3.153 \times 10^{-5})t^3$ (standard deviation, ± 0.12) and (ii) $t = -36.74 + 0.5078\Lambda^0_{H_2O} - (7.861 \times 10^{-4}).(\Lambda^0_{H_2O})^2 + (9.728 \times 10^{-7})(\Lambda^0_{H_2O})^3$ (standard deviation, ± 0.05) for $0° \geq t \geq 55°$]. These values (reported in Table III) are systematically lower than those evaluated from spectroscopic data (Figure 1). Neglect of the effect of obstruction that the relatively large, nearly spherical HMT molecules may cause to the motion of ions is a possible cause of this discrepancy.

Using the equation for the obstruction effect in the form[6]

$$\frac{\Lambda^0_{HMT}}{(\Lambda^0_{H_2O})_0} = \frac{1 - 1.5\Phi}{1 - \Phi} \quad (2)$$

where Φ is, in our case, the volume fraction of HMT, it was found that if a molar volume of 130 cm^3/mol is taken for HMT, the $(\Lambda^0_{H_2O})_0$ values happen to be, in each case, just those corresponding to the spectroscopic structural temperatures of the various HMT solutions examined (see t and t_{ir} values in Table III). It is interesting to point out that a volume of 130 cm^3/mol is a very reasonable value for HMT, compared with the solid-state value of 104 cm^3/mol[9] and the hydrodynamic value of 160–180 cm^3/mol obtained from diffusion and viscosity data.[3] Admittedly, the final agreement, which relies mainly on the soundness of the structural-temperature values as derived by a spectroscopic technique, may be to some extent fortuitous.

(9) G. W. Smith, J. Chem. Phys., 36, 3081 (1962).

The results reported here seem to favor the applicability of the concept of structural temperature as a means of explaining the behavior of aqueous solutions. This concept appears to be particularly applicable to the problem of the conductance of simple electrolytes in the presence of an excess of a nonionic third component. More extended studies along these lines might prove interesting.

An Asymmetry-Potential Effect across Gradient Permselective Membranes

by F. de Körösy

The Negev Institute for Arid Zone Research, Beersheva, Israel (*Received January 23, 1968*)

The preparation of gradient permselective membranes has been described. They are prepared by one-sided amination of PVC[1] (anionic) or by one-sided sulfochlorination of polyethylene (cationic), with subsequent quaternization or hydrolysis, respectively. Gradient membranes of about 100 kilohm cm[2] generate an emf and produce electrical energy between salt solutions of identical composition. This effect is due to the diffusion of solution to the edge of the membrane at the circumference of the measuring cell and to the concentration differences arising on this edge.

The work of Liquori and Botré on nonuniform selective membranes[2] explained how an electric potential difference can be temporarily established across such membranes when they are placed between two electrolyte solutions of the same composition. Their effect is due to different degrees of permselectivity of two sides of the membrane and to ions migrating into the internal, aqueous layers of the membrane from both of its sides.

Some time ago we also worked with permselective membranes in which there was a built-in concentration gradient of their active sites from one face toward the other. We also observed in some cases that a potential difference of up to 80 mV arises across these membranes when they are fitted into a cell between two solutions of, say, KCl, of the same concentration on their two sides. It was even possible to extract currents of up to some 10^{-7} A for several weeks from membranes about 5 cm[2] in surface area. Eventually it became possible to explain this mysterious source of energy. Our explanation of the phenomenon was different from that of Liquori and Botré and seems sufficiently interesting to warrant a short description.

Preparation of Gradient Permselective Membranes

Two entirely different methods were used, one for anion-selective and the other for cation-selective membranes.

In the first instance, a PVC[1] sheet without plastifier, about 0.1 mm thick, was pressed against a rubber sheet adjoining a metal plate. There was a hole across both the metal and the rubber, so that a small container was formed with the PVC sheet as its base. Tetraethylenepentamine was poured into this container[3] and the assembly was heated to 80° for various periods of time. The PVC sheet was aminated beginning from the side of its contact with the pentamine in a gradient toward the other side. This was evident from its color. It has originally been an opaque white, and upon amination it turned, successively, yellow, orange, and reddish brown. The side toward the amine became colored long before the other side and always remained darker than the other side. The amination gradient could also be established by nitrogen determination of razor scrapings from different layers, *e.g.*: surface layer of the light-colored side, 1.8% N; first layer below the surface, 2.5% N; second layer below the surface, 3.3% N; third layer below the surface, 3.7% N; surface layer of the deep-colored side, 9.4% N.

After amination the gradient membranes were left for 1 day in a 25% alcoholic solution of methyl bromide to alkylate their amino groups, whereby a certain number of quaternary amino groups were also formed. These impart strong anion-exchange properties to the membranes.

In the second instance, polyethylene sheets 0.02–0.1 mm in thickness were photochemically sulfochlorinated from one of their sides in a streaming gas mixture of sulfur dioxide and chlorine (2:1) in the light of one

(1) Polyvinyl chloride.

(2) (a) A. M. Liquori and C. Botré, *J. Phys. Chem.*, **71**, 3765 (1967);

(b) A. M. Liquori and C. Botré, *Ric. Sci.*, **6**, 71 (1964).

(3) F. de Körösy and Y. Shorr, *Dechema Monograph.*, **47**, 477 (1962).

or two 200-W incandescent lamps. The side of the sheet which was closed off from the gas stream was pressed against a vaseline-coated glass plate. The temperature rose to 50–60° during the illumination. The sulfochlorinated sheets were hydrolyzed either in 10% NaOH at about 90° for about 3 hr or in a 5% NaOH solution in 1:1 water–dioxane at room temperature overnight.

Properties of the Gradient Membranes

The electric resistance across these gradient membranes in salt solutions varied with the time of amination or of sulfochlorination, respectively. It was obvious that they remained insulators in the first stage of the reaction and eventually yielded normal good permselective membranes of low resistance (a few ohms per square centimeters) if the reaction time was lengthened sufficiently. We were interested in the stage in which conductivity began to emerge and the gradient remained steep. Therefore, we concentrated on membranes between 10,000- and some 100,000-ohm cm² resistance which could be obtained after 70–100 min of amination or after 2–6 hr of sulfochlorination (0.1–0.2 mm thick polyethylene presoaked in dekaline). The resistance across gradient membranes was never found to be appreciably dependent on the direction of the current; they never showed a rectifying effect.

Diffusion of NaCl solution across the membrane in distilled water was measured at 30° on two aminated PVC membranes of about a 1000-ohm cm² resistance. A slight but reproducible asymmetry was found between the two directions of diffusion (in units of equiv/cm² sec)

	1st membrane ($\times 10^{-11}$)	2nd membrane ($\times 10^{-11}$)
Salt on the darker side	2.4 ± 0.1	0.92 ± 0.03
Salt on the lighter side	2.9 ± 0.1	1.07 ± 0.04

The membrane swells to different degrees in salt solution and in distilled water, and this may well cause an asymmetry in its diffusive properties when the solutions are changed on both of its sides. Similar dissymmetry has been found by Rogers[4] on gradient plastic membranes for gases and for liquids.

The existence of an *asymmetry potential* between two sides of some of these membranes was by far their most interesting property. When placed between two KCl solutions of equal concentration, say 0.1 or 0.2 N on both sides, the emf between the two sides of the membrane was not zero, as it ought to have been. During the first hours there were irregular variations of this emf, but later it usually steadied to much more stable values which changed less and more slowly. According to the sample of membrane used and subject to influences which were only later understood, this emf varied between a few millivolts and, at most, about 80 mV. Its sign may have varied during the first day, but it eventually became negative on the more strongly

reacted side of the anion-selective membrane and positive on the same side of the cation-selective one. It was even possible to extract current, that is, actually to extract energy, from these cells for several successive weeks. There was no visible source of energy. Resistances made up of electrolytes of different, appropriate magnitudes were necessary as shunts to perform these experiments. KCl–agar bridges of different size and concentration were prepared to this end, and, of them, that bridge was selected which just lowered the voltage drop between the two halves of the cell to 0.5 of its open emf value. This was done because we assumed that the voltage decreases approximately linearly with the extracted current, and some sets of measurements proved the validity of this assumption. The maximum extracted energy was thus to be expected on the resistance which decreased the voltage to 0.5 of its open-cell value. Currents obtained from a few square centimeters of membrane surface amounted to some 10^{-7} A, so that the maximal wattage was 10^{-8} W.

A systematic search for the inexplicable source of energy revealed the following properties of these cells with gradient membranes.

1. The effect was independent of pressure differences of a column of solution (a few centimeters high) between the two half-cells.

2. The effect was independent of temperature differences between the two half-cells up to about 10°.

3. The effect did depend on the temperature of the cell, but changes with temperature were slow, of the order of 1 or 2 days, and they were neither regular nor reproducible. After having made observations in rooms roughly thermostated to temperatures between 5 and 30°, it seemed necessary to immerse the cell in a thermostated liquid.

4. During these experiments in the thermostat baths, it gradually became apparent that the edge of the membrane in contact with the water of the bath was influenced by the conductivity of the bath: there was a measurable potential difference between the cell halves and the bath. Afterward the water was exchanged for paraffin oil. The emf fell in a few days to a few millivolts. Later irregularities appeared and after another few days it became evident that some droplets of salt solution wetted the circular circumference of the membrane in the paraffin bath. The cell was duly lifted out of the bath and was cleaned around the edge. During this process the emf changed suddenly and irregularly by several tenths of 1 mV.

All this seemed to indicate that the edge of the gradient membrane protruding on the circumference of the cell may have been the seat of the curious effect. To test this assumption, the following experiments were performed.

(4) C. E. Rogers, *J. Polym. Sci.*, **C10**, 93 (1965).

1. The thermostat bath was filled with the same KCl solution which was within the two half-cells. The emf disappeared.

2. On withdrawing the cell from the KCl bath and allowing it to stand in the air, a strong emf developed, the strongly reacted side of the membrane being negative, as usual.

3. Careful drying of the edge around the cell made the emf vanish, but it returned within a few days.

4. Washing the circumference of the membrane edge all around the cell with distilled water changed the sign of the emf.

5. Sealing the dried edge all around the cell hermetically with Picein definitively annihilated the emf.

6. A PVC sheet was aminated within a circumference of only about 2 cm in diameter, while the PVC around this area remained unreacted and served as an insulating frame for the gradient membrane. When bathed in the same solution, *none* of these framed membranes evolved an emf between their two sides. During the first day of equilibration, irregular emf values would appear but they always disappeared after equilibration.

Discussion

In view of these results, it is felt that we have found the mysterious source of electrical energy. Solution migrates slowly within the membrane to its edges and loses water by evaporation. Thus the solution on the edge becomes more concentrated than the solution in the half-cells, and two diffusion potentials arise on the two faces of the permselective membranes between their edge and the solutions on their wet faces, along the surfaces closed by pressure against the cell frame.

Diffusion is easier on the more highly reacted and more conductive surface, so that the diffusion potential on this side would be larger than on the less reacted surface. The resistance across the membrane is too high to short-circuit this potential difference, and, consequently, the effect appears only on membranes with very high resistance. (As a matter of fact, the resistances measured in the standard measuring cells were far smaller than the real resistance, because the shunt around the edge was actually being measured.) A certain amount of (at least) surface conductivity is of course necessary in all cases.

If the membrane was anion selective, the concentrated solution around the edge made the more conductive, better reacted side of the membrane negative. If it was cation selective, the opposite was the case. If the edge was made more dilute than the interior by washing with distilled water, the direction of salt diffusion became inverted, namely, from the center to the edge. Hence the emf also changed its sign. If the edge was carefully dried or hermetically sealed against evaporation or diffusion of water, the whole emf effect naturally disappeared, because there was no longer any concentration gradient between edge and interior. Thus the source of energy of the gradient membrane cell has been found in the free energy of evaporation of water from around the open edge of the membrane or in the diffusion of salt from the cell into distilled water on its circumference. The second law of thermodynamics is obeyed.

Chemistry of Crystalline Aluminosilicates.   V.   Preparation of

Aluminum-Deficient Faujasites[1]

by George T. Kerr

*Mobil Research and Development Corporation, Central Research Division Laboratory,
Princeton, New Jersey   08540   (Received January 24, 1968)*

The slow addition of a dilute solution of ethylenediaminetetraacetic acid to sodium zeolite Y effects the removal of aluminum from the zeolite. A mechanism for the reaction is presented. The removal of up to about 50% of the aluminum yields highly crystalline products of improved thermal stability and increased sorptive capacity. As aluminum removal proceeds from about 60 to 100%, the crystallinity of the products decreases; aluminum-free products are completely amorphous.

Introduction

Removal of aluminum from clinoptiolite[2] and a synthetic erionite[3] by leaching with hydrochloric acid has been reported recently. Faujasite, having lower ratios of silicon to aluminum than either clinoptiolite or erionite, is prone to crystal lattice attack by strong mineral acids.[4] For synthetic faujasite, aluminum was removed by special thermal treatment of the hydrogen (acid) form of the zeolite, followed by cation exchange of aluminum by sodium using sodium hydroxide solution.[5] In the work reported here, aluminum is removed directly from sodium zeolite Y, a synthetic faujasite, by a special technique using ethylenediaminetetraacetic acid (H_4EDTA).

Experimental Section

The Siemens Crystalloflex II X-ray diffractometer was used, with a 1-radian camera, for the diffraction analyses. A Du Pont 900 differential thermal analyzer was used at a heating rate of $30°/min$ to determine the temperature at which crystal lattice collapse occurred.[6]

Reagents. Reagent grade chemicals were used throughout this study. The sodium zeolite Y had the following composition: ash, 75.7% (ignition at 1100°); Na_2O, 13.5%; Al_2O_3, 21.1%; and SiO_2, 65.2%.

Reaction Conditions. All reactions involving the zeolite and H_4EDTA were conducted at reflux using 20.0 g of the zeolite. This quantity of zeolite contains the following quantities of oxides, expressed as gram formula weight: 0.0331, Na_2O; 0.0314, Al_2O_3; and 0.1595, SiO_2.

For rapid addition of H_4EDTA to the zeolite, 9.6 g (0.033 mol) of the acid was added directly to a slurry of zeolite in 300 ml of water. The mixture was stirred for 6 hr. For slow addition of the acid to the zeolite, a Soxhlet extractor was used. The 20.0 g of zeolite and the 300 ml of water were contained in the boiling flask; the appropriate quantity of acid was contained in a Soxhlet thimble within the extractor. At least

18 hr was required for complete addition of the acid to the boiling flask. After filtration the samples were calcined with air or with nitrogen purge at 550–600° prior to sorption measurements.

Results

The Effect of Rate of Addition of Acid to Sodium Zeolite Y. The same quantities of reactants were used for both slow and rapid addition. The properties of the products and of the initial zeolite are summarized in Table I. Cyclohexane sorptive capacities and the quality of the powder photographs indicate that the product of slow addition is the more crystalline. Both aluminum-deficient products, however, are significantly more thermally stable than the normal sodium zeolite. Although about 50% of the tetrahedrally coordinated aluminum and the accompanying sodium ions were removed from the slow-addition product, the sorptive capacity and the powder photograph indicate that little, if any, loss of crystallinity occurred.

Composition of Aluminum-Deficient Products. A series of reactions were conducted using various quantities of H_4EDTA and the slow-addition technique. The results of this study are depicted in Figure 1. The straight line conforms to the stoichiometry of the general equation

$$xH_4EDTA + NaAlO_2(SiO_2)_y \longrightarrow$$

$$xNaAlEDTA \cdot H_2O + (NaAlO_2)_{1-x}(SiO_2)_y + xH_2O$$
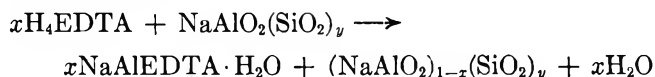
where $x \leq 1$ and $y \geq 2.5$. The close fit of the experimentally derived points to the line in Figure 1 shows that the above stoichiometry is very closely followed

(1) Part IV: G. T. Kerr, *J. Phys. Chem.*, **72**, 1385 (1968).

(2) R. M. Barrer and M. B. Makki, *Can. J. Chem.*, **42**, 1481 (1964).

(3) S. P. Zhdanov and B. G. Novikov, *Dokl. Akad. Nauk SSSR*, **166**, 1107 (1966).

(4) R. M. Barrer, *Proc. Chem. Soc.*, 99 (1958).

(5) G. T. Kerr, *J. Phys. Chem.*, **71**, 4155 (1967).

(6) A. S. Berger and L. K. Yakovlev, *Zh. Prikl. Khim.*, **38**, 1240 (1965).

Table I: Rapid and Slow Addition of Ethylenediaminetetraacetic Acid to Sodium Zeolite Y

	Product of rapid addition	Product of slow addition	Initial zeolite
Formula weight ratio			
Na₂O:Al₂O₃	0.89 (0.96)[a]	0.87 (1.16)[a]	1.05
SiO₂:Al₂O₃	13.2 (0.167)[a]	10.3 (0.164)[a]	5.26
Cyclohexane sorption			
Grams/100 g of activated sample	11.2	24.0	19.1
Grams/1 g of SiO₂ in activated sample	0.135	0.298	0.292
Fraction removed[b]			
Na	0.66	0.575	0
Al	0.60	0.515	0
Temperature of crystal collapse, °C	1040	1047	974

[a] Composition of aqueous-phase product given in parentheses.
[b] Assuming no loss of Si from zeolite.

In Table II is a resume of the compositions and properties of the samples shown in Figure 1.

Composition of Aqueous Product from Aluminum-Removal Reaction Mixtures. The aqueous phase from a slow-addition reaction in which 50% of the aluminum and sodium were removed from the zeolite was evaporated to a low volume. On cooling, the liquid yielded a crystalline solid which was filtered, was dried at 100°, and was analyzed.

Anal. Calcd for NaAlEDTA·H₂O: Na, 6.46; Al, 7.55; C, 33.8; H, 3.43; N, 7.86. Found: Na, 7.2; Al, 7.57; C, 34.4; H, 3.82; N, 8.03.

The X-ray diffraction powder photograph of this material was identical with that of an authentic sample of NaAlEDTA·H₂O prepared by treating Al with NaH₃EDTA in the ratio of 1 g-atom/1 mol. A trace of mercuric chloride was added to the aqueous phase to enhance the reactivity of the metallic Al. These findings also confirm the validity of the general equation proposed for the removal of aluminum from sodium zeolite Y.

Table II: The Stoichiometry and Composition of Aluminum-Deficient Zeolite Y

Moles of H₄EDTA used/ formula weight of NaY	Fraction removed		Grams of cyclohexane sorbed per		Temperature of crystal collapse, °C	Crystallinity by X-ray
	Na	Al	100 g of zeolite	1 g of SiO₂ in zeolite		
0	0	0	19.1	0.292	974	Good
0.25	0.393	0.263	21.4	0.293	1033	Good
0.50	0.575	0.515	24.0	0.298	1047	Good
0.50	0.59	0.51	23.6	0.295	1050	Good
0.675	0.74	0.70	24.8	0.284	993	Good
0.750	0.84	0.80	24.5	0.270	993	Nearly amorphous
1.00	1.0	1.0	21.8	0.224	Amorphous	Completely amorphous
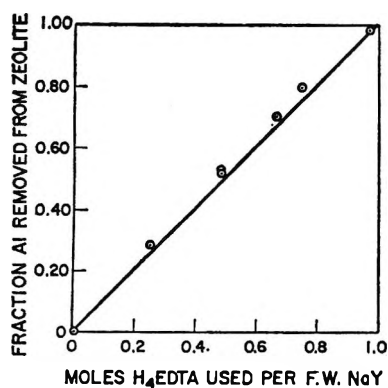
Figure 1. The stoichiometry of aluminum removal.

in practice. Therefore, any degree of aluminum removal can be easily achieved by use of the proper quantity of acid relative to the quantity of zeolite used.

Discussion

The Mechanism of Aluminum Removal. In an earlier article, a mechanism was proposed to explain the formation of cationic aluminum during conversion of hydrogen zeolite Y to a more stable substance.[5] Reaction 1 shows how the sodium zeolite is partially con-

$$2O—Al—O—Si—O \ (Na^+) + H_4EDTA \longrightarrow$$

$$2O—Al \ O—Si—O + Na_2H_2EDTA \quad (1)$$

$$
2O—Al \quad O—Si—O + 3H_2O \longrightarrow
$$

(with O, H, O above; O, O below)

$$
—OH \quad HO—Si—O + O—Al—O—Si—O + H_2O \quad (2)
$$

$$Al(OH)_2{}^+$$

$$
O—Al—O—Si—O + Na_2H_2EDTA \longrightarrow
$$

$$Al(OH)_2{}^+$$

$$
O—Al—O—Si—O + NaAlEDTA \cdot H_2O + H_2O \quad (3)
$$

$$Na^+$$

verted to the hydrogen form by H_4EDTA. The zeolite must be at least partially in the hydrogen form for removal of aluminum; no reaction occurs between the sodium zeolite and Na_2H_2EDTA. Reaction 2 is a composite of the two reactions presented in the earlier report.[5] This reaction involves hydrolysis of a tetrahedral aluminum adjacent to a Brønsted acid site, followed by neutralization of the resultant basic aluminum hydroxide by a Brønsted acid site to yield the cationic aluminum species and water. In reaction 3 the aluminum cation is exchanged by sodium ion and then chelated by the EDTA anion. By the mass action principle, the chelation effects essentially complete exchange of aluminum ions by sodium ions. In the earlier work the formation of the hydroxyaluminate ion, using sodium hydroxide solution, served this purpose.[5] The composite of the three proposed mechanistic reactions is in agreement with the general equation presented in the Results section.

Thermal Stability. Removal of a portion of the tetrahedrally coordinated aluminum from the zeolite framework has been shown[5] (and Table II) to increase its thermal stability. The reason for this increase in stability is not obvious, but it might be attributable to the formation of new Si–O–Si bonds.[5] The four hydroxyls in the product of reaction 2 are each bonded to silicon; on heating, these four groups would be expected to condense to yield water and Si–O–Si bonds. The

observed contraction of the unit-cell dimension on aluminum removal is in line with this proposal.[5]

The temperatures reported here at which lattice collapse occurs should not be considered as true transition points, such as melting. Berger and Yakovlev pointed out that a dehydrated zeolite, "having a large internal surface and excess of free energy, is in a state of unstable equilibrium and when the temperature is raised to a certain limit it undergoes sudden breakdown which leads to formation of an amorphous product and liberation of the excess energy in the form of heat."[6] Differential thermal analysis is a dynamic method and the heating rate affects the temperature of crystal loss in zeolites. As long as the rate is constant, dta can serve to compare the relative stabilities of zeolites.

For the particular sodium zeolite Y used in this study, the optimum removal of aluminum for thermal stability appears to be in the range of 25–50%. Above 50%, not only does the thermal stability decrease but also serious lattice collapse begins to occur; on complete removal of aluminum, the product is X-ray amorphous.

Sorptive Capacity. The sorptive data in Table II show that removal of aluminum generally increases the capacity for cyclohexane sorption on the basis of sample weight. However, the sorptive capacity per gram of SiO_2 in the zeolite remains nearly constant up to about 60–70% aluminum removal. If it is assumed that silicon remains intact in the framework on removal of aluminum, then the number of grams of silicon in a sample is proportional to the number of unit cells in the sample. If the cyclohexane capacity per unit cell is unchanged on removal of aluminum, then the number of grams of cyclohexane sorbed per gram of SiO_2 should be unchanged. The assumption that framework silicon is unaffected by aluminum removal is supported by the $SiO_2:Al_2O_3$ ratios in the aqueous phases shown in Table I. Our observations on the sorptive-capacity increase are in agreement with those of Zhdanov and Novikov who studied aluminum-deficient erionite.[3] The decrease in sorptive capacity (based on the number of grams of SiO_2 in the samples), from which more than about 70% of the aluminum was removed, is in line with the decrease in crystallinity as determined by X-ray diffraction.

Usually faujasites sorb only traces of cyclohexane on conversion from the crystalline to the amorphous state. The relatively high sorptive capacities of these amorphous products, containing almost no aluminum, behave more like silica gel than amorphous zeolites. This is not surprising, since the amorphous material obtained on complete aluminum removal is simply silica. The usual amorphous faujasite contains about 20% of Al_2O_3 and would not be expected to yield a silica-type product.

Disulfide Ions Produced in γ-Irradiated Organic Glasses

at −196°.   A Photochromism of the Anion[1]

by Tadamasa Shida

Rikagaku Kenkyusho, The Institute of Physical and Chemical Research, Honkomagome, Bunkyo-ku, Tokyo, Japan
(Received January 24, 1968)

Molecular positive and negative ions of alkyl and aromatic disulfides have been produced in rigid matrices γ irradiated at −196°. Disulfide anions absorb strongly at about 420 mμ, while the corresponding cations exhibit a weak absorption at 600–900 mμ. A photochromism was found for alkyl disulfide anions in nonprotic matrices, which has been ascribed to a rotational isomerization of the anion. In protic matrices the rotation is hindered by the hydrogen bridge. In contrast with the alkyl disulfide anions, photoexcitation of dibenzyl and dibenzhydryl disulfide anions results in the splitting of benzyl and benzhydryl radicals, respectively.

Introduction

γ irradiation of frozen organic solids produces reactive intermediates which are not obtained by conventional means, such as photolysis and electrolysis. When the concentration of the additive in a one-component matrix is small enough, the additive is not affected directly by radiation but is affected indirectly by a few processes, such as electron capturing and positive hole trapping. The indirect effects result in the formation of ionic intermediates derived from the additive. The intermediates can be studied spectroscopically in a systematic way, because in many cases a single species having absorption bands in the visible and near-infrared regions is produced predominantly.[2] In glassy matrices, most colored intermediates are found to be molecular ions of additives. Both cations and anions can be formed separately in different matrices.[2] If the previous work on molecular ions in glassy matrices is extended, disulfide ions are produced and their spectral features are discussed in relation to the nature of matrices. A photochromism was found for alkyl disulfide anions which is understood in terms of a rotational isomerization of the ion.

Experimental Section

Dimethyl disulfide from two commercial sources (K & K, Laboratories, Inc., and TCI Co. Ltd.) was purified by fractional distillation. Other liquid disulfides were distilled under reduced pressure. Glpc analysis using Carbowax and Apiezon columns showed no significant amount of impurity except for di-*t*-amyl disulfide (obtained from K & K) which contained an unknown impurity. Repeated distillations reduced the amount of the tenacious impurity, but complete removal was not achieved. Tetramethylene disulfide was prepared by the method described by Barltrop, *et al.*,[3] and was purified by sublimation to obtain a crystal melting at 31–32°. Dibenzhydryl disulfide was synthesized from thiobenzophenone and am-

monium hydrogen sulfide according to a standard method.[4]

The disulfides were dissolved in various solvents and were frozen to a glassy solid in an all-quartz (Suprasil) thin cell having the inner dimensions of 30 × 10 × 1.5 mm. Concentrations of the solutes ranged from 0.5 to 2 mol % and are indicated in the figure captions. Optical changes induced by γ irradiation at −196° were observed by measuring the absorption of the sample solid before and after irradiation. Optical measurements were carried out with a Cary 14R and a Shimadzu SV-50 spectrometer. For a selective photobleaching, Toshiba glass filters, VV-40 (transmitting 330–500 mμ) and VR-65 (>590 mμ), were used. Esr spectra were recorded at −196° on a JEOL spectrometer with a 100-kc modulation. Dosimetry was carried out by using the Fricke solution. The solution in an ampoule was placed in a dewar vessel, which served as a liquid-nitrogen container throughout the experiment. In order to correct the absorption of energy by liquid nitrogen, the ampoule of the Fricke solution was immersed in 1-butanol, whose density roughly matches that of liquid nitrogen. The volume contraction of liquid samples at −196° was properly corrected.

Results and Discussion

(I) Alkyl Disulfide Anions in Methyltetrahydrofuran Glass. In pure methyltetrahydrofuran (MTHF) glass at −196°, major events caused by γ irradiation are ionization, the protonation of cations, and the formation of solvated electrons

(1) This is part IX of a series "Molecular Ions." For the previous paper see: T. Shida, *J. Phys. Chem.*, **72**, 723 (1968).

(2) T. Shida and W. H. Hamill, *J. Chem. Phys.*, **44**, 4372 (1966).

(3) J. A. Barltrop, P. M. Hayes, and M. Calvin, *J. Amer. Chem. Soc.*, **76**, 4348 (1954).

(4) E. Müller, Ed., "Methoden der Organische Chemie," Vol. 9, 4th ed, Georg Thieme Verlag, Stuttgart, 1955, p 723.

$$C_5H_{10}O \xrightarrow{\gamma} C_5H_{10}O^+ + e^-_{mobile} \qquad (1)$$

$$C_5H_{10}O^+ + C_5H_{10}O \longrightarrow C_5H_{10}OH^+ + C_5H_9O \cdot \qquad (2)$$

$$e^-_{mobile} \longrightarrow e^-_{solvated} \qquad (3)$$
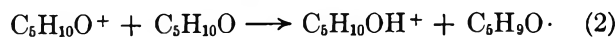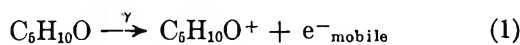
The solvated electron gives rise to a broad absorption band at about 1200 mμ.[5]

In agreement with Wendenburg's results,[6,7] disulfides eliminated the electron even at a concentration of 0.5 mol %, and a new band emerged at about 420 mμ for all disulfides tested. The result for dimethyl disulfide in MTHF is shown in curve 1 of Figure 1. It was suggested that the band might be due to the thiyl radical produced by the reaction[6]

$$RSSR + e^- \longrightarrow RS \cdot + RS^- \qquad (4)$$
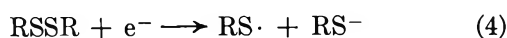
For the following reasons we attribute the band to the disulfide anion. Studying the pulse radiolysis of aqueous cysteamine and cystamine solutions, Adams, et al., claimed that a disulfide anion, $RSSR^-$ ($R = CH_2CH_2-NH_2$), absorbs strongly at 410 mμ.[8] The thiyl radical, on the other hand, has a characteristic esr spectrum, whereas the spectrum of the anion is a broad singlet.[9,10] The sample having the 420-mμ band (Figure 1, curve 1) exhibited a singlet which agreed with the reported spectrum of the anion.

When the irradiated dimethyl disulfide in MTHF glass was bleached with selective filters, spectral changes, shown by curves 1–4 of Figure 1, were observed. Illumination with blue light (330–500 mμ) for 10 min reduced the 420-mμ band to the optical density of less than 0.1, and broad bands appeared in the near-infrared region. Subsequent illumination with red light (>590 mμ) eliminated the ir bands within 1 min and the 420-mμ band was restored. The cyclic change could be effected without a significant loss of spectral intensity. Unless longer wavelengths of the tungsten lamp were carefully cut off in the first bleaching, the change from curve 1 to 2 was not induced, apparently because of the efficient backward action by the red light. Bleaching with full tungsten light diminished the 420-mμ band slowly without any significant change in the band shape. As the alkyl group of disulfide ascended from methyl to n-propyl, isopropyl, sec-butyl, and n-amyl, the loss of intensity after one cycle of bleaching became noticeable. For n-amyl disulfide the loss amounted to about 10%.

Since the reversible color change suggests an intramolecular process of the anion, we propose the rotational isomerization as shown in Figure 2. The dimethyl disulfide molecule has a twisted conformation whose dihedral angle is about 90°.[11] If we assume that the ground state of anion has a similar dihedral angle, absorption of photon $h\nu_1$ by the anion may cause the skeletal change to produce a metastable anion. The latter is further assumed to absorb photon $h\nu_2$ to restore the stable conformation. In order to substantiate the
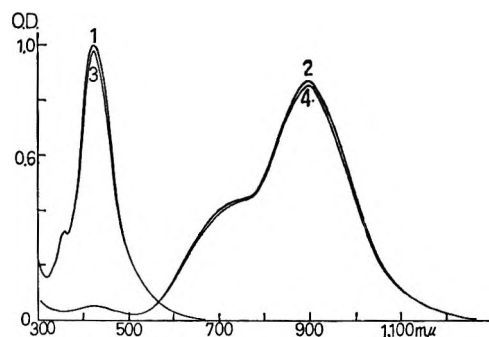
Figure 1. Absorption spectra of γ-irradiated dimethyl disulfide in MTHF (1 vol %) at −196° and a dose of 1.52 × 10^{19} eV/ml: curve 1, after γ irradiation; curve 2, sample after 10 min of bleaching with light of wavelength 330–500 mμ; curve 3, sample after 2 min of bleaching with light of wavelength 590 mμ; curve 4, sample after 10 min of bleaching with light of wavelength 330–500 mμ.
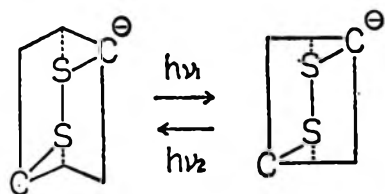
Figure 2. Proposed mechanism of rotational isomerization of the disulfide anion.

assumption, the energy diagram of the anion as a function of dihedral angle is required. For a polyatomic anion radical containing sulfur atoms, however, any accurate computation for the energy level is prohibitively difficult because of the uncertainty incidental to the integrals of electronic interaction. We infer that the highest occupied molecular orbital of the ground-state anion consists mainly of 4s atomic orbitals of sulfur[12,13] and that the total electronic energy depends little upon the dihedral angle, while in excited states the participation of directional 3d and 4p atomic orbitals makes the energy dependent upon the angle

(5) P. J. Dyne and O. A. Miller, Can. J. Chem., 43, 2696 (1965).

(6) J. Wendenburg, "Second Symposium on Radiation Chemistry," Tihany, Hungary, 1966, papers no. 0–34.

(7) J. Wendenburg, H. Moeckel, A. Granzow, and A. Henglein, Z. Naturforsch., 21, 632 (1966).

(8) G. S. McNaughton, G. E. Adams, and B. D. Michael in "Radiation Research," G. Silini, Ed., North-Holland Publishing Co., Amsterdam, The Netherlands, 1967, p 205. See also G. E. Adams, G. S. McNaughton, and B. D. Michael in "The Chemistry of Ionization and Excitation," G. R. A. Johnson and G. Scholes, Ed., Tailor and Francais, Ltd., London, 1967, pp 281–293.

(9) F. K. Truby, C. MacCallum, and J. E. Hesse, J. Chem. Phys., 37, 2777 (1962).

(10) S. B. Milliken, K. Morgan, and R. H. Johnsen, J. Phys. Chem., 71, 3238 (1967).

(11) D. W. Scott, H. L. Finke, J. P. McCullough, M. E. Gross, R. E. Pennington, and G. Waddington, J. Amer. Chem. Soc., 74, 2478 (1952).

(12) P. Palmieri and C. Zauli, J. Chem. Soc., A, 813 (1967).

(13) L. C. Cusachs and J. R. Linn, Jr., J. Chem. Phys., 46, 2919 (1967).

Photoexcitation will thus distort the anion as described above. The prediction was supported qualitatively by an extended Huckel MO calculation carried out for the dimethyl disulfide molecule.[14]

In striking contrast with the five disulfides mentioned above, the anions of di-t-alkyl (t-butyl and t-amyl) disulfides behaved differently toward photobleaching. They also yielded the strong absorption band of the anion at 420 mμ. The illumination with the blue light, however, did not induce the reversible color change but merely suppressed the intensity of the band, as shown in Figure 3, for di-t-butyl disulfide in MTHF. It seems that the stiff t-alkyl groups militate against the rotation of the anion. The uniform decay of the anion induced by the illumination (curves 2–4, Figure 3) might be due to the decomposition

$$\text{RSSR}^- \xrightarrow{h\nu \ (330-500 \text{ m}\mu)} \text{RS} \cdot + \text{RS}^- \qquad (5)$$
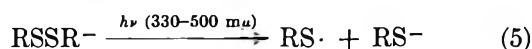
However, the thiyl radical was not detected by esr spectroscopy even after 1 hr of illumination with the blue light. The decay is attributed to the slow photoionization of the anion, the detached electron ultimately recombining with the positive species produced by reaction 2 in the matrix. As mentioned before, disulfides of longer alkyl chains, such as di-n-amyl disulfide, also lost gradually the intensity of the anion band after each cycle of optical bleaching. The decay is now ascribed to the photoionization competing with the isomerization.

The results obtained in the tetramethylene disulfide system are interesting in this context because the ring structure of the disulfide will prevent the anion from rotating to the $trans$ conformation. The disulfide in MTHF produced the anion band at 405 mμ similar to the 420-mμ band of the other disulfides (curve 1, Figure 4). Upon bleaching with light of wavelength 330–500 mμ. the 405-mμ band disappeared quickly, but instead of the ir bands only a weak band appeared irreversibly at about 520 mμ (curve 2, Figure 5). The ring strain of the anion may induce a decomposition, $e.g.$

$$(6)$$
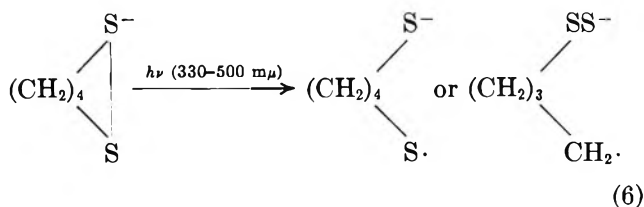
(II) *Aromatic Disulfide Anions in MTHF Glass.* Figure 5 shows the absorption spectra of irradiated aromatic disulfides in MTHF glass. The insignificant shift of λ_{max} reflects the localization of odd electron on the S–S bond in the aromatic system also. The anion bands for dibenzyl and dibenzhydryl disulfides are much weaker than that for diphenyl. For the former two, the known absorption bands of benzyl and benzhydryl radicals are seen in the near-ultraviolet region.[15,16]

Figure 3. Absorption spectra of γ-irradiated di-t-butyl disulfide in MTHF (1 vol %) at −196° and a dose of 2.84 × 10^{19} eV/ml: curve 1, after γ irradiation; curves 2–4, progressive illumination (10 min each) with light of wavelength 330–500 mμ.
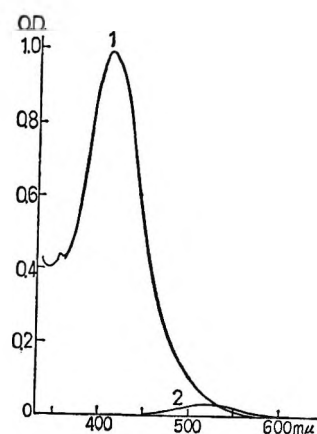
Figure 4. Absorption spectra of γ-irradiated 0.5 mol % tetramethylene disulfide in MTHF at −196° and a dose of 1.52 × 10^{19} eV/ml: curve 1, after γ irradiation; curve 2, sample after 10 min of bleaching with light of wavelength 330–500 mμ.

Assuming that the molar absorption coefficients are roughly the same for the three anions, the smaller yields of anions of benzyl and benzhydryl disulfides and the appearance of the radical bands are explained by the competing reaction

$$\text{BzSSBz} + \text{e}^- \longrightarrow \text{Bz} \cdot + \text{BzSS}^- \qquad (7)$$
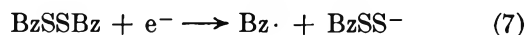
where Bz· stands for benzyl or benzhydryl radical. As curves 2 and 3 of Figure 5 show, illumination with the blue light eliminated the anion bands of benzyl and benzhydryl disulfides and enhanced the radical bands. The result is accounted for by the reaction

$$\text{BzSSBz}^- \xrightarrow{h\nu \ (330-500 \text{ m}\mu)} \text{Bz} \cdot + \text{BzSS}^- \qquad (8)$$
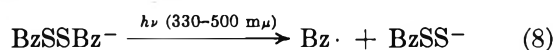
(14) The calculation was carried out using a program coded by Professors T. Yonezawa and H. Kato whose assistance the author wishes to acknowledge gratefully.

(15) G. Porter and E. Strachan, *Spectrochim. Acta*, 12, 299 (1958).

(16) G. Porter and E. Strachan, *Trans. Faraday Soc.*, 54, 1595 (1958).
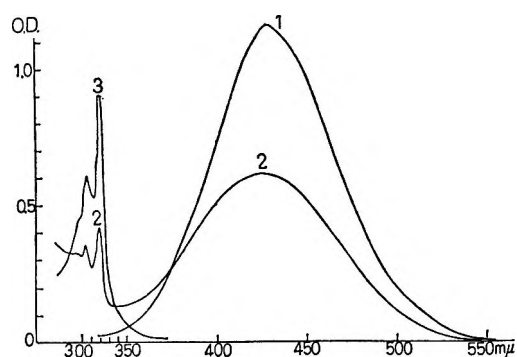
Figure 5. Absorption spectra of aromatic disulfides in MTHF at $-196°$ and a dose of 1.52×10^{19} eV/ml: curve 1, diphenyl disulfide (1 mol %); curve 2, dibenzyl disulfide (1 mol %); curve 3, dibenzyl disulfide after 10 min of bleaching with light of wavelength 330–500 mμ. Dibenzhydryl disulfide gave analogous results to those of dibenzyl, the bands of benzhydryl radical appearing at the reported wavelengths.[15,16]

Table I: λ_{max} of Disulfide Ions (in mμ)

	Anions in MTHF	Anions in alcoholic matrices[a]	Cations in sec-BuCl
Dimethyl	420	400	710
Di-n-propyl	420	410	730
Diisopropyl	419	403	. . .
Di-sec-butyl	425	413 (EtOH)	. . .
Di-n-amyl	420	409 (EtOH)	780
Di-t-butyl	430	415	720
Di-t-amyl	435	. . .	730
Tetramethylene	405	396	. . .
Diphenyl	427	415 (EtOH)	800
Dibenzyl	427	410	. . .
Dibenzhydryl	422	402 (methyl Cellosolve)	800

[a] Unless otherwise stated, methanol containing 2 vol % of water was used as the alcoholic matrix. Ethanol or methyl Cellosolve was used for its higher solvency.

Figure 6. Absorption spectra of dimethyl disulfide in hexanol (2 vol %) at $-196°$ and a dose of 1.52×10^{19} eV/ml: curves 1–3, see the corresponding part of the caption for Figure 1.

the resonance stabilization of the radical favoring the splitting. Photobleaching the diphenyl disulfide anion caused a slow decay similar to di-t-alkyl disulfides but produced no new bands. Thus the resonance energy of Bz· seems to be crucial in reaction 8, and the bulky phenyl group prevents the rotation of the anion.

(III) Disulfide Anions in Other Matrices. It is now established that a band at about 510 mμ in γ-irradiated alcohol glasses is due to the electron trapped by the matrix.[17] In the presence of disulfides the band failed to appear and a strong band at about 400 mμ was produced. Although the λ_{max} is about 20 mμ shorter than that in MTHF, the band is, in every respect, ascribable to the disulfide anion. The shift is associated with the solvent effect of alcoholic matrices stabilizing the ground-state anion (see Table I).

A remarkable contrast to the result in MTHF glass is that *any* anions did not show the photochromism in methanol or ethanol. The anion band merely diminished slowly, as observed for di-t-alkyl and diphenyl disulfides in MTHF. Since the photochromism is attributed to the rotation of the anion, the absence of the color change in alcohol indicates that the rotation is prevented by the hydrogen bridge to the negatively charged S–S bond. The results of disulfides in higher alcohols and amines are consistent with the above presumption. In higher alcohols, such as hexanol and t-amyl alcohol, the anion band appeared at about 410 mμ an intermediate of 400 mμ in methanol and 420 mμ in MTHF. As Figure 6 shows, photobleaching with the blue light for 10 min decreased the anion band to about 70%, compared with about 5% in MTHF (Figure 1), and produced the ir bands to a limited extent. In large alcohols some of the disulfide anions may be protected from hydrogen bonding on account of the bulky alkyl group of alcohol, and thus the rotation may again be allowed. Analogous results were obtained for a series of amine matrices. Tested are triethyla-

mine, diisopropylamine, sec-butylamine, and triethylenetetramine.

(IV) Disulfide Cations in Alkyl Chloride Glass. Alkyl chlorides have been repeatedly shown to be suitable matrices for the formation of solute cations.[18] Radiation-ejected electrons in the chloride are scavenged by the matrix itself

$$RCl + e^- \longrightarrow R\cdot + Cl^- \qquad (9)$$
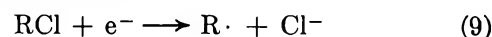
The counterpart positive hold is mobile at an early stage and is trapped by the matrix giving rise to a broad band at 400–600 mμ.[2]

Dimethyl disulfide in butyl chloride glass suppressed the band of the trapped hole and produced a weak band at 700–800 mμ (Figure 7). The 440-mμ band of trapped holes is coincidentally similar to the disulfide anion band in MTHF, but it cannot be due to the anion because of the efficient scavenging reaction 9.

(17) T. Shida and W. H. Hamill, *J. Amer. Chem. Soc.*, **88**, 3689 (1966).

(18) T. Shida and W. H. Hamill, *ibid.*, **88**, 5376 (1966).
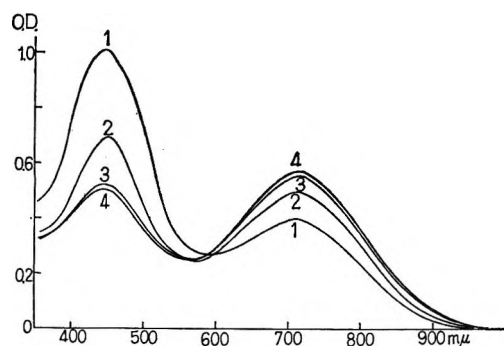
Figure 7. Absorption spectra of dimethyl disulfide in *sec*-butyl chloride (2 vol %) at −196° and a dose of 5.74 × 10^{19} eV/ml: curve 1, after γ irradiation; curves 2–4, see the corresponding part of the caption for Figure 3.

Other disulfides also yielded similar bands in the near-infrared region (Table I). The ir bands are ascribed to disulfide cations formed by accepting the migrating positive hole[2]

$$(BuCl^+)_{mobile} + RSSR \longrightarrow BuCl + RSSR^+ \quad (10)$$
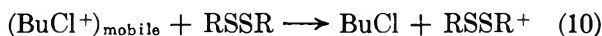
The difference of ionization potentials between butyl chloride and disulfides drives the reaction forward.

Photobleaching the trapped hole with light of wavelength 330–500 mμ diminished the band at 440 mμ and increased the ir bands. The result is consistently explained by the reaction

$$(BuCl^+)_{trapped} \xrightarrow{h\nu} (BuCl^+)_{mobile} \quad (11)$$
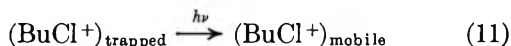
followed by eq 10. Disulfide cations, on the other hand, were stable toward illumination. Similar enhancement of the ir band was noticed transiently when the irradiated sample was warmed to thaw. The brown component (440 mμ) was lost and the sample became deeper blue, indicating that the matrix-trapped positive charge migrates to disulfide molecules in the
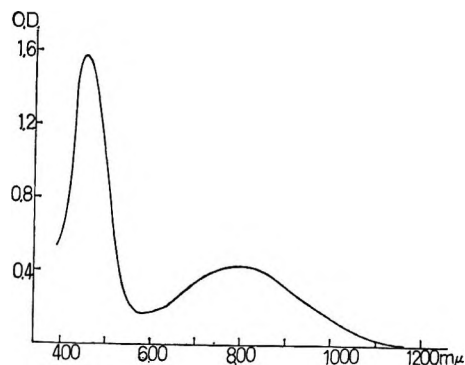
Figure 8. Absorption spectra of pure di-*n*-amyl disulfide at −196° and a dose of 2.20 × 10^{19} eV/ml.

less-rigid medium and adds to the disulfide cation. The sample, of course, lost any color when it was melted completely to liquid.

(*V*) *Pure Disulfide Glass.* Alkyl disulfides formed glassy solids at −196°, most of which were translucent. Because of its transparency, di-*n*-amyl disulfide glass was studied intensively. From the argument outlined above, γ-irradiated pure disulfide should exhibit both anion and cation bands at 420 and 700–800 mμ, respectively, provided the ions are kept stably in the disulfide matrix. Figure 8 demonstrates that both are formed. The presence of both anion and cation in irradiated pure disulfide glass has been proposed by Truby in the esr study of the system.[19] The photoinduced conversion of the anion band was observed also for the anion in pure disulfide glass.

(19) F. K. Truby, *J. Chem. Phys.*, **40**, 2768 (1964).

Kinetic Isotope Effects: Approximate Calculations[1]

by Paul C. Chang and Carole R. Gatz[2]

Chemistry Department, Portland State College, Portland, Oregon 97207 (Received January 25, 1968)

Treating the activated complex for unimolecular dissociation as uncoupled fragments simplifies the calculation of transition-state frequencies in the quasi-equilibrium-theory formulation of an isotopic rate-constant ratio. The general method is applied to the specific case of the intramolecular kinetic isotope effect in decarboxylation of malonic acid. The fragment models are further simplified by means of the "cutoff" approximation of Stern and Wolfsberg. These model calculations are in agreement with the presently available experimental results. Applicability to reactions involving simultaneous multiple bond rupture or formation is noted.

Introduction

The transition-state formulation for the ratio of rate constants for unimolecular reactions differing only in isotopic constitution is[3]

$$\frac{k'}{k} = \frac{\nu_X^{\pm\prime}}{\nu_X^{\pm}} \prod^{3n-6} \frac{u_i \sinh (u_i'/2)}{u_i' \sinh (u_i/2)} \prod^{3n-7} \frac{u_i^{\pm\prime} \sinh (u_i^{\pm}/2)}{u_i^{\pm} \sinh (u_i^{\pm\prime}/2)}$$

$$(1)$$

where primed and unprimed quantities refer to the two isotopic species and $\pm$ refers to the transition-state structure, $\gamma_X^{\pm}$ is the frequency (or average frequency) of motion in the reaction coordinate, and $u_i = hc\omega_i/kT$, where ω_i is a vibrational frequency. The appropriate symmetry numbers are assumed to be included in k'/k.

The vibrational frequencies of the activated complex are often calculated by Wilson's F–G matrix methods.[4] One assumes a structure for the activated complex, thus specifying G. The diagonal elements of F can be estimated from the assumed structure by analogy to stable molecules; the off-diagonal elements might be set equal to zero or adjusted to conform to assumptions about the nature of the reaction coordinate.[5,6] The vibrational frequencies are then obtained from the roots of the secular equation

$$|FG - E\lambda| = 0 \qquad (2)$$

where $\lambda_i = 4\pi^2 c^2 \omega_i^2$. The reactant frequencies may be obtained by a similar calculation or from spectroscopic data. However, the continued product involving reactant frequencies in eq 1 reduces to unity for an intramolecular isotope effect, where both reactant species are identical. An example is the decarboxylation of end-labeled malonic acid

$$
\begin{array}{l}
^{13}\text{COOH} \\
| \qquad\qquad \xrightarrow{k_3} \; ^{12}\text{CH}_3{}^{12}\text{COOH} + {}^{13}\text{CO}_2 \\
^{12}\text{CH}_2 \\
| \qquad\qquad \xrightarrow{k_4} \; ^{12}\text{CH}_3{}^{13}\text{COOH} + {}^{12}\text{CO}_2 \\
^{12}\text{COOH}
\end{array}
\qquad (3)
$$
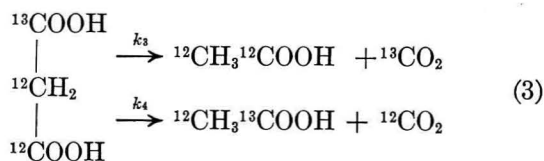
where k_4/k_3 is a measure of a carbon-12:carbon-13 intra-molecular isotope effect. Since the rate-constant ratio depends only on the vibrational frequencies of the activated complexes for this type of isotope effect, approximations and assumptions about the transition state that simplify the secular equation are particularly useful in these cases.

The Molecular-Fragment Approximation

If the assumption is made that the activated complex can be treated as vibrationally decoupled fragments, its secular equation is considerably simplified. Uncoupled, freely rotating models for the activated complex have been used in a number of absolute rate theory calculations of rate constants.[7] These applications have been limited, quite properly, to dissociations with abnormally large preexponential factors (and the reverse recombinations), since the change of several internal modes of vibration in the reactant to free rotations in the activated complex must be associated with abnormally large entropies of activation. However, in calculations of *ratios* of rate constants for isotopic molecules, the decoupled fragment approximation has a broader range of validity. If the activated complex has a "loose" structure, with weakly coupled fragments, motions between fragments involve vibrations of much lower frequency than motions within fragments. The approximate separation of high and low frequencies[8] can then be applied to factor the secular equation into intra- and interfragment parts. The low-frequency, interfragment vibrations, although very

(1) Presented at the Fifth Symposium on Stable Isotopes, Leipzig, Oct 1967.

(2) To whom reprint requests should be addressed.

(3) J. Bigeleisen and M. Wolfsberg, *Advan. Chem. Phys.*, **1**, 15 (1958).

(4) E. B. Wilson, J. C. Decius, and P. C. Cross, "Molecular Vibrations," McGraw-Hill Book Co., Inc., New York, N. Y., 1955.

(5) H. S. Johnston, W. A. Bonner, and D. J. Wilson, *J. Chem. Phys.* **26**, 1002 (1957).

(6) M. Wolfsberg and M. J. Stern, *Pure Appl. Chem.*, **8**, 225 (1964).

(7) Reviewed by B. S. Ravinovitch and D. W. Setser, *Adv. Photochem.*, **3**, 1 (1964).

(8) Reference 4, p 75.

important in calculations of an individual rate constant, have little effect on the continued product in eq 1, since $(u/2)^{-1} \sinh (u/2)$ approaches unity for small u. The rows and columns of the secular equation that correspond to interfragment motions can, therefore, be deleted, and the approximate frequencies of internal vibrations of the fragments, obtained from the reduced secular equation, can be used in eq 1.

For dissociation (or recombination) reactions involving rupture (or formation) of one bond, the activated complex is treated as two fragments, and the motion in the reaction coordinate is the change in the distance between the centers of mass of the two fragments. Thus $\nu_x^{\ddagger\prime}/\nu_x^{\ddagger}$ becomes the square root of the ratio of the reduced masses of the two fragments.

Reactions involving simultaneous rupture or formation of two (or more) bonds can also be treated by this type of model, in terms of three (or more) uncoupled fragments. General formulations of $\nu_x^{\ddagger\prime}/\nu_x^{\ddagger}$ for three-center models that have been previously developed[9] are applicable in these cases. However, the reaction coordinate can be treated only in terms of interfragment motions; the reaction coordinate as a linear combination of internal displacements, within as well as between fragments, cannot be incorporated in this approach.

The molecular-fragment approach, which assumes a "loose" activated complex, cannot be applied to reactions that do not involve bond rupture of formation in the rate-determining step. In addition, of course, an assumption of equilibrium between reactants and activated complexes is implicit in the general formulation of eq 1.

Despite these limitations molecular-fragment models have a wide range of application. This approach should be particularly useful and valuable in dealing with large, complicated structures, because it provides simple, pictorial representations for various reaction mechanisms and greatly simplifies the calculation of activated-complex vibrational frequencies. Thus the method could be used, as the next approximation beyond noting the presence or absence of kinetic isotope effects, in distinguishing between alternate mechanisms, such as concerted or stepwise rupture of two bonds. It could also be used to estimate substituent effects in a series of analogous isotopic reactions.

Molecular-Fragment Calculations for Malonic Acid

We have used molecular-fragment models to calculate k_4/k_3 for malonic acid decarboxylation. We assumed that one carbon–carbon bond was so weak in the transition state that this structure could be treated as two independent fragments.

The secular equation was further simplified by omission of the four hydrogen atoms from the transition-state models. This is an application of the "cutoff" approximation of Stern and Wolfsberg.[10] In this case one can argue that characteristic group frequencies for
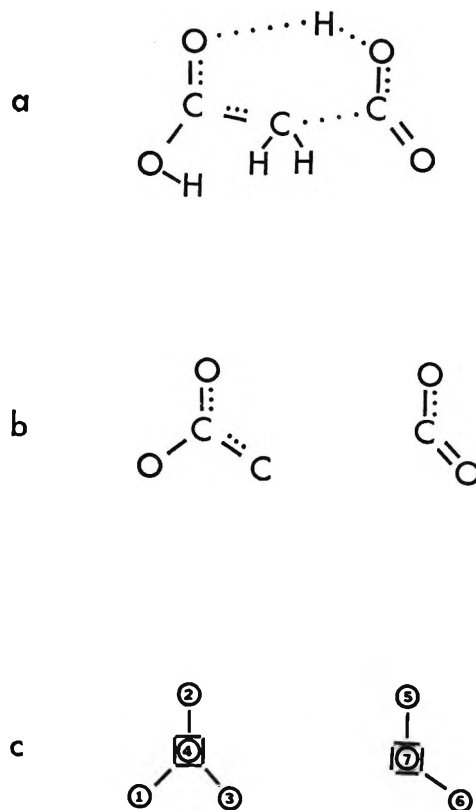
Figure 1. (a) Malonic acid transition-state model; (b) after cutoff and fragment approximations; (c) fragment model notation (boxed circles indicate sites of isotopic substitution).

hydrogen stretching and bending should be nearly identical for k_3 and k_4, since none of the hydrogens is bonded directly to either site of isotopic substitution. However, the proton masses were included in calculating the fragment reduced-mass ratio for $\nu_x^{\ddagger\prime}/\nu_x^{\ddagger}$.

With these "uncoupled" and "cutoff" approximations, the 11-center activated complex for malonic acid decarboxylation is treated as one four-center and one three-center fragment (Figure 1), and the 26th-order secular equation is reduced to one sixth-order and one third-order equation.

We have carried out model calculations for a number of fragment models of the type shown in Figure 1c. Specific models were selected by arbitrarily assigning a bond order to each bond and then empirically relating bond orders to bond lengths, bond angles, and force constants, according to the following procedure.

Assigned bond orders were: for the four-center fragment, 1 for bond 1–4, $2 - X$ for bond 2–4, and $1 + X$ for bond 3–4; for the three-center fragment, $1 + X$ for bond 5–7 and 2 for bond 6–7 (bonds are specified in terms of the notation of Figure 1c). A value of the parameter X, from 0 to 1, was specified

(9) J. Bigeleisen and M. Wolfsberg, *J. Chem. Phys.*, 21, 1972 (1953); 22, 1264 (1954); C. R. Gatz, *ibid.*, 44, 1861 (1966).

(10) M. J. Stern and M. Wolfsberg, *ibid.*, 45, 4105 (1966).

for each set of calculations; $X = 0$ corresponds to the reactant structure and $X = 1$ corresponds to the product structure, assuming enol formation in the rate-determining step.

The bond angle in the three-center fragment, ϕ_{576}, was assumed to be 120° for $X = 0$, 180° for $X = 1$, and a linear function of X for intermediate values. The four-center fragment was assumed to be planar, with all three bond angles equal to 120°, for all values of X.

Bond lengths for bond orders of 1 and 2 were estimated from compiled data[11] for stable molecules: 1.54 Å for C—C, 1.33 Å for C=C, 1.43 Å for C—O, and 1.22 Å for C=O. These bond lengths were assumed to vary linearly with bond orders between 1 and 2. In addition, small variations were made in the lengths of bonds 1-4 and 6-7. As X went from 0 to 1, r_{14} went from 1.37 to 1.43 Å and r_{67} went from 1.22 to 1.18 Å.

Similarly, stretching force constants were estimated for bond orders of 1 and 2 and were varied linearly with intermediate bond orders. The assigned stretching force constants,[12] in millidynes per ångstrøm, were 5.0 for C—C, 9.0 for C=C, 6.0 for C—O, and 13.0 for C=O. In addition, the C=O stretching force constant for bond 6-7 was varied from 13.0 to 15.0 mdyn/Å as X was varied from 0 to 1.

In assigning bending force constants, we assumed that for the four-center fragment all $f_{\phi\phi}/r_i r_j = 0.6$ mdyn/Å and that for the three-center fragment $f_{\phi\phi}/r_{57} r_{67}$ varied from 0.6 to 1.0 mdyn/Å, linearly with X. All interaction force constants were set equal to zero.

The above method for specifying fragment structures and force constants is arbitrary and empirical, and it is not intended to be accurate in detail. However, it does permit a systematic variation in transition-state models from reactant to product configurations in terms of the single parameter X. We have carried out calculations for a few models that did not fit this system and found that, in general, slight changes in the model produced correspondingly slight changes in the calculated isotope effect.

Three sets of models are shown in Figure 2. Bond lengths and stretching force constants and, for the three-center fragment, bond angle and bending force constant, are indicated in the figure. The fragment structures in model A approximate the corresponding portions of the reactant malonic acid. In model C they approximate the product structures, except that ϕ_{576} is 170°, rather than 180°, because our program was written for nonlinear structures. Model B is an intermediate case, with $X = 0.5$.

The calculated isotope effects for these models are compared with experiment in Table I. It can be seen that the intermediate set of fragment structures, model B, gives agreement with the experimental k_4/k_3. For this reaction, then, a molecular-fragment calculation
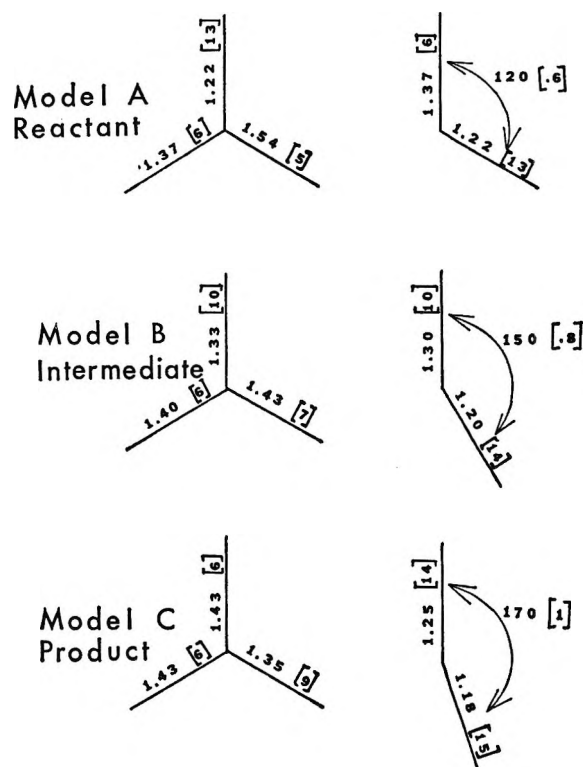
Figure 2. Malonic acid fragment models in calculations for Table I. Bond lengths (Å) and bond angles are shown with the corresponding force constants (mdyn/Å) in brackets. For four-center fragments, all angles are 120° and all $f_{\phi\phi}/r_i r_j = 0.6$ mdyn/Å.

for a chemically reasonable model is consistent with experiment. At present this is the most that can be claimed for any theoretical isotope-effect calculation.

Table I: Calculated and Experimental Values of k_4/k_3

	k_4/k_3 at		
	473°K	573°K	673°K
Model A	1.041	1.031	1.024
Model B	1.026	1.019	1.015
Model C	1.010	1.006	1.004
Experiment[a]	1.023 ± 0.004	1.017 ± 0.004	1.013 ± 0.004

[a] C. R. Gatz, Ph.D. Thesis, University of Illinois, Urbana, Ill., 1960.

(11) L. E. Sutton, Ed., "Tables of Interatomic Distances and Configurations in Molecules and Ions," Special Publication No. 11, The Chemical Society, London, 1958.

(12) Approximated from ref 4, p 175.

Stepwise Formation of Cyanide Complexes of Copper(I) in

Anion Exchangers[1]

by J. S. Coleman, R. George, L. Allaman,[2] and L. H. Jones

Los Alamos Scientific Laboratory, University of California, Los Alamos, New Mexico 87544   (*Received January 25, 1968*)

Strong-base anion exchanger in the cyanide form absorbs CuCN upon prolonged stirring of a slurry of the resin and solid CuCN in 0.0001 M HCN. Infrared spectra of samples cut from single resin beads exhibit peaks assignable to $Cu(CN)_4^{3-}$, $Cu(CN)_3^{2-}$, and $Cu(CN)_2^{-}$. The species $Cu(CN)_4^{3-}$ predominates when less than 0.3 mol of CuCN is absorbed per equivalent of exchange capacity. Titration with $HClO_4$ of anion exchanger containing absorbed CuCN yields estimates for the stepwise formation quotients within the resin. The values obtained are remarkably similar to those observed in aqueous solution.

Introduction

Absorption of complex ions by anion exchangers has proved to be a remarkably useful means for effecting separations.[3] The anion exchanger can be viewed as providing a separate phase with a high concentration of free ligand. The absorption of a given metal will reflect its tendency to form complex ions within the anion exchanger. The usefulness of this picture depends in large part on knowledge of the similarities and differences in complex formation in aqueous solutions and anion exchangers.

Information regarding complex formation within ion exchangers must be inferred very indirectly for most systems. For the present study, we have chosen a system suitable for direct spectroscopic examination and one in which essentially all of the absorbed metallic ion is retained by the anion exchanger over large changes in composition of the surrounding aqueous phase.

Our first purpose here is to demonstrate stepwise formation of complex ions within an anion exchanger on the basis of vibrational spectra of the individual species. Such a demonstration is uncommon even for formation of complex species in aqueous solution; some of the clearest evidence has come from studies of cyanide complexes[4] which exhibit narrow peaks in the infrared in a region relatively free of absorption by water. We draw for this purpose on the study of aqueous Cu(I)–cyanide complexes carried out at this laboratory.[5]

Our second purpose in the present study is to obtain estimates of the stepwise formation quotients for comparison with those obtained in aqueous solution. Titration with $HClO_4$ proved suitable for this purpose using anion exchanger containing various amounts of absorbed CuCN.

Experimental Section

Materials. The anion exchanger used throughout this study was a commercial preparation of the qua-

ternary ammonium type (Dowex 1-X10). Aqueous HCN was prepared by passing KCN through cation exchanger (Dowex 50) in the H^+ form; the cation exchanger columns were pretreated with NH_4SCN to remove the traces of iron typically present. Cuprous cyanide was prepared by dropwise addition of aqueous NaCN into a hot $CuSO_4$ solution.[6] Other reagents were of analytical reagent grade.

Absorption of CuCN. Prolonged stirring of a slurry of cyanide-form anion exchanger and solid CuCN in 0.0001 M HCN results in absorption of CuCN by the resin.

Cyanide-form anion exchanger was prepared by passing an excess of aqueous KCN through a column of resin initially in the chloride form; the resin was rinsed thoroughly with 0.0001 M HCN. The exchangeable CN^- was determined by displacement with NO_3^- and titration of the eluate with $AgNO_3$ to the AgI end point. We found 1.99 mmol of CN^-/g of air-dried chloride-form anion exchanger, a value equal to the exchange capacity of the chloride form determined in separate experiments.

Samples were prepared containing known amounts of CuCN and cyanide-form anion exchanger (50–100 mesh) slurried together in 0.0001 M HCN. The samples were stirred gently and examined from time to time with a microscope to see if the absorption of CuCN was complete. Complete absorption was noted after 2 days of stirring when 0.97 or less mole of CuCN was present per equivalent of exchange capacity.

(1) Work performed under the auspices of the U. S. Atomic Energy Commission.

(2) Participant in summer student program, LASL, 1961.

(3) F. Helfferich, "Ion Exchange," McGraw-Hill Book Co., Inc., New York, N. Y., 1962.

(4) J. M. Smith, L. H. Jones, I. K. Kressin, and R. A. Penneman, *Inorg. Chem.*, **4**, 369 (1965), and especially R. A. Penneman and L. H. Jones, *J. Chem. Phys.*, **24**, 293 (1956); **22**, 965 (1954).

(5) R. A. Penneman and L. H. Jones, *ibid.*, **24**, 293 (1956).

(6) H. J. Barber, *J. Chem. Soc.*, **79** (1943).

Absorption was incomplete for samples with 1.05 or more moles of CuCN per equivalent of exchange capacity even after 20 days of stirring. We conclude that cyanide-form anion exchanger absorbs CuCN until its composition corresponds to the $Cu(CN)_2^-$ form and that no further absorption occurs.

Infrared Spectra. Spectra of samples cut from single beads of anion exchanger were obtained using a Perkin-Elmer Model 112 spectrometer fitted with a commercial microscope attachment. Batches of cyanide-form anion exchanger were stirred with known amounts of CuCN to prepare resin samples containing the desired CN/Cu(I) ratios. Single beads were selected, surface dried, and immediately immersed in mineral oil. The beads were pressed into a section of Kel-F tubing for ease in handling. Flat surfaces were cut on the beads with a razor blade and the samples were ground to the desired thickness under oil using silicon carbide paper cemented to a microscope slide. Before use, the paper was leached with concentrated HCl and with 0.3 M KCN.

Spectra of samples containing various CN/Cu(I) ratios are shown in Figure 1. The $Cu(CN)_2^-$-form anion exchanger exhibits a single asymmetric peak with maximum absorption near 2100 cm^{-1}. At somewhat higher CN/Cu(I) ratios, a peak arises at 2091 cm^{-1}. With 3.4 CN per Cu(I), an additional, well-resolved peak is evident at 2069 cm^{-1}. Absorption at this last frequency predominates at higher ratios.

From micrometer measurements of sample thickness and the known exchange capacity of the resin, an extinction coefficient of about 190 M^{-1} cm^{-1} is estimated for the $Cu(CN)_2^-$ absorption maximum near 2100 cm^{-1}. The extinction coefficients at the maxima for the species absorbing at 2091 and 2069 cm^{-1} are estimated to be 5–8 times greater than for $Cu(CN)_2^-$. Cyanide-form anion exchanger exhibits an absorption maximum at 2071 cm^{-1} with an extinction coefficient of about 35 M^{-1} cm^{-1}. Some samples were dried over $Mg(ClO_4)_2$ before spectra were obtained; the peaks at 2100, 2091, and 2069 cm^{-1} were shifted to 2095, 2086, and 2063 cm^{-1}, respectively.

Although the principal features of the spectra illustrated in Figure 1 proved highly reproducible, we concluded that quantitative measurements of absorbance were not feasible. Over periods of several hours, increasing absorption arose at 2155 cm^{-1} which was eventually found to be due to formation of NCO^-. Further, the reproducibility in absolute peak heights proved unsatisfactory.

Titration of Cyanide-Form Anion Exchanger Containing Absorbed CuCN. Perchloric acid was added to about 500 ml of water in contact with 10 g of anion exchanger containing various amounts of absorbed CuCN. Our results are shown in Figure 2. We used a continuous flow system similar to that illustrated by Marcus and Maydan.[7] The resin and solution were
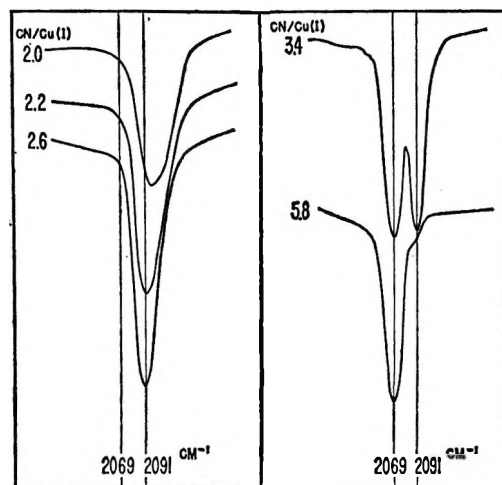
Figure 1. Infrared spectra of cyanide-form anion exchanger containing absorbed CuCN.
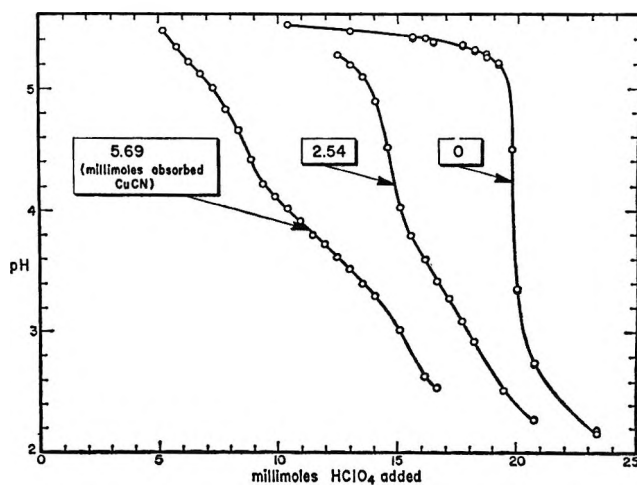
Figure 2. Titration of cyanide-form anion exchanger containing various amounts of absorbed CuCN; conditions: 10.0 g of anion exchanger in contact with about 500 ml of water at 25° with continuous circulation.

maintained in contact in a well-stirred flask. A portion of the solution was drawn continuously through a filter stick by a peristaltic pump, passed through a heat exchanger immersed in a 25° bath, and finally sprayed down the sides of the flask. The system was closed to the atmosphere. A Beckman Model G pH meter was used for the measurement of acidity.

Essentially all of the Cu(I) remained in the anion exchanger throughout the titration. We checked for removal of Cu(I) using a sodium polysulfide precipitation test. Sensitivity of the test was established using solutions of very sparingly soluble CuCN in 0.0001–0.01 M HCN. We conclude that less than 0.2% of the Cu(I) initially present appeared in the aqueous phase.

(7) Y. Marcus and D. Maydan, Israel Atomic Energy Commission Report 1A-764(1962).

Discussion

Assignment of Infrared Absorption. The absorption band at 2100 cm^{-1} may be assigned confidently to $Cu(CN)_2^-$ on the basis of the composition of the CuCN-saturated resin. Absorption bands at two other frequencies are observed as the CN/Cu(I) ratio is increased. The trends with CN/Cu(I) ratio are remarkably similar to those observed by Penneman and Jones[5] in the aqueous KCN–CuCN system. Using this analogy, we assign the absorption at 2091 cm^{-1} and 2069 cm^{-1} to $Cu(CN)_3^{2-}$ and $Cu(CN)_4^{3-}$, respectively.

The presence of the resin framework exerts no striking influence on either the frequencies or the intensities of the observed bands, though a slight shift toward lower frequencies may be noted. The absence of substantial effects attributable to the resin provides impressive evidence that the structure of the complex ions is essentially unaffected by absorption in anion exchangers.

Formation Curve for Cu(I)–Cyanide Complexes in Anion Exchanger. When $HClO_4$ is added to cyanide-form anion exchanger, HCN is formed and perchlorate ions go into the resin. The same thing happens when part of the CN$^-$ in the resin is tied up in complex ions, but now, as the titration curves of Figure 2 show, no sharp end point is observed. The titrations provide a direct measure of the average charge on the Cu(I) complexes within the anion exchanger, denoted here by $\bar{z}$. At any point in the titrations, the amount of ClO_4^- in the anion exchanger, n_{ClO_4}, may be calculated, and the additional negative charge to satisfy the exchange capacity must be distributed among the complex ions and free CN$^-$ in the resin. Over most of the pH range of these experiments, the concentration of free CN$^-$ is very small compared to that of the complex ions. The average charge is then given by

$$\bar{z} = (q - n_{ClO_4})/n_{Cu} \tag{1}$$

in which q is the exchange capacity in milliequivalents and n_{Cu} denotes the millimoles of absorbed CuCN.

To deduce formation quotients within the anion exchanger, we also need an estimate of the free CN$^-$ concentration in the resin at each point in the titration. For this we consider the exchange equilibrium

CN$^-$ (in anion exchanger) $+ H^+(aq) + ClO_4^-(aq) =$

   HCN(aq) $+ ClO_4^-$ (in anion exchanger) (2)
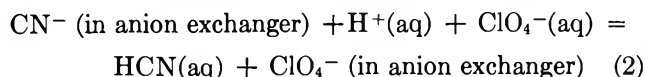
Over most of the pH range, the concentration of CN$^-$ in the aqueous phase, (CN$^-$), is much smaller than that of ClO_4^-. To maintain charge balance

$$(ClO_4^-) = (H^+)$$

since these are the only aqueous phase ions present in appreciable amounts in the pH range being considered. The concentration of ClO_4^- in the anion exchanger,

$\{ClO_4^-\}$, is related to the millimoles of titrant added, N, according to

$$w\{ClO_4^-\} = N - v(ClO_4^-) \tag{3}$$

where w and v are the weight of anion exchanger and volume of aqueous phase, respectively, and the concentration units for ions in the anion exchanger are millimoles per gram. The amount of HCN present is also given by $w\{ClO_4^-\}$; the HCN will be distributed between the two phases with a distribution constant, K_D, given by

$$K_D = \{HCN\}/(HCN) \tag{4}$$

We can thus set

$$(HCN) = w\{ClO_4^-\}/(v + wK_D) \tag{5}$$

The concentration of free CN$^-$ in the anion exchanger is given by

$$\log\{CN^-\} = -\log K_z\left(\frac{v}{w} + K_D\right) + 2\log\{ClO_4^-\} + 2pH \tag{6}$$

where K_z is the equilibrium constant for (2).

In applying these relations to our titrations, small corrections were necessary to account for volume changes, loss of reagents when samples were withdrawn for the pH measurements, and, at the higher pH values, for the presence of CN$^-$ in the solution and in the anion exchanger. Titrations of the Cu(I)-free anion exchanger were used to estimate $\log K_z [(v/w) + K_D]$ which appears in eq 6; we obtain 13.34 $\pm$ 0.14. Figure 3 shows $\bar{z}$ as a function of $\{CN^-\}$.

We may also express $\bar{z}$ in terms of the stepwise formation quotients K_3 and K_4, where

$$K_3 = \{Cu(CN)_3^{2-}\}/\{Cu(CN)_2^-\}\{CN^-\}$$
$$K_4 = \{Cu(CN)_4^{3-}\}/\{Cu(CN)_3^{2-}\}\{CN^-\}$$

so that

$$-\bar{z} = \frac{1 + 2K_3\{CN^-\} + 3K_3K_4\{CN^-\}^2}{1 + K_3\{CN^-\} + K_3K_4\{CN^-\}^2} \tag{7}$$

The curves in Figure 3 were constructed using eq 7. The titrations with 0.569 and 0.254 mmol of absorbed CuCN/g of anion exchanger give similar but slightly different formation curves. At the lower loading, we used $\log K_3 = 4.85$ and $\log K_4 = 1.85$; at the higher loading, we took $\log K_3 = 4.60$ and $\log K_4 = 2.03$.

It seems remarkable that these equilibria may be represented so simply. In the derivation of eq 6 and 7, we have assumed constancy of activity coefficients in the face of very high molalities and the expected major changes in the average charge on the anions. The formation curves in Figure 3 are the first to describe complex formation within an anion exchanger. They provide an encouraging basis for treatment of
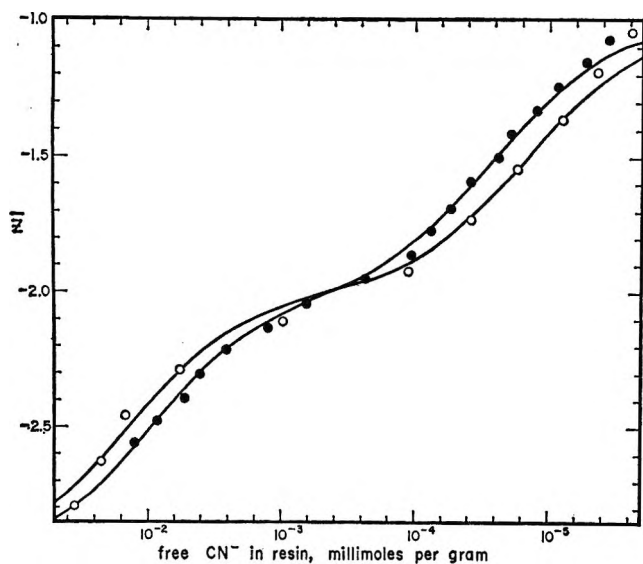
Figure 3. Formation curves for cyanide complexes of Cu(I) in anion exchanger; open circles, 0.254 and filled circles, 0.569 mmol of absorbed CuCN/g of air-dried anion exchanger.

Table I: Formation Quotients for $Cu(CN)_3{}^{2-}$ and $Cu(CN)_4{}^{3-}$ in Anion Exchanger and in Aqueous Solution at 25°

| | Anion exchanger | | |
	High loading[a]	Low loading[a]	Aqueous solution[a]
Log K_3/K_4	2.58	3.00	2.57
Log K_3	4.60	4.85	4.82
Log K_4	2.03	1.85	2.24

[a] Concentration units are millimoles per gram of air-dried resin for columns 2 and 3 and molarity for column 4.

complex formation within anion exchangers with the same formalism commonly applied to aqueous solutions.

Even more remarkable is the similarity of the formation quotients to those found by Penneman and Jones[5] in aqueous solutions. The clearest comparison is that of the K_3/K_4 ratios since in this case the concentration units cancel out. At the higher loading, we find log (K_3/K_4) = 2.57. Penneman and Jones[5] report that in aqueous solution at 25° log (K_3/K_4) = 2.58 as shown in Table I. We do not have satisfactory measurements of the amount of water taken up by the resin in the presence of absorbed CuCN for use in conversion of the measured K's to more rational concentration units. However, since the Cl^--form anion exchanger in water contains roughly 1 g of absorbed water/g of air-dry resin, the units used can be considered roughly equivalent to millimoles per gram of absorbed water (i.e., molality). The uncertainty in the water content is likely smaller than the uncertainty in log K_x $[(v/w) + K_D]$ which enters

directly into the separate evaluation of log K_3 and log K_4.

The close agreement of the formation quotients in aqueous and anion-exchanger systems must be somewhat fortuitous. The differences are small, for example, compared to those induced by modest temperature changes.[5] In our experiments, we calculate that the ratio of $Cu(CN)_4{}^{3-}$ to free CN^- was initially 5.9 in the highly loaded anion exchanger and 0.62 at the lower loading. In both cases, a major fraction of the exchange capacity was occupied by Cu(I) complexes.

Conclusions

We reach the following conclusions. (1) Stepwise formation of $Cu(CN)_2{}^-$, $Cu(CN)_3{}^{2-}$, and $Cu(CN)_4{}^{3-}$ occurs in quaternary amine anion exchangers. Formation of the lower complexes occurs at high levels of CuCN absorption and upon acidification of a surrounding aqueous phase. (2) The complex ions exhibit infrared absorption similar to that observed with the corresponding ions in aqueous solution, which indicates that their structure is not strongly affected by presence of the resin framework. (3) Formation of Cu(I) cyanide complexes in anion exchangers is well represented using formation quotients invariant with free CN^- concentration. (4) The magnitudes of the formation quotients are remarkably similar to the corresponding quotients in aqueous solution.

An X-Ray Study of the Participation of the Bulk Phase of

Cobalt Oxide in Oxidation Catalysis

by Richard M. Levy

Central Research Department, Monsanto Company, St. Louis, Missouri (*Received January 25, 1968*)

Although catalysis is ordinarily associated with surface reactions, certain metal oxides, such as cobalt oxide, exhibit profound changes in bulk-phase composition during catalytic oxidation. We have studied the bulk-phase transformations accompanying the oxidation of hydrocarbons using *in situ* X-ray diffraction, a method which allows measurement under reaction conditions, *i.e.*, high temperature and a reactive gas atmosphere. This technique permits us to perform successive measurements on the same solid sample at different conditions, and results in enormous time-saving over conventional X-ray diffraction. The data reveal a stable coexistence of Co_3O_4 and CoO in the presence of a hydrocarbon–air mixture. The proportion of these two phases is shown to vary in a regular fashion with temperature, hydrocarbon-to-air ratio, reaction initiation procedure, and precalcination temperature of the sample. This variation allows a computation of the activation energy for reorientation of the catalyst and indicates a very rapid ionic diffusion within the solid. From the data, it can be demonstrated that within a range of conditions determined by the prior treatment of the catalyst, a constancy exists in the order of the reaction between the solid and the gas phase.

Introduction

The equilibrium between oxides of two different oxidation states of a metal has been shown in numerous cases to depend solely upon temperature and oxygen pressure.[1] The equilibrium constant has been well characterized, univariant equilibrium occurring generally at temperatures above 900° for transition metal oxides. The kinetics of equilibration have been attributed to the rates of diffusion of ions through the metal oxide lattices.[2]

The readily characterizable equilibrium between a solid phase and a gaseous phase consisting only of oxygen suggests the possibility of adding a hydrocarbon to the vapor phase and studying the phase relations under conditions of temperature and pressure which lead to catalytic oxidation of the hydrocarbon over the metal oxide. Current hypotheses view this oxidation as primarily a surface phenomenon, with the relative rates of surface reduction and surface oxidation controlled by factors such as hydrocarbon-to-oxygen ratios, surface area, and temperature.[3] However, predicted and observed relationships between the details of the oxidation and the properties of the bulk solid[4] indicate that the bulk phase may indeed play a major role in hydrocarbon oxidation. Accordingly, one may hope to derive information on surface changes from details of bulk properties.

We have studied a simple hydrocarbon oxidation by observing the X-ray diffraction pattern of the bulk phase of a metal oxide under external conditions at which changes in the bulk composition occur. The measurements were made in a specially designed attachment to an ordinary XRD unit, which allowed us to record spectra of oxides equilibrated under various temperature and gas partial-pressure environments applied *in situ* in the XRD cell. This *in-situ* cell enabled us to monitor continuously the structure of the solid phases and resulted in enormous time-saving over the usual technique of preparing a sample in a separate reactor, quenching, crushing, and mounting in the X-ray diffraction apparatus.

Preliminary measurements showed that under typical oxidation conditions, approximately equal partial pressures of oxygen and hydrocarbon, and temperatures in the range 250–500°, several metal oxide systems exhibited multiple oxidation states equilibrated in proportions determined by the gas mixture. Using *in situ* X-ray diffraction, we determined, for example, that conditions could be found which lead to stable mixtures of differing oxidation states of manganese oxide and of iron oxide. The system $CuO-Cu_2O-Cu^0$ has previously been investigated by Russian workers,[5] as well as by our group,[6] using *in situ* X-ray diffraction techniques. We have chosen for detailed elucidation the system Co_3O_4-CoO, cobalt oxides being among the most active of the oxidation catalysts[7] and permitting the widest choice of convenient operating conditions.

(1) H. M. O'Bryan and G. Parravano, "Reactivity of Solids," Elsevier Publishing Co., Amsterdam, 1965, pp 256–268.

(2) H. M. O'Bryan, "Univariant Equilibrium Between the Oxides of Cobalt and Related Reaction Kinetics," Ph.D. Thesis, University of Michigan, 1963.

(3) G. L. Simard, J. F. Steger, R. J. Arnott, and L. A. Siegel, *Ind. Eng. Chem.*, 47, 1424 (1955).

(4) Ya. B. Gorokhovatskii, I. I. Vovyanko, and M. Ya. Rubanik, *Kinetika i Kataliz*, 7, 76 (1966).

(5) O. V. Isaev and M. Ya. Kushnerev, *Dokl. Akad. Nauk SSSR*, 124, 858 (1959).

(6) E. D. Pierron, J. A. Rashkin, and J. F. Roth, *J. Catalysis*, 9, 38 (1967).

As an indication of the appropriate operating conditions, an analysis of the ranges of stability of the various phases of cobalt and its oxides was performed using the *in-situ* reactor. The temperature limits and gas atmospheres requisite for the existence of various phases are shown graphically in Figure 1. All transformations in this system were practically instantaneous at the temperatures indicated.

Experimental Section

Starting catalysts of Co_3O_4 were prepared by the vacuum heating of reagent grade $Co(NO_3)_2 \cdot 6H_2O$ at 150° for 24 hr. The resultant Co_3O_4 was ground to pass a no. 325 mesh, slurried in benzene, and spread on a strip of platinum in a layer 1 cm² in area and about 0.5 mm thick. The platinum stage is mounted vertically in a parafocussing geometry in the X-ray unit and forms a low resistance electrical contact between the electrodes in the *in-situ* reactor. Temperatures up to 1000° could be achieved in the sample by applying currents of up to 100 A at a potential of 5 V. Temperatures were measured by a Pt–Rh thermocouple affixed to the Pt strip.

The reaction chamber was a Materials Research Corporation Model X-86-G high-temperature diffractometer attachment designed to fit onto a standard General Electric XRD-5 diffractometer. Beryllium windows allowed the passage of X-rays, and O-ring seals ensured a leak-proof gas flow through the reactor.

Gases were premixed at atmospheric pressure in quantitative proportions using calibrated flow meters. Phillips pure grade *n*-butane, or Matheson CP propylene, was mixed at room temperature with cylinder air and passed, at atmospheric pressure, over the heated catalyst at a total flow rate of 100 cc/min. Air-to-hydrocarbon mole ratios ranged from 5:1 to 1:1.

Spectra of the catalysts were taken at various temperatures and partial pressures using the Mo Kα line generated at 40 kV and 16 mA and filtered through zirconium foil. Periodic checks were made to ascertain that an invariant system had been attained and to compare the spectra taken at reaction conditions and at room temperature. Equilibration was always virtually instantaneous, and room temperature and reaction-condition spectra were always the same.

The per cent by volume of the coexistent phases in the catalyst was determined, according to the procedure described by Beu,[8] from the area under the diffraction peaks uniquely characteristic of the respective species, Co_3O_4 and CoO. Resolution of closely lying peaks as well as area measurements were facilitated by a Dupont Model 310 curve resolver.

The analytical peaks selected for Co_3O_4 and CoO were, respectively, at 26.42° 2θ (511 reflection) and 27.28° 2θ (220 reflection).[9] The response factors for these peaks were determined to be approximately equal, so that the integrated areas under the peaks could be used as a
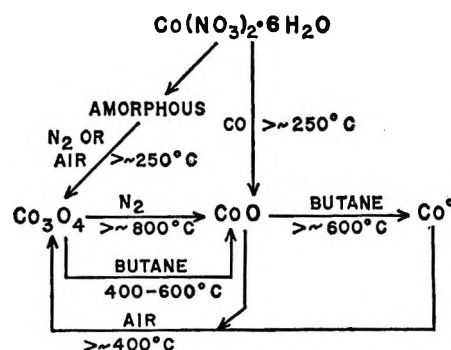
Figure 1. Phase relations of the decomposition products of cobalt nitrate in the presence of various gas atmospheres.

direct measure of the volume ratio of phases, $V_{Co_3O_4}/V_{CoO}$. The ratio of these areas was determined using the Dupont curve resolver. Background correction was estimated from the base line on either side of the peaks. The curve resolver was operated by combining symmetrical peaks which fit the line shapes of the pure components. The height and width of these symmetrical peaks were adjusted until the curve resolver gave, by visual judgment, the best match with experimental data. The total volume under both peaks was normalized to 100 and the relative contribution of each peak was read directly off the intensity gauge on the curve resolver.

The full width at half maximum for the peaks varied from 0.4° 2θ for over 50% of a given component to 0.5° 2θ for 10% of a given component. Thus, the best resolution was obtained at $V_{Co_3O_4}/V_{CoO} = 1$, and the worst where one component greatly exceeded the other in volume. The errors indicated in the accompanying figures are a measure of the changing resolution and the estimated uncertainty in the peak area determinations.

Data

The logarithm of $V_{Co_3O_4}/V_{CoO}$ has been plotted as a function of reciprocal temperature for a number of conditions. The data in Figure 2 typify the kind of information gained from the *in-situ* experiments. A sample of Co_3O_4 was placed in the cell and a mixture of butane and air passed over it at a total flow rate of 100 cc/min. The cobalt oxide temperature was linearly increased until CoO lines grew into the diffraction pattern due to reduction of the Co_3O_4 by the butane. The relative areas under the CoO and Co_3O_4 peaks were used to compute $V_{Co_3O_4}/V_{CoO}$ at several different temperatures. Each of the approximately parallel lines in Figure 2 represents data obtained as a function

(7) K. C. Stein, J. J. Feenan, L. J. E. Hofer, and R. B. Anderson, U. S. Bureau of Mines Bulletin 608, U. S. Government Printing Office, Washington, D. C., 1962.

(8) K. E. Beu in "The Encyclopedia of X-Rays and Gamma Rays," Reinhold Publishing Corp., New York, N. Y., 1963, p 72.

(9) National Bureau of Standards Circular 9, U. S. Government Printing Office, Washington, D. C., 1959, p 539.
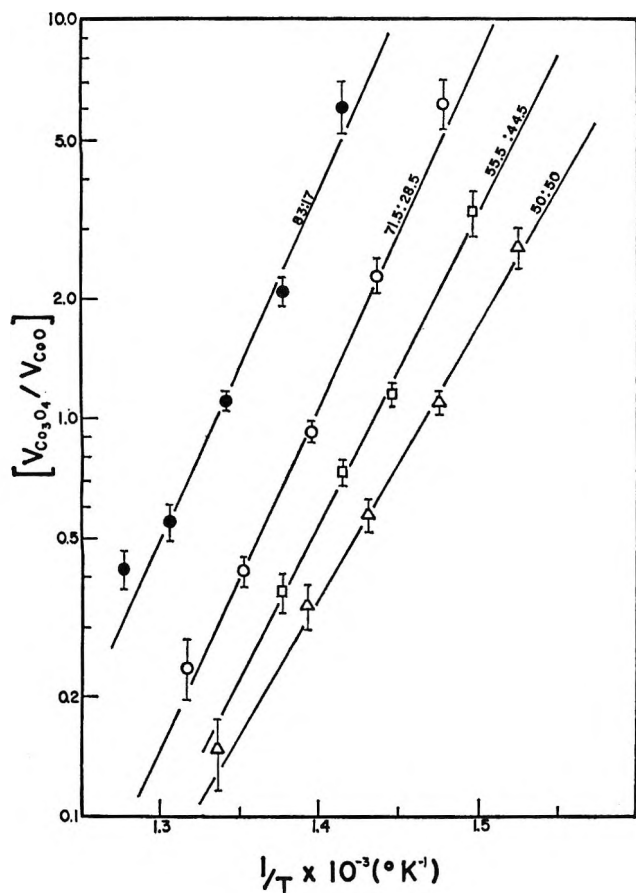
Figure 2. Semilogarithmic plots relating volume ratio of cobalt oxide phases to temperature. Air–butane flow rates, in cc/min, are indicated on the figure, each set of points representing the data from a fresh sample of cobalt oxide which had been precalcined at 600° in air.

Figure 3. Dependence of plots of log $V_{Co_3O_4}/V_{CoO}$ vs. $1/T$ on precalcination temperature. Precalcinations were carried out, at temperatures indicated on plots, for 20 min in air.

of temperature, using a different ratio of butane to air and a fresh catalyst charge.

All of the data in Figure 2 resulted from a starting charge of Co_3O_4 which had been pretreated by heating at 600° in air for 20 min. Analogous families of semilogarithmic plots were obtained for samples which had never previously been heated above 250°. Finally, runs were made for a single hydrocarbon-to-oxygen ratio on samples precalcined for 20 min at 700 and 800°. Data showing the dependence upon calcination temperature are plotted in Figure 3.

In each individual run, with a given gaseous environment and a fresh catalyst charge, an approximately straight line could be drawn in plotting log $[V_{Co_3O_4}/V_{CoO}]$ vs. $1/T$. However, probable errors in slope and intercept for each line, i.e., reproducibility, are estimated to be about ±18% and ±3%, respectively, due to slight differences in the initiation of the autothermal oxidation reaction (see below), the precision of the flow controllers, and the subjectivity in estimating the best straight line. For this reason, triplicate runs were taken for most of the data reported. The effective enthalpy, ΔH, calculated from the aver-

age of the slopes in the triplicate runs, and the average value of T at the point where $V_{Co_3O_4} = V_{CoO}$ are given in Table I. Estimated errors in the quoted values are ±10% and ±2%, respectively.

Table I: Summary of Cobalt Oxide Phase Relations

Pre-treatment temp, °C	Air flow, cc/min	Butane flow, cc/min	ΔH, kcal/mol	Temp for $V_{Co_3O_4} = V_{CoO}$, °C
250	83	17	19.8	439
250	71.5	28.5	19.8	400
250	55.5	44.5	20.4	383
250	50	50	20.1	370
600	83	17	32.2	479
600	71.5	28.5	32.8	441
600	55.5	44.4	30.8	423
600	50	50	30.4	410
700	83	17	81.4	412
800	83	17	132	467

It is important to note that in all of the above cases, operating conditions lead to regular incremental changes in the bulk properties, resulting in linear semilogarithmic plots. This is not always the case. When samples were reduced and then oxidized by alternating the direction of the temperature changes, decidedly irreversi-
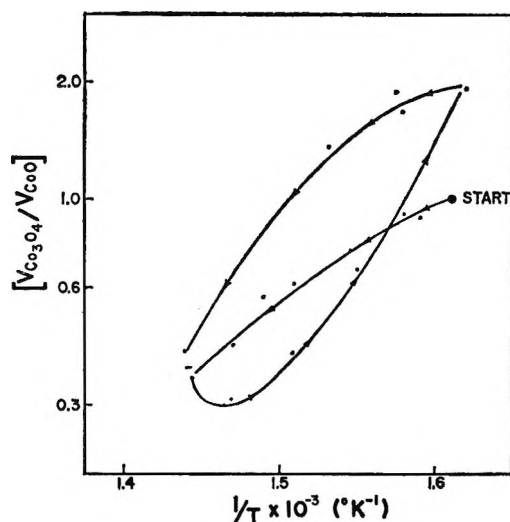
Figure 4. Evidence of irreversibility in plots of log $[V_{Co_3O_4}/V_{CoO}]$ vs. $1/T$. Butane and air flow rates were held at 28.5 and 71.5 cc/min, respectively. Pretreatment of sample consisted of four successive reductions and oxidations in butane and air, respectively, at 600°.

ble behavior was found, as illustrated in Figure 4. Even after four successive reductions and oxidations in butane and air, respectively, at 600°, this irreversibility remained.

A further complicating factor was the 50–200° exotherm observed when the autothermal oxidation commenced. To assess the effect of this exotherm upon bulk properties, mixtures of a highly reactive hydrocarbon, propylene, with air were passed over the catalyst, and temperatures were slowly increased. During the first 10–20 sec of the autothermal reaction, the degree of temperature rise in the catalyst could be controlled by external manipulation of current to the resistance heater in the *in-situ* cell. The temperatures could be allowed to rise to a very high value due to the reaction exotherm, then to fall quickly to a steady-state value within 20 sec, or could be controlled to rise asymptotically to the same constant value. In view of the sensitivity of the bulk phases to the past history of the catalyst, these diverse temperature conditions should affect the crystalline properties of the bulk phase. This emphatically occurs, as shown in Figure 5, where four different plots result from different degrees of temperature overshoot on the same catalyst subjected to the same air–propylene mixture. For all of the runs involving butane and air, the overshoot was constrained as carefully as possible to give an asymptotic approach to the constant exotherm.

Discussion

Ordinarily, in systems in which a metal oxide is reduced, the coexistence of phases would be ascribed to a vanishingly small reduction rate caused by diffusion limitations. This coexistence would represent a metastable equilibrium involving Co_3O_4, CoO, and O_2, and
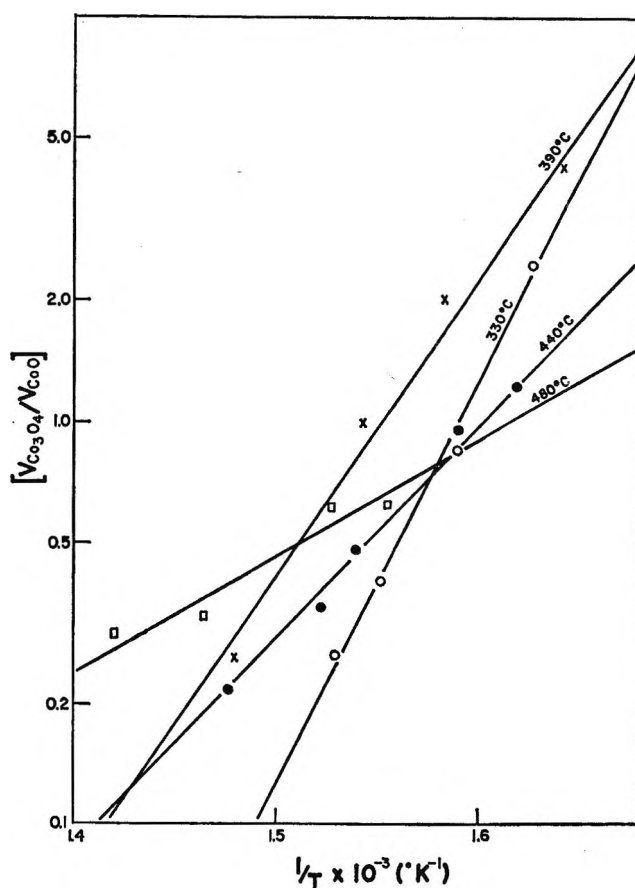
Figure 5. Temperature dependences of the volume ratio of phases, $V_{Co_3O_4}/V_{CoO}$, under a flowing atmosphere of 17 cc/min of propylene and 83 cc/min of air. Different temperatures indicated on the figure represent the maximum catalyst temperature immediately after the onset of the autothermal reaction. Equilibrium temperatures, recorded 1 min after the start of the reaction, always fell to around 330°.

at the temperatures of our work would occur at oxygen partial pressures of 10^{-8} atm or less.[2] Our data indicate that this is not the phenomenon we are observing with Co_3O_4–CoO prepared as stated. The system generates coexistent phases virtually instantaneously at much higher P_{O_2} and maintains an invariant value of $V_{Co_3O_4}/V_{CoO}$ for at least 2 hr under reaction conditions. Typical diffusion-limited systems would parabolically approach either complete reduction or a metastable configuration of two distinct valence states.

The stable, coexistent phases in cobalt oxide must accordingly arise from equal rates of oxidation of CoO and reduction of Co_3O_4 in the hydrocarbon–air mixture. Our data indicate, moreover, that these rates depend not only upon the partial pressures of gaseous reactants, but also upon the volumes of the cobalt oxide phases. Thus, we may write

$$\text{rate of oxidation} = k_1 f(V)[O_2]^n e^{-H_0^{\ddagger}/RT} \qquad (1)$$

$$\text{rate of reduction} = k_2 f'(V)[HC]^m e^{-H_r^{\ddagger}/RT} \qquad (2)$$

where $f(V)$ and $f'(V)$ are some functions of the volumes

of Co_3O_4 and/or CoO, k_1 and k_2 are constants, $[O_2]^n$ and $[HC]^m$ are partial pressures of oxygen and hydrocarbon raised to some power, and $H^{\ddagger}$ is an activation energy. Setting the rate of oxidation and the rate of reduction equal, and rewriting in a form consistent with our data, we have

$$[V_{Co_3O_4}/V_{CoO}] = k\frac{[O_2]^n}{[HC]^m}e^{-\Delta H/RT} \quad (3)$$

with $\Delta H = H_0^{\ddagger} - H_r^{\ddagger}$, $k = k_1/k_2$, and $[V_{Co_3O_4}/V_{CoO}] = f'(V)/f(V)$. Equation 3 is empirically derived and gives no direct indication of the exact form of $f(V)$ or $f'(V)$.

Two aspects of eq 3, the origin and magnitude of ΔH and the constancy of m and n (indicated by the linearity of the semilogarithmic plots), are of particular interest.

The values of ΔH allow us to distinguish between the two possible rate-determining factors in the oxidation and the reduction reactions. In an oxidation (or reduction) limited by the rate of the surface reaction, activation energies of less than 20 kcal/mol are common.[10] Our measured ΔH (Table I), the difference in activation energies, is clearly too large to reflect exclusively surface rates, and must derive in a large part from properties of the bulk phase, presumably from diffusion rates within the bulk.

Table I, for example, shows that oxidative precalcinations at temperatures from 250 to 800° lead to ΔH values ranging from 19 to 132 kcal/mol. The direction and magnitude of these changes point to a considerable thermodynamic stabilization of the bulk-phase Co_3O_4 with respect to the CoO formed from it. This stabilization of the lattice, corresponding to a progressive annealing of defects, is enhanced by time and high temperature. We may arbitrarily assign kinetic parameters to this reorganization of the cobalt oxide lattice by assuming an Arrhenius rate of reorganization

$$\frac{dH}{dt} = ke^{-H_{reorg}^{\ddagger}/RT} \quad (4)$$

and

$$\Delta H = e^{-H_{reorg}^{\ddagger}/RT}\int_0^t k(t)dt \quad (5)$$

The term under the integral accounts for the time variation in the enthalpy of the lattice. A plot of log ΔH vs. the $1/T$ values corresponding to calcination temperatures of 600, 700, and 800° gives a straight line indicating the approximate constancy of the integral in eq 5 and allowing a measure of the activation energy for lattice stabilization. The latter computation gives

$$H_{reorg}^{\ddagger} = 17 \text{ kcal/mol} \quad (6)$$

This value is consistent in magnitude with the activation energy for an order-disorder transformation in a typical solid.[11]

A similar treatment may also be applied to the data describing the effect of reaction initiation upon the ΔH associated with the phase transitions in the cobalt oxide. In this case, the overshoot temperature may be considered a momentary precalcination temperature. The atmosphere, in these "pretreatments," contains both hydrocarbon and air, so that we find now a growing temperature stabilization of CoO with respect to Co_3O_4, higher temperatures leading to lower ΔH values. A plot of log ΔH vs. the reciprocal of the overshoot temperature gives an approximately straight line with a slope corresponding to a reorganization activation energy of about 6 kcal/mol for the CoO. The relatively low value is probably due to the concurrent stabilization of both CoO and Co_3O_4, leading to only a slight change in the difference of their enthalpy contents.

The linearity of the semilogarithmic plots implies a constancy in the order of the reaction between gaseous components and the solid catalyst, i.e., m and n in eq 3. Thus, to the extent that the oxidation reaction involves a direct interaction of hydrocarbon and metal oxide, the reaction is one of constant selectivity. The ranges of conditions leading to this constancy vary with the history of the catalyst and must be taken into consideration when comparing catalysts. Typical temperature ranges for constant reaction order are shown in Table II.

Table II: Typical Temperature Ranges of Constant Reaction Order

Maximum pretreatment temp, °C	Pretreatment atmosphere	Temperature range, °C
250	Air	325–555
600	Air	400–550
700	Air	385–435
800	Air	445–485
330	Air–propylene	300–410
390	Air–propylene	310–430
400	Air–propylene	270–430
480	Air–propylene	180–510

The origin of the irreversibility (Figure 4) in this model cannot be determined from X-ray diffraction data alone. It could be (1) an experimental artifact arising from the growth of layers of oxide from the surface inward; (2) an indication of irreversible changes in physical properties such as pore volume and crystallite size; or (3) a measure of the defect concentrations in Co_3O_4 and CoO. Further study of these possibilities is warranted.

(10) F. S. Stone, R. Rudham, and R. L. Gale, Z. Elektrochem., 63, 129 (1959).

(11) W. Jost, "Diffusion in Solids, Liquids, and Gases," Academic Press, New York, N. Y., 1952, Chapters 2 and 3.

In summary, we consider the cobalt oxide system to be unique in that it supports a steady-state coexistence of two distinct phases in a hydrocarbon–air atmosphere. This is made possible by facile bulk-phase diffusion accompanying both oxidation and reduction. The data indicate that, although quite fast, diffusion in the solid is the rate-controlling step in the reactions of cobalt oxide with the gas phase. Furthermore, the order of the reaction between the gaseous components and the solid does not change in the regime of coexistent phases. It is shown that for systems such as cobalt oxide used as an oxidation catalyst, past history is extremely critical and must be carefully controlled.

Low-Frequency Raman Spectra of Aqueous Solutions of

Formates and Acetates[1]

by L. A. Blatz and Peter Waldstein

University of California, Los Alamos Scientific Laboratory, Los Alamos, New Mexico 87544   (*Received January 28, 1968*)

The Raman spectra of aqueous solutions of sodium and ammonium formate and acetate below 400 cm^{-1} can be largely attributed to the effects of primary hydration of the anions. Some spectral evidence of primary coordination between ammonium and formate ions has been found in concentrated ammonium formate solutions.

Introduction

Interactions between electrolytes and water in aqueous solutions have been the subject of considerable study by infrared and Raman techniques.[2–7] These interactions are sometimes classified as "structure making" (tending to promote order in the solvent water) if the spectrum of the solution at some temperature is like that of water at a lower temperature, or "structure-breaking" if the spectrum is like that of water at a higher temperature. A solution spectrum different in appearance, or in temperature behavior, from that of pure water can be taken as evidence of specific interactions (perhaps hydration of the ions) between the electrolyte and water.[2] The interpretation of the OH (or OD) stretching bands of water, often used for this kind of comparison, is somewhat ambiguous.[3,4,8] The spectral region below 1000 cm^{-1} is simpler.[2] In principle, a structure maker should simply intensify the water spectrum in this region and a structure breaker should simply decrease its intensity.

Sodium formate has been classified variously as a weak structure maker[4] or a weak structure breaker[5] and sodium acetate has been classified as a weak structure maker[4] or neither,[5] according to their effects on different OH stretching bands of solvent HOD. The presence of the carboxylic oxygens of the anions, which ought to be good electron donors for hydrogen bond-

ing, suggests that primary hydration of these ions might be considerable. Preliminary low-frequency spectra (below 400 cm^{-1}) of concentrated sodium formate and ammonium acetate solutions were quite different from (and much stronger than) the low-frequency spectrum of water, which suggested that further work might provide direct information about such interactions as ionic hydration. Here we report the low-frequency Raman spectra of solutions of sodium and ammonium formates and acetates (normal and deuterated) in H$_2$O and D$_2$O.

Experimental Section

The method of observing low-frequency Raman lines and the method of separating the lines from the con-

(1) Work done under the auspices of the U. S. Atomic Energy Commission. Presented in part at the Society for Applied Spectroscopy Symposium on Water and Aqueous Solutions, Chicago, Ill., May 1967.

(2) G. E. Walrafen, *J. Chem. Phys.*, **44**, 1546 (1966).

(3) T. T. Wall and D. F. Hornig, *ibid.*, **47**, 784 (1967).

(4) K. A. Hartman, *J. Phys. Chem.*, **70**, 270 (1966).

(5) J. D. Worley and I. M. Klotz, *J. Chem. Phys.*, **45**, 2868 (1966).

(6) H. Yamatera, B. Fitzpatrick, and G. Gordon, *J. Mol. Spectrosc.*, **14**, 268 (1964).

(7) R. E. Weston, *Spectrochim. Acta*, **18**, 1257 (1962).

(8) B. E. Conway, *Ann. Rev. Phys. Chem.*, **17**, 481 (1966). The first few pages of this review discuss some of the problems of interpretation.

tinuous background to determine line frequencies and relative intensities, are discussed elsewhere.[9-11]

Nominal peaks reported are maxima in intensity above the sloping background. For comparison of solutions of different concentration, an appropriate fraction of a reference water spectrum was subtracted from the spectrum of each solution; the peaks reported for the more dilute solutions are peaks in this difference spectrum. Relative intensities of the ammonium acetate and sodium formate solution lines were measured both from nominal peak heights and by integration of areas under the peaks from 0 to about 360 cm^{-1}. Both sets of measurements yielded the same results. The relative intensities were adjusted for the effects of varying light transmission and the intensity contributions of the water in the solutions but no attempt was made to apply refractive index corrections.[12,13] Although the spectra of the concentrated solutions were very reproducible, uncertainties in separating the lines from the background, in separating the lines from each other, in correcting for the intensity contributions of water to the spectrum, and in correcting for the effects of the baffle[10] limit the precision of the relative intensities obtained to perhaps ±10%.

The treatment of salt solutions with the adsorbent Spheron Grade-6 carbon (Godfrey L. Cabot, Inc., Boston, Mass.) to improve their light transmission is described elsewhere.[14] All concentrated (>0.5 M) salt solutions treated with the carbon showed increased light transmission at 4360 Å and decreased continuous backgrounds after treatment. Figure 1 shows the low-frequency spectrum of 10.2 M ammonium acetate before and after treatment with the carbon. One treatment with the carbon yielded a solution with a light transmission at 4360 Å of 96% (for 10-cm cells, relative to conductivity water), and further treatment with the carbon produced no further change in light transmission. The same results were obtained for 8.3 M sodium formate. Since other concentrated salt solutions treated with the carbon showed higher light transmissions at 4360 Å, it may be that ammonium acetate and sodium formate have small, but real, extinction coefficients at 4360 Å. All solutions used in this study were filtered through 0.01 μ pore size Millipore filters.

Anhydrous analytic grade reagents were used to prepare the concentrated solutions of sodium and ammonium formate and acetate, which were then diluted with a precision of about 1%. No attempt was made to establish the absolute concentrations accurately, and they may have been uncertain to as much as 10%.

The ammonium perdeuterioacetate, NH_4OOCCD_3, and the sodium perdeuterioformate, NaOOCD (International Chemical and Nuclear Corp.), were of 97–98% isotopic purity, and the sodium perdeute-
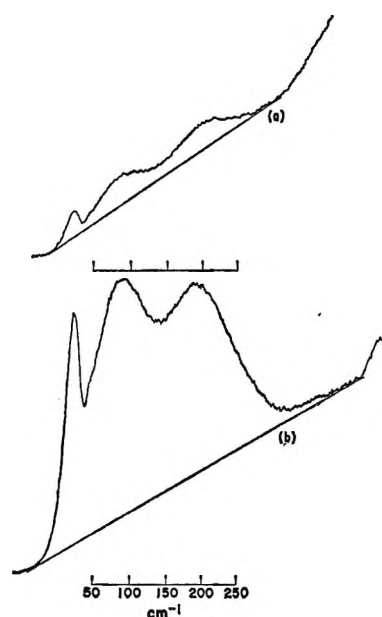
Figure 1. (a) Spectrum of 10.2 M $NH_4(CH_3COO)$ in H_2O before treatment with adsorbent carbon: scan rate = 10 cm^{-1} min^{-1}, time constant = 40 sec, relative gain = 0.7; (b) spectrum of the same solution after treatment with the carbon: scan rate = 20 cm^{-1} min^{-1}, time constant = 20 sec, relative gain = 1.0. For both traces: instrumental width = 25 cm^{-1}, baffle setting = 10.0 mm. The peak at the far left of each spectrum is the unbaffled shoulder of the Rayleigh line.

rioacetate, $NaOOCCD_3$ (Bio-Rad Laboratories), was of 98% isotopic purity. The ammonium perdeuterioformate, NH_4OOCD, solutions in H_2O were made by passing NH_3 gas into perdeuterioformic acid, DCOOD (Nuclear Research Chemicals, minimum 99% isotopic purity). The perdeuterioammonium acetate, $ND_4-OOCCH_3$, solutions in D_2O were made by passing perdeuterioammonia, ND_3, gas into a D_2O solution of acetic anhydride and then by diluting with D_2O. The 98% isotopically pure D_2O was heated several days with potassium permanganate, was distilled, and then was treated with the Spheron Grade-6 carbon. This combined treatment resulted in a 40-fold reduction in continuous background.

Spectra

Spectra of solutions of $NH_4(CH_3COO)$ in H_2O at several concentrations from 1.3 to 10.2 M were recorded. Isotope effects on the acetate spectra were determined from spectra of $NH_4(CD_3COO)$ solutions in H_2O and of $ND_4(CH_3COO)$ solutions in D_2O. (The ammonium

(9) L. A. Blatz, *Spectrochim. Acta*, 21, 1973 (1965).

(10) L. A. Blatz, *J. Chem. Phys.*, 47, 841 (1967).

(11) P. Waldstein and L. A. Blatz, *J. Phys. Chem.*, 71, 2271 (1967).

(12) T. T. Wall and D. F. Hornig, *J. Chem. Phys.*, 45, 3424 (1966).

(13) G. Eckhardt and W. G. Wagner, *J. Mol. Spectrosc.*, 19, 407 (1966).

(14) L. A. Blatz, *Anal. Chem.*, 33, 249 (1961).
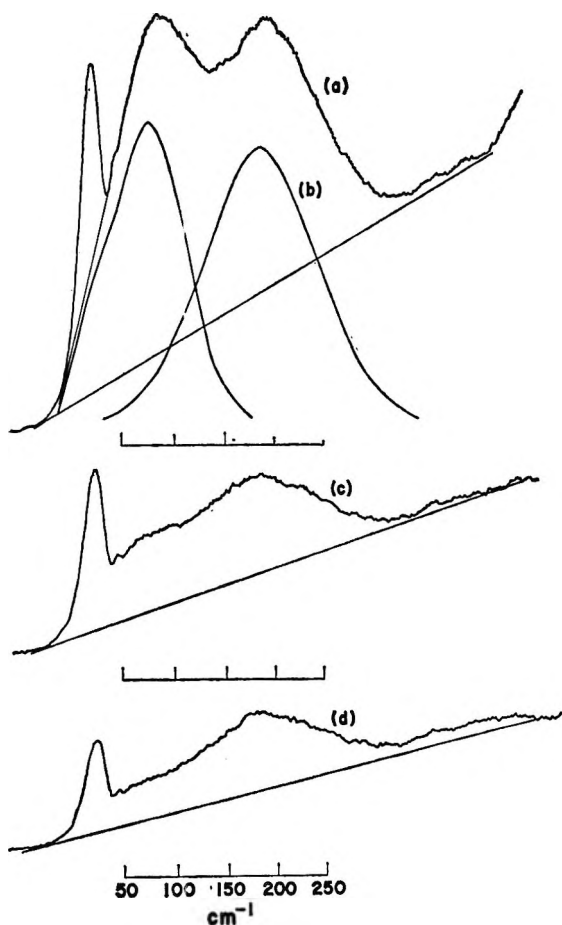
Figure 2. (a) Spectrum of 10.2 M $NH_4(CH_3COO)$ in H_2O; (b) spectrum a decomposed into two lines; (c) spectrum of 1.3 M $NH_4(CH_3COO)$ in H_2O; (d) spectrum of H_2O. All spectra were taken at the same gain and instrumental settings: instrumental width = 25 cm⁻¹, baffle setting = 10.0 mm, scan rate = 20 cm⁻¹ min⁻¹, time constant = 20 sec.

Figure 3. (a) Spectrum of 8.3 M Na(HCOO) in H_2O (relative gain = 0.8); (b) spectrum of 1.0 M Na(HCOO) in H_2O relative gain = 1.0); (c) spectrum of H_2O (relative gain = 1.0). For all spectra: instrumental width = 25 cm⁻¹, baffle setting = 10.0 mm, scan rate = 20 cm⁻¹ min⁻¹, time constant = 20 sec.

ion was deuterated to prevent protonation of the D_2O by exchange.) Spectra of $Na(CH_3COO)$ in H_2O were recorded to provide information about the effect of the cation. Solutions of Na(HCOO) in H_2O were examined at several concentrations between 1.0 and 8.3 M. Solutions of $NH_4(HCOO)$ between 4.0 and 10.7 M were also examined. Isotope effects were determined from the spectra of Na(HCOO) solutions in D_2O and of H_2O solutions of Na(DCOO) and $NH_4(DCOO)$.

All spectra reported here are depolarized within experimental error (ρ = 0.86 ± 0.08), and, except for the water spectrum, their intensities and frequencies are temperature independent between 9 and 53°. The spectra shown in the figures were all observed at 23°.

Acetates. The low-frequency spectrum of a 10.2 M solution of $NH_4(CH_3COO)$ in H_2O is shown in Figure 2a. There are two maxima of about equal intensity; the frequencies of the nominal maxima are 185 ± 1.5 and 88 ± 3 cm⁻¹. Figure 2b shows a decomposition of the spectrum into two lines. The upper line, assumed

to be symmetric, is about 130 cm⁻¹ wide (half-intensity width); the frequency of the resolved peak is 185 cm⁻¹. The frequency of the resolved lower peak is 78 ± 10 cm⁻¹. Its half-width is 80 cm⁻¹ and it is somewhat asymmetric, with excess intensity in the 20–40-cm⁻¹ region. The spectrum of 10 M $ND_4(CH_3COO)$ in D_2O is similar, but the upper maximum is shifted down 11 ± 2 cm⁻¹, or 6%. The lower (nominal) maximum is unshifted by deuterating the water, and neither maximum was shifted more than 2 cm⁻¹ by deuterating the methyl group of the acetate ion.

Figure 2c shows the spectrum of a 1.3 M solution of $NH_4(CH_3COO)$ in H_2O; Figure 2d shows the water spectrum for comparison. Spectra of 2.6, 5.2, 7.2, and 8.2 M solutions were also recorded. Their molar intensities (adjusted) were constant over the entire concentration range. The frequency of the 88-cm⁻¹ (nominal) maximum was independent of concentration. The frequency of the upper maximum (of the spectrum adjusted by subtracting an appropriate fraction of the
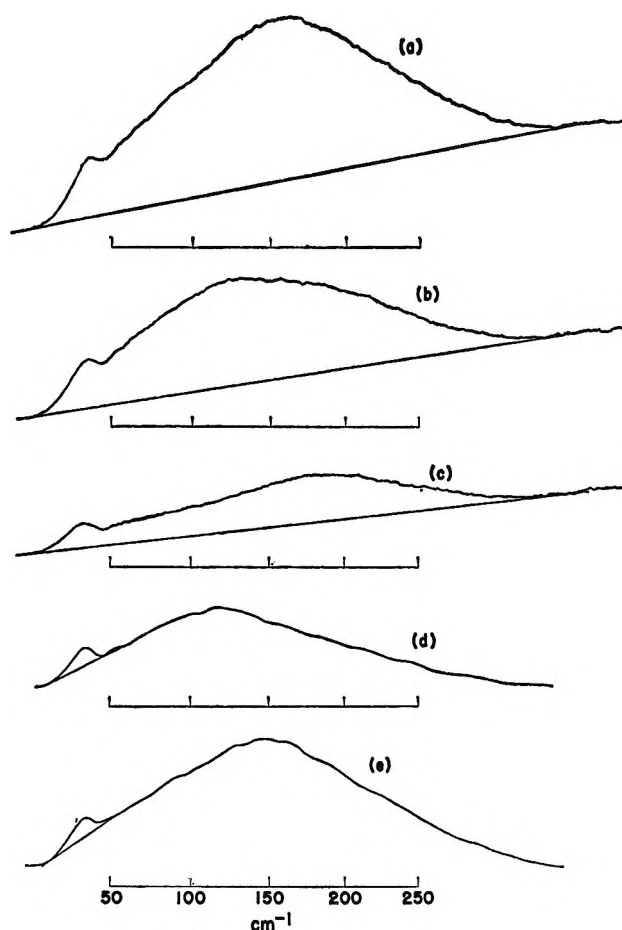
Figure 4. (a) Spectrum of 4.0 M NH$_4$(HCOO) in H$_2$O; (b) spectrum of 3.5 M NH$_4$(DCOO) in H$_2$O; (c) spectrum of H$_2$O; (d) spectrum b adjusted for intensity contribution of water; (e) spectrum a adjusted for intensity contributions of water. All spectra were taken at the same gain and instrumental settings: instrumental width = 25 cm^{-1}, baffle setting = 10.05 mm, scan rate = 10 cm^{-1} min^{-1}, time constant = 40 sec.

Figure 5. (a) Spectrum of 10.7 M NH$_4$(HCOO) in H$_2$O; (b) spectrum of 8.3 M NH$_4$(HCOO) in H$_2$O; (c) spectrum of 8.3 M Na(HCOO) in H$_2$O. For all spectra: instrumental width = 25 cm^{-1}, baffle setting = 10.05 mm, scan rate = 10 cm^{-1} min^{-1}, time constant = 40 sec.

water spectrum) decreased from 185 ± 2 cm^{-1} at 8.2 M to 157 ± 5 cm^{-1} at 1.2 M.

Spectra of sodium acetate solutions (4 M or less) were identical with those of ammonium acetate at the same concentration.

Formates. The low-frequency spectrum of an 8.3 M solution of Na(HCOO) in H$_2$O is shown in Figure 3a. It appears to consist of a single band, 190 cm^{-1} in half-width. Its center can be located reproducibly at 145.5 ± 1 cm^{-1} (with an absolute accuracy of ±3 cm^{-1}). Figure 3b shows the spectrum of a 1.0 M solution; spectra of 2.1 and 4.1 M solutions were also recorded. They all look about the same. The frequency of the band maximum drops about 5 cm^{-1} as the concentration of the solutions is lowered from 8.3 to 1.0 M. An increase of about 20% in molar intensity (adjusted) was observed in the spectra of the 1.0 and 2.1 M solutions. This increase may be real, but the experimental error can be as high as 20% at

these concentrations, where the total intensities are low and the adjusted intensities are sensitive to errors in determining the background in the spectra both of the water and of the solution.

Replacement of H$_2$O by D$_2$O in the sodium formate solutions shifts the band maximum down no more than 1 ± 1 cm^{-1}. Deuteration of the formate ion produces the changes shown in Figure 4. The maximum of the NH$_4$(HCOO) spectrum occurs at 145 cm^{-1}; the maximum of the NH$_4$(DCOO) spectrum occurs at 115 ± 5 cm^{-1}. The integrated molar intensity of the NH$_4$-(DCOO) spectrum is only 70 ± 5% that of the NH$_4$-(HCOO) spectrum, and the NH$_4$(DCOO) spectrum is clearly asymmetric.

Figure 5 shows the spectra of 10.7 and 8.3 M ammonium formate solutions, with the spectrum of an 8.3 M sodium formate solution for comparison. A shoulder at about 80 cm^{-1} can be discerned in the spectra of the solutions of ammonium formate but not in the spectrum of the solution of the sodium salt. At a lower concentration (4 M), no difference could be found between spectra of the sodium and ammonium
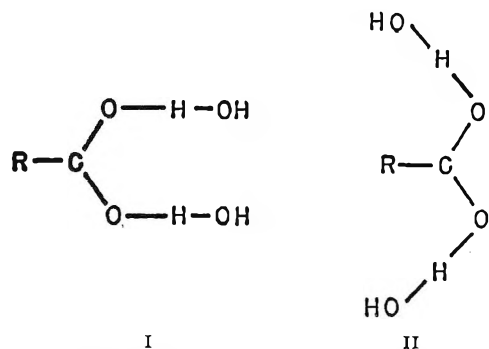
Figure 6. Two possible structures for a dihydrated anion. The terminal OH groups were treated as point masses.

salts. The 80-cm^{-1} shoulder was too weak to permit intensity vs. concentration studies.

Discussion and Conclusions

The spectra reported here cannot be attributed to internal vibrations of the acetate and formate ions. The fundamentals, which are well established,[15] are all (except for the CH_3 torsion of the acetate ion) above 450 cm^{-1}. Difference bands, which should involve an excited state at least 600 cm^{-1} above the ground state, should increase at least 30% in intensity between 9 and 53°; the intensities of the observed spectra are constant in this temperature range. So we attribute our spectra to the vibrations of complexes between the anions and some other species in the solution, presumably water. It is easy to imagine solvent water molecules hydrogen bonded to the carboxylic oxygens of the anions. We cannot specify what, if anything, is bonded to the other ends of the water molecules.

Crude, normal coordinate analyses were performed for the two hydrate structures shown in Figure 6. Other structures are also possible, but these two were felt to be geometrically extreme cases. Hydrogen-bonding force constants were taken from Miyazawa and Pitzer's analysis of carboxylic acid dimers.[16] Both the structures shown in Figure 6 led to approximately the same frequencies and to about the same estimates of isotope shifts, which were the basis of the following assignments.

Acetates. The 185-cm^{-1} line in $10.2\ M\ NH_4(CH_3COO)$ fits the picture of a hydrated acetate ion. The observed isotope shifts, <1% for $NH_4(CD_3COO)$ solutions in H_2O and 6% for $NH_4(CH_3COO)$ solutions in D_2O, are those expected for the stretch of a hydrogen bond between water and a carboxylic oxygen. The change in frequency with concentration can probably be attributed to changes in the environment of the other end of the hydrate water molecules or to increased hydration of the anion at lower concentrations. (A $10.2\ M$ ammonium acetate solution contains less than 2 water molecules/acetate ion.)

The lower line, nominally at 88 cm^{-1}, is more difficult to explain. Its isotope shifts are too small to be consistent with a torsion or a bend of the hydrate complex or with some kind of hindered rotation of the entire complex such as is reported in ref 10. A complex between cations and anions should be much more likely in a $10.2\ M$ solution (37 mol %) than in a $1.3\ M$ solution (1.9%), but the molar intensity of this line is constant throughout the concentration range.

Formates. The spectrum of $3.5\ M\ NH_4(DCOO)$ (Figure 4) is asymmetric. It appears to consist of at least two overlapping lines, the principal of which is centered around 115 cm^{-1}. The spectrum of $4.0\ M\ NH_4(HCOO)$ is presumably also a composite, with its principal component about 145 cm^{-1}. The isotope shifts of this component, 20% upon deuteration of the formate ion and <1% upon deuteration of the water, are those expected for the out-of-plane (B_1) bend of a formate hydrate complex. A 20% intensity loss can be expected for a line shifted down 20% in frequency, if the normal coordinates are unchanged by deuteration; this can account for a large part of the 30% intensity loss of the $NH_4(DCOO)$ spectrum. The weaker component of these spectra, presumably around 150 cm^{-1}, could be a hydrogen-bond stretch. Such an assignment is mostly conjecture, however, since this component is too poorly resolved to permit observation of any isotope effects.

The 80-cm^{-1} shoulder observed in the spectra of concentrated ammonium formate solutions is the only spectral feature observed in this work which depends upon the nature of the cation. Its specific intensity may also be concentration dependent. This behavior is not consistent with a vibration of a hydrated anion. It is, however, consistent with the vibration of a cation-anion complex. Particularly at high concentrations, where there is not enough water to completely coordinate the lone pairs of the formate oxygens, it seems reasonable that an ammonium ion could be hydrogen bonded to a formate ion. We believe this band is the first vibrational spectral evidence of ionic association in aqueous solution. Spectral evidence of ion pairing in nonaqueous solutions has been reported in the literature.[17,18]

(15) K. Ito and H. J. Bernstein, *Can. J. Chem.*, **34**, 170 (1956).

(16) T. Miyazawa and K. S. Pitzer, *J. Amer. Chem. Soc.*, **81**, 74 (1959).

(17) J. C. Evans and G. Y-S. Lo, *J. Phys. Chem.*, **69**, 3223 (1965).

(18) W. F. Edgell, A. T. Watts, J. Lyford, and W. M. Risen, *J. Amer. Chem. Soc.*, **88**, 1815 (1966).

Carbon-13 Nuclear Magnetic Resonance Studies of 2-Substituted Pyridines

by H. L. Retcofsky and R. A. Friedel

U. S. Department of the Interior, Bureau of Mines, Pittsburgh Coal Research Center, Pittsburgh, Pennsylvania 15213
(Received February 5, 1968)

Carbon-13 magnetic resonance spectra of ten 2-substituted pyridines have been obtained and analyzed. Substituents included both electron-releasing and electron-withdrawing groups. Only half of the 50 carbon shieldings measured yielded substituent effects that agree, within experimental error, with those found for the corresponding monosubstituted benzenes. Differences between substituent effects on the ring carbons for the two series of compounds ranged from −4.5 to 21.1 ppm, where a positive sign means that replacement of the hydrogen atom in the 2-position of pyridine by a substituent leads to smaller paramagnetic shifts (or larger diamagnetic ones) than replacing a hydrogen atom in benzene with the same substituent. These differences were found to be most pronounced for the carbons in the 2 position and, for these carbons, to correlate well with the electronegativity of the first atom of the substituent group. Paramagnetic shifts for the C-2 carbons were found to be much smaller than expected in those cases where considerable quantities of electronic charge had been removed by strongly electronegative groups. Shieldings of the carbon atoms in the 5 position, *i.e.*, *para* to the substituent, were found to reflect electron release or withdrawal by substituent groups. Substituent carbon atoms directly bonded to C-2 were all found to be less shielded than the corresponding ones in 3- and 4-substituted pyridines.

Introduction

Carbon-13 magnetic shieldings have been reported for various unsaturated heterocyclic molecules, including azines,[1,2] thiophene,[3] furan,[3] and pyrrole,[3] as well as selected methyl derivatives of each. Protonated diazines have also been investigated by ^{13}C nmr spectroscopy.[2] Shieldings of ^{13}C nuclei in a number of 3- and 4-substituted pyridines have recently been reported by this laboratory and constituted the first two phases of an investigation of carbon shieldings in monosubstituted pyridines.[4,5] We wish here to report carbon shieldings for ten 2-substituted pyridines which constitute the third and final phase of this investigation. The primary purpose of these studies was to obtain a collection of carbon-13 nmr spectra of nitrogen-containing heterocyclic molecules to be used in spectroscopic studies of the structure of coal, coal derivatives, and coal-like materials.

Experimental Section

Nuclear magnetic resonance spectra were obtained at a spectrometer operating frequency of 15.085 MHz and were of the rapid passage dispersion mode[6] variety. Details of the experimental procedure have been reported previously.[4] All chemical shifts are designated δ_c and are referred to that of carbon disulfide ($\delta_c = 0$). The compounds were all obtained from commercial sources and contained only naturally occurring carbon-13. 2-Aminopyridine was examined as a saturated solution in carbon tetrachloride; all other measurements were made on neat liquids. Extensive use of proton decoupling was made to facilitate assignments of spectral peaks to specific spin–spin multiplets.

Results and Spectral Assignments

Magnetic shieldings of all carbon atoms in the nine

2-substituted pyridines measured in this laboratory and Lauterbur's results[1] for pyridine and 2-picoline are given in Table I. Spectral assignments are unambiguous only for C-2 carbons, since, under the experimental conditions employed, these give single line resonances in all cases except that of the 2-fluoro compound. The large one-bond [13]C–[19]F spin–spin coupling constant (244 cps) plus the fact that the components of the doublet were essentially unaffected during proton decoupling experiments removed any ambiguity from this assignment. Remaining assignments were made using the method reported previously for the 3- and the 4-substituted compounds.[4,5]

Discussion

Ring-Carbon Shieldings. The effects on carbon shieldings when the hydrogen atom in the 2 position of pyridine is replaced by various substituents are listed in Table II. Also included are the corresponding ones for monosubstituted benzenes,[4,7–9] as well as differences between the two sets of data. Differences are significant only when they exceed the absolute value of the accumulative experimental error which is estimated to

(1) P. C. Lauterbur, *J. Chem. Phys.*, **43**, 370 (1965).

(2) A. Mathias and V. M. S. Gil, *Tetrahedron Lett.*, 3163 (1965).

(3) T. F. Page, T. Alger, and D. M. Grant, *J. Amer. Chem. Soc.*, **87**, 5333 (1965).

(4) H. L. Retcofsky and R. A. Friedel, *J. Phys. Chem.*, **71**, 3592 (1967).

(5) H. L. Retcofsky and R. A. Friedel, *ibid.*, **72**, 290 (1968).

(6) P. C. Lauterbur in "Determination of Organic Structures by Physical Methods," Vol. 2, F. C. Nachod and W. D. Phillips, Ed., Academic Press Inc., New York, N. Y., 1962, p 472.

(7) K. S. Dhami and J. B. Stothers, *Can. J. Chem.*, **43**, 479 (1965).

(8) H. Spiesecke and W. G. Schneider, *J. Chem. Phys.*, **35**, 731 (1961).

(9) R. A. Friedel and H. L. Retcofsky, *J. Amer. Chem. Soc.*, **85**, 1300 (1963).

Table I: ^{13}C Magnetic Shieldings in 2-Substituted Pyridines (ppm from CS_2)

Substituent	C-2	CH-3	CH-4	CH-5	CH-6	Other carbons
H[a]	43.1	69.2	57.3	69.2	43.1	
F	29.1	83.2	51.9	71.6	45.4	
OCH₃	28.9	82.3	55.5	76.8	45.7	140.6 (CH₃)
NH₂	33.3	84.2	55.6	79.7	44.7	
CHO	40.4	71.9	56.0	65.4	43.2	−0.2 (C=O)
COCH₃	39.4	72.2	56.3	66.7	45.2	−5.8 (C=O) 168.7 (CH₃)
Cl	41.7	68.9	54.3	70.4	43.1	
CH₂CH₃	29.8	71.8	57.4	71.8	43.9	161.7 (CH₂) 179.5 (CH₃)
Br	50.5	64.8	54.0	69.8	42.7	
CN	59.4	64.5	55.3	65.9	42.0	75.3 (CN)
CH₃[a]	33.8	70.3	56.5	71.7	43.9	168.6 (CH₃)

[a] Data taken from ref 1.

Table II: Substituent Effects on Ring-Carbon Shieldings in 2-Substituted Pyridines and Monosubstituted Benzenes[a]

Substituent	Pyridines (C-2)	Benzenes (C-X)	Diff	Pyridines (CH-3)	Benzenes (ortho)	Diff	Pyridines (CH-4)	Pyridines (CH-6)	Benzenes (meta)	Diff (CH-4)	Diff (CH-6)	Pyridines (CH-5)	Benzenes (para)	Diff
F	−14.0	−35.1	21.1	14.0	14.3	−0.3	−5.4	2.3	−0.9	−4.5	3.2	2.4	4.4	−2.0
OCH₃	−14.2	−30.2	16.0	13.1	14.7	−1.6	−1.8	2.6	−0.9	−0.9	3.5	7.6	8.1	−0.5
NH₂	−9.8	−19.2	9.4	15.0	12.4	2.6	−1.7	1.6	−1.3	−0.4	2.9	10.5	9.5	1.0
CHO	−2.7	−9.0	6.3	2.7	−1.2	3.9	−1.3	0.1	−1.2	−0.1	1.3	−3.8	−6.0	2.2
COCH₃	−3.7	−9.3	5.6	3.0	−0.2	3.2	−1.0	2.1	−0.2	−0.8	2.3	−2.5	−4.2	1.7
Cl	−1.4	−6.4	5.0	−0.3	−0.2	−0.1	−3.0	0	−1.0	−2.0	1.0	1.2	2.0	−0.8
CH₂CH₃	−13.3	−16.1	2.8	2.6	2.7	−0.1	0.1	0.8	−1.6	1.7	2.4	2.6	2.3	0.3
Br	7.4	5.4	2.0	−4.4	−3.3	−1.1	−3.3	−0.4	−2.2	−1.1	1.8	0.6	1.0	−0.4
CN	16.3	15.6	0.7	−4.7	−4.3	−0.4	−2.0	−1.1	−1.3	−0.7	0.2	−3.3	−4.3	1.0
CH₃[b]	−9.3	−9.1	−0.2	1.1	−0.3	1.4	−0.8	0.8	−0.3	−0.5	1.1	2.5	2.8	−0.3

[a] Data for monosubstituted benzenes taken from ref 4 and 7–9. [b] Carbon shieldings for 2-methylpyridine taken from ref 1.

be ±1.3 ppm.[7] Only half of the 50 measured substituent effects for the 2-substituted pyridines fall within this range.

The most interesting effects were those found for the carbon atoms bearing the substituent (C-2) and those located *para* to the substituents (CH-5). The latter carbons are far enough removed from the substituents to preclude any significant shielding contributions from inductive or magnetic anisotropy effects of substituents. The trend in the CH-5 carbon shieldings is essentially that found for the *para* carbons in mono-substituted benzenes and is consistent with that expected from variations in *para*-carbon charge densities arising from resonance effects of the substituents. The observed shieldings for both series of compounds are nearly linearly related to Hammett's chemical-reactivity parameters (σ_p). The substituent effects at CH-5 for the 2-substituted pyridines are plotted against σ_p in Figure 1. Also included in the plot are the corresponding values for the 3-substituted pyridines,[5] *i.e.*, those of CH-6. The plot suggests that electron

release or withdrawal at the *para* position is influenced little, if at all, by the proximity of the substituent to the heterocyclic nitrogen. With the exception of those of the formyl, acetyl, and fluoro substituents in the 2-substituted compounds and the chloro substituent in the 3-substituted ones, the effects agree within experimental error with those found for the corresponding monosubstituted benzenes. Jaffé and Doak have concluded from studies of basicities of 3- and 4-substituted pyridines that the Hammett equation is applicable to the prediction of substituent effects on chemical reactivity of these heterocyclic aromatic compounds.[10] The ^{13}C nmr data suggests that their conclusions can be extended to 2-substituted pyridines.

The relation between CH-5 carbon shieldings and σ_p was used to estimate a σ_p constant for the 2-pyridyl group. The ^{13}C spectrum of 2,2'-dipyridyl was obtained for this purpose. Carbon shieldings are given in Table III. Unfortunately, the shieldings at CH-5

(10) H. H. Jaffé and G. O. Doak, *J. Amer. Chem. Soc.*, **77**, 4441 (1955).
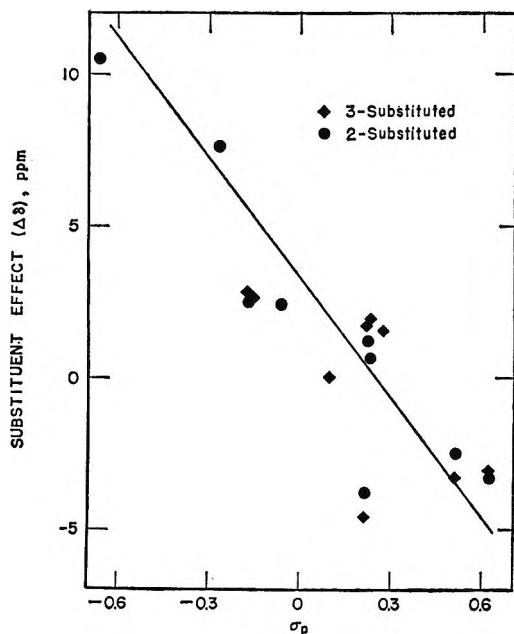
Figure 1. Magnetic shieldings of carbon atoms *para* to substituents in monosubstituted pyridines *vs.* Hammett σ_p constants.

and CH-3 differ by only 2.7 ppm and unambiguous assignments are not possible. Nevertheless, the substituent effects are rather small (-0.2 and 2.5 ppm) and both lead to positive σ_p constants (~0.2). Thus the ¹³C nmr data indicate the 2-pyridyl group to be a weak to moderate electron attracting *para* substituent.

Table III: ¹³C Magnetic Shieldings for 2,2′-Dipyridyl (Saturated Solution in CS₂)

Carbon	δ_c, ppm
C-2	36.3
CH-3	69.0 or 71.7
CH-4	56.2
CH-5	71.7 or 69.0
CH-6	43.3

The carbon shieldings at C-2 are of particular interest, in that the substituent effects are, with few exceptions, unusually small when compared to those found for the benzene series. For example, replacing one of the hydrogen atoms in benzene with fluorine produces a paramagnetic shift of 35.1 ppm for the carbon atom at the position of substitution. For the corresponding atom in the 2-substituted pyridine, the change in shielding is only -14.1 ppm, a difference of more than 20 ppm. All such differences at C-2 are either positive or, within experimental error, essentially zero. The C-2 shieldings in the pyridines are shown plotted against those of the corresponding carbons (C-X) in the benzene series in Figure 2. The solid line represents pyridine shieldings calculated by adding
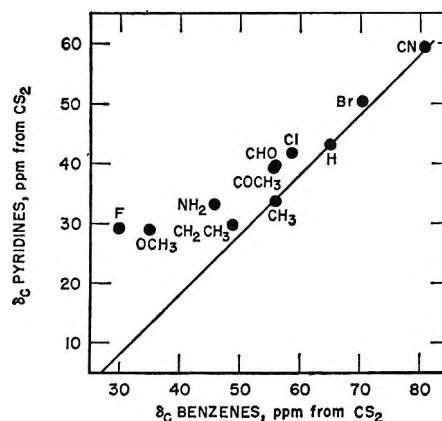
Figure 2. Magnetic shieldings of the *substituted carbon atoms* in 2-substituted pyridines and monosubstituted benzenes.
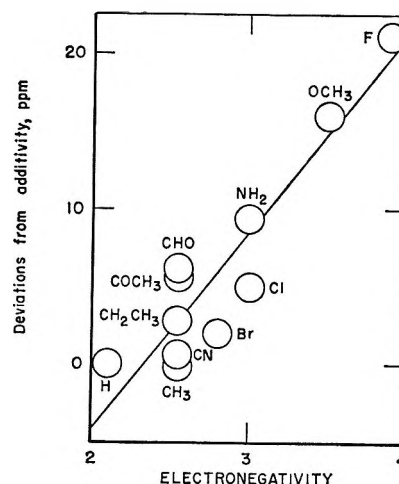
Figure 3. Deviations from additivity for C-2 carbon shields in 2-substituted pyridines *vs.* electronegativities of the first atom of the substituent.

the substituent effects for the appropriate benzenes to the C-2 shielding in pyridine. Deviations from this line are most pronounced for resonances which are found at low magnetic field.

On the basis of linear plots between carbon shieldings and charge densities or parameters reflecting charge densities,[1,8,11] this behavior would suggest incorrectly that the nitrogen atom in a 2-substituted pyridine is less effective than a carbon atom in a monosubstituted benzene in withdrawing charge from an adjacent substituted carbon atom. Clearly such linear relationships are not adequate to explain the large differences in substituent effects found at the site of substitution for the two classes of compounds. These differences do, however, correlate reasonably well with the electronegativity of the first atom of the substituent as can be seen in Figure 3; the largest differences are positive ones but are found for the most electronegative groups.

(11) H. Spiesecke and W. G. Schneider, *Tetrahedron Lett.*, 468 (1961).

Since the electronegativity of nitrogen is greater than that of carbon, it appears that the large withdrawal of charge from C-2 owing to the presence of a highly electronegative group as well as the presence of electronegative nitrogen, in some manner, diminishes the magnitude of the expected paramagnetic shift. These results are in agreement with the recent theoretical interpretation of carbon shieldings given in a study of carbon shieldings in six-membered ring nitrogen heterocyclics and protonated derivatives by Pugmire and Grant.[12] These workers found that the paramagnetic contributions (χ_p's) to carbon shieldings are related to orbital charge densities (q's) and effective nuclear charge parameters (ξ's) according to the expression

$$\chi_p = -12.07\xi^3[q - (q^2/2)]$$

They point out that the dependence of χ_p upon ξ^3 gives rise to the near-linear charge-density–chemical shift relationship proposed originally by Spiesecke and Schneider[11] and by Lauterbur,[13] provided that the carbon atom in question is not too positive. A plot of χ_p vs. q, prepared by Pugmire and Grant, shows that the carbon resonance will not continue to move to lower fields without bounds as electronic charge is removed but will eventually level off and then move again to higher fields as the net charge on carbon becomes highly positive. Although the lack of quantitative values of carbon atom charge densities precludes the actual calculation of shielding constants, the plot in Figure 2, by virtue of its positive slope, clearly indicates a dependence of carbon shieldings upon differences in charge density at C-2 owing to the presence or absence of the electronegative nitrogen atom just two bonds removed from the substituent. A least-squares treatment of the data shown graphically in Figure 2 indicates that the C-2 shieldings (δ_p^{C-2}) can be calculated within ±4 ppm from benzene substituent effects ($\Delta\delta_b^{C-X}$) if a correction for the electronegativity (ϵ) is made as follows

$$\delta_p^{C-2} = 14.2 + \Delta\delta_b^{C-X} + 12.4\epsilon$$

Observed shieldings and those calculated from this equation are given in Table IV.

In 2-substituted pyridines, two positions, CH-4 and CH-6, are *meta* to the substituents. Spiesecke and Schneider found substituent effects at carbon atoms *meta* to substituents in monosubstituted benzenes to be very small and uniform.[8] The effects at CH-4 in the

Table IV: Calculated and Observed C-2 Carbon Shieldings in 2-Substituted Pyridines

| Substit- | δ_c, ppm | | |
uent	Calcd	Obsd	Diff
F	27.6	29.1	1.5
OCH₃	27.5	28.9	1.4
NH₂	32.3	33.3	1.0
CHO	36.9	40.4	3.5
COCH₃	36.6	39.4	2.8
Cl	45.1	41.7	-3.4
CH₂CH₃	29.8	29.8	0
Br	54.4	50.5	-3.9
CN	61.5	59.4	-2.1
CH₃	36.8	33.8	-3.0
H	40.3	43.1	2.8

pyridines agree well with those at the *meta* carbons in the benzenes, with the exception of the fluoro compound which exhibits a large negative deviation and the ethyl and chloro compounds which show small positive and negative deviations, respectively. All deviations at CH-6 are either positive or essentially zero, as was found in the case of the C-2 carbon which are also adjacent to nitrogen. The deviations at CH-6, however, show only a very rough correlation with substituent electronegativity. Substituent effects at CH-3, *ortho* to substituents, are within ±4 ppm of those found for the corresponding benzenes, but no trend with any unique electronic property of substituent group is apparent.

Other Carbon Shieldings. Magnetic shieldings of carbon atoms which are parts of substituent groups are included in Table I. All resonances of substituent carbons which are directly bonded to C-2 are found at lower magnetic fields than the corresponding resonances in the 3- and 4- substituted pyridines.

(12) R. J. Pugmire and D. M. Grant, *J. Amer. Chem. Soc.,* **90**, 697 (1968).

(13) P. C. Lauterbur, *ibid.,* **83**, 1838 (1961).

Evidence for Electron Migration during γ Irradiation of Silica Gel:

Reactions of Adsorbed Electron Scavengers[1]

by P. K. Wong and J. E. Willard

Department of Chemistry, University of Wisconsin, Madison, Wisconsin 53706 (*Received February 5, 1968*)

To study whether long-range electron migration may occur in silica gel during γ irradiation, the yields of products of electron attachment to adsorbed alkyl halides, galvinoxyl, naphthalene, and biphenyl have been investigated as a function of concentration of these electron scavengers. The esr and optical spectra of the sorbed radical and anion products are directly identifiable with the spectra produced by γ irradiation or chemical reduction of the sorbate species in organic solution, except for the case of naphthalene. G values, calculated on the basis of total energy absorbed in the SiO_2, are all greater than unity and are nearly independent of concentration of the sorbate to concentrations at least as low (in the case of galvinoxyl) as 5×10^{-6} mol fraction. This is consistent with the conclusion that electrons ejected by the ionizing radiation migrate very extensively through the SiO_2 matrix. No radicals were generated when alkyl halides were added to silica gel following irradiation of the gel.

Introduction
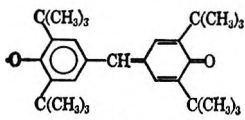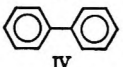
Ionizing radiation absorbed by a substrate such as silica gel may cause decomposition of sorbed molecules located several molecular diameters from the point of energy deposition.[2] This must involve transfer of energy, positive charge, or electrons through the substrate. The compounds for which this phenomenon has been most extensively studied are hydrocarbons and azoethane,[2] which have too low electron affinity to be decomposed by electron attack. However, N_2O, which can undergo dissociative electron attachment ($N_2O + e^- \rightarrow N_2 + O^-$) produces N_2 with $G = 3.5$ (based on total energy absorbed in $SiO_2 + N_2O$) when present as 0.05 monolayer on silica gel.[3] This result suggests the possibility that electrons ejected from the SiO_2 may travel many molecular diameters in the gel.

To further investigate whether long-range electron migration may occur in silica gel during irradiation, we have used three types of adsorbed electron scavengers, shown in Table I, at concentrations ranging from 5.2×10^{-6} mol fraction to 6.2×10^{-2} mol fraction relative to the SiO_2. These are: (I) alkyl halides, which undergo dissociative electron capture, producing alkyl radicals, which can be characterized and assayed by esr;[4] (II) galvinoxyl, a stable free radical[5] which undergoes quantitative changes in esr absorption and visible absorption proportional to the number of electrons captured; (III) napthalene, which in solution produces well-known anions assayable by their optical absorption[6] and by esr spectroscopy;[7] and (V) biphenyl, which in solution produces well-known anions assayable by their optical absorption[6] and by esr spectroscopy.

Experimental Methods

Materials. Davison Chemical Co. Grade 950 silica gel with a stated BET surface area of 700 m² g⁻¹ was

Table I: Reactions Used to Investigate e⁻ Yields from γ-Irradiated Silica Gel[a]

		Esr	Visible–uv
$RX + e^- \rightarrow R + X^-$ I		X	
II	$+ e^- \rightarrow II^-$	X	X
III	$+ e^- \rightarrow III^-$	X	X
IV	$+ e^- \rightarrow IV^-$	X	X

[a] I is CH_3Cl, CH_3Br, or C_2H_5Cl; II is galvinoxyl; III is naphthalene; and IV is biphenyl.

(1) This work has been supported by U. S. Atomic Energy Commission Contract No. AT(11-1)-1715 and by the W. F. Vilas Trust of the University of Wisconsin, Madison, Wis.

(2) J. G. Rabe, B. Rabe, and A. O. Allen, *J. Phys. Chem.*, **70**, 1098 (1966).

(3) (a) P. J. Dyne and N. H. Sagert, *Can. J. Chem.*, **45**, 615 (1966); (b) J. W. Sutherland and R. Goodrich, *J. Amer. Chem. Soc.*, **89**, 6779 (1967).

(4) (a) R. F. C. Claridge and J. E. Willard, *ibid.*, **87**, 4992 (1965); (b) D. W. Skelly, R. G. Hayes, and W. H. Hamill, *J. Chem. Phys.*, **43**, 2795 (1965); (c) M. Shirom and J. E. Willard, *J. Phys. Chem.*, **72**, 1702 (1968).

(5) G. M. Coppinger, *J. Amer. Chem. Soc.*, **79**, 501 (1957).

(6) (a) P. Balk, G. J. Hoijtink and J. W. H. Schreurs, *Rec. Trav. Chim.*, **76**, 813 (1957); (b) P. Balk, G. J. Hoijtink, and J. W. H. Schreurs, *ibid.*, **76**, 907 (1957).

(7) H. Nishiguchi, Y. Nakai, K. Nakamura, K. Ishizu, Y. Deguchi, and H. Takaki, *J. Chem. Phys.*, **40**, 241 (1964).

used after screening the 60–200 mesh size to 140–200. The stated composition of the gel is SiO_2, 99.85%; iron as Fe_2O_3, 0.007%; sodium as Na_2O, 0.004%; and heavy metal oxides, 0.106%. Galvinoxyl (2,6-di-t-butyl-α-[3,5-di-t-diene-1-ylidene]-p-tolyloxyl) from Aldrich Chemical Co.; CH_3Cl, CH_3Br, and C_2H_5Cl (99.5% purity) from the Matheson Chemical Co.; Eastman White Label CH_3I and biphenyl; and Baker and Adamson naphthalene were used as received. Eastman White Label C_2H_5I was further purified by aqueous sulfite wash and distillation. Both iodides used showed less than 0.5% impurity by gas chromatography. Phillips pure grade hexane was purified by passage through a 2-ft column of freshly activated silica gel immediately before use.

Preparation of Samples. Weighed samples (1–5 g) of silica gel were placed on the vacuum line in a bulb and maintained at a pressure of less than 10^{-3} torr at 460° for 24 hr. When a volatile sample of an alkyl halide was to be sorbed, a known aliquot of the vapor measured by PVT technique was admitted from a metering flask, after the halide had been degassed and passed through P_2O_5 and silver powder. Rapid and complete adsorption was indicated by the manometer reading. Greaseless stopcocks were used throughout the filling manifold. Mercury vapor from the manometer was prevented from reaching the sample by a trap of silver powder.

Weighed samples of biphenyl and of naphthalene were degassed at 195°K in a tube with a greaseless stopcock. This was then sealed to the vessel containing the silica gel and the latter was degassed at 460° for 24 hr; following this procedure, the combination was sealed from the vacuum line and placed in an oven at 100°. The aromatic compound vaporized and adsorption occurred rapidly.

Because the low volatility of galvinoxyl precludes vapor-phase addition to the silica gel, it was added, using a greaseless stopcock, to the degassed gel as a degassed solution in hexane. The yellow color of the solution disappeared immediately, indicating rapid adsorption, following which the hexane was pumped off to a residual pressure of less than 10^{-3} torr.

Following preparation of an adsorbed sample, the gel was mixed by shaking and was then poured, without breaking the vacuum, into a sample tube for γ irradiation and esr or optical observation. The sample tube was then sealed from the mixing reservoir. Electron spin resonance examination was made in 3 mm i.d. Suprasil tubes, attached by graded seal to a Pyrex section. To avoid inducing signals in the section used for esr examination, γ irradiation was done in the Pyrex section. For optical measurements, the sample tube contained a thin, flat rectangular Pyrex cell (*ca.* 0.07 × 1 × 3 cm) in place of the Suprasil tube. These cells were made by rapidly drawing down heated glass tubing on a metal form.

The concentrations of sorbed materials are expressed as mole fractions, using 60 for the molecular weight of SiO_2. A mole fraction of 10^{-6} is 0.018 μmol/g.

Irradiations. Irradiations were carried out at room temperature or 77°K using a ^{60}Co γ-ray source at absorbed dose rates of 1.7 × 10^{17} eV or 6.3 × 10^{17} eV g^{-1} min^{-1}. The dose rates were determined by Fricke dosimetry, with an extinction coefficient of ferric ion of 2160 M^{-1} cm^{-1} at 3050 Å at 22.5°, a temperature coefficient of 0.8 % deg, and a yield of 15.6 ferric ions/ 100 eV absorbed. The dose rate per gram in SiO_2 was taken as 0.9 of that in H_2O, in proportion to the number of electrons per gram.

Optical Measurements. Measurements of optical spectra were made with a Cary 14 recording spectrophotometer. At 77°K the sample cells were reproducibly positioned in the analyzing beam in a square quartz dewar. A neutral density filter or reference cell containing silica gel was used in the reference beam to balance the high optical density due to light scattering by the sample. The effective path length of the light through the sample was evaluated by the change in optical density produced by adsorption of a known amount of Cl_2 on the gel. Assuming the same extinction coefficient on the gel as in the gas phase gave 2.5 mm as the effective light path in a 0.7-mm cell. A similar determination using 8.6 × 10^4 M^{-1} cm^{-1} as the extinction coefficient for the 4200-Å line of galvinoxyl gave a value of 2.6 cm. (The density of the silica gel is 0.56 g cc^{-1}.)

Electron Spin Resonance Measurements. Electron spin resonance measurements were made with a Varian 4500 spectrometer using 100 kcps modulation. The sample tubes were intercalibrated. Absolute radical yields were determined by comparing the area under the esr absorption curve (obtained by integration of the first-derivative signal) with the area from benzene solutions of known concentration of galvinoxyl. For measurements at 77°K, the fourfold higher sensitivity than at 300°K was taken into account. Arrows on the figures which show esr spectra in this paper indicate the position of the resonance line of a pitch standard for which $g = 2.0028$.

Results and Discussion

Electron Spin Resonance and Optical Evidence for Electron Capture. For each of the electron scavengers adsorbed on silica gel (Table I), γ irradiation produces a change in the esr or optical spectrum, or both, consistent with the conclusion that electrons ejected from the SiO_2 are captured by the sorbate with a yield of $G = 1$ or higher. The yields are independent of wide variations in the concentration of sorbate. Figures 1–7 illustrate the signals observed.

The four-line esr signal of the methyl radical from CH_3Cl, CH_3Br, or CH_3I (Figure 1A) is unambiguous. Figure 8 shows the growth of this radical as a function

Figure 1. (A) Electron spin resonance spectrum of γ-irradiated CH_3Br on silica gel at 77°K (3.0 × 10⁻² mol fraction); (B) esr spectrum of γ-irradiated C_2H_5Cl on silica gel at 77°K (3.6 × 10⁻² mol fraction). The arrows indicate g = 2.0028.
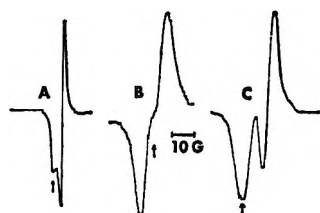

Figure 2. Electron spin resonance spectra of galvinoxyl at 300°K: (A) in hexane (4.5 × 10⁻⁷ mol fraction); (B) in hexane (6.0 × 10⁻⁵ mol fraction); (C) on silica gel (9.0 × 10⁻⁵ mol fraction). The arrows indicate g = 2.0028.
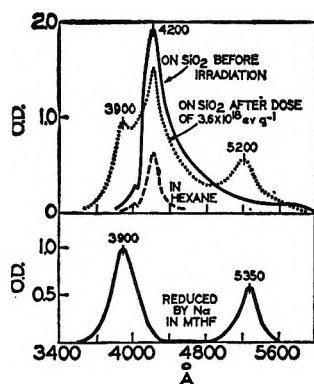

Figure 3. Optical spectra of galvinoxyl. Spectra on silica gel are for a 0.7 mm thick sample containing 2 × 10⁻⁷ mol fraction of galvinoxyl. Spectrum in hexane is for a 1-cm cell containing 4.4 × 10⁻⁷ mol fraction. Spectrum in methyltetrahydrofuran is for a 1.0-cm cell containing 10⁻⁵ mol fraction.

of dose at 77°K for several concentrations of CH_3Br on silica gel from 1.2 × 10⁻² mol fraction to 7.5 × 10⁻² mol fraction. The G values are 1.4 ± 0.2.

Both the esr and optical spectra of galvinoxyl on silica gel at room temperature are similar to those in solution (Figures 2 and 3). Irradiation of sorbed samples produces a linear decrease in the esr signal, until a high percentage of the stable radical has been consumed. Figure 9 shows this decrease for four samples with initial concentrations from 2.3 × 10⁻⁵ to 10⁻⁴ mol fraction. Other samples ranging in concen-
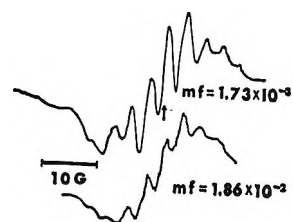
Figure 4. Electron spin resonance spectra of γ-irradiated (8.6 × 10¹⁹ eV g⁻¹) biphenyl on silica gel at 77°K at two mole fractions. The arrow indicates g = 2.0028.
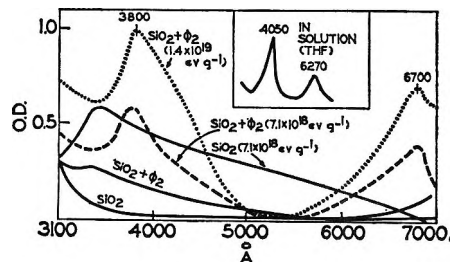
Figure 5. Optical spectra of γ-irradiated biphenyl on silica gel at 77°K and biphenylide anion in tetrahydrofuran at 77°K (insert). Spectra on silica gel are for a 0.7 mm thick sample containing 2 × 10⁻⁷ mol fraction of biphenyl.
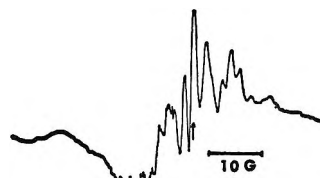
Figure 6. Electron spin resonance spectrum of γ-irradiated naphthalene on silica gel at 77°K (2.0 × 10⁻³ mol fraction, 6 × 10¹⁹ eV g⁻¹). The arrow indicates g = 2.0028.
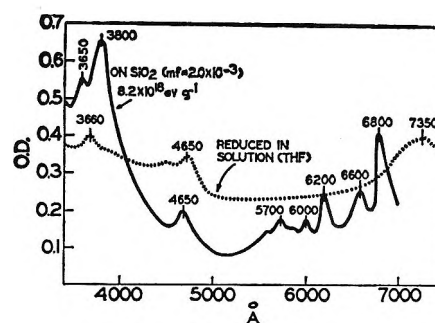
Figure 7. Optical spectra of γ-irradiated naphthalene on silica gel and naphthalenide anion in tetrahydrofuran solution. Spectra on silica gel are for a 0.7 mm thick sample.

tration down to 5 × 10⁻⁶ mol fraction gave similar plots. G values calculated from the linear portions of the plots are 4.7 ± 0.4, independent of mole fraction.

Figure 10 shows the decay of the 4200 Å galvinoxyl radical optical absorption peak and growth of the 3900- and 5200-Å anion peaks as a function of dose. For this plot the concentration of galvinoxyl before ir-
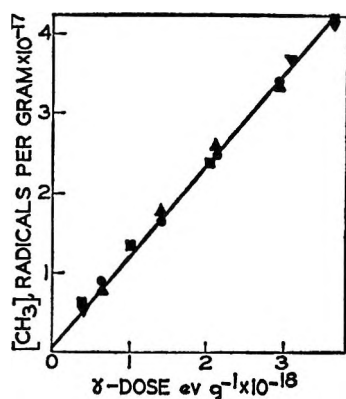
Figure 8. Yields of methyl radicals from the irradiation of CH_3Br on silica gel at 77°K, as a function of γ dose at different CH_3Br concentrations (mol fraction): ▼, 7.5×10^{-2}; ▲, 5.1×10^{-2}; ■, 3.1×10^{-2}; ●, 1.2×10^{-2}.

Figure 10. Decay of galvinoxyl radical and growth of galvinoxyl anion as a function of γ dose at 300°K: ●, 4200-Å radical peak; ▲, 5200-Å anion peak; ■, 3900-Å anion peak.

Figure 9. Effect of γ dose at 300°K on concentration of galvinoxyl adsorbed on silica gel at different concentrations.

Table II: Yields of Electron-Capture Reactions

Method of observation		Temp, °K	Yield per 100 eV absorbed by	
			SiO_2 + adsorbate	Adsorbate only
CH_3 + Br^-	Esr	77	1.4	$10^{2\,a}$
(Galvinoxyl)$^-$	Esr	300	4.7	$10^{5\,b}$
	Optical	300	4.6	$10^{5\,b}$
Naphthalene	Esr	77	2.1	$10^{3\,a}$
Biphenyl	Esr	77	2.1	$10^{3\,a}$

^{a} 10^{-4} mol fraction. ^{b} 10^{-6} mol fraction.

radiation is known from the weight of galvinoxyl and silica gel used, so the change in the 4200-Å peak with dose is a direct measure of the change in concentration. These data give a value of 4.6 for $G(-$galvinoxyl). The points of Figure 10 for the growth of the anion have been calculated on the assumption that the extinction coefficients at 3900 and 5200 Å are equal to the extinction coefficient at 4200 multiplied by the ratio of the change in optical density at 3900 or 5200 Å/unit dose to the change at 4200 Å. Both peaks grow linearly with dose.

For biphenyl and naphthalene, the similarity between spectra of the anions in solution and the species produced by irradiation on silica gel is not as great as for methyl radicals and galvinoxyl anions. It is, however, not inconsistent with the conclusion that the sorbed species are the same as those in solution, except for distorting effects resulting from interaction with the substrate.

Implication of G Values. It is reasonable to assume that G(ionization) in silica gel is of the order of 3, as it is for most substances for which measurements (necessarily gas phase) have been made. This being the case,

the data of Table II indicate that a considerable fraction of all of the electrons ejected from the silica gel used in this work can migrate so extensively through the matrix that they can be captured by as little as 5×10^{-6} mol fraction of scavenger. The G values in the last column of Table II, estimated on the basis that only that energy absorbed by the sorbate is effective, are impossibly high, dramatizing the fact that energy deposited in the adsorbent is predominantly responsible for the observed changes.

Temperature Effects. Methyl radicals produced by γ irradiation of methyl halides on silica gel (Figure 1) are indefinitely stable at 77°K and do not disappear rapidly below *ca.* 250°K. They cannot be observed at 300°K.

The species produced by irradiation of adsorbed biphenyl and naphthalene at 77°K (Figures 4–7) disappear rapidly on warming to 195°K. By contrast, irradiation does not change the intensity of the esr or optical spectra of sorbed galvinoxyl at 77°K but does change the intensity at 300°K, and the new species are stable at 300°K. This suggests (1) binding of the free radical to the surface at 77°K in a manner to preclude electron addition and (2) low mobility of the anion (as well as positive charge) at 300°K. When a sample of galvinoxyl on SiO_2 is warmed to 300°K following irradiation at 77°K, the spectrum remains identical with that of an unirradiated sample.

Galvinoxyl Spectra. The esr and optical spectra of galvinoxyl in hexane have been reported.[5] Additional information is given here.

The esr spectrum of adsorbed galvinoxyl on silica gel at 300°K (Figure 2) shows no saturation effects at powers up to at least 30 mW (−10 db), but at 77°K, onset of saturation occurs at about 0.5 mW and the signal height passes through a maximum at 1.2 mW. The line shape at 77°K is independent of the concentration of galvinoxyl on the silica gel from 5×10^{-7} to 10^{-5} mol fraction, indicating that there is no interaction between the adsorbed radicals, in contrast to hexane solutions where the shape changes with concentration (Figure 2). As the adsorbed radicals disappear during irradiation at 300°K, there is no change in line shape. Whereas the spectra of galvinoxyl in hexane and iso-octane are similar to that on silica gel, the shape and width are much different in benzene,[8] in C_2H_5I, and in CH_2Cl_2. We observe ten lines in each of these solvents, under the same conditions of measurement which gave the spectra of Figure 2.

As shown in Figure 3, the 4200-Å optical absorption peak previously observed in hexane solutions of galvinoxyl[5] is also found when it is adsorbed on silica gel. It decreases linearly as a function of γ dose, while the peaks at 3900 and 5200 Å (Figure 3) grow. Evidence that the latter peaks are attributable to the galvinoxyl anion has been obtained by dissolving sodium in 2-methyltetrahydrofuran containing galvinoxyl. In the absence of air, a cherry-red compound with absorption bands at 3900 and 5350 Å is produced. When air is admitted the 5350-Å peak shifts to 5800. The negative ion has also been prepared by reducing hydrogenated galvinoxyl in ethanol with sodium.[9a] The purple solution obtained showed absorption maxima at 2750 and 5750 Å.

Biphenylide Spectra. The resolution of the nine-line esr spectrum of biphenyl irradiated on silica gel improves as the concentration is decreased (Figure 4). It is similar to the spectra of the biphenylide ion produced by reduction of biphenyl in tetrahydrofuran with sodium.[7,9b] The proton hyperfine-coupling constants a_2 and a_4 appear to be 2.86 and 5.72, as compared to 2.65 and 5.29 for the anion in solution. As shown in Figure 5, the visible-uv spectrum of irradiated adsorbed biphenyl is similar to that reported for the biphenylide ion in solution. A similar spectrum has also been observed for biphenylide ion formed during the γ irradiation of biphenyl in 3-methylpentane glass at 77°K.[10]

Naphthalenide Spectra. The esr spectrum of naphthalenide ion prepared by chemical reduction in tetrahydrofuran contains 25 lines with a total spread of 27 G.[11a] Under less ideal conditions a partially resolved spectrum of 17 lines has been observed.[11b] The spectrum obtained by γ irradiation on silica gel shows nine less well-resolved lines with a spread of 41.5 G.

The a_1 and a_2 coupling constants of the major lines are larger than those of the solution spectrum[11] by about the factor of 41.5–27, by which the total spread is increased.

As indicated in Figure 7, the visible-uv spectrum obtained by irradiating naphthalene on silica gel at 77°K is different from that of the naphthalenide ion in solution,[6] except for peaks at 4650 and 3660 Å. The absorption spectrum produced by the γ irradiation of dilute solutions of naphthalene in 3-methylpentane (3-MP) at 77°K is, however, similar to that in solution.

Either naphthalenide is adsorbed on silica gel in such a way as to change its esr and optical spectra more drastically than the spectra of galvinoxyl anion and biphenylide are changed, or the irradiation yields a different type of product. The spectrum shows some similarity to that which has been attributed[12] to the naphthalene cation in γ-irradiated CCl_4 at 77°K.

Products from Adsorbed Alkyl Halides. CH_3Cl and CH_3I when γ irradiated on silica gel at 77°K give methyl radical esr spectra essentially the same as that of Figure 1A from CH_3Br. These are similar to the spectra produced by the photolysis of CH_3I on porous glass.[13,14] Ethyl chloride γ irradiated on silica gel at 77°K gives the spectrum of Figure 1B, which appears to be dominated by a 12-line ethyl radical spectrum similar to that observed from the γ irradiation of C_2H_5-Cl as a liquid[15] or solid[16] and from the photoionization of N,N,N′,N′-tetramethyl-p-phenylenediamine (TMPD) in 3-MP glass containing C_2H_5Cl.[4a]

The spectra of alkyl radicals adsorbed on silica gel have much narrower lines than those observed[4a,17] in glassy or polycrystalline matrices and, as noted earlier,[18] are usually somewhat asymmetric.

No radical esr signals were produced when 6×10^{-2} mol fraction of CH_3Cl or CH_3Br was added at 200°K, under vacuum, to silica gel which had been irradiated to a dose of 3×10^{19} eV g^{-1} at 77°K.

(8) C. Besev, L. T. Vanngard, and R. Hakansson, *Acta Chem. Scand.*, **17**, 2281 (1963).

(9) (a) M. S. Kharasch and B. S. Joshi, *J. Org. Chem.*, **22**, 1435 (1957); (b) E. de Boer and S. I. Weissman, *J. Amer. Chem. Soc.*, **80**, 4549 (1958).

(10) M. R. Ronayne, J. P. Guarino, and W. H. Hamill, *ibid.*, **84**, 4230 (1962).

(11) (a) A. Carrington, *J. Chem. Soc.*, 947 (1959); (b) S. I. Weissman T. R. Tuttle, Jr. and E. de Boer, *J. Phys. Chem.*, **61**, 28 (1957).

(12) T. Shida and W. H. Hamill, *J. Chem. Phys.*, **44**, 2375 (1966).

(13) J. Turkevich and Y. Fujita, *Science*, **152**, 1619 (1966).

(14) M. Fujimoto, H. D. Gesser, B. Garbutt, and A. Cohen, *ibid.*, **154**, 381 (1966).

(15) R. W. Fessenden and R. H. Schuler, *J. Chem. Phys.*, **39**, 2147 (1963).

(16) B. Smaller and M. S. Matheson, *ibid.*, **28**, 1169 (1958).

(17) H. W. Fenrick, S. V. Filseth, A. L. Hanson, and J. E. Willard, *J. Amer. Chem. Soc.*, **85**, 3731 (1963).

(18) V. B. Kasansky and G. B. Pariisky, *Intern. Congr. Catalysis, Amsterdam, 3rd*, 367 (1964).
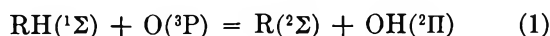
Activation Energies and Rate Constants Computed for Reactions

of Oxygen with Hydrocarbons

by S. W. Mayer and L. Schieler

Laboratories Division, Aerospace Corporation, El Segundo, California 90245 (*Received February 6, 1968*)

A study has been made of a procedure for computationally estimating activation energies and rate constants of bimolecular transfer reactions for atomic or molecular oxygen with hydrocarbons, hydrogen, and water in the gas phase. The procedure is modified from the Johnston–Parr bond-energy method, previously applied to abstraction by radicals in the doublet electronic state. One modification is based on the doubled spin repulsion that could arise in the activated complex because of the two parallel-spin electrons characteristic of triplet states such as those for atomic or molecular oxygen. The modified procedure based on doubled repulsion provides better agreement between computed and experimental activation energies or rate constants for abstraction by triplet O or O_2. A modification in which the alkyl radicals of the hydrocarbons are treated as point masses is also examined briefly. Computations of activation energies and rate constants are made for abstractions by the singlet excited states: $O(^1D_g)$, $O(^1S)$, $O_2(^1\Delta_g)$, and $O_2(^1\Sigma_g^+)$.

A chain-propagation step in the combustion process for a hydrocarbon is the abstraction by atomic oxygen of a hydrogen atom from the hydrocarbon. This reaction is written in the following equation with the ground electronic states indicated

$$RH(^1\Sigma) + O(^3P) = R(^2\Sigma) + OH(^2\Pi) \qquad (1)$$

During the past few years, rate measurements by improved techniques[1–3] have provided rather dependable activation-energy (E_0) and rate-constant (k) data for this important abstraction reaction in several cases where R was an alkyl, hydroxyl, or hydrogen radical. An objective of the present study was to compare these experimental values for E_0 and k with the values computed by a modification of the bond-energy–bond-order method[4–6] for calculating E_0 and k. This method is based on an activated-complex treatment using several trial postulates interrelating dissociation energy, bond order, and bond length. The method does not use adjustable parameters. Computations of kinetic data by the modified method are also reported herein for the abstraction of hydrogen by ground-state or excited molecular oxygen and by excited atomic oxygen, in addition to the abstraction by ground-state atomic oxygen shown in eq 1.

Modified Computation Procedure

The generalized hydrogen atom abstraction reaction can be written

$$RH + B = R \cdots H \cdots B = R + HB \qquad (2)$$
$$ _{n_1} _{n_2}$$
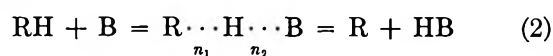
where n_1 and n_2 are the bond orders, in the transition state, of the breaking bond $R \cdots H$ and the forming bond $H \cdots B$, respectively. This study is concerned with cases in which the abstracting species B is an oxygen atom or molecule. The potential energy of forming the

transition state is postulated on a trial basis to be equal to the energy required to break the bond RH to $R \cdots H$ of bond order n_1 in the transition state, less the energy supplied by the forming of $H \cdots B$ to bond order n_2, plus a repulsion energy V_r arising from the parallel electron spins on R and B.[4] By using the trial postulate[4,5] that the bond energy at zero bond order corresponds to the binding energy of a noble gas diatomic pair, the potential energy of forming the transition state can be expressed as

$$V = D_{RH} - D_{RH}n_1{}^p - D_{HB}n_2{}^q + V_r \qquad (3)$$

where D is the bond dissociation energy, and p and q are the slopes of the log (dissociation energy) *vs.* log (bond order) lines. Equation 3 produced rather good agreement (*e.g.*, within 2 kcal/mol) between computed and experimental E_0 when it was tested for reactions where the radical B had only one unpaired electron.[4,5] In these cases B consisted of only univalent species such as atomic hydrogen, atomic halogens, CF_3, CH_3, or C_2H_5 radicals. The origin of the parallel spin repulsion in the transition state for such cases can be illustrated by the following representation of the reaction, where the arrows indicate the direction of electron spin

$$R{\uparrow}{\downarrow}H + {\uparrow}B = R{\uparrow} \cdots {\downarrow}H \cdots {\uparrow}B = R{\uparrow} + H{\downarrow}{\uparrow}B$$
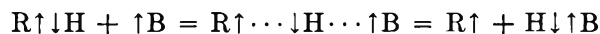
(1) A. A. Westenberg and N. de Haas, *J. Chem. Phys.*, **46**, 490 (1967).

(2) A. A. Westenberg and N. de Haas, *ibid.*, **47**, 1393 (1967).

(3) W. E. Wilson and A. A. Westenberg, Eleventh Symposium (International) on Combustion, The Combustion Institute, Pittsburgh, Pa., 1967, p 1143.

(4) H. S. Johnston and C. Parr, *J. Amer. Chem. Soc.*, **85**, 2544 (1963).

(5) H. S. Johnston, "Gas Phase Reaction Rate Theory," The Ronald Press Co., New York, N. Y., 1966.

(6) S. W. Mayer, L. Schieler, and H. S. Johnston, *J. Chem. Phys.*, **45**, 385 (1966).

In order to estimate the spin repulsion between R and B in the transition state, it was assumed on a trial basis that V_r is similar to that of the repulsive, triplet state of $H_2(^3\Sigma_u{}^+)$ and that V_r can be expressed as an anti-Morse function such as the one used by Sato for triplet H_2.[4]

When B has more than one unpaired electron (e.g., if B is triplet oxygen or quartet atomic nitrogen), the problem arises of choosing between using the Johnston–Parr method[4] of computing V_r or modifying it because of increased repulsion between R and B due to the two or three parallel-spin electrons on B. In the present study, the modification was adopted of doubling V_r if B had two parallel-spin electrons. This modification was applied to abstraction by $O(^3P)$ or $O_2(^3\Sigma_g{}^-)$; it restores the factor in the Sato type of expression to 1.0.[4]

Johnston (ref 5, p 221) has pointed out that experimental preexponential factors in abstraction reactions do not usually decrease greatly as the number of atoms in the radical R increases. This relative constancy of the preexponential factor can be attributed to the probability that most of the force constants for polyatomic R are not extensively altered in the transition state. The estimation of bending force constants in the transition state is not dependable when R or B are not monatomic.[5] For these reasons, in this study the modification of treating R and B simply as if they were monatomic mass points was tested as a convenient method of estimating the preexponential factors for comparison with experiment. This modification cannot be completely correct, but it is believed that in many reactions the net correction arising from changes in bending force constants of R in the transition state is small. For those reactions having exceptionally low steric factors,[5] this modification should be considered particularly undependable.

Molecular parameters used in the computations are summarized in Table I. The Morse parameter β used[4] for computing V_r can be calculated from the relationship

$$\beta = (1.2177 \times 10^7)\omega_e(\mu/D_e)^{1/2} \text{ cm}^{-1} \qquad (4)$$

where ω_e is the vibrational wave number (in cm^{-1}); D_e is the dissociation energy, in kcal/mol (to the minimum of the potential energy curve); and μ is the reduced mass, in atomic weight units.

Results and Discussion

In Table II, computed activation energies and rate constants are summarized for the abstraction reaction of ground state $O(^3P)$ with hydrogen, water, methane, ethane, n-propane, n-butane, and acetaldehyde in the gas phase. Activation energies computed by the modified procedure are presented in Table II for comparison with the experimental values. Also shown in Table II are the activation energies calculated by the

Table I: Properties[a] of the Bond Involving the Abstracted Hydrogen Atom

Compound	Bond-dissociation energy,[b] kcal/mol	Vibrational wave number, cm^{-1}	Bond length, $\times 10^{-8}$ cm
H$_2$	109.5	4405	0.742
H$_2$O	123.4	3760	0.96
OH	106.7	3735	0.971
O$_2$H	51.0	3600	0.96
CH$_4$	105.1	3000	1.09
C$_2$H$_6$	102	3000	1.09
n-C$_3$H$_8$	104	3000	1.09
n-C$_4$H$_{10}$	105	3000	1.09
CH$_3$CHO	93	3000	1.09

[a] Data from D. R. Stull, Ed., "JANAF Thermochemical Tables and Supplements," Dow Chemical Co., Thermal Research Laboratory, Midland, Mich., 1967; C. T. Mortimer, "Reaction Heats and Bond Strengths," Pergamon Press Inc., New York, N. Y., 1962. [b] This dissociation energy, D_e, includes the zero-point vibrational energy of the bond. For propane and butane, D_e is weighted for the presence of secondary hydrogen bonds. The D_e of acetaldehyde applies to the CH bond of the aldehyde group.

unmodified procedure in which the spin repulsion between R and $O(^3P)$ is assumed equal to that arising from only a single unpaired electron on the abstracting oxygen atom. Examination of the results for computed E_0 in the table shows that the modified procedure gave better agreement with experiment for each reaction. In the abstraction from ethane, for example, E_0 computed by the modified procedure was 0.7 kcal/mol higher than the experimental value of 6.8 kcal/mol, whereas the unmodified procedure produced an E_0 which was 3.3 kcal/mol lower than the experimental value. For all seven reactions, the mean value by which E_0 computed via the modified method differed from experimental E_0 was 0.8 kcal/mol. The unmodified method produced E_0 results which were lower than experimental E_0 by a mean of 2.6 kcal/mol.

This difference of 2 or 3 kcal/mol between computing procedures for E_0 is reflected in the rate constant results at 300°K, since the exponential factor is sensitive to such differences at 300°K in contrast with the decreased sensitivity at high temperatures.[6] In the aforementioned abstraction from ethane, the rate constant computed by the modified procedure is within a factor of 2 of the experimental value. The rate constant calculated on the basis of single repulsion, however, is a factor of 100 larger than that of the experimental k at 300°K. The tunneling effect[5] in hydrogen atom abstractions, moreover, would tend to raise the computed rate constants if a correction for tunneling were applied. No tunneling correction was used for the computations summarized in Table II, since there is considerable disagreement about the method of making this correction.[2,5] If the method[5] based on the unsymmetrical

Table II: Activation Energies and Rate Constants Computed by Modified Procedure and by Single Repulsion

Reaction	Activation energy, kcal/mol			Log k at 300°K, cc/mol sec			Log k at 1000°K, cc/mol sec		
	Exptl	Computed	Single[a]	Exptl	Computed	Single[a]	Exptl	Computed	Single[a]
$H_2 + O = H + OH$	10.2[b]	11.2	6.1	6.0	5.6	9.5	11.3	11.5	12.8
$HOH + O = 2OH$	19.5[c]	18.9	17.6	0.3	0.0	1.1	10.2	10.0	10.6
$CH_4 + O = CH_3 + OH$	8.7[b]	8.8	4.6	7.5	7.3	10.3	11.5	12.0	13.0
$C_2H_6 + O = C_2H_5 + OH$	6.1[b]	6.8	2.8	8.9	8.8	11.7	12.0	12.7	13.8
$n\text{-}C_3H_8 + O = C_3H_7 + OH$	5.7[d]	6.9	3.8	9.7	8.7	11.0	12.7	12.7	13.5
$n\text{-}C_4H_{10} + O = C_4H_9 + OH$	4.2[e]	4.5	2.3	10.5	10.6	12.2	12.6	13.3	14.1
$CH_3CHO + O = CH_3CO + OH$	2.3[d]	3.0	1.1	11.3	10.8	12.4	12.5	12.5	13.4

[a] V_r not doubled; spin repulsion assumed from only a single unpaired electron on $O(^3P)$. [b] Reference 1. [c] R. S. Brokaw, ref. 3, p 1071. [d] K. Schofield, *Planetary Space Sci.*, **15**, 643 (1967). [e] L. Elias and H. I. Schiff, *Can. J. Chem.*, **38**, 1657 (1960).

Eckart barrier is used for estimating a tunneling correction in the ethane abstraction, a mean tunneling correction factor of about 2 would be applied to the computed k's at 300°K listed in Table II. This tunneling factor would make k computed by the modified procedure about 60% larger than the experimental k. The k computed by the single-repulsion assumption would disagree with the experimental k at 300°K by a factor of 200 if this tunneling factor were applied.

The mean deviation between the experimental log k and the log k computed by the modified procedure is 0.37 at 300°K. Only in the case of the abstraction from propane is this deviation in log k greater than 0.5. If the propane case is omitted, the average excess of the experimental log k over this computed log k is only 0.23, which corresponds to deviation by a factor of 1.7. A small tunneling correction could improve the agreement further. Inasmuch as these rate constants were computed with the use of the modification that neglects any changes in the force constants for the radical R when it is in the transition state, the agreement with experimental k suggests that in some abstraction reactions it is feasible to treat R as a point mass. The case of propane may represent an example where R should not be so treated. Alternatively, in the case of propane the method may give relatively poor agreement because other trial postulates fail or, less probably, because the experimental results may not be accurate. In view of the unestablished dependability of the trial postulates, it clearly is highly probable that they would not be obeyed by some reactions. Rather, it is surprising that these very simple postulates can provide the good agreement seen in Table II and in previous studies.[4,6-8]

The computing procedure that assumes single repulsion produces rate constants at 300°K which exceed the observed rate constants by a mean factor of 100. This large disagreement is attributable mainly to the low E_0 computed when single repulsion is assumed for $O(^3P)$, since the trial postulate that R can be treated as a point mass was used throughout this study. At

1000°K, where the tunneling effect is generally negligible,[5] the disagreement between the single repulsion computed and the experimental k had dropped to a factor of 15 because the deviation in E_0 has a smaller effect at 1000°K than at 300°K. The modified procedure (*i.e.*, doubled V_r because of triplet oxygen) provided a mean deviation at 1000°K between the experimental and the computed log k of 0.33, which corresponds to a mean factor of 2.1. The propane reaction at 1000°K did not exhibit the marked disagreement noted at 300°K, apparently because of the aforementioned effect of higher temperatures in diminishing the importance of E_0.

To supplement the computations made for abstraction by $O(^3P)$, a set of calculations for abstraction by the singlet excited electronic states $O(^1D)$ and $O(^1S)$

Table III: Activation Energies and Rate Constants[a] Computed for Reactions with Ground-State and Excited Molecular Oxygen

|	$O_2(^3\Sigma_g^-)$	$O_2(^1\Delta_g)$	$O_2(^1\Sigma_g^+)$
	Reactant, Hydrogen		
E_0, kcal/mol	58	35	20
k (at 300°K)	4×10^{-30}	1×10^{-14}	1×10^{-6}
k (at 1000°K)	3	3×10^4	1×10^6
	Reactant, Water		
E_0, kcal/mol	72	49	34
k (at 300°K)	5×10^{-42}	4×10^{-25}	3×10^{-14}
k (at 1000°K)	3×10^{-4}	60	1×10^6
	Reactant, Methane		
E_0, kcal/mol	57	34	19
k (at 300°K)	6×10^{-30}	4×10^{-14}	2×10^{-6}
k (at 1000°K)	6	6×10^4	5×10^6

[a] The rate constant k, in units of cc/mol sec, for the reaction $RH + O_2 = R + HO_2$.

(7) S. W. Mayer, *J. Phys. Chem.*, **71**, 4159 (1967).

(8) S. W. Mayer, L. Schieler, and H. S. Johnson, ref 3, p 837.

was made for each reactant listed in Table II. Since singlet rather than triplet atomic oxygen was the abstracting species, V_r was not doubled in this set of calculations. The products and the RH reactant were again taken to be in their ground states. In each case, it was found that the computed activation energy did not exceed 1 kcal/mol. This result was not unexpected, since the energetic, excited states can usually supply the energy required by activation energies such as those shown in Table II. The computation also showed that the bending force constant in the transition state was less than 1.2×10^{-13} erg/rad^2 throughout this series of abstractions by O(^{1}D) or O(^{1}S). Therefore, as previously discussed,[6] these abstractions by singlet atomic oxygen should be treated by a collision method rather than a transition-state method. This result agrees with the viewpoint that abstraction by O(^{1}D) or O(^{1}S) is very rapid.[9]

Finally, a set of computations was made for the abstraction of hydrogen atoms by $O_2(^3\Sigma_g^-)$, O_2 ($^1\Delta_g$), or O_2 ($^1\Sigma_g^+$) to form ground state HO_2

$$RH + O_2 = R + HO_2 \qquad (5)$$
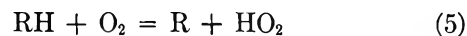
where RH was H_2, H_2O, or CH_4. (In view of the triplet nature of ground state $O_2(^3\Sigma_g^-)$, V_r was doubled as in the modified computing procedure.) For every reaction in this series of computations, it was found that the activation energy was within 1 kcal/mol of the endothermicity of the reaction. Computed rate constants (and activation energies) for H atom abstraction by molecular oxygen are presented in Table III. It is evident that the rate constants in Table III are much lower than the rate constants for abstraction by atomic oxygen (Table II). Consequently, these computations support the view that combustion initiates *via* reaction with atomic oxygen much more readily than by reaction with molecular oxygen.

Acknowledgment. The authors are grateful for the valuable correspondence with Professor H. S. Johnston of the University of California at Berkeley, Berkeley, California.

(9) W. B. DeMore, *J. Chem. Phys.*, **47**, 2777 (1967).

Reaction of Recoil Tritium with Methylsilanes

by Judith Witkin[1] and Richard Wolfgang

Department of Chemistry, Yale University, New Haven, Connecticut 06511 (*Received February 7, 1968*)

The reactions of hot hydrogen atoms, in the form of tritium recoiling from nuclear reactions, with methylsilanes have been studied. Reaction types found are similar to those with homologous hydrocarbons and are in accord with the previously postulated reaction models. A greater reactivity of silanes, especially for abstraction processes, appears related to the weakness of the Si–H bond. Yield patterns of reactions involving rupture of C–Si bonds correlate with known properties of silicon bonds and inertial restrictions on relaxation motions.

Introduction

The discovery that tritium recoiling from nuclear processes reacts as hot atoms[2] has led to an intensive study of this species. Nearly all work, from the initial characterization of the basic abstraction and displacement interactions[2] to the identification of the factors controlling these reactions, has been done using hydrocarbon systems.[3–6] The resultant body of information provides a prototype example of the nature of hot-atom chemistry. The present work was undertaken to determine whether the generalizations drawn from hydrocarbons are applicable to other systems. Silanes were chosen because the variety of possible products is sufficiently large that it should be possible to identify any significant changes in mechanism. Furthermore, while

silanes have obvious similarities to hydrocarbons, there are also some significant and interesting differences. Prominent among these is the greater size of the silicon atom, the relative weakness of the bonds it forms, and the possible availability of d orbitals which tends to stabilize distortion of its compounds from tetrahedral

(1) Work performed in partial satisfaction of the requirements for the M.S. degree.

(2) M. El-Sayed and R. Wolfgang, *J. Amer. Chem. Soc.*, **79**, 3286 (1957).

(3) D. Urch and R. Wolfgang, *ibid.*, **83**, 2982 (1961).

(4) W. Breckenridge, J. Root, and F. S. Rowland, *J. Chem. Phys.*, **39**, 2374 (1963); **43**, 3695 (1965).

(5) R. Wolfgang, *Progr. Reaction Kinetics*, **3**, 99 (1965).

(6) R. Wolfgang, *Ann. Rev. Phys. Chem.*, **16**, 15 (1965).

configuration. We find that these factors do indeed appear to modify the nature of hot-atom reactions with silanes.

The present work on methylsilanes was performed in 1962 but was not published then, in part because we considered it to be incomplete. However, recent studies of Cetini, et al.,[7,8] on the complementary systems, SiH_4 and Si_2H_6, tend to support and complete our work and lead to its publication at this time.

Experimental Section

Mixtures of the appropriate silane ($\sim$76 cm) together with ^3He ($\sim$2 cm) and, in certain cases, O_2 ($\sim$1 cm) were exposed to slow neutrons. The nuclear reaction ^3He (n, p)T produced tritium atoms of high energy which interacted with the silane to form labeled products. The oxygen was present as a possible scavenger for tritium reaching thermal energies, but as discussed below, probably did not act as such because of the high thermal reactivity of atomic hydrogen with silanes. With each batch of samples, an ampoule containing only butane and ^3He was irradiated to serve as a monitor for the amount of tritium produced. After irradiation, the tritium-labeled products in each sample were analyzed by radio gas chromatography.[9]

All of the above procedures have been described elsewhere.[10] Aspects of the method peculiar to this experiment are given below.

Silanes were obtained from Penninsular Chemical Co. They contained less than 0.1% of low-boiling impurities or were purified to that level by gas chromatography. Samples were contained in cylindrical quartz ampoules about 6 ml in volume. These were irradiated in the "instrument tunnel" of the Brookhaven graphite reactor at a temperature of $\sim$25° and a neutron flux $\sim$2 $\times$ 10⁹ neutrons/cm² sec for a time sufficient to yield (1–4) $\times$ 10⁶ disintegrations of tritium/min.

Separation of labeled products was done on a 10-ft silicone gas chromatographic column. This separates silanes from each other and from lower boiling compounds. HT and CH₃T were separated from each other and silanes by a 10-ft silica gel column. The identity of each labeled compound was determined by verifying that its elution characteristics were the same as that of the unlabeled carrier material.

No authentic sample of dimethylsilane was available. However, the probable elution time of this compound on the silicone column was estimated by plotting the boiling points of the silanes available against their elution volumes and interpolating, using the known boiling point of dimethylsilane. When dimethylsilane was expected as a product, a peak did appear at about the predicted elution volume. This activity was accordingly assigned to dimethylsilane. However, this identification cannot be regarded as completely certain.

Reproducibility of relative yields between similar samples was good, amounting to ±3% for major products and of the order of ±10% for minor peaks. At the time this work was done, monitoring techniques had not been fully developed; therefore, absolute yields are accurate only to about 20%.

Results

Yields of labeled compounds produced by reaction of tritium with methylsilanes are shown in Table I. They are expressed in terms of percentage of total observed volatile activity. Although the accuracy of monitoring was relatively low (as mentioned in the Experimental Section), the total observed volatile activity approximates the total tritium activity produced to within about 20%. Hence, Table I also provides a measure, within this accuracy, of the absolute yields.

By far, the greater part of the observed products are molecules which can be produced from the reacting silane by hydrogen abstraction, e.g.

$$T + CH_3SiH_3 \longrightarrow HT + \dot{C}SiH_5 \qquad (1)$$

or replacement of a hydrogen atom, e.g.

$$T + CH_3SiH_3 \longrightarrow CH_2TSiH_3$$
$$(or\ CH_3SiH_2T) + \dot{H} \qquad (2)$$
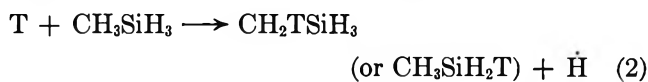
or replacement of a radical, e.g.

$$T + CH_3SiH_3 \longrightarrow CH_3T + \dot{S}iH_3 \qquad (3)$$

$$T + CH_3SiH_3 \longrightarrow SiH_3T + \dot{C}H_3 \qquad (4)$$

This finding was expected from the work on hydrocarbons, where essentially all nonradical products could be accounted for by analogous abstraction and replacement reactions.[3-6] It would thus appear that the basic model of hot-hydrogen reactions developed for hydrocarbons is substantially applicable to silanes.

In the case of tetramethylsilane, there are small but still significant yields of molecules which do not fall within the simple systematics outlined above. About 2% of a product tentatively identified as dimethylsilane and about 5% of a substance having an elution volume similar to ethane on a silica gel column were found. The possibility that these are experimental artifacts is not excluded. Thus the 5% yield could conceivably have its origin in decomposition of trace amounts of labeled silanes on the chemically active silica gel column. The dimethylsilane could arise from a tritiated radical produced by a double-displacement process

$$T + (CH_3)_4Si \longrightarrow (CH_3)_2\dot{S}iT + 2\dot{C}H_3$$
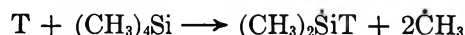
which subsequently acquires a hydrogen atom in a sec-

(7) G. Cetini, O. Gambino, M. Castiglioni, and P. Volpe, *J. Chem. Phys.*, **46**, 89 (1967); G. Cetini, O. Gambino, and B. Minasso, *Atti Acad. Sci. Torino: Classe Sci. Fis., Mat. Nat.*, **97**, 1137 (1963).

(8) G. Cetini, O. Gambino, M. Castiglioni, and P. Volpe, *ibid.*, **99**, 1093 (1965).

(9) R. Wolfgang and F. S. Rowland, *Anal. Chem.*, **30**, 903 (1958).

(10) D. Seewald and R. Wolfgang, *J. Chem. Phys.*, **47**, 143 (1967).

Table I: Yields of Labeled Products from Reaction of Recoil Tritium with Silanes[a]

Reacting compound	Scavenger	Labeled Product							
		H_2	CH_4	SiH_4	CH_3SiH_3	$(CH_3)_2SiH_2$[b]	$(CH_3)_3SiH$	$(CH_3)_4Si$	Uniden-tified[c]
CH_3SiH_3	...	64.0	5.4	2.1	27.2	...	...	...	1.3
	...	66.5	4.8	2.1	25.2	...	...	...	1.4
	O_2	61.7	5.4	2.1	28.6	...	...	...	2.2
$(CH_3)_3SiH$	...	64.0	5.2	...	...	2.2	28.8	...	...
	O_2	63.5	5.1	...	...	2.1	29.5	...	...
	O_2	64.8	5.0	...	...	2.2	27.6	...	0.4
$(CH_3)_4Si$	...	56.2	6.2	...	...	1.8	1.3	28.5	6.0[d]
	...	56.1	6.6	...	...	1.8	1.3	28.6	6.6[d]
	O_2	52.5	6.2	...	...	2.2	2.0	31.4	5.7[d]

[a] Expressed as per cent of total observed activity. [b] See the Experimental Section. [c] Or origin uncertain. [d] Includes about 5% of a substance having an elution volume on a silica gel column similar to that of ethane.

ondary process. This would, however, require that oxygen scavenger does not prevent the secondary reactions. A further possibility is that these unexpected products arise in rearrangements made possible because the time scale of a T–silane collision might be somewhat longer than that for a typical T–alkane collision (see below). In any case, conclusions which involve the character of these products must be regarded as highly tentative.

Discussion

We have noted that, with certain minor exceptions, the systematics of hot-hydrogen reactions with methylsilanes closely resemble those with alkanes. Processes of hydrogen abstraction (eq 1), T for H replacement (eq 2), and T for alkyl (or silyl) replacement (eq 3 and 4) account for nearly all products. There are, however, changes in yield patterns compared to the analogous hydrocarbons, which indicate that the mechanisms involved, though similar in outline, may differ significantly in detail. These differences appear to be reasonable when the differences between C and Si bonds, as given in Table II, are considered.

The total reactivity of silane systems is clearly much higher than that of analogous hydrocarbons. Compar-

Table II: Comparison of C and Si Bonding Constants[a]

	C–C	C–H	Si–C	Si–H
Bond length, Å	1.54	1.09	1.87	1.48
Bond strength, kcal	83	99	69	70
Bending vibration, cm^{-1}		1300		400

[a] Data are taken from L. Pauling, "The Nature of the Chemical Bond," 3rd ed, Cornell University Press, Ithaca, N. Y., 1960; G. Herzberg, "Molecular Spectra and Molecular Structure," Vol. II, D. Van Nostrand Co., Inc., Princeton, N. J., 1945. Values are typical for single bonds in simple molecules.

ison of absolute yields indicates that all products from the CH_3SiH_3 system (Table I) appear in greater yield than those from CH_3CH_3,[11,12] although the increase in the T- or H-replacement product is hardly outside experimental error. This is consistent with results of Cetini, et a.,[7] on SiH_4 compared to CH_4.[10] Table III shows yields in homologous hydrocarbon and silane reactants, relative to T for H substitution. It is apparent that most of the increase in silane reactivity is due to abstraction. A related finding (Table I) is that oxygen scavenger has relatively little effect on yields from methylsilanes, a fact also apparent in the study of the effect of I_2 on silane.[7]

The increase in HT yield accords with the finding of Rowland, et al.,[4] that abstraction efficiency depends on bond energy. The Si–H bond is so weak that HT formation is actually exoergic by about 30 kcal. However, the lack of effect of oxygen scavenger makes it difficult to decide whether the higher efficiency of this reaction is due to hot or thermal reaction of the tritium, or both. An increased hot reactivity would mean that few hydrogen atoms reach thermal energies. An increased thermal reactivity would have the result that the oxygen could not compete effectively for H atoms, i.e., the system would be "self-scavenging." Either way, oxygen scavenging would have little effect. This question could be resolved by extensive moderator and scavenger studies. In any case, the broad conclusion that abstraction in general is facilitated by the weakness of Si–H bonds is most reasonable.

The findings on the alkyl- vs. silyl-substitution reaction (Table III) provide the most interesting insight into how differences between the central atoms affect the model of hot hydrogen reactions. In these processes, a C–Si bond is broken and the tritium has a choice of combining with a methyl or silyl group. In

(11) D. Urch and M. Welch, Radiochim. Acta, 5, 202 (1966).
(12) R. T. K. Baker, private communication.

Table III: Relative Frequency of Abstraction and Substitution Processes in Homologous Hydrocarbons and Methylsilanes[a]

Reacting molecule	Abstraction (HT)	Substitution processes		T for $X(CH_3)_mH_{3-m}(CH_3T)$
		T for H	T for CH_3	
CH_3SiH_3	216	100 (CH_3SiH_3T)	7.3 (SiH_3T)	18.9
CH_3CH_3[b]	165	100 (CH_3CH_3T)	5.6[d] (CH_3T)	5.6[d]
$(CH_3)_3SiH$	225	100 ($Si(CH_3)_3HT$)	7.5 ($Si(CH_3)_2H_2T$)	17.7
$(CH_3)_3CH$[c]	192	100 $C(CH_3)_3HT$)	3.0 ($C(CH_3)_2H_2T$)	14.1
$(CH_3)_4Si$	167	100 ($Si(CH_3)_4T$)	6.3 ($Si(CH_3)_3HT$)	19.8
$(CH_3)_4C$[c]	139	100 ($C(CH_3)_4T$)	2.5 ($C(CH_3)_3HT$)	21.0

[a] Yields relative to 100 for H displacement in scavanged systems. Products shown in parentheses. [b] References 11 and 12. [c] Reference 3. [d] Actual yield 11.1; for purposes of comparison, half of this is listed in each column.

the case of CH_3SiH_3, the product ratio $CH_3T:SiHT_3$ favors CH_3T. Yet in a more complex silane, such as $(CH_3)_3SiH$, the ratio $CH_3T:Si(CH_3)_2HT$ is smaller than the corresponding ratio $CH_3T:C(CH_3)_2HT$ of products from reaction with $(CH_3)_3CH$.

A reasonable explanation for this apparently anomalous situation can be found in the differences in bond energies and steric factors, operating under inertial[3] restrictions on vibrational–rotational relaxation.[5,6,13] A statement of the "golden rule" of hydrogen hot-atom chemistry is that reactions which can only provide a strong bonding orbital for the incoming tritium by an intrinsically slow rotational–vibrational relaxation tend to be disfavored. Thus when a hot T atom attacks a C–C bond in $(CH_3)_3CCH_3$, the inertia of the system is such that the time of collision $\sim 10^{-14}$ sec[5,6] is insufficient for the CH_3 and $C(CH_3)_3$ groups to separate enough to let the T atom come between. However, the CH_3 group can reorient itself rapidly, primarily by rotation of the H atoms around the carbon, to provide a strong, tetrahedrally oriented orbital to capture the tritium. On the other hand, because of the greater mass of the CH_3 radical, the $C(CH_3)_3$ group requires a much longer time to reorient and make a strong bond available to the tritium. As a result, the yield of CH_3T is much greater than that of $C(CH_3)_3T$.[5,6,13]

Consider now attack of a T atom on a C–Si bond. A representative configuration for such a process is shown in Figure 1. In the case of CH_3SiH_3, both CH_3 and SiH_3 can relax to provide an optimally oriented orbital within the time of collision. Since the C–H bond is intrinsically much stronger than the Si–H bond, the greater yield of CH_3T is reasonable. Now consider the analogous situation in the case of attack on the C–Si linkages in $(CH_3)_3SiCH_3$ and the C–C linkages in $(CH_3)_3CCH_3$. In both cases because of the slowness of reorientation of the $Si(CH_3)_3$ and $C(CH_3)_3$ groups, respectively, formation of CH_3T is strongly preferred.
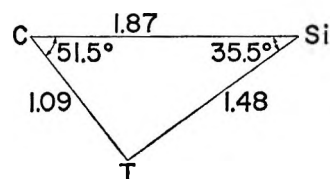
Figure 1. Representative configuration for attack by a tritium atom on a C–Si bond. Distances shown represent normal bond lengths for C–Si, C–H, and Si–H linkages (see Table II).

The fact that production of $Si(CH_3)_3T$ is less disfavored than that of $C(CH_3)_3T$ becomes reasonable on considering Figure 1. From this, it is evident that without rotational–vibrational relaxation of ligand methyl radicals, the T atom is closer to being at a normal bond angle to the Si than it is to the C. Further, the frequency of the bending motion of a Si–H bond is less than that of a C–H bond (Table II), meaning that distortion from tetrahedral symmetry has less weakening effect. Both these factors imply that upon initial impact the $Si(CH_3)_3$ radical can bind the tritium atom more strongly than can the $C(CH_3)_3$. Thus the chance that the proto-$Si(CH_3)_3T$ complex can retain the tritium atom until relaxation is complete is greater than for a proto-$C(CH_3)_3T$ complex.

In conclusion, it appears that the basic model for hot-hydrogen reactions, as developed for hydrocarbons, is also applicable to silanes. Differences between the two systems seem to follow naturally from known differences of bonding properties of silicon and carbon atoms.

(13) R. Odum and R. Wolfgang, *J. Amer. Chem. Soc.,* **85,** 1050 (1963).

The Mechanism of Hydrogen Formation in the γ Radiolysis of 1,4-Dioxane and Its Mixtures with Water

by Robert R. Hentz and Warren V. Sherman

Department of Chemistry and the Radiation Laboratory,[1] University of Notre Dame, Notre Dame, Indiana 46556
(Received February 8, 1968)

In the γ irradiation of pure liquid 1,4-dioxane, $G(H_2) = 1.31$ was obtained. The hydrogen yield is suppressed to a limit of $G(H_2) \approx 1.0$ by the H atom scavenger 1-hexene and by the electron scavengers N_2O and c-C_4F_8. Consequently, $G(H_2) \approx 1.0$ is attributed to molecular elimination from directly excited dioxane molecules. The yield of scavengeable electrons, as determined with N_2O and 0.1 N H_2SO_4, corresponds to $G = 3.1$–3.4. Thus $G(H_2) \approx 0.3$ results from H atoms produced with ~10% efficiency in the neutralization of dioxane cations by electrons. An enhancement of $G(H_2)$ by NH_3 is observed that indicates proton transfer from a dioxane cation to give NH_4^+, which on neutralization by an electron presumably yields H with unit efficiency. Water is considerably less effective than NH_3 in the enhancement of $G(H_2)$; the results suggest that the specific rate of proton transfer to H_2O is less than that to NH_3 in liquid dioxane. As the water–dioxane composition is varied over the whole range, $G(H_2)$ passes through a maximum. Such behavior is related to a change in the yield of free solvated electrons with change in the dielectric constant of the medium. The presence of dioxane in cyclohexane causes a suppression of $G(H_2)$, which is restored by the addition of methanol or NH_3. The results indicate that positive charge is transferred from cyclohexane cations to dioxane and that the added base scavenges cations of both cyclohexane and dioxane with about equal efficiency.

Introduction

In a preliminary communication, $G(H_2) = 1.4$ was reported for radiolysis of pure dioxane;[2] such a value is significantly smaller than the values generally observed for saturated ethers, alcohols, and hydrocarbons.[3] The small hydrogen yield in dioxane radiolysis cannot be attributed, as in the case of unsaturated compounds, to self-scavenging of hydrogen atoms. On the contrary, reaction of H with dioxane to give H_2 should be relatively efficient. Consequently, the low hydrogen yield must reflect a low probability of formation of H and H_2 in the primary processes. The aim of the present study was to clarify the mechanism of formation of the small hydrogen yield obtained in the radiolysis of 1,4-dioxane. The study of water–dioxane mixtures yielded somewhat surprising results of special interest.

Experimental Section

Materials. The 1,4-dioxane (Matheson Coleman and Bell spectroscopic reagent) was passed through a column of activated alumina to remove peroxides. Then it was refluxed over sodium under an atmosphere of dried nitrogen for ~16 hr and subsequently was distilled from sodium on a 3-ft Nester-Faust spinning-band column. The middle third of the distillate was retained and stored in a drybox under dry nitrogen. The uv spectrum of this dioxane has been reported.[2]

Methanol (Fisher) was refluxed with dinitrophenylhydrazine and sulfuric acid for approximately 24 hr and then was distilled on the Nester-Faust spinning-band column; both operations were carried out under dried nitrogen. The middle third of the distillate was re-

tained for use. Methanol-d (Merck Sharp and Dohme) was used as received. Cyclohexane (Fisher spectro-analyzed) was passed through a column of silica gel and stored over sodium. 1-Hexene (Aldrich Chemical Co.) was used after being passed through a column of activated alumina.

Ammonia, perfluorocyclobutane, and nitrous oxide, all obtained from Matheson Co., were purified by three trap-to-trap distillations under vacuum with rejection of head and tail fractions; the gases were stored on the vacuum line, and prior to use they were pumped for at least 30 min at −196°. Deuterium oxide (Columbia Organic Chemicals, 99.5%) was distilled from an alkaline permanganate solution and then was redistilled once in a system protected from atmospheric water and carbon dioxide by a drying tube containing sodium hydroxide. Triply distilled water used in all aqueous experiments was kindly supplied by Farhataziz. All other chemicals were of reagent grade and used as received.

Procedures. The solution (5 ml) to be irradiated was placed in a 13-mm o.d. Pyrex reaction tube fitted with a standard-taper joint and break-seal. The reaction tube was attached to a vacuum line, and the solution was thoroughly degassed by successive freeze-pump-

(1) The Radiation Laboratory of the University of Notre Dame is operated under contract with the U. S. Atomic Energy Commission. This is AEC Document No. COO-38-589.

(2) R. R. Hentz, F. W. Mellows, and W. V. Sherman, *J. Phys. Chem.*, 71, 3365 (1967).

(3) M. Haissinsky and M. Magat, "Radiolytic Yields," Pergamon Press Ltd., London, 1961.

thaw cycles. Gaseous solutes were admitted into an evacuated bulb of known volume to a desired pressure, and the gas was condensed into the reaction tube containing degassed solution at 77°K. The reaction tube then was sealed and was allowed to warm to room temperature; when a gaseous solute was present, the reaction tube was shaken vigorously for ∼10 min to ensure equilibration.

Samples were irradiated in a 4-kc ^{60}Co source. Over the period of the work, dose rates received by Fricke-dosimeter solutions, based on $G(Fe^{3+})$ = 15.6, were (1.82–1.64) × 10^{18} eV ml^{-1} min^{-1}. The dose received by a particular solution was calculated by correction for the electron density relative to that of the dosimeter.

After radiolysis the reaction tube was attached to a vacuum line. Gas products were collected with a Toepler pump, using two or three freeze–pump–thaw cycles, at −196 and −77° and their pressure was measured in a calibrated volume. The −196° fraction was analyzed for H_2, O_2, N_2, CH_4, and CO by gas chromatography using a Gow-Mac 9677 matched-thermistor detector, a column of molecular sieve (Linde 5A) at room temperature, and helium as the carrier gas; the −77° fraction was analyzed with a Consolidated 21-103A mass spectrometer. Hydrogen isotopes also were analyzed with the mass spectrometer. In a number of experiments, mass spectrometry was used as a cross-check on the gas chromatographic analyses. The agreement was better than ±5%.

Determination of Gas Solubilities. Because there was a dead volume above the liquid sample in the sealed reaction tube, calculation of the concentration of gaseous solutes required a determination of the gas solubilities. The solubilities were determined with the simple apparatus shown in Figure 1. The solvent (100 ml) was placed in bulb A and was degassed by repeated pumping (*via* stopcock 1) and shaking. With stopcock 1 closed, the solvent was allowed to equilibrate and the vapor pressure was measured with the manometer. Next, stopcock 2 was rotated to close off bulb A, and bulb B was evacuated and then filled with gas to a measured pressure. Stopcock 1 was closed, and the gas was condensed in the limb of B by cooling in liquid nitrogen. Stopcock 2 then was rotated, and the contents of A were tipped into B by raising A *via* the flexible tube. After closure of bulb A with stopcock 2, the contents of B were allowed to warm to room temperature and were equilibrated by vigorous shaking. Because the volume bounded by stopcocks 1 and 2 was previously measured (530 ml), measurement of the pressure permitted calculation of the Ostwald solubility coefficient, β.[4] Values of β for NH_3, N_2O, and c-C_4F_8 in dioxane and for NH_3 in cyclohexane were determined to be, with ∼10% accuracy, 17, 2.8, 1.3, and 2.0, respectively, at ∼24°. For N_2O, values of β equal to 2.8 and 1.3 were obtained at electron fractions
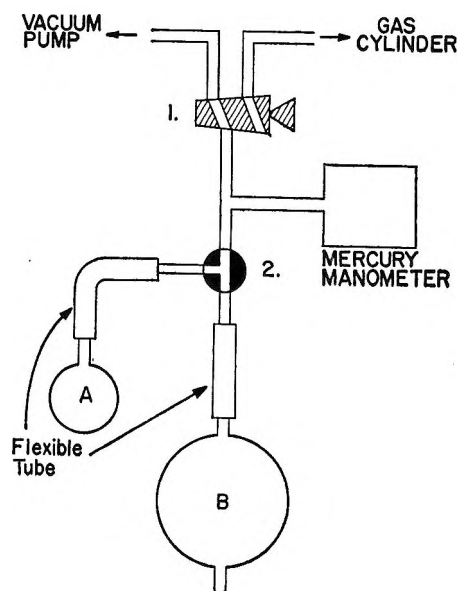
Figure 1. Apparatus for the determination of gas solubilities.

of water equal to 0.1 and 0.5, respectively. Gas concentrations in the irradiated liquids were calculated using these β values and a dead-space volume estimated to be equal to the volume occupied by the solution.

Results

Pure Dioxane. Gas products identified in the radiolysis of dioxane were hydrogen, carbon monoxide, ethylene, and traces (G < 0.05) of methane and ethane. No dose dependence of hydrogen and carbon monoxide yields was observed over the range 3.6 × 10^{18} to 4.9 × 10^{20} eV ml^{-1}. $G(H_2)$ = 1.31 ± 0.04 and $G(CO)$ = 0.18 ± 0.03 represent the results of eight experiments over this dose range. $G(C_2H_4)$ decreased with increasing dose over the same range; G values at the lowest and highest doses were 1.58 and 0.50, respectively. At a dose of 4.3 × 10^{21} eV ml^{-1}, the hydrogen and carbon monoxide yields also were lower; such a dose gave values of $G(H_2)$ = 0.99, $G(CO)$ = 0.08, and $G(C_2H_4)$ = 0.20.

Dioxane–Water Mixtures and the Effect of Solutes. The dependence of radiolysis yields (dose = 1.1 × 10^{20} eV ml^{-1}) on the electron fraction, F, of added water is shown in Figure 2. The effect of dose was checked for F = 0.1 and 0.5; no dose dependence was observed over the range from 9.2 × 10^{18} to 1.1 × 10^{20} eV ml^{-1}. Essentially identical yields of total hydrogen and other products were obtained with D_2O in place of H_2O; the isotopic composition of the hydrogen yields is presented in Table I. A further enhancement of hydrogen yields was observed in H_2O–dioxane mixtures with 0.1 N sulfuric acid present (Figure 2). The value of $G(H_2)$ = 4.1 ± 0.2 is essentially independent of the amount of water present over the range F = 0.1–0.9.

(4) β equals the ratio at equilibrium of the molar concentration of gas in the liquid phase to that in the gas phase.
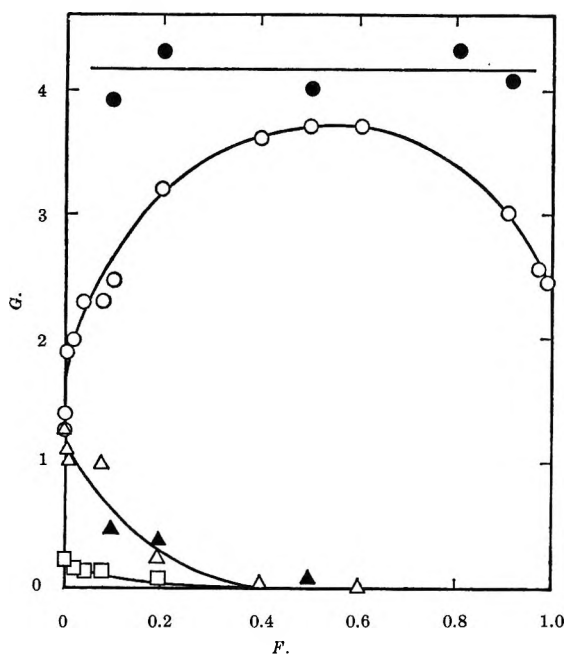
Figure 2. Yields in the radiolysis of dioxane-water mixtures ($\bigcirc$, $G(H_2)$; $\triangle$, $G(C_2H_4)$; $\square$, $G(CO)$) and in the presence of 0.1 N H_2SO_4 ($\bullet$, $G(H_2)$; $\blacktriangle$, $G(C_2H_4)$). Note: $M = 55.5F$ and mole fraction $X = 4.8F/(1 + 3.8F)$. F denotes the electron fraction of water.

Table I: Isotopic Composition of the Hydrogen Yields from D_2O-Dioxane Mixtures[a]

$F(D_2O)$	$G(H_2)$	$G(HD)$	$G(D_2)$
0	1.31	. . .	. . .
0.1	0.97[b]	1.53[b]	0.04
0.2	0.77	1.99	0.08
0.6	0.29	2.97	0.25
0.8	0.18	2.95	0.31

[a] Dose = 1.1 × 10²⁰ eV ml⁻¹. [b] Essentially identical results were obtained for a dose = 9.2 × 10¹⁸ eV ml⁻¹.

The effect of added ammonia on $G(H_2)$ was qualitatively similar to that of water but, as shown in Figure 3, a given concentration of ammonia up to 1 M (upper limit attainable at convenient working pressures) caused a significantly greater enhancement of $G(H_2)$. The presence of both water and ammonia had an additive effect on $G(H_2)$; thus the addition of 0.07 and 0.2 M NH_3 to a solution containing water at $F = 0.1$ increased $G(H_2)$ from 2.5 to 2.8 and 2.9, respectively.

The effect of nitrous oxide in pure dioxane and in solutions containing 0.1 and 0.5 electron fraction of water is shown in Figure 4. The initial slope of the $G(N_2)$ vs. [N_2O] curve increases with increasing water content, although similar values of $G(N_2)$ are attained near 0.25 M. The depression of $G(H_2)$ by a given concentration of nitrous oxide increases with water concentration; in all three solutions, $G(H_2)$ approaches a limiting value of 1.0 at higher N_2O concentrations.
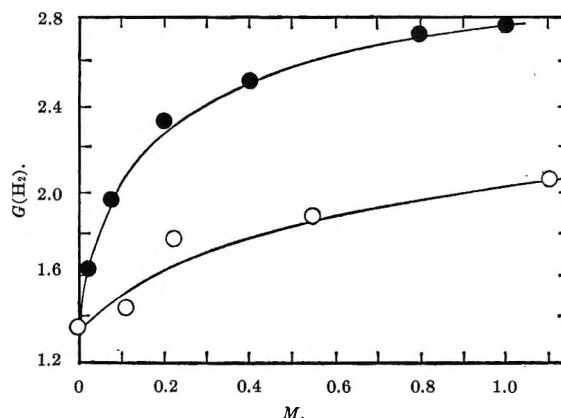
Figure 3. Hydrogen yields from dioxane as a function of the molarity, M, of ammonia ($\bullet$) or H_2O ($\bigcirc$).

A similar enhancement of $G(N_2)$ was not found with ammonia present in place of water. Radiolysis of a solution containing 7.5 × 10⁻² M N_2O and 1.0 M NH_3 gave $G(N_2) = 2.13$, essentially the same as that of a solution containing N_2O alone, and $G(H_2) = 1.14$.

The presence of 0.1 M benzene had no significant effect on $G(H_2)$ from dioxane. The effects of 1-hexene, perfluorocyclobutane, and iodine are shown in Table II. A concentration of 10⁻² M iodine reduced $G(H_2)$ in solutions containing 0.1 and 0.2 electron fraction of water to 1.98 and 2.57, respectively.

Table II: Effect of Solutes on the Hydrogen Yield from Dioxane[a]

Solute	Concn, M	$G(H_2)$
None	. . .	1.31
1-Hexene	0.064	1.08
	0.100	1.19
	0.160	0.95
	0.320	0.96
	0.640	1.02
c-C_4F_8	0.028	1.12
	0.057	1.08
	0.110	1.09
Iodine	0.010	1.26
	0.100	1.13

[a] Dose rate = 1.8 × 10¹⁸ eV ml⁻¹ min⁻¹; total dose = 2.7 × 10¹⁹ eV ml⁻¹.

Hydrogen Yields in Cyclohexane-Dioxane Mixtures. A progressive decrease in $G(H_2)$ was observed with increasing concentration of dioxane in cyclohexane (Figure 5). For solutions containing up to 0.05 M dioxane, the presence of 1 M methanol essentially restored $G(H_2)$ to the value of 5.4 ± 0.1 for pure cyclohexane. At higher dioxane concentrations, as shown in Figure 5, 1 M methanol only partly restored the hydrogen yield. Ammonia had a similar effect. The
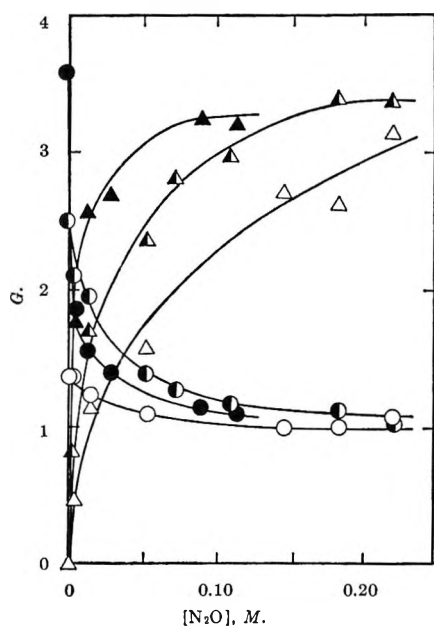
Figure 4. Hydrogen and nitrogen yields from dioxane and its mixtures with water as a function of the molarity of nitrous oxide: $F = 0$: O, $G(H_2)$; △, $G(N_2)$; $F = 0.10$: ◐, $G(H_2)$; ◭, $G(N_2)$; $F = 0.50$: ●, $G(H_2)$; ▲, $G(N_2)$.
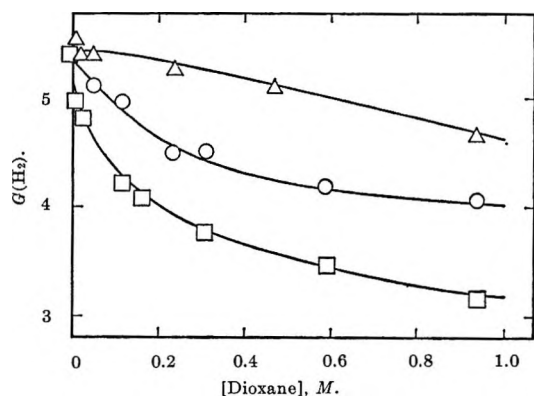

Figure 5. Effect of methanol or ammonia on $G(H_2)$ from solutions of dioxane in cyclohexane: □, $G(H_2)$ (with dioxane as the only solute); O, $G(H_2)$ (with 0.13 M ammonia present); △, $G(H_2)$ (with 1.0 M methanol present).

presence of 0.13 M ammonia restored $G(H_2)$ in solutions containing up to 0.024 M dioxane to the value for pure cyclohexane; at higher dioxane concentrations, the same concentration of ammonia only partly restored $G(H_2)$.

Figure 6 shows the isotopic composition of hydrogen yields from cyclohexane solutions containing 1.0 M methanol-d and various dioxane concentrations. In the absence of dioxane, the hydrogen yield was 30% HD and 70% H_2, as compared with 28% HD and 72% H_2 obtained by Buchanan and Williams[5] for cyclohexane containing 1.1 M C_2H_5OD. The yield of HD remains approximately constant with increasing dioxane concentration; thus the decrease in $G(H_2)$ almost completely accounts for the decrease in total hydrogen yield.
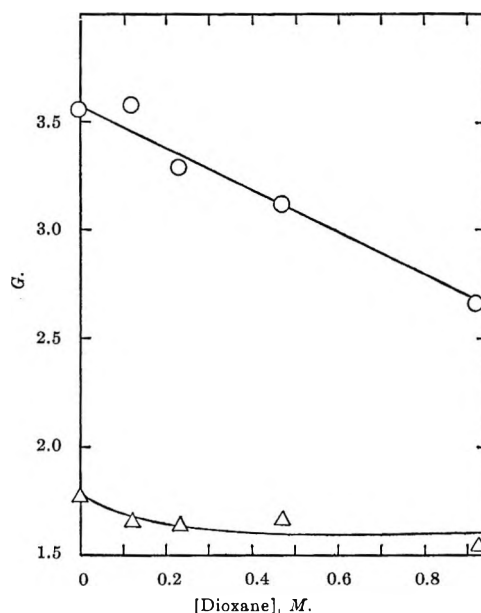
Figure 6. Isotopic composition of the hydrogen yields from cyclohexane solutions of dioxane and 1.0 M methanol-d: O, $G(H_2)$; △, $G(HD)$.

Discussion

Dioxane. The formation of N_2 in radiolysis of dioxane with added N_2O, as shown in Figure 4, is considered evidence for the formation of scavengeable electrons. $G(N_2)$, at corresponding concentrations of N_2O, is 20–50% lower than values obtained in cyclohexane.[6-8] Such a result may be attributable to suppression of the secondary reaction

$$O^- + N_2O \longrightarrow N_2 + O_2^- \tag{1}$$
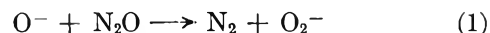
because of enhanced H abstraction by O^- from the more labile CH bonds in dioxane; if so, $G(N_2)$ in dioxane may correspond more closely to the yield of scavenged electrons. Attainment of a limiting $G(H_2) \approx 1.0$ with increase in N_2O concentration indicates that, unlike the situation in cyclohexane and other saturated solvents, only a small fraction ($\sim$24% corresponding to $\Delta G \approx -0.3$) of the hydrogen yield can be suppressed by N_2O. Thus with the assumption of a total $G(e^-) \approx 3$, only 10% of the scavengeable electrons ultimately yield H_2.

The effect of c-C_4F_8 on $G(H_2)$ was studied for confirmation of the N_2O results. The bond strengths of CF and HF are 152[9] and 136[10] kcal mol^{-1}, respectively. Consequently, abstraction of H from dioxane should

(5) J. W. Buchanan and Ff. Williams, *J. Chem. Phys.*, **44**, 4377 (1966).

(6) G. Scholes and M. Simic, *Nature*, **202**, 895 (1964).

(7) W. V. Sherman, *J. Chem. Soc.*, *A*, 599 (1966).

(8) S. Sato, R. Yugeta, K. Shinsaka, and T. Terao, *Bull. Chem. Soc. Jap.*, **39**, 156 (1966).

(9) M. M. Bibby and G. Carter, *Trans. Faraday Soc.*, **59**, 2455 (1963).

(10) S. W. Benson, *J. Chem. Educ.*, **42**, 502 (1965).

remain the predominant fate of thermal H at the concentrations of c-C_4F_8 used. Rajbenbach[11] has concluded that suppression of $G(H_2)$ by c-C_4F_8 in radiolysis of n-C_6H_{14} is attributable to the scavenging of electrons. The suppression of $G(H_2)$ in dioxane radiolysis by concentrations of c-C_4F_8 up to the maximum attainable at atmospheric pressure is shown in Table II. The results are consistent with the conclusions drawn from the N_2O experiments.

An olefin such as 1-hexene (IP = 9.46 eV[12]) does not scavenge electrons and cannot undergo charge transfer with an unexcited dioxane (IP = 9.13 eV[12]) cation. However, addition of thermal H to olefins is rapid,[13] and, therefore, the suppression of $G(H_2)$ by added 1-hexene to a limiting value of ~ 1.0 (cf. Table II) is consistent with a value of $G(H) \approx 0.3$ in the radiolysis of dioxane. Coincidence of the limiting values obtained with 1-hexene and the electron scavengers suggests that electrons are precursors of thermal H; i.e., it appears that the $\sim 10\%$ of scavengeable electrons that ultimately yield H_2 do so via the formation of thermal H. The results presented in Table II for I_2 as the solute, which presumably can scavenge both electrons and H, also are consistent with the view presented.

The major portion of the hydrogen yield obtained in γ radiolysis of dioxane, corresponding to $G(H_2) \approx 1.0$, apparently is formed in a molecular elimination process which does not have an electron precursor. Decomposition of a directly excited state is suggested as the source of this hydrogen yield, designated as $G^*(H_2)$. Failure of 0.1 M benzene to affect $G(H_2)$ requires that such an excited state have a lifetime less than $\sim 10^{-10}$ sec, assuming a diffusion-controlled excitation transfer. As expected, 0.1 M benzene (IP = 9.24 eV[12]) must have no effect on the ionic processes responsible for $G(H_2) \approx 0.3$, and benzene must be a less efficient scavenger of H than 1-hexene.

As shown in Figure 3, addition of NH_3 to dioxane produces an increase in $G(H_2)$. In accordance with the arguments of Williams,[14] such an effect is interpreted in terms of the reaction sequence

$$RH^+ + B \longrightarrow R + BH^+ \qquad (2)$$

$$BH^+ + e^- \longrightarrow B + H \qquad (3)$$

$$H + RH \longrightarrow R + H_2 \qquad (4)$$
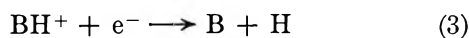
in which RH represents a solvent molecule and B represents a basic solute; reaction 3 is assumed to occur in each such neutralization (i.e., H is formed with unit efficiency). The yield of free ion pairs in dioxane is given by Hummel and Allen[15] as $G_{fi} = 0.04$. Consequently, the enhanced yield of hydrogen must result from a competition between reaction 2 and the rapid recombination (yielding H with only 10% efficiency) of those sibling cation–electron pairs of the solvent ($\sim 99\%$) whose members do not escape from their
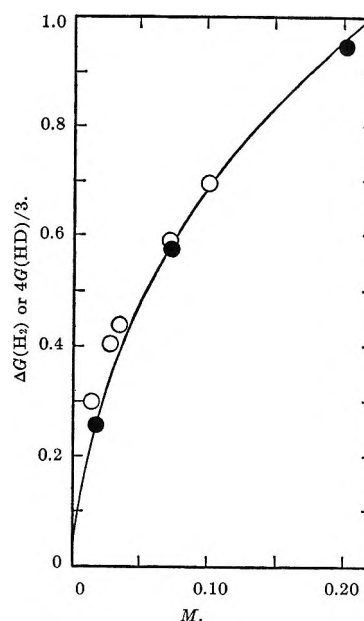

Figure 7. The enhancement of the hydrogen yield, $\Delta G(H_2)$, vs. the molarity of NH_3 in dioxane (●) compared with the yield of the proton transfer, $4G(HD)/3$, vs. the molarity of ND_3 in cyclohexane (○). (Cf. ref 14.)

mutual coulombic fields (hence are designated as geminate or coupled).

The presence of 0.075 M N_2O in a 1 M NH_3 solution gave the same $G(N_2) = 2.13$ as was obtained from 0.075 M N_2O in dioxane alone, but $G(H_2)$ was reduced to a value of 1.14 from $G(H_2) = 2.75$ in 1 M NH_3 solution without N_2O. Apparently the presence of 1 M NH_3 has a negligible effect on G_{fi} and on the over-all evolution of electron-neutralization processes which determines the efficiency of electron scavenging by a given concentration of N_2O.[16] Thus the observed reduction of $G(H_2)$ by 0.075 M N_2O in the 1 M NH_3 solution results from the scavenging of electrons in coupled ion pairs and replacement of the electron in reaction 3 by an anion which does not yield H or H_2 on neutralization by NH_4^+.

In Figure 7, the enhancement of $G(H_2)$ by NH_3 in dioxane is compared with Williams' results[14] for the yield of solvent cations scavenged by proton transfer to ND_3 in c-C_6H_{12}, this yield being taken as the measured $G(HD)$ multiplied by $^4/_3$. The comparison indicates

(11) L. A. Rajbenbach, J. Amer. Chem. Soc., 88, 4275 (1966).

(12) K. Watanabe, T. Nakayama, and J. Mottl, J. Quant. Spectrosc. Radiat. Transfer, 2, 369 (1962).

(13) See, e.g., J. L. McCrumb and R. H. Schuler, J. Phys. Chem., 71, 1953 (1967).

(14) F. Williams, J. Amer. Chem. Soc., 86, 3954 (1964).

(15) A. Hummel and A. O. Allen, J. Chem. Phys., 44, 3426 (1966).

(16) Presumably, the evolution of electron-neutralization processes is governed largely by the dielectric constant, ϵ, of the medium. See, e.g., ref 14 and G. R. Freeman and J. M. Fayadh, J. Chem. Phys., 43, 86 (1965). Assuming ϵ of the solution to be the molecular average of the component values, $\epsilon \approx 3.5$ is obtained for 1 M NH_3 in dioxane as compared to $\epsilon = 2.2$ for pure dioxane.

that the efficiency of ammonia as a scavenger of solvent cations is essentially the same in these two solvents of nearly equal dielectric constant.

Dioxane–Water Mixtures. Interpretation of the radiation chemistry of dioxane–water mixtures is fraught with difficulties. Both the dielectric constant[17] and the structure of the solution[17,18] undergo a continuous change with change in mixture composition. Because of the strong hydrogen-bonding propensities of water and dioxane, the solution structure at any composition appears to be determined by the equilibria between various water–dioxane complexes, the monomers, and "polymers" of water. At the water-rich end of the composition range, the radiation chemistry of dioxane–water mixtures involves the complications of water radiation chemistry as modified in several important respects by the presence of relatively large concentrations of dioxane. At the dioxane-rich end of the composition range, the radiation chemistry involves those complexities peculiar to a solvent of low dielectric constant.[14,19] In view of the complex character of water–dioxane mixtures, a detailed interpretation of the results obtained in this initial study is not attempted. Instead, the results are rationalized in terms of a general model which can be elaborated by further experimentation.

Somewhat surprisingly, as shown in Figure 3, water is considerably less effective than ammonia in the enhancement of hydrogen yields. Such a difference in behavior must be ascribed to a difference in the efficiency with which NH_3 and H_2O convert solvent cations into H atoms *via* reactions 2 and 3. The behavior of water, in particular, may be related to the manner in which water molecules are bound in the dioxane solutions, *i.e.*, to the structure of the solutions. At the lower H_2O concentrations, then, either the scavenging efficiency *via* reaction 2 is greatly reduced relative to that of NH_3 or reaction 3 occurs in a small fraction of the neutralizations. The latter explanation requires that the ratio of hydrogen-yield enhancements obtained in an NH_3 solution and an H_2O solution of the same concentration be independent of concentration and that a comparatively small limiting yield of $G(H_2)$ be approached at high concentrations of water; neither condition is satisfied by the data (see Figures 2 and 3). It is concluded that in dioxane solutions the value of k_2 for water as B is less than for NH_3, which results in a reduction of the efficiency with which reaction 2 competes with neutralization of the dioxane cation of a coupled ion pair.[20]

As the water concentration is increased, a greater fraction of the dioxane cations of coupled ion pairs would be scavenged in reaction 2 for a fixed value of k_2; the efficiency of such scavenging may be a complicated function of water concentration owing to concomitant changes in the value of k_2 as the solution structure changes. Another, perhaps more important, contri-

bution to an increase in $G(H_2)$ is the increase in direct ionization of water molecules which have other water molecules as nearest neighbors. Such a process leads, in every case, to H_3O^+ which on neutralization by the coupled electron is assumed to give H with unit efficiency. Thus an increase in $G(H_2)$ occurs which is determined by the fraction of total ionization occurrent in water molecules.

At 25°, the dielectric constant of a dioxane–water mixture[17] is only 10.1 at a mole fraction of water $X = 0.5$ ($F = 0.17$) and is 31.2 at $X = 0.8$ ($F = 0.45$). Consequently, a pronounced increase in G_{fi} must occur as water concentration is increased from $F = 0.45$ to 1. Such an increase in G_{fi} may account for the passage of $G(H_2)$ through a maximum near $F = 0.55$ (Figure 2). At the dose rates used, all free electrons will react either with small concentrations of impurities for which the specific rate of reaction is diffusion controlled or possibly with dioxane at a considerably smaller specific rate or both. If the net effect of such reactions is to yield less than one molecule of H_2 per free electron, as seems very likely, then the processes which tend to increase $G(H_2)$ on addition of water to dioxane are counteracted by the increase in G_{fi}. In solutions of $F > 0.9$, corresponding to dioxane concentrations below ~1 M, the continuing decrease in $G(H_2)$ must be almost entirely a manifestation of the radiation chemistry of dilute aqueous solutions.

As N_2O concentration is increased in pure dioxane (Figure 4), the gradual increase in $G(N_2)$ and complementary decrease in $G(H_2)$ are characteristic of the scavenging of electrons from coupled ion pairs.[6–8] With water present at $F = 0.1$, the scavenging efficiency of N_2O is increased, as reflected in the greater rates of increase and decrease of $G(N_2)$ and $G(H_2)$, respectively. Because little increase in G_{fi} would be expected ($\epsilon \approx 6.0$), the enhanced scavenging efficiency must be related almost entirely to an increase in the lifetimes of coupled ion pairs, owing to the somewhat larger dielectric constant.[14,19] The enhancement of N_2O scavenging efficiency is still more pronounced at $F = 0.5$. In addition to a further increase in the lifetimes of coupled ion pairs, a significant contribution of G_{fi} to $G(N_2)$ would be expected in this solution with $\epsilon \approx 35$. The present results are not adequate for disclosure of such a contribution. For all three solvent mixtures represented in Figure 4, $G(N_2)$ appears to be approaching an upper

(17) S. K. Garg and C. P. Smyth, *J. Chem. Phys.*, **43**, 2959 (1965).

(18) G. G. Hammes and W. Knoche, *ibid.*, **45**, 4041 (1966); J. R. Goates and R. J. Sullivan, *J. Phys. Chem.*, **62**, 188 (1958).

(19) G. R. Freeman, *J. Chem. Phys.*, **46**, 2822 (1967); A. Hummel and A. O. Allen. *ibid.*, **46**, 1602 (1967).

(20) The lower k_2 for water may be related to its lower proton affinity. A. P. Altshuller, *J. Amer. Chem. Soc.*, **77**, 3480 (1955), gives the gas-phase proton affinity of ammonia as 202 kcal mol⁻¹; that for water has been determined by V. L. Tal'roze and E. L. Frankevich, *ibid.*, **80**, 2344 (1958), to be 169 kcal mol⁻¹.

limit near 3.4, which may represent the yield of scavengeable electrons. The approach of $G(H_2)$ to a lower limit near unity in all three solvents (Figure 4) appears to be a coincidental result of the approximate equality of $G^*(H_2) = 1$ in dioxane radiolysis and the sum of H and H_2 "primary" yields in water radiolysis.[21]

The constancy of $G(H_2) = 4.1$ in 0.1 N H_2SO_4 solutions from $F = 0.1$ to 0.9 indicates that the yield of scavengeable electrons plus $G^*(H_2)$ in dioxane radiolysis approximates the sum of "primary" yields of e_{aq}^-, H, and H_2 in water radiolysis. The value of $G(H_2) = 4.1$ at $F = 0.9$ (~1 M dioxane) is near that expected for a water solution containing 0.1 N H_2SO_4 and an organic additive to convert all H into H_2.[22] At $F = 0.1$, for which ϵ and G_{fi} are small, 0.1 N H_2SO_4 must efficiently scavenge the electrons (with formation of H) of coupled ion pairs. Subtraction of $G^*(H_2) = 1$ from the value of $G(H_2) = 4.1$ gives $G = 3.1$ as the yield of scavenged electrons. Such a value is in reasonable agreement with the value of $G = 3.4$ obtained as the yield of scavengeable electrons with N_2O.

Another interesting aspect of the radiolysis of water-dioxane mixtures is evident in the isotopic composition of the hydrogen yields obtained with D_2O (Table I). Multiplication of $G^*(H_2) = 1$ by $1 - F$ gives values in rather close agreement with the measured values of $G(H_2)$. Such a result, particularly at $F(D_2O) = 0.1$ for which use of the electron fraction assumption is not critical, indicates that H atoms from dioxane (which would form H_2 in reaction 4) make little or no contribution to the enhanced hydrogen yield. The results of Baxendale and Rodgers,[23] obtained at $F(D_2O) < 0.05$, unequivocally support such a conclusion. Thus any HD_2O^+ formed in reaction 2 must undergo several exchanges with D_2O molecules prior to neutralization; alternatively, another mechanism may be involved such as that suggested by Baxendale and Rodgers.[23]

Cyclohexane–Dioxane Mixtures. Cyclohexane has an ionization potential of 9.88 eV.[12] Consequently, transfer of charge from a cyclohexane cation to dioxane is exothermic and, therefore, is expected to occur on each encounter; the transfer of a proton also may be possible. Because of the low efficiency with which ionic processes yield hydrogen in dioxane, corresponding to $G_i(H_2) \approx 0.3$ as compared to a value of $G_i(H_2) \approx 3$ in cyclohexane,[6-8] charge transfer to dioxane (reaction 5)

$$c\text{-}C_6H_{12}^+ + C_4H_8O_2 \longrightarrow c\text{-}C_6H_{12} + C_4H_8O_2^+ \quad (5)$$
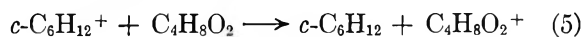
will result in a reduction in $G(H_2)$ greater than that expected on the basis of an electron fraction partition of the absorbed energy. In fact, because $G(H_2) = 1.3$ for dioxane as compared to $G(H_2) = 5.4$ for cyclohexane, any process that results in preferential localization of deposited energy on dioxane molecules will contribute to a reduction in $G(H_2)$ of the mixture.

Addition of dioxane to cyclohexane has the expected effect on $G(H_2)$ as shown in Figure 5. That the reduction in $G(H_2)$ is attributable to ionic processes only is shown by the effects of methanol and ammonia on $G(H_2)$ of the dioxane–cyclohexane mixtures. Such basic solutes (as shown for NH_3 in Figure 7) should scavenge cations of both cyclohexane and dioxane with about equal efficiency and, *via* reactions 2–4, yield a molecule of H_2 for each cation scavenged. If neutralization of a cyclohexane cation by an electron yields H or H_2 with unit efficiency, conversion of a cyclohexane cation to the protonated basic solute (reaction 2) has no effect on the hydrogen yield; however, replacement of a dioxane cation by the protonated basic solute exactly offsets the effect of reaction 5 on the hydrogen yield.

As shown in Figure 5, addition of ammonia or methanol to dioxane–cyclohexane mixtures enhances the hydrogen yield. When the concentration of added base is large relative to that of dioxane, $G(H_2)$ is restored to the value for pure cyclohexane; such is the case for 0.13 M NH_3 and 1 M CH_3OH in solutions of less than 0.024 and 0.05 M dioxane, respectively. It is clear that a simple competition between dioxane and base for cyclohexane cations is not involved; if this were the case, the curves in Figure 5 for a fixed concentration of base would converge at large dioxane concentrations. As expected, the base must scavenge cations of both cyclohexane and dioxane with about equal efficiency. Thus the fraction of total cations scavenged by a fixed concentration of base is independent of the composition of the cyclohexane–dioxane mixture. Such behavior is confirmed by the approximate constancy of $G(HD)$ shown in Figure 6 for 1 M CH_3OD and dioxane concentrations up to ~1 M. The net effect of increasing dioxane concentration is that an increasing fraction of those cations *not* scavenged by 1 M CH_3OD undergo reaction 5; the resultant decrease in $G(H_2)$ necessarily corresponds to the decrease in total hydrogen yield.

(21) R. R. Hentz, Farhataziz, and D. J. Milner, *J. Chem. Phys.*, **47**, 5381 (1967).

(22) A. O. Allen, "The Radiation Chemistry of Water and Aqueous Solutions," D. Van Nostrand Co., Inc., Princeton, N. J., 1961, p 41.

(23) J. H. Baxendale and M. A. J. Rodgers, *Trans. Faraday Soc.*, **63**, 2004 (1967).

The Oxidation of Chlorine Dioxide by Cobalt(III) in Perchlorate Solution

by Richard C. Thompson

Department of Chemistry, University of Missouri, Columbia, Missouri 65201   (*Received February 14, 1968*)

The kinetics of the reaction $Co(III) + Cl(IV) = Co(II) + Cl(V)$ have been studied in acid perchlorate solutions from 0.30 to 2.0 M $HClO_4$. The rate law is $-d[Cl(IV)]/dt = k''[Cl(IV)][Co(III)][H^+]^{-1.07\pm0.02}$ at 25°, where $k''[H^+]^{-1.07}$ is interpreted to equal $(k_0/[H^+])e^{\beta[H^+]}$. Values of ΔH^* and ΔS^* appropriate to the k_0 term were found to be 22.2 ± 0.3 kcal/mol and 24.9 ± 0.9 eu, respectively. The kinetic and oxygen-18 tracer data provide no evidence for the formation of a $Co(III)-Cl(IV)$ complex intermediate.

Introduction

The oxidation of a variety of metal ions by the oxychlorine species have been reported.[1-4] Many aspects of the mechanisms of these multiequivalent reactions have been elucidated, including the possible interactions of the oxychlorine species themselves.[5] An alternative approach utilizing metal ion oxidants is being explored in this laboratory. For example, preliminary studies indicate that the oxidation of chlorous acid by excess cobalt(III) to chlorate ion proceeds through the formation of a chlorine dioxide intermediate. This article reports a kinetic and oxygen-18 tracer study of the Cl-(IV)–Co(III) reaction in acid perchlorate solution.

Experimental Section

Reagents. The preparation and standardization of the Co(III), perchloric acid, and lithium perchlorate solutions have been described previously.[6] The chlorine dioxide was generated in an all-glass apparatus by allowing sodium chlorite to disproportionate in 2 M $HClO_4$. Only about 20% of the sodium chlorite was allowed to disproportionate—any chlorine produced would react very rapidly with the excess chlorite.[5] The chlorine dioxide was transferred from this solution in a stream of purified air and was collected in 2 M $HClO_4$. This stock solution was stored in the dark at 0°. Four fresh Cl(IV) stock solutions were used during the course of this study; each gave identical kinetic results within the precision of the measurements.

Procedures. The literature values of the molar extinction coefficients for chlorine dioxide (ϵ 1242 M^{-1} cm^{-1} at 3600 Å)[6] and cobalt(III) (ϵ 34.5 M^{-1} cm^{-1} at 6020 Å)[7] were used. Values of ϵ 98.5 M^{-1} cm^{-1} for chlorine dioxide and ϵ 252 M^{-1} cm^{-1} for cobalt(III) at 2800 Å in 0.80 M $HClO_4$ were determined. The chlorine dioxide is essentially transparent at 6020 Å.

The stoichiometry of the reaction

$$Co(III) + Cl(IV) = Co(II) + Cl(V) \qquad (1)$$

was determined spectrophotometrically using these molar extinction coefficients. The ratio of chlorine dioxide reacted:cobalt(III) reacted = 0.985 in 0.40 M

$HClO_4$ and 0.98$_0$ in 2.0 M $HClO_4$ at 25°. The initial presence of $NaClO_3$ at a concentration ten times that of the reactants did not affect these values. This result indicates that any possible reaction between the product Cl(V) and Co(III) is negligibly slow relative to reaction 1 in these experiments. The small deviation of the observed stoichiometry from that indicated for reaction 1 may be due to small errors in the values of the molar extinction coefficients used and/or a minor side path involving the oxidation of water by Co(III).

For the kinetics runs, all of the reagents but the Co(III) (except for the runs at 2800 and 6020 Å) were contained in either a 2- or 5-cm absorption cell in the thermostated compartment of the Cary Model 14 spectrophotometer. After temperature equilibration, an aliquot of the Co(III) stock solution at the working temperature was introduced into the cell. The reaction was usually monitored at the chlorine dioxide absorption maximum at 3600 Å. The [H$^+$] of the reaction mixture was determined by titration with the standard base after completion of the reaction.

The first observation was generally made within 20 sec after mixing, and the reaction was followed for at least 3 half-lives. The values reported for the rate constants were obtained from a least-squares adjustment of the data (20–30 OD,t data points/experiment) as previously described.[8]

Tracer Experiments. ClO_2 gas dried by bubbling through concentrated H_2SO_4 and by passing it over anhydrous $Mg(ClO_4)_2$ was bubbled through a solution ca. 0.15 M Co(III), enriched in H_2O^{18} (YEDA), and 2 M $HClO_4$ at 0°. After a nearly stoichiometric amount of the ClO_2 had been introduced and reacted,

(1) R. Thompson and G. Gordon, *Inorg. Chem.*, 5, 562 (1966).

(2) G. Gordon and P. Tewari, *J. Phys. Chem.*, 70, 200 (1966).

(3) T. Chen, *Anal. Chem.*, 39, 804 (1967).

(4) G. Gordon and F. Feldman, *Inorg. Chem.*, 3, 1728 (1964).

(5) F. Emmenegger and G. Gordon, *ibid.*, 6, 633 (1967).

(6) J. Sullivan and R. Thompson, *ibid.*, 6, 1795 (1967).

(7) R. Keiffer, Ph.D. Thesis, University of Maryland, College Park, Md., 1966.

(8) R. Thompson and J. Sullivan, *J. Amer. Chem. Soc.*, 89, 1096 (1967).

Table I: [H$^+$] and Temperature Dependencies of k' [a]

				Temp, °C			
	5		10		17		25
[H$^+$], M	k', M^{-1} sec^{-1}	[H$^+$], M	k', M^{-1} sec^{-1}	[H$^+$], M	k', M^{-1} sec^{-1}	[H$^+$], M	k', M^{-1} sec^{-1}
0.336	19.1 ± 0.2	0.333	40.2 ± 0.5	0.319	113 ± 0.3	0.258	376 ± 1.6
0.500	13.6 ± 0.1	0.545	24.7 ± 0.3	0.520	66.3 ± 0.9	0.443	235 ± 7.5
0.500	14.0 ± 0.1[b]	0.920	13.9 ± 0.1	0.907	37.7 ± 0.1	0.840	120 ± 3.1
0.907	6.67 ± 0.18	0.920	13.9 ± 0.1[d]	1.29	25.7 ± 0.4	0.829	116 ± 0.2[e]
1.36	4.20 ± 0.03	0.920	14.1 ± 0.1[e]	1.76	18.6 ± 0.4	0.834	118 ± 0.7[f]
1.74	3.09 ± 0.03	1.31	9.00 ± 0.20	2.11	14.7 ± 0.3	1.27	78.0 ± 1.0
2.10	2.38 ± 0.14	1.75	6.89 ± 0.11			1.65	56.8 ± 0.1
2.07	2.89 ± 0.10[c]	2.13	5.35 ± 0.06				

[a] $I = 2.1_0$ maintained with LiClO$_4$. Uncertainties are the average deviations. The Co(III) was prepared electrolytically unless otherwise noted. [ClO$_2$]$_0$ = 1.54 × 10^{-4} to 4.18 × 10^{-3} M. [Co^{3+}]$_0$ = 1.23 × 10^{-4} to 5.57 × 10^{-3} M. [b] Chemically prepared Co(III) (from the Co(III)–carbonate complex).[7] [c] 6020 Å, excess Co^{3+}. [d] 2800 Å. [e] [NaClO$_3$]$_0$ = 10^{-3} M. [f] [Co(ClO$_4$)$_2$]$_0$ = 10^{-3} M.

a portion of the reaction solution was saved for later solvent-enrichment determination. The remaining solution was nearly neutralized with solid KOH, the KClO$_4$ precipitate was filtered, and the metal ions were removed by ion-exchange techniques. A small amount of the chlorate is reduced by the resin in this procedure. The eluent, which contained perchloric, chloric, and a trace of hydrochloric acid, was neutralized with solid KOH, the KClO$_4$ was filtered, and the filtrate was converted to the silver salts by ion-exchange techniques. The trace of AgCl that was formed was removed. The eluent containing about equal concentrations of AgClO$_4$ and AgClO$_3$* was concentrated in a rotor evaporator at 50°, and the AgClO$_3$* was allowed to precipitate slowly at 0°. The AgClO$_3$* was collected and washed with a small amount of cold water. After careful drying, the solid was sealed in an ampoule under vacuum and was converted to predominantly oxygen gas and AgCl by heating at 325° for 2 hr. (*Caution!* In preliminary experiments, attempts to convert the AgClO$_3$ to CO$_2$ by the Anbar technique[9] were unsuccessful owing to detonation at *ca.* 100°.) The gas was collected from the ampoule maintained at liquid-air temperatures in a Toepler pump and was analyzed in an isotope-ratio mass spectrometer. The solvent water was distilled from the sample of the reaction mixture, and Ag$_2$O* was precipitated from the distillate by addition of dry AgNO$_3$ and NaOH (in amounts small relative to the volume of water). The Ag$_2$O* was carefully washed with the distillate, was dried, and was converted to oxygen and silver by heating at 350° for 2 hr. The enriched oxygen was collected and analyzed as before. A sample of standard oxygen was prepared in the same manner from triply distilled water of normal isotopic composition. In all the analyses the 34/(32 + 33) mass ratio was measured. The author is indebted to Professor R. K. Murmann for performing the mass spectrometric analyses.

Results

The Rate Law. The data at constant [H$^+$] were adequately correlated by the integrated form of the second-order rate law. The standard deviation for the rate parameter k' ranged from 0.1 to 0.9%. The reproducibility of replicate runs, as can be seen from the data in Table I, was between 1 and 6%.

The method of preparation of the Co(III) stock solutions did not affect the value of k' within the experimental uncertainties nor did the initial presence of 10^{-3} M NaClO$_3$ or 10^{-3} M Co(ClO$_4$)$_2$. k' was also invariant with the wavelength used to monitor the reaction (Co(III) is the predominantly absorbing species at 6020 and 2800 Å; at 3600 Å, ClO$_2$ accounts for nearly all the absorption). Room light did not change the rate constant from that measured in the dark.

An empirical form of the rate expression that summarizes the variation in k' with the change in the hydrogen ion concentration is

$$k' = k''[\text{H}^+]^n$$

Values determined for n, from a least-squares adjustment of all the data in Table I, are: -1.09 ± 0.03, -1.08 ± 0.01, -1.07 ± 0.01, and -1.07 ± 0.02 at 5, 10, 17, and 25°, respectively.

These values suggest that the rate is predominantly proportional to [H$^+$]$^{-1}$. The small deviations from this value can most simply be ascribed either to a contribution from a path proportional to [H$^+$]$^{-2}$ or to mild medium effects as the [H$^+$] is varied at constant ionic strength. Our calculations indicate that these interpretations correlate the data about equally well. We have chosen the latter of the two models. In terms of a Harned-type correction factor

(9) M. Anbar and S. Guttmann, *J. Appl. Radiat. Isotopes*, **5**, 233 (1959).

$$k' = \frac{k_0}{[\text{H}^+]} e^{\beta [\text{H}^+]}$$

the values for k_0 are: 6.75 ± 0.25, 14.0 ± 0.2, 36.5 ± 0.5, and 108 ± 3 at 5, 10, 17, and 25°, respectively. The corresponding values of β are: -0.083 ± 0.024, -0.085 ± 0.011, -0.071 ± 0.011, and $-0.081 \pm 0.025 \, M^{-1}$.

The activation energy for the net activation process

$$\text{Co}^{3+} + \text{ClO}_2 + \text{H}_2\text{O} = \text{CoOHClO}_2{}^{2+} + \text{H}^+$$
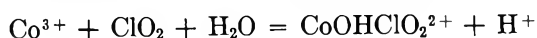
as calculated from this data is 22.7 ± 0.3 kcal/mol. Values of $\Delta H^* = 22.2 \pm 0.3$ kcal/mol and $\Delta S^*(25°) = 24.9 \pm 0.9$ eu were calculated by use of the expression from the absolute reaction rate theory[10]

$$k = \frac{ekT}{h} e^{-\Delta E/RT} e^{\Delta S^*/R}$$

where $\Delta H^* = \Delta E - RT$.

Tracer Results. In two independent experiments at 2.0 M HClO$_4$ and 0°, 1.07 ± 0.04 oxygens in the chlorate ion product had the same enrichment as the solvent water. No corrections for possible fractionation effects in the determination of the solvent enrichment were attempted.

Discussion

In a study of the reduction of ClO$_3{}^-$ by Cr(II), the formation of Cr(III) complexes with lower oxidation states of the oxychlorine species has been postulated.[1] The existence of these intermediates could not be demonstrated directly, presumably owing to their instability with respect to further reduction by Cr(II). Conocchioli, Nancollas, and Sutin[11] have reported the formation of CoCl^{2+} prior to subsequent oxidation of the Cl$^-$. One aspect of the present work was to test whether a Co(III)–ClO$_2$ inner-sphere complex is formed prior to the oxidation–reduction reaction; this would be analogous to a possible Cr(III)–ClO$_2$ complex in the Cr(II)–ClO$_3{}^-$ system.[1] No indication of the formation of the Co(III) complex was obtained. The probe used was to monitor the reaction at three widely separated wavelengths; if an appreciable concentration (the necessary amount depends on its molar extinction coefficient) were formed, its presence might be detected. However, the data in Table I give no such indication. It should be noted that a 50 times variation in the initial concentrations of the reactants was used. These results do not rule out the possibility of a Co(III)–ClO$_2$ complex intermediate in this system if its formation rather than decomposition to products is rate controlling.

The oxygen-18 tracer data provide no evidence for the formation of a complex. Indirect studies indicate

that the rate of oxygen exchange between ClO$_2$ and solvent is slow,[12] and a direct study shows that ClO$_3{}^-$ exchanges its oxygens very slowly.[13] It might reasonably be predicted, then, that in the conversion of the bent ClO$_2$ to the pyramidal ClO$_3{}^-$, one solvent oxygen would be incorporated into the ClO$_3{}^-$ product. However, if a fairly long-lived Co(III)–ClO$_2$ complex were an intermediate in this transformation by Co(III), then the ClO$_2$ oxygens might be labilized, with the net result that *more* than one solvent oxygen would be incorporated into the ClO$_3{}^-$ product.[14] However, the tracer results indicate that essentially one solvent oxygen appears in the ClO$_3{}^-$. This datum substantiates the earlier conclusion that ClO$_2$ oxygen exchange is slow, at least in the time required for the present reaction. Direct experiments on this exchange rate are in progress.

The kinetic data are consistent with the following reaction scheme

$$\text{Co(H}_2\text{O)}_6{}^{3+} \rightleftharpoons (\text{H}_2\text{O})_5\text{CoOH}^{2+} + \text{H}^+$$

$$\text{H}_2\text{O} + (\text{H}_2\text{O})_5\text{CoOH}^{2+} + \text{ClO}_2 \xrightarrow{k_0}$$
$$\text{Co(H}_2\text{O)}_6{}^{2+} + \text{ClO}_3{}^- + \text{H}^+$$
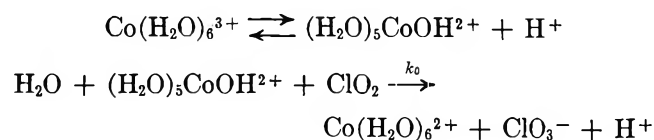
which invokes a rapid preequilibrium involving the hydrolysis of Co^{3+}. The hydrolysis constant for Co(III) is large, although its value is still a topic of debate.

If the value of the hydrolysis constant of Co^{3+} is 0.0175 M,[15] then the linear k' vs. $1/[\text{H}^+]$ plots obtained over the [H$^+$] range used in this study would be expected. If, however, the hydrolysis constant is 0.22 M as reported by Conocchioli, Nancollas, and Sutin,[11] then this reaction scheme must be modified.

(10) S. Glasstone, R. Laidler, and H. Eyring, "The Theory of Rate Processes," McGraw-Hill Book Co., Inc., New York, N. Y., 1941, pp 195–199.

(11) T. Conocchioli, G. Nancollas, and N. Sutin, *Inorg. Chem.*, **5**, 1 (1966).

(12) J. Halperin and H. Taube, *J. Amer. Chem. Soc.*, **74**, 375 (1952).

(13) T. Hoering, E. Ishimori, and H. McDonald, *ibid.*, **80**, 3876 (1958).

(14) Oxygen-exchange rates of oxyanions are generally increased by the acidity of the media (for example, J. O. Edwards, "Inorganic Reaction Mechanisms," W. A. Benjamin, Inc., New York, N. Y., pp 137, 138). With the provision that ClO$_2$ behaves like an oxyanion and that Cr(III) as a coordination site can exhibit acidic properties, then the complexed ClO$_2$ would be expected to exchange its oxygens more rapidly than the uncomplexed species. Direct evidence for such labilization has been obtained for the (NH$_3$)$_5$CoOReO$_3{}^{2+}$ complex (R. K. Murmann, private communication).

(15) L. H. Sutcliffe and J. R. Weber, *Trans. Faraday Soc.*, **52**, 1225 (1956).

The Isotope Effect on the Vapor Pressures of

H_2O–C_2H_5OH and D_2O–C_2H_5OD Mixtures

by C. U. Linderstrøm-Lang and Fred Vaslow[1a]

Chemistry Department, Danish Atomic Energy Commission, Risø, Denmark   (Received February 21, 1968)

The vapor pressure isotope effect in the liquid composition range 0–30 mol % ethanol has been studied by a static method that permits measurements to be obtained that are accurate to about 0.01 mm relative to the vapor pressure of water. The measuring system consists of a silicone-oil manometer, read with a long-range cathetometer. Small amounts of noncondensable gases in the vapor phase are swept from the sample vessel with sample vapor distilling into a CO_2 trap, and their contribution to the total vapor pressure is estimated on a Pirani gauge. The activity coefficients of the two components in both isotopic systems are calculated from the total-pressure data (by three different methods) and are checked by vapor-composition determinations. The isotope effects in terms of the logarithm of the activity-coefficient ratios show interesting trends (crossover phenomena) which are discussed on the basis of current ideas of the structure of alcohol-water mixtures.

Introduction

Comparative data on heavy- and light-water systems are of interest in connection with studies of the structure of aqueous solutions and, in general, of solvent mixtures containing water as one of the components.

A number of data on the mutual solubility of polar organic compounds and light water compared with those of the equivalent systems containing heavy water are available and show interesting features,[1b] which, however, are of somewhat limited use without support by other comparative information, notably the free energy of mixing. It was, therefore, felt of value to initiate a series of experiments on the vapor pressure isotope effect of water–nonelectrolyte mixtures.

In choosing a method, the guiding principle has been that the highest possible relative accuracy of the pressure measurements should be attained, while high absolute accuracy should be of less importance. This led to the choice of an essentially differential method based upon static measurements of the pressures. A truly differential system, i.e., one in which heavy and light systems of the same composition were compared, would have been ideal because of the possibility of employing modern highly sensitive, but narrow-ranged, pressure transducers; however, such a system would be difficult to operate or, whenever identical composition in the two systems was not obtained, difficult to interpret without an equally precise knowledge of the absolute-pressure curve. A compromise, with pressure measurements against the vapor pressure of a standard liquid in a reservoir, was, therefore, adopted.

A disadvantage of the static method is that sufficiently accurate vapor sampling is difficult to carry out, but this was not felt to be a serious obstacle, since any error occurring during the integration of the Duhem-Margules equation, which must be employed in the absence of vapor-composition data, would probably cancel for the greater part when light and heavy systems were compared—an expectation which appears to have been justified as shown later. Some provision for sampling the vapor phase was, however, included, which was essentially a microvariant of a system previously used by Hansen and Miller.[2] Since a number of features of the apparatus were novel, water–ethanol was chosen as the first system to be measured because of the availibility of data on light-water systems for comparison with our results, as well as the intrinsic interest of the system.

Experimental Section

The measuring system consists of a silicone-oil manometer which could be used in a differential or, at lower pressures, an absolute manner and in which the manometer fluid is separated from the sample vapor by a buffer column of air. Samples are put into the system under vacuum by injection with a hypodermic syringe through a rubber stopper. Noncondensable gases are swept from the sample-vessel gas volume, with the sample vapor distilling into a carbon dioxide cooled trap. A Pirani gauge connected to the trap is used to determine any contribution from noncondensable gases to the total pressure above the sample liquid.

A schematic diagram of the apparatus is shown in Figure 1. The manometer is asymmetric, with one arm about 1 m long and having a 3-mm bore and the other arm 5 cm long and having a 3-cm bore. The long column of oil is followed with a cathetometer to a

(1) (a) On assignment to Risø, 1966–1967. Permanent address: Chemistry Division, Oak Ridge National Laboratory, Oak Ridge, Tenn. 37830. (b) C. U. Linderstrøm-Lang, Acta Chem. Scand., 16, 1730 (1962); Pure Appl. Chem., 8, 259 (1964).

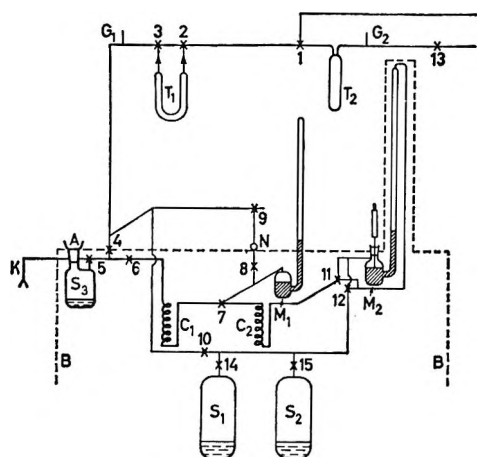(2) R. S. Hansen and F. A. Miller, J. Phys. Chem., 58, 193 (1954).

Figure 1. Vapor pressure apparatus: two-way stopcocks: X-1, X-4, X-6, X-8, X-10, X-14, X-15; three-way stopcocks: X-2, X-3, X-5, X-7, X-9, X-12; needle valve, N; pressure gauges: G_1, G_2; mercury manometer, M_1; oil manometer, M_2; removable trap, T_1; trap, T_2; 1-l. reference liquid reservoirs: S_1, S_2; 200-ml sample reservoir, S_3; 1 mm in diameter by 1 m long capillary tubes: C_1, C_2; thermostated bath, B.

precision of 0.1 mm, using a precision steel scale attached to the manometer as a reference point and a standard. The level in the wide arm of the manometer is measured with a micrometer by means of a long needle running through a lubricated and gas-tight seal in a rubber stopper. By observing from below (with a dentist's mirror), the position at which the needle first contacted the oil surface the level could be determined to within 0.02 mm. The manometer is surrounded by a thermostated water jacket at a slightly higher temperature than the main thermostat.

The density of the manometer oil (DC 200/10) was 0.934 g/cm³ or 0.068 times that of mercury. Although the vapor pressure of water calculated with this oil density was in excellent agreement with the literature value,[3] 23.77 cm, at the temperature of measurement (25.02°), in each experiment the manometer was directly calibrated at different levels in terms of the vapor pressure of pure water taken at its literature value.

The sample vessel has a short tube (A) ending in a ground-glass socket through which samples are injected. A raised rim surrounds the socket in order to allow the space below the stopper to be beneath the thermostat surface.

The two three-way stopcocks (X-11 and X-12) connected to the manometer provide for an interchange of connections to the sample vessel, the reservoir, and the vacuum system. In the present experiments, water or heavy water were used as standards and in all cases the standards (or vacuum) were connected to the long arm. The short arm was exposed only to the buffer gas, air, or vacuum.

To make a measurement, the pressure in the wide arm and C_1 are adjusted as closely as possible (using the

needle valve N and stopcock X-9, which gives access to either the vacuum or the atmosphere) to the pressure in S_1. The mercury manometer can be used for the initial estimation of pressure. C_2 is filled with vapor from the sample vessel (X-6 open) and the connection between the two capillaries (X-7) is kept closed. The long arm of the manometer is exposed either to the vacuum or to the reference vessel. After the manometer reading becomes constant or moves negligibly slowly, a connection is made at X-7 and the readings are made. A period of about 5 min is available before diffusion of gases starts to change the readings, and after the first 30 sec the reading is constant to 0.1 mm (0.007 mm of Hg).

The manometer zero is determined with pure water in S_3 and the water reference vapor in the long arm. With any pressure in S_3 greater than that of water and less than 70 mm, the manometer can be directly calibrated in terms of the difference between the reference water vapor and the vacuum in the long arm.

While initial degassing of the system and the manometer fluid could take as long as 24 hr, equilibrium pressures in a run were reached in 15-30 min. Degassing of injected samples was accomplished in 3-5 cycles over a 0.5-hr period in which S_3 was briefly opened (about 4 sec) to T_1, which was cooled with Dry Ice and the vacuum system was closed off at X-2. After the vapor was condensed, the residual pressure was measured at G_1, the gas then was pumped off, and the cycle was repeated, until the pressure was less than 5μ.

Since essentially the entire static-vapor volume of S_3 was pumped off in a cycle, the pressure at G_1 could give an upper limit to the noncondensable pressure in S_3. Similar cycles and measurements were made after each vapor pressure measurement to confirm that there was no significant amount of noncondensable gas in the sample vessel. Measurements with too high a residual pressure were rejected and were repeated rather than being corrected. All vapor from S_3 was collected in trap T_1 and after completion of measurements for each composition, the trap was removed and the content of ethanol and water was determined.

For vapor-phase analyses, samples were withdrawn to an evacuated and Dry-Ice-trapped, 0.5-ml removable vessel (K). In most experiments the lead tube had a constriction somewhat less than 0.1 mm in diameter. A calculation, which takes into account the effect of the rate of evaporation on the equilibrium pressure as well as the separation effect of the Knudsen component of the flow through the constriction, shows this diameter to be close to optimal and to lead to small, probably negligible, errors in sample composition. In the first experiment, a wider constriction in the lead tube was

(3) "Handbook of Chemistry and Physics," 39th ed, Chemical Rubber Publishing Co., Cleveland, Ohio, 1957, p 2146.

Table I: Experimental and Calculated Pressures and Composition of Ethanol-Water Mixtures (Calculations by Method 3)

Expt no.	$10^2 x_{alc}(l)$	P (exptl), mm	$10^2 P$ (exptl − calcd^a), mm	$10^2 y_{alc}(v)$ (calcd)	$10^3 y_{alc}(v)$ [(exptl − calcd)/ calcd^a]
		Light System			
3	0.000	23.77	0	0	
2	1.257	26.23	1	10.43	−13
1	1.444	26.55	−1	11.74	−13
2	2.459	28.35	0	18.09	1
1	2.817	28.94	−2	20.08	−9
1	4.146	31.18	3	26.64	−11
1	5.384	33.12	0	31.79	−6
1	6.645	35.02	−1	36.29	−3
2	7.238	35.91	1	38.16	1
1	7.844	36.74	−2	39.94	−6
2	11.57	41.33	0	48.27	−6
1	12.20	42.01	3	49.31	−4
2	15.57	44.76	−3	53.60	0
1	16.18	45.20	0	54.19	−5
2	19.21	46.86	−1	56.56	−3
1	19.69	47.13	4	56.87	−3
2	22.50	48.20	−1	58.43	−6
2	25.61	49.22	0	59.84	−11
2	28.48	50.03	0	61.01	−8
4	100.0	59.10	0	100.0	
		Heavy System			
4	0.000	20.51	0	0	. . .
3^b	1.170	22.67	0	10.54	−4
2	1.276	22.85	0	11.36	57
3	2.314	24.60	−1	18.50	−5
2	2.545	24.98	−1	19.92	4
1	2.798	25.45	4	21.40	(65)^c
3	3.414	26.35	−4	24.74	−16
2	3.747	26.90	−2	26.49	23
2	4.995	28.92	7	32.22	. . .
1	5.351	29.43	4	33.69	(−47)
2	6.350	30.86	−1	37.47	6
2	7.531	32.54	−1	41.35	13
3	7.770	32.86	−2	42.07	0
1	8.071	33.25	−4	42.94	(−31)
1	10.49	36.28	−3	48.40	(−31)
3	11.65	37.59	3	50.98	−5
2	12.00	37.96	4	51.57	4
1	14.52	40.10	−2	55.06	. . .
3	15.31	40.70	1	55.92	3
2	16.08	41.20	0	56.68	6
1	18.15	42.35	−3	58.37	(−25)
3	18.60	42.61	0	58.69	4
2	19.63	43.10	1	59.37	16
1	21.40	43.80	−2	60.39	(−25)
3	21.72	43.96	2	60.56	0
2	22.93	44.38	0	61.17	4
3	24.53	44.92	2	61.91	−2
1	24.76	44.94	4	62.01	(−26)
3	27.04	45.67	6	62.91	−5
1	27.67	45.75	−2	63.13	(−29)
5	100.0	56.02	0	100.0	0

^{a} Calculations by method 3. ^{b} C_2H_5OD made by the second method in experiment 3. ^{c} In experiment 1 with heavy water, vapor sampling was through a constriction having about 15 times the flow rate of the construction used in all other experiments.

used and an appreciable error was introduced. The differences between the analytical results and the thermodynamically calculated vapor compositions are given in Table I.

Initially for each run about 15 g of light or heavy water was injected into S_3 and the syringe was weighed before and after addition in order to determine the amount added. Suitable precautions were taken in order to prevent liquid losses or the introduction of excessive amounts of air into the system. After standardization of the manometer, samples of 0.7–2 g of ethanol (−OD or −OH) were added and the pressure measurements were made in duplicate. The second measurement was generally about 0.1–0.2 mm of oil lower in pressure, corresponding to the change in composition caused by pumping out the vessel.

Samples (10–30 mg) of vapor, taken as described earlier, were analyzed as follows. The alcohol was oxidized with excess standard dichromate and the excess was determined by thiosulfate titration. If special precautions were taken, the results were reproducible to about 0.5% of sample weight.

The ethanol used was an absolute grade alcohol with impurities other than water equal to less than 0.01%. The water content was determined separately by a Karl–Fischer titration.

Deuteration of the ethanol was performed in two ways: (1) according to the method of de Salas and Wilson,[4] which involves the preparation of diethanol sulfite, purification, and hydrolysis in heavy water; (2) by deuterium–protium exchange, with repeated shaking of ethanol (the same grade as used for the light experiments) with high-grade heavy water saturated with potassium carbonate. The loss of alcohol in the water phase was negligible. The alcohol phase contained about 10% water, which was removed by treatment with CaO. The product was distilled off and the residual water content was determined by the Karl Fischer method.

The errors in the pressure measurements are estimated on the basis of the reproducibility of the duplicate measurements made for each composition. Correcting for the composition change, the average agreement was ±0.1 mm of oil with a maximum difference of 0.3 mm. The manometer zero was reproducible to better than 0.1 mm and the calibrations agreed to within ±0.2 mm in 35 cm.

Since the composition was determined from a material balance, cumulative errors could occur in an uncertain manner. Individual measurements of amounts added were made to better than 0.1%, with losses in transfer believed to be not larger than 0.1%. In addition, pumping loses were possible, although they could not be detected in tests. Other uncertainties were in the

(4) S. E. de Salas and C. L. Wilson, *J. Chem. Soc.*, 319 (1938); G. L. P. Kyrides, *J. Amer. Chem. Soc.*, **66**, 1006 (1944).

removal and the weighing of the trap T_1 and in the analyses of its contents.

Comparing the calculated and the density-determined weight per cents of alcohol of the final solutions for the two light water runs, the results were, respectively, 38.68 and 38.53% for run 1 and 30.33 and 30.40% for run 2. Proportional corrections were made for intermediate concentrations on the basis of the density measurements.

The duplicate runs were compared graphically, first subtracting a quadratic-deviation function from all pressure data in order to permit the use of a larger scale, and the pressure generally agreed to within 0.02 mm. This also applies to runs with heavy alcohol prepared by the two different methods described above.

Results

The experimental and the calculated results for the pressure and the composition are given in Table I. All pressures are relative to that for H_2O at $25.02 \pm 0.01°$ taken as $P_{h-w} = 23.77$ mm. On the basis of the activity-coefficient calculations given later, the pressure (and the activities) are in agreement with those of Hansen and Miller[2] within the combined experimental error. The ratio of pressures P_{h-w}/P_{d-w} obtained here is 1.159 compared with 1.158 obtained by Combs, Googen, and Smith[5] and lower values obtained in earlier work.

The ratio of pressures P_{h-alc}/P_{d-alc} obtained is 1.055 compared with 1.055 obtained by Rabinowich[6] and 1.057 by Kiss,[7] et al.

In order to obtain the partial pressures and the activities, the data were treated in several ways. Large-scale plots of the data from which a suitable quadratic deviation function had been subtracted were constructed with the mole fraction of alcohol, x_{alc}, as the abscissa, and pressures were read at 0.01-mol fraction intervals and the Boissonnas procedure[8] was used to calculate the partial pressures and the activities (method 1). No corrections for gas imperfections were made.

In a second group of procedures, two different computer programs with and without gas corrections were used to calculate pressures and activities. The one method (method 2) involves a numerical integration (a Runge–Kutta procedure) of the Duhem–Margules equation (in a form similar to the one used in the Boissonnas procedure above) based on a minimax fit of Chebyshev polynomials either to the total-pressure data or to the "total fugacity," where total fugacity is defined as the sum of the component fugacities and is calculated from the total-pressure data using first-order imperfect gas corrections.

The other computer method (method 3) is similar to the one devised by Barker;[9] i.e., it determines, in an interative procedure, a least-squares fit of the total pressure, assuming the excess free energy of mixing to

be of the form $\Delta G^e = x(1 - x)[a + b(1 - 2x) + c \cdot (1 - 2x)^2 + \ldots]$ and also makes first-order imperfect gas corrections. A sufficiently accurate fit was given by an eight-parameter equation. An asymmetry parameter, as introduced by Myers,[10] did not appreciably improve the convergence of the solution in the present case.

Method 3 gave slightly better values than method 2 for P, and the deviations of these calculated total pressures from experiment are given in Table I. Results calculated by the three procedures are given in Table II for ΔG_{exc} (excess molal free energy) and in Figures 2 and 3 for $\ln (\gamma_{d-w}/\gamma_{h-w})$, i.e., $\Delta \ln \gamma_w$, and for $\ln (\gamma_{d-alc}/\gamma_{h-alc})$, i.e., $\Delta \ln \gamma_{alc}$, respectively. The disagreements between the methods are minor and are within a range that could be caused by the differences in the total-pressure curves used by the three methods.

Table II

| | $\Delta G_{exc}/RT$ | | | | | |
| | Method 1 | | Method 2 | | Method 3 | |
x_{alc}	Light	Heavy	Light	Heavy	Light	Heavy
0.00	0.0000	0.0000	0.0000	0.0000	0.0000	0.0000
0.02	0.0262	0.0258	0.0258	0.0257	0.0265	0.0262
0.04	0.0516	0.0510	0.0507	0.0504	0.0515	0.0510
0.06	0.0765	0.0757	0.0748	0.0744	0.0756	0.0751
0.08	0.1001	0.0994	0.0982	0.0977	0.0989	0.0984
0.10	0.1227	0.1222	0.1206	0.1202	0.1214	0.1210
0.12	0.1442	0.1440	0.1421	0.1418	0.1428	0.1426
0.14	0.1647	0.1647	0.1623	0.1623	0.1631	0.1631
0.16	0.1840	0.1843	0.1813	0.1815	0.1821	0.1823
0.18	0.2019	0.2024	0.1988	0.1992	0.1996	0.2000
0.20	0.2176	0.2185	0.2148	0.2154	0.2156	0.2162
0.22	0.2322	0.2333	0.2292	0.2300	0.2301	0.2310
0.24	0.2450	0.2463	0.2423	0.2433	0.2431	0.2442
0.26	0.2560	0.2576	0.2539	0.2551	0.2547	0.2561
0.28	0.2665	0.2693	0.2641	0.2655	0.2649	0.2665
0.30	...	...	(0.2728)	(0.2741)	(0.2738)	(0.2755)

A parameter study of the computer results, in which the experimental x and P data were varied at random, as well as systematically, showed that random errors as the cause of the isotope effect are very unlikely.

Systematic errors would have to operate mainly in the water-rich range, since the experimental vapor-composition data (see Table I), though inaccurate at low x_{alc}, support the calculated results at higher x_{alc}.

(5) R. L. Combs, J. M. Googen, and H. A. Smith, *J. Phys. Chem.* **58**, 1000 (1954).

(6) I. B. Rabinowich, N. A. Sokolov, and P. A. Artyakhin, *Dokl. Akad. Nauk SSSR*, **105**, 762 (1955).

(7) I. Kiss, Gy. Jakii, G. Jancso, and H. Illy, *Acta Chem. Acad. Sci. Hung.*, **51**, 65 (1967).

(8) J. Prigogine and R. Defay, "Chemical Thermodynamics," Longmans, Green and Co., London, 1954, p 347.

(9) J. A. Barker, *Aust. J. Chem.*, **6**, 207 (1953).

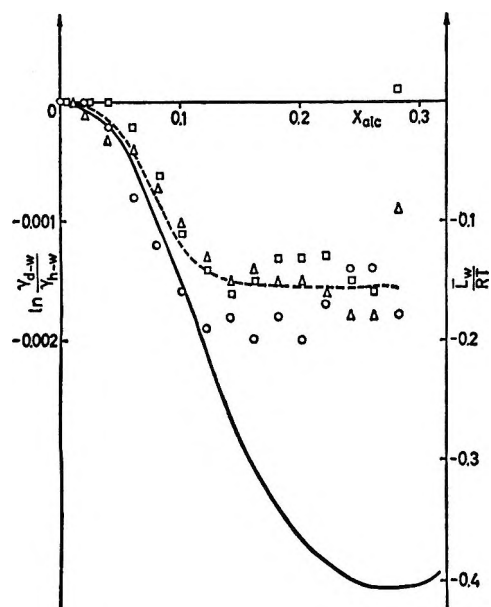(10) D. B. Myers and R. L. Scott, *Ind. Eng. Chem.*, **55**, No. 7, 43 (1963).

Figure 2. Logarithm of the activity-coefficient ratio for water as a function of the mole fraction of alcohol: O, method 1; □, method 2; △, method 3. Full line is the relative partial molal heat content of water, taken from R. F. Lama and B. C. J. Lee, *J. Chem. Eng. Data*, **10**, 216 (1965), and G. L. Bertrand, F. J. Millero, C. Wu, and L. G. Hepler, *J. Phys. Chem.*, **70**, 699 (1966).
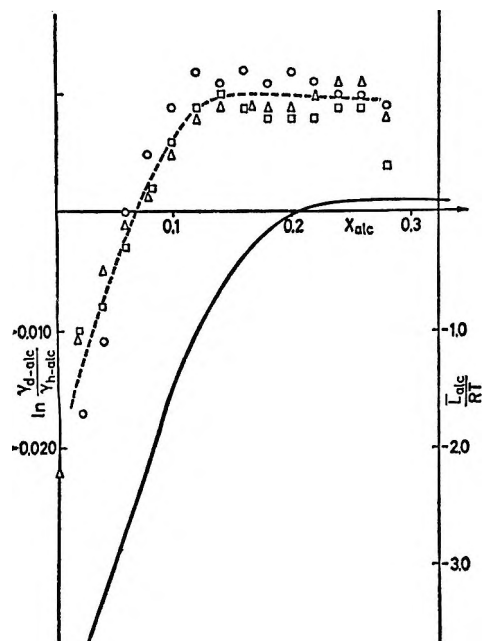

Figure 3. Logarithm of the activity-coefficient ratio for ethanol and the relative partial molal heat content of ethanol. Symbols the same as in Figure 2.

Also at higher x_{alc}, a $\gamma_{d-alc} > \gamma_{h-alc}$ is the expected effect if heavy water is to be the poorer solvent than light water, as often found. That this may apply to alcohol–water systems is indicated by our finding (unpublished result) that 1-butanol is about 5% less soluble in heavy water than in light water. On the

other hand, a systematic error in the water-rich range ($x_{alc} < 0.1$) of a magnitude sufficient to remove the isotope-effect shift with composition (*i.e.*, errors of the order of 0.03–0.05 mm) is very unlikely because the pressure measurements are most reliable there. Also, individual experiments for each system gave very similar results.

Discussion

The relative magnitudes of the isotope effects on ln γ_{alc} are not greatly different from the isotope effect on ln p of the pure-alcohol component and perhaps the most interesting feature of the results is the crossover in sign for Δ ln γ_{alc} at about $0.08x_{alc}$ and the relative constancy of Δ ln γ_w and Δ ln γ_{alc} above $x_{alc} \approx 0.12$. Similarly, the values of ΔG_{exc} for heavy and light systems cross at $x_{alc} = 0.14$. An attempt will be made in the following to relate these findings in a general way to the structure difference between light and heavy water and to its probable modification by the addition of alcohol molecules.

As pointed out in a recent review article by Franks and Ives,[11] a great many of the properties of alcohol–water mixtures have unique features, such as maxima or minima in this region. As an example of this, the relative partial molal heat contents for water and alcohol are included in Figures 2 and 3 to show the high degree of parallelism to the curves obtained here. The ideas reviewed and suggested by Franks and Ives can, in a general way, also be used here.

According to these general ideas, the addition of alcohol has a dual effect on water structure. On the one hand, the alcohol molecule forms hydrogen bonds with the surrounding water molecules. On the other hand, it promotes an increase in the order of the adjacent water structure similar to the one around inert molecules such as hydrocarbons, a change which often has been called the iceberg formation.[12] A typical feature is that the enthalpy and excess entropy of mixing are both negative, with the excess free energy much smaller and positive.

Since the hydrogen bonds broken in pure water and pure alcohol are replaced by new ones in the mixture, the net effect on ΔH of the direct changes in hydrogen bond number may be relatively small. The main contribution to ΔH may, therefore, come from an increase in the degree of hydrogen bonding between the water molecules surrounding the alcohol molecule and also an increased van der Waals energy from the filling of interstitial positions in the open water structure.

With increasing alcohol content, the spaces become filled and the order reaches a maximum until in the neighborhood of $x_{alc} = 0.1$ the structure becomes unstable and additional alcohol molecules have to find

(11) F. Franks and D. J. G. Ives, *Quart. Rev.* (London), **20**, 1 (1966).

(12) H. S. Frank and M. W. Evans, *J. Chem. Phys.*, **13**, 507 (1945).

accommodation in a different way. This new way will involve breaking of the original water structure and expenditure of energy (cf. Figure 2, where h_{alo} gradually becomes positive).

In order to relate these conclusions to the effect of isotopic substitution on activity coefficients, the properties of pure heavy and light water can be considered. On the basis of a substantially larger heat and entropy of vaporization as well as other evidence, it is considered that heavy water is the more structured substance. This would imply a greater number or greater stability of the interstitial spaces in heavy, as compared with light water, or, alternatively, a greater tendency to form such ordered domains under the influence of a foreign molecule. Thus it might be expected that initially heavy water would be an energetically favored host for the alcohol molecules and, in fact, the heat of solution of alcohol in heavy water is larger than in light water.[13] Although the entropy must also decrease, the relative decrease is evidently not as large in the heavy system as in the light-water system, and the free energy change is, therefore, more negative.

Somewhat similar ideas have recently been used by Vdovenko, et al.,[13] in a theory of water–ethanol solutions.

As the initial water structure becomes unstable with increasing alcohol, the resistance to change is greater for the heavy system and the free energy of transfer for this system is now the more positive as found experimentally.

It should be noted that the isotope effect on the hydrogen bonding in the alcohol phase compared with that of the alcohol in the water phase has been neglected above. How permissible this is depends upon the relative number of bonds broken and formed. At any rate, it is likely that the effect from these interactions contributes a fairly constant term to the total isotope effect and thus, even with this limitation in mind, the close link between the isotope effect and the partial molar heat of mixing, as described here, goes far to explain the very similar shape of the two sets of curves (cf. Figure 2).

(13) V. M. Vdovenko, Yu. V. G. Gurekov, and E. K. Legen, *Proc. Acad. Sci. USSR, Phys. Chem. Sect.*, **172**, 5 (1967).

Heat Capacity Changes in Ion-Exchange Reactions. The Exchange

of Tetra-*n*-butylammonium with Sodium Ion in

Cross-Linked Polystyrenesulfonate[1]

by G. E. Boyd, Q. V. Larson, and S. Lindenbaum

Oak Ridge National Laboratory, Oak Ridge, Tennessee 37830 (*Received February 23, 1968*)

Calorimetric measurements of the temperature dependence of the standard enthalpy of ion exchange, $\Delta H°$, were performed for the reaction in dilute aqueous solution of tetra-*n*-butylammonium with sodium ion in a lightly cross-linked sulfonated polystyrene type of cation exchanger. Between 15 and 35° the value of $\Delta H°$ decreased from 2.39 to 1.38 kcal equiv^{-1} corresponding to an average standard heat capacity change, $\Delta C_p° = -53 \pm 9$ cal equiv^{-1} deg^{-1}. The sign and magnitude of $\Delta C_p°$ are consistent with the hypothesis that large, singly charged organic cations such as the tetra-*n*-alkylammonium ions in aqueous solution produce an extensive ordering of the water structure in their vicinity. The prediction of $\Delta C_p°$ values for the exchange reactions in dilute solutions of singly charged cations (and anions) with one another is discussed.

Calorimetric[2-12] measurements on ion-exchange reactions between dilute aqueous electrolyte solutions and organic ion exchangers have shown that these reactions are accompanied by an enthalpy change, the magnitude of which is dependent on (a) the charge on the ions, (b) their electronic and/or molecular structures, (c) the nature of the ionogenic group, and (d) the cross-linking of the exchanger. The enthalpy change, if it is truly a thermodynamic property, must vary with the temperature so that ion-exchange reactions must also be accompanied by a heat capacity change.

Only fragmentary information is available on the sign and magnitude of the heat capacity change in ion-exchange reactions, and this comes entirely from temperature coefficient determinations. Measurements[13,14] with 8 and 16% DVB cross-linked polystyrenesulfonates on the variation of ion-exchange equilibria with temperature between 0 and 100° have shown that generally log K_a vs. T^{-1} curves are not linear and hence that the standard enthalpy change, $\Delta H°$, is not independent of temperature. The heat capacity change, $\Delta C_p°$, thus inferred from the change in $\Delta H°$, appears to be either zero or positive and small, although in the exchange of thallium with hydrogen ion $\Delta C_p° = 12$ cal equiv^{-1} deg^{-1}. Temperature coefficient measurements on cation-exchange reactions with 12% DVB cross-linked polystyrenesulfonate over a wider interval (*i.e.*, 0–200°) but with one ion only at tracer concentrations have been reported by Kraus and Raridon.[15] The $\Delta C_p'$ values obtained from a "least-squares best fit" of the data, assuming $\Delta C_p'$ itself was independent of temperature, were always positive and sometimes as large as 20 cal equiv^{-1} deg^{-1}. The temperature dependence of $\Delta H°$ revealed by the measurements of Bonner and the temperature coefficients recently

reported by Starobinets and Soldatov[16] suggest that $\Delta C_p°$ also varies with temperature. However, equilibrium constants were measured only at 20 to 25° intervals from 0 to 100°, and corrections for the temperature-dependent activity coefficient ratios of the ions in the aqueous phase either were ignored or were estimated crudely. The magnitude and even the sign of the temperature dependence of $\Delta C_p°$ therefore is highly uncertain.

In this research the calorimetric measurement of $\Delta H°$ at a series of temperatures near 25° was undertaken in an attempt to derive more reliable values of

(1) Research sponsored by the U. S. Atomic Energy Commission under contract with the Union Carbide Corp.

(2) (a) G. E. Boyd, F. Vaslow, and S. Lindenbaum, *J. Phys. Chem.*, **68**, 590 (1964); (b) S. Lindenbaum and G. E. Boyd, *ibid.*, **69**, 2374 (1965).

(3) F. Vaslow and G. E. Boyd, *ibid.*, **70**, 2295, 2507 (1966).

(4) K. E. Becker, S. Lindenbaum, and G. E. Boyd, *ibid.*, **70**, 3834 (1966).

(5) G. E. Boyd and A. Schwarz, *ibid.*, **71**, 1355 (1967).

(6) G. E. Boyd, F. Vaslow, and S. Lindenbaum, *ibid.*, **71**, 2214 (1967).

(7) G. E. Boyd and Q. V. Larson, *J. Amer. Chem. Soc.*, **89**, 6038 (1967).

(8) O. D. Bonner and J. R. Overton, *J. Phys. Chem.*, **65**, 1599 (1961).

(9) E. H. Cruickshank and P. Meares, *Trans. Faraday Soc.*, **53**, 1289 (1957).

(10) D. S. Flett and P. Meares, *ibid.*, **62**, 1469 (1966).

(11) W. R. Heuman and D. Patterson, *Can. J. Chem.*, **44**, 2139 (1966).

(12) J. S. Redhina and J. A. Kitchener, *Trans. Faraday Soc.*, **59**, 515 (1963).

(13) O. D. Bonner and L. L. Smith, *J. Phys. Chem.*, **61**, 1614 (1957).

(14) O. D. Bonner and R. R. Pruett, *ibid.*, **63**, 1417, 1420 (1959).

(15) K. A. Kraus and R. J. Raridon, *ibid.*, **63**, 1901 (1959).

(16) G. L. Starobinets and V. S. Soldatov, *Russ. J. Phys. Chem.*, **37**, 153 (1963).

$\Delta C_p{}^\circ$ and to determine if the latter showed a temperature dependence. The exchange reaction between tetra-n-butylammonium ion, Bu_4N^+, in 0.01 N aqueous solution with sodium ion in a sulfonated polystyrene exchanger was used. Because of the large size of the Bu_4N^+ ion, a lightly cross-linked (*i.e.*, 0.5% divinylbenzene) polystyrenesulfonate cation exchanger was employed that a rapid exchange reaction leading to the establishment of an equilibrium in which all the sulfonate groups participated would be realized.

Experimental Section

Heat Measurements. The calorimeter, thermal measurement techniques, and experimental procedure were closely similar to those described in earlier reports from this laboratory[7] except that less exchanger was used (*e.g.*, *ca.* 1 mequiv) and a smaller concentration in the aqueous electrolyte phase was employed (μ = 0.01 M) so that heat of dilution corrections, $\Delta\phi_L$, would be negligibly small compared with the integral heat of ion exchange. Measurements were performed at 15, 20, 25, 30, and 35° with the exchanger initially in an homoionic form (*i.e.*, as NaR or as Bu_4NR). Two and sometimes four determinations were made at each temperature. A correction of 0.011 cal exothermic was applied for the heat of opening of the pipet which initially contained the ion exchanger.

The calorimeter was submerged in a stirred 60-l. water bath whose temperature was maintained constant to ±0.001° for periods of 1–2 hr. Longer term temperature drifts were read to 0.002° on a 5° range Beckman thermometer. A calibrated NBS mercury-inglass thermometer (range, −1 to 51° in 0.1°) was used to estimate the absolute temperature of the thermostat. The temperature of the stirred calorimeter solution was set above that of the thermostat for convenience in establishing a uniform drift rate. This increment, ΔT, was determined from the difference in resistance, $\Delta R = R_0 - R_t$, of the calorimeter thermistor measured when immersed in the bath, R_0, and in the assembled and stirred calorimeter, R_t. The approximate equation, $\Delta T = (T^2/B)(\Delta R/R_0)$, was employed. A plot of log R_0 *vs.* T^{-1} was accurately linear from 15 to 35° and yielded a slope of $B = 0.389 \times 10^4$. The reaction temperatures thus are believed to have been known to ±0.05°.

The over-all reliability of the calorimeter system was established by measurements of the heat of solution of tris(hydroxymethyl)aminomethane (THAM) in 0.1 N HCl solution. After small heat of dilution and heat capacity corrections, a value of 7095 ± 7 cal mol^{-1} at 25.00° and 0.04 m final concentration was obtained which is in good agreement with the value of 7104 cal mol^{-1} by Irving and Wadsö[17] and of 7107 cal mol^{-1} by Gunn.[18] The temperature coefficient of the heat of solution of THAM estimated from calorimetric measurements[17] at 20, 25, and 30° is 40 cal deg^{-1} mol^{-1}.

As a further test of our calorimeter, the heat of solution of THAM was measured at 30°. A value of 6916 ± 30 was obtained in good agreement with the value 6904 ± 3 cal mol^{-1} by Irving and Wadsö.

Chemical Analyses. The number of milliequivalents of exchange reaction was determined on concluding the thermal measurements by analysis of the exchanger and the mixed aqueous electrolyte in the calorimeter for sodium and tetra-n-butylammonium ions. Sodium ion concentrations were determined by flame spectrophotometry with a precision of *ca.* ±1%; tetra-n-butylammonium ion was measured by amperometric titration[7] with sodium tetraphenylboron to *ca.* ±2%. The total milliequivalents of ion exchanger in the calorimeter were found by titration of the acid form after its quantitative recovery and conversion by elution with 100 ml of 0.2 N HNO$_3$. The purity of the ion-exchange reaction (*i.e.*, the absence of interferences from other ionic impurities) was established by material balances from the chemical analyses of the exchanger and aqueous electrolyte.

The source of the largest error in the calculated heats of exchange was in the determination of the milliequivalents of reaction. The uncertainty in the calorimetric measurements was 0.4% or less, while that in the analyses of the exchanger for the amount of Na$^+$ or Bu$_4$N$^+$ ion taken up varied from 1 to 2%. The precision of the heat of exchange therefore was *ca.* 2%, although at several temperatures the measurements were better than this.

Experimental Results

The experimentally determined heats of partial exchange, Q, were plotted as chords against the initial and final values of the equivalent fraction of Bu$_4$N$^+$ ion in the exchanger, $x_{Bu_4N^+}$, and the chord-area method was applied to find the differential heat of ion exchange, $\Delta\bar{H} = dQ/dx_{Bu_4N^+}$, and also the integral ion-exchange enthalpy, ΔH, defined by $\Delta H = \int_0^1 \Delta\bar{H}\, dx_{Bu_4N^+}$. The standard enthalpy change, ΔH°, for the hypothetical ion-exchange reaction in which the products and reactants are in their standard states

NaR(a = 1, equil with 0.1 N NaCl) +

$\quad$ Bu$_4$NCl(aq, a = 1) $\rightleftharpoons$ Bu$_4$NR(a = 1,

$\quad\quad$ equil with 0.1 N Bu$_4$NCl) +

$\quad\quad\quad$ NaCl(aq, a = 1) + nH$_2$O(a_w = 1)
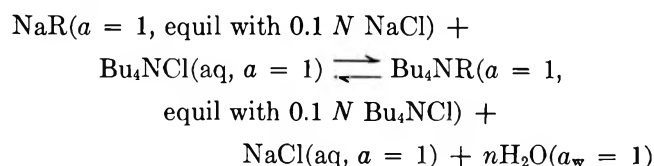
was obtained from the relation: $\Delta H^\circ = \Delta H + \Delta\phi_L$ where $\Delta\phi_L$ is the relative apparent molal heat content difference, ϕ_L(Bu$_4$NCl) − ϕ_L(NaCl), which was taken to be negligibly small for μ = 0.01 N solutions.

The values of ΔH° plotted against temperature in Figure 1 show that the standard enthalpy of exchange

(17) R. J. Irving and I. Wadsö, *Acta Chem. Scand.*, **18**, 195 (1964).
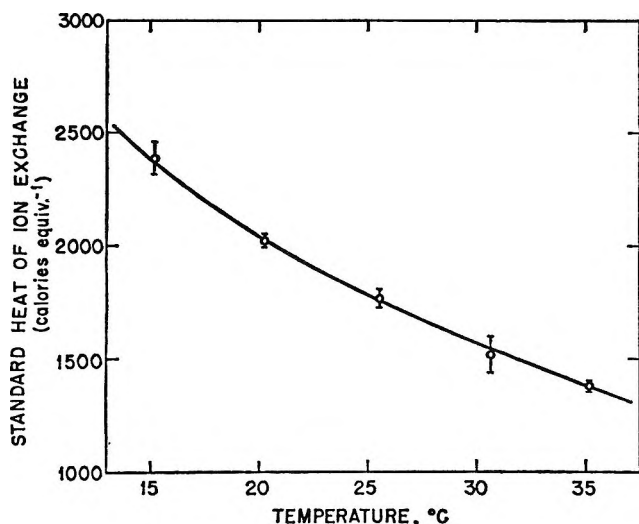(18) S. Gunn, *J. Phys. Chem.*, **69**, 2902 (1965).

Figure 1. Temperature dependence of the standard enthalpy of exchange, $\Delta H°$, of tetra-n-butylammonium with sodium ions in 0.5% divinylbenzene cross-linked polystyrenesulfonate.

of Bu_4N^+ with Na^+ ion decreased by approximately 1000 cal equiv^{-1} as the temperature increased from 15 to 35°. The decrease in $\Delta H°$ with temperature followed the least-squares quadratic equation

$$\Delta H° = 3605 - 92.7t + 0.804t^2$$

where t is the temperature in degrees Centigrade. The standard errors in the constants were 108, 9.1, and 0.179, respectively. The standard heat capacity change, $\Delta C_p°$, is given by

$$\Delta C_p° = d\Delta H°/dt = -92.7 + 1.6_1t$$

which, for 25°, gives $\Delta C_p° = -53 \pm 9$ cal deg^{-1} mol^{-1}. The heat capacity change itself is slightly temperature dependent and increases by approximately 1.6 eu deg^{-1}.

Discussion

The standard heat capacity change in the tetra-n-butylammonium–sodium ion-exchange reaction is unusually large and negative in contrast with all other reactions involving the exchange of singly charged cations in organic ion exchangers. However, the apparent molal heat capacity, ϕC_p, of aqueous solutions of Bu_4NBr are known from the measurements of Frank and Wen[19] to be quite large, whereas the ϕC_p for NaBr solutions is small (i.e., $\phi°C_p = -22.8$ eu). Accordingly, ΔC_p for the conversion of sodium form exchanger to the tetra-n-butylammonium form can be expected to be large provided other effects do not enter. The standard heat capacity change, $\Delta C_p°$, in the conversion in fact is simply related to the ϕC_p difference for the two resinates when the cross-linking of the ion exchanger is light

$$\Delta C_p° = \phi C_p(Bu_4NR) - \phi C_p(NaR) +$$
$$\phi°C_p(Na^+) - \phi°C_p(Bu_4N^+) \quad (1)$$

The standard apparent molal heat capacity for sodium ion is known,[20] $\phi°C_p(Na^+) = 11.1$ eu, while that for tetra-n-butylammonium ion may be derived from the experimental measurements of Wen.[21] However, an extrapolation to infinite dilution from the 25° value, $\phi C_p(Bu_4NBr) = 270 \pm 2$ cal deg^{-1} mol^{-1} at 0.1988 m, must be made. We have utilized the equation for a 1-1 electrolyte

$$\phi C_p - \phi°C_p = A_J m^{1/2}[(1 + m^{1/2})^{-1} -$$
$$\sigma(m^{1/2})/3] - 2.303RT^2[(2/T)(dB/dT) +$$
$$(d^2B/dT^2)]m \quad (2)$$

first proposed by Guggenheim and Prue[22] to join the available data to the limiting Debye–Hückel slope. The quantities, dB/dT and d^2B/dT^2, were estimated from the correlation diagrams of Pitzer and Brewer[23] with the value of $B = -0.25$ for aqueous solutions of Bu_4NBr estimated at $m = 0.1$ from the osmotic coefficient at this concentration[24] with the equation

$$1 - \phi = (2.303/3)A_\gamma m^{1/2}\sigma(m^{1/2}) - (2.303/2)Bm \quad (3)$$

where $A_\gamma = 0.511$. Thus, with $A_J = 10.4$ cal deg^{-1} mol^{-1}, $dB/dT = 7.2 \times 10^{-3}$, and $d^2B/dT^2 = -13.6 \times 10^{-5}$, one calculates for $m = 0.1988$

$$\phi C_p - \phi°C_p = 9.4 \text{ eu} \quad (4)$$

from which $\phi°C_p(Bu_4NBr) = 261 \pm 2$ eu. The value $\phi°C_p(Bu_4N^+) = 295 \pm 2$ eu is then obtained by subtracting the value for bromide ion[20] $\phi°C_p(Br^-) = -33.9$ eu from 261 ± 2 eu. Equation 1 becomes

$$\Delta C_p° = \phi C_p(Bu_4NR) - \phi C_p(NaR) - 284 \pm 2 \quad (1')$$

To estimate approximately the difference $\phi C_p(Bu_4NR) - \phi C_p(NaR) = \Delta\phi C_p$, we note that an examination of available heat capacity data for aqueous solutions of the alkali metal salts[20] shows that $\Delta\phi C_p$ is nearly independent of the nature of the anion over a wide concentration range. Thus, we shall assume $\phi C_p(NaR) \approx \phi C_p(NaBr)$ and $\phi C_p(Bu_4NR) \approx \phi C_p(Bu_4NBr)$, respectively. The concentration at which $\phi C_p(NaR)$ and $\phi C_p(Bu_4NR)$ are to be taken needs justification. There is reason to believe that the "effective concentration" in the double layer of cations about the negatively charged polyelectrolyte chains of the cation exchanger is of the order of 4-5 m based on heat of ion-exchange

(19) H. Frank and W. Y. Wen, *Discussions Faraday Soc.*, **24**, 136 (1957).

(20) V. B. Parker, "Thermal Properties of Aqueous Uni-univalent Electrolytes," National Standard Reference Data Series, NSRDS-NBS 2, National Bureau of Standards, U. S. Government Printing Office, Washington, D. C., 1965.

(21) W. Y. Wen, Ph.D. Thesis, University of Pittsburgh, 1957.

(22) E. A. Guggenheim and J. E. Prue, *Trans. Faraday Soc.*, **50**, 710 (1954).

(23) K. S. Pitzer and L. Brewer in G. N. Lewis and M. Randall, "Thermodynamics," McGraw-Hill Book Co., Inc., New York, N. Y., 1961, pp 396, 397.

(24) S. Lindenbaum and G. E. Boyd, *J. Phys. Chem.*, **68**, 911 (1964).

measurements[25] and other studies.[26] Therefore, assuming an effective localized concentration $m = 4.0$, the value $\phi C_p(\text{NaBr}) = 3.8$ may be taken from the literature, while $\phi C_p(\text{Bu}_4\text{NBr}) \approx 220$ eu may be found by extrapolating the 25° measurements of Frank and Wen.[19,21] Thus, $\Delta\phi C_p \approx 216$ eu and $\Delta C_p° \approx 216 - 284 \approx -68$ eu. If $m = 2.0$ is assumed, $\Delta C_p° \approx -40$ eu. It is clear therefore that a large and negative standard heat capacity change in the exchange reaction of Bu_4N^+ with Na^+ ion is to be expected.

It is of interest to note that only a relatively small fraction of the total heat capacity (i.e., 284 eu) of the Bu_4N^+ ion is released when it is bound by the ion exchanger. However, this large, complex hydrocarbon-like ion may be estimated to possess an internal heat capacity of as much as 150 eu; this will not be lost when the ion is taken up by the exchanger. Further, as Frank and Wen[19] have pointed out, the ca. 130-eu difference between the internal and the total heat capacity of the ion must be assigned to the interaction of the ion with water. This interaction decreases when Bu_4N^+ ion leaves its dilute solution and is bound by the exchanger. Actually, of course, this ion does not entirely leave its water environment; even when it is held by the polyelectrolyte it will interact with the water structure in its vicinity. An appreciable overlap of the "hydration" cospheres must occur, however, so that a negative and relatively large heat capacity change will accompany its replacement of sodium ion in an ion-exchange reaction. The relatively large increase in the standard entropy, $\Delta S°$, previously reported[7] and the large, negative $\Delta C_p°$ found in this research are consistent with the view of Frank that

tetra-n-butylammonium ion should be regarded as a "water-structure producer" of a special type.

In conclusion, we note that eq 1 may be employed to predict the approximate magnitude of $\Delta C_p°$ for many ion-exchange reactions in exchangers of large cross-linking. A comparison of predicted and observed values is presented in Table I where it was assumed that $\text{R}^- = \text{NO}_3^-$. All things considered, the agreement between columns 4 and 5 is surprisingly good, particularly when it is remembered that the "observed" $\Delta C_p'$ values were for the exchange of trace amounts of alkali metal ion in either the pure hydrogen or pure sodium form of cross-linked polystyrenesulfonate.

Table I: Estimation of Heat Capacity Changes at 298.2°K in Ion-Exchange Reactions with Eq 1 and the Apparent Molal Heat Capacities of Aqueous Nitrate Solutions

Reaction	$\Delta(\phi C_p)$	$\Delta(\phi° C_p)$	Calcd $\Delta C_p°$	Obsd[15] $\Delta C_p'$
Na–H[a]	25.8	11.1	14.7	9.3
K–H[a]	16.8	5.2	11.6	11.4
Rb–H[a]	15.3	3.3	12.0	11.3
Cs–H[a]	14.0	1.9	12.1	15.5
K–Na[b]	−6.0	−5.9	−0.1	1.1
Rb–Na[b]	−8.5	−7.8	−0.7	0.4
Cs–Na[b]	−9.5	−9.2	−0.3	0.9

[a] Computed for hydrogen resinate molality of 2.6. [b] Computed for NaR molality of 2.95.

(25) G. E. Boyd, F. Vaslow, A. Schwarz, and J. W. Chase, *J. Phys. Chem.*, **71**, 3879 (1967).

(26) O. D. Bonner and O. C. Roger, *ibid.*, **65**, 981 (1961).

Absorption Spectra of the Alkali Metals in Hexamethylphosphoramide

by Jon M. Brooks and Robert R. Dewald

Department of Chemistry, Tufts University, Medford, Massachusetts 02155 (*Received February 28, 1968*)

A qualitative study of the absorption spectra of dilute solutions of the alkali metals in hexamethylphosphoramide has been carried out at room temperature and at 10°. The five metals have an identical absorption peak at 2250 mμ. Sodium, potassium, and rubidium also have maxima at 750, 950, and 975 mμ, respectively. Lithium shows a peak at 760 mμ at 10°. Addition of alkali metal halide salts to the blue solutions confirmed the metal dependence of the visible and near-infrared peaks. With a decrease in temperature, the absorption curves are shifted to higher energies, and the intensities of the respective visible and near-infrared peaks increase with a corresponding decrease in the infrared peak.

Introduction

Solutions of the alkali metals in liquid ammonia exhibit a broad optical absorption band that peaks at approximately 1500 mμ at −65°, and the shapes of the absorption curves were found essentially the same for solutions of the different metals.[1,2] Metal–amine solutions, on the other hand, consistently show two or three absorption maxima, some of which are metal dependent.[3–6] Recently, Hurley, Tuttle, and Golden[7] have reported that the metal-dependent absorption at 660 mμ, frequently observed in metal–amine solutions other than sodium, is probably due to sodium contamination during the experiment.

A recent article has reviewed the versatility of hexamethylphosphoramide (Me$_2$N)$_3$PO, HMPA, as a solvent for organic oxidations, reductions, polymerizations, and other reactions.[8] The utility of this solvent is attributed to its high basicity, its relatively large dielectric constant[9] (30 at 25°), and its aprotic nature. A blue-black solution of sodium in HMPA was reported in 1964;[10] soon afterward, lithium and potassium were shown to be soluble.[11,12] The alkaline earth metals, except beryllium, also are reported to dissolve in HMPA.[13] The absorption spectra in the visible region up to 800 mμ have recently been reported for solutions of sodium, magnesium, calcium, strontium, and barium in HMPA.[13] Each of these metal solutions, exhibits an absorption maximum at 770 mμ which is not attributable to decomposition products.[8,13] Recently, Catterall, Stodulski, and Symons[14] reported that dilute solutions of sodium and potassium in HMPA show an absorption band in the 2130-mμ region while concentrated solutions have an additional band at 725 mμ.

Some investigators[8,15] have concluded, primarily on the basis of esr data, that when the metals dissolve in HMPA, solutions consisting of radical anions of the solvent and metal ions are formed. Other investigators[11,14] have suggested that solvated electrons are present, since these solutions are similar to those of the metals in ammonia and amines. This study was undertaken with the hope that a more complete investigation of the absorption spectra would yield information on the types of species present in solutions of the alkali metals in HMPA.

Experimental Section

Metals. The alkali metals were obtained in the highest purity from the following sources: sodium, potassium, and rubidium from the United Mineral and Chemical Corp.; lithium from the Foote Mineral Co.; and cesium as a gift from The Dow Chemical Co. Large samples of sodium, potassium, rubidium, and cesium were broken down as previously described by a double distillation process (*in vacuo*) into usable quantities contained in small vacuum-sealed ampoules.[3] Lithium was cut into small pieces under an argon atmosphere in a drybox described elsewhere.[16] The lithium samples were placed in break-seal tubes and

(1) R. C. Douthit and J. L. Dye, *J. Amer. Chem. Soc.*, **82**, 4472 (1960).

(2) M. Gold and W. L. Jolly, *Inorg. Chem.*, **1**, 818 (1962).

(3) R. R. Dewald and J. L. Dye, *J. Phys. Chem.*, **68**, 121 (1964).

(4) G. W. A. Fowles, W. R. McGregor, and M. C. R. Symons, *J. Chem. Soc.*, 3329 (1957).

(5) E. C. Evers, *J. Chem. Educ.*, **38**, 590 (1961).

(6) M. Ottolenghi, K. Bar-Eli, H. Linschitz, and T. R. Tuttle, Jr., *J. Chem. Phys.*, **40**, 3729 (1964).

(7) I. Hurley, T. R. Tuttle, Jr., and S. Golden, *ibid.*, in press.

(8) H. Normant, *Angew. Chem.*, **79**, 1029 (1967); *Angew. Chem. Int. Ed. Engl.*, **6**, 1046 (1967).

(9) J. E. Hofmann, A. Schriesheim, and D. D. Rosenfeld, *J. Amer. Chem. Soc.*, **87**, 2523 (1965).

(10) T. Cuvigny, J. Normant, and H. Normant, *C. R. Acad. Sci., Paris*, **C258**, 3503 (1964).

(11) G. Fraenkel, S. H. Ellis, and D. T. Dix, *J. Amer. Chem. Soc.*, **87**, 1406 (1965).

(12) H. Normant, T. Cuvigny, J. Normant, and B. Angelo, *Bull. Soc. Chim. Fr.*, 1561 (1965).

(13) M. Fontanille and P. Sigwalt, *C. R. Acad. Sci., Paris*, **C263**, 316 (1966).

(14) R. Catterall, L. P. Stodulski, and M. C. R. Symons, *J. Chem. Soc., A*, 437 (1968).

(15) H. Normant, T. Cuvigny, J. Normant, and B. Angelo, *Bull. Soc. Chim. Fr.*, 3441 (1965).

(16) T. R. P. Gibb, Jr., *Anal. Chem.*, **29**, 584 (1957).

transferred without atmospheric contamination to a
vacuum line. The assembly was evacuated for several
hours and then the break-seal tube containing the
lithium was sealed off.

Salts. Rubidium iodide (Fisher, Purified), cesium
chloride (Fisher, 99.9%), lithium chloride (Fisher,
Certified), sodium iodide (Matheson Coleman and
Bell, Reagent), and sodium chloride (Fisher, Biological)
were used without further chemical purification. A
weighed amount of the salt was transferred quickly to a
break-seal tube. The contents were heated *in vacuo*
(almost to melting), and after further evacuation for
4 hr, the tubes were sealed off.

Solvent. An all-Pyrex purification assembly, using
only break-seals and seal-offs, similar to that described
elsewhere,[17] was constructed. The entire system was
capable of evacuation to better than 5×10^{-6} torr
after flaming. HMPA (a gift from The Dow Chemical
Co.) was stored in contact with sodium metal for 1 week
and then was transferred to the stillpot and refluxed
under $\sim$0.5 torr of N_2 (Matheson, prepurified) for 24 hr.
The solvent was distilled through a 3-ft column packed
with helices; the middle fraction (*ca.* 450 ml) was col-
lected on a potassium mirror, immediately forming a
blue solution. About 2 days was required for complete
reaction of the excess metal. A second distillation (*in
vacuo*) was then carried out onto another potassium
mirror and likewise was allowed to stand for 2 days.
The solvent was finally distilled into the reservoir flask
and then transferred (*in vacuo*) to 25- and 50-ml am-
poules containing break-seals.

A Beckman Model DK-2 ratio recording spectro-
photometer was used to record the spectra of the blue
solutions from 320 to 3200 mμ. Pyrex optical cells
(American Instrument Co.) of nominal path lengths
0.1 and 0.01 cm were used. Pure solvent (*in vacuo*)
was used in the reference beam. A low-temperature
cell compartment was constructed similarly to that de-
scribed elsewhere.[1] A circulating system maintained
the temperature at $10 \pm 0.5°$. Room temperature
varied during the investigation but was assumed to
average about 25°.

Procedure. Standard high-vacuum techniques were
used and stringent precautions were taken to ensure
cleanliness of the glassware.[3] The apparatus, shown
in Figure 1 (excluding the solvent recovery trap), was
connected to the vacuum line with Apiezon W wax;
a metal ampoule was broken and introduced into the
metal still which was then sealed. The apparatus was
evacuated and flamed out until the pressure stabilized
at about 5×10^{-6} torr. In an effort to displace water
sorbed on the walls of the vessel, the apparatus was
exposed to pure ammonia vapor six times, each followed
by evacuation. The metal was distilled into the mixing
chamber and the seal-off to the vacuum line was closed.
The solvent was then tipped into the chamber and the
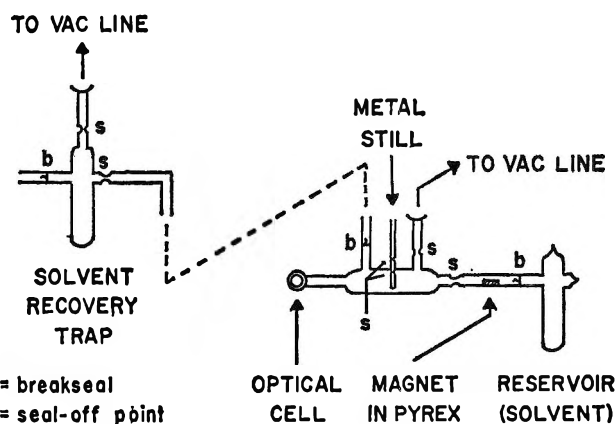
Figure 1. Apparatus for solution makeup and
solvent recovery.

reservoir was sealed off. The blue solutions formed
immediately.

Because of the difficulties encountered in distilling
and purifying HMPA in large quantities, the solvent
was recovered without exposure to the atmosphere after
each experiment. This was accomplished by sealing a
solvent recovery trap to the apparatus as shown in
Figure 1. The assembly was then evacuated, flamed,
and exposed to dry ammonia as described above. Fi-
nally after breaking the break-seal, the solvent was vac-
uum distilled into the recovery trap which was kept at
liquid nitrogen temperature.

Results

Table I shows absorption maxima at 25 and 10°
for the alkali metals in HMPA. It is difficult to define
the infrared peak positions exactly since they are quite
broad, having a half-width of approximately 1700 mμ.
In addition, HMPA possesses very intense absorption
bands in the 2100–2500-mμ region, so that this region is
inaccessible for quantitative measurements even with a
1-mm cell. With a 0.1-mm cell, however, the absorb-
ance of the most intense band (2270 mμ) is 0.3 for the
pure solvent. Decomposed solutions were found to
absorb only below 500 mμ. Since precise measure-
ments of the amount of metal and the volume of sol-
vent were not made, spectra were evaluated and com-
pared by plotting A/A_{max} *vs.* wavelength, where A is
absorbance. This procedure allowed a comparison of
peak positions and shapes in spite of varying rates of
decomposition. We estimate that the concentrations
of the dilute solutions were about 10^{-3} to 10^{-2} M,
except where noted otherwise. It was observed that
the blue solution in the optical cell did not visibly de-
compose any faster than that in the body of the ap-
paratus. This observation is contrary to the results
found for the alkali metal–ethylenediamine solutions.[3]

Lithium. Since handling techniques used in working
with lithium metal limited its purity and decomposition

(17) R. R. Dewald, Ph.D. Thesis, Michigan State University, East
Lansing, Mich., 1963.

of the metal solutions is enhanced by impurities,[18] the lithium solutions were the least stable. A visible peak was not found at room temperature; however, at 10° a small distinct peak was observed at about 760 mμ and its intensity was enhanced by the addition of lithium chloride to the solution. The infrared peak was estimated to be about ten times more intense than the visible peak at 10°. On addition of more lithium metal to the decomposed lithium solutions at 10°, the blue color reappeared and the infrared peak position shifted gradually to 2400 mμ.

Sodium. Solutions of sodium in HMPA appeared to be more stable than those of the other metals; about 5 hr was required for the dilute blue solutions to decompose at 10° and shorter times at 25°. The visible peak at 735 mμ was initially more intense than the infrared peak at 10°, while at room temperature the infrared peak was more intense. Figure 2 shows the absorption spectrum of a dilute sodium–HMPA solution. It was noted that the visible peak always decayed faster than the infrared peak. (For the metal solutions, the infrared peak consistently decomposed at a slower rate than other peaks given in Table I.) Addition of sodium chloride and sodium iodide to solutions of sodium, potassium, rubidium, and cesium in HMPA at room temperature always resulted in the appearance of a band peaking at 750 mμ. When the spectrum in Figure 2 is replotted as A/A_{max} vs. wave number, the curves of the two bands are about identical with broadening on the high-energy side, and the widths at halfheight are equal (3700 ± 200 cm^{-1}).

Potassium. Dilute potassium solutions in HMPA (less than 10^{-2} M, 25°) showed only the infrared peak, whereas in more concentrated solutions, a shoulder at about 950 mμ was observed. At 10° the dilute solutions in the 0.1-mm cell showed peaks at 935 and 2100 mμ. Potassium solutions appeared to be slightly less stable than those of sodium.

Rubidium. At room temperature, rubidium solutions showed a weak (but distinct) peak at 975 mμ and the broad infrared peak. At 10° the intensity of the visible peak was found to be about one-third that of the infrared peak. The characteristic band at about 975 mμ for rubidium was also observed when rubidium chloride was mixed with a sodium–HMPA solution. Stabilities of the rubidium solutions were comparable to those of potassium.

Cesium. Only the broad peak at 2300 mμ was observed for cesium solutions, even at fairly high metal concentrations using the 0.1-mm cell at 10°. It was noted that the visible tail of the infrared peak increased slightly when the temperature was changed from 25 to 10°. The decomposition rate of these solutions appeared to increase with greater metal concentration.

Salt Addition. Figure 3 illustrates the effect of adding salt to the metal solutions. In this case, sodium iodide was added to a potassium solution after its
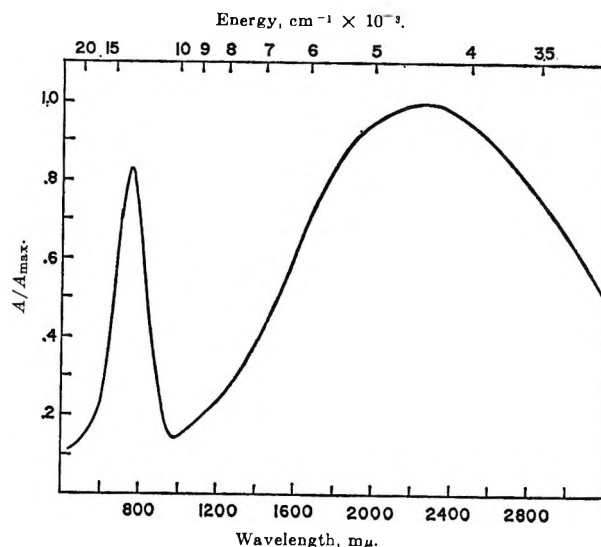
Figure 2. A plot of A/A_{max} vs. wavelength (mμ) for a sodium–HMPA solution.
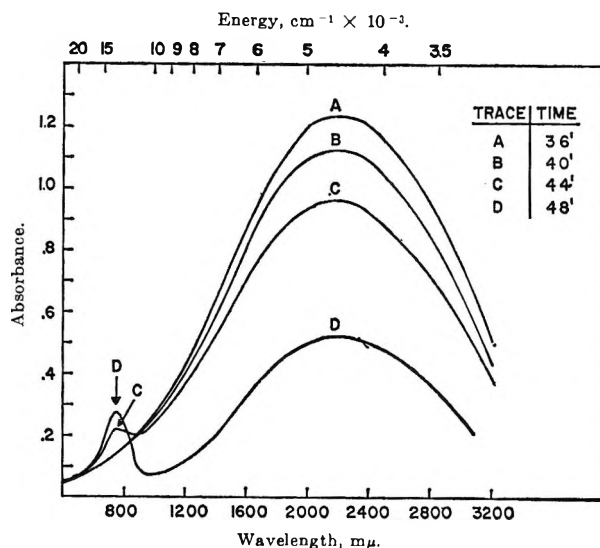
Figure 3. Illustration of salt addition: consecutive absorption curves of a potassium–HMPA solution to which sodium iodide was added after trace B. Normal rate of decomposition is shown by traces A and B.

characteristic 975-mμ peak had decomposed. Traces C and D show the appearance of a new peak at about 750 mμ similar to that observed for sodium–HMPA solutions. In all cases it was noted that the intensity of the visible–near-infrared peaks (experiments with sodium iodide and rubidium chloride) appeared at the expense of the infrared peak, beyond that due to reaction of the metal with the solvent. The addition of salt to the blue solutions did not significantly affect their stability.

Temperature Dependence. In all cases the blue solutions were found to be considerably more stable (a

(18) W. L. Jolly and C. J. Hallada in "Non-Aqueous Solvent Systems," T. C. Waddington, Ed., Academic Press Inc., New York, N. Y., 1965, p 37.

factor of 3 to 4) at 10° than at room temperature. In solutions of sodium, potassium, and rubidium it was found that the intensity of the visible–near-infrared band increased with a corresponding decrease in the infrared peak when cooled to 10. Figure 4 illustrates this for a sodium experiment. Table I also summarizes the results.

Table I: Absorption Maxima in Hexamethylphosphoramide[a]

Metal	Maximum absorbance (mμ)[b] at	
	25°	10°
Lithium	...	760
	2250	2150
Sodium	750	735
	2250	2150
Potassium	950 (sh)	935
	2220	2100
Rubidium	975	960
	2300	2175
Cesium	2250	2150

[a] Range scanned for all metals: 320–3200 mμ. [b] Average error: infrared peak, ± 50 mμ; visible–near-infrared peak, ± 5 mμ.

Discussion

Comparison of plots of A/A_{max} vs. wavelength for the broad absorption band peaking at about 2250 mμ shows that these absorption curves are the same for the different alkali metals. The visible–near-infrared peaks at 750, 950, and 975 mμ observed for sodium, potassium, and rubidium solutions, respectively, resemble one another in shape but are displaced in position. The addition of salts to metal solutions demonstrated that the appearance and position of the visible–near-infrared peaks are dependent on the presence of the particular metal ions. Fontanille and Sigwalt[13] reported the absorption spectra of sodium in HMPA up to 800 mμ and found a maximum at 770 mμ. Catterall, Stodulski, and Symons reported peaks at about 2130 mμ for dilute solutions of sodium and potassium and an additional peak at 725 mμ for more concentrated solutions. The previous results for sodium are in general agreement with this work, but for potassium solutions we observed a shoulder at about 950 mμ and no evidence of a peak at 725 mμ (Table I). However, when sodium iodide was added to a potassium solution, a peak at 750 mμ developed immediately.

The alkali metals in liquid ammonia show only a single absorption in the near-infrared.[1,2] This broad absorption band, tailing into the visible, is attributed to an electron in a cavity surrounded by polarized solvent molecules.[19,20] The infrared absorption band reported for metal–amine solutions is also very broad and extends into the visible.[3,6,21] The conductances of potassium, rubidium, and cesium in ethylenediamine support the assignment of the infrared absorbing species
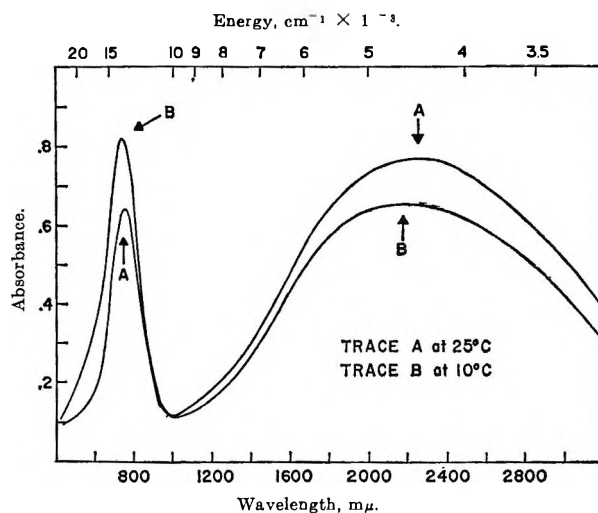
Figure 4. Absorption curves for sodium in HMPA at 25 and 10°.

to the solvated electron.[22,23] The infrared band in metal–HMPA solutions resembles that reported in metal–ammonia solutions. The visible–near-infrared bands observed for sodium, potassium, and rubidium in HMPA are also similar to those found for the respective metals in amine solvents.[24] These absorptions in amines have been attributed to dimers, but there is no agreement on their exact nature and more studies on the stoichiometry are needed to complete the identification.[6,14,23]

We can estimate from Table I an average peak shift with temperature of about -13 cm^{-1} deg^{-1} for both peaks from 10 to 25°. This temperature dependence on the spectra is similar to that reported for sodium and potassium in liquid ammonia.[1,2] In addition to the peak shift, as the temperature is lowered it was observed for sodium, potassium, and rubidium solutions that intensity of the respective visible–near-infrared peaks increased with a corresponding decrease in the intensity of the infrared peak. This indicates that an equilibrium exists between the species responsible for the different absorption bands.

It was suggested that the blue metal in HMPA solutions consisted of solvent radical anions[8,15]

$$M + O=P(NMe_2)_3 \longrightarrow [O \doteq P(NMe_3)_3]^- M^+$$
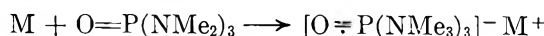
The absorption spectra reported in this study and in the work of Catterall, et al.,[14] suggest that these solutions are quite similar to metal–amine and –ammonia systems where studies have shown that solvated electrons rather

(19) J. Jortner, J. Chem. Phys., **30**, 839 (1959).

(20) J. Jortner, S. A. Rice, and E. G. Wilson, in "Metal–Ammonia Solutions," G. LePoutre and M. J. Sienko, Ed., W. A. Benjamin, Inc., New York, N. Y., 1964, p 222.

(21) H. Blades and J. W. Hodgins, Can. J. Chem., **33**, 411 (1955).

(22) R. R. Dewald and J. L. Dye, J. Phys. Chem., **68**, 128 (1964).

(23) L. R. Dalton, J. L. Dye, E. M. Fielden, and E. J. Hart, ibid., **70**, 3358 (1966).

(24) J. L. Dye and R. R. Dewald, ibid., **68**, 135 (1964).

than solvent radical anions are the dominant species in solutions.

NOTES

Direct Detection of the Hexaaquocobalt(II) Ion in Aqueous Solutions by Proton Magnetic Resonance Spectroscopy

by N. A. Matwiyoff and P. E. Darley

*Chemistry Department, Pennsylvania State University,
University Park, Pennsylvania 16802*
(Received January 29, 1968)

Nuclear magnetic resonance studies of the contact chemical shifts[1,2] and enhanced relaxation rates[3-8] induced in water molecules by paramagnetic ions have provided much valuable information concerning the hydration of cations.[9] Of these studies the ones which yield the most direct information about the hydration number of the cation are those which result in a distinction between the nmr signals of the water molecules within and those outside the first coordination sphere of the cation. Such a distinction is not easily obtained for aqueous solutions of paramagnetic cations owing to: the large water-exchange rates, the broad signals of the bonded water molecules, and the fact that the chemical shift between bonded and free water is not always large compared to the signal widths.

Connick and Fiat,[10] using ^{17}O nmr spectroscopy, observed a separate first-solvation-sphere signal for Ni(II) in aqueous solutions. Also separate solvation sphere proton signals have been observed for solutions of Co(ClO$_4$)$_2$ in methanol,[11] N,N-dimethylformamide,[12] and acetonitrile.[13] We wish to report here that at temperatures below $-38°$, it is possible to distinguish the pmr signal of water molecules within the primary coordination sphere of Co(II) in concentrated aqueous Co(ClO$_4$)$_2$ solutions. From the relative intensities of the bonded and free water signals, a primary hydration number of 6, within experimental error, is obtained for Co(II). Furthermore, we have been able to show that the primary hydration number is invariant with respect to solution composition in the temperature range -63 to $+67°$.[14]

A 100-MHz pmr spectrum of an aqueous Co(ClO$_4$)$_2$ solution at $-60°$ is represented in Figure 1. From the

dependence of the relative signal intensities upon the solution composition, the low-field resonance is assigned to water within, and the high-field resonance to water outside, the first hydration sphere of the Co(II) ion. The primary hydration numbers calculated from the relative signal intensities are listed in Table I, along with the signal line widths and relative chemical shifts.

The proton chemical shifts of Co(OH$_2$)$_6^{2+}$, $\Delta\nu_m$, with respect to those of bulk water are plotted *vs.* the reciprocal temperature in Figure 2. In the temperature range, $4.51 \leq 10^3/T \leq 4.78$, the shifts are a linear function of the reciprocal temperature and conform to the Bloembergen equation[15]

$$\frac{\Delta\nu_m}{\nu_I} = -\frac{A}{h}\frac{2\pi}{3}\frac{S(S+1)g\beta}{\gamma_I kT} \qquad (1)$$

where A/h is the proton–electron hyperfine coupling constant in hertz, ν_I is the resonance frequency, β is the Bohr magneton, γ_I is the proton magnetogyric ratio, and S is the electron spin of Co(II). At temperatures $10^3/T \leq 4.42$, the shifts deviate from the linear relation, owing to the onset of chemical exchange[4] which is also reflected in the line-width data in Table I.

(1) Z. Luz and R. G. Shulman, *J. Chem. Phys.*, **43**, 3750 (1965).

(2) B. B. Wayland and W. L. Rice, *Inorg. Chem.*, **5**, 54 (1966).

(3) R. A. Bernheim, T. H. Brown, H. S. Gutowsky, and D. E. Woessner, *J. Chem. Phys.*, **30**, 950 (1958).

(4) T. J. Swift and R. E. Connick, *ibid.*, **37**, 307 (1962).

(5) T. J. Swift and T. A. Stephenson, *Inorg. Chem.*, **5**, 1100 (1966).

(6) N. Bloembergen and L. O. Morgan, *J. Chem. Phys.*, **34**, 842 (1961).

(7) L. O. Morgan and A. W. Nolle, *ibid.*, **31**, 365 (1959).

(8) R. Hausser and C. Laukien, *Z. Phys.*, **153**, 394 (1959).

(9) For a general discussion of the nmr of paramagnetic molecules, see D. R. Eaton and W. D. Phillips, *Advan. Magnetic Res.*, **1**, 103 (1965).

(10) R. E. Connick and D. N. Fiat, *J. Chem. Phys.*, **44**, 4103 (1966).

(11) Z. Luz and S. Meiboom, *ibid.*, **40**, 1058 (1964).

(12) N. A. Matwiyoff, *Inorg. Chem.*, **5**, 788 (1966).

(13) N. A. Matwiyoff and S. V. Hooker, *ibid.*, **6**, 1127 (1967).

(14) In the temperature range -63 to $0°$, aqueous solutions of Co(ClO$_4$)$_2$ of the compositions used in this study are viscous but flow freely and are free of solids. No time dependence of these properties, or the nmr spectra, was noted over a 4-hr period.

(15) N. Bloembergen, *J. Chem. Phys.*, **27**, 595 (1957).

Table I: Solvation Numbers, Line Widths, and Relative Chemical Shifts for the Ion $Co(OH_2)_n^{2+}$ Derived from the 100-MHz Spectra of Aqueous $Co(ClO_4)_2$ Solutions

—Solution composition, mol—		Temp, °C	Solvation no. (± 0.3), n	Line widths[a]		Chemical shift[b]
[Co(II)]	[H₂O]			$\Delta\nu_c$	$\Delta\nu_f$	
1.00	18.0	−63.7	5.8	1450	400	10,000
		−60.0	5.7	1430	390	9,850
		−55.8	5.8	1440	430	9,650
		−51.5	5.9	1600	540	9,500
		−47.0	5.9	1900	800	9,150
		−42.8	5.8	2550	1200	8,700
		−38.0	6.1	4300	2000	7,530
1.00	16.0	−63.7	5.9	1490	410	10,050
1.00	23.1	−38.0	5.9	4100	1900	7,430

[a] Full width (in hertz, $\pm 1.0\%$) of the line at half the maximum height; $\Delta\nu_c$ refers to the coordinated water signal and $\Delta\nu_f$ to the free water signal. [b] Chemical shift (in hertz, $\pm 1.0\%$) of the coordinated water signal downfield with respect to free water.
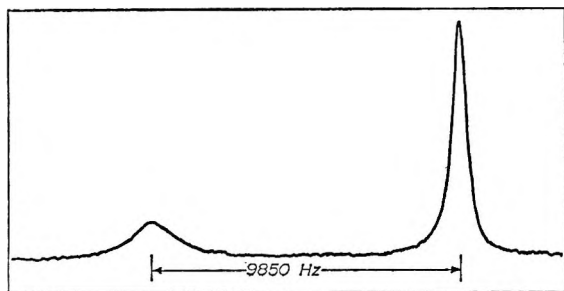
Figure 1. Proton magnetic resonance spectrum (100 MHz) of a 3.2 m solution of $Co(ClO_4)_2$ in water at $-60°$. The magnetic field increases from left to right.

Figure 2. The proton chemical shifts, $\Delta\nu_m$, of $Co(OH_2)_6^{2+}$ vs. $10^3/T$: ○, proton chemical shifts of $Co(OH_2)_6^{2+}$ at 100 MHz in the slow-exchange limit; ⊕, 60 MHz for a 1.020 m solution in the rapid-exchange limit; +, 60 MHz for a 0.309 m solution; □, 100 MHz for a 3.02 m solution; △, 100 MHz for a 0.400 m solution; I, 60 MHz for a 0.400 m solution.

Also included in Figure 2 are chemical shifts calculated from data obtained at high temperatures in the rapid chemical exchange limit (where a single exchange-averaged proton signal is distinguished) using the equation[4]

$$\Delta\nu = P\Delta\nu_m \qquad (2)$$

where P is the fraction of the total amount of water coordinated to Co(II) and $\Delta\nu$ is the difference in chemical shift between the exchange-averaged pmr signal of the $Co(ClO_4)_2$ solution and that for a solution of Mg-$(ClO_4)_2$,[16,17] each measured relative to the internal standard 3-(trimethylsilyl)-1-propanesulfonic acid sodium salt. The P values were calculated using a primary hydration number of 6 for Co(II). The shift measurements in the rapid-exchange limit were made under the following conditions (Figure 2) and all the shift data were adjusted to 100 MHz: 60 MHz for a 0.400 m solution, 100 MHz for a 0.400 m solution, 100 MHz for a 3.02 m solution, 60 MHz for a 0.309 m solution, and 60 MHz for a 1.020 m solution.

Because the shift data obtained in the rapid- and slow-exchange limits fall along the same straight line, we can conclude that the primary hydration number of Co(II) is 6 and that it is independent of the temperature and solution composition. However, in view of the

error limits for the shift measurements, we cannot exclude the formation of small amounts of species such as, $Co(OH_2)_5^{2+}$ or $Co(OH_2)_5ClO_4^+$, in these solutions. The coupling constant, A/h, calculated using the slope of the line in Figure 2 is $(3.7 \pm 0.1) \times 10^5$ Hz, in acceptable agreement with the value 3.9×10^5, obtained by Luz and Shulman[1] from measurements at 20 and 100°. Similar conclusions about the temperature independence of the coordination number of Co(II) in aqueous solutions of $Co(ClO_4)_2$ have been reported by Chmelnick and Fiat,[18] who studied the

(16) The primary hydration number of Mg(II) in aqueous solutions of $Mg(ClO_4)_2$ is 6.[17]

(17) N. A. Matwiyoff and H. Taube, J. Amer. Chem. Soc., in press.

(18) A. M. Chmelnick and D. Fiat, J. Chem. Phys., 47, 3986 (1967); in this paper, reference is made to unpublished work by D. Fiat, Z. Luz, and B. L. Silver, who observed the ^{17}O resonance for solvent molecules within the first coordination sphere of Co(II) in methanol-water mixtures.

water ^{17}O resonance over a wide temperature range in the rapid chemical exchange limit. Although the coordination number of Co(II) was not determined in that study, the water ^{17}O chemical shifts and line widths were found to be consistent with a constant coordination number for Co(II) over the temperature range from -10 to $+183°$.

Although the temperature dependence of the proton line widths in Table I is characteristic of that for a system undergoing chemical exchange, we have not attempted a detailed analysis because of our uncertainty about the magnitude and temperature dependence of the interionic electron–nuclear dipolar interactions. Such interactions must be large in these concentrated solutions.[19]

We can, however, estimate the electron-spin relaxation time of $Co(OH_2)_6{}^{2+}$, τ_s, from the line-width data at low temperatures ($\leq -55.8°$) where the chemical exchange of water is very slow. The Solomon[20] and Bloembergen[6] equations for the longitudinal and transverse relaxation rates, $1/T_{2M}$ and $1/T_{1M}$, of nuclei bonded to paramagnetic ions reduce to the following, under the conditions obtained in this study

$$\pi \Delta \nu_m = \frac{1}{T_{2M}} = \frac{1}{T_{1M}} =$$
$$\frac{4}{3}\frac{S(S + 1)\gamma_I{}^2 g^2 \beta^2}{r^6}\tau_s + \frac{2}{3}S(S + 1)\left(\frac{A}{\hbar}\right)^2 \tau_s \quad (3)$$

where r is the Co–H distance. The first term in eq 3 gives the contribution of the electron–nuclear dipolar relaxation to the line width and the second term that for isotropic spin exchange, which, in this case, accounts for less than 1% of the line width. Using a value of 2.1 Å for the Co–H distance and the pmr line width of $Co(OH_2)_6{}^{2+}$ at $-63.7°$, we obtain $\tau_s = 1.6 \times 10^{-13}$ sec. The value is substantially less than that calculated by Bloembergen and Morgan,[6] 5×10^{-13} sec, who used proton T_1 data obtained at 25°, and it is also smaller than that estimated from ^{17}O T_2 data, 1.7×10^{-12} sec at $-10°$.[18] The low value obtained in this study may be due to electron-spin exchange contributions to τ_s in the concentrated solutions employed.[21]

Experimental Section

Cobalt(II) perchlorate hexahydrate was prepared by treating $CoCl_2$ (Fisher) with a large excess of 70% $HClO_4$ (Baker) at 80° until a Cl^- ion test of the resulting solution with aqueous $AgNO_3$ was negative. The solid recovered after the $HClO_4$ solution had been concentrated by distillation was recrystallized from distilled water several times and was spectrophotometrically analyzed for Co(II) as the $CoCl_4{}^{2-}$ ion in 13 m HCl. The nmr spectra were obtained with the Varian A-60A and HA-100 spectrometers, the latter being operated in the HR mode. The measurements

were made and the systems were calibrated in the manner described previously.[12]

(19) The "free"-water line widths in concentrated diamagnetic solutions of $Mg(ClO_4)_2$ in water at $-70°$ are approximately 50 Hz, nearly a factor of 10 less than those for the corresponding $Co(ClO_4)_2$ solutions.[17]

(20) I. Solomon, Phys. Rev., 99, 559 (1955).

(21) The calculated τ_s is a sensitive function of r. In the determination of r, we assumed a dipolar coordination of H_2O to Co(II) in which all four atoms are coplanar. Angular coordination, in which Co(II) is bonded to a lone pair of oxygen electrons, results in smaller r (1.93 Å) and τ_s (9.5×10^{-14}) values.

Proton Magnetic Resonance Spectra of

DL- and LL-Phenylalanylvalines

by Vito J. Morlino and R. Bruce Martin

Chemistry Department, University of Virginia, Charlottesville, Virginia 22901 (Received November 27, 1967)

In a recent publication we reported on the chemical-shift nonequivalence of the methylene hydrogens observed in the pmr spectra of a series of dipeptide L-aminoacylglycines and some tripeptides.[1] A striking feature of this study was the downfield shift of one of the nonequivalent methylene hydrogen resonances of the glycyl residue in L-phenylalanylglycine upon ionization of an ammonium hydrogen. The observation of this downfield shift for only one of the nonequivalent methylene hydrogens suggested that a study of the diastereomeric LL- and DL-phenylalanylvalines would be informative. Results for the LL dipeptide are reported in the previous paper,[1] but because of its limited solubility in neutral solutions, no results were reported for the dipolar ion form of D-phenylalanyl-L-valine. We have recently obtained a 100-Mc nmr spectrometer, and the results obtained with the aid of a computer of average transients for the dipolar ion form of D-phenylalanyl-L-valine are recorded in Table I, along with the values obtained for the cationic and anionic forms. Though obtained with the use of external tetramethylsilane (TMS) as a lock signal, the values reported in Table I are converted to parts per million downfield from sodium (trimethylsilyl)-1-propanesulfonate (DSS) as an internal standard in order to be directly comparable with the values reported for the LL dipeptide. Values for the methyl resonances recorded in Table I are averages for the doublet produced by coupling of about 7 cps with α-CH.

Table I shows for the DL dipeptide a downfield shift for resonance of the α-CH of the valyl residue upon ionization of an ammonium hydrogen. Thus the unusual downfield shift of the high-field glycyl hy-

(1) V. J. Morlino and R. B. Martin, J. Amer. Chem. Soc., 89, 3107 (1967).

drogen resonance upon ammonium ionization in L-phenylalanylglycine is mimicked by a downfield shift of the valyl α-CH resonance in D-phenylalanyl-L-valine, in contrast to the normal upfield shift in the LL diastereomer. These results strongly support the earlier suggestion,[1] advanced on the basis of the higher

Table I: Valyl Resonances of Phenylalanylvalines[a]

Charge	α-CH		Methyls	
	DL	LL	DL	LL
+0	4.18	4.23	0.73	0.93
+-	3.95	4.05	0.76	0.92, 0.90
0-	3.97	4.03	0.65	0.85

[a] In parts per million downfield from DSS as an internal standard in D_2O.

field valyl α-CH resonance in the DL compared to the LL dipeptide, that the high-field resonance of the nonequivalent glycyl hydrogens in L-phenylalanylglycine is the one that would remain if the glycyl residue were stereoselectively deuterated so that the deuterium atom appears in the position of the side chain in a DL or LD dipeptide.

In both the DL and LL dipeptides, the valyl methyl resonances are relatively less affected by carboxylic acid ionizations on their own residues than by ammonium ionizations on the phenylalanyl residue. A consequence of this unusual behavior upon ionization is that the methyl resonances appear at unusually low field in the dipolar ion form of both dipeptides, but more so in the DL case. Indeed, there is even a low-field shift of the valyl methyl resonances, as shown in Table I, upon the carboxylic acid ionization in D-phenylalanyl-L-valine. Curiously, the valyl methyl groups exhibit chemical shift nonequivalence in the dipolar ion form of the LL dipeptide but, as shown in Table I, do not do so in the DL dipeptide.

The unusually low-field position of the methyl groups and the unusually high-field position of the α-CH resonance in the dipolar ion, as compared with the other charge forms of D-phenylalanyl-L-valine, suggest that in the dipolar ion form of the dipeptide an average conformation is adopted that places the methyl groups less and the valyl α-CH more subject to the shielding cone of the phenylalanyl residue than in the other two charged forms of the dipeptide. Examination of Courtauld's space-filling atomic models in conformations consistent with calculated nonbonding interactions[2] reveals that the chemical shift changes may be accounted for by adopting an average conformation that brings the positively and negatively charged groups slightly nearer to each other in the dipolar ion

compared to the singly charged forms of the DL dipeptide.

Thus the picture that appears to emerge is one where dipeptide conformations are determined primarily by nonbonded interactions and secondarily by some weighting of those conformations that bring opposite charges somewhat nearer in dipolar ion forms. It is our view that chemical shift nonequivalence in dipolar ion forms is not primarily the result of the above small weighting of rotamer distributions but is due predominantly to the field gradient produced by a zwitterion structure. Evidence in support of this view is the observation of methyl group nonequivalence in the dipolar ion form of L-phenylalanyl-L-valine, where the vector joining positive and negative charge centers passes near the methyl groups in the average conformation, and the absence of observable nonequivalence in the DL diastereomer where the vector is shorter and not so near the methyl groups.

In Table II the chemical shifts of glycyl methylene hydrogens are reported for several di- and tripeptides which exhibited little or no splitting on a 60-Mc instrument. The results reported in Table II were obtained on a 100-Mc instrument and demonstrate the magnetic

Table II: Chemical Shifts of Glycyl Methylene Protons in Di- and Tripeptides[a]

Peptide	Charge	ν_A	$(\nu_A + \nu_B)/2$	ν_B
Ala-Gly	+0		4.07	
	+-	3.84		3.74
	0-		3.76	
Ser-Gly	+-	3.86		3.77
Pro-Gly	+-	3.83		3.74
Ala-Gly-Gly	+0		4.05	
	+-	4.06		3.99
	0-		3.96	
Val-Gly-Gly	+-	4.08		3.99

[a] In parts per million downfield from DSS as an internal standard in D_2O. For tripeptides, values recorded refer only to the central glycyl residue.

nonequivalence of glycyl methylene hydrogens in the dipolar ion forms. Only the central glycyl residue of the tripeptides exhibits nonequivalent hydrogens. Especially noteworthy is the resolution achieved in the case of the alanyl peptides. With the smallest possible side chain that could lead to nonequivalence its observation in the alanyl peptides suggests that magnetic nonequivalence in glycyl residues is a general result whose observation is dependent upon an asymmetric center.

(2) S. J. Leach, G. Némethy, and H. A. Scheraga, *Biopolymers*, **4**, 369 (1966).

Viscosity of Mixtures of Electrolyte Solutions[1]

by Y. C. Wu[2]

*Chemistry Division, Oak Ridge National Laboratory,
Oak Ridge, Tennessee 37830*   (*Received February 8, 1968*)

The relative viscosity of binary electrolyte solutions is generally discussed in terms of the equation of Jones and Dole[3]

$$\eta/\eta_0 = 1 + a\sqrt{I} + bI \qquad (1)$$

where η is the viscosity of the solution, η_0 is that of the solvent, and I is the ionic strength in molar concentration units. (This equation is most often written in terms of the molar concentration c rather than ionic strength. The form used here is more convenient in discussing mixtures and in comparison with other limiting laws. For 1:1 electrolytes the two concentrations scales are the same.) The coefficient a has been identified as the slope of the limiting law of Falkenhagen.[4] The coefficient b has been shown to have the property of additivity[5] and has been discussed by several authorities on electrolyte solutions.[6]

Onsager and Fuoss[7] developed equations for the ionic contribution to the viscosity of multicomponent systems, η^*, which lead to a limiting law of the form

$$\eta^* \equiv \eta - \eta_0 = a'\sqrt{I} \qquad (2)$$

The limiting slopes in eq 1 and 2 are related by $a' = a\eta_0$.

It has been suggested that the additivity rule for the b coefficient of eq 1 can be extended to multicomponent mixtures.[6a] There appear to be no explicit tests of this rule.

In this communication, the viscosities of the systems LiCl–NaCl–H_2O, LiCl–KCl–H_2O, and NaCl–$MgCl_2$–H_2O at 25° and in the concentration range 0.01 to 1 ionic strength are reported. These results are compared by means of eq 1 with the a coefficients of the Onsager–Fuoss theory and the b coefficients obtained from the additivity rule.

Experimental Section

Stock solutions of LiCl, NaCl, KCl, and $MgCl_2$ were prepared from reagent grade chemicals which had been recrystallized and dried. The concentrations were verified by titration with $AgNO_3$. Dilutions and mixtures were made from these stock solutions.

Viscosities were measured with Cannon–Ubbelohde semimicroviscometers with efflux times of about 400 sec. The kinetic energy correction for this type of viscometer[8] is very small and was neglected for the systems studied here. The relative viscosity was determined from the densities and efflux times; the viscosity of water at 25° was taken as 0.8903 cP.[6b] The densities were measured with 5-ml pycnometers.

The efflux time was measured to 0.1 sec with an electric timer. The over-all reproducibility and accuracy is ±0.1%.

Results and Discussion

Viscosity measurements were made on solutions of LiCl, NaCl, and KCl and equimolar mixtures of LiCl–NaCl and LiCl–KCl. In addition, measurements were made on an NaCl–$MgCl_2$ mixture (88.06 mol % NaCl) having the Na:Mg ratio of sea water.[9] The results are shown in Table I.

Table I: Viscosities (cP) at 25°

I	KCl	LiCl–KCl 1:1	LiCl	LiCl–NaCl 1:1	NaCl
0.01		0.8912	0.8921	0.8918	0.8915
0.05		0.8944	0.8978	0.8964	0.8951
0.0625	0.8898	0.8951	0.8986		
0.10		0.8976	0.9045	0.9017	0.8991
0.125	0.8900	0.8988	0.9066		
0.25	0.8903	0.9078	0.9246		
0.50	0.8883	0.9214	0.9565	0.9400	0.9294
1.00	0.8875	0.9540	1.0250	0.9997	0.9664

I	NaCl–$MgCl_2$ 88.06 mol % NaCl
0.07034	0.8978
0.1407	0.9041
0.3517	0.9240
0.7034	0.9540
1.0551	0.9934
1.4068	1.0284

The Onsager–Fuoss theory[7] provides a means of calculating the coefficient a' of eq 2 and thus the limiting slope, a, of eq 1. The electrostatic contribution to the viscosity may be written as (ref 7, eq 3.7.2)

(1) Research sponsored by The Office of Saline Water, U. S. Department of the Interior, under Union Carbide Corporation's contract with the U. S. Atomic Energy Commission.

(2) U. S. Department of Commerce, National Bureau of Standards, Washington, D. C. 20234.

(3) G. Jones and M. Dole, *J. Am. Chem. Soc.*, **51**, 2950 (1929).

(4) H. Falkenhagen and M. Dole, *Physik. Z.*, **30**, 611 (1929); H. Falkenhagen, *ibid.*, **32**, 745 (1931); H. Falkenhagen and E. L. Vernon, *Phil. Mag.*, **14**, 537 (1932).

(5) W. M. Cox and J. H. Wolfenden, *Proc. Roy. Soc.* (London), **A145**, 475 (1934); E. Asmus, *Z. Naturforsch.*, **4a**, 589 (1949); R. W. Gurney, "Ionic Processes in Solution," McGraw-Hill Book Co., Inc., New York, N. Y., 1953; M. Kaminsky, *Discussions Faraday Soc.*, **24**, 171 (1957).

(6) (a) H. S. Harned and B. B. Owen, "The Physical Chemistry of Electrolytic Solutions," 3rd ed, Reinhold Publishing Corp., New York, N. Y., 1958; (b) R. A. Robinson and R. H. Stokes, "Electrolyte Solutions," 2nd ed revised, Butterworth and Co. Ltd., London, 1965; (c) R. H. Stokes and R. Mills, "Viscosity of Electrolytes and Related Properties," Pergamon Press Inc., New York, N. Y., 1965.

(7) L. Onsager and R. M. Fuoss, *J. Phys. Chem.*, **36**, 2689 (1932).

(8) M. R. Cannon, R. E. Manning, and J. D. Bell, *Anal. Chem.*, **32**, 355 (1960).

(9) K. S. Spiegler, "Salt-Water Purification," John Wiley and Sons, Inc., New York, N. Y., 1962.

$$\eta^* = A'(P - Q_n)\sqrt{I} = a'\sqrt{I} \qquad (3)$$

where

$$A' = 0.362\sqrt{2}(1/DT)^{1/2}$$

$$P = \sum_i^s x_i z_i / \lambda_i$$

$$Q_n = 4[R] \sum_{n=0}^{\infty} b_n S^{(n)}$$

and x_i is the ional fraction $c_i z_i^2 / \Sigma c_i z_i^2$, z_i the absolute value of the valence, and λ_i the ionic equivalent conductance for ion i; D is the dielectric constant for the solvent, T is the absolute temperature, b_n are the binomial coefficients, $[R]$ and $S^{(n)}$ are matrices whose elements are functions of ionic fractions and ionic mobilities, n is the number of recursions, and $A' = 0.00335$ for aqueous solutions at 25° with the viscosity in poise units. Values for P, Q_n, and a' calculated by eq 3 are given in Table II along with the resulting value of a for eq 1.

Figure 1. Viscosities of pure salt solutions.

Table II: Parameters of Eq 3

	P	Q_1	$a' \times 10^5$	a
KCl	0.01336	0.00000	4.47	0.00502
LiCl–KCl (1:1)	0.01641	0.00098	5.17	0.00580
LiCl	0.01947	0.00143	6.03	0.00678
LiCl–NaCl (1:1)	0.01800	0.00100	5.68	0.00638
NaCl	0.01653	0.00049	5.37	0.00603
NaCl–MgCl₂ᵃ	0.01665	0.00044	5.43	0.00610
MgCl₂	0.01693	0.00032	5.56	0.00624

ᵃ 88.06 mol % NaCl.

It can be seen from Table II that the P term is the main contribution to η^* and that it is dependent on the mixing ratio. The Q_n term is a small correction, but causes the limiting slope for mixtures to diverge from a linear combination of that of their components.

It has been shown[6] that the b coefficient of eq 1 for binary electrolyte solutions is an additive property of the constituent ions. It seemed reasonable that values of b for mixtures of electrolytes could be obtained from the values for the individual components; thus for a mixture of two electrolytes

$$b = y_A b_A + y_B b_B \qquad (4)$$

where y_J is the ionic strength fraction and b_J the linear coefficient of eq 1 for component J. Values of b for the pure salts and the mixtures are given in Table III. In this table, values for the pure salts were obtained from the ionic values[6b] and values for the mixtures were obtained from those for the pure salts combined according to eq 4. Since most of the b coefficients in the literature are on the molar scale, it is necessary to divide these coefficients by a valence factor (1 for 1:1

Figure 2. Viscosities of electrolyte mixtures.

Table III: Values of the b Coefficientᵃ

KCl	−0.014
LiCl–KCl (1:1)	0.0645
LiCl	0.143
LiCl–NaCl (1:1)	0.111
NaCl	0.079
NaCl–MgCl₂ᵇ	0.092
MgCl₂	0.371

ᵃ Ionic b coefficients (molar scale) used: Li⁺, 0.150; Na⁺, 0.086; K⁺, −0.007; Mg²⁺, 0.385; Cl⁻, −0.007. ᵇ 88.06 mol % NaCl; b coefficient converted to ionic strength scale.

electrolytes and 3 for 2:1 electrolytes) to convert them to ionic strength units for use in eq 4.

The experimental results are shown in Figures 1 and 2

as plots of $[(\eta/\eta_0) - 1]/\sqrt{I}$ vs. $\sqrt{I}$. The solid lines represent eq 1 with values of a from the Onsager–Fuoss theory (Table II) and values of b from the additivity rule (Table III). The agreement between the calculated curves and the experimental points is satisfactory, at least up to $I = 1$.

Acknowledgment. The author expresses his indebtedness to Dr. K. A. Kraus for his support, encouragement, and constructive criticism; his appreciation to Drs. J. S. Johnson, R. J. Raridon, and R. M. Rush for helpful discussion; and to Mr. J. Csurny for technical assistance. He also wishes to thank Professor H. L. Friedman of the State University of New York at Stony Brook for his stimulating discussion and valuable suggestions.

Ion Exchange with a Two-Phase Glass

by R. H. Doremus

General Electric Research and Development Center, Schenectady, New York (Received November 27, 1967)

Many borosilicate glasses separate into two interconnected, amorphous phases.[1,2] When the borate-rich phase is etched out, a porous glass of nearly pure silica (SiO_2) results, which when heated collapses to a compact glass (Vycor) resembling fused silica. There is some evidence that commercial Pyrex glass, which is a sodium borosilicate glass containing more silica than the glasses from which Vycor is made, also separates into two continuous amorphous phases.[2] However, no separation is observed in the electron microscope, nor can any phase be etched out from this glass, perhaps because the phase separation is on too fine a scale. In this work the exchange behavior of silver ions with Pyrex glass gives additional evidence that this glass contains two phases.

Pieces of Pyrex glass (80% SiO_2, 13% B_2O_3, 4.2% Na_2O, and 2% Al_2O_3, approximate composition in weight %) tubing were placed in mixed sodium nitrate–silver nitrate melts at 335° for several hours. Then layers of glass were etched off with 8% HF and were analyzed. Extrapolation of the profile of silver concentration to the glass surface gave the equilibrium concentration of silver that had exchanged with sodium ions in the glass. The exchange of silver ion in the melt with sodium ions in the glass can be represented by the equation

$$Ag^+(m) + Na^+(g) = Ag^+(g) + Na^+(m)$$
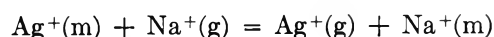
The exchange coefficient

$$K = \frac{a_{Na}C_{Ag}}{a_{Ag}C_{Na}} \quad (1)$$

was calculated from the results. In eq 1, a is the thermodynamic activity of the nitrate in the melt, referred to a pure solution as the standard state as taken from the measurements of Laity,[3] and C is the concentration of an ion in the glass. The measured K values for Pyrex glass are given in Table I.

Table I: Exchange of Silver Ions in a Sodium Nitrate Melt with Pyrex Glass

Mole fraction of silver nitrate in melt	Exchange coefficient, K
0.398	1.97
0.310	1.87
0.153	1.98
0.0475	2.05
0.0022	7.06
3×10^{-6}	12.2

If the solution of ions in the glass is ideal, K should be constant with concentration. This constancy has been found for silver exchange with sodium ions in soda lime glass (15% Na_2O) and in fused silica (3 atomic ppm of sodium ion),[4] both of which contain one homogeneous phase. Therefore, if the Pyrex glass were a single phase containing uniform sodium borosilicate groups, one would expect a constant K for this exchange, since the density of exchanging groups is even less than in the soda lime glass. Thus the change in K at lower silver concentrations, shown in Table I, is evidence that the glass separates into two different phases.

A two-phase glass can be treated as a mixture of two ideal phases, each with its appropriate exchange coefficient K_1 or K_2, invariant with ionic concentration, as defined in eq 1. In terms of the ionic concentrations in the two phases, numbered 1 and 2, the experimentally measured distribution coefficient K is

$$K = \frac{a_{Na}(C_{1Ag} + C_{2Ag})}{a_{Ag}(C_{1Na} + C_{2Na})} \quad (2)$$

In terms of the coefficients K_1 and K_2 this measured K is

$$K = \frac{rN_1(K_1 - K_2) + K_2(r + K_1)}{r + K_1 + N_1(K_2 - K_1)} \quad (3)$$

in which N_1 is the mole fraction of exchangeable ions in phase 1 (a constant for any given glass composition) and r is a_{Na}/a_{Ag}, the ratio of activities in the melt. Consistent values of the parameters in eq 3 for the data in Table I are $K_1 = 2.3 \times 10^2$, $K_2 = 1.6$, and $N_1 = 0.047$.

This treatment of ion exchange with two phases is formally equivalent to that with a single phase contain-

(1) M. E. Nordberg, *J. Am. Ceramic Soc.*, **27**, 299 (1944).

(2) R. J. Charles, *ibid.*, **47**, 559 (1964).

(3) R. W. Laity, *J. Am. Chem. Soc.*, **79**, 1849 (1957).

(4) R. H. Doremus, unpublished results.

ing two different types of sites (polyfunctional exchanger). Cornaz and Deuel[5] measured ion exchange with a bifunctional resin in water, and Barrer and Meier[6] presented results for bifunctional exchange in a zeolite, as well as equations similar to those given above.

The borosilicate glasses used to make Vycor glass separate into a high silica phase and one containing soda, borate, and some silica.[1,2] It seems likely that Pyrex glass also separates into silica and sodium borosilicate phases.[2] The partitioning of sodium between the two phases in Pyrex, as calculated from the exchange results, suggests that phase 2 is the sodium borosilicate phase, since it contains 95% of the sodium, and that phase 1 is the silica phase.

The coefficients K_1 and K_2 are consistent with this assignment and give further information about the compositions of the phases. Silver is bound strongly to the SiO^- or silicate group in a purely silicate lattice; for example, $K = 120$ (glass prefers silver) for silver–sodium exchange in a soda–lime glass.[4] Thus the high K value found for the silica phase in this study implies that the anionic groups in this phase are SiO^- groups, and that the boron concentration in it is low. Recent studies of surface adsorption on porous glass (a Vycor borosilicate from which the borate phase has been leached out) show that the boron remaining in the glass after leaching is concentrated at the internal surfaces of the glass.[7,8] Therefore there is little boron in the bulk of the silica phase, in agreement with the present deduction. The preference of the silica group for silver results from the high "field strength" (low effective anionic radius) of the group and the high polarizability of the silver ion. Groups with lower field strength, such as aluminosilicate and borosilicate, have lower affinity for silver ions compared to sodium. The value of $K_2 = 1.6$ for silver exchange with the sodium borosilicate phase is close to this coefficient for silver–sodium exchange on the aluminosilicate groups in fused silica,[4] in agreement with this prediction. The relations between the structure of anionic groups and their cation affinity are expounded in detail by Eisenman,[9] based on both experiment and theory.

The two-phase exchanger can be considered as a single nonideal phase, and the deviations caused by the presence of two phases absorbed in formal activities a'_{Ag} and a'_{Na} for the ions in the glass. A constant exchange coefficient K' is then defined as

$$K' = \frac{a'_{Ag}a_{Na}}{a'_{Na}a_{Ag}} = \frac{a'_{Ag}r}{a'_{Na}} \tag{4}$$

where the unprimed activities refer to the melt as before. From eq 3 and 4 and an integration of the relation between activities in the glass

$$C_{Ag}\frac{\partial(\ln a'_{Ag})}{\partial C_{Ag}} + C_{Na}\frac{\partial(\ln a'_{Na})}{\partial C_{Na}} = 0$$

the formal activities are found to be

$$\ln a'_{Ag} = \frac{1}{2}\ln\left[\frac{K_1K_2}{r^2 + (K_1 + K_2)r + K_1K_2}\right] + \left(\frac{N_2 - N_1}{2}\right)\ln\left(\frac{r + K_1}{r + K_2}\right)\frac{K_2}{K_1}$$

and

$$\ln a'_{Na} = \frac{1}{2}\ln\left[\frac{r^2}{r^2 + (K_1 + K_2)r + K_1K_2}\right] + \left(\frac{N_2 - N_1}{2}\right)\ln\left(\frac{r + K_1}{r + K_2}\right)$$

Therefore from eq 4

$$K' = \sqrt{K_1K_2}\left(\frac{K_2}{K_1}\right)^{(N_2 - N_1)/2}$$

and $K' = 1.8$ for the parameters given above. This K' can be used in equations for the membrane potential of a two-phase or bifunctional membrane.

(5) J. P. Cornaz and H. Deuel, *Helv. Chim. Acta*, **39**, 1220, 1227 (1956).

(6) R. M. Barrer and W. M. Meier, *Trans. Faraday Soc.*, **55**, 1301 (1959).

(7) M. L. Hair and I. D. Chapman, *J. Am. Ceramic Soc.*, **49**, 651 (1966).

(8) M. J. D. Low and N. Ramasubramanian, *J. Phys. Chem.*, **71**, 3077 (1967).

(9) G. Eisenman, *Biophys. J.*, **2**, 259 (1962); chapter in "Advances in Analytical Chemistry and Instrumentation," Vol. 4, C. N. Reilly, Ed., John Wiley and Sons, Inc., New York, N. Y., 1965, p 305.

The Nuclear Magnetic Resonance Spectrum of Chloromethylphosphine

by H. Goldwhite and D. G. Rowsell

Department of Chemistry, California State College at Los Angeles, Los Angeles, California 90032 (*Received February 14, 1968*)

Very few determinations of the signs of the coupling constants J_{HCP} in trivalent phosphorus compounds have been made.[1] Methods of sign determination involve either double resonance or the analysis of complex spectra. An initial investigation of the nmr spectrum of chloromethylphosphine showed that it was complex,[2] suggesting that a complete analysis would give the sign of J_{HCP} relative to J_{HP}.

Experimental Section

The nmr spectra were obtained using a Varian A60 spectrometer fitted with a variable temperature probe.

(1) G. Mavel, "Progress in Nuclear Magnetic Resonance Spectroscopy," Vol. 1, Pergamon Press, New York, N. Y., 1966, p 251.

(2) B. Fontal, H. Goldwhite, and D. G. Rowsell, *J. Org. Chem.*, **31**, 2424 (1966).
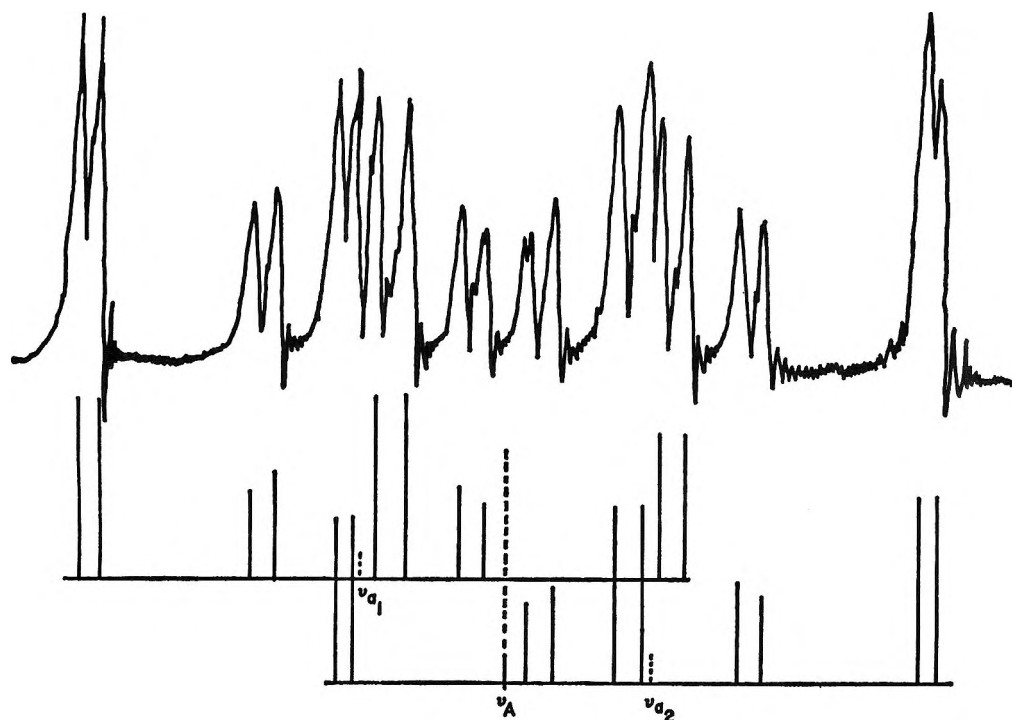
Figure 1. ^1H nmr spectrum of chloromethylphosphine: top, observed; bottom, calculated.

Chemical shifts are relative to internal tetramethyl-silane. Chloromethylphosphine was prepared by the thermal decomposition of chloromethylphosphinic acid.[2]

Results and Discussion

The ^1H nmr spectrum of chloromethylphosphine was observed to be complex, and a closer examination revealed that it was of the $AA'BB'X$ type. It has been pointed out[3] that use can often be made of the fact that the $AA'BB'$ part of an $AA'BB'X$ spectrum consists of two overlapping $aa'bb'$ subspectra with effective Larmor frequencies

$$\nu_a = \nu_A \pm \frac{1}{2}J_{AX}; \quad \nu_b = \nu_B \pm \frac{1}{2}J_{BX}$$

In the particular case of chloromethylphosphine, as $|J_{AX} - J_{BX}|$ is large, $|\nu_{a_1} - \nu_{b_1}|$ and $|\nu_{a_2} - \nu_{n_2}|$, the apparent relative shifts of the subspectra, are much larger than $|\nu_A - \nu_B|$. It is thus possible to treat each $aa'bb'$ subspectrum by a suitable approximate method. In the following calculations the results of a perturbation technique have been used.[4] The effective Larmor frequencies of the two $aa'bb'$ subspectra are given in Table I. Complete spectral parameters are summarized in Table II, and the experimental spectrum is compared with that calculated using restricted second-order corrections[5] in Figure 1.

The spectral analysis shows that J_{HOP} and J_{HP} have the same sign. J_{HP} in phosphines is generally considered to be positive,[6] so that J_{HCP} in chloromethylphosphine is also positive. Previous work[7,8] has shown that J_{HCP} is positive in methylphosphine, though the only determination upon a compound containing a

Table I: Effective Larmor Frequencies of Subspectra (Hz)

ν_A (ν_{CH_2Cl})	217.5
ν_B (ν_{H_2P})	200.7
ν_{a_1}	221.3
ν_{b_1}	300.4
ν_{a_2}	213.7
ν_{b_2}	101.0

Table II: Spectral Parameters for Chloromethylphosphine (Hz)

$\Delta\nu_{AB}$	16.8
$\left.\begin{array}{l}J_{AA'}\\J_{BB'}\end{array}\right\}$	10.4, 9.8
$\left.\begin{array}{l}J_{AB} = J_{A'B'}\\J_{AB'} = J_{A'B}\end{array}\right\}$	±10.2; ±4.9
J_{AX}	±7.6
J_{BX}	±199.4

CH_2P group (triethylphosphine) gave a small negative coupling constant.[1]

(3) R. G. Jones and R. L. Williams, *Spectrochim. Acta*, **23A**, 15 (1967).

(4) B. Gestblom and S. Rodmar, *Acta Chem. Scand.*, **18**, 1767 (1964).

(5) B. Gestblom, R. A. Hoffman, and S. Rodmar, *Mol. Phys.*, **8**, 425 (1964).

(6) A. H. Cowley, W. D. White, and S. Manatt, *J. Amer. Chem. Soc.*, **89**, 6433 (1967).

(7) G. M. Whitesides, J. L. Beauchamp, and J. D. Roberts, *ibid.*, **85**, 2665 (1963).

(8) S. L. Manatt, G. L. Juvinall, and D. D. Elleman, *ibid.*, **85**, 2664 (1963).

As the nmr spectrum of chloromethylphosphine is of the AA'BB'X type, it is clear that exchange or any process involving inversion of configuration at phosphorus must be slow on the nmr time scale.

If there is rapid rotation about the phosphorus–carbon bond, then there must be two averaged coupling constants between the methylene protons and the protons directly attached to phosphorus (cf. substituted ethanes).[9]

Variable temperature studies showed that inversion of configuration at phosphorus was slow even at 150°. However, traces of hydrogen chloride produced broadening of the spectral lines which would be consistent with an exchange process of the type

$$ClCH_2PH_2 + HCl \rightleftharpoons ClCH_2\overset{+}{P}H_3 + Cl^-$$
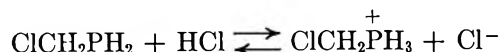
The low inversion rate for this primary phosphine, implying a high barrier to inversion, provides support for recent calculations which suggest an inversion barrier of about 30 kcal for PH_3 and a barrier of about 20 kcal for $(CH_3)_3P$.[10]

(9) J. A. Pople, W. G. Schneider, and H. J. Bernstein, "High Resolution Nuclear Magnetic Resonance," McGraw-Hill Book Co., Inc., New York, N. Y., 1959, p 379.

(10) G. W. Koeppl, D. S. Sagatys, G. S. Krishnamurthy, and S. I. Miller, J. Amer. Chem. Soc., 89, 3396 (1967).

Volumetric Behavior of Dilute Aqueous Solutions of Sodium Alkyl Sulfates[1]

by F. Franks, M. J. Quickenden, J. R. Ravenhill, and H. T. Smith

Biophysical Chemistry Laboratory, Unilever Research Laboratory, Colworth House, Sharnbrook, Bedford, England

In a previous study,[2] two of us showed that in submicellar solutions of sodium dodecyl sulfate there were indications of solute–solute interactions. These findings were based on density measurements with a precision of ±10 ppm. We now wish to present more extensive data on the volumetric properties of dilute solutions of sodium decyl (SDeS), sodium dodecyl (SDS), and sodium tetradecyl (STS) sulfates at 5 and 25°.

Experimental Section

Densities were measured by a high precision (better than 1 ppm) magnetic-float technique which has been described in detail.[3] The compressibility of SDS was determined using a 1-MHz ultrasound interferometer which allowed sound velocities to be measured with an accuracy of 1 part in 10^4.
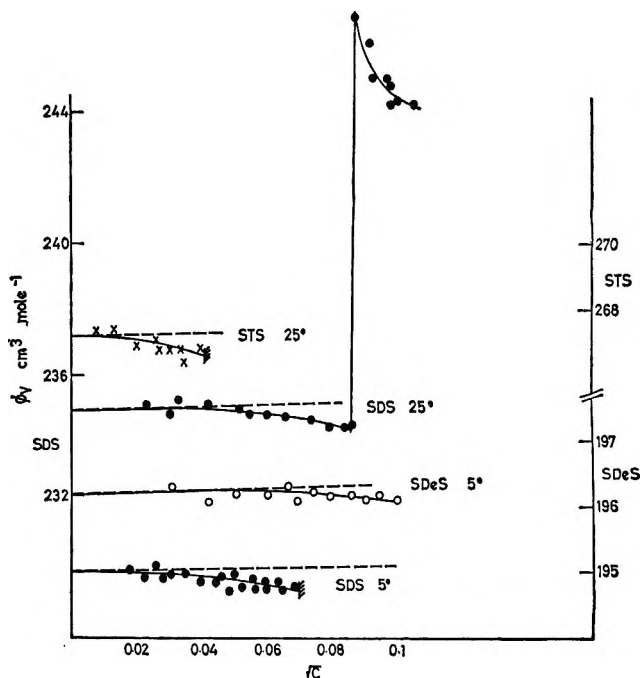
Figure 1. Apparent molal volumes, ϕ_V, of the C_{10}, C_{12}, and C_{14} sodium alkyl sulfates in aqueous solutions. The dotted line corresponds to the limiting-law slope.

Pure samples of the alkyl sulfates were kindly supplied by Dr. L. Shedlovsky. Deionized and degassed water was used throughout in preparation of the solutions.[3]

Results

Apparent molal volumes, ϕ_V, and apparent compressibilities, ϕ_K, were calculated from the relationships

$$\phi_V = \frac{1000}{m\rho\rho_0}(\rho_0 - \rho) + \frac{M}{\rho}$$

and

$$\phi_K = 10^3c^{-1}(\beta - \beta_0) + \beta_0\phi_V$$

where ρ and ρ_0 are the densities and β and β_0 are the adiabatic compressibilities of solution and solvent, respectively.

The ϕ_V data are summarized in Figure 1 and the concentration dependence of ϕ_K of SDS at 25° is shown in Figure 2. In only one case could the phenomenon of micellization be studied, because the other experimental runs were carried out below the Krafft points of the compounds employed.

Discussion

For a given experimental precision (in this case better than 1 ppm), the uncertainties in ϕ_V increase rapidly

(1) Presented at the 154th National Meeting of the American Chemical Society, Chicago, Ill., Sept 1967.

(2) F. Franks and H. T. Smith, J. Phys. Chem., 68, 3581 (1964).

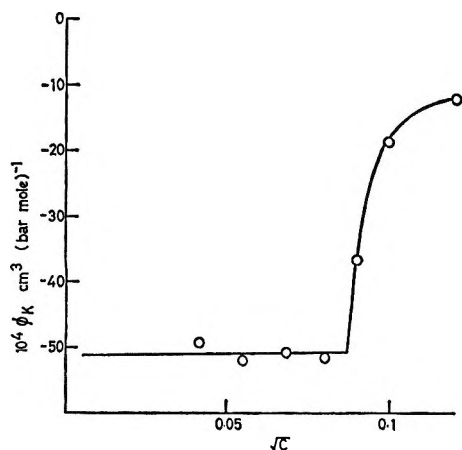(3) F. Franks and H. T. Smith, Trans. Faraday Soc., 63, 2586 (1967).

Figure 2. Apparent molar compressibility of SDS at 25°.

with decreasing concentration, so that extrapolations to infinite dilution ($\phi_v{}^0$) are difficult to carry out.[2] However, the Debye–Hückel limiting law predicts the limiting slope of the ϕ_v vs. $c^{1/2}$ plots, since

$$\phi_v = \phi_v{}^0 + kc^{1/2}$$

where k comprises some physical properties of the solvent which are known in the case of water.[4]

Examination of Figure 1 reveals two interesting features: below the critical micelle concentration (cmc), ϕ_v values exhibit negative deviations from the limiting-law behavior. Above micellization, which is accompanied by a large positive volume change, ϕ_v again falls off with increasing concentration. The former phenomenon, which is also observed in solutions of tetraalkylammonium halides[3] and other alkyl derivatives,[5] has been discussed in terms of ion pairing,[6,7] hydrophobic bonding,[2] micelle formation,[8] and cooperative interactions of hydrated ions of like charge.[9] We have discussed these alternatives in some length,[3] and although ion pairing cannot be ruled out, this is normally accompanied by positive ϕ_v deviations, whereas the behavior reported here for the alkyl sulfates is not one which is usually associated with electrolytes. Instead it is observed for most organic derivatives with large nonpolar residues and is believed to arise from cooperative hydrophobic hydration effects.[10]

The volume contribution of the CH_2 group toward the infinite dilution value of ϕ_v is 16 cm^3 mol^{-1}, which is consistent with published data.[3,11] The mean apparent expansibility, ϕ_E, of SDS at 15° is obtained as 0.25 cm^3 deg^{-1} mol^{-1}, which is about equal to that of $(n\text{-Bu})_4NBr$.[3]

The volume change accompanying micelle formation, +12 cm^3 mol^{-1}, is in good agreement with that found by Hamann,[12] from a study of the pressure dependence of the cmc. We cannot at the present time explain the decrease of ϕ_v above the cmc. This may be associated with hydration changes which arise from changes in the degree of counterion binding or from changes in the

distribution of micellar sizes. The volume behavior both below and above the cmc supports the concept of micellization as a process involving a complex series of equilibria[13] rather than a simple phase separation which would require ϕ_v below and above the cmc to be concentration independent,[11] apart from the $c^{1/2}$ dependence predicted by the Debye–Hückel limiting law.

Physical changes, probably in the nature of the micelles, just above the cmc are also indicated by the ϕ_K vs. $c^{1/2}$ plot for SDS, shown in Figure 2. Other published ultrasound-velocity data of aqueous sodium alkyl sulfates at 30° are not suitable for the evaluation of accurate ϕ_K data but do show, qualitatively, that ϕ_K is not constant immediately above the cmc.[14] If ϕ_K below the cmc is considered, the experimental error associated with the determination of the ultrasound velocity makes it impossible to determine, in the concentration range amenable to study, whether deviations from the predicted behavior of the ϕ_K vs. $c^{1/2}$ plot occur. However, the negative ϕ_K values are consistent with similar results for tetraalkylammonium halides,[15] which have been interpreted in terms of water structuring induced by alkyl residues.

(4) O. Redlich and D. M. Meyer, *Chem. Rev.*, **64**, 221 (1964).

(5) H. T. Smith, Ph.D. Thesis, University of Bradford, 1967.

(6) R. M. Diamond, *J. Phys. Chem.*, **67**, 2513 (1963).

(7) H. E. Wirth, *ibid.*, **71**, 2922 (1967).

(8) S. Lindenbaum and G. E. Boyd, *ibid.*, **68**, 3581 (1964).

(9) W. Y. Wen and S. Saito, *ibid.*, **68**, 2639 (1964).

(10) F. Franks and D. J. G. Ives, *Quart. Rev. Chem. Soc.*, **20**, 1 (1966).

(11) K. Shinoda and T. Soda, *J. Phys. Chem.*, **67**, 2072 (1963).

(12) S. D. Hamann, *ibid.*, **66**, 1359 (1962).

(13) P. Mukerjee, *Advan. Colloid Interface Sci.*, **1**, 241 (1967).

(14) K. Shigehara, *Bull. Chem. Soc. Jap.*, **38**, 1700 (1965).

(15) B. E. Conway and R. E. Verrall, *J. Phys. Chem.*, **70**, 3952 (1966).

An Electron Paramagnetic Resonance Study of Cupric Ion Tetrahedrally Coordinated by Nitrogen Atoms

by Denis Forster and Virgil W. Weiss

The Central Research Department, Monsanto Company, St. Louis, Missouri 63166 (*Received February 15, 1968*)

Numerous electron paramagnetic resonance studies of six-coordinated first row transition metal complexes have been reported.[1] However, epr data are scarce for

metals in a tetrahedral environment. The probable reason for this is that three of the species commonly found in tetrahedral coordination, Fe^{2+},[2] Co^{2+},[3] and Ni^{2+},[3] have very fast electron-spin relaxation times ($<10^{-11}$ sec), which allows observation of resonance only at very low temperatures (in practice, liquid helium temperature). However, the relaxation time of "tetrahedral" copper is relatively long and several studies have been reported. The epr spectrum of tetrahedral Cu has been examined both as pure $CuCl_4^{2-}$ and doped into a $ZnCl_4^{2-}$ lattice.[4,5] Also a study has been reported by Bates, et al.,[6] on copper (α,α'-dibromodipyrromethene)$_2$ where it has been proposed that the Cu is in a distorted tetrahedron of nitrogens. However, copper and/or ligand hyperfine structure was surprisingly absent from their observed spectrum. There has been an increased interest in tetrahedrally coordinated copper recently because of the postulate[7,8] that copper in cuproproteins is tetrahedrally coordinated by nitrogens. This biological interest as well as the absence of hyperfine structure in Cu(α,α'-dibromodipyrromethene)$_2$ led us to investigate Cu doped into a tetrahedral environment of nitrogens.

The system chosen for investigation was Cu doped into the $ZnHg(SCN)_4$ lattice. The zinc atoms in $ZnHg(SCN)_4$ are tetrahedrally coordinated by nitrogen atoms, since the compound is isomorphic[9] with $CoHg(SCN)_4$, which has been proven to contain cobalt in a slightly flattened tetrahedron by an X-ray diffraction study.[10] X-Ray diffraction studies[11-13] of $(CuZn)Hg(SCN)_4$ have shown that doping occurs without gross distortion of the lattice.

Experimental Section

Specimens of $ZnHg(SCN)_4$ doped with Cu^{2+} were prepared by adding aqueous solutions of $(NH_4)_2Hg(SCN)_4$ to mixed aqueous solutions of zinc nitrate and copper nitrate. The purple solids which precipitated were filtered and air dried.

The epr study was carried out at X-band ($\sim$9300 MHz) on a Varian V-4502-15 spectrometer employing a 12-in. magnet, a magnetic field modulation of 100 kHz, and a Mark II Fieldial. All spectra were obtained at 77°K on degassed powdered samples. DPPH was used as a g-value standard.[14]

Results and Discussion

The observed g values for $(Cu_zZn)Hg(SCN)_4$ as a function of the per cent of Cu are presented in Table I for four levels of doping and also for pure $CuHg(SCN)_4$. The g values for $CuHg(SCN)_4$ which contains Cu in a very distorted six-coordinate environment[15] are seen to be quite different from those of the $(Cu_zZn)Hg(SCN)_4$ system. However, as the Cu doping level is increased an absorption corresponding to about g 2.25 is observed (see Table I). It seems most likely that this impurity is $CuHg(SCN)_4$, since the $g_{||}$ values of the impurity and

that of pure $CuHg(SCN)_4$ agree. It is interesting that this is detected at such low levels of copper doping since its presence had not been detected in the X-ray studies up to about 40% Cu doping.[11]

Table I: The g Values of $(Cu_zZn_{1-z})Hg(SCN)_4$ and the Impurity as a Function of the Per Cent of Zn Sites Occupied by Cu

Value of z in (Cu_zZn_{1-z})-$Hg(SCN)_4$	$g_{||}$	$g_\perp$	g of impurity
0.0030	2.43 ± 0.02	2.07 ± 0.03	Not obsd
0.0057	2.40 ± 0.03	2.07 ± 0.03	2.24 ± 0.03
0.042	2.42 ± 0.02	2.07 ± 0.02	2.25 ± 0.02
0.080	2.44 ± 0.02	2.08 ± 0.02	2.25 ± 0.02
1.000	2.24 ± 0.02	2.07 ± 0.02	

Although the low-field g value of 2.43 is larger than that usually found for copper in distorted octahedral or planar environments, there are some recorded examples of six-coordinate copper exhibiting values as large as this,[1] and thus a ready distinction between tetrahedral and other coordination environments does not seem to be possible with certainty on the basis of a powder or solution epr spectrum.

The X-ray study of $CoHg(SCN)_4$ showed[11] that the Co–N–C–S grouping is essentially linear so that the point group of the $Co(NCS)_4$ (and, therefore, $Zn(NCS)_4$) entities can be represented fairly well by D_{2d}. Although X-ray studies indicate some distortion of the lattice may occur when Zn is replaced with Cu,[13] it appears that any rhombic distortion in the crystal field is small since $g_\perp$ was not resolved.

(1) B. R. McGarvey, "Transition Metal Chemistry," Vol. 3, R. L. Carlin, Ed., Marcel Dekker Inc., New York, N. Y., 1966, p 89.

(2) W. Low and M. Weger, Phys. Rev., 118, 1130 (1960).

(3) G. N. Lamar, J. Amer. Chem. Soc., 87, 3567 (1965).

(4) M. Sharnoff, J. Chem. Phys., 42, 3383 (1965).

(5) M. Sharnoff and C. W. Riemann, ibid., 43, 2993 (1965).

(6) C. A. Bates, W. S. Moore, K. J. Standley, and K. W. H. Stevens, Proc. Phys. Soc., 79, 73 (1962).

(7) A. S. Brill, R. B. Martin, and R. J. P. Williams in "Electronic Aspects of Biochemistry," B. Pullman, Ed., Academic Press Inc., New York, N. Y., 1964, p 519.

(8) E. Frieden, S. Osaki, and H. Kobayashi, J. Gen. Physiol., 49, 213 (1965).

(9) W. Stahl and M. Straumanis, Z. Physik. Chem. (Leipzig), 193, 121 (1944).

(10) J. W. Jeffery, Nature, 159, 610 (1947); Acta Crystallogr. Suppl., A66, 6 (1963).

(11) E. Ence and M. Straumanis, Z. Anorg. Allg. Chem., 228, 334 (1936).

(12) D. Forster and D. M. L. Goodgame, Inorg. Chem., 4, 823 (1965).

(13) D. E. Scaife, ibid., 6, 625 (1967).

(14) L. R. Dalton, J. D. Rynbrandt, E. M. Hansen, and J. L. Dye, J. Chem. Phys., 44, 3969 (1966).

(15) A. Korczynski, Rocz. Chem., 36, 1539 (1962).

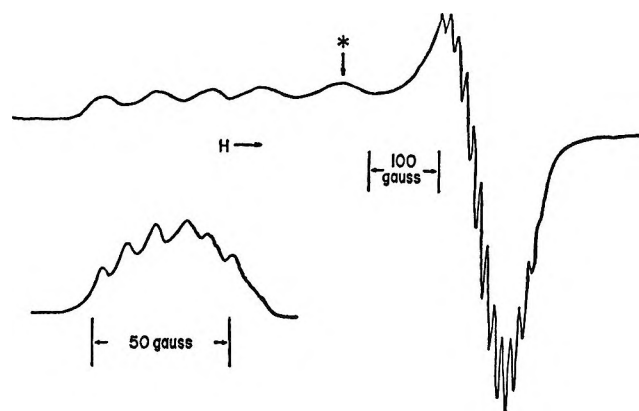Figure 1. The epr spectrum for $(Cu_xZn_{1-x})Hg(SCN)_4$ for $x = 0.57\%$ is shown. The transition denoted by an asterisk has been assigned to the impurity $CuHg(SCN)_4$. The insert is a magnification of the low-field component of the parallel copper hyperfine structure for $n = 0.30\%$. The nitrogen hyperfine structure can be readily discerned.

We were able to observe both ligands as well as copper hyperfine structure. The copper hyperfine interaction constants were found to be $|a_{||}{}^{Cu}| = 78 \pm 2$ G and $|A_{\perp}{}^{Cu}| = n(12 \pm 2)$ where $n = 1, 2,$ or 3. The nitrogen hyperfine interaction constants were found to be $|A_{||}{}^{N}| = 11 \pm 1$ G and $|A_{\perp}{}^{N}| = 12 \pm 1$ G. A typical spectrum which corresponds to 0.57% of the Zn sites occupied by Cu is shown in Figure 1. A magnification of the ligand hyperfine structure of the parallel component is also given. This was taken from the sample with 0.30% of the Zn sites occupied by Cu as shown in Figure 1.

The observed hyperfine parameters have several points of interest: (1) the copper hyperfine interaction constants are appreciably smaller than those usually observed for copper in distorted octahedral or square planar complexes; (2) the finding of both copper and ligand hyperfine structure contrasts markedly with the study of copper dipyrromethene,[6] where no fine structure could be resolved even at $1.4°K$;[16] (3) these values are similar to those reported[8] for oxidative copper enzymes; (4) however, the copper hyperfine interaction constants observed in this study are considerably different from those observed for copper in other types of tetrahedral environment.[4,17] It appears that the copper hyperfine splitting parameters are sensitive to small

(16) Bates, et al., attributed this effect to strong admixture of the 4p state into the 3d orbitals of the copper. The possibility of strong exchange narrowing was excluded because it was thought that the copper atoms would be at least 8 Å apart owing to the size of the ligands. This may be true in this instance, but reasoning based upon steric requirements of ligands should be used with caution, since it was suggested that the palladium in bis(α,α-dipyridyliminato) palladium(II) (which is closely related to the copper complex) should be tetrahedrally coordinated because of the steric requirements of the ligands, whereas a complete X-ray structural determination [H. C. Freeman and M. R. Snow, Acta Crystallogr., 18, 845 (1965)] showed the palladium to be surrounded by a square plane of nitrogens and that the ligands suffered gross distortion.

(17) R. E. Dietz, H. Kamimura, M. D. Sturge, and A. Yariv, Phys. Rev., 132, 1559 (1963).

changes in configuration mixing in tetrahedral environments.

Thus the results obtained here for copper in a distorted tetrahedron of nitrogens are not in conflict with the postulate of such an environment in copper oxidases, although we do not feel that this study provides an unambiguous proof of this structure.[18]

(18) It should be pointed out that an additional similarity exists between the blue cuproteins and $(Cu_xZn)Hg(SCN)_4$. The cuproteins display an intense electronic transition ($\epsilon \sim 10^3$–10^4 M^{-1} cm^{-1}) at about 16,000–18,000 cm^{-1} which has been attributed to a charge-transfer band of anomalously low energy. The $(CuZn)$-$Hg(SCN)_4$ system has[12] a charge-transfer band at 18,300 cm^{-1} and the intensity[12] of this transition in the related $Cu(NCS)_4{}^{2-}$ ion is of a similar magnitude to that reported for blue cuproteins.

Determination of Electron Affinities of Radicals and Bond Dissociation Energies by Electron-Attachment Studies at Thermal Energies—Electron Affinity of Acetate Radical

by W. E. Wentworth, Edward Chen, and Joe C. Steelhammer

Department of Chemistry, University of Houston, Houston, Texas 77004 (Received January 25, 1967)

In previous publications,[1-3] three mechanisms for electron attachment to molecules at thermal energies have been proposed. These mechanisms involve (I) formation of a stable molecular negative ion, (II) a single bimolecular electron-attachment step followed by immediate dissociation into a negative halide ion and an organic radical by way of a dissociative potential energy curve, and (III) a two-step dissociative process which first involves the formation of a molecular negative ion followed by a dissociative step giving generally a negative halide ion and an organic radical by way of a dissociative potential energy curve. The distinct difference of these three mechanisms can best be described in terms of potential energy diagrams as shown in an earlier publication.[3]

In this paper we wish to present data supporting a fourth mechanism (IV) which is identical with the third

(1) W. E. Wentworth and R. S. Becker, J. Amer. Chem. Soc., 84, 4263 (1962).

(2) W. E. Wentworth, E. Chen, and J. E. Lovelock, J. Phys. Chem., 70, 445 (1966).

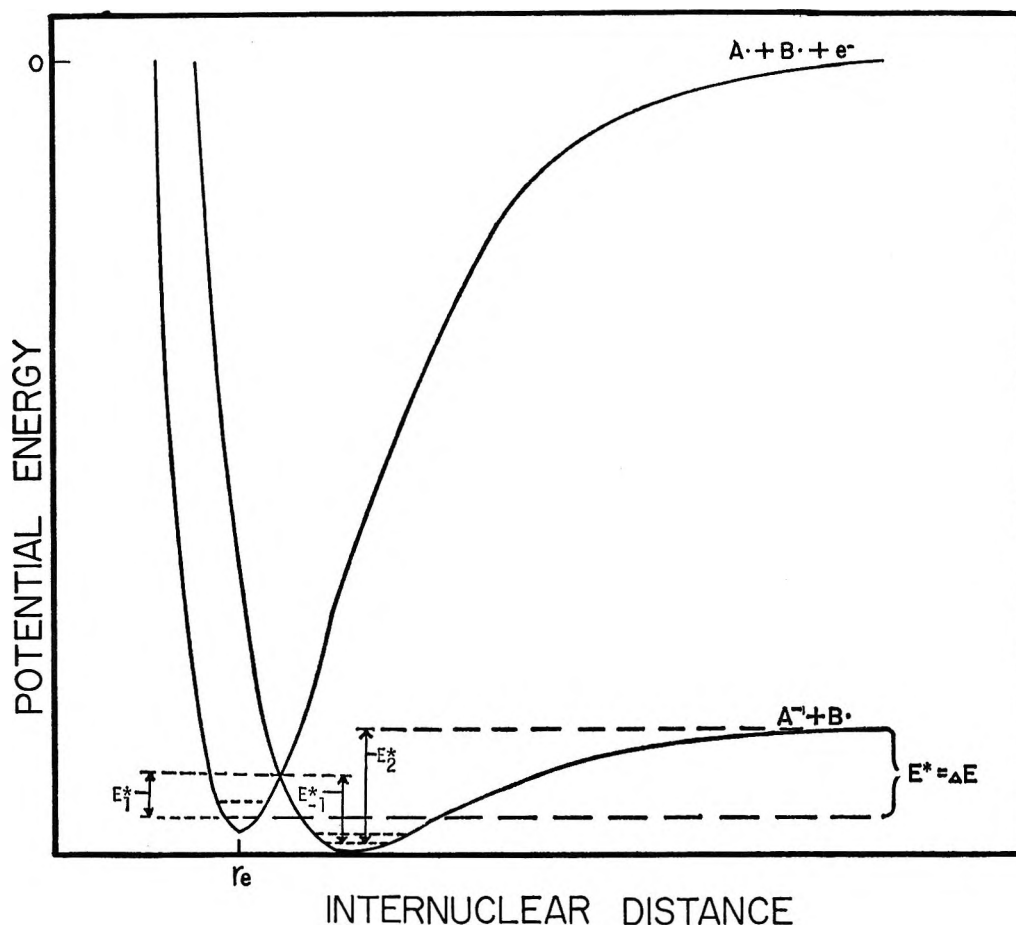(3) W. E. Wentworth, R. S. Becker, and R. Tung, ibid., 71, 1652 (1967).

Figure 1. Potential energy diagrams representing electron attachment according to mechanism IV.

mechanism above except that dissociation does *not* occur along a dissociative potential energy curve. This mechanism is shown in Figure 1. This fourth mechanism is important since the activation energy (E^*) is a *direct* measure of the difference in bond dissociation energy (D_{AB}) and the electron affinity of the radical (EA_A). If the compound being studied is sufficiently volatile, the activation energy can generally be determined with a standard error of ± 0.2–0.4 kcal/mol. Therefore, if one knows the bond energy rather precisely, this method would permit a precise determination of electron affinities of radicals. On the other hand, if the electron affinity of the radical were previously known, the bond dissociation energy could be determined. In another paper,[4] a technique for the determination of bond dissociation energies of some aliphatic halides is presented. However, that technique involves an empirical linear relationship between E^* and $(D_{AB} - EA_B)$, where B refers to the halide, which necessarily is an indirect method.

Of the existing experimental methods for the determination of the electron affinity of radicals probably the two most important are the electron impact and the magnetron methods. The magnetron method was first developed by Sutton and Mayer[5] and refined more recently by Page.[6] The precision of the electron impact method is generally on the order of ± 2–5 kcal/mol. The magnetron method is generally more precise than the electron impact method; however, interpretation of the results is often complicated by a complex mechanism which must be established and hence is always subject to error. If the correct mechanism is selected, then the magnetron method can give excellent results. The technique proposed in this paper should yield results which are both simple to interpret and have the desired precision.

In this paper the results of three compounds leading to the electron affinity of the acetate radical will be presented. This radical was selected since a rather reliable estimate of the electron affinity has been established.[7] Presently, compounds leading to the electron affinity of trifluoroacetate and nitro radicals are being investigated.

Experimental Section

The experimental procedure was essentially that

(4) W. E. Wentworth, H. Keith, and R. George, in preparation.

(5) P. P. Sutton and J. E. Mayer, *J. Chem. Phys.*, **2**, 145 (1934); **3**, 20 (1935).

(6) F. M. Page, *Trans. Faraday Soc.*, **56**, 1742 (1960).

(7) S. Tsuda and W. H. Hamill, "Advances in Mass Spectrometry," Vol. III, W. L. Mead, Ed., The Institute of Petroleum, London, 1966, pp 249–257.

used in previous studies of this nature.[2-4] A Microtek
2000-R gas chromatograph utilizing a 250-ft, 0.03-in.
i.d. stainless steel capillary column coated with poly-
phenyl ether (6 rings, 250° limit) was used for all com-
pounds. It was operated isothermally at the following
temperatures: acetic anhydride, 100°; benzyl acetate,
130°; ethyl acetate, 50°. Argon was used as the carrier
gas with methane added prior to the electron capture
cell to make up a 10% methane mixture. A pulse
width of 0.5 μsec at an interval of 1000 μsec was em-
ployed in the electron capture cell to collect the free
electrons.

The acetic anhydride was Baker reagent grade and
the ethyl and benzyl acetate were Eastman reagent
grade. The polyphenyl ether was obtained from Ap-
plied Science Laboratories. It was not necessary to
carry out a purification since this is accomplished satis-
factorily in the gas chromatograph prior to measure-
ment in the electron capture cell. Solutions of appro-
priate concentrations to inject 1–5-μl samples were pre-
pared using Mallinckrodt nanograde benzene.

The temperature of the electron capture cell was
generally elevated to the highest temperature ($\approx 230°$)
and measurements were made at successive intervals
as the temperature was allowed to drop. In the case of
acetic anhydride, the data at lower temperatures were
obtained at a later date and the data were adjusted to
the high-temperature data by four data points which
were common to the two regions. In all cases the span
correction b^0/b was used;[2] however, the correction was
generally on the order of 1.5 or less.

The areas under the chromatographic peaks were
obtained by using a Leeds and Northrup analog com-
puter which integrates the response $\int (b - [e^-]/[e^-])$
dx.[8]

Results and Discussion

The kinetic expression for this mechanism of electron
capture is identical with the mechanism identified
earlier in the paper as mechanism III. This expression
has been developed in a previous publication[3] where it
was referred to as the k_1k_2/k_{-1} mechanism. A more
general model was considered at that time and various
steps eliminated where they were shown to be negligible.
These approximations and simplifications will be made
in the present discussion. For mechanism IV the
products will be designated as A^- and $B^.$. The elec-
tron attachment and negative ion reaction steps for
this mechanism are

$$e^- + P^+ \xrightarrow{k_N'} \text{neutrals} \qquad (1)$$

$$e^- + R^. \xrightarrow{k_R'} R^- \xrightarrow{P^+} \text{neutrals} \qquad (2)$$

$$e^- + AB \underset{k_{-1}}{\overset{k_1}{\rightleftarrows}} AB^- \qquad (3)$$

$$AB^- \xrightarrow{k_2} A^- + B^. \qquad (4)$$

$$AB^- + P^+ \xrightarrow{k_{N1}'} \text{neutrals} \qquad (5)$$

$$AB^- + R^. \xrightarrow{k_{R1}'} AB + R^- \xrightarrow{P^+} \text{neutrals} \qquad (6)$$
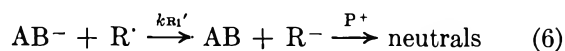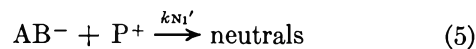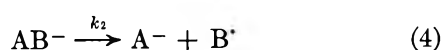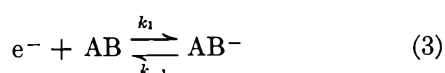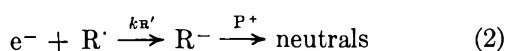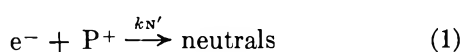
Assuming steady state for the $[e^-]$ and $[AB^-]$ and
an excess concentration of P^+, $R^.$, and capturing
species $[AB] = a$, the following expression can be
derived

$$\frac{b - [e^-]}{[e^-]} = Ka = \frac{1}{k_N + k_R} \times$$

$$\left[\frac{k_1k_2}{k_{-1}} + \frac{k_1(k_{N1} + k_{R1})}{k_{-1}} \right] a \qquad (7)$$

where b is the concentration of electrons when no
capturing species is present. $k_N = k_N'$ $[P^+]$, $k_R = k_R'$ $[R]$, etc., where k_N, k_R, k_{N1} and k_{R1} are pseudo-first-
order rate constants. The first term in the brackets is
the dissociative mechanism III or IV whereas the
second term corresponds to the stable negative ion
mechanism I.

The compounds acetic anhydride, benzyl acetate, and
ethyl acetate were run in this study and the temperature
dependence results are shown in Figure 2. The data
for acetic anhydride at higher temperatures define a
linear $\ln KT^{1/2}$ vs. $1/T$ plot with a negative slope cor-
responding to the dissociative mechanism. At lower
temperature there is an upward trend of the data away
from the negative slope. The data for benzyl and
ethyl acetate likewise show a negative slope at higher
temperatures; however, the departure at lower tem-
peratures leads to a positive slope in both cases. The
positive slope is associated with nondissociative electron
capture where the second term in eq 7 has now become
predominant. Since only the acetate radical has a
sufficient electron affinity relative to the bond dissoci-
ation energy in these compounds, only a single negative
ion potential energy curve is expected in the vicinity of
the ground state of the neutral molecule. We have
elected to classify this electron attachment phenomenon
involving a single negative ion potential energy curve as
mechanism IV. A similar temperature dependence
was observed for 1-chloronaphthalene;[3] however, two
negative ion potential energy curves are apparently
involved, and it has been classified as mechanism
III.

The two regions of temperature dependence shown
in Figure 2 are important in distinguishing this mech-
anism from mechanism II. In mechanism II the
activation energy for electron attachment, E_1^*, is
greater than $\Delta E = (D_{AB} - EA_B)$ and dissociation
should occur almost immediately upon electron attach-
ment to the vibrationally active molecule.

For mechanism II only a single negative slope should
be observed for the temperature dependence. The

(8) W. E. Wentworth and E. Chen, *J. Gas Chromatogr.*, **5**, 170 (1967).

Table I: Evaluation of Electron Affinity of Acetate Radical

(1) Compound	(2) Intercept	(3) −(negative slope × R), kcal	(4) Molecular EA, eV	(5) E*, kcal	(6) E*$_{298°}$, kcal	(7) D$_{AB,298°}$,^{a} kcal	(8) EA$_{CH_3CO_2}$, 298°, eV	(9) EA$_{CH_3CO_2}$, 0°, eV
Acetic anhydride	34.86 ± 0.14	7.82	<0.236	6.56	6.93 ± 0.12	(81.5 ± 2.3)^b	3.24 ± 0.10	3.20 ± 0.10
						(85.4 ± 2.3)^c	3.40 ± 0.10	3.36 ± 0.10
						(91.8 ± 2.2)^d	3.68 ± 0.09	3.64 ± 0.09
Benzyl acetate	33.76 ± 0.49	10.27	0.168 ± 0.004	8.94	9.38 ± 0.44	(81.6 ± 3.6)^e	3.13 ± 0.16	3.10 + 0.16
Ethyl acetate	32.00 ± 2.00	11.25	0.159 ± 0.004	9.79	10.35 ± 2.74^h	(82.0 ± 4.0)^f	3.11 ± 0.21	3.07 ± 0.21
						87.6 ± 2.0^{g,h}	3.35 ± 0.14	3.31 ± 0.14

Weighted av = 3.36 ± 0.05

^{a} Bond dissociation energies in parentheses were calculated by $D_{AB} = \Delta H_f°(A,g) + \Delta H_f°(B,g) - \Delta H_f°(AB,g)$. $\Delta H_f°$ of all radicals except acetyl were obtained from C. T. Mortimer, "Reaction Heads and Bond Strengths," Addison-Wesley Publishing Co., Reading, Mass., 1962, Chapter 7; $\Delta H_f°$ acetyl radical from R. I. Reed and J. C. D. Brand, *Trans. Faraday Soc.*, **54**, 478 (1958). ^{b} $\Delta H_f°(AB,g)$ from H_{comb}, H_{vap} in "Handbook of Chemistry and Physics," Chemical Rubber Publishing Co., Cleveland, Ohio, 1962. ^{c} $\Delta H_f°(AB,g)$ from H_{comb} from ref b and H_{vap} from John Perry, Ed., "Chemical Engineer's Handbook," McGraw-Hill Book Co., New York, N. Y., 1963, Sec. 3. ^{d} $\Delta H_f°(AB,g)$ from ref c. ^{e} $\Delta H_f°(AB,g)$ from H_{RX}, M. Fiorani, G. Barbieri, and L. Riccoboni, *Ric. Sci.*, **28**, 11 (1958). H_{vap} from V. V. Serpinski, S. A. Vortkevich, N. Yu. Lyuboshits, *Zh. Fiz. Khim.*, **28**, 810 (1954). ^{f} $\Delta H_f°(AB,g)$ from ref c. ^{g} D_{AB} calculated from appearance potential and ionization potential. *IP* from F. A. Elder, C. Giese, M. G. Inghram, and B. Steiner, ASTM Committee E-14 on Mass Spectrometry, 9th Annual Meeting, Chicago, Ill., June 4–9, 1961. *AP* from ref 7. ^{h} Error estimated.
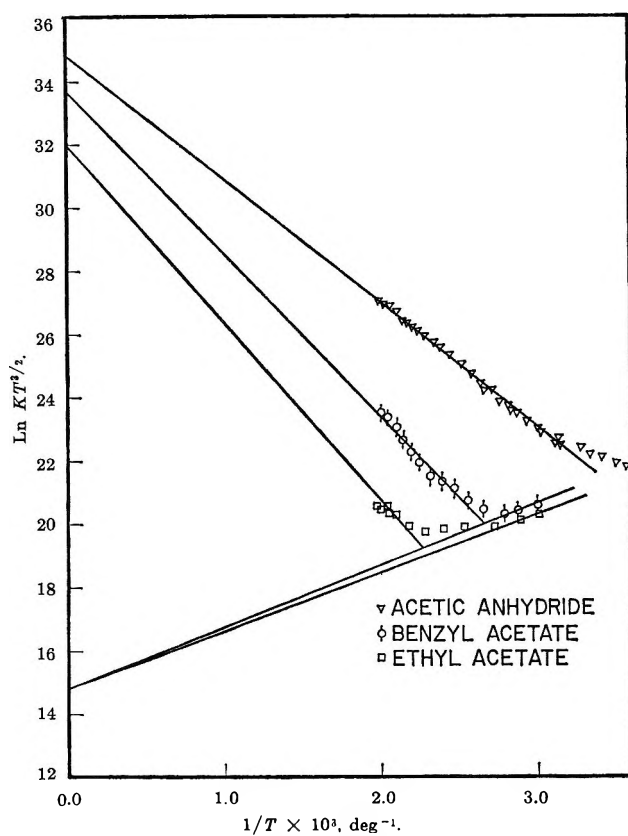

Figure 2. Temperature dependence of electron attachment.

subscripts on the activation energies in Figure 1 correspond to the rate constants defined in eq 3 and 4. On the other hand, in mechanism IV $E_1^* < \Delta E$ and the intermediate negative molecular ion should form prior to dissociation. In agreement with the data in Figure 2 and eq 7, two different temperature dependencies are

observed for mechanism IV. The actual shape of the ln $KT^{3/2}$ vs. $1/T$ curves are dependent upon the magnitudes of E_1^*, E_{-1}^*, E_2^*. Although the curves in Figure 2 are quite different, they are generally consistent with eq 7.

As stated previously, according to mechanism IV, $E^* = (D_{AB} - EA_A)$. Hence with an experimental E^* and knowledge of the bond dissociation energy, the electron affinity of the acetate radical can be calculated with the data for the three compounds. These results are shown in Table I. The −(negative slope × R) was determined by a least-squares adjustment[2,3] for acetic anhydride and benzyl acetate, and E^* corresponds to the activation energy for no preexponential temperature term,[3] i.e., the energy of activation from a ln K vs. $1/T$ graph. The data for ethyl acetate do not define the negative slope well and the curve in Figure 2 was drawn with an assumed intercept of 32. In general, the intercepts for the dissociative mechanism fall in the region 32–36. A relatively large error in the slope has been assigned to the E^* for ethyl acetate which is to account for the error in the assumed intercept. The correction of E^* to 298°K is given in column 6 and was made with $\Delta C_v = {}^3/_2R$. This ΔC_v was derived assuming ideal gas behavior, complete activation of the rotational modes, cancellation of the vibrational contributions of the molecule with those in the radical and negative ion products, and neglect of the vibrational mode leading to dissociation. The bond dissociation energies are given in column 7 at 298°K. In some cases values from more than one source are given when it is uncertain which value is to be preferred. The difference of columns 6 and 7 leads to the electron affinity of the radical at 298°K and is given in column 8. Finally, the electron affinities corrected

to 0°K are given in column 9 using $\Delta C_v = {}^3/_2 R$ for the difference in translational and rotational contributions to the heat capacities. One should note that the electron affinities for the acetate radical obtained from the various compounds are consistent within the experimental error. Furthermore, the weighted average of the values is 3.36 ± 0.05 which agrees favorably with the electron impact value of 3.3 eV obtained by Tsuda and Hamill.[7] This agreement clearly shows that E^* is equal to the change in internal energy for the process, $(D_{AB} - EA_A)$, and gives strong support for the proposed mechanism for dissociative electron attachment.

The molecular electron affinity estimates for benzyl acetate and ethyl acetate are also given in column 4 of Table I. They were obtained from a limited amount of data in the region suggestive of a positive slope. A least-squares adjustment using the common intercept method was carried out using a common intercept of 14.79 ± 0.11.[2,9] The molecular electron affinity values themselves are not of any specific significance with regard to the proposed mechanism. However, the fact that the data definitely suggest the formation of a stable negative ion at lower temperatures adds further support to the proposed mechanism. With the data for acetic anhydride it is difficult to establish a reliable estimate of the electron affinity. However, as mentioned previously, the upward trend of the data at lower temperatures is in agreement with the proposed mechanism.

The electron affinities of benzyl acetate and ethyl acetate are on the same order of magnitude, and one might expect this since the effect of ethyl and benzyl should be essentially inductive through the oxygen adjacent to the C=O group. The inductive effect of ethyl and benzyl should not differ greatly as indicated by the similarity of the Taft σ^* values of -0.10 and $+0.22$, respectively. This is a difference of 0.32 in the σ^* values. For comparison, the σ^* value of the acetyl group is 1.65.[10] This system gives positive values to those groups which are electron-withdrawing relative to the methyl group which is assigned the value zero. From these σ^* values, benzyl acetate would be expected to have a slightly higher electron affinity than ethyl acetate, which is in agreement with the results. Little can be said of the magnitude of the molecular electron affinities since no values have ever been reported for this class of compounds. The values obtained, however, do not seem unreasonable.

In conclusion, the agreement between the activation energy and the change in internal energy for the process supports the dissociative electron attachment mechanism which involves the formation of a stable negative ion intermediate but does not follow a dissociative potential energy curve. The activation energy is thus the difference in bond dissociation energy and electron affinity of the radical $(D_{AB} - EA_A)$ permitting the

evaluation of either of these two quantities providing the other is known.

Acknowledgment. The authors are appreciative of the financial support for this research which was received from the Robert A. Welch Foundation.

(9) W. E. Wentworth and E. Chen, *J. Phys. Chem.*, 71, 1929 (1967).
(10) J. Hine, "Physical Organic Chemistry," McGraw-Hill Book Co., Inc., New York, N. Y., 1962.

A Kinetic Study of the System ${}^{237}Np(V)\cdot Cr(III)-{}^{239}Np(V)$[1]
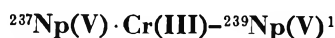
by James C. Sullivan and Mary J. Burkhart[2]

Argonne National Laboratory, Argonne, Illinois 60439
(Received February 16, 1968)

In a recent study of the reduction of Co(III) by the $Np(V)\cdot Cr(III)$ complex, evidence consistent with the interpretation that the electron-transfer reaction between Np(VI) and the complex did not proceed at a significant rate was presented.[3] The present investigation, *i.e.*, the exchange reaction

$$Np(V)^* + Np(V)\cdot Cr(III) \xrightarrow{k_1}$$
$$Np(V) + Np(V)^*\cdot Cr(III) \quad (1)$$
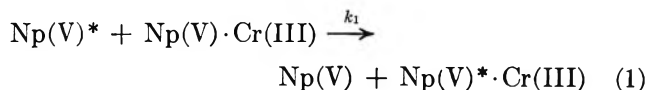
was undertaken as a necessary preliminary to a study of the $Np(VI)^*-Np(V)\cdot Cr(III)$ exchange. The results of a study of reaction 1, in addition, might reasonably be expected to provide additional information about the $Np(V)\cdot Cr(III)$ complex ion.

Experimental Section

A. Reagents. The ${}^{239}Np$ was separated from the parent ${}^{243}Am$ (*ca.* 1.3 g)[4] by two solvent-extraction procedures.[5] A half-life of 57 hr was determined for the ${}^{239}Np$, a value in good agreement with the more precise value of 56.6 ± 0.2 hr previously reported.[6] The carrier free ${}^{239}Np$ was then added to a solution containing ${}^{237}Np$, and the Np(V) stock solution was prepared as previously described.[7]

(1) Based on research performed under the auspices of the United States Atomic Energy Commission.
(2) Participant from East Texas State University in the CSUI-ANL Honors Program.
(3) J. C. Sullivan and R. C. Thompson, *Inorgan. Chem.*, 6, 1795 (1967).
(4) P. E. Horwitz, of this laboratory, graciously made the ${}^{243}Am$ sample available for this purpose.
(5) (a) P. E. Horwitz, personal communication, 1967; (b) D. F. Peppard, G. W. Mason, and R. J. Sironen, *J. Inorg. Nucl. Chem.*, 10, 1196 (1959); (c) kinetic results obtained with ${}^{239}Np$ from either extraction procedure were the same within the precision of our measurements.
(6) D. Cohen, J. C. Sullivan, and A. J. Zielen, *ibid.*, 11, 159 (1961).

Solutions of the $Np(V) \cdot Cr(III)$ complex were prepared just prior to the kinetic experiments by an ion-exchange procedure.[3]

The hydrogen ion concentrations of the spent reaction mixtures were determined by titration of a suitable aliquot with 0.1 M NaOH.

B. Procedures. The reagents, except the $Np(V)*$, were introduced into a volumetric flask which was allowed to come to temperature equilibrium in a water bath. The $Np(V)*$ was then introduced and *ca.* 2-ml samples were withdrawn at timed intervals. These samples were quickly injected into 15-ml centrifuge tubes (precooled in an ice–water bath) which contained *ca.* 2.5 ml Dowex 50W-X2 (200–400 mesh) resin and *ca.* 2 ml of water. The contents of the tube were mixed vigorously for 4 min, then centrifuged, and an aliquot of the supernatant liquid was plated on a planchet.

Between 15 and 20 such data points were obtained for each kinetic experiment. All experiments were carried out in duplicate and were followed to 90–95% of complete exchange. Infinite time values were determined from samples taken after the reaction mixture had been kept at *ca.* 100° for 24 hr.

A standard Geiger tube with sufficient absorber present to screen out the α particles from the ^{237}Np was used to determine the β^- activity. A proportional α counter was used to determine the α activity. All activities were determined to a statistical uncertainty of ±1%.

The separation procedure induced no exchange within the precision of the experimental methods. For example, the ratio of β^- activity : α activity for a solution initially containing only $Np(V)*$ was 0.909 after contact with the resin. Replication of this experiment with the addition of an aliquot of the $Np(V) \cdot Cr(III)$ complex resulted in a ratio of 0.907.

The ratios of the β^- activity (counts/min) : α activity (counts/min) on the same planchet were used to determine the fraction exchanged (F). The quantity $1 - F$ in terms of the observed ratios is

$$1 - F = \frac{(\beta/\alpha)_t - (\beta/\alpha)_\infty}{(\beta/\alpha)_0 - (\beta/\alpha)_\infty} \quad (2)$$

where $(\beta/\alpha)_t$ is the ratio at time t, $(\beta/\alpha)_0$ is the ratio at time zero, and $(\beta/\alpha)_\infty$ is the ratio at equilibrium.

Results and Discussion

Attempts to correlate the data in terms of dissociation plus exchange using the equations previously developed[8] demonstrated that the only change in the specific β^- activity of the $Np(V)$ with time was due to the dissociation of the complex. The data can, therefore, be used to determine a value for the specific rate constant k

$$Np(V) \cdot Cr(III) \xrightarrow{k} Np(V) + Cr(H_2O)_6{}^{3+} \quad (3)$$
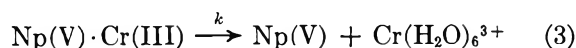
For this particular system, where all the β^- activity

is initially associated with the aquated $Np(V)$, the relation between F and k is

$$\ln \left[\frac{a^0}{b^0(1 - F)} + 1 \right] = kt + \ln \frac{a^0 + b^0}{b^0} \quad (4)$$

where a^0 and b^0 are the initial concentrations of $Np(V)*$ and the complex, respectively.

The computation of k in terms of eq 4 was carried out by a weighted least-squares adjustment of the data. A summary of the calculated first-order rate constants is presented in Table I.

Table I: Summary of Rate Constants for the Reaction
$Np(V) \cdot Cr(III) \xrightarrow{k} Np(V) + Cr(H_2O)_6{}^{3+}$ [a]

Temp, °C	$10^5 k$,[b] sec^{-1}	$10^4 [Np(V) \cdot Cr(III)]^0$, M	$10^5 [N_F(V)]^0$, M
25	0.218 ± 0.009	8.47	7.95
25	0.221 ± 0.007	4.24	8.83
35	1.15 ± 0.02	7.55	9.61
35	1.06 ± 0.03	4.52	9.61
35	1.18 ± 0.04	9.50	19.2
50	7.87 ± 0.14	6.34	19.4
50	8.08 ± 0.06	3.97	19.4
50	8.13 ± 0.43	4.88	30.96
50	7.71 ± 0.07	5.09	9.12
50	8.11 ± 0.13	8.44	9.07

[a] Values are for solution 2.0 M $HClO_4$ at an ionic strength of 2.0. [b] Uncertainties are the deviations from the mean of replicate determinations.

The invariance of the specific rate constants (all values at a given temperature overlap at the 95% confidence level) supports the original interpretation of the data. Additional evidence that the primary process occurring is the dissociation of the complex is provided by the following observations.

Results obtained in the spectrophotometric study[9] of reaction 3 displayed no large variations in the rate parameter with gross changes in solvent composition. Although the values presented in Table I are within 10–20% of those previously determined, a limited number of additional results were obtained to allow a comparison under the same experimental constraints.

At 50° in 1.00 M $HClO_4$ the average value of the rate parameter determined in this investigation was (7.50 ± 0.20) × 10^{-5} sec^{-1}, compared with the value of (9.43 ± 0.04) × 10^{-5} sec^{-1} previously determined. The difference between the values is larger than one would optimistically expect but not large enough to indicate a

(7) R. C. Thompson and J. C. Sullivan, *J. Amer. Chem. Soc.*, **89**, 1096 (1967).

(8) C. P. Luehr, G. E. Challenger, and B. J. Masters, *ibid.*, **78**, 1315 (1956).

(9) J. C. Sullivan, *Inorg. Chem.*, **3**, 315 (1964).

significant difference between the two types of experiments at a reasonable level of confidence.

At 25° in 1.00 M HClO₄ the average value of the rate parameter determined in this investigation was $(2.08 \pm 0.07) \times 10^{-6}$ sec⁻¹, as compared with the value of $(2.34 \pm 0.07) \times 10^{-6}$ sec⁻¹.

A value for the experimental activation energy $E = 25.8 \pm 0.3$ kcal/mol was computed from the data[10] at 2.00 M HClO₄ which is the same at the 95% confidence level as the previously determined value of $E = 28.3 \pm 0.8$ kcal/mol for the enthalpy of dissociation in a medium of 1.00 M HClO₄.

A value for k (eq 1) cannot be calculated from the present results. The data presented, however, are sufficient to allow an estimate of $t_{1/2} > 10^8$ sec for that reaction.

(10) The computations used in 18 independent values of k obtained in 2 M perchloric acid at the three temperatures. Weights were based on the standard deviations associated with the previously computed values of k.

The Thermal Decomposition of

Dimethyl Azodiformate

by A. Jones,

Chemistry Department, Leeds University, Leeds, England

E. R. Morris, and J. C. J. Thynne

Chemistry Department, Edinburgh University, Edinburgh, Scotland
(Received February 19, 1968)

The thermal decomposition in the gas and liquid phases of compounds of the type RN=NR to yield nitrogen and the free radical R is well known, data having been reported for systems where R is an alkyl,[1] alkoxyl,[2] or alkylamino[3] substituent.

$$RN=NR \longrightarrow N_2 + 2R \cdot \qquad (1)$$

The decompositions of formates[4-6] and carbonates[7] have demonstrated the instability of alkoxycarbonyl radicals, ĊOOR, which appear to decarboxylate quantitatively to generate an alkyl radical and carbon dioxide, and advantage has been taken of this reaction to generate free radicals not readily obtained by other methods

$$\dot{C}OOR \longrightarrow CO_2 + R \cdot \qquad (2)$$
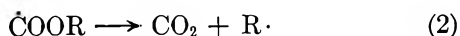
A class of compounds which combines both of the above features is the esters of azodiformic acid, ROOCN=NCOOR. These compounds are easily prepared, are reddish, and decompose at temperatures above about 120°. They may be useful as potential thermal and photochemical sources of alkyl radicals, since by

analogy with reactions 1 and 2 the following sequence of reactions might be expected

$$ROOCN=NCOOR \longrightarrow N_2 + 2\dot{C}OOR \qquad (3)$$

$$\dot{C}OOR \longrightarrow CO_2 + R \cdot \qquad (4)$$
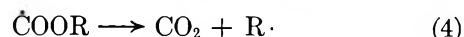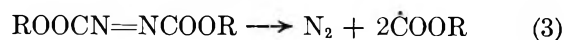
Although the use of these compounds in connection with the Diels–Alder reaction is well known, their decomposition appears not to have been examined. We have studied the thermal decomposition of dimethyl azodiformate in the gas phase and in dodecane solution.

Experimental Section

Materials. Dimethyl azodiformate was prepared by the method of Rodgman and Wright,[8] a fraction boiling at 80.5° at 6.5 mm being collected. This was subjected to several bulb-to-bulb distillations on a vacuum line before being stored in a blackened bulb. Gas chromatographic analysis showed the sample to be pure.

Apparatus. In the gas-phase study, the azodiformate was condensed into a cylindrical Pyrex reaction vessel (volume 180 cm³) equipped with a break-seal and sealed off under vacuum. The reaction vessel was then immersed in a thermostated oil bath capable of maintaining temperatures up to 200° to better than $\pm 1°$. The reaction was stopped by removing the vessel from the oil bath and plunging it into a bath at −80°.

The reaction vessel was then sealed onto a high-vacuum line and the break-seal was broken. The reaction products were expanded into an analytical train which was comprised of a liquid nitrogen trap, a gas buret, and a Macleod gauge. The products not condensable in liquid nitrogen were collected and measured in the gas buret before being analyzed mass spectrometrically. A second fraction was removed at −121° using a pentane–liquid nitrogen slush bath and was similarly analyzed.

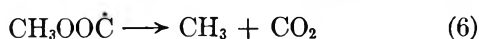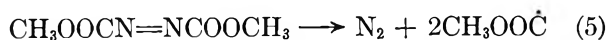In the liquid-phase study, the decomposition was investigated in dodecane with 10^{-2} M solutions being used. The reaction vessels were cylindrical Pyrex tubes (volume *ca.* 5 cm³) which could be filled with solution leaving only a small space above the liquid. The ampoules were sealed off and the runs and analysis were performed as described above.

A similar analytical procedure was used for the photolysis studies, the light source being the full beam of a Mazda ME/D250W medium-pressure mercury lamp.

(1) W. Forst and O. K. Rice, *Can. J. Chem.*, **41**, 562 (1963).

(2) J. R. Partington and C. C. Shah, *J. Chem. Soc.*, 2589 (1932).

(3) A. J. Waring and J. S. Watson, *Can. J. Chem.*, **38**, 298 (1960).

(4) J. C. J. Thynne, *Trans. Faraday Soc.*, **58**, 676 (1962).

(5) J. C. J. Thynne, *ibid.*, **58**, 1394 (1962).

(6) J. C. J. Thynne, *ibid.*, **58**, 1533 (1962).

(7) M. J. Yee Quee and J. C. J. Thynne, *ibid.*, **62**, 3154 (1966).

(8) A. Rodgman and G. F. Wright, *J. Org. Chem.*, **18**, 465 (1953).

Results and Discussion

Gas-Phase Decomposition. A series of runs were carried out at 162°. The noncondensable fraction contained no methane and consisted entirely of nitrogen. Analysis of the fraction volatile at $-121°$ showed it to contain only about 3% ethane, the remainder being carbon dioxide with traces of the azodiformate ester. A typical product analysis yielded the following values (in micromoles): N_2, 205; CO_2, 1.94; and C_2H_6, 0.06; *i.e.*, $N_2/CO_2 = 1.06$ and $2C_2H_6/CO_2 = 0.06$.

$$CH_3OOCN{=}NCOOCH_3 \longrightarrow N_2 + 2CH_3OO\dot{C} \quad (5)$$

$$CH_3OO\dot{C} \longrightarrow CH_3 + CO_2 \quad (6)$$

Decomposition of the ester according to reactions 5 and 6 would require that the ratios N_2/CO_2 and $\Sigma CH_3\cdot/CO_2$ would have the values 0.5 and 1, respectively. We interpret the divergence of our experimental values from these predicted values to indicate that only about half of the methoxycarbonyl radicals generated in reaction 5 decompose. It appears that approximately 6% of the methyl radicals produced in the decarboxylation reaction are accounted for by the reaction

$$2CH_3\cdot \longrightarrow C_2H_6 \quad (7)$$
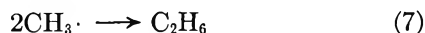
Methyl radicals have been shown to react very readily with azomethane[9] by addition to form trimethylhydrazine and tetramethylhydrazine. Our experimental results suggest that they may also react very readily with the azodiformate. It is likely also that some of the unaccounted for methoxycarbonyl radicals have reacted by addition to the N=N bond. Conjugation with the two carbonyl groups appears to have the effect of enhancing the rate of radical addition to the double bond. This reaction must be fast, since it is clearly competitive with reaction 6 and very much faster than the hydrogen atom abstraction reaction

$$CH_3\cdot + CH_3OOCN{=}NCOOCH_3 \longrightarrow$$
$$CH_4 + \cdot CH_2OOCN{=}NCOOCH_3 \quad (8)$$
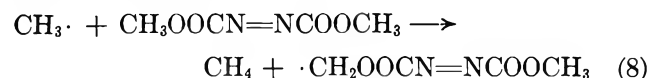
because no methane is detected.

Rate constants (based on nitrogen evolution) were measured for reaction 5 at 162°. The results of five repeat determinations yielded a value $k_5 = (6.4 \pm 0.9) \times 10^{-6} \text{ sec}^{-1}$, the error limit representing the average deviation of these runs. If a preexponential factor of 10^{14} sec^{-1} is assumed, this rate corresponds to an activation energy for reaction 5 of about 38 kcal mol^{-1}. This may be compared with a value of 34.6 kcal mol^{-1} for the activation energy reported[10] for the decomposition of tetramethyltetrazene, *i.e.*, where R is $(CH_3)_2N\cdot$ in reaction 1.

Decomposition in Dodecane Solution. When 10^{-2} M solutions in dodecane were decomposed thermally at temperatures in the range 120–170° or photochemically

at a lower temperature, a colorless sticky polymerlike solid was produced which went brown on standing. The bright red solution was rapidly bleached, suggesting complete consumption of the azodiformate, although the maximum yield of nitrogen indicated that only about 7% of the azodiformate had decomposed.

Analysis of the polymerlike solid showed it to contain C, 44.1%; N, 12.6%; H, 6.4%; and O, 36.8% (by difference). This corresponds to a formula of $C_{17}H_{30}O_{11}N_4$, the molecular weight of which is 466, in reasonable agreement with the molecular weight of 500 $\pm$ 20 determined directly using a vapor pressure osmometer.

We consider that these results may be interpreted in terms of a ready addition of the radicals produced in reactions 5 and 6 to the azo linkage. The resulting radical then undergoes an isomerization reaction

$$CH_3OOC\dot{N}N(R)COOCH_3 \longrightarrow$$
$$CH_3OC(\dot{O}){=}NN(R)COOCH_3$$
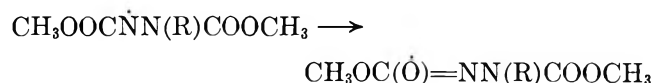
This radical in turn reacts by addition to the azodiformate and in this manner a repeating unit $(ON(COOCH_3)N{=}C(OCH_3)-)_n$ is built up. Our molecular weight determination suggests a value of about 3 or 4 for n. This ready addition reaction rapidly consumes all of the azodiformate and this explains why the solution is bleached, although actual thermal decomposition of dimethyl azodiformate based upon nitrogen evolution only accounts for a relatively small consumption of the ester.

It is clear that because of this complication the decomposition of azodiformate esters is not likely to be of use as a free-radical source.

(9) M. H. Jones and E. W. R. Steacie, *J. Chem. Phys.*, 21, 1018 (1953).

(10) A. Good and J. C. J. Thynne, *J. Chem. Soc.*, B, 684 (1967).

Some Observations on the Proton Magnetic Resonance Spectrum of Tetraethyl Ethylenebisphosphonate

by M. P. Williamson and C. E. Griffin

Department of Chemistry, University of Pittsburgh, Pittsburgh, Pennsylvania, and Mellon Institute, Carnegie Mellon University, Pittsburgh, Pennsylvania (*Received February 23, 1968*)

The salient features of the proton magnetic resonance spectra of a number of compounds containing the PCH_2CH_2P system (1) have been reported recently.[1,2]

(1) A. J. Carty and R. K. Harris, *Chem. Commun.*, 234 (1967).

(2) J. J. Brophy and M. J. Gallagher, *Austral. J. Chem.*, 20, 503 (1967).

For compounds in which the phosphorus atoms are symmetrically substituted, the methylene protons yield a deceptively simple spectrum which has been treated as being due to the X part of an $AXX'X''X'''A'$ spin system.[1] The spectrum normally observed is a triplet with the separation of the relatively sharp and intense outer lines equal to $|^2J_{PH} + {}^3J_{PH}|$, although the appearance of the spectrum is markedly dependent upon the nature of the substitution at phosphorus. The structure of the inner peak varies erratically from a sharp singlet to a broad singlet and even to a partially resolved multiplet.[1,2] Partial analyses of the spectra of a number of compounds of type 1 have been reported by Carty and Harris.[1] In an effort to obtain a complete analysis of one representative of this class, we have examined the pmr spectrum of tetraethyl ethylenebisphosphonate $[(CH_3CH_2O)_2P(O)CH_2CH_2P(O)(OCH_2CH_3)_2$ (2)] in some detail.

Experimental Section

Samples of 2 were kindly provided by Drs. D. J. Martin and R. L. K. Carr. The samples were degassed on a vacuum line and sealed in 5-mm nmr tubes after the addition of 3% tetramethylsilane (TMS).

The decoupling experiment was performed on a Varian HA-100 spectrometer which was frequency swept in the HA mode, the field frequency being locked to the internal TMS. The irradiating frequency was provided by a Hewlett-Packard 201CR audiooscillator. All the other spectra were recorded on a Varian A-60 spectrometer. The high- and low-temperature measurements were made using a Varian V-4060 variable-temperature controller and a V-6031B probe.

Discussion

The $-CH_2CH_2-$ portion of the pmr spectrum of 2 in carbon tetrachloride [25% (v/v) solution] at 37° is shown in Figure 1b. A spectrum of similar appearance has been reported by Brophy and Gallagher.[2] The observed separation (9.0 Hz, lit.[2] 9 Hz) of the two intense lines is of the expected magnitude for $|^2J_{PH} + {}^3J_{PH}|$.[2] Several trial calculations of the spectrum were performed using a program written specifically for the $AXX'X''X'''A'$ system.[3] It became apparent that the observed broadness of the lines was not being matched. This broadness was neither dependent on the source of the sample used nor could it be attributed to the viscosity of the sample; the broadness was found to persist even in dilute solutions. The resonances of the ester ethyl groups were also found to be unusually broad, particularly in the methylene region. It was thought that the broadness of the $-CH_2CH_2-$ region could have been due to either a mixing of the spin states of the phosphorus nuclei by coupling with the $-OCH_2-$ protons of the ethyl group, or possibly, a proton–proton coupling ($^5J_{HH}$) between $-CH_2CH_2-$ and $-OCH_2-$ protons. Brophy and Gallagher[2] have indicated longer
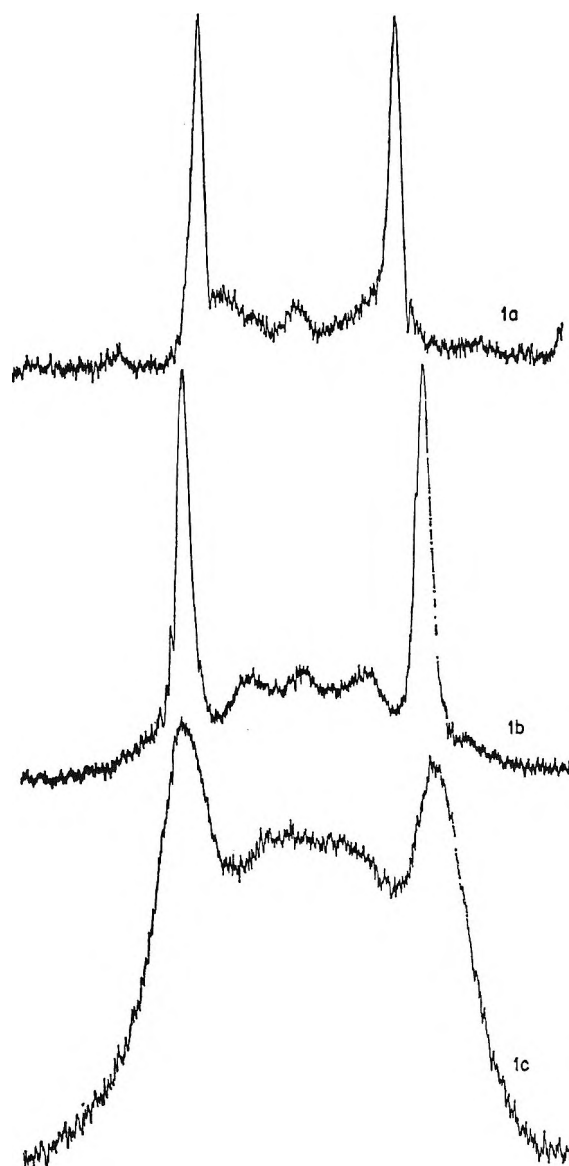

Figure 1. The PCH_2CH_2P region of the pmr spectrum of tetraethyl ethylenebisphosphonate as a 25% (v/v) solution: (a) in nitrobenzene at 180°; (b) in carbon tetrachloride at 37°; (c) in carbon disulfide at −50°.

range couplings to be a possible cause of line broadening in spectra of compounds of type 1. In order to test this postulation, a double-resonance experiment was carried out. Irradiation of the $-OCH_2-$ region of the spectrum at 100 MHz failed to affect the appearance of the $-CH_2CH_2-$ resonances; no line narrowing was observable. Under these conditions, the ester methyl resonance collapsed to a singlet, indicating that the ester methylene protons had, in fact, been decoupled.

A second possible explanation of the broadness of the lines in the spectrum of 2 was a lack of rotational averaging. The bulk of the $(CH_3CH_2O)_2P(O)-$ groups might be sufficient to cause a slow rotation about the

(3) A. A. Bothner-By, personal communication. The input data for this program accommodate different values for J_{HCCH} *gauche* and *trans*.

methylene carbon-carbon bond. In this event, it would be expected that the lines would narrow with an increase in temperature. However, even at 180° the spectrum of 2 in nitrobenzene [25% (v/v) solutions] failed to show any detectable line narrowing in either the $-CH_2CH_2-$ (Figure 1a) or the ester regions. If the premise of slow rotation were correct, this finding would indicate the barrier to rotation to be extremely high. In such a case, it should have been possible to freeze out one of the rotamers at low temperature. However, the spectrum of 2 in carbon disulfide [25% (v/v) solution] at −50° (Figure 1c) showed no line narrowing.

The effect of temperature on the spectrum of 2 is summarized in Table I. Further, the appearance of the spectrum changed only slightly on passing from the neat liquid to dilute solutions in carbon tetrachloride, carbon disulfide, nitrobenzene, acetone-d_6, and trifluoroacetic acid. Previous investigations have shown dialkyl alkylphosphonates to possess a modest solvent dependence, particularly for solutions in trifluoroacetic acid.[4] These changes may be the result of changes in rotamer populations.

Table I: Nmr Spectra of Tetraethyl Ethylenebisphosphonate

Solvent	Concn, % (v/v)	Temp, °C	$\lvert {}^2J_{PH} + {}^3J_{PH}\rvert$ Hz
CCl₄	25	37	9.0
Acetone-d_6	12.5	37	8.8
Trifluoroacetic acid	25	37	8.3
PhNO₂	25	37	8.4
		100	8.1
		150	7.6
		180	7.3
CS₂	10	37	8.7
	25	37	8.8
		−10	9.0
		−50	9.3

Although the results of this study are inconclusive, some possible explanations for the appearance of the spectra of symmetrical PCH_2CH_2P compounds are eliminated. A complete analysis of the spectra of this system must probably await the availability of stereospecifically deuterated compounds.

(4) M. Gordon, Ph.D. Thesis, University of Pittsburgh, Pittsburgh, Pa., 1965.

2-Aminopyridine as a Standard for Low-Wavelength Spectrofluorimetry

by R. Rusakowicz and A. C. Testa

Department of Chemistry, St. John's University, Jamaica, New York 11432 (*Received March 5, 1968*)

The use of fluorescent compounds to standardize photomultiplier-monochromator assemblies is commonplace in many laboratories today. In general, convenience dictates the use of such compounds. Quinine bisulfate (QBS) and Al–PBBR chelate have been used as reference compounds;[1,2] however, these compounds fluoresce above 390 mμ. Fluorescence in the low-wavelength region (300–400 mμ) has been given very little attention with regard to common acceptance of a reference compound. In view of this shortcoming, we report the results of experiments with 2-aminopyridine (AMP) in 0.1 N H_2SO_4 and suggest that it is a convenient fluorescence standard in the wavelength range 315–480 mμ.

Illustrated in Figure 1 is the single-peak envelope of the fluorescence spectrum of 2 AMP in 0.1 N H_2SO_4, resulting from excitation at 285 mμ. The data presented are an average of the emission spectra obtained at concentrations of 1.25×10^{-5} and 4.53×10^{-6} M and have been normalized to the fluorescence wavelength maximum at 367 mμ. The recorded fluorescence spectrum has been corrected for the wavelength sensitivity of our photomultiplier-monochromator system, which has been calibrated with a standard lamp of known irradiance ($\mu W/cm^2$ sec 10 Å). It is evident that there is no significant difference between the corrected and recorded fluorescence spectrum.[3] Since this is obviously an advantage in calibration, it is also convenient for quantum-yield determinations. An estimate of the difference between the area of the recorded and corrected spectra is ±10%.

The determination of the fluorescence quantum yield of 2-AMP was made by comparison to QBS in 0.1 N H_2SO_4. In order to justify 285-mμ excitation for QBS rather than the generally used 366-mμ excitation,[1] we determined the fluorescence area of QBS at these two excitation wavelengths. Although there is a small

(1) W. H. Melhuish, *J. Phys. Chem.*, **64**, 762 (1960).

(2) R. J. Argauer and C. E. White, *Anal. Chem.*, **36**, 368 (1964).

(3) Calibration of the 1P21 photomultiplier-monochromator system with a standard lamp in our laboratory indicated that the correction factors for wavelength sensitivity of the tube were unity in the region 315–360 mμ.

blue shift in the fluorescence of QBS with 285-mμ excitation relative to 366 mμ, it is not significant enough to change correction factors or quantum yields. The ratio of the fluorescence areas of QBS at the two wavelengths of excitation, A_{366}(QBS)/A_{285}(QBS), was determined to be 1.06 ± 0.03.
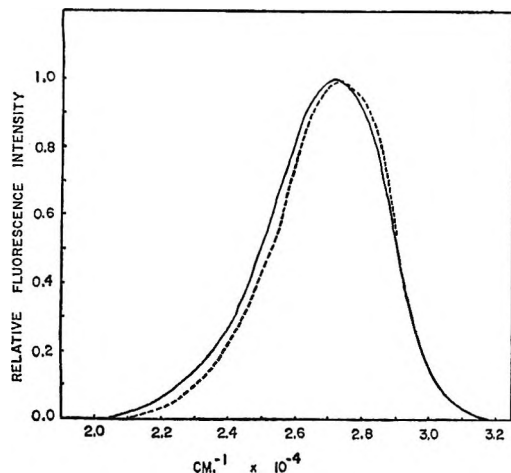

Figure 1. Fluorescence spectrum of 2-aminopyridine ($10^{-5} M$) in 0.1 N H$_2$SO$_4$ normalized to unity at $\bar{\nu}_{max} = 27,200$ cm^{-1}: ———, corrected fluorescence; – – – –, uncorrected fluorescence spectrum. (λ_{ex} 285 mμ, 1P21 photomultiplier.)

The ratio of fluorescence quantum yields at 285-mμ excitation, Φ_f(2-AMP)/Φ_f(QBS), was determined to be 1.40 ± 0.06 when the compounds were dissolved in 0.1 N H$_2$SO$_4$. It was observed that QBS and 2-AMP, each in 0.1 N H$_2$SO$_4$, have the same extinction coefficient at 285 mμ, i.e., 1.60 × 10^3 M^{-1} cm^{-1}, when measured with a Beckman DU spectrophotometer. The fraction of light absorbed in the fluorescence experiments, however, was determined with a single-beam photometer (vide infra). The absorption characteristics of the QBS and 2-AMP were equivalent over the transmission band of the 285-mμ interference filter used; consequently, the use of equal concentrations to compare their quantum yields was justified.

The fluorescence quantum yield of 2-AMP in 0.1 N H$_2$SO$_4$ was also determined by comparison with a degassed solution of 9,10-diphenylanthracene (DPA) in cyclohexane. Excitation with 285 mμ leads to a fluorescence quantum yield ratio, Φ_f(DPA)/Φ_f(2-AMP), of 1.80 ± 0.08. This value includes the correction for refractive indices of the solvents.[4] Using the value of unity and 0.46 for the fluorescence yields of DPA[5] and QBS,[6] respectively, the fluorescence quantum yield of 2-AMP was determined to be 0.60 ± 0.05. The agreement for the quantum-yield results of 2-AMP relative to 9,10-DPA and QBS is reassuring.

The high fluorescence yield, facile accessibility and recrystallization, stability of solutions, and the small

corrections factors arising from the 1P21 photomultiplier–monochromator system favor the use of 2-AMP in 0.1 N H$_2$SO$_4$ as a fluorescence standard. Solutions of 2-AMP (ca. 10^{-5} M) in 0.1 N H$_2$SO$_4$ are stable for long periods of time when stored in a refrigerator. During a period of 5 months there was no detectable change in either the absorption or fluorescence spectrum. The combined use of 2-AMP and QBS, each dissolved in 0.1 N H$_2$SO$_4$, permits fluorimeters to be calibrated over the wavelength range 315–580 mμ.

Experimental Section

An Aminco grating monochromator (5000-Å blaze) and an RCA 1P21 photomultiplier tube comprised the detection system. Fluorescence at room temperature from 1-cm quartz cells was observed in a direction perpendicular to the excitation beam. The 285-mμ excitation was achieved with an interference filter (10-mμ half-band width) from Thin Films Products, Cambridge, Mass., and 366-mμ excitation was achieved with a Schott interference filter (8-mμ half band width). 2-AMP from two supply houses (Aldrich and K & K) was recrystallized from n-hexane, with no measurable difference attributed to origin of the samples. 9,10-DPA and QBS were obtained from K & K Laboratories, Plainview, N. Y. The former was recrystallized three times from ethanol and chloroform and the latter three times from water.

The standard lamp was obtained from Electro Optics Associates, Palo Alto, Calif., and is accurate to ±5% relative to a NBS-certified Lamp.

The fraction of light absorbed was determined with a single-beam photometer employing the same excitation filter and high-pressure mercury lamp (Osram HBO 100W/2) used in the fluorescence experiments. The possibility of fluorescence emission interfering with the absorption measurements was excluded by using the following filter arrangement in front of the photomultiplier tube: 1 cm of saturated NiSO$_4$·6H$_2$O and a Corning No. CS 7-54 filter. The single-beam photometer was necessary because the determination of light absorbed with a spectrophotometer does not agree with the value measured with an interference filter, since the spectral bandwidths are different.

The linearity of fluorescence signal with concentration of 2-AMP in 0.1 N H$_2$SO$_4$ was obeyed up to 5 × 10^{-5} M for the right-angle detection system which was employed. The recommended upper limit of concentration for QBS was 3 × 10^{-5} M.

(4) (a) J. J. Hermans and S. Levinson, J. Opt. Soc. Amer., **41**, 460 (1951). (b) E. H. Gilmore, G. E. Gibson, and D. S. McClure, J. Chem. Phys., **23**, 399 (1955). The experimental fluorescence area was multiplied by the square of the refractive index.

(5) I. B. Berlman, "Handbook of Fluorescence Spectra of Aromatic Molecules," Academic Press Inc., New York, N. Y., 1965.

(6) R. Rusakowicz and A. C. Testa, J. Phys. Chem., **72**, 793 (1968).

Negative-Ion Mass Spectra of

Some Boron Hydrides[1]

by D. F. Munro, J. E. Ahnell, and W. S. Koski

Department of Chemistry, The Johns Hopkins University,
Baltimore, Maryland 21218 (Received January 31, 1968)

Figure 1.

While preparing equipment for a related investigation, we had occasion to observe the negative-ion mass spectra of some of the more common boron hydrides. In view of the dearth of mass spectral information on such ions and their importance in electron-impact processes, gas-discharge reactions, and radiation chemistry, we are reporting our results at this time for their potential interest to other workers in the field.

The important features of the experimental arrangement are shown diagrammatically in Figure 1. The sample gas flows from a bulb at room temperature through a Granville-Phillips variable leak to the ion source, which is similar in design to that described by Von Zahn,[2] having an electron-beam energy variable from 0–100 V. The ions are focused and accelerated to 50–100 V, and they then are mass analyzed by a quadrupole mass filter with electronically variable resolution. The quadrupole has a length of 10.0 in. (25.4 cm) and an r_0 of 0.27 in. (0.686 cm). Scanning is accomplished by varying the radiofrequency and direct current voltages applied to the mass filter. The ions are then accelerated to 600 V and are detected by a Bendix Channeltron continuous electron multiplier.

Because of the absence of slits in the mass spectrometer, the relatively open nature of the ion source, and the high sensitivity of the detector, it is necessary to reduce the background from scattered electrons. This is accomplished in two ways: first, by the establishment of a weak magnetic field to deflect the electrons preferentially and, second, by the use of pulse techniques. The ionizing beam is switched at 10 kcps through the application of a 40-V gating pulse to the first electron lens of the source. The beam "on" time is 10 μsec. After a delay of 5 μsec, the second generator sends a 1-V pulse to the detector gating circuitry, allowing only those signal pulses which arrive during the 20–30-μsec sampling interval to be sent on to the ratemeter. At the voltages used, most electrons arrive at the detector within 1–2 μsec; the flight time of the negative ions, however, is on the order of 10–20 μsec. Thus the detected signal is primarily due to negative ions, the electron background being reduced drastically.

The boron hydride samples were purified by trap-to-trap distillation on a vacuum system. Diborane was first collected at −196° and then was allowed to warm to −154°, with trapped pumping to eliminate hydrogen. Distillation was continued with traps at −89° to remove the higher boron hydrides, followed by final trap-
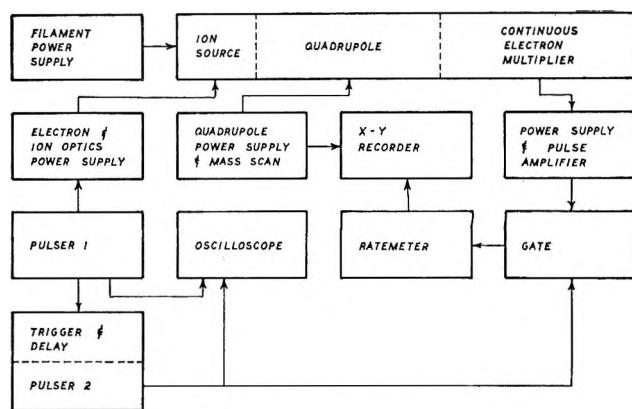
ping at −154°. The tetraborane was first trapped at −196°, was pumped on to remove hydrogen, and then was allowed to warm slowly to −130°, with trapped pumping to remove diborane. The residue was then passed through a trap at −95° to condense the pentaborane and higher boron hydrides. The tetraborane was then condensed at −196°. Pentaborane was similarly purified. Diborane and tetraborane were removed at −98°, followed by slow passage of the pentaborane fraction through a trap at −79° to remove any higher hydrides and then by condensation at −196°. The purified samples were stored in bulbs previously exposed to the respective hydrides to eliminate surface decomposition and were then kept at −79° until analysis.

The results obtained are compiled in Table I. All measurements were obtained with 70-V ionizing electrons. Monoisotopic mass spectra were computed, assuming the natural $^{10}B:^{11}B$ distribution of 20:80 and neglecting any isotope effects. In all cases the peak heights from which the monoisotopic spectra were calculated were an average of at least three measurements, with individual measurements in agreement within 10%. A check on the accuracy of the instrument was made by observing the positive-ion spectrum of B_2H_6. This was done by changing only the signs of the voltages in the ion optics and by accelerating the mass-analyzed positive ions to 3000 V before detection. The relative peak heights are compared with those obtained in published results in Table II. With a voltage-swept quadrupole, the resolution increases as the mass number increases. The result is an apparent mass discrimination for higher masses which sets in rapidly but is very slight before this onset. Thus by operating at a lower direct current:radiofrequency ratio of voltages, this effect can be greatly reduced, so that meaningful relative intensity measurements can still be made. The results shown in Table II seem to justify the use of

(1) This work was done under the auspices of the United States Atomic Energy Commission.

(2) V. Von Zahn, *Rev. Sci. Instrum.*, **34**, 1 (1963).

Table I: Relative Abundance of Ions in the Negative-Ion Mass Spectra of B_2H_6, B_4H_{10}, and B_5H_9

Negative ion	Relative abundance		
	B_2H_6	B_4H_{10}	B_5H_9
B	35.2		1.1
BH	23.5		0.7
BH_2	11.9		0.3
BH_3	15.7	0.1	0.1
BH_4	96.0	0.8	3.4
B_2	24.5		2.5
B_2H	10.6		2.2
B_2H_2	16.0	0.2	1.2
B_2H_3	100	1.1	9.1
B_2H_4	3.1	2.8	1.4
B_2H_5	25.6	0.3	3.1
B_3			2.7
B_3H			1.3
B_3H_2			14.4
B_3H_3			35.2
B_3H_4			16.7
B_3H_5		16.2	1.8
B_3H_6			
B_3H_7		100	13.1
B_4H			1.1
B_4H_2			4.4
B_4H_3			35.6
B_4H_4			3.3
B_4H_5			4.4
B_4H_6			24.6
B_4H_7		0.8	2.7
B_4H_8		0.5	
B_4H_9		5.5	
B_5H_5			0.9
B_5H_6			9.5
B_5H_7			5.3
B_5H_8			100
B_5H_9			2.6

Table II: Comparison of the Relative Abundance of Ions in the Positive-Ion Mass Spectra of B_2H_6

Mass	Our data	NBS[a]
10	6.8	6.31
11	25.4	28.4
11.5	0.6	0.46
12	14.5	18.1
13	20.2	24.4
14	[b]	0.72
15	[b]	0.10
20	0.6	0.16
21	1.7	1.94
21.2	[c]	0.06
22	12.5	11.2
22.2	[b]	0.15
23	52.5	45.7
24	89.0	89.6
25	64.5	56.7
26	100	100
27	100	97.4
28	[b]	0.25

[a] American Petroleum Institute Project 44, National Bureau of Standards No. 334 Mass Spectral Data, U. S. Government Printing Office, Washington, D. C., 1949. [b] Obscured by background. [c] Metastables not observed in a quadrupole mass spectrometer.

this technique. On the basis of such considerations, relative intensities referred to the most intense peak observed within a group of peaks, *e.g.*, $B_5H_9^-$, $P_5H_8^-$, $B_5H_7^-$, etc., should be accurate to 10%. The relative intensities throughout the series of spectra are probably correct to 25%.

Examination of the data in Table I shows that, corresponding to the positive-ion case, the parent-ion peaks are absent in both the diborane and tetraborane negative ion spectra, while the parent ion of pentaborane-9 is present in small amounts. The $B_4H_9^-$ ion is observed, whereas the $B_4H_8^+$ ion is the fragment of highest mass seen in the positive-ion spectrum of tetraborane. Similarly, $B_5H_8^-$ is the most intense peak in the pentaborane negative-ion spectrum, but $B_5H_8^+$ is not observed. This trend is generally followed for the rest of the spectra of the hydrides studied, although the effect is less marked in most cases.

There are several mechanisms by which negative ions may be formed:[3] (1) electron attachment, (2) dissociation electron attachment, and (3) ion-pair formati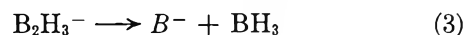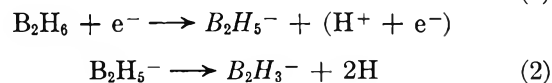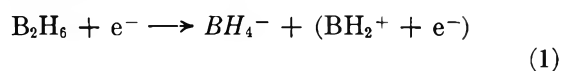on. The first two processes usually take place over a narrow range of low electron energies. The third requires electrons with energy exceeding a critical energy of about 20 eV. The excitation function for this process exhibits the same general features as that for the production of positive ions by ordinary electron impact. As the electron energy is increased, highly excited states can be produced, which in turn may decay into simpler ions.
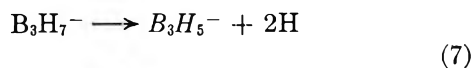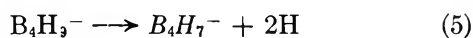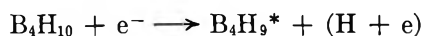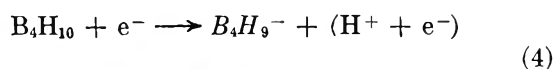
Using the above mechanisms, several tentative schemes are possible to explain the negative-ion spectra of the boron hydrides. A possible fragmentation scheme for diborane is

$$B_2H_6 + e^- \longrightarrow BH_4^- + (BH_2^+ + e^-) \tag{1}$$

$$B_2H_6 + e^- \longrightarrow B_2H_5^- + (H^+ + e^-) \tag{}$$

$$B_2H_5^- \longrightarrow B_2H_3^- + 2H \tag{2}$$

$$B_2H_3^- \longrightarrow B^- + BH_3 \tag{3}$$

The ions in italics are the four most intense in the diborane mass spectrum. The species given in parentheses may or may not be separate entities; *i.e.*, eq 1 may be a pair production process or a resonant dissociation attachment. In view of the electron energy used and the fact that the negative-ion yield was not a sensitive function of the electron energy from 40 to 100 eV, it would appear that the negative ions result primarily from pair ionization. A similar scheme for tetraborane might be written as

(3) E. W. McDaniel, "Collision Phenomena in Ionized Gases," John Wiley and Sons, Inc., New York, N. Y., 1964.

$$B_4H_{10} + e^- \longrightarrow B_4H_9^- + (H^+ + e^-) \tag{4}$$

$$B_4H_{10} + e^- \longrightarrow B_4H_9^* + (H + e) $$

$$B_4H_9^- \longrightarrow B_4H_7^- + 2H \tag{5}$$

$$B_4H_9^* \longrightarrow B_3H_7^- + BH_2^+ \tag{6}$$

$$B_3H_7^- \longrightarrow B_3H_5^- + 2H $$

$$B_3H_7^- \longrightarrow B_2H_4^- + BH_3 \tag{7}$$

This mechanism accounts for all peaks with an observed intensity greater than 1%, except $B_2H_3^-$. This peak was observed with 1.1% relative intensity, which could be due to a diborane impurity. A corresponding scheme can be prepared to explain the pentaborane negative-ion spectrum. It should be noted that the formation of BH_2^+ is favored over BH_3^+ in these schemes, owing to the fact that the 70-eV positive-ion spectrum of diborane[4] exhibits a BH_2^+ intensity of 19.1% and a BH_3^+ intensity of 0.59% relative to the most intense peak. The tetraborane results[5] are similar, giving 7.0 or 0.6%, respectively. Pentaborane[6] exhibits a BH_2^+ peak of 12.2% and a negligible BH_3^+.

The loss of BH_3 from neutral boron hydrides is well established in a number of reactions.[7] It is assumed that BH_3 may also be easily lost from negative boron hydride ions, a supposition included in the proposed mechanisms.

One of the most intense peaks in the negative-ion spectrum of diborane is due to BH_4^-. This is not too surprising, in view of the observed stability of this ion in the crystalline or solution state.[8] Analogously, one might have expected $B_3H_8^-$ to play a significant role in the tetraborane negative-ion spectrum, since it too shows considerable stability in solution and crystal studies.[8] Instead, $B_3H_7^-$ is the most prevalent ion in the B_4H_{10} spectrum. The mass assignment of this peak was repeatedly checked and is unlikely to be in error. In the tetraborane scheme, this ion was assumed to have its origin in a pair process arising from a highly excited $B_4H_9^*$ species. The reason for this is twofold. (1) The high electron energies could conceivably allow generation of the excited entity. (2) The $B_3H_7^-$ ion yield was relatively insensitive to electron energy from 40 to 100 V. Taken together, these facts would tend to preclude a resonant dissociative attachment leading to $B_3H_7^-$ and BH_3. Another possibility would be a simpler pair process such as

$$B_4H_{10} + e^- \longrightarrow B_3H_7^- + BH_3^+ + e^-$$

although the relative abundances of BH_3^+ and BH_2^+ seem to argue against it.

The absence of $B_3H_8^-$, which would be expected from a process as

$$B_4H_{10} + e^- \longrightarrow B_3H_8^- + BH_2^+$$
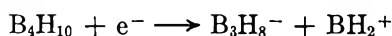
cannot be explained at this time and can only be resolved by further experimental and theoretical investigation.

Reese, Dibeler, and Mohler[9] have reported on the negative-ion spectrum of pentaborane, in which they observed the resonant attachment process for the parent ion. Although their relative intensities differ from those of this laboratory, such discrepancies may be attributed to the differing energies of the ionizing electrons in the two cases and do not appear surprising. Curiously, they do not report any of the lower fragments of pentaborane.

In conclusion, it is evident that the lower boron hydrides do form negative ions. Under favorable conditions, the abundance and lifetime of these ions may be great enough to warrant consideration in mass spectral, radiation, and gas-discharge phenomena.

(4) American Petroleum Institute Project 44, National Bureau of Standards No. 333 Mass Spectra Data, U. S. Government Printing Office, Washington, D. C., 1949.

(5) T. P. Fehlner and W. S. Koski, *J. Amer. Chem. Soc.,* **85,** 1905 (1963).

(6) American Petroleum Institute Project 44, National Bureau of Standards No. 334, Mass Spectra Data, U. S. Government Printing Office, Washington, D. C., 1949.

(7) T. P. Fehlner and W. S. Koski, *J. Amer. Chem. Soc.,* **86,** 2733 (1964).

(8) W. N. Lipscomb, "Boron Hydrides," W. A. Benjamin, Inc., New York, N. Y., 1963.

(9) R. M. Reese, V. H. Dibeler, and F. L. Mohler, *J. Res. Nat. Bur. Stand.,* **57,** 367 (1956).

Photolysis of Methylene Blue by a Giant-Pulse Ruby Laser

by Ikuzo Tanaka, Yuji Mori, Yoshisato Minagawa, and Eiichi Okutsu

Laboratory of Physical Chemistry, Tokyo Institute of Technology, Ohokayama, Meguro-ku, Tokyo (*Received December 19, 1967*)

Extensive studies of the photochemical reaction of methylene blue (MB) have already been reported.[1-4] The photoreduction of MB is accomplished through the interaction between the lowest triplet state of MB and the reducing agent. In the present paper, a giant-pulse ruby laser has been applied to the study of the photochemical reaction of MB, and as a result, it has

(1) R. M. Danziger, K. H. Bar-Eli, and K. Weiss, *J. Phys. Chem.,* **71,** 2633 (1967).

(2) S. Kato, M. Morita, and M. Koizumi, *Bull. Chem. Soc. Jap.,* **37,** 117 (1964).

(3) S. Matsumoto, *ibid.,* **35,** 1860 (1962).

(4) S. Matsumoto, *ibid.,* **37,** 491 (1964).

been shown that the excited triplet state of MB also plays an important role in the photoreduction owing to the exceedingly intense laser light.

The laser head is made by NEC in Japan. The ruby is 8 mm in diameter and its length is 150 mm. The Q switch consists of a solution of kryptocyanine in EtOH with a concentration of approximately 10^{-5} M. The cross-sectional area of the laser beam is about 0.25 cm². The giant pulse is a single pulse with a peak power of 5–8 MW and a half-width value of about 20 nsec. The output energy is about 150 mJ, which corresponds to 5.2×10^{17} photons. Some neutral filters whose per cent transmittances are calibrated for the laser light are used to reduce the light intensity. The cell used in this experiment has a 13-mm diameter and a length of 18 mm and is made of quartz. The quantum yield of photoreduction of MB in the presence of α-dimethylphenylglycine (DMPG) is known to be about 0.3. Althought other derivatives of N-phenylglycine or N-phenylalanine react in a way similar to DMPG, quantum yields in these cases are less than that of DMPG.[3] Dissolved O_2 is removed from the solution to prevent the oxidation of the reduced MB. Degassing of the sample is done by the use of an oil diffusion pump. In this experiment a buffer solution is used to keep pH at 8.0 because the quantum yield has a maximum value at pH 8. The quantity of the reduced MB is measured by the decrease of the optical density of the absorption peak of MB at 665 mμ. Using the values that the extinction coefficient of MB at 6943 Å is 10^4 and the length of the reaction cell is 18 mm, I_T/I_0 is calculated to be 0.66 for a 10^{-5} M solution, but more than 90% of the incident light is transmitted in the case of giant pulse as shown in Table I.

Table I[a]

I_0, mJ	I_T, mJ	I_T/I_0	
		Obsd	Calcd
101.0	98.0	0.97	0.66
45.0	42.8	0.95	0.66
4.4	3.9	0.89	0.66

[a] I_0, incident light and I_T, transmitted light. [MB] = 10^{-5} M.

As shown in Figure 1 in the region within 2% of the maximum intensity, the decrease of MB is proportional to the light intensity, but it deviates from the straight line in the region of higher laser-light intensity. These results suggest the fact that saturation of the laser-light absorption is realized when the concentration of the solution is 10^{-5} M.

Since the quantum yield for the reduction of MB in the absence of a reducing agent is negligibly small and the triplet state of MB has so long a lifetime as to be
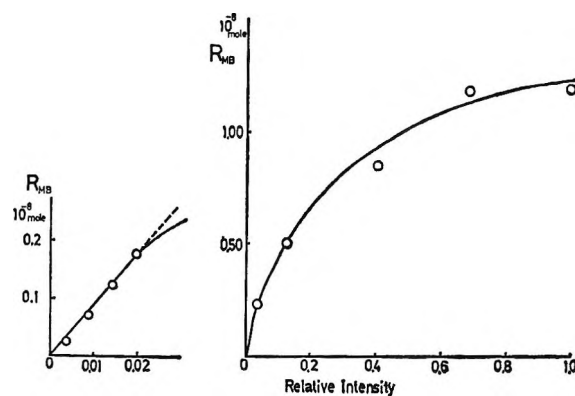

Figure 1. R_{MB} (the decrease of MB by five laser shots) vs. laser-light intensity, where the concentration of DMPG is 10^{-5} M.
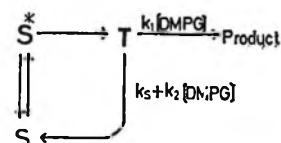

Figure 2. S, ground state of MB; S*, excited singlet state of MB; T, lowest triplet state of MB.

detected by the flash technique, the triplet state of MB reacts with DMPG predominantly.[5] Therefore, the mechanism shown in a simplified form in Figure 2 seems to be reasonable for the ordinary light. From this mechanism eq 1 can be derived.

$$A = T \frac{k_1[\text{DMPG}]}{(k_1 + k_2)[\text{DMPG}] + k_1} \tag{1}$$

where A is the quantity of the reduced MB and T is the total amount of MB converted to the triplet state. The following equation is derived from eq 1.

$$\frac{1}{A} = \frac{1}{T}\left\{\frac{k_s}{k_1}\frac{1}{[\text{DMPG}]} + \left(1 + \frac{k_2}{k_1}\right)\right\} \tag{2}$$

The reciprocal of the decrease of MB as a function of the reciprocal of the concentration of DMPG at various laser-light intensities is plotted in Figure 3. Equation 2 indicates that the reciprocal of the decrease of MB increases linearly with the reciprocal of the concentration of DMPG and also that the ratio of the intercept to the slope, $(k_1 + k_2)/k_s$, should be independent of the light intensity.

When the intensity is lowered to 4.4% of the maximum intensity, the value of $(k_1 + k_2)/k_s$ agrees with the experimental value for the ordinary light given by Matsumoto.[6] However, in the case of the maximum intensity, the experimental results requires k_1 to be a larger value, whereas k_1 should be independent of the

(5) G. Oster and N. Wotherspoon, J. Amer. Chem. Soc., **79**, 4836 (1957).

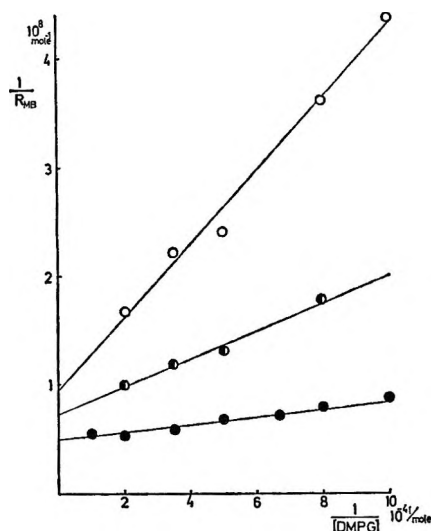(6) S. Matsumoto, Bull. Chem. Soc. Jap., **37**, 117 (1964), Table IV.

Figure 3. R_{MB} (the decrease of MB by five laser shots) vs. 1/[DMPG] (the reciprocal of the concentration of DMPG). The relative laser-light intensity is 1.00, 0.125, and 0.044 for ●, ◐, and ○, respectively.

light intensity. This inconsistency can be removed by considering the following mechanism. MB in the lowest triplet state absorbs the laser light during a pulse and is excited to an excited triplet state.[7] MB in this excited triplet state reacts with DMPG.[8] The possibility of the self-decomposition of MB in this excited triplet state should be excluded because of the fact that no decrease of MB can be detected in the absence of DMPG within experimental error. The rate of the process mentioned above is defined as k_3 [DMPG]. Therefore, the mechanism shown in Figure 4 is proposed. The S*–T intersystem crossing rate seems to be rapid enough to significantly populate the T level during the pulse. The laser flash produces T* and T such that,
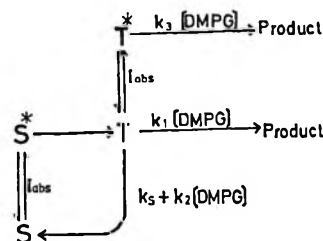

Figure 4. S, ground state of MB; S*, excited singlet state of MB; T, lowest triplet state of MB; T*, excited triplet state of MB.

at any given intensity, the ratio of the maximum amounts of these two species formed can be considered constant, i.e., (T*)/(T) = a. Considering the decay of T and T*, the differential equations, after integration and combination give

$$\frac{1}{A} = \frac{1}{T(1 + a)} \left\{ \frac{k_s}{k_1 + bk_3} \frac{1}{[DMPG]} + \left(1 + \frac{k_2}{k_1 + bk_3}\right) \right\} \quad (3)$$

where $b = \int (T^*) \, dt / \int (T) \, dt$ and a and b are the functions of the intensity. At low intensity $a \rightarrow 0$ and $b \rightarrow 0$, and the expression becomes identical with eq 2. It is understood by eq 3 that the slope of the line decreases at higher light intensity. At the highest intensity, the data indicate that $bk_3 \gg k_1$, and the limiting intercept with $k_2/(k_1 + bk_3) \approx 0$ is $[T(1 + a)]^{-1}$.

(7) The lowest triplet state shows absorption in the 7000-Å region, which corresponds to the transition between T and T*, as well as considerable absorption at lower wavelength (see ref 2 and 4).

(8) It does not seem to be important that multiphoton excitation of the substrate (DMPG) comes into play, since the substrate has no absorption band in the vicinity of 3470 Å.
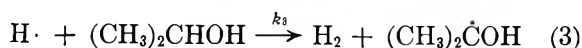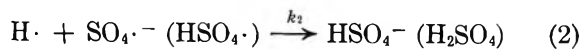
COMMUNICATIONS TO THE EDITOR

The Kinetics of the Reaction of Trapped

Hydrogen Atoms in Sulfuric Acid Glasses

Sir: We investigated the kinetics of the disappearance of trapped H atoms in a glassy matrix of 6 M H_2SO_4 in the absence and presence of isopropyl alcohol. The H atoms were produced by γ irradiation (^{60}Co, dose rate = 1.15 × 10^{16} eV/ml sec). In all experiments the concentration of H atoms was about 10^{-3} $M;$ the G(H) values were 2.3 and 0.9 in the absence and presence of

0.35 mol of 2-propanol, respectively. All measurements were carried out using an X-band esr spectrometer with a ruby crystal as the internal-cavity standard. The H atoms produced in the walls of quartz ampoules during irradiation were eliminated by using a technique described earlier.[1] The H atoms react according to

$$H \cdot + H \cdot \xrightarrow{k_1} H_2 \quad (1)$$
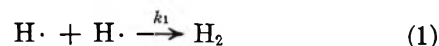
(1) K. Eiben and D. Schulte-Frohlinde, *Z. Phys. Chem.* (Frankfurt), **45**, 20 (1965).

$$H\cdot + SO_4\cdot^- (HSO_4\cdot) \xrightarrow{k_2} HSO_4^- (H_2SO_4) \quad (2)$$

$$H\cdot + (CH_3)_2CHOH \xrightarrow{k_3} H_2 + (CH_3)_2\dot{C}OH \quad (3)$$

In the absence of isopropyl alcohol, the H atoms disappeared completely at 90°K, while only 15% of the central part of the esr spectrum (attributed to $HSO_4\cdot$ or $SO_4\cdot^-$) diminished. Under these conditions most H atoms (approximately 85%) recombine *via* reaction 1 to yield H_2. Since reaction 2 is not very important compared with reaction 1, the kinetics should be second order. However, in the beginning the plot of $[H]_0/[H]$ *vs.* time (Figure 1) does not follow second-order kinetics. Since the ratio of the reactions 1 and 2 does not change with time, it can be ruled out that reaction 2 predominates in the initial period to cause the deviation obtained from the second-order kinetics.

Deviations of this kind have been explained by assuming an initial nonrandom distribution of the reacting species or different energetic depths of the traps in the matrix.[2,3] We show that under our experimental conditions, because of time-dependent rate constants, it is sufficient to assume an initial random distribution of the H atoms. Such a time dependence should always occur in a condensed system if the barrier for diffusion is greater than the barrier for reaction. In this case, the initial random distribution becomes nonrandom during the reaction with respect to the environment of every reacting particle. The result is a deviation from simple kinetic laws in the initial period. A mathematical treatment of this kinetic behavior was carried out by different authors.[4-6] We used the formula presented by Waite[6d] for an initial random distribution of the reacting particles

$$\frac{d[C_A]}{dt} = -\left(1 + \frac{r_0}{\sqrt{\pi Dt}}\right)4\pi r_0 D[C_A][C_B] \quad (4)$$

In formula 4, r_0 is the capture radius and D is the sum of the diffusion constants of both particles A and B. Following this formula, a straight line should be expected by plotting $\Delta_i([H]_0/[H])/\Delta_i t$ *vs.* $t^{-1/2}$. In fact, for the bimolecular reaction of H atoms, this equation is valid over the whole range of time, as can be seen from Figure 2.

Equation 4 can be applied also to a case of pseudo-first-order reaction.[6a] Approximately 82% of the H atoms react *via* reaction 3 in the presence of 0.35 mol of isopropyl alcohol in glassy 6 M H_2SO_4 at 77°K. In this case the disappearance of the H atoms should follow pseudo-first-order kinetics. Figure 1 shows that a straight line is not obtained by plotting log $[H]/[H]_0$ *vs.* t. Again, however, a plot of Δ_i log $([H]/[H]_0)/\Delta_i t$ *vs.* $t^{-1/2}$ yields a straight line over the whole range of time.

Equation 4 can be applied only if the reaction of the H atoms is diffusion controlled. Experiments with different scavengers show that this is indeed the case.
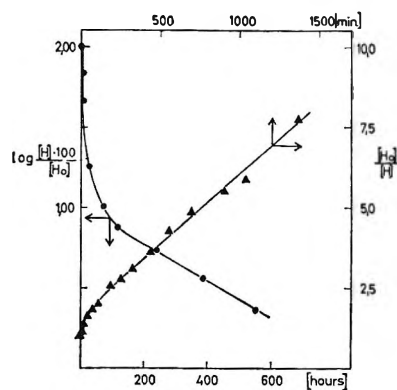

Figure 1. The disappearance of H· atoms in the absence (▲, 90°K) and presence (●, 77°K) of 0.35 mol of isopropyl alcohol.
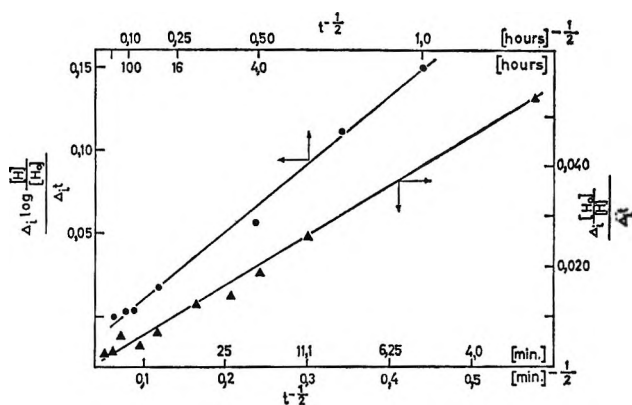

Figure 2. Data of Figure 1 using the diffusion-kinetic treatment.

At low temperatures the H atoms react with isopropyl alcohol or allyl alcohol in this matrix with the same rate constants. However, in the liquid phase in 0.8 M H_2SO_4 at 25° the H atoms react 35 times faster with allyl alcohol than with isopropyl alcohol, which shows that addition is preferable to abstraction. A similar conclusion can be made from the following fact. Regardless of the reaction mechanism (reaction 1 or 3), the activation energy measured for the disappearance of H atoms in glassy 6 M H_2SO_4 is the same (6.0 ± 0.2 kcal/mol) in the absence and in the presence of isopropyl alcohol.

A random distribution of trapped H atoms is in agreement with the dose dependence of esr relaxation

(2) V. N. Belevsky, L. T. Bugaenko, and V. B. Golubev, *Dokl. Akad. Nauk SSSR*, **168**, 122 (1966).

(3) J. M. Flournoy, L. H. Baum, and S. Siegel, *J. Chem. Phys.*, **36**, 2229 (1962); A. I. Mikhailov, Ya. S. Lebedev, and N. Ya. Buben, *Kinet. Katal.*, **6**, 48 (1965).

(4) M. V. Smoluchowski, *Z. Phys. Chem.* (Leipzig), **92**, 192 (1917).

(5) J. Yguerabide, M. A. Dillon, and M. Burton, *J. Chem. Phys.*, **40**, 3040 (1964).

(6) (a) T. R. Waite, *Phys. Rev.*, **107**, 463 (1957); (b) T. R. Waite, *ibid.*, **107**, 471 (1957); (c) T. R. Waite, *J. Chem. Phys.*, **28**, 103 (1958); (d) T. R. Waite, *ibid.*, **32**, 21 (1960).

published recently.[7] It was shown that most of the H atoms in this matrix are not trapped in a "spur."[7] Summarizing, we would like to emphasize that the occurrence of a rapid initial period and deviations from simple kinetics for bimolecular reactions in the condensed phase are not sufficient to postulate a nonrandom distribution of the reaction particles. In a forthcoming paper we shall show that this diffusion treatment provides an explanation of the socalled "stepwise" disappearance of trapped radicals in some cases.

(7) J. Zimbrick and L. Kevan, *Nature*, 214, 693 (1967).

INSTITUT FÜR STRAHLENCHEMIE   K. VACEK
KERNFORSCHUNGSZENTRUM,   D. SCHULTE-FROHLINDE
KARLSRUHE, WEST GERMANY
        ACCEPTED AND TRANSMITTED BY THE FARADAY SOCIETY
                    (NOVEMBER 30, 1967)

On the Purported Infrared Absorption at 21 μ of Carbon Monoxide Adsorbed on Silica-Supported Platinum

Sir: The purpose of this letter is to draw attention to the fact that the reported[1] infrared absorption at 476 cm^{-1} of carbon monoxide adsorbed on silica-supported platinum is an artifact. As alluded to in the article by Clarke, *et al.*,[1] the silica disks, even very thin, absorb very strongly in the region 400–1200 cm^{-1}. The 5% transmission at 475 cm^{-1} of the clean disk at room temperature may result from several causes. Apart from such probably dismissory effects as spectrometer stray light or incomplete blocking of the sample beam by the sample disk, the most probable reason for the apparent transmission is the emission of the sample slightly heated above the detector temperature by the undispersed radiation from the spectrometer source. The best confirmation of this mechanism is the apparent increase of transmission when the sample is deliberately heated to 250°. As silica is a strong absorber of radiation of 475 cm^{-1}, it will also be a strong emitter at this frequency. The effects of the apparent transmission change when carbon monoxide is admitted to the sample cell are related to the emissivity of the sample and cannot be directly related to absorption by the Pt–CO groups. Also, the temperature of a sample of small thermal conductivity is itself dependent on its emissivity. The particularly weak nature of the apparent absorption recorded by Clarke, *et al.*,[1] would imply that emission by the supposed Pt–CO groups would also be weak. The breadth of the presumed absorption (about 50 cm^{-1} at half height) provides another clue to the spurious nature of this absorption, as bands observed for carbon monoxide adsorbed on various substrates are generally much narrower. In fact, the

477-cm^{-1} band in the spectrum of Garland, *et al.*,[2] is by Clarke, *et al.*,[1] referred to as being relatively sharp. The large slit width used should still not obscure entirely any fine structure that might be spread over 50 or 70 cm^{-1}. Therefore, any deductions drawn from the position of the spurious 476-cm^{-1} band[1] are unfounded: of course, these criticisms do not specifically apply to spectra of other investigators. Whether or not the purported decrease in transmission[1] is in fact a real decrease in emission due to the adsorbed carbon monoxide remains to be proved by the obtaining of less doubtful spectral changes (*i.e.*, more intense difference spectra) concomitant with admission of carbon monoxide to the sample cell.

The emission from samples in the far-infrared (<700 cm^{-1}) is a common problem in spectroscopy, but one which can frequently be overcome by chopping the radiation between the source and the sample and not between the sample and the detector, as is not the practice in the Grubb–Parsons Spectromaster instrument.[1] A much more likely method of increasing, in some spectral regions, the transmittance of the silica samples would be to cool them near liquid nitrogen temperature.

(1) J. K. Clarke, G. M. Farren, and H. E. Rubalcava, *J. Phys. Chem.*, 72, 327 (1968).
(2) C. W. Garland, R. C. Lord, and P. F. Troiano, *ibid.*, 69, 1188 (1965).

DEPARTMENT OF CHEMISTRY   J. F. OGILVIE
MEMORIAL UNIVERSITY OF NEWFOUNDLAND
ST. JOHN'S, NEWFOUNDLAND, CANADA
                RECEIVED FEBRUARY 16, 1968

Infrared Absorption at 21 μ of Carbon Monoxide Adsorbed on Silica-Supported Platinum

Sir: Ogilvie[1] is mistaken in contending that we have erred in our interpretation of the 21-μ absorption of carbon monoxide adsorbed on silica-supported platinum.[2] At the outset, the possible artifacts arising from experimental procedures mentioned, *viz.*, stray light or faulty sample placement, can indeed be dismissed; normal precautions were taken to exclude such errors. Further, in recognition of Kirchoff's law, both sample spectra and backgrounds were obtained at the same temperature, which procedure would compensate for temperature-dependent optical effects of the substrate.

Ogilvie correctly states that a strong absorber is a strong emitter. Thus carbon monoxide adsorbed on the platinum would increase the emissivity of the disk in the vicinity of 470 cm^{-1}. If the disk had been

(1) J. F. Ogilvie, *J. Phys. Chem.*, 72, 2688 (1968).
(2) J. K. A. Clarke, G. M. Farren, and H. E. Rubalcava, *ibid.*, 72, 327 (1968).

virtually totally opaque, the increase in emissivity would have caused more light to fall on the detector. However, every separate experimental sequence which contributed to our published spectrum showed that less light fell on the detector when carbon monoxide was proved, by its 5-μ absorption, to be present. Therefore, it is quite clear that the radiation emanating from the disk was predominantly transmitted rather than emitted, and that the decrease in radiation incident on the detector when carbon monoxide was present as adsorbed species was largely due to absorption by the surface species. Furthermore, the relevance of Ogilvie's reference to strong silica absorption near 475 cm^{-1} is far from clear since he does not specify the conditions under which the datum was obtained. The relevant background spectrum is that of a very dry Cabosil disk under the conditions specified in our paper, not any other.

There is no basis for Ogilvie's suggestion that the low-frequency band should have a half-width similar to that of the high-frequency band. That the 470-cm^{-1} band should be wider than that near 2100 cm^{-1} is to be expected because the energy of the low-frequency level is much nearer to that of the platinum lattice modes than is the energy of the high-frequency level. Consequently, the low-frequency transition, which involves levels with a greater admixture of the low-lying lattice modes than does the high-frequency transition, will appear as an extra broad band.[3] Our spectrum is in accord with this, as are the pertinent spectra in the references cited in our paper.

The appearance of a band near 476 cm^{-1} due to adsorbed carbon monoxide is fully in accord with the results of earlier investigations: references 5 and 8 of our paper[2] report far-infrared absorption of carbon monoxide adsorbed on platinum, the former at 477 cm^{-1} and the latter at 476 cm^{-1}. Recently (after our paper was submitted for publication), Smith and Eckstrom[4] have reported a band at 460 cm^{-1} due to carbon monoxide adsorbed on nickel.

It appears necessary to reemphasise that the main conclusion stated in our paper concerns the relation between derived force constants and bond properties of adsorbed carbon monoxide. Not only does this conclusion apply to three separate investigations, but, as we explicitly stated, it holds even for relatively large changes in the value used for the position of the low-frequency band.

(3) Ogilvie quotes out of context our use of the expression "relatively sharp" for the 477-cm^{-1} band of Garland, et al.

(4) W. H. Smith and H. C. Eckstrom, paper read at the 9th European Congress on Molecular Spectroscopy, Madrid, Sept 1967.

(5) To whom correspondence regarding this communication should be addressed.

DEPARTMENT OF CHEMISTRY   J. K. A. CLARKE
UNIVERSITY COLLEGE   G. M. FARREN
DUBLIN 4, IRELAND   H. E. RUBALCAVA[5]

The Nature of Sites Formed on Zeolites by Addition of Water

Sir: Recent studies of zeolites have shown that small amounts of water enhance the catalytic activity.[1-3] The increased activity could be due to the interaction of water with the cation to yield $M^{n+}OH_2$ or $M^{n+}OH$ which function as protonic acid centers, where M is a mono-, di-, or trivalent cation.[4,5]

We have studied the infrared spectrum of chemisorbed pyridine[6] and of the structural hydroxyl groups of X and Y zeolites containing Na, Mg, Ca, and rare earth cations. The effects of water on the spectra have yielded interesting results. Pressed wafers of zeolite weighing about 0.05 g and 1 in. in diameter were used. Spectra were recorded on a Cary-White 90 spectrometer with a spectral slit width of 3 cm^{-1}. After calcination *in vacuo* for 6 hr at 450°, spectra of NaX or NaY show no structural hydroxyl groups. On chemisorption of pyridine, no band near 1545 cm^{-1} which could be attributed to the presence of protonic acid sites is observed.[6] As previously reported, addition of a small amount of water produces neither structural hydroxyl groups nor protonic acid sites.[7,8]

In marked contrast, after dehydration at 450°, Mg and CaY exhibit bands due to structural hydroxyl groups, similar to those found by previous workers.[7,9] For CaY, additional bands are observed at 3688 (AlOH groups?) and 3585 cm^{-1} (Figure 1a). On addition of pyridine and subsequent removal by evacuation at 250°, the pyridine only interacts with the 3642-cm^{-1} band (Figure 1b), and a band at 1545 cm^{-1}, and bands between 3300 and 2900 cm^{-1} characteristic of pyridinium ions,[6,7] due to pyridine adsorbed on protonic acid sites, are observed. A distinct band at 3530 cm^{-1} is also observed. On addition of water and subsequent evacuation at 150°, discrete absorption frequencies are observed at 3638, 3585, and 3530 cm^{-1} (Figure 1c). The usual water bending vibration at 1635 cm^{-1} was detected. In contrast to the initial spectrum, the 3585-cm^{-1} band is 5 times as intense as the 3638 cm^{-1}, suggesting a particular type of hydroxyl group is formed preferentially on hydration in the presence of pyridine. To see if the 3585-cm^{-1} band represents acidic hydroxyl groups, more pyridine was added. No interaction of the 3585-cm^{-1} band with

(1) H. W. Habgood and Z. M. George, Society of Chemical Industry Conference on Molecular Sieves, London, 1967.

(2) P. B. Venuto, L. A. Hamilton, and P. S. Landis, *J. Catal.*, **5**, 484 (1966).

(3) H. A. Benesi, *ibid.*, **8**, 368 (1967).

(4) A. E. Hirschler, *ibid.*, **2**, 428 (1963).

(5) L. Bertsch and H. W. Habgood, *J. Phys. Chem.*, **67**, 1621 (1963).

(6) E. P. Parry, *J. Catal.*, **2**, 371 (1963).

(7) P. E. Eberly, *J. Phys. Chem.*, **72**, 1042 (1968).

(8) J. W. Ward, *J. Catal.*, **10**, 34 (1968).

(9) C. L. Angell and P. C. Schaffer, *J. Phys. Chem.*, **69**, 3463 (1965).
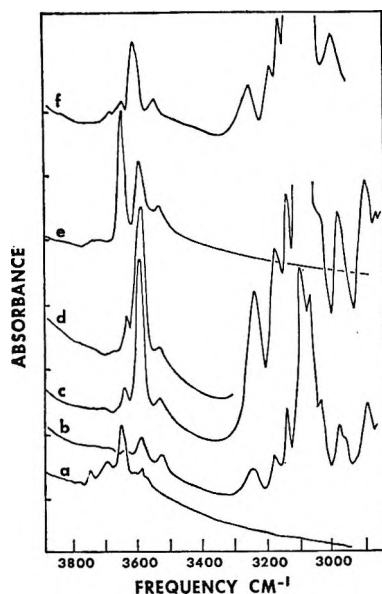
Figure 1. Spectra of calcium Y zeolite: a, zeolite calcined at 450° under vacuum; b, pyridine adsorbed and evacuated at 250°; c, water added and evacuated at 250°; d, further pyridine added and evacuated at 250°; e, water adsorbed on (a) and evacuated at 250°; f, pyridine adsorbed after (e) and evacuated at 250°.

the pyridine was observed at ambient or elevated temperature (Figure 1d). To further investigate the nature of the 3585-cm^{-1} band, a small amount of water was added to a second calcined CaY zeolite sample, with the results shown in Figure 1e. Both the 3642 and 3585 cm^{-1} increased in intensity by a factor of 3 compared with the dehydrated zeolite. The 3642-cm^{-1} band is about 1.5 times as intense as the 3585 cm^{-1}. On chemisorption of pyridine (Figure 1f) the 3585-cm^{-1} band was unaffected while the 3642-cm^{-1} band was decreased to 0.125 times its original intensity. Similar results were found with MgY, except the band appeared at 3595 cm^{-1} on water addition.

The results indicate that the 3642-cm^{-1} band type of hydroxyl groups are acidic, while the 3585 (3595)-cm^{-1} type are non acidic. By comparison with hydrogen Y zeolite, the 3642-cm^{-1} band probably represents the acidic SiOH groups.[6-8,10] The addition of water probably follows the previously proposed scheme[2,8,10]

$$MOH_2^{2+}$$

$$O \diagdown Si \diagup O \diagdown Al \diagup O \diagdown Si \diagup O \diagdown Al \diagup O \rightleftharpoons$$

$$MOH^+ \qquad H$$
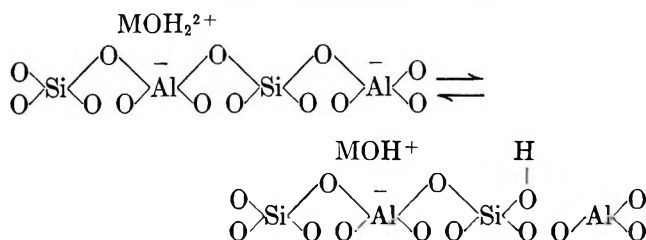
Whereas the proton from the adsorbed water can react directly with the lattice to give the 3642-cm^{-1} band type of hydroxyl group, in the presence of pyridine, it either reacts directly with the pyridine to give

pyridinium ion or reacts first with the lattice and is then rapidly transferred to the pyridine.

Because of its formation simultaneously with the 3642-cm^{-1} band and its variation in frequency with cation, the band near 3585 (3595) cm^{-1} is considered to represent the hydroxyl groups associated with the cation. If this is so, these observations show that this type of hydroxyl group is nonacidic (or possibly very weakly acidic) and hence unlikely to be important active centers for reactions involving carbonium ion mechanisms.

The results are supported by observations on sodium and rare earth zeolites. The absorption band near 3520 cm^{-1} in the spectra of rare earth zeolites has been attributed to hydroxyl groups associated with the cation.[11] Studies of the adsorption of pyridine showed these groups also to be nonacidic. In the spectra of NaY zeolites the band at 3694 cm^{-1} due to the MOH$_2$ groups is also nonacidic. Hence it appears that the increase of catalytic activity is due to the increase in population of the 3642-cm^{-1} type of hydroxyl groups which have been suggested as active centers previously[8] rather than hydroxyl groups associated with the cation, although the role of the MOH$^+$ type of hydroxyl groups as active centers cannot be completely ruled out at this time.

Further details of these observations and the influence of water on zeolite acidity will be reported later.

(10) W. K. Hall, *Chem. Eng. Progr. Symps. Ser.*, **63**, 68 (1967).

(11) J. A. Rabo, C. L. Angell, P. H. Kasai, and V. Schomaker, *Discussions Faraday Soc.*, **41**, 328 (1966).

UNION OIL COMPANY OF CALIFORNIA   JOHN W. WARD
UNION RESEARCH CENTER
BREA, CALIFORNIA 92621

The Spectra of Polyene–Iodine Complexes[1]

Sir: Lupinski has reported that iodine forms a complex with β-carotene.[2] As the complex forms, a new, narrow, intense absorption band appears at 1000 mμ which develops at the expense of the original polyene absorption. Two molecules of iodine are needed for the complex, and they add in such a fashion as to form this species [C$_{40}$H$_{56}$I]$^+$I$_3^-$. Lupinski postulates that the cation can be either carbonium ion or charge transfer in character. He concludes that the absorption band at 1000 mμ is attributable to charge transfer. In a recent letter, Ebrey suggested that the new band might be explained in terms of a shift in absorption maximum

(2) J. H. Lupinski, *J. Phys. Chem.*, **67**, 2725 (1963).

of β-carotene rather than a charge-transfer band.[3] He suggests that if the β-carotene–iodine complex is treated as a polymethine, its λ_{max}, calculated by FEMO, should occur at 1100 mμ.[4,5] It was also indicated that one test would be to examine the spectra of other polyene–iodine complexes and see if the observed wavelength agrees with the one predicted from FEMO calculations on a symmetrical polymethine. We have determined the spectrum of the iodine complex of the polyene anhydroretinol (1)[6] and report our findings here.

The iodine complex of anhydroretinol is relatively unstable at room temperature, and in order to obtain suitable spectra, samples were examined at $-27°$ by the following procedure. Required amounts of anhydroretinol and iodine were dissolved in purified, dry 1,2-dichloroethane[7] and allowed to cool to $-27°$. After cooling, the samples were rapidly mixed, inserted in a low-temperature cell holder along with a solvent reference and placed in a Beckman DK-2A double-beam spectrophotometer.

The spectrum of anhydroretinol in 1,2-dichloroethane at $-27°$ (Figure 1) shows fine structure with three separate bands which have λ_{max} values of 404, 382, and 361 mμ. Based on the absorbance of the 382 mμ peak, the half band width is about 4000 cm^{-1}. The spectrum of the resulting iodine complex is shown in Figure 2. In this spectrum, absorption at 492 mμ is attributable to iodine, whereas absorption at 630 mμ is attributable to the anhydroretinol–iodine complex. The half band width of the complex has decreased from about 4000 cm^{-1} to about 2000 cm^{-1}. The complexed species can be formulated in the following manner, where x may be either 1 or 3.[2]
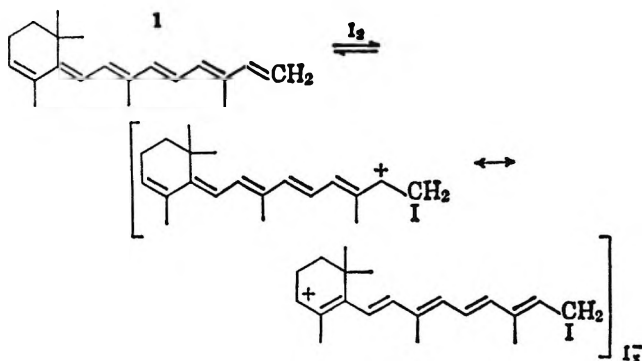
This conclusion is substantiated by comparison of these data with those for protonated anhydroretinol.[8] The proton was shown to add to the polyene in such a manner as to form a pentaenylic cation similar to the one shown here. The cation, formed in butanol–sulfuric acid at low temperature, has a λ_{max} value of 607 mμ and a half band width of about 2000 cm^{-1}. These values are in good agreement with those reported here for the anhydroretinol–iodine complex.

The wavelength of maximum absorption of the polyene–iodine complex can be calculated from the simple
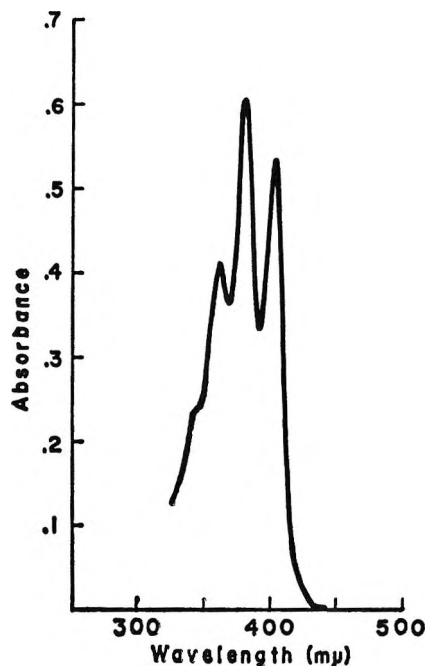

Figure 1. Anhydroretinol (1.5 $\times$ 10^{-5} mmol/ml) in 1-cm quartz cells at $-27°$.
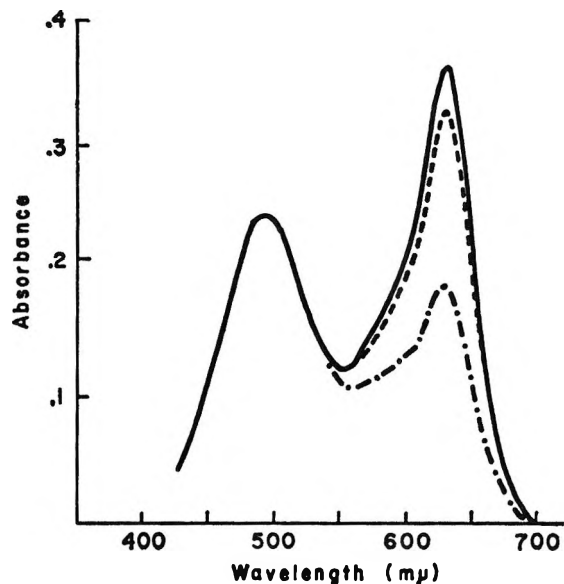
Figure 2. Anhydroretinol (4 $\times$ 10^{-5} mmol/ml plus I$_2$ 17 $\times$ 10^{-5} mmol/ml) in 1,2-dichloroethane in 1-cm Pyrex cells at $-26°$. — · — · —, 34 sec; ———, 174 sec; and — — — —, 319 sec after mixing.

formula $\lambda = 50(n)$, derived from FEMO considerations by Platt, where n is the number of carbon atoms in the

(3) T. G. Ebrey, *J. Phys Chem.*, 71, 1963 (1967).

(4) H. Kuhn, *J. Chem. Phys.*, 17, 1198 (1949).

(5) J. R. Platt, *Science*, 129, 372 (1959).

(6) E. M. Shantz, J. D. Cawley, and N. D. Embree, *J. Amer. Chem. Soc.*, 65, 901 (1943).

(7) L. F. Fieser, "Experiments in Organic Chemistry," 3rd ed, D. C. Heath and Co., Boston, Mass., 1955, p 288.

(8) P. E. Blatz and D. L. Pippert, *J. Amer. Chem. Soc.*, 90, 1296 (1968).

conjugated double bond sequence of the parent polyene. For a carotene with 11 double bonds, the λ_{max} of the complex is predicted to be 1100 mμ. For anhydroretinol with six double bonds, the λ_{max} of the complex is calculated to be 600 mμ. Consequently, the experimentally determined λ_{max} value of the iodine complex of anhydroretinol is in good agreement with a similar species obtained from protonation of anhydroretinol and also a calculated value from FEMO considerations. This evidence supports the suggestion of Ebrey that the new band might be explained in terms of a shift in absorption of the polyene band.

Department of Chemistry   P. E. Blatz
University of Wyoming   N. Baumgartner
Laramie, Wyoming 82070   S. Dewhurst

Received April 19, 1968

The Existence of Homogeneous

Oscillating Reactions

Sir: The communication entitled, "Homogeneous Periodic Reactions," by Shaw and Pritchard[1] contains a number of errors which we feel need correction. It is stated in the communication that two reactions which oscillate in homogeneous phase are known. It appears that the oscillating reaction of ceric ions, bromate, and malonic acid[2-4] and the oscillating reaction in the glycolytic pathways in cell free extracts of yeast[5] or heart muscle[6] have escaped the attention of Shaw and Pritchard. These authors also give a secondary reference to the explanation of the oscillations in cool flame combustion of hydrocarbons which was originally proposed by Day and Pease.[7] In their restatement of this explanation they miss the important point that the reaction is a branched-chain reaction, *i.e.*, an autocatalytic reaction. The negative temperature coefficient alone cannot lead to oscillations. It should also be mentioned that analogous oscillations are found in the gas-phase oxidation of hydrogen sulfide.[8]

Shaw and Pritchard also report some experiments on the oscillating reaction of hydrogen peroxide and iodate. We assume that they have not used periodate as they write; at least Bray[9] did not. They claim in italics that the exclusion of daylight suppressed the oscillation. It is possible that such an effect can be observed under their conditions. However, that the oscillations can readily occur in the dark has been demonstrated by one of us,[10] who studied this oscillating reaction spectrophotometrically, the only light present being the weak measuring beam. Though not reported, it was found that turning off the measuring light for a period of time did not produce any phase shift of the oscillation. Apparently, the oscillation went on in darkness

and the measuring light did not influence the reaction to any measurable degree. Since the oscillation was also found when Na_2O_2 or distilled H_2O_2 was used, the inhibitor added to commercial hydrogen peroxide can be disregarded in connection with the mechanism of the oscillation. The very high reproducibility of the oscillation also rules out any critical influence of dust contamination.[11] The additional finding that the oscillation does not depend on stirring would appear to rule out heterogeneous reactions. If the reaction were heterogeneous, there would have to be concentration gradients of reactants at the surface where the reaction takes place. Such gradients would be strongly influenced by stirring, and the time course of the reaction would depend on stirring. It may also be noted that stirring does not affect the oscillatory kinetics of the glycolytic intermediates in heart muscle extract.

Shaw and Pritchard's theoretical comments are misleading, to say the least. In his treatise, Bak[12] demonstrated that open or closed systems composed of only first-order reactions have real eigenvalues due to the condition of microscopic reversibility; such systems can exhibit only overshoot and undershoot phenomena in the approach to the stationary or equilibrium state. Bak also demonstrated that systems composed of only pseudo-first-order reactions could have complex eigenvalues leading to a damped oscillation in the approach to the stationary state. For general types of reaction schemes (*i.e.*, involving second-order reactions), Prigogine[13] has demonstrated that the equilibrium state for a closed system has real eigenvalues and consequently oscillations cannot occur in the neighborhood of the equilibrium state. However, this result cannot be extrapolated to the behavior of the system in the large, that is when the initial concentrations are far from the equilibrium concentrations. It is only within the past year that a satisfactory proof has been given that indefinitely sustained oscillations cannot occur in a closed system.[14,15] Nevertheless, both experiment and theory show clearly that closed homogeneous systems may

(1) D. H. Shaw and H. O. Pritchard, *J. Phys. Chem.*, **72**, 1403 (1968).
(2) B. P. Belousov, *Sb. ref. radiats. med. za 1958, Medgiz, Moscow,* 1959.
(3) A. M. Zhabotinskij, *Biofizika*, **9**, 306 (1964).
(4) H. Degn, *Nature*, **213**, 589 (1967).
(5) K. Pye and B. Chance, *Proc. Natl. Acad. Sci. U. S.*, **55**, 888 (1966).
(6) R. Frenkel, *Arch. Biochem. Biophys.*, **115**, 112 (1966).
(7) R. A. Day and R. N. Pease, *J. Amer. Chem. Soc.*, **62**, 2234 (1940).
(8) H. W. Thompson, *Nature*, **127**, 629 (1931).
(9) W. C. Bray, *J. Amer. Chem. Soc.*, **43**, 1262 (1921).
(10) H. Degn, *Acta Chem. Scand.*, **21**, 1057 (1967).
(11) F. O. Rice and M. Reiff, *J. Phys. Chem.*, **31**, 1352 (1927).
(12) T. A. Bak, "Contributions to the Theory of Chemical Kinetics," W. A. Benjamin, Inc., New York, N. Y., 1963.
(13) I. Prigogine, "Thermodynamics of Irreversible Processes," John Wiley and Sons, Inc., New York, N. Y., 1955.
(14) D. Shear, *J. Theoret. Biol.*, **16**, 212 (1967).
(15) J. Higgins, *ibid.*, in press.

exhibit prolonged series of oscillations, before approaching the final equilibrium state. This is due to the fact that a complex system will typically pass through a sequence of nearly stationary states in the approach to the equilibrium state.[16] As recognized by Prigogine,[13] indefinitely sustained oscillations can occur in open systems. For example, if hydrogen peroxide were supplied at a suitable constant rate, the oscillation would persist indefinitely in the hydrogen peroxide–iodate system.

As long ago as 1920, Lotka[17] proposed a reaction mechanism based on the law of mass action which could exhibit oscillations. Recent theoretical developments have dealt with the general requirements for oscillatory behavior in a chemical reaction scheme.[18–20] The simplicity of these requirements has led to the development of a wide variety of reaction schemes, based on known types of reactions, which can give rise to oscillatory kinetics without introducing any heterogeneous effects. In computer studies, qualitative reproduction of experimental results for the glycolytic system[18] and the hydrogen peroxide–iodate[21] system have been obtained.

While the mechanism of the hydrogen peroxide–iodate reaction may be complex, we believe that the heterogeneous and photochemical effects are so subtle that they can be ignored with regard to the mechanism of the oscillation. In our view, that reaction and the others mentioned are excellent examples of homogeneous reactions which can exhibit prolonged oscillations in closed homogeneous systems.

(16) J. Higgins in "Control of Energy Metabolism," B. Chance, R. W. Estabrook and J. R. Williamson, Ed., Academic Press, New York, N. Y., 1965.

(17) A. J. Lotka, J. Amer. Chem. Soc., 42, 1595 (1920).

(18) J. Higgins, Ind. Eng. Chem., 59, 18 (1967).

(19) E. E. Sel'kov in "Symposium on Oscillating Processes in Biological and Chemical Systems," Nauka, Moscow, 1967.

(20) R. A. Spangler and F. M. Snell, J. Theoret. Biol., 16, 381 (1967).

(21) P. Lindblad and H. Degn, Acta Chem. Scand., 21, 791 (1967).

JOHNSON FOUNDATION   H. DEGN
UNIVERSITY OF PENNSYLVANIA   J. HIGGINS
PHILADELPHIA, PENNSYLVANIA   19104

Homogeneous Periodic Reactions

Sir: Degn and Higgins[1] are indeed correct that we[2] accidentally ascribed periodic behavior to the reaction between periodate and peroxide; in fact, we used iodate as described by Bray. We too studied the reaction in a spectrophotometer, but in our instrument the cell space was too small for effective mechanical stirring.

Instead, we used streams of O_2 or N_2 and found that at low flow rates, the oscillatory behavior persisted; however, using rapid flows, we appeared to suppress the oscillations. We concluded that there was probably a periodic buildup in opacity due to bubble formation followed by sudden effervescence, masking any genuine variations in iodine concentration. Unfortunately, the work of Degn[3] escaped our attention, since it was published after we had completed these experiments.

Many theoretical reaction schemes[4] have been put forward in the past to account for periodic behavior. It is well known that some of these do not conserve particles (e.g., scheme I of ref 4 where the over-all reaction is the creation of B + C out of nothing); others conserve particles, but include creation (A → A + A) or annihilation (A + B → B) reactions. We have difficulty in envisaging how such processes can be microscopically reversible when they take place at the molecular level in a homogeneous phase and in a closed system (but accept that they may have symbolic relevance to heterogeneous and/or open systems). From our own work[5] on the Master Equation, we have learned that unless meticulous attention is paid to conservation of particles and of energy and to microscopic reversibility, spurious oscillatory or divergent behavior usually results in either the concentrations, or the total entropy, or both. Since it is always possible to symmetrize the Master Equation for a closed system, even when nonlinearities are present,[5] the eigenvalues are necessarily real throughout the process; these eigenvalues will be time dependent, but this effect cannot lead to sustained oscillation once any initial transients have died out.

Finally, it is clear that the evolution of a gas (either O_2 in the iodate–peroxide reaction, or CO_2 in the ceric–bromate–malonate system[6]) cannot in any case be regarded as homogeneous when considered from the point of view of microscopic reversibility—the reverse process must involve at least one heterogeneous step; basically, if one wants to regard the system as homogeneous, it must also be considered open—otherwise one has to regard it as a closed system (i.e., liquid plus vapor), in which case it is heterogeneous.

(1) H. Degn and J. Higgins, J. Phys. Chem., 72, 2692 (1968).

(2) D. H. Shaw and H. O. Pritchard, ibid., 72, 1403 (1968).

(3) H. Degn, Acta Chem. Scand., 21, 1057 (1967).

(4) P. Linbald and H. Degn, ibid., 21, 791 (1967).

(5) V. A. LoDato and H. O. Pritchard, "The Master Equation for the Dissociation of a Dilute Diatomic Gas," in preparation.

(6) H. Degn, Nature, 213, 589 (1967).

C.R.E.S.S.   D. H. SHAW
YORK UNIVERSITY   H. O. PRITCHARD
TORONTO, CANADA

Comment on "A Low-Temperature, High-Pressure Hydrate of n-Tetrabutylammonium Halides"

Sir: In a recent paper, Horne and Young[1] reported the formation of a hydrate of n-Bu$_4$NBr under high pressures, having a very low guest to host molar ratio ($\sim$1:530). They pointed out that the abrupt increase in the resistance of a 0.1 M solution of n-Bu$_4$NBr with increase of pressure could be due to a clathrate formation and not due to the freezing of the solvent since the equilibrium freezing point of the solution was much lower than the temperature at which the solid separated. Primarily, the possibility of the formation of a clathrate with such a low guest to host molar ratio seems remote since this composition would leave many of the cages in the host structure unfilled, thereby making the clathrate itself unstable (if it were to form at all) under the high pressures involved. The existence of many void spaces will tend to collapse the structure under high pressure. This will be evident if the composition and stability of the clathrates of tetra-n-butyl ammonium salts which were studied[2] in detail are considered. The steric requirements for the guest molecules and the host structure make it imperative that for maximum stability of the clathrate, most (if not all) of the polyhedral cages in the host network must be occupied by the guest molecules. It is our contention that in such a situation it is unlikely that a clathrate is formed under the experimental conditions.[1] On the other hand, there are reasons to believe that the solid that separates is just some polymorph of ice.

Evans,[3,4] while studying heterogeneous ice nucleation under pressure and in salt solution, finds that organic compounds which promote the nucleation of ice in supercooled water nucleate ice more effectively when the hydrostatic pressure is increased. He attributes this characteristic to the special thermodynamic properties of the monolayer of water in contact with the organic surface. Studying a variety of nucleators, he observes[4] that "under high pressure or in presence of dissolved salt the monolayer crystallizes at a temperature above the equilibrium freezing point of the bulk liquid phase and having crystallized, the monolayer provides a better substrate for the nucleation of bulk ice than does the original organic surface." Extensive measurements[4] on the freezing of water in the presence of phloroglucinol dihydrate under the influence of high pressure indicate that a monolayer of ice surrounding the organic nucleator becomes more crystalline with increase of pressure and since a "well crystallized" monolayer should prove to be a good nucleator for bulk ice, the supercooling required to freeze the solvent should decrease as the pressure is increased. It is found to be so;[4] the supercooling required at 1500 bars is zero whereas at atmospheric pressure it is 6.5°. This

does not indicate straightaway that the equilibrium freezing point would shift upward above 0°, but the studies[4] do indicate that the crystallinity of the monolayer persists ("memory effect"[3]) up to 0 ± 1°. Since the monolayer is responsible for the nucleation of bulk ice, it is not surprising if even at 0° bulk nucleation of ice occurs, since solutes like n-Bu$_4$N$^+$ salts which are strong "structure-makers" would help preserve the monolayer even at a temperature greater than 0°, depending on the efficiency of the salt. The thermodynamic instability of icebergs renders them highly sensitive to pressure and temperature. Inasmuch as the volume changes associated with the formation and melting of icebergs are considerable, temperature and pressure changes would be expected to influence chemical and biological processes at the solid–liquid interface.

It is reported[1] that the melting pressure and solidification pressure at a particular temperature are not the same. This is in accord with the observation of Evans[4] that if after melting the temperature is increased to >0°, the original supercooling is required to freeze the solution at the same pressure. In other words, after melting the solid solvent and heating it to a temperature beyond which the monolayer is unstable, extra pressure is required to freeze the solvent at the same temperature or a lowering of temperature is needed at the same pressure in order to facilitate the formation of monolayer which would further nucleate bulk ice. It is reasonable to expect the solvent to freeze out at a higher temperature if the pressure is very high since monolayer formation is dependent on the hydrostatic pressure.

More work on similar lines under higher pressures needs to be done with solutes like, for example, n-Pr$_4$N$^+$ salts which are structure-makers but for which no clathrate has so far been isolated in order to understand the nature of the solid that separates under high pressure. It would be very much revealing if a high-pressure X-ray analysis were done on the solid[1] that separates out.

(1) R. A. Horne and R. P. Young, *J. Phys. Chem.*, **72**, 376 (1968).

(2) (a) R. K. McMullan, M. Bonamico, and G. A. Jeffrey, *J. Chem. Phys.*, **39**, 3295 (1963); (b) G. Beurskens, G. A. Jeffrey, and R. K. McMullan, *ibid.*, **39**, 3311 (1963).

(3) L. F. Evans, *Nature*, **213**, 384 (1967).

(4) L. F. Evans, *Trans. Faraday Soc.*, **63**, 3060 (1967).

DEPARTMENT OF CHEMISTRY   S. SUBRAMANIAN
INDIAN INSTITUTE OF TECHNOLOGY
KANPUR, INDIA

The Pressure Dependence, Specific Volume, and Suggested Structure of Hydrophobic Hydration

Sir: In our paper on a high-pressure hydrate of n-tetrabutylammonium halides,[1] we do not draw the

conclusion ascribed to us by Subramanian,[2] namely, that the hydrate, if a clathrate, has a low guest to host ratio. On the contrary, the stability of this hydrate under pressure, the electrically conductive properties of solution permeated solids[3] and of aqueous tetraalkylammonium halide solutions[4] under pressure, and the partial molar volumes of the tetraalkylammonium cations in aqueous solution[5] all point to the conclusion that hydrophobic hydration such as that enveloping the n-tetrabutylammonium cation represents a low specific volume type of water structure. This in turn implies that, in order to achieve high density, if the structure is of a clathrate type, then the cages in the host structure surrounding the cations must be filled with one or more water molecules. Also the structure cannot be that of the ordinary hexagonal ice-I, a high specific volume form.

If the structure is not ice-like, there is no reason to expect it to facilitate ice formation in the bulk solution. Furthermore the nucleation of supercooled water is a rate, not an equilibrium phenomenon, and examination of Bridgman's phase diagram for water[6] shows that there are no stable forms in the temperature and pressure range of the experiments in question.

Thus we feel that some explanation other than the nucleation of ice-I must be proposed in explanation of Evans' results,[7,8] but we most heartily agree that, in view of the biological significance of the structure involved, further studies, such as X-ray examination, of these structures should prove to be worthwhile.

(1) R. A. Horne and R. P. Young, *J. Phys. Chem.*, **72**, 376 (1968).

(2) S. Subramanian, *ibid.*, **72**, 2694 (1968).

(3) R. A. Horne, A. F. Day, R. P. Young, and N. T. Yu, *Electrochim. Acta*, **13**, 397 (1968).

(4) R. A. Horne and R. P. Young, *J. Phys. Chem.*, in press.

(5) N. Y. Wen and S. Saito, *ibid.*, **68**, 2639 (1964).

(6) P. W. Bridgman, *J. Chem. Phys.*, **5**, 964 (1937).

(7) L. F. Evans, *Nature*, **213**, 384 (1967).

(8) L. F. Evans, *Trans Faraday Soc.*, **63**, 3060 (1967).

Arthur D. Little, Inc.   R. A. Horne
Cambridge, Massachusetts 02140   R. P. Young

Received May 13, 1968

The Pressure at the Maximum in Adsorption Isotherms at High Pressures

Sir: The maximum in adsorption isotherms at high pressures and above the critical temperature of the adsorbate has been observed in all cases where the measurements have been carried out to sufficiently high pressures, *e.g.*, CH_4 and H_2 on charcoal,[1] CO_2, N_2O, and SiF_4 on charcoal,[2] CH_4 on coal,[3-6] A and N_2 on active carbon,[7] N_2 and CO on alumina,[8,9] and CH_4 and C_2H_4 on silica gel.[10] According to the ordinary definition of

Table I: Comparison of $\tau^2 p_c$ with p_{max} from High-Pressure Adsorption Data

Gas	Adsorbent	Temp, °C	$\tau^2 p_c$, atm	p_{max}, atm	Ref
	A. Adsorbents of Second Structural Type				
CH_4	Coal	25	112	100–115	3–6
N_2	Alumina	−0.76	156	154	8
		25.1	188	200	
		50.0	220	227	
		74.9	256	260	
		99.7	293	300	
CO	Alumina	−0.77	142	146	9
		25.0	170	180	
		50.0	200	216	
CH_4	Silica gel	0	94	96	10
		−20	81	82	
		−40	68	63	
C_2H_4	Silica gel	25	56	52	10
CO_2	Porous plug of lampblack	32	73.6	74	13
	B. Adsorbents of First Structural Type				
CH_4	Charcoal	25	112	85	1
		50	131	100	
		100	175	124	
		180	258	132	
H_2	Charcoal	25	1169	80	1
CO_2	Coconut shell charcoal	35	75	44	2
		50	82	54	
		100	110	85	
N_2O	Coconut shell charcoal	60	83	52	2
		100	104	85	
SiF_4	Coconut shell charcoal	25	60	19	2
		50	71	28	
		100	94	41	
N_2	Active carbon	−76	82	60	7
		−25	130	80	
		0	157	95	
		20	181	120	
A	Active carbon	−76	85	60	7
		−25	134	95	
		0	163	105	
		20	187	120	
CH_4	Molecular sieve (Ca-substituted)	−78	48	32	14
N_2	Molecular sieve (Ca-substituted)	−78	80	57	14

adsorption, the amount adsorbed is the *excess* material present in the pores and on the surface of the adsorbent over and above that corresponding to the density of the

(1) P. K. Frolich and A. White, *Ind. Eng. Chem.*, **22**, 1058 (1950).

(2) A. S. Coolidge and H. J. Fornwalt, *J. Amer. Chem. Soc.*, **56**, 561 (1934).

(3) V. T. Palvelev, *Dokl. Akad. Nauk SSSR*, **62**, 779 (1948).

(4) V. V. Khodot, *Izv. Akad. Nauk SSSR, Otd. Tech. Nauk*, **733** (1948); 99 (1949); 1085 (1951).

(5) J. van der Sommen, P. Zwietering, B. J. M. Eillebrecht, and D. W. van Krevelen, *Fuel*, **34**, 444 (1955).

(6) D. H. Moffatt and K. E. Weale, *ibid.*, **34**, 449 (1955).

(7) A. von Antropoff, *Kolloid-Z.*, **137**, 105 (1955).

(8) A. Michels, P. G. Menon, and C. A. ten Seldam, *Rec. Trav. Chim.*, **80**, 485 (1961).

(9) P. G. Menon, *J. Amer. Chem. Soc.*, **87**, 3057 (1965).

(10) H. B. Gilmer and R. Kobayashi, *A.I.Ch.E. J.*, **10**, 797 (1964).

gas in the gas phase at that temperature and pressure. With increasing pressure this excess or differential adsorption soon reaches a maximum. As the pressure is increased further, the density of the gas phase (ρ_g) gradually approaches that of the adsorbed phase (ρ_a). This can continue till $\rho_g = \rho_a$ and the amount adsorbed, measured experimentally and calculated according to the above definition, must become zero.[11] Hence the high-pressure adsorption isotherms must exhibit a maximum even by elementary considerations.

In the application of Polanyi's potential theory of adsorption for gases above their critical temperatures, Dubinin[12] has shown that the filled volumes of adsorption space can be expressed as

$$W = ab \qquad (1)$$

where a is the amount adsorbed and b is the constant in the van der Waals equation, while the adsorption potential ϵ can be calculated from

$$\epsilon = 2.30RT \log (\tau^2 p_0/p) \qquad (2)$$

where $\tau = T/T_c$ is the reduced temperature and p_0 is the critical pressure of the adsorbate.

Application of eq 2 to high-pressure adsorption data shows that in many cases a is maximum when $\tau^2 p_0 = p$ and hence $\epsilon = 0$. The equilibrium pressure p_{max} at which the adsorption isotherm at any temperature exhibits a maximum can thus be calculated from critical temperature and pressure of the gas; it does not seem to depend on the type or nature of the adsorbent surface. In Table IA[13,14] the values of $\tau^2 p_c$ are compared with literature data on pressure p_{max} at which experimental adsorption isotherms exhibit a maximum. The agreement between the two is quite satisfactory especially in view of the numerous inaccuracies and uncertainties in usual high-pressure adsorption measurements,[15] and the added difficulty of locating p_{max} in cases where the maximum in the isotherm is not sharp but is rather flattened over a pressure range of 10–30 atm.

Adsorbents with extremely small micropores of molecular dimensions, e.g., charcoal, active carbon of high surface area, and molecular sieves, exhibit a dif-

ferent behavior (Table IB). In their case p_{max} is always much lower than $\tau^2 p_0$, the ratio of the two often being 0.6–0.8. These adsorbents for which the effect of increasing adsorption potentials as a result of overlapping of the fields of opposite walls of the pore is prominent, are designated by Dubinin[12] as adsorbents of the first structural type. In adsorbents with larger pores this overlapping of fields does not take place, and these are referred to as adsorbents of the second structural type. It is for this second type, given in Table IA, that the relation $\tau^2 p_0 = p_{max}$ holds good, although eq 2 has been found to be equally applicable[12] to adsorbents of both structural types.

A consequence of the relation $\tau^2 p_0 = p_{max}$ will be that $p_c = p_{max}$ when $T = T_c$. Thus p_{max} seems to have the role of a critical pressure for the gas adsorbed above its critical temperature, as if above this pressure the adsorbed gas forms a continuous film or "condensed" layer. An adsorption isotherm measured at the critical temperature of a gas should show a maximum at the critical pressure. The closest approach to critical temperature can be seen in the measurement of adsorption of CO_2 on a porous plug of lampblack[13] at 32° ($T_c = 31°$) where a maximum in the isotherm is observed at 74 atm, which agrees very well with the calculated value $\tau^2 p_0 = 73.6$ atm and the critical pressure of CO_2 of 73 atm.

(11) In practice, this has not been observed for any rigid noncompressible adsorbent. The behavior of the adsorption isotherms at very high pressures is quite different.[8,9]

(12) M. M. Dubinin, Chem. Rev., 60, 235 (1960); Russ. J. Phys. Chem., 39, 697 (1965).

(13) W. M. Jones, P. J. Isaac, and D. Phillips, Trans. Faraday Soc., 55, 1953 (1959).

(14) P. B. Lederman and B. Williams, A.I.Ch.E. J., 10, 30 (1964).

(15) P. G. Menon, Chem. Rev., 68, 277 (1968).

(16) Department of Chemical Engineering, Technological University Twente, Enschede, The Netherlands.

REGIONAL RESEARCH LABORATORY   P. G. MENON[16]
HYDERABAD 9, INDIA